Monopole Antennas

Melvin M. Weiner (retired)
The MITRE Corporation
Bedford, Massachusetts, U.S.A.

MARCEL DEKKER, INC. NEW YORK • BASEL

Marcel Dekker, Inc , and the author make no warranty with regard to the accompanying software, its accuracy or its suitability for any purpose other than as described in the *preface* This software is licensed solely on an 'as is' basis The only warranty made with respect to the accompanying software is that the diskette medium on which the software is recorded is free of defects Marcel Dekker, Inc , will replace a diskette found to be defective if such defect is not attributable to misuse by the purchaser or his agent The defective diskette must be returned within 10 days to Customer Service, Marcel Dekker, Inc , P O Box 5005 Cimarron Road Monticello, NY 12701 (914) 796-1919

Library of Congress Cataloging-in Publication Data
A catalog record for this book is available from the Library of Congress

ISBN: 0-8247-0496-7

This book is printed on acid-free paper

Headquarters
Marcel Dekker, Inc ,
270 Madison Avenue, New York, NY 10016
tel 212-696-9000 fax 212-685-4540

Eastern Hemisphere Distribution
Marcel Dekker AG
Hutgasse 4, Postfach 812, CH-4001 Basel, Switzerland
tel 41-61-260-6300 fax 41-61-260-6333

World Wide Web
http //www dekker com

The publisher offers discounts on this book when ordered in bulk quantities For more information write to Special Sales/Professional Marketing at the address below

Copyright © 2003 by Marcel Dekker, Inc. All Rights Reserved.

Neither this book nor any part may be reproduced or transmitted in any form or by any means, electronic or mechanical, including photocopying, microfilming, and recording, or by any information storage and retrieval system, without permission in writing from the publisher

Current printing (last digit)
10 9 8 7 6 5 4 3 2 1

PRINTED IN THE UNITED STATES OF AMERICA

In memory of

Jack H. Richmond (1922–1990)
Professor Emeritus,
The Ohio State University

and

James R. Wait (1924–1998)
Regents Professor,
University of Arizona

Preface

The primary intent of this book is to provide an industry standard for the modeling, testing, and application of airborne and ground-based monopole antennas. This standard is intended for engineers, scientists, practitioners, and students in the communication, radar, navigation, and government service industries. Most of the book is based on the original state-of-the-art work performed by the author at The MITRE Corporation in Bedford, Massachusetts with sponsorship by the U.S. Air Force and MITRE Independent Research Program. I did the work on surface-wave fields in Sec. 9.3 after my retirement from MITRE.

Part I is concerned with monopole antennas in free space. In this part of the book Earth parameters *do not* affect the antenna's electrical properties but *do* affect propagation losses (denoted as basic transmission loss $L_b(d)$ in Eq. (6.4.1)). This characteristic is realized if the base of the antenna is more than a quarter-wavelength above the earth's surface. The propagation mode is assumed to be the sum of direct and indirect waves through the troposphere by line of sight, reflection, refraction, and/or scattering—a typical mode and paths at frequencies above 30 MHz (see Sec. 6.5). An overview of the models, numerical results, applications, and computer programs in Part I is given in Chapter 1.

Part II is concerned with monopole antennas in proximity to flat earth. In Part II, Earth parameters *do* affect the antenna's electrical properties This

characteristic is realized if the base of the antenna is below the earth's surface or within a quarter-wavelength above the earth's surface Propagation modes are assumed to be a space wave within the radio horizon (with no earth dependent propagation losses), a space wave over the horizon by reflection from the ionosphere (with no earth-dependent propagation losses but with ionospheric propagation losses), or a surface wave through the earth (with earth-dependent propagation losses)—typical modes and paths at frequencies below 30 MHz (see discussion preceding and following Eq (13 1 3)) An overview of the models, numerical results, applications and computer programs in Part II is given in Chapter 7

This book is a greatly expanded version of an earlier book (MM Weiner, SP Cruze, CC Li, and WJ Wilson, *Monopole Elements on Circular Ground Planes*, Norwood, MA Artech House, 1987) that was restricted to discussion of structures in free space only The present book discusses structures in proximity to flat earth in addition to those in free space Chapters 1–5 and Appendices A 1–A 5, and B 1–B 5 are partially revised from the previous book except that the computer programs in Appendices B 1–B 5 are now provided on CD rather than as program printouts Entirely new material is in Chapters 6–13 and Appendices A 6–A 8, B 6–B 12, C and D

Although the monopole antenna is one of the oldest of antennas, its properties are neither well understood nor standardized, particularly for ground–plane radii that are small or comparable to a wavelength Most treatments idealize the monopole antenna by assuming a 'perfect" ground plane (of infinite extent and conductivity) Other treatments utilize asymptotic models that give approximate results only In this book, these deficiencies are addressed by providing an in depth treatment of the influence of both the finite extent and proximity to earth of the ground plane State of the art numerical methods, including Richmond's method of moments for disk ground planes and Lawrence Livermore Laboratory's Numerical Electromagnetics Code for radial-wire ground planes are featured to provide accurate results and an industry standard that were previously unavailable for monopole antennas A vertical cylindrical monopole element at the center of a horizontal circular ground plane has the simplest monopole antenna geometry because its structure and radiation pattern are both invariant in the azimuthal direction Such a structure is convenient for modeling, testing, and standardization

The electrical properties of monopole antennas with nonperfect ground planes *in free space* can be substantially different from those with a perfect ground plane For perfectly conducting structures in free space, the radiation efficiency is 100% However edge diffraction by the ground plane can reduce the input resistance (equal to the radiation resistance) by a factor of two peak directivity by as much as 3 3 dB and directivity in the plane of the ground plane by as much as 3 3 dB and increase the magnitude of the input reactance by an

infinite percentage from the value for a perfect ground plane (see Table 4 in Sec. 4.5). Furthermore, the direction of peak directivity can be tilted as much as 58 degrees above the plane of the ground plane compared with zero degrees for a perfect ground plane (see Fig. 5 in Sec. 4.5 and Table A2-22 in App. A.2).

Those same structures *in proximity to earth* can be substantially different from those in free space and from those with a perfect ground plane. Fresnel reflection causes a directivity null of minus infinity dB in the plane of the ground plane (see App. A.8). An electrically short monopole element in close proximity to dielectric earth can have a radiation efficiency of almost 0% and a peak directivity below earth of approximately +15 dB at a critical angle of approximately 20 degrees from the nadir direction (see Fig. 75 in Sec. 9.2.2 and Figs. 76 and 77 in Sec. 9.2.3). For quarterwave elements on electrically small ground planes resting on most types of earth except sea water, the peak directivity in the High Frequency (HF) band is not substantially different from that of a perfect ground plane but is tilted approximately 30 degrees above the plane of the ground plane compared to 0 degrees for a perfect ground plane (see Fig. 91 in Sec. 10.2 4) The input impedance is not as severely affected by edge diffraction (because the earth softens the edge of the ground plane) but is now affected by the decreased radiation efficiency (see Figs. A6-57 and A6-58 in Appendix A.6).

Part I is based on work performed for the U.S. Air Force SINCGARS radio program. The radio is a frequency-hopping antijamming radio in the Very High Frequency (VHF) band and utilizes an electrically short antenna to minimize aerodynamic drag on airborne platforms. The development of optimally efficient, electronically tunable antennas for this radio is of interest. Although the antenna ground plane is platform-dependent, it is usually small compared with a radio frequency (RF) wavelength. A circular ground plane provides a standardized ground-plane geometry with which to model and evaluate candidate antennas. Accordingly, a VHF antenna range with an eight-foot diameter ground plane was constructed at The MITRE Corporation and a theoretical study was initiated to evaluate candidate antennas. The system margin parameters of the SINCGARS radio were also investigated.

The results are reported in technical reports ESD-TR-86-241, ESD-TR-85-136, ESD-TR-88-270, and ESD-TR-82-400 prepared by MITRE for the Electronic Systems Division, Air Force Systems Command, Hanscom Air Force Base, Massachusetts under Project 6480, Contracts F19623-82-C-0001, F19628-84-C-0001 and F19628-86-C-0001. The book *Monopole Elements on Circular Ground Planes* and the present book's Chapters 1–5, Apps. A.1–A.5, and Apps. B.1–B.6 are from report ESD-TR-86-241. Sections 6.3, 6.4, and 6.5 are from reports ESD-TR-88-270, ESD-TR-85-136, and ESD-TR-82-400, respectively. Sec. 6.1 is from MITRE report M90-93 prepared under the MITRE Independent Research Program, Project 91260.

Part II is based on work sponsored by the MITRE Independent Research Program, Project Nos 91260 91030, and 91740, in support of the Advanced Over-the-Horizon (AOTH) radar program of the Defense Advanced Research Project Agency (DARPA) and the U S Air Force The proposed radar operates in the HF band with over-the-horizon space wave mode of propagation made possible by reflection from the ionosphere It would utilize a ground-based receiving array comprising hundreds or thousands of randomly spaced antenna elements Although an array with electrically large ground planes is desirable to increase radiation efficiency and reduce the elevation angle of peak directivity, they are prohibitively expensive to construct and maintain One approach is to use elements with electrically small ground planes A monopole element at the center of a circular ground plane provides a standardized geometry for evaluating candidate elements and ground planes Accordingly, a theoretical study was initiated to understand the electrical properties of monopole elements with circular ground planes in proximity to earth

The results are reported in MITRE reports MTR-10989 (Project 91260), M90-92 (Project 91260), M91-104 (Project 91030), MTR-92B0000089 (Project 91260), MTR 92B0000090 (Project 91260), MTR-11277 (Project 91030), MTR-11278 (Project 91030), MTR-11169 (Project 91030), MTR-93B000016 (Project 91740), and M91-82 by LW Parker (Project 91260) Sec 9 is in part from MTR-11277, Sec 10 and App A 6 are from M90 92, MTR-92B0000089, and MTR-92B0000090 Sec 11 and App A 7 are from M91-104 and MTR-11278, part of Sec 12 is from M91-82, Sec 13 1 is from MTR-10989 and MTR-93B0000169, Sec 13 2 is from MTR-11169, and Sec 13 3 is from MTR-11277

The above technical reports are in the public domain and are obtainable from the National Technical Information Service (NTIS)

The discussion of surface waves in Sec 9 3 represents new work I performed specifically for this book It includes approximate expressions for the case when the index of refraction is approximately unity, complementing work of earlier investigators for the case when the index of refraction is large

Melvin M Weiner

Acknowledgments

Several MITRE technical staff members and cooperative students contributed to this work. SP Cruze contributed to Sec. 3.5, wrote program LEITNER-SPENCE in App. B.03, and performed some of the early modeling in Sec. 6.3. CC Li contributed to Sec. 4.2, edited programs RICHMOND1 and RICHMOND2 in App. B.02, program AWADALLA in App. B.05, and wrote program BARDEEN in App. B.04. WJ Wilson contributed to Sec. 2 3 and Sec. 3.3. JE Kriegel derived the correct form of the continued fractions given in Eqs. (3.5.4) and (3 5.5), contributed to the evaluation of the limits in Eqs. (3.3.22–3.3.24), and confirmed the partial differential equation solution given in Eq. (C-27b). WC Corrieri (deceased) skillfully performed the measurements discussed in Chapter 5. K Pamidi contributed to the development of Eq. (3.3.16). LW Parker (deceased) developed the program for the computer plots in Sec. 6.1 and contributed Sec. 12.3.2. CR Sharpe obtained the computer plots in Sec. 6.1 and edited the RICHMOND3, RICHMOND4, RICHMOND5, RICHMOND6, and WAIT–SURTEES programs in App. B.06 and B.09-B.10. G Ploussios directed the design and development of electronically tuned helical monopole elements discussed in Sec. 6.2.9 and contributed Fig. 38. RD Parsons wrote the computer program SONF which produced the numerical results in Sec 6 4. C Korbani and SF McGrady wrote the computer program that produced the numerical results in Sec. 6.3. E Jappe and NJ Johnson

contributed to the numerical results in Sec 6 5 DJ Violette wrote the MODIFIED IMAGES program in App B 11 and obtained the numerical results in App A 8 L Giandomenico performed the computer runs that produced the numerical results in Sec 11 1 2 E Vlashi produced the computer plots in App A 6 S Zamoscianyk performed the computer runs and produced the computer plots in App A 7 JL Pearlman performed the MITRE code extensions of the NEC-3 NEC GS and NEC-31 programs discussed in Sec 11 1 JDR Kramer contributed Eq (D 3) in Appendix D GA Robertshaw contributed to the discussion in Sec 9 2 1 RL Lagace contributed to the discussion in Sec 11 1 3 and obtained extensive NEC 31 numerical results for electrically short elements and radial wire ground planes with a feed cable, including Table 42 in Sec 13 3 RI Millar WJ Wilson D Lamensdoff, and LJ Tieg reviewed the original manuscripts O Gray J Kalkert, SA Lamoureux, MP Lonergan M Massinger and EA Trottier typed most of the original manuscripts LC Nocca produced the photos in Figs 54 and 57

In Part I I am grateful to A Leitner of Rensselaer Polytechnic Institute for helpful conversations regarding his method of oblate spheroidal wave functions, JH Richmond (deceased) of Ohio State University for helpful conversations and magnetic tapes of his RICHMOND1, RICHMOND2 RICHMOND5, and RICHMOND6 method of moments programs K Awadalla of Menoufia University (Egypt) for helpful correspondence, including a listing of his program for the method-of-moments combined with the geometric theory of diffraction, GH Hufford, ME Johnson and WA Kissick of the Institute for Telecommunication Sciences (ITS) for software of the Longley–Rice and Johnson–Gierhart tropospheric propagation programs and GJ Burke of Lawrence Livermore National Laboratory (LLNL) for the NEC numerical results of Chapter 5 After I had obtained results by using the integral equation method and the method of oblate spheroidal functions it was possible to confirm the correctness of Richmond s method-of moment results, which were subsequently published (Ref 2)

In Part II, I am grateful to RP Ratuse of MIT s Lincoln Laboratory for helpful discussions on antenna structure fabrication remifications in Sec 8 3, RWP King of Harvard University for the Sommerfeld numerical results in Figs 76 and 77 in Sec 9 2 3 GJ Burke of LLNL for *NEC 3* numerical results (in Figs 75–77 of Sec 9 2 2 Table 19 of Sec 9 2 3 and Table 29 of Sec 12 2 2) *Mathematica* numerical results (in Figs 80–85 of Sec 9 3 3) and helpful discussion concerning the surface wave and the use of the NEC 3 and NEC GS programs GH Hagn of SRI International for Figs 66–69 and contributing to the feed cable discussion in Sec 11 1 3 JH Richmond (deceased) of Ohio State University for contributing his RICHMOND3 and RICHMOND4 method-of-moments programs and WAIT-SURTEES Program, JR wait (deceased) of the University of Arizona for preparing MITRE Report M90 79

"Antenna Performance Influenced by the Finite Extent and Conductivity of Ground Planes A Collection of Reprints by JR Wait, et al " which presents asymptotic results typical of the earlier literature, Lt J Fortney of the Rome Air Development Center for detecting an error in one of Wait's reprints, GA Thiele of the University of Dayton for his hybrid method of moments–geometric theory of diffraction program, CG Christodoulou of the University of Central Florida for his spectral domain conjugate algorithm for reflection from a planar mesh in free space, and GR Hand of ITS for permission to use the HFWIN32 ionospheric propagation programs

I am also grateful for the following MITRE management support

Project 6480 SINCGARS, GP Massa, Project Director

GP Massa perceived and supported the effort on antennas, propagation, and system margin, He brought to my attention the Institute for Telecommunication Sciences propagation programs and the work of GH Hagn on system margin

JF Sullivan (Department Head) supported the investigation of ways to reduce antenna Q without reducing antenna efficiency

RA McCown (Technical Director) motivated me to begin a serious study of monopole antennas after correctly pointing out that the radiation patterns of Leitner and Spence in Reference 3 were not normalized to give directivity

Major R Sutter (Air Force SINCGARS Program Office) gave constructive support to the MITRE effort

Project 91260 HF Antenna Element Modeling, MM Weiner, Principal Investigator

An outside Technical Advisory Group, organized by the Principal Investigator, assisted in refereeing technical issues and contributing to the results (see earlier acknowledgments) The Group comprised GJ Burke, CG Christodoulou, Lt J Fortney, GH Hagn, RWP King RP Rafuse, JH Richmond (deceased), GA Thiele, and JR Wait (deceased)

JF Sullivan (Department Head) correctly pointed out that the Fresnel Reflection Coefficient Model in Sec 12 does not account for the interconnectivity of the individual wire meshes comprising a groundscreen

RW Bush (Technical Director), CH Gager (Associate Technical Director), JDR Kramer (Consulting Engineer), RD Haggarty (Chief Engineer), and WE Sievers (Consulting Engineer) promoted the project effort

Project 91030 Experimental Site, EA Palo, Principal Investigator

EA Palo supported the study of the impact of candidate antenna elements on the performance of the HF West Texas Experimental Facility

Project 91740 High-Resolution Noise Mitigation Measurements, JDR Kramer, Principal Investigator

JDR Kramer contributed his signal processing expertise to the channel calibration of the MITRE West Texas Experimental Facility

Some of the material in this book has been published in book form and in refereed journals protected by copyright Receipt of waiver of copyright is gratefully acknowledged as follows

CHAPTERS 1–5

MM Weiner, SP Cruze, CC Li, WJ Wilson Monopole Elements on Circular Ground Planes, Norwood Artech House, 1987 (Copyright reverted to MM Weiner on Dec 29, 1998)

MM Weiner Monopole element at the center of a circular ground plane whose radius is small or comparable to a wavelength, IEEE Trans Antennas Propag, AP-35(5) 488–495, May 1987

MM Weiner Monopole element at the center of a circular ground plane of arbitrary radius, PIERS 1989 Proceedings, Boston July 25–26, 1989, p 216

CHAPTER 6

MM Weiner Electrically-small, quarterwave, and resonant monopole elements with disk ground planes in free space, PIERS 1991,Proceedings, Cambridge, Massachusetts, July 1–5, 1991, p 690

MM Weiner Noise factor of receiving systems with arbitrary antenna impedance mismatch, IEEE Trans Aerospace and Electron Sys, AES-24(2) 133–140, March 1988

MM Weiner Tuning stability of a digitally tuned, electrically-short monopole element on disk groundplanes of different radii Electromagn Waves Appl, 5(11) 1199–1215, 1991

MM Weiner Use of the Longley-Rice and Johnson-Gierhart tropospheric radio propagation programs 0 02-20 GHz, IEEE J Selected Areas Commun, SAC-4(2) 297–307, March 1986

CHAPTER 8

Figures 64-66 are reproduced from ITU-R P 527-3, Electrical Characteristics of the Surface of the Earth, (P Series—Part 1, 1997), International

Telecommunication Union, Place des Nations, CH-1211, Geneva 20, Switzerland.

CHAPTER 9

RWP King. On the Radiation Efficiency and Electromagnetic Field of a Vertical Electrical Dipole in the Air Above a Dielectric or Conducting Half-Space, Progress in Electromagnetic Research (PIER 4), New York: Elsevier, 1991, Chapter 1, pp 1–42.

JD Jackson. Classical Electrodynamics, 2nd ed, John Wiley and Sons, 1975, pp 316–317.

CHAPTER 10

MM Weiner. Radiation efficiency and directivity of monopole elements with disk ground planes on flat earth. Electron Lett, 28(25)·2282–2283, Dec. 3, 1992.

CHAPTER 11

MM Weiner, S Jamosciank, GJ Burke. Radiation efficiency and input impedance of monopole elementswith radial-wire ground planes in proximity to earth, Electroni Lett, 28(16) 1550–1551, July 30, 1992. Reply to JR Wait, ElectronLett, 28(25):2329, Dec. 30, 1992.

MM Weiner. Validation of the Numerical Electromagnetic Code (NEC) for Antenna Wire Elements in Proximity to Earth, Applied Comput Electromagn Soc J, 28(2)·44–71, 1993

Figure 99 is reproduced from GJ Burke, EK Miller. Numerical modeling of monopoles on radial-wire ground screens, Proceedings of 1989 IEEE Antennas and Propagation Society Symposium, 1:244–247, 1989.

CHAPTER 13

MM Weiner. Noise factor and antenna gains in the signal/noise equation for over-the-horizon radar. IEEE Trans Aerospace Electronic Sys, AES-27(6):886–890, Nov., 1991. Addendum, AES-30(2):648.

MM Weiner. Influence of non-homogeneous earth on the performance of high-frequency receiving arrays with electrically-small ground planes, Radio Sci, 29(1):55–71, Jan–Feb., 1994 (published by American Geophysical Union).

MM Weiner Performance of Ground-Based High-Frequency Receiving Arrays with Electrically Small Ground Planes, Progess in Electromagnetics Research (PIER 8), Cambridge, MA: EMW Publishing, 1994, Chapter 4, pp 109-159

The acquisition and production stages of this book were skillfully guided by BJ Clark and Brian Black of Marcel Dekker, Inc. The CD was resourcefully developed by H Rutledge of International Press, Inc.; S Mentzer of Objexx Engineering, and Y Kogan of Solid Applications, Inc.

Contents

Preface

Acknowledgments

Part I Monopole Elements on Disk Ground Planes in Free Space

1 Introduction

2 Circuit Representation
- 2.1 Geometry and Coordinate Systems
- 2.2 Directivity and Input Impedance
- 2 3 Relationship Between Radiation Resistance and Directivity on the Horizon
- 2.4 Characterization of Currents

3 Models in Which the Current Distribution on the Monopole Element is Initially Known
- 3.1 Boundary Conditions
- 3.2 Induced EMF Method, Ground Plane of Zero Extent
  - 3.2 1 Concept of a Ground Plane of Zero Extent

3 2 2 Near Fields
3 2 3 Far-Fields
3 2 4 Input Impedance
3 2 5 Summary of Results
3 3 Integral Equation $0 \leq ka \leq 2\ 75$
3 4 Method of Moments $0 \leq ka \leq 14$
3 5 Oblate Spheroidal Wave Functions $3\ 0 \leq ka \leq 6\ 5$
3 5 1 Form of Solution
3 5 2 Corrections
3 5 3 Regions of Calculation Validity
3 5 4 Accuracy
3 5 5 Numerical Results
3 6 Scalar Diffraction Theory and Geometric Theory of Diffraction $6\ 5 < ka < \infty$
3 7 Variational Method $30 \leq ka < \infty$
3 8 Method of Images $ka = \infty$
3 8 1 Near-Fields
3 8 2 Far Fields
3 8 3 Input Impedance
3 9 Summary of Results

4 Models in Which the Current Distributions on the Monopole Element and Ground Plane Are Both Initially Unknown
4 1 Boundary Conditions
4 2 Method of Moments $0 < ka \leq 14$
4 3 Method of Moments Combined with Geometric Theory of Diffraction $8\ 5 \leq ka < \infty$
4 4 Method of Images $ka = \infty$
4 5 Summary of Results

5 Comparison with Experimental Results

6 Applications Utilizing Electrically Small Elements
6 1 Electrically Small vs Quarter-Wave and Resonant Elements
6 2 Fundamental Limitations of Digitally Tuned Electrically Small Elements
6 2 1 Introduction
6 2 2 Definition of Problem
6 2 3 Radiation Regions
6 2 4 TM_{n0} Spherical Wave Modes
6 2 5 Equivalent Circuit of TM_{10} Mode
6 2 6 Q_{10} of TM_{10} Mode

6.2.7 Effect of Ground-Plane Size on Q_{10}
6.2.8 Bounds on Antenna System Performance
6.2.9 Unloaded Q of Monopole Elements
6.3 Tuning Stability of a Digitally-Tuned, Electrically Small Element on Disk Ground Planes of Different Radii
6.3.1 Introduction
6.3.2 Analytical Model
6.3.3 Numerical Results
6.3.4 Conclusions
6.4 Noise Factor of Receiving Systems with Arbitrary Antenna Impedance Mismatch
6.4.1 Introduction
6.4.2 Analytical Model
6.4.3 Numerical Results
6.4.4 Conclusions
6.5 Use of the Longley–Rice and Johnson–Gierhart Tropospheric Radio Propagation Programs: 0.02–20 GHz
6.5.1 Introduction
6.5.2 Basic Transmission Loss
6.5.3 Input Parameter Specification for the Longley–Rice Version 1.2.2 Prediction Program
6.5.4 Input Parameter Specification for Johnson–Gierhart IF-77 Prediction Program
6.6 Design and Qualification of a VHF Antenna Range
6.6.1 Requirements
6.6.2 Design Considerations
6.6.3 Qualification

Part II Monopole Elements on Disk, Radial-Wire, and Mesh Ground Planes in Proximity to Flat Earth

7 Influence of Proximity to Earth

8 Characterization of Antenna Parameters
8.1 Circuit Parameters
8.2 Earth Characteristics
8.3 Antenna Structure Fabrication Considerations

9 Models in the Absence of a Ground Plane
9.1 Introduction
9.2 Space-Wave Fields: Method of Images with Fresnel Reflection

9 2 1 Vertically Polarized Hertzian Dipole in Air Above Conducting Earth
9 2 2 Vertically Polarized Hertzian Dipole in Air Above Nonconducting Earth
9 2 3 Thin Monopole Element in Air Above Conducting Earth
9 3 Surface-Wave Fields Sommerfeld–King Integrals for Vertically Polarized Hertzian Dipole in Air Above Flat Earth
9 3 1 Hertz Potential in Air and Earth
9 3 2 Fields and Pseudo Fields in Air
9 3 3 Cases $|n^2| \gg 1$ and $|n^2| \approx 1$

10 Disk Ground Planes
10 1 Introduction
10 2 Method of Moments $0 \leq ka \leq 14$
10 2 1 Current Distribution and Input Impedance
10 2 2 Far Zone Field
10 2 3 Validation
10 2 4 Numerical Results
10 3 Variational Method $2 \leq ka \leq \infty$
10 4 Method of Images $ka = \infty$

11 Radial-Wire Ground Planes
11 1 Method of Moments $0 \leq ka \leq 250$
11 1 1 Model Description
11 1 2 Validation
11 1 3 Radiation Pattern Degradation by Feed Cable
11 1 4 Numerical Results
11 2 Variational Method $ka \geq 6 \quad N \geq 100$

12 Wire Mesh Ground Planes
12 1 Modeling Limitations
12 2 Method of Moments
12 2 1 Bonded Radial–Concentric Mesh
12 2 2 Rectangular Mesh
12 3 Space Wave Far Fields Method of Images with Fresnel Reflection $ka = \infty$
12 3 1 Fresnel Reflection Coefficient
12 3 2 Parallel-Wire Grid

13 System Performance
13 1 Noise Factor and Antenna Gains in the Signal/Noise Equation for Over the-Horizon Radar

13.1.1 Introduction and Summary
13.1.2 Recommended Form of the Signal-to-Noise Radar Equation
13.2 Influence of Nonhomogeneous Earth on the Performance of High-Frequency Receiving Arrays with Electrically Small Ground Planes
13.2.1 Introduction
13.2.2 Model
13.2.3 Numerical Results
13.2.4 Summary and Conclusions
13.3 Performance of Ground-Based High-Frequency Receiving Arrays with Electrically Small Ground Planes
13.3.1 Introduction
13.3.2 Element Directivity
13.3.3 System Operating Noise Factor
13.3.4 Array Factor Degradation by Nonhomogeneous Earth
13.3.5 Summary and Conclusions

Appendix A Computer Plots and Printouts of Numerical Results
A.1 Integral Equation
A.2 Method of Moments—Free Space
A.3 Oblate Spheroidal Wave Functions
A.4 Variational Method
A.5 Method of Moments Combined with Geometrical Theory of Diffraction
A.6 Method of Moments (Richmond)—Proximity to Earth
A.7 Method of Moments (NEC-GS)
A.8 Method of Images with Fresnel Reflection

Appendix B Computer Programs
B.01 BARDEEN (Integral Equation)
B.02 RICHMOND1, RICHMOND2 (Method of Moments—Free Space)
B.03 LEITNER-SPENCE (Oblate Spheroidal Wave Functions)
B.04 STORER (Variational Method—Free Space)
B.05 AWADALLA (Method of Moments with Geometrical Theory of Diffraction)
B.06 RICHMOND5, RICHMOND6 (Method of Images with Moments—Free Space)
B.07 LONGLEY–RICE (Tropospheric Propagation—Program ITM)
B.08 JOHNSON–GIERHART (Tropospheric Propagation—Program IF-77)

B 09 RICHMOND3, RICHMOND4 (Method of Moments—Proximity to Earth)
B 10 RICHMOND7 (Variational Method—Proximity to Earth)
B 11 MODIFIED IMAGES (Method of Images with Fresnel Reflection)
B 12 IONCAP (HF Ionospheric Propagation—Program HFWIN32)

Appendix C Evaluation of Sommerfeld–King Integrals for Surface-Wave Fields
C 1 Exact Integral Expressions for Pseudo-Surface Wave Fields
C 2 $|n^2| \gg 1$*, Approximate Closed-Form Expressions for Fields*
C 3 $|n^2| \approx 1$*, Approximate Closed-Form Expressions for Fields*

Appendix D Beam Pointing Errors Caused by a Nonhomogeneous Earth

References

Part I

Monopole Elements on Disk Ground Planes in Free Space

1

Introduction

Monopole antennas are commonly employed in airborne and ground-based communication systems at a wide range of frequencies. The electrical properties of such antennas are dependent upon the geometry of both the monopole element and the ground plane. Typically, the monopole element may be electrically short (length is much less than a quarter-wavelength) or near-resonant (length approximately a quarter-wavelength), and it may be thin (length-to-radius ratio is much greater than 10^4) or relatively thick (length-to-radius ratio of 10^1 to 10^4). In addition, the ground-plane dimensions may vary from a fraction of a wavelength to many wavelengths. Therefore, it is desirable to know how the input impedance and radiation pattern of the antenna change as the dimensions of the monopole element and the ground plane vary. The directivity on or near the radio horizon (the ground plane is assumed to be horizontal) is of particular interest because the maximum operational range of a communication system often depends on the directivity on the radio horizon.

This study is restricted to a monopole geometry consisting of a vertical cylindrical element at the center of a perfectly conducting, infinitely thin, circular ground plane in free space. This geometry is of interest because its radiation pattern is uniform in the azimuthal direction and because its electrical characteristics are primarily a function of only three parameters, namely, the *element length*, *the element radius*, *and the ground-plane radius*, when each is normalized to the excitation wavelength. Therefore, this geometry is conducive to analysis, experimental verification, and standardization.

A typical feed for the monopole antenna is a coaxial line with its inner conductor connected through a hole in the ground plane to the vertical monopole element and its outer conductor connected by means of a flange to the ground plane. Typically, the inner conductor's diameter is equal to the monopole

element's diameter and the outer conductor's diameter is equal to the ground-plane hole diameter. Unless stated otherwise, such a feed will be assumed in this study. The ratio of the coaxial line's outer-to-inner conductor diameters affects the antenna's input impedance, but only significantly for a relatively thick monopole element on a very small ground plane.

For the idealized case of a ground plane of infinite extent and infinite conductivity, the monopole antenna may be modeled by the method of images as a dipole with one-half the input impedance and double the peak directivity of the dipole. The infinite ground plane prevents monopole radiation into the hemisphere below the ground plane, but allows a radiation pattern identical to that of the dipole in the upper hemisphere. However, for a monopole element mounted on a ground plane of finite extent, the outer edge of the ground plane diffracts incident radiation in all directions, and consequently modifies the currents on the ground plane and the vertical element from those of an infinite ground plane. At the outer edge of the ground plane, the currents on its top and bottom faces are equal in magnitude but opposite in direction because the net current must be zero at the edge. Outer-edge diffraction becomes increasingly significant with decreasing size of the ground plane because of the increasing magnitude of the currents on the ground-plane faces at the outer edge. Edge diffraction can alter the input impedance by more than 3 dB and directivity in the plane of the ground plane by more than 6 dB from the values for a ground plane of infinite extent.

Theoretical models exist for predicting the effects of diffraction by the outer edge of the ground plane. The existing models may be classified into two categories, distinguished by whether the current distribution on the monopole element is initially known or unknown.

When the monopole element is very thin and not too long, its current distribution is approximately sinusoidal and independent of the radius of the ground plane. Consequently, the element's current distribution can be initially specified and we need only determine the ground plane's current distribution. For this category of monopoles, the theoretical models reported in the literature essentially consist of Bardeen's integral equation method for a ground-plane radius that is small compared to a wavelength [1], Richmond's method of moments (ground plane only) for a ground-plane radius that is not too large compared to a wavelength [2], Leitner and Spence's method of oblate spheroidal wave functions for a ground-plane radius that is comparable to a wavelength [3–5], Tang's scalar theory of diffraction [6] and the geometric theory of diffraction (GTD) for a ground-plane radius that is large compared to a wavelength, and Storer's variational method for a ground-plane radius that is very large compared to a wavelength [7,8].

When the monopole element is relatively thick, its current distribution is no longer sinusoidal, and the current distribution on both the monopole element and the ground plane consequently need to be determined as a function of

the ground-plane radius. For this category of monopoles, the theoretical models reported in the literature essentially consist of Richmond's method of moments for ground-plane radius that is not too large compared to a wavelength [2] and Awadalla-Maclean's method of moments (monopole element only) combined with the geometric theory of diffraction for ground-plane radius that is large or comparable to a wavelength [9,10]. Thiele and Newhouse have also reported a model that combines the method of moments with the geometric theory of diffraction, but their computer program is unavailable [11].

Each of the existing models is valid for different and sometimes overlapping sets of limited values of ground-plane radii. Some of the models require extensive numerical computation. Therefore, the collection of models taken as a whole has several deficiencies. In the open literature, results for input impedance and directivity have never been assembled as a continuous function of ground-plane radius for the entire range of values from zero to infinity. In regions where models overlap, it is sometimes unclear which models are more accurate. In some models, numerical results have been reported for only a few values of ground-plane radius. In one model, Bardeen's integral equation, the base of the monopole element has not been allowed to be in the same plane as the ground plane, which is our present case of interest. Computer programs are not available for some of the older models because they were developed before the advent of computers. One of the most versatile of the models, Richmond's method of moments, gives only the input impedance and not the radiation pattern. In another model, Leitner and Spence's oblate spheroidal wave functions, one of the published algorithms for computing the eigenvalues is incorrect. Finally, extensive numerical results for small ground planes and resonant monopoles with finite ground planes are not to be found in the open literature.

Chapters 2–5 attempt to correct these deficiencies. Computer programs and numerical results are presented for all of the models. The induced EMF method is utilized to determine the input impedance of a thin, idealized monopole element in the absence of a ground plane. In Bardeen's integral equation method, the excitation function for the ground-plane currents is extended to include the singularity that occurs when the base of the monopole element is in the same plane as the ground plane. Richmond's method of moments is extended to give the far-field radiation pattern. In Leitner and Spence's method of oblate spheroidal wave functions, we have corrected the published continued-fraction algorithm for computing the eigenvalues. Numerical results for input impedance and directivity are presented as a continuous function of ground-plane radius for arbitrary radius. Numerical results of various models are compared, and we identify the suspected best available results. Extensive numerical results are given for small ground planes and resonant monopoles on finite ground planes. New experimental data are presented and compared with numerical results.

Circuit representations of the monopole antenna are developed in Chapter 2. Theoretical models and numerical results are presented in Chapter 3 for the case in which the current distribution on the monopole element is initially known. In Chapter 4, theoretical models and numerical results are presented for the case in which the current distribution on both the monopole element and ground plane are initially unknown. The theoretical models are compared with experimental data in Chapter 5. Computer printouts of directivity, and the far-field elevation pattern are given in Appendices A.1 – A.5. Computer programs of the theoretical models are given in Appendices B.01 – B.06.

Some system applications of free-space models of monopole antennas, whose radiated energy propagates through the Earth's troposphere, are illustrated in Chapter 6. Sec. 6.1 compares the properties of small, quarter-wave, and resonant elements. Some fundamental limitations of electrically short monopole antennas are presented in Sec. 6.2. Sec. 6.3 discusses the tuning stability of a digitally tuned, electrically short monopole element on disk ground planes of different radii. The effect of the electrical properties of monopole antennas on the system margin of a receiving system (including effect of impedance mismatch on system noise factor) is discussed in Sec. 6.4. Appendices B.07 and B.08 present two versatile Institute for Telecommunication Sciences (ITS) computer programs for calculating propagation loss through the Earth's troposphere. The use of these two programs is discussed in Sec. 6.5. Sec. 6.6 concludes Part 1 with the design and qualification of a very high frequency (VHF) antenna range that simulates free-space conditions.

2

Circuit Representation

2.1 GEOMETRY AND COORDINATE SYSTEMS

Consider a monopole element of length h and radius b, which is located in free space at the center of an infinitely thin, circular ground plane of radius a and infinite conductivity (see Fig. 1). The ground-plane radius, when expressed in radians, is given by

$$\epsilon \equiv ka \tag{2.1.1}$$

where

$k = 2\pi/\lambda =$ wavenumber (m^{-1})
$\lambda =$ excitation wavelength (m)

The monopole element and ground plane have current distributions in real time given by

$$I_z(z,t) = \mathrm{Re}[I(z)\,\mathrm{e}^{j\omega t}], \quad I_\rho(\rho,t) = \mathrm{Re}[I(\rho)\,\mathrm{e}^{j\omega t}] \tag{2.1.2}$$

where

$\omega =$ radian frequency of the excitation $= 2\pi c/\lambda$ (rad/sec)
$c =$ wave velocity in free space $= 2.9979 \times 10^8$ m/sec
$I(z),\ I(\rho) =$ element and ground-plane current amplitude distributions, respectively, (A). The subscripts z and ρ are suppressed in our notation.

A field point $P(r, \theta, \phi)$, expressed in spherical coordinates, is shown in Fig. 1. The field is uniform in the azimuthal direction ϕ. The relationships between

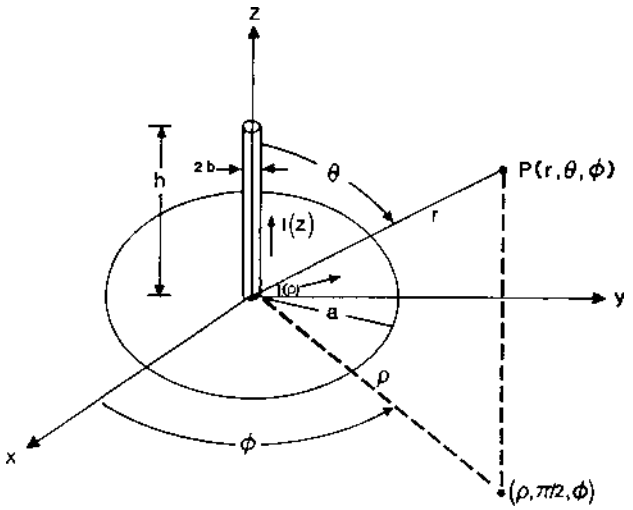

FIGURE 1 Monopole element at the center of a circular ground plane.

spherical, cylindrical, and oblate spheroidal coordinate systems are shown in Table 1. In the far-field, the elevation angle θ is related to the oblate spheroidal >angular coordinate η by $\eta \rightarrow \cos\theta$ as the spheroidal radial coordinate $\xi \rightarrow \infty$.

2.2 DIRECTIVITY AND INPUT IMPEDANCE

At a far-field observation point $P(r, \theta, \phi)$, the numeric directivity $d(\theta, \phi)$ of the antenna is defined as the ratio of its radiated power density $s(\theta, \phi)$ to its radiated

TABLE 1 Spherical, Cylindrical, and Oblate Spheroidal Coordinates

Coordinates	Spherical (r, θ, ϕ)	Cylindrical (ρ, z, ϕ)	Oblate spheroidal (ξ, η, ϕ)
Radius	r	$\rho = r\sin\theta$	$\rho = a[(1-\eta^2)(1+\xi^2)]^{1/2}$
Elevation	θ	$z = r\cos\theta$	$z = a\eta\xi$
Azimuth	ϕ	ϕ	ϕ

Note 1: In Table 1, the notation ξ, η is that of Leitner and Spence (L + S), *Franklin Institute Journal*, Vol. 249, No. 4, pp. 299–321, April 1950. This notation is related to that of Abramowitz and Stegun (A + S), *Handbook of Mathematical Functions*, National Bureau of Standards, Applied Mathematical Series, No. 55, p. 752, June 1964, by $\xi_{L+S} = (\xi^2_{A+S} - 1)^{1/2}$, $\eta_{L+S} = (1 - \eta^2_{A+S})^{1/2}$.
Note 2: The cylindrical coordinates (ρ, z, ϕ) are related to the rectangular coordinates (x, y, z) by $x = \rho\cos\phi$, $y = \rho\sin\phi$, $z = z$.

power density averaged over all directions. The radiated power density averaged over all directions is equivalent to the power density radiated by a hypothetical "isotropic" (ideal) antenna. Accordingly, the directivity $d(\theta, \phi)$, expressed in spherical coordinates with the origin at the antenna, is given by

$$d(\theta, \phi) = \frac{s(\theta, \phi)}{(1/4\pi)\int_0^{2\pi}\int_0^{\pi} s(\theta, \phi)\sin\theta \,\mathrm{d}\theta\,\mathrm{d}\phi} \tag{2.2.1}$$

For antenna patterns that are uniform in the azimuthal direction, such as for the antenna geometry of Fig. 1, Eq. (2.2.1) reduces to

$$d(\theta) = \frac{2s(\theta)}{\int_0^{\pi} s(\theta)\sin\theta \,\mathrm{d}\theta} = \frac{2s'(\eta)}{\int_{-1}^{1} s'(\eta)\,\mathrm{d}\eta} = d'(\eta) \tag{2.2.2}$$

where

$s(\theta) = (1/2)\sqrt{\mu_0/\epsilon_0}|H_\phi|^2 = (1/2)\sqrt{\epsilon_0/\mu_0}|E_\theta|^2$
H_ϕ, E_θ = far-field magnetic and electric field intensities, respectively
$s'(\eta)$, $d'(\eta)$ = radiation power density and directive gain, respectively, in oblate spheroidal coordinates
$\sqrt{\mu_0/\epsilon_0}$ = wave impedance in free space

The numeric directivity $d(\theta, \phi)$ is related to the directivity $D(\theta, \phi)$, expressed in dBi, by

$$D(\theta, \phi) = 10\log_{10} d(\theta, \phi) \quad \text{(dBi)} \tag{2.2.3}$$

The total time-averaged radiated power P_{total} of the antenna is given by

$$\begin{aligned} P_{\text{total}} &= \int_0^{2\pi}\int_0^{\pi} s(\theta, \phi) r^2 \sin\theta \,\mathrm{d}\theta\,\mathrm{d}\phi \\ &= 2\pi r^2 \int_0^{\pi} s(\theta)\sin\theta \,\mathrm{d}\theta = 2\pi r^2 \int_{-1}^{1} s'(\eta)\,\mathrm{d}\eta \end{aligned} \tag{2.2.4}$$

The antenna radiation resistance R_{rad}, referred to the complex amplitude $I(z = 0)$ of the antenna base current, is defined by

$$R_{\text{rad}} = 2P_{\text{total}}/|I(z = 0)|^2 \tag{2.2.5}$$

By substituting Eqs. (2.2.4) and (2.2.5) in Eq. (2.2.2), we have

$$\begin{aligned} d(\theta) &= s(\theta)\, 8\pi r^2/[R_{\text{rad}}|I(z = 0)|^2] \\ &= s'(\eta)\, 8\pi r^2/[R_{\text{rad}}|I(z = 0)|^2] = d'(\eta) \end{aligned} \tag{2.2.6}$$

The antenna input impedance, Z_{in}, is given by

$$Z_{in} = V(z = 0)/I(z = 0) = R_{in} + jX_{in} \tag{2.2.7}$$

where

$V(z = 0)$ = complex amplitude of the excitation voltage across the aperture of the coaxial-line feed to the antenna (V)
R_{in} = input resistance (Ω)
X_{in} = input reactance (Ω)

The input resistance R_{in}, is related to the radiation resistance R_{rad} by

$$R_{in} = R_{rad} + R_{ohmic} \tag{2.2.8}$$

where R_{ohmic} is the ohmic loss resistance of the antenna for finite conductivity of either the monopole element or the ground plane. Here, $R_{ohmic} = 0$ because the monopole element and ground plane are assumed to be of infinite conductivity. Accordingly,

$$R_{in} = R_{rad}, \quad R_{ohmic} = 0 \tag{2.2.9}$$

Equation (2.2.9) is a statement that the antenna is assumed to have an efficiency of unity.

2.3 RELATIONSHIP BETWEEN RADIATION RESISTANCE AND DIRECTIVITY ON THE HORIZON

For a vertical monopole element with a finite ground plane, the far-field radiated power density on the radio horizon, $s(\theta = \pi/2)$, is determined only by the current distribution on the monopole element (and not the ground-plane current) because only the vertical monopole element has a component of electron acceleration normal to the radio horizon. (This statement is not true for a ground plane of infinite extent because a far-field point on the radio horizon is then on the ground plane.) Identical monopole elements with identical current distributions, but mounted on ground planes of different finite radii, will consequently have identical far-field radiated power densities on the radio horizon. Accordingly,

$$s_\epsilon(\theta = \pi/2) = s_0(\theta = \pi/2) \tag{2.3.1}$$

for identical monopole element, identical element current distribution, and ground plane of finite extent, where the subscript ϵ denotes the radius in radians of the ground plane of arbitrary but finite extent ($\epsilon < \infty$), and the subscript 0 denotes a ground plane of zero extent ($\epsilon = 0$).

If we substitute Eq. (2.2.6) in Eq. (2.3.1) and compute the quantity $s(\theta = \pi/2)|I(z=0)|^2/8\pi r^2$, we obtain the following relationship between radiation resistance R_{rad} and numeric directivity on the horizon $d(\theta = \pi/2)$:

$$d_\epsilon(\theta = \pi/2)R_{\text{rad}\,\epsilon} = d_0(\theta = \pi/2)R_{\text{rad}\,0} = \text{constant} \tag{2.3.2}$$

for identical monopole elements, identical element current distributions, and ground plane of finite extent.

In Eqs. (2.3.1) and (2.3.2), the condition of identical element current distributions for ground planes of different radii is generally not satisfied by the use of monopole antennas. The element current distribution $I(z)$ is generally dependent on the ground-plane current $I(\rho)$, which, in turn, is a function of the ground-plane radius. However, for monopole elements that are sufficiently thin electrically and not too long, the element current distribution $I(z)$ is approximately sinusoidal and independent of the ground-plane current $I(\rho)$ (see Sec. 3.1). Expressions for $d_0(\theta = \pi/2)$ and R_{rad}, for elements with a sinusoidal current distribution, are determined in Sec. 3.2. Substitution of those expressions in Eq. (2.3.2), for the case of an infinitely thin monopole element ($b = 0$), yields

$$d(\theta = \pi/2)R_{\text{rad}} = (\eta/4\pi)[1 - \cos(kh)]^2/\sin^2(kh); \quad b = 0 \tag{2.3.3}$$

for a sinusoidal element current distribution and ground planes of finite extent, where

η = wave impedance of free space = 376.73 Ω
h = length of the monopole element

The condition $b = 0$ may be removed from Eq. (2.3.3) without substantially altering the result because the radiation pattern and radiation resistance of electrically thin elements that are not too long are weakly dependent upon the element radius (see Sec. 3.2).

2.4 CHARACTERIZATION OF CURRENTS

The characterization of the currents on the monopole element, ground plane, and coaxial-line-feed is illustrated in Fig. 2. The physical realization, circuit representation, and two circuit idealizations of the currents are shown in Fig. 2(a)–(d), respectively. In Fig. 2(b), the coaxial-line excitation of Fig. 2(a) is replaced by equivalent electric and magnetic currents on a conductor completely enclosing the coaxial line. In Fig. 2(c), the normalized ferrite attenuation distance $h_1/\lambda \ll 1$ is idealized to be zero. In Fig. 2(d), the magnetic frill M_ϕ is assumed to be negligible.

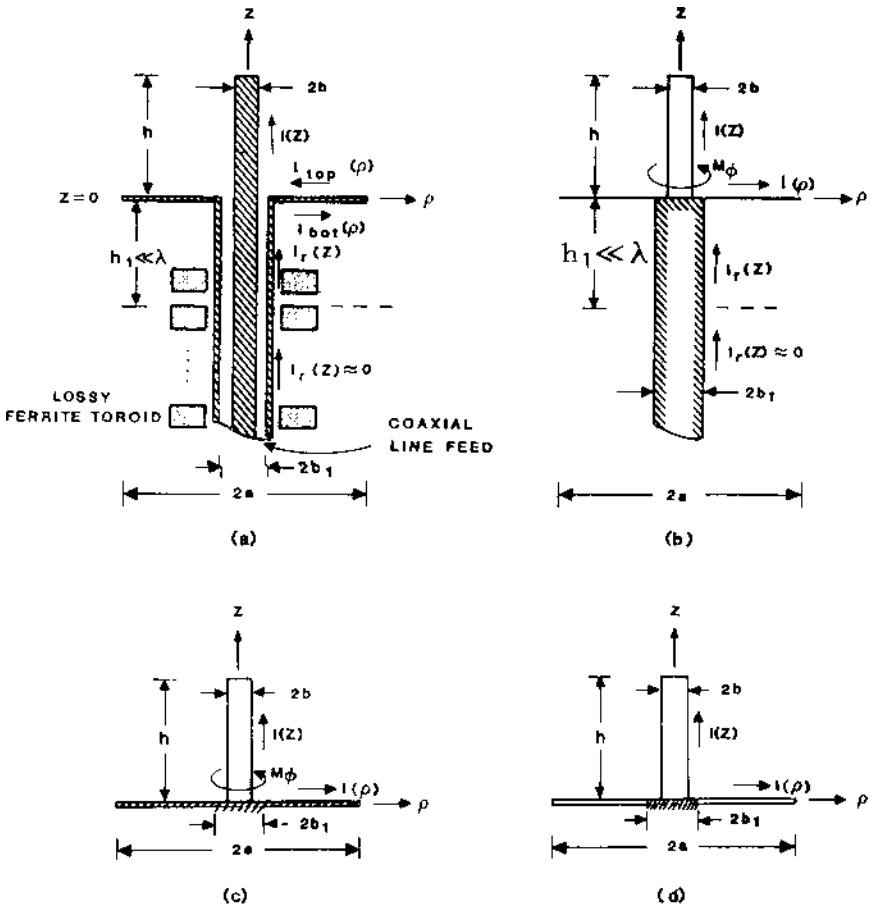

FIGURE 2 Characterization of currents on monopole element, ground plane, and coaxial-line feed: (a) physical realization; (b) circuit representation; (c) idealization of circuit ($h_1/\lambda = 0$); and (d) idealization of circuit ($h_1/\lambda = 0, \quad kb_1 \ll 1$, where $I(z)$ or $I(\rho)$ initially known).

The currents of interest are the element current $I(z)$ (positive in the $+z$ direction), the return current $I_r(z)$ on the outside of the coaxial-line outer conductor (positive in the $+z$ direction), the current $I_{bot}(\rho)$ on the bottom face of the ground plane (positive in the $+\rho$ direction, and the current $I_{top}(\rho)$ on the top face of the ground plane (positive in the $-\rho$ direction). A net ground-plane current $I(\rho)$ (positive in the $-\rho$ direction) is defined as

$$I(\rho) = I_{bot}(\rho) - I_{top}(\rho) \tag{2.4.1}$$

In the physical realization of the currents [Fig. 2(a)], lossy ferrite toroids are mounted along the outside of the coaxial-line's outer conductor. Such a procedure is commonly utilized on antenna ranges to reduce the radiation or pickup of unwanted signals from currents induced on the outside of the transmitter or receiver coaxial cables. For a sufficient number of ferrite toroids near the terminal end of the coaxial line, the return current $I_r(z)$ is approximately zero at distances greater than the l/e attenuation distance h_1 from the termination of the line. Here, we assume the ferrite toroids to be sufficiently lossy, so that

$$h_1 \ll \lambda \tag{2.4.2}$$

where λ is the excitation wavelength.

The radii of the outer and inner conductors of the coaxial line are b_1 and b, respectively, where b is also the radius of the monopole element. The wall thickness of the coaxial-line's outer conductor is assumed to be much less than its diameter. Consequently, the return current $I_r(z)$ occurs at the radial coordinate $\rho \approx b_1$.

The constraints on the various currents are given as follows:

Element:

$$I(z = h) = 0 \tag{2.4.3}$$

Ground Plane:

$$I(\rho = a) = 0 \tag{2.4.4}$$

Coaxial Line:

$$I_r(z) \approx 0, \quad -\infty < z < -h_1 \tag{2.4.5}$$

Element Ground-Plane:

$$I(z = 0) = -I(\rho = b) \tag{2.4.6}$$

Ground-Plane Coaxial Line:

$$I_{bot}(\rho = b_1) = I_r(z = 0) \tag{2.4.7}$$

The element and ground-plane constraints are a consequence of an open circuit at the end of the element and the ground plane. The coaxial-line constraint is a consequence of the lossy ferrites. The element ground-plane constraint is a consequence of conservation of charge (Kirchhoff's current law) at a node. The ground-plane coaxial-line constraint is a consequence of conservation of charge along a conductor.

By the use of the equivalence principle [12], the coaxial-line feed excitation may be replaced by equivalent tangential field excitations defined along a surface completely enclosing the coaxial line. At field points external to

this surface, the equivalent field excitations will give the same field as the original source excitation. In the circuit representation of the monopole antenna currents [Fig. 2(b)], the coaxial-aperture excitation is replaced by an equivalent surface magnetic current density (magnetic frill) M_ϕ, which sits on top of a thick ground plane of radius b_1. The magnetic frill M_ϕ is defined to be positive in the positive azimuthal direction, and is given by

$$M_\phi = \begin{cases} -V(0)/[\rho \ln(b_1/b)], & b \le \rho \le b_1 \\ 0, \quad \rho < b, & \rho > b_1 \end{cases} \tag{2.4.8}$$

Equation (2.4.8) is derived as follows. The radial field E of the coaxial-line aperture, assuming a TEM-mode excitation, is given by

$$E_\rho = \begin{cases} V(0)/[\rho \ln(b_1/b)], & b \le \rho \le b_1 \\ 0, & \rho < b \end{cases} \tag{2.4.9}$$

where $V(0)$ is the positive voltage at $z = 0$ across the aperture with the coaxial outer conductor at zero potential. By way of the equivalence principle [12], an aperture field may be replaced by a magnetic frill $\mathbf{M}$ that sits on top of a ground plane congruent with the aperture surface, and which is defined as

$$\mathbf{M} = \mathbf{E}_{\text{tangential}} \times \mathbf{n} \tag{2.4.10}$$

where $\mathbf{n}$ is the outward normal to the aperture surface and $\mathbf{E}_{\text{tangential}}$ is the tangential field at the aperture surface. By substituting Eq. (2.4.9) in Eq. (2.4.10), we have

$$\mathbf{M} = (\hat{u}_\rho E_\rho) \times \hat{u}_z = -E_\rho \hat{u}_\phi = \hat{u}_\phi M_\phi \tag{2.4.11}$$

where M_ϕ is given by Eq. (2.4.8). Equation (2.4.8) agrees with the result obtained by Richmond [2].

In the circuit representation of Fig. 2(b), the net ground-plane current $I(\rho)$ is the same as defined by Eq. (2.4.1), with the additional current constraint:

$$I_{\text{bot}}(\rho) = 0, \quad 0 \le \rho < b_1 \tag{2.4.12}$$

If the circuit representation of the monopole antenna in Fig. 2 is now idealized by setting the ferrite l/e attenuation distance $h_1/\lambda = 0$, then,

$$I_{\text{r}}(z) \approx 0; \quad z < 0, \quad h_1/\lambda = 0 \tag{2.4.13}$$

Consequently, the coaxial-line's outer conductor may be removed from the circuit as shown in Fig. 2(c). The ground-plane coaxial-line current constraint of (2.4.7) is not disturbed by such an idealization. Because it has already been assumed that $h_1 \ll \lambda$, the idealization $h_1 = 0$ does not appreciably alter either

the radiation pattern or the input impedance of the monopole antenna, provided that the monopole length $h \gg h_1$. Finite currents on an aperture that is small compared to the excitation wavelength contribute little to the far-field and input impedance. (Compare with the results for an electrically small dipole.) Experimental radiation patterns and measurements of input impedance (see Chapter 5) confirm that the use of lossy ferrite toroids along the coaxial-line's outer conductor yields results which are in close agreement with theoretical results for the circuit idealization condition of Eq. (2.4.13)—even for electrically small ground planes.

In the idealization of the monopole antenna circuit, the magnetic frill M_ϕ may be removed [Fig. 2(d)] without appreciably altering the radiation pattern or input impedance, provided that

$$kb_1 \ll 1 \tag{2.4.14}$$

and $I(z)$ or $I(\rho)$ is initially known, which constitute the conditions for neglecting the magnetic frill.

The condition $kb_1 \ll 1$ corresponds to the condition for TEM-mode excitation of the coaxial line and negligible power radiated from the coaxial-line aperture. If either $I(z)$ or $I(\rho)$ is initially known, then the one which is not known may be determined from the other, without requiring knowledge of the original coaxial-line excitation or its equivalent, provided that the field radiated by the known current distribution is the predominant field incident on the conductor of unknown current distribution. When neither $I(z)$ nor $I(\rho)$ is known, then the original source excitation or its equivalent (in this case, the magnetic frill M_ϕ) must be specified to determine the unknown radiated fields.

3

Models in Which the Current Distribution on the Monopole Element is Initially Known

3.1 BOUNDARY CONDITIONS

The current amplitudes, $I(z)$ and $I(\rho)$, on the monopole element and ground plane, respectively, are generally complex and initially unknown quantities (see Fig. 1). Consider now the case where the current distribution on the monopole element is assumed to be sinusoidal. For such a case and for the waveform dependence given in Eq. (2.1.2), we have

$$I(z) = \frac{I(0)}{\sin(kh)} \sin[k(h - z)], \quad 0 \leq z \leq h \tag{3.1.1}$$

where

h = monopole length (m)
$k = 2\pi/\lambda$ = wave number (m^{-1})
$I(0)$ = current amplitude of the monopole base current at $z = 0$ (A)

From Eq. (3.1.1)

$$\arg I(z) = \text{constant}, \quad 0 \leq z \leq h \tag{3.1.2}$$

Although a sinusoidal distribution of current is not possible, even for an infinitely thin antenna, Eq. (3.1.1) is most likely a fair approximation to the current if the monopole element is sufficiently thin electrically and not too long [13]. For a center-fed dipole of radius b and total length $2h$, Elliot [14] gives examples where the current distribution is approximately sinusoidal and of approximately constant argument for $b/\lambda = 1.0 \times 10^{-4}$ and $h/\lambda = 0.125, 0.25$.

However, for $b/\lambda = 1.0 \times 10^{-4}$ and $h/\lambda = 0.375, 0.5$, Elliot demonstrates that the current distribution is no longer sinusoidal near the center of the dipole, nor is $\arg z$ approximately constant. Balanis [15] shows that for $b/\lambda = 2.0 \times 10^{-4}$ and $h/\lambda = 0.25, 0.5$, the current distribution is not sinusoidal near the center of the dipole. Elliot and Balanis also demonstrate that for $b/\lambda = 1.0 \times 10^{-2}$ and $h/\lambda = 0.125, 0.25, 0.375, 0.50$, the current distribution is neither sinusoidal, nor of constant phase, and that the deviations from Eqs. (3.1.1) and (3.1.2) increase with increase in values of h/λ and b/λ. On the basis of the above results, it appears that Eqs. (3.1.1) and (3.1.2) are approximately valid for the conditions:

$$b/\lambda < 10^{-4}, \quad h/\lambda \lesssim 0.25 \tag{3.1.3}$$

In addition to the constraint on $I(z)$ given by Eq. (3.1.1), assume that the return current $I_r(z)$ on the outside of the coaxial-line's outer conductor (see Fig. 2) is given by

$$I_r(z) \approx 0, \quad z < 0 \tag{3.1.4}$$

The constraint of Eq. (3.1.4) corresponds to the idealized condition that the ferrite toroids have a $1/e$ current attenuation distance h_1, given by

$$h_1/\lambda = 0 \tag{3.1.5}$$

It should be noted that Eqs. (3.1.4) and (3.1.5) do not alter the constraint $I_r(z = 0) = I_{bot}(\rho = b_1)$ given by Eq. (2.3.7), nor do they impose any constraints on $I_{bot}(\rho = b_1)$, where $I_{bot}(\rho = b_1)$ is the current on the bottom of the ground plane at a radius equal to that of the outer conductor.

Combining the current constraints given by Eqs. (3.1.1) and (3.1.4) with those given by Eqs. (2.4.3)–(2.4.7) and Eq. (2.4.12), the current constraints on the monopole antenna are given by

Element:

$$I(z) = [I(0)/\sin(kh)] \sin[k(h - z)], \quad 0 \leq z \leq h \tag{3.1.6}$$

Ground Plane:

$$I(\rho = a) = 0 \tag{3.1.7}$$

$$I_{bot}(\rho) = 0, \quad 0 \leq \rho \leq b_1 \tag{3.1.8}$$

Coaxial Line:

$$I_r(z) \approx 0, \quad z < 0 \tag{3.1.9}$$

Element Ground Plane:

$$I(z = 0) = -I(\rho = b) \tag{3.1.10}$$

Ground-Plane Coaxial Line:

$$I_{\text{bot}}(\rho) = I_{\text{r}}(z = 0) \tag{3.1.11}$$

In Chapter 3, we will assume that all models satisfy the current constraints given by Eqs. (3.1.6)–(3.1.11). The results are expected to be approximately correct if the monopole element is sufficiently thin electrically and not too long [conditions (3.1.3)] and if the ferrite toroids are sufficiently lossy [$h_1/\lambda \ll 1$, idealized by condition (3.1.5)]. For these conditions, the circuit representation of the monopole antenna is shown in Fig. 2(d).

For the current constraints of Eqs. (3.1.6)–(3.1.11), the total magnetic and electric field intensities $\mathbf{H}^{(\text{total})}$, $\mathbf{E}^{(\text{total})}$ at an arbitrary field point $P(x, y, z)$ external to the element-excitation-source points are simply the vector sum of the fields resulting from the element current and the current induced on the ground plane by the fields incident by the element.

Accordingly,

$$\begin{aligned} \mathbf{H}^{(\text{total})} &= \mathbf{H}^{(\text{e})} + \mathbf{H}^{(\text{g})}[\mathbf{E}^{(\text{e})}, \mathbf{H}^{(\text{e})}] \\ \mathbf{E}^{(\text{total})} &= \mathbf{E}^{(\text{e})} + \mathbf{E}^{(\text{g})}[\mathbf{E}^{(\text{e})}, \mathbf{H}^{(\text{e})}] \end{aligned} \tag{3.1.12}$$

for the current constraints of Eqs. (3.1.6)–(3.1.11), where

$\mathbf{H}^{(\text{e})}$, $\mathbf{E}^{(\text{e})}$ = magnetic and electric field intensities, respectively, generated by the element current

$\mathbf{H}^{(\text{g})}$, $\mathbf{E}^{(\text{g})}$ = magnetic and electric field intensities, respectively, generated by the ground-plane current induced by the element incident fields.

The element fields $\mathbf{H}^{(\text{e})}$, $\mathbf{E}^{(\text{e})}$ are determined in Sec. 3.2. The ground-plane fields $\mathbf{H}^{(\text{g})}$, $\mathbf{E}^{(\text{g})}$ are determined in Secs. 3.3–3.8 for ground-plane radii of various extents.

3.2 INDUCED EMF METHOD, GROUND PLANE OF ZERO EXTENT

3.2.1 Concept of a Ground Plane of Zero Extent

Consider a monopole antenna excited by a coaxial line with an outer conductor of radius b_1 that is terminated by free space, rather than by a ground plane [Fig. 3(a)]. The ground plane for such an antenna is denoted as being of *zero extent*. As was shown in Sec. 2.4, the coaxial-line excitation may be replaced by an equivalent magnetic current (frill) M_ϕ sitting on top of a thick ground plane of

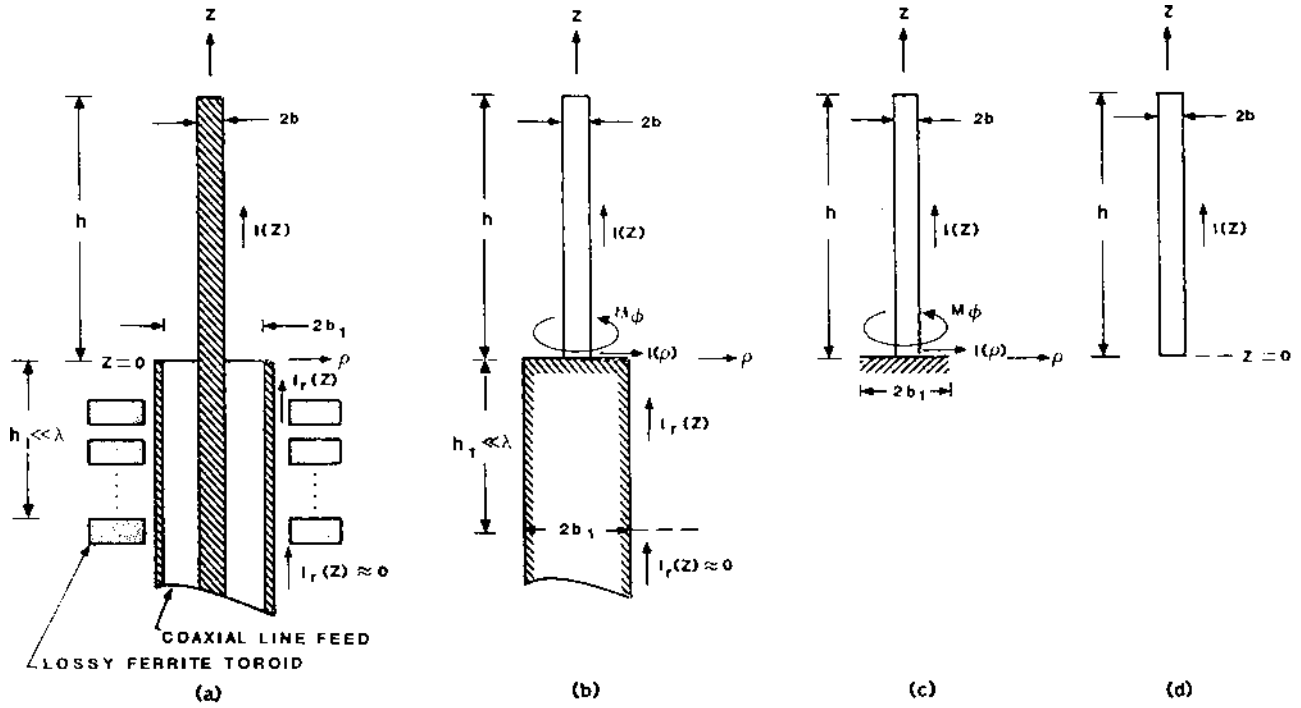

FIGURE 3 Characterization of currents for monopole antenna with ground plane of zero extent: (a) physical realization, (b) circuit representation, (c) idealization of circuit ($h_1/\lambda = 0$), (d) idealization of circuit ($h_1/\lambda = 0, \quad k_{b1} \ll$, where $I(z)$ or $I(\rho)$ initially known).

radius $\rho = b_1$ [Fig. 3(b)]. For sufficiently lossy ferrite toroids along the outside of the coaxial line, the current on the exterior of the coaxial-line's outer conductor may be neglected [Fig. 3(c)]. The magnetic frill may be removed from the circuit without appreciably affecting the results because $kb_1 \ll 1$ for the assumed sinusoidal current distribution on the monopole element [see Eq. (3.1.3) and the discussion concerning the circuit idealization of Fig. 2(d)]. Finally, the ground plane of radius b_1 may be removed from the circuit without appreciably affecting the results because a finite current on an electrically small conductor does not radiate an appreciable amount of power compared with that radiated by a monopole element of length $h \gg b_1$. The circuit idealization of a monopole antenna with a ground plane of zero extent is therefore an electrically thin monopole element with no ground plane [Fig. 3(d)].

The near-fields, far-fields, and input impedance of an electrically thin monopole element are derived and summarized in the remainder of Sec. 3.2. The input impedance is derived by way of the induced EMF method.

3.2.2 Near-Fields

Consider a monopole element of length h with a sinusoidal current distribution $I(z') = [I(0)/\sin(kh)]\sin[k(h - z')]$, $0 \le z' \le h$, at points $Q(x', y', z')$ on the surface of the element (Fig. 4). For an electrically thin element with a known

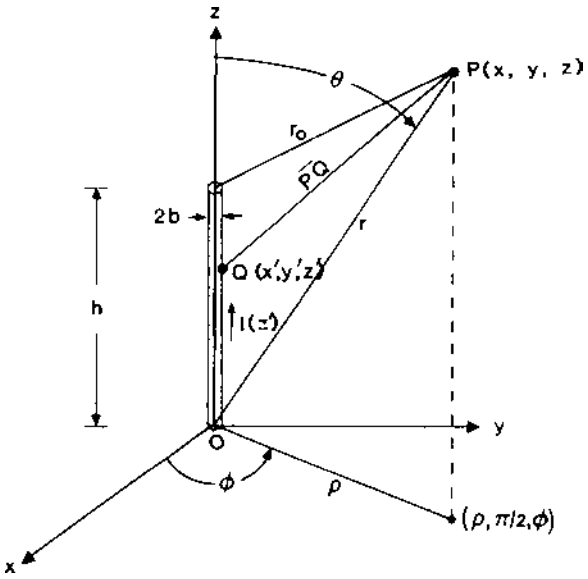

FIGURE 4 Monopole element geometry.

current distribution, the fields at arbitrary points $P(x, y, z)$ external to the element may be determined almost exactly by approximating the source points to lie on the element axis, that is, $Q(x', y', z') \approx Q(0, 0, z')$. For the current waveform of Eq. (2.1.2), the magnetic vector potential **A** is given by [16]:

$$\begin{aligned}\mathbf{A}(x, y, z) &= \hat{u}_z A_z \\ &= \hat{u}_z \frac{\mu_0 I(0)}{4\pi \sin(kh)} \int_0^h \frac{\sin[k(h - z')] \exp(-jk\overline{PQ})}{\overline{PQ}} \mathrm{d}z' \end{aligned} \tag{3.2.1}$$

where

$$\begin{aligned}\mu_0 &= \text{permeability of free space} = 4\pi \times 10^{-7}\ \text{H/m} \\ \overline{PQ} &= [(x - x')^2 + (y - y')^2 + (z - z')^2]^{1/2} \\ &\approx [x^2 + y^2 + (z - z')^2]^{1/2} \\ &= [\rho^2 + (z - z')^2]^{1/2} \\ \hat{u}_\rho,\ \hat{u}_\phi,\ \hat{u}_z &= \text{unit vectors in the radial, azimuthal, and axial cylindrical directions, respectively}\end{aligned}$$

The magnetic and electric field intensities, **H** and **E**, respectively, are given by

$$\mathbf{H} = \frac{1}{\mu_0}(\nabla \times \mathbf{A}) = -\hat{u}_\phi \frac{1}{\mu_0} \frac{\partial A_z}{\partial \rho} \tag{3.2.2}$$

$$\mathbf{E} = \frac{1}{j\omega\epsilon_0}(\nabla \times \mathbf{H}) = -\hat{u}_\rho \frac{1}{j\omega\epsilon_0} \frac{\partial H_\phi}{\partial z} + \hat{u}_z \frac{1}{j\omega\epsilon_0} \frac{1}{\rho} \frac{\partial}{\partial \rho}(\rho H_\phi) \tag{3.2.3}$$

where $\epsilon_0 =$ permittivity of free space $= 8.854 \times 10^{-12}$ F/m.

Exact closed-form expressions of **A, H, E,** and radiation resistance were first obtained for an infinitely thin element by Brillouin [17] and are summarized by Stratton [18]. The magnetic and electric fields are given by

$$\begin{aligned}H_\phi = \frac{jI(0)}{4\pi\rho \sin(kh)} &\left[\exp(-jkr_0) - \cos(kh) \exp(-jkr)\right. \\ &\left. - (jz/r) \sin(kh) \times \exp(-jkr)\right]\end{aligned} \tag{3.2.4}$$

$$\begin{aligned}E_\rho &= \frac{jI(0)\eta}{4\pi\rho \sin(kh)} \left\{\frac{(z - h) \exp(-jkr_0)}{r_0} - \frac{z}{r} \cos(kh) \exp(-jkr)\right. \\ &\quad \left. + \sin(kh) \frac{\partial}{\partial z}\left[\frac{z}{kr} \exp(-jkr)\right]\right\} \\ &= \frac{jI(0)\eta}{4\pi\rho \sin(kh)} \left[\frac{(z - h) \exp(-jkr_0)}{r_0} - \frac{z}{r} \cos(kh) \exp(-jkr)\right. \\ &\quad \left. + \sin(kh) \exp(-jkr)\left(\frac{1}{kr} - \frac{z^2}{kr^3} - \frac{jz^2}{r^2}\right)\right]\end{aligned} \tag{3.2.5}$$

$$E_z = \frac{-jI(0)\eta}{4\pi \sin(kh)} \left\{ \frac{\exp(-jkr_0)}{r_0} - \cos(kh) \frac{\exp(-jkr)}{r} + \sin(kh) \frac{\partial}{\partial z} \left[\frac{\exp(-jkr)}{kr} \right] \right\}$$

$$E_z = \frac{-jI(0)\eta}{4\pi \sin(kh)} \left[\frac{\exp(-jkr_0)}{r_0} - \cos(kh) \frac{\exp(-jkr)}{r} - z \sin(kh) \exp(-jkr) \left(\frac{j}{r^2} + \frac{1}{kr^3} \right) \right] \tag{3.2.6}$$

where

$$\eta = k/\omega\epsilon_0 = \text{wave impedance of free space} = 376.73\,\Omega$$
$$r_0 = [\rho^2 + (z - h)^2]^{1/2}$$
$$r = (\rho^2 + z^2)^{1/2}$$

Equations (3.2.4)–(3.2.6) are identical to the results given by Stratton [$\xi_2 = h,\ \xi_1 = 0,\ l = h,\ \alpha = kh,\ r_2 = r_0,\ r_1 = r,\ I_0 = -I(0)/[\sin(kh)]$ after the substitution of $-j$ for j to account for the $\exp(-j\omega t)$ waveform of Stratton, instead of the $\exp(j\omega t)$ waveform of Eq. (2.1.2). The fields given by Eqs. (3.2.4)–(3.2.6) are exact for an infinitely thin element, and they are almost exact for an electrically thin element with the same sinusoidal current distribution.

3.2.3 Far-Fields

Consider a field point P at a sufficiently large radial distance r, which satisfies both the far radiation zone and Fraunhofer diffraction conditions given by

$$h \ll r, \quad kr \gg 1 \tag{3.2.7}$$

for the far radiation zone conditions, and

$$kh^2/2r \ll 2\pi \tag{3.2.8}$$

for the Fraunhofer diffraction condition. For these conditions, we write

$$\exp(-jkr_0) \approx \exp[-kj(r - h\cos\theta)], \qquad h \ll r, \quad (kh^2/2r) \ll 2\pi$$
$$1/r_0 \approx 1/r, \quad h \ll r \tag{3.2.9}$$
$$z - h \approx z = r\cos\theta, \quad h \ll r$$

$$(1/kr) - (z^2/kr^3) - (jz^2/r^2) \approx -j\cos^2\theta, \quad kr \gg 1$$

$$(j/r^2) + (1/kr^3) \approx (j/r^2), \quad kr \gg 1$$

For the approximations of Eq. (3.2.9), the "exact" fields given by Eqs. (3.2.4)–(3.2.6) reduce to the far-fields given by

$$H_\phi = \frac{jI(0)\exp(-jkr)}{4\pi r \sin\theta \sin(kh)}[\exp(jkh\cos\theta) - \cos(kh) - j\cos\theta\sin(kh)] \tag{3.2.10}$$

$$E_\rho = \frac{jI(0)\eta\cos\theta\exp(-jkr)}{4\pi r \sin\theta\sin(kh)}[\exp(jkh\cos\theta) - j\cos\theta\sin(kh)] \tag{3.2.11}$$

$$E_z = \frac{-jI(0)\eta\exp(-jkr)}{4\pi r \sin(kh)}[\exp(jkh\cos\theta) - j\cos\theta\sin(kh)] \tag{3.2.12}$$

The resultant electric field $\mathbf{E} = \hat{u_\rho}E_\rho + \hat{u_z}E_z$ reduces in the far-field to

$$\mathbf{E} = \hat{u}_\theta E_\theta \quad \text{(far-field)} \tag{3.2.13}$$

where

$$\hat{u_\theta} = \hat{u_\rho}\cos\theta - \hat{u_z}\sin\theta$$
$$E_\theta = \frac{jI(0)\eta\exp(-jkr)}{4\pi r \sin\theta\sin(kh)}[\exp(jkh\cos\theta) - \cos(\mathrm{kh}) - j\cos\theta\sin(\mathrm{kh})]$$

The time-averaged Poynting vector $\mathbf{S} = (1/2)(\mathbf{E}\times\mathbf{H}) = (1/2)(\hat{u_\theta}E_\theta \times \hat{u_\phi}H_\phi) = \hat{u_r}s(\theta)$, with a time-averaged radiated power density $s(\theta)$ given by

$$s(\theta) = |E_\theta|^2/(2\eta) = (\eta/2)|H_\phi|^2 = \frac{\eta|I(0)|^2 f(\theta)}{32\pi^2 r^2 \sin^2(kh)} \tag{3.2.14}$$

where

$$f(\theta) \equiv \frac{[\cos(kh\cos\theta) - \cos(kh)]^2 + [\sin(kh\cos\theta) - \cos\theta\sin(kh)]^2}{\sin^2\theta}$$

The direction of maximum radiated power is $\theta = \pi/2$ rad.

By substituting Eq. (3.2.14) in Eqs. (2.2.4) and (2.2.5), the radiation resistance R, referred to the base current, is given for an infinitely thin element by

$$\begin{aligned} R_{\text{rad}} &= \frac{\eta \int_0^{\pi} f(\theta) \sin\theta \, \mathrm{d}\theta}{8\pi \sin^2(kh)} (\Omega) \\ &= \frac{\eta}{4\pi \sin^2(kh)} [\text{Cin}(2kh) - \sin^2(kh)], \quad b = 0 \end{aligned} \tag{3.2.15}$$

where $\text{Cin}(z)$ is the modified cosine integral [19]:

$$\int_0^z \frac{\mathrm{d}t}{t} (1 - \cos t)$$

The result given for the definite integral of Eq. (3.2.15) is readily obtained by letting $t = \cos\theta$, and noting that

$$\frac{1}{1 - t^2} = \frac{1}{2} \left(\frac{1}{x} + \frac{1}{y} \right)$$

where $x = 1 + t$ and $y = 1 - t$.

By substituting Eqs. (3.2.14) and (3.2.15) in Eq. (2.2.8), the numeric directivity $d(\theta)$ is given by

$$d(\theta) = \frac{f(\theta)}{\text{Cin}(2kh) - \sin^2(kh)} \tag{3.2.16}$$

where $f(\theta)$ is as defined in Eq. (3.2.14).

For electrically short monopole elements ($kh \ll 1$) and for $\eta = 376.73 \approx 120\pi\,(\Omega)$, Eqs. (3.2.14)–(3.2.16) reduce to

$$f(\theta) = \frac{1}{4} (kh)^4 \sin^2\theta, \quad kh \ll 1 \tag{3.2.17}$$

$$s(\theta) = \frac{15}{16} \frac{|I(0)|^2 (kh)^2 \sin^2\theta}{\pi r^2}, \quad kh \ll 1 \tag{3.2.18}$$

$$R_{\text{rad}} = 5(kh)^2 \quad (\Omega), \quad kh \ll 1, \quad b = 0 \tag{3.2.19}$$

$$d(\theta) = \frac{3}{2} \sin^2\theta, \quad kh \ll 1 \tag{3.2.20}$$

The relative power-radiation pattern $s(\theta)/s_{\max} = s(\theta)/s(\pi/2)$, radiation resistance R, and the directivity $d(\theta)$ are tabulated in App. A.1, Tables A1-1, A1-14, A1-26, and A1-38 for $h/\lambda = 1/4$, 1/10, 1/40, and 1/100, respectively. The numeric directivity pattern $d(\theta)$ for a quarter-wave monopole element [see Fig. 8(a) in Sec. 3.9] is similar to that of a half-wave dipole, except that its

peak directivity is less (1.88 vs. 1.76 dBi) and its 3 dB beamwidth is more (94 vs. 78°).

3.2.4 Input Impedance

The input impedance may be determined by the induced EMF method introduced by Brillouin [17]. With reference to Fig. 4, the input impedance Z_{in} is given by [20]:

$$Z_{\text{in}} = -(1/I(0)I_m)\int_0^h I_z(\rho=b, z=z')\, E_z(\rho=b, z=z')\mathrm{d}z', \quad b>0 \tag{3.2.21}$$

where

$$I_m = I(0)/\sin(kh)$$

The induced EMF method is indeterminate for collinear current elements unless the elements are of radius $b > 0$. For sufficiently thin elements, the current I_z is given by Eq. (3.1.1) and the electric near-field E_z is given almost exactly by Eq. (3.2.6). By substituting Eqs. (3.1.1) and (3.2.6) in Eq. (3.2.21), we have

$$Z_{\text{in}} = \frac{j\eta}{4\pi\sin(kh)}\int_0^h \mathrm{d}z' \sin[k(h-z')] \times\left\{\frac{\exp(-jkr_0)}{r_0} - \cos(kh)\frac{\exp(-jkr)}{r} + \sin(kh)\frac{\partial}{\partial z'}\left[\frac{\exp(-jkr)}{r}\right]\right\} \tag{3.2.22}$$

where

$$r_0 = [b^2 + (z' - h)^2]^{1/2}$$
$$r = (b^2 + z'2)^{1/2}$$

Each of the three terms of the integrand of Eq. (3.2.22) may be integrated using the methods summarized by Stratton [18]. However, the third term of the integrand should first be integrated by parts. Accordingly,

$$Z_{\text{in}} = R_{\text{in}} + jX_{\text{in}} = Z_1 + Z_2 + Z_3 \tag{3.2.23}$$

where

$$Z_1 = \frac{j\eta}{4\pi\sin^2(kh)}\int_0^h \mathrm{d}z'\left\{\sin[k(h-z)]\frac{\exp(-jkr_0)}{r_0}\right\}$$
$$= R_1 + jX_1 \tag{3.2.24}$$

$$R_1 = \frac{\eta}{4\pi \sin^2(kh)} \left[\frac{1}{2} \mathrm{Cin}(x_1) + \frac{1}{2} \mathrm{Cin}(x_2) - \mathrm{Cin}(x_3) \right] \tag{3.2.25}$$

$$X_1 = \frac{\eta}{4\pi \sin^2(kh)} \left[\frac{1}{2} \mathrm{Si}(x_1) + \frac{1}{2} \mathrm{Si}(x_2) - \mathrm{Si}(x_3) \right] \tag{3.2.26}$$

$$\begin{aligned} Z_2 &= \frac{j\eta}{4\pi \sin^2(kh)} \int_0^h - \mathrm{d}z' \left\{ \sin[k(h - z')] \cos(kh) \frac{\exp(-jkr)}{r} \right\} \\ &= R_2 + jX_2 \end{aligned} \tag{3.2.27}$$

$$\begin{aligned} R_2 = \frac{\eta}{4\pi \sin^2(kh)} \Bigg\{ & \frac{-\sin(2kh)}{4} [\mathrm{Si}(x_1) - \mathrm{Si}(x_2)] \\ & + \cos^2(kh) \left[-\mathrm{Cin}(x_3) + \frac{1}{2} \mathrm{Cin}(x_2) + \frac{1}{2} \mathrm{Cin}(x_1) \right] \Bigg\} \end{aligned} \tag{3.2.28}$$

$$\begin{aligned} X_2 = \frac{\eta}{4\pi \sin^2(kh)} \Bigg\{ & \frac{-\sin(2kh)}{4} [\mathrm{Cin}(x_2) - \mathrm{Cin}(x_1) \\ & + \ln(x_1/x_2)] + \frac{\cos^2(kh)}{2} [\mathrm{Si}(x_1) + \mathrm{Si}(x_2) - 2\,\mathrm{Si}(x_3)] \Bigg\} \end{aligned} \tag{3.2.29}$$

$$\begin{aligned} Z_3 &= \frac{j\eta}{4\pi \sin^2(kh)} \int_0^h \mathrm{d}z' \left\{ \sin[k(h - z')] \sin(kh) \frac{\partial}{\partial z'} \left[\frac{\exp(-jkr)}{r} \right] \right\} \\ &= R_3 + jX_3 \end{aligned} \tag{3.2.30}$$

$$\begin{aligned} R_3 = \frac{\eta}{4\pi \sin^2(kh)} \Bigg\{ & \frac{\sin^2(kh)}{2} \Bigg[\mathrm{Cin}(x_1) + \mathrm{Cin}(x_2) - 2\,\mathrm{Cin}(x_3) \\ & + \frac{2(x_1 + x_2)(\sin x_1 + \sin x_2)}{x_1^2 + x_2^2 + 2(kb)^2} - \frac{4x_3 \sin x_3}{x_3^2 + (kb)^2} \Bigg] - \frac{\sin(2kh)}{4} \\ & \times \left[\mathrm{Si}(x_2) - \mathrm{Si}(x_1) - \frac{2(x_1 + x_2)(\cos x_1 - \cos x_2)}{x_1^2 + x_2^2 + 2(kb)^2} \right] \Bigg\} \end{aligned} \tag{3.2.31}$$

$$
\begin{aligned}
X_3 = \frac{\eta}{4\pi \sin^2(kh)} \Bigg\{ & \frac{\sin^2(kh)}{2} \Bigg[\mathrm{Si}(x_1) + \mathrm{Si}(x_2) \\
& - 2\,\mathrm{Si}(x_3) + \frac{2(x_1 + x_2)(\cos x_1 + \cos x_2)}{x_1^2 + x_2^2 + 2(kb)^2} - \frac{4x_3 \cos x_3}{x_3^2 + (kb)} \Bigg] \Bigg\} \\
& + \frac{\sin(2kh)}{4} \Bigg[- \mathrm{Cin}(x_1) + \mathrm{Cin}(x_2) + \ln(x_1/x_2) \\
& - \frac{2(x_1 + x_2)(\sin x_1 - \sin x_2)}{x_1^2 + x_2^2 + 2(kb)^2} \Bigg]
\end{aligned}
\tag{3.2.32}
$$

where

$$
\begin{aligned}
x_1 &= k[(b^2 + h^2)^{1/2} + h] \\
x_2 &= k[(b^2 + h^2)^{1/2} - h] \\
x_3 &= kb
\end{aligned}
$$

As before, $\mathrm{Cin}(x)$ is the modified cosine integral [19]:

$$
\int_0^x \frac{\mathrm{d}t}{t}(1 - \cos t)
$$

and $\mathrm{Si}(x)$ is the sine integral [19]:

$$
\int_0^x \frac{\sin t}{t}\,\mathrm{d}t
$$

Then, summing Eqs. (3.2.23)–(3.2.32), we have

$$
\begin{aligned}
R_{\mathrm{in}} = \frac{\eta}{4\pi \sin^2(kh)} \Bigg\{ & \mathrm{Cin}(x_1) + \mathrm{Cin}(x_2) - 2\,\mathrm{Cin}(x_3) \\
& + \frac{\sin(2kh)}{2} \left[\frac{(x_1 + x_2)(\cos x_1 - \cos x_2)}{x_1^2 + x_2^2 + 2x_3^2} \right] \\
& + \sin^2(kh) \left[\frac{(x_1 + x_2)(\sin x_1 + \sin x_2)}{x_1^2 + x_2^2 + 2x_3^2} - \frac{\sin x_3}{x_3} \right] \Bigg\}
\end{aligned}
\tag{3.2.33}
$$

$$X_{\text{in}} = \frac{\eta}{4\pi \sin^2(kh)} \left\{ \text{Si}(x_1) + \text{Si}(x_2) - 2\,\text{Si}(x_3) \right.$$

$$- \frac{\sin(2kh)}{2} \left[\frac{(x_1 + x_2)(\sin x_1 - \sin x_2)}{x_1^2 + x_2^2 + 2x_3^2} \right] \tag{3.2.34}$$

$$\left. + \sin^2(kh) \left[\frac{(x_1 + x_2)(\cos x_1 + \cos x_2)}{x_1^2 + x_2^2 + 2x_3^2} - \frac{\cos x_3}{x_3} \right] \right\}$$

where

$$x_1 = k[(b^2 + h^2)]^{1/2} + h], \quad x_2 = k[(b^2 + h^2)^{1/2} - h], \quad x_3 = kb$$

For $b = 0$, Eqs. (3.2.33) and (3.2.34) reduce to

$$R_{\text{in}} = \frac{\eta}{4\pi \sin^2(kh)} [\text{Cin}(2kh) - \sin^2(kh)], \quad b = 0 \tag{3.2.35}$$

$$X_{\text{in}} = \frac{\eta}{4\pi \sin^2(kh)} \left[\text{Si}(2kh) - \frac{\sin^2(kh)}{kb} \right], \quad b \to 0 \tag{3.2.36}$$

Equation (3.2.35) agrees with the result for radiation resistance given by Eq. (3.2.15). A comparison of Eq. (3.2.33) with Eq. (3.2.35) reveals that the input resistance is relatively insensitive to the monopole element radius b for $kb \ll 1$. The input resistance given by Eq. (3.2.35) is plotted in Fig. 5. For $kh = \pi/2$ rad, $R_{\text{in}} = 19.4\,\Omega$.

The input reactance is sensitive to the element radius b as can be seen in Eq. (3.2.36). For $b = 0$, the input reactance is given by

$$X_{\text{in}} = \begin{cases} -\infty; & kh \neq n\pi, \quad n = 1, 2, 3, \ldots; \quad b = 0 \\ \infty; & kh = n\pi, \quad n = 1, 2, 3, \ldots; \quad b = 0 \end{cases} \tag{3.2.37}$$

From Eq. (3.2.36), resonance ($X_{\text{in}} = 0$) occurs for

$$(kh)_{\text{resonance}} \approx n\pi \pm [kb\,\text{Si}(2n\pi)]^{1/2}, \quad n = 1, 2, 3, \ldots \tag{3.2.38}$$

The input resistance at resonance, for kh given by Eq. (3.2.38), is found from Eq. (3.2.35) to be

$$(R_{\text{in}})_{\text{resonance}} \approx \frac{\eta}{4\pi} \left[\frac{\text{Cin}(2n\pi)}{kb\,\text{Si}(2n\pi)} - 1 \right] \tag{3.2.39}$$

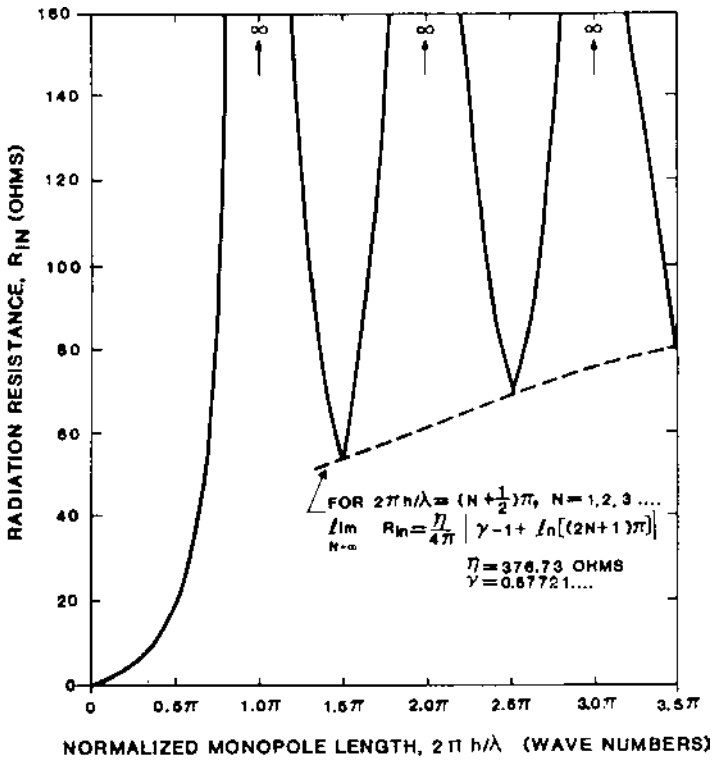

FIGURE 5 Radiation resistance of electrically thin ($kb \ll 1$) monopole elements.

Minima of input resistance occur for kh, given by

$$(kh)_{\text{minima}} \approx \left(N + \frac{1}{2}\right)\pi, \quad N = 1, 2, 3, \ldots \tag{3.2.40}$$

The input resistance at these minima element lengths is found from Eq. (3.2.35) to be

$$(R_{\text{in}})_{\text{minima}} \approx \frac{\eta}{4\pi}[\gamma - 1 + \ln[(2N+1)\pi] \tag{3.2.41}$$

where

$$\gamma = \text{Euler's constant} = 0.57721$$

The accuracy of Eq. (3.2.40) increases as $N \to \infty$.

3.2.5 Summary of Results

The input impedance and directivity properties of quarter-wave and electrically short monopole elements with zero, large, and infinite extent ground planes are compared in Table 4 of Sec. 3.9. The peak directivity is approximately 3 dB *less* with ground planes of zero extent than with ground planes of large extent. However, the directivity on the horizon is approximately 3 dB *more* with ground planes of zero extent than with ground planes of large, but finite, extent. The radiation resistance with ground planes of zero extent is approximately one-half that with ground planes of large extent.

Unlike dipole elements in free space where the first resonance occurs for dipole half-lengths that are approximately equal to a quarter-wavelength, monopole elements with ground planes of zero extent have a first resonance for an element length that is approximately equal to a half-wavelength.

3.3 INTEGRAL EQUATION: $0 \leq ka \leq 2.75$

The fields generated by the monopole element were determined in Sec. 3.2. These fields impinge on the ground plane and induce a ground-plane current. For sufficiently small ground planes, the fields generated by the ground-plane current may be determined by Bardeen's integral equation method [1].

In Bardeen's method, a cylindrically symmetrical electromagnetic wave (generated by the element) is incident on the ground-plane disk. The fields generated by the induced ground-plane current are required and the solution depends on solving an integral equation of the first kind. For arbitrary ground-plane radii, the integral equation cannot be readily solved because it contains two integrals. However, for sufficiently small ground-plane radii, Bardeen neglects one of the integrals so that the equation may be solved explicitly.

Although Bardeen gives a general formulation of the solution for the resulting single-integrand integral equation, his only explicit results are for the case in which the incident wave is generated by an infinitely thin dipole element having a base that is at a nonzero height above the center of the ground plane. Bardeen restricted his solution to elements at a nonzero height above the ground plane in order to avoid having a source point (the base of the element) located at a near-field point of interest, which, for the integral equation method, includes the center of the ground plane. The total field is then given by the vector sum of the incident and induced fields [see Eq. (3.1.12)].

The present case of interest is that of a monopole element having a base that is in the plane of the ground plane (i.e., at a vertical height $v = 0$ above the center of the ground plane (see Fig. 6). For this case, the total magnetic field may be determined by first evaluating the field with the element at an arbitrary height $v > 0$, and then by evaluating the resulting expression in the $\lim v \to 0$. By using

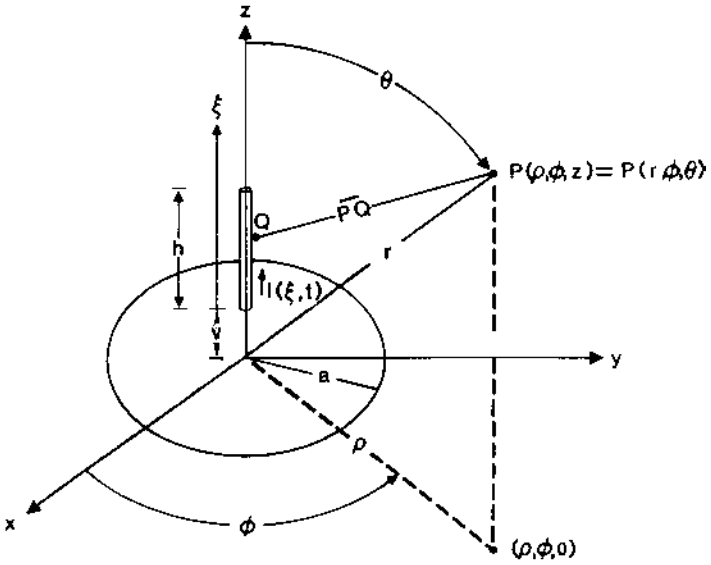

FIGURE 6 Thin monopole element, the base of which is above the center of a circular ground plane.

such a procedure, we avoid an indeterminate expression for the field generated by the induced ground-plane current.

Accordingly, the total magnetic field intensity $H_\phi^{(\text{total})}$ [see Eq. (3.1.12)], in the $\lim v \to 0$, is given by

$$\lim_{v\to 0} H_\phi^{(\text{total})} = \lim_{v\to 0} H_\phi^{(\text{e})} + \lim_{v\to 0} H_\phi^{(\text{g})} \tag{3.3.1}$$

where $H_\phi^{(\text{e})}$ and $H_\phi^{(\text{g})}$ are the magnetic field intensities generated by the element and ground-plane currents, respectively. In the following evaluation of the two terms of Eq. (3.3.1), the fields are assumed to have an $\exp(j\omega t)$ time dependence [see Eq. (2.1.2)], unlike the $\exp(-j\omega t)$ time dependence assumed by Bardeen.

The first term of Eq. (3.3.1) is given exactly, for an infinitely thin element, by [see Eq. (3.2.4)]:

$$\lim_{v\to 0} H_\phi^{(\text{e})} = \frac{jI(0)}{4\pi\rho\sin(kh)}\left[\exp(-jkr_0) - \cos(kh)\exp(-jkr) - \frac{jz}{r}\sin(kh)\exp(-jkr)\right] \tag{3.3.2}$$

In the far-field, Eq. (3.3.2) reduces to [see Eq. (3.2.10)]:

$$\lim_{\nu\to 0} H_\phi^{(e)} = A_0[\, j\exp(\, jkh\cos\theta) + j\cos(kh) + \cos\theta\sin(kh)], \quad \text{(far-field)} \tag{3.3.3}$$

where

$$A_0 = \frac{-I(0)\exp(-jkr)}{4\pi r\sin\theta\sin(kh)}$$

The second term of Eq. (3.3.1) may be evaluated by utilizing Bardeen's equation [1, Eq. (31)] for $H_\phi^{(g)}$, which he obtained as a solution to his single-integrand integral equation. For an infinitely thin element and sufficiently small ground planes ($ka \lesssim 1$), $H_\phi^{(g)}$ is given by Bardeen's equation [1, Eq. (31)] as

$$H_\phi^{(g)} = \operatorname{sgn}(z)\frac{-j\omega\epsilon_0}{k\rho}\int_0^a F(s)\,K(s)\,\mathrm{d}s, \quad ka \lesssim 1 \tag{3.3.4}$$

where

$$K(s) = \frac{\exp(-jkA_1)\sinh(kB_1)\sinh(ks) - \exp(-jkA_2)\sinh(kB_2)\sinh(ka)}{\sinh(ka)}$$

$$\operatorname{sgn}(z) = \begin{cases} +1, & z \geq 0 \\ -1, & z < 0 \end{cases}$$

$\epsilon_0 =$ permittivity of free space (F/m)

$$A_1 - jB_1 = \{\rho^2 + [-ja + z\operatorname{sgn}(z)]^2\}^{1/2} = [r^2 - \operatorname{sgn}(z)\,2jra\cos\theta - a^2]^{1/2}$$

$$A_2 - jB_2 = \{\rho^2 + [-js + z\operatorname{sgn}(z)]^2\}^{1/2} = [r^2 - \operatorname{sgn}(z)\,2jrs\cos\theta - s^2]^{1/2}$$

$s =$ dummy variable having the dimension of length

$F(s) =$ excitation function related to the radial electric near-field intensity $E_r^{(e)}|_{z=0}$, which is incident on the ground plane

The second term of Eq. (3.3.1) is therefore given by

$$\lim_{\nu\to 0} H_\phi^{(g)} = \operatorname{sgn}(z)\frac{-j\omega\epsilon_0}{k\rho}\lim_{\nu\to 0}\int_0^a F(s)\,K(s)\,\mathrm{d}s, \quad ka \lesssim 1$$

$$\lim_{\nu\to 0} H_\phi^{(g)} = \operatorname{sgn}(z)\frac{-j\omega\epsilon_0}{k\rho}\int_0^a \left[\lim_{\nu\to 0} F(s)\right] K(s)\,\mathrm{d}s, \quad ka \lesssim 1 \tag{3.3.5}$$

The excitation function $F(s)$ is given by Bardeen [1, Eq. (35)] as

$$F(s) = -\frac{2}{\pi}\int_0^\infty ph(p)\frac{\sin[s(p^2-k^2)^{1/2}]}{(p^2-k^2)^{1/2}}\,\mathrm{d}p \tag{3.3.6}$$

where

p = dummy variable having the dimensions of (length)$^{-1}$
$h(p)$ = function of the radial electric near-field intensity $E_\rho^{(\mathrm{e})}|_{z=0}$, which is incident on the ground plane

The function $h(p)$ is given by Bardeen [1, Eq. (33)] as

$$-E_\rho^{(\mathrm{e})}|_{z=0} = \int_0^\infty h(p)J_1(\rho p)\,\mathrm{d}p \tag{3.3.7}$$

where $J_1(x)$ = Bessel function of the first kind.

The electric field intensity $E_\rho^{(\mathrm{e})}|_{z=0}$, incident on the ground plane, is given by

$$E_\rho^{(\mathrm{e})}\bigg|_{z=0} = \hat{u}_\rho\cdot\frac{[\nabla x(\nabla x\mathbf{A}^{(\mathrm{e})})]}{j\omega\mu_0\epsilon_0}\bigg|_{z=0} \tag{3.3.8}$$

where

$\mathbf{A}^{(\mathrm{e})}$ = magnetic vector potential generated by the monopole source points
μ_0 = permeability of free space (H/m)
$\hat{u}_\rho$ = unit vector in the cylindrical radial direction

The magnetic vector potential $\mathbf{A}^{(\mathrm{e})}$ for the element base at an arbitrary height v is given by [16]:

$$\mathbf{A}^{(\mathrm{e})} = \hat{u}_z(\mu_0/4\pi)\int_0^h I(\xi)(1/\overline{PQ})\exp(-jk\overline{PQ})\,\mathrm{d}\xi \tag{3.3.9}$$

where

$\hat{u}_z$ = unit vector along the z axis
$\overline{PQ}$ = distance from source point Q to field point $P \approx [\rho^2 + (z-\xi-v)^2]^{1/2}$, $\quad Q(x', y', \xi) \approx Q(0, 0, \xi)$
$I(\xi)$ = monopole current distribution = $[I(0)/\sin(kh)]\sin[k(h-\xi)]$

In order to facilitate the evaluation of $h(p)$ in Eq. (3.3.7), it is convenient to express the factor $(1/\overline{PQ})\exp(-jk\overline{PQ})$ in terms of Bessel functions. By using Sommerfeld's formula [21] and the dummy variable p introduced in Eq. (3.3.6), we write

$$\frac{\mathrm{e}^{-jk\overline{PQ}}}{\overline{PQ}} = \int_0^\infty \frac{J_0(p\rho)\exp[-|z-\xi-v|\sqrt{p^2-k^2}]p\,\mathrm{d}p}{(p^2-k^2)^{1/2}}; \tag{3.3.10}$$

$$-(\pi/2) < \arg\sqrt{p^2-k^2} \le (\pi/2), \quad -\pi < \arg k \le 0$$

By substituting Eq. (3.3.10) in Eq. (3.3.9), we have

$$\mathbf{A}^{(e)} = \frac{\mu_0 I(0)}{4\pi \sin(kh)} \hat{u}_z \int_0^h \mathrm{d}\xi \sin[k(\xi - h)]$$

$$\times \int_0^\infty \frac{J_0(p\rho) \exp[-|z - \xi - v|\sqrt{p^2 - k^2}]}{(p^2 - k^2)^{1/2}} p \, \mathrm{d}p; \tag{3.3.11}$$

$$-(\pi/2) < \arg\sqrt{p^2 - k^2} \leq (\pi/2), \quad -\pi < \arg k \leq 0$$

Because we are interested in evaluating $E_\rho^{(e)}|_{z=0}$, consider the case of $z < \xi + v$. By substituting Eq. (3.3.11), for such a case, in Eq. (3.3.8), and noting that

$$\mathbf{A}^{(e)} \hat{u}_z = A_z \quad \text{and} \quad \frac{\partial J_0(p\rho)}{\partial \rho} = -pJ_1(p\rho)$$

$$E_\rho^{(e)}\Big|_{z=0} = \frac{1}{-j\omega\mu_0\epsilon_0} \frac{\partial^2 A_z}{\partial z \partial \rho}\Big|_{z=0}$$

$$E_\rho^{(e)}\Big|_{z=0} = \frac{I(0)}{-j4\pi\omega\epsilon_0 \sin(kh)} \int_0^\infty p^2 J_1(p\rho)$$

$$\times \exp[(z - v)\sqrt{p^2 - k^2}] B(p) \, \mathrm{d}p\Big|_{z=0} \tag{3.3.12}$$

where

$$B(p) = \int_0^h \sin[k(h - \xi)] \exp[-\xi\sqrt{p^2 - k^2}] \, \mathrm{d}\xi$$

$$= \frac{k \exp[-h\sqrt{p^2 - k^2}] + \sqrt{p^2 - k^2} \sin(kh) - k\cos(kh)}{p^2} \tag{3.3.13}$$

By substituting Eq. (3.3.13) in Eq. (3.3.12), and letting $z = 0$, we have

$$E_\rho^{(e)}|_{z=0} = \frac{I(0)}{-j4\pi\omega\epsilon_0 \sin(kh)} \int_0^\infty \mathrm{d}p \{J_1(p\rho) \exp(-v\sqrt{p^2 - k^2})$$

$$\times [\exp(-h\sqrt{p^2 - k^2}) + \sqrt{p^2 - k^2} \sin(kh)$$

$$- k\cos(kh)]\} \tag{3.3.14}$$

Comparison of Eq. (3.3.14) with Eq. (3.3.7) yields

$$h(p) = \frac{I(0)}{j4\pi\omega\epsilon_0 \sin(kh)} [k \exp(-(h+v)\sqrt{p^2 - k^2}\,) + \sqrt{p^2 - k^2} \sin(kh) \exp(-v\sqrt{p^2 - k^2}) - k\cos(kh) \exp(-v\sqrt{p^2 - k^2})] \tag{3.3.15}$$

By substituting Eq. (3.3.15) in Eq. (3.3.6), we have

$$F(s) = \frac{-2Ck}{\pi} \left[I_1 + \frac{\sin(kh)}{k} I_2 - \cos(kh) I_3 \right] \tag{3.3.16}$$

where

$$C \equiv \frac{I(0)}{j4\pi\omega\epsilon_0 \sin(kh)}$$

$$I_1 = \int_0^\infty \frac{p \exp(-(h+v)\sqrt{p^2 - k^2}) \sin(s\sqrt{p^2 - k^2})\, \mathrm{d}p}{(p^2 - k^2)^{1/2}}$$

$$I_2 = \int_0^\infty p \sin(s\sqrt{p^2 - k^2}) \exp(-v\sqrt{p^2 - k^2})\, \mathrm{d}p$$

$$I_3 = \int_0^\infty \frac{p \sin(s\sqrt{p^2 - k^2}) \exp(-v\sqrt{p^2 - k^2})\, \mathrm{d}p}{(p^2 - k^2)^{1/2}}$$

We introduce in integrals I_1, I_2, and I_3 a change in variable p to y, given by

$$y = (p^2 - k^2)^{1/2}, \quad -(\pi/2) < \arg y \leq (\pi/2) \tag{3.3.17}$$

where the condition on y follows from the conditions of Eq. (3.3.10).

It follows (from Integral 2.663.1 [22]) that I_1 is given by

$$\begin{aligned} I_1 &= \int_{jk}^\infty \exp(-(h+v)y) \sin(sy)\, \mathrm{d}y \\ &= \frac{\exp(-(h+v)y)}{(h+v)^2 + s^2} [-(h+v)\sin(sy) - s\cos(sy)] \Big|_{jk}^\infty \\ &= \frac{-\exp(-k(h+v))}{(v+h)^2 + s^2} [-j(h+v)\sinh(ks) - s\cosh(ks)] \end{aligned} \tag{3.3.18}$$

It follows (from Integral 2.667.5 [22]) that I_2 is given by

$$\begin{aligned} I_2 &= \int_{jk}^{\infty} y \sin(sy) \exp(-vy)\, \mathrm{d}y \\ &= \frac{\exp(-vy)}{v^2+s^2}\left[\left(-vy + \frac{s^2-v^2}{v^2+s^2}\right)\sin(sy) - \left(sy + \frac{2vs}{s^2+v^2}\right)\cos(sy)\right]\Bigg|_{jk}^{\infty} \\ &= \frac{-\exp(-jkv)}{s^2+v^2}\left[kv\sinh(ks) - jks\cosh(ks)\right. \\ &\qquad \left. - \frac{j(v^2-s^2)\sinh(ks) - 2vs\cosh(ks)}{s^2+v^2}\right] \end{aligned} \tag{3.3.19}$$

It follows (from Integral 2.663.1 [22]) that I_3 is given by

$$I_3 = \int_{jk}^{\infty} \sin(sy)\exp(-vy)\,\mathrm{d}y = \exp(-vy)\left[\frac{-v\sin(sy) - s\cos(sy)}{s^2+v^2}\right]\Bigg|_{jk}^{\infty}$$

$$= -\exp(-jkv)\left[\frac{-jv\sinh(ks) - s\cosh(ks)}{s^2+v^2}\right] \tag{3.3.20}$$

Consider now the limits of I_1, I_2, and I_3 as $v \longrightarrow 0$. Thus,

$$\lim_{v\to 0} I_1 = \frac{\exp(-jkh)}{h^2+s^2}[-jh\sinh(ks) - s\cosh(ks)] \tag{3.3.21}$$

$$\begin{aligned} \lim_{v\to 0} I_2 &= -\pi k\delta(s)\sinh(ks) + \frac{jk\cosh(ks)}{s} + j\pi^2\delta^2(s)\sinh(ks) \\ &\qquad - \frac{j\sinh(ks)}{s^2} - \pi\delta'(s)\cosh(ks) \end{aligned} \tag{3.3.22}$$

$$\lim_{v\to 0} I_3 = j\pi\delta(s)\sinh(ks) + \frac{\cosh(ks)}{s} \tag{3.2.23}$$

where [23]

$$\delta(x) = \text{Dirac delta function} = \lim_{v\to 0}\left[\frac{1}{\pi}\frac{v}{v^2+x^2}\right]$$

$$\int_a^b \delta(x-x_0)\,\mathrm{d}x = \begin{cases} 1, & a < x_0 < b \\ 1/2, & a = x_0 < b \quad \text{or} \quad a < x = b \\ 0, & x_0 < a \quad \text{or} \quad x_0 > b \end{cases}$$

$$\delta'(x) = \frac{\mathrm{d}}{\mathrm{d}x}[\delta(x)] = \lim_{\nu\to 0}\frac{\partial}{\partial x}\left[\frac{1}{\pi}\frac{\nu}{\nu^2+x^2}\right] = \lim_{\nu\to 0}\left[-\frac{1}{\pi}\frac{2\nu x}{(\nu^2+x^2)^2}\right]$$

In Eqs. (3.3.22) and (3.3.23), those terms containing the product $\delta(s)\sinh(ks)$ may be set equal to zero because [from Eq. (B.2-12) [23]] $x\delta(x) = 0$.

The $\lim(\nu \to 0)F(s)$ is found by substituting Eqs. (3.3.21)–(3.3.23) in Eq. (3.3.16). Accordingly,

$$\begin{aligned}\lim_{\nu\to 0} F(s) = {} & \frac{2Ck}{\pi}\frac{\exp(-jkh)}{h^2+s^2}[-jh\sinh(ks) - s\cosh(ks)] \\ & + \frac{2C\sin(kh)}{\pi}\left[\frac{-jk\cosh(ks)}{s} - \frac{j\sinh(ks)}{s^2} + \pi\delta'(s)\cosh(ks)\right] \\ & + \frac{2Ck\cos(kh)}{\pi}\frac{\cosh(ks)}{s}\end{aligned} \tag{3.3.24}$$

The magnetic field intensity generated by the ground-plane current, for the case $\nu \to 0$, is found by substituting Eq. (3.3.24) in Eq. (3.3.5). The total magnetic field is explicitly determined by numerical evaluation of Eqs.(3.3.1)–(3.3.5).

In the far-field, the factor $K(s)$ and the parameters A_1, A_2, B_1, and B_2 in Eqs. (3.3.4) and (3.3.5) reduce to a simpler form.

In the far-field, when $r \to \infty$, then $a \ll r$ and $s \ll r$. For these conditions, we write

$$\begin{aligned}A_1 - jB_1 &\approx [r^2 - \mathrm{sgn}(z)\,2jra\cos\theta - a^2\cos^2\theta]^{1/2} \\ &= r - \mathrm{sgn}(z)\,ja\cos\theta, \quad a \ll r\end{aligned} \tag{3.3.25}$$

$$\begin{aligned}A_2 - jB_2 &\approx [r^2 - \mathrm{sgn}(z)\,2jra\cos\theta - s^2\cos^2\theta]^{1/2} \\ &= r - \mathrm{sgn}(z)\,js\cos\theta, \quad s \ll r\end{aligned} \tag{3.3.26}$$

If we equate the real and imaginary parts in Eqs. (3.3.25) and (3.3.26), then

$$A_1 = A_2 = r, \quad a \ll r, \quad s \ll r \tag{3.3.27}$$

$$B_1 = \mathrm{sgn}(z)\,a\cos\theta, \quad a \ll \rho \tag{3.3.28}$$

$$B_2 = \mathrm{sgn}(z)\,s\cos\theta, \quad s \ll \rho \tag{3.3.29}$$

By substituting Eqs. (3.3.27), (3.3.28), and (3.3.29) in Eqs. (3.3.4) and (3.3.5), the magnetic far-field intensity due to the ground-plane current,

for the case $v \rightarrow 0$, is given by

$$\lim_{v\to 0} H_{\phi}^{(g)} = \frac{-j\omega\epsilon_0 \exp(-jkr)}{kr \sin\theta} \int_0^a \left[\lim_{v\to 0} F(s)\right] g(s)\, ds \qquad (3.3.30)$$

$$\text{far-field}, \quad ka \lesssim 1$$

where

$$g(s) = \frac{\sinh(ka\cos\theta)\sinh(ks) - \sinh(ks\cos\theta)\sinh(ka)}{\sinh(ka)}$$

and $\lim(v \rightarrow 0)F(s)$ is given by Eq. (3.3.24).

Equation (3.3.30) can be further reduced by utilizing the properties of the Dirac delta function [from Eq. (B.2-7) [23]] and the relation:

$$\int_0^a \delta'(x) f(x)\, dx = -\frac{1}{2} f'(0^+)$$

It follows that Eq. (3.3.30) reduces to

$$\lim_{v\to 0} H_{\phi}^{(g)} = \frac{2A_0}{\pi} \int_0^a ds\, g(s) \left\{ \frac{\exp(-jkh)}{h^2 + s^2} [-jh\sinh(ks) - s\cosh(ks)] \right.$$

$$\left. + \sin(kh) \frac{-j\cosh(ks)}{s} + \frac{j}{ks^2}\sinh(ks) + \frac{\cos(kh)\cosh(ks)}{s} \right\} \qquad (3.3.31)$$

$$- A_0 \sin(kh) \left[\frac{\sinh(ka\cos\theta) - \cos\theta \sinh(ka)}{\sinh(ka)} \right];$$

$$\text{far-field}, \quad ka \lesssim 1$$

where A_0 and $g(s)$ are defined in Eqs. (3.3.3) and (3.3.30), respectively.

The total magnetic far-field intensity generated by the element and ground-plane currents, for the case $v \rightarrow 0$, is found by substituting Eqs. (3.3.3) and (3.3.31) in Eq. (3.3.1). The resulting expression for $\lim(v \rightarrow 0)H_{\phi}^{(\text{total})}$ is in a form suitable for computer evaluation.

The radiated power density $s(\theta)$, directivity $d(\theta)$, and radiation resistance R_{rad} are found from (2.2.2) and (2.2.5). These quantities are computed in program *BARDEEN* of App. B.01. Computer printouts of the relative power-radiation pattern $s(\theta)/s_{\max}$, radiation resistance R_{rad}, and the directivity $d(\theta)$ are given in Tables A1-1–A1-13, A1-14–A1-25, A1-26–A1-37, A1-38–A1-49 for normalized element lengths $h/\lambda = 0.25$, 0.1, 0.040, 0.01, respectively, and normalized ground-plane radii = 0, 0.25, 0.50, …, 3.0 rad.

The radiation patterns have no appreciable change in shape for ground-plane radii $0 \leq ka \lesssim 1.75$, and resemble that of a dipole in free space, with peak gains approximately in the direction of the horizon and directivities less than that of a dipole for which the total element length is twice that of the monopole element. For a quarter-wave monopole element, the directivity on the horizon decreases from 1.88 dBi for $ka = 0$ to 1.23 dBi for $ka = 1.75$.

In Table 5 of Sec. 3.9, the radiation resistances obtained by the integral equation method are compared with those from the method of moments for a quarter-wave element and ground-plane radii $0 \leq ka \leq 3.0$. The values obtained with the integral equation method differ from those obtained using the method of moments by less than 1% for $0 \leq ka \leq 1.75$ and by less than 10% for $0 \leq ka \leq 2.75$. These results suggest that the integral equation method is accurate for ground-plane radii $0 \leq ka \leq 1.75$, and also that it is useful for $0 \leq ka \leq 2.75$. We suspect that the best available results are obtained by using the integral equation method for $0 \leq ka \leq 1.0$.

3.4 METHOD OF MOMENTS: $0 < ka \leq 14$

We saw in Sec. 3.3 that the integral equation method, which is used for determining the fields generated by the ground-plane current when the current distribution on the monopole element is initially specified, is accurate only for ground-plane radii of less than approximately 1.75 wave numbers. We will show in Sec. 3.5 that the algorithms utilized in the oblate spheroidal wave function method are accurate only for ground-plane radii which are no smaller than 3.0 rad. A question thus arises. What method is accurate over a range of ground-plane radii that includes the region $1.75 < ka < 3.0$?

We have found that Richmond's method of moments [2] is the only method in the currently available literature to be accurate over a range of ground-plane radii that includes the region $1.75 < ka < 3.0$. Although this method is primarily intended to be used when the current distribution on the monopole element is initially unknown, it is also applicable when the element is specified to have a sinusoidal current distribution.

Richmond's method of moments is discussed in Sec. 4.2. In this method, the element is subdivided into N equal segments and the ground plane is subdivided into M concentric annular zones of equal width. The unknown current distributions on the element and ground plane are expanded as a series of $N + M$ overlapping sinusoidal dipole modes (sinusoidal-Galerkin method), each with an unknown current distribution. The $N + M$ currents are determined by the Crout substitution method of solution of a $(N + M) \times (N + M)$ matrix. The numbers of subdivisions, N and M, are limited by the cost of computation time and the precision of the computer. The accuracy of the solution can be appreciably decreased if either N or M is

too small or too large. The method of moments converges to a solution when an increase or decrease of unity in the value of N or M does not appreciably alter the solution for input impedance.

A particularly useful property of the sinusoidal-Galerkin method is the sinusoidal current distribution that is imposed on the element by setting $N = 1$.

The input impedance and radiation pattern of thin quarter-wave elements ($b/\lambda = 10^{-6}$, $h/\lambda = 0.25$), for ground-plane radii $0 < ka \leq 14$ wave numbers, were determined by Richmond's method of moments utilizing MITRE's programs *RICHMD1* and *RICHMD2*, which are discussed in Sec. 4.2 and listed in App. B.5. With $N = 1$, convergent solutions were obtained for values of M given by

$$M = 3, \quad ka = 0.25$$

$$M = 7, \quad ka = 0.50$$

$$M = 16, \quad ka = 0.75, 1.0, \ldots, 8.5$$

$$M = 3\,ka, \quad ka = 8.75, 9.0, \ldots, 14.0$$

Computer printouts of the input admittance, ground-plane current distribution, radiation resistance, directivity, and radiation patterns are given in App. A.5.

The input resistance and reactance, as determined by the method of moments, or other methods which give similar results, are plotted for thin quarter-wave elements on ground planes of radii $0 \leq ka \leq 14$ in Figs. 9 and 10 of Sec. 3.9. The directivity on the horizon, peak directivity, and elevation angle of the peak directivity, given by the computer printouts of App. A.5, are plotted in Figs. 11–13 of Sec. 3.9.

The input impedance of thin elements with a sinusoidal current distribution were also determined for element lengths $h/\lambda = 0.1$ and 0.025 and ground-plane radii $0 < ka \leq 8.0$ rad by utilizing program RICHMD1 with $N = 1$. The radiation resistance of these elements is compared in Fig. 14 of Sec. 3.9 with those of a quarter-wave element. In Fig. 14, the radiation resistance is normalized to the value of radiation resistance of each element for $ka = 0$.

Values of the radiation resistance for quarter-wave elements are determined in App. A.5 by computing the input impedance (program RICHMD1) and also by the far-field radiation pattern (program RICHMD2). The values determined from the two methods differ by less than 1% for small ground-plane radii and less than 3% for the larger ground-plane radii.

The values of radiation resistance obtained from program RICHMD2 are compared in Table 5 of Sec. 3.9 with the values obtained by the integral equation method and the oblate spheroidal wave function method. Richmond's method of moments gives useful results over the entire range of $0 < ka \leq 14$, and it provides good agreement with the integral equation method for $0 < ka \leq 1.75$ and the oblate spheroidal wave function method for $3.0 \leq ka \leq 6.5$. Whereas the method of moments gives useful results in the regions $1.75 < ka < 3.0$ and $6.5 < ka \leq 14$, the other methods fail in these regions. For $ka > 14$, Richmond's method of moments is not as useful because of increased computation time and decreased accuracy. We suspect that for thin monopole elements the best available results are obtained by the method of moments for $1.25 \leq ka \leq 2.75$ and $6.75 \leq ka \leq 14$. For relatively thick monopole elements, Richmond's method of moments gives the best available results for ground-plane radii $0 < ka \leq 14$, as discussed in Sec. 4.2.

3.5 OBLATE SPHEROIDAL WAVE-FUNCTIONS: $3.0 \leq ka \leq 6.5$

Oblate spheroidal coordinates (see Table 1 in Sec. 2.1) are particularly convenient for handling the boundary conditions of the magnetic field intensity on the ground plane. The requirement for constant tangential magnetic field intensity across the upper and lower hemispheres at the ground-plane interface may be specified at all points of the ground-plane disk by a boundary condition at only the oblate *radial* coordinate $\xi = 0$.

For ground-plane radii of the same order of magnitude as the excitation wavelength, Leitner and Spence [3–5] utilized oblate spheroidal wave functions to determine the ground-plane current induced by a thin quarter-wave element with a sinusoidal current distribution. Leitner and Spence give numerical values of the ground-plane current distribution, radiation resistance, and far-field power density (at constant element base current) for ground-plane radii $ka = 3, 4, 5$, and $\sqrt{42}$ rad. The complex current distributions are reported on both the top and bottom faces of the ground plane.

In this section, we report the results of a computer program *MONOPL*, based on the theory of Leitner and Spence, which calculates the directivity pattern and radiation resistance for ground-plane radii including the cases of $ka = 3, 4, 5$, and $\sqrt{42}$ rad. Our results are consistent with, but not identical to, the results reported by Leitner and Spence. The form of the solution, corrections, regions of validity for the calculations, accuracy, and numerical results of program MONOPL are discussed in the remainder of this section.

3.5.1 Form of Solution

For a quarter-wave monopole ($h = \lambda/4$), the far-field power density $s'(\eta)$ and radiation resistance R_{rad}, expressed in oblate spheroidal wave functions, are given with reference to Fig. 1 of Sec. 2.1, by [5]:

$$s'(\eta) = [I^2(0)/8\pi^2 r^2](\mu_0/\epsilon_0)^{1/2}\epsilon^4 \left| \sum_{l=1}^{\infty} B_l u_{l1}(\eta) \right|^2 \tag{3.5.1}$$

$$R_{\text{rad}} = (1/2\pi)(\mu_0/\epsilon_0)^{1/2}\epsilon^4 \sum_{l=1}^{\infty} N_{l1}|B_l|^2 \tag{3.5.2}$$

where

$$\begin{aligned}
(\mu_0/\epsilon_0)^{1/2} &= \text{wave impedance in free space } (\Omega) \\
\epsilon \equiv ka = 2\pi a/\lambda &= \text{ground-plane radius (rad)} \\
u_{l1}(\eta) &= \text{angular oblate spheroidal wave function of order 1 and degree } l \\
N_{l1} &= \int_{-1}^{1} u_{l1}^2(\eta)\,\mathrm{d}\eta = \text{norm of } u_{l1}(\eta) \\
{}_2w_{l1}(\xi) &= (1+\xi^2)^{1/2}\ {}_2v_{l1}(\xi) \\
B_l &= (-1)^{l-1}\ {}_2w_{l1}(\pi/2\epsilon)/\alpha_{l1}N_{l1}q_{l1}\ {}^{(3)}v'_{l1}(0)
\end{aligned}$$

The reader is referred to Leitner and Spence [3] for a definition of the oblate spheroidal wave functions α_{l1}, q_{l1}, ${}^{(3)}v'_{l1}(\xi)$, and ${}_2v_{l1}(\xi)$.

Substitution of Eqs. (3.5.1) and (3.5.2) in Eq. (2.2.4) yields the directivity $d'(\eta)$, given by

$$d'(\eta) = 2\left| \sum_{l=1}^{\infty} B_l u_{l1}(\eta) \right|^2 \Big/ \sum_{l=1}^{\infty} N_{l1}|B_l|^2 \tag{3.5.3}$$

3.5.2 Corrections

Problems were encountered in generating the eigenvalues of the oblate spheroidal wave functions. These problems were narrowed down to the continued fractions that generate the eigenvalues. Said continued fractions were derived from the recurrence relations, which, in turn, come from the differential equation. A discrepancy was discovered between our derived continued fractions and the published continued fractions [3]. The corrected continued fractions appear below.

For $l-$ m even:

$$\gamma_{lm}=\frac{-(l+m)(l-m)\ \epsilon^2}{2(2l-1)+\gamma_{lm}\ +\ \dfrac{(l+m-2)(l-m-2)\ \epsilon^2}{4(2l-3)+\gamma_{lm}\ +\ \dfrac{(l+m-4)(l-m-4)\ \epsilon^2}{6(2l-5)+\gamma_{lm}\ +}}}$$
$$+\frac{(l+m+2)(l-m+2)\ \epsilon^2}{2(2l+3)-\gamma_{lm}\ +\ \dfrac{(l+m+4)(l-m-4)\ \epsilon^2}{4(2l+5)-\gamma_{lm}\ +\ \dfrac{(l+m+6)(l-m+6)\ \epsilon^2}{6(2l+7)-\gamma_{lm}\ +}}} \tag{3.5.4}$$

For $l-m$ odd:

$$\gamma_{lm}=\frac{-(l+m-1)(l-m-1)\ \epsilon^2}{2(2l-1)+\gamma_{lm}\ +\ \dfrac{(l+m-3)(l-m-3)\ \epsilon^2}{4(2l-3)+\gamma_{lm}\ +\ \dfrac{(l+m-5)(l-m-5)\ \epsilon^2}{6(2l-5)+\gamma_{lm}\ +}}}$$
$$+\frac{(l+m+1)(l-m+1)\ \epsilon^2}{2(2l+3)-\gamma_{lm}\ +\ \dfrac{(l+m+3)(l-m+3)\epsilon^2}{4(2l+5)-\gamma_{lm}\ +\ \dfrac{(l+m+5)(l-m+5)\ \epsilon^2}{6(2l+7)-\gamma_{lm}\ +}}} \tag{3.5.5}$$

The eigenvalues can also be expressed in terms of a series expansion, which has the form:

$$\gamma_{lm}=\sum_{k=1}^{\infty} f_{2k}^{lm}\epsilon^{2k} \tag{3.5.6}$$

The first two terms in this expansion were checked against the continued fractions and found to agree. This is important because the continued fraction method by which values of the eigenvalues are obtained depends on the accuracy of the roots γ_{lm} in Eq. (3.5.6).

3.5.3 Regions of Calculation Validity

A lower bound on the value of $\epsilon = 2\pi a/\lambda$ for which the calculations are valid depends on the following equations (see Eqs. (34) and (48), [3]):

$$^{(1)}v_{l1}(\xi)=(1+\xi^2)^{1/2}\sum_{n=0,1}^{\infty} a_n^{l1}\xi^n, \quad \text{for} \quad \xi=\pi/2\epsilon \tag{3.5.7}$$

and

$$g_{l1}(\xi) = (1+\xi^2)^{-1/2} \sum_{n=0,1}{}' b_n^{l1} \xi^n, \quad \text{for} \quad \xi = \pi/2\epsilon \tag{3.5.8}$$

where the prime indicates summation over alternate n, starting with $n = 0$ if $(l-1)$ is even, and $n = 1$ if $(l-1)$ is odd.

Equation (3.5.7) is the expression for the first-order radial spheroidal wave function of the first kind. Equation (3.5.8) is used in another expression to obtain the first-order radial spheroidal wave function of the second kind. As ϵ becomes small, ξ becomes large, so more terms are needed in Eqs. (3.5.7) and (3.5.8). In theory, Eqs. (3.5.7) and (3.5.8) converge for all real values of $\xi = \pi/2\epsilon$. Computationally, however, because of the finite accuracy of the computer, Eqs. (3.5.7) and (3.5.8) will not converge for all real values of $\xi = \pi/2\epsilon$. To be cautious, we can restrict ξ so that it is less than unity. We obtain from this assumption the computational constraint $\xi = \pi/2\epsilon < 1$, which implies a lower bound on ϵ, given by $\epsilon > \pi/2 \approx 1.57$.

An even tighter lower bound on ϵ is obtained by observing what happens in the algorithm that is used to derive the eigenvalues. However, this algorithm is not well behaved for values of ϵ less than $\epsilon = 2.5$. Therefore, a lower bound for ϵ is given by $\epsilon \geq 2.5$. For accurate values of radiation resistance, a lower bound for ϵ would be $\epsilon \geq 3.0$. (see Table5 of Sec. 3.9).

An upper bound on ϵ is obtained by observing what happens in the continued fraction algorithm that is used to derive the eigenvalues. For values of ϵ greater than 6.5, the series expansion for the eigenvalues, given by Eq. (3.5.6), does not give a sufficiently accurate answer by using only the first four terms. The resulting eigenvalues are so far from the correct eigenvalues as to cause the continued fraction algorithm of Eqs. (3.5.4) and (3.5.5) to converge to a root that is not the correct value. As a consequence, erroneous values of radiation resistance can be obtained for $\epsilon > 6.5$ (see Table 5 of Sec. 3.9).

Consequently, the useful range of ϵ for Leitner and Spence's method of oblate spheroidal wave functions is $2.5 \leq \epsilon \leq 6.5$. We suspect that the best available results are obtained by the oblate spheroidal wave function method for $3.0 \leq \epsilon \leq 6.5$.

Suggestions for extending the method of oblate spheroidal wave functions to the entire range $0 \leq \epsilon < \infty$ are as follows.

$0 \leq \epsilon < 3.0$

In determining the eigenvalues γ_{lm}, bypass the subroutine IMPROV. In determining the radial eigenfunctions ${}_2w_{l1}(\xi)$, substitute (65) and (66) for (34) and (48) of Ref. 3. Program MONOPL now utilizes (34) and (48) of Ref. 3.

$3 \leq \epsilon \leq 6.5$

Use Program MONOPL in its present form.

$6.5 < \epsilon < \infty$

In determining the eigenvalue γ_{lm}, use the asymptotic expansion given by (21.8.2) of Ref. 19 to obtain a raw value and then use subroutine IMPROV to obtain a refined value. In determining the eigenfunctions, use the present routines in Program MONOPL.

3.5.4 Accuracy

The calculation of directivity and radiation resistance is comprised of many equations. Some of these equations involve series expansions. When we varied the number of terms in these series, the radiation resistance was found to vary only in the fifth or sixth significant term.

Another problem mentioned previously was the accuracy by which Eqs. (3.5.6) computes the eigenvalues. Because of computational reasons, we used only the first four terms in Eq. (3.5.6). As a result, a raw eigenvalue is computed by using Eq. (3.5.6), which is then used as an initial guess in the continued fractions. The continued fractions have many roots in γ_{lm}. The number of roots is dependent on the number of fractional terms used in the continued fraction. However, only one of these roots can be the eigenvalue. If the raw eigenvalue is sufficiently far from the correct eigenvalue, then the continued fraction will converge to a root that is not an eigenvalue. This will produce incorrect results.

The computed eigenvalues were checked against published values [24]. The computed values were found to be within the percentage error of the published values.

The computed eigenvalues of directivity on the horizon and radiation resistance, for different values of ground-plane extent, were found to agree with the relationship given by (2.3.3) to at least five decimal places with the free-space wave impedance $\eta = 376.73037\,\Omega$.

3.5.5 Numerical Results

The far-field power density $s'(\eta)$, radiation resistance R, and directivity $d'(\eta)$ of quarter-wave elements given by Eqs. (3.5.1), (3.5.2), and (3.5.3), respectively, were numerically evaluated by program MONOPL written in FORTRAN 77 language for use on a DEC PDP-11/70 computer. The program listing is given in App. B.03. Numerical values are obtained for the cases of $2.5 \leq ka \leq \sqrt{42}$.

The computed eigenvalues are given in Table 2. Computer printouts of the directivity patterns are given in App. A.3 for $ka = 3$, 4, 5, and $\sqrt{42}$. The patterns are plotted in Fig. 8 of Sec. 3.9 as polar graphs on the same linear scale. The total radiated power is held constant in these plots.

TABLE 2 Eigenvalues γ_{l1} for $2\pi a/\lambda = 3, 4, 5, \sqrt{42}$

	γ_{l1}			
l	$2\pi a/\lambda = \epsilon = 3$	$\epsilon = 4$	$\epsilon = 5$	$\epsilon = \sqrt{42}$
1	6.7305791912	11.0907992567	15.056611686	21.687439619
2	4.8215414322	8.1301387077	11.872162474	17.738230003
3	5.0070741733	9.4059031099	15.750367134	28.127723151
4	4.7772522576	8.6287184908	13.694959245	23.237303490
5	4.6896340053	8.4462229270	13.439315734	23.585994650
6	4.6368101196	8.3210439564	13.161309568	22.624607030
7	4.6032991570	8.2427831207	12.999910517	22.234563635
8	4.5807102835	8.1899480807	12.890952874	21.960565094
9	4.5647761329	8.1526212369	12.814155253	21.770549914
10	4.5531234272	8.1252813999	12.757940027	21.632114595

The directivity on the horizon, radiation resistance, and peak directivity are summarized in Table 3.

3.6 SCALAR DIFFRACTION THEORY AND GEOMETRIC THEORY OF DIFFRACTION: $6.5 < ka < \infty$

For an element on a ground plane of sufficiently large radius, Tang [6] utilized a scalar theory of diffraction to calculate the far-field elevation pattern. For elevation angles near the horizon ($\theta \approx \pi/2$), the magnetic far-field intensity is determined by linear extrapolation to the result for the element itself given by Eq. (3.2.10) with $\theta = \pi/2$ rad. Tang's method for the radiation pattern is more accurate than that obtained by the variational method of Sec. 3.7 because it includes an additional term in the expansion for the total magnetic field intensity. Because the variational method is useful for ground-plane radii as small as $ka = 30$ rad, Tang's method should be useful for even smaller ground-plane radii, provided that $ka \gg 1$.

The geometric theory of diffraction (GTD) is another method applicable for sufficiently large ground-plane radii. In GTD, the fields are determined by ray optics (an incident ray plus a reflected ray) and diffraction by the edge. However, the effect of edge diffraction is only approximated in GTD because the edge is treated point by point as though it were a straight knife-edge of infinite extent. Therefore, GTD may be applied to an element at the center of a circular ground plane only when said ground plane is of sufficiently large radius. The GTD method is reviewed by Balanis [25], who also gives a computer program for calculating the diffraction coefficient.

TABLE 3 Directivity on Horizon and Radiation Resistance of Quarter-Wave Element, $2.5 \leq 2\pi a/\lambda \leq \sqrt{42}$

	Directivity on horizon		Radiation resistance		Peak directivity	
Ground-plane radius, $\epsilon = 2\pi a/\lambda$ (rad)	$d(\pi/2)$ (numeric)	$D(\pi/2) = 10\log_{10} d(\pi/2)$ (dBi)	R_{rad} (ohms) Program MONOPL	R_{rad} (ohms) Leitner[a]	D_{peak} (dBi)	θ_{peak} (°)
2.5	1.09745	0.40383	27.31731			
3.0	0.79995	−0.96938	37.47646	39.32	2.52250	46
3.4	0.66233	−1.78923	45.26299			
3.5	0.65086	−1.86515	46.06128			
3.6	0.64812	−1.88346	46.25589			
3.7	0.65316	−1.84980	45.89866			
4.0	0.70254	−1.53326	42.67237	42.10	3.89943	40
4.5	0.82743	−0.82271	36.23191			
5.0	0.92059	−0.35934	32.56526	31.87	3.37175	36
5.25	0.93879	−0.27430	31.93379			
5.5	0.93294	−0.30146	32.13410			
6.0	0.85088	−0.70134	35.23337			
$\sqrt{42}$	0.74637	−1.27045	40.16661	39.88	2.55213	56

[a] A. Leitner, Research Report No. EM-19, New York University, New York, April 1950.

In Sec. 4.3, the method of moments combined with GTD yields results for input impedance that are useful for ground planes of radii $ka \gtrsim 6$ rad and accurate for $ka > 8$. Therefore, when the element current distribution is constrained to be sinusoidal, the GTD method is expected to give useful results for ground-plane radii $ka \gtrsim 6.5$ rad, over which range the oblate spheroidal wave function method does not give useful results.

3.7 VARIATIONAL METHOD: $30 \lesssim ka < \infty$

For an element on a ground plane of very large radius ($ka \gtrsim 30$ rad), differences in the input impedance and radiation pattern from the values for a ground plane of infinite extent may be determined by utilizing a variational method of Storer [7,8].

With reference to Fig. 1 of Sec. 2.1, for a sinusoidal current distribution on the element as given by Eqs. (3.1.1), the input impedance difference is [from Eq. (20) of Ref. 7]:

$$Z_{\text{in}} - Z_\infty = \frac{-j\eta \exp(j2ka)}{4\pi ka}\left[\frac{1-\cos(kh)}{\sin(kh)}\right]^2 \times \left\{1 + \frac{\exp[j(2ka + 3\pi/4)]}{(4\pi ka)^{1/2}}\right\}^{-1}, \quad ka \gtrsim 30 \tag{3.7.1}$$

where

Z_{in} = input impedance for an element on a ground plane of radius ka rad (Ω)
Z_∞ = input impedance for the same element on a ground plane of radius $ka = \infty$ rad (Ω)
η = wave impedance in free space = 376.73037 Ω.

Because $(4\pi ka)^{1/2} \gg 1$ for $ka \gtrsim 30$, the difference of input resistance $R_{\text{in}} - R_\infty$ and input reactance $X_{\text{in}} - X_\infty$ are given approximately by

$$R_{\text{in}} - R_\infty \approx \left[\frac{1-\cos(kh)}{\sin(kh)}\right]^2 \frac{\sin(2ka)}{4\pi ka}, \quad ka \gtrsim 30 \tag{3.7.2}$$

$$X_{\text{in}} - X_\infty \approx \left[\frac{1-\cos(kh)}{\sin(kh)}\right]^2 \frac{\cos(2ka)}{4\pi ka}, \quad ka \gtrsim 30 \tag{3.7.3}$$

The maxima, nulls, and minima of $R_{\text{in}} - R_\infty$ occur for values of ka given

approximately by

$$ka = \begin{cases} \left(2N + \frac{1}{2}\right)(\pi/2) & \text{(maxima)}, \quad N = 0, 1, 2, \ldots \\ N\pi/2 \quad \text{(nulls)}, & N = 0, 1, 2, \ldots \\ \left(2N + \frac{3}{2}\right)(\pi/2) & \text{(minima)}, \quad N = 0, 1, 2, \ldots \end{cases} \tag{3.7.4}$$

The input impedance $Z_{\text{in}} - Z_\infty$ given by Eq. (3.7.1) is calculated in computer program *MONOSTOR* (also called *STORER*), the description of which is given in App. B.04.

For very thin quarter-wave elements, $R_\infty = 36.54\,\Omega$ and $X_\infty = 21.26\,\Omega$ (see Sec. 3.8). The numeric directivity on the horizon, $d(\pi/2)$, is related to the radiation resistance $R_{\text{rad}} = R_{\text{in}}$ by Eq. (2.3.2). Computer printouts of the maxima and minima of $R_{\text{in}} - R_\infty$, as well as for $X_{\text{in}} - X_\infty$, are given in App. A.4. For very thin quarter-wave elements, App. A.5 also gives computer printouts of R_{in}, X_{in}, $d(\pi/2)$, and $D(\pi/2) = 10 \log_{10} d(\pi/2)$.

Differences in the far-field radiation pattern from that for a ground plane of infinite extent are given by Storer [8]. For the waveform of Eq. (2.1.2) and a sinusoidal current distribution $I(z)$ for the elements (see Fig. 1 of Sec. 2.1), the difference in the far-field magnetic field intensity is [from Eq. (6) of Ref. 8]:

$$H_\phi - H_\phi|_{ka=\infty} = \operatorname{sgn}(\theta) \left\{ \frac{jI(0) \exp(-jkr)[1 - \cos(kh)]}{[\sin(kh) 2\pi r][2\pi\sqrt{2}]} \right\} \times \left\{ \int_0^{2\pi} \frac{\exp[-jka(1 - \sin\theta \cos\phi)] \cos\phi}{(1 - \sin\theta \cos\phi)^{1/2}} \, d\phi \right\}, \quad ka \gtrsim 30 \tag{3.7.5}$$

where

H_ϕ = magnetic far-field intensity for an element on a ground plane of radius ka rad (A/m)

$H_\phi|_{ka=\infty}$ = magnetic far-field intensity for an element on a ground plane of infinite extent (A/m)

and

$$\operatorname{sgn}\theta = \begin{cases} +1, & 0 \le \theta < \pi/2 \\ 0 & \\ -1, & \pi/2 < \theta \le \pi \end{cases}$$

The magnetic field intensity $H_\phi|_{ka=\infty}$ is given by (see Sec. 3.8):

$$H_\phi|_{ka=\infty} = \begin{cases} \dfrac{jI(0)\exp(-jkr)}{\sin(kh) 2\pi r} \left[\dfrac{\cos(kh\cos\theta) - \cos(kh)}{\sin\theta} \right], & 0 \le \theta \le \pi/2 \\ 0, & \pi/2 < \theta \le \pi \end{cases} \tag{3.7.6}$$

The electric far-field intensity $E_\theta = \eta H_\phi$, where H_ϕ is given by Eq. (3.7.5) and η is the free-space wave impedance.

One of the distinguishing features of the far-field radiation pattern for ground plane of large radii is the occurrence of a fine-structured lobing pattern, $H_\phi - H_\phi|_{ka=\infty}$, superimposed on the pattern for a ground plane of infinite extent. The lobing pattern, given by Eq. (3.7.5), is symmetrical about the horizon (except for a phase shift of π rad) with the most prominent lobes near the zenith and nadir directions. The nth maximum of the lobing pattern in each quadrant decreases with increase in values of n, where $n = 1$ corresponds to the lobe nearest to either the zenith or nadir direction.

The lobing structure is characterized [8] by the elevation angle θ_n of the nth maxima, the angular separation $\Delta\theta$ between lobes, the angle $\theta_{\max}$ within which all prominent maxima occur, and the number N of prominent lobes. The elevation angle θ_n in radians is given approximately by

$$\theta_n \approx \begin{cases} 0.59(\pi/ka); & n = 1, \quad ka \gtrsim 30 \\ (n + 0.75)(\pi/ka); & n = 2, 3, \ldots, N; \quad ka \gtrsim 30 \end{cases} \tag{3.7.7}$$

The angular separation $\Delta\theta$ in radians is given approximately by

$$\Delta\theta \approx \begin{cases} 1.16(\pi/ka); & n = 1, \quad ka \gtrsim 30 \\ \pi/ka; & n = 2, 3, \ldots, N; \quad ka \gtrsim 30 \end{cases} \tag{3.7.8}$$

Prominent lobes are defined [8] as lobes having maxima that are less than one-fourth the amplitude for the case of a ground plane of infinite extent. The angle $\theta_{\max}$ in radians is given approximately by

$$\theta_{\max} \approx 1.87(\pi/ka)^{1/3} \left[\frac{1 - \cos(kh)}{kh \sin(kh)}\right]^{2/3}, \quad ka \gtrsim 30 \tag{3.7.9}$$

The number N of prominent lobes is determined by

$$\theta_{\max} = \theta_1 + (\Delta\theta)_{n=1} + (N - 2)(\Delta\theta)_{n\neq 1}, \quad ka \gtrsim 30 \tag{3.7.10}$$

where θ_1, $\Delta\theta$, and $\theta_{\max}$ are given by Eqs. (3.7.7)–(3.7.9), respectively. Solving for N, we have

$$N = [\theta_{\max}/(\pi/ka)] - 0.25 = 1.87(\pi/ka)^{-2/3} - 0.25, \quad ka \gtrsim 30 \tag{3.7.11}$$

3.8 METHOD OF IMAGES: $ka = \infty$

For the idealized case of a monopole element mounted on a ground plane of infinite extent and infinite conductivity, the monopole antenna may be modeled,

by using the method of images, as a dipole with one-half of the input impedance and double the peak numeric directivity of the dipole [26]. The infinite ground plane prevents monopole radiation into the hemisphere below the ground plane, but it allows a radiation pattern identical to that of the dipole in the upper hemisphere.

In this section, we assume that the current has a waveform as given by (2.1.2), and a current distribution $I(z)$ on the element and its image (see Fig. 7) of the form:

$$I(z) = \begin{cases} [I(0)/\sin(kh)]\sin[k(h-z)], & 0 \le z \le h \quad \text{(element)} \\ [I(0)/\sin(kh)]\sin[k(h+z)], & -h \le z \le 0 \quad \text{(image)} \end{cases} \tag{3.8.1}$$

The near-fields, far-fields, and input impedance of an electrically thin element on a ground plane of infinite extent are summarized in the remainder of this section.

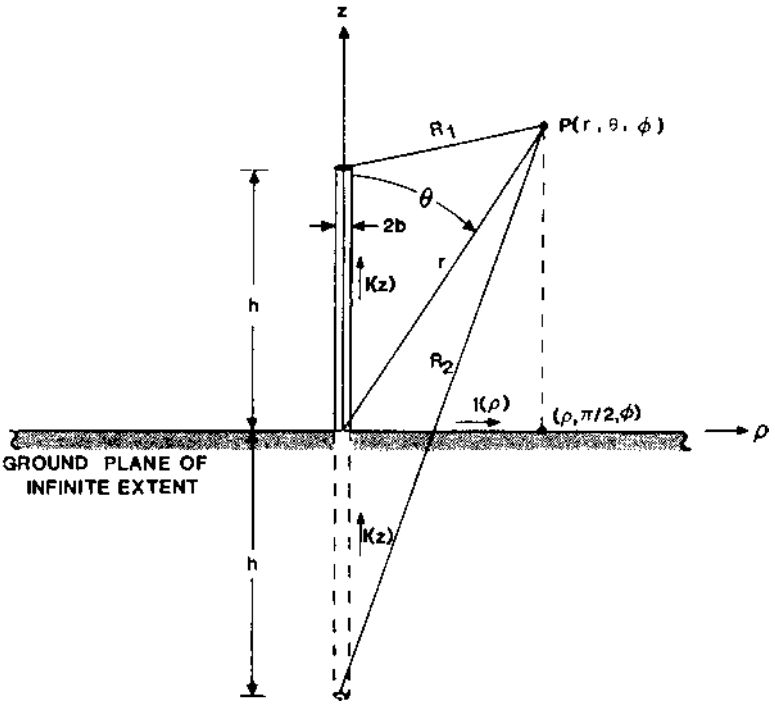

FIGURE 7 Method of images for a monopole element at the center of a circular ground plane of infinite extent.

3.8.1 Near-Fields

The exact magnetic field intensity $\mathbf{H} = \hat{u}_\phi H_\phi$ and electric field intensity $\mathbf{E} = \hat{u}_\rho E_\rho + \hat{u}_z E_z$ for an infinitely thin element are given [from Eqs. (7–15) and (7–17) of Ref. 25] as

$$H_\phi = \frac{jI(0)}{4\pi\rho\sin(kh)}[\exp(-jkR_1) + \exp(-jkR_2) - 2\cos(kh)\exp(-jkr)], \quad z \geq 0 \tag{3.8.2a}$$

$$= 0, \quad z < 0 \tag{3.8.2b}$$

$$E_\rho = \frac{j\eta I(0)}{4\pi\rho\sin(kh)}\left[\frac{(z-h)\exp(-jkR_1)}{R_1} + \frac{(z+h)\exp(-jkR_2)}{R_2} - 2z\cos(kh)\frac{\exp(-jkr)}{r}\right], \quad z \geq 0 \tag{3.8.3a}$$

$$= 0, \quad z < 0 \tag{3.8.3b}$$

$$E_z = \frac{-j\eta I(0)}{4\pi\sin(kh)}\left[\frac{\exp(-jkR_1)}{R_1} + \frac{\exp(-jkR_2)}{R_2} - 2\cos(kh)\frac{\exp(-jkr)}{r}\right], \quad z \geq 0 \tag{3.8.4a}$$

$$= 0, \quad z < 0 \tag{3.8.4b}$$

where

$$R_1 = [\rho^2 + (z-h)^2]^{1/2}$$
$$R_2 = [\rho^2 + (z+h)^2]^{1/2}$$

The magnetic field intensities at the top and bottom surfaces of the ground plane are respectively given by Eqs. (3.8.2a) and (3.8.2b) as

$$H_\phi|_{z=0_+} = \frac{jI(0)}{2\pi\rho\sin(kh)}[\exp(-jkR_3) - \cos(kh)\exp(-jk\rho)] \quad \text{(top of ground plane)} \tag{3.8.5}$$

$$H_\phi|_{z=0_-} = 0 \quad \text{(bottom of ground plane)} \tag{3.8.6}$$

where

$$R_3 = (\rho^2 + h^2)^{1/2}$$

The incremental ground-plane current $\Delta I(\rho)$ contained a differential azimuthal angle $\mathrm{d}\phi$ may be determined from Eqs. (3.8.5), (3.8.6), and Ampere's circuit law applied to a closed path along the top and bottom surfaces of the ground plane for arc lengths within $\mathrm{d}\phi$. Because the ground-plane current $I(\rho)$ is defined to be positive in the $+\rho$ direction (see Fig. 1 of Sec. 2.1), the path is taken in the clockwise direction. Accordingly,

$$\begin{aligned}\Delta I(\rho) &= (-\hat{u}_\phi \cdot \mathbf{H}_{\text{top}} + \hat{u}_\phi \cdot \mathbf{H}_{\text{bottom}})\rho\,\mathrm{d}\phi \\ &= [-H_\phi|_{z=0_+} + H_\phi|_{z=0_-}]\rho\,\mathrm{d}\phi\end{aligned} \tag{3.8.7}$$

The total ground-plane current $I(\rho)$ is given by

$$\begin{aligned}I(\rho) &= \int_0^{2\pi} \Delta I(\rho)\,\mathrm{d}\phi = 2\pi\rho[-H_\phi|_{z=0_+} + H_\phi|_{z=0_-}] \\ &= \frac{jI(0)}{\sin(kh)}[\cos(kh)\exp(-jk\rho) - \exp(-jkR_3)]\end{aligned} \tag{3.8.8}$$

Equation (3.8.8) agrees with that given by Richmond [Eq. (33) of Ref. 2].

3.8.2 Far-Fields

For the far-field conditions given by Eqs. (3.2.7) and (3.2.8), the relations (3.8.2a)–(3.8.4b) reduce to the far-fields $\mathbf{H} = \hat{u}_\phi H_\phi$ and $\mathbf{E} = \hat{u}_\theta E_\theta = \hat{u}_\theta \eta H_\theta$, where [from Eq. (4–62) of Ref. 25], H_ϕ is given by

$$H_\phi = \begin{cases} \dfrac{jI(0)\exp(-jkr)}{\sin(kh)2\pi r}\left[\dfrac{\cos(kh\cos\theta) - \cos(kh)}{\sin\theta}\right], & 0 \le \theta \le \pi/2 \\ 0, & \pi/2 < \theta \le \pi \end{cases} \tag{3.8.9}$$

The time-averaged radiated power density $s(\theta) = (\eta/2)|H_\phi|^2$ is given by

$$s(\theta) = \begin{cases} \dfrac{\eta|I(0)|^2 f(\theta)}{8\pi^2 r^2 \sin^2(kh)}, & 0 \le \theta \le \pi/2 \\ 0, & \pi/2 < \theta \le \pi \end{cases} \tag{3.8.10}$$

where

$$f(\theta) = \left[\frac{\cos(kh\cos\theta) - \cos(kh)}{\sin\theta}\right]^2$$

The direction of maximum radiated power is $\theta = \pi/2$ rad.

The input impedance of a monopole element of length h on a ground plane of infinite extent is one-half that of a dipole of total length $2h$ in free space. Accordingly, the radiation resistance R_{rad} of an infinitely thin element on a ground plane of infinite extent is given by [compare with Eqs.(4-70) and (4-79) of Ref. 26]:

$$R_{\text{rad}} = \frac{\eta}{4\pi\sin^2(kh)}\left\{\text{Cin}(2kh) + \frac{1}{2}\sin(2kh)[\text{Si}(4kh) - 2\,\text{Si}(2kh)]\right.$$
$$\left. + \frac{1}{2}\cos(2kh)[2\,\text{Cin}(2kh) - \text{Cin}(4kh)]\right\}, \quad b = 0 \tag{3.8.11}$$

where $\text{Si}(x)$ and $\text{Cin}(x)$ are the sine integral and modified cosine integrals, respectively, which are defined according to Eq. (3.2.32). Equation (3.8.9) is also approximately valid for thin elements ($kb \ll 1$). (For example, compare Eqs. (3.2.33) and (3.2.35) for a thin monopole element in the absence of a ground plane.)

By substituting Eqs. (3.8.10) and (3.8.11) in (2.2.6), the numeric directivity $d(\theta)$ is given by

$$d(\theta) = \frac{4f(\theta)}{B} \tag{3.8.12}$$

where

$$B \equiv \text{Cin}(2kh) + \frac{1}{2}\sin(2kh)[\text{Si}(4kh) - 2\,\text{Si}(2kh)]$$
$$+ \frac{1}{2}\cos(2kh)[2\,\text{Cin}(2kh) - \text{Cin}(4kh)]$$

For a quarter-wave monopole element ($kh = \pi/2$), Eqs. (3.8.11) and (3.8.12) reduce to

$$R_{\text{rad}} = \frac{\eta}{4\pi}\frac{\text{Cin}(2\pi)}{2} = 36.5395\,\Omega; \quad kh = \pi/2, \quad b = 0 \tag{3.8.13}$$

$$f(\theta) = \frac{\cos^2[(\pi/2)\cos\theta]}{\sin^2\theta}, \quad kh = \pi/2 \tag{3.8.14}$$

$$d(\theta) = \frac{4\cos^2[(\pi/2)\cos\theta]}{\sin^2\theta}\frac{2}{\mathrm{Cin}(2\pi)}, \quad kh = \pi/2 \tag{3.8.15}$$

The peak directivity $d(\pi/2) = 3.2818$ (numeric) corresponding to $D(\pi/2) = 10\log_{10} d(\pi/2) = 5.1612\,\mathrm{dBi}$. The `directivity` is plotted in Fig. 8(f) of Sec. 3.9.

For an electrically short monopole element ($kh \ll 1$) and $\eta \approx 120\pi(\Omega)$, Eqs. (3.8.11) and (3.8.12) reduce to

$$R_{\mathrm{rad}} = 10(kh)^2, \quad (kh) \ll 1 \tag{3.8.16}$$

$$f(\theta) = \frac{(kh)^4}{4}\sin^2\theta, \quad (kh) \ll 1 \tag{3.8.17}$$

$$d(\theta) = \begin{cases} 3\sin^2\theta, & \mathrm{kh} \ll 1, \quad 0 \le \theta \le \pi/2 \\ 0, & -\pi/2 \le \theta < 0 \end{cases} \tag{3.8.18}$$

The peak directivity $d(\pi/2) = 3.0$ (numeric) corresponding to $D(\pi/2) = 10\log_{10} d(\pi/2) = 4.7712\,\mathrm{dBi}$.

3.8.3 Input Impedance

The input resistance R_{in} is given by Eq. (3.8.11), which is exact for an infinitely thin element and approximately correct for thin elements, provided that the current distribution of the elements is sinusoidal.

The input reactance X_{in} for thin elements ($kb \ll 1$) is given by [compare with Eqs. (7-33) and (7-30) of Ref. 25]:

$$\begin{aligned} X_{\mathrm{in}} = \frac{\eta}{4\pi\sin^2(kh)}\Big\{ & \mathrm{Si}(2kh) + \cos(2kh)[\mathrm{Si}(2kh) - \frac{1}{2}\mathrm{Si}(4kh)] \\ & - \sin(2kh)[\ln(h/b) - \mathrm{Cin}(2kh) + \frac{1}{2}\mathrm{Cin}(4kh) + \frac{1}{2}\mathrm{Cin}(kb^2/h)]\Big\} \end{aligned} \tag{3.8.19}$$

For a quarter-wave element, for any value of b, Eq. (3.8.19) gives an input reactance $X_{\mathrm{in}} = 21.2576\,\Omega$. In Eq. (3.8.19), $X_{\mathrm{in}} = 0$ for element lengths that are slightly less than $kh = (2n-1)(\pi/2)$, $n = 1,2,3,\ldots$, which are approximately one-half of the resonant lengths for a monopole element in the absence of a ground plane [see Eq. (3.2.38)].

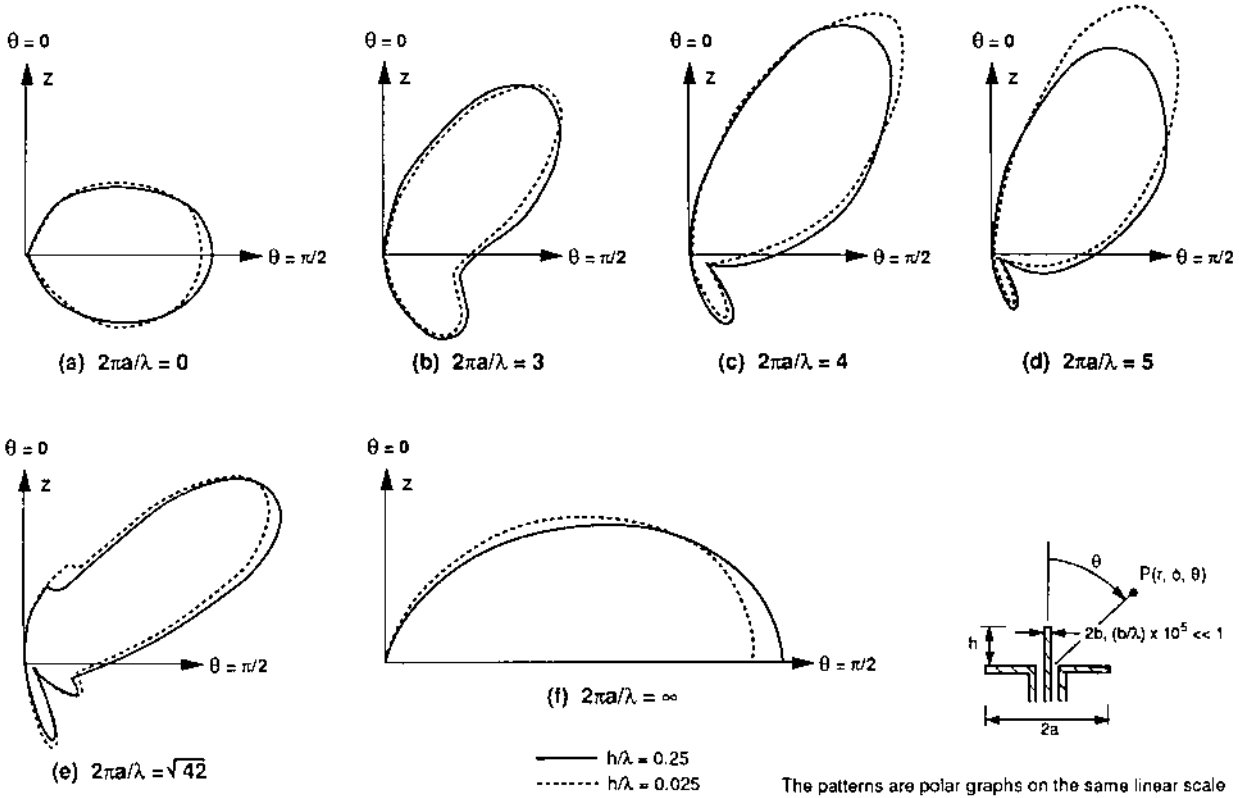

FIGURE 8 Elevation directivity patterns, for any azimuthal direction, of quarter-wave and electrically-short-elements mounted on a ground-plane radius a.

3.9 SUMMARY OF RESULTS

In Chapter 3, a sinusoidal current distribution is assumed on the monopole element. Although such a current distribution is never exactly realized, even for an infinitely thin element (see Sec. 3.1), it is a useful approximation for sufficiently thin elements. As an example, for a quarter-wave element of radius $b = 10^{-6}\lambda$, comparison of the input impedances computed by determining the actual current distribution of the elements with that computed by assuming a sinusoidal current distribution yields a difference of not more than 5% for ground-plane radii $ka = 6-14$ (compare Table 7 of Sec. 4.5 with Tables A2-24–A2-42 of App. A). The assumption of a sinusoidal current distribution of the elements allows computationally simpler models to determine input impedance and radiation patterns than those models that follow in Chapter 4. The results of these simpler models are summarized in this section.

The electrical properties of electrically short and quarter-wave monopole elements on zero, large, and infinite extent ground planes are compared in Table 4 with the corresponding properties of electrically short and half-wave dipoles. The peak directivity of a quarter-wave monopole is 1.88 and 5.16 dBi for zero and infinite extent ground planes, respectively. The directivity on the horizon of a quarter-wave monopole is 1.88 and -0.86 dBi for ground planes of zero extent and very large but finite extent, respectively. Slightly smaller directivities are obtained for electrically short elements than is the case for quarter-wave elements.

The radiation resistances obtained by different methods are compared in Table 5 for a thin quarter-wave element on a ground plane of radius $0 \leq ka \leq 8.5$ rad. The suspected best available results are obtained by the integral equation method for $0 \leq ka \leq 1.0$, by the method of moments ($N = 1$) for $1 < ka < 3.0$, by the oblate spheroidal wave function method for $3.00 \leq ka \leq 6.5$, and by the method of moments ($N = 1$) for $6.5 < ka \leq 14$. The result obtained by the method of moments is in good agreement with the suspected best available results obtained by other methods.

The numeric directivity patterns of quarterwave and electrically short elements on ground planes of radii $ka = 0, 3, 4, 5, \sqrt{42},$ and ∞ rad are plotted in Fig. 8. These polar graphs of directivity should not be confused with the polar graphs of radiated power density plotted by Leitner and Spence [5] for constant base current. It should be noted that the peak directivity and its direction are not monotonic functions of the ground-plane radius.

The input impedance of a thin quarter-wave element is plotted in Figs. 9 and 10 for ground-plane radii $0 \leq ka \leq 14$ rad. The input resistance varies between 19.4 and 46.1 Ω, and asymptotically approaches 36.5 Ω for increasingly large ground-plane radii. The input reactance varies between $-\infty$ and 32.5 Ω, and asymptotically approaches 21.3 Ω for increasingly large ground-plane radii.

TABLE 4 Electrical Properties of Very Thin Monopole Elements on Ground Planes of Zero, Large, and Infinite Extent

Antenna structure	Ground-plane radius (rad), $2\pi a/\lambda$	Element length (wavelengths), h/λ	Peak directivity[b]		Directivity on horizon		Input impedance		Reference equations
			$d(\theta_p)$ (numeric)	$D(\theta_p)$ (dBi)	$d(\theta = \pi/2)$ (numeric)	$D(\theta = \pi/2)$ (dBi)	Radiation resistance (Ω)	Reactance[b] (Ω)	
Monopole	0	$\ll 1$	1.500	1.761	1.500	1.761	$20\pi^2(h/\lambda)^2$	$-\infty$	(3.2.19), (3.2.20)
	0	0.25	1.543	1.882	1.543	1.882	19.43	$-\infty$	(3.2.15), (3.2.16)
	$\gg 1$, FINITE	$\ll 1$	3.000	4.771	0.750	-1.249	$40\pi^2(h/\lambda)^2$	$-\infty$	(3.7.1), (3.8.18), (2.3.2)
	$\gg 1$, FINITE	0.25	3.282	5.161	0.820	-0.859	36.54	21.26	(3.7.1), (3.8.15), (2.3.2)
	∞	$\ll 1$	3.000	4.771	3.000	4.771	$40\pi^2(h/\lambda)^2$	$-\infty$	(3.8.16), (3.8.18), (3.8.19)

TABLE 4 Continued

Antenna structure	Ground-plane radius (rad), $2\pi a/\lambda$	Element length (wavelengths), h/λ	Peak directivity[b]		Directivity on horizon		Input impedance		Reference equations
			$d(\theta_p)$ (numeric)	$D(\theta_p)$ (dBi)	$d(\theta = \pi/2)$ (numeric)	$D(\theta = \pi/2)$ (dBi)	Radiation resistance (Ω)	Reactance[b] (Ω)	
	∞	0.25	3.282	5.161	3.282	5.161	36.54	21.26	(3.8.13), (3.8.15), (3.8.19)
Dipole[c]	0	$\ll 1$	1.500	1.761	1.500	1.761	$80\pi^2(h/\lambda)^2$	$-\infty$	Balanis [15], pp. 108, 112, 131, 132
	0	0.25	1.641	2.151	1.641	2.151	73.08	42.52	
Idealized isotropic radiator			1.000	0	1.000	0	—	—	—

[a] Direction of peak directivity is $\theta_p = \pi/2$ rad, except for monopole elements on ground planes of finite but nonzero extent, in which case $\theta_p < \pi/2$ rad.
[b] Reactance is in the limit of an infinitely thin element.
[c] Very thin dipole of half-length h.

TABLE 5 Radiation Resistance of a Thin Quarter-Wave Element at the Center of a Circular Ground Plane of Radius $0 \leq ka \leq 8.5$ rad (Sinusoidal Current Distribution Assumed on Element)

	Radiation resistance (Ω)		
Normalized ground -plane radius, $2\pi a/\lambda$	Integral equation method	Oblate spheroidal wave-function method	Method of moments
0	19.43[a]		
0.25	19.48[a]		19.49
0.50	19.62[a]		19.62
0.75	19.86[a]		19.86
1.00	20.23[a]		20.21
1.25	20.76		20.71[a]
1.50	21.51		21.25[a]
1.75	22.59		22.44[a]
2.00	24.15		23.89[a]
2.25	26.46		25.99[a]
2.50	29.95	27.32	29.02[a]
2.75	35.44	31.92	33.24[a]
3.00	44.60	37.48[a]	38.62
3.25		43.01[a]	44.12
3.50		46.06[a]	47.57
3.75		45.55[a]	47.35
4.00		42.67[a]	44.43
4.25		39.23[a]	40.58
4.50		36.23[a]	37.13
4.75		34.00[a]	34.46
5.00		32.57[a]	32.68
5.25		31.93[a]	31.70
5.50		32.13[a]	31.53
5.75		33.23[a]	32.26
6.00		35.23[a]	34.04
6.25		37.85[a]	36.94
6.50		40.33[a]	40.56
6.75		30.12	43.53[a]
7.00		30.09	44.20[a]
7.25			42.30[a]
7.50			39.10[a]
7.75			35.96[a]
8.00			33.50[a]
8.25			31.88[a]
8.50			31.16[a]

[a] Suspected best available result.

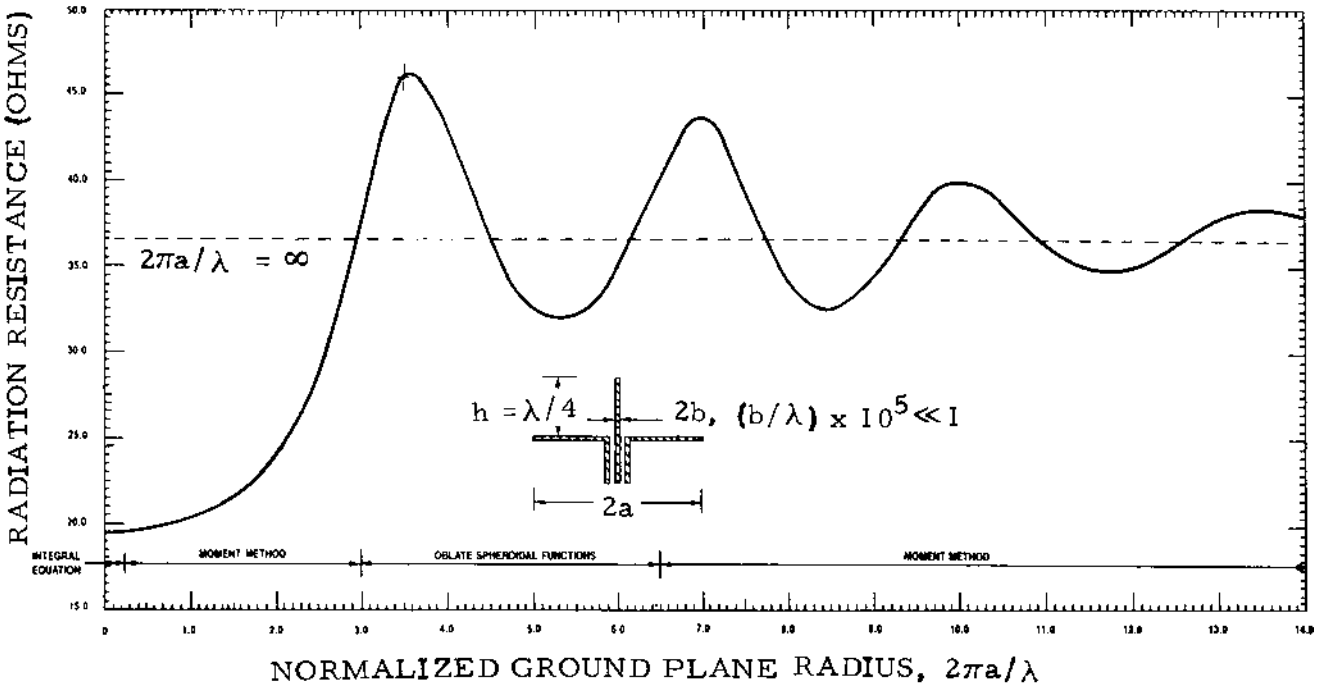

FIGURE 9 Radiation resistance of a thin quarter-wave element at the center of a circular ground plane on radius $0 \leq ka \leq 14$ rad.

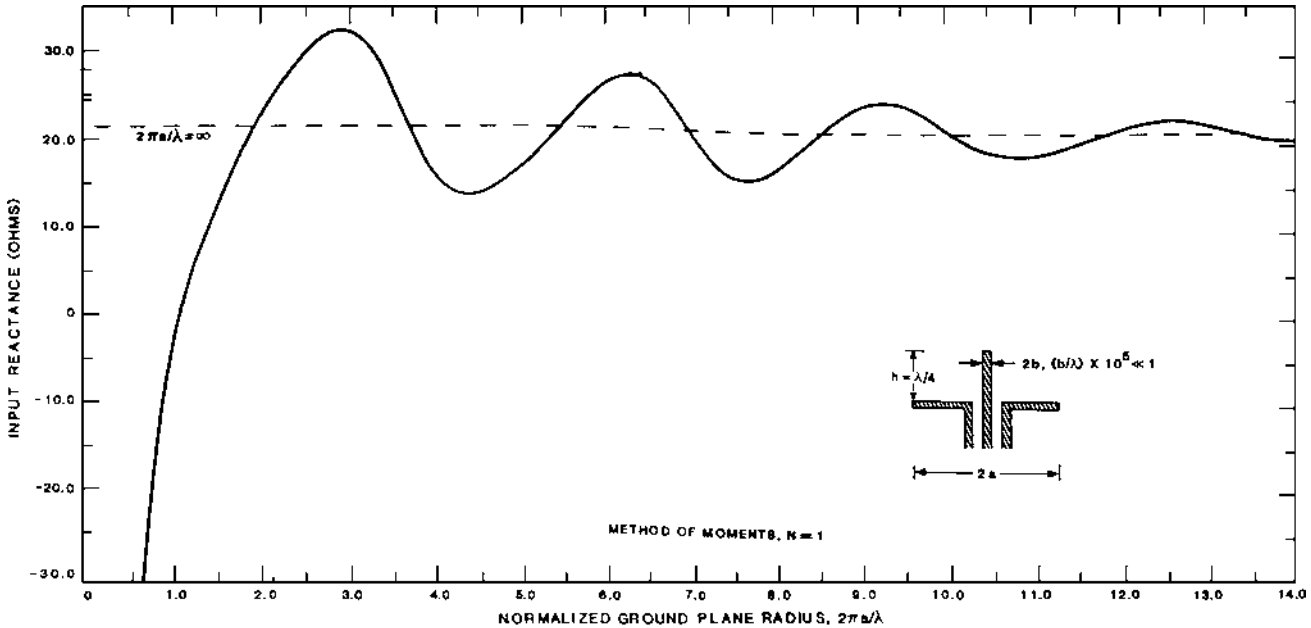

FIGURE 10 Input reactance of a thin quarter-wave element at the center of a circular ground plane of radius $0 \leq ka \leq 14$ rad.

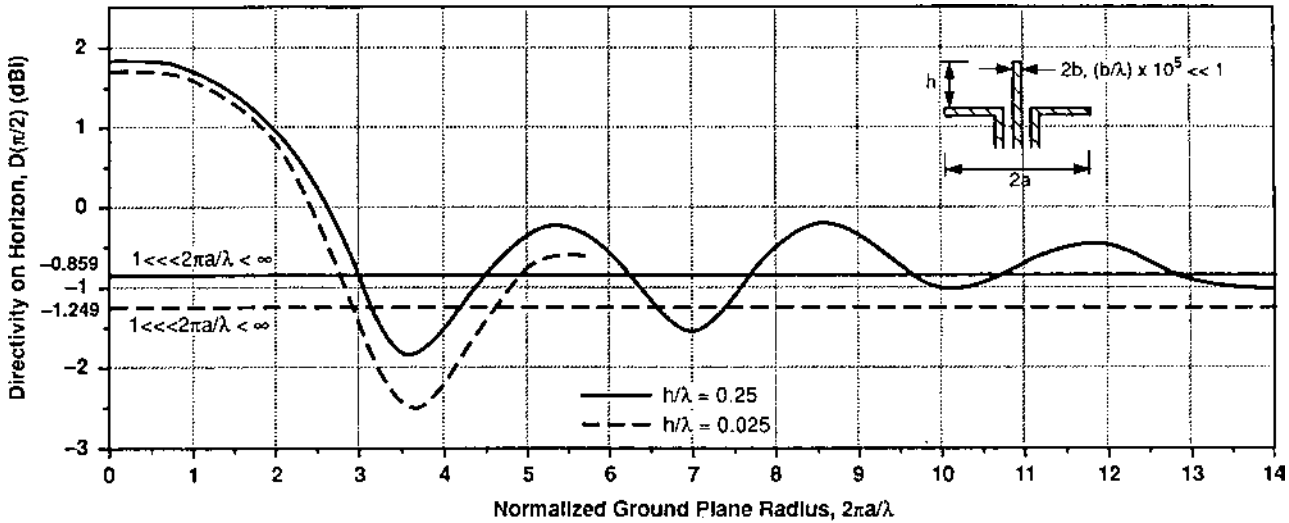

FIGURE 11 Directivity on the horizon of thin quarter-wave and electrically short elements at the center of a circular ground plane of radius $0 \leq ka \leq 14$ rad.

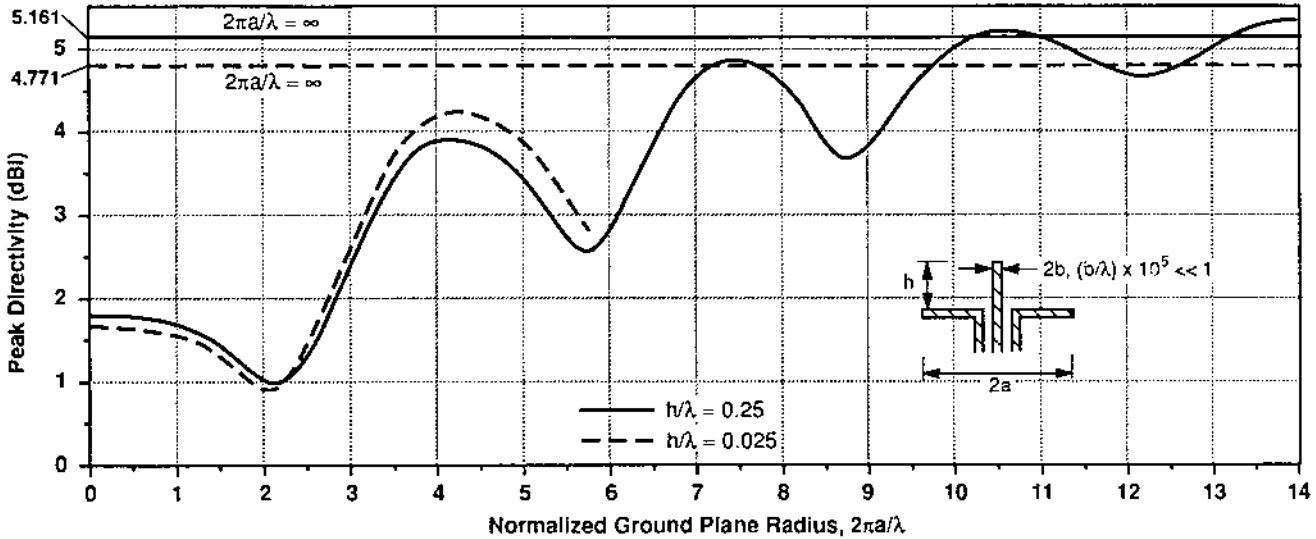

FIGURE 12 Peak directivity of thin quarter-wave and electrically short elements at the center of a circular ground plane of radius $0 \leq ka \leq 14$ rad.

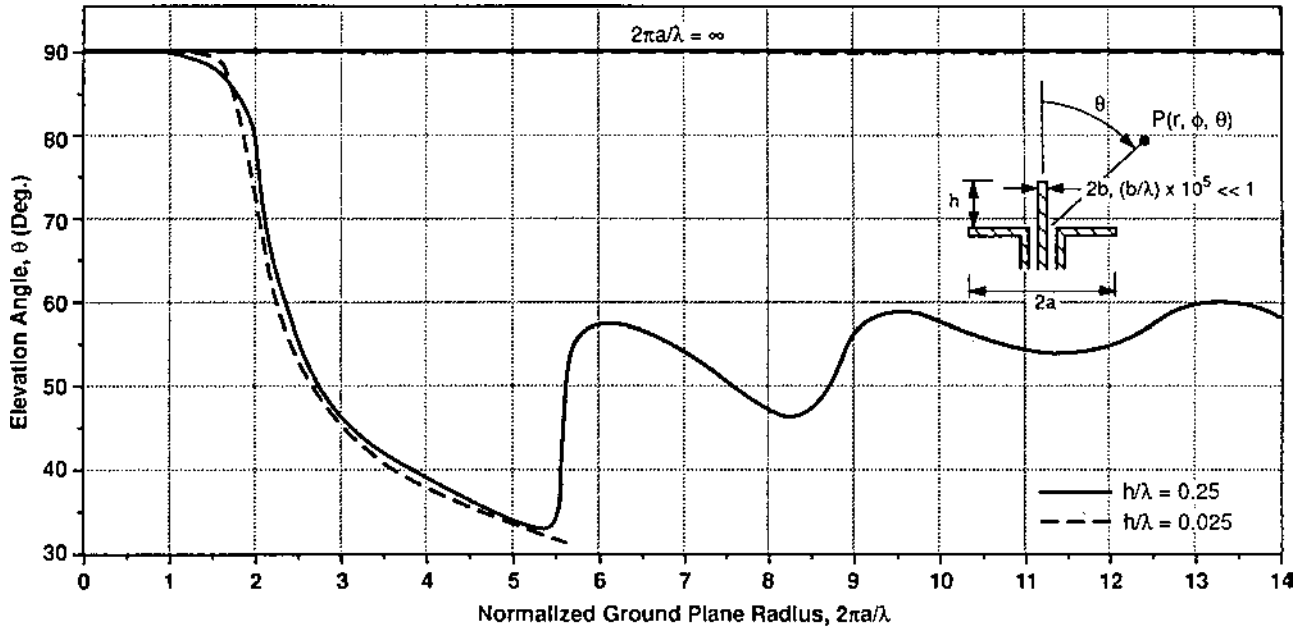

FIGURE 13 Elevation angle of peak directivity for thin quarter-wave and electrically short elements at the center of a circular ground plane of radius $0 \leq ka \leq 14$ rad.

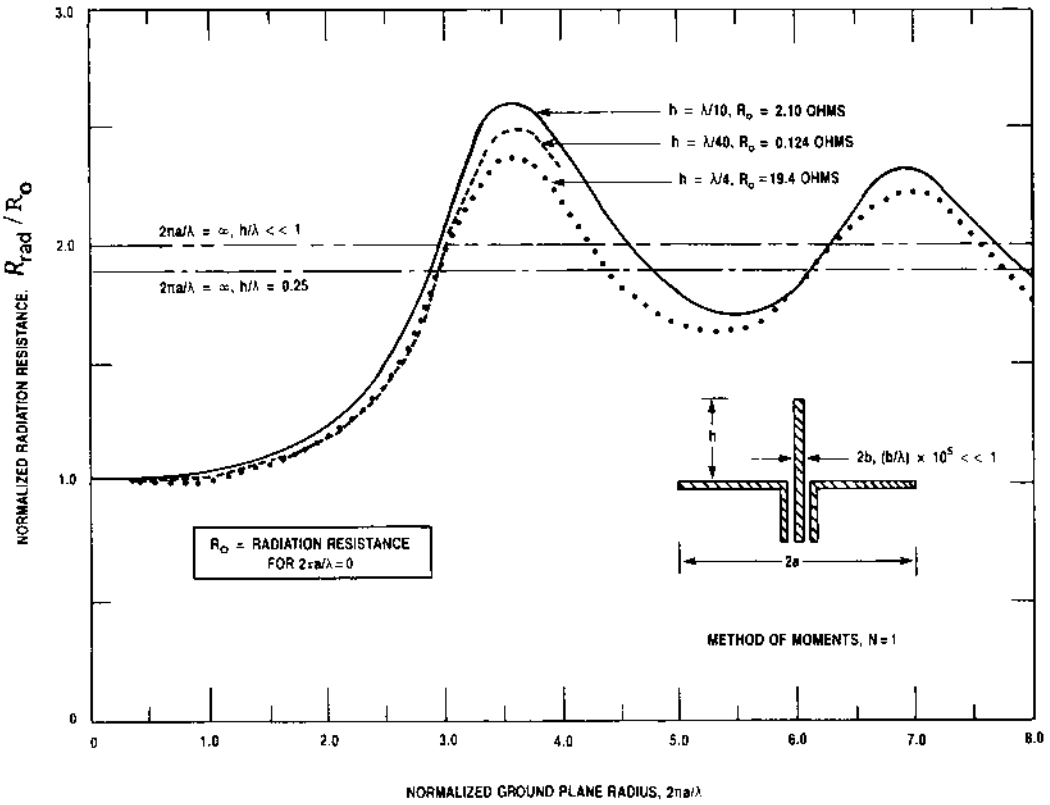

FIGURE 14 Radiation resistance for thin elements of various lengths at the center of a circular ground plane in free space.

The directivity on the horizon, peak directivity, and elevation angle of the peak directivity for a quarter-wave element are plotted in Figs. 11–13 with ground-plane radii of $0 \leq ka \leq 14$ rad. The directivity on the horizon varies between 1.9 and -1.9 dBi, and asymptotically approaches -0.86 dBi for increasingly large but finite ground-plane radii. The peak directivity varies between 1.0 and 5.3 dBi, and asymptotically approaches 5.2 dBi for increasingly large ground-plane radii. The elevation angle of the peak directivity varies between 33 and 90°, and asymptotically approaches 90° for increasingly large ground-plane radii.

The radiation resistances for thin elements of length $h/\lambda = 0.25$, 0.1, and 0.025 with ground-plane radii of $0 \leq ka \leq 8$ rad are compared in Fig. 14. The radiation resistance of each element is normalized to that for a ground plane of zero extent. The normalized radiation resistance, as a function of the ground-plane radius, is approximately independent of the element length. The directivity properties for electrically short elements are not appreciably different from those for quarter-wave elements as shown in Figs. 11–13.

4

Models in Which the Current Distributions on the Monopole Element and Ground Plane Are Both Initially Unknown

4.1 BOUNDARY CONDITIONS

In Chapter 3, the total field at an arbitrary field point could be simply expressed as the vector sum of an incident field and an induced field [see Eq. (3.1.12)] because the incident field was specified from the initially known current distribution on the monopole element. In this chapter, such a procedure is not possible because the current distributions on the element and ground plane are both initially unknown. Instead, the total field is determined here by representing the unknown current distribution on either the element, ground plane, or both by a finite series of overlapping modes with unknown current amplitudes. The current amplitudes are determined by matrix algebra, subject to boundary conditions that comprise current constraints and the excitation voltage across the coaxial line feed.

The antenna geometry is shown in Fig. 1 of Sec. 2.1. The current waveform is given by Eq. (2.1.2). The models which follow in this chapter are based on the current characterization and circuit idealization of Fig. 2(c) from Sec. 2.4.

The coaxial line feed and the excitation voltage, which is not explicitly shown in Fig. 1, are characterized in Fig. 2(c) by a surface magnetic current density (magnetic frill) M_ϕ, which sits on top of a thick ground plane of radius b_1, where b_1 is the radius of the outer conductor of the coaxial line feed. The magnetic frill M_ϕ is defined over the ground plane by Eq. (2.4.8).

Constraints on the various circuit currents of Fig. 2(c) are given by Eqs. (2.4.3)–(2.4.7). These constraints, together with the magnetic frill, constitute the boundary conditions on the current amplitudes.

4.2 METHOD OF MOMENTS: $0 < ka \leq 14$

When the element and ground-plane current distribution are initially unknown, the current distributions may be determined by a sinusoidal-Galerkin method of moments as employed by Richmond [2]. The antenna geometry is shown in Fig. 1 of Chapter 2.

In the method of moments, the element is divided into N equal segments (see Fig. 15) of length d' given by

$$d' = h/N \tag{4.2.1}$$

where N is a positive integer and h is the element length. The ground plane is

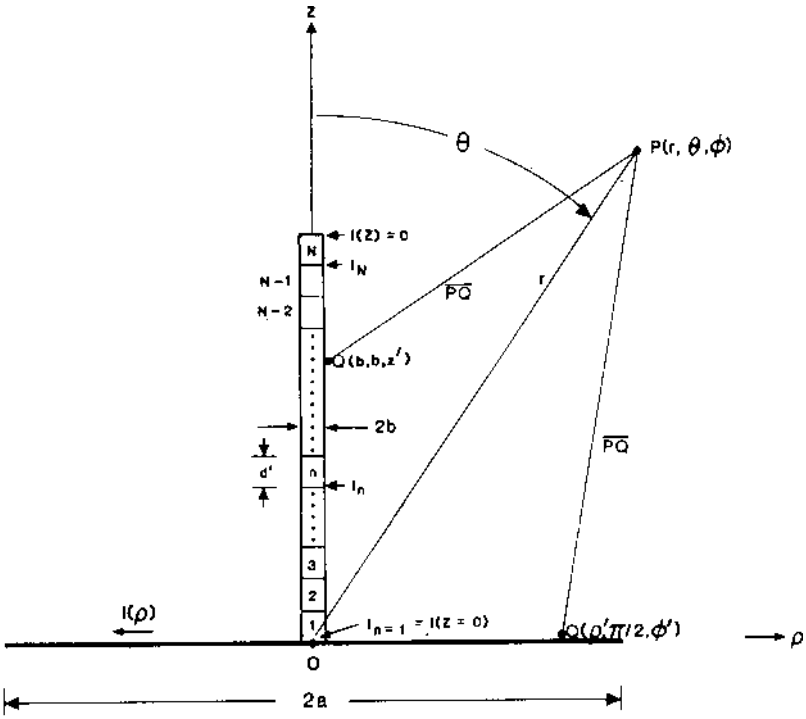

FIGURE 15 Element with N equal segments of length d'.

divided into M concentric annular zones (see Fig. 16) of width d, given by

$$d = (a - b)/M > b_1 - b \tag{4.2.2}$$

where M is a positive integer, a, the ground-plane radius, b, the element radius, and b_1, the radius of the outer conductor of the coaxial line feed. The ground plane extends from the coaxial line's inner conductor because of the equivalent circuit representation of the coaxial line excitation in Fig. 2(b). The element current distribution $I(z)$ and ground-plane current distribution $I(\rho)$ are the sum of the current distributions on each element segment and ground-plane annular zone, respectively, which are given by

$$I(z) = \sum_{n=1}^{N} I_n(z) \tag{4.2.3}$$

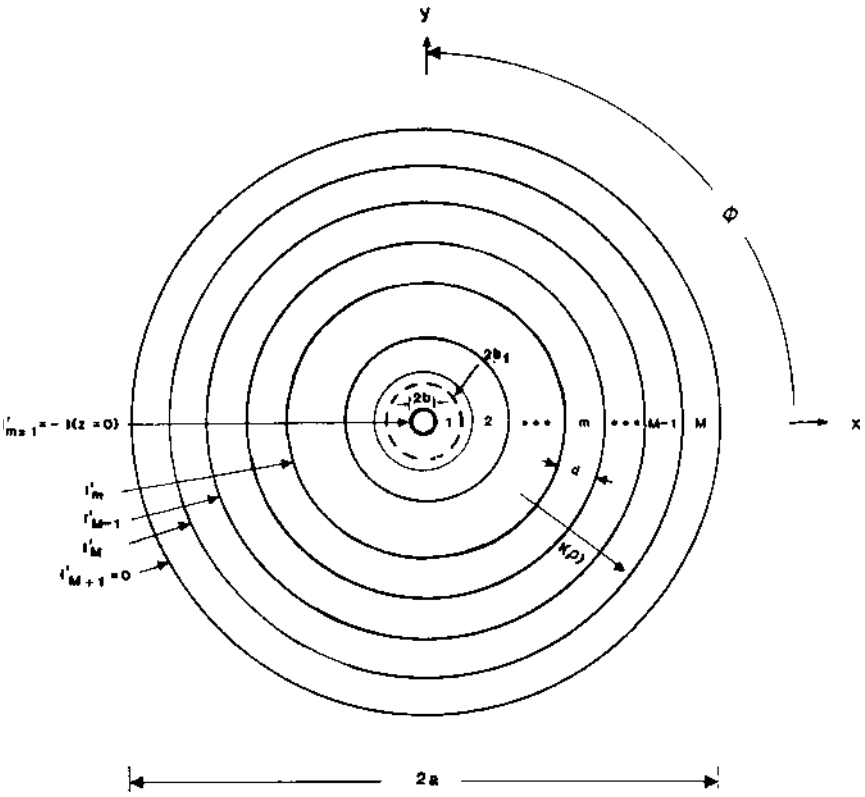

FIGURE 16 Ground plane with M annular zones of width d.

$$I(\rho) = \sum_{m=1}^{M} I'_m(\rho) \tag{4.2.4}$$

where $I_n(z)$ and $I'_m(\rho)$ are the current distributions on the nth segment and mth annular zone, respectively.

In the sinusoidal-Galerkin method, the current distribution $I_n(z)$ on the nth element segment is approximated by

$$I_n(z) \approx \frac{I_n \sin[k(nd' - z)] + I_{n+1} \sin\{k[z - (n-1)]d'\}}{\sin(kd')}; \tag{4.2.5}$$

$$(n-1)d' \le z \le nd'; \quad n = 1, 2, 3, \ldots, N$$

where $I_{n=1} = I(z = 0)$ and $I_{N+1} = 0$.

The current distribution $I'_m(\rho)$ on the mth annular zone is approximated by

$$I'_m(\rho) \approx \frac{I'_m \sin\{k[md + b - \rho]\} + I'_{m-1} \sin\{k[\rho - (m-1)]d - b\}}{\sin(kd)}; \tag{4.2.6}$$

$$b + (m-1)d \le \rho \le b + md; \quad m = 1, 2, 3, \ldots, M$$

where $I'_{m=1} = -I_{n=1} = -I(z = 0)$ and $I'_{M+1} = 0$.

The current distribution on each segment and annular zone is therefore the sum of two overlapping dipole modes, except for the segment and annular zone adjacent to the base of the element. The *base* mode may be thought of as a dipole mode comprising an element monopole mode ($n = 1$) and a ground-plane monopole mode ($m = 1$) with terminals along the circumference of the element's base. The element and ground-plane dipole modes are functionally tied to each other by means of the base-mode amplitude constraint $I_{n=1} = -I'_{m=1} = I(z = 0)$.

The element and ground-plane current distributions are represented in Eqs. (4.2.3)–(4.2.6) as a series of $N + M$ overlapping sinusoidal dipole modes with $N + M$ unknown complex current amplitudes. The $N + M$ amplitudes are determined in Richmond's method of moments by the Crout substitution method of solution of a $(N + M) \times (N + M)$ matrix, subject to the boundary conditions discussed in Sec. 4.1. The constraint $I_{n=1} = -I'_{m=1}$ reduces the matrix size to $(N + M - 1) \times (N + M - 1)$.

The numbers of subdivisions, N and M, are limited by the cost of computation time and the precision of the computer. The accuracy of the solution can be appreciably decreased if either N or M is too small or too large. The method of moments converges to a solution when an increase or decrease of unity in the value of N or M does not appreciably alter the solution for input impedance.

A method-of-moments computer program for a monopole element at the center of a circular ground plane in free space was obtained from

Professor J. H. Richmond of Ohio State University. The program computes the input impedance and the $N + M$ complex current amplitudes on the element and ground plane for a voltage input $V(0) = 1$ V. The program, written in FORTRAN IV language and in single precision, was edited and converted by the MITRE Corp. to double precision for use on a DEC VAX 11/780 computer. A description of the MITRE version, designated *RICHMD1* (also called RICHMOND1), is given in App. B.02.

The authors' experience with this program suggests the following constraints on its use. At least double precision is required to give convergent results. Meaningful results were obtained for element radii of $b/\lambda \geq 10^{-10}$ and ground-plane radii of $ka > 0.25$. As a rule of thumb, $N = 2\text{–}3kh$ and $M = 2\text{–}3ka$ give reasonably accurate and convergent results. The amount of central processing unit (CPU) time on the VAX 11/780 is approximately 2 min for $N + M = 20$, 6 min for $N + M = 30$, 34 min for $N + M = 60$, and 50 min for $N + M = 75$.

The versatility of a sinusoidal-Galerkin method of moments is illustrated by the case of $N = 1$. A sinusoidal current distribution is imposed on the element by setting $N = 1$ [see Eq. (4.2.5)].

The element and ground-plane current distributions obtained from program RICHMD1 can be utilized to obtain the far-field radiation pattern in the following manner.

The magnetic field intensity $\mathbf{H}(P)$ at a far-field point $P(r, \theta, \phi)$ and for an $e^{j\omega t}$ waveform is related to the magnetic vector potential $\mathbf{A}(P)$ by [27]:

$$\mathbf{H}(P) = -j(1/\eta)\omega\, \hat{u}_r \times \mathbf{A}(P) \tag{4.2.7}$$

where $\hat{u}_r$ is a unit vector in the radial direction and η is the free-space wave impedance. The magnetic vector potential $\mathbf{A}(P)$ at the far-field point P resulting from a current source point $Q(x', y', z') = Q(b, b, z')$ on the element or a source point $Q(\rho', \pi/2, \phi')$ on the ground plane (see Fig. 4) is given by [27]:

$$\begin{aligned} \mathbf{A}(P) &= (\mu_0/4\pi) \int_v J(Q) \exp(-jk\overline{PQ})(1/\overline{PQ})\, \mathrm{d}v \\ &\approx [\mu_0 \exp(-jkr)/4\pi r] \int_v J(Q) \exp(jk\hat{u}_r \cdot \mathbf{OQ})\, \mathrm{d}v \end{aligned} \tag{4.2.8}$$

where

$$\begin{aligned} \overline{\mathrm{PQ}} &= [r^2 - 2r\hat{u}_r \cdot \mathbf{OQ} + x'^2 + y'^2 + z'^2]^{1/2} \approx \mathbf{r} - \hat{u}_r \cdot \mathbf{OQ}, \\ &\quad r \gg (x'^2 + y'^2 + z'^2)^{1/2} \\ \hat{u}_r \cdot \mathbf{OQ} &= x' \sin\theta \cos\phi + y' \sin\theta \sin\phi + z' \cos\theta \\ \mu_0 1 &= \text{permeability of free space} = 4\pi \times 10^{-7}\ (\text{H/m}) \\ J(Q) &= \text{source surface current density at an arbitrary source point } Q \text{ on} \\ &\quad \text{either the element or ground plane (A/m)} \end{aligned}$$

$r = \overline{\text{OP}} =$ radial distance between the origin $O(0, 0, 0)$and the far − field point $P(r, \theta, \phi)$

$\mathrm{d}v =$ differential surface area containing the current source points $Q(\text{m}^2)$

By substituting Eq. (4.2.3) into (4.2.8), the magnetic far-field intensity $H_\phi^{(e)}$, resulting from the monopole current distribution, is given by

$$H_\phi^{(e)} = \frac{j \exp(-jkr) \sin\theta}{4\pi r} \int_0^h \sum_{n=1}^{N} I_n(z') \exp(jkz' \cos\theta)\, \mathrm{d}z'$$

$$\begin{aligned} H_\phi^{(e)} = \frac{j \exp(-jkr)}{4\pi r \sin\theta \sin(kd')} \Bigg\{ \Bigg[\sum_{n=1}^{N} I_n \exp(jnkd' \cos\theta) \Bigg] \\ \times [1 - \cos(kd')\cos(kd'\cos\theta) - \cos\theta \sin(kd')\sin(kd'\cos\theta)\} \\ + j\cos(kd')\sin(kd'\cos\theta) - j\cos\theta\sin(kd')\cos(kd'\cos\theta)] \\ - \Bigg\{ \sum_{n=2}^{N} I_n \exp[j(n-2)kd'\cos\theta] \Bigg\} [\cos(kd')\cos(kd'\cos\theta) \\ + \cos\theta\sin(kd')\sin(kd'\cos\theta) - 1 + j\cos(kd')\sin(kd'\cos\theta) \\ - j\cos\theta\sin(kd')\cos(kd'\cos\theta)] \Bigg\} \end{aligned} \tag{4.2.9}$$

By substituting Eq. (4.2.4) into (4.2.8), the magnetic far-field intensity $H_\phi^{(g)}$, resulting from the ground-plane current distribution, is given by

$$\begin{aligned} H_\phi^{(g)} = \frac{-j \exp(-jkr)}{4\pi r} \int_0^a \int_0^{2\pi} \frac{1}{2\pi} \sum_{m=1}^{M} I'_m(\rho') \\ \times \exp[jk\rho' \cos(\phi - \phi)] \cos\theta \cos(\phi' - \phi)\, \mathrm{d}\phi' \mathrm{d}\rho' \end{aligned} \tag{4.2.10}$$

Equation (4.2.10) is not readily evaluated when Eq. (4.2.6) is substituted into it. An approximate simplified solution can be found when each annular zone of the ground plane is subdivided into X smaller annular zones of width $\Delta\rho = d/X$ so that the current distribution in each subdivided zone is almost constant and approximately equal to its average current. The total number J of subdivided

annular zones on the entire ground plane is given by

$$J = XM \tag{4.2.11}$$

The average current I_u in the uth subdivided zone is given by

$$I_u = \frac{1}{\Delta\rho}\int_{(u-1)\Delta\rho+b}^{u\Delta\rho+b} \frac{I'_m \sin[k(md+b-\rho)] + I'_{m+1}\sin\{k[\rho-(m-1)d-b]\}}{\sin(kd)}\,\mathrm{d}\rho, \tag{4.2.12}$$

$$[b+(m-1)d] < \rho < (b+md)$$

The current distribution $I(\rho)$ on the ground plane is therefore given approximately by

$$I(\rho) \approx \sum_{u=1}^{J} I_u \tag{4.2.13}$$

By substituting $I_u(\rho')$ for $I_m(\rho')$ in Eq. (4.2.10), we have

$$\begin{aligned} H_\phi^{(g)} \approx{}& \frac{-j\exp(-jkr)}{4\pi r}\int_0^a\int_0^{2\pi} \\ &\times\frac{1}{2\pi}\left\{\sum_{u=1}^{J} I_u(\rho')\exp[jk\rho'\cos(\phi'-\phi)]\right\} \\ &\times\cos\theta\cos(\phi'-\phi)\,\mathrm{d}\phi'\mathrm{d}\rho' = \frac{\exp(-jkr)\cos\theta}{4\pi r\sin\theta}\sum_{u=1}^{J} I_u(\rho') \\ &\times\{J_0[k\sin\theta((u-1)\Delta\rho+b)] - J_0[k\sin\theta(u\Delta\rho+b)]\} \end{aligned} \tag{4.2.14}$$

where J_0 is the zero-order Bessel function of the first kind.

The total magnetic far-field intensity $H_\phi^{(\text{total})}$ is given by

$$H_\phi^{(\text{total})} = H_\phi^{(e)} + H_\phi^{(g)} \tag{4.2.15}$$

where $H_\phi^{(e)}$ and $H_\phi^{(g)}$ are given by Eqs. (4.2.9) and (4.2.14), respectively.

The time-averaged radiated power density $s(\theta)$, directive gain $d(\theta)$, and radiation resistance R are found from Eqs. (2.2.2) and (2.2.5), where $H_\phi^{(\text{total})}$ is given by Eq. (4.2.15) and $I(z=0) = I_{n=1}$. Numerical evaluation of $s(\theta)$, $d(\theta)$, and R is implemented by means of MITRE's computer program *RICHMD2*, written in FORTRAN language for use on a DEC VAX 11/780 computer. A description of program RICHMD2 (also called RICHMOND2) is given in App. B.02.

A discussion of the results obtained by the method of moments for a sinusoidal current distribution on the element ($N = 1$) is given in Sec. 3.4.

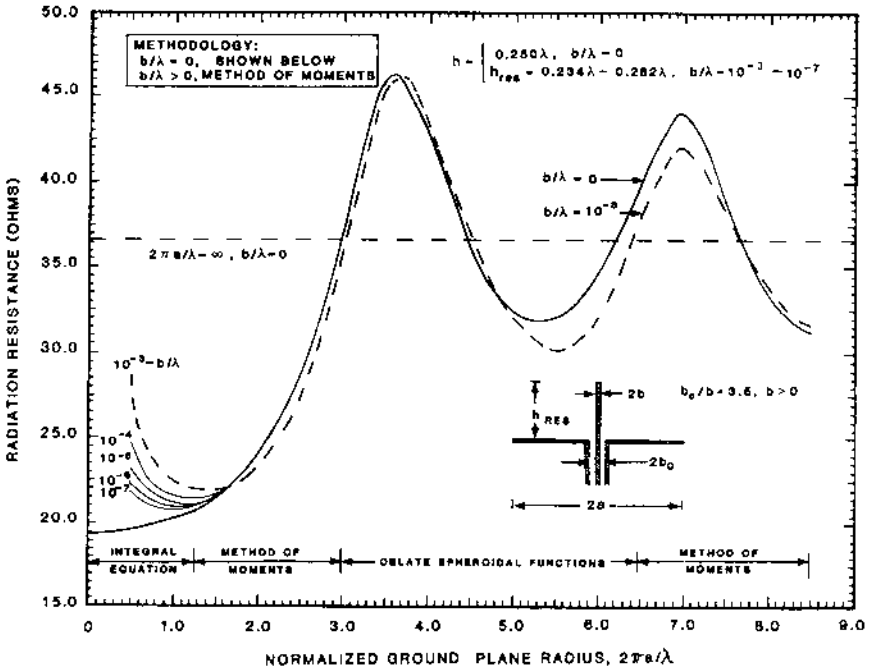

FIGURE 17 Radiation resistances of resonant elements of various diameters and an infinitely thin quarter-wave element at the center of a circular ground plane of radius $0 \leq ka \leq 8.5$ rad.

Computer printouts of the directive gain and far-field radiation pattern of the experimental monopole antennas discussed in Chapter 5 were obtained by the method of moments and are given in App. A.2.

The input impedance determined by the method of moments ($N = 4$, $M = 3ka$) for a quarter-wave element of radius $b = 10^{-6}\lambda$ and ground-plane radii of $6 \leq ka \leq 30$ rad is compared in Table 7 of Sec. 4.5 with that obtained by the method of moments combined with the geometric theory of diffraction. For $ka > 14$, Richmond's method of moments is inaccurate. In addition to the large amount of CPU time required (greater than 30 min for $ka > 14$), convergent results are difficult to obtain for $ka > 14$. It is most likely that the usefulness of Richmond's method of moments could be extended to significantly larger ground-plane radii if a more efficient method of matrix inversion were utilized, rather than the Crout method employed by Richmond. When the element's current distribution is not assumed, Richmond's method of moments gives the best currently available results for ground-plane radii of $ka \leq 14$ rad.

The lower limit of ka has not been firmly established for accurate results with Richmond's method of moments. For an element segment number $N > 1$, we have obtained useful results for ka as small as 0.25 rad, but not for ground planes of zero extent. For $N = 1$, accurate results were obtained, subject to the constraint of a sinusoidal current distribution of the elements, for ground planes of zero extent.

The radiation resistance for resonant (zero input reactance) elements of various diameters is compared in Fig. 17 of Sec. 4.5 with the radiation resistance of an infinitely thin quarter-wave element for ground-plane radii of $0 \leq ka \leq 8.5$ rad. For $ka \rightarrow 0$, the radiation resistance of the resonant elements is appreciably different from that of the infinitely thin quarter-wave element because an infinitely thin element on a ground plane of zero extent is resonant for an element length that is equal to 0.5λ, not 0.25λ [see Eq. (3.2.38)].

The lengths and radiation resistances for resonant elements of various diameters, for ground planes of radii $0.25 \leq ka \leq 7$ rad are plotted in Figs. 18 and 19 of Sec. 4.5.

4.3 METHOD OF MOMENTS COMBINED WITH GEOMETRIC THEORY OF DIFFRACTION: $8.5 \leq ka < \infty$

The method of moments, when used to determine the current distributions on both the element and the ground plane, can require considerable computation time for large ground-plane radii. For example, Richmond's method of moments requires approximately 1.5 hr of CPU time on the VAX 11/780 for a ground-plane radius $ka = 20$ with $N = 4$ element segments and $M = 60$ ground-plane annular zones (see Sec. 4.2). Although it may be possible to reduce the computation time by using a more efficient program than the one employed by Richmond, it is of interest to find an alternative method for large ground planes.

Awadalla and Maclean [9,10] have reduced the computation time for large ground planes by combining the method of moments with the geometric theory of diffraction. The element's current distribution is determined by the method of moments and the effect on input impedance due to ground-plane edge diffraction is determined by GTD.

The antenna geometry is shown in Fig. 1 of Sec. 2.1. The method of Awadalla and Maclean is described [9] for determining the input impedance and the radiation pattern [10].

A fictitious magnetic edge current is defined and expressed in terms of a GTD coefficient to account for diffraction by the edge of the ground plane. The GTD method is valid only for sufficiently large ground-plane radii. Unfortunately, this method, as applied by Awadalla and Maclean, does not determine the ground plane's current distribution.

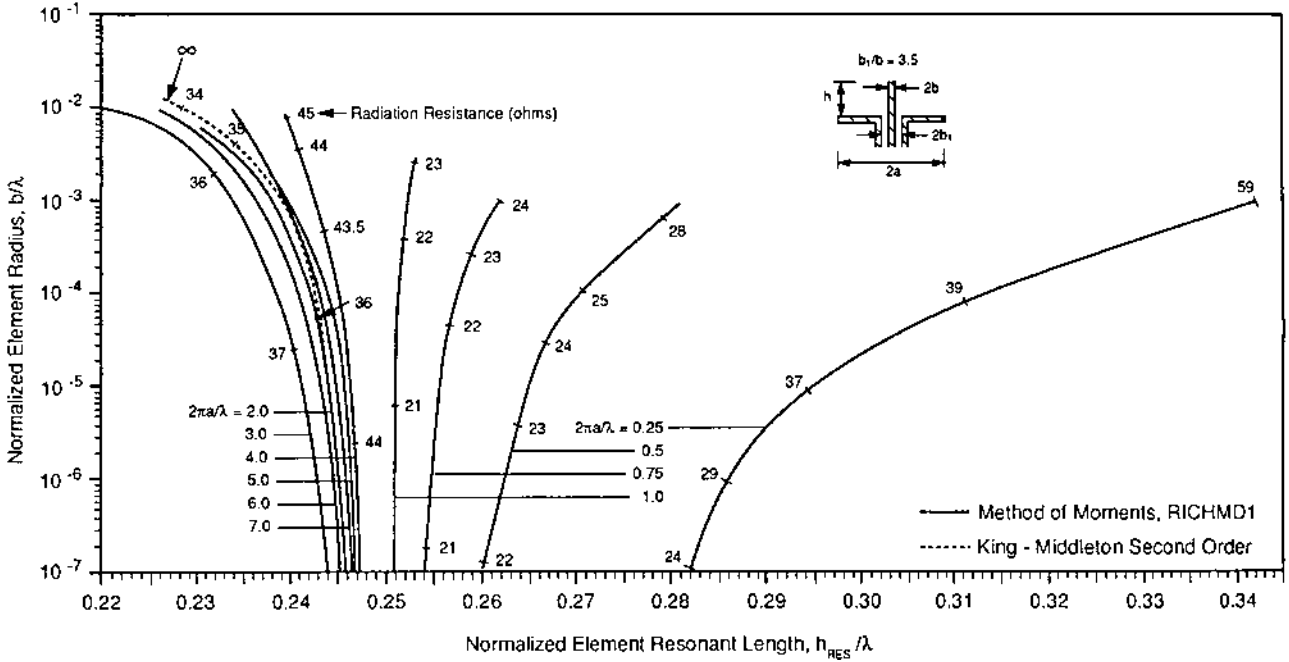

FIGURE 18 Resonant length of elements of various diameters at the center of a circular ground plane of radius $0.25 \leq ka \leq 7$ rad.

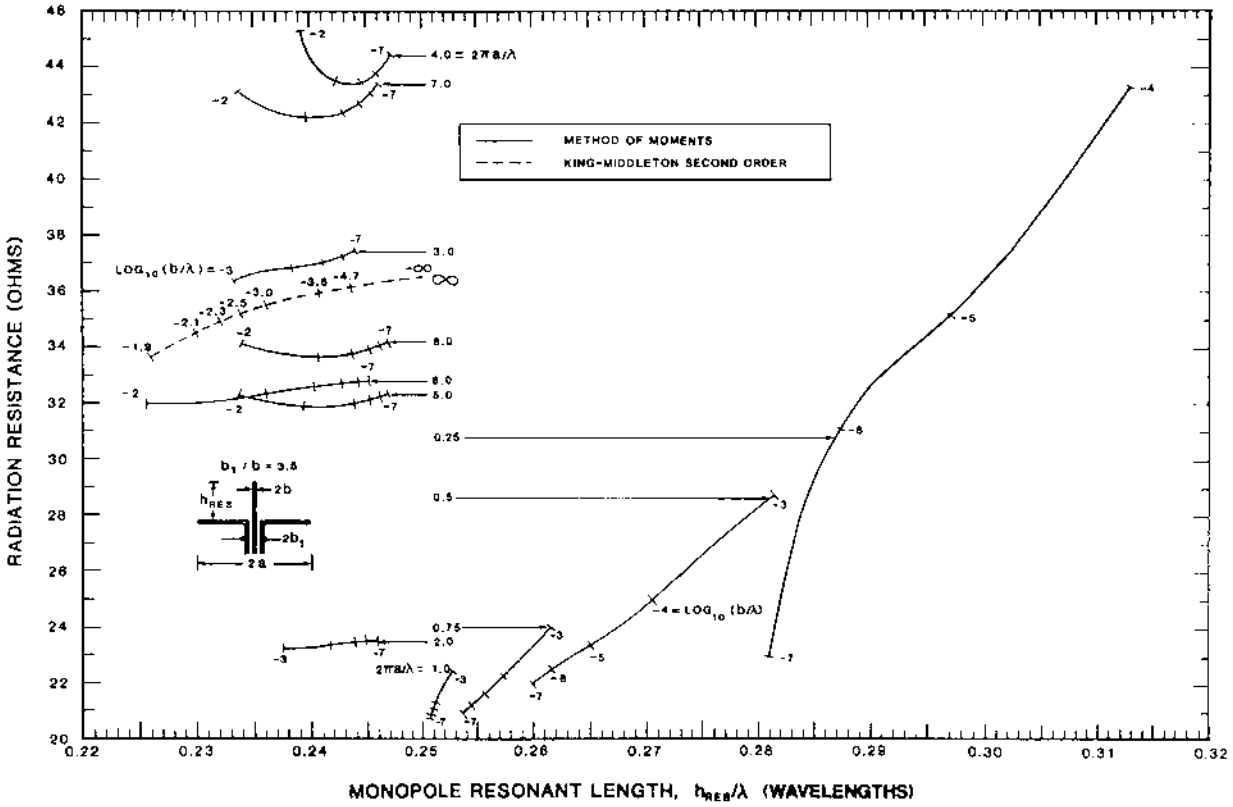

FIGURE 19 Radiation resistances and lengths of resonant elements of various diameters at the center of a circular ground plane of radius $0.25 \leq ka \leq 7$ rad.

The ground plane's current distribution is idealized by Awadalla and Maclean in determining the radiation pattern. The current distribution on the top of the ground plane is assumed to be that for an infinite ground plane, but it is defined only over the finite extent of the ground plane. The net current at the edge of the ground plane is set equal to zero. This constraint satisfies the boundary condition given by Eq. (2.4.4), and requires, at the edge of the ground plane, that the current on the bottom be equal, but in the opposite direction, to that on the top. The current distribution on the bottom of the ground plane is then assumed to decrease linearly from the edge of the ground plane to zero at the base of the element.

The method of moments employed by Awadalla and Maclean is not a sinusoidal-Galerkin method. Consequently, we cannot impose a sinusoidal current distribution on the element by setting the number of element segments to be $N = 1$ as a test case for purposes of comparison with other models.

A program listing was obtained from Professor K. H. Awadalla and edited at the MITRE Corp. The edited program *AWADALLA* is given in App. A.05. Program AWADALLA is written in FORTRAN language for use on a DEC VAX 11/780 computer. The CPU time for $N = 30$ element segments is less than 10 sec.

Program AWADALLA was utilized to obtain the input impedance, directivity, and far-field elevation pattern of a quarter-wave element of radius $b = 10^{-6}\lambda$ on ground plane of radii $8 \leq ka \leq 50$ rad. The results for input impedance are given in Table 6. These results are compared in Table 7 of Sec. 4.5 with those obtained by the method of moments ($N = 4$). As concerns the input impedance, the method of moments combined with GTD gives useful results for $ka \gtrsim 6$, accurate results for $ka > 8$, and the suspected best available results for $14 < ka < \infty$.

A sample computer printout of directive gain and the far-field elevation pattern obtained by program AWADALLA for $ka = 20$ is given in App. A.05. Unfortunately, the idealizations made by Awadalla and Maclean in characterizing the ground-plane current distribution yield unrealistic peak directivities and elevation patterns. For example, a peak directivity of 7.5 dBi was obtained for $ka = 49$. This result for a thin quarter-wave element seems unlikely because such an element with a sinusoidal current distribution that is mounted on a ground plane of infinite extent has a peak directivity of only 5.2 dBi.

The method of moments combined with GTD by using the definition of a fictitious magnetic edge current has also been reported by Thiele and Newhouse [11] for computing input impedance and by Stutzman and Thiele [28] for computing the far-field radiation pattern. In the method of Stutzman and Thiele [28], the far-field pattern is determined without idealization of the ground-plane current distribution.

TABLE 6 Input Impedance of a Quarter-Wave Element of Radius $b = 10^{-6}\lambda$ at the Center of a Circular Ground Plane of Radius $8 \leq ka \leq 50$ rad (Method of Moments Combined with Geometric Theory of Diffraction)

ka	Input resistance (Ω)	Input reactance (Ω)
8	35.96	18.28
9	36.55	24.45
10	41.45	21.82
11	37.54	18.67
12	36.30	23.08
13	40.49	22.51
14	38.44	19.17
15	36.36	22.18
16	39.72	22.82
17	38.99	19.70
18	36.58	21.51
19	39.09	22.89
20	36.87	21.05
22	38.58	22.84
23	39.45	20.63
24	37.20	20.73
25	38.17	22.67
26	39.48	21.06
27	37.55	20.56
28	37.87	22.46
29	39.41	21.40
30	37.88	20.47
31	37.67	22.19
32	39.27	21.68
33	38.19	20.49
34	37.55	21.93
35	39.08	21.90
36	38.45	20.56
37	37.51	21.65
38	38.87	22.06
39	38.66	20.68
40	37.54	21.42
41	38.64	22.13
42	38.82	20.86
43	37.62	21.21
44	38.43	22.14
45	38.92	21.05
46	37.75	21.04
47	38.23	22.10

TABLE 6 Continued

ka	Input resistance (Ω)	Input reactance (Ω)
48	38.96	21.26
49	37.91	20.93
50	38.06	21.99

4.4 METHOD OF IMAGES: $ka = \infty$

For the idealized case of a monopole element mounted on a ground plane of infinite extent and infinite conductivity, a monopole antenna of length h may be modeled by the method of images as a dipole of total length $2h$, but with one-half of the input impedance and double the peak numeric directivity of the dipole (see Sec. 3.8). The infinite ground plane prevents radiation into the hemisphere below it, but the ground plane generates fields in the upper hemisphere that are identical to those of a dipole.

A detailed treatment of the fields and input impedance of a dipole is given by King [13]. An excellent summary of the current state of dipole theory, including plots of input impedance as a function of dipole length and radius, is given by Elliot [14].

J. Richmond (deceased) of Ohio State University has written a program RICHMD5 that uses the method of images and a sinusoidal-Galerkin method of moments to compute the input impedance and current distribution of a monopole element on a ground plane of infinite extent, subject to the constraint that the element radius is much less than a wavelength. The current distribution of RICHMD5 is then used in program RICHMD6 to obtain the far-zone field. These programs are reproduced in Appendix B.06. Numerical results obtained by MITRE are in reasonable agreement with those from King-Middleton theory [29]. For example, for $h/\lambda = 0.25$ (corresponding to $kh = \pi/2$) and $h/b = 16.56$ (corresponding to the King-Middleton parameter = 7), the RICHMD5 result for the monopole input impedance in $Z_{in} = 46.52 + j15.97\,\Omega$ which differs from the King-Middleton result of $Z_{in} = 47.85 + j18.50\,\Omega$ by 2.8 and 13.7% for input resistance and input reactance, respectively. The method of moments result is the suspected best available result. For the same example, the RICHMD6 result for directivity is almost identical to the well-known results given in Sec. 3.8 for a thin, quarter-wave monopole on a perfect ground plane. Sec. 10.4 provides further validation of programs RICHMD5 and RICHMD6.

TABLE 7 Input Impedance of a Quarter-Wave Element at the Center of a Circular Ground Plane of Radius $6 \leq ka \leq 30$ rad ($h/\lambda = 0.25$, $b/\lambda = 10^{-6}$)

	Input resistance (Ω)			Input reactance (Ω)		
Normalized ground-plane radius, ka	(1) Method of moments	(2) Method of moments with GTD	$\frac{\lvert(1)-(2)\rvert}{(1)} \times 100$	(1) Method of moments	(2) Method of moments with GTD	$\frac{\lvert(1)-(2)\rvert}{(1)} \times 100$
6	35.2988[a]	37.7258	6.88	26.7927[a]	26.6729	0.45
7	45.7499[a]	42.6747	6.72	20.5664[a]	20.2537	1.52
8	35.7335[a]	35.9640	0.65	17.1839[a]	18.2823	6.39
9	36.2886	36.5496[a]	0.72	24.7424	24.4496[a]	1.16
10	42.0987	41.4538[a]	1.53	21.5758	21.8225[a]	1.14
11	38.1401	37.5375[a]	1.58	18.8073	18.6728[a]	0.72
12	36.7590	36.2962[a]	1.26	22.0824	23.0841[a]	4.54
13	39.7689	40.4928[a]	1.82	22.6158	22.5061[a]	0.49
14	39.6986	38.4400[a]	2.60	20.3449	19.1676[a]	5.79
15	38.3512	36.3630[a]	5.18	20.0026	22.1845[a]	10.91
20	38.4250	39.3019[a]	2.28	22.2706	20.1706[a]	9.43
25	39.0594	38.1746[a]	2.26	21.5934	22.6704[a]	4.99
30	38.8703	37.8798[a]	2.55	21.0052	20.4663[a]	2.57

[a]Suspected best available result: (1) Richmond's method of moments ($N = 4$, $M = 3ka$), (2) Awadalla and Maclean, method of moments combined with geometric theory of diffraction ($N = 30$).

4.5 SUMMARY OF RESULTS

In Chapter 4, the current distribution on the element is determined by the method of moments, rather than being assumed, as was the case in Chapter 3. The determination of the element's current distribution is particularly important for element radii of $b > 10^{-4}\lambda$.

The essential difference between the two models utilized in Chapter 4 is the treatment of the ground plane's current distribution. In Richmond's model, the ground plane's current distribution is determined by the method of moments. Useful results are obtained for $0 < ka \leq 14$ rad. In the model of Awadalla and Maclean for large but finite ground planes, the input impedance is accurately computed by the introduction of a fictitious magnetic edge current, which is determined by the GTD. However, in that model, the ground-plane current distribution is not determined, but rather idealized, thus causing unrealistic peak directivities and far-field radiation patterns.

The input impedances, determined by the method of moments and the method of moments combined with GTD, are compared in Table 7 for a quarter-wave element of radius $b = 10^{-6}\lambda$ and ground-plane radii of $6 \leq ka \leq 30$ rad. The suspected best available results for input impedance are obtained by the method of moments for $0 < ka \lesssim 8.5$ and by the method of moments combined with GTD for $8.5 \lesssim ka < \infty$. The method of moments combined with GTD is inaccurate for $ka \leq 8$ (approximately 6% error in input reactance for $ka = 8$ and approximately 7% error in input resistance for $ka = 6$). Richmond's method of moments is inaccurate for $14 \lesssim ka < \infty$ (approximately 11% error in input reactance and approximately 5% error in input resistance, both for $ka = 15$). Richmond's method of moments (RICHMD6) is the suspected best available result for $ka = \infty$.

The radiation resistance for resonant (zero input reactance) elements of various diameters is compared in Fig. 17 with the radiation resistance of an infinitely thin quarter-wave element for ground plane of radii $0 \leq ka \leq 8.5$ rad. The radiation resistance of the resonant elements is not appreciably different from that of the quarter-wave element for $ka > 1$ rad. However, as $ka \rightarrow 0$, the radiation resistances of the resonant elements become increasingly different from that of the infinitely thin element because such an element on a ground plane of zero extent is resonant for an element length that is equal to 0.5λ, not 0.25λ [see Eq. (3.2.38)].

The lengths and radiation resistance of resonant elements with various diameters for ground plane of radii $0.25 \leq ka \leq 7$ rad are plotted in Figs. 18 and 19. For these ground-plane radii, the element's resonant length h_{res}/λ varies from approximately 0.22 to 0.34λ for element radii of $10^{-7} \leq b/\lambda < 10^{-2}\lambda$. The resonant radiation resistance, for these ground-plane and element radii, varies from approximately 21 to 65 Ω.

5

Comparison with Experimental Results

The input impedance and elevation patterns of several monopole antennas were measured, each at a different frequency within the 30–254 MHz band, on the MITRE Corp. VHF antenna range. Each antenna consisted of a tubular element of radius $b = 0.25$ in. mounted at the center of a ground plane of radius $a = 4$ ft, and fed by a 50-Ω RG-214 coaxial cable with a type N panel connector and a 50-Ω tapered adapter to the element. The length h of each element was approximately a quarter-wavelength. The exact length of each element was chosen to be resonant (input reactance equals zero ohms) for a ground plane of infinite extent. On a ground plane of finite extent, the input reactance is expected to approach zero asymptotically as $ka \rightarrow \infty$.

For better wind resistance, the ground plane was constructed of $N = 16$ uniformly-spaced radial-wires, of radius $b_w = 0.25$ in., connected circumferentially by 1/16 in. diameter wires at 2, 3, and 4 ft radial distances, with a 2 ft on-a-side square plate at the center of the ground plane (see Fig. 57 of Sec. 6.6).

The VHF antenna range is located on a roof. The transmitting and receiving antennas are at a height of 27 ft above the roof and separated by approximately 40 ft. A conducting fence, 16 ft high and 48 ft wide, is located on the roof midway between the transmitting and receiving antennas to minimize multipath reflections from the roof. Lossy ferrite toroids (Ferronics, type-B material, 0.540-in. inner diameter × 0.870 in. outer diameter × 0.25 in.) are spaced along the receiving and transmitting cables to minimize currents on the outside of the cables. Outside RF interference is reduced to at least 40 dB below the desired signal as a result of the use of narrowband RF filters.

The monopole test antenna was operated in the receiving mode to obtain elevation patterns on the same platform used for input impedance measurements.

The monopole ground plane was supported by a 10-ft wooden vertical mast, mounted on an antenna pedestal.

The input impedance was measured with a Hewlett-Packard HP-8754A network analyzer with a computerized printout. The measurement test setup is shown in Fig. 20.

The predicted input impedance of each experimental monopole antenna was determined using program (1) RICHMD1 for a disk ground plane; (2) NEC4 for a 16 radial-wire ground plane with three circumferential wires; (3) NEC-GS for a 16 radial-wire ground plane; and (4) NEC-GS for a 256 radial-wire ground plane. NEC4 and NEC-GS are Lawrence Livermore Laboratory Numerical Electromagnetics Code (NEC) programs for antenna wire elements and are described in Section 11.1 with numerical results in Table 29, Sec. 12.2.1.

The measured input impedances differ from RICHMD1 predicted values by 0.8–9.7% for resistance and 2.3–11.9 Ω for reactance, over a range of normalized ground-plane radii 0.77–6.5 rad (see Table 8). We do not make a percentage comparison for input reactance because some of the predicted values are near resonance.

The measured input impedances differ from NEC-GS predicted values, over the same range of normalized ground plane radii, in Case (2) by 1.4–64.9% for resistance and 0.4–40.6 Ω for reactance; in Case (3) by 2.0–38.0% for resistance and 0.7–20.2 Ω for reactance; and in Case (4) by 1.4–20.1% for resistance and 0–11.2 Ω for reactance. The RICHMD1 predicted values for a disk ground plane give the best overall agreement with measured values, apparently because it includes the effect of the square plate at the center of the ground plane.

Measured elevation patterns for most of the test monopole antennas specified in Table 8 are compared in Figs. 21–29 with theoretical patterns predicted by the method of moments (see App. A.2 for the computer printouts). Allowing for some multipath distortion of the VHF test range, the received patterns are in good agreement with the predicted pattern. We should note that the measured pattern for $ka = 0.766$ is not appreciably different from the predicted pattern for the monopole element itself. The effect of the ground plane on the shape of the pattern is not readily apparent until $ka \gtrsim 2.0$.

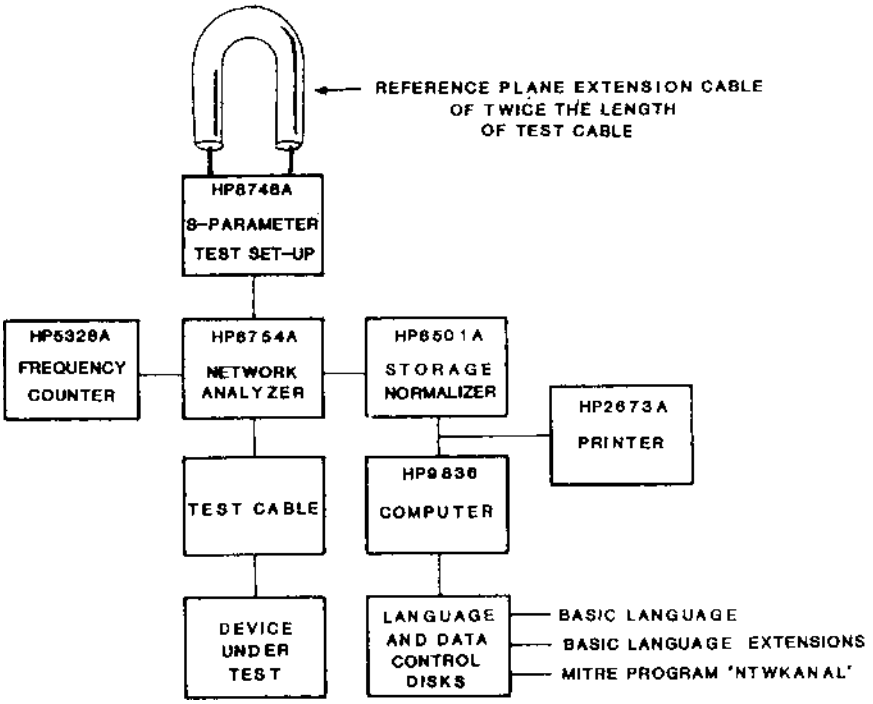

FIGURE 20 Input impedance test setup.

TABLE 8 Input Impedance of 0.50-in.-Diameter Monopole Elements on an 8-ft.-Diameter Ground Plane (Comparison of Method of Moments Predictions with MITRE Measurements)

					Input resistance, R_{in} (Ω)			Input reactance[a], X_{in} (Ω)		
Frequency (MHz) [wavelength, λ (in.)]	Element length, [a] h (in.)	Normalized ground plane radius, ka	Normalized element radius $(b/\lambda) \times 10^4$	Normalized element length, h/λ	Predicted by method of moments (1)	Measured by MITRE[a] (2)	Percentage difference $\frac{(1)-(2)}{(1)} \times 100$	Predicted by method of moments (3)	Measured by MITRE[b] (4)	Difference[a] (3)–(4)(Ω)
30.3 [393.43]	94.26	0.766	6.35	0.2396	17.76	17.62	0.8	−35.97	−30.92	−5.1
36.0 [327.86]	78.55	0.919	7.63	0.2396	18.35	18.57	−1.2	−25.48	−13.59	−11.9
43.0 [274.48]	65.46	1.097	9.11	0.2385	18.77	19.05	−1.5	−19.33	−16.38	−3.0
54.0 [218.57]	52.07	1.379	11.43	0.2382	19.93	20.15	−1.1	−12.11	−5.92	−6.2
62.4 [189.15]	45.00	1.593	12.21	0.2379	20.80	22.82	−9.7	−4.73	−8.48	−4.3
75.0 [157.37]	37.36	1.915	15.89	0.2374	22.95	23.23	−1.2	−0.43	1.60	−2.3
86.0 [137.24]	32.48	2.197	18.22	0.2366	25.35	27.63	−9.0	3.34	7.39	−4.1
89.7 [131.58]	31.13	2.300	19.00	0.2366	26.59	28.16	−5.9	4.99	−1.05	6.0
97.5 [121.05]	28.60	2.500	20.65	0.2363	29.41	31.22	−6.2	7.29	11.05	−3.8
117.0 [100.88]	23.76	3.000	24.78	0.2355	39.27	40.50	−3.1	8.27	15.21	−6.9
136.5 [86.47]	20.34	3.500	28.91	0.2352	45.76	46.23	−1.0	0.84	7.18	−6.3
156.0 [75.66]	17.75	4.000	33.04	0.2346	40.39	38.59	4.7	−8.16	−1.09	−7.1
175.5 [67.25]	15.77	4.500	37.17	0.2344	34.00	30.94	9.0	−7.45	−1.91	−5.5
195.0 [60.53]	14.14	5.000	41.30	0.2335	30.54	28.58	6.4	−4.36	0.51	−4.9
214.5 [55.02]	12.82	5.500	45.44	0.2330	30.33	28.28	6.8	−0.18	4.87	−5.1
234.0 [50.44]	11.74	6.000	49.56	0.2328	33.69	31.44	6.7	3.64	5.56	−1.9
253.6 [46.56]	10.87	6.500	53.69	0.2335	40.25	41.13	2.2	3.91	6.57	−2.7

[a] The element lengths were selected to be resonant when mounted on a ground plane of infinite extent [see R.W.P. King, *Theory of Linear Antennas* (Cambridge, MA: Harvard University Press, 1956) Figure 30.7a]. On ground planes of finite extent, the input reactance is expected to approach zero asymptotically as $ka \rightarrow \infty$.

[b] MITRE measurements were made on Jan. 7 and 10, 1985 utilizing computerized printout of network analyzer.

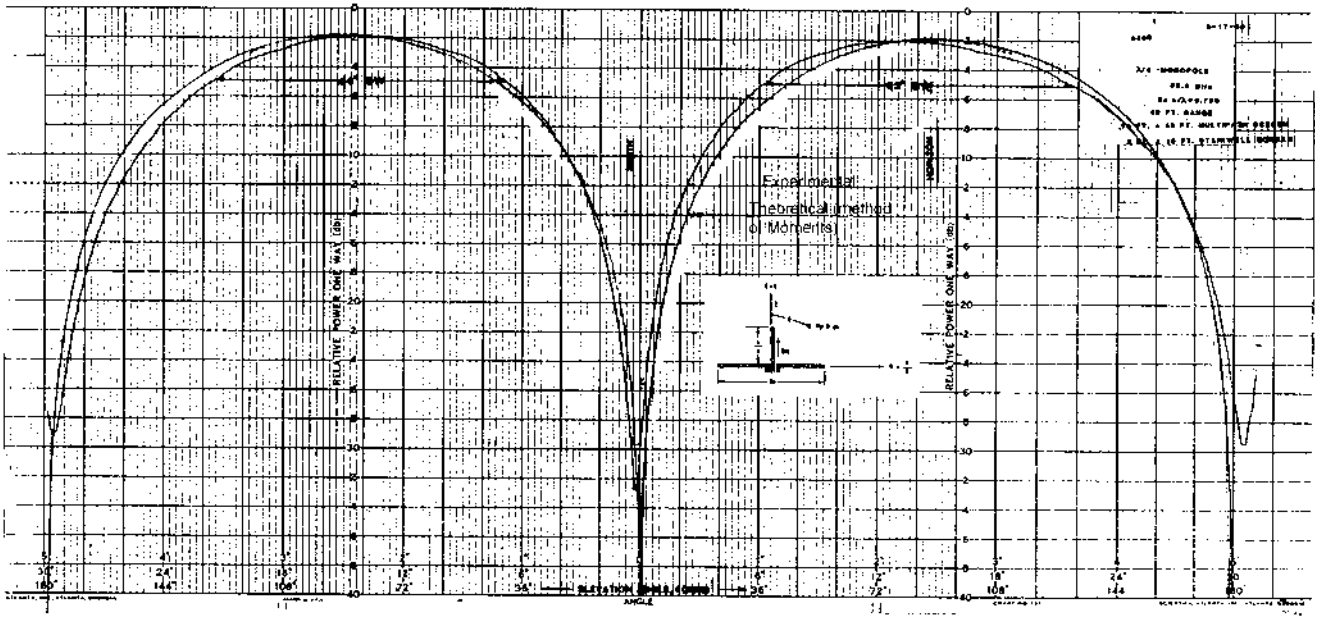

FIGURE 21 Measured and theoretical elevation patterns, 30 MHz ($h/\lambda = 0.2396$, $b/\lambda = 6.35 \times 10^{-4}$, $ka = 0.766$).

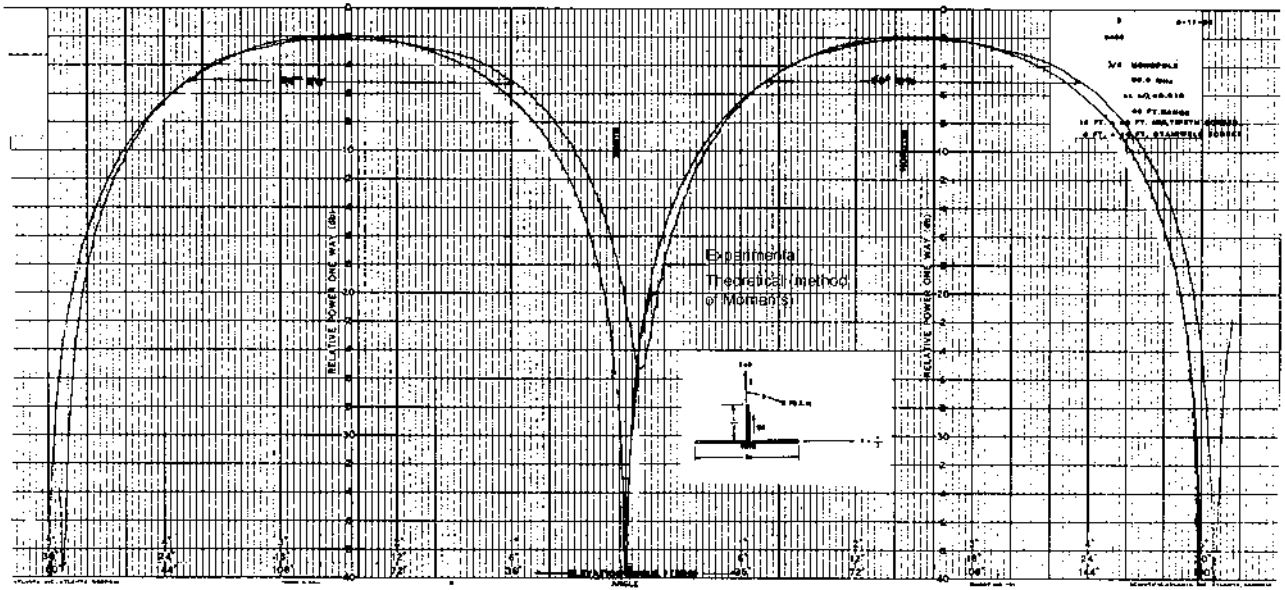

FIGURE 22 Measured and theoretical elevation patterns, 36 MHz ($h/\lambda = 0.2396$, $b/\lambda = 7.63 \times 10^{-4}$, $ka = 0.919$).

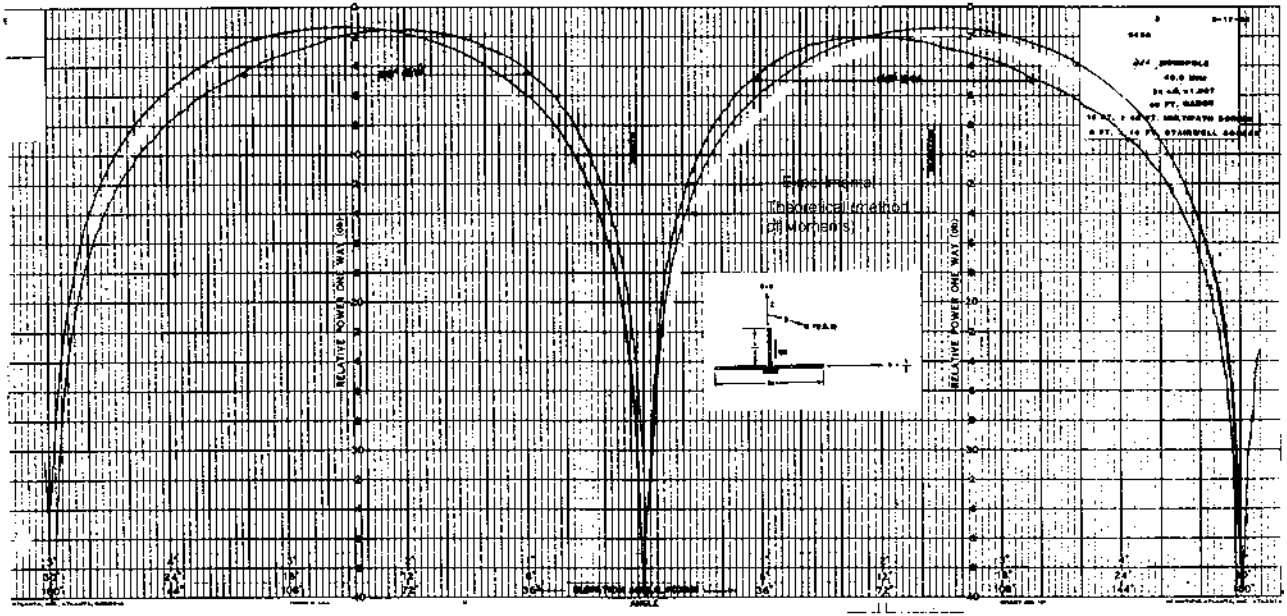

FIGURE 23 Measured and theoretical elevation patterns, 43 MHz ($h/\lambda = 0.2385$, $b/\lambda = 9.11 \times 10^{-4}$, $ka = 1.097$).

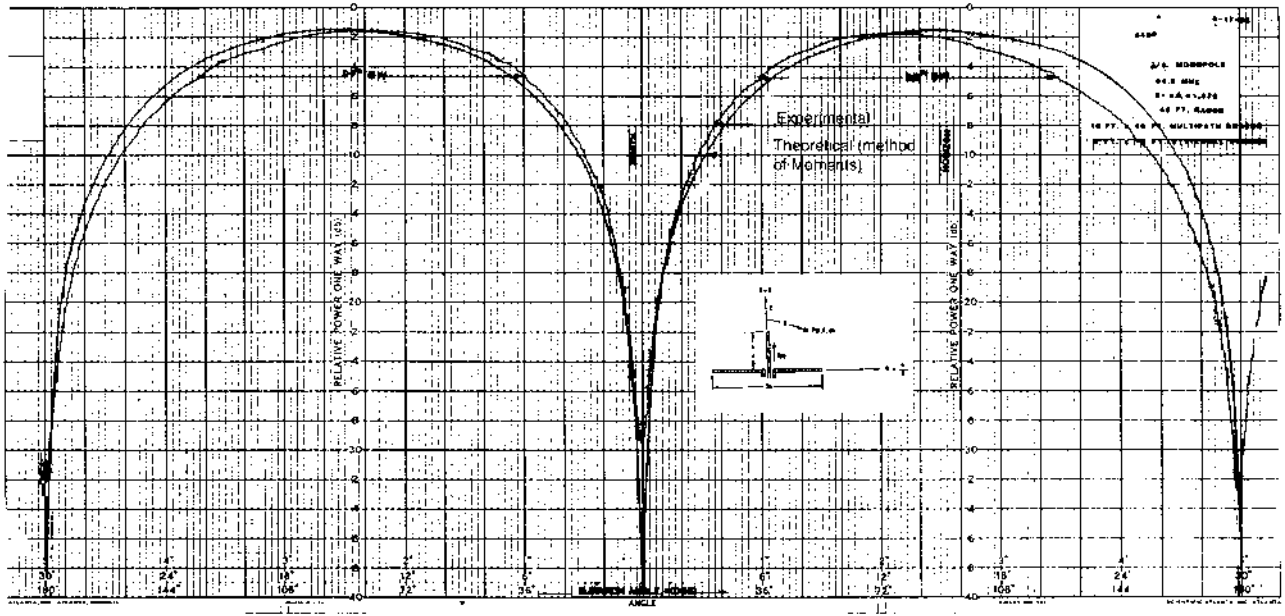

FIGURE 24 Measured and theoretical elevation patterns, 54 MHz ($h/\lambda = 0.2382$, $b/\lambda = 11.43 \times 10^{-4}$, $ka = 1.379$).

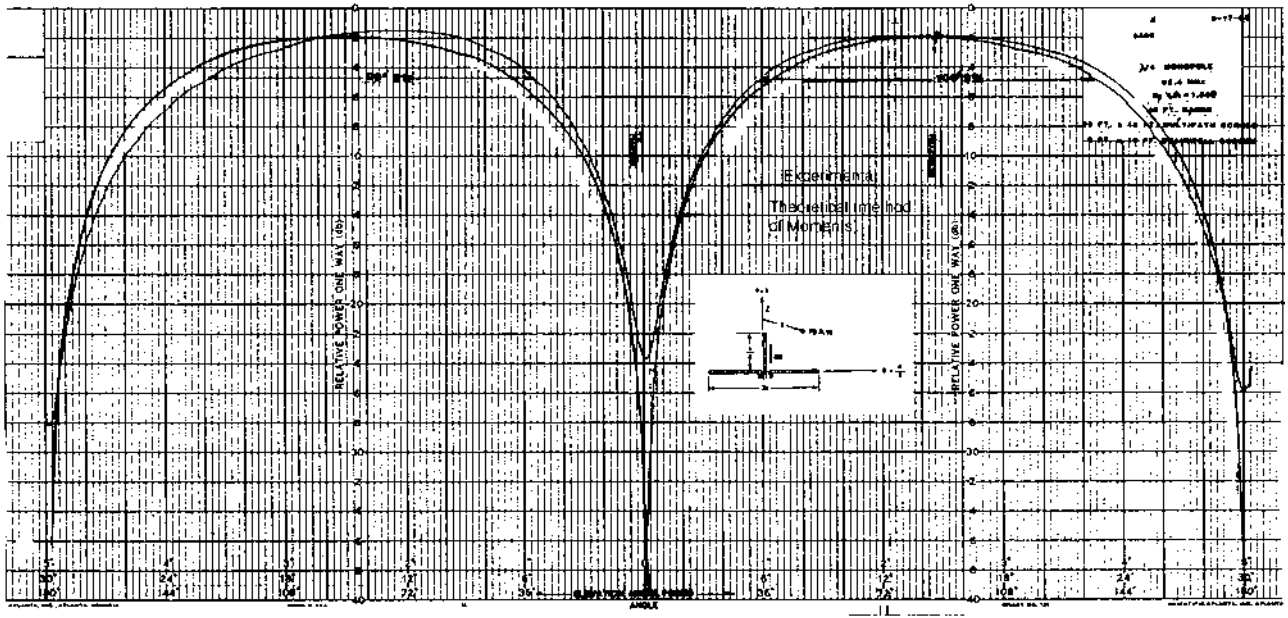

FIGURE 25 Measured and theoretical elevation patterns, 62.4 MHz ($h/\lambda = 0.2379$, $b/\lambda = 13.21 \times 10^{-4}$, $ka = 1.593$).

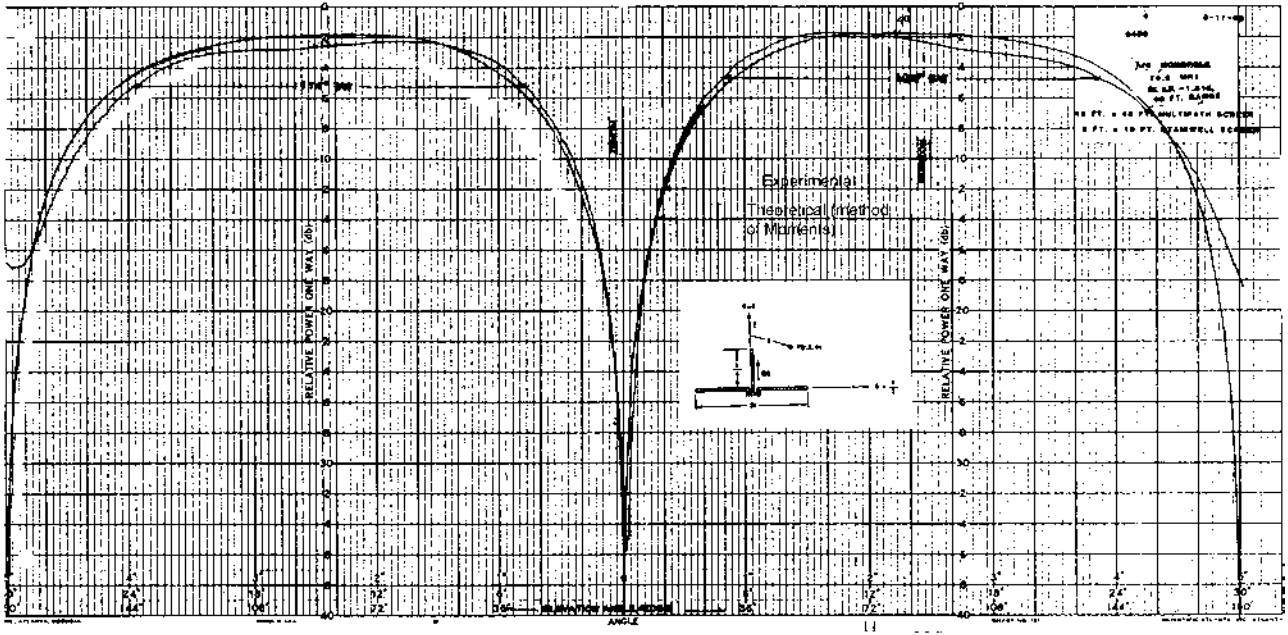

FIGURE 26 Measured and theoretical elevation patterns, 75 MHz ($h/\lambda = 0.2374$, $b/\lambda = 15.89 \times 10^{-4}$, $ka = 1.915$).

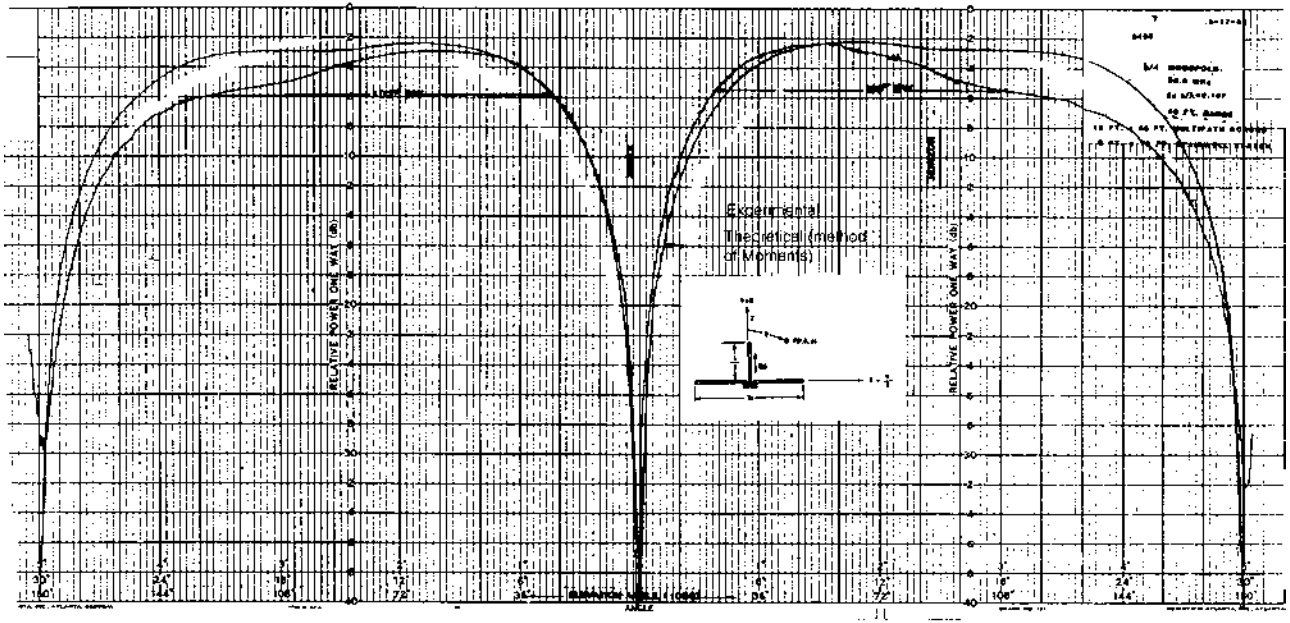

FIGURE 27 Measured and theoretical elevation patterns, 86 MHz ($h/\lambda = 0.2366$, $b/\lambda = 18.22 \times 10^{-4}$, $ka = 2.197$).

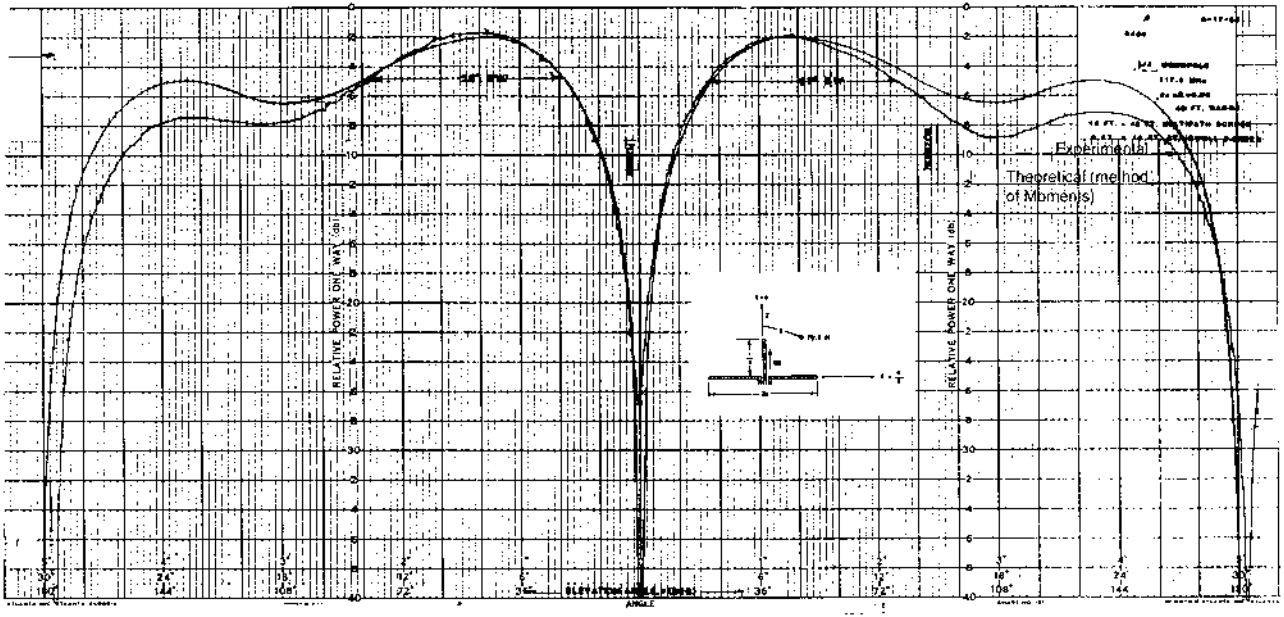

FIGURE 28 Measured and theoretical elevation patterns, 117 MHz ($h/\lambda = 0.2355$, $b/\lambda = 24.78 \times 10^{-4}$, $ka = 3.000$).

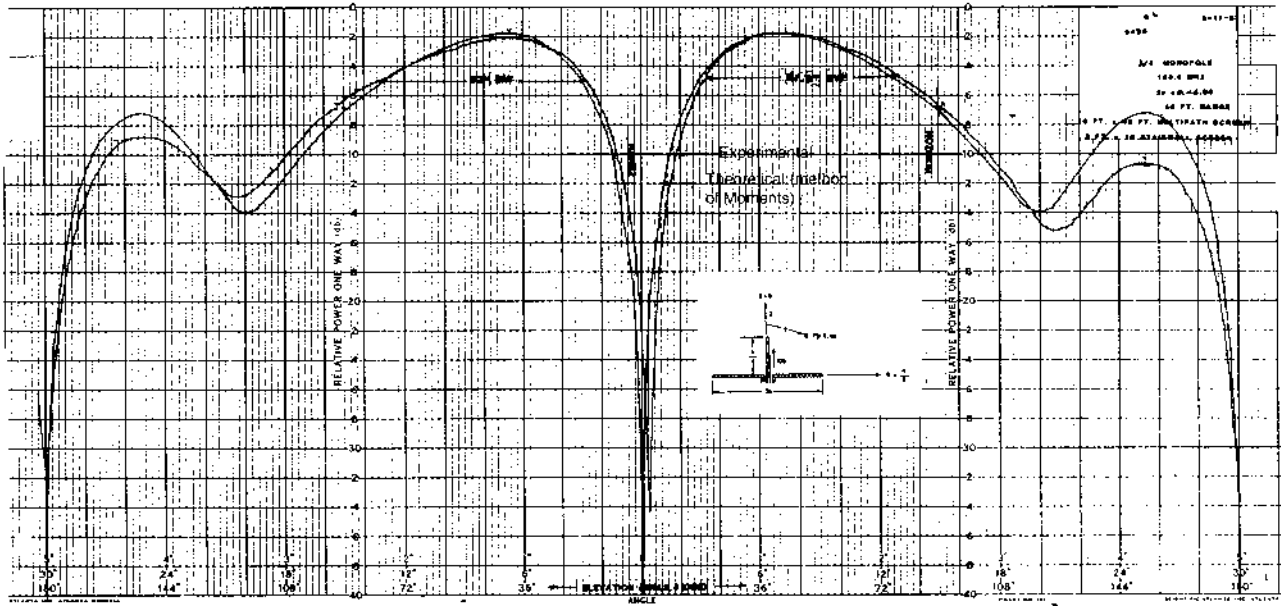

FIGURE 29 Measured and theoretical elevation patterns, 156 MHz ($h/\lambda = 0.2346$, $b/\lambda = 33.04 \times 10^{-4}$, $ka = 4.000$).

6

Applications Utilizing Electrically Small Elements

6.1 ELECTRICALLY SMALL VS. QUARTER-WAVE AND RESONANT ELEMENTS

At long wavelengths, electrically short elements are often desirable for minimizing aerodynamic drag, size, exposure, weight, or cost. The directivity properties of electrically short elements are not appreciably different from those of quarter-wave elements (see Sec. 3.9). The disadvantage of electrically short elements is the large magnitude of their input reactance, often necessitating the use of matching networks. Matching networks can also suffer from the problems of aerodynamic drag, size, exposure, weight, or cost. However, the main disadvantages of matching networks are that they often introduce ohmic loss into the antenna circuit (thus reducing radiation efficiency) and, if they are not very lossy, are matched only over a narrow band of frequencies.

It is therefore of interest to examine the input impedance properties of monopole antennas as a function of element length and radius. The fundamental limitations of electrically short monopole antennas are discussed in Sec. 6.2. The tuning stability of a digitally tuned, electrically short monopole element on disk ground planes of different radii is discussed in Sec. 6.3. This section presents numerical results, obtained from program RICHMD1, of input impedance as a function of element length and radius.

Elements are defined to be resonant or anti-resonant for the condition of zero input reactance or peak input resistance, respectively. Peak input resistance is usually accompanied by a minimum in input reactance centered between maximum positive and negative reactances for slightly different element lengths.

Increasing order of the resonance or anti-resonance corresponds to increasing element length. First-order resonance occurs when the element length is approximately a quarter-wave. The exact element length for resonance may differ by as much as 30% from the nominal value and is dependent upon the ground plane and element radii (see Sec. 4.5).

The input reactance for element lengths of 0.25 and 0.025 wavelengths is shown in Fig. 30 as a function of ground-plane radius. In Fig. 30, the input reactances are normalized to the reactances for a perfect ground plane, namely $21.26\,\Omega$ and $-3456\,\Omega$ for element lengths of 0.25 and 0.025 wavelengths, respectively. For the quarter-wave element, the input reactance is inductive for normalized ground-plane radii greater than approximately 1 rad, capacitive for ground-plane radii less than approximately 1 rad, and approaches $-\infty\ \Omega$ as the ground-plane radius approaches zero. For the electrically short element, the input inductance is capacitive for all ground-plane radii, approximately independent of ground-plane radius for ground-plane radii greater than the element length, and approaches minus infinity ohms as the ground-plane radius approaches zero.

The real and imaginary parts of input impedance for normalized ground-plane radii of 0.25, 0.025, and 0 rad are plotted as a function of element length in Figs. 31–33, respectively. Whereas resonances and anti-resonances both occur for a normalized ground-plane radius of 0.25 rad, only anti-resonances occur for normalized ground-plane radii of 0.025 and 0 rad. The element lengths for first-order resonance, first-order anti-resonance, second-order resonance, and second-order anti-resonance are approximately 0.25, 0.5. 0.75. and 1.0 wavelengths, respectively, if such resonances do occur.

6.2 FUNDAMENTAL LIMITATIONS OF DIGITALLY-TUNED, ELECTRICALLY SMALL ELEMENTS

6.2.1 Introduction

Efficient, electrically small antennas have instantaneous percentage bandwidths which are inherently narrow. By loading the antenna or its impedance matching network with sufficient ohmic loss, large bandwidths can be achieved but at the expense of appreciably reduced efficiency. An alternative method for obtaining potentially much larger efficiency is electronic tuning of the antenna system. The loaded antenna system comprises the antenna and its impedance matching network.

However, this alternative method requires that the unloaded antenna's instantaneous percentage bandwidth $(\Delta f/f)_{\text{unloaded}}$ be made as large as possible to facilitate high efficiency, stable tuning under changing environmental conditions, with a minimum number of tuning bits, where f is the band center

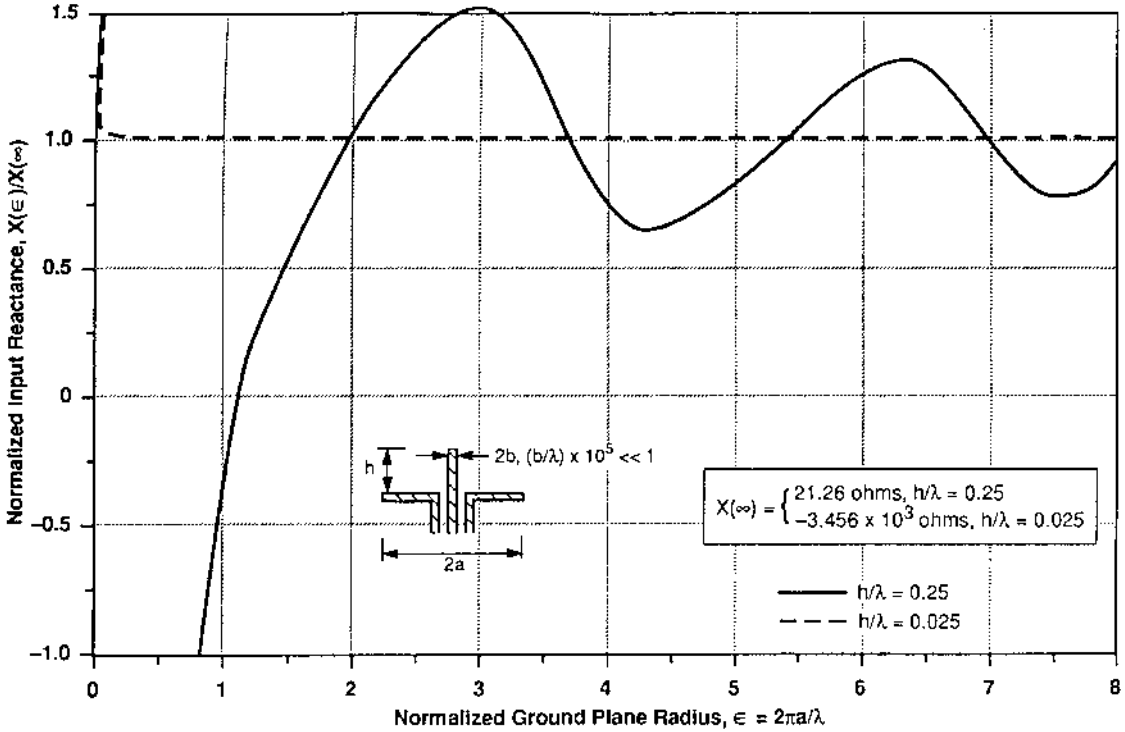

FIGURE 30 Input reactance of thin quarter-wave and electrically short elements at the center of a disk ground plane of normalized radius $ka = 0-8$ rad.

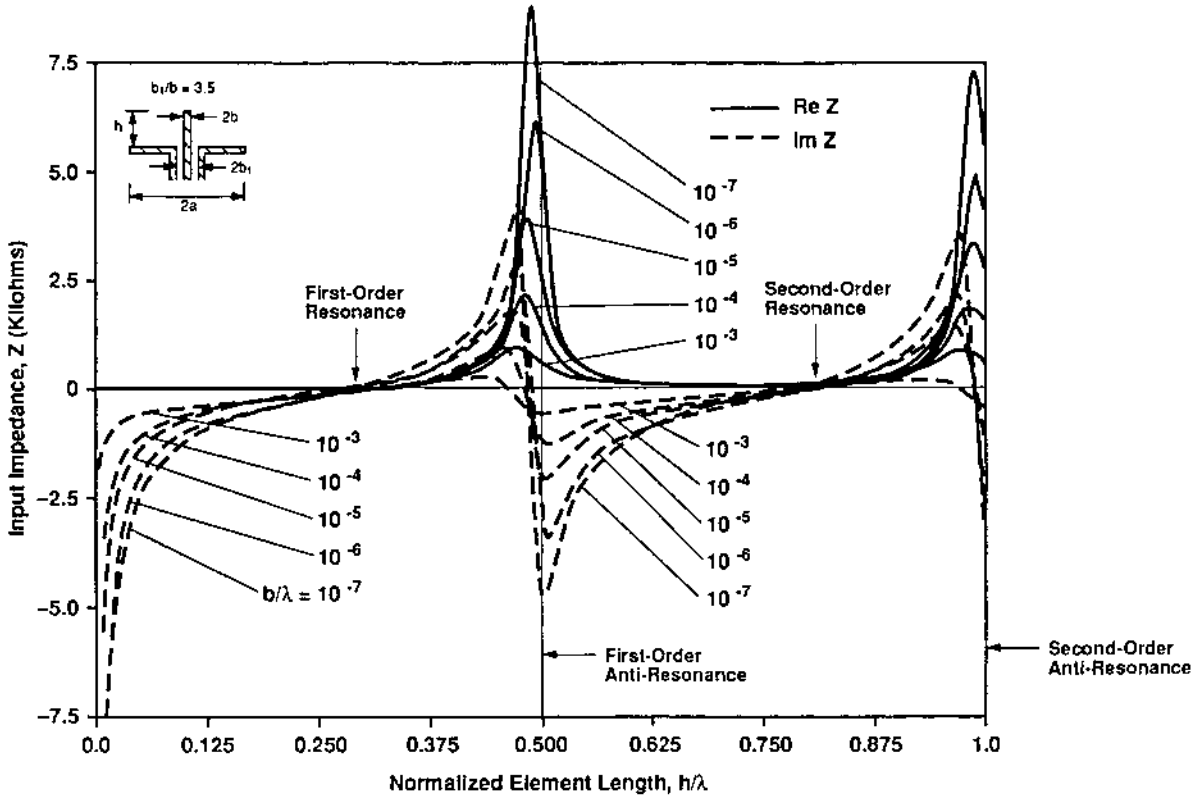

FIGURE 31 Input impedance for elements, of length 0–1 wavelengths, at the center of a disk ground plane of normalized radius $ka = 0.25$ rad.

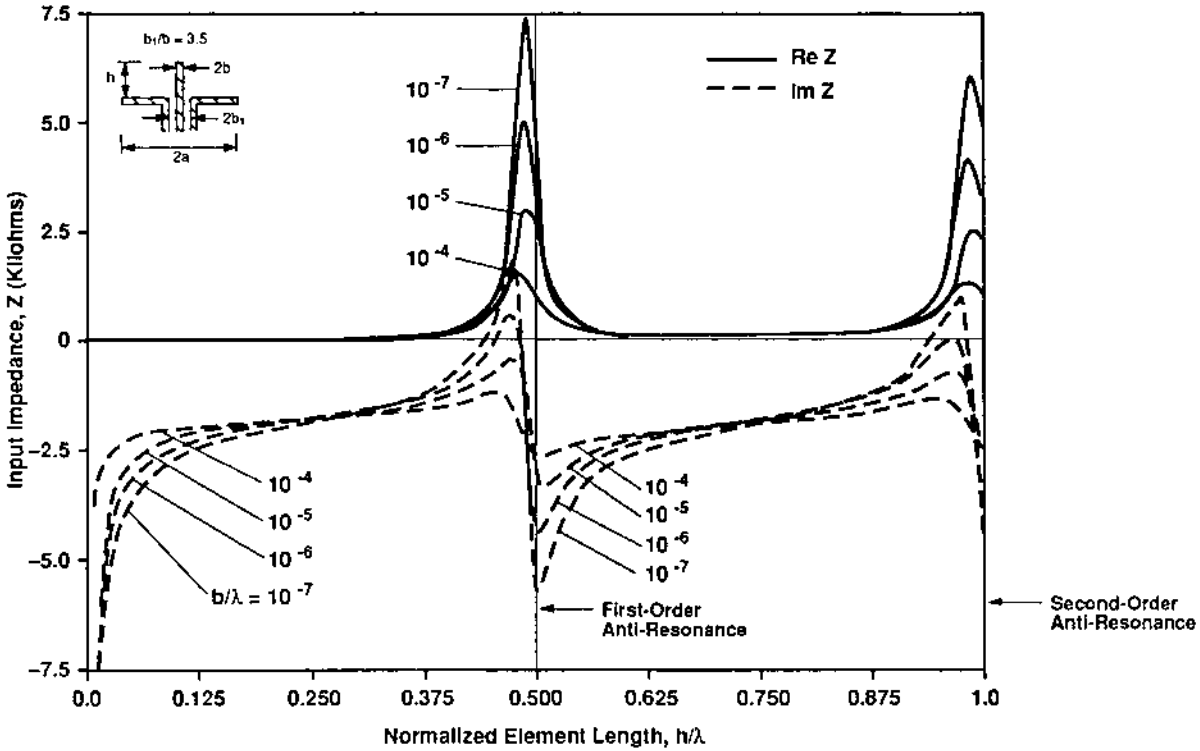

FIGURE 32 Input impedance for elements, of length 0–1 wavelengths, at the center of a disk ground plane of normalized radius $ka = 0.025$ rad.

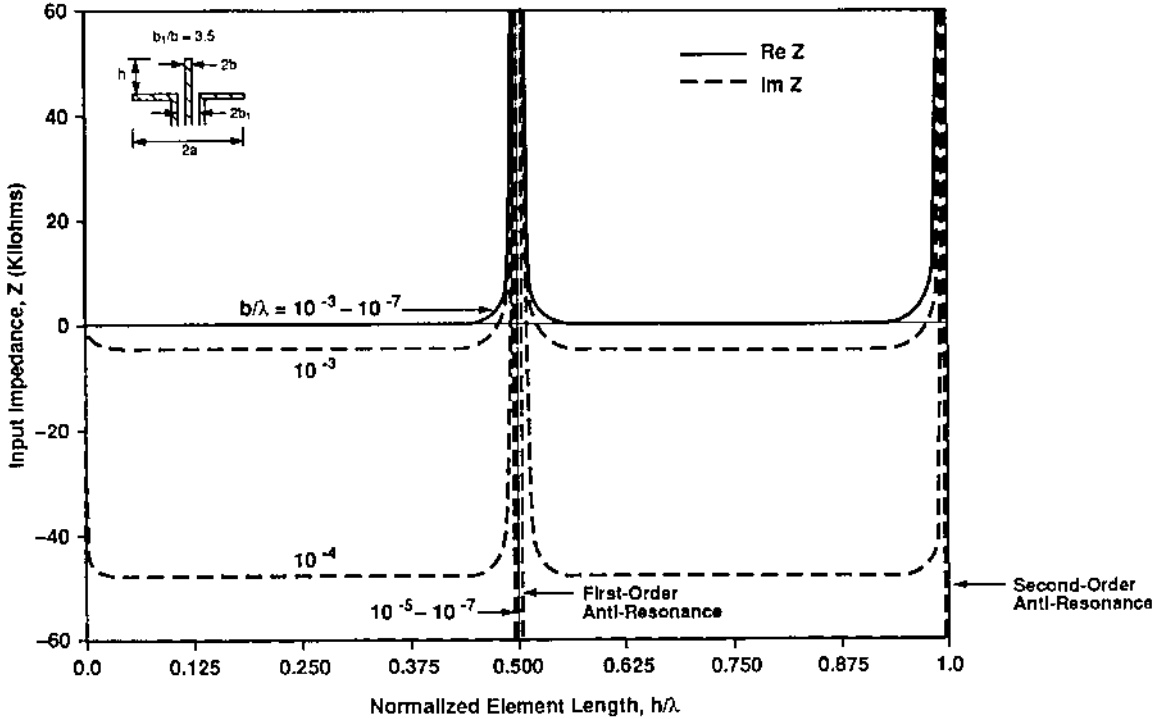

FIGURE 33 Input impedance for elements, of length 0–1 wavelengths, at the center of a disk ground plane of normalized radius $ka = 0$ rad.

frequency and Δf is the 3 dB bandwidth. For electrically small antennas and an idealized lossless matching network,

$$(\Delta f/f)_{\text{unloaded}} = (1/2)(\Delta f/f)_{\text{loaded}} \approx 1/Q_{\text{unloaded}} \ll 1 \tag{6.2.1}$$

where Q_{unloaded} is defined as the ratio of reactance magnitude to resistance of the unloaded antenna's input impedance.

Radome and ground-plane size constraints impose fundamental limitations on how small Q_{unloaded} can be made. These same constraints also impose fundamental limitations on directivity and radiation resistance. It is of interest to determine these fundamental limitations since they can be utilized as a basis for evaluating the performance of any candidate antenna contained within the same radome and ground-plane envelope.

Fundamental limitations of electrically small antennas, whose envelope is constrained to be within the smallest spherical volume enclosing the antenna, have been developed by Chu [30] who developed an equivalent circuit of the TM_{10} spherical wave mode evaluated on the surface of the smallest sphere enclosing the radiating structure. Harrington [31] employed Chu's equivalent circuit to develop a simple algebraic expression for Q_{10} of the TM_{10} mode. Later, Hansen [32] obtained an incorrect result which for electrically small antennas does not differ appreciably from that of Harrington. McLean [33] confirmed the correctness of Harrington's result. Fundamental limitations, for envelope shapes other than spherical, are not found in the literature. However, Chu–Harrington demonstrated that Q_{unloaded} of any antenna structure contained within the smallest spherical volume enclosing the structure will always be larger than Q_{10} of the TM_{10} spherical wave mode evaluated on that spherical surface.

In Sec. 6.2, the Chu–Harrington Q_{10} is utilized to determine the limit on the lowest possible Q_{unloaded} of any monopole element whose envelope is constrained to be within a blade radome. The limit Q_{10} is determined by constructing the smallest sphere enclosing the blade radome and its effective ground-plane image. The effective ground-plane image is determined from Sec. 3 numerical results.

6.2.2 Definition of Problem

For any electrically small antenna structure of zero ohmic loss and whose envelope is within given radome and ground-plane size constraints, the problem is to determine the limitations on:

1. Minimum antenna $Q_{\text{unloaded}} = f/\Delta f$
2. Maximum gain on horizon
3. Maximum peak gain

4. Maximum radiation resistance
5. Minimum number M of bits required to tune over a given band

A solution has been obtained subject to the following additional boundary conditions:

Vertical polarization
Omnidirectionality in azimuth
Spherical radome
Ground-plane options:

1. Very small compared to a wavelength and radome height
2. Small compared to wavelength but large compared to radome height
3. Large compared to a wavelength and radome height

6.2.3 Radiation Regions

The volume, within the smallest envelope surface S_1 enclosing the radiating structure, is designated the *antenna region* (see Fig. 34). When the surface S_1 is specified, but the radiating region within S_1 is not specified, the minimum possible antenna Q_{unloaded} is determined by computing the ratio of peak-stored electric power to the time-averaged radiated power outside the antenna region. The time-averaged radiated power emanating outward from the antenna region is equal to that from any surface enclosing the antenna region but the peak-stored electric power within the antenna region is greater than that from any closed surface outside the antenna region.

Consider now the smallest spherical surface S_2, of radius r_o that encloses the antenna region. The energy stored within S_2 is generally less than that stored external to the antenna region because of the additional stored energy in the region between S_2 and S_1.

6.2.4 TM_{n0} Spherical-Wave Modes

The solution of the vector Helmholtz equation in spherical co-ordinates, subject to the constraints of vertical polarization, outward traveling waves, and an omnidirectional pattern in the azimuthal direction, is a set of orthogonal TM_{n0} spherical-wave modes. The resulting fields evaluated at a radius $r = r_o$ are given

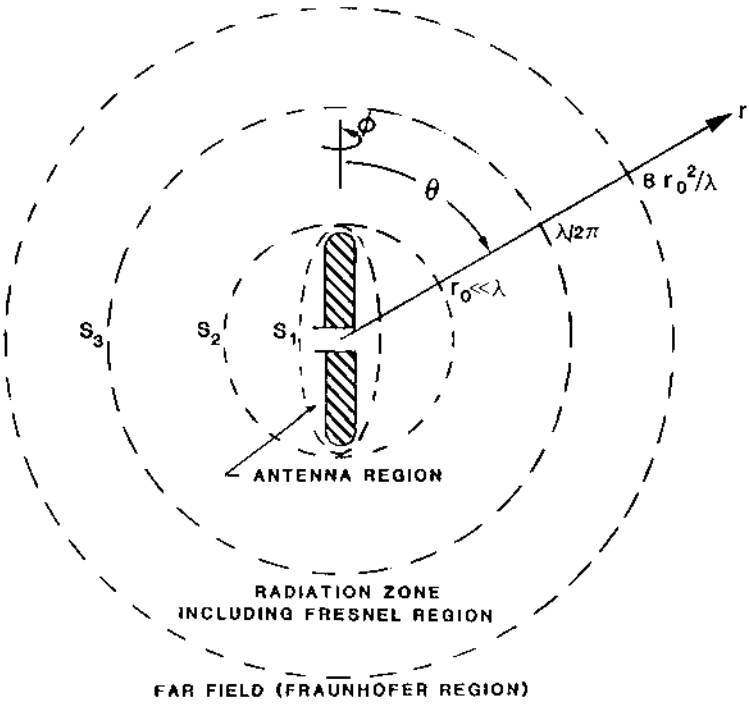

FIGURE 34 Radiating regions.

by

$$
\begin{aligned}
H_\phi &= \sum_{n=1}^{\infty} A_n P_n^{(1)}(\cos\theta) h_n(\rho) \\
E_\mathrm{r} &= -i\sqrt{\mu/\varepsilon}\sum_{\infty^{n=1}}^{\infty} A_n n(n+1) P_n(\cos\theta) h_n(\rho)/\rho \\
E_\theta &= i\sqrt{\mu/\varepsilon}\sum_{n=1} A_n \mathrm{P}_n^{(1)}(\cos\theta)(\rho h_n)'/\rho
\end{aligned}
\tag{6.2.2}
$$

where

$$
\rho \equiv (2\pi/\lambda) r_o \quad , \quad (\rho h_n)' \equiv \tfrac{\mathrm{d}}{\mathrm{d}\rho}(\rho h_n)
$$

$P_n(\cos\theta) =$ Legendre polynomial of order n

$$P_n^{(1)}(\cos\theta) = \text{first associated Legendre polynomial}$$

$$h_n(\rho) = \sqrt{\frac{\pi}{2\rho}} H^{(2)}_{n+\frac{1}{2}}(\rho) = \text{spherical Hankel function of the second kind of order } n$$

The radial wave-impedance $Z_{n0}(\rho)$ of the Poynting vector in the outward radial direction for each mode is defined as

$$Z_{n0}(\rho) = (E_\theta/H_\phi)_n = i\sqrt{\mu/\varepsilon}(\rho h_n)'/\rho h_n \tag{6.2.3}$$

The Poynting vector is not sufficient to characterize the mode Q_{n0} because its imaginary part is proportional to the difference (rather than the sum) of electric and magnetic stored energies. The radial wave impedance and all its derivatives with respect to frequency are sufficient but not convenient to characterize Q_{n0} of the TM_{n0} mode.

6.2.5 Equivalent Circuit of TM_{10} Mode

A more convenient determination of Q_{n0} is possible for a spherical-wave mode because its wave impedance can be expanded as a finite continued fraction given by

$$\begin{aligned} Z_{n0}(\rho) &= \sqrt{\mu/\varepsilon}\left\{ \frac{\sum_{k=0}^{n-1} \frac{(n+k-1)!(2i\rho)^{-k}}{k!(n-k-1)!}}{\sum_{k=0}^{n} \frac{(n+k)!(2i\rho)^{-k}}{k!(n-k)!}} + n/i\rho \right\} \\ &= \frac{n}{i\omega\varepsilon\rho} + \cfrac{1}{\frac{2n-1}{i\omega\mu\rho} + \cfrac{1}{\frac{2n-3}{i\omega\varepsilon\rho} + \ddots + \cfrac{1}{\frac{1}{i\omega\mu\rho} + \frac{1}{(\mu/\varepsilon)^{1/2}}}}} \end{aligned} \tag{6.2.4}$$

The terms of Eq. (6.2.3) can be identified with the elements of an LC ladder network terminated in a resistance R equal to the wave impedance of the lossless medium in which the antenna is imbedded (see Fig. 35). The wave impedance $R = (\mu/\epsilon)^{1/2}$ where μ and ϵ are the permeability and permittivity, respectively, of the lossless medium enclosed by S_2. For an envelope radius r_o which is small compared to the wavelength in the medium, the dominant TM mode is the TM_{10}

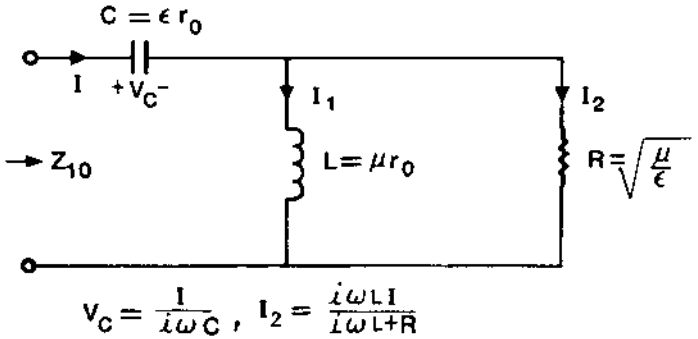

FIGURE 35 Equivalent circuit of TM_{10} mode.

mode. The equivalent circuit of the TM_{10} mode is similar to that of an electrically-short dipole.

6.2.6 Q_{10} of TM_{10} Mode

A simple algebraic expression for Q_{10} of the TM_{10} mode is readily found by computing the ratio of the peak-stored electric power to the time-averaged radiated power in the equivalent circuit of Fig. 35. Assuming a steady-state sinusoidal waveform of radian frequency ω, the peak-stored electric power $=$ (2 ω)(time-averaged stored electric energy). It follows that

$$Q_{10} = \frac{2\omega(\text{TIME–AVERAGED STORED ELECTRIC ENERGY})}{\text{TIME–AVERAGED RADIATED POWER}} = \frac{2\omega\frac{1}{4}C|V_C|^2}{\frac{1}{2}R|I_2|^2} = \left(\frac{2\pi r_o}{\lambda}\right)^{-3} + \left(\frac{2\pi r_o}{\lambda}\right)^{-1} \tag{6.2.5}$$

The same result can be obtained by direct evaluation of the spherical Hankel functions in the expression for Q_{10}, as attempted by Hansen [32]. For large values of Q_{10}, Eq. (6.2.5) reduces to

$$Q_{10} \approx (2\pi r_o/\lambda)^{-3}, \quad Q_{10} \gg 1 \tag{6.2.6}$$

6.2.7 Effect of Ground-Plane Size on Q_{10}

The radius r_o of the smallest spherical envelope, enclosing a blade radome and its effective ground-plane image, is a function of the ground-plane size (see Fig. 36). The blade radome is of height h (equal to the height of a potential antenna

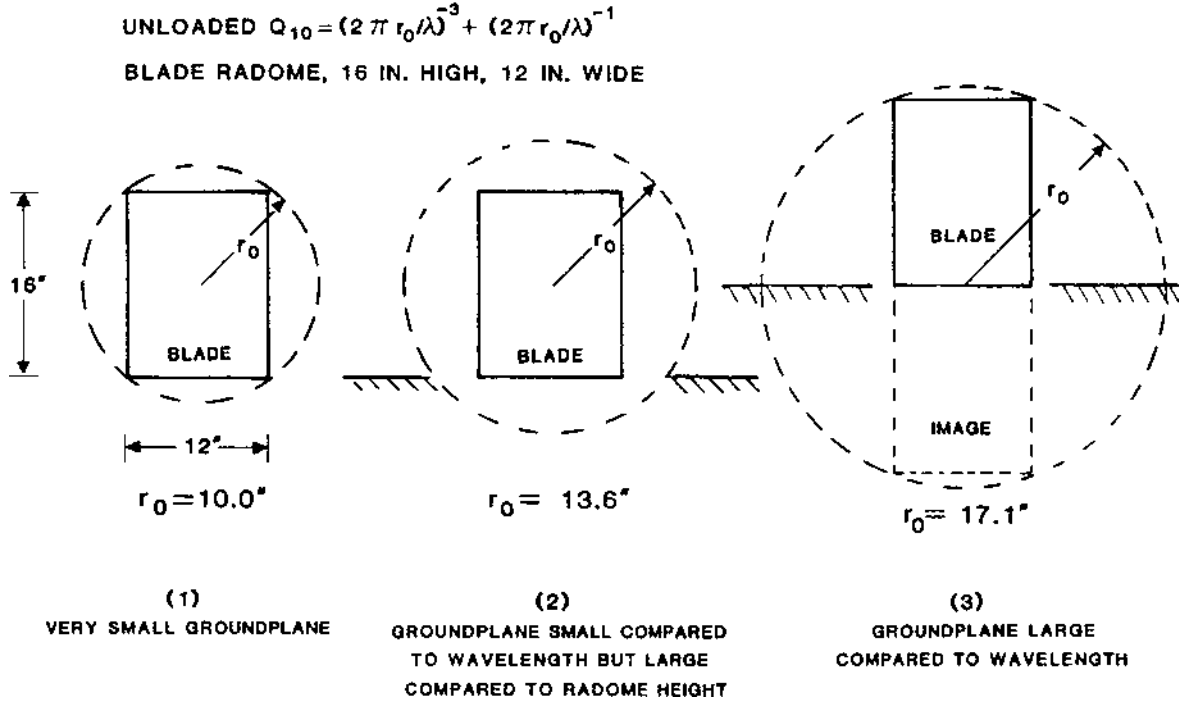

FIGURE 36 Effect of ground-plane size on Q_{10}.

element), width w, and thickness much less than h and w. The three cases considered in Fig. 36 are ground planes: (1) very small compared to wavelength and radome height; (2) small compared to wavelength but large compared to radome height; and (3) large compared to wavelength and radome height. In Case (1), the radius r_o is approximately that of the smallest sphere enclosing the blade radome (since there is virtually no ground plane), and is given by

$$r_o = (h/2)^2 + (w/2)^{2\,1/2}, \quad \text{Case (1)} \tag{6.2.7}$$

In Case (3), the radius r_o is that of the smallest sphere enclosing the blade radome and its image, and is given by

$$r_o = h^2 + (w/2)^{2\,1/2}, \quad \text{Case (3)} \tag{6.2.8}$$

In Case (2), assuming similar ground-plane characteristics as for a monopole element, the input reactance is approximately the same as for an infinite ground plane (see Fig. 30 in Sec. 6.1) whereas the radiation resistance is approximately one-half that for an infinite ground plane (see Fig. 14 in Sec. 3.9). From Eq. (6.2.1), it follows that Q_{unloaded} of Case (2) is twice that of Case (3) and therefore from Eq. (6.2.6) it follows that r_o of Case (2) is $2^{-1/3}$ that of Case (3). Accordingly,

$$r_o = 2^{-1/3}h^2 + (w/2)^{2\,1/2}, \quad \text{Case (2)} \tag{6.2.9}$$

6.2.8 Bounds on Antenna System Performance

The lower bound on the minimum number M of binary tuning bits, of a lossless matching network required to tune over the desired frequency band, is given by

$$M = (2\ln 2)^{-1}\ln\left[\int_{\rho_2}^{\rho_1} \rho^{-1} Q_{10}(\rho)\,\mathrm{d}\rho\right] \tag{6.2.10}$$

where ρ is defined in Eq. (6.2.2), $Q_{10}(\rho)$ is given by Eq. (6.2.5), and the subscripts 1 and 2 denote the low and high ends, respectively, of the frequency band. Since Eq. (6.2.10) generally does not yield a whole number, the result given by Eq. (6.2.10) should be rounded off to the nearest larger integer.

Bounds on antenna system performance, subject to the boundary conditions of Sec. 6.2.2, are given in Table 9 for any antenna enclosed within a blade radome of height $h = 16$ in., width $w = 12$ in., and operating over the frequency band 30–150 MHz. In Table 9, the performance bounds are determined by evaluating Q_{10} of the TM_{10} spherical wave mode on the surface of the smallest sphere enclosing the blade radome and its effective ground-plane image. The radius r_o of the sphere is given in Fig. 36 for the three ground-plane cases that are considered.

TABLE 9 Bounds on Antenna System Performance

Antenna system characteristic	Performance bound			Reference
	Very small ground-plane-1	Small ground plane-2	Large ground plane-3	
Polarization	Vertical	Vertical	Vertical	Sec. 6.2.2
Azimuthal pattern	Omnidirectional	Omnidirectional	Omnidirectional	Sec. 6.2.2
Directive gain on horizon	≤ 1.76 dBi	≤ 1.76 dBi	$\lesssim -1.25$ dBi[a]	30, Table 4
Peak directive gain	≤ 1.76 dBi	≤ 1.76 dBi	$\lesssim 4.77$ dBi	30, Table 4
Radiation resistance	$\leq 9.4\,\Omega$, 30 MHz $\leq 146.6\,\Omega$, 150 MHz	$\leq 9.4\,\Omega$, 30 MHz $\leq 146.6\,\Omega$, 150 MHz	$\leq 13.1\,\Omega$, 30 MHz $\leq 122.6\,\Omega$, 150 MHz	Eq. (6.2.3)
Unloaded Q	>251.8, 30 MHz >3.2, 150 MHz	>105.6, 30 MHz >2.2, 150 MHz	>52.8, 30 MHz >1.1, 150 MHz	Eq. (6.2.5)
Loaded half-power relative bandwidth, $\Delta f/f$	$<0.79\%$, 30 MHz $<62.5\%$, 150 MHz	$<1.9\%$, 30 MHz $<88.8\%$, 150 MHz	$<3.8\%$, 30 MHz $<177.6\%$, 150 MHz	Eqs. (6.2.1) and (6.2.5)
Number of tuning bits for VSWR $\leq 2.3{:}1$	≥ 6 (binary)	≥ 5 (binary)	≥ 4 (binary)	Eq. (6.2.10)

Radome: blade, 16 in. high, 12 in. wide.
Frequency band: 30–150 MHz.
Spherical wave mode: TM_{10}.
Ohmic loss of antenna system: zero.
Ground plane: (1)very small compared to a wavelength and the radome height, (2)small compared to a wavelength but large compared to the radome height, (3)finite, large compared to a wavelength.
[a] Dependent upon shape of ground plane. Value given is for a disc.

6.2.9 Unloaded *Q* of Monopole Elements

In Fig. 37, the unloaded Q of a rod monopole element on a disk ground plane is plotted as a function of element radius and is compared with the fundamental limitation Q_{10} of the TM_{10} spherical wave mode. The unloaded Q is more than an order of magnitude larger than Q_{10} for small element radii but approaches that of Q_{10} for large element radii. For a monopole element of elliptical cross-section with major and minor axes of 6 and 2 in., respectively, the effective element

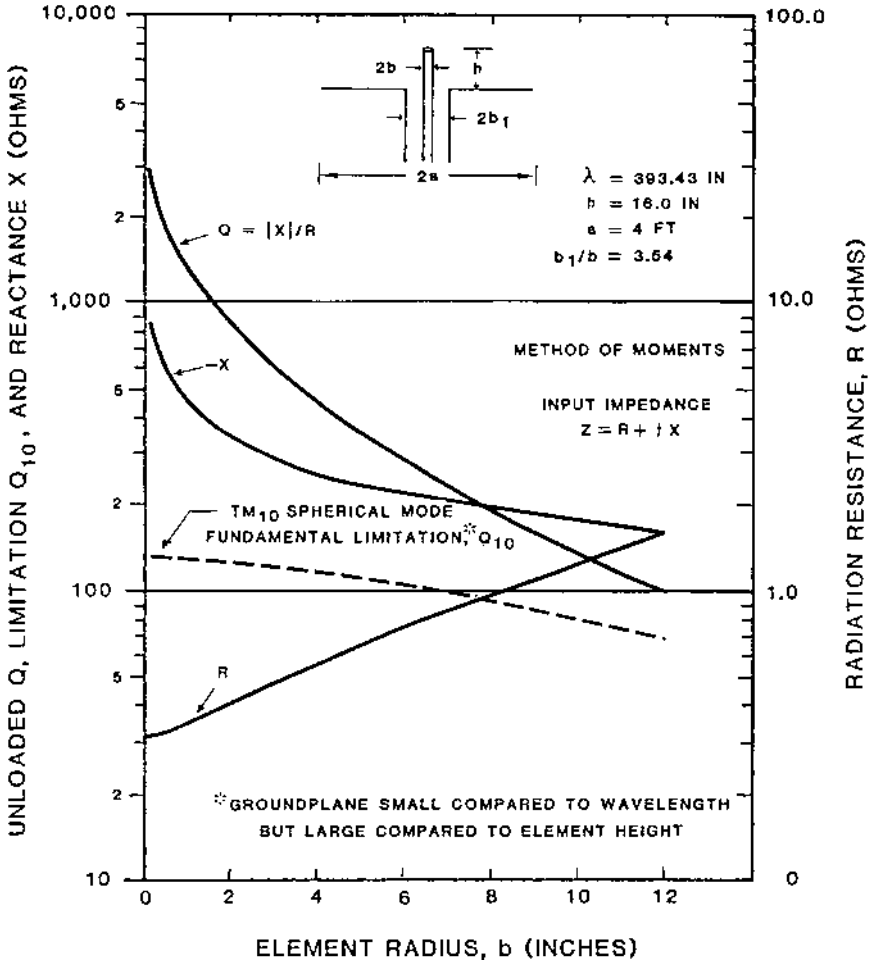

FIGURE 37 Unloaded Q of monopole antennas with rod elements.

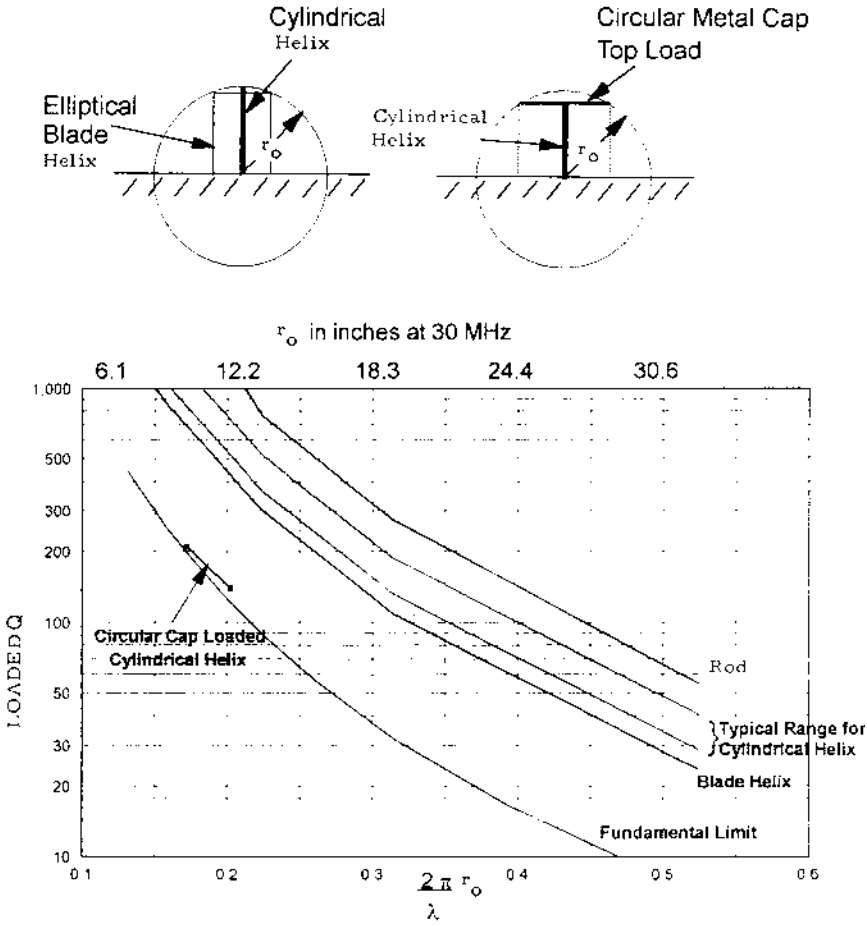

FIGURE 38 Loaded Q of monopole antennas with helical cylindrical elements (Courtesy of G. Ploussios, GS Inc.).

radius is approximately 4 in. The unloaded Q in Fig. 37 for a rod element of radius 4 in. is approximately four times that of Q_{10}. If a thin rod element were top-loaded with a nonradiating cap to provide a more uniform current along the vertical element, the difference between unloaded Q and Q_{10} would decrease significantly.

However, even if an electrically small monopole element of elliptical cross section could be designed to have an unloaded Q approaching that of Q_{10}, the problem still remains of designing an electronically tuned matching network that

is inductive, efficient (small ohmic loss), and is contained within the radome envelope. One solution to this problem is a helical coil monopole element shunted by diodes at M tapping points, corresponding to the number M of tuning bits required over the operating band. The helical cross-section is sufficiently small so that the peak directivity is normal (for a perfect ground plane) to the axis of the helix and may be shaped to match the radome cross-section. The helical element, which serves as both the radiating element and the matching network, could also be top-loaded if desired. The diode dc bias voltages must be fed in such a way that the bias circuit neither radiates nor introduces too much shunt capacitance.

G. Ploussios [34,35] has successfully designed and tested monopole antennas with efficient electronically tunable helical elements. The loaded Q of the helical elements, for zero ohmic loss and an electrically large ground plane, is compared in Fig. 38 with that for a rod element of the same height and radius and also with that of the TM_{10} spherical wave mode fundamental limit. For a sphere of radius $r_o = 17.1$ in., corresponding to Case (3) in Fig. 36 of the smallest sphere that encloses the blade radome and its ground-plane image, the loaded Q of an elliptical helical element is approximately 2.5 times less than that for the rod element and approximately four times more than that of the fundamental limit Q_{10}. A cylindrical top-loaded helical element, of even modest element radius, can attain a loaded Q that approaches the fundamental limit (see Fig. 38).

6.3 TUNING STABILITY OF A DIGITALLY-TUNED, ELECTRICALLY SMALL ELEMENT ON DISK GROUND PLANES OF DIFFERENT RADII

6.3.1 Introduction

Vertically polarized, omnidirectional, high-power transmitting antennas that will fit inside an electrically small radome and that will accommodate frequency hopping over a large frequency range are of interest to designers of airborne very high frequency (VHF) communication systems that operate in an interference environment. This section investigates the tuning stability of a digitally tuned, electrically short monopole element mounted at the center of different-sized disk ground planes whose radii vary from a fraction of a wavelength to several wavelengths. In particular, double- and single-parameter tuning are investigated to determine the range of ground-plane radii for which the same tuning words can be utilized in maintaining a specified antenna gain (including mismatch losses) over a 5:1 frequency band.

Efficient, electrically small antennas have instantaneous percentage bandwidths that are inherently narrow [30,31]. By loading the antenna or its impedance matching network with sufficient ohmic loss, large bandwidths can be

achieved, but at the expense of appreciably reduced efficiency. An alternative method for obtaining potentially much larger efficiency is electronic tuning of the impedance-matching network.

Generally, two parameters in the impedance-matching network must be varied (designated "double-parameter tuning") to provide impedance matching of both the real and imaginary parts of the antenna input impedance. However, single-parameter tuning is sufficient provided the radiation resistance is proportional to the square of the frequency, large compared to the ohmic loss resistance, and small compared to the source impedance [36]. These conditions for perfect impedance matching with single-parameter tuning are generally not realizable over large frequency bands for monopole elements on finite size ground planes, as will be shown in this paper.

Impedance matching of the *imaginary* part of the antenna input impedance may usually be achieved by digital switching of appropriate inductances from a fixed inductance bank in series with the antenna element. Impedance matching of the *real* part of the antenna input impedance may usually be achieved with double-parameter tuning by feeding the inductances at a variable (digitally switched) tap point. The set of switching bits, which achieves an impedance match at a given frequency when the monopole element is mounted on the reference ground plane, is denoted the "tuning word" for that frequency.

Edge diffraction by the circular ground plane significantly alters the antenna input impedance so that it is generally not possible to provide a good impedance match with the same tuning word for ground-plane radii appreciably different from the radius of the reference ground plane. Although directive gain and radiation efficiency are functions of the ground-plane size, it is shown in this paper that the matching efficiency is particularly sensitive to ground-plane size. It is found that the range of ground-plane radii, for good impedance matching with fixed tuning words, is generally not significantly larger with double-parameter tuning than with single-parameter tuning. It is concluded that it may not be possible to use the same tuning words for all ground-plane radii of interest without a substantial loss in antenna gain, particularly at the low end of the frequency band.

The analytical model is described in Sec. 6.3.2. Numerical results and conclusions are given in Secs. 6.3.3 and 6.3.4, respectively.

6.3.2 Analytical Model

With reference to Fig. 39, consider an electrically short, electrically thin monopole element, of height h (= 16 in. = 0.04–0.20 wavelengths) and radius b (= 0.5 in. = 0.00125–0.006 wavelengths), which is mounted at the center of various disk ground planes with an 80:1 range of radius a (= 0.5–40 ft = 0.015–4.1 wavelengths) in a 5:1 frequency band (30–150 megahertz (MHz)).

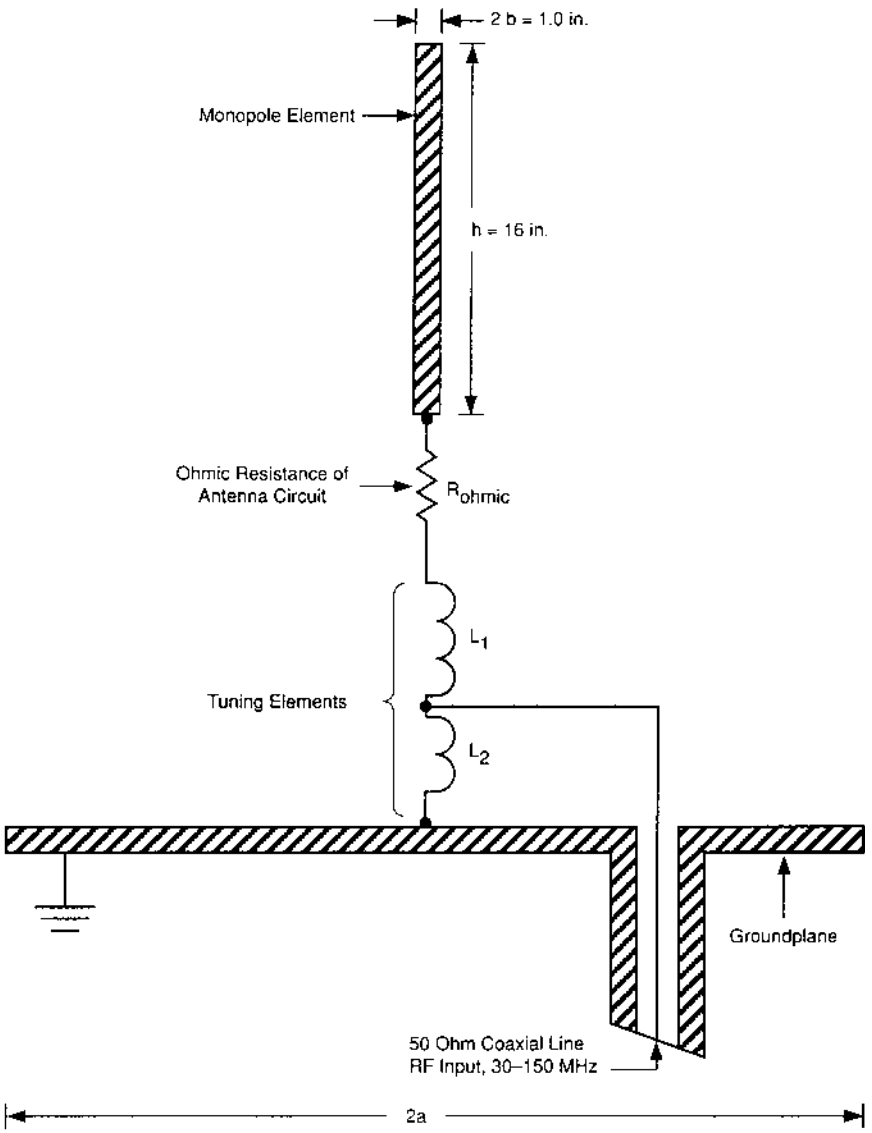

FIGURE 39 Monopole antenna with impedance–matching network.

The element is in series with an impedance-matching network comprising the inductances L_1 and L_2 of a tapped coil, one end of which is connected to the ground plane. The coil tap point is fed by the center conductor of a low-loss coaxial line whose outer conductor is also connected to the ground plane. The ohmic resistance of the coil and antenna is approximated by a resistance R_{ohmic} in series with L_1. The tapped coil is treated as a lumped circuit that does not radiate.

The equivalent circuit of the monopole antenna and its impedance-matching network is shown in Fig. 40. In double-parameter tuning, both L_1 and L_2 are variable with the radian frequency, ω [Fig. 40(a)]. In single-parameter tuning, only L_1 is variable with frequency [see Fig. 40(b)]. The monopole antenna has an

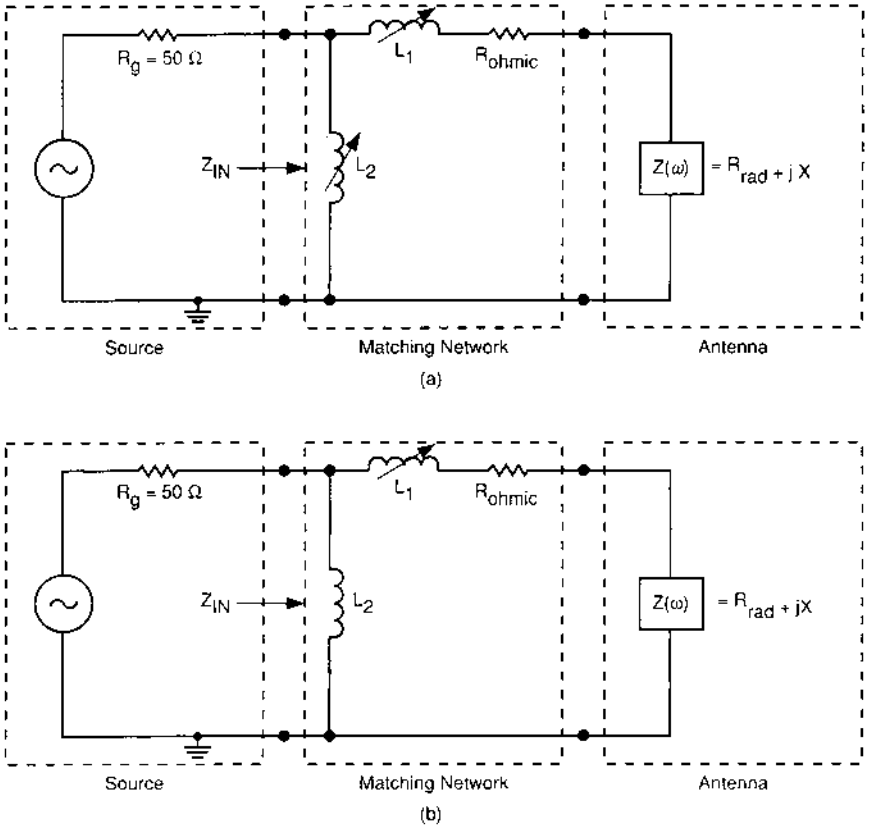

FIGURE 40 Equivalent circuit with (a) double-parameter tuning and (b) single-parameter tuning.

input impedance $Z(\omega)$. The transmission line has a characteristic impedance of $50\,\Omega$, which is matched to the output impedance $Z_g = R_g = 50\,\Omega$ of the source generator. The input impedance Z_{IN} to the matching network is a function of the antenna input impedance $Z(\omega)$, R_{ohmic}, and the assigned values of L_1 and L_2 at any given frequency.

The central issue is the range of ground-plane sizes for which the same tuning "words" can be utilized in maintaining a specified antenna gain over the frequency band. In double-parameter tuning, the tuning words (values of the inductances L_1 and L_2 at each frequency) are chosen so that when the monopole element is mounted on a reference ground plane of radius $a = 4\,\text{ft}$, $Z_{IN} = R_g = 50\,\Omega$ at each of these frequencies. In single-parameter tuning, the tuning words are chosen so that, when the monopole element is mounted on a reference ground plane of radius $a = 4\,\text{ft}$, $\text{Im}\,(Z_{IN}) = 0$ at each frequency and $\text{Re}\,(Z_{IN}) = R_g = 50\,\Omega$ at 30 MHz. No constraints are placed on the maximum impedance mismatch that can be attained except for the above matching constraints.

With single-parameter tuning, both the real and imaginary parts of the input impedance can be matched at generally only one selected frequency. At other frequencies, only the real or imaginary part of the input impedance can be matched. The imaginary part was chosen to be matched at each frequency because, for electrically short antennas, the input reactance contributes more to impedance mismatch than the input resistance. The real part was selected to be matched at 30 MHz because the input resistance has the largest impedance mismatch at the lowest end of the frequency band.

6.3.2.1 Input Impedance

The input impedance $Z(\omega)$ of the monopole antenna is given by

$$Z(\omega) = R_{rad} + jX \tag{6.3.1}$$

where R_{rad} is the antenna radiation resistance and X is the antenna reactance.

The input impedance $Z(\omega)$ of the monopole antenna was determined by Richmond's method of moments RICHMD1 program for each of the above ground planes. The radiation resistance varies from 0.3 to $0.6\,\Omega$ at 30 MHz and 10 to $30\,\Omega$ at 150 MHz (see Fig. 41). The reactance varies from -500 to $-750\,\Omega$ at 30 MHz and -20 to $-90\,\Omega$ at 150 MHz (see Fig. 41).

6.3.2.2 Determination of the Tuning Words

The input impedance Z_{IN} to the matching network is given by

$$Z_{IN} = j\omega L_2 \| [j\omega L_1 + R_{ohmic} + Z(\omega)] = \text{Re}(Z_{IN}) + j\,\text{Im}(Z_{IN}) \tag{6.3.2}$$

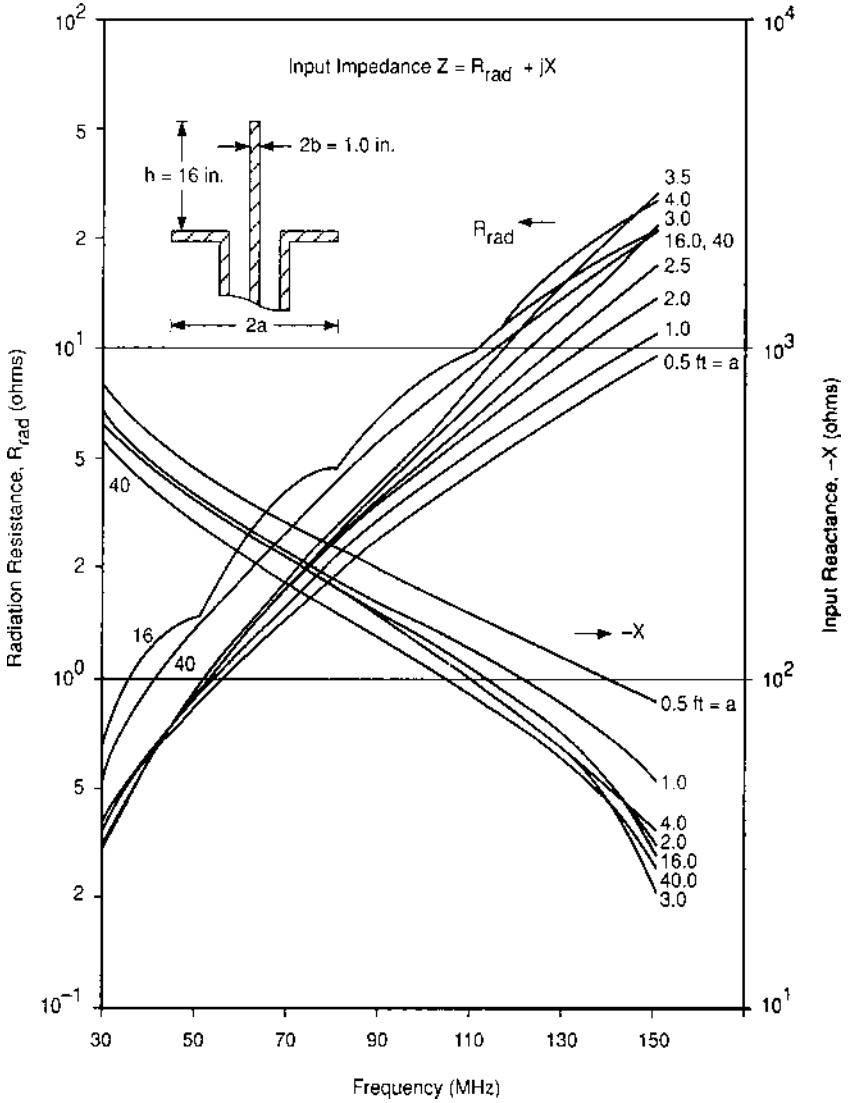

FIGURE 41 Input impedance, for zero ohmic loss, of electrically small element on ground plane of radius $a = 0.5–40$ ft.

where

$$\| \equiv \text{“in parallel with”}$$

$$\mathrm{Re}(Z_{\mathrm{IN}}) = \frac{\omega^2 L_2^2 R}{(\omega L_2 + B)^2 + R^2} \tag{6.3.3}$$

$$\mathrm{Im}(Z_{\mathrm{IN}}) = \frac{\omega L_2 [B(\omega L_2 + B) + R^2]}{(\omega L_2 + B)^2 + R^2} \tag{6.3.4}$$

$$R \equiv R_{\mathrm{rad}} + R_{\mathrm{ohmic}} \tag{6.3.5}$$

$$B \equiv \omega L_1 + X \tag{6.3.6}$$

The voltage reflection coefficient ρ is given by

$$\rho = \frac{Z_{\mathrm{IN}} - Z_{\mathrm{g}}}{Z_{\mathrm{IN}} + Z_{\mathrm{g}}} \tag{6.3.7}$$

The parameters L_1 and L_2 must be positive real quantities, which are determined by requiring, when the monopole element is mounted on a reference ground plane (of radius $a = 4$ ft), that (1) $\mathrm{Im}(Z_{\mathrm{IN}}) = 0$ at each frequency of interest and (2) $\mathrm{Re}(Z_{\mathrm{IN}}) = R_{\mathrm{g}} = 50\,\Omega$ at each frequency of interest for double-parameter tuning and only at $\omega_A/2\pi = 30$ MHz for single-parameter tuning. Let the subscript o denote the reference ground plane. Thus, ρ_o, $Z_{\mathrm{IN}o}$, L_{1o}, L_{2o}, B_o, R_o, and X_o denote the quantities Z_{IN}, L_1, L_2, B, R, and X, respectively, when the monopole element is mounted on the reference ground plane.

Accordingly, the algorithms for determining L_{1o} and L_{2o} are given by double-parameter tuning:

$$L_{2o} = L_{2o}(\omega) = \begin{cases} \frac{1}{\omega}\left[\frac{R_{\mathrm{g}} R_o(\omega)}{1 - \frac{R_o(\omega)}{50}}\right]^{1/2}, & 0 \le R_o(\omega) \le R_{\mathrm{g}}\,\Omega \\ \text{not realizable}, & R_o(\omega) > R_{\mathrm{g}}\,\Omega \end{cases} \tag{6.3.8}$$

$$L_{1o} = L_{1o}(\omega) = \begin{cases} -\frac{X_o(\omega)}{\omega} - \frac{L_{2o}}{2} - \left[\left(\frac{L_{2o}}{2}\right)^2 - \frac{R_o^2(\omega)}{\omega^2}\right]^{1/2}, \\ \qquad 0 \le R_o(\omega) \le R_{\mathrm{g}}/2\,\Omega \\ -\frac{X_o}{\omega} - \frac{L_{2o}}{2} + \left[\left(\frac{L_{2o}}{2}\right)^2 - \frac{R_o^2(\omega)}{\omega^2}\right]^{1/2}, \\ \qquad R_{\mathrm{g}}/2 < R_o(\omega) < R_{\mathrm{g}}\,\Omega. \end{cases} \tag{6.3.9}$$

single-parameter tuning:

$$L_{2o} = L_{2o}(\omega_A) = \begin{cases} \frac{1}{\omega_A}\left[\frac{R_{\mathrm{g}} R_o(\omega_A)}{1 - \frac{R_o(\omega_A)}{R_{\mathrm{g}}}}\right]^{1/2}, & 0 \le R_o(\omega_A) \le R_g\,\Omega \\ \text{not realizable}, & R_o(\omega_A) > R_{\mathrm{g}}\,\Omega \end{cases} \tag{6.3.10}$$

where $\omega_A/2\pi = 30\,\text{MHz}$.

$$L_{1o} = L_{1o}(\omega)$$

$$= \begin{cases} -\frac{X_o(\omega)}{\omega} - \frac{L_{2o}}{2} \pm \left[\left(\frac{L_{2o}}{2}\right)^2 - \frac{R_o^2(\omega)}{\omega^2}\right]^{1/2} \\ \text{(choose root that yields } L_{1o}0 \geq 0 \\ \textit{and} \text{ that yields the smaller value of } |\rho_o|), \quad R_o(\omega) \leq \omega L_{2o}/2 \\ -\frac{X_o}{\omega} - \frac{L_{2o}}{2} \qquad\qquad\qquad\qquad\qquad\qquad R_o(\omega) > \omega L_{2o}/2 \end{cases} \tag{6.3.11}$$

When the monopole element is mounted on the reference ground plane and $R_o(\omega) \leq R_g\,\Omega$, then it is always possible with double-parameter tuning to provide over the operating band a perfect match of the antenna input impedance $Z(\omega)$ to the generator source impedance R_g. It is generally not possible with single-parameter tuning.

There is a case, however, for which impedance matching over the operating band can be obtained with single-parameter tuning. Consider the case in which the radiation resistance is proportional to the square of the frequency, large compared to ohmic loss resistances, and small compared to the source impedance. This case is often assumed in the literature [36], but the conditions for the realization of this case are difficult to realize over large frequency bands on ground planes of finite extent. Stated algebraically, these conditions are

$$R_\text{ohmic} \ll R_\text{rad} = K\omega^2 \gg R_g \tag{6.3.12}$$

where K is a constant. For conditions (6.3.12), the double-parameter tuning Eqs. (6.3.8) and (6.3.9) reduce to

$$L_{2o} \sim \frac{1}{\omega}[R_\text{g} R_o(\omega)]^{1/2} \sim \frac{1}{\omega}[R_\text{g} R_\text{rad}]^{1/2} = [R_\text{g} K\,]^{1/2} \tag{6.3.13}$$

$$L_{1o} \sim -\frac{X_o(\omega)}{\omega} - \frac{L_{2o}}{2} - \left[\left(\frac{L_{2o}}{2}\right)^2 - K\omega^2\right]^{1/2} \tag{6.3.14}$$

Since L_{2o} in Eq. (6.3.13) is approximately independent of frequency, an approximately perfect match over the operating band can be obtained with single-parameter tuning if conditions (6.3.12) are satisfied over the operating band.

At the high end of the band, the condition $R_\text{rad} \ll R_\text{g}$ is not satisfied for $R_\text{g} = 50\,\Omega$ (see Fig. 41). Furthermore, the condition $R_\text{rad} = K\omega^2$ is not physically realizable over large operating bands (see Fig. 42). In Fig. 42, the radiation resistance of Fig. 41 is replotted on log paper whose abscissa corresponds to

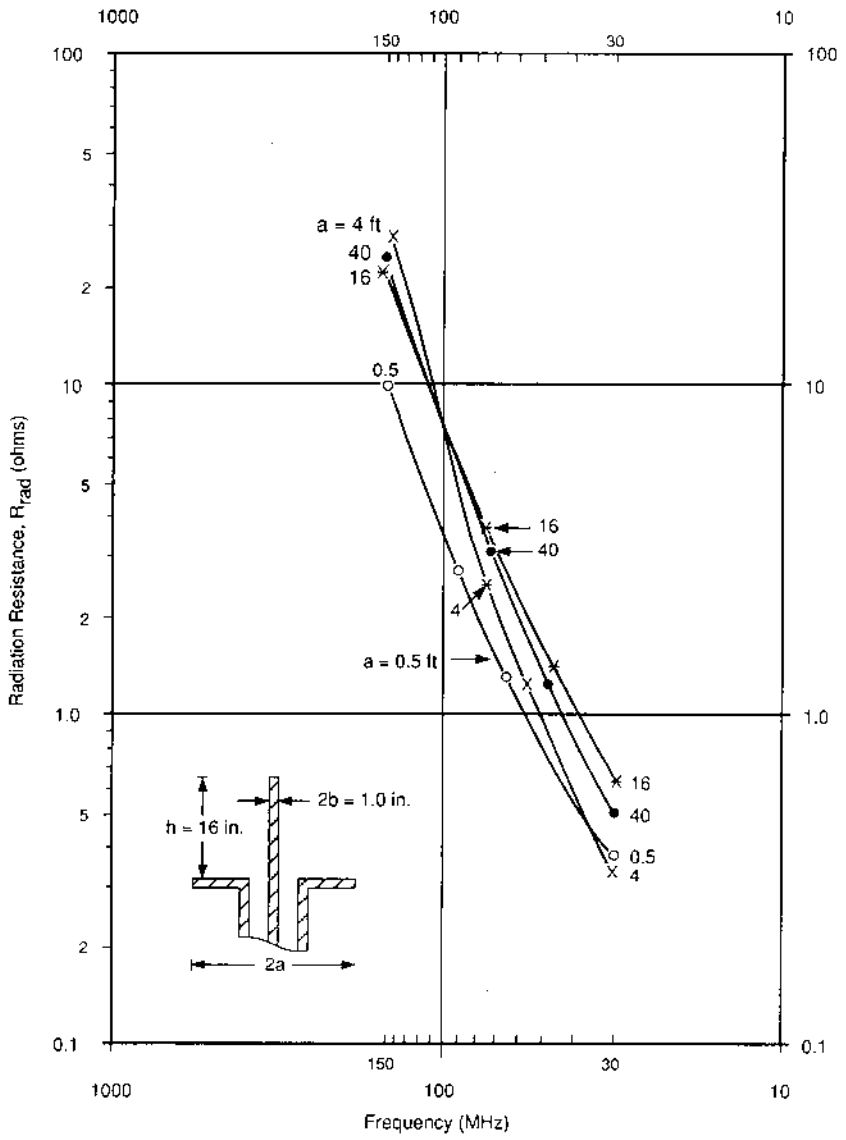

FIGURE 42 Frequency dependence of radiation resistance.

decreasing values of frequency. It will be noted that the plots are not straight lines with a slope of two, as would be the case if the radiation resistance were proportional to the square of the frequency. However, for electrically short, electrically thin, low-loss monopole elements mounted on ground planes that are very much larger than a wavelength, the radiation resistance is approximately proportional to the square of the frequency. For such a case, the constant K is given by Table 4:

$$K = K_{\epsilon \gg 1} = \frac{\eta h^2}{12\pi c^2} \sim 10h^2/c^2; \quad h \ll \lambda, \quad a \gg \lambda, \quad b \ll \lambda \tag{6.3.15}$$

$\epsilon \equiv 2\pi a/\lambda$
$\eta =$ wave impedance of free space $= 376.73\,\Omega \approx 120\pi\,\Omega$
$c =$ wave velocity in free space $= 2.9979 \times 10^8$ m/sec
$h =$ element length
$b =$ element width
$a =$ ground-plane radius.

For the same monopole elements, the condition $R_{\text{rad}} = K\omega^2$ is also physically realizable over small operating bands for ground-plane radii $\epsilon = 2\pi a/\lambda = 0$, 3.6, 5.3, 7.0, 8.5, 10.0, 11.8,... rad for which the derivative of radiation resistance with respect to ground-plane radius (in radians) is zero (see Fig. 9).

The proportionality constant K_ϵ for each of the above ground-plane radii is given by

$$K_\epsilon/K_{\epsilon \gg 1} = d_{\epsilon \gg 1}/d_\epsilon = 0.750/d_\epsilon, \epsilon$$
$$= 0, 3.6, 5.3, 7.0, 8.5, 10.0, 11.8, \ldots \tag{6.3.16}$$

where d_ϵ is the numeric directive gain on the horizon for an electrically short monopole element mounted on a ground plane of radius ϵ (in radians) and where $K_{\epsilon \gg 1}$ is given by Eq. (6.3.15). For $\epsilon = 0$, $K_\epsilon/K_{\epsilon \gg 1} = 0.5$ since $d_0 = 1.5$ (see Table 4).

In summary, single-parameter tuning cannot provide a perfect impedance match over a 5:1 operating band (30–150 MHz) on a ground plane whose radius is either electrically small or comparable to a wavelength. When the monopole element is mounted on the reference ground plane, double-parameter tuning can provide a perfect impedance match over the operating band, whereas in single-parameter tuning, the tuning words can be chosen to provide a perfect impedance match only at one frequency (30 MHz) and to provide zero input reactance at other frequencies.

6.3.2.3 Antenna Gain

It is of interest to determine the antenna gain (including mismatch loss) on the radio horizon (elevation angle $\theta = \pi/2$ rad) as a function of ground-plane radius for the same tuning words that are selected when the monopole element is mounted on the reference ground plane. The antenna gain, $G(\pi/2)$ (decibels relative to isotropic (dBi)), on the radio horizon is given by

$$G(\pi/2) = D(\pi/2) + M + \eta(\text{dBi}) \tag{6.3.17}$$

where

$D(\pi/2)$ = directivity on the horizon of the monopole antenna (dBi)
η = radiation efficiency of the antenna circuit (dB)
M = mismatch gain (= − mismatch loss) of the antenna circuit (dB).

The directivity $D(\pi/2)$ is determined in Sec. 6.3.3 by the method of moments RICHMD2 program

The radiation efficiency, η, is given by

$$\eta = 10\log_{10}\frac{R_{\text{rad}}}{R_{\text{rad}} + R_{\text{ohmic}}}(\text{dB}) \tag{6.3.18}$$

where

R_{ohmic} = series ohmic resistance of antenna system (ohms)
R_{rad} = radiation resistance of the monopole antenna (ohms).

The mismatch gain M is given by

$$M = 10\log_{10}(1 - |\rho|^2)(\text{dB}) \tag{6.3.19}$$

where ρ is the voltage reflection coefficient given by Eq. (6.3.7).

Although the mismatch gain M is determined by specifying the voltage reflection coefficient ρ, it may also be determined by specifying the equivalent voltage standing wave ratio (VSWR) that would be measured along a transmission line between the source generator and the impedance-matching network. The VSWR, ρ, and M are related by

$$\text{VSWR} = \frac{1 + |\rho|}{1 - |\rho|} \tag{6.3.20}$$

$$M = 10\log_{10}\frac{4\text{VSWR}}{(\text{VSWR} + 1)^2}(\text{dB}) \tag{6.3.21}$$

The analytical model does not include the effect of any impedance pad that might be placed between the source generator and the impedance-matching network. A two-port impedance pad between the source generator and

the impedance-matching network does not improve the mismatch gain of the antenna but does help protect the source generator from being damaged by the reflected power from the antenna. The impedance pad reduces the amount of power reflected back to the source generator but also reduces the antenna gain by an amount equal to the insertion loss L (dB) of the pad (for a pad whose input and output impedances are equal to the source impedance when the opposite port is terminated in the source impedance). For example, a pad of 3 dB insertion loss will ensure a VSWR $\leq$ 3:1 between the generator and the pad for any load impedance at the output of the pad. However, the antenna gain will be reduced by 3 dB since the voltage reflection coefficient of the input to the impedance-matching network will be unchanged by the presence of the pad and the power delivered to the antenna will be reduced by 3 dB. For this reason, impedance pads are generally not used in high-power transmitting antennas.

6.3.3 Numerical Results

6.3.3.1 Directivity on the Horizon

The directivity of the monopole antenna was determined by the method of moments RICHMD2 program [4] for each of the above ground planes. The directivity, $D(\pi/2)$, on the radio horizon (elevation angle $\theta = \pi/2$ rad) varies from 1.76 to -0.95 dBi at 30 MHz and 1.81 to -1.95 dBi at 150 MHz (see Fig. 43). For a given ground-plane size, the elevation pattern for the 16 in. length element is within approximately 0.4 dB of that for a quarter-wave element. An electrically short thin element has a directivity on the radio horizon that is less than that of a quarter-wave element by 0.12 dB for very small ground planes and by 0.39 dB for very large ground planes (see Table 4).

6.3.3.2 Radiation Efficiency

The radiation efficiency η of the antenna circuit was determined by substituting into Eq. (6.3.18) the values of radiation resistance R_{rad} plotted in Fig. 44.

Numerical results are given for $R_{\text{ohmic}} = 0$, 1.7 and 7.8 Ω. The matching coil ohmic resistance $R_{\text{ohmic}} = 0$, 1.7, and 7.8 Ω yields radiation efficiencies of 0, -8, and -14 dB, respectively, of the matching network at 30 MHz when the monopole element is mounted on a ground plane of radius $a = 4.0$ ft. The radiation efficiency improves significantly (by several dB) with increasing frequency but is only weakly dependent (varies by approximately 2 dB) upon ground-plane radius (see Fig. 44).

6.3.3.3 Mismatch Gain

The mismatch gain M at 30 MHz as a function of ground-plane radius is plotted in Fig. 45 for the tuning conditions given by Eqs. (6.3.10) and (6.3.11). The range of

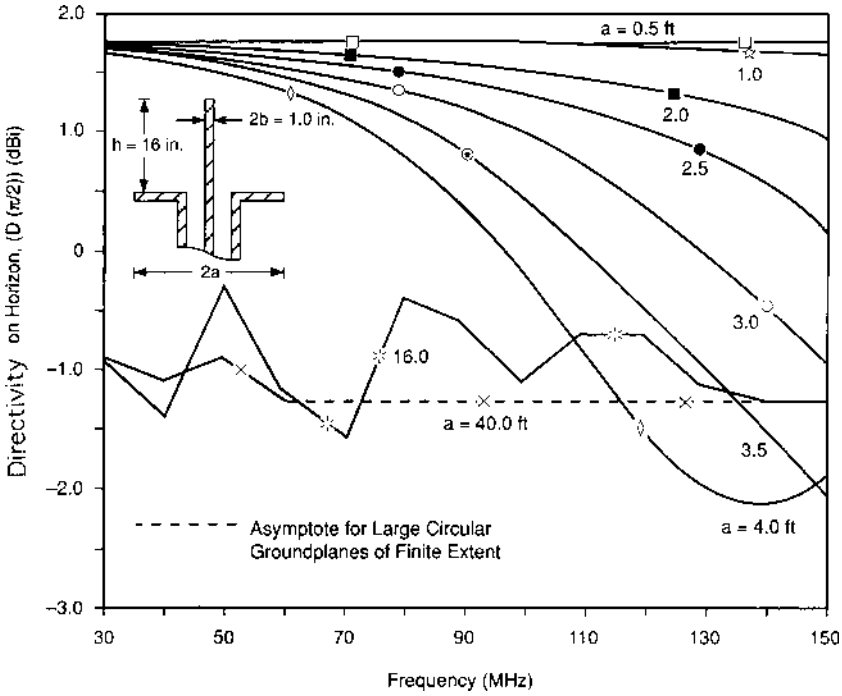

FIGURE 43 Directivity on horizon of electrically small element on ground plane of radius $a = 0.5$–40 ft.

ground-plane radii, for which the mismatch loss (= − mismatch gain in dB) does not exceed a specified level, increases with increasing ohmic resistance. The range of ground-plane radii, for which the mismatch loss is within 3 dB, is approximately 4–16, 3–16, and 2–16 ft for $R_{\text{ohmic}} = 0$, 1.7, and 7.8 Ω, respectively. With very small and very large ground-plane radii, the mismatch loss can exceed 90 dB for $R_{\text{ohmic}} = 0\,\Omega$.

6.3.3.4 Antenna Gain on the Horizon

The antenna gain on the radio horizon, $G(\pi/2)$, at 30 MHz is plotted in Fig. 46 as a function of ground-plane radius. Although the antenna gain is plotted as a continuous curve, please note the discontinuities in the abscissa and that the only data points for ground-plane radii $a \geq 4$ ft are for $a = 4$, 16, and 40 ft. At 30 MHz, the antenna horizon gain as a function of ground-plane radii is a maximum for ground-plane radii approximately equal to that of the reference ground plane with gains of 2, −6, and −12 dBi for $R_{\text{ohmic}} = 0$, 1.7, and 7.8 Ω,

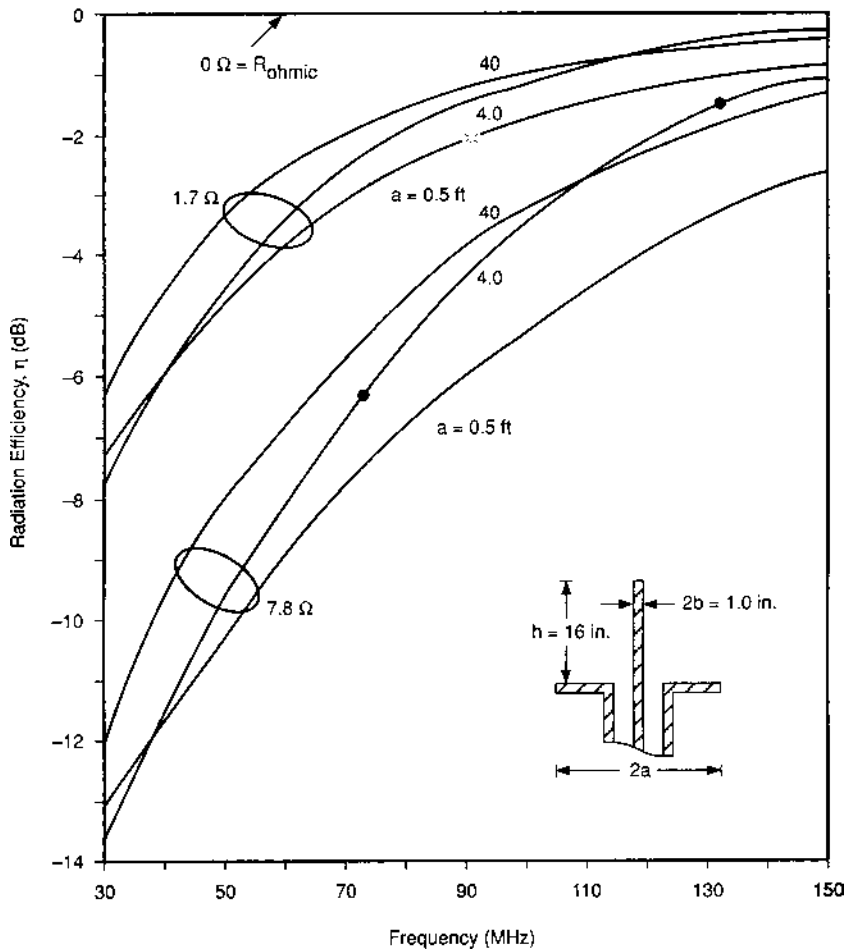

FIGURE 44 Radiation efficiency for system ohmic resistances of 0, 1.7, and 7.8 Ω.

respectively. The range of ground-plane radii a, for which the horizon gain is within 3 dB of the maximum horizon gain, is $4 \leq a \leq 16$, $3 \leq a \leq 16$, and $2 \leq a \leq 16$ ft for $R_{\text{ohmic}} = 0$, 1.7, and 7.8 Ω, respectively. These results are independent of whether double- or single-parameter tuning is utilized, because at 30 MHz the tuning words are identical for double- and single-parameter tuning. The maximum antenna gain on the horizon as a function of ground-plane radius generally *decreases* with increasing values of R_{ohmic}, whereas the range of

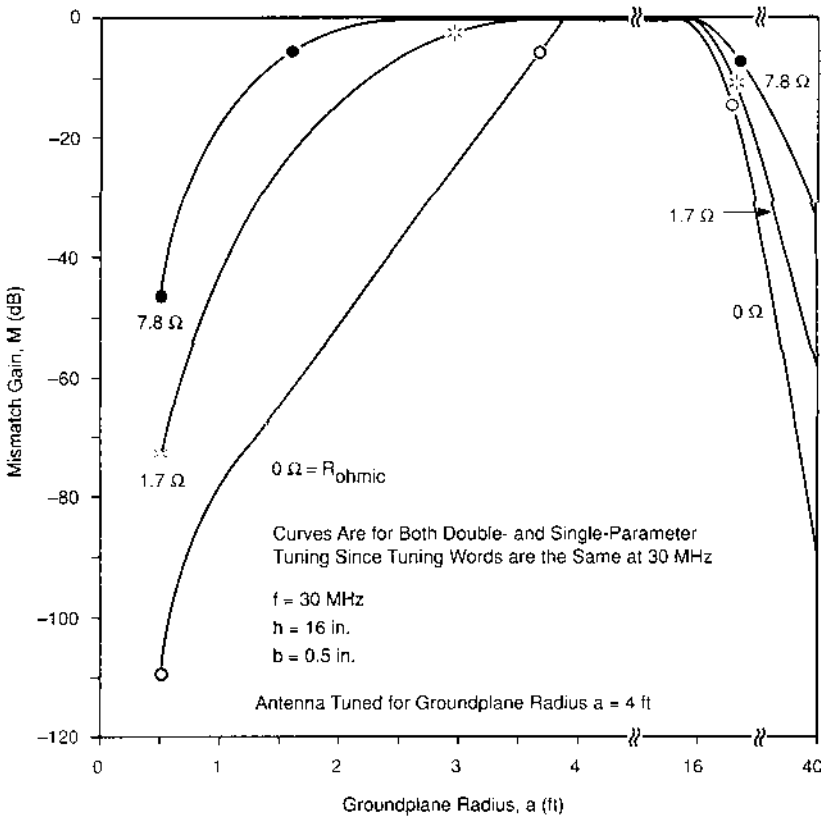

FIGURE 45 Mismatch gain at 30 MHz.

ground-plane radii for which the gain is within 3 dB of the maximum gain generally *increases* with increasing values of R_{ohmic}.

The antenna gain on the radio horizon for the monopole element mounted on the reference ground plane of radius $a = 4$ ft is plotted as a function of frequency in Fig. 47. The discontinuity in antenna gain for single-parameter tuning at 110 MHz for $R_{\text{ohmic}} = 7.8\,\Omega$ is because of a change in the algorithm for L_{1o} when $R_o(\omega) > \omega L_{2o}/2$ (see (11)). The antenna gain at any frequency over the frequency band is larger with double-parameter tuning than with single-parameter tuning. For zero-ohmic loss, $G(\pi/2)$ over the entire frequency band is greater than -2 and -7 dBi with double-parameter and single-parameter tuning, respectively. Unfortunately, as we mentioned earlier, the tuning stability as

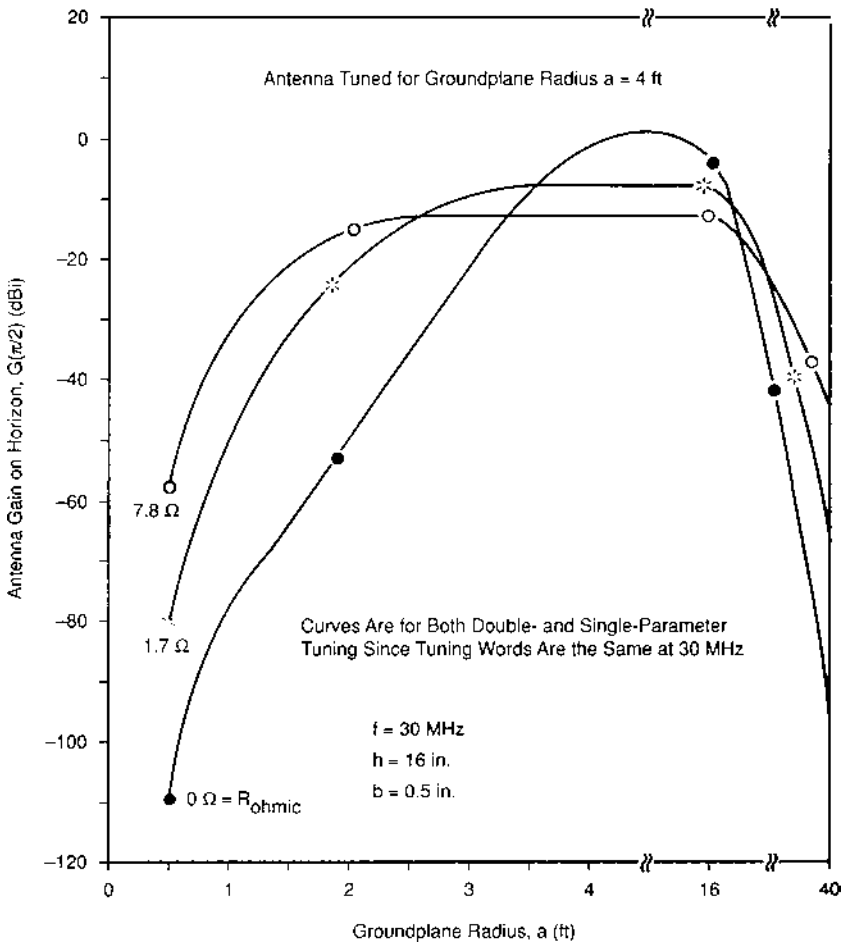

FIGURE 46 Antenna gain on horizon at 30 MHz.

a function of ground-plane radius is not significantly better with double-parameter tuning than with single-parameter tuning.

6.3.4 Conclusions

Double-parameter and single-parameter tuning of an electrically short monopole antenna are investigated above to determine the range of ground-plane radii for which the same tuning words can be utilized in maintaining a specified antenna gain over the 30–150 MHz frequency band.

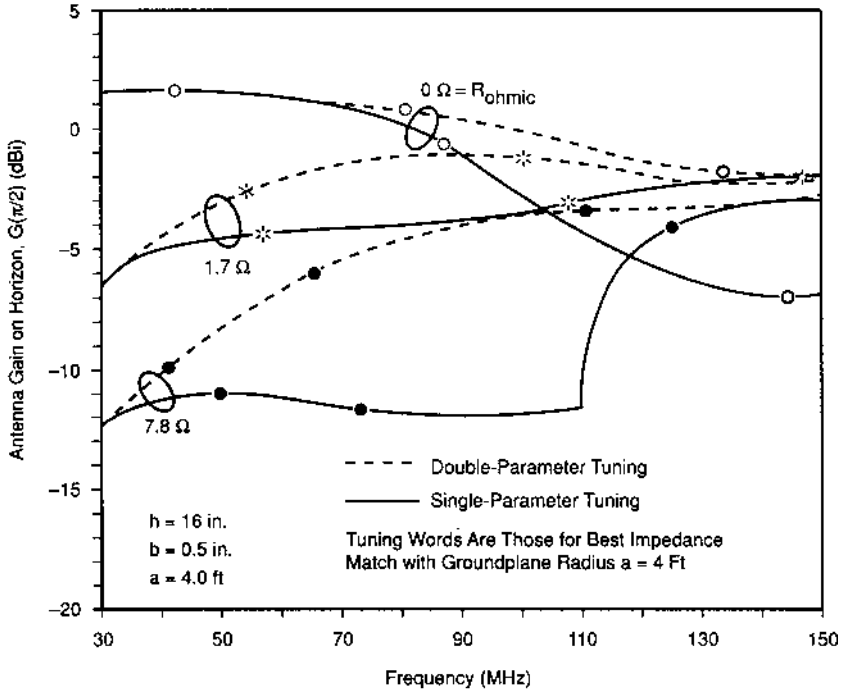

FIGURE 47 Antenna gain on horizon, $a = 4.0$ ft.

In double-parameter tuning, the tuning words are chosen by varying two inductances of the impedance-matching network to provide a perfect impedance match at each frequency of interest when the antenna is mounted on a reference ground plane of 4 ft in radius. In single-parameter tuning, the tuning words are chosen by varying one inductance to provide a perfect impedance match at 30 MHz and zero input reactance at other frequencies when the antenna is mounted on a ground plane of 4 ft in radius.

Edge diffraction by the circular ground plane significantly alters the antenna input impedance so that it is not possible to utilize the same tuning words to provide a good impedance match for ground-plane radii appreciably different from the radius of the reference ground plane and, in the case of single-parameter tuning, even for the reference ground plane.

The maximum antenna gain on the horizon as a function of ground-plane radius is generally greater with double-parameter tuning than with single-parameter tuning. The range of ground-plane radii for which the gain is within

3 dB of the maximum gain, however, is generally not significantly increased with double-parameter tuning.

The maximum antenna gain on the horizon as a function of ground-plane radius generally decreases with increasing ohmic resistance R_{ohmic} of the antenna circuit, whereas the range of ground-plane radii for which the gain is within 3 dB of the maximum gain generally increases with increasing values of R_{ohmic}.

The antenna gain on the horizon as a function of ground-plane radius is a maximum at 30 MHz for any given ground plane except the reference ground plane. For example, the antenna gain is 40–100 dB less at 30 MHz than at 150 MHz for ground-plane radii much less or greater than the radius of the reference ground plane [5]. Obviously, such large mismatch losses are not tolerable, either for a transmitting antenna or for a receiving system whose external noise factor is comparable to or less than the mismatch loss.

At 3 MHz the antenna gain on the horizon as a function of ground-plane radius is a maximum for ground-plane radii approximately equal to the radius of the reference ground plane with gains of 2, -6, and -12 dBi for $R_{\text{ohmic}} = 0$, 1.7, and 7.8 Ω, respectively. At 30 MHz, the range of ground-plane radii a, for which the horizon gain is within 3 dB of the maximum horizon gain, is $4 \leq a \leq 16$, $3 \leq a \leq 16$ and $2 \leq a \leq 16$ ft for $R_{\text{ohmic}} = 0$, 1.7, and 7.8 Ω, respectively.

It is concluded that it may not be possible to use the same tuning words for all ground planes of interest without a substantial loss in antenna gain because of mismatch loss at some frequencies, particularly at the lower end of the band. Therefore, it may be necessary to have different tuning words for different ground planes.

Different tuning words for different ground planes may be implemented by utilizing more than one antenna configuration or by sensing in real time the impedance mismatch and then modifying the tuning word at a given frequency to minimize the impedance mismatch.

The latter method is preferable, because it would

1. Eliminate the difficult logistics problem of having to field several antenna configurations for different ground planes.
2. Solve the problem of tuning instabilities arising from environmental changes in humidity and temperature in addition to that of ground-plane size.
3. Improve the antenna radiation efficiency, since it would not be necessary to load the antenna circuit with antenna loss in order to provide tuning stability.

An alternative to the implementation of different tuning words for different platforms might be to utilize a different antenna element, such as a dipole, whose input impedance might not be as sensitive to ground-plane size as that of a monopole. However, even if such an element would prove to have better tuning

stability with varying ground-plane size and to have the desired gain pattern characteristics, it is not clear how such an alternative would solve the problem of tuning instabilities arising from changes in humidity and temperature without having to load the antenna circuit with antenna loss in order to provide tuning stability.

Consequently, implementation of different tuning words, by sensing in real time, the impedance mismatch and then modifying the tuning word at a given frequency to minimize the impedance mismatch, is a preferable design objective. Such an objective has been realized at HF frequencies and for a radio frequency (RF) power level of 400 W with sensing and tuning times of approximately 20 μsec and 1 sec, respectively, by a circuit comprising a directional coupler, digital processor, and electromechanical switches. The substitution of p-type/-intrinsic type/n-type (PIN) diode switches for the electromechanical switches might prove to be a feasible technique for achieving such an objective with a tuning time of less than 1 msec, provided that the intermodulation products generated by the use of such switches are not excessive for the intended application.

Electronically tunable helical elements utilizing PIN diode switches (see Sec. 6.2.9) have been successfully designed and tested in an open loop mode with an RF power level of 10 W at VHF frequencies and 400 W at HF frequencies [35]. Closed-loop operation is compatible with the fast tuning capability of PIN diode switches but its realization has not yet been reported in the open literature.

6.4 NOISE FACTOR OF RECEIVING SYSTEMS WITH ARBITRARY ANTENNA IMPEDANCE MISMATCH

6.4.1 Introduction

The system operating noise factor of a receiving system whose antenna is impedance-matched to the transmission line feeding the receiver is usually limited by the receiver noise factor at frequencies above 100–300 MHz and by the antenna external noise factor at frequencies below 100–300 MHz [37,38]. However, for large impedance mismatch, the noise factors of the transmission line and receiver [39,40] can be significantly increased. For such a case, the system operating noise factor can be limited by the transmission line or receiver noise factors. This case is of particular interest to VHF and HF receiving systems with electrically short antennas.

The noise factor of the transmission line increases with increasing mismatch source impedance of the line to its characteristic impedance, because of the decreased available signal power at the output of the line.

The noise factor of the receiver, as in any linear two-port network, increases with increasing difference of its source impedance from that designed (usually 50 Ω if fed by a transmission line with 50 Ω characteristic impedance) for minimum noise factor. This property is a consequence of the equivalent circuit representation, of any two-port network with internally generated noise, by a complex noise current generator and a complex noise voltage generator in parallel and series, respectively, with the noise-free two-port network [40]. Thus, a large impedance mismatch at the antenna transmission line interface may cause the source impedance of the receiver to be substantially different from 50 Ω and consequently may cause an appreciably increased noise factor of the receiver.

Although the qualitative effects of antenna impedance mismatch on the noise factors of the transmission line and receiver are generally recognized, quantitative analyses of the combined effects are not readily found in the literature. For example, it is common to find in such analyses that the noise factor dependency upon source impedance of either the transmission line or receiver or both is ignored [41].

Sec. 6.4 presents a detailed model of the system operating noise factor in a receiving system with arbitrary antenna impedance mismatch. The increases in the noise factors of the transmission line and the receiver with increasing mismatch are considered. The stochastic nature of the external noise factor is also considered. The amount of mismatch that can be tolerated before the internal system noise factor exceeds the external noise factor is determined. Numerical results are presented for a VHF–FM radio receiving system with an electrically short monopole antenna.

6.4.2 Analytical Model

6.4.2.1 System Operating Noise Factor

With reference to Fig. 48, the predetection system margin $M(d, r_i)$ (in dB) of a radio system for a propagation path distance d and message quality r_i is given by

$$M(d, r_i) = \overbrace{P_T - l_{n,T} + G_T - L_b(d) + D_R}^{S(d)} - N - R_r(r_i) \tag{6.4.1}$$

where

$S(d)$ = available signal power at the output terminals of the equivalent lossless receiving antenna (dBm)

P_T = transmitter–carrier available output power (dBm)

$L_{N,T}$ = insertion loss of transmitter transmission line (including reflection losses, if any) (dB)

G_T = transmitter antenna gain (including ohmic losses of matching network, if any) (dB)

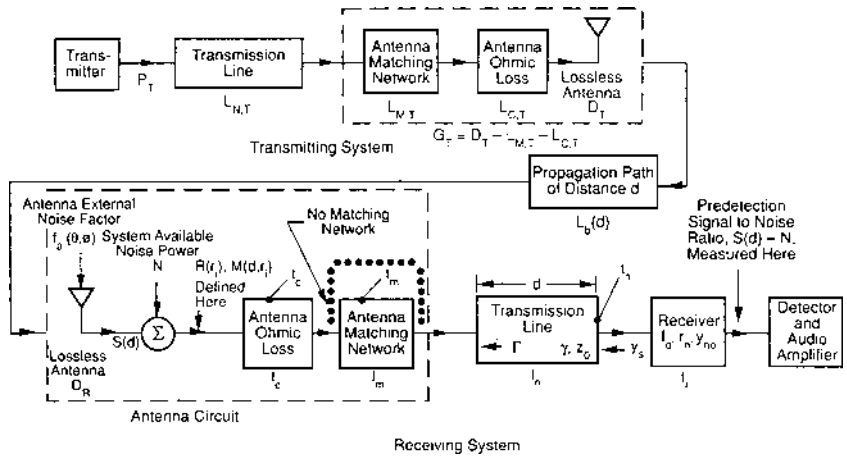

FIGURE 48 System margin parameters of radio system.

$L_b(d)$ = basic transmission loss of propagation path (dB)

D_R = directivity of the receiving antenna (dBi)

N = system-available noise power referred to the output terminals of the equivalent lossless receiving antenna (dBm)

$R_r(r_i)$ = predetection signal-to-noise ratio for a required message quality r_i (dB). For example, for a digital signal input, r_i is the required message bit error probability.

The convention is followed that capitalized margin parameters are in units of decibels whereas uncapitalized margin parameters refer to their numerical values. In Fig. 48, the signal-to-noise ratio referred to the output terminals of the equivalent lossless antenna is defined to be equal to the predetection signal-to-noise ratio of the receiver.

The system-available noise power N in Eq. (6.4.1) referred to the output terminals of the equivalent lossless receiving antenna (see Fig. 48) is the time-averaged power contributed by all noise sources, both internal and external to the receiver system, that would be delivered by the lossless antenna to a load if the load impedance were set equal to the conjugate output impedance of the lossless antenna. Examples of external noise sources are the atmosphere, stars, man-made environment (power lines, automobile ignition systems, etc.), and jammers both hostile and friendly. Internal noise sources are the receiver, antenna matching network, and transmission line of the receiving system.

The system-available noise power N (dBm) may be expressed as

$$N = N_{\text{ref}} + F \tag{6.4.2}$$

where N_{ref} is the system reference noise power (dBm), and F is the system operating noise figure, referenced to N_{ref} (dB). The system reference noise power N_{ref} is given by

$$N_{\text{ref}} = 30 + 10\log_{10}(kt_{\text{ref}}b)\ \ (\text{dBm}) \tag{6.4.3}$$

where k is Boltzmann's constant $= 1.38 \times 10^{-23}$ J/K, t_{ref} is the reference noise temperature $= 288$K, and b is the receiver noise power effective bandwidth (Hz). It is convenient to set $t_{\text{ref}} = 288$K because measurements of atmospheric noise and man-made environmental noise are usually referenced to thermal noise at that temperature and because $10\log_{10} kt_{\text{ref}} = -204.0059$ dB relative to one joule is approximately a whole number [42].

The system operating noise figure F may be expressed as

$$F = 10\log_{10} f \tag{6.4.4}$$

where

$f = [s_i/n_{\text{ref}}]/[s_0/n_0]$ = system operating noise factor (numeric)
$s_i = s(d)$ = available signal power at the input to the receiving system (W)
$n_{\text{ref}} = kt_{\text{ref}}b$ = reference noise power (W)
s_0 = available signal power at the output of the receiver (W)
n_0 = available noise power at the output of the receiver (W)

With reference to Fig. 48, the system operating noise factor f is given by [42].

$$f = f_{\text{a}} + (l_{\text{c}} - 1)\frac{t_{\text{c}}}{t_{\text{ref}}} + l_{\text{c}}(l_{\text{m}} - 1)\frac{t_{\text{m}}}{t_{\text{ref}}} + l_{\text{c}}\, l_{\text{m}}(l_{\text{n}} - 1)\frac{t_{\text{n}}}{t_{\text{ref}}}$$
$$+ l_{\text{c}}\, l_{\text{m}}\, l_{\text{n}}(f_{\text{r}} - 1) \tag{6.4.5}$$

where f_{a} is the receiving antenna external noise factor integrated over the antenna pattern function (numeric), l_{c}, l_{m}, l_{n} are the available loss factors of the receiving antenna, matching network, and transmission line, respectively (numeric), t_{c}, t_{m}, t_{n} are the ambient temperatures of the receiving antenna, matching network, and transmission line, respectively (degrees Kelvin), and f_{r} is the receiver noise factor (numeric). If the ambient temperatures of the antenna, matching network, and transmission line are equal to the reference temperature t_{ref}, then Eq. (6.4.5) reduces to

$$f = f_{\text{a}} - 1 + l_{\text{c}}\, l_{\text{m}}\, l_{\text{n}} f_{\text{r}}; \quad t_{\text{c}} = t_{\text{m}} = t_{\text{n}} = t_{\text{ref}} \tag{6.4.6}$$

6.4.2.2 Statistical Dependence

The parameters of Eq. (6.4.5) are treated as deterministic quantities with the exception of the antenna external noise factor f_a, which is treated as a stochastic variable. Examples of stochastic external noise sources are the atmosphere and man-made noise sources such as power lines and automobile ignitions. Expected values and standard deviations of man-made noise for business, residential, and rural areas are given in [38].

The expected value $\langle f \rangle$ and standard deviation σ_f of the operating noise factor f are therefore given by

$$\langle f \rangle = \langle f_a \rangle + (l_c - 1)\frac{t_c}{t_{ref}} + l_c(l_m - 1)\frac{t_m}{t_{ref}} + l_c\, l_m(l_n - 1)\frac{t_n}{t_{ref}} + l_c\, l_m\, l_n(f_r - 1) \tag{6.4.7}$$

$$\sigma_f = \sigma_{f_a} \tag{6.4.8}$$

where $\langle f_a \rangle$ and σ_{f_a} are the expected value and standard deviation, respectively, of the external noise factor f_a.

The external noise factor f_a is related by definition to the external noise figure F_a (in dB) by

$$f_a \equiv 10^{(F_a/10)}; \quad F_a \equiv 10\log_{10} f_a \tag{6.4.9}$$

When man-made noise is the dominant noise source, F_a (dB) is approximately two-piecewise normally distributed with a breakpoint at the median value [40]. Nevertheless, if the external noise F_a is assumed to be approximately normally distributed, then from Eq. (6.4.9), the external noise factor f_a is lognormally distributed. For such distributions, the expected values and standard deviations of the two distributions are related by [43]

$$\langle f_a \rangle = 10^{[(\langle F_a \rangle/10)+(1/2)\ln 10(\sigma_{F_a}/10)^2]} \tag{6.4.10}$$

$$\sigma_{f_a} = \langle f_a \rangle [10^{\ln 10(\sigma_{F_a}/10)^2} - 1]^{1/2} \tag{6.4.11}$$

Similarly, if the operating noise factor f is assumed to be approximately lognormally distributed, then from Eq. (6.4.4), the operating noise figure F is normally distributed. For such distributions, the expected values and standard

deviations of the two distributions are related by

$$\langle F\rangle = 10\left[\log_{10}\langle f\rangle - \frac{1}{2}\ln 10\left(\frac{\sigma_F}{10}\right)^2\right] \tag{6.4.12}$$

$$\sigma_F = 10\left\{\frac{1}{\ln 10}\log_{10}\left[1+\left(\frac{\sigma_f}{\langle f\rangle}\right)^2\right]\right\}^{1/2} \tag{6.4.13}$$

where $\langle f\rangle$ and σ_f are given by Eqs. (6.4.7) and (6.4.8).

For the purpose of distinguishing between external and internal noise, it is useful to define a receiving system noise degradation figure ΔF (dB) by

$$\Delta F \equiv F - F_a(\text{dB}) \tag{6.4.14}$$

The noise degradation figure ΔF is the system operating noise figure relative to the antenna external noise figure and is a measure of the contribution of the internal noise sources to the system operating noise figure. The expected value $\langle \Delta F\rangle$ is given by

$$\langle \Delta F\rangle = \langle F\rangle - \langle F_a\rangle(\text{dB}) \tag{6.4.15}$$

where $\langle F\rangle$ is given by Eq. (6.4.12).

The external noise which is incident on the receiving antenna within a differential solid angle at an elevation angle θ and azimuthal angle ϕ (see Fig. 48) must be integrated over the entire sphere of the directional gain pattern of the antenna to obtain the total external noise at the output terminals of the equivalent lossless antenna. Accordingly, the external noise factor $\langle f_a\rangle$ is given by

$$\langle f_a\rangle = \frac{1}{4\pi}\int_0^{2\pi}\int_{-\pi/2}^{\pi/2}\langle f_a(\theta,\phi)\rangle d_r(\theta,\phi)\ \sin\theta\ d\theta\ d\phi \tag{6.4.16}$$

where $d_r(\theta,\phi)$ is the receiver directive gain in the elevation and azimuthal directions θ and ϕ, respectively (numeric), and $\langle f_a(\theta,\phi)\rangle$ is the expected value of the antenna noise factor in the elevation and azimuthal directions θ and ϕ, respectively (numeric).

The factor $\sin\theta$ is included in the integrand because the integration is in spherical coordinates.

6.4.2.3 Available Loss Factors

The receiving system available loss factors l_c, l_m, l_n of the antenna, matching network, and transmission line, respectively, are given by

$$l_c = 1 + \frac{r_c}{r_a} \tag{6.4.17}$$

$$l_m = 1 + \frac{r_m + r_s}{r_a + r_c} \tag{6.4.18}$$

$$l_n = \frac{\exp(2\alpha d)\{1 - |\Gamma|^2 \exp(-4\alpha d) - 2[\mathrm{Im}(z_0)/\mathrm{Re}(z_0)]\mathrm{Im}[\Gamma \exp(-2\gamma d)]\}}{1 - |\Gamma|^2 - 2[\mathrm{Im}(z_0)/\mathrm{Re}(z_0)]\mathrm{Im}(\Gamma)} \tag{6.4.19}$$

where r_a, r_c, r_m, r_s, z_0, $\gamma = \alpha + j\beta$, d, Γ, and z are circuit parameters defined in Fig. 49 of the impedance equivalent circuit of the receiving system.

In Eq. (6.4.19) the transmission line available loss factor l_n increases with increasing modulus of the voltage reflection coefficient at the antenna

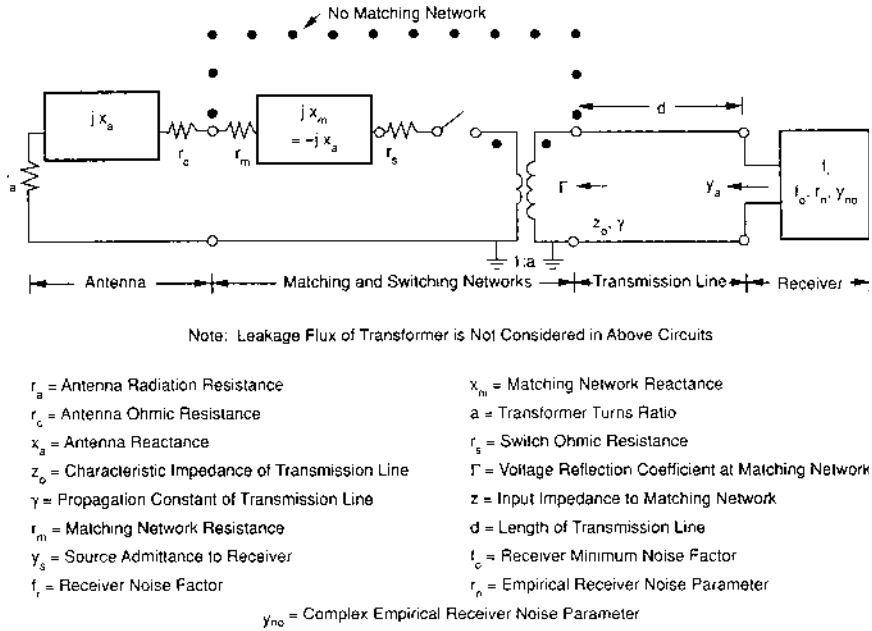
No Matching Network
j x_a
r_c
r_m
j x_m
= −j x_a
r_s
d
Γ
y_a
f_c, r_n, y_no
z_0, γ
1:a
Antenna
Matching and Switching Networks
Transmission Line
Receiver
Note: Leakage Flux of Transformer is Not Considered in Above Circuits
r_a = Antenna Radiation Resistance
r_c = Antenna Ohmic Resistance
x_a = Antenna Reactance
z_o = Characteristic Impedance of Transmission Line
γ = Propagation Constant of Transmission Line
r_m = Matching Network Resistance
y_s = Source Admittance to Receiver
f_r = Receiver Noise Factor
x_m = Matching Network Reactance
a = Transformer Turns Ratio
r_s = Switch Ohmic Resistance
Γ = Voltage Reflection Coefficient at Matching Network
z = Input Impedance to Matching Network
d = Length of Transmission Line
f_c = Receiver Minimum Noise Factor
r_n = Empirical Receiver Noise Parameter
y_no = Complex Empirical Receiver Noise Parameter

FIGURE 49 Impedance equivalent circuit of receiving system.

transmission line interface. For $\Gamma = 0$, $l_n = \exp(2\alpha d)$. For $\Gamma \rightarrow 1 + j0$

$$\lim l_n = \begin{cases} \infty, & \alpha d \neq 0 \\ 1, & \alpha d = 0 \end{cases}$$

The reason for these limits is that l_n is a function of available powers and not transmitted powers.

The voltage reflection coefficient Γ is given by

$$\Gamma = \frac{z - z_0}{z + z_0} \tag{6.4.20}$$

The input impedance z to the antenna circuit, including the matching network, is given by

$$\begin{aligned} z &= a^2[(r_a + r_c + r_m + r_s) + j(x_a + x_m)] \\ &= \begin{cases} z_0, & \text{antenna conjugate–matched to transmission line.} \\ r_a + r_c + jx_a, & \text{no matching network} \end{cases} \end{aligned} \tag{6.4.21}$$

When the antenna is conjugate impedance matched ($\Gamma = 0$) to a transmission line by the matching network, then the matching network parameters x_m and a are given by

$$\begin{aligned} x_m &= -x_a + \frac{1}{a^2}\mathrm{Im}(z_0) \\ a &= \left[\frac{\mathrm{Re}(z_0)}{r_a + r_c + r_m + r_s}\right]^{1/2} \end{aligned} \tag{6.4.22}$$

where $\Gamma = 0$. In the absence of any matching network,

$$\begin{aligned} x_m &= 0 = r_m = r_s \\ a &= 1 \end{aligned} \tag{6.4.23}$$

where there is no matching network.

6.4.2.4 Receiver Noise Factor

The receiver noise factor f_r is a function of the source admittance y_s seen by the receiver looking back at the transmission line (see Fig. 49) and consequently is

a function of antenna impedance mismatch. The source admittance y_s is given by

$$y_s = \frac{1}{z_0}\left[\frac{1-\Gamma\exp(-2\gamma d)}{1+\Gamma\exp(-2\gamma d)}\right] \tag{6.4.24}$$

where z_0, Γ, γ, and d are defined in Fig. 49.

The receiver noise factor f_r, for an arbitrary source admittance y_s at an ambient temperature equal to the reference temperature t_{ref}, is given by [39],[40]

$$f_r = f_0 + \frac{r_n}{\mathrm{Re}(y_s)}|y_s - y_{n0}|^2 \tag{6.4.25}$$

where f_0 is the minimum noise factor of the receiver for any possible source admittance y_s at an ambient temperature equal to the reference temperature t_{ref}, $y_{n0} = g_{n0} + jb_{n0}$ is the complex empirical receiver noise parameter with the dimensions of admittance (ohms), and r_n is the empirical receiver noise parameter with the dimensions of resistance, which accounts for the sensitivity of the receiver noise factor to the receiver source impedance (ohms).

The receiver noise factor f_r has a minimum value f_0 for a source admittance $y_s = y_{n0}$. Most receivers are designed to have a minimum noise factor f_0 for a source admittance $y_s = 1/z_0$. For such a condition, the receiver input impedance is generally not matched to the characteristic impedance of the transmission line, and the receiver noise factor f_r increases with increasing impedance mismatch of the antenna to the transmission line. For $|\Gamma| = 0$, $f_r = f_0$, whereas for $|\Gamma| = 1$, $f_0 \le f_r < \infty$. In particular for the case $|\Gamma| = 1$,

$$\lim f_r = \begin{cases} f_0, & \alpha d \to \infty \\ \infty, & \gamma d \to 0 + j0 \end{cases} \tag{6.4.26}$$

For $\alpha d = \infty$ and $|\Gamma| = 1$, the receiver noise factor is a minimum, whereas the transmission line noise factor is a maximum [see the limits following Eq. (6.4.19)].

6.4.3 Numerical Results

The effect of antenna impedance mismatch on the operating noise figure of a radio receiving system is numerically evaluated for the case of a VHF–FM receiver with an electrically short monopole antenna. For such a case, in the absence of a matching network, the real part of the antenna input impedance can be of the order of one ohm or less and the imaginary part can be of the order of several hundred ohms or more. Therefore, the antenna presents a large impedance mismatch to a 50 Ω transmission line. When matched, the VHF–FM receiving system is generally limited by external environmental noise which may be two or three orders of magnitude larger than receiver noise. Consequently, such a case is

a severe test of the effect of antenna impedance mismatch on the system operating noise figure.

Numerical evaluation of the theoretical model of the second section for the above case was facilitated by the MITRE computer program system operating noise figure (SONF), Numerical values are calculated at 30, 50, and 88 MHz for man-made environmental noise in rural, residential, and business area locations. The system comprises a monopole antenna of 10 in. in length and 1.4 in. in diameter, a matching network solenoid of 1.5 in. in length and 0.5 in. in diameter, a PIN diode switch of 0.25 Ω series resistance, a 10 m length of RG-58/U coaxial transmission line, and a receiver with noise parameters $f_0 = 5$ and $r_n = 100\ \Omega$.

The receiving system noise and available loss factors are summarized in Table 10. The modulus $|\Gamma|$ of the voltage reflection coefficient, at the transmission-line/antenna interface and looking in the direction of the antenna, is $|\Gamma| = 0.9966 - 0.9991$ without a matching network and $|\Gamma| = 0$ with a matching network over the frequency range 30–88 MHz. In the presence of a matching network, the system operating noise factor $\langle f \rangle$ is approximately equal to the antenna external noise factor $\langle f_a \rangle$. However, in the absence of a matching network, the system operating noise factor is appreciably larger than the antenna external noise because the product $f_r l_n \gg \langle f_a \rangle$ where f_r is the receiver noise factor and l_n is the transmission line available loss factor.

The system noise degradation figure $\langle \Delta F \rangle$ is 26.0–5.8 dB without a matching network and 1.23–0.01 dB with a matching network (see Table 11). In the absence of a matching network, the noise degradation figure decreases with increasing man-made noise because $\langle \Delta F \rangle$ is defined relative to man-made noise. The noise degradation figure decreases with increasing frequency because $|\Gamma|$ decreases with increasing frequency.

For a large mismatch of the antenna impedance to the transmission line, the combined noise figure of the transmission line and receiver remains large regardless of line length (see Fig. 50). Smaller line lengths result in a smaller transmission-line noise figure (because of less ohmic loss) but a larger receiver noise figure (because of less padding by the transmission line of the antenna impedance mismatch). When the antenna impedance is matched to the transmission line, the transmission-line noise figure is limited to that resulting from the ordinary exponential attenuation loss of the transmission line. For arbitrary values of the receiver noise parameter r_n there exists a line length for which the combined noise figure of the transmission line and receiver is minimized. In Fig. 50, it is fortuitous for $r_n = 100$ ohm that the combined noise figure is approximately independent of line length for line lengths less than 0.1 wavelength.

TABLE 10 Noise Parameter Factors for Receiving System with Electrically Short Monopole Antenna

		Noise factor (Relative to 288K thermal noise			Available loss factors			
Frequency (MHz)	Man-made noise location	System operating $\langle f \rangle$	Antenna external $\langle f_a \rangle$	Receiver $\langle f_r \rangle$	Antenna ohmic (l_c)	Matching network (l_m)	Transmission line (l_n)	Voltage reflection coefficient $\lvert\Gamma\rvert$
Without matching network								
	Business	209400.0	41860.0	22.71	1.004	1.0	7348.0	
30	Residential	176600.0	9106.0	22.71	1.004	1.0	7348.0	0.9991
	Rural	168600.0	1096.0	22.71	1.004	1.0	7348.0	
	Business	42990.0	20560.0	17.81	1.002	1.0	1257.0	
50	Residential	24920.0	2488.0	17.81	1.002	1.0	1257.0	0.9986
	Rural	22600.0	1720.0	17.81	1.002	1.0	1257.0	
	Business	5016.0	2551.0	13.44	1.001	1.0	183.4	
88	Residential	2831.0	366.4	13.44	1.001	1.0	183.4	0.9966
	Rural	2515.0	49.9	13.44	1.001	1.0	183.4	
With matching network								
	Business	41940.0	41860.0	5.03	1.004	12.88	1.208	
30	Residential	9184.0	9106.0	5.03	1.004	12.88	1.208	0
	Rural	1174.0	1096.0	5.03	1.004	12.88	1.208	
	Business	20580.0	20560.0	5.03	1.002	3.18	1.278	
50	Residential	2507.0	2488.0	5.03	1.002	3.18	1.278	0
	Rural	1915.0	1720.0	5.03	1.002	3.18	1.278	
	Business	2559.0	2551.0	5.03	1.001	1.367	1.39	
88	Residential	375.0	366.4	5.03	1.001	1.367	1.39	0
	Rural	58.5	49.9	5.03	1.001	1.367	1.39	

$\langle f \rangle = \langle f_a \rangle - 1 + l_c l_m l_n f_r$.
Antenna: 10 in. monopole 1.4 in. diameter.
Matching network: coil, 0.5 in. diameter, single-layer, 1.5 in. length.
Switch: PIN diode, 0.25 Ω resistance.
Transmission line: RG-58 Coaxial line,10 m length.
Receiver: $f_a = 5$, $r_n = 100\,\Omega$

TABLE 11 System Noise Degradation Figure for a Receiver with an Electrically Short Monopole Antenna

Frequency f(MHz)	Expected value of noise degradation figure $\langle \Delta F \rangle = \langle F\acute{A} - \langle F_a \rangle$ (dB)					
	With matching network			No matching network		
	Rural	Residential	Business	Rural	Residential	Business
30	0.547	0.073	0.016	26.0	20.7	13.6
50	0.753	0.067	0.008	23.4	17.6	6.4
88	1.229	0.197	0.029	20.7	15.1	5.8

Antenna: 10 in. monopole, 1.4 in. diameter.
Matching network: coil, 0.5 in. diameter, single layer, 1.5 in. length.
Switch: PIN diode, 0.25 Ω resistance.
Transmission line: RG-58/U Coaxial line, 10 m length.
Receiver: $f_0 = 5$, $r_n = 100\,\Omega$.

6.4.4 Conclusions

A large impedance mismatch at the antenna/transmission-line interface of a radio receiving system can cause a significant increase in the system internal noise factor (more than a 50 dB increase for a voltage reflection coefficient of 0.999). This conclusion is supported by numerical results for a VHF–FM radio receiving system with an electrically short monopole antenna. In the absence of a matching network, the limiting noise of the system is generated within the system (by the transmission line and receiver) and can be more than 20 dB larger than the external man-made noise. With a matching network, the limiting noise of the system is external man-made noise.

Antenna impedance mismatch significantly affects the transmission line noise figure and to a lesser extent the receiver noise figure when the voltage reflection coefficient $|\Gamma| \geq 0.5$ as illustrated in Fig. 51 for $\mathrm{Im}\Gamma = 0$ and a transmission line length of 10 m at 30 MHz. For $|\Gamma| = 0.9991$, the transmission line noise figure is approximately 22 dB in Fig. 51 because $\mathrm{Im}\Gamma = 0$ and 39 dB in Fig. 50(a) because $\mathrm{Im}\Gamma = -\mathrm{j}0.09965$. However, for an external noise figure of 26 dB, the system operating noise figure is not significantly affected by antenna impedance mismatch until the voltage reflection coefficient $|\Gamma| \geq 0.98$. Consequently, VHF and HF receiving systems with electrically small antennas require some impedance matching, but only a modest amount, so that the system margin remains external-noise-limited.

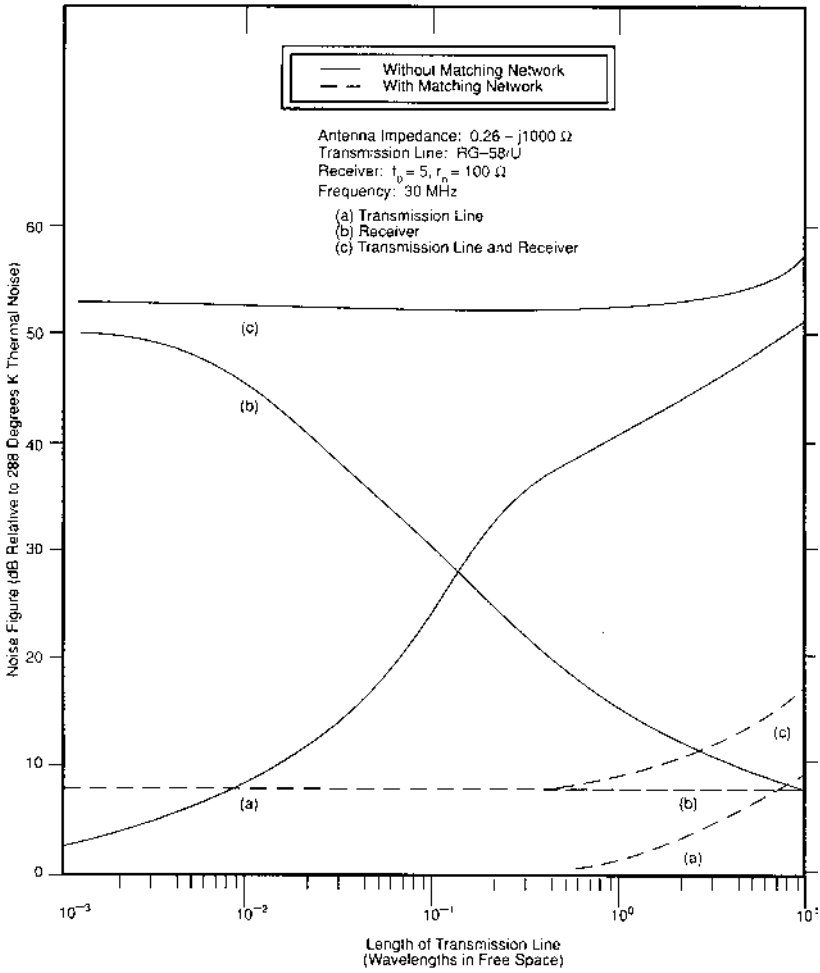

FIGURE 50 Transmission line and receiver noise figures.

6.5 USE OF THE LONGLEY–RICE AND JOHNSON–GIERHART TROPOSPHERIC RADIO PROPAGATION PROGRAMS: 0.02–20 GHZ

6.5.1 Introduction

The Longley–Rice [44–46,63,65] and Johnson–Gierhart [47–49] prediction programs of the Institute for Telecommunication Sciences (ITS) are statistical/semiempirical models of tropospheric radio propagation for low- and

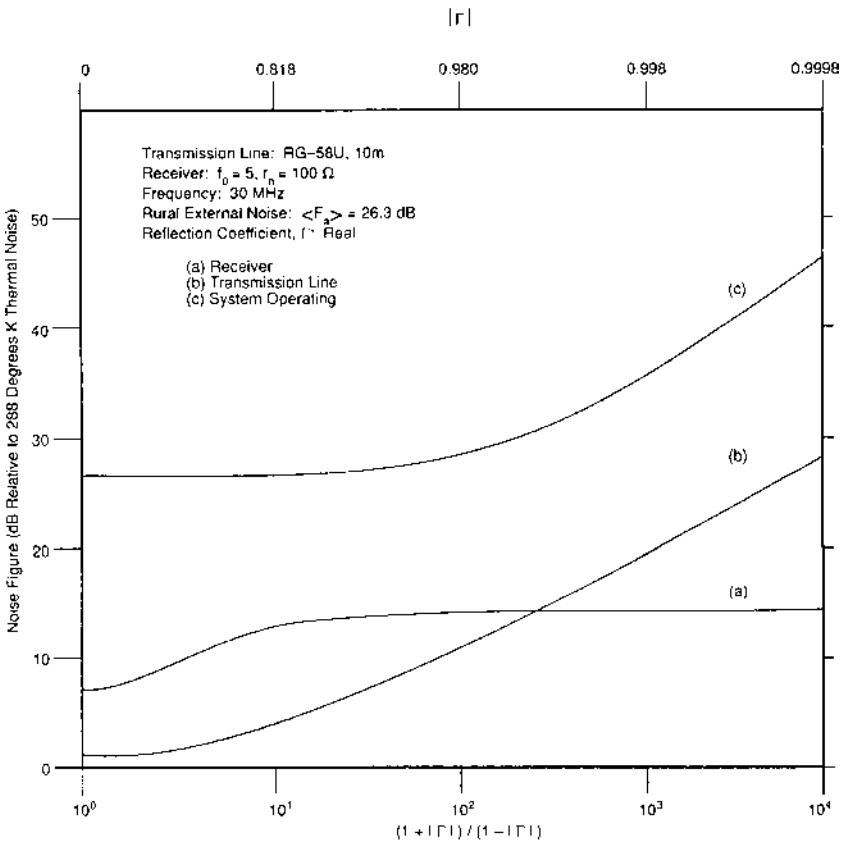

FIGURE 51 Effect of voltage reflection coefficient $|\Gamma|$ on noise figure.

high-altitude scenarios, respectively, in the frequency range of 0.02–20 GHz. These programs are restricted to frequencies above 20 MHz because "sky" and "ground" wave propagation paths, which can be dominant propagation paths at frequencies less than 20 MHz, are not included in these programs. These programs are restricted to frequencies less than 20 GHz because the empirical database does not include absorption and refractivity of the atmosphere or ground at wavelengths shorter than 1 cm.

These models are particularly useful in predicting propagation losses over irregular terrain for which knife-edge diffraction losses are significant. These programs use an empirical database to statistically weigh knife-edge diffraction

losses with losses from multipath interference, smooth-spherical Earth diffraction, and troposcatter modes of propagation.

Propagation paths over irregular terrain are commonly encountered in ground-to-ground, air-to-ground, and air-to-air military tactical scenarios. In tactical scenarios, propagation paths of interest are usually for specified classes of paths with location and time variabilities, rather than for a specific deterministic path. For example, one class of paths might be characterized as having rolling plains, average ground permittivity, and random siting. The propagation path loss for such environments is best characterized by statistical quantities which are semiempirically determined. For this reason, the Longley–Rice and Johnson–Gierhart programs are well-suited for military tactical scenarios. Other statistical propagation programs, such as EPM-73 [66] and TIREM [67] of the Department of Defense Electromagnetic Compatibility Analysis Center, may be less complex but usually rely either for modeling or validation on the empirical database of the Longley–Rice program.

The Longley–Rice program, in the point-by-point profile mode of operation, is also capable of predicting statistical propagation losses for a deterministic propagation path whose terrain profile is specified. For such propagation paths, deterministic propagation programs may also be used. For example, MIT Lincoln Laboratory has recently developed the deterministic propagation program Spherical Earth Knife-Edge (SEKE) and performed measurements to validate this program [69–72].

The theory, computer programs, and user's guides for the Longley–Rice and Johnson–Gierhart prediction models are given in [44–49,63,65] and may also be obtained on-line by clicking "Telecommunication Analysis Services" at the ITS home page address http:/www.its.bldrdoc.gov/Home.html. However, an explicit comparison of the properties and regions of applicability of the two models is not given. Furthermore, with the exception of [68], extensive numerical results for various scenarios and ranges of input parameters are not given. Consequently, the selection and utility of these models, as well as their input parameter specification, may be somewhat bewildering to the potential user. Section 6.5 attempts to address these deficiencies.

Version 1.2.1 of the Longley–Rice model and the air-to-air (ATOA) version of the Johnson–Gierhart model were acquired several years ago by The MITRE Corporation from ITS for prediction of propagation path loss in radio scenarios. ITS no longer supports versions 1.2.1 and ATOA but instead presently supports Longley–Rice version 1.2.2 and Johnson–Gierhart version IF-77. Although the numerical results of this Sec. 6.5 were obtained from versions 1.2.1 and ATOA, the results given are similar to those that would be obtained from versions 1.2.2. and IF-77.

The computer programs for version 1.2.2 of the Longley–Rice model and the IF-77 version of the Johnson–Gierhart model are described in Apps. B.07 and B.08, respectively.

The outputs of these programs are statistical values of "basic transmission loss." Sec. 6.5.2 defines basic transmission loss and discusses the particular quantities of basic transmission loss evaluated by these programs. Numerical results are given for various scenarios and ranges of input parameters. Results for a particular scenario are compared to other theoretical models. Secs. 6.5.3 and 6.5.4 discuss input parameter specifications for the Longley–Rice and Johnson–Gierhart models, respectively.

6.5.2 Basic Transmission Loss

Basic transmission loss $L_b(d)$ in Eq. (6.4.1) is a system margin parameter that is a stochastic function of the propagation range of great circle distance d between the transmitting and receiving antennas. More specifically, "the basic transmission loss (sometimes called path loss) of a radio circuit is the transmission loss expected between ideal, loss-free, isotropic, transmitting and receiving antennas at the same locations as the actual transmitting and receiving antennas" [50].

The basic transmission loss $L_b(d)$ (dB) may be expressed as

$$L_b(d) = L_{bo}(d) + U(d) + V(d) \tag{6.5.1}$$

where

$L_{bo}(d)$ = Local path propagation loss for a path with no buildings or significant vegetation in the immediate vicinity of the antennas (hourly median value, in dB).

$U(d)$ = Urban area propagation loss term resulting from buildings in the immediate vicinity of the antennas (hourly median value, in dB).

$V(d)$ = Vegetative propagation loss term resulting from significant vegetation in the immediate vicinity of the antennas (hourly median value, in dB).

Since $L_b(d)$ is defined for idealized isotropic antennas, its measurement is best approximated when made with antennas that are electrically small.

The propagation path loss given by Eq. (6.5.1) does not include rapid fading, about the hourly median value, of the received signal that results from multipath interference (vertical lobing) for a small change in range (of the order of a carrier wavelength) in a mobile system operating over irregular terrain. Instead of superimposing the distributions of hourly median and rapid fading propagation losses, the effects of multipath rapid fading can be included in the system margin model by increasing the value of the required predetection

signal-to-noise ratio $R_r(r_i)$ necessary to obtain a specified channel quality r_i in the presence of rapid fading [51].

The local path propagation loss $L_{bo}(d)$ may be expressed as

$$L_{bo}(d) = L_{bf}(d) + A(d) \tag{6.5.2}$$

where

$L_{bf}(d)$ = Free-space propagation loss (dB)= $10\log_{10}\left(\frac{4\pi d}{\lambda}\right)^2 = 10\log_{10}\left(\frac{4\pi df}{c}\right)^2 = 32.447 + 20\log_{10} f_{MHz} + 20\log_{10} d_{km}$.

d_{km} = Great circle distance between transmitter and receiver antennas (km).

λ = RF carrier wavelength (in units of d).

f_{MHz} = RF carrier frequency (MHz).

c = Free-space velocity of propagation = 0.29979 km/μsec.

$A(d)$ = Excess propagation loss over that of free-space for a path with no buildings or significant vegetation in the immediate vicinity of the antennas (hourly median value in dB). This term is usually modeled by semiempirical methods.

The Longley–Rice and Johnson–Gierhart prediction programs are concerned with estimating the hourly median values of excess propagation loss $A(d)$ defined by Eq. (6.5.2). The urban loss $U(d)$ and vegetative loss $V(d)$ terms in Eq. (6.5.1) are not predicted by these programs. The rapid fading, about the hourly median values, is also not predicted by the Longley–Rice program but is an available vertical lobing option in the Johnson–Gierhart program. Before discussing the excess loss $A(d)$, a brief review is given here of the urban loss $U(d)$ and vegetative loss $V(d)$ terms in Eq. (6.5.1).

The urban area propagation loss term $U(d)$ in Eq. (6.5.1) has been estimated to have a median value $U(d,50\%)$ given by [52]

$$U(d, 50\%) = \begin{cases} 16.5 + 15\log_{10}(f_{MHz}/100) - 0.12\ d_{km}, \text{urban area} \\ 0, \text{both antennas are in open areas} \end{cases} \tag{6.5.3}$$

which agrees within 1 dB with empirical data at 100–300 MHz and distances 10–70 km. The median value $U(d, 50\%)$ given by Eq. (6.5.3) is the difference in the median values of excess propagation loss reported by Okumura [53] for urban areas and by Longley–Rice [45] for open areas. Eq. (6.5.3) is based on data for which the receiver antenna was near ground level (at a height of 3 m) and the transmitter antenna was at various elevated heights of 30–600 m. At a frequency of 88 MHz and a distance of 35 km, the median value of the additional transmission loss from urban area clutter is found from Eq. (6.5.3) to be 11.5 dB.

The vegetative propagation loss term $V(d)$ in Eq. (6.5.1) is appreciably less at VHF frequencies than at higher frequencies because vegetation is appreciably more transparent at longer wavelengths and because obstacles, such as vegetation, diffract more energy into shadow zones at longer wavelengths [52]. Only vegetation in the immediate vicinity of the antennas should be considered in estimating $V(d)$ in Eq. (6.5.1), because knife-edge diffraction by vegetation distant from the antennas is usually included in the semiempirical methods used for estimating the excess propagation loss $A(d)$. The loss term $V(d)$ is the lesser of the absorptive path loss through the vegetation and the diffractive path loss over the vegetation.

When one of the antennas is placed near a grove of trees or in a jungle, vertically polarized VHF radio waves are attenuated appreciably more than horizontally polarized waves. For example, at 30 and 100 MHz, the average loss from nearby trees was reported to be 2–3 and 5–10 dB, respectively, for vertical polarization and approximately 0 and 2–3 dB, respectively, for horizontally polarized signals [52,54]. In dense jungles, vertically polarized waves can be attenuated about 15 dB more than horizontally polarized waves [52,54]. At higher frequencies, the effects of polarization on vegetative loss are not as pronounced.

La Grone [56] conducted propagation experiments of horizontally polarized waves behind a grove of 3 m tall live oak and blackberry trees on flat ground in Texas, at frequencies 0.5–3 GHz and at distances greater than five times the tree height. Measurements of path loss were in good agreement with theoretical predictions of diffraction over an ideal knife-edge assuming distances and heights the same as those in the measurements. For such a case, the loss term $V(d)$ may be interpreted as the difference in losses between knife-edge (tree) diffraction and smooth-spherical Earth diffraction with losses expressed in dB. Approximate numerical values, deduced from data for the above case, are $V(d) = -4$, -2, and $+2$ dB for receiver heights above local terrain of 2, 10, and 18 m respectively; a frequency of 82 MHz; transmitter-to-receiver distance $d = 67$ km; transmitter height of 424 m; and receiver-to-grove distance of 111 m.

Estimates of the excess propagation loss $A(d)$ defined in Eq. (6.5.2) can be as formidable to calculate as the estimates for urban area and vegetative propagation losses because of the semiempirical nature of the required models.

The excess propagation loss $A(d)$ is generally a stochastic quantity because the scenarios of interest are generally not for deterministic propagation paths, but for specified classes of propagation paths. For example, the propagation paths may be specified as being over irregular terrain characterized by rolling plains, average ground permittivity, and random siting.

Radio waves generally may be propagated (1) through or along the surface of the Earth (ground wave), (2) through the lower atmosphere of the Earth beneath the ionosphere (tropospheric propagation), or (3) by reflection or scatter in the upper atmosphere (sky wave) for natural reflectors (ionosphere, aurora) or

artificial reflectors (satellites). At frequencies greater than 20 MHz, ground wave propagation losses (except for very short paths within the radio horizon and along the Earth's surface) and sky wave propagation losses (except for very long propagation paths beyond the radio horizon) are usually very much larger than tropospheric propagation losses. The Longley–Rice and Johnson–Gierhart programs consider only tropospheric propagation paths.

For tropospheric propagation over irregular terrain, the possible modes of propagation may be categorized as

1. Multipath interference
2. Multipath–diffraction transition
3. Diffraction (smooth-SEKE)
4. Diffraction–tropospheric scatter transition
5. Tropospheric scatter

The regions for these propagation modes are shown in Fig. 52.

Mode 1 is the dominant mode of propagation for line-of-sight paths which clear the radio horizon by greater than approximately 1/4 of a Fresnel number, where the Fresnel number is the number of half-wavelengths of the path difference between the direct ray and the indirect ray specularly reflected from the ground [57]. Mode 2 occurs for line-of-sight propagation paths within 1/4 of a Fresnel number of the radio horizon. Mode 3 occurs for propagation paths beyond the radio horizon by more than 1/4 of a Fresnel number, but less than that for

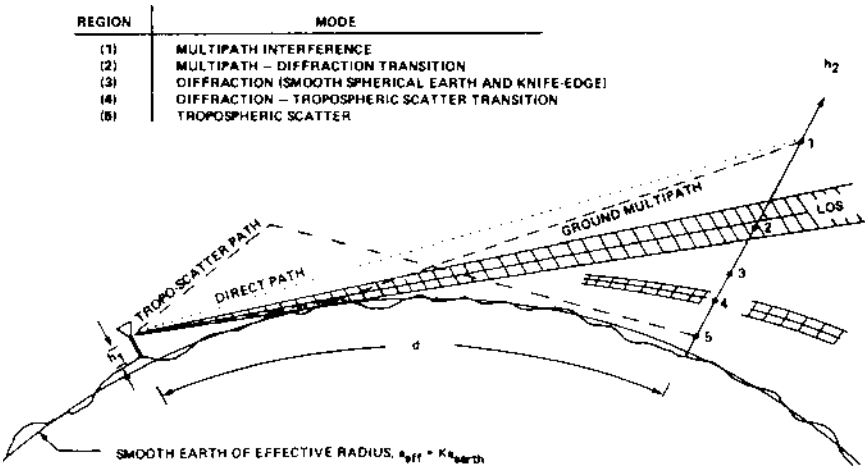

FIGURE 52 Regions of various tropospheric propagation modes over irregular terrain.

which tropospheric scatter starts to become significant. Mode 4 is a transition mode between diffraction and troposcatter modes. Mode 5 occurs for propagation paths sufficiently beyond the radio horizon where tropospheric scatter losses are less than diffractive losses. Except for mode 1 lobing, the excess propagation loss $A(d)$ generally increases with decreasing height h_2 as the dominant mode of propagation progresses from 1 to 5.

As an example of tropospheric modes 1 and 2, consider the various scenarios shown in Table 12. For smooth Earth, all of the Table 12 scenarios correspond to radio links within or on the radio horizon. However, for random siting of the ground-based radio on irregular terrain, the radio line-of-sight to low-altitude aircraft will often be obstructed. In the case of nonobstructed radio line-of-sight over smooth terrain, the principal mode of propagation is smooth-spherical Earth diffraction coupled with multipath interference between the direct and indirect signals reflected by the terrain to the receiver. In the case of an obstructed radio line-of-sight over irregular terrain, the principal mode of propagation is smooth-spherical Earth diffraction coupled with knife-edge diffraction by the obstructing terrain. Multipath interference is the dominant mode of propagation in scenario numbers 3b, 7b1, and 8 which clear the radio horizon for a smooth Earth by at least 1/8 of a Fresnel number. All of the other scenarios in Table 12, which clear the radio horizon by less than 0.01 Fresnel number, correspond to the multipath–diffraction transition mode.

In the multipath–diffraction transition mode, the propagation path loss is significantly larger than the free-space loss. In the case of multipath interference, the interference is almost totally destructive because (1) the Fresnel amplitude reflection coefficient is approximately -1 at low grazing angles of incidence, (2) the surface roughness reflection coefficient is approximately unity at sufficiently low grazing angles of incidence, and (3) the path length difference between the direct and indirect signals is much less than a wavelength.

In the case of diffraction, the path loss increases exponentially with increasing distance of the transmitter or receiver into the shadow region of the obstructing terrain. For a given distance into the shadow region, the sharpness of the obstructing terrain appreciably alters the path loss in a diffraction mode. Therefore, for a diffraction mode of propagation, slope and height distribution of the obstructing terrain affect the path loss.

The Longley–Rice and Johnson–Gierhart statistical, semiempirical programs are particularly useful in modeling propagation loss over irregular terrain in the transition modes 2 and 4 of Fig. 52. The propagation loss for mode 2 is found from empirical data and from extrapolations between theoretical models for multipath interference and smooth-spherical Earth diffraction. The propagation loss for mode 4 is found from empirical data and from extrapolations between theoretical models for smooth-spherical Earth diffraction and tropospheric scatter.

TABLE 12 Basic Transmission Loss for Low- and High-Altitude Scenarios, $f = 50$ MHz

No.	h_1 (m)	h_2 (m)	Desired maximum operational range, d (km)	Grazing angle (mrad)	Number of Fresnel zones clearance	Free space loss, L_{bf} (dB)	BASIC transmission loss, L_b (dB)					
							$\Delta h = 90$ m		$\Delta h = 225$ m		$\Delta h = 500$ m	
							$\langle L_b \rangle$	σ_{L_b}	$\langle L_b \rangle$	σ_{L_b}	$\langle L_b \rangle$	σ_{L_b}
1	2.5	305	35	4.0	0.014	97.4	112.7	11.0	118.0	11.9	126.8	12.2
2	2.5	75	28	1.1	0.0029	95.4	124.9	10.9	126.5	11.8	134.2	12.2
3a	30	75	56	0.22	0.032	101.4	131.5	11.1	132.3	11.7	135.0	12.0
3b	915	75	56	9.5	1.30	101.4	101.5	11.2	105.4	11.9	106.4	12.2
4a	2.5	150	28	1.9	0.0097	95.7	118.2	11.0	119.2	11.8	127.4	12.2
4b	2.5	150	46	1.0	0.00084	99.7	130.5	11.0	133.6	11.8	144.1	12.1
5	2.5	61	28	0.86	0.0022	95.4	126.7	10.9	129.0	11.7	136.5	12.2
6a	2.5	150	46	1.0	0.00084	99.7	130.5	11.0	133.6	11.8	144.1	12.1
6b	2.5	1070	112	3.1	0.0017	107.4	136.1	11.2	154.6	12.1	154.6	12.1
7a1	2.5	5500	185	11.9	0.050	111.8	118.9	1.4	128.2	1.6	150.2	1.8
7a2	2.5	5500	230	8.6	0.040	113.7	128.8	2.6	145.0	2.7	158.1	2.8
7b1	2.5	6100	92	31.5	0.111	105.7	107.9	0.0	106.7	0.0	115.4	0.0
7b2	2.5	6100	140	19.6	0.073	109.3	114.3	0.3	112.4	0.3	140.8	0.8
7c1	2.5	4600	185	9.7	0.041	111.8	120.7	1.7	144.2	2.0	154.5	1.9
7c2	2.5	4600	230	6.5	0.033	113.7	134.0	3.0	151.7	3.2	160.3	3.2
8a1	9	9200	140	31.0	0.40	109.3	110.4	0.0	110.0	0.0	109.7	0.0
8a2	9	9200	230	17.0	0.24	113.7	117.7	1.4	116.9	1.5	118.8	1.4
8b1	915	9200	260	19.5	20.33	114.7	113.9	1.3	114.2	1.4	114.9	1.6
8b2	915	9200	300	15.8	13.64	116.0	115.7	2.0	115.7	2.0	115.2	2.0
9a	2.5	61	30	0.67	0.0017	96.0	128.5	10.9	130.5	11.7	138.7	12.1
9b1	2.5	150	37	1.56	0.0034	97.8	124.7	11.0	126.7	11.8	136.0	12.1
9b2	2.5	150	46	1.0	0.00084	99.7	130.5	11.0	133.6	11.8	144.1	12.1

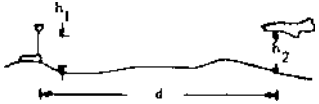

Average ground, random siting, 4/3 Earth radius, temperate climate, vertical polarization, and isotropic antennaa in a nonvegetative open area are assumed.
Δh = interdecile terrain roughness.

The Longley–Rice prediction program is applicable to scenarios where both the transmitter and receiver antennas are at heights above local ground between 0.5 m and 3 km (which we shall designate as "low altitude" scenarios). The Johnson–Gierhart program is applicable to "high altitude" scenarios in which (1) the lower antenna is at a height above local ground between 0.5 m and approximately 3 km, (2) the higher antenna is less than 100 km but at a sufficient height above local ground that the elevation angle at the lower antenna of the terrain-limited radio horizon is less than the elevation angle of the higher antenna, and (3) the terrain-limited radio horizon for the higher antenna is taken either as a common horizon with the lower antenna or as a smooth Earth horizon with the same elevation as the lower antenna effective reflecting plane. These altitude restrictions and the use of these programs are based on the following considerations:

1. Whereas two-ray multipath interference models are adequate for path clearances greater than 1/4 of a Fresnel number and whereas smooth Earth spherical diffraction models are adequate for transhorizon paths well beyond the radio horizon, an extrapolation between these models, even for a smooth Earth, is presently required for modeling of propagation paths near the radio horizon [57]. Reference 57 gives a deterministic computer program for such an extrapolation. However, for path loss averaged over random paths above irregular terrain near the radio horizon, a semiempirical, stochastic extrapolation is required. The empirical weighting accounts for knife-edge diffraction effects over a rough Earth. The Longley–Rice semiempirical prediction program does such an extrapolation and allows for double horizon diffraction for both random and specific terrain profiles.
2. Probabilistic predictions of path loss are possible because the database includes many samples for various locations, time of year, and experimental situations. Much of the database for the Longley–Rice program is for double horizon diffraction paths and was obtained in the frequency range of 20–100 MHz [58]. Much of the database for the Johnson–Gierhart program is from 200 single horizon diffraction paths contained in the data of Longley et al. [59].
3. The Longley–Rice program assumes a uniform atmosphere (linear refractive gradient) and is, therefore, not applicable to propagation paths in standard exponential atmosphere at elevations above 3000 m. The Longley–Rice program is also restricted at each antenna to path elevation angles less than 12°. For path elevation angles greater than 12°, time variability of path loss caused by atmospheric refraction is appreciably less than that of the empirical database (which is limited to refractive effects at elevation angles less than 12°).

4. The Johnson–Gierhart prediction program is restricted to single-horizon diffraction which allows for ray tracing in standard atmospheres from the horizon back to the antenna site. The Johnson–Gierhart program is, therefore, applicable to paths at high elevations and steep elevation angles, but is not applicable at low elevations where double-horizon diffraction may be significant.

In the Longley–Rice and Johnson–Gierhart programs, ionospheric propagation and auroral scatter effects are assumed to be negligible. This assumption is valid at frequencies above 100 MHz and is expected to be valid at frequencies of 20–100 MHz for sufficiently short path lengths. In the Longley–Rice program, a printout warning is issued at frequencies less than 40 MHz to remind the user that sky wave effects may be important at sufficiently long path lengths. The Johnson–Gierhart program can be extended to frequencies as low as 20 MHz provided that sky wave effects are negligible.

Both of these prediction programs restrict antenna sites to locations for which the ratio of the distance to the terrain-limited radio horizon to that for a smooth-spherical Earth is greater than 0.1 and less than 3.0. This restriction applies to both antenna sites in the Longley–Rice program, and only to the lower antenna in the ATOA program. For example, these programs would not be applicable to a scenario in which the ground site is at the bottom of a steeply rising hill because the weighted extrapolation of models in these programs does not allow for severe knife-edge diffraction. The hourly median basic transmission loss computed by the programs does not include losses resulting from foliage or buildings.

In Fig. 53, the cumulative distribution functions of path loss are plotted on normal probability paper for both high- and low-altitude scenarios. The path loss for the low-altitude scenario of Table 12 (scenario no. 9a) was predicted using the Longley–Rice model, whereas the path loss for the high-altitude scenario (scenario no. 7c2) was predicted using the Johnson–Gierhart model. Longley–Rice program predictions of path loss for low-altitude scenarios are approximately normally distributed when path loss is expressed in dB. However, Johnson–Gierhart program predictions of path loss for high-elevation scenarios are two-piecewise normally distributed with a breakpoint at the median value as explained below. Location, time, and situation (model) uncertainties contribute to path loss variability. In the Longley–Rice program, location variability is usually the dominant path loss variability because diffraction by terrain at both ends of the link is considered. In the Johnson–Gierhart program, time variability is usually the dominant path loss variability because diffraction by terrain at only the low-altitude end of the link is considered. Location and time variabilities are one-piecewise and two-piecewise, respectively, normally distributed in both programs.

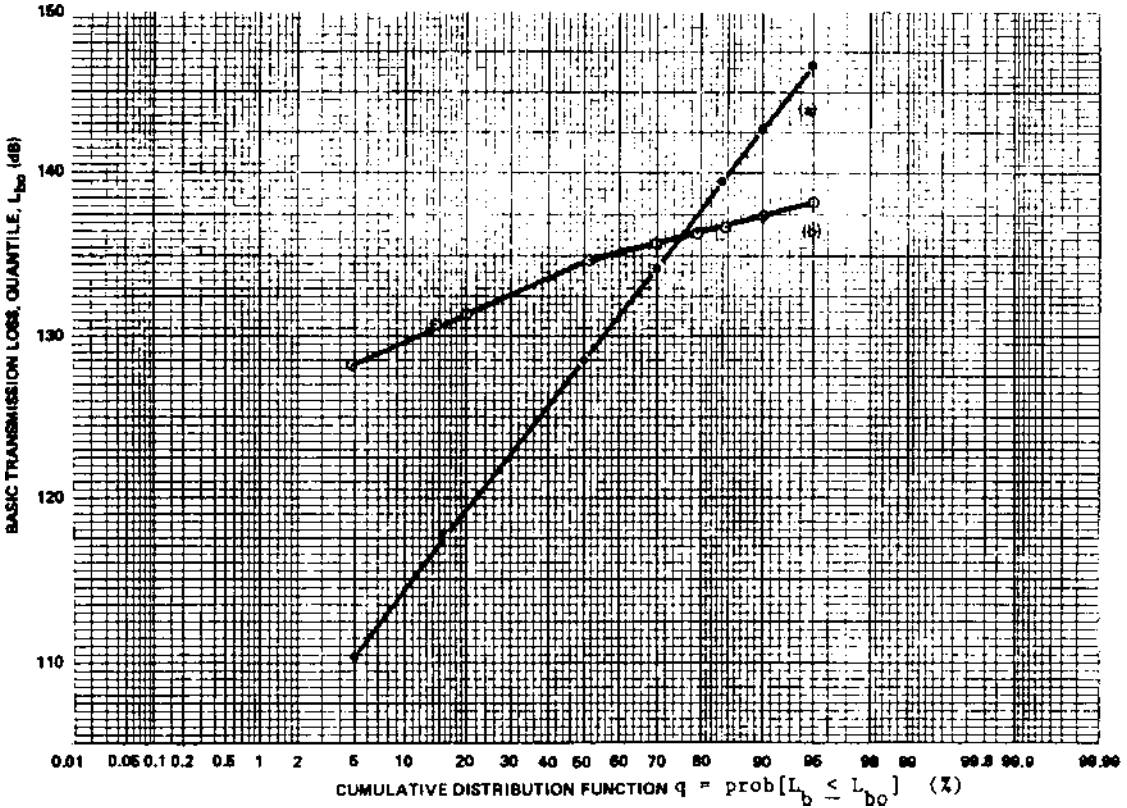

FIGURE 53 Cumulative distribution function of basic transmission loss $f = 50$ MHz. (a) Longley-rice ($h_1 = 2.5$ m, $h_2 = 61$ m, $d = 30$ km). (b) Johnson–Gierhart ($h_1 = 2.5$ m, $h_2 = 4600$ m, $d = 225$ km).

The Longley–Rice and Johnson–Gierhart programs predict the hourly median quantities $L_{bo}(d,q)$ of the basic transmission $L_b(d)$ as a function of the path distance d and the cumulative distribution function (confidence level) $q = \text{prob}[L_b(d) \leq L_{bo}(d)]$. The single-variate probability q, in which marginal probabilities of time, location, and situation (model uncertainty) are combined, is the only statistical service (designated single-message service) available in the Johnson–Gierhart program. In the Longley–Rice program, other statistical services are also available [64, Sec. 3.0, Table 5].

For the Johnson–Gierhart program, in which path loss $L_b(d)$ is two-piecewise normally distributed with a breakpoint at the median value $L_b(d,50\%)$, the expected value $\langle L_b(d)\rangle$, and standard deviation $\sigma_{L_b(d)}$ are given by

$$\langle L_b\rangle = L_{bo}(50\%) + 0.312[L_{bo}(90\%) + L_{bo}(10\%) - 2L_{bo}(50\%)], \quad \text{two-piecewise normal} \tag{6.5.4}$$

$$\sigma_{L_b} = \frac{1}{1.28}\left\{\frac{1}{2}[L_{bo}(90\%) - L_{bo}(50\%)]^2 + \frac{1}{2}[L_{bo}(50\%) - L_{bo}(10\%)]^2 - \frac{1}{2\pi}[L_{bo}(90\%) + L_{bo}(10\%) - 2L_{bo}(50\%)]^2\right\}^{1/2}, \quad \text{two-piecewise normal} \tag{6.5.5}$$

In Eqs. (6.5.4) and (6.5.5), the parameter d has been suppressed in order to condense the notation.

For the Longley–Rice program, in which path loss $L_b(d)$ for the low-altitude scenarios is normally distributed, $\langle L_b(d)\rangle$ and $\sigma_{L_b}(d)$ are given by

$$\langle L_b(d)\rangle = L_{bo}(d, 50\%), \quad \text{normal} \tag{6.5.6}$$

$$\sigma_{L_b(d)} = \frac{1}{1.28}[L_{bo}(d, 90\%) - L_{bo}(d, 50\%)] = L_{bo}(d, 84.1\%) - L_{bo}(d, 50\%), \quad \text{normal} \tag{6.5.7}$$

Equations (6.5.4) and (6.5.5) reduce to Eqs. (6.5.6) and (6.5.7), respectively, for $L_{bo}(90\%) - L_{bo}(50\%) = L_{bo}(50\%) - L_{bo}(10\%)$.

Both the Longley–Rice and Johnson–Gierhart programs use information based on the same statistical–empirical study of various terrain profiles and propagation measurements conducted primarily in the United States. In that study, each terrain profile was characterized by its interdecile height h and distance to the radio horizon. The interdecile height is the difference in heights corresponding to the 90 and 10% values of the cumulative distribution function

for the height deviation from the mean surface level of average terrain slope. When random siting is specified for an antenna above a surface of specified interdecile height, the programs again assign a median distance to the radio horizon on the basis of information derived from the statistical–empirical study.

The statistical parameters $L_b(d)$ and $\sigma_{L_b(d)}$ are tabulated in Table 12. The basic transmission loss is tabulated for interdecile terrain heights $\Delta h = 90$, 225, and 500 m, corresponding, respectively, to hills (U.S. average terrain), mountains (slightly shorter than those in the Fulda gap of Germany), and rugged mountains (slightly taller than those in Korea). The results of Table 12 are for average ground permittivity, random siting of the antennas, atmospheric refractivity at the Earth's surface equivalent to an effective Earth radius equal to 4/3 of the Earth's geometric radius, temperate climate, vertical polarization, and isotropic antennas in a nonvegetative open area.

The expected value of the basic transmission loss exceeds the free-space loss, for $\Delta h = 90$, 225, and 500 m, by 1.1, 0.7, and 0.4 dB, respectively, for the high-altitude scenario no. 8a1, and by 32.5, 34.5, and 42.7 dB, respectively, for the low-altitude scenario no. 9a. The standard deviation $\sigma_{L_b(d)}$ is 0–3 dB for the high-altitude scenarios of Table 12 and 10.9–12.2 dB for the low-altitude scenarios.

Longley–Rice predictions of basic transmission loss for worldwide environmental conditions are tabulated in Table 13 for scenario no. 9a of Table 12. Variations in terrain roughness and surface permittivity appreciably affect the expected value of transmission loss. Very careful siting of the ground antenna can reduce transmission loss by approximately 6 dB over that for random siting. Variations in climate and atmospheric refractivity have relatively little effect on transmission loss for this scenario. In nonvegetated areas, vertically polarized waves have less path loss than for horizontal polarization. In vegetated areas, however, the reverse may be true (see earlier discussion of vegetative loss term).

Transmission loss decreases with increasing terrain roughness for terrain roughness less than or comparable to the higher antenna height above the ground, but increases with increasing terrain roughness for terrain appreciably larger than the higher antenna height. The reason is that obstructions with small interdecile heights do not appreciably reduce path clearance, but instead enhance propagation by knife-edge diffraction. For obstructions with large interdecile heights, the exponential increase of the path loss with increasing distance into the shadow region of the obstructing terrain exceeds any reduction in path loss obtained by the knife-edges of the obstructing terrain. When smooth-spherical Earth diffraction is the dominant mode of propagation, surface permittivity, and particularly ground conductivity, appreciably affect the distribution of energy above and below the Earth's surface. For example, in Table 13, the transmission

TABLE 13 Basic Transmission Loss for Worldwide Environmental Conditions

Environmental parameter		Basic transmission loss L_b (dB)	
		$\langle L_b \rangle$	σ_{L_b}
Terrain roughness, Δh (m)			
0	(Perfectly smooth)	132.6	7.1
5	(Water or very smooth plains)	131.1	7.5
30	(Slightly rolling plains)	129.2	9.3
60	(Rolling plains)	128.6	10.3
90[a]	(United States average)	128.5	10.9
225	(Mountains)	130.5	11.5
500	(Rugged mountains)	138.7	12.1
700	(Extremely rugged mountains)	145.5	12.5
Surface permittivity			
ϵ $\sigma(S/m)$			
4 0.001	(Poor ground)	130.9	10.9
15[a] 0.005	(Average ground)	128.5	10.9
25 0.02	(Good ground)	127.3	10.9
81 5.0	(Sea water)	113.4	10.9
81 0.01	(Fresh water)	124.4	10.9
Siting criteria for ground facility			
Random siting[a]		128.5	10.9
Careful siting		125.1	10.9
Very careful siting		122.6	10.9
Climate			
Equatorial		128.8	10.9
Continental subtropical		128.5	10.9
Maritime subtropical		128.5	10.9
Desert		129.0	10.9
Continental temperate[a]		128.5	10.9
Maritime temperate overland		128.6	10.8
Maritime temperate oversea		128.5	10.9
Atmospheric Refractivity			
K (*Earth radius*)	N_S (N-units)		
1.23	250	129.0	10.9
1.33[a]	301	128.5	10.9
1.49	350	127.9	10.9
1.77	400	127.2	10.9
Polarization			
Vertical[a]		128.5	10.9
Horizontal		133.2	10.9

Scenario parameters: $h_1 = 2.5$ m, $h_2 = 61$ m, $d = 30$ km, $f = 50$ MHz, nonvegetated open area.
[a] Baseline environmental parameters: $\Delta h = 90$ m, average ground permittivity, random siting, $K = 4/3$ Earth radius, temperate climate, vertical polarization.

loss is approximately 17 dB less for propagation paths over sea water than for over very dry (poor) ground.

For nonvegetated open areas, the expected value and standard deviation of the excess propagation loss $A(d)$ are relatively frequency insensitive, over the frequency range 30–88 MHz, when compared to the variation of free-space loss over this frequency range (see Table 14).

A comparison of theoretical models with Longley–Rice predicted values is given in Table 15 for scenario no. 9a of Table 12 and an interdecile terrain roughness $\Delta h = 0$. The theoretical models considered are free space, plane Earth multipath, and spherical Earth multipath. The semiempirical model gives an expected value that exceeds the free-space loss by 35.4–37.5 dB over the frequency range 30–88 MHz. The plane Earth multipath model predicts a loss 1–6 dB larger than that predicted by the Longley–Rice model. The spherical Earth multipath model predicts a loss that is appreciably less than that predicted by the Longley–Rice model, but more than the free-space loss. The close agreement, between the results for the multipath plane Earth model and those of the Longley–Rice model, should be viewed as just a coincidence. The multipath plane Earth model is only an idealized limit of the more physical spherical Earth multipath model, which in turn is inappropriate for radio propagation paths that clear the radio horizon by less than 1/4 of a Fresnel number. The incremental path loss (expressed as a numeric rather than in units of dB) increases with incremental range to the second, fourth, and greater than fifth powers for the free-space, plane Earth multipath, and Table 13 Longley–Rice models, respectively.

The Longley–Rice semiempirical model has been compared to theoretical models and to empirical data in a multipath interference mode of propagation [60–62]. Both the Longley–Rice semiempirical model and a statistical model, in which the surface height is assumed to be exponentially distributed, agree well with experimental data for coherent scatter in the forward-scattered direction for both terrain and sea surfaces. The theoretical model for the particular mode of propagation has the advantages of providing a theoretical basis for the results, and better agreement with data for very smooth surfaces and possible very rough surfaces. However, for the multipath–diffraction transition mode of propagation near the radio horizon over an irregular terrain, the Longley–Rice semiempirical model appears to be the best available model because presently, there is no adequate theoretical model.

6.5.3 Input Parameter Specification for the Longley–Rice Version 1.2.2 Prediction Program

The Longley–Rice version 1.2.2 propagation program predicts long-term (hourly) median radio transmission loss over irregular terrain. The output of

TABLE 14 Frequency Scaling of Propagation Loss in Excess of Free-Space Loss

Interdecile terrain roughness, Δh (m)	Excess propagation loss, $A(d)$ (dB)							
	$\langle A(d) \rangle$				$\sigma_{A(d)} = \sigma_{L_b(d)}$			
	30 MHz	50 MHz	88 MHz	$\lvert\langle A(d) \rangle - \langle A_{50\,\mathrm{MHz}} \rangle\rvert$	30 MHz	50 MHz	88 MHz	$\lvert\sigma_{A(d)} - \sigma_{A_{50\,\mathrm{MHz}}}\rvert$
60	33.9	32.6	31.2	1.4	9.6	10.3	11.0	0.7
225	35.1	34.5	34.4	0.6	11.4	11.7	12.0	0.3
500	41.5	42.7	45.7	3.0	11.9	12.1	12.2	0.2

Scenario parameters: $h_1 = 2.5\,\mathrm{m}$, $h_2 = 61\,\mathrm{m}$, $d = 30\,\mathrm{km}$, average ground permittivity, random siting, $K = 4/3$ Earth radius, temperate climate, vertical polarization, nonvegetated open area.

TABLE 15 Comparison of Models for Basic Transmission Loss ($h_1 = 2.5$ m, $h_2 = 61$ m, $d = 30$ km, average ground, random siting, terrain roughness $\Delta h = 0$ m, effective Earth radius $K = 4/3$, temperate climate, vertical polarization)

	Basic transmission loss, L_b (dB)		
Model	30 MHz	50 MHz	88 MHz
Longley–Rice, 50% confidence level	129.0	132.6	136.3
Free space	91.5	96.0	100.9
Plane earth multipath, $R = 1$	135.4	135.4	135.4
Spherical earth multipath, $R = R_o D$	101.3	105.8	110.7

Free space

$$L_{bf}(d) = 20\log_{10}\ (4\pi d/\lambda)$$

$$= 32.447 + 20\log_{10} f + 20\log_{10} d\ \text{(dB)}$$

Multipath mode over a plane Earth at low grazing angles and with an amplitude reflection coefficient $R = -1$

$$L_b(d) = -20\log_{10}\ (h_1 h_2/d^2)\ \text{(dB)}$$

(From W. C. Jakes, Jr., "Microwave Mobile Communications," John Wiley, NY, 1974, Eq. 2.1–8).
Multipath mode over a smooth spherical Earth

$$L_b(d) = L_{bf}(d) - 20\log_{10}|1 + e^{j\Delta}|\ \text{(dB)}$$

where

$L_{bf}(d)$ = free-space loss
$R = R_o D$ = amplitude reflection coefficient
R_o = Fresnel amplitude reflection coefficient (Eq. 11–1)
D = Divergence coefficient (Monogram F)
Δ = Phase difference between direct and indirect ray (Monogram D)

(From P. Beckmann and A. Spizzichino, "The Scattering of Electromagnetic Waves from Rough Surfaces," Pergammon Press, Oxford, 1963, Chapter 11.)

the program is basic transmission loss. The program combines well-established propagation theory with empirical data to predict propagation losses. The prediction program is applicable for RF above 20 MHz. For frequencies below 40 MHz, a warning is automatically printed out, regardless of path distance, to remind the user that the sky wave may be significant for sufficiently long paths. The program may be used either with terrain profiles that are representative of

median terrain characteristics for a given area (the area-prediction mode) or with detailed terrain profiles for actual paths (the point-to-point mode).

The empirical database is for wide ranges of frequency, antenna height and distance, and for all types of terrain from very smooth plains to extremely rugged mountains. The database includes more than 500 long-term recordings at fixed locations throughout the world in the frequency range 40 MHz – 10 GHz, and several thousand mobile recordings in the United States at frequencies from 20 MHz to 1 GHz. Much of the empirical database is in the VHF frequency band 30 – 100 MHz.

The program is intended for use within the following ranges:

The elevation angles and radio horizon distances are not program input parameters, but are computed internally by the program.

Parameter	Range
Frequency	20 – 20000 MHz
Antenna heights	0.5 – 3000 m
Distance	1 – 2000 km
Surface refractivity	250 – 400 N units
Elevation angle, of the irregular terrain radio horizon ray above the horizontal, at each antenna	0 – 12 °
Relative distance, from each antenna to its terrain horizon, normalized to the corresponding smooth-Earth distance	0.1 – 3.0

Version 1.2.2 is written in ANSI Fortran language and is therefore compatible with any large-scale computer.

The input parameter specifications for version 1.2.2 are given in [64, table 5], which includes numerical ranges of parameters and the numerical values for which a warning is automatically printed out. An asterisk denotes the numerical value that will be assumed for a parameter if the user does not specify a particular value.

Version 1.2.2 offers two program modes whose selection depends upon how the user wishes to specify the terrain surface profile: the area prediction mode, designated “QKAREA”; and the point-to-point mode, designated “QKPFL.” The area-prediction mode is characterized by specifying the interdecile height Δh, the antenna siting criteria, and the great circle distances for which the basic transmission loss $L_b(d)$ is printed out. The point-to-point mode is characterized by specifying the elevation matrix of the terrain profile.

In the area-prediction mode, the interdecile terrain height and antenna siting criteria determine the expected values of the antenna effective heights, the elevation angles, and the terrain horizon distances by means of the stored empirical database. The point-to-point mode computes the elevation angles and distance to the radio horizon for each antenna and the antenna effective height by considering whether or not the antenna is near or on a hill. Except for these differences, the QKAREA and QKFPL programs are identical.

6.5.4 Input Parameter Specification for Johnson–Gierhart IF-77 Prediction Program

The Johnson–Gierhart IF-77 prediction program is similar in many respects to the Longley–Rice prediction program. The IF-77 program predicts radio transmission loss over irregular terrain. The output of the program is basic transmission loss. The program combines well-established propagation theory with empirical data to predict propagation losses that have been tested against a large number of propagation measurements [73–76]. It is applicable to RF 100 MHz–20 GHz, but can also be used at frequencies as low as 20 MHz, provided that the propagation paths are sufficiently short, so that the sky wave is insignificant. The program is used with terrain profiles that are representative of median terrain characteristics for a given area (similar to the area-prediction mode of version 1.2.2 of the Longley–Rice program), but without detailed terrain profiles for actual paths.

The Johnson–Gierhart IF-77 prediction program differs from the Longley–Rice program principally in the following ways.

1. Only single-horizon diffraction rather than double-horizon diffraction is considered.
2. A standard exponential atmosphere rather than a uniform gradient atmosphere is assumed (the index of refraction decreases exponentially rather than linearly with increasing height).
3. Plotting routines and various output options are available in the original CDC computer versions of the IF-77 program.
4. Basic transmission loss options exist for specifying whether surface reflection multipath and tropospheric multipath contribute to instantaneous levels exceeded or hourly median levels exceeded, and whether it contributes to variability (standard deviation) or median level (50% confidence level).

The empirical database comprises 200 single-horizon paths from [59]. Double-horizon paths are not included in the empirical database.

The program is intended for use within the following ranges.

Parameter	Range
Frequency	100–20000 MHz
Lower antenna height	0.5–3000 m
Higher antenna height	≥ radio horizon height of lower antenna
Surface refractivity	200–400 *N* units
Elevation angle, of the irregular terrain radio horizon ray above the horizontal, at the lower antenna only	0–12°
Distance, from the lower antenna to its terrain horizon, normalized to the corresponding smooth Earth distance	0.1–3.0

The input parameter specifications for the IF-77 program are given in [64, table 8]. An asterisk denotes the numerical value that will be assumed for a parameter by the programmer if the user does not specify a particular value. Unlike the Longley–Rice version 1.2.2 program, the asterisk values are not program-automatic default values, but must be specified by the programmer. The elevation angle of the horizon at the facility (lower antenna) and the distance from the lower antenna to its radio horizon are not program-input parameters, but are calculated internally by the program.

6.6 DESIGN AND QUALIFICATION OF A VHF ANTENNA RANGE

6.6.1 Requirements

Measurement of an electrically small monopole antenna's free-space far-field radiation pattern is difficult to achieve in the VHF band because of multipath reflection from the surface below the propagation path. A VHF antenna range was constructed on the roof of MITRE E-building to evaluate candidate antennas for the AF SINCGARS radio (see Fig. 54). The range was required to: (1) Approximate free-space far-field propagation conditions in the frequency band 30–156 MHz, without varying the range geometry, by minimizing roof and building multipath and by minimizing RF interference from TV and radio, (2) Accomodate low-gain VHF test receiving antennas with or without ground planes, and (3) Measure E-plane test patterns with horizontal polarization of the transmitting antenna and H-plane test patterns with vertical polarization of the transmitting antenna.

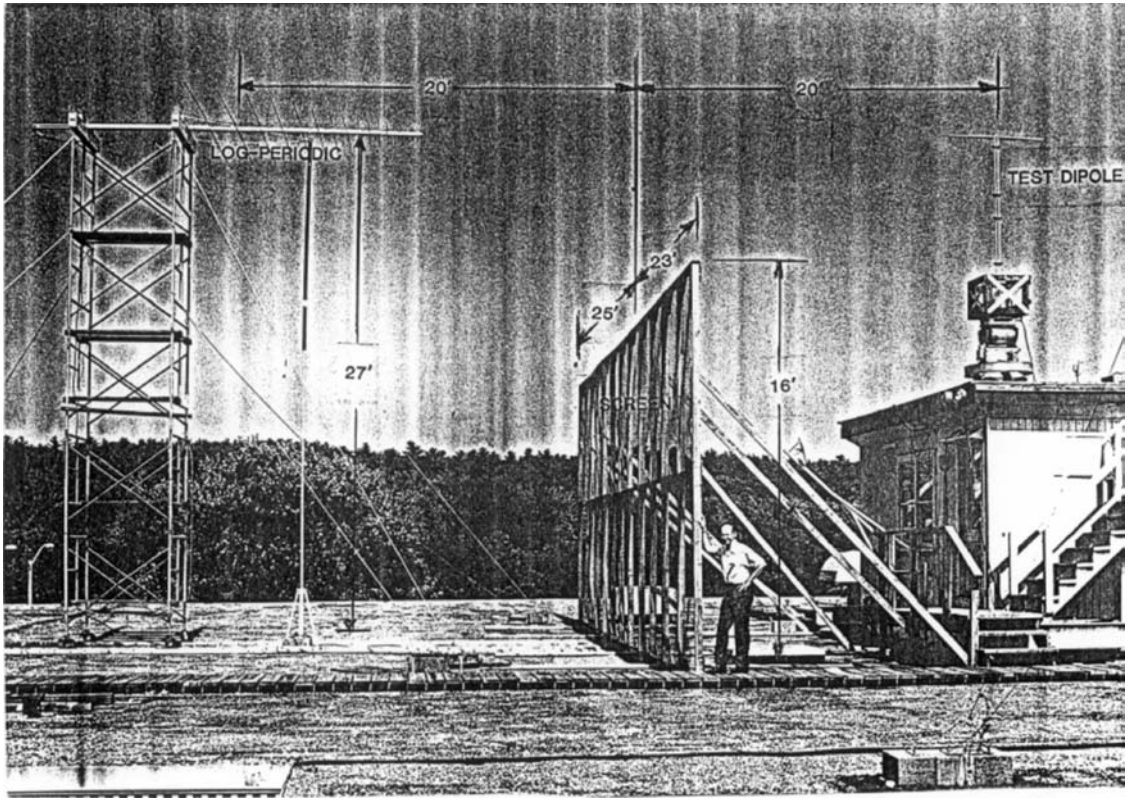

FIGURE 54 VHF Test range on roof of MITRE E-building.

6.6.2 Design Considerations

The first requirement of approximating free-space propagation conditions was realized by (1) propitious choice of the height and separation of the transmitting and receiving antennas and (2) insertion of a conducting fence midway between the transmitting and receiving antennas.

6.6.2.1 Range Dimensions

The separation $AB = 40\,\text{ft}$, between transmitting antenna T_x and receiving antenna R_x at A and B respectively at a height $h = 27\,\text{ft}$, is a design compromise between two opposing constraints as illustrated in Fig. 55. The separation should be sufficiently large (much greater than 5 ft) so that the transmitting and receiving antennas are in the far-field radiation zone of each other. On the other hand, the separation should be much less than $2h = 54\,\text{ft}$ so that the propagation path distance, and hence attenuation, of the multipath specular ray is much greater than the direct path specular ray. The height $h = 27\,\text{ft}$ of the antennas was the maximum attainable height without incurring significant additional expense for staging and safety. The free-space attenuation of the multipath specular ray relative to the direct path ray is 4.5 dB (see Fig. 56).

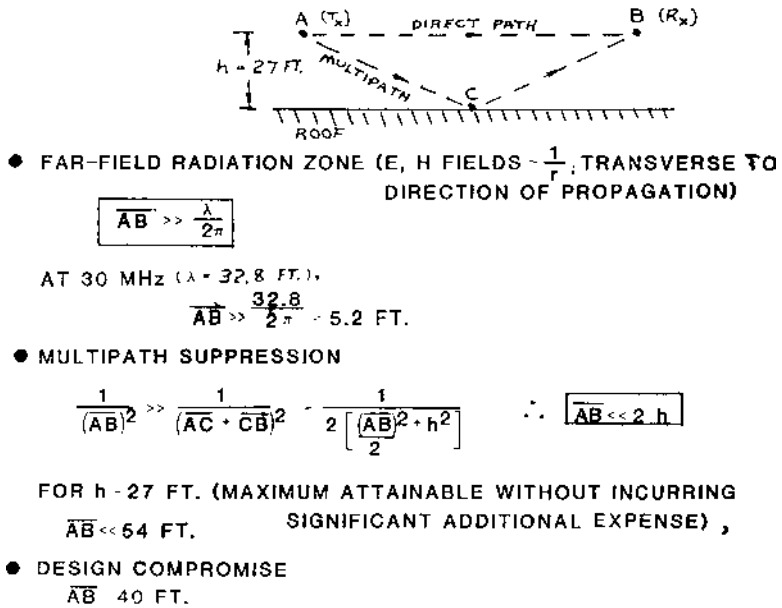
A (Tx)
DIRECT PATH
B (Rx)
h = 27 FT.
MULTIPATH
C
ROOF
• FAR-FIELD RADIATION ZONE (E, H FIELDS ~ 1/r; TRANSVERSE TO DIRECTION OF PROPAGATION)
AB >> λ/2π
AT 30 MHz (λ = 32.8 FT.),
AB >> 32.8/2π = 5.2 FT.
• MULTIPATH SUPPRESSION
1/(AB)² >> 1/(AC + CB)² ≈ 1/2[(AB/2)² + h²]
∴ AB << 2h
FOR h = 27 FT. (MAXIMUM ATTAINABLE WITHOUT INCURRING SIGNIFICANT ADDITIONAL EXPENSE),
AB << 54 FT.
• DESIGN COMPROMISE
AB 40 FT.

FIGURE 55 Height and separation of transmitting and receiving antennas.

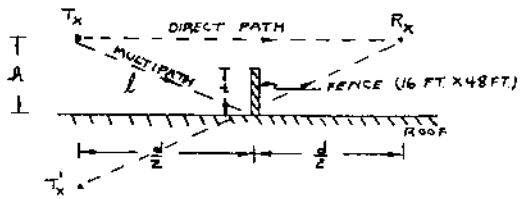

- FENCE HEIGHT t=16 FT. MAXIMIZES THE ATTENUATION OF MULTIPATH SPECULAR RAY WITH RESPECT TO DIRECT RAY

$$A = A_o + A_{diff.}\,(dB) = \text{TOTAL ATTENUATION} = 15.6\ dB$$

WHERE

A_o = FREE SPACE ATTENUATION = $10 \log_{10} \left(\frac{2l}{d}\right)^2 = 4.5$ dB

A_{diff} = ADDITIONAL DIFFRACTION ATTENUATION WITH FENCE = 11.1 dB

- FENCE WIDTH W = 48 FT. IS EQUAL TO LENGTH OF MAJOR AXIS OF FIRST FRESNEL ZONE ELLIPSE SUBTENDED BY FENCE FOR A SOURCE AT T_x' AND RECEIVER AT R_x.
- FENCE DESIGN

  16 FT. HIGH X 48 FT. WIDE

FIGURE 56 Multipath-suppression fence.

6.6.2.2 Multipath-Suppression Fence

Knife-edge diffraction by an upright conducting fence, resting on the roof midway between the transmitting and receiving antennas, serves to attenuate more the multipath quasi-planar wavefront than the direct path quasi-planar wavefront. If t is the height of the fence and h is the height of the antennas, then the direct path specular ray is at a distance $-(h - t)$ into the shadow zone whereas the multipath specular ray is at a distance $+$t into the shadow zone (see Fig. 56). For $h = 27$ ft, the height $t = 16$ ft maximizes the diffraction attenuation of the multipath wavefront relative to the diffraction attenuation of the direct path. The diffraction attenuation of the multipath wavefront relative to the direct path wavefront is 11.1 dB, assuming that the number of Fresnel zones subtended by the width of the fence is infinite.

Since most of the energy of the multipath wavefront incident on the fence is contained within the first Fresnel zone, the fence width $w = 48$ ft was chosen equal to the length of the major axis of the first Fresnel zone ellipse subtended by the fence.

The total attenuation of the multipath wavefront with respect to the direct path wavefront is the sum of the free-space and diffraction attenuations $= 4.5 + 11.1 = 15.6$ dB.

6.6.2.3 Other Design Features

Radio-frequency interference was designed to be at least 40 dB below the peak of a test radiation pattern. This requirement was achieved by (1) increasing the transmitter power to the maximum allowed by Federal Communication Commission regulations, (2) utilizing a receiver with narrow bandpass filters, and (3) utilizing a wideband log periodic transmitting antenna to reduce impedance mismatch power loss over the frequency band of interest.

Induced currents, on the exterior of the outermost conductor of the transmitter and receiver coaxial cables, were minimized to give improved repeatability, reciprocity, and fidelity of the radiation patterns. Minimization of the induced currents was achieved by utilizing (1) baluns on the transmitter and receiver line feeds, (2) lossy ferrite cores on the transmitter and receiver cables, and (3) straight and trim cable runs.

Improved durability of the antenna range to outdoor weather conditions was achieved by utilizing (1) lightweight antenna mounts, (2) a radial-wire ground plane for test monopole elements (see Fig. 57 and description in Chapter 5), (3) a wire-mesh multipath suppression fence, and (4) reinforced supports for the antenna mounts and fence.

The mount for the transmitting antenna was designed so that the antenna's polarization could be changed without dismounting the antenna.

6.6.3 Qualification

Radiation patterns of half-wave dipole antennas and quarter-wave monopole antennas were obtained for E-plane and H-plane polarizations over the frequency band 30–156 MHz. The E-plane patterns of the monopole antennas at nine frequencies within the band are shown in Figs. 21–29 of Chapter 5. The E-Plane patterns of the dipole antennas at 30, 54, 86, 117, and 156 MHz are shown in Figs. 58–62, respectively. The H-plane monopole and dipole patterns were uniform as expected for rotationally uniform antennas.

All the E-plane patterns closely approximate theoretical patterns in free space. The 3 dB beamwidth is within 10% of theoretical with the exception of 29% for a monopole at 88 MHz. The null in the zenith direction is at least 20 dB down from the peak directivity. Since the monopole and dipole antenna geometries have symmetry about the zenith direction, their free-space radiation patterns should be symmetrical about the zenith direction. The two peak directivities about the zenith direction are within 1 dB of each other. The angle of the zenith null on the radiation pattern occurs within $\pm 6^\circ$ of boresight.

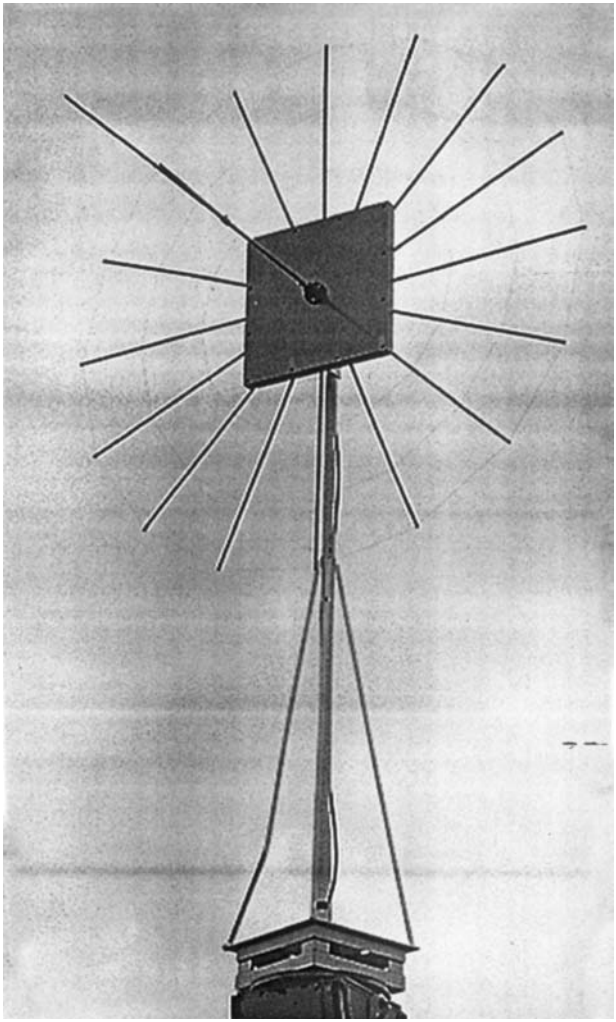

FIGURE 57 Ground plane with test monopole element.

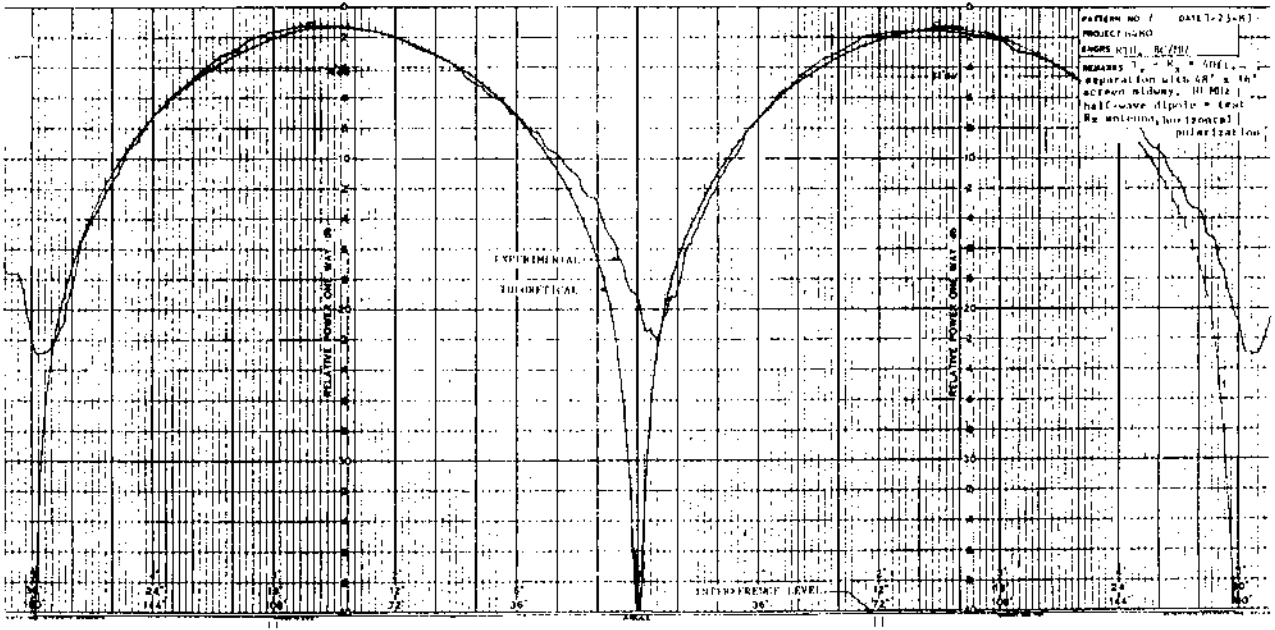

FIGURE 58 Half-wave dipole E-plane test pattern, 30.0 MHz.

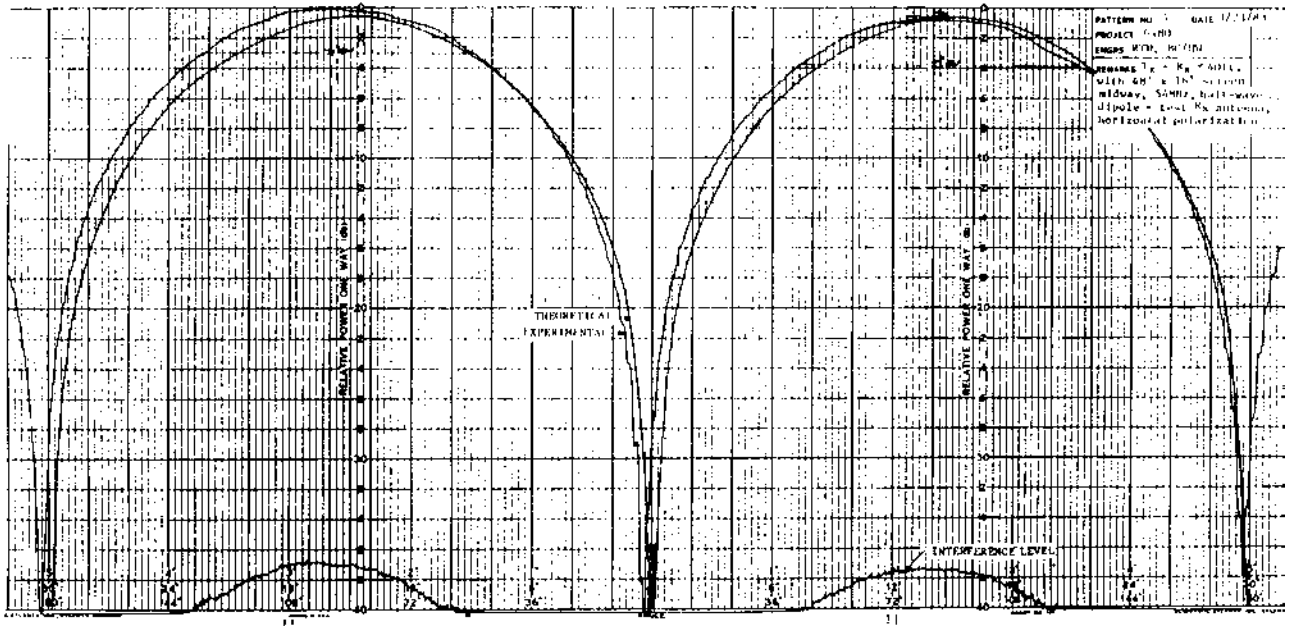

FIGURE 59 Half-wave dipole E-plane test pattern, 54.0 MHz.

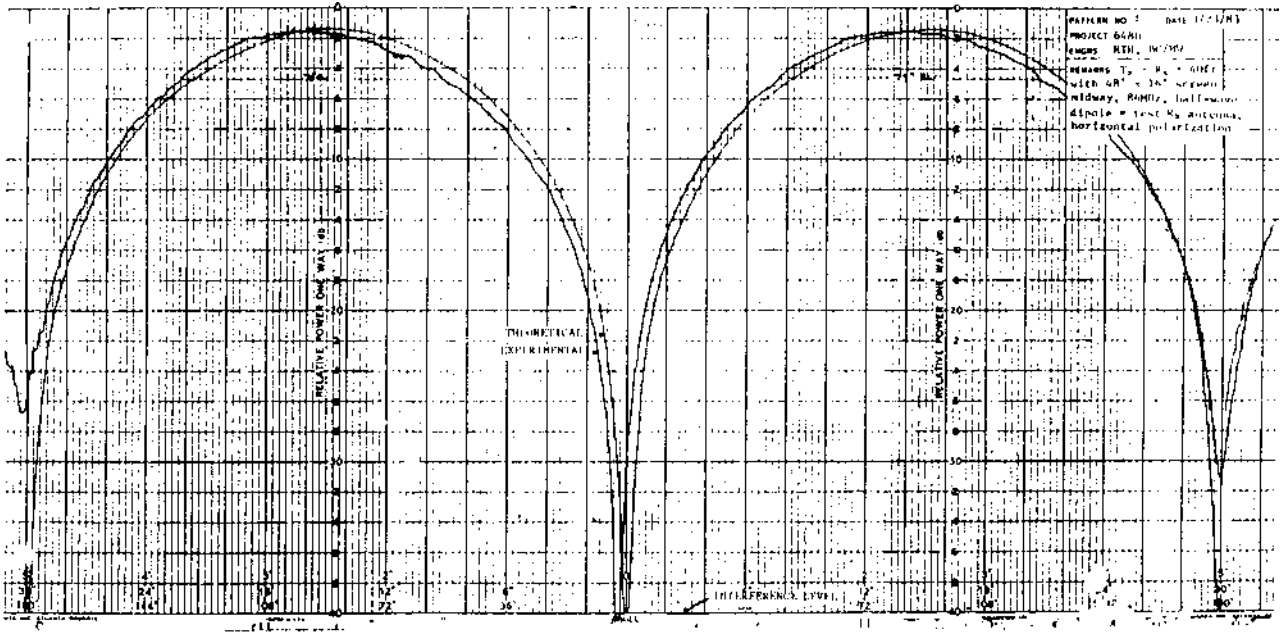

FIGURE 60 Half-wave dipole E-plane test pattern, 86.0 MHz.

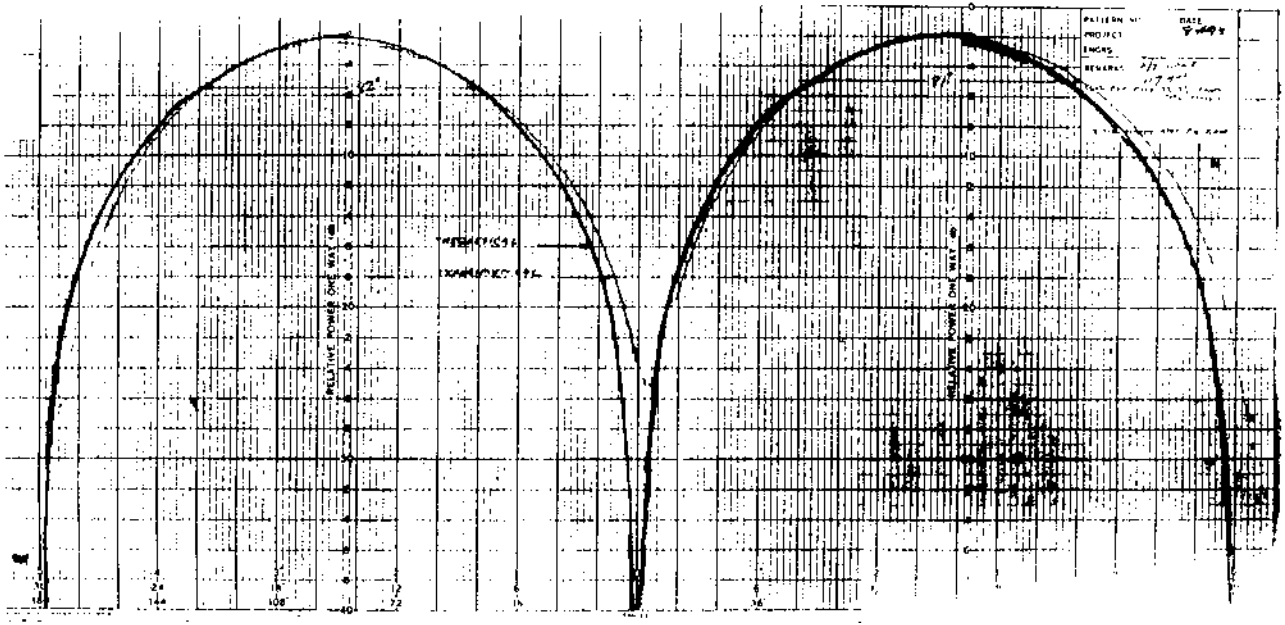

FIGURE 61 Half-wave dipole E-plane test pattern, 117 MHz.

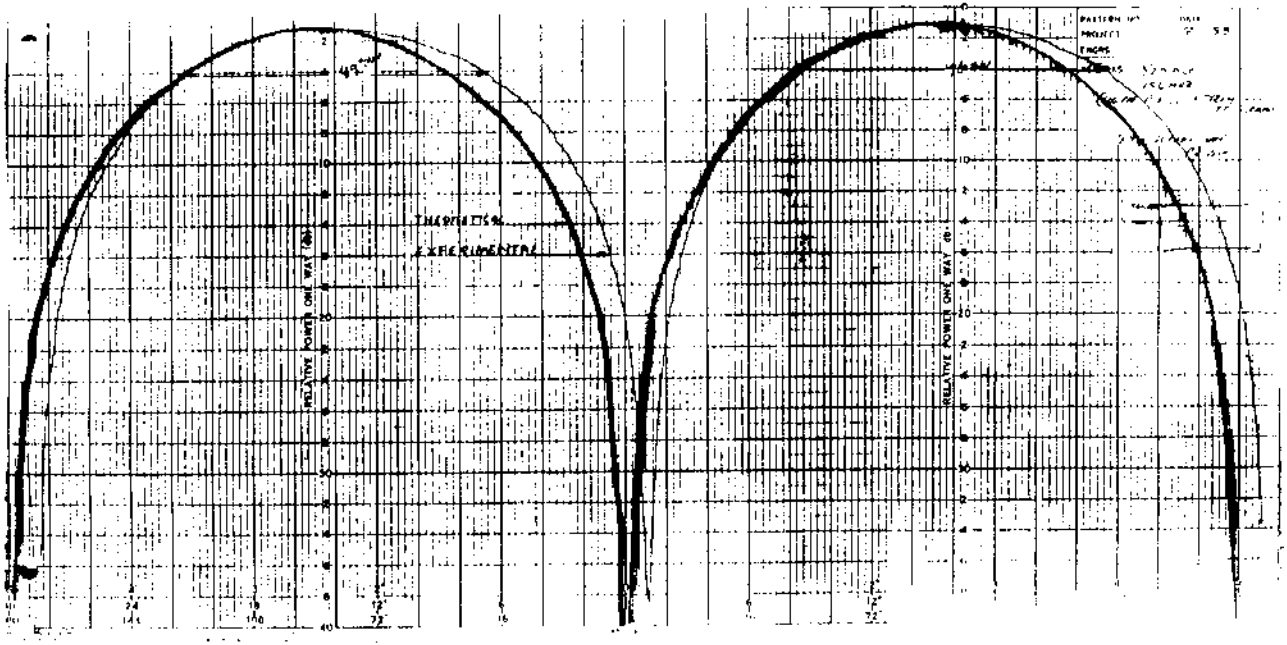

FIGURE 62 Half-wave dipole E-plane test pattern, 156 MHz.

Part II

Monopole Elements on Disk, Radial-Wire, and Mesh Ground Planes in Proximity to Flat Earth

7

Influence of Proximity to Earth

In Part 1, the currents on the monopole element and ground plane were assumed to be independent of earth parameters. This assumption is a reasonably good approximation provided the base of the element is more than a quarter-wavelength above the earth's surface. In such a case, the influence of the earth is lumped into the wave propagation factor or basic transmission loss $L_b(d)$ where d is the great circle propagation path distance between the transmitting and receiving antennas, as discussed in Secs. 6.4 and 6.5. The basic transmission loss is approximately independent of antenna characteristics (unless either one of the antennas has a very narrow beam width) and is usually based on data obtained with electrically small antennas (see Sec. 6.5). The mode of propagation is assumed to be a space wave equal to the sum of direct and indirect waves through the troposphere by line-of-sight, reflection, refraction, and/or scattering (with free-space and earth-dependent propagation losses). This mode and paths of propagation are typical for applications at frequencies above 30 MHz and for antenna platforms that are either airborne or elevated above the earth's surface.

In Part 2, the monopole antenna currents and mode of propagation are influenced by the antenna's proximity to the earth. The antenna's electrical characteristics are functions of earth parameters when the base of the antenna is either below the earth's surface or within a quarter-wavelength above the earth's surface. In such cases, the earth is treated as a part of the antenna structure.

The input impedance is not as severely affected by ground plane edge diffraction (because the earth's proximity softens the edge) but is now affected by the decreased radiation efficiency.

The modeling of monopole antenna performance, when the radiating structure is in proximity to earth, has developed in three progressive stages.

The first stage of model development is concerned with evaluation of the direct, indirect, and surface waves generated by a vertically polarized Hertzian (infinitesimally small) dipole in proximity to the earth's surface. One approach has been the use of Sommerfeld integrals [77,78] for the Hertz vector potential and, by differentiation, the field strength. Sommerfeld represented the total field as the sum of fields from a primary (direct) wave and a secondary wave. The Sommerfeld secondary wave integral is not readily evaluated in the form of an exact closed-form expression and has not lent itself to easy physical interpretation or application. For the purpose of mathematical simplification of terms, later investigators, such as Norton [79,80], Banos [81], Wait and Campbell [82], and King [84,85], represented the total fields as the sum of fields from two waves that they called a "space" wave and a "surface" wave but which we shall call a "pseudo-space" wave and a "pseudo-surface" wave. The pseudo-space wave is defined as the sum of the direct wave and an image wave reflected from a perfectly conducting earth even though the earth is generally imperfectly conducting. The pseudo-surface wave is defined as the wave to account for the near fields not accounted for by the direct and image waves. Norton [79,80], among others, has produced approximate evaluations of the pseudo-surface wave term. Banos [81] and Wait and Campbell [82] developed approximate formulas for the pseudo-surface wave term in restricted, nonoverlapping regions of space. Hansen [83] determined the radiation efficiency for vertical Hertzian and half-wave dipoles above lossy earth. King [84,85] has obtained approximate closed-form expressions for the fields of the pseudo-space wave and pseudo-surface wave at almost all points in space, subject to the constraint that the absolute value of the wave number (or index of refraction) in the earth is at least three times larger than that in free space.

In this book, the space wave (also called "sky wave") is defined as the sum of the direct wave and an indirect wave determined by Fresnel reflection from an imperfectly conducting earth. The surface wave is defined as the wave to account for the near fields not accounted for by the space wave.

Another approach, to modeling a Hertzian dipole in proximity to the earth's surface, is the decomposition of the spherical wavefront into an angular spectrum of plane waves. Booker and Clemmow [86,87] determined the equivalent aperture distribution in the vertical plane that gives the direct, image, and pseudo-surface fields in the air medium above the earth. The aperture distribution consists of the dipole, its image, and an infinite line source extending downward from the image corresponding to the sources for the direct, image, and pseudo-surface waves, respectively. The line source disappears when the earth is perfectly conducting. The aperture distribution yields an angular spectrum of reflected plane waves whose complex amplitude is determined by the Fresnel reflection coefficient for each of the spectrum. The amplitude spectrum of the Fresnel coefficients is the Fourier transform of

the aperture distribution. Brekhovskikh [88] combines the method of steepest descents (saddle points) with the decomposition of a spherical wavefront into an angular spectrum of plane waves to give a complete description of the direct, image, and surface waves at all points in space for a wide variety of cases, including the optical Goos-Hanchen effect of lateral displacement for total internal reflection.

The second stage of model development analyzes the performance of actual structures utilizing models based either on the Sommerfeld attenuation function [89] or variational models based on the Monteath compensation theorem [90–95]. These models give asymptotic or approximate expressions subject to several constraints on the validity of application. Although the Monteath compensation theorem may be conceptually correct, its implementation by analytical methods often involves an approximation such as setting the current or tangential magnetic field on the ground plane equal to that for a perfect ground plane [96] which reduces the theorem to a variational method. The Monteath compensation theorem can also be used to obtain an integral equation for the ground plane current (or fields) but the solution usually requires numerical methods. These models usually do not determine directivity and radiation efficiency as separate entities but instead lump them together as a product to yield the antenna gain, often expressed in dB relative to that for a Hertzian dipole. A more complete survey of this second stage of model development is given in a collection of reprints by Wait et al. [97] and by the references contained within these reprints.

The third and most recent stage of model development is dependent upon numerical methods, and in particular, the methods of moments. There are presently two method-of-moments models that evaluate monopole antenna performance influenced by the structure's proximity to earth. One model, for elements with disk ground planes, is Richmond's [98] computer program RICHMOND3 for disk ground planes that gives the input impedance and current distributions on the element and ground plane. This model is an extension of program RICHMOND1 that is discussed in Secs. 3.3 and 4.2. The other method of moments model, applicable to elements with no ground plane or with a radial ground plane, is the Lawrence Livermore National Laboratory (LLNL) Numerical Electromagnetics Code (NEC) programs for antenna wire elements [99–102]. The NEC programs give the input impedance, current distributions, near and far-zone fields, directivity, and radiation efficiency.

By 1986, the above models for structures in proximity to earth had either been reported in the literature or, in the case of King [85] and Burke and Miller [102], were nearing completion. At that time, the model development described in Part 1 for monopole antennas in free space had been completed by Weiner et al.

[103]. An effort to extend those models to structures in proximity to earth was initiated with the following objectives:

1. Develop models and obtain extensive numerical results for the directivity and radiation efficiency of elements in the absence of ground planes.
2. Develop closed form expressions for the space- and surface-wave fields of a vertically polarized Hertzian dipole in proximity to earth of arbitrary permittivity.
3. Obtain extensive numerical results for input impedance using program RICHMOND3 for elements with disk ground planes.
4. Utilize the current distributions obtained from RICHMOND3 to develop a model and obtain extensive numerical results for the far-field, directivity, and radiation efficiency of elements with disk ground planes.
5. Obtain extensive numerical results using program NEC-GS for input impedance, directivity, and radiation efficiency of elements with radial-wire ground planes.
6. Assess the validity of the Fresnel coefficient models for elements with mesh ground planes.
7. Utilize these models in evaluating the system performance of high-frequency (HF) receiving arrays for over-the-horizon (OTH) radar.

Part 2 describes the results of this effort. Circuit and earth parameters are characterized in Chapter 8. Space- and surface-wave fields are modeled in Chapter 9 for elements in the absence of a ground plane. Richmond's method of moments and the Wait–Surtees variational method are presented in Chapter 10 for elements with disk ground planes. The Numerical Electromagnetics Code (NEC-GS) and the Wait–Pope variational method are presented in Chapter 11 for elements with radial-wire ground planes including the feed cable. Method-of-moments and Fresnel coefficient models are assessed in Chapter 12 for elements with mesh ground planes. Chapter 13 applies Part 2 models to the system performance of OTH radar and ground-based HF receiving arrays. Numerical results of Part 2 models are found in Appendices A.6–A.8. Computer programs (on the attached software disk) of Part 2 models are briefly described in Appendices B.09–B.012. The Sommerfeld–King integrals in Sec. 9.3.3 and beam-pointing errors in Sec. 13.2.2 are evaluated in Appendices C and D, respectively.

8

Characterization of Antenna Parameters

8.1 CIRCUIT PARAMETERS

Monopole antennas, with a vertical element at the center of a disk ground plane in proximity to flat earth, are characterized by at least six parameters: three antenna structure parameters (element length, element radius, and ground plane radius in wavelengths) and three earth parameters (dielectric constant, loss tangent, and height in wavelengths of the ground plane above the earth's surface). In contrast, only three parameters are required when the structure is in free space (see Sec. 2.1). The additional three parameters not only increase the complexity of modeling antenna performance but also increase the difficulty of obtaining sufficient numerical results for standardization of antenna performance.

Consider first the case of a monopole antenna with a disk ground plane in air above nonmagnetic flat earth. The antenna excitation has a time dependence $\exp(j\omega t)$ at a radian frequency $\omega = 2\pi f$ (rad/sec) of corresponding frequency f(Hz) and free-space wavelength $\lambda = c/f$ where c is the free-space velocity of light. The antenna geometry consists of a vertical monopole element, of length h and radius b, on a ground plane of radius a at a height z_0 above earth (see Fig. 63).

In Part 2, circuit parameters in the air and earth mediums are denoted by the subscripts 0 and 1, respectively. However, to simplify the notation, the subscripts 0 and 1 may be dropped in some cases if it is clear from the text to what medium the parameter refers.

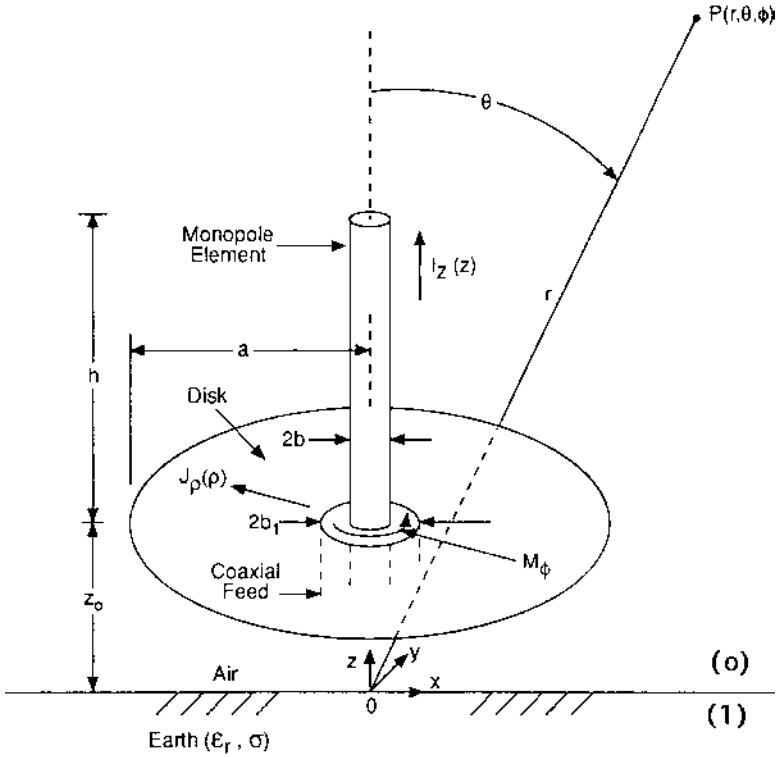

FIGURE 63 Monopole element on a disk ground plane above flat earth.

The earth, with a dielectric constant ε_r and conductivity σ (S/m), has a complex relative permittivity $\varepsilon_1/\varepsilon_0$ given by

$$\varepsilon_1/\varepsilon_0 = n^2 = \varepsilon_r[1 - j(\sigma/\omega\varepsilon_0\varepsilon_r)] = \varepsilon_r(1 - j\tan\delta) \tag{8.1.1}$$

where

$$\tan\delta = \text{loss tangent (dissipation factor)} = (\sigma/\omega\varepsilon_0\varepsilon_r) = (60\lambda\sigma/\varepsilon_r)$$
$$n^2 = (\text{complex index of refraction of earth})^2 = \varepsilon_r[1 - j(\sigma/\omega\varepsilon_0\varepsilon_r)]$$

The wave numbers k_0 and k_1 in air and earth, respectively, are given by

$$k_0 = \omega(\mu_0\varepsilon_0)^{1/2} = 2\pi/\lambda\,(\text{m}^{-1}) \quad \text{(air)} \tag{8.1.2}$$

$$k_1 = n\omega(\mu_0\varepsilon_0)^{1/2} = 2\pi/\lambda_1\,(\text{m}^{-1}) \quad \text{(earth)} \tag{8.1.3}$$

where λ_1 is the wavelength in earth. The wave impedances Z_0 and Z_1 in air and earth, respectively, are given by

$$Z_0 = (\mu_0/\varepsilon_0)^{1/2} \quad \text{(air)} \tag{8.1.4}$$

$$Z_1 = (1/n)(\mu_0/\varepsilon_0)^{1/2} \quad \text{(earth)} \tag{8.1.5}$$

The element and ground plane are assumed to have infinite conductivity. The location of an arbitrary observation point P is designated by spherical coordinates (r, θ, ϕ) with origin at O at the air–earth interface below the element. The point P is at an elevation grazing angle ψ at a distance ρ along the earth's surface.

For antennas with disk ground planes, the six parameters h/λ, b/λ, a/λ, ε_r, σ, z_0/λ sufficiently define the antenna's circuit parameters. For radial-wire ground planes, with uniformly spaced wires in the circumferential direction, additional parameters are the number N and radius b_w of the wires. For mesh-screen ground planes, the mesh shape, spacing, and wire radius are additional parameters.

The feed for the monopole antenna is described in Sec. 2.4. The feed is a coaxial line whose inner conductor extends through a hole of radius b_1 in the ground plane and is connected to the element (see Fig. 2). The outer conductor is connected by means of a flange to the ground plane. The inner conductor's radius is equal to the element radius b and the outer conductor's radius is equal to the ground-plane hole radius b_1. The current on the outside of the coaxial-line feed is assumed to be zero because of the current's attenuation by lossy ferrite toroids along the exterior of the coaxial-line feed. The coaxial-line feed excitation may be replaced by an equivalent surface magnetic current density M_ϕ (magnetic frill) given by Eq. (2.4.8).

The magnetic frill excitation gives rise to an element current distribution $I_z(z)$ along the z axis of the element and a ground-plane current density distribution $J_\rho(\rho)$ in the radial direction. The current density $J_\rho(\rho)$ is the net current density on the top and bottom of the ground plane and is given by Eq. (2.4.1).

The total power P_r radiated into the far-field (at distances r sufficiently large so that the electric field is inversely proportional to r) is given by

$$\begin{aligned} P_r &= (\pi/Z_0)\int_0^{\pi/2} IE_\theta(r, \theta) I^2 r^2 \sin\theta \, d\theta, \quad \sigma > 0; \\ &= (\pi/Z_0)\int_0^{\pi} IE_\theta(r, \theta) I^2 r^2 \sin\theta \, d\theta, \quad \sigma = 0 \end{aligned} \tag{8.1.6}$$

where $E_\theta(r, \theta)$ is the far-zone electric field. For the case of $\sigma > 0$, the integrand in Eq. (8.1.6) is integrated only over the hemisphere above the earth because, in conducting earth, the field is attenuated at a rate greater than $(1/r)$ at large radial distances.

The directivity $d(\theta)$ expressed as a numeric is given by

$$d(\theta) = 2\pi r^2 I E_\theta(r, \theta) I^2/(Z_0 P_r). \tag{8.1.7}$$

The directivity $D(\theta)$ expressed in decibels relative to an isotropic radiator is given by

$$D(\theta) = 10 \log_{10} d(\theta) \quad \text{(dBi)}. \tag{8.1.8}$$

The input power P_{in} to the monopole element is given by

$$P_{in} = (1/2)\,\mathrm{Re}[V(0)\mathrm{I}^*(0)] \tag{8.1.9}$$

where

$V(0)$ = peak input voltage (volts). The input voltage $V(0)$ is usually set equal to 1 volt in the moment-method analysis
$\mathrm{I}^*(0)$ = conjugate of the peak input current $I(0)$ at the base of the monopole element

The input impedance Z_{in} is given by

$$Z_{in} = R_{in} + jX_{in} = V(0)/I(0) \tag{8.1.10}$$

where R_{in} and X_{in} are the input resistance and reactance, respectively.

The radiation resistance R_{rad} is defined as

$$R_{rad} = 2P_r/|I(0)|^2 \tag{8.1.11}$$

The radiation efficiency η is defined as

$$\eta = P_r/P_{in} = [1 + (R_{rad}/R_{in})]^{-1}. \tag{8.1.12}$$

For earth of conductivity $\sigma = 0$, the radiation efficiency $\eta = 1$ because the element and ground plane conductivities are assumed to be infinite. For earth of conductivity $\sigma < \infty$, the radiation efficiency $\eta < 1$.

It is useful to also define a *modified radiation efficiency* η_d by

$$\eta_d = P_{air}/(P_{air} + P_{earth}) \tag{8.1.13}$$

where

P_{air} = far-field power radiated into the upper hemisphere (air)
P_{earth} = far-field power radiated into the lower hemisphere (earth)

For earth conductivity $\sigma = 0$, the radiation efficiency $\eta = 1$ but the modified radiation efficiency $\eta_d < 1$. For $\varepsilon_r = 1$ and $\sigma = 0$, the modified radiation efficiency $\eta_d = 0.5$.

8.2 EARTH CHARACTERISTICS

Recommendation P.527-3 of the International Telecommunication Union (ITU) [104] gives the relative dielectric constant, conductivity, and penetration depth of several generic classifications of earth, over the frequency range 10 kHz–300 GHz (see Figs. 64–66). These values are based largely on measurements and extrapolations performed more than 20 years earlier. The values at HF frequencies are summarized in Table 16. The ITU values of dielectric constant and conductivity fail to display frequency dispersion at HF frequencies because the HF values are extrapolated from measurements made mostly at medium frequency (MF) wavelengths. Hagn [105,106] at SRI International has corrected this deficiency in the HF band by developing values of the dielectric constant, conductivity, skin depth, and dissipation factor, over the frequency range 2–30 MHz, for several SRI categories of terrain (see Figs. 67–70).

The ITU values of penetration depth δ and the Hagn values of skin depth δ_s refer to the depth in earth at which the electromagnetic *field* has attenuated to $(1/e)$ of its value on the underside surface of the earth. In other words, $\delta = \delta_s = 1/\alpha$ where α is the propagation attenuation constant in earth. For magnetic earth of relative permeability constant μ_r and zero magnetic loss (i.e., the magnetic conductivity $\sigma_m = 0$), the skin depth δ_s is given by [105–107]

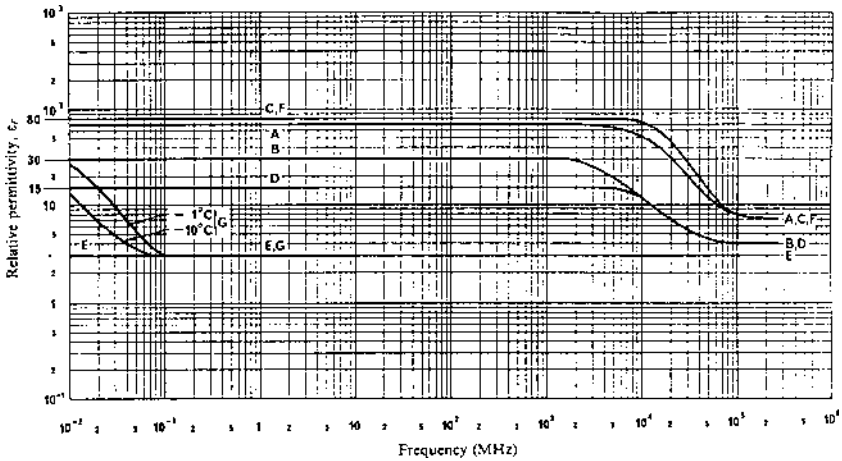

FIGURE 64 Dielectric constant of CCIR classifications of earth, 10 kHz–300 GHz (CCIR, Rec. 527-1): (A) sea water (average salinity), 20°C; (B) wet ground; (C) fresh water, 20°C; (D) medium dry ground; (E) very dry ground; (F) pure water, 20°C; and (G) ice (fresh water, −1°C and −10°C).

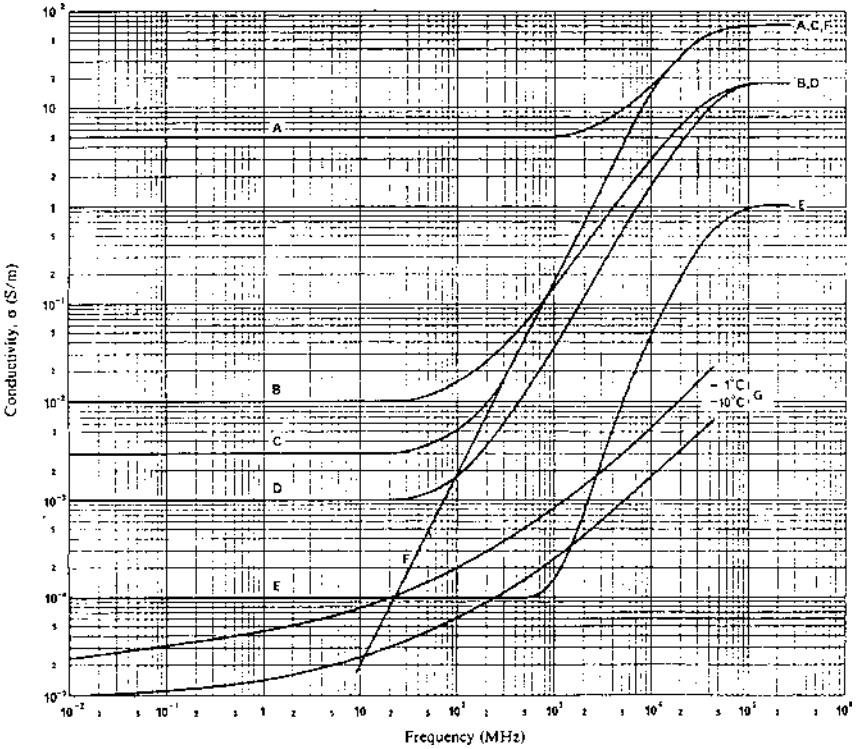

FIGURE 65 Conductivity of ITU classifications of earth, 10 kHz–300 GHz (ITU, Recommendation P.527-3): (A) sea water (average salinity), 20°C; (B) wet ground; (C) fresh water, 20°C; (D) medium dry ground; (E) very dry ground; (F) pure water, 20°C; and (G) ice (fresh water, −1°C and −10°C).

as

$$\delta_s = [(\omega^4 \mu_r^2 \varepsilon_r^2/4c^4) + (\sigma^2 \omega^2 \mu_r^2 \mu_0^2/4)^{1/2} - (\omega^2 \mu_r \varepsilon_r/2c^2)]^{-1/2}, \qquad \sigma_m = 0 \tag{8.2.1}$$

where $c = (\varepsilon_0 \mu_0)^{-1/2}$ = velocity of light in free space. For the ITU classifications of earth in Table 16, $\mu_r = 1$.

At HF frequencies, the skin depth in various types of soil is of the order of 1–100 m (see Fig. 69). Consequently, the electrical properties of monopole antennas in proximity to earth can be influenced by the properties of earth well below the earth's surface. For example, a dry salt flat (that at one time was a salt lake)

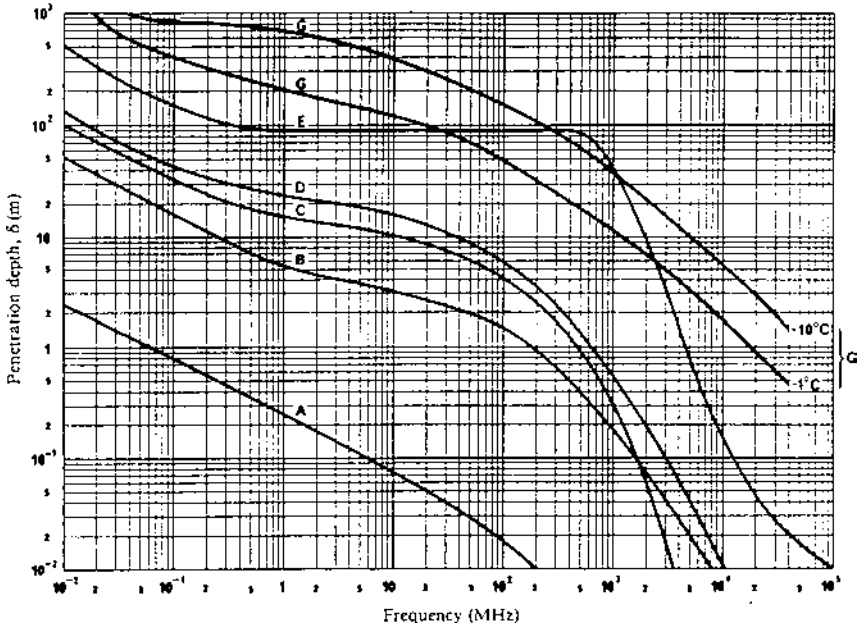

FIGURE 66 Penetration depth of ITU classifications of earth, 10 kHz–300 GHz (ITU, Recommendation P.527-3): (A) sea water (average salinity), 20°C; (B) wet ground; (C) fresh water, 20°C; (D) medium dry ground; (E) very dry ground; (F) pure water, 20°C; and (G) ice (fresh water, −1°C and −10°C).

may have poor conductivity on its surface but excellent conductivity within a skin depth of its surface.

The IEEE [108] has recommended radio methods for measuring ground conductivity. Among these methods are:

1. Electric field vs. distance and frequency,
2. Coplanar loop,
3. Inverted monopole,
4. Inverted monopole with parasitics,
5. Two-conductor open-wire line (OWL),
6. Four-probe (e.g., Wenner),
7. Wave tilt.

These methods usually involve measurements made near the soil surface. The assumption is usually made that the soil is homogeneous within a skin depth. This assumption is often not valid at HF or lower frequencies because of the large

TABLE 16 High-Frequency Permittivity, Loss Tangent, and Penetration Depth of ITU-R P.527-3 Classifications of Earth

			Loss tangent $\sigma/(\omega\varepsilon_r\varepsilon_0) = (60\lambda)(\sigma/\varepsilon_r)$			Penetration depth δ (m)		
	Constants		Frequency (MHz) [wavelength (m)]			Frequency (MHz) [wavelength (m)]		
Cases	ε_r	σ (S/m)	3 [99.93]	15 [19.986]	30 [9.993]	3 [99.93]	15 [19.986]	30 [9.993]
(1) Perfect ground	1.0	∞	∞	∞	∞	0	0	0
(2) Sea water (average salinity 20°C)	70.0	5.0	4.282×10^{2}	8.425×10^{1}	4.283×10^{1}	1.3×10^{-1}	5.8×10^{-2}	4.1×10^{-2}
(3) Fresh water	80.0	3.0×10^{-2}	2.251×10^{0}	4.497×10^{-1}	2.248×10^{-1}	2.1×10^{0}	1.6×10^{0}	1.6×10^{0}
(4) Wet ground	30.0	1.0×10^{-2}	1.999×10^{0}	3.997×10^{-1}	1.999×10^{-1}	3.7×10^{0}	3.0×10^{0}	2.9×10^{0}
(5) Medium dry ground	15.0	1.0×10^{-3}	3.997×10^{-1}	7.995×10^{-2}	3.997×10^{-2}	2.1×10^{1}	2.1×10^{1}	2.1×10^{1}
(6) Very dry ground	3.0	1.0×10^{-4}	1.999×10^{-1}	3.997×10^{-2}	1.999×10^{-2}	9.2×10^{1}	9.2×10^{1}	9.2×10^{1}
(7) Pure water, 20°C	80.0	1.8×10^{-6}	1.350×10^{-4}	—	—	2.6×10^{4}	—	—
		5.0×10^{-4}	—	7.495×10^{-3}	—	—	9.4×10^{2}	—
		1.7×10^{-3}	—	—	1.274×10^{-2}	—	—	2.7×10^{1}
(8) Ice (fresh water, −1°C)	3.0	6.0×10^{-5}	1.199×10^{-1}	—	—	1.5×10^{2}	—	—
		9.0×10^{-5}	—	3.597×10^{-2}	—	—	1.0×10^{2}	
		1.0×10^{-4}	—	—	1.999×10^{-2}	—	—	9.2×10^{1}
(9) Ice (fresh water, −10°C)	3.0	1.8×10^{-5}	3.597×10^{-2}	—	—	5.1×10^{2}	—	—
		2.7×10^{-5}	—	1.079×10^{-2}	—	—	3.4×10^{2}	—
		3.5×10^{-5}	—	—	6.995×10^{-3}	—	—	2.6×10^{2}
(10) Average land (TCI)	10.0	5.0×10^{-3}	2.998×10^{0}	5.996×10^{-1}	2.998×10^{-1}	4.8×10^{0}	1.6×10^{0}	3.4×10^{0}
(11) Free space	1.0	0	0	0	0	∞	∞	∞

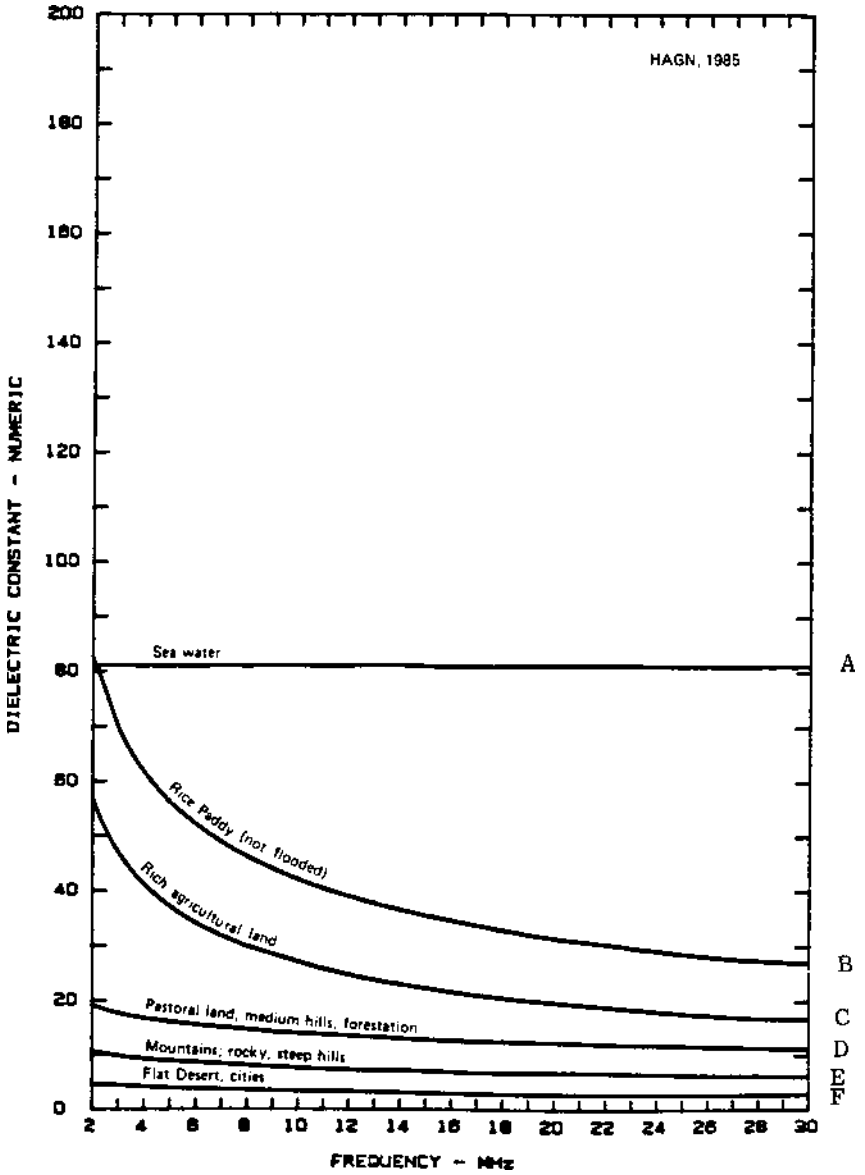

FIGURE 67 Dielectric constant of SRI categories of terrain, 2–30 MHz (Hagn, 1985): (A) sea water; (B) rice paddy (not flooded); (C) rich agricultural land; (D) pastoral land, medium hills, forestation; (E) mountains; rocky, steep hills; and (F) flat desert, cities.

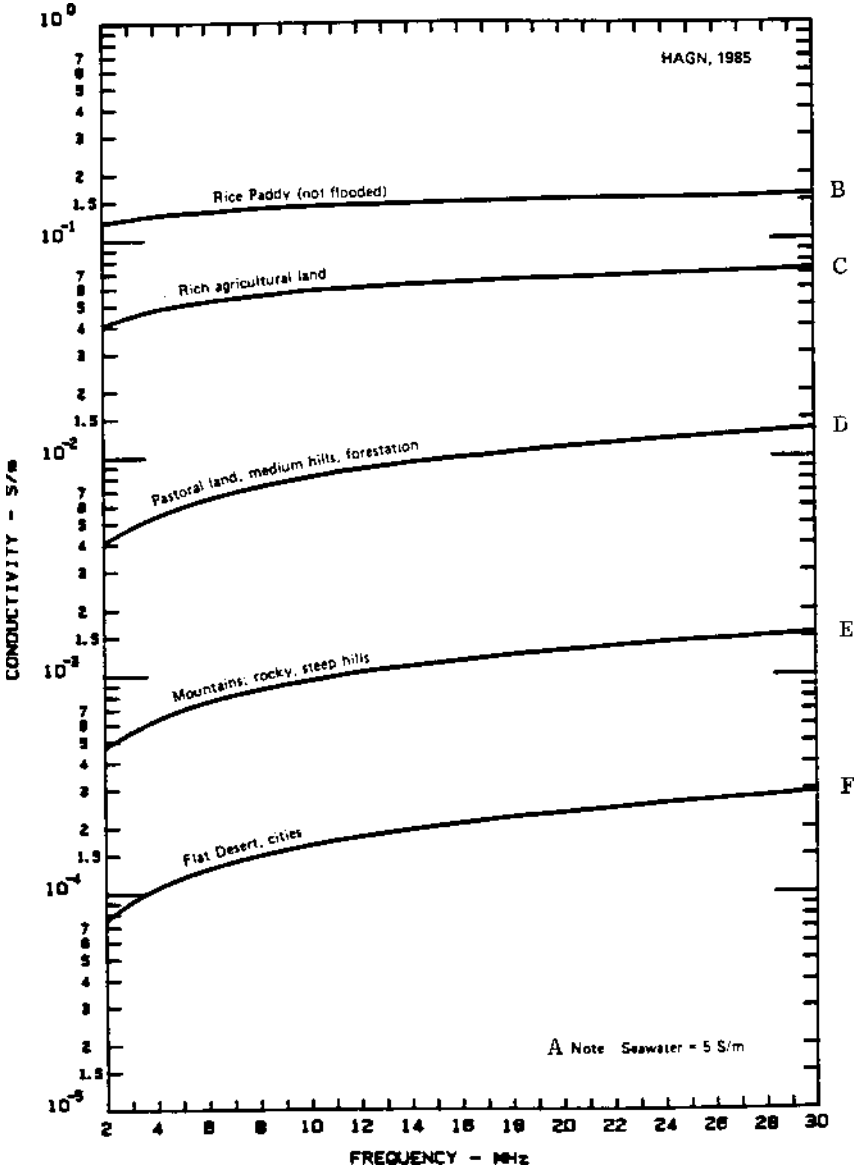

FIGURE 68 Conductivity of SRI categories of terrain, 2–30 MHz (Hagn, 1985): (A) sea water = 5 S/m; (B) rice paddy (not flooded); (C) rich agricultural land; (D) pastoral land, medium hills, forestation; (E) mountains; rocky, steep hills; and (F) flat desert, cities.

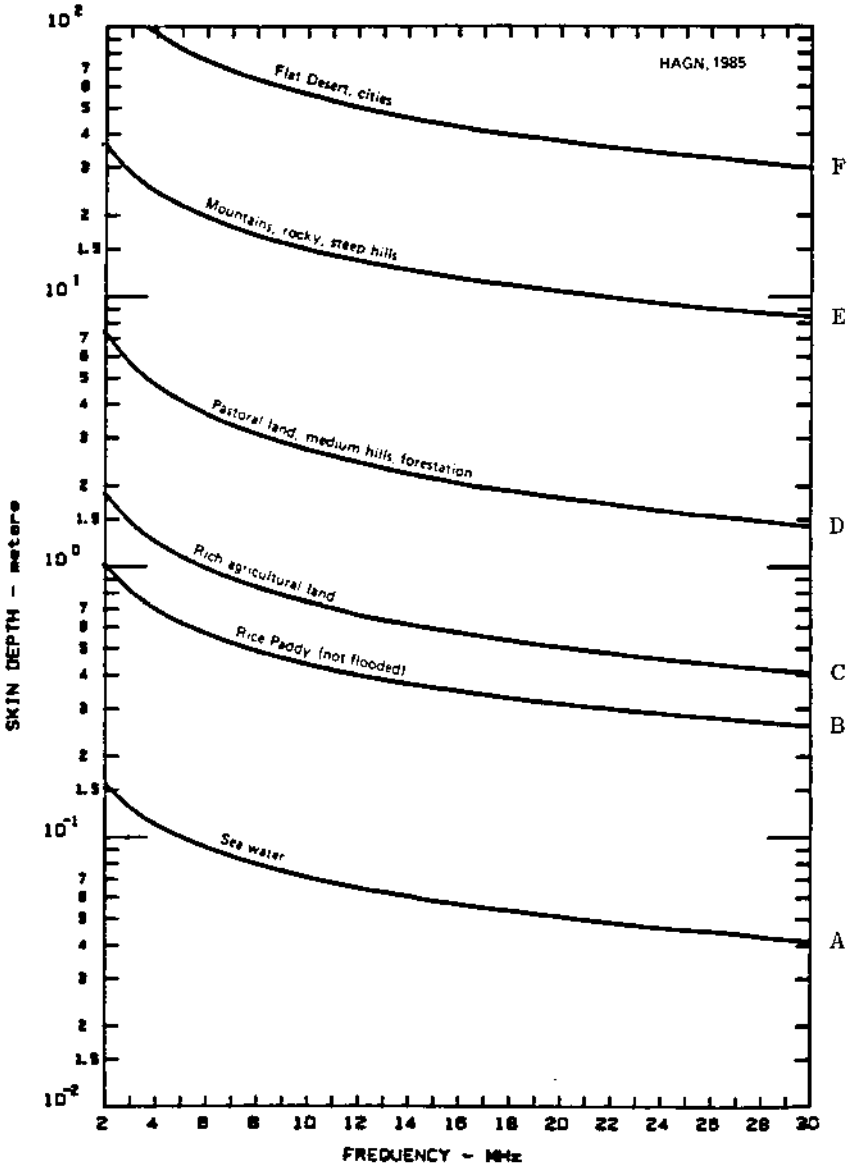

FIGURE 69 Skin depth of SRI categories of terrain, 2–30 MHz (Hagn, 1985): (A) sea water; (B) rice paddy (not flooded); (C) rich agricultural land; (D) pastoral land, medium hills, forestation; (E) mountains; rocky, steep hills; and (F) flat desert, cities.

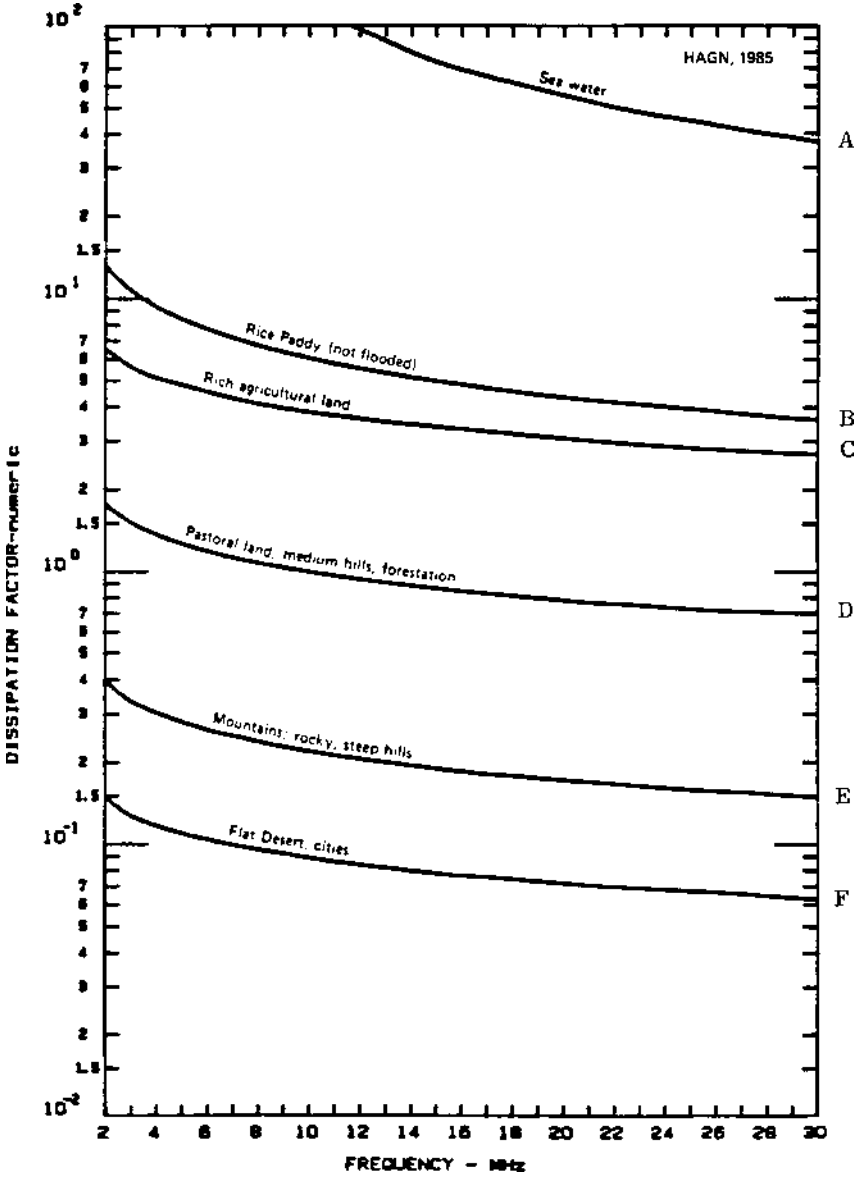

FIGURE 70 Dissipation factor (loss tangent) of SRI categories of terrain, 2–30 MHz (Hagn, 1985): (A) sea water; (B) rice paddy (not flooded); (C) rich agricultural land; (D) pastoral land, medium hills, forestation; (E) mountains; rocky, steep hills; and (F) flat desert, cities.

skin depths at those frequencies and because the moisture content can vary significantly within a skin depth.

8.3 ANTENNA STRUCTURE FABRICATION CONSIDERATIONS

In this book, antenna parameter characterization and modeling of monopole antennas are concerned with "zero-order" antenna design, i.e., the design of antennas for performance under ideal operating and environmental conditions. For antennas that are protected from the environment by a radome, zero-order design may be sufficient. However, for large ground-based antennas, such as HF antenna arrays for over-the-horizon (OTH) radar, poor structural design and fabrication of the antenna elements and their associated ground planes and/or back screens may cause substantial reductions in performance from that expected based on zero-order design.

Antenna structural design is particularly critical in radars that look down at the ground to detect targets. In such cases, the clutter echo power can be 60–80 dB larger than the target echo power. The target is detected by measuring the difference in returns from one pulse to the next. This method is based on the underlying assumption that the clutter echo power and the radar system are stable between pulses. The degree of stability is defined as the subclutter visibility (SCV), i.e., the ratio by which the target echo power may be weaker than the coincident clutter echo power and still be detected with specified detection and false alarm probabilities [109]. Faulty antenna fabrication and poor structural design can cause a decrease in subclutter visibility and an increase in radio-frequency (RF) interference because of radar system instability between pulses. Furthermore, faulty antenna fabrication and poor structural design can cause a decrease in antenna radiation efficiency and a decrease in antenna directivity at low grazing angles because of poor connectivity of mesh ground plane panels.

Antenna-related mechanisms that may reduce system performance are:

1. Motion, induced by wind forces or land vibration, of antenna elements, backscreens, or ground planes,
2. Breaking of electrical contacts (either permanently or temporarily from wind, humidity, temperature, moisture, salt, ice and snow, land vibrations, and dissimilar metals) at the joints that fasten the many panels comprising the ground planes and backscreens,
3. Corona plumes, characterized by a *high* conductivity electrical discharge during transmit at the junctions between antenna elements and their insulated support cables, caused by wind-induced breakage and/or improper design of corona-protection rings at the junctions,

4. Arcing, characterized by a *low* conductivity electrical discharge during transmit at the junctions between antenna elements and their insulated support cables, caused by poor and loose contacts of dissimilar-metal clevice and pin joints at the junctions; also, arcing during transmit at temperature-expansion junctions between sections of a transmission line, caused by poor or loose contacts of dissimilar metal junctions.

For example, ground screens constructed of copper mesh panels joined together by brazing may be required for nonideal environmental conditions whereas galvanized-steel mesh panels fastened together by crimped cadmium-plated copper clips may be sufficient for ideal environmental conditions. Under nonideal environmental conditions, the latter type of fabrication can cause a several order-of-magnitude decrease in subclutter visibility and a 10–20 dB decrease in one-way antenna gain at very low grazing angles.

As another example, transmitter elements of 6-in. diameter and 0.25-in. wall thickness may be designed to yield a maximum element deflection of 0.5 in. under nonideal operating conditions. If it is assumed that deflection is inversely proportional to [(outer diameter)^4 − (inner diameter)^4], then weaker transmitter elements of 4-in. diameter with a 0.125-in. wall thickness would cause a deflection of 2.6 in. under the same environmental conditions, resulting in a substantial reduction in subclutter visibility.

9

Models in the Absence of a Ground Plane

9.1 INTRODUCTION

The concept of monopole elements with a ground plane of zero extent is discussed in Sec. 3.2.

The modeling of monopole elements in air (free space) but in proximity to earth is complicated by the effect of earth on input impedance and the generation of a surface wave in addition to the usual space wave. This chapter presents three models for monopole elements in the absence of a ground plane. The three models are the method of images modified by Fresnel coefficients (presented in Sec. 9.2), the Sommerfeld integral (presented in Sec. 9.3), and the Numerical Electromagnetics Code (presented in Sec. 9.4).

The method of images modified by Fresnel coefficients is accurate for the space-wave portion of the fields but does not account for the surface-wave portion of the fields. The far-field amplitudes of the space wave and surface wave are inversely proportional to distance and (distance)^2, respectively, from the radiating source (see Sec. 9.3). Consequently, the far-field amplitude of the surface wave is small compared to that of the space wave except on the surface of imperfectly conducting earth where the space-wave amplitude is zero.

The method of images modified by the Fresnel coefficients is therefore accurate for modeling the far-field, directivity, and the space wave portion of the near-field in the air medium above earth but is not adequate for modeling radiation efficiency because it ignores the effect of surface wave on total radiated power and dissipated power in the earth medium.

The method of images with Fresnel reflection is presented first because of its simplicity and accuracy in modeling the space wave. Secs. 9.2.1 and 9.2.2

consider a vertically polarized Hertzian dipole in air above *conducting* and *nonconducting* earth, respectively. Sec. 9.2.3 considers a monopole element in air above nonconducting earth.

The second model is the Sommerfeld integral for a vertically polarized Hertzian dipole in air above flat earth. Sec. 9.3.1 presents integral expressions for the Hertz potential of the primary and secondary waves which are then regrouped as a space wave (sum of direct and indirect waves) and a surface wave. Sec. 9.3.2 gives the relationships between the fields and pseudo-fields in air. Approximate closed-form expressions for the surface-wave fields in air are developed in Sec. 9.3.3 for the cases of the earth's relative permittivity either large or approximately equal to unity.

9.2 SPACE-WAVE FIELDS: METHOD OF IMAGES WITH FRESNEL REFLECTION

9.2.1 Vertically Polarized Hertzian Dipole in Air Above Conducting Earth

9.2.1.1 Dipole Moment

With reference to Fig. 4 of Sec. 3.2.2, a vertically polarized electrically thin monopole element, of length h and base current $I(0)$, has a current distribution given by Eq. (3.1.1). The mean current I_{av} is found by integrating the current distribution over the length h and dividing by h. Accordingly,

$$I_{\text{av}} = I(0)[1 - \cos(kh)]/[kh \sin(kh)] \tag{9.2.1}$$

For $kh \ll 1$ and retaining the first three terms in the Taylor series expansion, Eq. (9.2.1) reduces to

$$I_{\text{av}} = I(0)/2, \quad kh \ll 1 \tag{9.2.2}$$

In the limit of $h \rightarrow 0$ with the product $[I_{\text{av}}h]$ held constant, the monopole element reduces to a vertically polarized Hertzian dipole of moment $\mathbf{p}$ given by

$$\mathbf{p} = \mathbf{u}_z p \tag{9.2.3}$$

where

$\mathbf{u}_z$ = unit vector along the z axis
$p = \lim_{h\rightarrow 0}[I_{\text{av}}h] = (1/2)\lim_{h\rightarrow 0}[I(0)h]$ (A m).

9.2.1.2 Far-Fields in Air

At a far-field point $P(r, \theta, \phi)$ of radial distance r, elevation angle θ, and azimuthal angle ϕ, the electric field $\boldsymbol{E} = \boldsymbol{u}_\theta E_\theta$ of a monopole element in free space in the absence of earth is given by Eq. (3.2.13). In the limit $h \rightarrow 0$ and retaining the first

three terms in the Taylor series expansion of vanishing small quantities, Eq. (3.2.13) reduces to

$$E_\theta = A \sin\theta, \quad \text{absence of earth} \tag{9.2.4}$$

where

$$A = j[(Z_0 k_0 p)/(4\pi r)] \exp(-jk_0 r) \quad (\mathrm{V/m})$$

$$Z_0 = (\mu_0/\varepsilon_0)^{1/2} = \text{wave impedance in free space (ohms)}$$

$$k_0 = \omega(\mu_0\varepsilon_0)^{1/2} = \text{wave number in free space } (\mathrm{m}^{-1})$$

Equation (9.2.4) is the far-field electric field intensity, *in the absence of earth*, of a vertically polarized Hertzian dipole of moment **p**. The corresponding magnetic field intensity $H_\phi = (1/Z_0)E_\theta$.

Consider now a vertically polarized Hertzian dipole of moment **p** in air at a point $P_1(0, 0, z_0)$ at a height z_0 above earth of dielectric constant ε_r and conductivity σ (see Fig. 71). In this section and throughout Part 2, the air medium is treated as though it were free space. The far-fields, of the space wave and surface wave in conducting earth, are attenuated to zero at a rate greater than

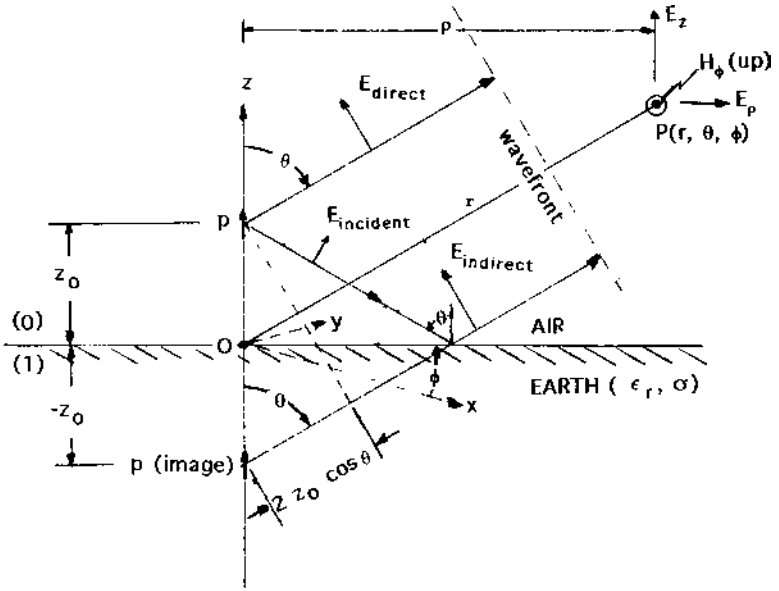

FIGURE 71 Direct and indirect rays of space wave, at a far-field point $P(r, \theta, \phi)$ in air, from a vertically polarized hertzian dipole above earth.

$(1/r)$. In the free-space medium above earth, the far-field amplitudes of the space wave and surface wave are proportional to $(1/r)$ and $(1/r)^2$, respectively (see Sec. 9.3). Consequently, in the free-space medium above earth, the space wave is the only significant wave in the far-field.

For the far-field conditions $z_0 \ll r$ and $k_0 r \gg 1$ (see Eq. 9.2.39a in the following subsection), the space wave at a far-field point $P(r, \theta, \phi)$ in air above earth is the sum of a direct wave and an indirect wave, both propagating in the same direction with electric fields in the θ direction and magnetic fields in the ϕ direction (see Fig. 71). The indirect wave is modified by the plane-wave Fresnel reflection coefficient $R_v(\theta)$ defined as the ratio of the reflected magnetic field $\mathbf{H}_r$ to that of the incident magnetic field $\mathbf{H}_i$ (equal to the ratio of the negative of the reflected electric field $\mathbf{E}_r$ to that of the incident electric field $\mathbf{E}_i$) for the polarization of $\mathbf{E}_i$ parallel to the plane of incidence and for the directions of the direct and indirect electric fields defined in Fig. 72. The Fresnel reflection coefficient $R_v(\theta)$ is given by [110] as

$$R_v(\theta) = \mathbf{H}_r/\mathbf{H}_i = -\mathbf{E}_r/\mathbf{E}_i = \frac{n\cos\theta - (1 - n^{-2}\sin^2\theta)^{1/2}}{n\cos\theta + (1 - n^{-2}\sin^2\theta)^{1/2}} \tag{9.2.5}$$

where n is the complex index of refraction of earth given by Eq. (8.1.1). Equation (9.2.5) was obtained from [110] by multiplying the numerator and denominator in [110] by n^2 and is identical to that given by [111]. The quantity n^2 is generally

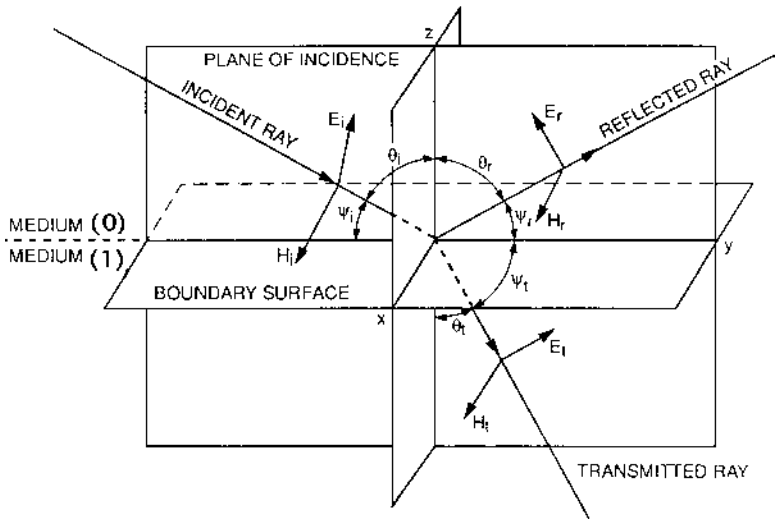

FIGURE 72 Incident, reflected, and transmitted rays for parallel polarization of a plane wave incident on a semi-unbounded medium.

a complex number. The positive root or principal value of $(1 - n^{-2}\sin^2\theta)^{1/2}$ is intended (see discussion in Sec. 11.2). The subscript v denotes parallel polarization but also serves here as a reminder that the source is a *vertically* polarized monopole element or Hertzian dipole. In some textbooks, $R_v(\theta)$ is given as the negative of that given in Eq. (9.2.5) because $R_v(\theta)$ is defined as $\mathbf{E}_r/\mathbf{E}_i$ rather than $-\mathbf{E}_r/\mathbf{E}_i$. Also in some textbooks, the directions of the incident and reflected fields are defined 180° out of phase from that shown in Figs. 71 and 72.

The far-field electric field $\mathbf{E} = \mathbf{u}_\theta E_\theta$ with E_θ given by

$$\begin{aligned} E_\theta &= (\mathbf{E}_{\text{direct}} + \mathbf{E}_{\text{indirect}}) \\ &= A\sin\theta\exp(jk_0z_0\cos\theta)[1 + R_v(\theta)\exp(-j2k_0z_0\cos\theta)], \\ &\quad 0 \le \theta \le \pi/2; \\ &= 0, \quad \pi/2 < \theta \le \pi, \quad \sigma > 0 \end{aligned} \tag{9.2.6}$$

where

$$\begin{aligned} \mathbf{E}_{\text{direct}} &= A\sin\theta\exp(jk_0z_0\cos\theta), \quad 0 \le \theta \le \pi/2; \\ &= 0, \quad \pi/2 < \theta \le \pi, \quad \sigma > 0 \\ \mathbf{E}_{\text{indirect}} &= A\sin\theta R_v(\theta)\exp(-jk_0z_0\cos\theta), \quad 0 \le \theta \le \pi/2; \\ &= 0, \quad \pi/2 < \theta \le \pi, \quad \sigma > 0 \\ A &= j[(Z_0k_0p)/(4\pi r)]\exp(-jk_0r) \text{ as defined in Eq. (9.2.4)} \end{aligned}$$

The far-field magnetic field $\mathbf{H}$ is given by

$$\mathbf{H} = \mathbf{u}_\phi(1/Z_0)E_\theta \tag{9.2.7}$$

where Z_0 is defined in Eq. (8.1.4) and E_θ is given by Eq. (9.2.6).

9.2.1.3 Directivity

In the absence of earth, the numeric directivity $d(\theta)$ of a vertically polarized Hertzian dipole is found by substituting Eq. (9.2.3) into Eq. (3.2.20). Accordingly,

$$d(\theta) = (3/2)\sin^2\theta, \quad \text{absence of earth} \tag{9.2.8}$$

In the presence of conducting earth, the numeric directivity $d(\theta)$ of a vertically polarized Hertzian dipole is found by substituting Eq. (9.2.6) in

Eq. (8.1.7). Accordingly,

$$d(\theta) = \frac{2\sin^2\theta \exp(j2k_0 z_0 \cos\theta)\,|1 + R_v(\theta)\exp(-j2k_0 z_0\cos\theta)|^2}{\int_0^{\pi/2} \sin^3\theta \exp(j2k_0 z_0\cos\theta)\,|1 + R_v(\theta)\exp(-j2k_0 z_0\cos\theta)|^2\, d\theta}, \quad 0 \le \theta \le \pi/2; \\ = 0, \quad \pi/2 < \theta \le \pi, \quad \sigma > 0 \tag{9.2.9}$$

As an example, consider the case when $z_0 = 0$ so that the Hertzian dipole is in air just above the earth's surface. Equation (9.2.9) reduces to

$$d(\theta) = \frac{2\sin^2\theta\,|1 + R_v(\theta)|^2}{\int_0^{\pi/2} \sin^3\theta\,|1 + R_v(\theta)|^2\, d\theta}, \quad 0 \le \theta \le \pi/2, \quad z_0 = 0; \\ = 0, \quad \pi/2 < \theta \le \pi, \quad \sigma > 0 \tag{9.2.10}$$

For $\sigma = \infty$, the Fresnel reflection coefficient $R_v(\theta) = +1$ and Eq. (9.2.10) reduces to

$$d(\theta) = \frac{4 \times 2\sin^2\theta}{4\int_0^{\pi/2} \sin^3\theta\, d\theta} = \frac{4 \times 2\sin^2\theta}{4 \times (2/3)} \\ = 3\sin^2\theta, \quad 0 \le \theta \le \pi/2; \quad \sigma = \infty; \quad z_0 = 0; \\ = 0, \quad \pi/2 < \theta \le \pi, \quad \sigma = \infty \tag{9.2.11}$$

which is identical to Eq. (3.8.18) for an electrically short monopole element with a perfect ground plane. The directivity is twice that given by Eq. (9.2.4) for a Hertzian dipole in free space and has a peak numeric directivity $d(\pi/2) = 3.0$ on the horizon.

For $0 \le \sigma < \infty$ and $\varepsilon_r > 1$, the Fresnel reflection coefficient $R_v(\pi/2) = -1$ which, when substituted into Eq. (9.2.10), gives the result that the far-field radiation pattern has a null on the horizon with a directivity $d(\pi/2) = 0$.

For $\sigma = 0$ and $\varepsilon_r = 1$, the Fresnel reflection coefficient $R_v(\theta) = 0$ and the directivity is given by Eq. (9.2.4).

Numerical results of Eq. (9.2.10), for the directivity pattern of a vertically polarized Hertzian dipole just above the surface of conducting earth, are tabulated in App. A.8 for HF frequencies and ITU classifications of earth given in Table 16. App. A.8 gives the directivity of a monopole element of various lengths h. The tables that apply to a Hertzian dipole are for $N = (h/0.05\lambda) = 0$ where N is the number of segments of the monopole element. The tables corresponding to $N = 0$ are Tables A8-1, A8-7, A8-13, A8-19, A8-25, A8-31, A8-37, A8-43,

TABLE 17 Peak Directivity of a Vertically Polarized Hertzian Dipole at Zero Height Above Earth for ITU-R P.527-3 Classifications of Earth

	6.0 MHz		15.0 MHz		30.0 MHz	
Earth classification	D_{peak} (dBi)	ψ_{peak} (°)	D_{peak} (dBi)	ψ_{peak} (°)	D_{peak} (dBi)	ψ_{peak} (°)
(1) Perfect ground	4.77	0	4.77	0	4.77	0
(2) Sea water	4.69	10	4.68	12	4.68	14
(3) Fresh water	4.78	24	4.80	24	4.80	24
(4) Wet ground	4.86	26	4.89	28	4.89	28
(5) Medium dry ground	4.96	30	4.97	30	4.97	30
(6) Very dry ground	5.11	32	5.11	32	5.11	32
(7) Pure water, 20°C	4.81	24	4.81	24	4.81	24
(8) Ice, −1°C	5.11	32	5.11	32	5.11	32
(9) Ice, −10°C	5.11	32	5.11	32	5.11	32
(10) Average land (TCI)	4.95	30	4.99	30	5.00	30
(11) Free space	1.76	0	1.76	0	1.76	0

A8-49, and A8-55. The peak directivity D_{peak} (dBi) and the corresponding grazing angle ψ_{peak} (°) from those tables are summarized in Table 17. Except for the case of sea water, the peak directivities are slightly more than that for a perfect ground and the corresponding grazing angles are 24–32° above the horizon. For the case of sea water, the peak directivities are slightly less than that for the case of a perfect ground and the corresponding grazing angles are 10–14° above the horizon.

9.2.1.4 Radiation Efficiency Neglecting Surface Wave

The tables in App. A.8 also print out "radiation efficiency." The radiation efficiency is defined in Eq. (8.1.12) as the ratio of the far-field total radiated power to the antenna input power. This quantity is computed in App. A by the method of images modified by Fresnel reflection neglecting the effect of surface wave on the fraction of the input power that is dissipated in the earth medium. The App. A.8 values of radiation efficiency have been printed out so that a comparison can be made with the more accurate results given in Sec. 9.4.

In App. A.8, the numeric radiation efficiency $\eta = P_r/P_{in}$ where P_r is the total radiated power found by integrating Eq. (9.2.6) over the upper hemisphere for the case $z_0 = 0$ and P_{in} is the total input power. If it is assumed that P_{in} is equal to the total output power of a Hertzian dipole in free space in the absence of earth, then P_{in} is found by substituting Eq. (9.2.4) in Eq. (8.1.6) and integrating

over then upper and lower hemispheres. Accordingly,

$$P_{\mathrm{r}} = (\pi/Z_0)\mathrm{r}^2|A|^2 \int_0^{\pi/2} \sin^3\theta\,|1 + R_{\mathrm{v}}(\theta)|^2 \mathrm{d}\theta, \quad z_0 = 0, \quad \sigma > 0 \tag{9.2.12}$$

$$P_{\mathrm{in}} = (\pi/Z_0)r^2|A|^2(8/3) \tag{9.2.13}$$

$$\eta = P_{\mathrm{r}}/P_{\mathrm{in}} = (3/8) \int_0^{\pi/2} \sin^3\theta\,|1 + R_{\mathrm{v}}(\theta)|^2 \mathrm{d}\theta, \quad z_0 = 0, \quad \sigma > 0, \text{ surface wave neglected} \tag{9.2.14}$$

The input power P_{in} given by Eq. (9.2.13) is the same result found by integrating Eq. (9.2.6) over the upper hemisphere for the case $z_0 = 0$ and $R_{\mathrm{v}}(\theta) = +1$ for a perfectly conducting earth. The decibel radiation efficiently H in App. A.8 is given by

$$H = 10 \log_{10} \eta \quad (\mathrm{dB}) \tag{9.2.15}$$

The accurate value of radiation efficiency, for a Hertzian dipole just above conducting earth, is $\eta = 0.0000$, unless the earth is a perfect conductor in which case $\eta = 1.0000$ (see Sec. 9.4). In Tables A8-1, A8-7, and A8-55, for the cases of a perfect conductor, sea water, and average land, $\eta = 1.0000$, 0.9250, and 0.3517, respectively. Therefore, App. A.8 values for radiation efficiency are larger than the accurate values, except for the case in which earth is a perfect conductor.

9.2.1.5 Near-Fields in Air

Consider first, in the absence of earth, a vertically polarized electrically thin monopole element of length h with base at the origin $O(0, 0, 0)$ (see Fig. 4 of Sec. 3.2.2). The element has a base current $I(0)$ and an average current I_{av} given by Eq. (9.2.1). At a near-field point $P(\rho, z, \phi) = P(r, \theta, \phi)$ where $\rho = r \sin\theta$, $z = r\cos\theta$, and $r = (\rho^2 + z^2)^{1/2}$, a vertically polarized electrically thin monopole element has near-fields given by Eqs. (3.2.4)–(3.2.6).

In the limit $h \to 0$, with the product $(I_{\mathrm{av}}h)$ held constant, the monopole element reduces to a vertically polarized Hertzian dipole of moment $\mathbf{p} = \mathbf{u}_z p$ where $p = [I(0)/2]$ [see Eq. (9.2.3)]. The near-fields, of the vertically polarized Hertzian dipole in the absence of earth, are found by expanding the terms of Eqs. (3.2.4)–(3.2.6) in a Taylor series, retaining all terms of zero, first, and second order in h, and then taking the limit as $h \to 0$. Accordingly, the near-fields in cylindrical coordinates are $\mathbf{H} = \mathbf{u}_\phi H_\phi$ and $\mathbf{E} = \mathbf{u}_\rho E_\rho + \mathbf{u}_z E_z$ with components

given by

$$H_\phi = (1/Z_0)\,A \sin\theta\,[1 + (jk_0 r)^{-1}], \tag{9.2.16}$$

$$E_\rho = A \sin\theta \cos\theta\,[1 + 3(jk_0 r)^{-1} + 3(jk_0 r)^{-2}] \tag{9.2.17}$$

$$E_z = A[-\sin^2\theta + (3\cos^2\theta - 1)(jk_0 r)^{-1} + (3\cos^2\theta - 1)(jk_0 r)^{-2}] \tag{9.2.18}$$

where A, k_0, and Z_0 are defined in Eq. (9.2.4).

The corresponding near-fields in spherical coordinates are found from Eqs. (9.2.16)–(9.2.18) by use of the unit vector transformations

$$\mathbf{u}_\mathrm{r} = (\mathbf{u}_z \cos\theta + \mathbf{u}_\rho \sin\theta) \tag{9.2.19a}$$

$$\mathbf{u}_\theta = (\mathbf{u}_\rho \cos\theta - \mathbf{u}_z \sin\theta) \tag{9.2.19b}$$

$$\mathbf{u}_\phi = \mathbf{u}_\phi \tag{9.2.19c}$$

Accordingly, the near-fields in spherical coordinates are $\mathbf{H} = \mathbf{u}_\phi H_\phi$ and $\mathbf{E} = \mathbf{u}_\mathrm{r}\mathbf{E}_\mathrm{r} + \mathbf{u}_\theta E_\theta$ with components given by

$$H_\phi = (1/Z_0)\,A \sin\theta\,[1 + (jk_0 r)^{-1}] \tag{9.2.20}$$

$$E_\mathrm{r} = 2\,\mathrm{A}\cos\theta\,[(jk_0 r)^{-1} + (jk_0 r)^{-2}] \tag{9.2.21}$$

$$E_\theta = A \sin\theta[1 + (jk_0 r)^{-1} + (jk_0 r)^{-2}] \tag{9.2.22}$$

Equations (9.2.16)–(9.2.22) are consistent with the results given in [112] for the near-fields of a vertically polarized Hertzian dipole in the absence of earth. For $k_0\mathrm{r} \gg 1$, $H_\Phi = (1/Z_0)E_\theta$, $\mathbf{E}_\mathrm{r} = 0$, and $E_\theta = A\sin\theta$ which agree with the far-fields given by Eq. (9.2.4).

Consider now a vertically polarized Hertzian dipole of moment $\mathbf{p} = \mathbf{u}_z p$ on the z-axis at a height z_0 above conducting earth of relative dielectric constant ε_r and conductivity $\sigma > 0$ (see Fig. 73). The near-fields, at a point $P(\rho, z, \phi)$ in cylindrical coordinates of $P(r, \theta, \phi)$ in spherical coordinates, are the sum of the fields from the space and surface waves. In this section, the space-wave fields are determined by the method of images modified by the Fresnel reflection coefficient whereas in Sec. 9.3 both the space-wave and surface-wave fields are considered. Although the surface wave is negligible in the far-field, it is not negligible in the near-field.

The space-wave field at $P(r, \theta, \phi)$ above conducting earth is the sum of the fields from a direct ray and an indirect ray (see Fig. 73). The direct ray subtends an elevation angle θ_0 and has a path length r_0 given by

$$r_0 = [\rho^2 + (z - z_0)^2]^{1/2} \tag{9.2.23}$$

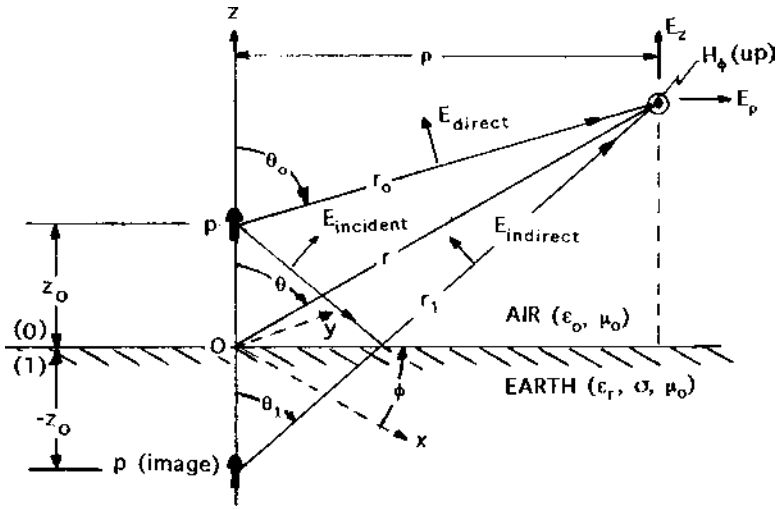

FIGURE 73 Direct and indirect rays of space wave, at a near-field point $P(r, \theta, \phi)$ in air, from a vertically polarized hertzian dipole above earth.

where

$$\rho = r \sin \theta$$

$$z = r \cos \theta$$

$$z - z_0 = r_0 \cos \theta_0$$

The indirect ray (also known as the "reflected ray") subtends an elevation angle θ_1 and has a path length r_1 given by

$$r_1 = [\rho^2 + (z + z_0)^2]^{1/2} \tag{9.2.24}$$

where $z + z_0 = r_1 \cos \theta_1$.

The cylindrical-coordinate components of the near-field direct wave in the air medium are found by substituting θ_0 for θ and r_0 for r in Eqs. (9.2.16)–(9.2.18). Accordingly, $\mathbf{H}_{\text{direct}} = \mathbf{u}_\phi H_{\phi\,\text{direct}}$ and $\mathbf{E}_{\text{direct}} = \mathbf{u}_\rho E_{\rho\,\text{direct}} + \mathbf{u}_z E_{z\,\text{direct}}$ with components given by

$$H_{\phi\,\text{direct}} = (1/Z_0) A_0 \sin \theta_0 [1 + (jk_0 r_0)^{-1}], \quad z \geq 0 \tag{9.2.25}$$

$$E_{\rho\,\text{direct}} = A_0 \sin \theta_0 \cos \theta_0 [1 + 3(jk_0 r_0)^{-1} + 3(jk_0 r_0)^{-2}], \quad z \geq 0 \tag{9.2.26}$$

$$\begin{aligned} E_{z\,\text{direct}} = A_0 [&-\sin^2 \theta_0 + (3 \cos^2 \theta_0 - 1)(jk_0 r_0)^{-1} \\ &+ (3 \cos^2 \theta_0 - 1)(jk_0 r_0)^{-2}], \quad z \geq 0 \end{aligned} \tag{9.2.27}$$

where $A_0 = j[(Z_0 k_0 p)/(4\pi r_0)] \exp(-jk_0 r_0)$.

The spherical-coordinate components of the near-field direct wave in the air medium are found by substituting θ_0 for θ and r_0 for r in Eqs. (9.2.20)–(9.2.22). Accordingly, $\mathbf{H}_{\text{direct}} = \mathbf{u}_\phi H_{\phi\,\text{direct}}$ and $\mathbf{E}_{\text{direct}} = \mathbf{u}_r E_{r\,\text{direct}} + \mathbf{u}_\theta E_{\theta\,\text{direct}}$ with components given by

$$H_{\phi\,\text{direct}} = (1/Z_0) A_0 \sin\theta_0 [1 + (jk_0 r_0)^{-1}], \quad z \geq 0 \tag{9.2.28}$$

$$E_{r\,\text{direct}} = 2A_0 \cos\theta_0 [(jk_0 r_0)^{-1} + (jk_0 r_0)^{-2}], \quad z \geq 0 \tag{9.2.29}$$

$$E_{\theta\,\text{direct}} = A_0 \sin\theta_0 [1 + (jk_0 r_0)^{-1} + (jk_0 r_0)^{-2}], \quad z \geq 0 \tag{9.2.30}$$

where A_0 is defined above.

The cylindrical-coordinate components of the near-field indirect wave in the air medium are found by substituting θ_1 for θ and r_1 for r in Eqs. (9.2.16)–(9.2.18) and by multiplying Eqs. (9.2.16)–(9.2.18) by the Fresnel reflection coefficient $R_v(\theta_1)$ where $R_v(\theta_1)$ is given by Eq. (9.2.5) except that θ_1 is substituted for θ. Accordingly, $\mathbf{H}_{\text{indirect}} = \mathbf{u}_\phi H_{\phi\,\text{indirect}} = R_v(\theta_1)\mathbf{H}_{\text{image}}$ and $\mathbf{E}_{\text{indirect}} = \mathbf{u}_\rho E_{\rho\,\text{indirect}} + \mathbf{u}_z E_{z\,\text{indirect}} = R_v(\theta_1)\mathbf{E}_{\text{image}}$ with cylindrical-coordinate components given by

$$\begin{aligned} H_{\phi\,\text{indirect}} &= (1/Z_0) A_1 R_v(\theta_1) \sin\theta_1 [1 + (jk_0 r_1)^{-1}] \\ &= R_v(\theta_1) H_{\phi\,\text{image}}, \quad z \geq 0 \end{aligned} \tag{9.2.31}$$

$$\begin{aligned} E_{\rho\,\text{indirect}} &= A_1 R_v(\theta_1) \sin\theta_1 \cos\theta_1 [1 + 3(jk_0 r_1)^{-1} + 3(jk_0 r_1)^{-2}] \\ &= R_v(\theta_1) E_{\rho\,\text{image}}, \quad z \geq 0 \end{aligned} \tag{9.2.32}$$

$$\begin{aligned} E_{z\,\text{indirect}} &= A_1 R_v(\theta_1)[-\sin^2\theta_1 + (3\cos^2\theta_1 - 1)(jk_0 r_1)^{-1} \\ &\quad + (3\cos^2\theta_1 - 1)(jk_0 r_1)^{-2}] \\ &= R_v(\theta_1) E_{z\,\text{image}}, \quad z \geq 0 \end{aligned} \tag{9.2.33}$$

where

$H_{\phi\,\text{image}}$, $E_{\rho\,\text{image}}$, $E_{z\,\text{image}}$ are defined by Eqs. (9.2.31)–(9.2.33)

$$A_1 = j[(Z_0 k_0 p)/(4\pi r_1)] \exp(-jk_0 r_1)$$

$$R_v(\theta_1) = [n\cos\theta_1 - (1 - n^{-2}\sin^2\theta_1)^{1/2}]/[n\cos\theta_1 - (1 - n^{-2}\sin^2\theta_1)^{1/2}]$$

The concept of using locally the plane-wave Fresnel reflection coefficient for determining the indirect space-wave near-fields is not new and had been used

correctly by Beckmann and Spizzochino for the scattering of electromagnetic waves from rough surfaces [113]. The indirect space-wave fields are defined to include the higher-order ${r_1}^{-2}$ and ${r_1}^{-3}$ terms in order to agree with the method of images for the case of a perfect ground plane ($|n^2| = \infty$) whose surface-wave fields are constrained to be zero.

The corresponding spherical-coordinate components of the near-field indirect wave are found from Eqs. (9.2.20)–(9.2.22) in the same manner. Accordingly, $\mathbf{H}_{\text{indirect}} = \mathbf{u}_\phi H_{\phi\,\text{indirect}} = R_{\text{v}}(\theta_1)\mathbf{H}_{\text{image}}$ and $\mathbf{E}_{\text{indirect}} = \mathbf{u}_r E_{r\,\text{indirect}} + \mathbf{u}_\theta E_{\theta\,\text{indirect}} = R_{\text{v}}(\theta_1)\mathbf{E}_{\text{image}}$ with components given by

$$\begin{aligned} H_{\phi\,\text{indirect}} &= (1/Z_0)A_1 R_{\text{v}}(\theta_1)\sin\theta_1\,[1 + (jk_0r_1)^{-1}] \\ &= R_{\text{v}}(\theta_1)H_{\phi\,\text{image}}, \quad z \geq 0 \end{aligned} \tag{9.2.34}$$

$$\begin{aligned} E_{r\,\text{indirect}} &= 2A_1 R_{\text{v}}(\theta_1)\cos\theta_1\,[(jk_0r_1)^{-1} + (jk_0r_1)^{-2}] \\ &= R_{\text{v}}(\theta_1)E_{r\,\text{image}}, \quad z \geq 0 \end{aligned} \tag{9.2.35}$$

$$\begin{aligned} E_{\theta\,\text{indirect}} &= A_1 R_{\text{v}}(\theta_1)\sin\theta_1\,[1 + (jk_0r_1)^{-1} + (jk_0r_1)^{-2}] \\ &= R_{\text{v}}(\theta_1)E_{\theta\,\text{image}}, \quad z \geq 0 \end{aligned} \tag{9.2.36}$$

where $H_{\phi\,\text{image}}, E_{r\,\text{image}}, E_{\theta\,\text{image}}$, are defined by Eqs. (9.2.34)–(9.2.36) and A_1 and $R_{\text{v}}(\theta_1)$ are defined above.

The total space-wave near-fields $\mathbf{H}_{\text{space}}$ and $\mathbf{E}_{\text{space}}$ in air are the sum of the direct and indirect space-wave near-fields. Accordingly,

$$\mathbf{H}_{\text{space}} = \mathbf{H}_{\text{direct}} + \mathbf{H}_{\text{indirect}} = \mathbf{H}_{\text{direct}} + R_{\text{v}}(\theta_1)\mathbf{H}_{\text{image}}, \quad z \geq 0 \tag{9.2.37}$$

$$\mathbf{E}_{\text{space}} = \mathbf{E}_{\text{direct}} + \mathbf{E}_{\text{indirect}} = \mathbf{E}_{\text{direct}} + R_{\text{v}}(\theta_1)\mathbf{E}_{\text{image}}, \quad z \geq 0 \tag{9.2.38}$$

where

$\mathbf{H}_{\text{direct}}, \mathbf{E}_{\text{direct}}$ are given by
  Eqs. (9.2.25)–(9.2.27) (cylindrical-coordinate components)
  Eqs. (9.2.28)–(9.2.30) (spherical-coordinate components)
$\mathbf{H}_{\text{indirect}}, \mathbf{E}_{\text{indirect}}$ are given by
  Eqs. (9.2.31)–(9.2.33) (cylindrical-coordinate components)
  Eqs. (9.2.34)–(9.2.36) (spherical-coordinate components)

Equations (9.2.37) and (9.2.38) reduce to Eqs. (9.2.6) and (9.2.7) for the far-field conditions

$$r \gg z_0, \quad k_0 r \gg 1 \tag{9.2.39a}$$

The above expressions for the space-wave near-fields are exact. The total near-fields are the sum of the space-wave fields and the surface-wave fields. Approximate closed-form expressions for the surface-wave fields are obtained in Sec. 9.3 and more exact numerical evaluations of the surface-wave fields are obtained in Sec. 9.4.

9.2.2 Vertically Polarized Hertzian Dipole in Air Above Nonconducting Earth

9.2.2.1 Near-Fields in Air and Earth

Consider a vertically polarized Hertzian dipole of moment $\mathbf{p} = \mathbf{u}_z p$ in air, at a height z_0 above the surface of nonconducting earth ($\sigma = 0$) of relative dielectric constant ε_r (see Fig. 74). For nonconducting earth, the index of refraction n is a real number and is given by $n = (\varepsilon_r)^{1/2}$. The dipole is located in spherical coordinates at a point $Q(z_0, 0, \phi) = Q(0, z_0, \phi)$ in cylindrical coordinates.

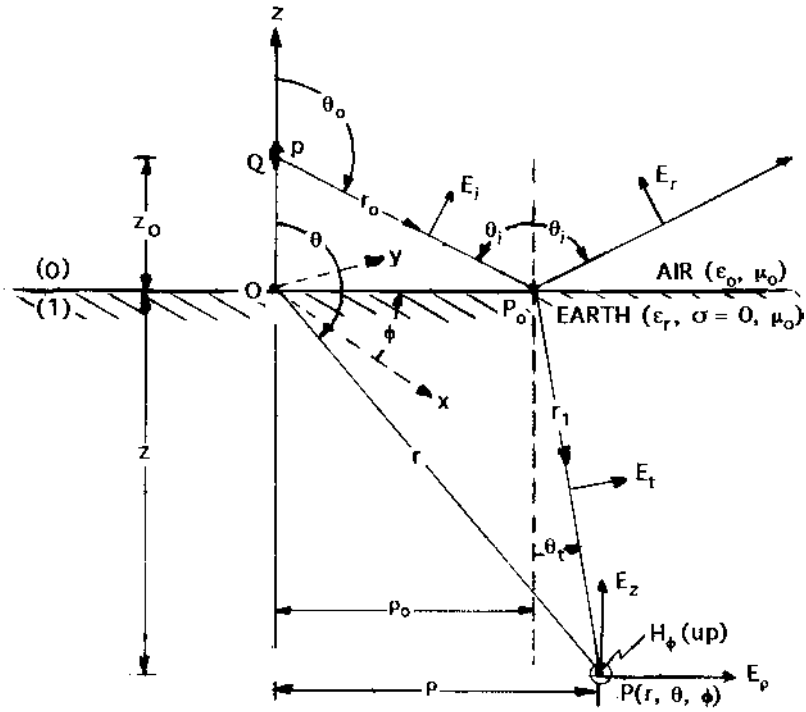

FIGURE 74 Space-wave ray, at a field point $P(r, \theta, \phi)$ in nonconducting earth, from a vertically polarized Hertzian dipole in air above the earth.

For near-field points $P(r, \theta, \phi)$ in air and for $0 \leq \theta \leq \pi/2$ (see Fig. 73), the space-wave near-fields are the sum of direct and indirect fields given by Eqs. (9.2.37) and (9.2.38).

For near-field points $P(r, \theta, \phi)$ in earth and for $\pi/2 < \theta \leq \pi$, the space-wave near-fields are propagated along a path QP_0 in air and a path P_0P in earth (see Fig. 74). Consider the ray in air that is propagated along the path QP_0 at an elevation angle θ_0 for $\pi/2 < \theta_0 \leq \pi$. The ray is incident on earth at an angle of incidence θ_i given by

$$\theta_i = \pi - \theta_0, \quad \pi/2 < \theta_0 \leq \pi \tag{9.2.39b}$$

where θ_i is measured from the normal to the earth's surface (see Fig. 74). The ray is incident on earth at a near-field point $P_0(r_0, \pi/2, \phi)$ (spherical coordinates)$= P_0(\rho_0, 0, \phi)$ (cylindrical coordinates) where

$$r_0 = z_0/\cos\theta_i = z_0/\cos(\pi - \theta_0) = -z_0/\cos\theta_0 \tag{9.2.40}$$

$$\rho_0 = z_0/\sin\theta_i = z_0/\sin(\pi - \theta_0) = z_0/\sin\theta_0 \tag{9.2.41}$$

The incident near-fields in air at P_0 are the space-wave direct fields given in spherical components by Eqs. (9.2.28)–(9.2.30).

The space-wave near-fields in earth at a near-field point $P(r, \theta, \phi)$ (spherical coordinates)$= P(\rho, z, \phi)$ (cylindrical coordinates), at a distance $r_1 = P_0P$ from P_0, are by definition the incident fields at P_0, modified by the Fresnel transmission coefficient, and propagated along the path P_0P at an angle of refraction θ_t given by Snell's law as

$$\begin{aligned}\theta_t &= \sin^{-1}[(1/n)\sin\theta_i] = \sin^{-1}[(1/n)\sin(\pi - \theta_i)] \\ &= \sin^{-1}[(1/n)\sin\theta_0]\end{aligned} \tag{9.2.42}$$

where θ_t is measured from the normal to the earth's surface (see Fig. 74).

From the law of cosines for solution of the triangle OP_0P, given the sides $OP_0 = \rho_0$ and $P_0P = r_1$ and the included angle $\angle OP_0P = \pi/2 + \theta_t$, the spherical coordinate r is given by

$$\begin{aligned}r &= \{\rho_0^2 + r_1^2 - 2\rho_0 r_1 \cos[(\pi/2) + \theta_t]\}^{1/2} \\ &= [\rho_0^2 + r_1^2 - 2\rho_0 r_1 \sin\theta_t]^{1/2}\end{aligned} \tag{9.2.43}$$

where θ_t is given by Eq. (9.2.42).

From the law of cosines, $\angle POP_0 = \cos^{-1}[(r^2 + \rho_0^2 - r_1^2)/(2\rho_0 r)]$. The spherical coordinate θ is given by

$$\theta = (\pi/2) + \angle OP_0P = (\pi/2) + \cos^{-1}[(r^2 + \rho_0^2 - r_1^2)/(2\rho_0 r)] \tag{9.2.44}$$

The cylindrical coordinates ρ and z are given by

$$\rho = r \sin\theta \tag{9.2.45}$$

$$z = r\cos\theta \tag{9.2.46}$$

where r and θ are given by Eqs. (9.2.43) and (9.2.44), respectively.

The transmitted space-wave near-fields at $P(r, \theta, \phi)$ are $\mathbf{H}_\mathrm{t} = \mathbf{u}_\phi H_{\phi,\mathrm{t}}$ and $\mathbf{E}_\mathrm{t} = \mathbf{u}_\mathrm{r}\mathbf{E}_{\mathrm{r,t}} + \mathbf{u}_\theta E_{\theta,\mathrm{t}}$ with spherical-coordinate components given by Eqs. (9.2.28)–(9.2.30) but modified by the Fresnel transmission coefficient $T_\mathrm{v}(\theta_\mathrm{i})$, additional path length r_1, and phase advance $k_1 r_1$ in the earth medium. Accordingly,

$$\begin{aligned} H_{\phi,\mathrm{t}} =& (1/Z_0) A_0 \sin\theta_0 \,[r_0/(r_0 + r_1)] T_\mathrm{v}(\theta_\mathrm{i}) \exp(-jk_1 r_1) \\ & \times [1 + (jb)^{-1}], \quad z \le 0,\ \sigma = 0 \end{aligned} \tag{9.2.47}$$

$$\begin{aligned} \mathbf{E}_{r,\mathrm{t}} =& 2A_0 \cos\theta_0 \,[r_0/(r_0 + r_1)] T_\mathrm{v}(\theta_i) \exp(-jk_1 r_1) \\ & \times [(jb)^{-1} + (jb)^{-2}], \quad z \le 0,\ \sigma = 0 \end{aligned} \tag{9.2.48}$$

$$\begin{aligned} E_{\theta,\mathrm{t}} =& A_0 \sin\theta_0 \,[r_0/(r_0 + r_1)] T_\mathrm{v}(\theta_i) \exp(-jk_1 r_1) \\ & \times [1 + (jb)^{-1} + (jb)^{-2}], \quad z \le 0,\ \sigma = 0 \end{aligned} \tag{9.2.49}$$

where

$$\begin{aligned} A_0 &= j[(Z_0 k_0 p)/(4\pi r_0)] \exp(-jk_0 r_0) \\ b &= k_0 r_0 + k_1 r_1 \\ k_1 &= \text{wave number in earth} = 2\pi/\lambda_1 = n k_0 \\ T_\mathrm{v}(\theta_\mathrm{i}) &= \text{Fresnel transmission coefficient defined below} \end{aligned}$$

The Fresnel transmission coefficient $T_\mathrm{v}(\theta_\mathrm{i})$ is defined as the ratio of the transmitted magnetic field $\mathbf{H}_\mathrm{t}$ to that of the incident magnetic field H_i for the electric fields polarized parallel to the plane of incidence and for the directions of the incident and transmitted magnetic fields defined to be in the same direction (see Fig. 72). Since the tangential magnetic fields must be continuous at the boundary, then

$$\mathbf{H}_\mathrm{t} = H_\mathrm{i} + H_\mathrm{r} \tag{9.2.50}$$

Dividing both sides of Eq. (9.2.50) by H_i,

$$\mathbf{H}_\mathrm{t}/H_i = T_\mathrm{v}(\theta_\mathrm{i}) = 1 + (H_\mathrm{r}/H_\mathrm{i}) = 1 + R_\mathrm{v}(\theta_\mathrm{i}) \tag{9.2.51}$$

Substituting, Eq. (9.2.5) for $R_\mathrm{v}(\theta_\mathrm{i})$ and Eq. (9.2.39b) for θ_i, into Eq. (9.2.51), it

follows that

$$T_v(\theta_i) = 1 + [n^2 \cos\theta_i - (n^2 - \sin^2\theta_i)^{1/2}]/[n^2 \cos\theta_i + (n^2 - \sin^2\theta_i)^{1/2}]$$
$$= (2n^2 \cos\theta_i)/[n^2 \cos\theta_i + (n^2 - \sin^2\theta_i)^{1/2}] \quad (9.2.52)$$

where $n = (\varepsilon_r)^{1/2}$ for nonconducting earth.

Again, the subscript v denotes that the electric fields are polarized parallel to the plane of incidence and also serves here as a reminder that the Hertzian dipole is vertically polarized. The concept, of utilizing the uniform plane-wave Fresnel reflection and transmission coefficients for the space-wave component of the near-fields when the incident wave is not a plane wave but is a spherical wave, is permissible because by definition the surface wave accounts for any deficiency not accounted for by the space wave. At far-field points, the surface-wave correction for the fields is of the order of $(1/r^2)$ and is therefore negligible.

9.2.2.2 Far-Fields in Air and Earth

A field point $P(r, \theta, \phi)$, in the far-field of a vertically polarized Hertzian dipole in air above nonconducting earth, is in air if $0 \le \theta \le \pi/2$ and is in earth if $\pi/2 < \theta \le \pi$ (see Fig. 74). For far-field points $P(r, \theta, \phi)$ in air, the far-fields are the sum of direct and indirect fields (see Fig. 71) and are given by Eqs. (9.2.6) and (9.2.7).

For far-field points in earth, the far-fields are found by applying far-field conditions to Eqs. (9.2.47)–(9.2.50) for the space-wave near-fields in earth. With reference to Fig. 74, the far-field conditions are

$$r \gg r_0 \quad (9.2.53a)$$

$$k_0 r_0 + k_1 r_1 \gg 1 \quad (9.2.53b)$$

For condition (9.2.53a), it follows that

$$r \approx r_0 + r_1 \quad (9.2.54a)$$

$$\angle \mathrm{OPP}_0 \approx 0 \quad (9.2.54b)$$

The condition $\angle \mathrm{OPP}_0 \approx 0$ implies that $\mathrm{P}_0\mathrm{P}$ is approximately parallel to OP at an elevation angle θ. Consequently,

$$\theta_t \approx \pi - \theta \quad (9.2.55)$$

Substituting Eq. (9.2.55) into Eq. (9.2.42), it follows that

$$\theta_i = \sin^{-1}(n \sin\theta_t) \approx \sin^{-1}[n(\pi - \theta)] \quad (9.2.56a)$$

$$\sin\theta_i = n \sin\theta_t \approx n(\pi - \theta) \quad (9.2.56b)$$

$$\cos\theta_i = (1 - \sin^2\theta_i)^{1/2} \approx [1 - n^2(\pi - \theta)]^{1/2} \quad (9.2.56c)$$

Substituting Eq. (9.2.56a) into Eqs. (9.2.39a) and (9.2.39b), it follows that

$$\theta_0 = \pi - \theta_\mathrm{i} \approx \pi - \sin^{-1}[n(\pi - \theta)] \tag{9.2.57a}$$

$$\sin\theta_0 \approx \sin\{\pi - \sin^{-1}[n(\pi - \theta)]\} = n(\pi - \theta) \tag{9.2.57b}$$

$$\cos\theta_0 = (1 - \sin^2\theta_0)^{1/2} \approx [1 - n^2(\pi - \theta)^2]^{1/2} \tag{9.2.57c}$$

For conditions (9.2.53a) and (9.2.53b), it follows that Eqs. (9.2.47)–(9.2.50) reduce to $\mathbf{H}_\mathrm{t} = \mathbf{u}_\phi H_{\phi,\mathrm{t}}$ and $\mathbf{E}_\mathrm{t} = \mathbf{u}_\theta E_{\theta,\mathrm{t}}$ with $H_{\phi,\mathrm{t}}$ and $E_{\theta,\mathrm{t}}$ given by

$$\begin{aligned} H_{\phi,\mathrm{t}} =& (1/z_0) A_2 \sin\theta_0 T_\mathrm{v}(\theta_\mathrm{i}) = (1/z_0) A_2\, n(\pi - \theta) T_\mathrm{v}(\theta_\mathrm{i}), \\ & z < 0,\ \sigma = 0 \end{aligned} \tag{9.2.58}$$

$$E_{\theta,\mathrm{t}} = A_2 \sin\theta_0 T_\mathrm{v}(\theta_\mathrm{i}) = A_2 n(\pi - \theta) T_\mathrm{v}(\theta_\mathrm{i}), \quad z < 0,\ \sigma = 0 \tag{9.2.59}$$

where

$$\begin{aligned} A_2 =& A_0[r_0/(r_0 + r_1)]\exp(-jk_1 r_1) \\ =& j[(Z_0 k_0 \rho)/(4\pi r)]\exp[-j(k_0 r_0 + k_1 r_1)] \end{aligned}$$

$$\begin{aligned} T_\mathrm{v}(\theta_\mathrm{i}) =& (2n^2\cos\theta_\mathrm{i})/[n^2\cos\theta_\mathrm{i} + (n^2 - \sin^2\theta_\mathrm{i})^{1/2}] \\ =& \{2n^2[1 - n^2(\pi - \theta)]^{1/2}\}/\{\mathrm{n}^2[1 - \mathrm{n}^2(\pi - \theta)]^{1/2} + n[1 + (\pi - \theta)^2]^{1/2}\} \\ =& \{2n[1 - n^2(\pi - \theta)]^{1/2}\}/\{n[1 - n^2(\pi - \theta)]^{1/2} + [1 + (\pi - \theta)^2]^{1/2}\} \end{aligned}$$

9.2.2.3 Directivity

For nonconducting earth, the radiated power P_r is found by integrating the time-averaged far-field power over the upper and lower hemispheres and is given by Eq. (8.1.6) for $\sigma = 0$. The radiated power P_r of a vertically polarized Hertzian dipole in air above nonconducting earth is found by substituting into Eq. (8.1.6) the far-field $E_\theta(r, \theta)$ given by Eq. (9.2.6) for $0 \le \theta \le \pi/2$ and by Eq. (9.2.59) for $\pi/2 < \theta_0 \le \pi$. Accordingly,

$$\begin{aligned} P_\mathrm{r} =& (\pi/z_0)|A|^2 r^2 \int_0^{\pi/2} \sin^3\theta\, |1 + R_\mathrm{v}(\theta)\exp(-j2k_0 z_0\cos\theta)|^2 \mathrm{d}\theta \\ &+ (\pi/\mathrm{z}_0)|A_2|^2 r^2 \int_{\pi/2}^{\pi} n^2(\pi - \theta)^3 |\mathrm{T}_\mathrm{v}(\theta_\mathrm{i})|^2 \sin\theta\, \mathrm{d}\theta \end{aligned} \tag{9.2.60}$$

where

$$|A| = |A_2| = [(Z_0 k_0 p)/(4\pi r)]$$

$$R_v(\theta) = [n^2 \cos\theta - (n^2 - \sin^2\theta)^{1/2}]/[n^2 \cos\theta + (n^2 - \sin^2\theta)^{1/2}]$$

$$n^2 = \varepsilon_r$$

$$T_v(\theta_i) = \{2n^2[1 - n^2(\pi - \theta)]^{1/2}\}/\{n^2[1 - n^2(\pi - \theta)]^{1/2} + n[1 + (\pi - \theta)^2]^{1/2}\}$$

The directivity $d(\theta)$ is found by substituting into Eq. (8.1.7) the far-field $E_\theta(r, \theta)$ given by Eq. (9.2.6) for $0 \le \theta \le \pi/2$ and by Eq. (9.2.59) for $\pi/2 < \theta \le \pi$. Accordingly,

$$d(\theta) = [(2\pi r^2)/(Z_0 P_r)]|A|^2 \sin^2\theta\,|1 + R_v(\theta)\exp(-j2k_0 z_0 \cos\theta)|^2,$$

$$0 \le \theta \le \pi/2; \tag{9.2.61}$$

$$= [(2\pi r^2)/(Z_0 P_r)]|A_2|^2\, n^2(\pi - \theta)^2 |T_v(\theta_i)|^2, \quad \pi/2 < \theta \le \pi$$

where P_r, $|A|^2$, $R_v(\theta)$, $T_v(\theta_i)$, and θ_i are given in Eq. (9.2.60).

Eq. (9.2.61) may be written in more concise form as

$$d(\theta) = (1/C_0)2\sin^2\theta\,|1 + \mathrm{R}_v(\theta)\exp(-j2k_0 z_0 \cos\theta)|^2,$$

$$0 \le \theta \le \pi/2; \tag{9.2.62}$$

$$= (1/C_0)2n^2(\pi - \theta)^2 |T_v(\theta_i)|^2, \quad \pi/2 < \theta \le \pi$$

where

$$C_0 = \int_0^{\pi/2} \sin^3\theta\,|1 + R_v(\theta)\exp(-j2k_0 z_0 \cos\theta)|^2 \mathrm{d}\theta$$

$$+ \int_{\pi/2}^{\pi} n^2(\pi - \theta)^2 |T_v(\theta_i)|^2 \sin\theta\,\mathrm{d}\theta$$

When the Hertzian dipole is in air at a height $z_0 = 0$, Eq. (9.2.62) reduces to

$$d(\theta) = (1/C_1)2\sin^2\theta\,|T_v(\theta)|^2,$$

$$0 \le \theta \le \pi/2, \quad z_0 = 0; \tag{9.2.63}$$

$$= (1/C_1)2n^2(\pi - \theta)^2 |T_v(\theta_i)|^2, \quad \pi/2 < \theta \le \pi, \quad z_0 = 0$$

where

$$C_1 = \int_0^{\pi/2} \sin^3\theta |T_v(\theta)|^2 d\theta + \int_{\pi/2}^{\pi} n^2(\pi - \theta)^2 |T_v(\theta_i)|^2 \sin\theta \, d\theta$$

$$T_v(\theta) = 1 + R_v(\theta) = (2n^2 \cos\theta)/[n^2 \cos\theta + (n^2 - \sin^2\theta)^{1/2}]$$

$$T_v(\theta_i) = 1 + R_v(\theta_i) = \{2n^2[1 - n^2(\pi - \theta)]^{1/2}\}/\{n^2[1 - n^2(\pi - \theta)]^{1/2} + n[1 + (\pi - \theta)^2]^{1/2}\}$$

As a numerical example of Eq. (9.2.63), consider the directivity pattern $D(\theta) = 10\log_{10} d(\theta)$ (dBi), of a vertically polarized Hertzian dipole in air at a height z_0 above nonconducting earth of relative dielectric constant $\varepsilon_r = 9.0$ (see Fig. 75). The peak directivities in earth and air are $+15.5$ and -4.2 dBi, respectively. The peak directivity in earth occurs at an angle of refraction $\theta_t = \theta_c = \sin^{-1}(1/n) = \sin^{-1}(1/3) = 0.3398$ rad $= 19.47°$ where θ_c is the critical angle of total internal reflection. The corresponding angle of incidence θ_i from Eq. (9.2.56a) is $\theta_i = \sin^{-1}(n \sin\theta_c) = \sin^{-1}(1.0) = \pi/2$ rad $= 90°$.

This result can be understood by applying the principal of reciprocity. Uniform plane waves incident *from* earth onto the less dense medium of air, at angles of incidence less than or equal to the critical angle θ_c, will not be transmitted into air but instead will be totally reflected back into earth. A ray incident from earth at the critical angle θ_c will be transmitted parallel to the air–earth interface. Consequently, most of the energy radiated to the far-field by the dipole in air is radiated in earth rather than air. In the example of Fig. 75, 89.7% of the radiated power is in earth and 10.3% is in air.

Although the directivity pattern of Fig. 75 is presumably that given by Eq. (9.2.63), the pattern was actually obtained by the Numerical Electromagnetic Code NEC-3 in the Sommerfeld option for a monopole element of length $h/\lambda = 2 \times 10^{-4}$, width $b/\lambda = 1 \times 10^{-6}$, number of element segments $N = 31$ of which the first segment is a voltage source $= 1\,\text{V}\exp(j\omega t)$ between the base of the element and earth, and integration steps $\Delta\theta = 0.01°$. Since the total radiated power of the space-wave $1/r$ field was determined by integrating the directivity pattern over both the upper and lower hemispheres, the result does not depend upon the surface-wave fields (cf. [116], pp. 132–133) and the same result probably would have been obtained using NEC-3 in the Fresnel option as suggested by Eq. (9.2.63).

9.2.2.4 Modified Radiation Efficiency

A vertically polarized Hertzian dipole in air above nonconducting earth has a radiation efficiency $\eta = 1$ because there are no dissipative power losses in

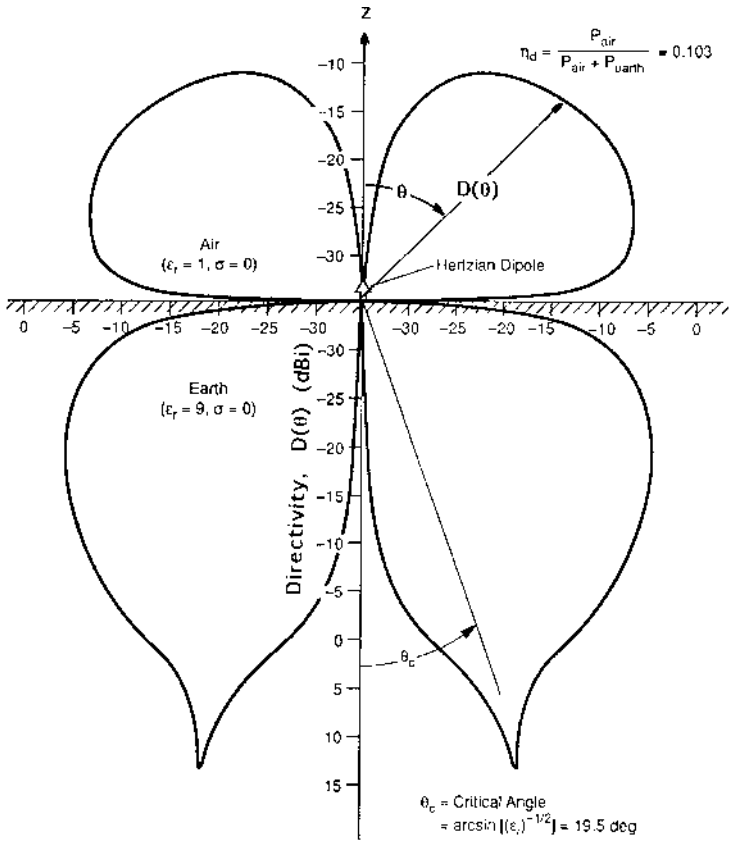

FIGURE 75 Directivity (in any azimuthal plane) of a vertically polarized Hertzian dipole in air at zero height above nonconducting earth, $\varepsilon_r = 9$ (NEC-3 in Sommerfeld option, $h/\lambda = 2 \times 10^{-4}$, $b/\lambda = 1 \times 10^{-6}$, $N = 31$, $\Delta\theta = 0.01°$, voltage source $= 1$ V $\exp(j\omega t)$ between base of monopole element and earth).

the earth, unlike the case of imperfectly conducting earth for which the radiation efficiency can be as small as $\eta = 0$.

For nonconducting earth, it is useful to define a modified radiation efficiency η_d defined in Eq. (8.1.13) as the ratio of the (far-field) radiated power in air to the total (far-field) radiated power. From Eq. (9.2.62), it follows that η_d is given by

$$\eta_d = (1/C_0) \int_0^{\pi/2} \sin^3\theta \, |1 + R_v(\theta) \exp(-j2k_0 z_0 \cos\theta)|^2 \, d\theta \qquad (9.2.64)$$

where C_0 is defined in Eq. (9.2.62).

For $z_0 = 0$ and $\varepsilon_r = 9.0$ (see Fig. 75), the modified radiation efficiency obtained using NEC-3 is $\eta_d = 0.103$. Presumably, Eq. (9.2.64) would yield the same result.

For $z_0 = \infty$, the modified radiation efficiency $\eta_d = 1.0$ because the intensity of the radiation incident on the earth is zero. This result does not follow from Eq. (9.2.64) because the condition $z_0 = \infty$ does not satisfy the far-field condition Eq. (9.2.53a).

For $z_0 = 0$, the modified radiation efficiency decreases monotonically from $\eta_d = 0.5$ for $\varepsilon_r = 1.0$ to $\eta_d = 0$ for $\varepsilon_r = \infty$ (see Fig. 76). The modified radiation efficiency η_d increases with increasing height z_0 of the dipole above earth but the increase is not monotonic (see Fig. 77). The data of Figs. 76 and 77 were generated by King [114] and Burke [115]. King's results, based on an evaluation of the Sommerfeld integral, are approximate because King's evaluation is subject to the condition $\varepsilon_r \gg 1$ (or equivalently, $k_1/k_0 \geq 3$) and lead to only approximately correct results in the far-field. Burke's results are more accurate and were obtained with NEC-3 in the Sommerfeld option (see Sec. 9.4) by

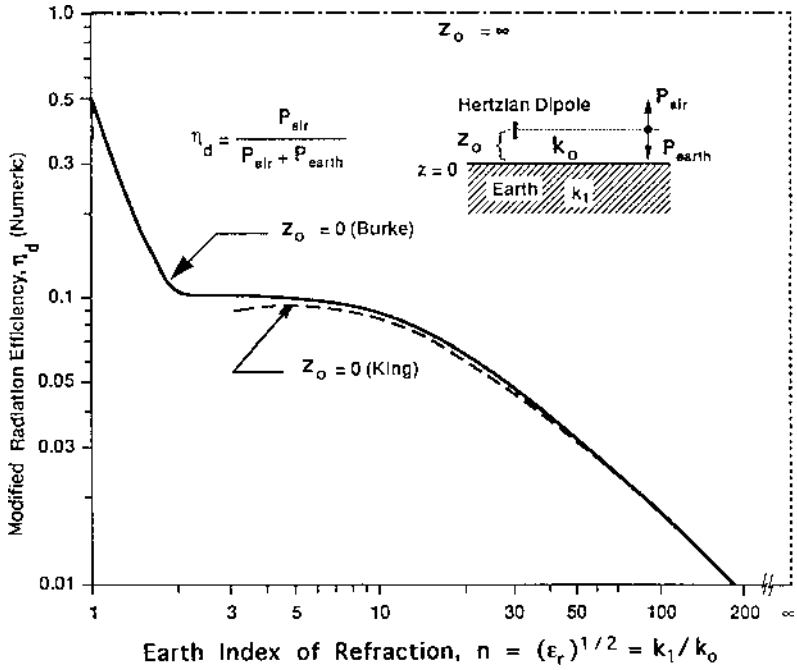

FIGURE 76 Modified radiation efficiency of a vertically polarized Hertzian dipole in air at zero height above nonconducting earth, $z_0 = 0$ and $z_0 = \infty$.

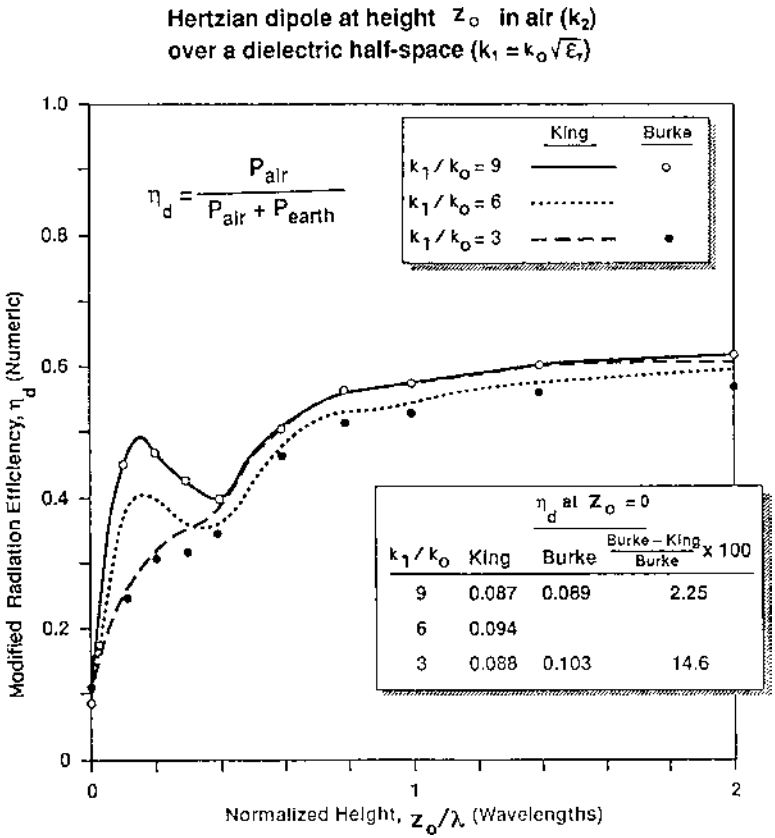

FIGURE 77 Modified radiation efficiency of a vertically polarized Hertzian dipole in air above nonconducting earth, $0 \leq z_0/\lambda \leq 2$.

approximating the Hertzian dipole by a center-fed dipole of total length $h/\lambda = 2 \times 10^{-4}$, width $b/\lambda = 1 \times 10^{-6}$, number of element segments $N = 11$ with the sixth segment a voltage source $= 1\,\text{V}\exp(j\omega t)$ at the input to the dipole, integration steps $\Delta\theta = 1.0°$ in air only, and with total radiated power equal to the input power.

The exact closed-form expression of Eq. (9.2.64), for the modified radiation efficiency, is developed solely from considerations of the far-field space wave. The result that most of the radiated power is in the nonconducting earth rather than in air is a far-field space wave effect and is not a surface-wave effect as was previously thought [116].

9.2.3 Thin Monopole Element in Air Above Conducting Earth

9.2.3.1 Far-Fields in Air

In the absence of earth, an electrically thin monopole element with a sinusoidal-current distribution has far-field electric and magnetic fields given by Eq. (3.2.13) and a directivity pattern given by Eq. (3.2.16). Consider now an electrically thin monopole element of length h, comprising N electrically short segments each of length $\Delta h = h/N$, whose base is at a height z_0 above *conducting* earth of relative dielectric constant ε_r and conductivity $\sigma > 0$ (see Fig. 78). The midpoint of the ith segment is at a height z_i above earth. Assuming the sinusoidal-current distribution of Eq. (3.1.1), the current $I(z_i')$ at the ith segment is given by

$$I(z_i') = [I(0)/\sin(k_0 h)]\sin[k_0(h - z_i')], \quad 0 \le z_i' \le h \tag{9.2.65}$$

where $z' = z - z_0$.

The far-field electric field is found by summing the fields from each segment. Substituting $[I(z_i')\Delta h/2]$ for p in Eq. (9.2.6), the far-field electric field

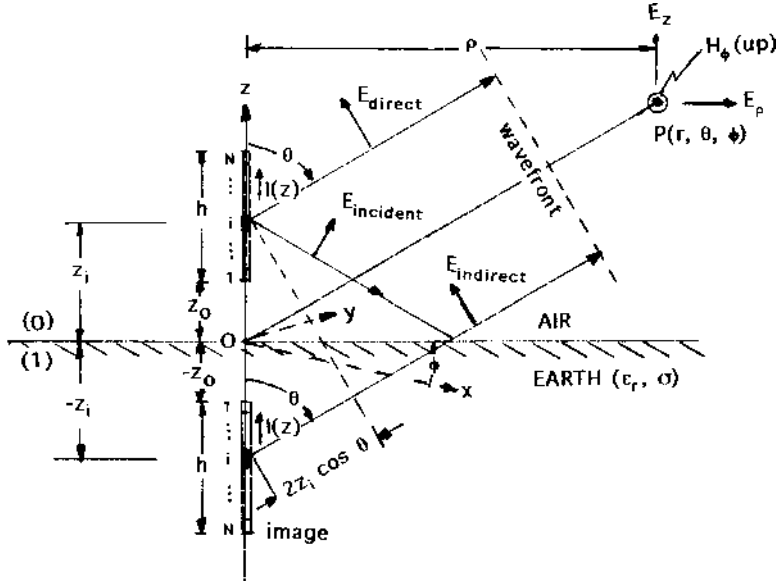

FIGURE 78 Direct and indirect rays of space wave, at a far-field point $P(r, \theta, \phi)$ in air, from the ith segment of a thin monopole element in air above conducting earth.

E is given by

$$\mathbf{E} = \mathbf{u}_\theta E_\theta = \mathbf{u}_\theta BC(\theta)\sin\theta,$$

$$0 \le \theta \le \pi/2; \tag{9.2.66}$$

$$= 0, \quad \pi/2 < \theta \le \pi, \quad \sigma > 0$$

where

$$B = j[I(0)\Delta h/2\sin(k_0 h)](Z_0 k_0/4\pi r)\exp(-jk_0 r)$$

$$C(\theta) = \sum_{i=1}^{N}\{\sin[k_0(h - z_i')]\exp(jk_0 z_i\cos\theta)[1 + R_v(\theta)\exp(-j2k_0 z_i\cos\theta)]\}$$

The far-field magnetic field **H** is given by

$$\mathbf{H} = \mathbf{u}_\phi(1/Z_0)E_\theta \tag{9.2.67}$$

where Z_0 is defined in Eq. (8.1.4) and E_θ is given by Eq. (9.2.17).

9.2.3.2 Directivity

The numeric directivity $d(\theta)$ is found by substituting Eq. (9.2.66) into Eq. (8.1.7). Accordingly,

$$d(\theta) = \frac{2\sin^2\theta|C(\theta)|^2}{\int_0^{\pi/2}\sin^3\theta|C(\theta)|^2 d\theta}, \quad 0 \le \theta \le \pi/2;$$

$$= 0, \quad \pi/2 < \theta \le \pi, \quad \sigma > 0 \tag{9.2.68}$$

where $C(\theta)$ is defined in Eq. (9.2.66).

Numerical results of Eq. (9.2.68), for the directivity $d(\theta)$ of a thin monopole element at height $z_0 = 0$ above earth at HF frequencies and for ICU-R P.527-3 classifications of earth, are given in App. A.8 for element lengths $h/\lambda = 0, 0.05, 0.10, 0.15, 0.20, 0.25$. The results were obtained by computer program MODIFIED IMAGES in App. B.11. As an example, the tables that apply to a quarterwave element are those for $N = (h/0.05\lambda) = 5$ where N is the amount of segments of the monopole element. The tables corresponding to $N = 5$ are Tables A8-6, A8-12, A8-18, A8-24, A8-30, A8-36, A8-42, A8-48, A8-54, and A8-60. The peak directivity D_{peak} (dBi) and the corresponding grazing angle ψ_{peak} (°) from those tables are summarized in Table 18. The peak directivities are within 0.15 dB of that for a perfect ground plane and the corresponding angles are 9–20° above the horizon.

The method of modified images, for the directivity of monopole elements in the absence of ground planes, gives almost identical results as those obtained by the method-of-moments programs NEC-3 (Sommerfeld option) and

TABLE 18 Peak Directivity of a Thin Quarter-Wave Monopole Element at Zero Height Above Earth for ITU-R P.527-3 Classifications of Earth

	6.0 MHz		15.0 MHz		30.0 MHz	
Earth classification	D_{peak} (dBi)	ψ_{peak} (°)	D_{peak} (dBi)	ψ_{peak} (°)	D_{peak} (dBi)	ψ_{peak} (°)
(1) Perfect ground	5.17	0	5.17	0	5.17	0
(2) Sea water	5.05	9	5.04	10	5.02	12
(3) Fresh water	5.03	20	5.03	22	5.03	22
(4) Wet ground	5.07	24	5.07	24	5.07	24
(5) Medium dry ground	5.11	26	5.11	26	5.11	26
(6) Very dry ground	5.21	30	5.21	30	5.21	30
(7) Pure water, 20°C	5.03	22	5.03	22	5.03	22
(8) Ice, −1°C	5.21	30	5.21	30	5.21	30
(9) Ice, −10°C	5.21	30	5.21	30	5.21	30
(10) Average land (TCI)	5.13	26	5.13	26	5.14	28
(11) Free space	1.88	0	1.88	0	1.88	0

RICHMD4 (see Table 19). These three models yield values, for the directivity of a thin quarterwave monopole element at height $z_0 = 0$ above medium dry earth at 15 MHz, that are within 0.03 dB of each other.

9.2.3.3 Radiation Efficiency Neglecting Surface Wave

As was pointed out in Sec. 9.2.1, the method of images modified by Fresnel reflection yields values of radiation efficiency that are larger than the accurate values obtained by considering the surface-wave fields (see Sec. 9.4). For a thin monopole element just above conducting earth, the radiation efficiency is determined, neglecting surface-wave fields, by the method of images modified by Fresnel reflection in the manner as described for a Hertzian dipole in Sec. 9.2.1. Accordingly,

$$\eta = \frac{\int_0^{\pi/2} \sin^3\theta |C(\theta)|^2 d\theta}{\int_0^{\pi/2} \sin^3\theta |C(\theta)_{R_v(\theta)=1}|^2 d\theta}, \quad z_0 = 0, \quad \sigma > 0; \tag{9.2.69}$$

Numerical results of Eq. (9.2.69), for the radiation efficiency of a thin monopole element at height $z_0 = 0$ above earth and for ICU-R P.527-3 classifications of earth, are given in App. A.8 for element lengths $h/\lambda = 0, 0.05, 0.10, 0.15, 0.20, 0.25$. The results were obtained by computer program MODIFIED IMAGES in App. B.11. The results for a thin quarter-wave element are summarized in Table 20. The method of modified images yields values of radiation efficiency that are significantly larger than the more accurate results

TABLE 19 Directivity of a Thin Quarter-Wave Monopole at Zero Height Above Medium Dry Ground, 15 MHz

Angle of incidence, θ (°)	Directivity (dBi)			Angle of incidence, θ (°)	Directivity (dBi)		
	NEC-3 (Sommerfeld option)[a]	Richmond (method of moments)[b]	Modified images (Fresnel coefficients)[c]		NEC-3 (Sommerfeld option)[a]	Richmond (method of moments)[b]	Modified images (Fresnel coefficients)[c]
0	$-\infty$	$-\infty$	$-\infty$	46	3.80	3.78	3.80
2	−22.90	−22.88	−22.88	48	4.07	4.05	4.07
4	−16.88	−16.86	−16.86	50	4.31	4.29	4.31
6	−13.35	−13.34	−13.34	52	4.53	4.50	4.53
8	−10.86	−10.85	−10.84	54	4.71	4.69	4.71
10	−8.92	−8.91	−8.91	56	4.86	4.84	4.86
12	−7.34	−7.33	−7.33	58	4.98	4.96	4.98
14	−6.00	−5.99	−5.99	60	5.07	5.04	5.06
16	−4.85	−4.84	−4.84	62	5.11	5.08	5.11
18	−3.83	−3.82	−3.82	64	5.12	5.09	5.11
20	−2.92	−2.92	−2.91	66	5.07	5.04	5.07
22	−2.10	−2.10	−2.09	68	4.98	4.95	4.98
24	−1.36	−1.36	−1.35	70	4.82	4.79	4.82
26	−0.68	−0.68	−0.67	72	4.59	4.56	4.59
28	−0.06	−0.06	−0.05	74	4.27	4.23	4.26
30	0.52	0.52	0.53	76	3.83	3.80	3.83
32	1.05	1.05	1.06	78	3.24	3.21	3.24
34	1.54	1.54	1.55	80	2.44	2.40	2.44
36	2.00	1.99	2.00	82	1.33	1.29	1.32
38	2.42	2.41	2.42	84	−0.29	−0.33	−0.29
40	2.81	2.80	2.81	86	−2.86	−2.90	−2.87
42	3.17	3.16	3.17	88	−7.85	−7.89	−7.85
44	3.50	3.48	3.50	90	$-\infty$	$-\infty$	$-\infty$

Medium dry earth ($\varepsilon_r = 15$, $\sigma = 1.0 \times 10^{-3}$).

[a] Voltage excitation source between the earth and the base of the element.

[b] Program RICHMD4 with small ground plane of normalized radius $2\pi a/\lambda = 0.025$ wave numbers.

[c] Program MODIFIED IMAGES assumes Fresnel reflection coefficient and sinusoidal-current distribution on element.

TABLE 20 Radiation Efficiency of a Thin Quarter-Wave Monopole Element at Zero Height Above Earth, 15 MHz

Earth classification (CCIR 527-1)	Radiation efficiency, η (numeric)	
	Modified Images	RICHMOND4[a]
(1) Perfect ground	1.000	1.000
(2) Sea water	0.914	0.766
(3) Fresh water	0.531	0.347
(4) Wet ground	0.404	0.229
(5) Medium dry ground	0.302	0.210
(6) Very dry ground	0.176	0.145
(7) Pure water	0.495	0.378
(8) Ice (-1°C)	0.177	0.148
(9) Ice (-10°C)	0.179	0.171
(10) Average land	0.299	0.105

[a] More accurate result.
RICHMOND 4 result is for ground plane radius $2\pi a/\lambda = 0.025$ wavenumbers.

obtained by considering surface-wave fields as is done in Richmond's method of moments program RICHMOND4 (see Table 20). For example, for average land, the method of modified images over-estimates the radiation efficiency by $(0.299 - 0.105)/0.105\text{x} = 185\%$.

In conclusion, for monopole elements in proximity to earth and in the absence of ground planes, the method of modified images is accurate for determining the far-field and directivity but inaccurate for determining radiation efficiency. In the far field, the space wave is dominant with fields proportional to $(1/r)$. On the surface of imperfectly conducting earth, the space-wave far-field is zero and, as shown in the following section, the surface wave dominates with far-fields proportional to $(1/r)^2$.

9.3 SURFACE-WAVE FIELDS: SOMMERFELD–KING INTEGRALS FOR VERTICALLY POLARIZED HERTZIAN DIPOLE IN AIR ABOVE FLAT EARTH

9.3.1 Hertz Potential in Air and Earth

9.3.1.1 Primary and Secondary Waves

Consider a vertically polarized Hertzian dipole of moment $\mathbf{p} = u_z\mathbf{p}$ with time dependence $\exp(j\omega t)$ at a height z_0 above earth of relative permittivity ε_r,

conductivity σ, and magnetic permeability μ_0 (see Fig. 79). Of interest are the fields at an arbitrary point $P(r_1, \theta_1, \phi)$.

Exact integral expressions for the fields at $P(r_1, \theta_1, \phi)$ were given in 1909 by Sommerfeld [77] and elucidated by Wait [117]. Following Wait, the electric field $\mathbf{E} = \mathbf{u}_\rho E_\rho + \mathbf{u}_\phi E_\phi + \mathbf{u}_z E_z$ and magnetic field $\mathbf{H} = \mathbf{u}_\rho H_\rho + \mathbf{u}_\phi H_\phi + \mathbf{u}_z H_z$ have cylindrical-coordinate field components given by

$$E_\rho = \partial^2 \Pi_z / \partial \rho \partial z, \quad E_\phi = 0, \quad E_z = k^2 \Pi_z + \partial^2 \Pi_z / \partial z^2 \tag{9.3.1}$$

$$H_\rho = 0, \quad H_\phi = (k^2 / j\mu_0 \omega)\, \partial \Pi_z / \partial \rho, \quad H_z = 0 \tag{9.3.2}$$

where $\Pi_z = z$-component of the Hertz vector potential Π.

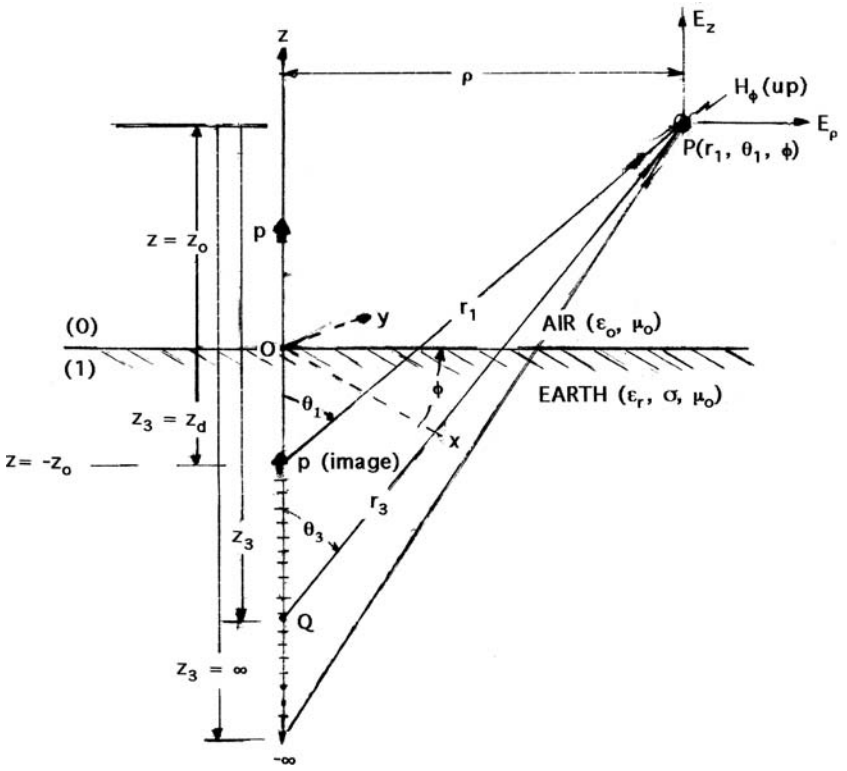

FIGURE 79 Surface-wave rays, at a near-field point $P(r_1, \theta_1, \phi)$ in air, from an image line-source ($z_d \leq z_3 \leq \infty$) generated by a vertically polarized Hertzian dipole at a height z_0 above earth.

The wave number k is defined as

$$k = nk_0 = n\omega(\varepsilon_0\mu_0)^{1/2} \tag{9.3.3}$$

where

$k_0 = \omega(\varepsilon_0\mu_0)^{1/2}$ = wave number in free space
$n^2 = \varepsilon_1/\varepsilon_0$ = relative permittivity of earth = $\varepsilon_r[1 - j(\sigma/\omega\varepsilon_0\varepsilon_r)]$

In the absence of the conducting half-space, the only wave incident at $P(r_1, \theta_1, \phi)$ is a primary wave. Accordingly, the Hertz potential $\Pi_z = \Pi_{z\,\text{primary}}$ where $\Pi_{z\,\text{primary}}$ is the Hertz potential of the primary wave and is given by

$$\begin{aligned}\Pi_{z\,\text{primary}} &= (p/4\pi j\omega\varepsilon_0)\int_0^\infty J_0(\lambda\rho)(j\gamma_0)^{-1}\exp(-j\gamma_0|z - z_0|)\lambda\,d\lambda \\ &= (p/4\pi j\omega\varepsilon_0)(1/r_0)\exp(-jk_0r_0)\end{aligned} \tag{9.3.4}$$

where

$r_0 = [\rho^2 + (z - z_0)^2]^{1/2}$
$\gamma_0 = (k_0^2 - \lambda^2)^{1/2}$
$J_0(x)$ = Bessel function of first kind of order zero
λ = eigen parameter of the eigenfunction $J_0(\lambda\rho)\exp[\pm j(k^2 - \lambda^2)^{1/2}z]$ and is a function of the wave number k_0 since k is a function of k_0 [see Eq. (9.3.3)]. The parameter λ should not be confused with that used elsewhere to designate wavelength

In the presence of the conducting half-space, it is convenient to express the resulting Hertz potential in the air medium (that is, $z > 0$) as the sum of the primary-wave term and a secondary-wave term. Thus,

$$\Pi_z = \Pi_{z\,\text{primary}} + \Pi_{z\,\text{secondary}}, \quad z \geq 0 \tag{9.3.5}$$

where $\Pi_{z\,\text{primary}}$ is given by Eq. (9.3.4).

The term $\Pi_{z\,\text{secondary}}$ is given by

$$\begin{aligned}\Pi_{z\,\text{secondary}} =& (p/4\pi j\omega\varepsilon_0)\int_0^\infty (j\gamma_0)^{-1}R(\lambda)J_0(\lambda\rho) \\ &\times\exp[-j\gamma_0(z + z_0)]\lambda\,d\lambda, \quad z \geq 0\end{aligned} \tag{9.3.6}$$

where

$$R(\lambda) = (n^2\gamma_0 - \gamma_1)/(n^2\gamma_0 + \gamma_1)$$
$$\gamma_1 = (k_1^2 - \lambda^2)^{1/2}$$

In the conducting half-space (i.e., $z < 0$), the Hertz potential component Π_z consists of a single term given by

$$\Pi_z = (p/4\pi j\omega\varepsilon_0 n^2)\int_0^\infty \gamma_0^{-1} T(\lambda) J_0(\lambda\rho)\exp(-j\gamma_1 z)\lambda\,\mathrm{d}\lambda, \quad z<0 \tag{9.3.7}$$

where $T(\lambda) = (2n^2\gamma_0)/(n^2\gamma_0 + \gamma_1)$.

Since the integrals of Eqs. (9.3.4), (9.3.6), and (9.3.7) are integrated between the limits $\lambda = 0$ and ∞ and since the integrands contain an exponential function, the question arises as to whether the Sommerfeld integrals given by Eqs. (9.3.4), (9.3.6), and (9.3.7) may be interpreted as inverse Laplace transforms or, with a change of variable, as Fourier integrals. Unfortunately, Eqs. (9.3.6) and (9.3.7) are not found evaluated in tables of definite integrals including those of Laplace transforms or Fourier integrals.

9.3.1.2 Space and Surface Waves

Instead of expressing the Hertz potential in the air half-space as the sum of potentials resulting from a primary wave and a secondary wave, it is convenient to express the Hertz potential as the sum of potentials resulting from a space wave and a surface wave. By definition, the space wave is the sum of the primary wave (also called *direct* wave) and an *indirect* wave (equal to the portion of the secondary wave field that reduces in the far-field to the direct-wave field multiplied by the Fresnel reflection coefficient for direct-wave field incident on the earth of interest). The surface wave is the wave that accounts for the portion of the secondary-wave fields not accounted for by the space-wave fields.

The space-wave fields in the half-space above the earth are given exactly by Eqs. (9.2.37) and (9.2.38) of Sec. 9.2.1. Accordingly, the Hertz potential Π_z may be expressed as

$$\begin{aligned}\Pi_z &= \Pi_{z\,\mathrm{space}} + \Pi_{z\,\mathrm{surface}}, \quad z \geq 0\\ &= (\Pi_{z\,\mathrm{direct}} + \Pi_{z\,\mathrm{indirect}}) + \Pi_{z\,\mathrm{surface}}, \quad z \geq 0\end{aligned} \tag{9.3.8}$$

where $\Pi_{z\,\mathrm{space}} = \Pi_{z\,\mathrm{direct}} + \Pi_{z\,\mathrm{indirect}}$.

By analogy to Eqs. (9.3.4) and (9.3.5), the Hertz potentials $\Pi_{z\,\mathrm{direct}}$ and $\Pi_{z\,\mathrm{indirect}}$ are given by

$$\begin{aligned}\Pi_{z\,\mathrm{direct}} &= \Pi_{z\,\mathrm{primary}} = (p/4\pi j\omega\varepsilon_0)(1/r_0)\exp(-jk_0 r_0), \quad z \geq 0;\\ &= (p/4\pi j\omega\varepsilon_0)\int_0^\infty J_0(\lambda\rho)\gamma_0^{-1}\exp(-j\gamma_0 Iz - z_0 I)\lambda\,\mathrm{d}\lambda\end{aligned} \tag{9.3.9}$$

$$\begin{aligned}\Pi_{z\,\mathrm{indirect}} &= (p/4\pi j\omega\varepsilon_0)(1/r_1)R_\mathrm{v}(\theta_1)\exp(-jk_0 r_1), \quad z \geq 0;\\ &= (p/4\pi j\omega\varepsilon_0)R_\mathrm{v}(\theta_1)\int_0^\infty J_0(\lambda\rho)(j\gamma_0)^{-1}\exp[-j\gamma_0(z+z_0)]\lambda\,\mathrm{d}\lambda\end{aligned} \tag{9.3.10}$$

where

$$\rho = r_1 \sin\theta_1 = r_0 \sin\theta_0$$
$$R_v(\theta_1) = [n\cos\theta_1 - (1 - n^{-2}\sin^2\theta_1)^{1/2}]/[n\cos\theta_1 + (1 - n^{-2}\sin^2\theta_1)^{1/2}]$$
$$r_1 = [\rho^2 + (z + z_0)^2]^{1/2}$$
$$r_0 = [\rho^2 + (z - z_0)^2]^{1/2}$$

Substituting Eq. (9.3.8) into Eq. (9.3.5) and noting that $\Pi_{z\,\text{primary}} = \Pi_{z\,\text{direct}}$, it follows that

$$\Pi_{z\,\text{surface}} = \Pi_{z\,\text{secondary}} - \Pi_{z\,\text{indirect}}$$

$$= (p/4\pi j\omega\varepsilon_0)\int_0^\infty (j\gamma_0)^{-1}[R(\lambda) - R_v(\theta_1)]J_0(\lambda\rho)\exp[-j\gamma_0(z+z_0)]\lambda\,d\lambda \tag{9.3.11}$$

$$= (p/4\pi j\omega\varepsilon_0)(P_1 - P_2), \quad z \geq 0$$

where $P_1 = \int_0^\infty [1 - R_v(\theta_1)](j\gamma_0 + jk_0\varepsilon)^{-1}J_0(\lambda\rho)\exp[-j\gamma_0(z+z_0)]\lambda\,d\lambda$

$$P_2 = -jk_0\int_0^\infty [1 + R_v(\theta_1)](\gamma_0)^{-1}(\gamma_0 + k_0\varepsilon)^{-1}\varepsilon J_0(\lambda\rho) \times\exp[-j\gamma_0(z + z_0)]\lambda\,d\lambda$$

$$R(\lambda) - R_v(\theta_1) = (\gamma_0 + k_0\varepsilon)^{-1}\{\gamma_0[1 - R_v(\theta_1)] - k_0\varepsilon[1 + R_v(\theta_1)]\}$$

$$\varepsilon = \gamma_1/(k_0 n^2) = (n^2 k_0^2 - \lambda^2)^{1/2}/(k_0 n^2) = n^{-1}[1 + (\lambda/jk_0 n)^2]^{1/2}$$

The parameter ε (not to be confused with permittivity) is equal to the parameter Δ of Wait [117] and is identical to that of King [85] and that used in Eq. (C-21) of App. C.

If $n = 1$, then $R_v(\theta_1) = 0$, $\varepsilon = \gamma_0/k_0$, $R(\lambda) = 0$, $P_1 - P_2 = 0$, $\Pi_{z\,\text{surface}} = 0$, and $\Pi_z = \Pi_{z\,\text{direct}}$.

If $\sigma = \infty$ so that $|n| = \infty$, then $R_v(\theta_1) = +1, \varepsilon = 0, R(\lambda) = 1, P_1 - P_2 = 0$, $\Pi_{z\,\text{surface}} = 0$ and $\Pi_z = \Pi_{z\,\text{direct}} + \Pi_{z\,\text{image}}$ where $\Pi_{z\,\text{image}} = \Pi_{z\,\text{indirect},R_v(\theta_1)=+1}$.

Consequently,

$$\Pi_{z\,\text{surface}} = 0, \quad n = 1 \text{ or } \sigma = \infty \tag{9.3.12}$$

The surface wave, as defined in Eq. (9.3.8), has the desirable property that it vanishes when either the earth is free space or a perfect conductor. For those conditions, only the space wave exists.

9.3.1.3 Waves and Pseudo-waves

The space and surface waves, as defined in Eq. (9.3.8), yield individual Hertz potentials given by Eqs. (9.3.9)–(9.3.11) that differ from those of earlier investigators (such as Norton [79], Wait [117], and King [85]) but whose total Hertz potential (and thus the total field) remains the same. Earlier investigators define the total wave to be the sum of a *pseudo-space* wave and a *pseudo-surface* wave. The pseudo-space wave is equal to the sum of the *direct* wave and an *image* wave. The image wave is the indirect wave whose field is equal to that of the direct wave multiplied by the Fresnel reflection coefficient for a perfectly-conducting earth [$R_v(\theta_1) = +1$]. The *pseudo-surface* wave is the difference between the total wave and the pseudo-space wave.

Since real earths are imperfectly conducting, the *image* wave, pseudo-space wave, and *pseudo-surface* wave of earlier investigators correspond to nonphysical waves or *pseudo*-waves. The pseudo-surface waves do have the advantage that their corresponding integral expressions for the Hertz potentials are of simpler mathematical form as will now be shown.

The Hertz potential Π_z may be expressed as

$$\begin{aligned}\Pi_z &= \Pi_{z\,\text{pseudo-space}} + \Pi_{z\,\text{pseudo-surface}} \\ &= (\Pi_{z\,\text{direct}} + \Pi_{z\,\text{image}}) + \Pi_{z\,\text{pseudo-surface}}, \quad z \geq 0\end{aligned} \tag{9.3.13}$$

where $\Pi_{z\,\text{pseudo-space}} = \Pi_{z\,\text{direct}} + \Pi_{z\,\text{image}}$.

The potential $\Pi_{z\,\text{direct}}$ is given by Eq. (9.3.9). The potential $\Pi_{z\,\text{image}}$ is found from Eq. (9.3.10) by setting $R_v(\theta_1) = +1$. Accordingly,

$$\begin{aligned}\Pi_{z\,\text{image}} &= (p/4\pi j\omega\varepsilon_0)(1/r_1)\exp(-jk_0 r_1) \\ &= (p/4\pi j\omega\varepsilon_0)\int_0^\infty J_0(\lambda\rho)(j\gamma_0)^{-1}\exp[-j\gamma_0(z+z_0)]\lambda\,d\lambda, \quad z \geq 0\end{aligned} \tag{9.3.14}$$

Substituting Eq. (9.3.13) into Eq. (9.3.5), it follows that

$$\begin{aligned}\Pi_{z\text{pseudo-surface}} &= \Pi_{z\text{secondary}} - \Pi_{z\text{image}} \\ &= (p/4\pi j\omega\varepsilon_0)\int_0^\infty \gamma_0^{-1}[R(\lambda)-1]J_0(\gamma\rho)\exp[-j\gamma_0(z+z_0)]\lambda\,d\lambda \\ &= (p/4\pi j\omega\varepsilon_0)(-2P), \; z \geq 0\end{aligned} \tag{9.3.15}$$

where

$$P = jk_0\int_0^\infty \gamma_0^{-1}(\gamma_0 + k_0\varepsilon)^{-1}\varepsilon J_0(\lambda\rho)\exp(-j\gamma_0(z+z_0)]\lambda\,d\lambda$$

$$R(\lambda) - 1 = -2k_0\varepsilon/(\gamma_0 + k_0\varepsilon)$$
$$\varepsilon = \gamma_1/(k_0 n^2) = (1/n)[1 + (\lambda/jk_0 n)^2]^{1/2}$$

If $n = 1$, then $R_v(\theta_1) = 0$, $\varepsilon = \gamma_1/k_0$, $R(\lambda) = 0$, $P = -(p/4\pi j\omega\varepsilon_0)^{-1} \times (\Pi_{z\,\text{image}}/2)$, $\Pi_{z\,\text{pseudo-surface}} = -\Pi_{z\,\text{image}}$, and $\Pi_z = \Pi_{z\,\text{direct}}$ where p is the dipole moment, ω is the radian frequency, and ε_0 is the permittivity of free space.

If $\sigma = \infty$ so that $|n| = \infty$, then $R_v(\theta_1) = +1$, $\varepsilon = 0$, $R(\lambda) = 1$, $P = 0$, $\Pi_{z\,\text{pseudo-surface}} = 0$, and $\Pi_z = \Pi_{z\,\text{direct}} + \Pi_{z\,\text{image}}$. Consequently,

$$\begin{aligned} \Pi_{z\,\text{pseudo-surface}} &= -\Pi_{z\,\text{image}}, \quad n = 1; \\ &= 0, \quad \sigma = \infty \end{aligned} \tag{9.3.16}$$

The pseudo-surface wave as defined in Eq. (9.3.13) is a nonphysical wave because even though it vanishes when the earth is a perfect conductor, it is nonvanishing (equal to a negative image wave) when the earth is free space. The surface wave as defined in Eq. (9.3.11) is a physical wave because it vanishes both when the earth is free space or a perfect conductor.

From Eqs. (9.3.11) and (9.3.15), it follows that

$$\begin{aligned} \Pi_{z\,\text{surface}} &= \Pi_{z\,\text{pseudo-surface}} + (\Pi_{z\,\text{image}} - \Pi_{z\,\text{indirect}}) \\ &= \{p/4\pi j\omega\varepsilon_0\}\{-2P + [1 - R_v(\theta_1)](1/r_1)\exp(-jk_0 r_1)\}, \quad z \geq 0 \end{aligned} \tag{9.3.17}$$

where

$$\Pi_{z\,\text{image}} - \Pi_{z\,\text{indirect}} = [p/4\pi j\omega\varepsilon_0][1 - R_v(\theta_1)](1/r_1)\exp(-jk_0 r_1)$$

From Eq. (9.3.17) it is seen that the surface-wave Hertz potential is given explicitly once the pseudo-surface wave Hertz potential is determined.

An exact closed-form evaluation of the integral expression given by Eq. (9.3.15) for the pseudo-surface wave Hertz potential has never been obtained. Approximate closed-form expressions for the Hertz potentials and fields, subject to the condition $|n^2| \gg 1$ where n is the earth index of refraction, have been obtained at restricted field points by Norton [79,80], Wait [82,94], and Banos [81] and at all field points (except in the immediate vicinity of the dipole) by King [85,118]. King obtained his approximate closed-form expressions by first developing exact integral expressions (which we shall denote as the "Sommerfeld–King integrals") for the pseudo-surface wave fields. None of the above approximate closed-form expressions reduce to the well-known case for free-space ($n = 1$) because of the approximations that were made in restricting n to the case $|n^2| \gg 1$. Approximate closed-form expressions for the case $|n^2| \approx 1$ are not given by the above investigators but are given in Sec. 9.3.3.

9.3.2 Fields and Pseudo-Fields in Air

The fields **E** and **H**, corresponding to the Hertzian potential Π_z of Eq. (9.3.8) at an arbitrary field point $P(r_1, \theta_1, \phi)$ in the half-space above earth, are given by

$$\mathbf{H} = \mathbf{H}_{\text{space}} + \mathbf{H}_{\text{surface}}, \quad z \geq 0 \tag{9.3.18}$$

$$\mathbf{E} = \mathbf{E}_{\text{space}} + \mathbf{E}_{\text{surface}}, \quad z \geq 0 \tag{9.3.19}$$

The space and surface-wave fields are related to the pseudo-space and pseudo-surface wave fields in air by

$$\mathbf{E}_{\text{space}} = \mathbf{E}_{\text{pseudo-space}} - [1 - R_{\text{v}}(\theta_1)]\mathbf{E}_{\text{image}} \tag{9.3.20}$$

$$\mathbf{H}_{\text{space}} = \mathbf{H}_{\text{pseudo-space}} - [1 - R_{\text{v}}(\theta_1)]\mathbf{H}_{\text{image}} \tag{9.3.21}$$

$$\mathbf{E}_{\text{surface}} = \mathbf{E}_{\text{pseudo-surface}} + [1 - R_{\text{v}}(\theta_1)]\mathbf{E}_{\text{image}} \tag{9.3.22}$$

$$\mathbf{H}_{\text{surface}} = \mathbf{H}_{\text{pseudo-surface}} + [1 - R_{\text{v}}(\theta_1)]\mathbf{H}_{\text{image}} \tag{9.3.23}$$

In Eqs. (9.3.20)–(9.3.23), the image field term follows from the definitions of the various waves. The image field term corresponds exactly to the field that is obtained when the Hertz potential term ($\Pi_{z\,\text{image}} - \Pi_{z\,\text{indirect}}$) in Eq. (9.3.17) is substituted into Eqs. (9.3.1) and (9.3.2) with the Fresnel reflection coefficient $R_{\text{v}}(\theta_1)$ treated as a constant during differentiation.

The image fields $\mathbf{H}_{\text{image}} = \mathbf{u}_\phi H_{\phi\,\text{image}}$ and $\mathbf{E}_{\text{image}} = \mathbf{u}_\rho E_{\rho\,\text{image}} + \mathbf{u}_z E_{z\,\text{image}}$ have cylindrical-coordinate components given by Eqs. (9.2.31)–(9.2.33) for $R_{\text{v}}(\theta_1) = +1$, in agreement with those given by King [85]. Accordingly,

$$\begin{aligned} H_{\phi\,\text{image}} &= (1/Z_0)A_1 \sin\theta_1[1 + (jk_0r_1)^{-1}] \\ &= H_{\phi 1\,\text{image}} + H_{\phi 2\,\text{image}}, \quad z \geq 0 \end{aligned} \tag{9.3.24}$$

$$\begin{aligned} E_{\rho\,\text{image}} &= A_1 \sin\theta_1 \cos\theta_1[1 + 3(jk_0r_1)^{-1} + 3(jk_0r_1)^{-2}] \\ &= E_{\rho 1\,\text{image}} + E_{\rho 2\,\text{image}} + E_{\rho 3\,\text{image}}, \quad z \geq 0 \end{aligned} \tag{9.3.25}$$

$$\begin{aligned} E_{z\,\text{image}} &= -A_1[\sin^2\theta_1 + (1 - 3\cos^2\theta_1)(jk_0r_1)^{-1} + (1 - 3\cos^2\theta_1)(jk_0r_1)^{-2}] \\ &= E_{z1\,\text{image}} + E_{z2\,\text{image}} + E_{z3\,\text{image}}, \quad z \geq 0 \end{aligned} \tag{9.3.26}$$

where

$$\begin{aligned} A_1 &= j[(Z_0k_0p)/(4\pi r_1)]\exp(-jk_0r_1) \\ H_{\phi 1\,\text{image}} &= (1/Z_0)A_1 \sin\theta_1 \end{aligned}$$

$$H_{\phi 2\,\text{image}} = (jk_0r_1)^{-1}(1/Z_0)A_1 \sin\theta_1$$
$$E_{\rho 1\,\text{image}} = A_1 \sin\theta_1 \cos\theta_1$$
$$E_{\rho 2\,\text{image}} = A_1 \sin\theta_1 \cos\theta_1[3(jk_0r_1)^{-1}]$$
$$E_{\rho 3\,\text{image}} = A_1 \sin\theta_1 \cos\theta_1[3(jk_0r_1)^{-2}]$$
$$E_{z1\,\text{image}} = -A_1 \sin^2\theta_1$$
$$E_{z2\,\text{image}} = -A_1(1 - 3\cos^2\theta_1)(jk_0r_1)^{-1}$$
$$E_{z3\,\text{image}} = -A_1(1 - 3\cos^2\theta_1)(jk_0r_1)^{-2}$$

The corresponding spherical-coordinate components of the image fields are found from Eqs. (9.2.34)–(9.2.36) for $R_v(\theta_1) = +1$. Accordingly, $\mathbf{H}_{\text{image}} = \mathbf{u}_\phi H_{\phi\,\text{image}}$ and $\mathbf{E}_{\text{image}} = \mathbf{u}_r E_{r\,\text{image}} + \mathbf{u}_\theta E_{\theta\,\text{image}}$ where

$$H_{\phi\,\text{image}} = (1/Z_0)A_1 \sin\theta_1[1 + (jk_0r_1)^{-1}], \quad z \geq 0 \tag{9.3.27}$$

$$E_{r\,\text{image}} = 2A_1 \cos\theta_1[(jk_0r_1)^{-1} + (jk_0r_1)^{-2}], \quad z \geq 0 \tag{9.3.28}$$

$$E_{\theta\,\text{image}} = A_1 \sin\theta_1[1 + (jk_0r_1)^{-1} + (jk_0r_1)^{-2}], \quad z \geq 0 \tag{9.3.29}$$

where A_1 is defined above.

The space-wave fields are given by Eqs. (9.2.37) and (9.2.38) and are repeated below.

$$\mathbf{H}_{\text{space}} = \mathbf{H}_{\text{direct}} + \mathbf{H}_{\text{indirect}} = \mathbf{H}_{\text{direct}} + R_v(\theta_1)\mathbf{H}_{\text{image}} \tag{9.3.30}$$

$$\mathbf{E}_{\text{space}} = \mathbf{E}_{\text{direct}} + \mathbf{E}_{\text{indirect}} = \mathbf{E}_{\text{direct}} + R_v(\theta_1)\mathbf{E}_{\text{image}} \tag{9.3.31}$$

where $\mathbf{H}_{\text{direct}}$ and $\mathbf{E}_{\text{direct}}$ have cylindrical-coordinate components given by Eqs. (9.2.25)–(9.2.27) and spherical-coordinate components given by Eqs. (9.2.28)–(9.2.31).

The space-wave pseudo-fields are found from Eqs. (9.3.20), (9.3.21), (9.3.31), and (9.3.32) and, in agreement with King [85], are

$$\mathbf{H}_{\text{pseudo-space}} = \mathbf{H}_{\text{space}} + [1 - R_v(\theta_1)]\mathbf{H}_{\text{image}} = \mathbf{H}_{\text{direct}} + \mathbf{H}_{\text{image}} \tag{9.3.32}$$

$$\mathbf{E}_{\text{pseudo-space}} = \mathbf{E}_{\text{space}} + [1 - R_v(\theta_1)]\mathbf{E}_{\text{image}} = \mathbf{E}_{\text{direct}} + \mathbf{E}_{\text{image}} \tag{9.3.33}$$

9.3.3 Cases $|n^2| \gg 1$ and $|n^2| \approx 1$

Our approach in evaluating the Sommerfeld–King integral expressions for the pseudo-surface wave fields is similar to the methodology of Ref. 85 but with the following differences:

1. For $|n^2| \gg 1$, a modified variational method is utilized to evaluate the variational parameter ε introduced in Eq. (A12) of Ref. 85. Instead of setting $\varepsilon = \varepsilon(0) = n^{-1}$, as is done in Ref. 85 consistent with the value obtained by a conventional variational method of Storer [119],

the parameter ε is evaluated more exactly by requiring that the far-field asymptotic expressions for the surface-wave fields vanish for the lowest-order term proportional to $(k_0 r_1)^{-1}$. This new methodology is possible because $\varepsilon \approx \varepsilon(0)$ at all angles of incidence θ_1.

2. For $|n^2| \approx 1$, the functional form of the fields is determined utilizing a modified variational method to evaluate a new variational parameter $\varepsilon' = \varepsilon - (\gamma_0/k_0)$ but the argument of the functional form is determined utilizing the value $\varepsilon' = \varepsilon'(0) = n^{-1} - 1$ obtained from the conventional variational method. This difference in methodology is necessitated because $\varepsilon' \approx \varepsilon'(0)$ only at small angles of incidence θ_1.
3. The concept of *surface-wave fields* vs. conventional *pseudo surface-wave fields* is utilized to account for higher-order terms proportional to $(k_0 r_1)^{-2}$ and $(k_0 r_1)^{-3}$ that were previously neglected in expressions for the asymptotic surface-wave fields.

The Sommerfeld–King integrals [85] are evaluated in App. C. The exact integrals reduce to approximate integrals with a dummy variable of integration z_3, integrated over the range $z_d \leq z_3 \leq \infty$ [see Eqs. (C-63)–(C-65)]. These integrals may be conceptualized as surface-wave rays originating from an image line-source ($z_d \leq z_3 \leq \infty$) when z_3 is real (see Fig. 79). The amplitude distribution of the rays along the line source is approximated at all points of the line source by the amplitude at the dipole image point ($z_3 = z_d$) at the beginning of the line source. This conceptualization for the source of the surface-wave fields is somewhat similar to that of Booker and Clemmow [86,87] when z_3 is real but more like that of Lindell and Alanen [123] when z_3 is complex. The App. C methodology is attractive because:

1. It provides approximate closed-form expressions of the surface-wave fields at all points of the air medium, for both small and large relative permittivities of the earth.
2. The expressions for large relative permittivities agree with the previous most accurately known results; the expressions for small relative permittivities are new and reduce for the case $n = 1$ to those for free space.

9.3.3.1 $|n^2| \gg 1$

For the case $|n^2| \gg 1$, the surface-wave fields $H_{\phi\,\text{surface}}$, $E_{\rho\,\text{surface}}$, and $E_{z\,\text{surface}}$ are given by Eqs. (C-108)–(C-110) of App. C as

$$H_{\phi\,\text{surface}} = H_{\phi 1\,\text{image}}[1 - R_v(\theta_1)]\{1 - (j\pi s_0)\exp[j(\pi/2)s_0^2]\mathcal{F}^*(s_0)\} + H_{\phi 2\,\text{image}}[1 - R_v(\theta_1)], \quad |n^2| \gg 1 \tag{9.3.34}$$

$$E_{\rho\,\text{surface}} = -E_{\rho 1\,\text{image}}[1 - R_v(\theta_1)]^2[1 + R_v(\theta_1)]^{-1}$$
$$\times \{1 - (j\pi s_0)\exp[j(\pi/2)s_0^2]\mathcal{F}^*(s_0)\} \tag{9.3.35}$$
$$+ (E_{\rho 2\,\text{image}} + E_{\rho 3\,\text{image}})[1 - R_v(\theta_1)], \quad |n^2| \gg 1$$

$$E_{z\,\text{surface}} = E_{z1\,\text{image}}[1 - R_v(\theta_1)]\{1 - (j\pi s_0)\exp[j(\pi/2)s_0^2]\mathcal{F}^*(s_0)\}$$
$$+ (E_{z2\,\text{image}} + E_{z3\,\text{image}})[1 - R_v(\theta_1)], \quad |n^2| \gg 1 \tag{9.3.36}$$

where

$s_0 = 2\cot\theta_1[1 + R_v(\theta_1)]^{-1}(k_0 r_1/\pi)^{1/2}$
$\mathcal{F}^*(s_0) =$ complimentary conjugate Fresnel integral $= F^*(\infty) - F^*(s_0)$
$= \int_{s_0}^{\infty}\exp[-j(\pi/2)s^2]\mathrm{d}s$
$F^*(\infty) = \int_0^{\infty}\exp[-j(\pi/2)s^2]\mathrm{d}s \quad [= (1-j)/2,\ s \text{ real}]$
$F^*(s_0) =$ conjugate Fresnel integral $= \int_0^{s_0}\exp[-j\pi/2)s^2]\,\mathrm{d}s$
$R_v(\theta_1) =$ Fresnel reflection coefficient for parallel polarization
$= [n\cos\theta_1 - (1 - n^{-2}\sin^2\theta_1)^{1/2}]/[n\cos\theta_1 + (1 - n^{-2}\sin^2\theta_1)^{1/2}]$
$H_{\phi 1\,\text{image}}$, $H_{\phi 2\,\text{image}}$, $E_{\rho 1\,\text{image}}$, $E_{\rho 2\,\text{image}}$, $E_{\rho 3\,\text{image}}$, $E_{z1\,\text{image}}$, $E_{z2\,\text{image}}$, $E_{z3\,\text{image}}$ are given by Eqs. (9.3.24)–(9.3.26).

The pseudo-surface wave fields $H_{\phi\,\text{pseudo-surface}}$, $E_{\rho\,\text{pseudo-surface}}$, and $E_{z\,\text{pseudo-surface}}$ are given by Eqs. (C-105)–(C-107) of App. C as

$$H_{\phi\,\text{pseudo-surface}} \approx -H_{\phi 1\,\text{image}}[1 - R_v(\theta_1)](j\pi s_0)$$
$$\times \exp[j(\pi/2)s_0^2]\mathcal{F}^*(s_0), \quad |n^2| \gg 1 \tag{9.3.37}$$

$$E_{\rho\,\text{pseudo-surface}} \approx -2E_{\rho 1\,\text{image}}[1 - R_v(\theta_1)][1 + R_v(\theta_1)]^{-1}$$
$$\times \{1 - (1/2)[1 - R_v(\theta_1)](j\pi s_0) \tag{9.3.38}$$
$$\times \exp[j(\pi/2)s_0^2]\mathcal{F}^*(s_0)\}, \quad |n^2| \gg 1$$

$$E_{z\,\text{pseudo-surface}} \approx -E_{z1\,\text{image}}[1 - R_v(\theta_1)](j\pi s_0)$$
$$\times \exp[j(\pi/2)s_0^2]\mathcal{F}^*(s_0) \tag{9.3.39}$$

It should be noted that the index of refraction n does not enter Eqs. (9.3.34)–(9.3.39) directly but only indirectly through the Fresnel reflection

coefficient $R_v(\theta_1)$. Some relevant functions of $R_v(\theta_1)$ are given in Table 21(a) and (b). In particular, for $|n^2| \gg 1$,

$$R_v(\theta_1) \approx (n\cos\theta_1 - 1)(n\cos\theta_1 + 1)^{-1}, \quad 1 \ll |n^2| < \infty = 1, \quad |n^2| = \infty \tag{9.3.40}$$

$$1 - R_v(\theta_1) \approx 2(n\cos\theta_1 + 1)^{-1}, \quad 1 \ll |n^2| < \infty = 0, \quad |n^2| = \infty \tag{9.3.41}$$

$$[1 + R_v(\theta_1)]^{-1} \approx (n\cos\theta_1 + 1)(2n\cos\theta_1)^{-1}, \quad 1 \ll |n^2| < \infty = 1/2, |n^2| = \infty, \quad \theta_1 = \pi/2\,\text{rad} \tag{9.3.42}$$

$$s_0 \approx (n\cos\theta_1 + 1)(n\sin\theta_1)^{-1}(k_0 r_1/\pi)^{1/2}, \quad 1 \ll |n^2| < \infty = 0, \quad |n^2| = \infty, \quad \theta_1 = \pi/2\,\text{rad} \tag{9.3.43}$$

Substituting Eqs. (9.3.24)–(9.3.26) and (9.3.40)–(9.3.43) into Eqs. (9.3.37) and (9.3.39), the cylindrical-coordinate components of the pseudo-surface wave fields reduce to

$$H_{\phi\,\text{pseudo-surface}} \approx (pk_0/2\pi r_1 n)(\pi k_0 r_1)^{1/2}\exp(-jk_0 r_1) \times \exp[j(\pi/2)s_0^2]\mathcal{F}^*(s_0), \quad |n^2| \gg 1 \tag{9.3.44}$$

$$E_{\rho\,\text{pseudo-surface}} \approx -j(pZ_0 k_0/2\pi r_1 n)\exp(-jk_0 r_1)\sin\theta_1 \times \{1 - (j/n\sin\theta_1)(\pi k_0 r_1)^{1/2}\exp[j(\pi/2)s_0^2]\mathcal{F}^*(s_0)\}, \quad |n^2| \gg 1 \tag{9.3.45}$$

$$E_{z\,\text{pseudo-surface}} \approx (pZ_0 k_0/2\pi r_1 n)(\pi k_0 r_1)^{1/2}(1/\sin\theta_1)\exp(-jk_0 r_1) \times \exp[j(\pi/2)s_0^2]\mathcal{F}^*(s_0), \quad |n^2| \gg 1 \tag{9.3.46}$$

where

TABLE 21 Functions of the Fresnel Reflection Coefficient $R_v(\theta_1)$. (a) Exact Formulae and Values and (b) Approximate Formulae and Values

			Exact values					
			$\theta_1 = \pi/2$ rad or $A = 0$, $B = (1 - n^{-2})^{1/2}$			$\theta_1 = 0$ rad or $A = n$, $B = 1$		
			n			n		
No.	Function	Exact formulae	∞	$\neq 1$, $\neq \infty$	1	∞	Arbitrary	1
(a)								
1	$R_v(\theta_1)$	$(A - B)/(A + B)$	1	-1	0	1	$(n - 1)/(n + 1)$	0
2	$1 - R_v(\theta_1)$	$2B/(A + B)$	0	2	1	0	$2/(n + 1)$	1
3	$1 + R_v(\theta_1)$	$2A/(A + B)$	2	0	1	2	$2n/(n + 1)$	1
4	$[1 - R_v(\theta_1)]/[1 + R_v(\theta_1)]$	B/A	0	∞	1	0	$1/n$	1
5	$[1 - R_v(\theta_1)][1 + R_v(\theta_1)]$	$4AB/(A + B)^2$	0	0	1	0	$4n/(n + 1)^2$	1
6	$[1 + R_v(\theta_1)]^2$	$4A^2/(A + B)^2$	4	0	1	4	$4n^2/(n + 1)^2$	1
7	$[1 - R_v(\theta_1)]^2$	$4B^2/(A + B)^2$	0	4	1	0	$4/(n + 1)^2$	1
8	$[1 + R_v(\theta_1)]^2[1 - R_v(\theta_1)]^{-2}$	A^2/B^2	∞	0	1	∞	n^2	1
9	$[1 - R_v(\theta_1)]/R_v(\theta_1)$	$2B/(A - B)$	0	-2	∞	0	$2/(n - 1)$	∞
10	$R_v(\theta_1)/[1 + R_v(\theta_1)]$	$(A - B)/2A$	0.5	$-\infty$	0	0.5	$(n - 1)/2n$	0
11	$\cot \theta_1/[1 + R_v(\theta_1)]$	$\sec \theta_1(A + B)/2n$	0	*	0	∞	∞	∞

No.	Function	Approximate formulae and values		
			$\lvert n^2\rvert \approx 1$	
		$\lvert n^2\rvert \gg 1$ or $B \approx 1$	$\tan\theta_1 \ll [2(n-1)]^{-1/2}$ or $B \approx \cos\theta_1$	$\tan\theta_1 \gg [2(n-1)]^{-1/2}$ or $A \approx 1$, $B \approx (1-n^{-2})^{1/2}$
(b)				
1	$R_v(\theta_1)$	$(A-1)/(A+1)$	$(n-1)/(n+1)$	-1
2	$1-R_v(\theta_1)$	$2/(A+1)$	$2/(n+1)$	2
3	$1+R_v(\theta_1)$	$2A/(A+1)$	$2n/(n+1)$	0
4	$[1-R_v(\theta_1)]/[1+R_v(\theta_1)$	$1/A$	$1/n$	∞
5	$[1-R_v(\theta_1)][1+R_v(\theta_1)]$	$4A/(A+1)^2$	$4n/(n+1)^2$	0
6	$[1+R_v(\theta_1)]^2$	$4A^2/(A+1)^2$	$4n^2/(n+1)^2$	0
7	$[1-R_v(\theta_1)]^2$	$4/(A+1)^2$	$4/(n+1)^2$	4
8	$[1+R_v(\theta_1)]^2[1-R_v(\theta_1)]^{-2}$	A^2	n^2	0
9	$[1-R_v(\theta_1)]/R_v(\theta_1)$	$2/(A-1)$	$2/(n-1)$	-2
10	$R_v(\theta_1)/[1+R_v(\theta_1)]$	$(A-1)/2A$	$(n-1)/2n$	$-\infty$
11	$\cot\theta_1/[1+R_v(\theta_1)]$	$\sec\theta_1(A+1)/2n$	$\cot\theta_1(n+1)/2n$	∞

$A = n\cos\theta_1$.
$B = (1-n^{-2}\sin^2\theta_1)^{1/2}$, principal value.
$* = (2n)^{-1}(1-n^{-2})^{1/2}$, principal value.

p = moment of the Hertzian dipole
k_0,k_1 = wave numbers in air and earth, respectively ($n = k_1/k_0$)
$Z_0 k_0 = \omega\mu_0$
$\cos\theta_1 = (z + z_0)/r_1$
$\sin\theta_1 = \rho/r_1$

Equation (9.3.44) for $H_{\phi\,\text{pseudo-surface}}$, when multiplied by the free-space permeability μ_0, agrees with the King's Eq. (22) in Ref. 85. Equation (9.3.45) for $E_{\rho\,\text{pseudo-surface}}$ agrees with King's Eq. (23). Equation (9.3.46) for $E_{z\,\text{pseudo-surface}}$ agrees with King's Eq. (24). The differences in *notation* between King's results and those of App. C are summarized in Table C-1. In particular, please note that King's Fresnel integrals are of the form $F_2(x)$ whereas those of App. C are of the more conventional form $F(x) = F_2[(\pi/2)x^2]$ as defined in Ref. 124 and illustrated in lines 15–17 of Table C-1.

For $R_v(\theta_1) = +1$ (corresponding to earth of infinite conductivity), the pseudo-surface wave fields and surface-wave fields both vanish.

For $s_0 \gg 1$ (corresponding to $(k_0 r_1)^{1/2} \gg 1$), $\mathcal{F}^*(s_0)$ is given by Eq. (C-101) of App. C as

$$\begin{aligned}\mathcal{F}^*(s_0) =& (j\pi s_0)^{-1} \exp[-j(\pi/2)s_0^2]\{1 - [(1\cdot3)(\pi s_0^2)^{-2}] \\ &+ [(1\cdot3\cdot5\cdot7)(\pi s_0^2)^{-4}] - \cdots\} + (\pi s_0)^{-1}(\pi s_0^2)^{-1} \\ &\times \exp[-j(\pi/2)s_0^2]\{[1 - [(1.3.5)(\pi s_0^2)^{-2}] + \cdots\}, \quad s_0 \gg 1\end{aligned} \tag{9.3.47}$$

Substituting Eq. (9.3.47) into Eqs. (9.3.34)–(9.3.36),

$$\begin{aligned}H_{\phi\,\text{surface}} \approx& H_{\phi 1\,\text{image}}[1 - R_v(\theta_1)][\{[(1\cdot3)(\pi s_0^2)^{-2}] - [(1\cdot3\cdot5\cdot7)(\pi s_0^2)^{-4}] \\ &+ \cdots\} - j(\pi s_0^2)^{-1}\{[1 - [(1\cdot3\cdot5)(\pi s_0^2)^{-2}] + \cdots\}] \\ &+ H_{\phi 2\,\text{image}}[1 - R_v(\theta_1)]; \quad s_0 \gg 1, \quad |n^2| \gg 1\end{aligned} \tag{9.3.48}$$

$$\begin{aligned}E_{\rho\,\text{surface}} \approx& - E_{\rho 1\,\text{image}}[1 - R_v(\theta_1)]^2[1 + R_v(\theta_1)]^{-1}[\{[(1\cdot3)(\pi s_0^2)^{-2}] \\ &- [(1\cdot3\cdot5\cdot7)(\pi s_0^2)^{-4}] + \cdots\} - j(\pi s_0^2)^{-1} \\ &\times \{[1 - [(1\cdot3\cdot5)(\pi s_0^2)^{-2}] + \cdots\}] \\ &+ (E_{\rho 2\,\text{image}} + E_{\rho 3\,\text{image}})[1 - R_v(\theta_1)]; \\ &s_0 \gg 1, \quad |n^2| \gg 1\end{aligned} \tag{9.3.49}$$

$$E_{z\,\text{surface}} \approx E_{z1\,\text{image}}[1 - R_v(\theta_1)][\{[(1\cdot3)(\pi s_0^2)^{-2}] - [(1\cdot3\cdot5\cdot7)(\pi s_0^2)^{-4}] + \cdots\} - j(\pi s_0^2)^{-1}\{[1 - [(1\cdot3\cdot5)(\pi s_0^2)^{-2}] + \cdots\}] + (E_{z2\,\text{image}} + E_{z3\,\text{image}})[1 - R_v(\theta_1)]; \quad s_0 \gg 1, \quad |n^2| \gg 1 \tag{9.3.50}$$

In the far-field ($k_0 r_1 \gg 1$), the amplitudes of the surface-wave fields decrease with increasing distance approximately as $(k_0 r_1)^{-2}$ since the product of $H_{\phi 1\,\text{image}}$, $E_{\rho 1\,\text{image}}$, or $E_{z1\,\text{image}}$ with $-j(\pi s_0^2)^{-1}$ is proportional to $(k_0 r_1)^{-2}$ and also because $H_{\phi 2\,\text{image}}$, $E_{\rho 2\,\text{image}}$, $E_{z2\,\text{image}}$ are proportional to $(k_0 r_1)^{-2}$. For $\theta_1 = \pi/2$, the function $1 - R_v(\pi/2) = 2$ for $0 < |n^2| < \infty$ and 0 for $|n^2| = \infty$.

For $s_0 \ll 1$ (corresponding to $(k_0 r_1)^{1/2} \ll 1$), the series expansion of $\mathcal{F}^*(s_0)$ is given by Ref. 121 as

$$\mathcal{F}^*(s_0) = F^*(\infty) - [s_0 - (1/5)(\pi/2)^2 s_0^5 + \cdots] + j[(1/3)(\pi/2)s_0^3 - (1/42)(\pi/2)^3 s_0^7 + \cdots] \approx F^*(\infty), \quad s_0 \ll 1 \tag{9.3.51}$$

Substituting Eq. (9.3.51) into Eqs. (9.3.34)–(9.3.36),

$$H_{\phi\,\text{surface}} \approx H_{\phi 1\,\text{image}}[1 - R_v(\theta_1)]\{1 - (j\pi s_0)\exp(j\pi s_0^2/2)F^*(\infty)\} + H_{\phi 2\,\text{image}}[1 - R_v(\theta_1)]; \quad s_0 \ll 1, \quad |n^2| \gg 1 \tag{9.3.52}$$

$$E_{\rho\,\text{surface}} \approx -E_{\rho 1\,\text{image}}[1 - R_v(\theta_1)]^2][1 + R_v(\theta_1)]^{-1} \{1 - (j\pi s_0)\exp(j\pi s_0^2/2)\,F^*(\infty)\} + (E_{\rho 2\,\text{image}} + E_{\rho 3\,\text{image}})[1 - R_v(\theta_1)]; \quad s_0 \ll 1, \quad |n^2| \gg 1 \tag{9.3.53}$$

$$E_{z\,\text{surface}} \approx E_{z1\,\text{image}}[1 - R_v(\theta_1)]\{1 - (j\pi s_0)\exp(j\pi s_0^2/2)F^*(\infty)\} + (E_{z2\,\text{image}} + E_{z3\,\text{image}})[1 - R_v(\theta_1)]; \quad s_0 \ll 1, \quad |n^2| \gg 1 \tag{9.3.54}$$

In the very near-field $[(k_0 r_1)^{1/2} \ll 1]$, the amplitudes of the surface-wave fields decrease with increasing distance approximately as that of the image fields $H_{\phi 2\,\text{image}}$, $E_{z2\,\text{image}}$, $E_{z3\,\text{image}}$ where "approximately" is emphasized because of the asymptotic approximations made in Eqs. (C-62c) and (C-62d) of App. C. Again, for $\theta_1 = \pi/2$, the function $1 - R_v(\pi/2) = 2$ for $0 < |n^2| < \infty$ and 0 for $|n^2| = \infty$.

For $z_0 = 0$ (the dipole is in the air medium but on the earth's surface), the field point $P(r_1, \theta_1, \phi)$ of Fig. 79 reduces to the field point $P(r, \theta, \phi)$ of Fig. 73 in Sec. 9.2.1. The fields are given by Eqs. (9.3.18)–(9.3.54) but z_d, r_1, θ_1 reduce to

$$z_d = z_0 + z = z, \quad z_0 = 0 \tag{9.3.55a}$$

$$r_1 = (z_d^2 + \rho^2)^{1/2} = (z^2 + \rho^2)^{1/2} = r, \quad z_0 = 0 \tag{9.3.55b}$$

$$\theta_1 = \cot^{-1}(z_d/\rho) = \cot^{-1}(z/\rho) = \theta, \quad z_0 = 0 \tag{9.3.55c}$$

For $z_0 = 0$ and $z = 0$ (both the dipole and the field point are on the earth's surface), the field point $P(r_1, \theta_1, \phi)$ of Fig. 79 reduces to the field point $P(\rho, \pi/2, \phi)$ of Fig. 73 in Sec. 9.2.1. The fields are given by Eqs. (9.3.18)–(9.3.54) but z_d, r_1, and θ_1 reduce to

$$z_d = z_0 + z = 0, \quad z_0 = z = 0 \tag{9.3.56a}$$

$$r_1 = (z_d^2 + \rho^2)^{1/2} = \rho, \quad z_0 = z = 0 \tag{9.3.56b}$$

$$\theta_1 = \cot^{-1}(z_d/\rho) = \cot^{-1}(0) = \pi/2 \text{ rad}, \quad z_0 = z = 0 \tag{9.3.56c}$$

The ratio of the surface-wave radial electric field to the surface-wave's other field components provide a convenient measure of the earth's index of refraction. In particular, consider the wave tilt β defined by

$$\begin{aligned} \beta &= -[E_{\rho\,\text{surface}}/Z_0 H_{\phi\,\text{surface}}];\ \theta_1 = \pi/2, \quad k_0 r_1 \gg 1 \\ &= [E_{\rho\,\text{surface}}/E_{z\,\text{surface}}];\ \theta_1 = \pi/2, \quad k_0 r_1 \gg 1 \end{aligned} \tag{9.3.57}$$

Substituting Eqs. (9.3.34) and (9.3.35) into Eq. (9.3.57),

$$\beta = n^{-1}(1 - n^{-2})^{1/2}, \quad |n^2| \gg 1 \tag{9.3.58}$$

where

$$\cos\theta_1[1 + R_v(\theta_1)]^{-1} = (2n)^{-1}(1 - n^{-2})^{1/2}, \quad \theta_1 = \pi/2$$

$$1 - R_v(\theta_1) = 2, \quad \theta_1 = \pi/2, \quad 1 < |n^2| < \infty$$

The wave tilt β given by Eq. (9.3.58) agrees with that given by Norton (1937) [79].

Equations (9.3.34)–(9.3.36), for the surface-wave field components may be written as

$$H_{\phi\,\text{surface}} = [1 - R_v(\theta_1)][H_{\phi 1\,\text{image}}\,\mathcal{A}(s_0) + H_{\phi 2\,\text{image}}], \quad |n^2| \gg 1 \tag{9.3.59}$$

$$E_{\rho\,\text{surface}} = -E_{\rho 1\,\text{image}}[1 - R_{\text{v}}(\theta_1)]^2[1 + R_{\text{v}}(\theta_1)]^{-1}\mathcal{A}(s_0) + (E_{\rho 2\,\text{image}} + E_{\rho 3\,\text{image}})[1 - R_{\text{v}}(\theta_1)], \quad |n^2| \gg 1 \tag{9.3.60}$$

$$E_{z\,\text{surface}} = [1 - R_{\text{v}}(\theta_1)][E_{z1\,\text{image}}\mathcal{A}(s_0) + (E_{z2\,\text{image}} + E_{z3\,\text{image}})], \quad |n^2| \gg 1 \tag{9.3.61}$$

where

$$\mathcal{A}(s_0) = \text{amplitude attenuation function} = 1 - (j\pi s_0)\exp[j(\pi/2)\text{s}_\text{o}^2]\mathcal{F}^*(s_0) \tag{9.3.62}$$

The function $\mathcal{A}(s_0)$ may be written in a form recognizable as Sommerfeld's attenuation function [125] by introducing parameters $t_0 = (j\pi/2)^{1/2} \times (s_0)$, $w_0 = -t_o^2$, and the complimentary error function erfc(t_0). Accordingly,

$$\begin{aligned}\text{erfc}(t_0) &= \text{complimentary error function [126]} \\ &= 1 - \text{erf}(t_0) = 1 - 2\pi^{-1/2}\int_0^{t_0}\exp(-t^2)\ \text{d}t \\ &= 2\pi^{-1/2}\int_{t_0}^{\infty}\exp(-t^2)\text{d}t\end{aligned} \tag{9.3.63}$$

where

$$t = (j\pi/2)^{1/2}s \tag{9.3.64}$$

$$t_0 = (j\pi/2)^{1/2}s_0 \tag{9.3.65}$$

$$\text{dt} = (j\pi/2)^{1/2}\text{ds} \tag{9.3.66}$$

Substituting Eqs. (9.3.64)–(9.3.66) into Eq. (9.3.63),

$$\begin{aligned}\text{erfc}(t_0) &= \text{erfc}[(j\pi/2)^{1/2}s_0] \\ &= 2\pi^{-1/2}(j\pi/2)^{1/2}\int_{s_0}^{\infty}\exp[-j(\pi/2)s^2]\text{d}s \\ &= (2j)^{1/2}\int_{s_0}^{\infty}\exp[-j(\pi/2)\text{s}^2]\text{d}s = (2j)^{1/2}\mathcal{F}^*(s_0)\end{aligned} \tag{9.3.67}$$

From Eq. (9.3.67),

$$\mathcal{F}^*(s_0) = j^{-1/2}\text{erfc}(t_0) = (2j)^{-1/2} \quad \text{erfc}(jw_0)^{1/2} \tag{9.3.68}$$

where

$$w_0 = -t_0^2 = -(j\pi/2)s_0^2 = -j2k_0r_1[1 + R_v(\theta_1)]^{-2}\cot^2\theta_1 \tag{9.3.69}$$

Substituting Eqs. (9.3.68) and (9.3.69) into Eq. (9.3.62),

$$\begin{aligned} \mathcal{A}(s_0) &= 1 - [j\pi(j\pi/2)^{-1/2}jw_0][\exp(-w_0)][(2j)^{-1/2}\text{erfc}(jw_0^{1/2})] \\ &= 1 - j(\pi w_0)^{1/2}\exp(-w_0)\text{erfc}(jw_0^{1/2}) \\ &= A_{\text{sommerfeld}}(w_0) = \text{Sommerfeld's attenuation function [125]} \end{aligned} \tag{9.3.70}$$

The Sommerfeld attenuation function $A_{\text{sommerfeld}}$ (w_0) of Eq. (9.3.70) is of identical form as the Sommerfeld attenuation function given by Eq. (23.62) in [125]. However, a significant difference is that the parameter w_0 in Eq. (9.3.70) is applicable to any field point in the air medium whereas Eq. (23.62) in Ref. 125 is restricted to field points on the earth's surface in the far-field.

For $z = z_0 = 0$ (corresponding to $\theta_1 = \pi/2$ rad), the total electric field component E_z is given by Eqs. (9.2.37), (9.3.26), (9.3.61), and (9.3.70) as

$$\begin{aligned} E_z &= E_{z\,\text{space}} + E_{z\,\text{surface}} \\ &= [E_{z\,\text{direct}} + R_v(\pi/2)\,E_{z\,\text{image}}] + [1 - R_v(\pi/2)] \\ &\quad \times E_{z1\,\text{image}}A_{\text{sommerfeld}}(w_0) + (E_{z2\,\text{image}} + E_{z3\,\text{image}})] \\ &= -2A_0[A_{\text{sommerfeld}}(w_0) + (jk_0\rho)^{-1} + (jk_0\rho)^{-2}], \quad |n^2| \gg 1 \end{aligned} \tag{9.3.71}$$

where

$$E_{z\,\text{direct}} = -A_0[1 + (jk_0\rho)^{-1} + (jk_0\rho)^{-2}], \quad z = z_0 = 0$$

$$E_{z\text{image}} = -A_1[1 + (jk_0\rho)^{-1} + (jk_0\rho)^{-2}], \quad z = z_0 = 0$$

$$E_{z\,\text{space}} = 0, \quad z = z_0 = 0$$

$$A_0 = A_1 = j(\omega\mu_0 p/4\pi\rho)\ \exp(-jk_0\rho), \quad z = z_0 = 0$$

$$R_v(\pi/2) = +1, \quad |n^2| = \infty; = -1, \quad 1 < |n^2| < \infty$$

$$w_0 = -j\ (k_0\rho/2)n^{-2}(1 - n^{-2}), \quad z = z_0 = 0$$

[see Table 21(a), line 11].If $|n^2| = \infty$, then $A_{\text{sommerfeld}}(w_0) = 1$ and E_z, given by Eq. (9.3.71), reduces to a space-wave field equal to twice that of the direct field. If $1 \ll |n^2| < \infty$, then the space-wave field is zero on the earth's surface and

the total field consists solely of a surface-wave field. Eq. (9.3.71) agrees with a result given by Wait [129, Eq. (36)]. Numerical values of the Sommerfeld attenuation function $A_{\text{sommerfeld}}(w_0)$ have been published by Norton [79] for a range of values of $|w_0|$ and $\angle w_0$.

9.3.3.2 $|n^2| \approx 1$

For $|n^2| \approx 1$, the surface-wave fields $H_{\phi\,\text{surface}}$, $E_{\rho\,\text{surface}}$, $E_{z\,\text{surface}}$ and pseudo-surface wave fields $H_{\phi\,\text{pseudo-surface}}$, $E_{\rho\,\text{pseudo-surface}}$, $E_{z\,\text{pseudo-surface}}$ are given by Eqs. (C-163)–(C-168) and (C-170) of App. C as

$$H_{\phi\,\text{surface}} = -H_{\phi 1\,\text{image}} R_{\text{v}}(\theta_1)\{1 - (j\pi s_1)\exp[(j\pi/2)s_1^2]\mathcal{F}^*(s_1)\} - H_{\phi 2\,\text{image}} R_{\text{v}}(\theta_1), \quad |n^2| \approx 1 \tag{9.3.72}$$

$$E_{\rho\,\text{surface}} = -E_{\rho 1\,\text{image}}[R_{\text{v}}(\theta_1)]^2[1 + R_{\text{v}}(\theta_1)]^{-1}\{1 - (j\pi s_1)\exp[j(\pi/2)s_1^2] \times \mathcal{F}^*(s_1)\} - (E_{\rho 2\,\text{image}} + E_{\rho 3\,\text{image}})\ R_{\text{v}}(\theta_1), \quad |n^2| \approx 1 \tag{9.3.73}$$

$$E_{z\,\text{surface}} = -E_{z1\,\text{image}} R_{\text{v}}(\theta_1)\{1 - (j\pi s_1)\exp[j(\pi/2)s_1^2]\,\mathcal{F}^*(s_1)\} - (E_{z2\,\text{image}} + E_{z3\,\text{image}})\,R_{\text{v}}(\theta_1), \quad |n^2| \approx 1 \tag{9.3.74}$$

$$H_{\phi\,\text{pseudo-surface}} = -H_{\phi 1\text{image}}[R_{\text{v}}(\theta_1)](j\pi s_1)\exp[j(\pi/2)s_1^2]\mathcal{F}^*(s_1) - (H_{\phi 1\,\text{image}} + \text{H}_{\phi 2\,\text{image}}), \quad |n^2| \approx 1 \tag{9.3.75}$$

$$E_{\rho\,\text{pseudo-surface}} = E_{\rho 1\,\text{image}}[R_{\text{v}}(\theta_1)][1 + R_{\text{v}}(\theta_1)]^{-1} \times \{1 + [R_{\text{v}}(\theta_1)](j\pi s_1)\exp[j(\pi/2)s_1^2]\mathcal{F}^*(s_1)\} - (E_{\rho 1\,\text{image}} + E_{\rho 2\,\text{image}} + E_{\rho 3\,\text{image}}), \quad |n^2| \approx 1 \tag{9.3.76}$$

$$E_{z\,\text{pseudo-surface}} = -E_{z1\,\text{image}}[R_{\text{v}}(\theta_1)]\{(j\pi s_1)\exp[j(\pi/2)s_1^2]\mathcal{F}^*(s_1)\} - (E_{z1\,\text{image}} + E_{z2\,\text{image}} + E_{z3\,\text{image}}), \quad |n^2| \approx 1 \tag{9.3.77}$$

where

$$s_1 = (1/2)(n^{-1} - 1)(k_0 r_1/\pi)^{1/2}$$

$\mathcal{F}^*(s_1)$ = complimentary conjugate Fresnel integral = $F^*(\infty) - F^*(s_1) = \int_{s_1}^{\infty} \exp[-j(\pi/2)s^2]\text{d}s$

$F^*(\infty) = \int_0^\infty \exp[-j(\pi/2)s^2]\mathrm{d}s \qquad [= (1-j)/2,\ s \text{ real}]$

$F^*(s_1) =$conjugate Fresnel integral$= \int_0^{s_1} \exp[-j(\pi/2)s^2]\mathrm{d}s$

$H_{\phi 1\,\text{image}}$, $H_{\phi 2\,\text{image}}$, $E_{\rho 1\,\text{image}}$, $E_{\rho 2\,\text{image}}$, $E_{\rho 3\,\text{image}}$, $E_{z1\,\text{image}}$, $E_{z2\,\text{image}}$, $E_{z3\,\text{image}}$ are given by Eqs. (9.3.24)–(9.3.26).

The index of refraction n does not enter Eqs. (9.3.72)–(9.3.77) directly but only indirectly through the Fresnel reflection coefficient $R_{\text{v}}(\theta_1)$ and s_1.

For $R_{\text{v}}(\theta_1) = 0$ (corresponding to $n = 1$ for earth identical to that of free space), the surface-wave fields vanish but the pseudo-surface wave fields reduce to the negative of the image field defined for that for an earth of infinite conductivity. Surface-wave fields, as defined herein, have the attractive feature that they vanish for earth of either infinite conductivity or free space, unlike pseudo-surface-wave fields that vanish only for earth of infinite conductivity. Space-wave fields (as defined herein) have the attractive feature that they reduce in the absence of earth to the free-space fields, unlike pseudo-space-wave fields that always include the image field defined for an earth of infinite conductivity even though the earth is of finite conductivity.

For $s_1 \gg 1$ (corresponding to $(k_0 r_1)^{1/2} \gg 1$), $\mathcal{F}^*(s_1)$ is similar to Eq. (9.3.47) but with argument s_1 instead of s_0. Accordingly,

$$\begin{aligned}\mathcal{F}^*(s_1) =& (j\pi s_1)^{-1}\exp[-j(\pi/2)s_1^2]\{1 - [(1\cdot 3)(\pi s_1^2)^{-2}] \\ &+ [(1\cdot 3\cdot 5\cdot 7)(\pi s_1)^{-4}] - \cdots\} + (\pi s_1)^{-1}(\pi s_1)^{-1}\exp[-j(\pi/2)s_1^2] \\ &\times \{[1 - [(1\cdot 3\cdot 5)(\pi s_1^2)^{-2}] + \cdots\}, \quad s_1 \gg 1\end{aligned} \tag{9.3.78}$$

Substituting Eq. (9.3.78) into Eqs. (9.3.75)–(9.3.77),

$$\begin{aligned}H_{\phi\,\text{surface}} \approx& - H_{\phi 1\,\text{image}} R_{\text{v}}(\theta_1)[\{[(1\cdot 3)(\pi s_1^2)^{-2}] - [(1\cdot 3\cdot 5\cdot 7)(\pi s_1^2)^{-4}] + \cdots\} \\ &- j(\pi s_1^2)^{-1}\{[1 - [(1\cdot 3\cdot 5)(\pi s_1^2)^{-2}] + \cdots\}] - H_{\phi 2\,\text{image}} R_{\text{v}}(\theta_1); \\ & s_1 \gg 1, \quad |n^2| \approx 1\end{aligned} \tag{9.3.79}$$

$$\begin{aligned}E_{\rho\,\text{surface}} \approx& - E_{\rho 1\,\text{image}}[R_{\text{v}}(\theta_1)]^2[1 + R_{\text{v}}(\theta_1)]^{-1}[\{[(1\cdot 3)(\pi s_1^2)^{-2}] \\ &- [(1\cdot 3\cdot 5\cdot 7)(\pi s_1^2)^{-4}] + \cdots\} - j(\pi s_1^2)^{-1}\{[1 - [(1\cdot 3\cdot 5)(\pi s_1^2)^{-2}] \\ &+ \cdots\}] - (E_{\rho 2\,\text{image}} + E_{\rho 3\,\text{image}}) R_{\text{v}}(\theta_1); \quad s_1 \gg 1, \quad |n^2| \approx 1\end{aligned} \tag{9.3.80}$$

$$E_{z\,\text{surface}} \approx -E_{z1\,\text{image}} R_{\text{v}}(\theta_1)[\{[(1\cdot 3)(\pi s_1^2)^{-2}] - [(1\cdot 3\cdot 5\cdot 7)(\pi s_1^2)^{-4}] + \cdots\}$$
$$- j(\pi s_1^2)^{-1}\{[1 - [(1\cdot 3\cdot 5)(\pi s_1^2)^{-2}] + \cdots\}] \tag{9.3.81}$$
$$- (E_{z2\,\text{image}} + E_{z3\,\text{image}}) R_{\text{v}}(\theta_1); \quad s_1 \gg 1, \quad |n^2| \approx 1$$

In the far-field ($k_0 r_1 \gg 1$), the amplitudes of the surface-wave fields decrease with increasing distance approximately as $(k_0 r_1)^{-2}$ since the product of $H_{\phi 1\,\text{image}}$, $E_{\rho 1\,\text{image}}$, or $E_{z1\,\text{image}}$ with $-j(\pi s_1^2)^{-1}$ is proportional to $(k_0 r_1)^{-2}$ and also because $\text{H}_{\phi 2\,\text{image}}$, $E_{\rho 2\,\text{image}}$, $E_{z2\,\text{image}}$ are proportional to $(k_0 r_1)^{-2}$.

For $s_1 \ll 1$ (corresponding to $(k_0 r_1)^{1/2} \ll 1$), the series expansion of $\mathcal{F}^*(s_1)$ is given by Eq. (9.3.51) but with argument s_1. Substituting Eq. (9.3.51) into Eqs. (9.3.72)–(9.3.74),

$$H_{\phi\,\text{surface}} \approx -H_{\phi 1\,\text{image}} R_{\text{v}}(\theta_1)[1 - (j\pi s_1)\exp(j\pi s_1^2/2)\,\text{F}^*(\infty)]$$
$$- H_{\phi 2\,\text{image}} R_{\text{v}}(\theta_1); \quad s_1 \ll 1, \quad |n^2| \approx 1 \tag{9.3.82}$$

$$E_{\rho\,\text{surface}} \approx -E_{\rho 1\,\text{image}}[R_{\text{v}}(\theta_1)]^2[1 + R_{\text{v}}(\theta_1)]^{-1}$$
$$\times \{1 - (j\pi s_1)\exp(j\pi s_1^2/2)\,\text{F}^*(\infty)\} \tag{9.3.83}$$
$$- (E_{\rho 2\,\text{image}} + E_{\rho 3\,\text{image}}) R_{\text{v}}(\theta_1); \quad s_1 \ll 1, \quad |n^2| \approx 1$$

$$E_{z\,\text{surface}} \approx -E_{z1\,\text{image}} R_{\text{v}}(\theta_1)\{1 - (j\pi s_1)\exp(j\pi s_1^2/2)\,\text{F}^*(\infty)\}$$
$$- (E_{z2\,\text{image}} + E_{z3\,\text{image}}) R_{\text{v}}(\theta_1); \quad s_1 \ll 1, \quad |n^2| \approx 1 \tag{9.3.84}$$

For $z_0 = 0$ (the dipole is in the air medium but on the earth's surface), the field point $P(r_1, \theta_1, \phi)$ of Fig. 79 reduces to the field point $P(r, \theta, \phi)$ of Fig. 73 in Sec. 9.2.1. The fields are given by Eqs. (9.3.18)–(9.3.33) and Eqs. (9.3.72)–(9.3.84) where $z_{\text{d}}, r_1, \theta_1$ reduce to those given by Eqs. (9.3.55a)–(9.3.55c).

For $z_0 = 0$ and $z = 0$ (both the dipole and the field point are on the earth's surface), the field point $P(r_1, \theta_1, \phi)$ of Fig. 79 reduces to the field point $P(\rho, \pi/2, \phi)$ of Fig. 73 in Sec. 9.2.1. The fields are given by Eqs. (9.3.18)–(9.3.33) and Eqs. (9.3.93)–(9.3.99) where $z_{\text{d}}, r_1, \theta_1$ reduce to those given by Eqs. (9.3.56a)–(9.3.56c).

Substituting Eqs. (9.3.72)–(9.3.75) into Eq. (9.3.57), the wave tilt β is given by

$$\beta = (2n)^{-1}(1 - n^{-2})^{1/2}, \quad |n^2| \approx 1 \tag{9.3.85}$$

The wave tilt β given by Eq. (9.3.85) is one-half that for the case $|n^2| \gg 1$

[cf. Eq. (9.3.58)]. It would be of interest to compare Eq. (9.3.85) with experimental data or with numerical results obtained by numerical integration of the Sommerfeld integral but such data is presently unavailable for $|n^2| \approx 1$.

Eqs. (9.3.72)–(9.3.74) may be written as

$$H_{\phi\,\text{surface}} = -R_{\text{v}}(\theta_1)[H_{\phi 1\,\text{image}}\mathcal{A}(s_1) + H_{\phi 2\,\text{image}}], \quad |n^2| \approx 1 \tag{9.3.86}$$

$$\begin{aligned} E_{\rho\,\text{surface}} = &- E_{\rho 1\,\text{image}}[R_{\text{v}}(\theta_1)]^2[1 + R_{\text{v}}(\theta_1)]^{-1}\mathcal{A}(s_1) \\ &- (E_{\rho 2\,\text{image}} + E_{\rho 3\,\text{image}})R_{\text{v}}(\theta_1), \quad |n^2| \approx 1 \end{aligned} \tag{9.3.87}$$

$$\begin{aligned} E_{z\,\text{surface}} = &-R_{\text{v}}(\theta_1)[E_{z1\,\text{surface}}\mathcal{A}(s_1) + (E_{z2\,\text{image}} \\ &+ E_{z3\,\text{image}})], \quad |n^2| \approx 1 \end{aligned} \tag{9.3.88}$$

where

$$\begin{aligned} \mathcal{A}(s_1) &= \text{amplitude attenuation function} \\ &= 1 - (j\pi s_1^2)\exp[\text{j}(\pi/2)s_1]\mathcal{F}^*(s_1) \end{aligned} \tag{9.3.89}$$

The function $\mathcal{A}(s_1)$ is equal to Sommerfeld's attenuation function $A_{\text{sommerfeld}}(w_1)$ and is defined by Eq. (9.3.62) as

$$\mathcal{A}(s_1) = A_{\text{sommerfeld}}(w_1) = 1 - j(\pi w_1)^{1/2}\exp(-w_1)\text{erfc}(jw_1^{1/2}) \tag{9.3.90}$$

where from comparison with Eq. (9.3.69)

$$w_1 = -(j\pi/2)s_1^2 = -j(k_0 r_1/8)(n^{-1} - 1)^2, \quad |n^2| \approx 1 \tag{9.3.91}$$

Previous results by other investigators (see review by Wait [129]) have been restricted to the case $|n^2| \gg 1$.

For $z = z_0 = 0$ (corresponding to $\theta_1 = \pi/2$ rad), the total electric field $\mathbf{E} = u_z E_z$ where E_z is given by Eqs. (9.2.37), (9.3.26), (9.3.88)–(9.3.91) as

$$\begin{aligned} E_z =& E_{z\,\text{space}} + E_{z\,\text{surface}} = [E_{z\,\text{direct}} + R_{\text{v}}(\pi/2)E_{z\,\text{image}}] \\ &- E_{z1\,\text{image}}A_{\text{sommerfeld}}(w_1) + (E_{z2\,\text{image}} + E_{z3\,\text{image}}) \\ =& -A_0[A_{\text{sommerfeld}}(w_1) + (jk_0\rho)^{-1} + (jk_0\rho)^{-2}], \quad |n^2| \approx 1 \end{aligned} \tag{9.3.92}$$

where

$$E_{z\,\text{direct}} = -A_0[1 + (jk_0\rho)^{-1} + (jk_0\rho)^{-2}], \quad z = z_0 = 0$$

$$E_{z\,\text{image}} = -A_1[1 + (jk_0\rho)^{-1} + (jk_0\rho)^{-2}], \quad z = z_0 = 0$$

$$A_0 = A_1 = j(\omega\mu_0 \text{p}/4\pi\rho)\exp(-jk_0\rho), \quad z = z_0 = 0$$

$$R_{\text{v}}(\pi/2) = 0, \quad |n^2| = 1$$

$$R_{\text{v}}(\pi/2) = -1, \quad |n^2| \neq 1, \ \infty$$

$$w_1 = -j(k_0\rho/8)(1 - n^{-1})^2, \quad z = z_0 = 0$$

If $|n^2| = 1$, then the total field given by Eq. (9.3.92) reduces to the free-space field equal to the direct field. If $|n^2| \neq 1$ or ∞, then the space-wave field is zero on the earth's surface and the total field consists solely of a surface-wave field. Equation (9.3.92) is new to the literature because previous results have been restricted to the case $|n^2| \gg 1$.

Equation (9.3.92) for the case $|n^2| \approx 1$ is of similar functional form as Eq. (9.3.71) for the case $|n^2| \gg 1$ but has an initial amplitude, one-half that of Eq. (9.3.71) and decays with increasing ρ, much slower than that of Eq. (9.3.71).

9.3.3.3 Accuracy

Except for the treatment of the variational method, the same methodology is utilized in App. C to obtain the surface-wave fields for $|n^2| \gg 1$ (Case I) as for $|n^2| \approx 1$ (Case II). Three approximations are made in both Cases I and II. The first approximation is a *variational* method [see Eq. (C-42) in Case I and Eqs. (C-137a)–(C-137b) in Case II]. The second approximation is the method of *stationary phase*(see Eqs. (C-75) and (C-76) in Case I and Eqs. (C-143)–(C-145) in Case II). The third approximation neglects higher-order $(jk_0\rho)^{-2}$ and $(jk_0\rho)^{-3}$ amplitude terms [see Eqs. (C-62c) and (C-62d)]. The only difference in methodology is that Eqs. (C-42) and (C-137a) utilize a modified variational method whereas Eq. (C-137b) utilizes a *conventional* variational method.

The variational method reduces exact integral equations to more-readily-solvable approximate integral equations for small variations about known exact solutions. In the present instance, exact solutions are known for two values of the parameter n, namely, $|n^2| = \infty$ and $n = 1$. As a consequence of the variational method, approximate solutions are obtained for only a restricted range of values of n, namely $|n^2| \gg 1$ and $|n^2| \approx 1$. A second consequence, suggested by Burke [127], is that the approximate solutions for Cases I and II fail to produce undulating interference patterns caused by the proximity of two saddle points,

when the dipole source and the field point are both near the interface of low-loss earth (see Figs. 82 and 83). These effects have been predicted for a horizontal dipole in earth near the earth's surface [128] and are not to be confused with mistaken interference effects associated with the Zenneck surface wave controversy and an incorrect sign associated with Sommerfeld's 1909 paper [129]. Whereas the exact integrals of Eqs. (C-25), (C-28), and (C-31) contain a pole and *two* saddle points, the approximate integrals of Eqs. (C-43)–(C-45) in Case I and Eqs. (C-138)–(C-140) in Case II contain a pole and only a *single* saddle point.

The conventional variational method of Storer [119] integrates by parts an exact integral and then discards the integral containing the derivative of one of the parts (see the discussion following Eq. (18) in [119]). The *modified* variational method of App. C is similar to that of Storer but utilizes a far-field constraint to approximate the part of integration that was previously neglected. Consequently, the modified variational method (when applicable) gives more accurate results over a wider range of index of refraction n than the conventional variational method.

In Fig. 79, the surface-wave rays are depicted as emanating from an image line-source, beginning at the dipole image at $z_3 = z_d$ and continuing along the z_3 axis to $z_3 = \infty$. Such a depiction is a consequence of the approximate image theory introduced by the variational method and the resulting dummy variable of integration z_3 in App. C. For earth of complex permittivity, the dummy variable z_3 is a complex quantity and therefore the z_3 axis in Fig. 79 actually corresponds to a curved line in complex space. For nonconducting earth, the dummy variable z_3 is a real quantity and the z_3 axis lies along the z axis in real space. By replacing the image line source in real space by a line source in *complex* space, Lindell and Alanen [123] obtained a Hertz potential in the form of an exact integral that appears simpler to evaluate than the Sommerfeld integral but still requires numerical methods of evaluation.

The second approximation made in App. C is the method of *stationary phase (uniform phase)*, designated as such because integration in the complex plane is along a path of constant phase. Consider an exact integral, whose integrand is the product of an amplitude function $A(\omega)$ and a phase function $\exp[i\phi(\omega)]$. The method of stationary phase reduces the exact integral to an approximate integral equal to the product of the amplitude function $A(\omega_s)$ and an integrand containing only a modified phase function $\exp[i\varphi(\omega\text{-}\omega_s)^2]$ where ω_s is an extremum of the exact integrand, as discussed in App. C. The method of stationary phase is more intuitive but less rigorous than the method of *steepest descent* [121]. Nevertheless, the method of stationary phase employed in App. C provides quantitative results for Case 1 as good as any results previously obtained using the method of steepest descent.

The third approximation, of neglecting higher order $(jk_0\rho)^{-2}$ and $(jk_0\rho)^{-3}$ amplitude terms in the integrands of Eqs. (C-52)–(C-54), improves the accuracy of the method of stationary phase by reducing the variation in $A(\omega)$ *at small values* $k_0\rho$.

Some milestones, in improving the accuracy of closed-form expressions for the total field of a vertically polarized Hertzian dipole source above a half-space of complex relative permittivity n^2, are summarized in Table 22. Exact expressions of the space-wave fields are given by Fresnel (1832) for a plane-wave source and by Hertz (1888) for an infinitesimal dipole source. Until recently, approximate expressions for the pseudo surface-wave fields have been limited to the case $|n^2| \gg 1$, progressing from those of Sommerfeld (1909, 1926, 1935) at restricted field points, Norton (1936–1941), Wait (1953, 1963), Banos (1966) at less-restricted field points; and King (1982, 1990) at unrestricted field points (except very close to the dipole source). Approximate closed-form expressions for the surface-wave fields and pseudo surface-wave fields are given by Weiner (2003) at unrestricted field points for the cases $|n^2| \gg 1$ and $|n^2| \approx 1$. Exact closed-form expressions for the surface-wave fields and pseudo surface-wave fields have yet to be achieved.

Equations (9.3.34)–(9.3.36) and (9.3.72)–(9.3.74) for the surface-wave fields have assumed a plane earth. In actuality, the earth is not planar but is spherical with a nominal radius $a = 6378$ km. The planar-earth approximation is applicable for field-points at radial distances ρ less than approximately ρ_c where [133]

$$\rho_c = a(k_0 a/2)^{-1/3} \tag{9.3.93}$$

For example, at frequencies $f = 10^4$ Hz and 3×10^7 Hz, $\rho_c = 729$ and 50 km, respectively. Approximate formulae for the fields above a spherical earth, at radial distances $\rho > \rho_c$, are given by King and Harrison [134] after Houdzoumis [133].

In assessing the accuracy of the surface-wave fields given by Eqs. (9.3.59)–(9.3.61) for $|n^2| \gg 1$ and Eqs. (9.3.72)–(9.3.74) for $|n^2| \approx 1$, consider the total electric field component E_z for the case $z = z_0 = 0$. For this case, $E_z(\rho,\pi/2)$ is given by Eq. (9.3.71) for $|n^2| \gg 1$ and by Eq. (9.3.92) for $|n^2| \gg 1$.

The approximate closed-form expressions of Eqs. (9.3.71) and (9.3.92), designated *Weiner* ($|n^2| \gg 1$) and *Weiner* ($|n^2| \approx 1$), respectively, are compared in Table 23 with those of *Collin*, *Wait1*, *Wait2*, *Wait3*, and with exact expressions for the limiting cases of perfectly conducting earth and free space. *Wait1*, *Wait2*, and *Wait3* from a 1998 review paper on ground-wave propagation by Wait [129], are of successively increasing accuracy with *Wait3* being the most accurate.

Weiner ($|n^2| \gg 1$) is identical to that of *Wait3* derived using a different methodology. K. A. Norton implied an identical result in a classified 1942 report

TABLE 22 Some Milestones in Closed-Form Expressions for the Total Field of a Vertically Polarized Hertzian Dipole Above a Half-Space of Complex Relative Permittivity n^2

Date	Investigator	Expression	Characteristics	Ref.
1832	A. Fresnel	Space-wave fields from a plane-wave source	Exact reflection and transmission coefficients	[130]
1888	H. Hertz	Space-wave fields from infinitesimal dipole source	Exact closed-form	[131]
1909, 1926, 1935	A. Sommerfeld	Pseudo surface-wave Hertz potential	Exact integral; approximate attenuation function, $\|n^2\| \gg 1$, restricted field points	[77,77,78]
1936, 1937, 1953, 1963, 1966	K. A. Norton, J. R. Wait, A. Banos	Pseudo surface-wave fields	Approximate closed-form, $\|n^2\| \gg 1$, less-restricted field points	[79,82,94,81]
1982, 1990	R. W. P. King	Pseudo surface-wave fields	Exact integrals; approximate closed-form $\|n^2\| \gg 1$, almost all field points	[84,85]
2003	M. M. Weiner	Pseudo surface-wave fields, surface-wave fields	Approximate closed-form, $\|n^2\| \gg 1$, or $\|n^2\| \approx 1$, unrestricted field points	[132]
[a]	[a]	Surface-wave fields	Exact closed-form	[a]

[a] Not yet achieved.

[135] that gave corrections to his 1937 paper [37] but, upon recapitulation of the corrected result, neglected the $(jk_0\rho)^{-2}$ and $(jk_0\rho)^{-3}$ higher-order terms. After declassification of the report, Norton never published the results but referenced the report in the open literature [162]. In 1969, Ray J. King [137] published Norton's recapitulated result.

TABLE 23 Comparison of Closed-Form Expressions for the Total Electric Field $E_z(\rho, (\pi/2)$ at Height $z = 0$ and Excited by a Vertically Polarized Hertzian Dipole at Height $z_0 = 0$

1	Weiner[a] ($\lvert n^2\rvert \gg 1$); *Wait3*[b]	$E_z(\rho, \pi/2) = -jpZ_0k_0(2\pi\rho)^{-1}\exp(-jk_0\rho)[A_{\text{sommerfeld}}(w_0) + (jk_0\rho)^{-1} + (jk_0\rho)^{-2}]$
2	Weiner[c] ($\lvert n_2\rvert \approx 1$)	$E_z(\rho, \pi/2) = -jpZ_0k_0(4\pi\rho)^{-1}\exp(-jk_0\rho)[A_{\text{sommerfeld}}(w_1) + (jk_0\rho)^{-1} + (jk_0\rho)^{-2}]$
3	*Wait2*[d]	$E_z(\rho, \pi/2) = -jpZ_0k_0(2\pi\rho)^{-1}\exp(-jk_0\rho)A_{\text{sommerfeld}}(w_0)$
4	*Wait1*[e]	$E_z(\rho, \pi/2) = -jpZ_0k_0(2\pi\rho)^{-1}\exp(-jk_0\rho)A_{\text{sommerfeld}}(w_3)$
5	Collin[f]	$E_z(\rho, \pi/2) = -jpZ_0k_0(2\pi\rho)^{-1}\exp(-jk_0\rho)n^{-2}(1 - n^2)A_{\text{sommerfeld}}(w_0)$
6	Free-space ($\lvert n^2\rvert = 1$)	$E_z(\rho, \pi/2) = -jpZ_0k_0(4\pi\rho)^{-1}\exp(-jk_0\rho)[1 + (jk_0\rho)^{-1} + (jk_0\rho)^{-2}]$
7	Perfectly conducting earth ($\lvert n^2\rvert = \infty$)	$E_z(\rho, \pi/2) = -jpZ_0k_0(2\pi\rho)^{-1}\exp(-jk_0\rho)[1 + (jk_0\rho)^{-1} + (jk_0\rho)^{-2}]$

p = Dipole moment (amp-m), $\exp(j\omega(t)$ =time dependence, Z_0 = free-space impedance (ohms), n^2 = earth relative permittivity, $w_0 = -j(k_0\rho/2)n^{-2}(1 - n^{-2})$, $w_1 = -j(k_0\rho/8)n^{-2}(1 - n^{-1})^2$, $w_3 = w_0/(1 - n^{-2}) = -j(k_0\rho/2)n^{-2}$, k_0 = free-space wave number (m^{-1}), $A_{\text{sommerfeld}}(z) = 1 - j(\pi z)^{1/2}\exp(-z)\,\text{erfc}(jz^{1/2})$.

[a] Equation (9.3.71).

[b] Wait [129], Eq. (36).

[c] Equation (9.3.111).

[d] Wait [129], Eq. (32).

[e] Wait [129], Eq. (24).

[f] Collin [138].

Collin (Table 23, no. 5) is the least accurate of the various expressions because of his inclusion in [138] of an additional factor $n^{-2}(1 - n^2)$ which also gives the wrong sign. Collin's inclusion of the factor $n^{-2}(1 - n^2)$ does not agree with Chapter 23, Eq. 23.33 of his earlier book [117], as editor with Zucker, that contains the *Wait 2* equation (Table 23, no. 3) after Wait [139].

Wait1 [Table 23, no. 4] after Sommerfeld [77], [78] and Norton [79] *Wait1*, *Wait2*, and *Wait3* denote, in sequential order and increasing accuracy three expressions from a 1998 paper in ground-wave propagation by Wait [15] who reviews the various methodologies but does not give numerical results. Norton [79] is identical to that obtained by R. W. P. King [85].

Weiner ($|n^2| \gg 1$); *Wait3* [Table 23, no. 1] correctly reduces to *Perfectly Conducting earth* (Table 23, no. 7) when $|n^2| = \infty$, unlike *Wait2*, *Wait1*, and *Collin* who neglect the higher-order image terms.

Weiner ($|n^2| \approx 1$); (Table 23, no. 2) is the only entry in Table 23 that correctly reduces to *Free Space* (Table 23, no. 6) when $|n^2| = 1$.

Numerical results for the various closed-form expressions of Table 23 are compared in Figs. 80–85 where each figure is for a different value of relative permittivity n^2. These results were obtained by Burke [140] using Mathematica software. Also shown in Figs. 80–85 are results labeled *Sommerfeld*. Burke obtained the *Sommerfeld* results by numerically integrating the Sommerfeld integral for the surface wave Hertz potential given by Eq. (9.3.11), after first symbolically differentiating the integral to obtain the surface-wave field [see Eq. (9.3.1)]. The ordinate in all the graphs is $(\rho/\lambda)(\lambda^2/p)|E_z(\rho, \pi/2)|$. The ordinate contains the factor (ρ/λ) so that graphs of the space-wave fields *Free-Space* and *Perfect Conductor* are horizontal lines for $(\rho/\lambda) \gg 1$. The ordinate contains the factor (λ^2/p) so that the results are independent of the wavelength λ and dipole moment p.

In Figs. 80–82, results are shown for $n^2 = 10 - j100$, $n^2 = 2 - j2$, and $n^2 = 2 - j0$, respectively, corresponding to the case $|n^2| \gg 1$. *Collin* and *Wait1* are in the poorest agreement with *Sommerfeld*. *Wait2* and *Weiner* ($|n^2| \gg 1$) are in the best agreement with *Sommerfeld* and asymptotically approach *Sommerfeld*. Please note the undulating behavior of *Sommerfeld* for $n^2 = 2 - j0$ in Fig. 82.

In Fig. 83, results are shown for $n^2 = 1.2 - j0.012$. *Collin*, *Wait1*, and *Wait2* are in poor agreement with *Sommerfeld*. For $\rho/\lambda < 6$, *Weiner* ($|n^2| \approx 1$) gives the best agreement with *Sommerfeld*. For $\rho/\lambda \geq 6$, *Weiner* ($|n^2| \gg 1$) gives the best agreement with *Sommerfeld* and asymptotically approaches *Sommerfeld*. Please not the undulating behavior of *Sommerfeld*.

In Figs. 84 and 85, results are shown for $n^2 = 1.05 - j0$ and $n^2 = 1.01 - j0$, respectively, corresponding to the case $|n^2| \approx 1$). *Collin*, *Wait1* *Wait2*, and *Weiner* ($|n^2| \gg 1$) are in poor agreement with *Sommerfeld*. *Weiner* ($|n^2| \approx 1$) is in reasonably good agreement with *Sommerfeld* over a depicted range of ρ/λ that is not sufficiently large to determine whether or not there is

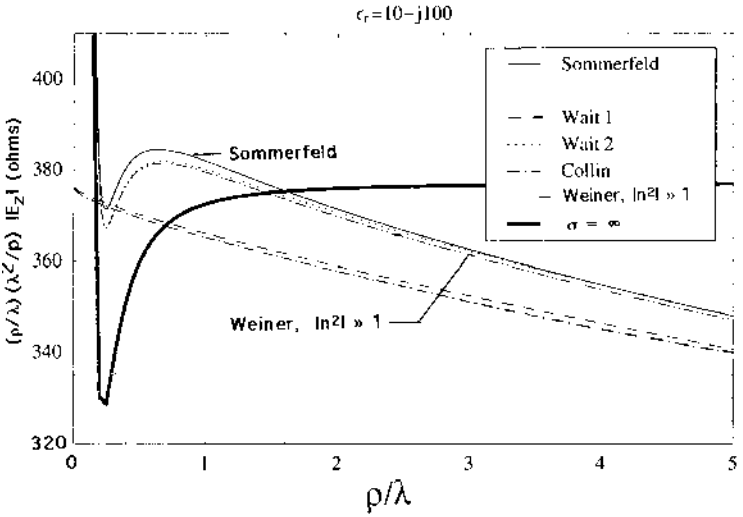

FIGURE 80 Total electric field $E_z(\rho, \pi/2)$ at height $z = 0$ above earth of relative permittivity $n^2 = 10 - j100$ excited by a vertically polarized Hertzian dipole of moment p and wavelength λ at height $z_0 = 0$.

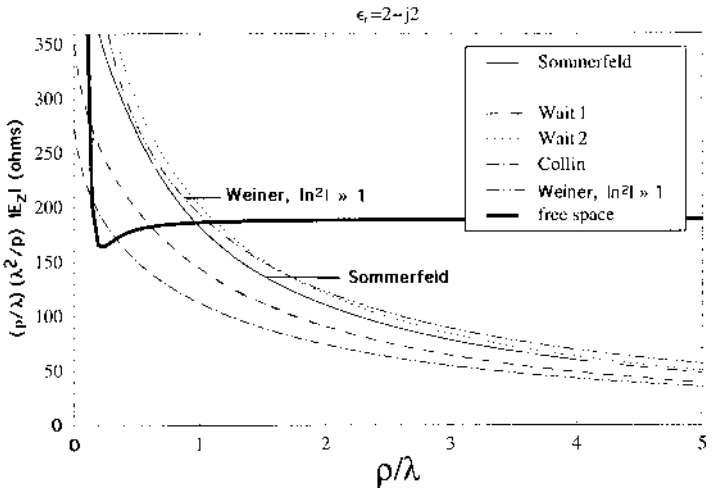

FIGURE 81 Total electric field $E_z(\rho, \pi/2)$ at height $z = 0$ above earth of relative permittivity $n^2 = 2 - j2$ excited by a vertically polarized Hertzian dipole of moment p and wavelength λ at height $z_0 = 0$.

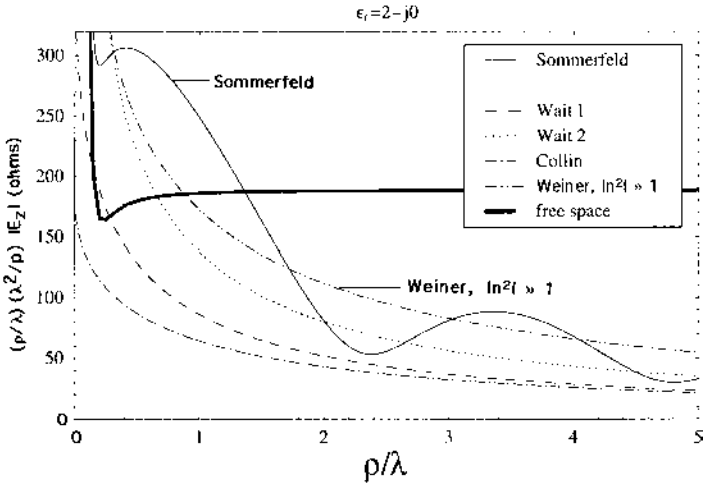

FIGURE 82 Total electric field $E_z(\rho, \pi/2)$ at height $z = 0$ above earth of relative permittivity $n^2 = 2 - j0$ excited by a vertically polarized Hertzian dipole of moment p and wavelength λ at height $z_0 = 0$.

asymptotic agreement. For $\rho/\lambda = 17.5$ and $n^2 = 1.01$ in Fig. 85, Free-Space has attained its asymptotic value whereas *Weiner* ($|n^2| \approx 1$) and *Sommerfeld* have not yet begun to attenuate appreciably.

On the basis of Figs. 80–85 and the closed-form expressions of Table 23, the best agreement with *Sommerfeld* is obtained by *Weiner* ($|n^2| \gg 1$) for $1.2 \leq |n^2| \leq \infty$ and *Weiner* ($|n^2| \approx 1$) for $0.95 \leq |n^2| \leq 1.05$.

9.3.3.4 Numerical Distance and Proximity Region

The surface-wave fields, given by Eqs. (9.3.59)–(9.3.61) for $|n^2| \gg 1$ and Eqs. (9.3.72)–(9.3.74) for $|n^2| \approx 1$, decrease in magnitude with increasing distance r_1 of the field point from the Hertzian dipole image point and with increasing height z_0 of the dipole source above the air–earth interface. Each of those surface-wave fields is a function of an image field, a Fresnel coefficient function, and an attenuation function. Those surface-wave fields may be expressed symbolically as

$$H_{\phi\,\text{surface}} = f_{\phi}[H_{\phi 1\,\text{image}} A_{\text{sommerfeld}}(w_j) + H_{\phi 2\,\text{image}}] \tag{9.3.94}$$

$$E_{\rho\,\text{surface}} = f_{\rho 1} E_{\rho 1\,\text{image}} A_{\text{sommerfeld}}(w_j) + f_{\rho 2}(E_{\rho 2\,\text{image}} + E_{\rho 3\,\text{image}}) \tag{9.3.95}$$

$$E_{z\,\text{surface}} = f_{z}[E_{z1\,\text{image}} A_{\text{sommerfeld}}(w_j) + (E_{z2\,\text{image}} + E_{z3\,\text{image}})] \tag{9.3.96}$$

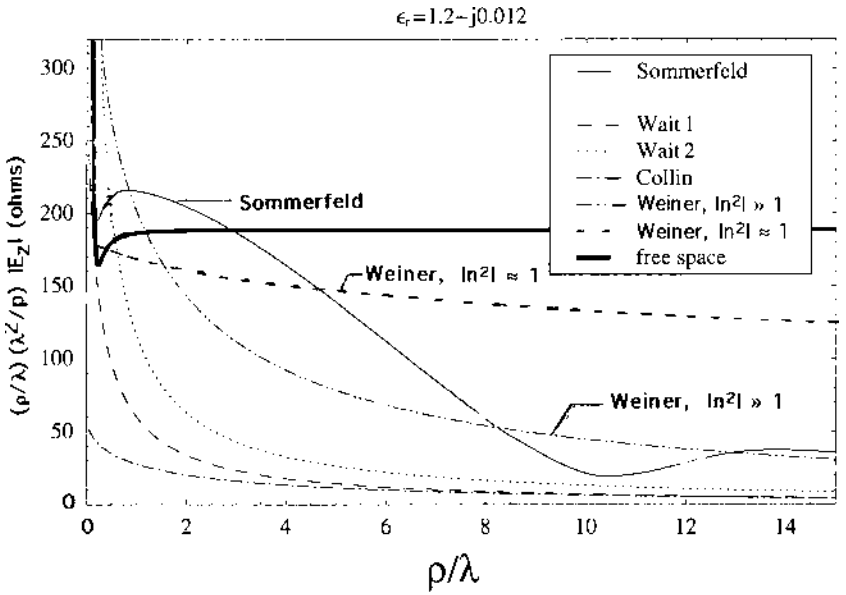

FIGURE 83 Total electric field $E_z(\rho, \pi/2)$ at height $z = 0$ above earth of relative permittivity $n^2 = 1.2 - j0.012$ excited by a vertically polarized Hertzian dipole of moment p and wavelength λ at height $z_0 = 0$.

where $H_{\phi 1\,\text{image}}, H_{\phi 2\,\text{image}}, E_{\rho 1\,\text{image}}, E_{\rho 2\,\text{image}}, E_{\rho 3\,\text{image}}, E_{z1\,\text{image}}, E_{z2\,\text{image}}\ E_{z3\,\text{image}}$, are given by Eqs. (9.3.24)–(9.3.26)

$$f_\phi = f_z = 1 - R_v(\theta_1), \quad |n^2| \gg 1 \tag{9.3.97a}$$

$$= -R_v(\theta_1), \quad |n^2| \approx 1 \tag{9.3.97b}$$

$$f_{\rho 1} = -[1 - R_v(\theta_1)]^2[1 + R_v(\theta_1)]^{-1}, \quad |n^2| \gg 1 \tag{9.3.98a}$$

$$= -[R_v(\theta_1)]^2[1 + R_v(\theta_1)]^{-1}, \quad |n^2| \approx 1 \tag{9.3.98b}$$

$$f_{\rho 2} = 1 - R_v(\theta_1), \quad |n^2| \gg 1 \tag{9.3.99a}$$

$$= -R_v(\theta_1), \quad |n^2| \approx 1 \tag{9.3.99b}$$

$$A_{\text{sommerfeld}}(w_j) = 1 - j(\pi w_j)^{1/2} \exp(-w_j)\,\text{erfc}(jw_j^{1/2}) \tag{9.3.100}$$

$$w_j = w_0 = -j2k_0 r_1[1 + R_v(\theta_1)]^{-2}\cot^2\theta_1, \quad |n^2| \gg 1 \tag{9.3.101a}$$

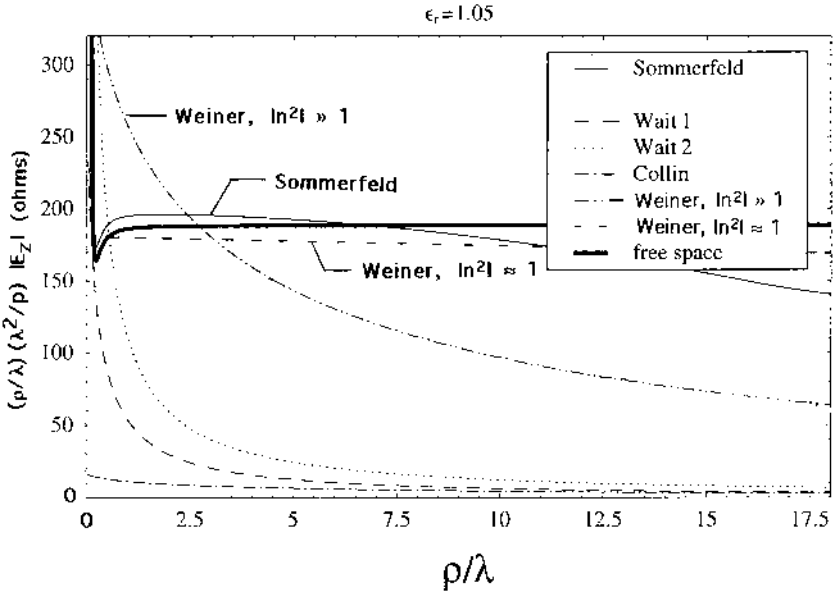

FIGURE 84 Total electric field $E_z(\rho, \pi/2)$ at height $z = 0$ above earth of relative permittivity $n^2 = 1.05 - j0$ excited by a vertically polarized Hertzian dipole of moment p and wavelength λ at height $z_0 = 0$.

$$= w_1 = -j(k_0 r_1/8)(1 - n^{-1})^2, \quad |n^2| \approx 1 \tag{9.3.101b}$$

The subscript $j = 0$ designates the case $|n^2| \gg 1$ whereas the subscript $j = 1$ designates the case $|n^2| \approx 1$.

In Eqs. (9.3.94)–(9.3.96), the Sommerfeld attenuation function $A_{\text{sommerfeld}}(w_j)$ has been substituted for the amplitude attenuation function $\mathcal{A}(s_j)$. Although the two attenuation functions are equal to each other [see Eqs. (9.3.70) and (9.3.90)], $A_{\text{sommerfeld}}(w_j)$ is generally easier to evaluate numerically because the complimentary error function is tabulated for complex arguments whereas the complimentary Fresnel integral is usually not found tabulated for complex arguments [135]. The properties of the Sommerfeld attenuation function $A_{\text{sommerfeld}}(w_j)$ is now discussed, followed by a brief discussion of the amplitude attenuation function $\mathcal{A}(s_j)$.

The complex argument w_j may be written as

$$w_j = |w_j| \angle w_j = |w_j| \exp(j \angle w_j) \tag{9.3.102}$$

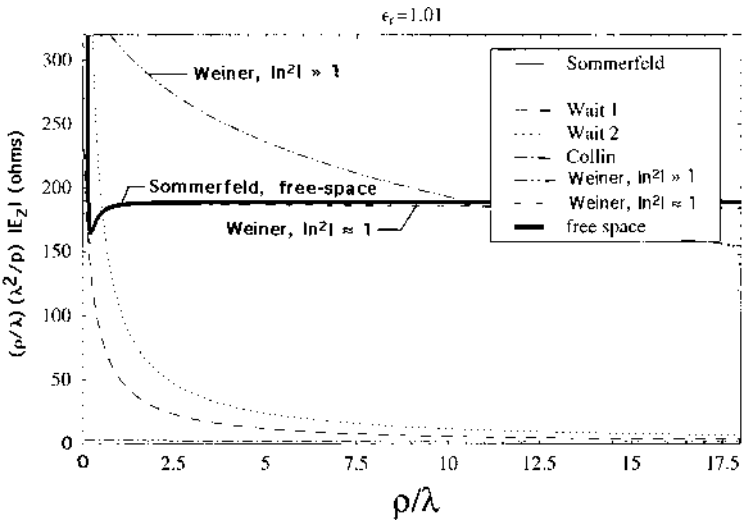

FIGURE 85 Total electric field $E_z(\rho, \pi/2)$ at height $z = 0$ above earth of relative permittivity $n^2 = 1.01 - j0$ excited by a vertically polarized hertzian dipole of moment p and wavelength λ at height $z_0 = 0$.

where

$|w_j|$ = "numerical distance" (dimensionless)

$$= \begin{cases} |w_0| = 2k_0 r_1 \, |1 + R_v(\theta_1)|^{-2} \cot^2 \theta_1, & |n^2| \gg 1 \\ |w_1| = (k_0 r_1/8) \, |1 - n^{-1}|^2, & |n^2| \approx 1 \end{cases} \tag{9.3.103}$$

$$\angle w_j = \text{phase angle of argument } w_j \text{ (rad or } ^\circ) \tag{9.3.104}$$

The phase angle $\angle w_j$ is restricted to the quadrant $-90^\circ \le \angle w_j \le 0^\circ$ provided $\varepsilon_r \ge 0$ and $\tan\delta = \sigma/\omega\varepsilon_0\varepsilon_r \ge 0$ for earth of relative permittivity $n^2 = \varepsilon_r(1 - j\tan\delta)$. For a lossless dielectric ($\tan\delta = 0$), $\angle w_j = -90^\circ$. For a good conductor ($\tan\delta \gg 1$), $\angle w_j \approx 0^\circ$.

At x-ray and higher frequencies, or at lower frequencies when the wavelength is comparable to the distance between lattice planes (particularly at angles of incidence $\theta_1 \approx \pi/2$ rad), the dielectric constant ε_r can be slightly *less* than unity. The surface-wave fields for such an application are particularly well approximated by Eqs. (9.3.72)–(9.3.74). (For a discussion of the propagation of the *space* wave in semi-unbounded continuous or discrete media at x-ray wavelengths or wavelengths comparable to the distance between lattice planes, see Weiner [136].)

The Sommerfeld attenuation function magnitude $|A_{\text{sommerfeld}}|$ is plotted in Fig. 86 for $|w_j| = 0.01-1000$ and $\angle w_j = 0, -30, -60, -90°$. Although Fig. 86 is for flat earth, the values are accurate for a spherical earth at radial distances $\rho \leq \rho_c$ where ρ_c is given by Eq. (9.3.93). The set of curves in Fig. 86 is similar to curves found in the literature but with different notations for the argument w_j (for example, in Collin [136], $p = |w_j|$ and $b = -\angle w_j$ where $0 \leq b \leq 90°$).

As a numerical example, consider a vertically polarized Hertzian dipole in air at a height $z_0 = 0$ above medium dry ground, a radiation frequency $f = 3\,\text{MHz}$ (wavelength $\lambda = 100\,\text{m}$), and a field point at height $z_0 = 0$ and radial distance ρ. With reference to Table 16 in Sec. 8.2, the relative permittivity $n^2 = 15.0(1 - j0.4)$. Since $z = z_0 = 0$, then $r_1 = \rho$, $\theta_1 = \pi/2$ rad, $R_v(\pi/2) = -1$, and $\cot^2\theta_1[1 + R_v(\pi/2)]^{-2} = (1/4)n^{-2}(1 - n^{-2})$ (see Table 21, entry no. 11, $\theta_1 = \pi/2$ rad, $1 < |n^2| < \infty$). The argument w_0 is given by Eq. (9.3.71) as

$$\begin{aligned} w_0 &= -j(1/2)n^{-2}(1 - n^{-2})k_0\rho \\ &= -j(1/2)[15.0(1 - j\,0.4)]^{-1}\{1 - [15.0(1 - j\,0.4)]^{-1}\}k_0\rho \\ &= (1\angle -90°)(1/2)[0.0619\angle 21.8°][0.942\angle -1.4°]k_0\rho \\ &= (2.92 \times 10^{-2}k_0\rho)\angle -69.6°; \quad \text{medium dry ground, } 3\,\text{Mhz} \end{aligned} \tag{9.3.105}$$

For the conditions of Eq. (9.3.105) and with reference to Eq. (9.3.97a), the surface-wave Fresnel coefficient function $f_z[R_v(\pi/2)] = 1 - R_v(\pi/2) = 2$ and the total electric field $E_z(\rho, \pi/2) = E_{z\,\text{surface}}(\rho, \pi/2) = 2E_{z\,\text{image}}(\rho, \pi/2)$ $A_{\text{sommerfeld}}(w_0)$. For w_0 given by Eq. (9.3.69) and for $k_0\rho > 100$, $A_{\text{sommerfeld}}(w_0)$ is approximately proportional to $(k_0\rho)^{-1}$ (see Fig. 86). For $k_0\rho > 100$, $E_{z\,\text{image}}$ is also approximately proportional to $(k_0\rho)^{-1}$ [see Eq. (9.3.26)]. Consequently, for w_0 given by Eq. (9.3.105), $E_z(\rho, \pi/2)$ is approximately proportional to $(k_0\rho)^{-2}$ for $k_0\rho > 100$.

In the above example, the numerical distance $|w_j|$ determines the relative amplitude of the surface-wave field given specified values of r_1/λ, θ_1, and n^2. Consider now the inverse problem of determining the region of field points enclosed in the air medium by an isometric contour of the numerical distance $|w_j|$ for a specified value of n^2 and $|w_j|$.

Consider the set of numerical distances $|w_j(m)|$ defined by

$$|w_j(m)| = m(\pi/2); \quad m = 1, 2, 3, \ldots, \infty; \quad n^2 = \text{constant} \tag{9.3.106}$$

Each numerical distance $|w_j|$ has associated with it an isometric contour ("isonumeric") that is a polar plot of r_1/λ as a function of θ_1 in the z–ρ plane,

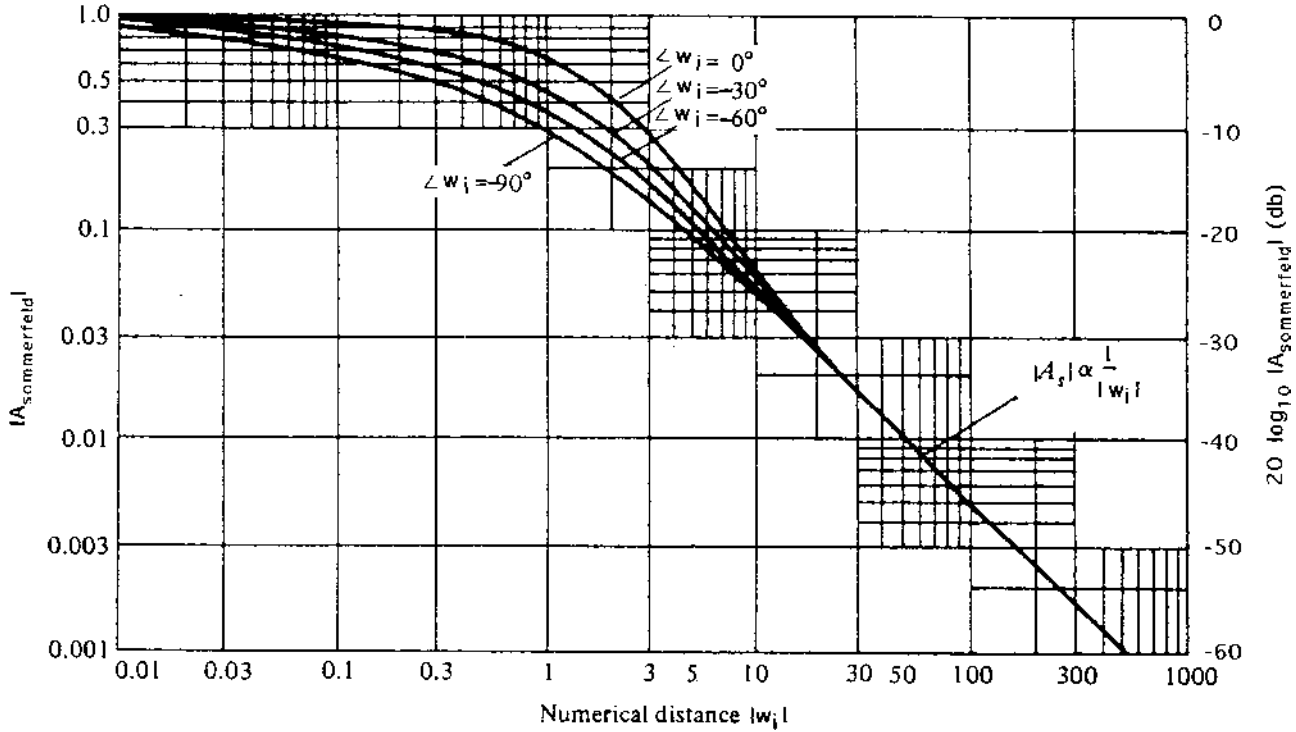

FIGURE 86 Sommerfeld attenuation function $|A_{\text{sommerfeld}}(w_j)|$.

with axes $(z+z_0)/\lambda$ and ρ/λ, and with the origin at the dipole image point $Q(z=z_0,\rho=0)$ where $z, z_0, \rho, r_1, \theta_1$ are defined in Fig. 79. The isonumerics are given by Eqs. (9.3.103) and (9.3.106) as

$$r_1(m)/\lambda = \begin{cases} (m/8)|1+R_v(\theta_1)|^2 \tan^2\theta_1; & m=1,2,3,\ldots,\infty \quad |n^2| \gg 1 \\ 2m|1-n^{-1}|^{-2}; & m=1,2,3,\ldots,\infty \quad |n^2| \approx 1 \end{cases} \tag{9.3.107}$$

In particular, consider the isonumeric $r_1(1)/\lambda$. The numeric distance $|w_j(1)| = \pi/2 = 1.57$. The magnitude $|A_{\text{sommerfeld}}[w_j(1)]| = |A_{\text{sommerfeld}}(1.57)|$ is found from Fig. 86 to be

$$|A_{\text{sommerfeld}}(1.57)| = \begin{cases} 0.50 = -3.0\,\text{dB}, & \angle w_j \approx 0^\circ \\ 0.23 = -12.8\,\text{dB}, & \angle w_j = -90^\circ \end{cases} \tag{9.3.108}$$

The isonumeric $r_1(1)/\lambda$ therefore corresponds to the -3.0-dB and -12.8-dB contours of $|A_{\text{sommerfeld}}|^2$ for a highly conducting earth $(\tan\delta \gg 1)$ and a lossless dielectric earth $(\tan\delta = 0)$, respectively. The region in the air medium, bounded by the isonumeric $r_1(1)/\lambda$ and the air–earth interface, is defined as the *proximity region*. At field points in the air medium but outside the proximity region, the surface wave will have a relative magnitude $|A_{\text{sommerfeld}}(w_j)| < |A_{\text{sommerfeld}}(1.57)|$. If the dipole source is at a height z_0 greater than a critical height h_0 above the interface, then no field points in the air medium will be within the proximity region. If there is at least one field point in the air medium that is within the proximity region (i.e., the numerical region is not a null set), then the dipole is defined to be in proximity to the interface.

The isonumeric $r_1(1)/\lambda$ is pancake-shaped (see Fig. 87) with its projection $\sin\theta_1\, r_1(1)/\lambda$ onto the ρ/λ axis much greater than its projection $\cos\theta_1\, r_1(1)/\lambda$ onto the z/λ axis. At $\theta_1 = 90^\circ$, the isonumeric $r_1(1)/\lambda$ has a maximum value $r_{1o}(1)/\lambda$ found from Eq. (9.3.107) and line 11 of Table 21 to be

$$r_{1o}(1)/\lambda = \begin{cases} (1/8)[1+R_v(\pi/2)]^2 \tan^2(\pi/2) = (1/2)|n^2/(1-n^{-2})|, & |n^2| \gg 1 \\ 2|1-n^{-1}|^{-2}, & |n^2| \approx 1 \end{cases} \tag{9.3.109}$$

The maximum value $r_{1o}(1)$ for $|n^2| \gg 1$ is approximately two orders of magnitude greater than the critical height h_0.

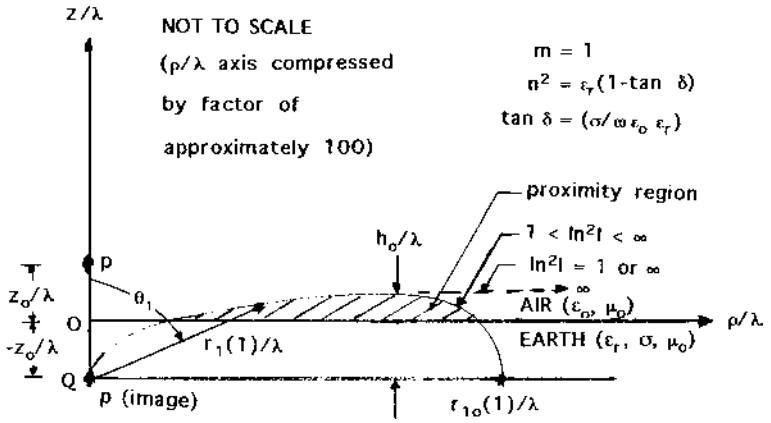

FIGURE 87 Surface-wave isonumeric $r_1(1)/\lambda$ and proximity region for a vertically polarized Hertzian dipole at a height z_0 above earth.

The proximity region is maximized for $z_0 = 0$ and is a null set when $z_0 > h_0$ as is evident from Fig. 87. For the limiting cases $|n^2| = \infty$ (corresponding to $R_v(\theta_1) = +1$ and $|n^2| = 1$ (corresponding to $R_v(\theta_1) = 0$) and for $m = 1$, Eq. (9.3.107) reduces to

$$r_1(1)/\lambda = \begin{cases} (1/2)\tan^2\theta_1, & |n^2| = \infty \\ \infty, & |n^2| = 1 \end{cases} \tag{9.3.110}$$

The isonumeric $r_1(1)/\lambda$, for the limiting cases $|n^2| = 1$ and $|n^2| = \infty$, serves as an envelope for the cases $1 < |n^2| < \infty$ and $0 < |n^2| < 1$.

The isonumeric $r_1(1)/\lambda$, is difficult to draw to scale because of its pancake shape. Numerical values of $r_1(1)/\lambda$ are given in Table 24 for (1) medium dry ground at a frequency $f = 15$ MHz, (2) sea water at a frequency $f = 15$ MHz, and (3) free-space or earth of infinite conductivity. For medium dry ground, $r_{1o}(1)/\lambda = 12.5$ and $h_0/\lambda = 0.471$ ($\theta_1 = 80°$). For sea water, $r_{1o}(1)/\lambda = 2948.8$ and $h_0/\lambda = 11.02$ ($\theta_1 = 89°$). For the limiting cases of free-space or earth of infinite conductivity, $r_{1o}(1)/\lambda = \infty$, $h_0/\lambda = \infty$ ($\theta_1 = 90°$), and $r_{1o}(1)/h_0 \rightarrow \infty$ ($\theta_1 = 90°$).

In Eqs. (9.3.94)–(9.3.96), the amplitude attenuation function $\mathcal{A}(s_j)$ may be substituted for the Sommerfeld attenuation function $A_{\text{sommerfeld}}(w_j)$. For lossless dielectrics, $\mathcal{A}(s_j)$ may be more convenient to tabulate than $A_{\text{sommerfeld}}(w_j)$ because the argument s_j is real whereas the argument w_j is imaginary. The amplitude

TABLE 24 Isonumeric $r_1(1)/\lambda$ for a Vertically Polarized Dipole at a Height z_0 Above Earth of Relative Permittivity n^2

	Case (a)			Case (b)			Case (c)		
θ_1 (°)	$r_1(1)/\lambda$	ρ/λ	$(z+z_0)/\lambda$	$r_1(1)/\lambda$	ρ/λ	$(z+z_0)/\lambda$	$r_1(1)/\lambda$	ρ/λ	$(z+z_0)/\lambda$
0	0	0	0	0	0	0	0	0	0
10	0.010	0.002	0.010	0.015	0.003	0.015	0.016	0.003	0.015
20	0.041	0.014	0.038	0.065	0.022	0.061	0.066	0.023	0.062
30	0.099	0.099	0.086	0.163	0.082	0.163	0.167	0.083	0.144
40	0.199	0.128	0.152	0.344	0.221	0.263	0.352	0.226	0.270
50	0.366	0.280	0.235	0.690	0.529	0.444	0.710	0.544	0.456
60	0.664	0.576	0.332	1.446	1.252	0.723	1.500	1.299	0.750
70	1.260	1.118	0.431	3.58	3.26	1.223	3.77	3.55	1.291
80	2.71	2.67	0.471	14.46	14.25	2.51	16.08	15.84	2.79
85	4.39	4.37	0.382	52.7	52.5	4.59	65.3	65.1	5.69
86	4.89	4.88	0.341	78.8	78.6	5.50	102.2	102.0	7.13
87	5.49	5.48	0.287	129.0	128.8	6.75	182.0	181.8	9.53
88	6.19	6.19	0.216	246.5	246.4	8.60	410.0	409.8	14.30
89	7.05	7.05	0.123	631.3	631.2	11.02	1641	1641	28.6
89.5	7.52	7.52	0.066	1240	1240	10.82	1.6(5)	1.6(5)	286.4
90	12.5	112.5	0	2949	2949	0	∞	∞	∞

Cases (a) and (b): $r_1(1)/\lambda = (1/8)[1 + R_v(\theta_1)]^2 \tan^2\theta_1$.
Case (c): $r_1(1)/\lambda = (1/2)\tan^2\theta_1$.
(a) $n^2 = 15(1 - j\,0.08)$; medium dry ground, $f = 15$ MHz, (b) $n^2 = 70(1 - j\,84.3)$; seawater, $f = 15$ MHz, and (c) $|n^2| = 1$ or ∞; free-space or earth of infinite conductivity.

TABLE 25 Complimentary Conjugate Fresnel Integral $\mathcal{F}^*(s_j)$, s_j Real

	Conjugate Fresnel integral $F^*(s_j)$		Complementary conjugate Fresnel integral $\mathcal{F}^*(s_j)$	
s_j	$\mathrm{Re}\,F^* + j\,\mathrm{Im}\,F^*$	$\lvert F^*\rvert \angle F^*$ rad	$\mathrm{Re}\mathcal{F}^* + j\,\mathrm{Im}\,\mathcal{F}^*$	$\lvert\mathcal{F}^*\rvert\angle\mathcal{F}^*$ rad
0.0	$0.000 - j0.000$	$0.000\angle -0.000$	$0.500 - j0.500$	$0.777\angle -0.785$
0.2	$0.200 - j0.004$	$0.200\angle -0.020$	$0.300 - j0.496$	$0.580\angle -1.027$
0.4	$0.398 - j0.023$	$0.399\angle -0.083$	$0.102 - j0.467$	$0.478\angle -1.356$
0.6	$0.581 - j0.111$	$0.592\angle -0.189$	$-0.081 - j0.389$	$0.397\angle -1.776$
0.8	$0.723 - j0.249$	$0.765\angle -0.332$	$-0.223 - j0.251$	$0.336\angle -2.297$
1.0	$0.780 - j0.438$	$0.895\angle -0.512$	$-0.280 - j0.062$	$0.287\angle -2.924$
1.2	$0.715 - j0.623$	$0.948\angle -0.717$	$-0.215 + j0.123$	$0.248\angle 2.622$
1.4	$0.543 - j0.714$	$0.897\angle -0.921$	$-0.043 + j0.214$	$0.218\angle 1.769$
1.6	$0.366 - j0.638$	$0.736\angle -1.050$	$0.134 + j0.138$	$0.192\angle 0.800$
1.8	$0.334 - j0.451$	$0.561\angle -0.933$	$0.166 - j0.049$	$0.173\angle -0.287$
2.0	$0.488 - j0.343$	$0.596\angle -0.613$	$0.012 - j0.157$	$0.157\angle -1.495$
2.5	$0.457 - j0.619$	$0.769\angle -0.935$	$0.043 + j0.119$	$0.127\angle 1.224$
3.0	$0.606 - j0.496$	$0.783\angle -0.686$	$-0.106 - j0.004$	$0.106\angle -3.104$
3.5	$0.5326 - j0.4152$	$0.6753\angle -0.662$	$-0.033 - j0.085$	$0.0912\angle -1.941$
4.0	$0.4984 - j0.4205$	$0.6521\angle -0.701$	$0.002 - j0.080$	$0.0800\angle -1.546$
∞	$0.500 - j0.500$	$0.707\angle -0.785$	$0.000 + j0.000$	$0.000\angle 0.000$

$F^*(s_j) = \int_0^{s_j} \exp[-j(\pi/2)s^2]\mathrm{d}s$.
$\mathcal{F}^*(s_j) = F^*(\infty) - F^*(s_j) = \int_{s_j}^{\infty} \exp[-j(\pi/2)s^2]\mathrm{d}s$.
In the present application: $s_j = s_0 = 2\cot\theta_1[1 + R_v(\theta_1)]^{-1}(k_0 r_1/\pi)^{1/2}, \quad |n^2| \gg 1; \quad s_j = s_1 = s_0/2 = \cot\theta_1[1 + R_v(\theta_1)]^{-1}(k_0 r_1/\pi)^{1/2}, \quad |n^2| \approx 1.$

attenuation function $\mathcal{A}(s_j)$ is given by Eqs. (9.3.62) and (9.3.89) as

$$\mathcal{A}(s_j) = 1 - (j\pi s_j)\exp[j(\pi/2)s_j^2]\mathcal{F}^*(s_j) \tag{9.3.111}$$

where

$$s_j = \begin{cases} s_0 = 2\cot\theta_1[1 + R_v(\theta_1)]^{-1}(k_0 r_1/\pi)^{1/2}, & |n^2| \gg 1 \\ s_1 = (1/2)(n^{-1} - 1)(k_0 r_1/\pi)^{1/2}, & |n^2| \approx 1 \end{cases} \tag{9.3.112}$$

The complimentary conjugate Fresnel integral $\mathcal{F}^*(s_j)$ and the amplitude attenuation function $\mathcal{A}(s_j)$ are tabulated in Tables 25 and 26, respectively, for s_j real. The argument s_j is related to the argument w_j [see Eqs. (9.3.69) and (9.3.91)] by

$$s_j^2 = j(2/\pi)w_j = |s_j^2|\angle s_j^2 = |s_j^2|\exp(j\angle s_j^2) \tag{9.3.113}$$

TABLE 26 Amplitude Attenuation Function $\mathcal{A}(s_j)$, s_j Real

	$\mathcal{A}(s_j)$		
s_j	$\mathrm{Re}\,\mathcal{A}(s_j) + j\,\mathrm{Im}\,\mathcal{A}(s_j)$	$\lvert\mathcal{A}(s_j)\rvert\angle\mathcal{A}(s_j)$ rad	$20\log\lvert\mathcal{A}(s_j)\rvert$ (dB)
0.0	$1.000 - j0.000$	$1.000\angle -0.000$	-0.00
0.2	$0.701 - j0.208$	$0.731\angle -0.288$	-2.72
0.4	$0.463 - j0.270$	$0.536\angle -0.528$	-5.42
0.6	$0.300 - j0.264$	$0.340\angle -0.722$	-7.97
0.8	$0.189 - j0.232$	$0.299\angle -0.887$	-10.5
1.0	$0.119 - j0.195$	$0.228\angle -1.023$	-12.8
1.2	$0.079 - j0.160$	$0.178\angle -1.112$	-15.0
1.4	$0.050 - j0.130$	$0.139\angle -1.204$	-17.1
1.6	$0.041 - j0.105$	$0.113\angle -1.199$	-19.0
1.8	$0.026 - j0.088$	$0.092\angle -1.284$	-20.7
2.0	$0.017 - j0.075$	$0.077\angle -1.348$	-22.3
2.5	$0.004 - j0.045$	$0.045\angle -1.482$	-26.9
3.0	$0.002 - j0.038$	$0.038\angle -1.518$	-28.4
3.5	$0.0019 - j0.0257$	$0.0259\angle -1.4959$	-31.8
4.0	$0.0011 - j0.0203$	$0.0204\angle -1.5148$	-33.8
∞	$0.000 - j0.0000$	$0.0000\angle -0.0000$	$-\infty$

$\mathcal{A}(s_j) = 1 - (j\pi s_j)\exp[j(\pi/2)s_j^2]\mathcal{F}^*(s_j)$.
$s_j = s_0 = 2\cot\theta_1[1 + R_v(\theta_1)]^{-1}(k_0 r_1/\pi)^{1/2}, \quad |n^2| \gg 1.$
$s_j = s_1 = s_0/2 = \cot\theta_1[1 + R_v(\theta_1)]^{-1}(k_0 r_1/\pi)^{1/2}, \quad |n^2| \approx 1.$

where

$$|s_i^2| = (2/\pi)|w_j| = \text{modified numerical distance} \tag{9.3.114}$$

$$\angle s_j^2 = \angle w_j + (\pi/2) \text{ (rad)} \quad \text{or} \quad \angle w_j + 90 \quad (^\circ) \tag{9.3.115}$$

The set of modified numerical distances defined by

$$|s_j^2| = m; \quad m = 1, 2, 3, \ldots, \infty \tag{9.3.116}$$

has isometric contours identical to the isonumerics $r_1(m)/\lambda$ given by Eq. (9.3.107).

10

Disk Ground Planes

10.1 INTRODUCTION

The modeling of monopole elements with circular ground planes in proximity to earth has been greatly enhanced in recent years by method-of-moments programs developed by Richmond for disk ground planes [98] and by Burke et al. for radial-wire ground planes [99,100,101].

The method-of-moments models have the following advantages over variational models based on the Monteath compensation theorem [90,91,93,143,144] or Sommerfeld's attenuation function [89]:

1. Current on the ground plane is computed rather than approximated by that for a ground plane.
2. Results are valid not only for moderately large ground planes, but also for electrically small ground planes.
3. Ground-plane edge diffraction is determined directly rather than neglected or obtained by perturbation methods.
4. Analytical restrictions on evaluating Sommerfeld's integral [such as requiring that the earth's relative permittivity have a modulus much greater than unity or approximately equal to unity (see Sec. 9.3.3)] are avoided.
5. Directivity and radiation efficiency are determined as separate entities, rather than being lumped together as a product to yield the antenna gain.

Although the Monteath compensation theorem may be conceptually correct, its implementation by analytical methods often involves an approximation such as setting the current or tangential magnetic field on

the ground plane equal to that for a perfect ground plane [145] which reduces the theorem to a variational method.

Nevertheless, models based on Monteath's compensation theorem or Sommerfeld's attenuation function are useful for validating method-of-moments numerical results and for treating large ground planes whose segmentation in method-of-moments models would exceed computer computational capacity and precision. The relative merits of method-of-moments models vs. models based on the Monteath compensation theorem have been discussed by Weiner et al. [146] with comment by Wait and reply by Weiner [146] and again by Weiner [147].

Richmond has developed a method-of-moments computer program RICHMD1 (now called RICHMOND1) for the current distribution and input impedance of a monopole element on a disk ground plane in free space [2]. Weiner et al. [103,148] utilized the current distribution determined from RICHMD1 to develop a computer program RICHMD2 (now called RICHMOND2) for the far-zone field, directivity, and radiation efficiency. Those efforts are described in Part 1, Secs. 3.4 and 4.2.

Richmond [98] has also developed a method-of-moments program (now called RICHMOND3) for the current distribution and input impedance of a monopole element on a disk ground plane in proximity to flat earth. Richmond, Weiner et al. [147] utilized the current distribution determined from RICHMD3 to develop a computer program RICHMOND4 for the far-zone field, directivity, and radiation efficiency. This latter effort is described in Sec 10.2.

Chapter 10 concludes with a discussion of the Wait–Surtees variational method in Sec. 10.3 and the method-of-images in Sec. 10.4.

10.2 METHOD OF MOMENTS: $0 \leq ka \leq 14$

10.2.1 Current Distribution and Input Impedance

The antenna geometry consists of a vertical monopole element (length h and radius b), on an infinitely thin disk ground plane of radius a at a height z_0 above flat earth (see Sec. 8.1, Fig. 63). The antenna excitation has a time dependence $\exp(j\omega t)$ at radian frequency $\omega = 2\pi f$ (rad/sec) of frequency f (Hz) and free-space wavelength $\lambda = c/f$ where c is the free-space velocity of light. The earth, with a dielectric constant ε_r and conductivity σ (S/m), has a complex relative permittivity $\varepsilon^*/\varepsilon_0 = \varepsilon_r(1 - j\tan\delta)$ where $\tan\delta =$ loss tangent $= \sigma/(\varepsilon_r\varepsilon_0) = 60\lambda\sigma/\varepsilon_r$. The monopole element and disk are assumed to of be infinite conductivity. An arbitrary far-zone observation point $P(r, \theta, \phi)$ is designated by spherical coordinates r, θ, ϕ with origin O at the air–earth interface below the monopole element.

The feed for the monopole antenna is coaxial line with its inner conductor connected through a hole of radius b_1 in the ground plane to the vertical

monopole element and its outer conductor by means of a flange to the ground plane. The inner conductor's diameter is equal to the monopole element's diameter $2b_1$. The current on the outside of the coxial-line feed is assumed to be zero because of the attenuation by lossy ferrite toroids along the exterior of the coaxial-line feed [see Sec. 2.4, Fig. 2(a)]. The coaxial-line feed excitation may be replaced by an equivalent surface magnetic current density (magnetic frill) M_ϕ [see Sec. 2.4, Fig. 2(b)].

The magnetic frill excitation gives rise to a monopole element current distribution $I_z(z)$ along the z-axis of the monopole element and a disk current density distribution $J_\rho(\rho)$ in the radial direction ρ in the plane of the disk. The current density $J_\rho(\rho)$ is the net current density on the top and bottom of the disk. Richmond's method-of-moments solution for the distributions $I_z(z)$ and $J_\rho(\rho)$ when the structure is above flat earth is described in Ref. 98.

The methodology for determining the distributions $I_z(z)$ and $J_\rho(\rho)$ is similar to that described in Sec. 4.2 except that near-field reflection and transmission coefficients at the air–earth interface are introduced to account for the proximity of the earth. The near-field reflection and transmission coefficients are expressed as a function of an unknown propagation constant by requiring that the tangential electric and magnetic fields be continuous at the air–earth interface [see Ref. 98, Eqs. (14) and (15)]. The incident, reflected, and transmitted fields at the air–earth interface are the total fields consisting of both the space-wave and surface-wave fields. For an input voltage $V(0)$ ($= 1$ V), the current $I_z(z)$ at each of L monopole element segments and current density $J_\rho(\rho)$ at each of M disc annular zones are solved simultaneously in Richmond's method-of-moments program RICHMOND3. The resulting value for the input current $I(0)$ at $z = 0$ is utilized to determine the input impedance $Z_{\text{in}} = V(0)/I(0)$. The values of $I_z(z)$ at each segment and $J_\rho(\rho)$ at each annular zone are utilized in determining the far-zone field at $P(r, \theta, \phi)$.

10.2.2 Far-Zone Field

The theory in this section is from a report by Richmond [149] except for some changes in notation.

> The far-zone electric field intensity of the monopole/disk antenna may be regarded as the sum of the field E^{J} radiated from the electric currents and the field E^{M} radiated from the magnetic frill current at the antenna terminals. To calculate these fields we consider the electric current density J, the magnetic current density M radiating in free space, and the field reflected from the air–earth interface. In these calculations, the perfectly conducting antenna structure is removed with the equivalent currents J and M.

One successful but tedious approach to the far-zone fields starts with the rigorous expressions in terms of Sommerfeld integrals. This formulation is interpreted as a plane-wave expansion that includes a finite spectrum of uniform "space" waves plus an infinite spectrum of evanescent plane "surface" waves. Since the evanescent waves attenuate approximately exponentially with their height above the earth, and since their peak amplitude relative to that of the space waves approach zero with increasing distance into the far-field, they are deleted in the far-zone field derivations. Finally, the method-of-stationary phase is applied to evaluate the remaining integrals asymptotically as the observation point recedes to infinity.

The same far-zone field expressions can be derived via Carson's reciprocity theorem [150,151]. To accomplish this, we $(\boldsymbol{E}^{\mathrm{t}}, \boldsymbol{H}^{\mathrm{t}})$ denote the total field in the vicinity of the origin produced by an infinitesimal electric test dipole located at the far-zone point $P(r, \theta, \phi)$ in the plane $\phi = 0$. If the dipole is oriented in the θ direction and has a dipole moment p, its field in the vicinity (x, y, z) of the origin is

$$\boldsymbol{E}_0^{\mathrm{t}}(x, y, z) = \frac{-\hat{\theta} jk\eta_0 p \exp(-jkR')}{4\pi r} \tag{10.2.1}$$

$$R' = r - (x \sin\theta + z\cos\theta) \tag{10.2.2}$$

With this field incident on the air–earth interface, the total magnetic field above the earth in the vicinity of the origin is

$$\begin{aligned} \boldsymbol{H}^{\mathrm{t}}(x, y, z) = &\frac{\hat{y} jkp \exp(-jkr)\exp(jkx\sin\theta)}{4\pi r} \\ &\times [\exp(jkz\cos\theta) + \Re \exp(-jkz\cos\theta)] \end{aligned} \tag{10.2.3}$$

where $\Re$ denotes the plane-wave Fresnel reflection coefficient at the air–earth interface.

The earth conductivity, permeability, and dielectric constant are denoted by $(\sigma, \mu_2, \varepsilon_{\mathrm{r}})$. We let $\mu_2 = \mu_0$, in which case reflection coefficient $\Re$ (for parallel polarization) is given by

$$\Re = \Re_{\parallel} = \frac{(\varepsilon^*/\varepsilon_0)\cos\theta - \sqrt{(\varepsilon^*/\varepsilon_0) - \sin^2\theta}}{(\varepsilon^*/\varepsilon_0)\cos\theta + \sqrt{(\varepsilon^*/\varepsilon_0) - \sin^2\theta}} \tag{10.2.4}$$

identical to the Fresnel reflection coefficient $R_{\mathrm{v}}(\theta)$ given by Eq. (9.2.5).

The complex relative permittivity of the earth is

$$(\varepsilon^*/\varepsilon_0) = \varepsilon_{\mathrm{r}} - j\sigma/(\omega\varepsilon_0) \tag{10.2.5}$$

From Eq. (10.2.3) and Maxwell's curl equations, the total electric field intensity above the earth in the vicinity of the origin is

$$E_x^{\mathrm{t}} = \frac{-jk\eta_0 p \exp(-jkr)\exp(jkx\sin\theta)\cos\theta}{4\pi r} \times [\exp(jkz\cos\theta) - \Re\exp(-jkz\cos\theta)] \tag{10.2.6}$$

$$E_y^{\mathrm{t}} = 0 \tag{10.2.7}$$

$$E_z^{\mathrm{t}} = \frac{-jk\eta_0 p \exp(-jkr)\exp(jkx\sin\theta)\cos\theta}{4\pi r} \times [\exp(jkz\cos\theta) + \Re\exp(-jkz\cos\theta)] \tag{10.2.8}$$

Carson's reciprocity theorem states that

$$\int \boldsymbol{I}^{\mathrm{t}}\cdot\boldsymbol{E}\,\mathrm{d}l = \iint (\boldsymbol{J}\cdot\boldsymbol{E}^{\mathrm{t}} - \boldsymbol{M}\cdot\boldsymbol{H}^{\mathrm{t}})\,\mathrm{d}s \tag{10.2.9}$$

where $\boldsymbol{E}$ is the total far-zone field at (r, θ, ϕ).

On the right-hand side of this equation, $\boldsymbol{J}$ and $\boldsymbol{M}$ denote surface-current densities on the perfectly conducting monopole/disk antenna and the integration extends over the surface of the monopole/disk antenna. On the left side the integration extends over the infinitesimal test dipole and is readily evaluated to be $pE_\theta(r, \theta, \phi)$, so the reciprocity theorem reduces to

$$\boldsymbol{E}_\theta(r, \theta, \phi) = (1/p)\iint (\boldsymbol{J}\cdot\boldsymbol{E}^{\mathrm{t}} - \boldsymbol{M}\cdot\boldsymbol{H}^{\mathrm{t}})\,\mathrm{d}s \tag{10.2.10}$$

where p is the dipole moment.

The magnetic frill current $\boldsymbol{M}$ is given. Upon completion of the moment-method analysis, the electric current density $\boldsymbol{J}$ is known on the vertical wire monopole and the horizontal conducting disk. The test dipole fields are given above, so Eq. (10.2.10) contains no unknown quantities. Thus, evaluation of the far-zone field $E_\theta(r, \theta, \phi)$ of the monopole/disk antenna is now simply a matter of performing the integrations in Eq. (10.2.10). If we start with a $\hat{\boldsymbol{\phi}}$-oriented test dipole, a similar analysis shows that the resulting far-zone ϕ component of the monopole/disk antenna is $E_\phi(r, \theta, \phi) = 0$.

10.2.2.1 The Field from the Monopole Element

In far-zone field calculations for the vertical wire monopole, the tubular surface-current density $\boldsymbol{J}$ can be replaced with a filamentary line source $I(z)$ on the z-axis. From Eqs. (10.2.8) and (10.2.10), the far-zone field from the vertical wire is

given by

$$E_\theta^{\mathrm{w}}(r,\theta,\phi) = \frac{jk\eta_0 \exp(-jkr)\sin\theta}{4\pi r}\int_{z_0}^{z_0+h} I(z)[\exp(jkz\cos\theta) + \Re\exp(-jkz\cos\theta)]\,\mathrm{d}z \tag{10.2.11}$$

The vertical wire monopole is divided into L segments with length $d' = L/h$. A typical segment (segment ℓ) extends from z_1^ℓ to z_2^ℓ on the z-axis, with the following current distribution:

$$I^\ell(z) = \frac{I_1^\ell \sin k(z_2^\ell - z) + I_2^\ell \sin k(z - z_1^\ell)}{\sin kd'} \tag{10.2.12}$$

The current entering the segment at the bottom is $I_2^\ell = I(z_1^\ell)$, and the current leaving the segment at the top is $I_2^\ell = I(z_2^\ell)$.

From Eqs. (10.2.11) and (10.2.12), the far-zone field of the wire monopole is given by

$$\begin{aligned} E_\theta^{\mathrm{w}}(r,\theta,\phi) =& C\sum_{\ell=1}^{L} I_1^\ell \left\{\exp(jkz_2^\ell\cos\theta) - A\exp(jkz_1^\ell\cos\theta)\right. \\ &\left. +\Re\left[\exp(-jkz_2^\ell\cos\theta) - B\exp(-jkz_1^\ell\cos\theta)\right]\right\} \\ &+ C\sum_{\ell=1}^{L} I_2^\ell \left\{\exp(jkz_1^\ell\cos\theta) - B\exp(jkz_2^\ell\cos\theta)\right. \\ &\left. +\Re\left[\exp(-jkz_1^\ell\cos\theta) - A\exp(-jkz_2^\ell\cos\theta)\right]\right\} \end{aligned} \tag{10.2.13}$$

where

$$A = \cos(kd) + j\cos\theta\sin(kd) \tag{10.2.14}$$

$$B = \cos(kd) - j\cos\theta\sin(kd) \tag{10.2.15}$$

$$C = \frac{j\eta_0\exp(-jkr)}{4\pi r\sin(kd)\sin\theta} \tag{10.2.16}$$

On the lowest wire segment ($\ell = 1$), the current at the bottom is $I_1^{\mathrm{t}} = I_1$. On the highest segment ($\ell = L$) the endpoint currents are $I_1^{\mathrm{t}} = I_N$ and $I_2^{\mathrm{t}} = 0$, where N denotes the number of equations and the number of unknowns in the moment-method solution for the monopole/disk antenna.

10.2.2.2 The Field from the Disk Ground Plane

The electric current density $J_\rho(\rho)$ on the perfectly conducting circular disk is radially directed and independent of the azimuthal angle ϕ. The disk lies in the plane $z = z_0$. If (ρ', ϕ', z_0) denotes the cylindrical coordinates of a source point on the disk, the far-zone disk field is obtained from Eqs. (10.2.6), (10.2.7), and (10.2.10) as follows:

$$\begin{aligned} E_\theta^{\mathrm{d}}(r, \theta, \phi) = & \frac{-jk\eta_0 \exp(-jkr)\cos\theta}{4\pi r} \\ & \times [\exp(jkz_0\cos\theta) - \Re\exp(-jkz_0\cos\theta)] \\ & \times \int_b^a \int_{-\pi}^{\pi} J_\rho(\rho)' \cos\phi'' \exp(jk\rho'\cos\phi''\sin\theta)\rho' \mathrm{d}\phi'' \mathrm{d}\rho' \end{aligned} \tag{10.2.17}$$

$$\phi'' = \phi' - \phi \tag{10.2.18}$$

Since the disk current density J_ρ is independent of ϕ', one integration can be evaluated as follows:

$$\int_{-\pi}^{\pi} \cos\phi \exp(jx\cos\phi)\,\mathrm{d}\phi = 2\pi j J_1(x) \tag{10.2.19}$$

where $J_1(x)$ denotes the Bessel function. Beginning at this point, it is convenient to let ρ (instead of ρ') denote the radial coordinate of a source point on the disk. From Eqs. (10.2.11) and (10.2.12), the far-zone field of the circular disk is

$$\begin{aligned} E_\phi^{\mathrm{d}} = & 0.5k\eta_0[\exp(-jkr)/r]\cos\theta\,[\exp(jkz_0\cos\theta) \\ & - \Re\exp(-jkz_0\cos\theta)]\int_b^a \rho J_\rho(\rho) J_1(k\rho\sin\theta)\,\mathrm{d}\rho \end{aligned} \tag{10.2.20}$$

The perfectly conducting circular disk is divided into M concentric annual zones. A typical zone (zone m) has an inner radius ρ_1^m, an outer radius ρ_2^m, and a width $d = \rho_2^m - \rho_1^m = (a-b)/M$. Let I_1^m denote the electric current entering the zone at ρ_1^m, and I_2^m the current leaving at ρ_2^m. Then the electric surface-current density on this zone is

$$J_\rho^m(\rho) = \frac{I_1^m \sin k(\rho_2^m - \rho) + I_2^m \sin k(\rho - \rho_1^m)}{2\pi\rho\sin kd} \tag{10.2.21}$$

From Eqs. (10.2.20) and (10.2.21), the far-zone field of the circular disk is given by

$$E_\theta^{\mathrm{d}}(r,\theta,\phi) = \frac{\eta_0 \exp(-jkr)\cos\theta}{4\pi r \sin(kd)}[\exp(jkz_0\cos\theta) - \Re\exp(-jkz_0\cos\theta)]$$
$$\times \sum_{m=1}^{M} \int_{k\rho_1^m}^{k\rho_2^m} [I_1^m \sin k(\rho_2^m - \rho) + I_2^m \sin k(\rho - \rho_1^m)] \quad (10.2.22)$$
$$\times J_1(k\rho\sin\theta)d(k\rho)$$

On the first zone ($m = 1$), the endpoint currents are $I_1^m = -I_1$ and $I_2^m = I_2$. On the last zone ($m = M$), the endpoint currents are $I_1^m = I_M$ and $I_2^m = 0$. Numerical integration techniques are required in evaluating this expression.

10.2.2.3 The Field from the Magnetic Frill

The perfectly conducting circular disk and the coaxial-fed monopole are replaced (via Schelkunoff's equivalence principle) with equivalent electric and magnetic surface currents radiating in free space over the flat earth. The equivalent magnetic surface-current density (magnetic frill) is given by [see Eq. (2.4.8)]

$$M_\phi = \begin{cases} -V/[\rho\ln(b_1/b)], & b \le \rho \le b_1 \\ 0, & \rho \text{ elsewhere} \end{cases} \quad (10.2.23)$$

This "magnetic frill," located at $z = z_0$, is centered on the z-axis and has inner and outer radii of b and b_1, respectively. The antenna is considered to be transmitting, with a voltage generator (of V peak volts) at the terminals and the coaxial outer conductor at zero potential. The free-space field of the magnetic frill is analyzed by Tsai [152,153]. From Eqs. (10.2.3) and (10.2.10) the far zone of the frill is given by

$$E_\theta^M(r,\theta,\phi) = \frac{-jk\exp(-jkr)}{4\pi r}[\exp(jkz_0\cos\theta) + \Re\exp(-jkz_0\cos\theta)] \quad (10.2.24)$$
$$\times \int_b^{b_1}\int_{-\pi}^{\pi} M_\phi(\rho')\cos\phi''\exp(jk\rho'\cos\phi''\sin\theta)\rho'\,\mathrm{d}\phi''\,\mathrm{d}\rho'$$

Since the magnetic current density is independent of ϕ', one integration can be performed with the aid of Eqs.(10.2.19) and (10.2.23) to obtain

$$E_\theta^M = \frac{-kV\exp(-jkr)}{2r\ln(b_1/b)}[\exp(jkz_0\cos\theta) + \Re\exp(-jkz_0\cos\theta)] \quad (10.2.25)$$
$$\times \int_b^{b_1} J_1(k\rho\sin\theta)\,\mathrm{d}\rho$$

The final integration is performed as follows:

$$\int J_1(\beta x)\,\mathrm{d}x = -J_0\beta x/\beta \tag{10.2.26}$$

Thus, the field of the magnetic frill is given by

$$\begin{aligned} E_\theta^M = {} & \frac{V\exp(-jkr)}{2r\ln(b_1/b)}[\exp(jkz_0\cos\theta) + \Re\exp(-jkz_0\cos\theta)] \\ & \times [J_0(kb\sin\theta) - J_0(ka\sin\theta)]/\sin\theta \end{aligned} \tag{10.2.27}$$

This expression can be simplified with the following:

$$J_0(x) \approx 1 - x^2/4, \quad x \ll 1. \tag{10.2.28}$$

From Eqs. (10.2.27) and (10.2.28), the far-zone field of the magnetic frill is given by

$$\begin{aligned} E_\theta^m(r,\theta,\phi) = {} & \frac{k^2V(b^2 - b_1^2)\exp(-jkr)}{8r\ln(b_1/b)}[\exp(jkz_0\cos\theta) \\ & + \Re\exp(-jkz_0\cos\theta)]\sin\theta, \quad kb_1 \ll 1 \end{aligned} \tag{10.2.29}$$

10.2.2.4 The Total Far-Zone Field

The total far-zone field $E_\theta(r,\theta,\phi)$ defined by Eq. (10.2.10) in the free-space region is the sum of the fields from the monopole element, the disk ground plane, and the magnetic frill. Accordingly, the total far-zone field in the free-space (air) region is given by

$$E_\theta(r,\theta,\phi) = E_\theta(r,\theta) = E_\theta^{\mathrm{w}}(r,\theta) + E_\theta^{\mathrm{d}}(r,\theta) + E_\theta^M(r,\theta) \tag{10.2.30}$$

where $E_\theta^{\mathrm{w}}, E_\theta^{\mathrm{d}}, E_\theta^M$ are given by Eqs. (10.2.13), (10.2.22), and (10.2.29), respectively. The fields $E_\theta, E_\theta^{\mathrm{w}}, E_\theta^{\mathrm{d}}$, and E_θ^M are uniform with azimuthal angle ϕ because of the azimuthal symmetry of the antenna geometry in Fig. 63.

The total radiated power P_{r}, antenna directivity $d(\theta)$ (numeric), antenna directivity $D(\theta)$ (dB), input power P_{in}, input impedance Z_{in}, antenna radiation resistance R_{rad}, antenna radiation efficiency η, and modified radiation efficiency η_{d} are defined in Sec.8.1, Eqs. (8.1.6)–(8.1.13), respectively.

10.2.3 Validation

Several approaches have been used in validating the numerical results from the programs RICHMOND3 and RICHMOND4. These approaches include validation by comparison with results from the limiting case of disk ground

planes in free space; the limiting case of ground planes of zero extent in proximity to earth; the limiting case of a perfect ground plane of infinite extent; Wait–Surtees model for input impedance; Wait–Walters model for gain; and the Numerical Electromagnetics Code (NEC) for radiation efficiency.

10.2.3.1 Limiting Case of Disk Ground Planes in Free Space

In the limiting case of disk ground planes in free space, numerical results from programs RICHMOND3 and RICHMOND4 agree with results from programs RICHMD1 and RICHMD2. The method-of-moments programs RICHMD1 and RICHMD2, for a monopole element on a disk ground plane in free space, are validated in Part 1. In Part 1, numerical results for electrically thin monopole elements were compared with results from Brillouin–Stratton induced electromotive force (EMF) method for ground planes of zero extent; Bardeen's integral equation method for ground-plane radii $0 \leq ka \leq 2.75$ wavenumbers; Leitner–Spence method of oblate spheroidal wave functions for ground-plane radii $3.0 \leq ka \leq 6.5$ wave numbers; Awadalla–McClean moment method combined with the geometric theory of diffraction for ground-plane radii $8.5 \leq ka < \infty$ wave numbers; and the method of images for $ka = \infty$. Consistent and excellent agreements of results were achieved by the RICHMD1 and RICHMD2 programs.

10.2.3.2 Limiting Case of Ground Planes of Zero Extent

In the limiting case of ground planes of zero extent in proximity to earth, program RICHMOND4 results for the directivity of a quarter-wave monopole element with a disk ground plane of radius $ka = 0.025$ wave number resting on medium dry earth are compared in Table 19 of Sec. 9.2 with results from a Fresnel reflection model (MITRE Program MODIFIED IMAGES) and Lawrence Livermore Laboratory's method-of-moments program NEC-3 using the Sommerfeld option. Programs RICHMOND4, MODIFIED IMAGES, and NEC-3 gave identical directivity patterns with absolute values of directivity that agreed to within 0.04 dBi. The reason for the close agreement is that the directivity does not depend upon the absolute accuracy of the antenna input current.

Radiation resistance and radiation efficiency do depend upon the absolute accuracy of the antenna input current. RICHMOND4 results of radiation resistance and radiation efficiency, for the above case and various types of earth, are compared in Table 27 with results from NEC-3 (but not MODIFIED IMAGES because the omission of the surface wave in the Fresnel coefficient model affects the radiation efficiency and radiation resistance, but not directivity). The results differ by approximately 10% for radiation resistance and by more than 25% for radiation efficiency. These differences are attributable to the difference in charge density at the base of the monopole element by a factor of 4000 resulting from the different configurations of the two models [154]. In NEC-3, the current produced

TABLE 27 Radiation Resistance and Efficiency of a Vertical, Quarter-Wave Monopole Element on a Flat Earth; $f = 15$ MHz, $b/\lambda = 1.0 \times 10^{-6}$

	Radiation resistance (Ω)			Radiation efficiency (numeric)		
Earth classification (ε_r, σ S/m)	NEC-3[a]	RICHMD4[b]	Percent difference[c]	NEC-3[a]	RICHMD4[b]	Percent difference[c]
Sea water (70, 5)	34.0	29.5	15.0	0.823	0.799	29.4
Fresh water (80, 3.0×10^{-2})	19.1	17.3	10.4	0.273	0.347	34.3
Wet ground (30, 1.0×10^{-2})	14.5	13.2	10.3	0.144	0.229	36.9
Medium dry ground (15, 1.0×10^{-3})	11.5	10.5	10.3	0.163	0.210	22.2
Very dry ground (3, 1.0×10^{-4})	6.2	5.7	9.6	0.091	0.145	37.6
Pure water, 20°C (80, 1.7×10^{-3})	19.1	17.3	9.4	0.375	0.378	0.8
Ice (−1°C) (3, 9.0×10^{-5})	6.2	5.7	9.6	0.091	0.148	38.8
Ice (−10°C) (3, 2.7×10^{-5})	6.2	5.7	9.5	0.136	0.171	20.8
Average land (10, 5.0×10^{-3})	9.9	9.0	10.3	0.044	0.105	58.3

[a] Number of element segments, $N = 25$; voltage source excitation at $N = 1$.
[b] Disk ground-plane radius, $2\pi a/\lambda = 0.025$ wave numbers.
[c] |(NEC-3 − RICHMD4)/RICHMD4| × 100.

by charge distribution is discharged into the earth through an element of radius 10^{-6} wavelengths, whereas in RICHMOND4 the current is discharged into the earth through a ground plane of radius 4×10^{-3} wavelengths. An increase in the number of monopole segments from 4 to 20 in RICHMOND4 has no significant effect in modifying the Table 27 results for radiation efficiency.

10.2.3.3 Limiting Case of a Ground Plane of Infinite Extent

In the limiting case of a perfect ground plane of infinite extent, the monopole element of length h may be modeled by the method of images as a free-space dipole of half-length h, but with twice the dipole input current, one-half the dipole impedance, twice the dipole directivity in the upper hemisphere, and zero times the dipole directivity in the lower hemisphere. Richmond has written a program, RICHMD6, that uses a sinusoidal-Galerkin method of moments to compute the input impedance, current distribution, and far-zone field of the equivalent free-space dipole. Program RICHMD6 is discussed in Sec. 10.4. Numerical results for input impedance are in reasonable agreement with those from King-Middleton theory [155]. For example, for $h/\lambda = 0.25$ (corresponding to $h/\lambda = \pi/2$) and $h/b = 16.56$ (corresponding to $\Omega = 7$), RICHMD6 results for the monopole input impedance are $Z_{\text{in}} = 46.52 + j15.97\,\Omega$ which differ from the King-Middleton results of $Z_{\text{in}} = 47.85 + j18.50\,\Omega$ by 2.8 and 13.7% for input resistance and input reactance, respectively. RICHMD6 results for directivity are almost identical to the Table 4 values for a thin quarter-wave monopole on a perfect ground plane.

10.2.3.4 Comparison with Wait–Surtees Model for Input Impedance

Program RICHMOND4 results for the input impedance of a monopole element with a disk ground plane resting on flat earth have been compared by RICHMOND [98] with those obtained from a Wait–Surtees model [91]. In Ref. 98, the Wait–Surtees results for input reactance are inadvertently given for a disk ground plane in free space rather than for a disk ground plane on flat earth. RICHMOND4 results for input resistance and input reactance are compared in Figs. 88 and 89, respectively, with those obtained from a program Wait–SURTEES written by Richmond and based on the Wait–Surtees model. Program WAIT–SURTEES, described in Sec. 10.3, incorporates results from program RICHMOND5 for the input impedance of a monopole element on a perfect ground plane. The RICHMOND4 results are in close agreement with WAIT–SURTEES results, except at small ground-plane radii less than approximately $ka = 1.0$ wave number for which Wait–Surtees model is not accurate. The RICHMOND4 results in Fig. 18 for input reactance should not have a local minimum at $ka = 0.75$. A nonconvergent result was obtained at $ka = 0.75$

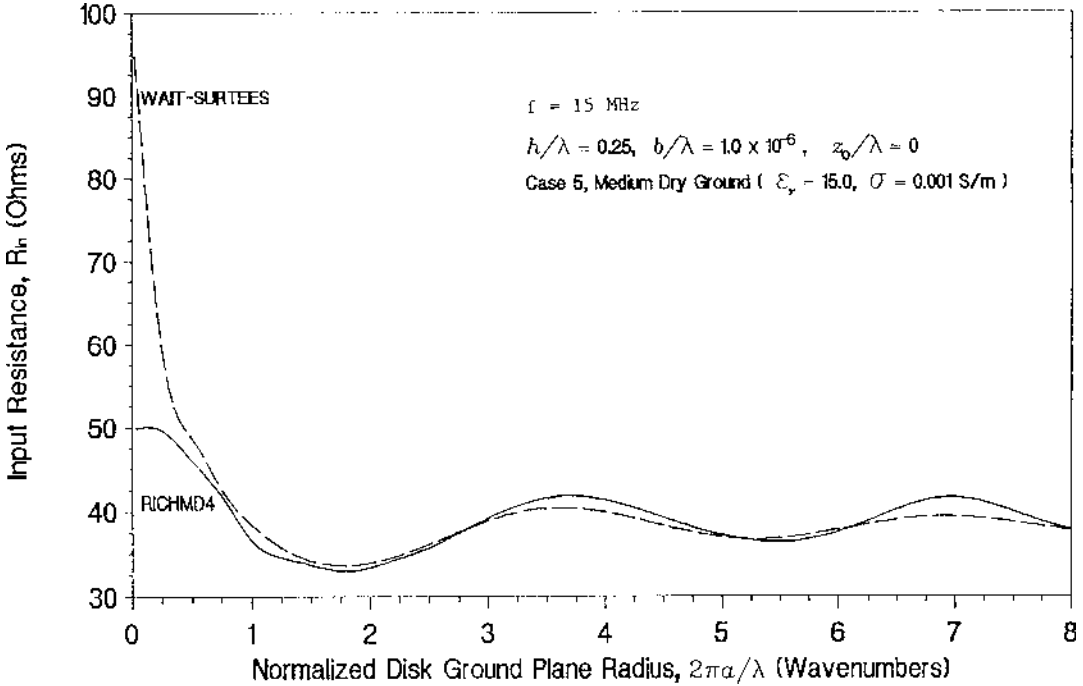

FIGURE 88 Comparison of WAIT–SURTEES and RICHMD4 numerical values for input resistance of quarter-wave monopole element with a disk ground plane on flat earth.

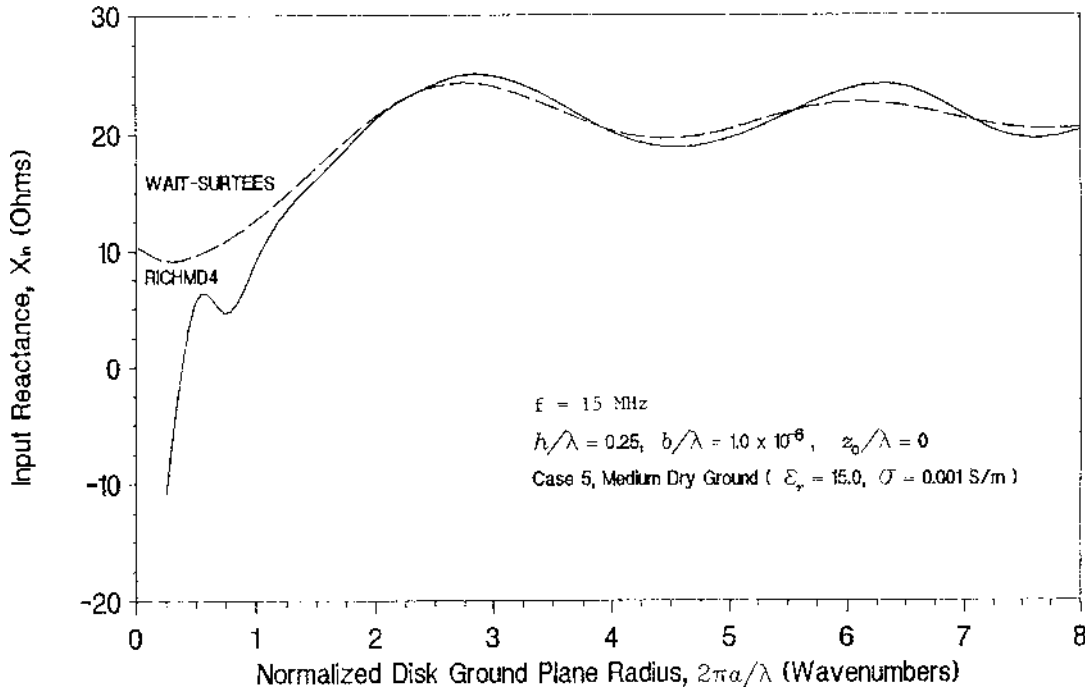

FIGURE 89 Comparison of WAIT–SURTEES and RICHMD4 numerical values for input reactance of quarter-wave monopole element with a disk ground plane on flat earth.

because of over-segmentation of the disk when the number of disk annular zones was abruptly increased from 7 at $ka = 0.5$ to 16 at $ka = 0.75$.

10.2.3.5 Comparison with Wait–Walters Model for Gain

Numerical results of directivity and radiation efficiency from Richmond's method-of-moments program RICHMOND4 cannot be validated against models based on Monteath's compensation theorem [90,92,93,98,117] and Sommerfeld's attenuation function [89]. Those models yield only the gain (the product of directivity and radiation efficiency) rather than directivity and radiation efficiency as separate entities. Nevertheless, it is of interest to compare RICHMOND4 results for gain with those from the Wait–Walters model [92,93,117,143] based on Monteath's compensation theorem.

First consider the Wait–Walters model. The gain $G(ka, \psi) - G(0, \psi)$ (dB) of an electrically short monopole element on a disk ground plane with radius ka wave numbers relative to that without a disk ground plane ($ka = 0$) is shown in Fig. 2 of Ref. 143 and in Fig. 23.26 of Ref. 117 for $ka = 10$, $\varepsilon_r = 9$, and $\sigma = 0$. The Wait–Walters model of Ref. 143 computes the magnetic field intensity $H(ka, \psi)$ with a disk ground plane as a function of the grazing angle ψ (the complement of the angle of incidence θ) relative to that with no ground plane. At a grazing angle $\psi = 2°$, the Wait–Walters model gives a relative gain of $G(10, 2) - G(0, 2) = 4.5$ dB.

Now consider the Richmond model. Program RICHMOND4 results for a quarter-wave monopole element on a disk ground plane of radius $ka = 8$ wave numbers on medium dry ground ($\varepsilon_r = 15.0$, $\sigma = 0.001$ S/m) gives a directivity at a grazing angle $\psi = 2°$, $D(8, 2) = -8.6$ dBi (see Fig. A6-136) and a radiation efficiency $\eta = 0.69 = -1.6$ dB (see Fig. A6-143). The gain $G(8, 2) = -8.6$ dBi $- 1.6$ dB $= -10.2$ dBi; for $ka = 0$ and $\psi = 2°$, $D(0, 2) = -7.9$ dBi (see Fig. A6-143) and the radiation efficiency $\eta = 0.21 = -6.8$ dB (see Fig. A6-136). The gain $G(0, 2) = -7.9$ dBi $- 6.8$ dBi $= -14.7$ dBi. The relative gain $G(8, 2) - G(0, 2) = -10.2$ dBi $+ 14.7$ dBi $= 4.5$ dB. Figs. A6-136 and A6-143 are found in App. A.6.

The RICHMOND4 and Wait–Walters results of 4.5 dB for relative gain are identical for these similar cases.

10.2.3.6 Comparison with NEC for Radiation Efficiency

Numerical results of radiation efficiency obtained from programs RICHMOND4, NEC-3, and NEC-GS are compared in Fig. 90 for the radiation efficiency of a quarter-wave monopole element with small ground planes on or just above medium dry earth as a function of the ground-plane radius. RICHMOND4 results are for disk ground planes (see Fig. A6-143). NEC-3 results are for ground plane of zero extent (see Table 27). NEC-GS results are for radial-wire ground planes whose wires have a radius $b_w = 10^{-5}$ wavelengths (see Sec. 11.2). The results for

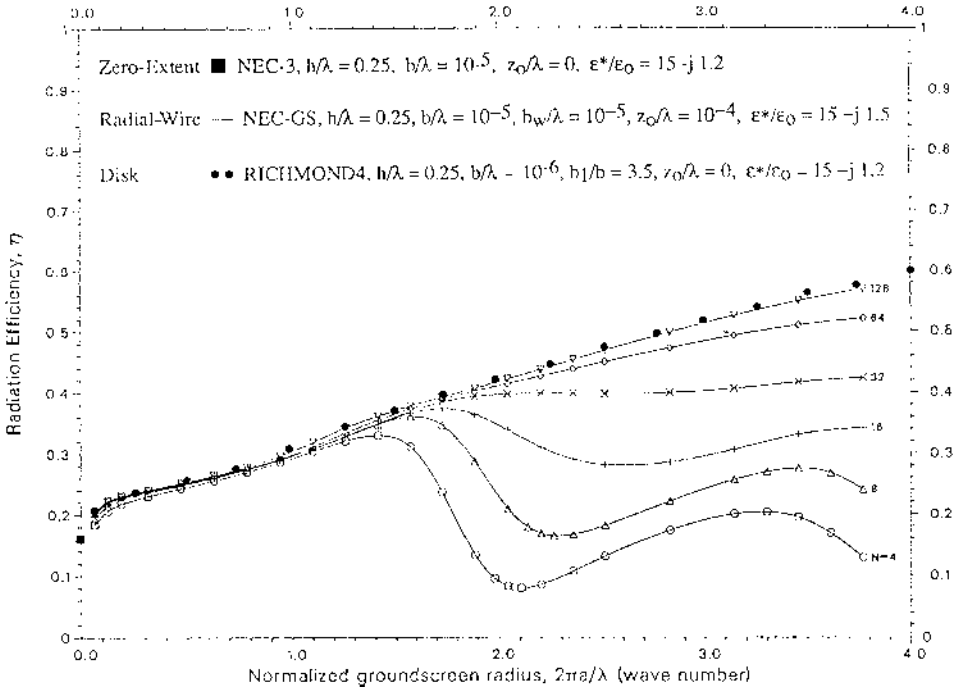

FIGURE 90 Radiation of efficiency of a quarter-wave monopole element with different (zero-extent, radial-wire, and disk) ground planes on or just above medium dry earth.

disk ground planes are in close agreement with those for ground planes with 128 radial wires.

10.2.4 Numerical Results

Numerical evaluation of the far-zone field, directivity, radiation resistance, and radiation efficiency is executed by Richmond's computer program RICHMOND4 written in FORTRAN 77. The program RICHMOND4 uses subroutines from Richmond's computer program RICHMOND3 that determines the current distributions on the monopole element and disk ground plane, as well as the input current and input impedance. Brief descriptions of programs RICHMOND3 and RICHMOND4 are given in App. B.9. Programs RICHMOND3 and RICHMOND4 are extensions of programs RICHMOND1 and RICHMOND2, respectively, described in Part 1 for a monopole element on a disk ground plane in free space.

Numerical results, in the form of an atlas of computer plots, are presented in App. A.6 (Figs. A6-1–A6-160). The results are for a thin quarter-wave monopole element on a small to moderately large disk ground plane resting on earth ($z_0 = 0$), for each of the earth classifications in Table 16 (Cases 2–10) at a frequency $f = 15$ MHz. In each plot, results are compared to those for a perfect ground plane (Case 1) and free space (Case 11). A comparison of results for sea water and medium dry ground (Figs. A6-145–A6-160) is designated as Case 12.

The coaxial-line feed ($b_1/b = 3.5$) has negligible effect on the far-zone field and input current because its equivalent magnetic frill of outer diameter $2b_1/\lambda$ ($= 7 \times 10^{-6}$ wavelengths) has a radiation resistance that is small compared to that of the monopole element of length h/λ ($= 0.25$ wavelengths). In the numerical results, the monopole element was divided into four segments. The disk was segmented into equal-width annular zones, whose numbers varied from 7 for $ka = 0.025,\ 0.25,\ 0.5$; 16 for $ka = 0.75$–5.25; 17 for $ka = 5.5$; 18 for $ka = 5.75$ and 6.00; 19 for $ka = 6.25$; 20 for $ka = 6.5$; 21 for $ka = 6.75,\ 7.0$; 22 for $ka = 7.25$; 23 for $ka = 7.50$; and 24 for $ka = 7.75,\ 8.0$.

The elevation numeric directivity patterns are shown as polar plots on the same linear scale for disk radii $2\pi a/\lambda = 0.025,\ 3.0,\ 4.0,\ 5.0$ and 6.5 wave numbers. For Cases 2–10 and the ground planes resting on earth, the directivity patterns are approximately independent of disk radius unlike Case 11 when the ground planes are in free space. The earth, in effect, softens the edge of the ground plane, thus minimizing changes in directivity resulting from ground plane edge diffraction.

For Cases 2–10, the peak directivity is approximately independent of disk radius and is approximately equal to that of a perfect ground plane with a numeric directivity of $3.282 = 5.161$ dBi. For those cases, except for sea water (Case 2), the elevation angle of the peak directivity is approximately 30° above the horizon,

independent of ground-plane radius. Sea Water (Case 2) is effective in reducing the elevation angle of peak directivity to approximately 8° above the horizon (see Figs. A6-145–A6-149). Otherwise, in Cases 3–10, a disk radius of $ka > 60$ is required to bring the elevation angle of peak directivity to within 8° of the horizon [89].

The directivities for Cases 2–10, at elevation angles near the horizon, show no improvement over that for no ground plane at all (see, e.g., Figs. A6-156–A6-160). The directivity at angles of incidence $\theta = 82,\ 84,\ 86,\ 88,$ and $90°$ are approximately 4, 5, 7, 13, and ∞ dB, respectively, below peak directivity. For Cases 2–10, the directivity on the horizon is $-\infty$ dBi because of the space wave multipath null (corresponding to a Fresnel reflection coefficient $= -1$). The near field on the horizon in not zero because of the presence of the surface-wave field (see Sec. 9.3).

The numeric directivity, of electrically short monopole elements on disk ground planes resting on earth may be approximated by an empirical expression of the form [116]

$$d_r(\theta) = \begin{cases} A\cos^m\theta\sin^n\theta; & 0 \le \theta \le \pi/2\,\text{rad},\ \ m > 0,\ \ n > 1 \\ 0, & -\pi/2 \le \theta \le 0\,\text{rad} \end{cases} \tag{10.2.31}$$

The exponents m and n are chosen to yield a peak directivity in a desired direction, and a null at $\theta = 0$ and $\pi/2$ rad. The coefficient A is chosen to satisfy the condition

$$(1/4\pi)\int_0^{2\pi}\int_0^{\pi/2} d_r(\theta)\sin\theta\,d\theta\,d\phi = 1 \tag{10.2.32}$$

Accordingly,

$$A = 2\left[\int_0^{\pi/2}\cos^m\theta\sin^{n+1}\theta\,d\theta\right]^{-1} \tag{10.2.33}$$

Equation (10.2.31), when combined with Eq. (10.2.33), has a null in the direction of zenith and a peak directivity comparable to that for a perfect ground plane. The directivity patterns for Cases 3–10 (sea water is excluded) of App. A.6, are approximated by Eqs. (10.2.31) and(10.2.33) if $m = 1$ and $n = 3$. Accordingly,

$$d_r(\theta) \approx \begin{cases} 10\cos\theta\sin^3\theta, & 0 \le \theta \le \pi/2\,\text{rad} \\ 0, & -\pi/2 \le \theta \le 0\,\text{rad} \end{cases} \qquad \text{Cases } 3\text{–}10 \tag{10.2.34}$$

As an example, the directivity pattern for medium dry ground (Case 5) and $ka = 3.0$ from Fig. A6-50 gives reasonably good agreement with that given by Eq. (10.2.34) (see Fig. 91).

The radiation efficiency increases monotonically with increasing disc radius. For free space (Case 11), the radiation efficiency should be exactly unity

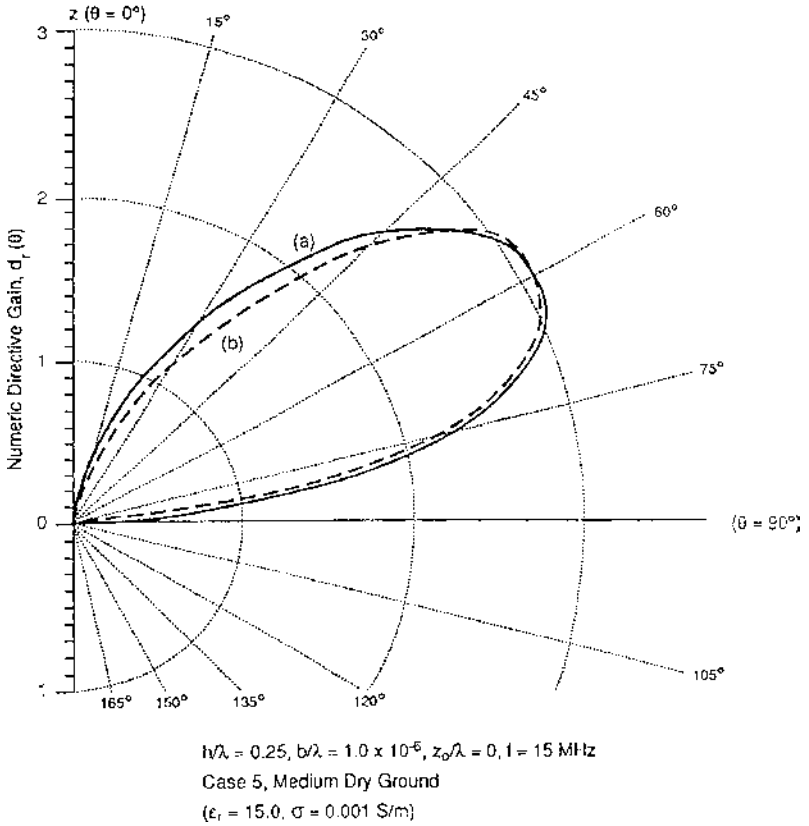

FIGURE 91 Numeric directivity of a quarter-wave element on a disk ground plane resting on medium dry ground, $ka = 3.0$ (a) RICHMOND4; (b) $10\cos\theta\sin^3\theta$.

for infinite conductivity of the monopole element and disk ground plane. The free-space numerical results for radiation efficiency differ slightly from unity at the larger disk radii because of uncorrected errors in the RICHMOND3 and RICHMOND4 computer programs. Apparently for the same reason, the sea water (Case 2) radiation efficiency is not a strictly increasing monotonic function with increasing disc radius (see Fig. A6-8).

The radiation resistance increases aperiodically with increasing disk radius. The input resistance decreases aperiodically with increasing disk radius to an asymptotic value of approximately 36 Ω. The input reactance increases aperiodically with increasing disk radius to an asymptotic value of approximately 21 Ω.

10.3 VARIATIONAL METHOD: $2 \leq ka \leq \infty$

The input impedance $Z_{in} = R_{in} + jX_{in}$ of a vertical monopole antenna centered on a disk ground plane over flat earth can be estimated by utilizing a variational method after Wait and Surtees [91]. The geometry and circuit parameters are the same as described in Sec. 10.2.1. The method determines the difference ΔZ of input impedance from that with a perfect ground plane. If Z_{inf} denotes the input impedance of a vertical monopole antenna with a perfect ground plane, then

$$Z_{in} = \Delta Z + Z_{inf} \tag{10.3.1}$$

Richmond has written a computer program RICHMOND7 for determining Z_{im} (previously called WAIT–SURTEES) that combines the Wait–Surtees variational method for determining ΔZ with his own method-of-moments program RICHMOND5 (previously called RICHMD5) for determining Z_{inf}. Program RICHMOND5 is discussed in Secs. 4.4 and 10.4. Program RICHMOND7 is described briefly in App. B.10 based on a report by Richmond [156].

In the theory of Wait and Surtees, the monopole is assumed to have a sinusoidal current distribution. Since the current distribution departs significantly from the sinusoidal form when the monopole length exceeds one-half wavelength, ΔZ may begin to lose reliability as the monopole length increases. This possible problem has not been investigated.

Program RICHMOND7 numerical results for input resistance R_{in} and input reactance X_{in} are valid for disk ground-plane radii $2 \leq ka \leq \infty$ wave numbers based on a comparison with numerical results from the method-of-moments program RICHMOND3 (see Sec. 10.2.3, Figs. 88 and 89). The suspected best available results for input impedance are RICHMOND3 for $0 \leq ka \leq 8$ and RICHMOND7 for $ka > 8$, based on a comparison of input impedance results obtained by the method-of-moments and by the geometric theory of diffraction (see Table 7 in Sec. 4.5). The method-of-moments RICHMOND3 is not applicable to very large ground planes because of precision errors in solving increasingly larger numbers of simultaneous equations. The variational method RICHMOND7 is not applicable to very small ground planes because of conceptual errors in approximating the ground plane current distribution to be that for an infinite ground plane.

10.4 METHOD OF IMAGES: $ka = \infty$

Consider an idealized monopole antenna consisting of a vertical monopole element mounted on a perfect ground plane above flat earth. The geometry and circuit parameters are the same as described in Sec. 10.2.1 but restricted to a normalized disk ground-plane radius $ka = \infty$ wave numbers. The presence of a flat earth has no effect on the electrical properties of the antenna because

the ground plane shields the earth from the fields generated by the current distributions on both the monopole element and ground plane. The current is zero on the underneath side of the ground plane.

The antenna may be modeled, therefore, by the method-of-images described in Sec. 4.4 for a monopole element on a perfect ground plane in free space. In the method of images, the electrical properties are first determined for a dipole antenna, of twice the length of the monopole element and with no ground plane. The monopole antenna has one-half the input impedance and double the peak numeric directivity of the dipole antenna. Furthermore, the monopole antenna has zero field below the ground plane whereas the dipole antenna has fields that are symmetrical about the horizon.

J. Richmond has written a program RICHMOND5 (previously called RICHMD5) that utilizes the method of images and the method of moments to compute the current distribution and input impedance of a monopole element on a ground plane of infinite extent. The current distribution determined in RICHMOND5 is then used in program RICHMOND6 (previously called RICHMD6) to obtain the far-field. Programs RICHMOND5 and RICHMOND6 are described in App. B.6. The validations of RICHMOND5 and RICHMOND6 are discussed in Sec. 4.4.

In calculating the input impedance Z_{in} (denoted as Z_{inf} for a perfect ground plane in Sec. 10.3), RICHMOND5 divides the monopole element into segments of equal length and the unknown current distribution $I(z)$ is expanded in overlapping sinusoidal basis functions (sinusoidal-Galerken method). Thus, $I(z)$ is taken to be piecewise sinusoidal. The source of excitation is the magnetic frill and boundary matching is enforced on the surface of the monopole element rather on its axis. The element radius b is assumed to be much smaller than the wavelength λ. The monopole element may be assigned perfect conductivity or finite conductivity as desired. With Galerkin's method, the calculated input impedance Z_{in} is believed to be accurate for short, medium, and long monopole elements. If the element length exceeds six wavelengths, however, one may wish to increase the dimension IDM in the main program and subroutine TSPAR.

11

Radial-Wire Ground Planes

11.1 METHOD OF MOMENTS: $0 \leq ka \leq 250$

11.1.1 Model Description

The antenna geometry consists of a vertical monopole element, of length h and radius b, with a ground plane consisting of N equally spaced radial wires, of length a and radius b_w, at a depth z_0 below a flat earth surface (see Fig. 92). The antenna excitation has a time dependence $\exp(j\omega t)$ at a radian frequency $\omega = 2\pi f$ (rad/sec) of frequency f (Hz) and free-space wavelength $\lambda = c/f$ where c is the free-space velocity of light. The earth, with a dielectric constant ε_r and conductivity σ (S/m), has a complex relative permittivity $\varepsilon^*/\varepsilon_0 = \varepsilon_r(1 - j\tan\delta)$ where $\tan\delta =$ loss tangent $= \sigma/(\omega\varepsilon_r\varepsilon_0) = 60\lambda\sigma/\varepsilon_r$. The monopole element and radial wires are assumed to be of infinite conductivity. An arbitrary field point $P(r, \theta, \phi)$ is designated by spherical coordinates r, θ, ϕ with origin O at the base of the monopole element.

G. J. Burke of Lawrence Livermore National Laboratory has developed a method-of-moments program NEC-GS for determining the electrical properties specifically for an antenna with that geometry [102,157,158]. For wire antennas that have rotational symmetry in the azimuthal direction, NEC-GS is more efficient than NEC-3 because the input parameter specification is simplified and the matrix size (total number of wire segments or current variables) is reduced. For example, instead of specifying the coordinates for each segment of N radial wires, it is only necessary to specify the segment coordinate for a single wire. Furthermore, the matrix size for N radial wires with k segments/wire is reduced from kN to k when the number of rotations M equals N.

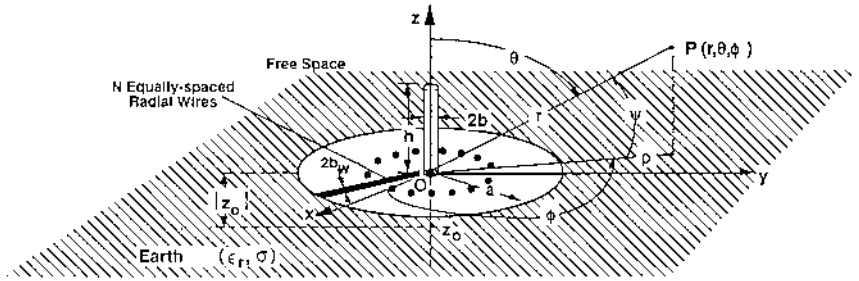

FIGURE 92 Monopole element on a radial-wire ground plane above flat earth.

The maximum matrix size for NEC-GS, as implemented by LLNL, limits the number of unknown current variables (or wire segments) to $N = 50$. The MITRE Corporation extended the maximum matrix size by a factor of 10 to $N = 500$ for NEC-GS [169]. As a rule of thumb, the method of moments gives reasonably accurate and convergent results for $N = 2\text{–}3\,ka$ (see Sec. 4.2). For $N = 500$, the maximum ground plane radius in wavenumbers is $ka \approx 250$.

Input parameter guidelines to NEC-GS are given in [158]. The following guidelines [159] may also be of interest to the user:

1. Wire intersections are assumed to be connected if two wires are within each other by 1/1000 of a segment length.
2. Horizontal wires on the air side of the earth interface should not approach the earth's surface to within the greater of $10^{-6}\lambda$ or 2–3 times the wire radius.
3. A monopole segment that is connected to a horizontal wire should be at least as short as the height of the horizontal wire above the earth's surface.
4. The physical junction of several radial wires with a vertical element is modeled as a singular point (a node) without regard as to whether or not the radial wires are conically tapered to physically fit around the vertical element.
5. The wire currents at a mode are constrained to satisfy Kirchhoff's current law without regard for current leakage into the earth.
6. The format for the field of input parameters, as illustrated on page 5 of [158], should be meticulously followed. For example, in the GR card that specifies the integer number of ground radials, the omission of the concluding comma increases the number of radials by a factor of 10.
7. In the NEC-3 and NEC-GS programs, the segment length should be at least four times longer than the segment radius. If not, the extended

kernal option (IK card) should be used for segment lengths as small as one segment radius.

8. The difference in radii of two adjoining wire segments (or two wires at a junction) should be minimized. A method for minimizing the difference in radii is the tapering of segment radii along one of the adjoining wires.
9. In the rotational model, a vertical monopole element of radius b may be represented by a cage of M vertical elements each of radius b_w along a circumference of radius b. Best results are obtained by $b_w = b/M$ so that the rotational elements have a group surface area equal to that of the original element [160,161]. Rotational model representations of a vertical dipole element, a vertical monopole element with no ground plane, and a monopole element with a radial wire ground plane—all in proximity to earth—are shown in Figs. 93–95, respectively. In the rotational model for a radial wire ground plane, the number of rotations M is equal to the number of radial wires, and the radius of the rotational vertical elements is equal to the radius b_w of the radial wires (see Fig. 95).

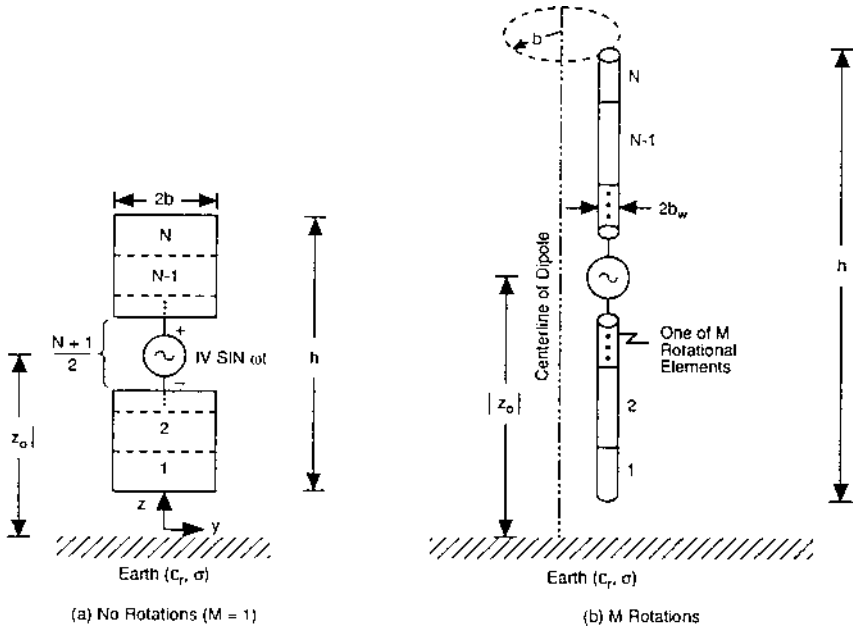

FIGURE 93 Rotational model representation of a vertical dipole element in proximity to earth.

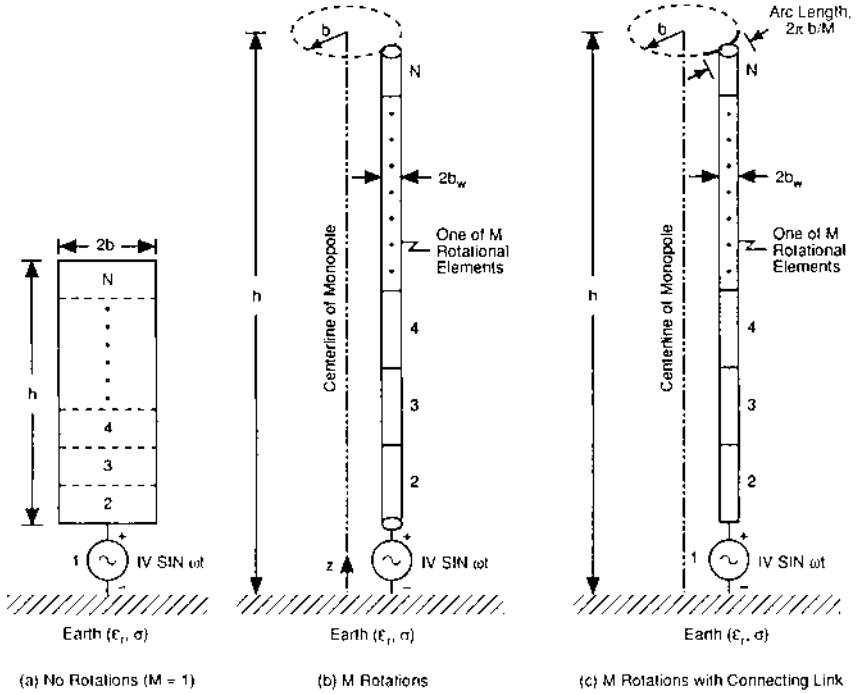

FIGURE 94 Rotational model representation of a vertical monopole element in proximity to earth.

When the rotational model is not used ($M = 1$), the output parameters represent those of the physical antenna. However, when the rotational model is used, the output parameters are those of the rotational elements and not those of the physical antenna. The algebraic operations required on the rotational model output parameters to obtain the output parameters for the physical antenna are summarized in Table 28.

11.1.2 Validation

The Numerical Electromagnetics Code (NEC) is a method-of-moments computer program by Lawrence Livermore National Laboratory (LLNL) for predicting the performance of wire-element antennas above or buried in flat earth [99,100]. In an early version (NEC-1), the effect of the air–ground interface was included by applying a plane-wave Fresnel reflection coefficient approximation to the field of a point source [162,163]. The NEC-2 version, while still retaining the Fresnel reflection coefficient model as an option, provides a more accurate option by

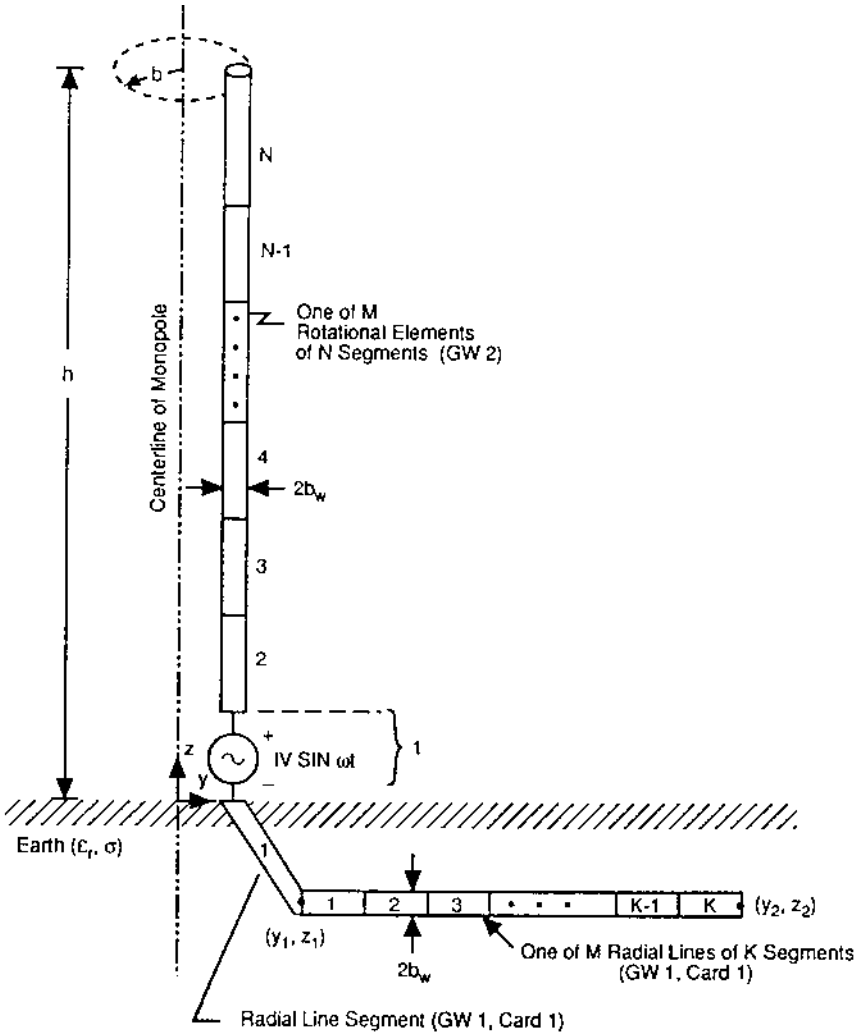

FIGURE 95 Rotational model representation of a monopole element of radius b with a ground plane of M radial wires of radius b_w in proximity to earth.

numerically evaluating Sommerfeld integrals [99,100]. Version NEC-3 extends the NEC-2 version to cases where bare wire segments are below the air–earth interface [164]. Version NEC-GS is a more efficient version of NEC-3 for wire antennas that have rotational symmetry in the azimuthal direction, such as a monopole element with uniform radial-wire ground plane [102,157,158]. Version

TABLE 28 Algebraic Operations to Obtain Output Parameters of Physical Antenna When Using a NEC-GS Rotational Modal with M Rotations

Output parameter of physical antenna	Operation required on the rotational model output parameter
Current on vertical element (amperes)	Multiply by M
Current on radial wire (amperes)	As printed out
Input impedance of vertical element (ohms)	Divide by M
Input admittance of vertical element (mhos)	Multiply by M
Radiation efficiency[a] (numeric)	Divide by M
Gain (dB)	Subtract $10 \log_{10} M$

[a] Radiation efficiency = one-half of printed out value of average power gain for cases when the antenna is in proximity to lossy earth.

NEC-3I extends NEC-3 to include the case of insulated wire [165,166]. Version NEC-4 avoids loss of precision when modeling electrically small structures and provides accurate modeling of stepped-radius wires and junctions of tightly coupled wires [167].

The NEC-2 program is available to the public, whereas the NEC-3, NEC-GS, NEC-3I, and NEC-4 programs are presently available to the U.S. Department of Defense contractors after completion and approval of a NEC order form obtainable from LLNL.

Code documentation has been produced by LLNL for the NEC-2 version and, in a more limited form, for the NEC-3, NEC-GS, NEC-3I, and NEC-4 versions. The NEC-2 documentation consists of theory, code, and a user's guide [99]. The NEC-3 [164], NEC-GS [158], NEC-3I [165], and NEC-4 [167] are in the form of user's guide supplements. The NEC-2 user's guide and NEC-3, NEC-GS, and NEC-4 user's guide supplements give examples of input and output files for most of the options available.

Code validation efforts by LLNL, for antennas near ground, are summarized in [168]. Additional validation efforts by the MITRE Corporation are discussed in [169]. Validation efforts pertaining specifically to NEC-GS are now reviewed.

LLNL [168] has compared NEC-GS numerical results with theoretical results from the variational method of Wait and Pope [90] for the input impedance of a quarter-wave monopole element on a buried, radial-wire ground plane. The Wait–Pope variational method is an approximate implementation of the compensation theorem. Good agreement was obtained between the two models only for those cases where implementation of the variational method is expected to be valid, namely for ground planes of sufficient density (the number N of radial

wires is large) and of sufficient extent (the length a of the radial wires are at least a wavelength in earth). Unlike the NEC-GS method-of-moments model, the variational method never solves for the current on the radial-wire ground plane, but instead approximates the current distribution with that for a perfect ground plane (but truncated because of the finite extent of the radial wires). Consequently, the Wait–Pope variational method yields inaccurate results of input impedance for *small* ground planes in proximity to earth (see Sec. 11.3).

The NEC-GS method-of-moments program is probably the best available model for monopole elements with radial-wire ground planes (just as Richmond's method-of-moments program is the best available model for monopole elements with disk ground planes), provided that the ground planes are not so large to cause precision errors.

In the NEC-GS user's guide [158], the test case is for a quarter-wave monopole element with six buried ground plane radial wires. Test case numerical results obtained from NEC-GS with no rotations ($M = 1$) agree to within 0.01% to those obtained from NEC-3 (see [169], Table 8).

Numerical results obtained from NEC-GS—for a dipole element, for a monopole element, and for thin and thick monopole elements with six buried ground plane radial wires, with the rotational geometries of Figs. 93–95, respectively—are in close agreement with those from the NEC-3 Sommerfeld integral option provided that the total surface area of the vertical rotational elements is equal to the surface area of the physical monopole element (see [169], Tables 9–11).

For a sufficiently large number N of radial wires, NEC-GS numerical results should approach those of RICHMOND4 for the same antenna geometry but with a disk ground plane. Close agreement for radiation efficiency is obtained with $N = 128$, for ground planes in close proximity to earth and ground plane radii as large as $ka = 4$ wavenumbers (see Sec. 10.2.3, Fig. 90).

11.1.3 Radiation Pattern Degradation by Feed Cable

The typical feed for a monopole antenna is a coaxial line of length/whose inner conductor is connected—through a hole at the center of the ground plane—to the monopole element and whose outer conductor is connected—by means of a flange—to the ground plane. The condition of zero current on the external surface of the outer conductor of the coaxial line feed cable (or its shield cable) is never realized for monopole elements with imperfect ground planes. However, this condition is approximated in practice with lossy ferrite toroidal cores around the feed cable (see Sec. 2.4, Fig. 2). The ferrite toroids must extend a sufficient distance along the cable so that (1) the monopole element field, impinging upon the cable, is weak and (2) the current, edge diffracted underneath the ground plane to the external surface outer conductor of the feed, is adequately attenuated.

When the monopole antenna is in proximity to earth, the monopole element field impinging upon the cable (and the resultant induced current on the cable) can be minimized by burying the cable at a sufficient depth below the surface of the earth. The reradiated field from the induced current is further attenuated by the earth above the cable. The cable need not be buried to a depth as large as the earth skin depth to be effectively shielded by the earth. For example, the penetration depth for a plane wave incident normally on Medium Dry Ground at 15 MHz is 21 m (see Sec. 8.2, Table 16). If the feed cable is buried at a depth of 21 cm (1/100 of the penetration depth), most of the current on the exterior surface of the outer conductor of the feed cable will not be reradiated into the air medium but instead will be leaked off into the earth (see Fig. 96).

The smaller and less dense the ground plane, the more severe is the radiation pattern degradation by the feed cable. A radial-wire ground plane, being less dense than a disk ground plane, is therefore more susceptible to effects of the feed cable. A perfect ground plane provides complete protection against pattern degradation by the feed cable.

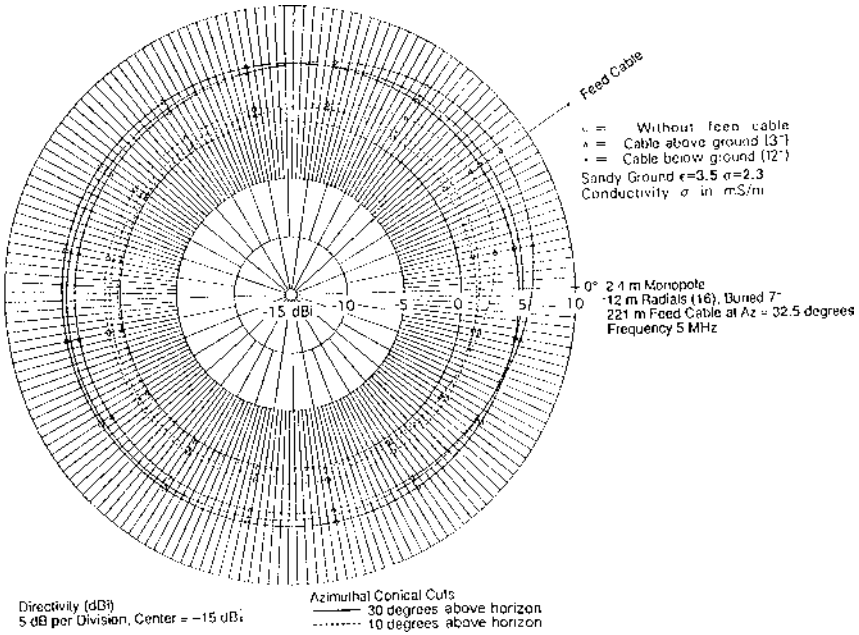

FIGURE 96 Feed-cable effects on directivity (azimuthal variation at 30° and 10° above horizon) of a 2.4 m monopole element with a 16 radial-wire ground plane buried in sandy Soil at 5 MHz (Lagace [170], Fig. 40, 1991).

Improved repeatability, reciprocity, and fidelity of antenna pattern measurements—at The MITRE Corporation VHF antenna range—were achieved with the aid of baluns; lossy ferrite cores on the transmitter and receiver cables; and trim cable runs (see Sec. 6.6.2, Fig. 54).

The feed cable can be modeled as a radial wire in the NEC-GS program for a monopole element with a radial-wire ground plane. Extensive NEC-GS numerical results of the effect of buried and unburied feed cables have been obtained in the HF band by R. L. Lagace [170,171] for an electrically short monopole element with a 16 radial-wire ground plane buried in various types of earth. A feed cable of normalized length $I/\lambda = 3.7$ wavelengths at 5 MHz causes an otherwise omnidirectional azimuthal directivity pattern at 10° above the horizon to have a maximum directivity change of +3 dB at the cable azimuthal direction when the cable is 3 in. *above* sandy soil (see Fig. 96). When the same cable is 12 in. *below* the soil, the increase in directivity at the cable azimuthal direction is reduced to less than 1 dB. The same feed cable causes a change in field phase at all azimuthal angles, except at ±90° from the cable azimuthal direction, with a maximum phase change of +13.6° at the cable azimuthal direction when the cable is 3 in. above sandy soil (see Fig. 97). When the same cable is 12 in. below the soil, the maximum phase change at the cable azimuthal direction is increased to +15.6°.

Full-scale radiation pattern measurements of ground-based monopole antennas have been obtained by G. H. Hagn [172–174] utilizing an airborne RELODOP measurement system [173] and an open-wire line (OWL) ground constants measurement kit [174]. The azimuthal pattern of a 7.5 ft monopole element with a 16 radial-wire ground plane buried in sandy soil at 28 MHz, measured by Hagn in clockwise and counter-clockwise flights at 8.9° above the horizon, is approximately omnidirectional (within 1 dB attributable to terrain roughness) except for a 3 dB increase in directivity at the cable approximate direction (see Fig. 98). The 700 ft feed cable in Fig. 98 is buried except for the first 75 ft (= 2.12 wavelengths) that rested on terrain that was flat in the NE direction of the cable.

11.1.4 Numerical Results

NEC-GS numerical results for radial-wire ground planes, have been reported by Burke et al. [102,157] and Weiner et al. [146]. Extensive NEC-GS numerical results for electrically short monopole elements with radial-wire ground planes have been obtained by Lagace [170,171]. Additional NEC-GS numerical results of radiation efficiency and input impedance are presented in Figs. A7-1–A7-36 of App. A.7 for quarter-wave elements with electrically small ground planes. G. J. Burke of Lawrence Livermore National Laboratory provided the data for

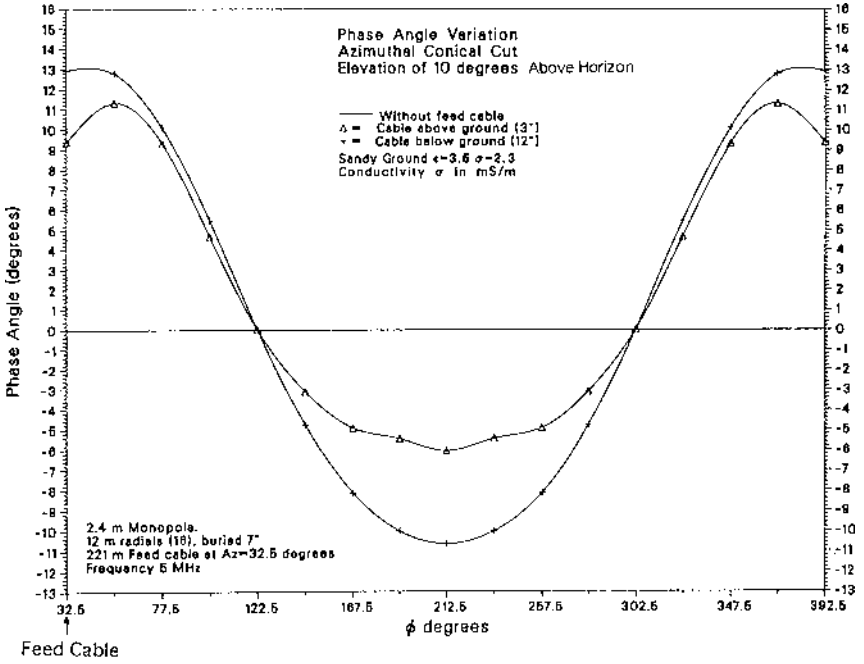

FIGURE 97 Feed-cable effects on field phase (azimuthal variation at 30° above horizon) of a 2.4 m monopole element with a 16 radial-wire ground plane buried in sandy soil at 5 MHz (Lagace [170], Fig. 45, 1991).

App. A.7 and S. Zamosciank of The MITRE coorporation developed the computer plots of the data.

Numerical results of directivity are not presented in App. A.7 because, for electrically small ground planes in close proximity to earth, the directivity is not appreciably different from the results presented in App. A.6 for disk ground planes. In App. A.6, the directivity for quarter-wave elements on disk ground planes varies by less than 1 dBi as the normalized ground plane radius is varied from 0 to 8 wavenumbers.

Numerical results for input impedance and radiation efficiency are given in App. A.7 for ground planes at normalized depths $z_0/\lambda = 10^{-4}$, -10^{-4}, and -10^{-2} below earth where the notation $z_0/\lambda = -10^{-4}$ designates that the ground plane is at a height 10^{-4} wavelengths above earth. The antenna parameters are defined in Sec. 11.1. The results are independent of frequency because all parameters, including the earth's complex relative permittivity $\varepsilon/\varepsilon_0$, are normalized to the free-space wavelength λ. Results are presented for $\varepsilon/\varepsilon_0 = 15 - j1.5$, $15 - j15$, $15 - j150$, $15 - j1500$ and for parameters with fixed values

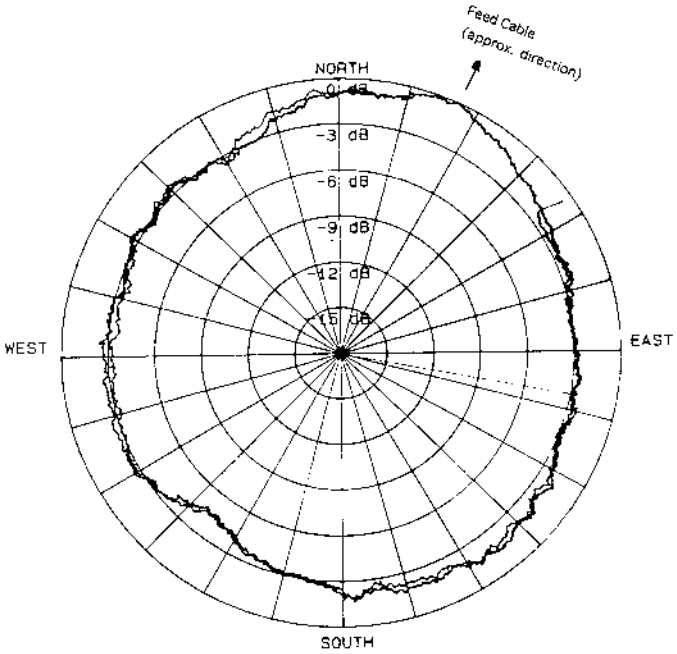

Monopole Element: 7.5 ft.
Ground Plane: 16 symmetrical 40-ft. radial wires buried at a depth of 7 in. in sandy soil
Feed Cable: 700-ft. coaxial line (first 75 ft. unburied and the remaining 625 ft. buried 3 ft. in sandy soil) in an approximate direction 27 deg. NE (compass reading of 32 deg. NE corrected for magnetic declination of 1 deg. 45 minutes W at Eglin AFB, FL and uncertainty in location of first 75 ft. of cable)
Measured Soil: $\varepsilon = 3.5$, $\sigma = 2.3 \times 10^{-3}$ S/m
Frequency: 27.925 MHz

FIGURE 98 Measured azimuthal pattern (at 8.9° above horizon) of a 7.5 ft. monopole element with a 16 radial-wire ground plane buried in sandy soil at 28 MHz (Hagn, 1990).

$h/\lambda = 0.25$, $b/\lambda = 10^{-5}$, $b_w/\lambda = 10^{-5}$. In each figure, results are given for $N = 4$, 8, 16, 32, 64, and 128 where N is the number of radial wires.

The radiation efficiency η is the ratio of the far-field radiated power to the available input power. The far-field radiation is confined to the air medium for earth conductivity $\sigma > 0$. The radiation efficiency is a measure of the power loss in the earth because the monopole element and radial wires are assumed to be of infinite conductivity. With increasing number of the radial wires, the radiation efficiency increases monitonically and approaches that for a disk ground plane

(cf. Sec. 10.2.3, Fig. 90). The radiation efficiency also increases monotonically with increasing length of the monopole element (not shown in App. A.7 but see App. A.8). The radiation efficiency exhibits resonances with increasing wire length for a sparse number of radial wires.

The input resistance and input reactance asymptotically approach the values for a disk ground plane as the ground plane density approaches infinity, i.e., as the number of radial wires $N \rightarrow \infty$, as seen by comparing the results of Apps. A.6 and A.7. A unique characteristic of radial-wire ground planes is the resonances in input impedance and radiation efficiency that occur for a sparse number of radial wires provided the earth is not of high conductivity. These resonances occur apparently because the currents on the wires are not closely coupled, unlike the case for a high density of radial wires or the case of a disk ground plane.

11.2 VARIATIONAL METHOD: $ka \geq 6$; $N \geq 100$

The input impedance $Z_{\text{in}} = R_{\text{in}} + jX_{\text{in}}$ of a vertical monopole element centered on a radial-wire ground plane, at a height $z_0 = 0$ above flat earth, can be estimated by utilizing a variational method after Wait and Pope [90]. The ground plane is assumed to be at the surface of the earth but in the earth medium. The geometry and circuit parameters are the same as described in Sec. 11.1.1. The method determines the difference $\Delta Z_T = \Delta Z + \Delta Z_s$ of input impedance from that with a perfect ground plane where ΔZ is the difference in input impedance of a monopole element with a disk ground plane from that with a perfect ground plane and ΔZ_s is the difference in input impedance of a monopole element with a radial-wire ground plane from that with a disk ground plane. If Z_{inf} denotes the input impedance of a monopole element with a perfect ground plane, then

$$Z_{\text{in}} = \Delta Z_T + Z_{\text{inf}} = \Delta Z + \Delta Z_s + Z_{\text{inf}}. \tag{11.2.1}$$

The difference ΔZ of input impedance of a monopole element with a disk ground plane from that with a perfect ground plane is determined by the Wait–Surtees variational method as discussed in Sec. 10.3. The input impedance Z_{inf} of a monopole element with a perfect ground plane is determined by the method of images combined with the method of moments as discussed in Sec. 10.4.

In both the Wait–Surtees and Wait–Pope variational methods, the monopole element is assumed to have a sinusoidal current distribution. Since the current distribution departs significantly from a sinusoidal form when the element is thick and exceeds one-half wavelength, the variational methods may not be reliable under those circumstances. This potential problem has not been investigated.

Both the Wait–Surtees and Wait–Pope variational methods are approximate implementations of the Monteath compensation theorem [95]

which in principle is exact but its implementation usually involves approximations. Unlike the method of moments, the variational methods never solve for the current on the radial-wire ground plane, but instead, approximate the current distribution with that for a perfect ground plane (but truncated because of the finite extent of the radial wires).

The difference ΔZ_s of input impedance of a monopole element with a radial ground plane from that with a disk ground plane is given approximately by Eq. (10) of [90] as

$$\Delta Z_s \approx (1/I_0)^2 \int_0^a Z_{\text{eff}}[H_\phi^\infty(\rho,\, \pi/2)]^2 2\pi\rho \, \mathrm{d}\rho \tag{11.2.2}$$

where

$I_0 =$ input current at the base of the monopole element (A)

$H_\phi^\infty(\rho,\, \pi/2) =$ magnetic field intensity at a radial distance ρ and elevation angle $\theta = \pi/2$ rad for a monopole element with a perfect ground plane (A/m)

$Z_{\text{eff}} =$ effective impedance of the radial-wire grid ground plane in parallel with the wave impedance of the earth (ohm).

For a monopole element with a sinusoidal current distribution and no top loading, the magnetic field intensity $H_\phi^\infty(\rho,\, \pi/2)$ is given by Eq. (5) of [90] as

$$H_\phi^\infty(\rho,\, \pi/2) = -jI_0[2\pi\rho \sin(2\pi h/\lambda)]^{-1}[\exp(-j2\pi r/\lambda) - \cos(2\pi h/\lambda)\exp(-j2\pi\rho/\lambda)] \tag{11.2.3}$$

where $r = (h^2 + \rho^2)^{1/2}$.

If each radial-wire segment, at a radial distance ρ is assumed to be approximately parallel to the corresponding segment of the adjoining radial wires and its wire radius b_{w} is small compared to the spacing $s = (2\pi/N)\rho$, then the effective impedance Z_{eff} is given by Eq. (7) of [90] (see also Sec. 12.3) as

$$Z_{\text{eff}} = Z_g(0)Z_e/[Z_g(0) + Z_e];\ \text{locally parallel wires}, \quad b_{\text{w}} \ll s \tag{11.2.4}$$

where

$Z_g(0) =$ parallel-wire grid intrinsic impedance at normal incidence ($\theta = 0$) or at height $Z_0 = 0$ (ohms)

$$= j(\mu_0/\varepsilon_0)^{1/2}(s/\lambda)\ln(s/2\pi b_{\text{w}}) \tag{11.2.5}$$

$Z_e =$ earth intrinsic impedance (ohms)

$$= (\mu_0/\varepsilon_0)^{1/2}\,[\varepsilon_{\text{r}}(1 - j60\lambda\sigma/_{\varepsilon})]^{1/2}. \tag{11.2.6}$$

(©1989 IEEE)

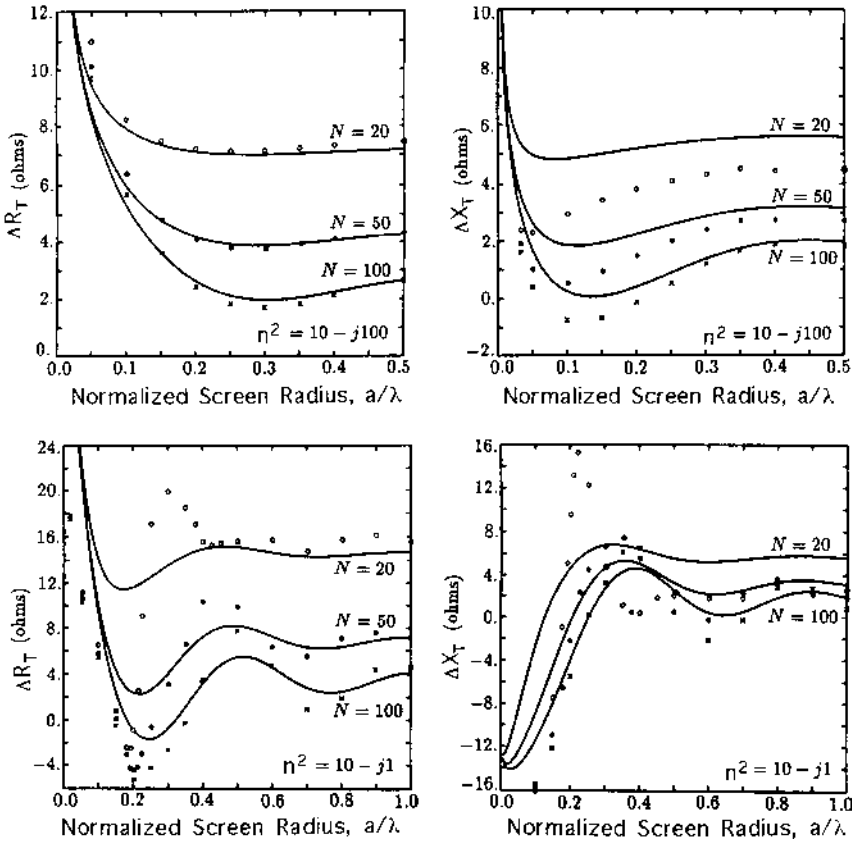

FIGURE 99 NEC-GS (circles) and Wait-Pope (solid line) values of input impedance difference $\Delta Z_T = \Delta R_T + j\Delta X_T$, from that with a perfect ground plane, for a thin ($b/\lambda = 10^{-6}$) quarter-wave monopole element with a thin ($b_w/\lambda = 10^{-6}$) buried radial-wire ground plane at depth $Z_0 = 0$ below earth (Burke and Miller, 1989).

Burke and Miller [102] have compared the input impedance difference $\Delta Z_T = \Delta R_T + j\Delta X_T$ obtained by the Wait–Pope variational method with that obtained by the method-of-moments NEC-GS. The results obtained by the two methods for a thin quarter-wave monopole element are in good agreement provided that the number N of radial wires is $N \geq 100$ and the normalized ground-plane radius ka is $ka \geq 6$ (see Fig. 99). Since NEC-GS is valid for N as

small as $N = 3$ and ka as small as $ka = 0$, then it is concluded that the Wait–Pope variational method is valid for $N \geq 100$ and $ka \geq 6$. In the Wait–Pope variational method the ground-plane radius a should be at least as large as one wavelength in earth.

12

Wire-Mesh Ground Planes

12.1 MODELING LIMITATIONS

The antenna geometry consists of a vertical monopole element (length h and radius b) on a wire-mesh ground plane of radius a at a height z_0 above flat earth. The parameter z_0 may be positive either when the ground plane is *above* earth (as in Sec. 8.1, Fig. 63) or *below* earth (as in Sec. 11.1, Fig. 92). The antenna excitation has a time dependence $\exp(j\omega t)$ at a radian frequency $\omega = 2\pi f$ (rad/sec) of frequency f (Hz) and free-space wavelength $\lambda = c/f$ where c is the free-space velocity of light. The earth, with a dielectric constant ε_r and conductivity σ (S/m), has a complex relative permittivity $\varepsilon^*/\varepsilon_0 = \varepsilon_r(1 - j\tan\delta)$ where $\tan\delta =$ loss tangent $= \sigma/(\omega\varepsilon_r\varepsilon_0) = 60\lambda\sigma/\varepsilon_r$. The monopole element and ground plane are assumed to be of infinite conductivity unless stated otherwise. An arbitrary field point $P(r, \theta, \phi)$ is designated by spherical coordinates r, θ, ϕ with origin O either at the air–earth interface below the monopole element (as in Sec. 8.1, Fig. 63) or at the base of the monopole element above the air–earth interface (as in Sec. 11.1, Fig. 92).

The wire-mesh ground-plane geometry is one of the following forms: (1) bonded radial–concentric mesh, (2) parallel-wire grid, (3) unbonded rectangular mesh, and (4) bonded rectangular mesh (see Fig. 100).

A grid of wires is considered *bonded* to another grid of wires if the electric-field differential between the two grids is zero at each intersection of the two grids. In such a case, the two grids form a bonded mesh in which each intersection is an electrical node common to both grids whose currents, into (+) and away (−) from the node, sum to zero. At each intersection of *unbonded* mesh, the current is continuous along each grid wire, and its electric field and current differ

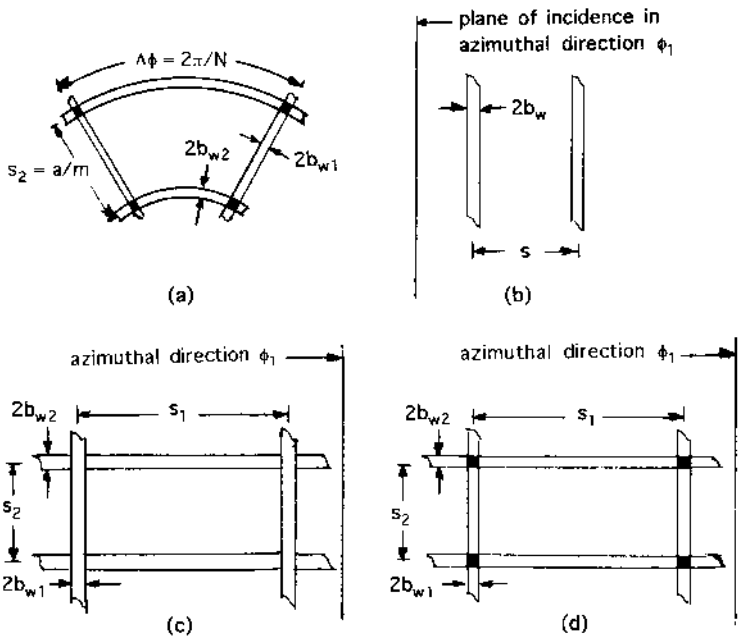

FIGURE 100 Wire-mesh ground-plane geometries: (a) bonded radial–concentric mesh; (b) parallel-wire grid; (c) unbonded rectangular mesh; (d) bonded rectangular mesh.

from those of the other intersecting grid wire. In unbonded mesh, the mutual coupling of currents from one grid to the other is minimized when the two grids are orthogonal to one another. Both a bonded-mesh ground plane and an unbonded-mesh ground plane have vastly different electrical properties from those of a ground plane fabricated from mesh panels that are bonded but are electrically disconnected at the junctions between panels.

Progressing from (a) to (d) in Fig. 100, the bonded radial–concentric mesh ground plane [Fig. 100(a)] is similar to a radial ground plane of radius a, with N wires of radius b_{w1} and azimuthal spacing $\Delta\phi = 2\pi/N$ rad, except that the radial wires are connected by m concentric wires of radius b_{w2} and spacing $s_2 = a/m$.

The parallel-wire grid ground planes [Fig. 100(b)], of wire spacing s and radius b_w, are in a plane perpendicular to the plane of incidence with wires assumed to be parallel to the plane of incidence in the azimuthal direction ϕ_1.

The rectangular-mesh ground planes [Fig. 100(c) and (d)], in a plane perpendicular to the plane of incidence, consist of two parallel-wire grids, one in the azimuthal direction ϕ_1 and the other in the azimuthal direction $\phi_1 + 90°$.

The first wire grid consists of wires of spacing s_1 and radius b_{w1} and the second wire grid consists of wires of spacing s_2 and radius b_{w2}. The rectangular-mesh ground plane is unbonded [Fig. 100(c)] or bonded [Fig. 100(d)] if the two parallel-wire grids are electrically disconnected or connected, respectively, to one another.

In applications requiring physically large ground planes, a bonded radial–concentric mesh ground plane may offer advantages in fabrication, cost, or maintainability. For example, an 8-ft diameter ground plane, of bonded radial–concentric mesh, on an outdoor roof-top VHF antenna range may offer better resistance to wind damage than a disk ground plane (see Chapter 5 and Sec. 6.6, Fig. 57). On the other hand, large ground planes constructed from bonded-mesh *panels* may offer an advantage in fabrication but a disadvantage in maintainability, particularly if adverse environmental conditions degrade the electrical connections between panels (see Sec. 8.3).

A monopole element with a wire-mesh ground plane may be modeled by the method of moments, to determine all electrical properties of the antenna (Sec. 12.2), and the method of images with Fresnel reflection, to determine the space-wave far-fields (Sec. 12.3).

The method of moments Numerical Electromagnetics Code (NEC) for wire elements, of Lawrence Livermore National Laboratory, is well suited for modeling wire-mesh ground planes that are not too large. The method of moments has the capability of determining the antenna's near fields, far-field elevation patterns, directivity, radiation efficiency, and input impedance. Its main disadvantage is that each wire segment of the mesh ground plane requires at least one unknown current variable that must be solved by the NEC program. Therefore, large ground planes require programs of large matrix size. Although the NEC programs are each configured for a particular maximum matrix size, they can be reconfigured to handle a larger matrix size. The maximum matrix size is inherently limited by the computing speed of the computer and the precision of the program. With double precision and well-conditioned matrices, the maximum matrix size is inherently limited by the computing speed of the computer. Bonded radial–concentric mesh ground planes (Sec. 12.2.1) are best modeled with NEC-GS program that minimizes matrix size by taking advantage of the azimuthal symmetry of the ground plane. Rectangular-mesh ground planes (Sec. 12.2.2) are best modeled with NEC-4 program that is suitable for insulated (unbonded) wires, bare (bonded) wires, and ground planes with no azimuthal symmetry.

In the absence of a ground plane, the method of images with Fresnel reflection determines the antenna's far-field elevation pattern (uniform in the azimuthal direction), directivity, and *approximate* radiation efficiency (see Sec. 9.2). In the presence of a mesh ground plane of infinite extent, the method of images with Fresnel reflection is limited to determining the space-wave fields at a far-field point $P(r, \theta, \phi)$ in only certain azimuthal directions related to

the orientation of the wire-mesh. The Fresnel reflection coefficient $R_v(\theta)$ is a function of the wire-mesh impedance Z_g in parallel with the intrinsic impedance Z_e of earth (Sec. 12.3.1). The wire-mesh impedance Z_g for a parallel-wire grid is determined in Sec. 12.3.2.

12.2 METHOD OF MOMENTS

12.2.1 Bonded Radial–Concentric Mesh

The antenna geometry consists of a monopole element with a bonded radial–concentric mesh ground plane in proximity to earth. The antenna parameters are described in Sec. 12.1.

The method of moments Numerical Electromagnetics Code (NEC-GS) provides the most accurate and complete modeling of the antenna's electrical properties provided the normalized radius ka of the ground plane is sufficiently small so that the maximum matrix size of the computer program is not exceeded. The input parameters for NEG-GS program, in the absence of the m concentric wires that are bonded to the radial wires of the ground plane, are described in Sec. 11.1.1. The NEC-GS input parameters for the m concentric wires consist of specifying *along one radial wire only*: (1) each concentric wire's location at the radial distance ρ, (2) its *half-length* $= (2\pi/N)(\rho/2)$ between the two adjoining radial wires, and (3) its wire radius b_{w2}. Each half-length should be divided into a sufficient number of segments so that no one segment exceeds approximately one-tenth of a wavelength. Each segment current is an unknown variable that must be solved for by the program. Although NEC-GS has no provision for bonding the two half-lengths of each concentric wire, the half-lengths are electrically connected because the ground-plane azimuthal symmetry imposes a null current midway along the concentric wire connecting the two adjoining radial wires.

If a radial wire is modeled by N_s segments and if the half-length of the i th concentric wire is modeled by m_{si} segments, then the number of ground-plane current variables that must be solved is $N_s + (m_{s1} + m_{s2} + \cdots + m_{sm})$. The computational time $t_f(s)$ to solve for the current variables is given by

$$t_f = (1/S)[N_s + (m_{s1} + m_{s2} + \cdots + m_{sm})]^3 \tag{12.2.1}$$

where

$S =$ computational speed of the computer (Hz)

As an example, consider the case where $m_{s1} = m_{s2} \ldots = m_{sm} = 1$, $m = N_s$, and $N_s = (a/0.1\lambda)$. For that case, $t_f = (1/S)(2a/0.1\lambda)^3$. If $S = 10^9$ Hz and $t_f = 60$ sec, then $ka = 1.23 \times 10^4$. The method of moments NEC-GS program is therefore inherently capable of solving for the unknown currents of a bonded

radial–concentric mesh ground plane of normalized radius $ka = 1.0 \times 10^4$ in a computational time of less than 1 min on a laptop computer with a computational speed of 1 GHz. The matrix fill time t_m, which is proportional to N_s^2 instead of N_s^3, should also be added to the total calculation time [158].

The NEC-GS maximum matrix size, as implemented by Lawrence Livermore National Laboratory, limits the number of unknown current variables (or wire segments) to 50. With modern computers, NEC-GS is inherently capable of solving for orders-of-magnitude more current variables. However, its maximum matrix size must be reconfigured to handle larger matrix sizes.

The input impedance, $Z_{in} = R_{in} + jX_{in}$, is significantly altered when concentric wires are bonded to a radial-wire ground plane of radius $ka \geq 1$ (see Table 29). The reason is that the concentric-wire currents can be appreciable when the wire's half-length between two adjoining radials exceeds approximately 1/20 of a wavelength—even though azimuthal symmetry of the ground plane constrains the current on each concentric wire to be zero midway between two adjoining radial wires. The numerical results in Table 29 were obtained by Burke [175] utilizing NEC-GS and NEC-3 programs for the radial-wire ground plane and radial–concentric mesh ground planes, respectively. The parameters in Table 29 correspond to those of the test antennas employed on The MITRE Corporation VHF test range (see Sec. 6.6) and to those in Table 8 of Chapter 5. The removal of the three concentric wires causes a change in input impedance $\Delta R_{in}/R_{in} = 2.2\%$, $\Delta X_{in}/X_{in} = -28.2\%$ for $ka = 0.766$ (30 MHz) and $\Delta R_{in}/R_{in} = 90.2\%$, $\Delta X_{in}/X_{in} = 307.9\%$ for $ka = 6.5$ (253.5 MHz).

12.2.2 Rectangular Mesh

The antenna geometry consists of a monopole element with a rectangular-mesh ground plane in proximity to earth. The antenna parameters are described in Sec. 12.1.

The method of moments Numerical Electromagnetics Code (NEC-4) provides the most accurate and complete modeling of the antenna's electrical properties provided the ground plane is sufficiently small so that the maximum matrix size of the computer program is not exceeded. The maximum matrix size is inherently limited by the computing speed of the computer rather than by the precision of the program when written in double precision with well-conditioned matrices.

The NEC-4 program is well suited for modeling ground planes that lack azimuthal symmetry, such as rectangular-mesh ground planes. In addition to being able to model bare wires, NEC-4 includes the NEC-3I feature of being able to model insulated wires. Therefore, NEC-4 is well suited for modeling both bonded and unbonded rectangular-mesh ground planes. The NEC-4 input parameters are described in Ref. 167. For modeling accuracy,

TABLE 29 Input Impedance of Quarter-Wave Monopole Element on a 16-Radial Wire Ground Plane With or Without 3-Concentric Wires Bonded to Radials Computed by NEC-GS and NEC-4, Respectively (after Burke [175])

	Input impedance, $Z_{in} = R_{in} + jX_{in}$ (Ω)					
	16 Radials, 3 concentric		16 Radials only		Percentage difference	
Frequency (MHz)	(1) R_{in}	(2) X_{in}	(3) R_{in}	(4) X_{in}	(5) $= \frac{(1)-(3)}{(1)}\ \Delta R_{in}/R_{in}$	(6) $= \frac{(2)-(4)}{(2)}\ \Delta X_{in}/X_{in}$
30	18.9	−36.8	18.5	−47.1	0.022	−0.282
36	19.7	−24.9	19.2	−33.8	0.023	−0.358
43	20.2	−16.8	19.7	−24.6	0.026	−0.465
54	21.6	−5.5	20.9	−12.5	0.035	−1.268
62.4	22.9	1.1	21.9	−57.7	0.047	0.636
75	25.7	9.7	23.7	2.4	0.077	0.753
86	29.7	16.4	26.0	8.1	0.126	0.507
89.7	31.9	19.0	27.1	10.2	0.150	0.462
97.5	38.0	24.1	29.9	14.3	0.214	0.404
117	71.0	24.2	43.1	23.0	0.393	−0.087
136.5	60.9	−24.1	67.3	15.0	−0.105	1.622
156	32.8	−16.7	62.2	−16.2	−0.898	0.031
175.5	26.6	−1.1	41.7	−18.9	−0.565	−0.747
195	29.8	17.3	32.0	−10.2	−0.073	1.589
214.5	80.5	34.9	29.7	0.2	0.632	0.994
234	48.6	−35.1	33.8	11.8	0.306	1.342
253.5	27.5	−10.7	52.3	22.3	−0.902	3.079

Monopole element: h (approx. quarter-wave, see Table 8), $b = 1/4$ in.
Radial wires: $N = 16$, $a = 4$ ft, $b_{w1} = 1/4$ in.
Concentric wires: $m = 3$, $b_{w2} = 1/32$ in. at $\rho = 2, 3, 4$ ft.

the rectangular-mesh spacings s_1 and s_2 should be subdivided into m_{s1} and m_{s2} segments, respectively, which do not exceed 0.1λ where λ is the free-space wavelength.

For a rectangular-mesh circular ground plane of radius a, the total number of wire-modeling segments is $(\pi/4)(4a^2)/(m_{s1}m_{s2}s_1s_2) = (\pi a^2)/(m_{s1}m_{s2}s_1s_2)$. Therefore, the number of ground-plane current variables that must be solved is $(\pi a^2)/(m_{s1}m_{s2}s_1s_2)$. The computational time $t_f(s)$ to solve for the current variables is given by

$$t_f = (1/S)[(\pi a^2)/(m_{s1}m_{s2}s_1s_2)]^3 \tag{12.2.2}$$

where S is the computational speed of the computer.

As an example, consider the case where $m_{s1} = m_{s2} = 1$ and $s_1 = s_2$. For that case, $t_f = (1/S)[(\pi(a/s_1)^2]^3$. If $S = 10^9$ Hz, $s_1 = 0.1\lambda$, and $t_f = 60$ sec, then $ka = 22.15$. For the same computational time, laptop computer, and maximum wire-segment length, the ka capability of the NEC-4 program for a rectangular-mesh ground plane is almost two orders of magnitude *less* than the ka capability of NEC-GS for a bonded radial–concentric mesh ground plane (compare with the numerical example in Sec. 12.2.1).

12.3 SPACE-WAVE FAR-FIELDS: METHOD OF IMAGES WITH FRESNEL REFLECTION, $ka = \infty$

12.3.1 Fresnel Reflection Coefficient

The antenna geometry consists of a vertically polarized Hertzian dipole of moment p at a height z_0 in air medium (0) above a half-space (1). The half-space (1) comprises: (1) the earth and (2) a wire-mesh ground plane of infinite extent ($ka = \infty$) at a height z_1 above earth (see Fig. 101). The antenna excitation has a time dependence $\exp(j\omega t)$ at a radian frequency $\omega = 2\pi f$ (rad/sec) of frequency f (Hz), free-space wavelength $\lambda = c/f$, and wavenumber $k_0 = 2\pi/\lambda$ where c is the free-space velocity of light. The earth, with a dielectric constant ε_r and conductivity σ (S/m), has a complex relative permittivity, $\varepsilon^*/\varepsilon_0 = n^2 = \varepsilon_r(1 - j\tan\delta)$ where $\tan\delta =$ loss tangent $= \sigma/(\omega\varepsilon_r\varepsilon_0) = 60\lambda\sigma/\varepsilon_r$. The wire mesh is assumed to be of infinite conductivity unless stated otherwise. The mesh-earth half-space has a complex permittivity $\varepsilon_{eff} = \varepsilon_0 n_{eff}^2$ where n_{eff} is the effective index of refraction of half-space (1) and is the subject of investigation in this Sec. 12.3. The wire-mesh parameters are described in Sec. 12.1.

The space-wave electric field $E = u_\theta E_\theta$ and magnetic field $H = u_\phi H_\phi$ at a far-field point $P(r, \theta, \phi)$ above the half-space (1) have components given by

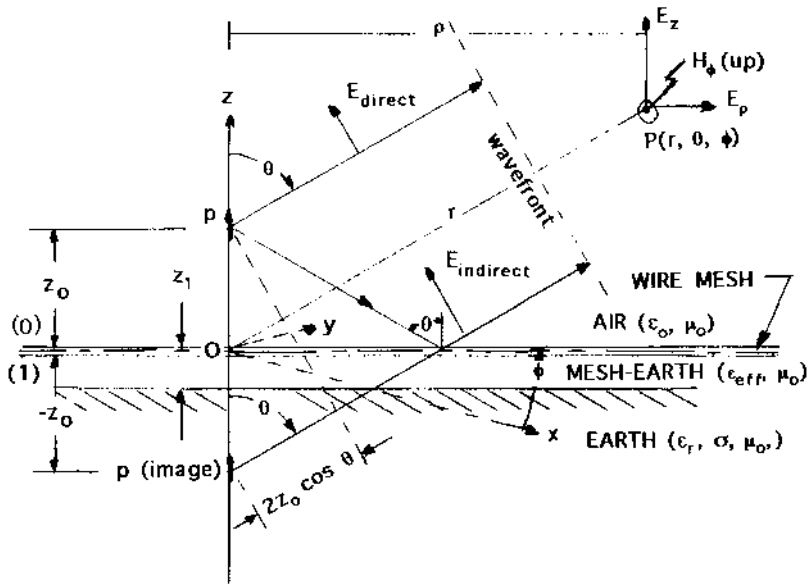

FIGURE 101 Direct and indirect rays of space wave, at a far-field point $P(r,\theta,\phi)$ in air, from a vertically polarized hertzian dipole above a half-space comprising a wire-mesh and earth.

Eqs. (9.2.6) and (9.2.7) as

$$E_\theta = A \sin\theta \exp(jk_0 z_0 \cos\theta)[1 + R_v(\theta)\exp(-j2k_0 z_0 \cos\theta)] \tag{12.3.1}$$

$$H_\phi = (1/Z_0)E_\theta \tag{12.3.2}$$

where

$A = j[(Z_0 k_0 p)/4\pi r)]\exp(-jk_0 r)$
$Z_0 =$ intrinsic impedance of free-space $= (\mu_0/\varepsilon_0)^{1/2}$
$R_v(\theta) =$ Fresnel reflection coefficient for parallel polarization

Substituting n_{eff} for n in Eq. (9.2.5),

$$R_v(\theta) = \frac{n_{\text{eff}} \cos\theta - (1 - n_{\text{eff}}^{-2}\sin^2\theta)^{1/2}}{n_{\text{eff}} \cos\theta + (1 - n_{\text{eff}}^{-2}\sin^2\theta)^{1/2}} \tag{12.3.3}$$

Defining an effective impedance $Z_{\text{eff}} = (\mu_0/\varepsilon_{\text{eff}})^{1/2} = Z_0/n_{\text{eff}}$ and dividing both numerator and denominator of Eq. (12.3.3) by n_{eff}, Eq. (12.3.3) may be expressed

as

$$R_v(\theta) = \frac{\cos\theta - (Z_{eff}/Z_0)[1 - (Z_{eff}/Z_0)^2 \sin^2\theta]^{1/2}}{\cos\theta + (Z_{eff}/Z_0)[1 - (Z_{eff}/Z_0)^2 \sin^2\theta]^{1/2}} \tag{12.3.4}$$

The correct branch in Eq. (12.3.4), of the complex quantity Z_{eff}/Z_0, is its principal value [169].

For a plane wave incident at an elevation angle θ on thin grid wires that are in a plane parallel to earth at a height z_1 above earth, the impedance Z_{eff} may be modeled after Wait [176] as a wire-grid impedance $Z_g(\theta, z_1)$ in shunt with the intrinsic impedance Z_e of earth. Accordingly,

$$Z_{eff} = Z_g Z_e/(Z_g + Z_e) \tag{12.3.5}$$

where

$$Z_e = \text{intrinsic impedance of earth (ohms)} = (\mu_0/\varepsilon^*)^{1/2}$$

$$= (1/n)Z_0 \tag{12.3.6}$$

In the absence of earth (the grid is in free-space), $z_1 = \infty$ and $Z_e = Z_0$. In the absence of the grid, the origin O is on the earth's surface, $Z_g = \infty$, and $Z_{eff} = Z_e$. The wire-grid impedance Z_g for a parallel-wire grid in proximity to earth is determined in Sec. 12.3.2.

12.3.2 Parallel-Wire Grid

Consider the case when the wire-mesh ground plane in the x–y plane (see Fig. 101) consists of a single grid of parallel wires of infinite extent in both the x and y directions where each wire is parallel to the plane of incidence in the azimuthal direction ϕ. The wires are of spacing s, radius b_w, and conductivity σ_w [see Fig. 100(b)].

The wire-grid impedance Z_g in Eq. (12.3.5) may be expressed after Wait [176] for a parallel-wire grid as

$$Z_g = jZ_0\delta(\theta)\cos^2\theta \tag{12.3.7}$$

where

Z_0 = intrinsic impedance of free-space (ohms) = $(\mu_0/\varepsilon_0)^{1/2}$
$\delta(\theta)$ = ground-plane (screen) parameter that must be determined

Although the screen parameter $\delta(\theta)$ is a function of several geometrical and electrical parameters, its dependence upon the elevation angle θ is indicated as

a reminder that Z_g is a more complicated function of θ than $\cos^2\theta$. For example, $Z_g \neq 0$ when $\theta = \pi/2$ rad.

The methodology for determining the screen parameter, as reviewed by Parker [177], usually follows three main steps:

1. Expand in series, e.g.:
   - Hankel series used by Wait [176,178]
   - Waveguide mode series used by Fan [179]
   - Floquet/Fourier series used by Otteni [180]
   - Fourier series by Skwirzynski and Thackray [181].
2. Determine series coefficients by matching electric-field tangential components at the wire surfaces so that the net value of this component vanishes; this gives the currents.
3. Calculate screen parameter in terms of series coefficients.

The full expansion after Wait [176] for the screen parameter $\delta(\theta)$ is

$$\delta(\theta) = (s/\lambda)\cos^2\theta\{\ln(s/2\pi b_w) - R_0 \ln[1 - \exp(-4\pi z_1 s^{-1} - 2\pi b_w s^{-1})] + \Delta\} + sZ_i \tag{12.3.8}$$

where

$$\begin{aligned}
R_0 &= [(1+A^2)(1-B^2) + (1-A^2)^2\sin^2\theta]/[(1+A^2)(1+B^2) \\
&\quad - (1-A^2)^2\sin^2\theta] \\
A^2 &= n^{-2}B^2 \\
B^2 &= [1 - (Z_{\text{eff}}/Z_0)^2\sin^2\theta]^{-2}\cos^2\theta \\
Z_i &= \text{internal wire impedance (ohms)} \\
&\approx (\mu_0\omega/2\sigma_w)^{1/2}(1+j)/(2\pi b_w) = (1+j)(f_{\text{MHz}}/10\sigma_w)^{1/2} \\
\Delta &= \sum \Delta_m \text{ summed from } m = 1 \text{ to } m = \infty \\
\Delta_m &= M^{-1}[1 + R_m \exp(-4\pi M z_1/s)] - m^{-1} \\
&\quad [1 + R_0 \exp(-4\pi m z_1/s)] \\
M &= [m^2 - (s/\lambda)^2\cos^2\theta]^{1/2} \\
R_m &= [(M + M_2A^2)(M - M_2B^2) + m^2(1-A^2)^2\sin^2\theta][(M + M_2A^2) \\
&\quad \times (M + M_2B^2) - m^2(1-A^2)^2\sin^2\theta]^{-1} \\
M_2 &= [m^2 - (s/\lambda)^2 n^2 C_2^2]^{1/2} \\
C_2^2 &= 1 - n^{-2}\sin^2\theta
\end{aligned}$$

In the absence of earth ($z_1 = \infty$), Eq. (12.3.8) reduces to

$$\delta(\theta) = \delta_0 + (s/\lambda)\sum\{ -(1/m) + [m^2 - (s/\lambda)^2 \cos^2\theta]^{-1/2}\} \tag{12.3.9}$$

summed from $m = 1$ to $m = \infty$, $\quad z_1 = \infty$

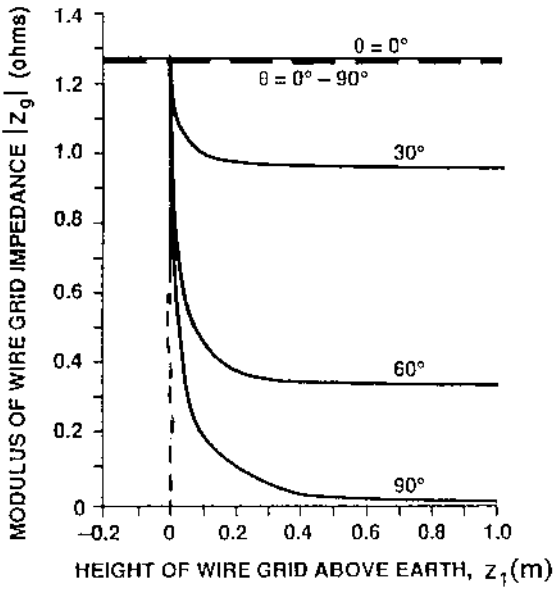

model: Wall (1962)
grid: s = 2m, $b_w = 2 \times 10^{-3}$m, $\sigma_w = \infty$
earth: $\varepsilon_r = 15$, $\sigma = 5 \times 10^{-2}$ mhos/m
frequency: f = 0.1 MHz

_____ $\delta(\theta)$, full-model screen parameter given by Eq. (12.3.8)
---- δ_σ, simplified-model screen parameter given by Eq. (12.3.10)

FIGURE 102 Parallel-wire grid impedance Z_g as a function of grid height z_1 and angle of incidence θ (Parker, 1991).

where

$$\delta_0 = \text{simplified-model screen parameter}$$

$$= (s/\lambda)[\ln(s/2\pi b_w) + (1+j)(s/b_w) \times (f_{MHz}/10\sigma_w)^{1/2}] \tag{12.3.10}$$

On the earth's surface ($z_1 = 0$) and for normal incidence ($\theta = 0$), Eq. (12.3.8) reduces to

$$\delta(\theta) = \delta_0 + (s/\lambda)\sum\{-(1/m) + 2/[[m^2 - (s/\lambda)^2]^{1/2} + [(m^2 - (s/\lambda)^2 n^2]^{1/2}]\} \tag{12.3.11}$$

summed from $m = 1$ to $m = \infty$; $\quad z_1 = 0, \quad \theta = 0$

Numerical results for the full-model screen parameter $\delta(\theta)$ and the simplified-model screen parameter δ_0 were obtained by Parker [177] and are reproduced in Figs. 102–106. The results are for the Wait (1962) model and case parameters.

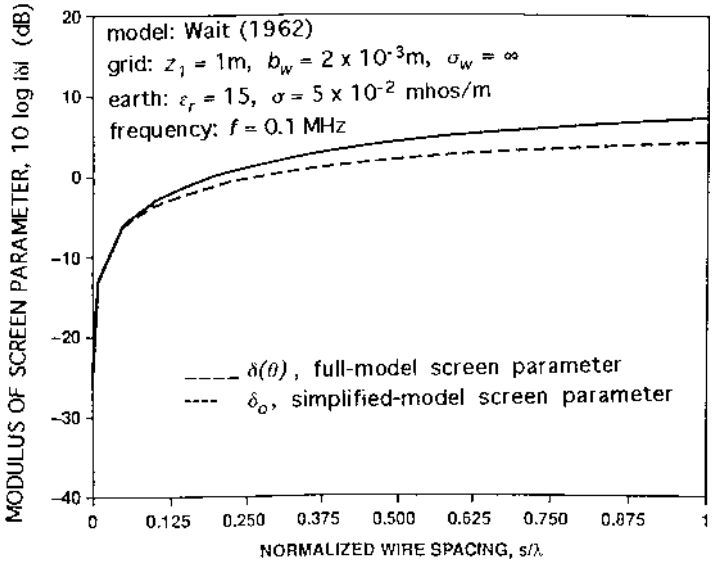

FIGURE 103 Screen parameter δ for parallel-wire grid, as a function of wire-spacing s, at angle of incidence $\theta = 0°$ (Parker, 1991).

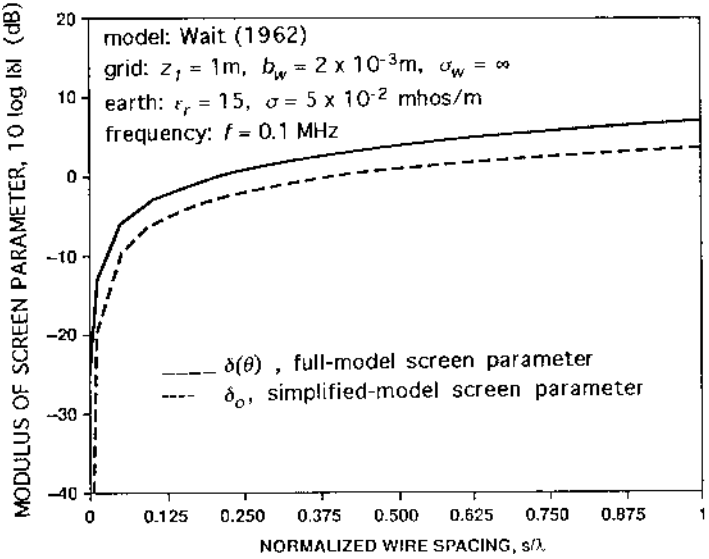

FIGURE 104 Screen parameter δ for parallel-wire grid, as a function of wire-spacing s, at angle of incidence $\theta = 90°$ (Parker, 1991).

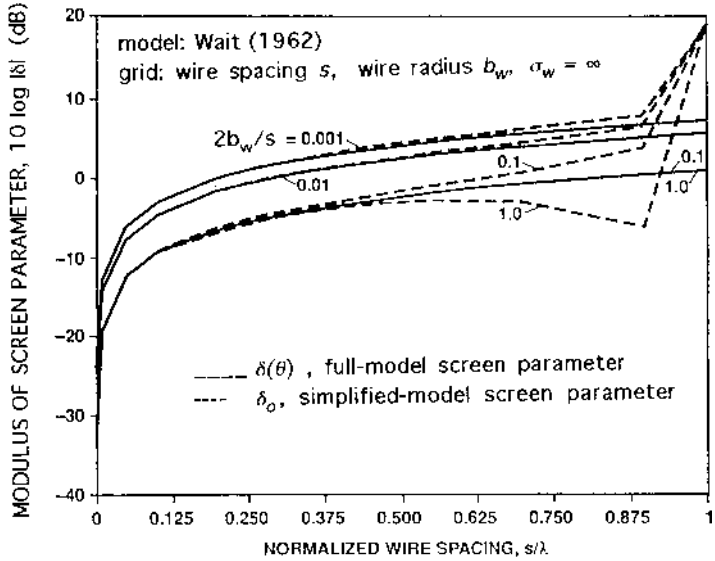

FIGURE 105 Screen parameter δ for parallel-wire grid at height $z_1 = \infty$ and for angle of incidence $\theta = 0°$ (Parker, 1991).

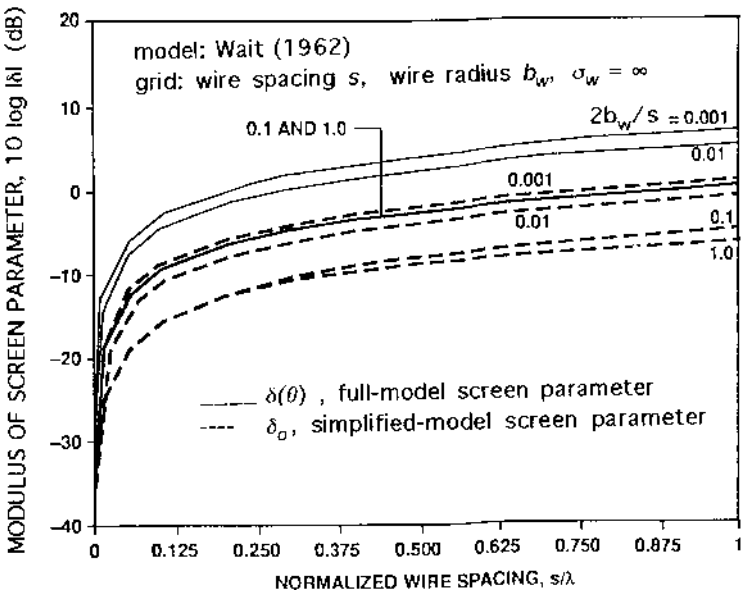

FIGURE 106 Screen parameter δ for parallel-wire grid at height $z_1 = \infty$ and for angle of incidence $\theta = 60^\circ$ (Parker, 1991).

On the basis of the numerical results, it is concluded that: $\delta(\theta) \approx \delta_0$ for $b_w/s \ll 1$ if:

1. the grid is on (or slightly below) the earth's surface, regardless of the angle of incidence, and $s/\lambda < 1$; or
2. the earth is absent ($z_1 = \infty$), the angle of incidence is normal ($\theta = 0$), and $s/\lambda \ll 1$.

13

System Performance

13.1 NOISE FACTOR AND ANTENNA GAINS IN THE SIGNAL/NOISE EQUATION FOR OVER-THE-HORIZON RADAR

13.1.1 Introduction and Summary

The predetection signal-to-noise ratio (SNR) of a radar or communication system is proportional to the *power* gain of the transmit antenna and the *directive* gain of the receive antenna, and is inversely proportional to the operating noise factor of the receiving system. The operating noise factor is approximately equal to the product of the external noise factor and the signal/noise processing factor when the system is external noise-limited, as is usually the case for over-the-horizon (OTH) radar. Unfortunately, the form of the signal/noise equation that is employed for some applications, particularly OTH radar, often does not explicitly yield these results. It is recommended that the form of the signal/noise equation be amended to explicitly yield these results rather than equivalent implicit results.

The recommended form of the signal-to-noise equation that includes both internal and external system noise and signal processing losses is discussed in Sec. 13.1.2. The recommended form conforms to the internationally-accepted definition of system operating noise factor and effective noise bandwidth but extended to include a digital receiver and signal/noise processing.

13.1.2 Recommended Form of the Signal-to-Noise Radar Equation

With reference to Fig. 107, the predetection SNR s/n of a bistatic radar system is given by

$$\frac{s}{n} = \overbrace{\frac{p_t g_t}{4\pi \ell_{p1} r_1^2} \quad \frac{\sigma_T}{4\pi \ell_{p2} r_2^2} \quad \frac{d_r \lambda^2}{4\pi}}^{s} \quad \underbrace{\frac{1}{kt_{ref} bf}}_{n} \tag{13.1.1}$$

where

$\frac{p_t g_t}{4\pi \ell_{p1} r_1^2}$ = incident power density on target

$\frac{\sigma_T}{4\pi \ell_{p2} r_2^2}$ = fraction of reflected power returned

$\frac{d_r \lambda^2}{4\pi}$ = collecting area of receive antenna

s = available signal power at the output terminals of the equivalent lossless receiving antenna (W)

n = system available noise power, after signal processing, but before threshold detection, referred to the output terminals of the equivalent lossless receiving antenna (W) = $kt_{ref} bf$

p_t = average power delivered to the transmit antenna (W) = p_0 / a_{nt}

p_0 = transmitter available average power (W)

a_{nt} = transmit transmission line loss factor accounting for the line absorption loss and the antenna reflection loss (numeric ≥ 1). The factor a_{nt}, is evaluated in Eq. (13.1.2)

g_t = transmit antenna power gain, in the direction of the target, averaged over the angle through which the target moves during a coherent integration time (numeric)

r_1 = free-space slant range from the transmit antenna to the target (m)

ℓ_{p1} = excess propagation loss factor, over that of free space loss factor $4\pi r_1^2$, from the transmit antenna to the target (numeric)

σ_T = bistatic target radar cross-section (m^2) for a bistatic angle β.

r_2 = free-space slant range from the target to the receive antenna (m)

ℓ_{p2} = excess propagation loss factor, over that of free space loss factor $4\pi r_2^2$, from the target to the receive antenna (numeric)

d_r = receive antenna directive gain, in the direction of the target, averaged over the angle through which the target moves during a coherent integration time (numeric)

λ = rf wavelength (m)

k = Boltzmann's constant = 1.38×10^{-23} (J/K)

t_{ref} = arbitrary reference noise temperature (K)

b' = effective noise bandwidth of the receiving system (Hz) = bf_p

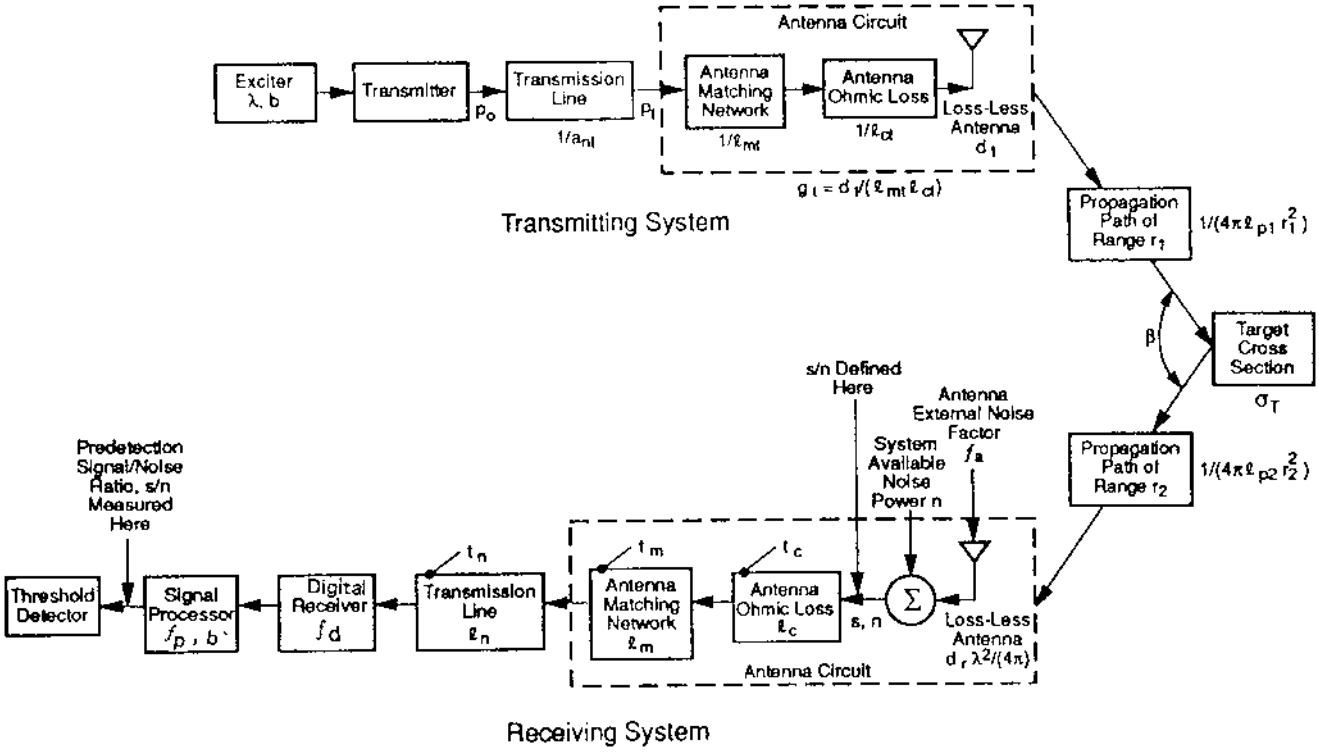

FIGURE 107 Signal/noise equivalent circuit of a bistatic radar system.

f_p = processing factor (numeric)

b = noise bandwidth of exciter and front-end (amplifier) of receiver (Hz) $= (1/g_0)\int_{\upsilon_a}^{\upsilon_b} g_{0\upsilon}\, d\upsilon$

g_0 = maximum gain of the receiving system gain $g_{0\upsilon}$ within the frequency band $\upsilon_b - \upsilon_a$ of the principal response of the receiving system (numeric)

f = system operating noise factor of the receiving system (numeric)

We follow the convention that lower case letters denote numeric values of the parameters and that upper case letters denote the parameters when expressed in dB [i.e., $10\log_{10}$ (numeric value)]. The parameters of the transmitting system have been denoted by the subscript t to distinguish them from those of the receiving system.

Equation (13.1.1) is similar to that for a radio communication system [see Eq. (6.4.1) of Sec. 6.4.2] except that Eq. (13.1.1) contains the signal factor $(\sigma_T/4\pi\ell_{p2}r_2^2)$, the signal-processing noise bandwidth factor b', and digital-receiver noise factor f_d.

Equation (13.1.1) is a simplistic representation of the signal/noise equation for OTH radar systems. The parameters are assumed to be deterministic whereas in practice the parameters ℓ_{p1}, ℓ_{p2}, σ_T, and f are usually nonstationary stochastic variables. The receiving system is treated as though it had a single receiver, whereas in practice the receiving system is comprised of many independent receivers. Furthermore, OTH radar systems are usually limited in performance by residual clutter rather than noise. The inclusion of these physical realities into the signal/noise equation is beyond the scope of this section.

For an OTH radar system, the bistatic slant ranges r_1 and r_2 are approximately equal and the bistatic angle $\beta \approx 0$. Furthermore, the terrestrial propagation path losses are usually included in the parameters g_t, d_r, and σ_T rather than in the parameters ℓ_{p1} and ℓ_{p2}. Accordingly,

$$r_1 \approx r_2 = r \tag{13.1.2}$$

$\ell_{p1} \approx \ell_{p2}$ = one-way ionospheric excess propagation loss factor including focusing gain by a spherical ionosphere

(13.1.3)

$\sigma_T \approx$ monostatic target radar cross-section (m^2) in the backscatter direction ($\beta = 0$).

The earth multipath pattern (including the null on the radio horizon) in the vicinity of the transmit and receive antennas is included in the respective gains g_t

and d_r by considering the earth as part of their respective antenna ground-plane systems. The earth multipath pattern in the vicinity of the target is included in the target radar cross-section σ_T. Power absorption by the transmit antenna earth–ground system is also included in g_t. The gains g_t and d_r also include the effects of array element weighting to achieve a desired sidelobe pattern.

The system operating noise factor f, which includes both external and internal noises and is based on an International Radio Consultative Committee (CCIR) definition of noise factor [42], is given by

$$\begin{aligned} f = {} & f_a + (\ell_c - 1)(t_c/t_{ref}) + \ell_c(\ell_m - 1)(t_m/t_{ref}) \\ & + \ell_c\ell_m(\ell_n - 1)(t_n/t_{ref}) + \ell_c\ell_m\ell_n(f_d - 1) \end{aligned} \tag{13.1.4}$$

where f_a is the receive antenna external noise factor integrated over the antenna pattern function (numeric); ℓ_c, ℓ_m, ℓ_n are the available loss factors of the receive antenna, matching network, and transmission line, respectively (numeric ≥ 1); t_c, t_m, t_n are the ambient temperatures (K) of the receive antenna, matching network, and transmission line, respectively; and f_d is the digital receiver noise factor (numeric ≥ 1). The signal/noise processing factor f_p (or simply, processing factor) is not included in the noise factors f or f_d, as was done earlier [182], but instead is more properly included as part of the effective noise bandwidth b' because f_p is not a function of the digital receiver front-end gain g_r as are the noise factors of the analog/digital (A/D) converter or finite impulse response filter (FIR) that follow the digital receiver front end. If the ambient temperatures of the antenna, matching network, and transmission line are equal to the reference temperature t_{ref}, then Eq. (13.1.4) reduces to

$$f = f_a - 1 + \ell_c\ell_m\ell_n f_d; \quad t_c = t_m = t_n = t_{ref} \tag{13.1.5}$$

The digital receiver consists of a front-end analog receiver, an A/D converter at the output of the analog receiver, and a FIR filter at the output of the A/D converter. The noise factor f_d (numeric) of the digital receiver is given by

$$f_d = f_r + (f_{A/D} - 1)(1/g_r) + (f_{FIR} - 1)(l_{A/D}/g_r) \tag{13.1.6}$$

where

f_r = noise factor of front-end analog receiver for a source impedance Z_g (numeric ≥ 1)
$f_{A/D}$ = noise factor of A/D converter (numeric ≥ 1)
g_r = power gain of analog front end (numeric)
f_{FIR} = noise factor of FIR filter (numeric ≥ 1)
$l_{A/D}$ = available loss factor of A/D converter (numeric ≥ 1)
= 1 if there is no appreciable ohmic loss associated with the A/D converter

The A/D converter noise factor $f_{A/D}$ is given by

$$f_{A/D} = 1 + [(1/12)(v_F/2^{m-1})^2(1/Z_g)][kt_{ref}b]^{-1} \tag{13.1.7}$$

where

v_F = full-scale peak voltage at input of A/D converter (V)
m = noise quantization number of bits of A/D converter (numeric)
k = Boltzmann's constant = 1.38×10^{-23} (J/K)
t_{ref} = reference noise temperature to which the noise factor is normalized (K)
b = system bandwidth *preceding* A/D converter (Hz)
Z_g = receiver source impedance (ohm).

If the A/D converter has a bipolar input range of $(+/-)$ v_F, then an input sinusoidal waveform of full-scale peak amplitude v_F will produce a digitized output signal over a period of time that contains 2^m levels whose numerical values vary in increments of unity from a value of -2^{m-1} for the first level (corresponding to $-|v_F|$ V), to 0 for the $2^{m-1} + 1$ level (corresponding to 0 V), to $2^{m-1} - 1$ for the 2^m level (corresponding to $+|v_F|$ V). It should be noted that there are 2^{m-1} levels with negative values, 1 level with a value of zero, and $2^{m-1} - 1$ levels with a positive value.

The FIR filter noise factor f_{FIR} is given by

$$f_{FIR} = 1 + [(1/12)(v_F/2^{M-1})^2(1/Z_g)][kt_{ref}b]^{-1} \tag{13.1.8}$$

where

M = noise quantization number of bits of FIR filter (numeric)

The number of bits M of the FIR filter is generally designed to be sufficiently greater than the number of bits m of the A/D converter so that the noise factor of the FIR filter is much less than that of the A/D converter.

It is convenient to set $t_{ref} = 288$K because measurements of atmospheric noise and man-made environmental noise are usually referenced to thermal noise at that temperature and because at that temperature $10\log_{10} kt_{ref} = -204.0059$ dBj is approximately a whole number.

The available loss factors ℓ_c, ℓ_m, ℓ_n and the receiver noise factor f_r are given by Eqs. (6.4.17)–(6.4.19), and (6.4.25), respectively, of Sec. 6.4.2. The available loss factors ℓ_c, ℓ_m, ℓ_n are a function of the impedance parameters and source impedances of the respective circuits and are equal to the reciprocal of the respective circuit efficiencies. The available loss factor ℓ_c of the receive antenna includes the ohmic loss of its earth–ground system. The receiver noise factor f_r is

a function of the receiver source admittance and the characteristic noise parameters f_0, r_n, y_{n0} of the receiver where

f_0 = the minimum noise factor for any possible source impedance
r_n = empirical noise parameters, with the dimension of resistance, which is a measure of the noise factor sensitivity to a change in source impedance
y_{n0} = source admittance for which $f_r = f_0$

The transmit transmission line loss factor a_{nt} is given by

$$a_{nt} = |1 - \Gamma_t \exp(-2\gamma_t d_{nt})|^2 \ell_{nt} \tag{13.1.9}$$

where

Γ_t = voltage reflection coefficient at the transmit transmission line–matching network interface (numeric)
γ_t = complex propagation constant of the transmit transmission line (m^{-1})
d_{nt} = length of transmit transmission line (m)
ℓ_{nt} = available loss factor of the transmit transmission line (numeric) given by Eq. (6.4.19) of Sec. 6.4.2 after substitution of corresponding transmitter parameters

The processing factor f_p (numeric ≥ 1) is the available power SNR at the output of a signal processor with a *matched* filter to that for the same signal processor but with a *weighted* filter. The processing factor includes range and Doppler frequency processing and is restricted to processing before threshold detection. Threshold detection is defined at the point at which radio-frequency (rf) phase information is lost. The processing factor f_p, for a radar system with range and Doppler frequency processing, is given by

$$f_p = f_{range} f_{Doppler} \tag{13.1.10}$$

where [184,185]

f_{range} = range processing factor (numeric ≥ 1) $= \left[\tau_r \int_0^{\tau_r} w_r^2(\tau)\mathrm{d}t\right] \Big/ \left[\int_0^{\tau_r} w_r(t)\mathrm{d}t\right]^2$
$f_{Doppler}$ = Doppler frequency processing factor (numeric ≥ 1)
$= \left[\tau \int_0^{\tau} w_D^2(\tau)\mathrm{d}t\right] \Big/ \left[\int_0^{\tau} w_D(t)\mathrm{d}t\right]^2$
$w_r(t)$ = weighting function (numeric) of range processing filter
$w_D(t)$ = weighting function (numeric) of Doppler frequency processing filter
τ_r = range window processing time interval (s)
τ = coherent integration processing time interval (s)

For an external noise-limited system, the system operating noise factor given by Eq. (13.1.4) reduces to

$$f \approx f_a f_p, \quad f_a \gg \ell_c \ell_m \ell_n f_d - 1 \tag{13.1.11}$$

where ℓ_c, ℓ_m, ℓ_n, and f_d are system internal noise parameters generated by the receiving system hardware. Substituting Eq. (13.1.11) into Eq. (13.1.1), the predetection SNR reduces to

$$\frac{s}{n} = \frac{p_t g_t}{4\pi \ell_{p1} r_1^2} \frac{\sigma_T}{4\pi \ell_{p2} r_2^2} \frac{d_r \lambda^2}{4\pi} \frac{1}{f_p} \frac{1}{k t_{ref \cdot b'} f_a}, \; f_a \gg \ell_c \ell_m \ell_n f_d - 1 \tag{13.1.12}$$

It should be noted in Eq. (13.1.12) that for an external noise-limited system, the predetection SNR is proportional to the transmit antenna *power* gain and receive antenna *directive* gain, and is inversely proportional to the antenna *external* noise factor. Equation (13.1.12) is a particularly useful form of the signal/noise equation for OTH radar since OTH radar systems are usually designed to be external noise-limited. However, Eq. (13.1.1) is a preferred form of the signal/noise equation for any radar system because it utilizes an internationally-accepted convention for defining the system operating noise factor that includes both externally and internally-generated noise.

The external noise factor f_a is given by Eq. (6.4.16) as

$$f_a = t_a / t_{ref} = (1/4\pi) \int_0^{2\pi} \int_{-\pi/2}^{\pi/2} f_s(\theta, \phi) d_r(\theta, \phi) \sin\theta \, d\theta \, d\phi \tag{13.1.13}$$

where

t_a = effective sky temperature (K)
$f_s(\theta,\phi) = t_s(\theta,\phi)/t_{ref}$ = external noise factor angular distribution (numeric)
$t_s(\theta,\phi)$ = sky temperature angular distribution (K)

The International Radio Consultative Committee [CCIR (French)] has published statistical values of f_a for atmospheric noise based on measurements in the frequency range 0.01–20 MHz as a function of location, hour, and season [186,187] and man-made noise based on measurements in the frequency range 0.25–250 MHz as a function of type of location [188]. CCIR claims that their values of f_a [denoted $(f_a)_{CCIR}$] are normalized to correspond to those that would be measured with an electrically-short vertical monopole element mounted on a ground plane of infinite extent and infinite conductivity. The directive gain of

such an antenna is given by Eq. (3.8.18) of Sec. 3.8.2 as

$$[d_r(\theta,\phi)]_{CCIR} = \begin{cases} 3\sin^2\theta, & 0 \le \theta \le \pi/2 \text{ rad} \\ 0, & -\pi/2 \le \theta < 0 \text{ rad} \end{cases} \tag{13.1.14}$$

Substituting Eq. (13.1.14) into Eq. (13.1.13), the CCIR external noise factor $(f_a)_{CCIR}$ is given by

$$(f_a)_{CCIR} = (1/4\pi)\int_0^{2\pi}\int_0^{\pi/2}[f_s(\theta,\phi)]_{CCIR}\ 3\sin^3\theta\,d\theta\,d\phi \tag{13.1.15}$$

where

$$[f_s(\theta,\phi)]_{CCIR} = \text{CCIR external noise factor angular distribution (numeric).}$$

A receiving system's external noise factor f_a, expressed in terms of CCIR external noise factor $(f_a)_{CCIR}$, is found from Eqs. (13.1.13) and (13.1.15) to be

$$\begin{aligned} f_a &= (f_a)_{CCIR}\cdot[f_a/(f_a)_{CCIR}] \\ &= (f_a)_{CCIR}\frac{\int_0^{2\pi}\int_{-\pi/2}^{\pi/2} f_s(\theta,\phi)\,d_r(\theta,\phi)\sin\theta\,d\theta\,d\phi}{\int_0^{2\pi}\int_0^{\pi/2}[f_s(\theta,\phi)]_{CCIR}\,3\sin^3\theta\,d\theta\,d\phi} \end{aligned} \tag{13.1.16}$$

where $f_s(\theta,\phi)$ is the actual external noise factor angular distribution at the receiving system.

For isotropic external noise with a constant sky temperature angular distribution t_{s0},

$$\begin{aligned} f_a &= (f_a)_{CCIR} = f_{s0}, \\ f_s(\theta,\phi) &= [f_s(\theta,\phi)]_{CCIR} = \text{constant} = f_{s0} \end{aligned} \tag{13.1.17}$$

where

$$f_{s0} = t_{s0}/t_{ref}$$

because, by definition of directive gain,

$$\int_0^{2\pi}\int_{-\pi/2}^{\pi/2} d_r\sin\theta\,d\theta\,d\phi = \int_0^{2\pi}\int_{-\pi/2}^{\pi/2}(d_r)_{CCIR}\sin\theta\,d\theta\,d\phi = 4\pi \tag{13.1.18}$$

It should be noted that in OTH radar systems the directive gain $d_r(\theta,\phi)$ generally has a null on the horizon ($\theta = \pi/2$ rad) because of earth multipath. The directive gain of an OTH receiving antenna is therefore appreciably different at angles near the horizon from that given by Eq. (13.1.14) which has a maximum on

the horizon. The external noise factor f_a can therefore be appreciably different from $(f_a)_{CCIR}$ even if $f_s(\theta, \phi) = [f_s(\theta, \phi)]_{CCIR} \neq$ constant (see Table 43 in Sec. 13.3.3 regarding the calibration of CCIR noise measurements).

At least six of the parameters in the signal/noise Eq. (13.1.1) are dependent upon antenna characteristics. The average power p_t delivered to the transmit antenna is dependent upon the mismatch input impedance of the transmit antenna. The transmit antenna power gain g_t is a function of the radiation pattern and ohmic losses of the transmit antenna (including its ground-plane system). The receive antenna directive gain d_r is a function of the radiation pattern of the receive antenna (including its ground-plane system). The excess propagation loss factors ℓ_p, and ℓ_{p2} are functions of the gain patterns of the transmit and receive antennas, respectively. The system operating noise factor f is a function of the radiation pattern and ohmic losses of the receive antenna. The target radar cross-section σ_T is a function of the radiation patterns of both the transmit and receive antennas since earth multipath in the vicinity of the target has been included as part of the target radar cross-section. In OTH radar systems, the parameters p_t, g_t, d_r, and f are strongly dependent upon antenna characteristics, whereas the parameters ℓ_p, ℓ_{p2}, and σ_T are weakly dependent upon antenna characteristics for a given mode of propagation. The parameters ℓ_{p1}, ℓ_{p2}, and σ_T are usually approximated by considering only the central ray in the scanned direction.

13.2 INFLUENCE OF NONHOMOGENEOUS EARTH ON THE PERFORMANCE OF HIGH-FREQUENCY RECEIVING ARRAYS WITH ELECTRICALLY SMALL GROUND PLANES

13.2.1 Introduction

The performance of ground-based HF antenna arrays is reduced when the array elements have electrically-small ground planes. Performance degradations include: (1) a decrease in directive gain near the horizon (caused by earth multipath), (2) a decrease in radiation efficiency and an increase in internal noise (caused by ground losses), (3) an array RMS phase error (caused by field-induced exterior currents on element feed cables), and (4) an array RMS phase error and beam pointing errors (caused by nonuniform Fresnel reflection from a nonhomogeneous earth). These degradations are summarized in Sec. 13.3.

Sec. 13.2 models the array RMS phase error and beam-pointing errors caused by nonuniform Fresnel reflection from a nonhomogeneous earth. Numerical results are presented for cases of randomly-distributed and systematically-distributed earth nonhomogeneities, where one-half of vertically-polarized array elements are located in proximity to one type of earth and the remaining half are located in proximity to a second type of earth. It is found,

for the cases examined, that the maximum expected values of RMS phase error are 18 and 9° for randomly-distributed and systematically-distributed nonhomogeneities, respectively. The maximum expected values of the beam-pointing error are 0 and 0.3 beamwidths from randomly-distributed and systematically-distributed nonhomogeneities, respectively.

The performance degradation, caused by nonuniform Fresnel reflection by a nonhomogeneous earth is modeled in Sec. 13.2.2. Numerical results are presented in Sec. 13.2.3. The summary and conclusions are given in Sec. 13.2.4.

13.2.2 Model

Consider a sparse HF receiving array of m vertically-polarized elements with ground planes, of radius a, pseudo-randomly distributed on flat earth over a circular area of radius $r_A \gg a$. The elements, in close proximity to earth, are identical except that the earth below each element may vary from element to element. The element length ℓ and ground-plane radius a are assumed to be electrically small ($\ell \ll \lambda_0, a \ll \lambda_0$ where λ_0 is the RF wavelength in free space). The midpoint of each element is at a height h above the earth.

Consider now a plane wave incident from the true direction (θ, Φ) where θ is the elevation angle of incident with respect to zenith (the z axis) and Φ is the azimuthal angle with respect to the x axis. The electric field at the midpoint of the kth element, in the absence of mutual coupling among elements, is the sum of the fields from a direct ray incident from the direction (θ, Φ) and an indirect ("multipath") ray reflected at a point P_k at a horizontal distance $h \tan \theta$ from the element local origin O_k (see Fig. 108). We assume that the ground plane is sufficiently small so that the indirect ray is reflected from the earth rather than from the ground plane. Accordingly, the radius of the ground plane satisfies the condition $a < h \tan \theta$. (At angles of incidence $\theta < 60°$ this condition is more stringent than the condition $a \ll \lambda_0$.)

The radiation pattern of the kth element is then approximately identical to that of a vertically-polarized Hertzian dipole at height h above flat earth (see Fig. 108).

The relative permittivity $\varepsilon_k^*/\varepsilon_0$ of the earth at the kth element is given by

$$\varepsilon_k^*/\varepsilon_0 = \varepsilon_{rk} - j60\lambda_0\sigma_k \tag{13.2.1}$$

where

ε_{rk} = dielectric constant of the earth at the kth element (numeric)
σ_k = conductivity of the earth at the kth element (S/m)
λ_0 = RF wavelength in free space (m)

For homogeneous earth,

$$\varepsilon^*/\varepsilon_0 = \varepsilon_r - j60\lambda_0\sigma. \tag{13.2.2}$$

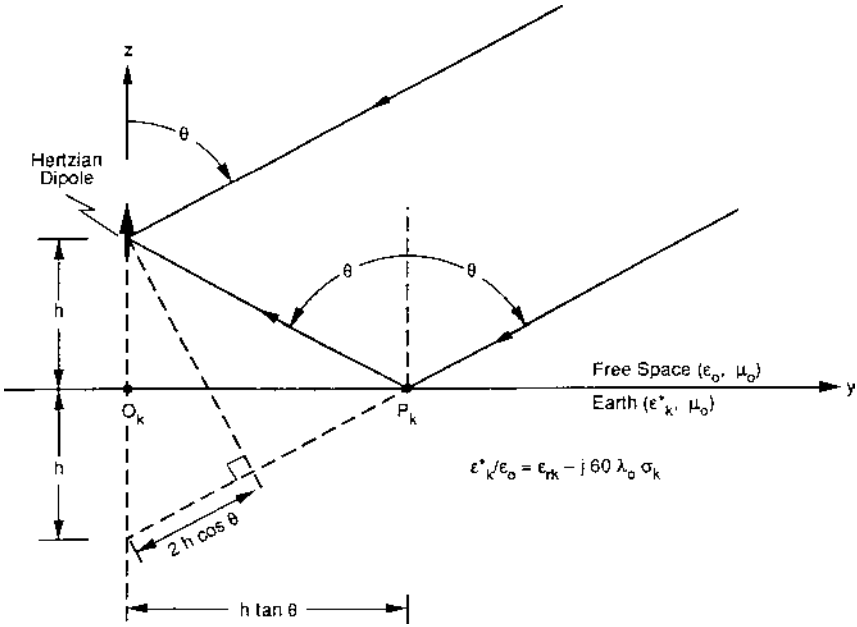

FIGURE 108 The kth element approximated by a vertically-polarized Hertzian dipole above flat earth.

The ground constants ε_r and σ, loss tangent, and penetration depth δ, for the CCIR 527-1 classifications of homogeneous earth, are summarized in Table 16.

The field $E_k(\theta, \phi)$ at the kth element, after elimination of the true phase advance of the direct field at each element relative to that at the origin, is given by

$$E_k(\theta) = A \sin\theta \{1 + R_{k,v} \exp[-j(2\pi/\lambda_0)2h\cos\theta]\}, \quad 0 \le \theta \le \pi/2 \text{ rad} \tag{13.2.3}$$

where

A = constant (V/m)
θ = angle of incidence (measured from zenith) of the direct ray (deg)
$R_{k,v} = |R_{k,v}| \exp[j(\text{angle } R_{k,v})]$ = Fresnel reflection coefficient of the earth at the kth element for a vertically-polarized direct wave incident from the direction (θ, ϕ).

Equation (13.2.3) is valid for computing the indirect field in air relative to the direct field in air. The single ray (plane wave) Fresnel reflection coefficient model

of Eq. (13.2.3) is not valid for calculating the amplitude A of the direct wave because the model does not include the substantial surface wave near-field losses in the earth.

The Fresnel reflection $R_{k,\mathrm{v}}$ for parallel (vertical) polarization (the E-field is parallel to the plane of incidence) is given by Eq. (9.2.5) as

$$R_{k,\mathrm{v}} = \frac{(\varepsilon_k^*/\varepsilon_0)\cos\theta - [(\varepsilon_k^*/\varepsilon_0) - \sin^2\theta]^{1/2}}{(\varepsilon_k^*/\varepsilon_0)\cos\theta + [(\varepsilon_k^*/\varepsilon_0) - \sin^2\theta]^{1/2}} \tag{13.2.4}$$

where ε_k^* is given by Eq. (13.2.1). The Fresnel reflection coefficient $R_{k,\mathrm{v}}$ is a function of k and θ. For homogeneous earth, Eq. (13.2.4) reduces to

$$\begin{aligned} R_{k,\mathrm{v}} &= R_{\mathrm{v}} \\ &= \frac{(\varepsilon^*/\varepsilon_0)\cos\theta - [(\varepsilon^*/\varepsilon_0) - \sin^2\theta]^{1/2}}{(\varepsilon^*/\varepsilon_0)\cos\theta + [(\varepsilon^*/\varepsilon_0) - \sin^2\theta]^{1/2}}, \text{ homogeneous earth} \end{aligned} \tag{13.2.5}$$

where $\varepsilon_k^*/\varepsilon_0$ is given by Eq. (13.2.2). For homogeneous earth, R_{v} is a function only of the angle of incidence θ and the relative permittivity $\varepsilon^*/\varepsilon_0$. The Fresnel reflection coefficient R_{v}, computed by MITRE program MODIFIED IMAGES, is given in App. A.8, $N = 0$ at 6, 15, and 30 MHz for the ground constants specified in Table 16. The coefficient R_{v} is tabulated as a function of the grazing angle ψ (with respect to zenith) Please note that $\psi = (\pi/2) - \theta$(rad) or $\psi = 90 - \theta$ (deg).

The numeric directive gain $d(\theta)$ of a vertically-polarized Hertzian dipole at a height h above flat homogeneous *lossy* earth is given by Eq. (2.2.2) of Sec. 2.2 as

$$d(\theta) = \begin{cases} \dfrac{2|E(\theta)|^2}{\int_0^{\pi/2} |E(\theta)|^2 \sin\theta \, \mathrm{d}\theta}, & 0 \le \theta \le \pi/2 \\ & \text{lossy earth} \\ 0, & -\pi/2 \le \theta \le 0 \end{cases} \tag{13.2.6}$$

where $E(\theta)$ is given by Eq. (13.2.3) (with the subscript k suppressed). The integration in the elevation plane is restricted to the upper hemisphere because, for a lossy earth, there is no far-field radiation in the lower hemisphere. The directive gain $D(\theta) = 10\log_{10} d(\theta)$ (dBi), computed by MITRE program MODIFIED IMAGES, is tabulated in App. A.8, $N = 0$.

The field $E_k(\theta)$, given by Eq. (13.2.2), may be written as

$$E_k/A \sin\theta = (1 + |R_{k,\mathrm{v}}| \cos\beta_\kappa) + j|R_{k,\mathrm{v}}| \sin\beta_\kappa \tag{13.2.7}$$

where

β_κ = phase delay of the indirect array with respect to the direct ray

$$= \begin{cases} \beta_\kappa(\text{rad}) = \text{angle } R_{k,\text{v}}(\text{rad}) - (2\pi/\lambda_0)2h\cos\theta \\ \beta_\kappa(\text{deg}) = \text{angle } R_{k,\text{v}}(\text{rad}) - (180/\pi)(2\pi/\lambda_0)2h\cos\theta \end{cases} \tag{13.2.8}$$

The argument α_k, of the complex quantity $E_k/A\sin\theta$, is given by

$$\alpha_k(\theta) = \arctan[|R_{k,\text{v}}|\sin\beta_\kappa/(1+|R_{k,\text{v}}|\cos\beta_\kappa)] \tag{13.2.9}$$

For homogeneous earth, $\alpha_k \equiv \alpha$ and $\beta_k = \beta$. The phase delay β and argument α are given in Tables 30–32 for homogeneous very dry ground, medium dry ground, and wet ground, respectively. Numerical values are given at 6 MHz for $h/\lambda_0 = 0, 0.054$ and at 30 MHz for $\lambda_0 = 0, 0.270$. The normalized heights $h/\lambda_0 = 0, 0.054$, and 0.270 correspond to the mid-point at 6 and 30 MHz, respectively, of a vertical monopole of length $\ell = 5.4$ m.

The mean argument $\bar{\alpha}(\theta)$, averaged over the m elements of the array for a plane wave incident from the direction θ, is given by

$$\bar{\alpha}(\theta) = (1/m)\sum_{k=1}^{m} \alpha_k(\theta), \tag{13.2.10}$$

The variability of the argument α_k from element to element causes an array RMS phase error α_{kms} and beam-pointing errors B_θ, B_ϕ. The RMS phase error, at the diffraction focus of the array [190], is given by

$$\alpha_{\text{rms}}(\theta) = \left\{ \left(\sum_{k=1}^{m} (1/m)[\alpha_k(\theta) - \bar{\alpha}(\theta)]^2 \right) - \alpha_{\text{B}}^2(\theta) \right\}^{1/2} \tag{13.2.11}$$

where $\alpha_{\text{B}}(\theta)$ is the RMS phase error caused by a linear phase shift resulting from beam-pointing errors. The rms phase error $\alpha_{\text{B}}(\theta)$ is given by Eq. (D-13) of App. D as

$$\alpha_{\text{B}} = \left\{ \frac{(1/m)\left[\sum_{k=1}^{m}(x_k/r_A)(\alpha_k - \bar{\alpha})\right]^2}{\sum_{k=1}^{m}(x_k/r_A)^2} + \frac{(1/m)\left[\sum_{k=1}^{m}(y_k/r_A)(\alpha_k - \bar{\alpha})\right]^2}{\sum_{k=1}^{m}(y_k/r_A)^2} \right\}^{1/2} \quad x_k, y_k \text{ are uncorrelated} \tag{13.2.12}$$

TABLE 30 Argument α, Very Dry Ground ($\varepsilon_r = 3.0$, $\sigma = 1.0 \times 10^{-4}$ S/m)

Grazing angle, ψ (deg)	$\lvert R_v \rvert$	Angle R_v (rad)	β (rad)		(1) $\lvert R_v \rvert \sin\beta$		(2) $1 + \lvert R_v \rvert \cos\beta$		α (rad) = arctan[(1)/(2)]	
			$h/\lambda_0 = 0$	$h/\lambda_0 = 0.054$	$h/\lambda_0 = 0$	$h/\lambda_0 = 0.054$	$h/\lambda_0 = 0$	$h/\lambda_0 = 0.054$	$h/\lambda_0 = 0$	$h/\lambda_0 = 0.054$
6 MHz ($\lambda_0 = 50$ m)										
0	1.000	$-\pi$	$-\pi$	$-\pi$	0.000	0.000	0.000.	0.000	$-\pi/2$	$-\pi/2$
5	0.689	−3.132	−3.132	−3.191	−0.007	0.034	0.311	0.312	−0.023	0.109
10	0.465	−3.119	−3.119	−3.157	−0.011	0.007	0.535	0.535	−0.021	0.109
16	0.271	−3.094	−3.094	−3.281	−0.013	0.038	0.729	0.732	−0.018	0.052
20	0.173	−3.060	−3.060	−3.292	−0.014	0.026	0.828	0.829	−0.017	0.031
26	0.061	−2.880	−2.880	−3.177	−0.016	−0.002	0.942	0.939	−0.017	−0.002
30	0.017	−1.554	−1.554	−1.893	−0.017	−0.016	1.000	0.995	−0.017	−0.016

Grazing angle, ψ (deg)	$\lvert R_v \rvert$	Angle R_v (rad)	β (rad)		(1) $\lvert R_v \rvert \sin\beta$		(2) $1 + \lvert R_v \rvert \cos\beta$		α(rad) = arctan[(1)/(2)]	
			$h/\lambda_0 = 0$	$h/\lambda_0 = 0.270$	$h/\lambda_0 = 0$	$h/\lambda_0 = 0.270$	$h/\lambda_0 = 0$	$h/\lambda_0 = 0.270$	$h/\lambda_0 = 0$	$h/\lambda_0 = 0.270$
30 MHz ($\lambda_0 = 10$ m)										
0	1.000	$-\pi$	$-\pi$	$-\pi$	0.000	0.000	0.000	0.000	$-\pi/2$	$-\pi/2$
5	0.689	−3.140	−3.140	−3.436	−0.001	0.200	0.311	0.341	−0.003	0.530
10	0.465	−3.137	−3.137	−3.726	−0.002	0.257	0.535	0.612	−0.004	0.398
16	0.271	−3.132	−3.132	−4.067	−0.003	0.216	0.729	0.837	−0.004	0.253
20	0.173	−3.125	−3.125	−4.285	−0.003	0.157	0.827	0.928	−0.004	0.168
26	0.059	−3.088	−3.088	−4.575	−0.003	0.058	0.941	0.992	−0.003	0.058
30	0.003	−1.567	−1.567	−3.263	−0.003	0.000	0.997	0.997	−0.003	0.000

β (rad) = angle R_v (rad) $- (2\pi/\lambda_0)2h \sin\psi$.
$\alpha = \arctan[R_v \sin\beta/(1 + R_v \cos\beta)]$.

TABLE 31 Argument α, Medium Dry Ground ($\varepsilon_r = 15.0$, $\sigma = 1.0 \times 10^{-3}$ S/m)

Grazing angle, ψ (deg)	$\lvert R_v \rvert$	Angle R_v (rad)	β (rad)		(1) $\lvert R_v \rvert \sin\beta$		(2) $1 + \lvert R_v \rvert \cos\beta$		α(rad) = arctan[(1)/(2)]	
			$h/\lambda_0 = 0$	$h/\lambda_0 = 0.054$	$h/\lambda_0 = 0$	$h/\lambda_0 = 0.054$	$h/\lambda_0 = 0$	$h/\lambda_0 = 0.054$	$h/\lambda_0 = 0$	$h/\lambda_0 = 0.054$
6 MHz ($\lambda_0 = 50$ m)										
0	1.000	π	π	π	0.000	0.000	0.000	0.000	$-\pi/2$	$-\pi/2$
5	0.481	−3.068	−3.068	−3.127	−0.035	−0.007	0.520	0.519	−0.067	−0.013
10	0.182	−2.893	−2.893	−3.011	−0.045	−0.024	0.824	0.820	−0.055	−0.029
16	0.070	−0.717	−0.717	−0.904	−0.046	−0.055	1.053	1.043	−0.044	−0.053
20	0.165	−0.277	−0.277	−0.509	−0.045	−0.080	1.159	1.144	−0.039	−0.070
26	0.279	−0.155	−0.155	−0.452	−0.043	−0.126	1.276	1.251	−0.034	−0.100
30	0.338	−0.124	−0.124	−0.463	−0.042	−0.151	1.335	1.334	−0.031	−0.113
Grazing angle, ψ (deg)	$\lvert R_v \rvert$	Angle R_v (rad)	β (rad)		(1) $\lvert R_v \rvert \sin\beta$		(2) $1 + \lvert R_v \rvert \cos\beta$		α(rad) = arctan[(1)/(2)]	
			$h/\lambda_0 = 0$	$h/\lambda_0 = 0.270$	$h/\lambda_0 = 0$	$h/\lambda_0 = 0.270$	$h/\lambda_0 = 0$	$h/\lambda_0 = 0.270$	$h/\lambda_0 = 0$	$h/\lambda_0 = 0.270$
30 MHz ($\lambda_0 = 10$ m)										
0	1.000	π	π	π	0.000	0.000	0.000	0.000	$-\pi/2$	$-\pi/2$
5	0.482	−3.127	−3.127	−3.423	−0.026	−0.134	0.518	0.537	−0.050	0.245
10	0.180	−3.091	−3.091	−3.680	−0.010	−0.092	0.820	0.845	−0.012	0.108
16	0.050	−0.189	−0.189	−1.124	−0.000	−0.045	1.049	1.022	0.000	0.044
20	0.155	−0.059	−0.059	−3.452	−0.000	−0.047	1.155	0.852	0.000	0.055
26	0.272	−0.032	−0.032	−1.519	−0.000	−0.272	1.272	1.014	0.000	−0.268
30	0.331	−0.026	−0.026	−1.727	−0.000	−0.327	1.331	0.950	0.000	−0.332

β(rad) = angle R_v (rad) $- (2\pi/\lambda_0)2h \sin\psi$.
$\alpha = \arctan[R_v \sin\beta/(1 + R_v \cos\beta)]$.

TABLE 32 Argument α, Wet Ground ($\varepsilon_r = 30.0$, $\sigma = 1.0 \times 10^{-2}$ S/m)

Grazing angle, ψ (deg)	$\lvert R_v \rvert$	Angle R_v (rad)	β (rad)		(1) $\lvert R_v \rvert \sin\beta$		(2) $1 + \lvert R_v \rvert \cos\beta$		α(rad) = arctan[(1)/(2)]	
			$h/\lambda_0 = 0$	$h/\lambda_0 = 0.054$	$h/\lambda_0 = 0$	$h/\lambda_0 = 0.054$	$h/\lambda_0 = 0$	$h/\lambda_0 = 0.054$	$h/\lambda_0 = 0$	$h/\lambda_0 = 0.054$
6 MHz ($\lambda_0 = 50$ m)										
0	1.000	$-\pi$	$-\pi$	$-\pi$	0.000	0.000	0.000.	0.000	$-\pi/2$	$-\pi/2$
5	0.334	−2.573	−2.573	−2.632	−0.180	−0.163	0.719	0.708	−0.245	−0.226
10	0.205	−1.233	−1.233	−1.351	−0.193	−0.200	1.068	1.045	−0.179	−0.189
16	0.347	−0.539	−0.539	−0.726	−0.178	−0.230	1.298	1.259	−0.136	−0.181
20	0.429	−0.396	−0.396	−0.628	−0.165	−0.252	1.396	1.347	−0.118	−0.185
26	0.519	−0.290	−0.290	−0.587	−0.148	−0.287	1.497	1.432	−0.099	−0.198
30	0.564	−0.248	−0.248	−0.587	−0.138	−0.312	1.547	1.470	−0.089	−0.209

Grazing angle, ψ (deg)	$\lvert R_v \rvert$	Angle R_v (rad)	β (rad)		(1) $\lvert R_v \rvert \sin\beta$		(2) $1 + \lvert R_v \rvert \cos\beta$		α(rad) = arctan[(1)/(2)]	
			$h/\lambda_0 = 0$	$h/\lambda_0 = 0.270$	$h/\lambda_0 = 0$	$h/\lambda_0 = 0.270$	$h/\lambda_0 = 0$	$h/\lambda_0 = 0.270$	$h/\lambda_0 = 0$	$h/\lambda_0 = 0.270$
30 MHz ($\lambda_0 = 10$ m)										
0	1.000	$-\pi$	$-\pi$	$-\pi$	0.000	0.000	0.000	0.000	$-\pi/2$	$-\pi/2$
5	0.346	−3.019	−3.019	−3.315	−0.042	−0.060	0.659	0.659	−0.064	−0.091
10	0.049	−1.822	−1.822	−2.411	−0.047	−0.033	1.988	0.964	−0.048	−0.034
16	0.220	−0.209	−0.209	−1.144	−0.046	−0.200	1.215	1.091	−0.038	−0.181
20	0.318	−0.136	−0.136	−1.296	−0.043	−0.306	1.315	1.086	−0.033	−0.275
26	0.424	−0.093	−0.093	−1.580	−0.039	−0.424	1.422	0.996	−0.027	−0.402
30	0.476	−0.079	−0.079	−1.775	−0.003	−0.466	1.475	0.903	−0.002	−0.476

β(rad) = angle R_v (rad) $- (2\pi/\lambda_0)2h \sin\psi$.
$\alpha = \arctan[R_v \sin\beta/(1 + R_v \cos\beta)]$.

where

x_k, y_k = projections of the kth element location onto the x and y axes, respectively, whose origin is at the center of the array.

The nonhomogeneous earth causes beam pointing errors B_θ and B_ϕ, in the elevation and azimuthal directions, respectively. The beam pointing errors, for a plane wave incident from the true direction (θ, ϕ) are given by Eqs. (D-20) and (D-21) as

$$\begin{aligned} B_\theta &= \theta_{\text{apparent}} - \theta \\ &= -(1/\cos\theta)[(\hat{u} - u)\cos\phi + (\hat{v} - v)\sin\phi], \quad B_\theta \ll 1 \text{ rad} \end{aligned} \tag{13.2.13}$$

$$\begin{aligned} B_\phi &= \phi_{\text{apparent}} - \phi \\ &= -(1/\sin\theta)[(\hat{u} - u)\sin\phi + (\hat{v} - v)\cos\phi], \quad B_\phi \ll 1 \text{ rad} \end{aligned} \tag{13.2.14}$$

where $(\theta_{\text{apparent}}, \phi_{\text{apparent}})$ is the apparent beam direction when the beam has a true direction (θ, ϕ). The quantities $(\hat{u} - u)$ and $(\hat{v} - v)$ are given by Eqs. (D-9) and (D-10), respectively, as

$$\hat{u} - u = (\lambda_0/2\pi r_A)\sum_{k=1}^{m}(x_k/r_A)(\alpha_k - \bar{\alpha})/\sum_{k=1}^{m}(x_k/r_A)^2 \tag{13.2.15}$$

$$\hat{v} - v = (\lambda_0/2\pi r_A)\sum_{k=1}^{m}(y_k/r_A)(\alpha_k - \bar{\alpha})/\sum_{k=1}^{m}(y_k/r_A)^2 \tag{13.2.16}$$

where x_k, y_k are assumed to be uncorrelated.

The parameters α_B, B_θ, B_ϕ, $\hat{u} - u$, and $\hat{v} - v$ are zero for the cases: (1) homogeneous earth $(\alpha_k = \bar{\alpha})$ and (2) nonhomogeneous earth with randomly-distributed nonhomogeneities and elements $(\sum x_k(\alpha_k - \bar{\alpha}) = \sum y_k(\alpha_k - \bar{\alpha}) = 0)$. However, for nonhomogeneous earth with systematically-distributed nonhomogeneities or elements $(\sum x_k(\alpha_k - \bar{\alpha}) \neq 0, \ \sum y_k(\alpha_k - \bar{\alpha}) \neq 0)$, then α_B, B_θ, B_ϕ, $\hat{u} - u$, and $\hat{v} - v$ are nonzero.

13.2.3 Numerical Results

Numerical results for the RMS phase error α_{rms} and boresight errors B_θ, B_ϕ, are given in this section for cases where a fraction of the elements are located in proximity to earth of permittivity ε_{I}^* and the remaining fraction are in proximity to earth of permittivity $\varepsilon_{\text{II}}^*$. This type of nonhomogeneous earth is designated as "two-level" nonhomogeneous earth. Accordingly, the parameters ε_k^*, γ_k, β_k, and

$R_{k,\mathrm{v}}$ at the kth element are given by

$$\varepsilon_{k\mathrm{u}}^{*}, \alpha_k, \beta_k, R_{k,\mathrm{v}} = \begin{cases} \varepsilon_{\mathrm{I}}^{*}, \alpha_{\mathrm{I}}, R_{\mathrm{I,V}} \text{ at } p \text{ elements, two-level nonhomogeneous earth} \\ \varepsilon_{\mathrm{II}}^{*}, \alpha_{\mathrm{II}}, R_{\mathrm{II,V}} \text{ at } m-p \text{ elements} \end{cases} \tag{13.2.17}$$

Furthermore, it is assumed that the elements are randomly distributed over the circular area of radius r_A and that projections x_k and y_k of the kth element onto the x and y axes, respectively, are uncorrelated.

13.2.3.1 Randomly-Distributed Two-Level Nonhomogeneous earth

Consider first the case the two permittivities $\varepsilon_{\mathrm{I}}^{*}$ and $\varepsilon_{\mathrm{II}}^{*}$ are randomly distributed with occurrence frequencies p/m for $\varepsilon_{\mathrm{I}}^{*}$ and $1-(p/m)$ for $\varepsilon_{\mathrm{II}}^{*}$. Consequently,

$$\sum_{k=1}^{m} x_k \alpha_k = \sum_{k=1}^{m} y_k \alpha_k = 0, \tag{13.2.18}$$

randomly distributed nonhomogenities and elements

For this case, Eqs. (13.2.10)–(13.2.16) reduce to

$$\bar{\alpha}(\theta) = (p/m)\alpha_{\mathrm{I}}(\theta) + [1-(p/m)]\alpha_{\mathrm{II}}(\theta), \tag{13.2.19}$$

two-level nonhomogeneous earth

$$\alpha_{\mathrm{rms}}(\theta) = \{(p/m)\{\alpha_{\mathrm{I}}(\theta) - \bar{\alpha}(\theta)]^2 + [1-(p/m)][\alpha_{\mathrm{II}}(\theta) - \bar{\alpha}(\theta)]^2\}^{1/2}, \tag{13.2.20}$$

two-level nonhomogeneous earth, randomly-distributed elements and nonhomogenities

$$\alpha_{\mathrm{B}} = B_\theta = B_\phi = \hat{u} - u = \hat{v} - v = 0, \tag{13.2.21}$$

randomly distributed elements and earth nonhomogenities

Numerical values of the RMS phase error $\alpha_{\mathrm{rms}}(\theta)$ are given in Tables 33–35 for three compositions of two-level randomly-distributed nonhomogeneous earth for $p/m = 0.5$ and elevation angles $60 \le \theta \le 90°$. Table 33 is for very dry ground/medium dry ground. Table 34 is for medium dry ground/wet ground. Table 35 is for very dry ground/wet ground. Numerical values are given at 6 MHz for normalized height $h/\lambda_0 = 0, 0.054$ and at 30 MHz for $h/\lambda_0 = 0, 0.270$.

The RMS phase errors of Tables 33–35 are summarized in Table 36. The largest phase errors occur for very dry ground/wet ground. At 6 MHz,

TABLE 33 RMS Phase Error α_{rms} (Very Dry Ground/Medium Dry Ground, $p/m = 0.5$, Randomly-Distributed Nonhomogeneities)

Grazing angle,	α_I (rad) Very dry ground		α_{II} (rad) Medium dry ground		$\bar{\alpha}$ (rad)		α_{rms} (rad)		α_{rms} (deg)	
ψ (deg)	$h/\lambda_0 = 0$	$h/\lambda_0 = 0.054$	$h/\lambda_0 = 0$	$h/\lambda_0 = 0.054$	$h/\lambda_0 = 0$	$h/\lambda_0 = 0.054$	$h/\lambda_0 = 0$	$h/\lambda_0 = 0.054$	$h/\lambda_0 = 0$	$h/\lambda_0 = 0.054$
6 MHz ($\lambda_0 = 50$ m)										
0	$-\pi/2$	$-\pi/2$	$-\pi/2$	$-\pi/2$	$-\pi/2$	$-\pi/2$	0	0	0	0
5	−0.023	0.109	−0.067	−0.013	−0.045	0.048	0.022	0.065	1.26	3.72
10	−0.021	0.109	−0.055	−0.029	−0.038	0.040	0.017	0.069	0.97	3.95
16	−0.018	0.052	−0.044	−0.053	−0.040	−0.001	0.016	0.053	0.92	3.04
20	−0.017	0.031	−0.039	−0.070	−0.028	−0.020	0.011	0.051	0.63	2.92
26	−0.017	−0.002	−0.034	−0.100	−0.026	−0.051	0.009	0.049	0.52	2.81
30	−0.017	−0.016	−0.031	−0.113	−0.024	−0.065	0.007	0.049	0.40	2.81

Grazing angle,	α_I (rad) Very dry ground		α_{II} (rad) Medium dry ground		$\bar{\alpha}$ (rad)		α_{rms} (rad)		α_{rms} (deg)	
ψ (deg)	$h/\lambda_0 = 0$	$h/\lambda_0 = 0.270$	$h/\lambda_0 = 0$	$h/\lambda_0 = 0.270$	$h/\lambda_0 = 0$	$h/\lambda_0 = 0.270$	$h/\lambda_0 = 0$	$h/\lambda_0 = 0.270$	$h/\lambda_0 = 0$	$h/\lambda_0 = 0.270$
30 MHz ($\lambda_0 = 10$ m)										
0	$-\pi/2$	$-\pi/2$	$-\pi/2$	$-\pi/2$	$-\pi/2$	$-\pi/2$	0	0	0	0
5	−0.003	0.530	−0.050	0.245	−0.027	0.388	0.023	0.143	1.32	8.19
10	−0.004	0.398	−0.012	0.108	−0.008	0.253	0.004	0.145	0.23	8.31
16	−0.004	0.253	0.000	0.044	−0.002	0.149	0.002	0.105	0.11	6.02
20	−0.004	0.168	0.000	0.055	−0.002	0.112	0.002	0.057	0.11	3.27
26	−0.003	0.058	0.000	−0.268	−0.002	−0.105	0.002	0.163	0.11	9.33
30	−0.003	0.000	0.000	−0.332	−0.002	−0.166	0.002	0.166	0.11	9.51

$\bar{\alpha} = 0.5(\alpha_I + \alpha_{II})$.
$\bar{\alpha}_{rms} = (0.5[(\alpha_I - \bar{\alpha})^2 + (\alpha_{II} - \bar{\alpha})^2])^{1/2}$.

TABLE 34 RMS Phase Error α_{rms} (Medium Dry Ground/Wet Ground, $p/m = 0.5$, Randomly-Distributed Nonhomogeneities)

Grazing angle,	α_I (rad) Medium dry ground		α_{II} (rad) Wet ground		$\bar{\alpha}$ (rad)		α_{rms} (rad)		α_{rms} (deg)	
ψ (deg)	$h/\lambda_0 = 0$	$h/\lambda_0 = 0.054$	$h/\lambda_0 = 0$	$h/\lambda_0 = 0.054$	$h/\lambda_0 = 0$	$h/\lambda_0 = 0.054$	$h/\lambda_0 = 0$	$h/\lambda_0 = 0.054$	$h/\lambda_0 = 0$	$h/\lambda_0 = 0.054$
6 MHz ($\lambda_0 = 50$ m)										
0	$-\pi/2$	$-\pi/2$	$-\pi/2$	$-\pi/2$	$-\pi/2$	$-\pi/2$	0	0	0	0
5	−0.067	−0.013	−0.245	−0.226	−0.156	−0.120	0.089	0.168	5.10	9.64
10	−0.055	−0.029	−0.179	−0.189	−0.117	−0.109	0.062	0.080	3.52	4.58
16	−0.044	−0.053	−0.136	−0.181	−0.090	−0.117	0.046	0.064	2.63	3.67
20	−0.039	−0.070	−0.118	−0.185	−0.079	−0.128	0.040	0.057	2.29	3.27
26	−0.034	−0.100	−0.099	−0.198	−0.067	−0.149	0.033	0.052	1.89	2.98
30	−0.031	−0.113	−0.089	−0.209	−0.060	−0.161	0.029	0.051	1.66	2.92

Grazing angle,	α_I (rad) Medium dry ground		α_{II} (rad) Wet ground		$\bar{\alpha}$ (rad)		α_{rms} (rad)		α_{rms} (deg)	
ψ (deg)	$h/\lambda_0 = 0$	$h/\lambda_0 = 0.270$	$h/\lambda_0 = 0$	$h/\lambda_0 = 0.270$	$h/\lambda_0 = 0$	$h/\lambda_0 = 0.270$	$h/\lambda_0 = 0$	$h/\lambda_0 = 0.270$	$h/\lambda_0 = 0$	$h/\lambda_0 = 0.270$
30 MHz ($\lambda_0 = 10$ m)										
0	$-\pi/2$	$-\pi/2$	$-\pi/2$	$-\pi/2$	$-\pi/2$	$-\pi/2$	0	0	0	0
5	−0.050	0.245	−0.064	−0.091	−0.057	0.077	0.007	0.168	0.40	9.62
10	−0.012	0.108	−0.048	−0.034	−0.030	0.037	0.018	0.071	1.03	4.07
16	0.000	0.044	−0.038	−0.181	−0.019	−0.069	0.019	0.113	1.09	6.47
20	0.000	0.055	−0.033	−0.275	−0.017	−0.110	0.017	0.165	0.97	9.45
26	0.000	−0.268	−0.027	−0.402	−0.014	−0.335	0.017	0.067	0.80	3.83
30	0.000	−0.332	−0.002	−0.476	−0.001	−0.404	0.001	0.072	0.06	4.13

$\bar{\alpha} = 0.5(\alpha_I + \alpha_{II})$.
$\bar{\alpha}_{rms} = (0.5[(\alpha_I - \bar{\alpha})^2 + (\alpha_{II} - \bar{\alpha})^2])^{1/2}$.

TABLE 35 RMS Phase Error α_{rms} (Very Dry Ground/Wet Ground, $p/m = 0.5$, Randomly-Distributed Nonhomogeneities)

Grazing angle,	α_I (rad) Very dry ground		α_{II} (rad) Wet ground		$\bar{\alpha}$ (rad)		α_{rms} (rad)		α_{rms} (deg)	
ψ (deg)	$h/\lambda_0 = 0$	$h/\lambda_0 = 0.054$	$h/\lambda_0 = 0$	$h/\lambda_0 = 0.054$	$h/\lambda_0 = 0$	$h/\lambda_0 = 0.054$	$h/\lambda_0 = 0$	$h/\lambda_0 = 0.054$	$h/\lambda_0 = 0$	$h/\lambda_0 = 0.054$
6 MHz ($\lambda_0 = 50$ m)										
0	$-\pi/2$	$-\pi/2$	$-\pi/2$	$-\pi/2$	$-\pi/2$	$-\pi/2$	0	0	0	0
5	−0.023	0.109	−0.245	−0.226	−0.134	−0.059	0.111	0.168	6.36	9.62
10	−0.021	0.109	−0.179	−0.189	−0.100	−0.040	0.080	0.149	4.58	8.54
16	−0.018	0.052	−0.136	−0.181	−0.077	−0.065	0.059	0.117	3.38	6.70
20	−0.017	0.031	−0.118	−0.185	−0.068	−0.077	0.051	0.108	2.92	6.19
26	−0.017	−0.002	−0.099	−0.198	−0.058	−0.100	0.041	0.098	2.35	5.61
30	−0.017	−0.016	−0.089	−0.209	−0.053	−0.113	0.036	0.097	2.06	5.56
Grazing angle,	α_I (rad) Very dry ground		α_{II} (rad) Wet ground		$\bar{\alpha}$ (rad)		α_{rms} (rad)		α_{rms} (deg)	
ψ (deg)	$h/\lambda_0 = 0$	$h/\lambda_0 = 0.270$	$h/\lambda_0 = 0$	$h/\lambda_0 = 0.270$	$h/\lambda_0 = 0$	$h/\lambda_0 = 0.270$	$h/\lambda_0 = 0$	$h/\lambda_0 = 0.270$	$h/\lambda_0 = 0$	$h/\lambda_0 = 0.270$
30 MHz ($\lambda_0 = 10$ m)										
0	$-\pi/2$	$-\pi/2$	$-\pi/2$	$-\pi/2$	$-\pi/2$	$-\pi/2$	0	0	0	0
5	−0.003	0.530	−0.064	−0.091	−0.034	0.220	0.031	0.311	1.78	17.8
10	−0.004	0.398	−0.048	−0.034	−0.026	0.182	0.022	0.216	1.26	12.4
16	−0.004	0.253	−0.038	−0.181	−0.021	0.036	0.017	0.217	0.97	12.4
20	−0.004	0.168	−0.033	−0.275	−0.019	−0.054	0.015	0.222	0.86	12.7
26	−0.003	0.058	−0.027	−0.402	−0.015	−0.172	0.012	0.230	0.69	13.2
30	−0.003	0.000	−0.002	−0.476	−0.003	−0.238	0.001	0.238	0.57	13.6

$\bar{\alpha} = 0.5(\alpha_I + \alpha_{II})$.
$\bar{\alpha}_{rms} = (0.5[(\alpha_I - \bar{\alpha})^2 + (\alpha_{II} - \bar{\alpha})^2])^{1/2}$.

the maximum RMS phase error is 10° and occurs for $\theta = 85°$, $h/\lambda_0 = 0, 0.054$. At 30 MHz, the maximum RMS phase error is 18° and occurs for $\theta = 85°$, $h/\lambda_0 = 0, 0.270$. The RMS phase error generally increases with increasing values of h/λ_0 (for modest value of h/λ_0). The dependence of RMS phase error upon θ is generally nonmonotonic.

13.2.3.2 Systematically-Distributed Two-Level Nonhomogeneous earth

Consider now the case where the two permittivities $\varepsilon_{\mathrm{I}}^*$ and $\varepsilon_{\mathrm{II}}^*$ are *not* randomly distributed over the array area of radius r_A. In particular, consider the case where

TABLE 36 Summary of RMS Phase Errors ($p/m = 0.5$, Randomly Distributed Two-Level Nonhomogeneous Earth)

Angle of incidence, θ (deg)	RMS phase error, α_{RMS} (deg)					
	Very dry ground/ medium dry ground		Medium dry ground/ wet ground		Very dry ground/ wet ground	
	$h/\lambda_0 = 0$	$h/\lambda_0 = 0.054$	$h/\lambda_0 = 0$	$h/\lambda_0 = 0.054$	$sh/\lambda_0 = 0$	$h/\lambda_0 = 0.054$
6 MHz ($\lambda_0 = 50$ m)						
60	0.4	2.8	1.7	2.9	2.1	5.6
64	0.5	2.8	1.9	3.0	2.3	5.6
70	0.6	2.9	2.3	3.3	2.9	6.2
74	0.9	3.0	2.6	3.7	3.4	6.7
80	1.0	4.0	3.5	4.6	4.6	8.5
85	1.3	3.7	5.1	9.6	6.4	9.6
90	0	0	0	0	0	0

Angle of incidence, θ (deg)	RMS phase error, α_{RMS} (deg)					
	Very dry ground/ medium dry ground		Medium dry ground/ wet ground		Very dry ground/ wet ground	
	$h/\lambda_0 = 0$	$h/\lambda_0 = 0.270$	$h/\lambda_0 = 0$	$h/\lambda_0 = 0.270$	$h/\lambda_0 = 0$	$h/\lambda_0 = 0.270$
30 MHz ($\lambda_0 = 10$ m)						
60	0.1	9.5	0.1	4.1	0.6	13.6
64	0.1	9.3	0.8	3.8	0.7	13.2
70	0.1	3.3	1.0	9.5	0.9	12.7
74	0.1	6.0	1.1	6.5	1.0	12.4
80	0.2	8.3	1.0	4.1	1.3	12.4
85	1.3	8.2	0.4	9.6	1.8	17.8
90	0	0	0	0	0	0

the left half of the array of $p = m/2$ elements is over earth with a permittivity $\varepsilon_{\mathrm{I}}^{*}$ and the right-half of the array of $m - p = m/2$ elements is over earth with a permittivity $\varepsilon_{\mathrm{II}}^{*}$. Accordingly, $p/m = 0.5$ and

$$\varepsilon_{ku}^{*}, \alpha_k, \beta_k, R_{k,\mathrm{v}} = \begin{cases} \varepsilon_{\mathrm{I}}^{*}, \alpha_{\mathrm{I}}, \beta_{\mathrm{I}}, R_{\mathrm{I,V}} \text{ at } (m/2) \text{ elements}, & -r_A \le x_k \le 0 \\ \varepsilon_{\mathrm{II}}^{*}, \alpha_{\mathrm{II,v}}, \beta_{\mathrm{II}}, R_{\mathrm{II,v}} \text{ at } (m/2) \text{ elements}, & 0 \le x_k \le r_A \end{cases} \tag{13.2.22}$$

If the probability densities of the spacing of element location projections on the x and y axes were specified, then the cumulative probabilities, of the RMS phase error and beam pointing errors exceeding specified values, could be determined [191]. In this study, only the expected value of the RMS phase error and beam pointing errors are determined.

The expected value $\langle s \rangle$ of the spacing between element location projections x_k, x_{k+1} on the y axis, is given by

$$\langle s \rangle = r_A/(m-1) \tag{13.2.23}$$

For $m \gg 1$

$$\langle s \rangle / r_A \ll \langle |x_k| \rangle / r_A \, \langle |y_k| \rangle / r_A \ll 1 \tag{13.2.24}$$

Denoting the ordered projections of x_k on the negative and positive x axes as x_q then

$$\langle (x_k)_{\text{ordered}} \rangle = \langle x_q \rangle = \begin{cases} -q \langle s \rangle; q = 1, 2, \ldots, m/2; & -r_A \le x_q < 0 \\ & m \gg 1 \\ q \langle s \rangle; q = 1, 2, \ldots, m/2; & 0 \le x_q \le r_A \end{cases} \tag{13.2.25}$$

For α_k and x_k given by Eqs. (13.2.22) and (13.2.25), respectively,

$$\begin{aligned} \sum_{k=1}^{m} (x_k/r_A)(\alpha_k - \bar{\alpha}) &= \frac{1}{m-1} \left[(\alpha_{\mathrm{I}} - \bar{\alpha}) \sum_{q=1}^{m/2} -q + (\alpha_{\mathrm{II}} - \bar{\alpha}) \sum_{q=1}^{m/2} q \right] \\ &= \frac{1}{m-1} (\alpha_{\mathrm{II}} - \alpha_{\mathrm{I}}) \frac{(m/2)[(m/2)+1]}{2} \\ &= \frac{m(m+2)}{q(m-1)} (\alpha_{\mathrm{II}} - \alpha_{\mathrm{I}}) \end{aligned} \tag{13.2.26}$$

$$\sum_{k=1}^{m}(y_k/r_A)(\alpha_k-\bar{\alpha})=0;\ y_k \text{ and } x_k \text{ are randomly distributed} \tag{13.2.27}$$

$$\begin{aligned}\sum_{k=1}^{m}(x_k/r_A)^2&=\sum_{k=1}^{m}(y_k/r_A)^2=2\sum_{q=1}^{m/2}(x_q/r_A)^2\\&=\frac{2}{(m-1)^2}\sum_{q=1}^{m/2}q^2=\frac{2}{(m-1)^2}\frac{(m/2)[(m/2)+1](m+1)}{6}\\&=\frac{m(m+1)(m+2)}{12(m-1)^2}\end{aligned} \tag{13.2.28}$$

Substituting Eqs. (13.2.26)–(13.2.28) into Eqs. (13.2.10)–(13.2.16),

$$\bar{\alpha}(\theta)=(\alpha_{\mathrm{I}}+\alpha_{\mathrm{II}})/2 \tag{13.2.29}$$

$$\alpha_{\mathrm{rms}}(\theta)=\{0.5[(\alpha_{\mathrm{I}}-\bar{\alpha})^2+(\alpha_{\mathrm{II}}-\bar{\alpha})^2]-\alpha_{\mathrm{B}}^2\}^{1/2} \tag{13.2.30}$$

$$\begin{aligned}\alpha_{\mathrm{B}}&=\left\{\frac{1}{m}\left[\frac{m(m+2)(\alpha_{\mathrm{II}}-\alpha_{\mathrm{I}})}{8(m-1)}\right]^2\frac{12(m-1)^2}{m(m+1)(m+2)}\right\}^{1/2}\\&=\left[\frac{3}{16}\frac{(m+2)(\alpha_{\mathrm{II}}-\alpha_{\mathrm{I}})^2}{(m+1)}\right]^{1/2}=[(3/16)(m+2)/(m+1)]^{1/2}|\alpha_{\mathrm{II}}-\alpha_{\mathrm{I}}|\end{aligned} \tag{13.2.31}$$

$$\begin{aligned}\hat{u}-u&=\frac{\lambda_0}{2\pi r_A}\frac{m(m+2)(\alpha_{\mathrm{II}}-\alpha_{\mathrm{I}})}{8(m-1)}\frac{12(m-1)^2}{m(m+1)(m+2)}\\&=\frac{\lambda_0}{r_A}\frac{3}{4\pi}\frac{(m-1)(\alpha_{\mathrm{II}}-\alpha_{\mathrm{I}})}{(m+1)}\end{aligned} \tag{13.2.32}$$

$$\hat{v}-v=0 \tag{13.2.33}$$

$$\begin{aligned}B_\theta&=-\frac{1}{\cos\theta}(\hat{u}-u)\cos\phi=-\frac{\lambda_0}{r_A}\frac{3}{4\pi}\frac{(m-1)(\alpha_{\mathrm{II}}-\alpha_{\mathrm{I}})}{(m+1)}\\&\approx-(\mathrm{BW})_{\theta,3\,\mathrm{dB}}\frac{3}{2\pi}\frac{(m-1)(\alpha_{\mathrm{II}}-\alpha_{\mathrm{I}})\cos\phi}{(m+1)},\quad B_\theta\ll 1\,\mathrm{rad}\end{aligned} \tag{13.2.34}$$

where

$$(\mathrm{BW})_{\theta,3\,\mathrm{dB}} = \text{elevation beamwidth of the array main beam at its half-power points} = (1.02\lambda_0/2r_A\cos\theta)\,\mathrm{rad} \tag{13.2.35}$$

$$B_\phi = \frac{1}{\sin\theta}(\hat{u}-u)\sin\phi = \frac{\sin\phi}{\sin\theta}\frac{\lambda_0}{r_A}\frac{3}{4\pi}\frac{(m-1)(\alpha_{\mathrm{II}}-\alpha_{\mathrm{I}})}{(m+1)}$$
$$\approx (\mathrm{BW})_{\phi,3\,\mathrm{dB}}\frac{3}{2\pi}\frac{(m-1)(\alpha_{\mathrm{II}}-\alpha_{\mathrm{I}})}{(m+1)}\frac{\sin\phi}{\sin\theta},\quad B_\phi \ll 1\,\mathrm{rad} \tag{13.2.36}$$

where

$$(\mathrm{BW})_{\theta,3\,\mathrm{dB}} = \text{azimuth beamwidth of the array main beam at its half-power points} = (1.02\lambda_0/2r_A\,\mathrm{rad}) \tag{13.2.37}$$

Numerical values of the RMS phase error α_{rms} and beam pointing errors B_θ, B_ϕ are given in Tables 37–39 for systematically-distributed nonhomogeneous very dry ground/medium dry ground, medium dry ground/wet ground, and very dry ground/wet ground, respectively. The RMS phase errors are approximately 50% less than those given in Tables 33–35 for randomly-distributed nonhomogeneous earth. The elevation and azimuthal beam-pointing errors are approximately one-tenth the 3 dB beamwidths of the array main beam.

The expected values of the RMS phase error and elevation beam-pointing error of Tables 37–39 are summarized in Tables 40 and 41, respectively. The largest RMS phase error is 9°. The largest beam-pointing error is 0.3 of a beamwidth. The maximum errors occur for $\theta = 85°$, 30 MHz, $h/\lambda = 0.270$, and very dry ground/wet ground.

13.2.4 Summary and Conclusions

The electric field, at each element of a ground-based HF receiving array, is the sum of a direct field and an indirect (multipath) field. For elements with sufficiently-small ground planes, the indirect field is reflected not from the ground plane but from the earth in proximity to that element. The indirect field, relative to the direct field, is the product of the earth Fresnel reflection coefficient and a path-length phase delay that is proportional to the height of the element above the earth. If the earth beneath the array is not homogeneous, then the argument of the total electric field at each element (after allowance for the true phase advance of the direct field at each element) is not uniform from element to element. The nonuniform argument causes an array rms phase error. The nonuniform argument also causes beam pointing errors when the nonhomogeneous earth is systematically-distributed.

TABLE 37 RMS Phase Error and Beam Pointing Errors (Very Dry ground/Medium Dry ground, $p/m = 0.5$, Earth Nonhomogeneities Systematically Distributed so that Each half of Array is over Different Earth, $m = 96$ Elements)

Grazing angle, ψ (deg)	$\alpha_{II} - \alpha_I$ (rad)		Pointing RMS phase error α_B (rad)		RMS phase error α_{RMS} (rad)		Elevation pointing error $B_\theta/(BW)_{\theta,3\,dB}$, $\phi = 0$ rad		Azimuthal pointing error $B_\phi/(BW)_{\phi,3\,dB}$, $\phi = \pi/2$ rad	
	$h/\lambda_0 = 0$	$h/\lambda_0 = 0.054$	$h/\lambda_0 = 0$	$h/\lambda_0 = 0.054$	$h/\lambda_0 = 0$	$h/\lambda_0 = 0.054$	$h/\lambda_0 = 0$	$h/\lambda_0 = 0.054$	$h/\lambda_0 = 0$	$h/\lambda_0 = 0.054$
6 MHz ($\lambda_0 = 50m$)										
0	0	0	0	0	0	0	0	0	0	0
5	−0.044	−0.122	0.008	0.023	0.020	0.061	0.021	0.057	−0.021	−0.057
10	−0.034	−0.138	0.006	0.026	0.016	0.064	0.016	0.065	−0.016	−0.057
16	−0.026	−0.101	0.005	0.020	0.015	0.049	0.0012	0.049	−0.012	−0.051
20	−0.022	−0.101	0.004	0.019	0.010	0.047	0.010	0.047	−0.011	−0.050
26	−0.017	−0.098	0.003	0.019	0.008	0.045	0.008	0.046	−0.009	−0.051
30	−0.014	−0.097	0.003	0.018	0.006	0.046	0.007	0.045	−0.008	−0.052

Grazing angle, ψ (deg)	$\alpha_{II} - \alpha_I$ (rad)		Pointing RMS phase error α_B (rad)		RMS phase error α_{RMS} (rad)		Elevation pointing error $B_\theta/(BW)_{\theta,3\,dB}$, $\phi = 0$ rad		Azimuthal pointing error $B_\phi/(BW)_{\phi,3\,dB}$, $\phi = \pi/2$ rad	
	$h/\lambda_0 = 0$	$h/\lambda_0 = 0.270$	$h/\lambda_0 = 0$	$h/\lambda_0 = 0.270$	$h/\lambda_0 = 0$	$h/\lambda_0 = 0.270$	$h/\lambda_0 = 0$	$h/\lambda_0 = 0.270$	$h/\lambda_0 = 0$	$h/\lambda_0 = 0.270$
30 MHz ($\lambda_0 = 10$ m)										
0	0	0	0	0	0	0	0	0	0	0
5	−0.047	−0.285	0.009	0.054	0.021	0.132	0.022	0.133	−0.022	−0.132
10	−0.008	−0.290	0.002	0.055	0.003	0.134	0.004	0.136	−0.044	−0.138
16	0.004	−0.209	0.001	0.040	0.002	0.097	−0.002	0.098	0.002	−0.102
20	0.004	−0.113	0.001	0.021	0.002	0.053	−0.002	0.053	0.002	−0.056
26	0.003	−0.326	0.001	0.062	0.002	0.151	−0.001	0.152	0.001	−0.169
30	0.003	−0.332	0.001	0.063	0.002	0.154	−0.001	0.155	0.001	−0.179

$\alpha_B = [(3/16)(m+2)(m+1)]^{1/2}|a_{II} - \alpha_I|$, $\alpha_{rms} = (\alpha^2_{rms,\alpha_B=0} - \alpha^2_B)^{1/2}$.

$\frac{B_\theta}{(BW)_{\theta,3\,dB}} = \frac{-3}{2\pi}\frac{m-1}{m+1}(\alpha_{II} - \alpha_I)\cos\phi$, $\frac{B_\theta}{(BW)_{\theta,3\,dB}} = \frac{3}{2\pi}\frac{m-1}{m+1}\frac{\sin\phi}{\sin\theta}(\alpha_{II} - \alpha_I)$.

TABLE 38 RMS Phase Error and Beam Pointing Errors (Medium Dry Ground/Wet Ground, $p/m = 0.5$, Earth Nonhomogeneities Systematically Distributed so that Each Half of Array is over Different Earth, $m = 96$ Elements)

Grazing angle, ψ (deg)	$\alpha_{II} - \alpha_I$ (rad)		Pointing RMS phase error α_B (rad)		RMS phase error α_{RMS} (rad)		Elevation pointing error $B\theta/(BW)_{\theta,3\,dB}$, $\phi = 0$ rad		Azimuthal pointing error $B\phi/(BW)_{\theta,3\,dB}$, $\phi = \pi/2$ rad	
	$h/\lambda_0 = 0$	$h/\lambda_0 = 0.054$	$h/\lambda_0 = 0$	$h/\lambda_0 = 0.054$	$h/\lambda_0 = 0$	$h/\lambda_0 = 0.054$	$h/\lambda_0 = 0$	$h/\lambda_0 = 0.054$	$h/\lambda_0 = 0$	$h/\lambda_0 = 0.054$
6 MHz ($\lambda_0 = 50$ m										
0	0	0	0	0	0	0	0	0	0	0
5	−0.178	−0.213	0.077	0.093	0.045	0.140	0.083	0.100	−0.083	−0.100
10	−0.124	−0.160	0.054	0.070	0.030	0.039	0.058	0.075	−0.059	−0.076
16	−0.092	−0.128	0.040	0.056	0.023	0.031	0.043	0.060	−0.045	−0.062
20	−0.079	−0.115	0.034	0.050	0.021	0.027	0.037	0.054	−0.039	−0.057
26	−0.065	−0.098	0.028	0.043	0.021	0.029	0.030	0.046	−0.033	−0.051
30	−0.058	−0.096	0.025	0.042	0.015	0.029	0.027	0.045	−0.031	−0.052

Grazing angle, ψ (deg)	$\alpha_{II} - \alpha_I$ (rad)		Pointing RMS phase error α_B (rad)		RMS phase error α_{RMS} (rad)		Elevation pointing error $B_\theta/(BW)_{\theta,3\,dB}$, $\phi = 0$ rad		Azimuthal pointing error $B_\phi/(BW)_{\phi,3\,dB}$, $\phi = \pi/2$ rad	
	$h/\lambda_0 = 0$	$h/\lambda_0 = 0.270$	$h/\lambda_0 = 0$	$h/\lambda_0 = 0.270$	$h/\lambda_0 = 0$	$h/\lambda_0 = 0.270$	$h/\lambda_0 = 0$	$h/\lambda_0 = 0.270$	$h/\lambda_0 = 0$	$h/\lambda_0 = 0.270$
30 MHz ($\lambda_0 = 10$ m)										
0	0	0	0	0	0	0	0	0	0	0
5	−0.014	−0.336	0.006	0.146	0.004	0.083	0.007	0.157	−0.007	−0.157
10	−0.036	−0.142	0.016	0.062	0.008	0.035	0.017	0.066	−0.017	−0.067
16	−0.038	−0.225	0.017	0.098	0.008	0.056	0.018	0.105	−0.018	−0.109
20	−0.033	−0.330	0.014	0.144	0.010	0.081	0.015	0.154	−0.016	−0.164
26	−0.027	−0.134	0.012	0.058	0.007	0.034	0.013	0.063	−0.014	−0.070
30	−0.002	−0.144	0.001	0.063	0	0.035	0.001	0.067	−0.001	−0.077

$\alpha_B = [(3/16)(m+2)(m+1)]^{1/2}|a_{II} - \alpha_I|$, $\alpha_{rms} = (\alpha^2_{rms,\alpha_B=0} - \alpha^2_B)^{1/2}$.

$\frac{B_\theta}{(BW)_{\theta,3\,dB}} = \frac{-3}{2\pi}\frac{m-1}{m+1}(\alpha_{II} - \alpha_I)\cos\phi$, $\frac{B_\phi}{(BW)_{\phi,3\,dB}} = \frac{3}{2\pi}\frac{m-1}{m+1}\frac{\sin\phi}{\sin\theta}(\alpha_{II} - \alpha_I)$.

TABLE 39 RMS Phase Error and Beam Pointing Errors (Very Dry Ground/Wet Ground, $p/m = 0.5$, Earth Nonhomogeneities Systematically Distributed so that Each Half of Array is over Different Earth, $m = 96$ Elements)

	$\alpha_{II} - \alpha_I$ (rad)		Pointing RMS phase error α_B (rad)		RMS phase error α_{RMS} (rad)		Elevation pointing error $B_\theta/(BW)_{\theta,3\,dB}$, $\phi = 0$ rad		Azimuthal pointing error $B_\phi/(BW)_{\phi,3\,dB}$, $\phi = \pi/2$ rad	
Grazing angle, ψ (deg)	$h/\lambda_0 = 0$	$h/\lambda_0 = 0.054$	$h/\lambda_0 = 0$	$h/\lambda_0 = 0.054$	$h/\lambda_0 = 0$	$h/\lambda_0 = 0.054$	$h/\lambda_0 = 0$	$h/\lambda_0 = 0.054$	$h/\lambda_0 = 0$	$h/\lambda_0 = 0.054$
6 MHz ($\lambda_0 = 50$ m)										
0	0	0	0	0	0	0	0	0	0	0
5	−0.222	−0.335	0.097	0.146	0.054	0.083	0.104	0.157	−0.0104	−0.158
10	−0.158	−0.298	0.069	0.130	0.040	0.073	0.074	0.139	−0.075	−0.141
16	−0.118	−0.233	0.051	0.101	0.030	0.059	0.055	0.109	−0.057	0.113
20	−0.101	−0.216	0.044	0.094	0.026	0.053	0.047	0.101	−0.050	−0.107
26	−0.082	−0.196	0.036	0.085	0.020	0.050	0.038	0.092	−0.042	−0.102
30	−0.072	−0.193	0.031	0.084	0.018	0.049	0.034	0.090	−0.039	−0.104

	$\alpha_{II} - \alpha_I$ (rad)		Pointing RMS phase error α_B (rad)		RMS phase error α_{RMS} (rad)		Elevation pointing error $B_\theta/(BW)_{\theta,3\,dB}$, $\phi = 0$ rad		Azimuthal pointing error $B_\phi/(BW)_{\phi,3\,dB}$, $\phi = \pi/2$ rad	
Grazing angle, ψ (deg)	$h/\lambda_0 = 0$	$h/\lambda_0 = 0.270$	$h/\lambda_0 = 0$	$h/\lambda_0 = 0.270$	$h/\lambda_0 = 0$	$h/\lambda_0 = 0.270$	$h/\lambda_0 = 0$	$h/\lambda_0 = 0.270$	$h/\lambda_0 = 0$	$h/\lambda_0 = 0.270$
30 MHz ($\lambda_0 = 10$ m)										
0	0	0	0	0	0	0	0	0	0	0
5	−0.061	−0.621	0.027	0.270	0.015	0.154	0.029	0.290	−0.029	−0.291
10	−0.044	−0.432	0.019	0.188	0.011	0.106	0.021	0.021	−0.021	−0.025
16	−0.034	−0.434	0.015	0.189	0.008	0.107	0.016	0.202	−0.017	−0.210
20	−0.029	−0.443	0.013	0.193	0.007	0.110	0.014	0.207	−0.015	−0.220
26	−0.024	0.460	0.010	0.200	0.007	0.114	0.011	−0.215	−0.012	−0.239
30	−0.001	0.476	0.000	0.207	0.001	0.117	0.000	−0.0223	0.000	0.248

$\alpha_B = [(3/16)(m+2)(m+1)]^{1/2}|a_{II} - \alpha_I|$, $\alpha_{rms} = (\alpha^2_{rms,\alpha_B=0} - \alpha^2_B)^{1/2}$.
$\frac{B_\theta}{(BW)_{\theta,3\,dB}} = \frac{-3}{2\pi}\frac{m-1}{m+1}(\alpha_{II} - \alpha_I)\cos\phi$, $\frac{B_\phi}{(BW)_{\phi,3\,dB}} = \frac{3}{2\pi}\frac{m-1}{m+1}\frac{\sin\phi}{\sin\theta}(\alpha_{II} - \alpha_I)$.

TABLE 40 Summary of RMS Phase Errors ($p/m = 0.5$, Two-Level Nonhomogeneous Earth Systematically Distributed so that Each Half of Array is over Different Earth)

Angle of incidence, θ (deg)	RMS phase error, α_{RMS} (deg)					
	Very dry ground/ medium dry ground		Medium dry ground/ wet ground		Very dry ground/ wet ground	
	$h/\lambda_0 = 0$	$h/\lambda_0 = 0.054$	$h/\lambda_0 = 0$	$h/\lambda_0 = 0.054$	$h/\lambda_0 = 0$	$h/\lambda_0 = 0.054$
6 MHz ($\lambda_0 = 50$ m)						
60	0.3	2.6	0.9	1.7	1.0	4.8
64	0.5	2.6	1.2	1.7	1.1	4.2
70	0.6	2.7	1.2	1.5	1.5	3.4
74	0.9	2.8	1.3	1.8	1.7	3.0
80	0.9	3.7	1.7	2.2	2.3	2.9
85	1.1	3.5	2.6	8.0	3.1	2.8
90	0	0	0	0	0	0

Angle of incidence, θ(deg)	RMS phase error, α_{RMS} (deg)					
	Very dry ground/ medium dry ground		Medium dry ground/ wet ground		Very dry ground/ wet ground	
	$h/\lambda_0 = 0$	$h/\lambda_0 = 0.270$	$h/\lambda_0 = 0$	$h/\lambda_0 = 0.270$	$h/\lambda_0 = 0$	$h/\lambda_0 = 0.270$
30 MHz ($\lambda_0 = 10$ m)						
60	0.1	8.8	0.3	4.8	0.9	6.7
64	0.1	8.7	0.5	2.0	0.6	6.5
70	0.1	3.0	0.5	3.2	0.5	6.3
74	0.1	5.6	0.6	4.6	0.4	6.3
80	0.2	7.7	0.4	1.9	0.4	6.1
85	1.2	7.5	0	2.0	0.1	8.8
90	0	0	0	0	0	0

The earth Fresnel reflection coefficients and the arguments of the total field, for a vertically-polarized Hertzian dipole at height h above the earth, are tabulated in this paper for CCIR 527-1 classifications of earth and $h/\lambda_0 = 0$, 0.054, and 0.270. The normalized heights $h/\lambda_0 = 0.054$ and 0.270 correspond to the midpoint at 6 and 30 MHz, respectively, of a 5.4 m length vertical monopole. The RMS phase errors and beam pointing errors are modeled for arbitrary distributions of nonhomogeneous earth.

Numerical results are presented for randomly-distributed and systematically-distributed earth nonhomogeneities for cases where one-half of the array elements are located in proximity to one type of earth and the remaining half are located in proximity to a second type of earth. The combinations of earth types

TABLE 41 Summary of Elevation Beam Pointing Errors ($p/m = 0.5$, Two-Level Nonhomogeneous Earth Systematically Distributed so that Each Half of Array is over Different Earth)

Angle of incidence, θ (deg)	Elevation beam pointing error, $B_\theta/(\mathrm{BW})_{\theta,3\,\mathrm{dB}}$					
	Very dry ground/ medium dry ground		Medium dry ground/ wet ground		Very dry ground/ wet ground	
	$h/\lambda_0 = 0$	$h/\lambda_0 = 0.054$	$h/\lambda_0 = 0$	$h/\lambda_0 = 0.054$	$h/\lambda_0 = 0$	$h/\lambda_0 = 0.054$
6 MHz ($\lambda_0 = 50$ m)						
60	0.01	0.05	0.03	0.05	0.03	0.16
64	0.01	0.05	0.03	0.05	0.04	0.14
70	0.01	0.05	0.04	0.05	0.05	0.11
74	0.01	0.05	0.04	0.06	0.06	0.10
80	0.02	0.07	0.06	0.08	0.07	0.09
85	0.02	0.06	0.08	0.10	0.10	0.09
90	0	0	0	0	0	0

Angle of incidence, θ(deg)	Elevation beam pointing error, $B_\theta/(\mathrm{BW})_{\theta,3\,\mathrm{dB}}$					
	Very dry ground/ medium dry ground		Medium dry ground/ wet ground		Very dry ground/ wet ground	
	$h/\lambda_0 = 0$	$h/\lambda_0 = 0.270$	$h/\lambda_0 = 0$	$h/\lambda_0 = 0.270$	$h/\lambda_0 = 0$	$h/\lambda_0 = 0.270$
30 MHz ($\lambda_0 = 10$ m)						
60	−0.001	0.16	0.001	0.07	0.00	−0.22
64	−0.001	0.15	0.01	0.06	0.01	−0.22
70	−0.002	0.05	0.02	0.02	0.01	0.21
74	−0.002	0.10	0.02	0.11	0.02	0.20
80	0.004	0.14	0.02	0.07	0.02	0.20
85	0.02	0.13	0.01	0.16	0.03	0.29
90	0	0	0	0	0	0

that are considered are very dry ground/medium dry ground, medium dry ground/wet ground, and very dry ground/wet ground.

The RMS phase error is an increasing monotonic function of h/λ_0 (for modest values of h/λ_0). The RMS phase error is generally a nonmonotonic function of the angle of incidence θ.

The maximum expected values of the RMS phase errors at the best diffraction focus of the array for the cases examined, are 18 and 9° for randomly-distributed and systematically-distributed nonhomogeneities, respectively. The RMS phase error is less for systematically-distributed nonhomogeneities because the linear phase error caused by beam pointing errors has been subtracted from

the RMS phase error. The maximum expected values of the beam-pointing error (in elevation and in azimuth) are 0 and 0.3 beamwidths for randomly-distributed and systematically-distributed nonhomogeneities, respectively. The maximum RMS phase errors and beam pointing errors occur for very dry ground/wet ground, $\theta = 85°$, $h/\lambda_0 = 0.270$.

The above numerical results suggest that the influence of nonhomogeneous earth is appreciable, but not significant, on the performance of HF receiving arrays with electrically-small ground planes that do not require very low sidelobes.

13.3 PERFORMANCE OF GROUND-BASED HIGH-FREQUENCY RECEIVING ARRAYS WITH ELECTRICALLY SMALL GROUND PLANES

13.3.1 Introduction

High-frequency (HF) antenna elements for OTH receiving arrays often consist of some form of a vertical monopole element with a ground plane resting on the earth or in close proximity to it. Its proximity to earth causes a far-field multipath pattern null on the horizon; multipath ground losses; a critical angle space wave (see Fig. 75 of Sec. 9.2.2) which directs energy into the earth, but not the air medium, causing additional ground losses; and a near-field nonuniform multipath reflection from a nonhomogeneous earth.

The output of each antenna element (including its matching network, if any) is usually transmitted to its own receiver by means of a transmission line (hereafter referred to as a "feed cable"). Exterior currents are induced on the element feed cables by the tangential component of the monopole clement field incident on the cables and by ground-plane currents diffracted by the edge of the ground plane.

Antenna performance degradation by the earth and by external currents on the feed cables are mitigated by employing ground planes that are as large as is economically feasible. Large ground planes bring the peak of the multipath pattern closer to the horizon, reduce near-field ground losses, provide uniform near-field ground reflection from element-to-element, shield the cables from the element fields, and minimize the ground-plane current incident on the edge of the ground plane.

In the design of very large OTH receiving arrays (comprising hundreds or thousands of elements), electrically large metallic ground planes are prohibitively expensive to construct and maintain. One alternative approach is to employ salt-water ground planes; however, suitable salt-water sites are not readily available and they have unique problems. In this section, we discuss

another alternative approach, using elements with electrically small ground planes; and we also estimate the performance degradations that can result from it.

Performance degradations caused by electrically small ground planes include: (1) a reduction in element directivity near the horizon (caused by earth multipath) and distortion of the azimuthal pattern (caused by exterior currents on element feed cables), (2) a decrease in element radiation efficiency with a consequential increase in system internal noise (caused by ground losses), (3) an increase in the array factor root-mean-squared (rms) phase error (caused by nonuniform Fresnel reflection from nonhomogeneous earth and exterior currents on element feed cables), and (4) an increase in the array factor beam-pointing errors (caused by nonuniform Fresnel reflection from nonhomogeneous earth).

These performance degradations may be grouped according to their affect on element directivity, the system operating noise factor, and the array factor. The predetection SNR of a receiving system is proportional to the receive antenna directivity (which is proportional to the element directivity and the array factor) and is inversely proportional to the system operating noise factor (see Sec. 13.1).

For ground-based HF radar or communication systems, the earth excess propagation loss factor is usually included in the antenna ground-plane system rather than in the propagation path. Ohmic losses of the receive antenna (including its ground-plane system and matching network) are incorporated as part of the system operating noise factor in accordance with CCIR convention.

13.3.2 Element Directivity

Monopole elements with perfect ground planes (of infinite extent, conductivity, and density) have a radiation pattern that has its peak on the horizon and is omnidirectional in azimuth. Furthermore, the current on the exterior of the element feed cable is zero. For this case, the interference of the element and the image fields is totally constructive in the direction of the horizon, the feed cable is completely shielded from the element fields, and the current on the bottom surface of the ground plane is zero.

For imperfect ground planes, the direction of peak directivity is at an angle above the horizon. The directivity on the horizon is approximately -6 and $-\infty$ dBi when the ground plane is in free space and when it is in proximity to flat earth, respectively. Furthermore, the current on the exterior of the element feed cable is nonzero because the feed cable is not completely shielded from the element fields, and the current on the bottom surface of the ground plane at the feed cable is also nonzero.

The directivity of monopole elements on electrically small *disk* ground planes resting on flat earth is determined in Sec. 10.2 using Richmond's method-of-moments computer program. Numerical results for various types of earth are given in App. A.6. The peak directivity is approximately independent of disk

radius and approximately equal to that for a perfect ground plane. The angle of incidence of the peak directivity for ground-plane radii less than a couple of wavelengths is approximately independent of ground-plane radius and approximately 30° above the horizon except for sea water for which the peak directivity is within 10° of the horizon. The earth softens the edge of the ground plane and minimizes changes in directivity resulting from ground-plane edge diffraction. With the exception of seawater, a disk radius of greater than 10 wavelengths is required so that the angle of incidence of the peak directivity is within 8° of the horizon.

The directivity of monopole elements on electrically-small *radial-wire* ground planes in proximity to flat earth is determined using the Lawrence Livermore National Laboratory method-of-moments for wire elements known as Numerical Electromagnetics Code (NEC). Numerical results for various types of earth are given in App. A.7. The directivity is approximately the same as that for a disk ground plane of the same radius.

The condition of zero exterior current on the feed cable is never realized for monopole elements with imperfect ground planes. However, this condition is approximated in practice with lossy ferrite toroidal cases around the feed cable (see Sec. 2.4). The ferrite toroids must extend along the cable to a distance so that the element field impinging upon the cable is sufficiently weak and the current (edge-diffracted underneath the ground plane to the feed cable) is adequately attenuated.

The exterior current on the feed cable may also be minimized by burying the cable below the surface of the earth at a sufficient depth. The depth can be much less than the field penetration depth. For example, the penetration depth for a plane wave incident normally on medium dry ground at 15 MHz is 21 m (see Table 16). If the feed cable is buried at a depth of 21 cm (1/100 of the penetration depth), most of the exterior current that is generated on the feed cable will not be reradiated into the air medium; instead, it will be leaked off into the earth (see Sec. 11.1.3).

13.3.3 System Operating Noise Factor

The predetection SNR of a receiving system is inversely proportional to the system operating noise factor f. If the ambient temperatures of the receiving antenna, matching network, and transmission line are equal to the reference temperature, then Eq. (13.1.4) reduces to

$$f = f_a - 1 + \ell_c \ell_m \ell_n f_d \tag{13.3.1}$$

where

f_a = receive antenna external noise factor integrated over the antenna pattern function (numeric)

ℓ_c, ℓ_m, ℓ_n = available loss factors of the receive antenna, matching network, and transmission line, respectively (numeric ≥ 1)

f_r = receiver noise factor (numeric)

f_p = signal-to-noise processing factor (numeric)

For an external noise-limited system, the system operating noise factor given by Eq. (13.1.4) reduces to

$$f \approx f_a, \quad f_a \gg \ell_c \ell_m \ell_n f_d - 1 \tag{13.3.2}$$

where ℓ_c, ℓ_m, ℓ_n, and f_d are internal noise parameters generated by the receiving system. When the receiving system is externally noise-limited, which is one of the design objectives of the HF receiving system, the system operating noise factor is minimized and the predetection SNR is maximized.

The external noise factor f_a is a function of the directivity of the receive antenna [see Eq. (13.1.13)]. The available loss factors ℓ_c, ℓ_m, ℓ_n and the receiver noise factor f_r are evaluated in Sec. 13.1.2 as functions of the circuit impedance parameters and source impedances of the respective circuits. The available loss factors are equal to the ratio of the input to output available powers of the respective circuits, which is unity when the ohmic loss of the circuit is zero. The ohmic loss of the receive antenna earth–ground system is conventionally included in the available loss factor ℓ_c of the receive antenna (rather than in the excess propagation loss factor) in HF receive systems [see Eq. (6.4.17)]. The receiver noise factor f_d is a function of the noise factors of the receiver front end, A/D converter, and FIR filter [see Eq. (13.1.13)].

The parameters f_a, ℓ_c, ℓ_m, ℓ_n, and f_d are all functions of the extent, conductivity, and density of the receive antenna ground plane. The parameters ℓ_m, ℓ_n, and f_d, which are indirect functions of these ground-plane parameters, become stabilized (as a function of ground-plane radius and earth permittivity) for small ground planes. The antenna available loss factor ℓ_c, a direct monotonic function of these ground-plane parameters, requires a much larger ground plane before becoming stabilized.

The antenna available loss factor ℓ_c is defined as the ratio of the available power at the input of the antenna to the radiated far-field power. For an antenna in free space or in proximity to dielectric earth ($\sigma = 0$), the far-field power is radiated into the hemispheres above and below the antenna. However, for an antenna in proximity to lossy earth ($\sigma > 0$), the radiated far-field power is confined to the hemisphere above the earth because any power radiated downward into lossy earth is attenuated at large distances at a rate greater than $1/r^2$. The antenna available loss factor ℓ_c is given by Eq. (6.4.17) as

$$\ell_c = 1/\eta = R_{in}/R_{rad} = 1 + (R_c/R_{rad}) \tag{13.3.3}$$

where

η = antenna radiation efficiency = fraction of the available input power that is radiated to the far field (numeric ≤ 1)
R_{in} = antenna input resistance = $R_c + R_{rad}$ (ohm)
R_{rad} = antenna radiation resistance (ohm)
R_c = series resistance due to ohmic losses of the antenna circuit including ground losses, but excluding losses in the matching network (ohm). The series resistance R_c is only from ohmic losses in the earth if the element and ground plane are assumed to be fabricated from metal of infinite conductivity

The radiation efficiency of a vertical dipole above lossy earth increases nonmonotonically with increasing height above earth, nonmonotonically with increasing length of the dipole, and nonmonotonically with increasing conductivity of the earth (see Sec. 9.2.3). For lossy earth ($\sigma > 0$), computer runs of the NEC-3 program using the Sommerfeld option yield a minimum radiation efficiency $\eta = 0$ in the limit of the dipole length h and the dipole height $|z_0|$ both approaching zero (see Table 20). The radiation efficiency of monopole elements in proximity to earth is tabulated in Appendices A.6 and A.7 for a quarterwave element and in Table 42 (after Lagace [171]) for an electrically short element.

The available loss factors of the receive antenna, matching network, and transmission line (ℓ_c, ℓ_m, ℓ_n, respectively), and the receiver noise factor f_d are functions of the source impedance of each of the respective circuits (see Sec. 6.4.2). Consequently, these parameters are a function of the receive antenna input impedance which, in turn, is a function of the receive antenna ground-plane system.

Antenna impedance mismatch can cause a significant increase in the internal noise factor (see Sec. 6.4.3). This problem is particularly acute in HF receiving systems because they usually employ electrically short elements that must operate over a wide range of frequencies. Therefore, there is interest in stabilizing the antenna receive mode input impedance so that the system remains externally noise-limited.

The antenna input impedance is a function of the normalized element length h/λ (the most influential parameter), the ground-plane system, and the normalized element radius b/λ which influences input reactance more than input resistance. The normalized ground-plane radius $2\pi a/\lambda$, groundscreen density (or number N of radial wires), normalized ground-plane height z_0/λ of the earth's surface relative to the ground plane, and earth relative permittivity ϵ^*/ϵ_0 also affect input impedance.

Normalized ground-plane radii of at least $2\pi a/\lambda = 2$ rad are required to stabilize the input impedance of quarter-wave elements with high-density ground planes to within 20% of that for a perfect ground plane (See Apps. A.6 and A.7).

TABLE 42 Radiation Efficiency η and Noise Figure NF $= 10 \log \eta$ of Electrically Short Monopole Element ($h = 5.4$ m, $f = 5$–30 MHz) with Buried Radial-Wire Ground Plane ($N = 16$, $a = 12$ m, $b_w = 10^{-3}$ m, $|z_0| = 0.178$ m) (Lagace [171], 1991)

	Soil characteristics									
	Very good (wet ground)		Good (moist clay)		Average (medium dry ground)		Fair (sand)		Poor (very dry ground)	
	$\epsilon_r = 30$, $\sigma = 15$ mS/m		$\epsilon_r = 10$, $\sigma = 15$ mS/m		$\epsilon_r = 10$, $\sigma = 1.5$ mS/m		$\epsilon_r = 4$, $\sigma = 1.5$ mS/m		$\epsilon_r = 4$, $\sigma = 0.15$ mS/m	
Frequency (MHz)	η (%)	NF (dB)	η (%)	NF (dB)	η (%)	NF (dB)	η (%)	NF (dB)	η (%)	NF (dB)
5.0	28.9	5.4	29.7	5.3	18.2	7.4	15.3	8.2	20.2	6.9
7.5	29.3	5.3	28.5	5.4	20.5	6.9	19.1	7.2	26.6	5.8
10.0	31.0	5.1	28.7	5.4	22.9	6.4	21.9	6.6	24.7	6.1
12.5	32.1	4.9	28.6	5.4	24.4	6.1	23.8	6.2	28.1	5.5
15.0	32.6	4.9	27.8	5.6	25.0	6.0	22.4	6.5	20.2	6.9
17.5	33.2	4.8	27.0	5.7	25.3	6.0	21.6	6.7	21.3	6.7
20.0	33.7	4.7	26.3	5.8	26.4	5.8	22.5	6.5	23.4	6.3
22.5	34.5	4.6	26.3	5.8	27.8	5.6	24.2	6.2	24.4	6.1
25.0	35.8	4.5	27.1	5.7	30.2	5.2	26.8	5.7	27.7	5.6
27.5	38.1	4.2	29.9	5.2	34.8	4.6	32.4	4.9	33.6	4.7
30.0	42.1	3.8	36.6	4.4	42.4	3.7	42.9	3.7	45.0	3.5

The minimum number of radial wires required to achieve this degree of stabilization is approximately $N = 32$. The input impedance of monopole antennas with low-density ground planes is stabilized with ground-plane radii smaller than those required for high-density ground planes.

The external noise factor f_a in Eq. (13.1.13) is a function of the directivity (and, consequently, ground-plane characteristics) of the receive antenna unless the angular distribution $f(\theta, \phi)$ of the external noise is uniform in the hemisphere above lossy earth.

For an antenna in proximity to lossy earth, $f(\theta, \phi) = 0$ and $d_r(\theta, \phi) = 0$ in the hemisphere below the ground. Therefore, Eq. (13.1.13) reduces to

$$f_a = \frac{1}{4\pi} \int_0^{2\pi} \int_0^{2\pi} f(\theta, \phi) d_r(\theta, \phi) \sin\theta \, d\theta \, d\phi, \tag{13.3.4}$$

antenna in proximity to lossy earth

Since the directivity $d_r(\theta, \phi)$ of a monopole element with a circular ground plane is approximately independent of the ground-plane radius for normalized ground-plane radii $ka \leq 8$ rad, the external noise factor f_a is approximately independent of ground plane radius for normalized ground-plane radii at least as small as 8 rad.

The CCIR (French) published statistical values of f_a for atmospheric noise in the frequency range 0.01–20 MHz based on measurements as a function of location, time of day, and season [187] and man-made noise in the frequency range 0.25–250 MHz based on measurements as a function of type of location [188]. These values, denoted by f_{aCCIR}, are claimed to be normalized to correspond to those values that would be measured with an electrically short vertically polarized monopole element mounted on a perfect ground plane [187,188]. It should be noted, however, that the antenna used for the CCIR measurements is a monopole element 21.75 ft long and a ground plane consisting of 90 radial wires (each 100 ft long and situated 8 ft above the ground) [192]. The HF CCIR values most likely correspond to those values that would be measured with an electrically short vertically polarized monopole element mounted on an electrically small ground plane in proximity to lossy earth.

If the values of f_{aCCIR} have been normalized to correspond to those values that would be measured with an electrically short monopole element on a perfect ground plane, then

$$d_{rCCIR}(\theta) = \begin{cases} 3\sin^2\theta, & 0 \leq \theta \leq \pi/2 \\ 0, & -\pi/2 \leq \theta < 0; \text{ perfect ground plane} \end{cases} \tag{13.3.5}$$

However, the values of f_{aCCIR} in the HF band correspond more closely to those values that would be measured with an electrically small ground plane.

The ground plane radial wires used to obtain the CCIR database are of length $a = 100\,\text{ft}$, corresponding to $2\pi a/\lambda = 1.9$ and 19 rad at 3 and 30 MHz, respectively. The CCIR database [187,188] in the HF band is better approximated by that for an electrically small ground plane for normalized ground-plane radii $0 \le 2\pi a/\lambda \le 8.0\,\text{rad}$ and possibly larger radii. Accordingly, $d_{\text{rCCIR}}(\theta)$ is better approximated by Eq. (10.2.34); namely,

$$d_{\text{rCCIR}}(\theta) = \begin{cases} 10\cos\theta\sin^3\theta, & 0 \le \theta \le \pi/2 \\ 0, & -\pi/2 \le \theta < 0; \end{cases} \qquad (13.3.6)$$

electrically small ground planes on lossy earth,

$0 \le 2\pi a/\lambda \le 8.0\,\text{rad}$.

The spatial distribution $f_s(\theta, \phi)$ of the CCIR external noise database at any specific site location was not measured and therefore remains unknown. If $f_s(\theta, \phi)$ were uniform [$f_s(\theta, \phi) = \text{constant}$], then the external noise factor f_a given by Eq. (13.3.4) reduces to $f_a = f_s(\theta, \phi) = \text{constant}$ and f_a is unaffected by whether Eqs. (13.3.5) or (13.3.6) were assumed for the directive gain $d_r(\theta, \phi)$. However, if $f_s(\theta, \phi) \neq \text{constant}$, then the external noise factor f_a can be appreciably different from the tabulated values $f_{a\text{CCIR}}$, depending upon the values of $d_r(\theta, \phi)$ and $f_s(\theta, \phi)$ that were assumed in calibrating the CCIR database (see Table 43). For example, if the actual directive gain of the CCIR antenna is given by Eq. (13.3.6) but that of Eq. (13.3.5) were assumed in calibrating the data and if the angular noise distribution had a peak on the horizon (Case 3 in Table 43), then

TABLE 43 Comparison of External Noise Factor f_a with CCIR Measured Values $f_{a\text{CCIR}}$

Case		Angular distribution of CCIR external noise $f_{\text{CCIR}}(\theta)/f_{a\text{CCIR}}$		External Noise Factor $f_a/f_{a\text{CCIR}}$	
No.	CCIR noise distribution	CCIR antenna (1)	CCIR antenna (2)	CCIR antenna (1)	CCIR antenna (2)
1	Uniform	1.00	1.00	1.00	1.00
2	Peak on horizon	$1.805\sin^8\theta$	$2.6\sin^8\theta$	0.69	1.00
3	Peak at $\theta = 60°$	$4.667\cos\theta\sin^3\theta$	$3.9\cos\theta\sin^3\theta$	1.19	1.00
4	Point source on horizon	$0.667\,\delta[\theta - (\pi/2)]$,	$A\delta[\theta - (\pi/2)]$, $A = \infty$	0	1.00

Receive antenna: Electrically-short monopole element with an electrically-small ground plane resting on lossy earth $d_r(\theta) = 10\cos\theta\sin^3\theta$; $0 \le \theta \le \pi/2$ rad, zero otherwise.

CCIR antenna (1): Electrically-short monopole element with a perfect ground plane $d_{\text{rCCIR}}(\theta) = 3\sin^2\theta$; $0 \le \theta \le \pi/2$ rad, zero otherwise.

CClR antenna (2): Electrically-short monopole element with an electrically-small ground plane resting on lossy earth $d_{\text{rCCIR}}(\theta) = 10\cos\theta\sin^3\theta$; $0 \le \theta \le \pi/2$ rad, zero otherwise

the actual noise factor $f_a = 0.69 f_{aCCIR}$. For a point source on the horizon (Case 4 in Table 43), $f_a = 0 f_{aCCIR}$.

13.3.4 Array Factor Degradation by Nonhomogeneous Earth

The electric field, at each element of a ground-based HF receiving array, is the sum of a direct field and an indirect (multipath) field. For elements with sufficiently small ground planes, the indirect field is not reflected from the ground plane; instead, it is reflected from the earth in proximity to that element. The indirect field, relative to the direct field, is the product of the earth Fresnel reflection coefficient and a pathlength phase delay that is proportional to the height of the element above the earth. If the earth beneath the array is nonhomogeneous, then the argument of the total electric field at each element (after allowance for the true phase advance of the direct field at each element) is not uniform from element-to-element. The nonuniform argument causes an array rms phase error and beam-pointing errors when the nonhomogeneous earth is systematically distributed. The rms phase errors and elevation beam-pointing errors are modeled in Sec. 13.2 for either randomly or systematically distributed nonhomogeneous earth. Numerical results are summarized in Tables 36, 40, and 42 of Sec. 13.2.3.

The maximum expected values of the rms phase errors at the best diffraction focus of the array for the cases examined are 18 and 9° for randomly distributed and systematically distributed inhomogeneities, respectively. The rms phase error is less for systematically distributed inhomogeneities because the linear phase error caused by beam-pointing errors has been subtracted. The maximum expected values of the beam-pointing error (in elevation and in azimuth) are zero and 0.3 beamwidths for randomly distributed and systematically distributed inhomogeneities, respectively. The maximum rms phase errors and beam-pointing errors occur for very dry ground/wet ground, $\theta = 85°$, $h/\lambda = 0.270$.

13.3.5 Summary and Conclusions

Ground-based HF receiving arrays often employ some form of a vertical monopole element with a ground plane that is made as large as is economically feasible to mitigate the effects of the earth and feed-cable exterior current on system performance. In the design of very large ground-based HF receiving arrays comprising hundreds or thousands of elements, electrically large metallic ground planes are prohibitively expensive to construct and maintain. Economically, electrically small ground planes are a relatively low-cost solution

to this problem, provided the system performance is not too adversely affected. The performance of HF receiving arrays with electrically small ground planes is investigated herein.

Electrically small ground planes do degrade the performance of ground-based HF receiving arrays by reducing element directivity near the horizon, distorting the element azimuthal pattern, increasing the system internal noise factor, and increasing the array factor rms phase error and beam-pointing errors. These performance degradations, however, are not significant for most applications.

earth multipath reduces the directivity near the horizon. The peak directivity is approximately the same as that for a perfect ground plane except that the peak directivity is approximately 30° above the horizon instead of near the horizon. The directivity pattern is unaffected by the size of the ground plane for normalized ground-plane radii at least as large as $0 \leq 2\pi a/\lambda \leq 8$ rad. The numeric directivity, of electrically short monopole elements with electrically small ground planes resting on lossy earth, is given approximately by $d_r(\theta) = 10\cos\theta\sin^3\theta$; $0 \leq \theta \leq 90°$ zero otherwise. At angles near the horizon and for normalized ground-plane radii at least as large as 8 rad, the directivity is reduced from the peak directivity by approximately 4 dB at $\theta = 82°$, 5 dB at 84°, 7 dB at 86°, 12 dB at 88°, and ∞ dB at 90°.

The exterior current on the element feed cable distorts the element azimuthal pattern and modifies the phase center of the element.

The system internal noise factor is increased by increased ground losses and antenna impedance mismatch. Whenever the antenna proximity to earth is not mitigated (by an electrically large ground plane), the element ground losses are increased because of the generation of a critical angle space wave that directs energy into the earth, but not into the air medium. The radiation efficiency of a vertically polarized Hertzian dipole resting on earth is zero if the earth is lossy, and is approximately 10% if the earth is a perfect dielectric. The radiation efficiency of monopole antennas increases monotonically with increasing radius and density of the ground planes, and increasing length of the monopole element; it increases quasi-monotonically with increasing height of the ground plane above the earth.

Antenna impedance mismatch can cause a significant increase in the system internal noise factor, particularly in HF receiving systems, because such systems usually employ electrically short elements that must operate over a wide range of frequencies. Normalized ground-plane radii of at least $2\pi a/\lambda = 2$ rad are required to stabilize the input impedance of quarter-wave elements with a high-density ground plane to within 20% of that for a perfect ground plane. The input impedance for a low-density ground plane is stabilized by ground-plane radii smaller than those for a high-density ground plane. Impedance-matching networks are generally necessary to achieve impedance matching over a wide

range of frequencies. The ohmic loss of the matching network should be minimized so that the reduction in internal noise factor achieved by reduced mismatch loss is not offset by an increase in internal noise factor caused by those ohmic losses.

The external noise factor of HF receiving systems with electrically small ground planes is expected to be comparable to CCIR predicted values. Although CCIR claims that their predicted values have been normalized to those for an electrically short monopole element on a perfect ground plane, the ground-plane radial wires used to obtain the database are of length $a = 100$ ft, corresponding to $2\pi a/\lambda = 1.9$ and 19 rad at 3 and 30 MHz, respectively. The ground-plane radii are too small to yield a directivity pattern at HF wavelengths that is appreciably different from that of a vertically polarized Hertzian dipole resting on lossy earth. It is doubtful that the CCIR values of the external noise factor are normalized to correspond to those for a perfect ground plane. This kind of normalization would require a knowledge of the elevation angular distribution of external noise, which was not experimentally determinable; it would also require knowledge of the directivity of monopole elements with electrically small ground planes resting on lossy earth, but that was not known theoretically until recently.

The electric field at each element of a ground-based HF receiving array is the sum of a direct field and an indirect (multipath) field. For elements with electrically small ground planes in proximity to inhomogeneous earth, the indirect field causes an array rms phase error and beam-pointing errors when the earth inhomogeneities are systematically distributed. The maximum expected values of rms phase error, at the best diffraction focus of the array for very dry/wet inhomogeneous earth, are 18 and 9° for randomly distributed and systematically distributed inhomogeneities, respectively. The maximum expected value of the beam-pointing error is zero and 0.3 beamwidths for randomly distributed and systematically distributed nonhomogeneities, respectively.

The most significant performance degradation is the reduced directivity at angles near the horizon. For applications that require better directivity at those angles, the ground plane must be made electrically large unless the ground planes are in proximity to sea water.

Appendix A

Computer Plots and Printouts of Numerical Results

A.1 INTEGRAL EQUATION

TABLE A1-1

INTEGRAL EQUATION METHOD
EPSILON= 0.0 (NORMALIZED GROUNDPLANE RADIUS)
MONOPOLE LENGTH= 0.250000(WAVELENGTH)
INFINITELY THIN MONOPOLE RADIUS
RADIATION RESISTANCE = 19.434878 (OHMS)

ELEVATION ANGLE θ (DEG)	DIRECTIVITY (NUMERIC)	DIRECTIVITY (DBI)	RELATIVE POWER (DB)	ELEVATION ANGLE (DEG)	DIRECTIVITY (NUMERIC)	DIRECTIVITY (DBI)	RELATIVE POWER (DB)
0	0.00000	-INFINITY	-INFINITY				
2.0	0.00163	-27.88102	-28.76341	92.0	1.54010	1.87635	-0.00804
4.0	0.00651	-21.86343	-23.74582	94.0	1.53389	1.85821	-0.02418
6.0	0.01463	-18.34684	-20.22903	96.0	1.52334	1.82796	-0.05443
8.0	0.02597	-15.85494	-17.73733	98.0	1.50853	1.78553	-0.09686
10.0	0.04050	-13.92589	-15.80828	100.0	1.48966	1.73087	-0.15152
12.0	0.05816	-12.35353	-14.23592	102.0	1.46686	1.66389	-0.21850
14.0	0.07892	-11.02803	-12.91042	104.0	1.44028	1.58446	-0.29793
16.0	0.10271	-9.88386	-11.76625	106.0	1.41009	1.49247	-0.38992
18.0	0.12946	-8.87877	-10.76116	108.0	1.37649	1.38774	-0.49464
20.0	0.15908	-7.98396	-9.86635	110.0	1.33971	1.27010	-0.61229
22.0	0.19147	-7.17889	-9.06128	112.0	1.29996	1.13930	-0.74309
24.0	0.22654	-6.44846	-8.33085	114.0	1.25751	0.99511	-0.88728
26.0	0.26417	-5.78120	-7.66359	116.0	1.21261	0.83722	-1.04517
28.0	0.30421	-5.16823	-7.05062	118.0	1.16554	0.66528	-1.21711
30.0	0.34653	-4.60256	-6.48495	120.0	1.11659	0.47892	-1.40347
32.0	0.39097	-4.07857	-5.96096	122.0	1.06603	0.27788	-1.60471
34.0	0.43735	-3.59167	-5.47406	124.0	1.01415	0.06104	-1.82135
36.0	0.48550	-3.13812	-5.02050	126.0	0.96126	-0.17158	-2.05397
38.0	0.53521	-2.71478	-4.59717	128.0	0.90764	-0.42085	-2.30324
40.0	0.58627	-2.31905	-4.20143	130.0	0.85358	-0.68756	-2.56995
42.0	0.63845	-1.94870	-3.83109	132.0	0.79936	-0.97259	-2.85498
44.0	0.69153	-1.60168	-3.48427	134.0	0.74525	-1.27697	-3.15936
46.0	0.74525	-1.27697	-3.15936	136.0	0.69153	-1.60188	-3.48427
48.0	0.79936	-0.97259	-2.85498	138.0	0.63845	-1.94870	-3.83109
50.0	0.85358	-0.68756	-2.56995	140.0	0.58627	-2.31905	-4.20143
52.0	0.90764	-0.42085	-2.30324	142.0	0.53521	-2.71478	-4.59717
54.0	0.96126	-0.17158	-2.05397	144.0	0.48550	-3.13812	-5.02050
56.0	1.01415	0.06104	-1.82135	146.0	0.43735	-3.59167	-5.47406
58.0	1.06603	0.27788	-1.60471	148.0	0.39097	-4.07857	-5.96096
60.0	1.11659	0.47892	-1.40347	150.0	0.34653	-4.60256	-6.48495
62.0	1.16554	0.66528	-1.21711	152.0	0.30421	-5.16823	-7.05062
64.0	1.21261	0.83722	-1.04517	154.0	0.26417	-5.78120	-7.66359
66.0	1.25751	0.99511	-0.88728	156.0	0.22654	-6.44846	-8.33085
68.0	1.29996	1.13930	-0.74309	158.0	0.19147	-7.17889	-9.06128
70.0	1.33971	1.27010	-0.61229	160.0	0.15908	-7.98396	-9.86635
72.0	1.37649	1.38774	-0.49464	162.0	0.12946	-8.87877	-10.76116
74.0	1.41009	1.49247	-0.38992	164.0	0.10271	-9.88386	-11.76625
76.0	1.44028	1.58446	-0.29793	166.0	0.07892	-11.02803	-12.91042
78.0	1.46686	1.66389	-0.21850	168.0	0.05816	-12.35353	-14.23592
80.0	1.48966	1.73087	-0.15152	170.0	0.04050	-13.92589	-15.80828
82.0	1.50853	1.78553	-0.09686	172.0	0.02597	-15.85494	-17.73733
84.0	1.52334	1.82796	-0.05443	174.0	0.01463	-18.34684	-20.22903
86.0	1.53389	1.85821	-0.02418	176.0	0.00651	-21.86343	-23.74582
88.0	1.54010	1.87635	-0.00604	178.0	0.00163	-27.88102	-29.76341
90.0	1.54209	1.88239	0.0	180	0.00000	-INFINITY	-INFINITY

$h/\lambda = 0.25,\ 0 \le ka \le 3.0$.

TABLE A1-2

INTEGRAL EQUATION METHOD
EPSILON= 0.2500(NORMALIZED GROUNDPLANE RADIUS)
MONOPOLE LENGTH= 0.250000(WAVELENGTH)
INFINITELY THIN MONOPOLE RADIUS
RADIATION RESISTANCE = 19.480016 (OHMS)

ELEVATION ANGLE (DEG)	DIRECTIVITY (NUMERIC)	DIRECTIVITY (DBI)	RELATIVE POWER (DB)	ELEVATION ANGLE (DEG)	DIRECTIVITY (NUMERIC)	DIRECTIVITY (DBI)	RELATIVE POWER (DB)
0	0.00000	-INFINITY	-INFINITY				
2.0	0.00164	-27.83892	-29.71123	92.0	1.53686	1.86634	-0.00598
4.0	0.00657	-21.82152	-23.69383	94.0	1.53052	1.84839	-0.02393
6.0	0.01477	-18.30504	-20.17735	96.0	1.52000	1.81845	-0.05387
8.0	0.02622	-15.81378	-17.68610	98.0	1.50538	1.77646	-0.09586
10.0	0.04088	-13.88530	-15.75762	100.0	1.48674	1.72236	-0.14996
12.0	0.05870	-12.31364	-14.18595	102.0	1.46421	1.65605	-0.21627
14.0	0.07964	-10.98695	-12.85126	104.0	1.43794	1.57742	-0.29490
16.0	0.10362	-9.84569	-11.71801	106.0	1.40810	1.48633	-0.38599
18.0	0.13057	-8.84163	-10.71395	108.0	1.37487	1.38262	-0.48970
20.0	0.16040	-7.94795	-9.82026	110.0	1.33847	1.26608	-0.60623
22.0	0.19301	-7.14411	-9.01642	112.0	1.29912	1.13650	-0.73581
24.0	0.22830	-6.41499	-8.28731	114.0	1.25707	0.99361	-0.87871
26.0	0.26613	-5.74914	-7.62145	116.0	1.21256	0.83710	-1.03521
28.0	0.30636	-5.13766	-7.00997	118.0	1.16591	0.66664	-1.20568
30.0	0.34886	-4.57354	-6.44586	120.0	1.11733	0.48181	-1.39050
32.0	0.39344	-4.05116	-5.92348	122.0	1.06713	0.28217	-1.59014
34.0	0.43995	-3.56594	-5.43825	124.0	1.01559	0.06720	-1.80512
36.0	0.48819	-3.11410	-4.98642	126.0	0.96300	-0.16372	-2.03603
38.0	0.53796	-2.69252	-4.56484	128.0	0.90965	-0.41124	-2.28356
40.0	0.58904	-2.29858	-4.17089	130.0	0.85582	-0.67617	-2.54849
42.0	0.64120	-1.93004	-3.80236	132.0	0.80179	-0.95940	-2.83171
44.0	0.69422	-1.58504	-3.45735	134.0	0.74783	-1.26196	-3.13427
46.0	0.74783	-1.26185	-3.13426	136.0	0.69422	-1.58505	-3.45736
48.0	0.80179	-0.95939	-2.83170	138.0	0.64120	-1.93005	-3.80237
50.0	0.85582	-0.67616	-2.54847	140.0	0.58904	-2.29859	-4.17090
52.0	0.90965	-0.41123	-2.28355	142.0	0.53796	-2.69254	-4.56485
54.0	0.96301	-0.16371	-2.03602	144.0	0.48819	-3.11411	-4.98643
56.0	1.01559	0.06720	-1.80511	146.0	0.43995	-3.56595	-5.43827
58.0	1.06713	0.28218	-1.59013	148.0	0.39344	-4.05118	-5.92349
60.0	1.11733	0.48182	-1.39049	150.0	0.34865	-4.57356	-6.44587
62.0	1.16591	0.66665	-1.20567	152.0	0.30636	-5.13767	-7.00999
64.0	1.21258	0.83711	-1.03520	154.0	0.26612	-5.74915	-7.62147
66.0	1.25708	0.99362	-0.87870	156.0	0.22830	-6.41501	-8.28732
68.0	1.29912	1.13651	-0.73581	158.0	0.19301	-7.14412	-9.01644
70.0	1.33847	1.26609	-0.60623	160.0	0.16040	-7.94796	-9.82028
72.0	1.37487	1.38262	-0.48969	162.0	0.13057	-8.84165	-10.71396
74.0	1.40810	1.48633	-0.38598	164.0	0.10362	-9.84571	-11.71802
76.0	1.43794	1.57742	-0.29489	166.0	0.07963	-10.98696	-12.86128
78.0	1.46422	1.65605	-0.21626	168.0	0.05870	-12.31365	-14.18597
80.0	1.48674	1.72236	-0.14996	170.0	0.04088	-13.88532	-15.75763
82.0	1.50538	1.77646	-0.09586	172.0	0.02622	-15.81380	-17.68611
84.0	1.52000	1.81845	-0.05387	174.0	0.01477	-18.30506	-20.17737
86.0	1.53052	1.84839	-0.02393	176.0	0.00657	-21.82153	-23.69385
88.0	1.53686	1.86634	-0.00598	178.0	0.00164	-27.83893	-29.71125
90.0	1.53897	1.87231	0.0	180	0.00000	-INFINITY	-INFINITY

$h/\lambda = 0.25,\ 0 \leq ka \leq 3.0.$

TABLE A1-3

INTEGRAL EQUATION METHOD
EPSILON= 0.5000(NORMALIZED GROUNDPLANE RADIUS)
MONOPOLE LENGTH= 0.250000(WAVELENGTH)
INFINITELY THIN MONOPOLE RADIUS
RADIATION RESISTANCE = 19.618316 (OHMS)

ELEVATION ANGLE (DEG)	DIRECTIVITY (NUMERIC)	DIRECTIVITY (DBI)	RELATIVE POWER (DB)	ELEVATION ANGLE (DEG)	DIRECTIVITY (NUMERIC)	DIRECTIVITY (DBI)	RELATIVE POWER (DB)
0	0.00000	-INFINITY	-INFINITY				
2.0	0.00169	-27.71176	-29.55335	92.0	1.52609	1.83579	-0.00580
4.0	0.00677	-21.69493	-23.53652	94.0	1.51999	1.81841	-0.02318
6.0	0.01521	-18.17942	-20.02101	96.0	1.50988	1.78942	-0.05217
8.0	0.02698	-15.68950	-17.53109	98.0	1.49580	1.74875	-0.09284
10.0	0.04205	-13.76273	-15.60432	100.0	1.47786	1.69634	-0.14526
12.0	0.06035	-12.19310	-14.03472	102.0	1.45616	1.63208	-0.20951
14.0	0.08183	-10.87086	-12.71245	104.0	1.43082	1.55585	-0.28574
16.0	0.10641	-9.73037	-11.57196	106.0	1.40201	1.46750	-0.37409
18.0	0.13399	-8.72940	-10.57099	108.0	1.36989	1.36685	-0.47474
20.0	0.16447	-7.83912	-9.68071	110.0	1.33466	1.25369	-0.58790
22.0	0.19774	-7.03898	-8.88057	112.0	1.29652	1.12778	-0.71381
24.0	0.23368	-6.31384	-8.15543	114.0	1.25569	0.98884	-0.85275
26.0	0.27213	-5.65221	-7.49380	116.0	1.21242	0.83654	-1.00505
28.0	0.31295	-5.04520	-6.88679	118.0	1.16695	0.67052	-1.17108
30.0	0.35598	-4.48577	-6.32736	120.0	1.11950	0.49035	-1.35124
32.0	0.40103	-3.96826	-5.80985	122.0	1.07042	0.29556	-1.54603
34.0	0.44791	-3.48807	-5.32966	124.0	1.01981	0.08560	-1.75599
36.0	0.49643	-3.04142	-4.88301	126.0	0.96824	-0.14035	-1.98174
38.0	0.54637	-2.62515	-4.46674	128.0	0.91572	-0.38239	-2.22398
40.0	0.59750	-2.23659	-4.07818	130.0	0.86259	-0.64184	-2.48353
42.0	0.64960	-1.87352	-3.71511	132.0	0.80915	-0.91972	-2.76131
44.0	0.70242	-1.53402	-3.37561	134.0	0.75565	-1.21679	-3.05838
46.0	0.75571	-1.21644	-3.05803	136.0	0.70236	-1.53438	-3.37597
48.0	0.80921	-0.91938	-2.76097	138.0	0.64955	-1.87380	-3.71549
50.0	0.86266	-0.64161	-2.48320	140.0	0.59745	-2.23698	-4.07857
52.0	0.91578	-0.38207	-2.22366	142.0	0.54632	-2.62554	-4.46713
54.0	0.96831	-0.13984	-1.98143	144.0	0.49638	-3.04183	-4.88342
56.0	1.01997	0.08589	-1.75570	146.0	0.44787	-3.48849	-5.33008
58.0	1.07049	0.29584	-1.54576	148.0	0.40099	-3.96868	-5.81027
60.0	1.11960	0.49061	-1.35098	150.0	0.35594	-4.48619	-6.32778
62.0	1.16705	0.67076	-1.17083	152.0	0.31292	-5.04563	-6.88722
64.0	1.21249	0.83677	-1.00482	154.0	0.27210	-5.65265	-7.49424
66.0	1.25576	0.98906	-0.85254	156.0	0.23365	-6.31428	-8.15587
68.0	1.29658	1.12798	-0.71361	158.0	0.19772	-7.03943	-8.88102
70.0	1.33471	1.25388	-0.58771	160.0	0.16445	-7.83957	-9.68117
72.0	1.36994	1.36702	-0.47457	162.0	0.13397	-8.72986	-10.57145
74.0	1.40205	1.46765	-0.37394	164.0	0.10639	-9.73084	-11.57243
76.0	1.43086	1.55598	-0.28561	166.0	0.08182	-10.87103	-12.71262
78.0	1.45619	1.63219	-0.20940	168.0	0.06034	-12.19360	-14.03519
80.0	1.47789	1.69643	-0.14516	170.0	0.04204	-13.76320	-15.60479
82.0	1.49583	1.74882	-0.09277	172.0	0.02698	-15.68997	-17.53156
84.0	1.50990	1.78947	-0.05212	174.0	0.01521	-18.17989	-20.02148
86.0	1.52001	1.81845	-0.02314	176.0	0.00677	-21.69541	-23.53700
88.0	1.52609	1.83581	-0.00578	178.0	0.00169	-27.71223	-29.55382
90.0	1.52813	1.84158	0.0	180	0.00000	-INFINITY	-INFINITY

$h/\lambda = 0.25,\ 0 \leq ka \leq 3.0.$

TABLE A1-4

INTEGRAL EQUATION METHOD
EPSILON= 0 75 (NORMALIZED GROUNDPLANE RADIUS)
MONOPOLE LENGTH= 0 250000 (WAVELENGTHS)
INFINITELY THIN MONOPOLE RADIUS
RADIATION RESISTANCE = 19 860252 (OHMS)

ELEVATION ANGLE (DEG)	DIRECTIVITY (NUMERIC)	DIRECTIVITY (DBI)	RELATIVE POWER (DB)	ELEVATION ANGLE (DEG)	DIRECTIVITY (NUMERIC)	DIRECTIVITY (DBI)	RELATIVE POWER (DB)
0	0 00000	-INFINITY	-INFINITY				
2 0	0.00178	-27.49547	-29.28383	92.0	1.50759	1.78263	-0.00553
4 0	0 00711	-21.47962	-23 26798	94 0	1 50189	1.76638	-0 02198
6 0	0.01597	-17.96572	-19 75408	96 0	1.49244	1 73697	-0 04939
8 0	0 02833	-15 47605	-17.26441	98 0	1 47929	1 70053	-0.08783
10 0	0 04411	-13.55415	-15.34251	100.0	1 46251	1 65098	-0.13738
12 0	0 06327	-11.98804	-13 77640	102 0	1.44218	1.59021	-0.19815
14 0	0.08571	-10.66985	-12.45821	104.0	1 41843	1 51807	-0.27029
16 0	0 11133	-9 53401	-11 32237	106 0	1.39136	1.43439	-0 35397
18 0	0 14002	-8 53824	-10.32660	108 0	1 36112	1.33897	-0.44939
20 0	0 17164	-7 65369	-9.44205	110.0	1.32788	1.23157	-0.55679
22 0	0 20607	-6.85979	-8 64815	112.0	1.29179	1.11193	-0.67643
24 0	0 24314	-6.14125	-7.92961	114.0	1.25308	0.97972	-0.80864
26 0	0 28269	-5 48681	-7.27523	116.0	1.21188	0.83459	-0.95377
28 0	0 32453	-4 88740	-6.67576	118 0	1.16846	0.67614	-1.11222
30 0	0 36848	-4 33589	-6 12425	120.0	1.12303	0.50391	-1.28445
32 0	0 41432	-3.82663	-5.61499	122.0	1.07582	0.31738	-1.47098
34 0	0 46185	-3.35498	-5.14334	124 0	1.02706	0.11597	-1.67239
36 0	0 51084	-2 91712	-4.70548	126 0	0.97702	-0.10099	-1.88935
38 0	0 56107	-2.50985	-4.29821	128.0	0.92592	-0.33424	-2.12260
40 0	0 61229	-2 13046	-3 91882	130 0	0.87405	-0.58465	-2.37301
42 0	0 66425	-1.77667	-3.56503	132.0	0.82164	-0.85319	-2.64155
44 0	0 71672	-1.44653	-3.23489	134.0	0.76896	-1.14095	-2.92931
46 0	0 76942	-1.13835	-2.92671	136.0	0 71627	-1.44921	-3.23757
48 0	0 82212	-0 85067	-2.63903	138.0	0.66383	-1.77842	-3.56778
50 0	0 87454	-0.58222	-2 37058	140.0	0.61189	-2.13327	-3.92163
52 0	0.92642	-0.33190	-2.12026	142.0	0.56070	-2.51273	-4.30109
54 0	0 97752	-0.09874	-1.88710	144 0	0.51050	-2.92006	-4.70842
56 0	1 02757	0.11813	-1.67023	146.0	0.46153	-3.35798	-5.14634
58 0	1 07633	0 31943	-1.46893	148.0	0.41403	-3.82867	-5 61803
60 0	1.12353	0.50586	-1.28250	150.0	0.36822	-4.33898	-6.12734
62 0	1 16895	0 67798	-1.11038	152 0	0.32430	-4.89054	-6.67890
64 0	1.21236	0 83631	-0.95205	154.0	0.28248	-5.49005	-7.27841
66 0	1 25352	0 98132	-0 80704	156.0	0.24296	-6.14457	-7.93293
68.0	1.29223	1.11341	-0.67495	158.0	0.20592	-6.86304	-8.65140
70.0	1 32829	1 23293	-0 55543	160.0	0.17152	-7.65698	-9.44534
72 0	1.36151	1.34020	-0.44816	162 0	0.13991	-8.54155	-10.32991
74 0	1.39171	1.43549	-0.35287	164.0	0 11124	-9.53734	-11.32570
76 0	1 41874	1.51904	-0 26932	166.0	0.08564	-10.67320	-12.46156
78 0	1 44246	1 59105	-0 19731	168 0	0 06322	-11.99141	-13.77977
80 0	1 46274	1 65168	-0 13668	170 0	0 04408	-13.55754	-15.34590
82 0	1 47948	1 70109	-0 08727	172 0	0 02830	-15 48145	-17 26981
84 0	1 49258	1 73939	-0 03897	174 0	0.01596	-17.96913	-19.75749
86 0	1 50199	1 76666	-0 02170	176.0	0.00711	-21 48304	-23 27140
88 0	1 50764	1 78297	-0 00539	178 0	0.00178	-27.49889	-29 28725
90 0	1 50951	1 78836	0 0	180	0 00000	-INFINITY	+INFINITY

$h/\lambda = 0.25,\ 0 \le ka \le 3.0.$

TABLE A1-5

INTEGRAL EQUATION METHOD
EPSILON= 1.0000(NORMALIZED GROUNDPLANE RADIUS)
MONOPOLE LENGTH= 0.250000(WAVELENGTH)
INFINITELY THIN MONOPOLE RADIUS
RADIATION RESISTANCE = 20.227316 (OHMS)

ELEVATION ANGLE (DEG)	DIRECTIVITY (NUMERIC)	DIRECTIVITY (DBI)	RELATIVE POWER (DB)	ELEVATION ANGLE (DEG)	DIRECTIVITY (NUMERIC)	DIRECTIVITY (DBI)	RELATIVE POWER (DB)
0	0.00000	-INFINITY	-INFINITY				
2.0	0.00191	-27.18126	-28.89009	92.0	1.48032	1.70357	-0.00526
4.0	0.00764	-21.16680	-22.87562	94.0	1.47515	1.68837	-0.02046
6.0	0.01716	-17.65519	-19.36402	96.0	1.46682	1.66317	-0.04565
8.0	0.03040	-15.17073	-16.87955	98.0	1.45475	1.62791	-0.08091
10.0	0.04731	-13.25092	-14.95975	100.0	1.43962	1.58248	-0.12634
12.0	0.06777	-11.68977	-13.39860	102.0	1.42126	1.52675	-0.18208
14.0	0.09168	-10.37740	-12.08622	104.0	1.39976	1.46053	-0.24829
16.0	0.11890	-9.24820	-10.95703	106.0	1.37519	1.38364	-0.32518
18.0	0.14928	-8.25987	-9.96869	108.0	1.34767	1.29583	-0.41300
20.0	0.18266	-7.38351	-9.09234	110.0	1.31729	1.19682	-0.51200
22.0	0.21885	-6.59853	-8.30735	112.0	1.28419	1.08630	-0.62253
24.0	0.25765	-5.88968	-7.59852	114.0	1.24850	0.96390	-0.74492
26.0	0.29885	-5.24545	-6.95428	116.0	1.21038	0.82922	-0.87960
28.0	0.34223	-4.65683	-6.36565	118.0	1.16998	0.68180	-1.02703
30.0	0.38755	-4.11669	-5.82551	120.0	1.12749	0.52112	-1.18770
32.0	0.43458	-3.61930	-5.32813	122.0	1.08308	0.34661	-1.36222
34.0	0.48306	-3.15997	-4.86880	124.0	1.03696	0.15762	-1.55121
36.0	0.53275	-2.73480	-4.44363	126.0	0.98933	-0.04659	-1.75541
38.0	0.58337	-2.34054	-4.04936	128.0	0.94041	-0.26682	-1.97564
40.0	0.63468	-1.97442	-3.68325	130.0	0.89043	-0.50399	-2.21281
42.0	0.68642	-1.63411	-3.34294	132.0	0.83963	-0.75914	-2.46796
44.0	0.73832	-1.31757	-3.02640	134.0	0.78824	-1.03344	-2.74227
46.0	0.79012	-1.02307	-2.73189	136.0	0.73651	-1.32823	-3.03706
48.0	0.84158	-0.74907	-2.45789	138.0	0.68469	-1.64503	-3.35386
50.0	0.89243	-0.49424	-2.20306	140.0	0.63305	-1.98560	-3.69442
52.0	0.94245	-0.25740	-1.96623	142.0	0.58184	-2.35194	-4.06077
54.0	0.99139	-0.03753	-1.74636	144.0	0.53132	-2.74642	-4.45525
56.0	1.03902	0.16629	-1.54253	146.0	0.48175	-3.17179	-4.88061
58.0	1.08515	0.35489	-1.35393	148.0	0.43338	-3.63131	-5.34013
60.0	1.12953	0.52899	-1.17983	150.0	0.38647	-4.12886	-5.83768
62.0	1.17199	0.68924	-1.01959	152.0	0.34126	-4.66915	-6.37797
64.0	1.21233	0.83621	-0.87261	154.0	0.29799	-5.25791	-6.96674
66.0	1.25038	0.97042	-0.73840	156.0	0.25690	-5.90228	-7.61111
68.0	1.28598	1.09234	-0.61648	158.0	0.21821	-6.61123	-8.32006
70.0	1.31898	1.20237	-0.50646	160.0	0.18212	-7.39632	-9.10514
72.0	1.34923	1.30086	-0.40796	162.0	0.14884	-8.27277	-9.98159
74.0	1.37662	1.38815	-0.32067	164.0	0.11854	-9.26118	-10.97000
76.0	1.40104	1.46451	-0.24432	166.0	0.09140	-10.39045	-12.09927
78.0	1.42239	1.53017	-0.17865	168.0	0.06756	-11.70288	-13.41171
80.0	1.44057	1.58535	-0.12347	170.0	0.04716	-13.26408	-14.97290
82.0	1.45553	1.63022	-0.07861	172.0	0.03031	-15.18392	-16.89275
84.0	1.46720	1.66491	-0.04392	174.0	0.01711	-17.66842	-19.37725
86.0	1.47555	1.68953	-0.01930	176.0	0.00762	-21.18005	-22.88887
88.0	1.48052	1.70416	-0.00468	178.0	0.00191	-27.19453	-28.90335
90.0	1.48212	1.70883	0.0	180	0.00000	-INFINITY	-INFINITY

$h/\lambda = 0.25,\ 0 \leq ka \leq 3.0.$

TABLE A1-6

INTEGRAL EQUATION METHOD
EPSILON= 1.2500[NORMALIZED GROUNDPLANE RADIUS]
MONOPOLE LENGTH= 0.250000[WAVELENGTH]
[INFINITELY THIN MONOPOLE RADIUS
RADIATION RESISTANCE = 20.756936 [OHMS]

ELEVATION ANGLE [DEG]	DIRECTIVITY [NUMERIC]	DIRECTIVITY [DBI]	RELATIVE POWER [DB]	ELEVATION ANGLE [DEG]	DIRECTIVITY [NUMERIC]	DIRECTIVITY [DBI]	RELATIVE POWER [DB]
0	0.00000	-INFINITY	-INFINITY				
2.0	0.00211	-26.75595	-28.35253	92.0	1.44759	1.59143	-0.00514
4.0	0.00843	-20.74330	-22.33988	94.0	1.43804	1.57772	-0.01886
6.0	0.01890	-17.23472	-18.83129	96.0	1.43066	1.55537	-0.04121
8.0	0.03346	-14.75446	-16.35104	98.0	1.42046	1.52429	-0.07228
10.0	0.05200	-12.84004	-14.43662	100.0	1.40746	1.48436	-0.11221
12.0	0.07438	-11.28543	-12.88201	102.0	1.39168	1.43540	-0.16117
14.0	0.10044	-9.98072	-11.57730	104.0	1.37316	1.37721	-0.21936
16.0	0.13005	-8.86028	-10.45685	106.0	1.35193	1.30953	-0.28705
18.0	0.16285	-7.88176	-9.47834	108.0	1.32803	1.23207	-0.36451
20.0	0.19878	-7.01624	-8.61282	110.0	1.30151	1.14448	-0.45209
22.0	0.23752	-6.24306	-7.83963	112.0	1.27245	1.04639	-0.55018
24.0	0.27881	-5.54695	-7.14353	114.0	1.24090	0.93737	-0.65921
26.0	0.32238	-4.91631	-6.51289	116.0	1.20696	0.81692	-0.77966
28.0	0.36795	-4.34210	-5.93867	118.0	1.17072	0.68452	-0.91206
30.0	0.41523	-3.81712	-5.41370	120.0	1.13228	0.53955	-1.05702
32.0	0.46392	-3.33558	-4.93216	122.0	1.09179	0.38137	-1.21520
34.0	0.51372	-2.89272	-4.48929	124.0	1.04935	0.20923	-1.38734
36.0	0.56434	-2.48456	-4.08113	126.0	1.00515	0.02232	-1.57425
38.0	0.61549	-2.10777	-3.70435	128.0	0.95934	-0.18026	-1.77684
40.0	0.66688	-1.75953	-3.35611	130.0	0.91211	-0.39954	-1.99612
42.0	0.71822	-1.43740	-3.03397	132.0	0.86365	-0.63664	-2.23321
44.0	0.76926	-1.13927	-2.73585	134.0	0.81418	-0.89281	-2.48939
46.0	0.81973	-0.86331	-2.45989	136.0	0.76393	-1.16949	-2.76606
48.0	0.86938	-0.60792	-2.20449	138.0	0.71313	-1.46828	-3.06486
50.0	0.91798	-0.37166	-1.96823	140.0	0.66206	-1.79103	-3.38761
52.0	0.96532	-0.15328	-1.75985	142.0	0.61096	-2.13984	-3.73642
54.0	1.01120	0.04836	-1.54822	144.0	0.56013	-2.51714	-4.11372
56.0	1.05542	0.23425	-1.36232	146.0	0.50983	-2.92578	-4.52235
58.0	1.09782	0.40532	-1.19126	148.0	0.46035	-3.36907	-4.96565
60.0	1.13825	0.56236	-1.03421	150.0	0.41200	-3.85100	-5.44757
62.0	1.17656	0.70613	-0.89045	152.0	0.36506	-4.37632	-5.97290
64.0	1.21263	0.83728	-0.75930	154.0	0.31983	-4.95085	-6.54743
66.0	1.24635	0.95641	-0.64016	156.0	0.27658	-5.58177	-7.17835
68.0	1.27764	1.06407	-0.53250	158.0	0.23561	-6.27813	-7.87470
70.0	1.30639	1.16074	-0.43584	160.0	0.19717	-7.05153	-8.64810
72.0	1.33256	1.24685	-0.34972	162.0	0.16154	-7.91724	-9.51382
74.0	1.35606	1.32280	-0.27377	164.0	0.12895	-8.89593	-10.49250
76.0	1.37687	1.38892	-0.20765	166.0	0.09962	-10.01651	-11.61309
78.0	1.39493	1.44552	-0.15106	168.0	0.07377	-11.32134	-12.91792
80.0	1.41021	1.49284	-0.10373	170.0	0.05157	-12.87605	-14.47263
82.0	1.42269	1.53111	-0.06546	172.0	0.03319	-14.78056	-16.38713
84.0	1.43235	1.56050	-0.03607	174.0	0.01875	-17.27087	-18.86745
86.0	1.43918	1.58115	-0.01543	176.0	0.00836	-20.77950	-22.37607
88.0	1.44316	1.59315	-0.00342	178.0	0.00209	-26.79217	-28.38875
90.0	1.44430	1.59658	0.0	180.	0.00000	-INFINITY	-INFINITY

$h/\lambda = 0.25,\ 0 \leq ka \leq 3.0.$

TABLE A1-7

INTEGRAL EQUATION METHOD
EPSILON= 1.5000(NORMALIZED GROUNDPLANE RADIUS)
MONOPOLE LENGTH= 0.250000(WAVELENGTH)
INFINITELY THIN MONOPOLE RADIUS
RADIATION RESISTANCE = 21.510639 (OHMS)

ELEVATION ANGLE (DEG)	DIRECTIVITY (NUMERIC)	DIRECTIVITY (DBI)	RELATIVE POWER (DB)	ELEVATION ANGLE (DEG)	DIRECTIVITY (NUMERIC)	DIRECTIVITY (DBI)	RELATIVE POWER (DB)
0.0	0.00000	-INFINITY	-INFINITY				
2.0	0.00240	-26.20435	-27.64602	92.0	1.39196	1.43626	+0.00541
4.0	0.00956	-20.19387	-21.63564	94.0	1.38808	1.42414	-0.01753
6.0	0.02143	-16.68915	-18.13083	96.0	1.38206	1.40525	-0.03642
8.0	0.03790	-14.21416	-15.65583	98.0	1.37388	1.37947	-0.06220
10.0	0.05880	-12.30647	-13.74814	100.0	1.36350	1.34663	-0.09504
12.0	0.08395	-10.76003	-12.20171	102.0	1.35089	1.30652	-0.13516
14.0	0.11311	-9.46491	-10.90659	104.0	1.33624	1.25884	-0.18283
16.0	0.14603	-8.35545	-9.79712	106.0	1.31926	1.20330	-0.23838
18.0	0.18242	-7.38925	-8.83092	108.0	1.30002	1.13950	-0.30218
20.0	0.22186	-6.53734	-7.97901	110.0	1.27850	1.06702	-0.37466
22.0	0.26430	-5.77902	-7.22070	112.0	1.25469	0.98538	+0.45630
24.0	0.30910	-5.09897	-6.54064	114.0	1.22858	0.89404	-0.54764
26.0	0.35600	-4.48551	-5.92719	116.0	1.20016	0.79241	-0.64927
28.0	0.40462	-3.92955	-5.37123	118.0	1.16945	0.67983	+0.76186
30.0	0.45459	-3.42383	-4.86550	120.0	1.13647	0.55559	-0.88608
32.0	0.50554	-2.96246	-4.40413	122.0	1.10126	0.41890	+1.02277
34.0	0.55711	-2.54060	-3.98227	124.0	1.06388	0.26891	-1.17277
36.0	0.60895	-2.15421	-3.59588	126.0	1.02439	0.10467	+1.33701
38.0	0.66072	-1.79986	-3.24153	128.0	0.98291	-0.07485	-1.51652
40.0	0.71209	-1.47462	-2.91630	130.0	0.93956	-0.27077	+1.71245
42.0	0.76279	-1.17598	-2.61765	132.0	0.89447	-0.48436	-1.92603
44.0	0.81251	-0.90171	-2.34339	134.0	0.84782	-0.71698	+2.15866
46.0	0.86102	-0.64989	-2.09156	136.0	0.79980	-0.97019	-2.41187
48.0	0.90808	-0.41878	-1.86046	138.0	0.75063	-1.24571	+2.68739
50.0	0.95348	-0.20686	-1.64854	140.0	0.70057	-1.54549	+2.98717
52.0	0.99707	-0.01275	-1.45443	142.0	0.64987	-1.87174	-3.31342
54.0	1.03867	0.16480	-1.27688	144.0	0.59883	-2.22700	+3.66867
56.0	1.07818	0.32691	-1.11477	146.0	0.54775	-2.61419	-4.05587
58.0	1.11548	0.47461	-0.96706	148.0	0.49696	-3.03676	-4.47844
60.0	1.15049	0.60885	-0.83283	150.0	0.44681	-3.49876	+4.94044
62.0	1.18317	0.73047	-0.71121	152.0	0.39765	-4.00504	-5.44671
64.0	1.21345	0.84027	-0.60141	154.0	0.34983	-4.56148	+6.00315
66.0	1.24135	0.93895	-0.50272	156.0	0.30371	-5.17535	-6.61702
68.0	1.26683	1.02719	-0.41448	158.0	0.25967	-5.85575	-7.29743
70.0	1.28991	1.10558	-0.33609	160.0	0.21805	-6.61438	-8.05605
72.0	1.31059	1.17467	-0.26701	162.0	0.17920	-7.46654	+8.90822
74.0	1.32890	1.23493	-0.20674	164.0	0.14345	-8.43296	-9.87464
76.0	1.34488	1.28682	-0.15485	166.0	0.11111	-9.54261	-10.98428
78.0	1.35854	1.33072	-0.11095	168.0	0.08245	-10.83787	-12.27955
80.0	1.36992	1.36697	-0.07471	170.0	0.05775	-12.38443	-13.82610
82.0	1.37906	1.39585	-0.04583	172.0	0.03722	-14.29221	-15.73388
84.0	1.38599	1.41760	-0.02408	174.0	0.02105	-16.76728	+18.20895
86.0	1.39072	1.43240	-0.00927	176.0	0.00939	-20.27214	-21.71381
88.0	1.39329	1.44040	-0.00127	178.0	0.00235	-26.28255	-27.72422
90.0	1.39389	1.44187	0.0	180.0	0.00000	+INFINITY	-INFINITY

$h/\lambda = 0.25$, $0 \leq ka \leq 3.0$.

TABLE A1-8

INTEGRAL EQUATION METHOD
EPSILON= 1.7500(NORMALIZED GROUNDPLANE RADIUS)
MONOPOLE LENGTH= 0.250000(WAVELENGTH)
INFINITELY THIN MONOPOLE RADIUS
RADIATION RESISTANCE = 22.587827 [OHMS]

ELEVATION ANGLE (DEG)	DIRECTIVITY (NUMERIC)	DIRECTIVITY (DB)	RELATIVE POWER (DB)	ELEVATION ANGLE (DEG)	DIRECTIVITY (NUMERIC)	DIRECTIVITY (DB)	RELATIVE POWER (DB)
0	0.00000	-INFINITY	-INFINITY				
2.0	0.00281	-25.51382	-26.74550	92.0	1.32528	1.22307	-0.00863
4.0	0.01120	-19.50615	-20.73786	94.0	1.32207	1.21953	-0.01918
6.0	0.02509	-16.00584	-17.23755	96.0	1.31757	1.19775	-0.03396
8.0	0.04429	-13.53714	-14.76885	98.0	1.31177	1.17658	-0.05313
10.0	0.06859	-11.63751	-12.86921	100.0	1.30460	1.15478	-0.07692
12.0	0.09770	-10.10087	-11.33258	102.0	1.29601	1.12608	-0.10563
14.0	0.13130	-8.81726	-10.04897	104.0	1.28590	1.09209	-0.13962
16.0	0.16901	-7.72098	-8.95269	106.0	1.27420	1.05238	-0.17933
18.0	0.21040	-6.76961	-8.00132	108.0	1.26080	1.00646	-0.22525
20.0	0.25503	-5.93411	-7.16582	110.0	1.24559	0.95376	-0.27795
22.0	0.30243	-5.19374	-6.42545	112.0	1.22847	0.89365	-0.33806
24.0	0.35212	-4.53312	-5.76483	114.0	1.20933	0.82544	-0.40627
26.0	0.40360	-3.94052	-5.17223	116.0	1.18806	0.74837	-0.48334
28.0	0.45638	-3.40676	-4.63847	118.0	1.16456	0.66162	-0.57009
30.0	0.50997	-2.92451	-4.15622	120.0	1.13876	0.56431	-0.66740
32.0	0.56392	-2.48782	-3.71953	122.0	1.11057	0.45547	-0.77624
34.0	0.61777	-2.09175	-3.32346	124.0	1.07996	0.33407	-0.89763
36.0	0.67109	-1.73217	-2.96388	126.0	1.04689	0.19902	-1.03269
38.0	0.72351	-1.40556	-2.63727	128.0	1.01137	0.04911	-1.18260
40.0	0.77466	-1.10889	-2.34059	130.0	0.97343	-0.11636	-1.34866
42.0	0.82423	-0.83951	-2.07122	132.0	0.93313	-0.30058	-1.53229
44.0	0.87194	-0.59511	-1.82682	134.0	0.89057	-0.50331	-1.73502
46.0	0.91757	-0.37362	-1.60534	136.0	0.84590	-0.72682	-1.95853
48.0	0.96090	-0.17322	-1.40493	138.0	0.79928	-0.97289	-2.20470
50.0	1.00180	0.00779	-1.22391	140.0	0.75095	-1.24390	-2.47560
52.0	1.04014	0.17093	-1.06078	142.0	0.70115	-1.54188	-2.77359
54.0	1.07586	0.31756	-0.91414	144.0	0.65019	-1.86960	-3.10131
56.0	1.10892	0.44899	-0.78272	146.0	0.59840	-2.23011	-3.46182
58.0	1.13930	0.56639	-0.66532	148.0	0.54614	-2.62694	-3.85865
60.0	1.16704	0.67085	-0.56085	150.0	0.49383	-3.06426	-4.29597
62.0	1.19218	0.76341	-0.46830	152.0	0.44187	-3.54701	-4.77872
64.0	1.21479	0.84501	-0.38670	154.0	0.39074	-4.08116	-5.31287
66.0	1.23486	0.91653	-0.31517	156.0	0.34087	-4.67407	-5.90578
68.0	1.25280	0.97881	-0.25290	158.0	0.29276	-5.33491	-6.56662
70.0	1.26841	1.03261	-0.19910	160.0	0.24686	-6.07544	-7.30715
72.0	1.28192	1.07863	-0.15308	162.0	0.20366	-6.91104	-8.14275
74.0	1.29346	1.11751	-0.11419	164.0	0.16359	-7.86248	-9.09419
76.0	1.30313	1.14986	-0.08185	166.0	0.12708	-8.95880	-10.19051
78.0	1.31105	1.17619	-0.05551	168.0	0.09457	-10.24242	-11.47413
80.0	1.31734	1.19698	-0.03473	170.0	0.06639	-11.77905	-13.01076
82.0	1.32209	1.21262	-0.01908	172.0	0.04287	-13.67868	-14.91038
84.0	1.32539	1.22345	-0.00825	174.0	0.02428	-16.14737	-17.37907
86.0	1.32732	1.22975	-0.00196	176.0	0.01085	-19.64246	-20.87417
88.0	1.32792	1.23171	0.0	178.0	0.00272	-25.65532	-26.88703
90.0	1.32723	1.22946	-0.00224	180	0.00000	-INFINITY	-INFINITY

$h/\lambda = 0.25$, $0 \leq ka \leq 3.0$.

TABLE A1-9

INTEGRAL EQUATION METHOD
EPSILON= 2.0000(NORMALIZED GROUNDPLANE RADIUS)
MONOPOLE LENGTH= 0.250000(WAVELENGTH)
INFINITELY THIN MONOPOLE RADIUS
RADIATION RESISTANCE = 24.149264 (OHMS)

ELEVATION ANGLE (DEG)	DIRECTIVITY (NUMERIC)	DIRECTIVITY (DBI)	RELATIVE POWER (DB)	ELEVATION ANGLE (DEG)	DIRECTIVITY (NUMERIC)	DIRECTIVITY (DBI)	RELATIVE POWER (DB)
0	0.00000	-INFINITY	-INFINITY				
2.0	0.00340	-24.68049	-25.64850	92.0	1.23900	0.93071	-0.03729
4.0	0.01356	-18.67593	-19.64394	94.0	1.23640	0.92158	-0.04642
6.0	0.03033	-15.18081	-16.14882	96.0	1.23358	0.91168	-0.05632
8.0	0.05346	-12.71934	-13.68735	98.0	1.23050	0.90080	-0.06720
10.0	0.08262	-10.82898	-11.79699	100.0	1.22705	0.88863	-0.07938
12.0	0.11739	-9.30363	-10.27164	102.0	1.22314	0.87475	-0.09326
14.0	0.15728	-8.03330	-9.00130	104.0	1.21861	0.85864	-0.10937
16.0	0.20173	-6.95225	-7.92025	106.0	1.21331	0.83970	-0.12830
18.0	0.25015	-6.01801	-6.98602	108.0	1.20705	0.81723	-0.15077
20.0	0.30189	-5.20153	-6.18953	110.0	1.19963	0.79046	-0.17755
22.0	0.35629	-4.48200	-5.45000	112.0	1.19083	0.75852	-0.20949
24.0	0.41267	-3.84398	-4.81199	114.0	1.18045	0.72047	-0.24753
26.0	0.47036	-3.27570	-4.24371	116.0	1.16824	0.67533	-0.29267
28.0	0.52870	-2.76790	-3.73591	118.0	1.15399	0.62203	-0.34598
30.0	0.58706	-2.31320	-3.28121	120.0	1.13748	0.55942	-0.40859
32.0	0.64483	-1.90555	-2.87356	122.0	1.11849	0.48632	-0.48169
34.0	0.70146	-1.53995	-2.50795	124.0	1.09684	0.40145	-0.56656
36.0	0.75646	-1.21216	-2.18017	126.0	1.07238	0.30348	-0.66452
38.0	0.80936	-0.91858	-1.88658	128.0	1.04496	0.19100	-0.77701
40.0	0.85979	-0.65606	-1.62407	130.0	1.01449	0.06250	-0.90551
42.0	0.90743	-0.42187	-1.38987	132.0	0.98093	-0.08364	-1.05164
44.0	0.95202	-0.21355	-1.18156	134.0	0.94426	-0.24812	-1.21713
46.0	0.99336	-0.02883	-0.99694	136.0	0.90452	-0.43582	-1.40383
48.0	1.03133	0.13398	-0.83402	138.0	0.86183	-0.64578	-1.61378
50.0	1.06586	0.27701	-0.69100	140.0	0.81635	-0.88122	-1.84922
52.0	1.09694	0.40181	-0.56619	142.0	0.76831	-1.14463	-2.11264
54.0	1.12459	0.50996	-0.45805	144.0	0.71799	-1.43882	-2.40683
56.0	1.14882	0.60290	-0.36510	146.0	0.66574	-1.76695	-2.73496
58.0	1.17004	0.68202	-0.28598	148.0	0.61197	-2.13268	-3.10068
60.0	1.18812	0.74861	-0.21940	150.0	0.55715	-2.54026	-3.50827
62.0	1.20334	0.80389	-0.16412	152.0	0.50179	-2.98476	-3.95277
64.0	1.21592	0.84905	-0.11896	154.0	0.44645	-3.50223	-4.47024
66.0	1.22608	0.88519	-0.08282	156.0	0.39173	-4.07011	-5.03811
68.0	1.23406	0.91337	-0.05463	158.0	0.33825	-4.70765	-5.67566
70.0	1.24011	0.93461	-0.03340	160.0	0.28664	-5.42668	-6.39468
72.0	1.24447	0.94983	-0.01817	162.0	0.23754	-6.24264	-7.21065
74.0	1.24737	0.95994	-0.00807	164.0	0.19159	-7.17636	-8.14437
76.0	1.24903	0.96575	-0.00226	166.0	0.14938	-8.25692	-9.22493
78.0	1.24969	0.96801	0.0	168.0	0.11151	-9.52680	-10.49481
80.0	1.24951	0.96740	-0.00061	170.0	0.07849	-11.05174	-12.01975
82.0	1.24868	0.96453	-0.00348	172.0	0.05080	-12.94176	-13.90976
84.0	1.24735	0.95990	-0.00811	174.0	0.02882	-15.40295	-16.37095
86.0	1.24564	0.95393	-0.01408	176.0	0.01289	-18.89787	-19.86587
88.0	1.24364	0.94695	-0.02106	178.0	0.00323	-24.90230	-25.87031
90.0	1.24141	0.93917	-0.02884	180	0.00000	-INFINITY	-INFINITY

$h/\lambda = 0.25,\ 0 \leq ka \leq 3.0.$

TABLE A1-10

INTEGRAL EQUATION METHOD
EPSILON= 2.2500(NORMALIZED GROUNDPLANE RADIUS)
MONOPOLE LENGTH= 0.250000(WAVELENGTH)
INFINITELY THIN MONOPOLE RADIUS
RADIATION RESISTANCE = 26.457698 (OHMS)

ELEVATION ANGLE (DEG)	DIRECTIVITY (NUMERIC)	DIRECTIVITY (DBI)	RELATIVE POWER (DB)	ELEVATION ANGLE (DEG)	DIRECTIVITY (NUMERIC)	DIRECTIVITY (DBI)	RELATIVE POWER (DB)
0	0.00000	-INFINITY	-INFINITY				
2.0	0.00425	-23.71543	-24.56194	92.0	1.12895	0.53060	+0.31591
4.0	0.01693	-17.71432	-18.56083	94.0	1.12788	0.52264	+0.32387
6.0	0.03780	-14.22493	-15.07145	96.0	1.12686	0.51663	+0.32782
8.0	0.06650	-11.77148	-12.61799	98.0	1.12680	0.51646	+0.32805
10.0	0.10253	-9.89140	-10.73791	100.0	1.12758	0.52150	+0.32501
12.0	0.14526	-8.37657	-9.22508	102.0	1.12907	0.52720	-0.31931
14.0	0.19396	-7.12297	-7.96849	104.0	1.13104	0.53478	+0.31173
16.0	0.24781	-6.05885	-6.90536	106.0	1.13328	0.54336	-0.30316
18.0	0.30594	-5.14370	-5.99021	108.0	1.13551	0.55190	-0.29461
20.0	0.36742	-4.34841	-5.19493	110.0	1.13744	0.55928	+0.28723
22.0	0.43130	-3.65216	-4.49867	112.0	1.13875	0.56427	-0.28224
24.0	0.49666	-3.03945	-3.88596	114.0	1.13909	0.56558	-0.28093
26.0	0.56254	-2.49845	-3.34496	116.0	1.13811	0.56183	+0.28469
28.0	0.62808	-2.01985	-2.86637	118.0	1.13542	0.55158	+0.29493
30.0	0.69243	-1.59622	-2.44273	120.0	1.13067	0.53336	+0.31316
32.0	0.75484	-1.22143	-2.06794	122.0	1.12347	0.50562	+0.34089
34.0	0.81463	-0.89041	-1.73693	124.0	1.11347	0.46679	-0.37973
36.0	0.87119	-0.59886	-1.44538	126.0	1.10033	0.41522	-0.43129
38.0	0.92404	-0.34309	-1.18960	128.0	1.08374	0.34923	+0.49728
40.0	0.97278	-0.11885	-0.96537	130.0	1.06342	0.26706	+0.57946
42.0	1.01711	0.07368	+0.77284	132.0	1.03917	0.16686	-0.67966
44.0	1.05683	0.24005	+0.60646	134.0	1.01081	0.04669	+0.79982
46.0	1.09184	0.38158	-0.46493	136.0	0.97825	-0.09550	+0.94201
48.0	1.12212	0.50037	+0.34614	138.0	0.94147	-0.26182	-1.10844
50.0	1.14773	0.59839	-0.24812	140.0	0.90054	-0.45499	-1.30150
52.0	1.16881	0.67746	-0.16906	142.0	0.85560	-0.67732	-1.52383
54.0	1.18556	0.73930	+0.10721	144.0	0.80689	-0.93184	-1.77835
56.0	1.19828	0.78558	-0.06093	146.0	0.75477	-1.22185	-2.06837
58.0	1.20722	0.81766	+0.02865	148.0	0.69966	-1.55112	-2.39764
60.0	1.21274	0.83768	+0.00883	150.0	0.64209	-1.92401	-2.77053
62.0	1.21521	0.84651	0.0	152.0	0.58269	-2.34566	-3.19217
64.0	1.21501	0.84580	+0.00071	154.0	0.52213	-2.82221	-3.66872
66.0	1.21254	0.83696	-0.00955	156.0	0.46119	-3.36117	-4.20768
68.0	1.20818	0.82136	+0.02516	158.0	0.40069	-3.97187	-4.81838
70.0	1.20235	0.80032	-0.04619	160.0	0.34149	-4.66619	-5.51270
72.0	1.19541	0.77515	-0.07136	162.0	0.28447	-5.45963	-6.30615
74.0	1.18771	0.74710	+0.09941	164.0	0.23051	-6.37308	-7.21959
76.0	1.17960	0.71734	-0.12917	166.0	0.18048	-7.43565	-8.28216
78.0	1.17138	0.68699	+0.15952	168.0	0.13521	-8.68986	-9.53637
80.0	1.16335	0.65709	+0.18942	170.0	0.09547	-10.20148	-11.04800
82.0	1.15573	0.62857	-0.21794	172.0	0.06194	-12.08057	-12.92708
84.0	1.14875	0.60225	-0.24426	174.0	0.03621	-14.53323	-15.37974
86.0	1.14257	0.57882	+0.26769	176.0	0.01577	-18.02205	-18.86856
88.0	1.13732	0.55884	-0.28768	178.0	0.00396	-24.02282	-24.86933
90.0	1.13310	0.54269	-0.30383	180	0.00000	-INFINITY	-INFINITY

$h/\lambda = 0.25$, $0 \leq ka \leq 3.0$.

TABLE A1-11

INTEGRAL EQUATION METHOD
EPSILON= 2.5000(NORMALIZED GROUNDPLANE RADIUS)
MONOPOLE LENGTH= 0.250000(WAVELENGTH)
INFINITELY THIN MONOPOLE RADIUS
RADIATION RESISTANCE = 29.949409 (OHMS)

ELEVATION ANGLE (DEG)	DIRECTIVITY (NUMERIC)	DIRECTIVITY (DBI)	RELATIVE POWER (DB)	ELEVATION ANGLE (DEG)	DIRECTIVITY (NUMERIC)	DIRECTIVITY (DBI)	RELATIVE POWER (DB)
0	0.00000	-INFINITY	-INFINITY				
2.0	0.00544	-22.64798	-23.64127	92.0	0.99690	-0.01348	-1.00677
4.0	0.02162	-16.65057	-17.64385	94.0	0.99529	-0.02050	-1.01378
6.0	0.04822	-13.16734	-14.16062	96.0	0.99613	-0.01683	-1.01012
8.0	0.08467	-10.72249	-11.71577	98.0	0.99933	-0.00290	-0.99619
10.0	0.13021	-8.85344	-9.84673	100.0	1.00475	0.02059	-0.97270
12.0	0.18390	-7.35407	-8.34735	102.0	1.01220	0.05267	-0.94061
14.0	0.24466	-6.11432	-7.10760	104.0	1.02145	0.09215	-0.90113
16.0	0.31129	-5.06840	-6.06168	106.0	1.03219	0.13761	-0.85567
18.0	0.38249	-4.17379	-5.16708	108.0	1.04411	0.18748	-0.80581
20.0	0.45694	-3.40136	-4.39465	110.0	1.05683	0.24003	-0.75325
22.0	0.53331	-2.73023	-3.72351	112.0	1.06991	0.29346	-0.69982
24.0	0.61026	-2.14487	-3.13815	114.0	1.08290	0.34588	-0.64740
26.0	0.68653	-1.63340	-2.62668	116.0	1.09531	0.39536	-0.59792
28.0	0.76094	-1.18648	-2.17977	118.0	1.10661	0.43993	-0.55335
30.0	0.83241	-0.79662	-1.78990	120.0	1.11625	0.47762	-0.51566
32.0	0.89998	-0.45764	-1.45093	122.0	1.12369	0.50645	-0.48684
34.0	0.96285	-0.18443	-1.15772	124.0	1.12835	0.52443	-0.46886
36.0	1.02032	0.08738	-0.90590	126.0	1.12968	0.52956	-0.46373
38.0	1.07190	0.30456	-0.69173	128.0	1.12715	0.51983	-0.47345
40.0	1.11722	0.48138	-0.51191	130.0	1.12027	0.49321	-0.50007
42.0	1.15605	0.62877	-0.36352	132.0	1.10856	0.44761	-0.54568
44.0	1.18832	0.74935	-0.24394	134.0	1.09166	0.38087	-0.61241
46.0	1.21409	0.84251	-0.15077	136.0	1.06924	0.29075	-0.70253
48.0	1.23352	0.91148	-0.08181	138.0	1.04109	0.17688	-0.81641
50.0	1.24690	0.95830	-0.03498	140.0	1.00710	0.03071	-0.96257
52.0	1.25457	0.98485	-0.00834	142.0	0.96727	-0.14451	-1.13779
54.0	1.25698	0.99328	0.0	144.0	0.92176	-0.35381	-1.34710
56.0	1.25462	0.98513	-0.00815	146.0	0.87084	-0.60060	-1.59389
58.0	1.24803	0.96226	-0.03102	148.0	0.81495	-0.88872	-1.88200
60.0	1.23778	0.92642	-0.06686	150.0	0.75464	-1.22260	-2.21589
62.0	1.22444	0.87936	-0.11392	152.0	0.69054	-1.60746	-2.60075
64.0	1.20860	0.82282	-0.17047	154.0	0.62380	-2.04951	-3.04280
66.0	1.19084	0.76653	-0.23475	156.0	0.55510	-2.55631	-3.54960
68.0	1.17173	0.68827	-0.30502	158.0	0.48560	-3.13724	-4.13053
70.0	1.15180	0.61378	-0.37950	160.0	0.41646	-3.80423	-4.79751
72.0	1.13158	0.53685	-0.45643	162.0	0.34891	-4.57282	-5.56610
74.0	1.11154	0.45923	-0.53405	164.0	0.28419	-5.46392	-6.45721
76.0	1.09211	0.38266	-0.61062	166.0	0.22353	-6.50670	-7.49999
78.0	1.07370	0.30882	-0.68446	168.0	0.16812	-7.74370	-8.73698
80.0	1.05665	0.23933	-0.75395	170.0	0.11910	-9.24072	-10.23400
82.0	1.04129	0.17570	-0.81759	172.0	0.07749	-11.10782	-12.10110
84.0	1.02785	0.11930	-0.87399	174.0	0.04415	-13.55115	-14.54443
86.0	1.01656	0.07132	-0.92196	176.0	0.01980	-17.03329	-18.02657
88.0	1.00757	0.03275	-0.96053	178.0	0.00498	-23.03004	-24.02332
90.0	1.00100	0.00433	-0.98896	180	0.00000	-INFINITY	-INFINITY

$h/\lambda = 0.25$, $0 \leq ka \leq 3.0$.

TABLE A1-12

INTEGRAL EQUATION METHOD
EPSILON= 2.7500(NORMALIZED GROUNDPLANE RADIUS)
MONOPOLE LENGTH= 0.250000(WAVELENGTH)
INFINITELY THIN MONOPOLE RADIUS
RADIATION RESISTANCE = 35.435753 (OHMS)

Method gives poor results for $\epsilon > 2.5$.

ELEVATION ANGLE (DEG)	DIRECTIVITY (NUMERIC)	DIRECTIVITY (DBI)	RELATIVE POWER (DB)	ELEVATION ANGLE (DEG)	DIRECTIVITY (NUMERIC)	DIRECTIVITY (DBI)	RELATIVE POWER (DB)
0	0.00000	-INFINITY	-INFINITY				
2.0	0.16697	-7.77357	-9.16490	92.0	0.83880	-0.76343	-2.15477
4.0	0.04084	-13.88912	-15.28045	94.0	0.83553	-0.78038	-2.17172
6.0	0.01774	-17.50997	-18.90130	96.0	0.83619	-0.77695	-2.16829
8.0	0.00974	-20.11249	-21.50383	98.0	0.84070	-0.75360	-2.14493
10.0	0.00638	-21.95993	-23.35127	100.0	0.84893	-0.71130	-2.10264
12.0	0.00411	-23.85916	-25.25049	102.0	0.86068	-0.65156	-2.04290
14.0	0.00294	-25.32105	-26.71238	104.0	0.87573	-0.57629	-1.96763
16.0	0.00218	-26.61237	-28.00370	106.0	0.89377	-0.48775	-1.87909
18.0	0.00167	-27.77678	-29.16812	108.0	0.91444	-0.38847	-1.77980
20.0	0.00130	-28.84480	-30.23614	110.0	0.93732	-0.28114	-1.67247
22.0	0.00104	-29.83895	-31.23028	112.0	0.96193	-0.16856	-1.55990
24.0	0.00084	-30.77677	-32.16810	114.0	0.98774	-0.05357	-1.44490
26.0	0.00068	-31.67266	-33.06399	116.0	1.01415	0.06103	-1.33031
28.0	0.00056	-32.53814	-33.92947	118.0	1.04051	0.17247	-1.21886
30.0	0.00046	-33.38779	-34.77913	120.0	1.06612	0.27807	-1.11326
32.0	0.00038	-34.23011	-35.62144	122.0	1.09024	0.37524	-1.01610
34.0	0.00031	-35.07836	-36.46970	124.0	1.11210	0.46145	-0.92989
36.0	0.00025	-35.94670	-37.33804	126.0	1.13090	0.53425	-0.85708
38.0	0.00021	-36.85281	-38.24414	128.0	1.14585	0.59127	-0.80007
40.0	0.00017	-37.82054	-39.21187	130.0	1.15615	0.63014	-0.76119
42.0	0.00013	-38.88502	-40.27635	132.0	1.16106	0.64853	-0.74280
44.0	0.00010	-40.10317	-41.49450	134.0	1.15986	0.64406	-0.74727
46.0	0.00007	-41.57970	-42.97103	136.0	1.15195	0.61432	-0.77701
48.0	0.00004	-43.54736	-44.93870	138.0	1.13678	0.55678	-0.83455
50.0	0.00002	-46.74541	-48.13675	140.0	1.11398	0.46878	-0.92255
52.0	1.37763	1.39133	0.0	142.0	1.08329	0.34747	-1.04387
54.0	1.36140	1.33985	-0.05148	144.0	1.04465	0.18971	-1.20163
56.0	1.33969	1.27006	-0.12128	146.0	0.99817	-0.00796	-1.39930
58.0	1.31335	1.18381	-0.20752	148.0	0.94418	-0.24946	-1.64079
60.0	1.28321	1.08298	-0.30836	150.0	0.88323	-0.53928	-1.93061
62.0	1.25010	0.96946	-0.42188	152.0	0.81608	-0.88268	-2.27401
64.0	1.21484	0.84520	-0.54614	154.0	0.74372	-1.28592	-2.67726
66.0	1.17821	0.71221	-0.67913	156.0	0.66733	-1.75662	-3.14795
68.0	1.14093	0.57260	-0.81873	158.0	0.58828	-2.30418	-3.69551
70.0	1.10371	0.42856	-0.96277	160.0	0.50809	-2.94057	-4.33191
72.0	1.06718	0.28239	-1.10895	162.0	0.42841	-3.68138	-5.07271
74.0	1.03192	0.13646	-1.25487	164.0	0.35095	-4.54754	-5.93887
76.0	0.99845	-0.00674	-1.39808	166.0	0.27744	-5.56824	-6.95957
78.0	0.96723	-0.14470	-1.53603	168.0	0.20960	-6.78605	-8.17739
80.0	0.93857	-0.27485	-1.66619	170.0	0.14905	-8.26680	-9.65814
82.0	0.91312	-0.39470	-1.78603	172.0	0.09726	-10.12057	-11.51190
84.0	0.89087	-0.50184	-1.89317	174.0	0.05555	-12.55350	-13.94484
86.0	0.87216	-0.59404	-1.98537	176.0	0.02496	-16.02821	-17.41954
88.0	0.85716	-0.66936	-2.06069	178.0	0.00628	-22.02051	-23.41184
90.0	0.84602	-0.72621	-2.11754	180	0.00000	-INFINITY	-INFINITY

$h/\lambda = 0.25,\ 0 \leq ka \leq 3.0.$

TABLE A1-13

TABLE A1-13 $2\pi a/\lambda = 3.00$, $h/\lambda = 0.25$

Method gives poor results for $\epsilon > 2.5$.

INTEGRAL EQUATION METHOD
EPSILON= 3.0000(NORMALIZED GROUNDPLANE RADIUS)
MONOPOLE LENGTH= 0.250000(WAVELENGTH)
INFINITELY THIN MONOPOLE RADIUS
RADIATION RESISTANCE = 44.59867J (OHMS)

ELEVATION ANGLE (DEG)	DIRECTIVITY (NUMERIC)	DIRECTIVITY (DBI)	RELATIVE POWER (DB)	ELEVATION ANGLE (DEG)	DIRECTIVITY (NUMERIC)	DIRECTIVITY (DBI)	RELATIVE POWER (DB)
0	0.00000	-INFINITY	-INFINITY				
2.0	0.26737	-5.72891	-6.58895	92.0	0.00007	-41.44714	-42.30817
4.0	0.06676	-11.75511	-12.61614	94.0	0.00006	-42.32503	-43.18607
6.0	0.02964	-15.28085	-16.14189	96.0	0.00004	-43.47261	-44.33365
8.0	0.01666	-17.78195	-18.64298	98.0	0.00003	-45.12107	-45.98211
10.0	0.01066	-19.72094	-20.58197	100.0	0.00002	-48.00829	-48.86933
12.0	0.00741	-21.30390	-22.16494	102.0	0.67468	-1.70899	-2.57002
14.0	0.00544	-22.64081	-23.50185	104.0	0.69294	-1.59303	-2.45407
16.0	0.00417	-23.79734	-24.65838	106.0	0.71581	-1.45200	-2.31303
18.0	0.00330	-24.81589	-25.67693	108.0	0.74299	-1.29018	-2.15121
20.0	0.00268	-25.72545	-26.58649	110.0	0.77408	-1.11214	-1.97317
22.0	0.00221	-26.54673	-27.40776	112.0	0.80863	-0.92250	-1.78353
24.0	0.00186	-27.29504	-28.15607	114.0	0.84610	-0.72580	-1.58683
26.0	0.00159	-27.98207	-28.84310	116.0	0.88586	-0.52636	-1.38740
28.0	0.00138	-28.61692	-29.47795	118.0	0.92720	-0.32827	-1.18930
30.0	0.00120	-29.20685	-30.06788	120.0	0.96933	-0.13531	-0.99634
32.0	0.00106	-29.75775	-30.61878	122.0	1.01125	0.04902	-0.81201
34.0	0.00094	-30.27448	-31.13551	124.0	1.05232	0.22148	-0.63956
36.0	0.00084	-30.76111	-31.62214	126.0	1.09120	0.37805	-0.48297
38.0	0.00075	-31.22109	-32.08212	128.0	1.12692	0.51894	-0.34210
40.0	0.00068	-31.65739	-32.51842	130.0	1.15826	0.63843	-0.22260
42.0	0.00062	-32.07261	-32.93364	132.0	1.18439	0.73494	-0.12609
44.0	0.00057	-32.46903	-33.33007	134.0	1.20391	0.80593	-0.05510
46.0	0.00052	-32.84870	-33.70974	136.0	1.21586	0.84883	-0.01220
48.0	0.00048	-33.21348	-34.07452	138.0	1.21928	0.86103	0.0
50.0	0.00044	-33.56508	-34.42611	140.0	1.21333	0.83979	-0.02124
52.0	0.00041	-33.90509	-34.76613	142.0	1.19735	0.78320	-0.07883
54.0	0.00038	-34.23504	-35.09607	144.0	1.17087	0.68509	-0.17694
56.0	0.00035	-34.55638	-35.41741	146.0	1.13370	0.54497	-0.31607
58.0	0.00033	-34.87057	-35.73160	148.0	1.08589	0.35788	-0.50316
60.0	0.00030	-35.17904	-36.04008	150.0	1.02785	0.11530	-0.74173
62.0	0.00028	-35.48329	-36.34432	152.0	0.96028	-0.17604	-1.03307
64.0	0.00026	-35.78486	-36.64589	154.0	0.88421	-0.53442	-1.39546
66.0	0.00025	-36.08539	-36.94643	156.0	0.80104	-0.98348	-1.82451
68.0	0.00023	-36.38670	-37.24773	158.0	0.71242	-1.47265	-2.33368
70.0	0.00021	-36.69077	-37.55180	160.0	0.62031	-2.07391	-2.93494
72.0	0.00020	-36.99987	-37.86090	162.0	0.52688	-2.78287	-3.64390
74.0	0.00019	-37.31664	-38.17768	164.0	0.43446	-3.62048	-4.48151
76.0	0.00017	-37.64420	-38.50523	166.0	0.34547	-4.61593	-5.47697
78.0	0.00016	-37.98631	-38.84735	168.0	0.26231	-5.81185	-6.67288
80.0	0.00015	-38.34765	-39.20868	170.0	0.18733	-7.27404	-8.13507
82.0	0.00013	-38.73414	-39.59517	172.0	0.12267	-9.11260	-9.97363
84.0	0.00012	-39.15351	-40.01454	174.0	0.07025	-11.53370	-12.39473
86.0	0.00011	-39.61614	-40.47718	176.0	0.03162	-14.99995	-15.86098
88.0	0.00010	-40.12656	-40.98760	178.0	0.00797	-20.98716	-21.84820
90.0	0.00008	-40.73596	-41.59699	180	0.00000	-INFINITY	-INFINITY

$h/\lambda = 0.25$, $0 \leq ka \leq 3.0$.

TABLE A1-14

INTEGRAL EQUATION METHOD
EPSILON= 0.0 (NORMALIZED GROUNDPLANE RADIUS)
MONOPOLE LENGTH= 0.100000(WAVELENGTH)
INFINITELY THIN MONOPOLE RADIUS
RADIATION RESISTANCE = 2.100720 (OHMS)

ELEVATION ANGLE θ (DEG)	DIRECTIVITY (NUMERIC)	DIRECTIVITY (DBI)	RELATIVE POWER (DB)	ELEVATION ANGLE (DEG)	DIRECTIVITY (NUMERIC)	DIRECTIVITY (DBI)	RELATIVE POWER (DB)
0	0.00000	-INFINITY	-INFINITY				
2.0	0.00179	-27.45943	-29.23947	92.0	1.50375	1.77464	-0.00541
4.0	0.00717	-21.44377	-23.22382	94.0	1.49913	1.75840	-0.02165
6.0	0.01611	-17.93019	-19.71023	96.0	1.48980	1.73129	-0.04876
8.0	0.02856	-15.44296	-17.22301	98.0	1.47681	1.69324	-0.08680
10.0	0.04447	-13.51963	-15.29967	100.0	1.46022	1.64418	-0.13586
12.0	0.06376	-11.95420	-13.73424	102.0	1.44012	1.58399	-0.19606
14.0	0.08636	-10.63680	-12.41685	104.0	1.41661	1.51252	-0.26753
16.0	0.11215	-9.50187	-11.28191	106.0	1.38982	1.42960	-0.35045
18.0	0.14102	-8.50711	-10.28715	108.0	1.35988	1.33502	-0.44503
20.0	0.17284	-7.62366	-9.40370	110.0	1.32695	1.22855	-0.55150
22.0	0.20745	-6.83094	-8.61098	112.0	1.29119	1.10991	-0.67014
24.0	0.24469	-6.11377	-7.89381	114.0	1.25279	0.97879	-0.80126
26.0	0.28441	-5.46063	-7.24067	116.0	1.21194	0.82482	-0.94522
28.0	0.32639	-4.86257	-6.64262	118.0	1.16886	0.67761	-1.10244
30.0	0.37047	-4.31251	-6.09256	120.0	1.12375	0.50669	-1.27336
32.0	0.41641	-3.80476	-5.58481	122.0	1.07684	0.32153	-1.45852
34.0	0.46402	-3.33466	-5.11471	124.0	1.02838	0.12154	-1.65850
36.0	0.51305	-2.89837	-4.67842	126.0	0.97860	-0.09393	-1.87398
38.0	0.56329	-2.49268	-4.27273	128.0	0.92776	-0.32566	-2.10571
40.0	0.61448	-2.11490	-3.89494	130.0	0.87609	-0.57450	-2.35455
42.0	0.66639	-1.76271	-3.54276	132.0	0.82387	-0.84143	-2.62147
44.0	0.71876	-1.43416	-3.21421	134.0	0.77134	-1.12756	-2.90760
46.0	0.77134	-1.12756	-2.90760	136.0	0.71876	-1.43416	-3.21421
48.0	0.82387	-0.84143	-2.62147	138.0	0.66639	-1.76271	-3.54276
50.0	0.87609	-0.57450	-2.35455	140.0	0.61448	-2.11490	-3.89494
52.0	0.92776	-0.32566	-2.10571	142.0	0.56329	-2.49268	-4.27273
54.0	0.97860	-0.09393	-1.87398	144.0	0.51305	-2.89837	-4.67842
56.0	1.02838	0.12154	-1.65850	146.0	0.46402	-3.33466	-5.11471
58.0	1.07684	0.32153	-1.45852	148.0	0.41641	-3.80476	-5.58481
60.0	1.12375	0.50669	-1.27336	150.0	0.37047	-4.31251	-6.09256
62.0	1.16886	0.67761	-1.10244	152.0	0.32639	-4.86257	-6.64262
64.0	1.21194	0.83482	-0.94522	154.0	0.28441	-5.46063	-7.24067
66.0	1.25279	0.97879	-0.80126	156.0	0.24469	-6.11377	-7.89381
68.0	1.29119	1.10991	-0.67014	158.0	0.20745	-6.83094	-8.61098
70.0	1.32695	1.22855	-0.55150	160.0	0.17284	-7.62366	-9.40370
72.0	1.35988	1.33502	-0.44503	162.0	0.14102	-8.50711	-10.28715
74.0	1.38982	1.42960	-0.35045	164.0	0.11215	-9.50187	-11.28191
76.0	1.41661	1.51252	-0.26753	166.0	0.08636	-10.63680	-12.41685
78.0	1.44012	1.58399	-0.19606	168.0	0.06376	-11.95420	-13.73424
80.0	1.46022	1.64418	-0.13586	170.0	0.04447	-13.51963	-15.29967
82.0	1.47681	1.69324	-0.08680	172.0	0.02856	-15.44296	-17.22301
84.0	1.48980	1.73129	-0.04876	174.0	0.01611	-17.93019	-19.71023
86.0	1.49913	1.75840	-0.02165	176.0	0.00717	-21.44377	-23.22382
88.0	1.50475	1.77464	-0.00541	178.0	0.00179	-27.45943	-29.23947
90.0	1.50662	1.78005	0.0	180.	0.00000	-INFINITY	-INFINITY

$h/\lambda = 0.10,\ 0 \le ka \le 3.0.$

TABLE A1-15

INTEGRAL EQUATION METHOD
EPSILON= 0.2500(NORMALIZED GROUNDPLANE RADIUS)
MONOPOLE LENGTH= 0.100000(WAVELENGTH)
INFINITELY THIN MONOPOLE RADIUS
RADIATION RESISTANCE = 2.105873 (OHMS)

ELEVATION ANGLE (DEG)	DIRECTIVITY (NUMERIC)	DIRECTIVITY (DBI)	RELATIVE POWER (DB)	ELEVATION ANGLE (DEG)	DIRECTIVITY (NUMERIC)	DIRECTIVITY (DBI)	RELATIVE POWER (DB)
0	0.00000	-INFINITY	-INFINITY				
2.0	0.00181	-27.41673	-29.18613	92.0	1.50109	1.76406	-0.00534
4.0	0.00724	-21.40126	-23.17067	94.0	1.49555	1.74802	-0.02139
6.0	0.01626	-17.88800	-19.65741	96.0	1.48636	1.72123	-0.04818
8.0	0.02883	-15.40123	-17.17064	98.0	1.47355	1.68364	-0.08577
10.0	0.04489	-13.47847	-15.24788	100.0	1.45719	1.63515	-0.13425
12.0	0.06436	-11.91374	-13.68315	102.0	1.43736	1.57566	-0.19375
14.0	0.08715	-10.59717	-12.36657	104.0	1.41417	1.50500	-0.26441
16.0	0.11316	-9.46316	-11.23257	106.0	1.38772	1.42301	-0.34640
18.0	0.14225	-8.46944	-10.23885	108.0	1.35815	1.32948	-0.43993
20.0	0.17430	-7.58714	-9.35654	110.0	1.32561	1.22415	-0.54526
22.0	0.20914	-6.79567	-8.56507	112.0	1.29026	1.10676	-0.66265
24.0	0.24661	-6.07984	-7.84925	114.0	1.25227	0.97698	-0.79243
26.0	0.28654	-5.42813	-7.19753	116.0	1.21184	0.83444	-0.93496
28.0	0.32873	-4.83158	-6.60098	118.0	1.16916	0.67874	-1.09067
30.0	0.37298	-4.28310	-6.05251	120.0	1.12445	0.50939	-1.26002
32.0	0.41908	-3.77689	-5.54640	122.0	1.07792	0.32588	-1.44353
34.0	0.46681	-3.30860	-5.07800	124.0	1.02982	0.12760	-1.64181
36.0	0.51593	-2.87406	-4.64347	126.0	0.98036	-0.08613	-1.85554
38.0	0.56622	-2.47016	-4.23957	128.0	0.92981	-0.31607	-2.08547
40.0	0.61742	-2.09420	-3.86361	130.0	0.87840	-0.56308	-2.33249
42.0	0.66929	-1.74386	-3.51327	132.0	0.82639	-0.82816	-2.59757
44.0	0.72158	-1.41717	-3.18658	134.0	0.77403	-1.11243	-2.88184
46.0	0.77403	-1.11243	-2.88184	136.0	0.72158	-1.41718	-3.18658
48.0	0.82639	-0.82816	-2.59757	138.0	0.66929	-1.74387	-3.51327
50.0	0.87840	-0.56308	-2.33249	140.0	0.61742	-2.09421	-3.86361
52.0	0.92981	-0.31606	-2.08547	142.0	0.56622	-2.47017	-4.23958
54.0	0.98036	-0.08613	-1.85553	144.0	0.51593	-2.87406	-4.64347
56.0	1.02982	0.12760	-1.64181	146.0	0.46681	-3.30860	-5.07801
58.0	1.07792	0.32588	-1.44353	148.0	0.41908	-3.77700	-5.54641
60.0	1.12445	0.50940	-1.26001	150.0	0.37298	-4.28311	-6.05251
62.0	1.16916	0.67874	-1.09067	152.0	0.32873	-4.83158	-6.60099
64.0	1.21184	0.83445	-0.93496	154.0	0.28654	-5.42813	-7.19754
66.0	1.25227	0.97698	-0.79243	156.0	0.24661	-6.07985	-7.84925
68.0	1.29026	1.10676	-0.66264	158.0	0.20914	-6.79567	-8.56508
70.0	1.32561	1.22415	-0.54525	160.0	0.17430	-7.58714	-9.35655
72.0	1.35815	1.32948	-0.43993	162.0	0.14225	-8.46945	-10.23885
74.0	1.38772	1.42301	-0.34639	164.0	0.11316	-9.46316	-11.23257
76.0	1.41417	1.50500	-0.26440	166.0	0.08715	-10.59717	-12.36657
78.0	1.43736	1.57566	-0.19375	168.0	0.06436	-11.91374	-13.68315
80.0	1.45719	1.63516	-0.13425	170.0	0.04489	-13.47848	-15.24788
82.0	1.47355	1.68364	-0.08577	172.0	0.02883	-15.40123	-17.17064
84.0	1.48636	1.72123	-0.04818	174.0	0.01626	-17.88901	-19.65742
86.0	1.49555	1.74802	-0.02139	176.0	0.00724	-21.40127	-23.17068
88.0	1.50109	1.76406	-0.00534	178.0	0.00181	-27.41673	-29.18614
90.0	1.50294	1.76941	0.0	180	0.00000	-INFINITY	-INFINITY

$h/\lambda = 0.10$, $0 \leq ka \leq 3.0$.

TABLE A1-16

INTEGRAL EQUATION METHOD
EPSILON= 0.5000[NORMALIZED GROUNDPLANE RADIUS]
#MONOPOLE LENGTH= 0.100000[WAVELENGTH]
[NFINITELY THIN MONOPOLE RADIUS
#RADIATION RESISTANCE = 2.120811 [OHMS]

ELEVATION ANGLE (DEG)	DIRECTIVITY (NUMERIC)	DIRECTIVITY (DBI)	RELATIVE POWER (DB)	ELEVATION ANGLE (DEG)	DIRECTIVITY (NUMERIC)	DIRECTIVITY (DBI)	RELATIVE POWER (DB)
0	0.00000	-INFINITY	-INFINITY				
2.0	0.00186	-27.29481	-29.03352	92.0	1.49058	1.73355	-0.00916
4.0	0.00745	-21.27990	-23.01861	94.0	1.48527	1.71806	-0.02065
6.0	0.01672	-17.76756	-19.50627	96.0	1.47645	1.69220	-0.04651
8.0	0.02963	-15.28207	-17.02078	98.0	1.46417	1.65590	-0.08281
10.0	0.04612	-13.36095	-15.09966	100.0	1.44846	1.60907	-0.12964
12.0	0.06610	-11.79820	-13.53691	102.0	1.42941	1.55188	-0.18713
14.0	0.08946	-10.48395	-12.22266	104.0	1.40711	1.48327	-0.25544
16.0	0.11608	-9.35260	-11.09131	106.0	1.38164	1.40395	-0.33476
18.0	0.14582	-8.36185	-10.10056	108.0	1.35313	1.31341	-0.42530
20.0	0.17853	-7.48281	-9.22152	110.0	1.32171	1.21137	-0.52733
22.0	0.21405	-6.69490	-8.43360	112.0	1.28753	1.09756	-0.64115
24.0	0.25218	-5.98289	-7.72160	114.0	1.25073	0.97163	-0.76708
26.0	0.29274	-5.33524	-7.07395	116.0	1.21149	0.83318	-0.90552
28.0	0.33551	-4.74299	-6.48170	118.0	1.16998	0.68180	-1.05681
30.0	0.38028	-4.19902	-5.93773	120.0	1.12642	0.51693	-1.22172
32.0	0.42681	-3.69761	-5.43632	122.0	1.08098	0.33819	-1.40052
34.0	0.47489	-3.23407	-4.97276	124.0	1.03390	0.14478	-1.59392
36.0	0.52426	-2.80453	-4.54324	126.0	0.98539	-0.06393	-1.80264
38.0	0.57468	-2.40575	-4.14446	128.0	0.93568	-0.28874	-2.02745
40.0	0.62589	-2.03500	-3.77371	130.0	0.88501	-0.53054	-2.26925
42.0	0.67765	-1.68993	-3.42864	132.0	0.83362	-0.79034	-2.52905
44.0	0.72970	-1.36856	-3.10727	134.0	0.78176	-1.06929	-2.80800
46.0	0.78178	-1.06915	-2.80786	136.0	0.72967	-1.36871	-3.10742
48.0	0.83364	-0.79020	-2.52891	138.0	0.67763	-1.69009	-3.42880
50.0	0.88503	-0.53040	-2.26911	140.0	0.62587	-2.03516	-3.77386
52.0	0.93571	-0.28861	-2.02732	142.0	0.57466	-2.40592	-4.14462
54.0	0.98542	-0.06380	-1.80251	144.0	0.52424	-2.80470	-4.54341
56.0	1.03393	0.14490	-1.59381	146.0	0.47487	-3.23424	-4.97295
58.0	1.08101	0.33830	-1.40041	148.0	0.42680	-3.69778	-5.43649
60.0	1.12644	0.51709	-1.22162	150.0	0.38026	-4.19920	-5.93791
62.0	1.17001	0.68190	-1.05681	152.0	0.33549	-4.74317	-6.48188
64.0	1.21151	0.83328	-0.90543	154.0	0.29272	-5.33543	-7.07414
66.0	1.25075	0.97171	-0.76700	156.0	0.25217	-5.98307	-7.72178
68.0	1.28755	1.09764	-0.64107	158.0	0.21404	-6.69509	-8.43379
70.0	1.32174	1.21145	-0.52726	160.0	0.17853	-7.48301	-9.22172
72.0	1.35315	1.31347	-0.42524	162.0	0.14581	-8.36204	-10.10075
74.0	1.38166	1.40401	-0.33470	164.0	0.11607	-9.35280	-11.09151
76.0	1.40712	1.48332	-0.25539	166.0	0.08945	-10.48415	-12.22286
78.0	1.42943	1.55162	-0.18709	168.0	0.06609	-11.79840	-13.53711
80.0	1.44847	1.60911	-0.12960	170.0	0.04612	-13.36115	-15.09986
82.0	1.46418	1.65593	-0.08278	172.0	0.02963	-15.28227	-17.02098
84.0	1.47645	1.69222	-0.04649	174.0	0.01672	-17.76777	-19.50647
86.0	1.48528	1.71807	-0.02064	176.0	0.00745	-21.28010	-23.01881
88.0	1.49068	1.73356	-0.00515	178.0	0.00186	-27.29501	-29.03372
90.0	1.49235	1.73831	0.0	180	0.00000	-INFINITY	-INFINITY

$h/\lambda = 0.10,\ 0 \le ka \le 3.0.$

TABLE A1-17

[NTEGRAL EQUATION METHOD
EPSILON= 0 7500[NORMALIZED GROUNDPLANE RADIUS]
MONOPOLE LENGTH= 0 100000[WAVELENGTH]
INFINITELY THIN MONOPOLE RADIUS
RADIATION RESISTANCE = 2.146484 [OHMS]

ELEVATION ANGLE (DEG)	DIRECTIVITY (NUMERIC)	DIRECTIVITY (DBI)	RELATIVE POWER (DB)	ELEVATION ANGLE (DEG)	DIRECTIVITY (NUMERIC)	DIRECTIVITY (DBI)	RELATIVE POWE (DB)
0	0 00000	-INFINITY	-INFINITY				
2 0	0 00195	-27 09141	-28 77786	92 0	1 47285	1 68158	-0 00487
4 0	0 00780	-21 07742	-22 76387	94 0	1 46792	1 66702	-0 01943
6 0	0 01761	-17 56660	-19 25305	96 0	1 45973	1 64271	-0 04374
8 0	0 03102	-15 08323	-16 76968	98 0	1 44830	1 60859	-0 07787
10 0	0 04825	-13 16482	-14 85127	100 0	1 43368	1 56453	-0 12182
12 0	0 06910	-11 60536	-13 29181	102 0	1 41593	1 51041	-0 17604
14 0	0 09343	-10 29395	-11 98140	104 0	1 39510	1 44605	-0 24040
16 0	0 12112	-9 16799	-10 85544	106 0	1 37127	1 37124	-0 31521
18 0	0 15198	-8 18215	-9 86860	108 0	1 34454	1 28573	-0 40072
20 0	0 18584	-7 30853	-8 99498	110 0	1 31500	1 18925	-0 49721
22 0	0 22251	-6 52650	-8 21295	112 0	1 28276	1 08146	-0 60500
24 0	0 26177	-5 82083	-7 50728	114 0	1 24796	0 96199	-0 72446
26 0	0 30339	-5 17994	-6 86639	116 0	1 21072	0 83044	-0 85601
28 0	0 34715	-4 59383	-6 28128	118 0	1 17120	0 68632	-1 00013
30 0	0 39279	-4 05835	-5 74480	120 0	1 12957	0 52912	-1 15733
32 0	0 44007	-3 56475	-5 25120	122 0	1 08598	0 35824	-1 32822
34 0	0 48873	-3 10930	-4 79575	124 0	1 04064	0 17301	-1 51344
36 0	0 53851	-2 68809	-4 37454	126 0	0 99374	-0 02729	-1 71374
38 0	0 58914	-2 29785	-3 98430	128 0	0 94547	-0 24351	-1 92996
40 0	0 64036	-1 93579	-3 62224	130 0	0 89607	-0 47655	-2 16303
42 0	0 69190	-1 59954	-3 28599	132 0	0 84576	-0 72755	-2 41400
44 0	0 74352	-1 28705	-2 97350	134 0	0 79476	-0 99762	-2 68407
46 0	0 79496	-0 99657	-2 68302	136 0	0 74334	-1 28814	-2 97459
48 0	0 84595	-0 72653	-2 41298	138 0	0 69173	-1 60066	-3 28711
50 0	0 89627	-0 47560	-2 16205	140 0	0 64019	-1 93694	-3 62339
52 0	0 94568	-0 24257	-1 92902	142 0	0 58897	-2 29903	-3 98549
54 0	0 99394	-0 02639	-1 71284	144 0	0 53836	-2 68931	-4 37576
56 0	1 04085	0 17387	-1 51258	146 0	0 48859	-3 11054	-4 79699
58 0	1 08619	0 35805	-1 32740	148 0	0 43995	-3 56602	-5 25247
60 0	1 12977	0 52989	-1 15656	150 0	0 39268	-4 05964	-5 74609
62 0	1 17140	0 68705	-0 99940	152 0	0 34705	-4 59614	-6 28259
64 0	1 21091	0 83112	-0 85533	154 0	0 30330	-5 18127	-6 86772
66 0	1 24814	0 96263	-0 72383	156 0	0 26168	-5 82218	-7 50863
68 0	1 28293	1 08204	-0 60441	158 0	0 22244	-6 52787	-8 21432
70 0	1 31516	1 18978	-0 49667	160 0	0 18578	-7 30992	-8 99637
72 0	1 34469	1 28622	-0 40023	162 0	0 15193	-8 18355	-9 87000
74 0	1 37149	1 37167	-0 31478	164 0	0 12108	-9 16940	-10 85586
76 0	1 39522	1 44643	-0 24002	166 0	0 09340	-10 29628	-11 98283
78 0	1 41603	1 51074	-0 17571	168 0	0 06908	-11 60679	-13 29334
80 0	1 43377	1 56481	-0 12164	170 0	0 04824	-13 16526	-14 85181
82 0	1 44837	1 60881	-0 07765	172 0	0 03101	-15 08468	-16 77123
84 0	1 45978	1 64288	-0 04357	174 0	0 01751	-17 56805	-19 25460
86 0	1 46796	1 66713	-0 01932	176 0	0 00780	-21 07887	-22 76533
88 0	1 47287	1 68164	-0 00481	178 0	0 00195	-27 09287	-28 77933
90 0	1 47450	1 68645	0 0	180	0 00000	-INFINITY	-INFINITY

$h/\lambda = 0.10$, $0 \leq ka \leq 3.0$.

TABLE A1-18

INTEGRAL EQUATION METHOD
EPSILON= 1.0000(NORMALIZED GROUNDPLANE RADIUS)
MONOPOLE LENGTH= 0.100000(WAVELENGTH)
INFINITELY THIN MONOPOLE RADIUS
RADIATION RESISTANCE = 2.185235 (OHMS)

ELEVATION ANGLE (DEG)	DIRECTIVITY (NUMERIC)	DIRECTIVITY (DBI)	RELATIVE POWER (DB)	ELEVATION ANGLE (DEG)	DIRECTIVITY (NUMERIC)	DIRECTIVITY (DBI)	RELATIVE POWER (DB)
0	0.00000	-INFINITY	-INFINITY				
2.0	0.00209	-26.79818	-28.40693	92.0	1.44686	1.60426	-0.00449
4.0	0.00835	-20.78549	-22.39424	94.0	1.44245	1.59101	-0.01774
6.0	0.01872	-17.27683	-18.88558	96.0	1.43514	1.56894	-0.03980
8.0	0.03314	-14.79647	-16.40522	98.0	1.42484	1.53797	-0.07078
10.0	0.05150	-12.88191	-14.49066	100.0	1.41188	1.49797	-0.11078
12.0	0.07367	-11.32713	-12.93587	102.0	1.39597	1.44877	-0.15998
14.0	0.09949	-10.02219	-11.63094	104.0	1.37726	1.39017	-0.21857
16.0	0.12878	-8.90148	-10.51023	106.0	1.35580	1.32194	-0.28680
18.0	0.16134	-7.92264	-9.53139	108.0	1.33162	1.24380	-0.36495
20.0	0.19694	-7.05674	-8.66549	110.0	1.30473	1.15541	-0.45333
22.0	0.23534	-6.28311	-7.89186	112.0	1.27539	1.05642	-0.55233
24.0	0.27628	-5.58649	-7.19524	114.0	1.24348	0.94640	-0.66235
26.0	0.31950	-4.95526	-6.56400	116.0	1.20917	0.82489	-0.78386
28.0	0.36472	-4.38036	-5.98911	118.0	1.17256	0.69136	-0.91738
30.0	0.41166	-3.85462	-5.46337	120.0	1.13377	0.54524	-1.06351
32.0	0.46002	-3.37232	-4.98097	122.0	1.09297	0.38587	-1.22287
34.0	0.50952	-2.92839	-4.53714	124.0	1.05016	0.21254	-1.39621
36.0	0.55987	-2.51917	-4.12791	126.0	1.00564	0.02444	-1.58431
38.0	0.61077	-2.14121	-3.74996	128.0	0.95955	-0.17933	-1.78808
40.0	0.66195	-1.79168	-3.40043	130.0	0.91206	-0.39976	-2.00850
42.0	0.71315	-1.46816	-3.07691	132.0	0.86338	-0.63796	-2.24671
44.0	0.76409	-1.16853	-2.77728	134.0	0.81373	-0.89520	-2.50395
46.0	0.81452	-0.89097	-2.49972	136.0	0.76333	-1.17290	-2.78164
48.0	0.86420	-0.63387	-2.24262	138.0	0.71242	-1.47265	-3.08139
50.0	0.91289	-0.39581	-2.00455	140.0	0.66126	-1.79629	-3.40503
52.0	0.96039	-0.17553	-1.78428	142.0	0.61011	-2.14592	-3.75467
54.0	1.00649	0.02808	-1.58067	144.0	0.55924	-2.52398	-4.13273
56.0	1.05100	0.21602	-1.39273	146.0	0.50894	-2.93331	-4.54205
58.0	1.09375	0.38919	-1.21956	148.0	0.45949	-3.37723	-4.98597
60.0	1.13459	0.54838	-1.06037	150.0	0.41118	-3.85971	-5.46846
62.0	1.17336	0.69432	-0.91442	152.0	0.36429	-4.38553	-5.99428
64.0	1.20995	0.82766	-0.78108	154.0	0.31912	-4.96050	-6.56925
66.0	1.24422	0.94898	-0.65976	156.0	0.27594	-5.59180	-7.20055
68.0	1.27609	1.05881	-0.54994	158.0	0.23505	-6.28649	-7.89524
70.0	1.30545	1.15760	-0.45115	160.0	0.19669	-7.06217	-8.67092
72.0	1.33223	1.24578	-0.36297	162.0	0.16113	-7.92813	-9.53687
74.0	1.35635	1.32372	-0.28503	164.0	0.12862	-8.90701	-10.51576
76.0	1.37776	1.39173	-0.21701	166.0	0.09936	-10.02776	-11.63651
78.0	1.39640	1.45011	-0.15864	168.0	0.07357	-11.33273	-12.94147
80.0	1.41224	1.49908	-0.10966	170.0	0.05143	-12.88754	-14.49628
82.0	1.42524	1.53887	-0.06987	172.0	0.03310	-14.80213	-16.41087
84.0	1.43536	1.56962	-0.03913	174.0	0.01870	-17.28250	-18.89125
86.0	1.44260	1.59146	-0.01728	176.0	0.00833	-20.79117	-22.39992
88.0	1.44693	1.60449	-0.00426	178.0	0.00209	-26.80387	-28.41262
90.0	1.44835	1.60875	0.0	180	0.00000	-INFINITY	-INFINITY

$h/\lambda = 0.10$, $0 \leq ka \leq 3.0$.

TABLE A1-19

INTEGRAL EQUATION METHOD
EPSILON= 1.2500(NORMALIZED GROUNDPLANE RADIUS)
MONOPOLE LENGTH= 0.100000(WAVELENGTH)
INFINITELY THIN MONOPOLE RADIUS
RADIATION RESISTANCE = 2.241091 (OHMS)

ELEVATION ANGLE θ (DEG)	DIRECTIVITY (NUMERIC)	DIRECTIVITY (DBI)	RELATIVE POWER (DB)	ELEVATION ANGLE (DEG)	DIRECTIVITY (NUMERIC)	DIRECTIVITY (DBI)	RELATIVE POWER (DB)
0	0.00000	-INFINITY	-INFINITY				
2.0	0.00229	-26.40280	-27.90193	92.0	1.41094	1.49508	+0.00405
4.0	0.00914	-20.39182	-21.89095	94.0	1.40720	1.48357	-0.01557
6.0	0.02048	-16.88601	-18.38515	96.0	1.40105	1.46453	+0.03461
8.0	0.03623	-14.40963	-15.90877	98.0	1.39247	1.43786	-0.06128
10.0	0.05623	-12.50016	-13.99929	100.0	1.38147	1.40340	+0.09573
12.0	0.08032	-10.95154	-12.45068	102.0	1.36803	1.36097	-0.13816
14.0	0.10830	-9.65365	-11.15298	104.0	1.35217	1.31032	+0.18882
16.0	0.13991	-8.54141	-10.04054	106.0	1.33388	1.25116	-0.24798
18.0	0.17491	-7.57184	-9.07098	108.0	1.31315	1.18315	+0.31598
20.0	0.21300	-6.71618	-8.21531	110.0	1.29001	1.10582	-0.39321
22.0	0.25388	-5.95071	-7.45284	112.0	1.26446	1.01903	-0.48010
24.0	0.29723	-5.26911	-6.76825	114.0	1.23652	0.92200	-0.57713
26.0	0.34271	-4.65073	-6.14987	116.0	1.20623	0.81429	+0.68485
28.0	0.38999	-4.08947	-5.58860	118.0	1.17362	0.69528	-0.80384
30.0	0.43873	-3.57806	-5.07720	120.0	1.13877	0.56435	-0.93479
32.0	0.48858	-3.11065	-4.60978	122.0	1.10172	0.42073	+1.07841
34.0	0.53921	-2.68239	-4.18152	124.0	1.06258	0.26363	+1.23551
36.0	0.59030	-2.28925	-3.78838	126.0	1.02145	0.09216	+1.40698
38.0	0.64153	-1.92780	-3.42696	128.0	0.97844	-0.09466	-1.59380
40.0	0.69260	-1.59521	-3.09434	130.0	0.93370	-0.29792	+1.79706
42.0	0.74321	-1.28888	-2.78801	132.0	0.88740	-0.51882	-2.01795
44.0	0.79311	-1.00666	-2.50578	134.0	0.83971	-0.75670	+2.25583
46.0	0.84205	-0.74663	-2.24577	136.0	0.79085	-1.01906	-2.51820
48.0	0.88979	-0.50711	-2.00625	138.0	0.74104	-1.30160	+2.80073
50.0	0.93614	-0.28660	-1.78573	140.0	0.69052	-1.60823	-3.10736
52.0	0.98090	-0.08374	-1.58288	142.0	0.63957	-1.94113	+3.44027
54.0	1.02392	0.10266	+1.39648	144.0	0.58846	-2.30282	-3.80195
56.0	1.06505	0.27369	-1.22545	146.0	0.53750	-2.69620	+4.19533
58.0	1.10416	0.43033	+1.06881	148.0	0.48700	-3.12468	-4.62382
60.0	1.14116	0.57346	-0.92567	150.0	0.43729	-3.59230	-5.09144
62.0	1.17595	0.70390	-0.79523	152.0	0.38870	-4.10390	-5.60304
64.0	1.20848	0.82238	-0.67675	154.0	0.34156	-4.66535	-6.16448
66.0	1.23867	0.92955	-0.56958	156.0	0.29622	-5.28389	+6.78302
68.0	1.26649	1.02603	-0.47311	158.0	0.25301	-5.96862	-7.46776
70.0	1.29191	1.11234	-0.38680	160.0	0.21226	-6.73123	-8.23038
72.0	1.31491	1.18897	-0.31016	162.0	0.17430	-7.58701	-9.08615
74.0	1.33548	1.25637	-0.24276	164.0	0.13942	-8.55668	-10.05582
76.0	1.35360	1.31491	-0.18422	166.0	0.10781	-9.66921	-11.16834
78.0	1.36928	1.36493	-0.13420	168.0	0.08004	-10.96698	-12.46612
80.0	1.38252	1.40672	-0.09241	170.0	0.05603	-12.51566	-14.01480
82.0	1.39332	1.44052	-0.05861	172.0	0.03610	-14.42519	-15.92432
84.0	1.40169	1.46653	-0.03260	174.0	0.02041	-16.90161	-18.40075
86.0	1.40764	1.48491	-0.01423	176.0	0.00910	-20.40745	-21.90658
88.0	1.41116	1.49575	-0.00338	178.0	0.00228	-26.41844	-27.91758
90.0	1.41226	1.49913	0.0	180	0.00000	-INFINITY	-INFINITY

$h/\lambda = 0.10$, $0 \leq ka \leq 3.0$.

TABLE A1-20

INTEGRAL EQUATION METHOD
EPSILON= 1.5000(NORMALIZED GROUNDPLANE RADIUS)
MONOPOLE LENGTH= 0.100000(WAVELENGTH)
(INFINITELY THIN MONOPOLE RADIUS
RADIATION RESISTANCE = 2.320740 (OHMS)

ELEVATION ANGLE (DEG)	DIRECTIVITY (NUMERIC)	DIRECTIVITY (DBI)	RELATIVE POWER (DB)	ELEVATION ANGLE (DEG)	DIRECTIVITY (NUMERIC)	DIRECTIVITY (DBI)	RELATIVE POWER (DB)
0	0.00000	-INFINITY	-INFINITY				
2.0	0.00258	-25.89000	-27.23747	92.0	1.36265	1.34383	-0.00363
4.0	0.01028	-19.88819	-21.22865	94.0	1.35973	1.33453	-0.01293
6.0	0.02302	-16.37897	-17.72644	96.0	1.35503	1.31948	-0.02789
8.0	0.04067	-13.90760	-15.25506	98.0	1.34851	1.29854	-0.04893
10.0	0.06303	-12.00453	-13.35200	100.0	1.34014	1.27151	-0.07595
12.0	0.08987	-10.46371	-11.81118	102.0	1.32989	1.23817	-0.10930
14.0	0.12092	-9.17516	-10.52262	104.0	1.31771	1.19819	-0.14927
16.0	0.15584	-8.07318	-9.42064	106.0	1.30354	1.15123	-0.19624
18.0	0.19430	-7.11535	-8.46281	108.0	1.28732	1.09686	-0.25060
20.0	0.23590	-6.27266	-7.62012	110.0	1.26900	1.03463	-0.31284
22.0	0.28026	-5.52435	-6.87182	112.0	1.24853	0.96399	-0.38348
24.0	0.32686	-4.85506	-6.20253	114.0	1.22585	0.88436	-0.46310
26.0	0.37557	-4.25307	-5.60053	116.0	1.20091	0.79510	-0.55236
28.0	0.42568	-3.70920	-5.05666	118.0	1.17368	0.69550	-0.65197
30.0	0.47685	-3.21614	-4.56361	120.0	1.14414	0.58477	-0.76269
32.0	0.52869	-2.76795	-4.11541	122.0	1.11226	0.46208	-0.88538
34.0	0.58080	-2.35972	-3.70718	124.0	1.07808	0.32650	-1.02097
36.0	0.63280	-1.98732	-3.33478	126.0	1.04160	0.17701	-1.17045
38.0	0.68434	-1.64726	-2.99472	128.0	1.00288	0.01254	-1.33483
40.0	0.73510	-1.33655	-2.68401	130.0	0.96202	-0.16814	-1.51561
42.0	0.78477	-1.05257	-2.40004	132.0	0.91911	-0.36634	-1.71380
44.0	0.83310	-0.79305	-2.14051	134.0	0.87428	-0.58051	-1.93097
46.0	0.87984	-0.55596	-1.90343	136.0	0.82770	-0.82127	-2.16873
48.0	0.92480	-0.33952	-1.68698	138.0	0.77958	-1.08142	-2.42888
50.0	0.96781	-0.14210	-1.48956	140.0	0.73013	-1.36597	-2.71344
52.0	1.00873	0.03775	-1.30972	142.0	0.67964	-1.67722	-3.02468
54.0	1.04745	0.20134	-1.14612	144.0	0.62838	-2.01777	-3.36523
56.0	1.08390	0.34988	-0.99758	146.0	0.57668	-2.38061	-3.73808
58.0	1.11801	0.48447	-0.86300	148.0	0.52490	-2.79926	-4.14672
60.0	1.14977	0.60610	-0.74136	150.0	0.47339	-3.24782	-4.59529
62.0	1.17916	0.71572	-0.63175	152.0	0.42255	-3.74122	-5.08868
64.0	1.20619	0.81416	-0.53331	154.0	0.37279	-4.28540	-5.63286
66.0	1.23089	0.90220	-0.44527	156.0	0.32451	-4.88767	-6.23513
68.0	1.25330	0.98055	-0.36692	158.0	0.27815	-5.55720	-6.90467
70.0	1.27346	1.04986	-0.29760	160.0	0.23411	-6.30573	-7.65319
72.0	1.29144	1.11073	-0.23674	162.0	0.19281	-7.14861	-8.49608
74.0	1.30728	1.16367	-0.18379	164.0	0.15465	-8.10661	-9.45407
76.0	1.32105	1.20918	-0.13828	166.0	0.11998	-9.20873	-10.55620
78.0	1.33280	1.24766	-0.09981	168.0	0.08918	-10.48741	-11.84487
80.0	1.34260	1.27948	-0.06799	170.0	0.06254	-12.03834	-13.39580
82.0	1.35050	1.30494	-0.04253	172.0	0.04035	-13.94148	-15.29895
84.0	1.35653	1.32430	-0.02316	174.0	0.02284	-16.41292	-17.76039
86.0	1.36074	1.33776	-0.00971	176.0	0.01020	-19.91518	-21.26264
88.0	1.36315	1.34545	-0.00202	178.0	0.00256	-25.92402	-27.27148
90.0	1.36379	1.34745	0.0	180	0.00000	-INFINITY	-INFINITY

$h/\lambda = 0.10,\ 0 \leq ka \leq 3.0.$

TABLE A1-21

INTEGRAL EQUATION METHOD
EPSILON= 1.7500(NORMALIZED GROUNDPLANE RADIUS)
MONOPOLE LENGTH= 0.100000(WAVELENGTH)
INFINITELY THIN MONOPOLE RADIUS
RADIATION RESISTANCE = 2.405146 (OHMS)

ELEVATION ANGLE (DEG)	DIRECTIVITY (NUMERIC)	DIRECTIVITY (DBI)	RELATIVE POWER (DB)	ELEVATION ANGLE (DEG)	DIRECTIVITY (NUMERIC)	DIRECTIVITY (DBI)	RELATIVE POWER (DB)
0	0.00000	-INFINITY	-INFINITY				
2.0	0.00299	-25.24458	-26.38355	92.0	1.29873	1.13520	-0.00337
4.0	0.01192	-19.23878	-20.37735	94.0	1.29679	1.12869	-0.00988
6.0	0.02666	-15.73092	-16.87949	96.0	1.29385	1.11885	-0.01872
8.0	0.04704	-13.27562	-14.41419	98.0	1.28968	1.10550	-0.03306
10.0	0.07277	-11.38034	-12.51890	100.0	1.28481	1.08839	-0.05017
12.0	0.10354	-9.84898	-10.98754	102.0	1.27855	1.06719	-0.07137
14.0	0.13895	-8.57154	-9.71010	104.0	1.27101	1.04151	-0.09706
16.0	0.17855	-7.48229	-8.62086	106.0	1.26208	1.01086	-0.12771
18.0	0.22188	-6.53879	-7.67735	108.0	1.25162	0.97472	-0.16385
20.0	0.26841	-5.71195	-6.85052	110.0	1.23950	0.93248	-0.20609
22.0	0.31762	-4.98099	-6.11955	112.0	1.22559	0.88346	-0.25510
24.0	0.36893	-4.33047	-5.46904	114.0	1.20974	0.82694	-0.31163
26.0	0.42183	-3.74862	-4.88718	116.0	1.19182	0.76209	-0.37647
28.0	0.47575	-3.22620	-4.36476	118.0	1.17167	0.68806	-0.45050
30.0	0.53017	-2.75582	-3.89439	120.0	1.14919	0.60390	-0.53466
32.0	0.58459	-2.33146	-3.47003	122.0	1.12424	0.50861	-0.62996
34.0	0.63854	-1.94813	-3.08670	124.0	1.09675	0.40109	-0.73748
36.0	0.69157	-1.60161	-2.74018	126.0	1.06664	0.28017	-0.85839
38.0	0.74331	-1.28831	-2.42688	128.0	1.03386	0.14451	-0.99396
40.0	0.79339	-1.00514	-2.14370	130.0	0.99840	0.00696	-1.13553
42.0	0.84152	-0.74936	-1.88793	132.0	0.96028	-0.17601	-1.31458
44.0	0.88744	-0.51859	-1.65716	134.0	0.91957	-0.36414	-1.50271
46.0	0.93096	-0.31069	-1.44926	136.0	0.87637	-0.57310	-1.71167
48.0	0.97191	-0.12372	-1.26229	138.0	0.83084	-0.80483	-1.94339
50.0	1.01020	0.04405	-1.09451	140.0	0.78317	-1.06146	-2.20003
52.0	1.04574	0.19423	-0.94434	142.0	0.73360	-1.34541	-2.48398
54.0	1.07852	0.32828	-0.81028	144.0	0.68243	-1.65940	-2.79797
56.0	1.10855	0.44755	-0.69102	146.0	0.63001	-2.00653	-3.14510
58.0	1.13587	0.55330	-0.58527	148.0	0.57671	-2.39041	-3.52898
60.0	1.16056	0.64668	-0.49189	150.0	0.52297	-2.81525	-3.95382
62.0	1.18271	0.72879	-0.40977	152.0	0.46924	-3.28605	-4.42462
64.0	1.20244	0.80064	-0.33793	154.0	0.41602	-3.80885	-4.94743
66.0	1.21988	0.86316	-0.27540	156.0	0.36383	-4.39102	-5.52959
68.0	1.23516	0.91724	-0.22133	158.0	0.31320	-5.04182	-6.18039
70.0	1.24844	0.96367	-0.17490	160.0	0.26467	-5.77302	-6.91159
72.0	1.25985	1.00320	-0.13537	162.0	0.21877	-6.60007	-7.73863
74.0	1.26955	1.03651	-0.10206	164.0	0.17605	-7.54375	-8.68232
76.0	1.27768	1.06421	-0.07436	166.0	0.13698	-8.63314	-9.77171
78.0	1.28436	1.08686	-0.05171	168.0	0.10208	-9.91070	-11.04927
80.0	1.28971	1.10492	-0.03364	170.0	0.07174	-11.44216	-12.58073
82.0	1.29385	1.11882	-0.01974	172.0	0.04637	-13.33752	-14.47609
84.0	1.29685	1.12890	-0.00967	174.0	0.02629	-15.80288	-16.94145
86.0	1.29880	1.13541	-0.00315	176.0	0.01175	-19.30078	-20.43935
88.0	1.29974	1.13857	0.0	178.0	0.00295	-25.30701	-26.44558
90.0	1.29971	1.13848	-0.00009	180.0	0.00000	-INFINITY	-INFINITY

$h/\lambda = 0.10$, $0 \leq ka \leq 3.0$.

TABLE A1-22

INTEGRAL EQUATION METHOD
EPSILON= 2 0000(NORMALIZED GROUNDPLANE RADIUS)
MONOPOLE LENGTH= 0 100000(WAVELENGTH)
INFINITELY THIN MONOPOLE RADIUS
RADIATION RESISTANCE = 2 602246 (OHMS)

ELEVATION ANGLE (DEG)	DIRECTIVITY (NUMERIC)	DIRECTIVITY (DBI)	RELATIVE POWER (DB)	ELEVATION ANGLE (DEG)	DIRECTIVITY (NUMERIC)	DIRECTIVITY (DBI)	RELATIVE POWER (DB)
0	0 00000	-INFINITY	-INFINITY				
2 0	0 00358	-24 45939	-25 32544	92 0	1 21539	0 84716	-0 01889
4 0	0 01427	-18 45624	-19 32230	94 0	1 21457	0 84422	-0 02183
6 0	0 03189	-14 96346	-15 82951	96 0	1 21375	0 84128	-0 02477
8 0	0 05617	-12 50525	-13 37131	98 0	1 21286	0 83809	-0 02796
10 0	0 08671	-10 61906	-11 48511	100 0	1 21180	0 83429	-0 03176
12 0	0 12306	-9 09877	-9 96482	102 0	1 21044	0 82943	-0 03662
14 0	0 16465	-7 83435	-8 70040	104 0	1 20863	0 82295	-0 04310
16 0	0 21086	-6 76004	-7 62609	106 0	1 20620	0 81420	-0 05185
18 0	0 26101	-5 83335	-6 69940	108 0	1 20294	0 80244	-0 06361
20 0	0 31440	-5 02518	-5 89123	110 0	1 19863	0 78686	-0 07919
22 0	0 37028	-4 31487	-5 18092	112 0	1 19304	0 76656	-0 09950
24 0	0 42792	-3 68636	-4 55241	114 0	1 18592	0 74056	-0 12549
26 0	0 48659	-3 12839	-3 99444	116 0	1 17702	0 70783	-0 15822
28 0	0 54557	-2 63147	-3 49752	118 0	1 16607	0 66726	-0 19879
30 0	0 60421	-2 18815	-3 05420	120 0	1 15284	0 61768	-0 24838
32 0	0 66185	-1 79232	-2 65838	122 0	1 13706	0 55783	-0 30822
34 0	0 71797	-1 43891	-2 30496	124 0	1 11852	0 48643	-0 37963
36 0	0 77204	-1 12361	-1 98966	126 0	1 09700	0 40207	-0 46399
38 0	0 82362	-0 84273	-1 70878	128 0	1 07233	0 30329	-0 56276
40 0	0 87236	-0 59306	-1 45911	130 0	1 04437	0 18855	-0 67750
42 0	0 91796	-0 37178	-1 23783	132 0	1 01302	0 05618	-0 80988
44 0	0 96021	-0 17635	-1 04240	134 0	0 97823	-0 08560	-0 96165
46 0	0 99886	-0 00450	-0 87055	136 0	0 94001	-0 26869	-1 13475
48 0	1 03415	0 14584	-0 72022	138 0	0 89842	-0 46520	-1 33125
50 0	1 06575	0 27656	-0 58949	140 0	0 85361	-0 68740	-1 55345
52 0	1 09381	0 38943	-0 47662	142 0	0 80578	-0 93784	-1 80390
54 0	1 11843	0 48610	-0 37995	144 0	0 75520	-1 21937	-2 08542
56 0	1 13975	0 56810	-0 29795	146 0	0 70223	-1 53520	-2 40126
58 0	1 15794	0 63687	-0 22918	148 0	0 64728	-1 88805	-2 75511
60 0	1 17322	0 69380	-0 17225	150 0	0 59085	-2 28523	-3 15128
62 0	1 18582	0 74019	-0 12586	152 0	0 53348	-2 72882	-3 59487
64 0	1 19598	0 77726	-0 08880	154 0	0 47578	-3 22595	-4 09200
66 0	1 20398	0 80618	-0 05987	156 0	0 41840	-3 78407	-4 65012
68 0	1 21006	0 82807	-0 03798	158 0	0 36204	-4 41249	-5 27854
70 0	1 21450	0 84396	-0 02209	160 0	0 30739	-5 12307	-5 98912
72 0	1 21754	0 85483	-0 01122	162 0	0 25519	-5 93129	-6 79734
74 0	1 21944	0 86160	-0 00446	164 0	0 20616	-6 85800	-7 72405
76 0	1 22042	0 86508	-0 00097	166 0	0 16096	-7 93231	-8 79836
78 0	1 22069	0 86605	0 0	168 0	0 12032	-9 19673	-10 06278
80 0	1 22044	0 86518	-0 00088	170 0	0 08478	-10 71701	-11 58306
82 0	1 21984	0 86304	-0 00301	172 0	0 05491	-12 60319	-13 46924
84 0	1 21903	0 86014	-0 00591	174 0	0 03116	-15 06138	-15 92743
86 0	1 21811	0 85686	-0 00919	176 0	0 01395	-18 55415	-19 42020
88 0	1 21717	0 85350	-0 01255	178 0	0 00350	-24 55729	-25 42334
90 0	1 21625	0 85025	-0 01581	180	0 00000	-INFINITY	-INFINITY

$h/\lambda = 0.10,\ 0 \le ka \le 3.0.$

TABLE A1-23

INTEGRAL EQUATION METHOD
EPSILON= 2.2500(NORMALIZED GROUNDPLANE RADIUS)
MONOPOLE LENGTH= 0.100000(WAVELENGTH)
INFINITELY THIN MONOPOLE RADIUS
RADIATION RESISTANCE = 2.851602 (OHMS)

ELEVATION ANGLE (DEG)	DIRECTIVITY (NUMERIC)	DIRECTIVITY (DBI)	RELATIVE POWER (DB)	ELEVATION ANGLE (DEG)	DIRECTIVITY (NUMERIC)	DIRECTIVITY (DBI)	RELATIVE POWER (DB)
0	0.00000	-INFINITY	-INFINITY				
2.0	0.00443	-23.53888	-24.28243	92.0	1.10914	0.44975	-0.29381
4.0	0.01762	-17.53915	-18.28271	94.0	1.10955	0.45148	-0.29207
6.0	0.03934	-14.05206	-14.79562	96.0	1.11118	0.45784	-0.28571
8.0	0.06915	-11.60181	-12.34537	98.0	1.11380	0.46844	-0.27511
10.0	0.10652	-9.72583	-10.46939	100.0	1.11757	0.48276	-0.26080
12.0	0.15073	-8.21798	-8.96154	102.0	1.12204	0.50009	-0.24346
14.0	0.20099	-6.96821	-7.71177	104.0	1.12710	0.51963	-0.22393
16.0	0.25640	-5.91074	-6.65430	106.0	1.13251	0.54041	-0.20315
18.0	0.31601	-5.00304	-5.74660	108.0	1.13798	0.56136	-0.18218
20.0	0.37879	-4.21598	-4.95953	110.0	1.14323	0.58133	-0.16223
22.0	0.44375	-3.52866	-4.27222	112.0	1.14790	0.59904	-0.14451
24.0	0.50985	-2.92557	-3.66913	114.0	1.15164	0.61319	-0.13037
26.0	0.57613	-2.38482	-3.12838	116.0	1.15408	0.62236	-0.12120
28.0	0.64164	-1.89705	-2.64061	118.0	1.15481	0.62510	-0.11846
30.0	0.70554	-1.45475	-2.19831	120.0	1.15343	0.61991	-0.12365
32.0	0.76705	-1.05176	-1.79532	122.0	1.14954	0.60523	-0.13832
34.0	0.82548	-0.68291	-1.42647	124.0	1.14274	0.57946	-0.16410
36.0	0.88027	-0.35084	-1.09440	126.0	1.13264	0.54093	-0.20263
38.0	0.93095	-0.05437	-0.79793	128.0	1.11890	0.48793	-0.25563
40.0	0.97716	0.20076	-0.54282	130.0	1.10120	0.41866	-0.32490
42.0	1.01866	0.08029	-0.66327	132.0	1.07926	0.33125	-0.41230
44.0	1.05532	0.23383	-0.50973	134.0	1.05287	0.22374	-0.51982
46.0	1.08709	0.36266	-0.38089	136.0	1.02189	0.09402	-0.64954
48.0	1.11404	0.46901	-0.27454	138.0	0.98624	-0.06015	-0.80371
50.0	1.13630	0.55493	-0.18863	140.0	0.94597	-0.24122	-0.98477
52.0	1.15408	0.62235	-0.12120	142.0	0.90119	-0.45184	-1.19540
54.0	1.16765	0.67311	-0.07044	144.0	0.85212	-0.69500	-1.43855
56.0	1.17732	0.70896	-0.03460	146.0	0.79910	-0.97401	-1.71757
58.0	1.18347	0.73158	-0.01198	148.0	0.74256	-1.29269	-2.03625
60.0	1.18647	0.74258	-0.00097	150.0	0.68306	-1.65544	-2.39899
62.0	1.18674	0.74356	0.0	152.0	0.62124	-2.06742	-2.81098
64.0	1.18468	0.73602	+0.00754	154.0	0.55785	-2.53482	-3.27838
66.0	1.18071	0.72145	+0.02211	156.0	0.49372	-3.06519	-3.80874
68.0	1.17525	0.70129	-0.04227	158.0	0.42975	-3.66787	-4.41142
70.0	1.16867	0.67692	+0.06664	160.0	0.36688	-4.35477	-5.09833
72.0	1.16136	0.64966	-0.09389	162.0	0.30610	-5.14143	-5.88499
74.0	1.15366	0.62079	+0.12276	164.0	0.24839	-6.04874	-6.79230
76.0	1.14591	0.59150	-0.15205	166.0	0.19472	-7.10585	-7.84941
78.0	1.13838	0.56288	-0.18067	168.0	0.14604	-8.35529	-9.09885
80.0	1.13134	0.53585	-0.20761	170.0	0.10321	-9.86286	-10.60642
82.0	1.12501	0.51158	-0.23198	172.0	0.06701	-11.73860	-12.48216
84.0	1.11958	0.49055	-0.25301	174.0	0.03812	-14.18866	-14.93221
86.0	1.11518	0.47346	-0.27010	176.0	0.01708	-17.67561	-18.41916
88.0	1.11193	0.46079	-0.28277	178.0	0.00429	-23.67525	-24.41881
90.0	1.10990	0.45284	-0.29072	180	0.00000	-INFINITY	-INFINITY

$h/\lambda = 0.10$, $0 \leq ka \leq 3.0$.

TABLE A1-24

INTEGRAL EQUATION METHOD
EPSILON= 2 5000(NORMALIZED GROUNDPLANE RADIUS)
MONOPOLE LENGTH= 0 100000(WAVELENGTH)
INFINITELY THIN MONOPOLE RADIUS
RADIATION RESISTANCE = 3 232568 (OHMS)

ELEVATION ANGLE (DEG)	DIRECTIVITY (NUMERIC)	DIRECTIVITY (DBI)	RELATIVE POWER (DB)	ELEVATION ANGLE (DEG)	DIRECTIVITY (NUMERIC)	DIRECTIVITY (DBI)	RELATIVE POWER (DB)
0	0 00000	-INFINITY	-INFINITY				
2 0	0 00561	-22.50875	-23 39219	92 0	0 97835	-0 09507	-0.97852
4 0	0 02232	-16.51271	-17 39616	94 0	0 98017	-0 08698	-0 97044
6 0	0 04975	-13 03178	-13 91522	96 0	0 98450	-0 06783	-0.95127
8 0	0 08729	-10 59013	-11 47357	98 0	0 89125	-0 03818	-0.92162
10 0	0 13412	-8.72519	-9 60863	100 0	1 00025	0 00110	-0.88234
12 0	0.18920	-7.23080	-8 11424	102 0	1 01132	0 04889	-0.83455
14 0	0 25137	-5 99690	-6 88034	104 0	1 02421	0 10389	-0.77956
16 0	0 31932	-4 95768	-5 84113	106 0	1 03863	0 16460	-0 71884
18 0	0 39169	-4 07060	-4 95405	108 0	1 05424	0 22939	-0.65405
20 0	0 46704	-3 30649	-4 18993	110 0	1 07066	0 29652	-0 58692
22 0	0.54395	-2 64443	-3 52788	112 0	1 08747	0 36417	-0.51926
24 0	0 62103	-2 06888	-2 95232	114 0	1 10419	0 43044	-0 45300
26 0	0.69696	-1 56790	-2 45133	116 0	1 12032	0.49342	-0.39002
28 0	0.77053	-1 13210	-2 01554	118 0	1 13532	0 55117	-0 33227
30 0	0 84063	-0 75393	-1 63737	120 0	1 14861	0 60174	-0.28170
32 0	0 90632	-0 42717	-1 31061	122 0	1.15962	0 64317	-0 24028
34 0	0 96680	-0 14661	-1 03006	124 0	1 16774	0 67348	-0.20996
36 0	1 02145	0 09217	-0 79127	126 0	1 17238	0 69070	-0 19274
38 0	1 06980	0 29302	-0 59042	128 0	1 17296	0 69283	-0 19062
40 0	1 11156	0 45932	-0.42413	130 0	1 16891	0 67782	-0.20562
42 0	1 14659	0 59408	-0 28937	132 0	1.15974	0.64360	-0 23984
44 0	1 17491	0 70002	-0 18341	134 0	1.14499	0.58800	-0 29544
46 0	1 19665	0 77968	-0 10377	136 0	1 12429	0.50877	-0 37467
48 0	1 21209	0 83535	-0 04809	138 0	1 09737	0 40352	-0 47992
50 0	1 22159	0 86925	-0 01420	140 0	1 06407	0 26969	-0 61376
52 0	1 22559	0 88344	0 0	142 0	1 02435	0.10449	-0 77895
54 0	1 22460	0 87986	-0 00349	144 0	0 97834	-0.09512	-0 97857
56 0	1 21920	0 86074	-0 02270	146 0	0 92628	-0.33257	-1 21602
58 0	1 20986	0 82771	-0 05573	148 0	0 86861	-0 61173	-1 49518
60 0	1 19750	0 78276	-0 10068	150 0	0 80592	-0 93707	-1 82051
62 0	1 18243	0.72776	-0 15568	152 0	0 73896	-1.31381	-2 19726
64 0	1 16536	0 66460	-0 21884	154 0	0.66862	-1.74820	-2 63165
66 0	1 14687	0 59515	-0 28830	156 0	0 59596	-2.24781	-3 13126
68 0	1 12753	0 52126	-0 36218	158 0	0 52215	-2.82206	-3 70550
70 0	1 10785	0 44481	-0 43863	160 0	0 44845	-3 48287	-4 36631
72 0	1 08834	0.36764	-0.51580	162 0	0 37620	-4.24582	-5 12927
74 0	1 06944	0 29156	-0 59188	164 0	0 30677	-5 13184	-6 01529
76 0	1 05155	0.21832	-0 66513	166 0	0 24154	-6.17010	-7 05354
78 0	1 03505	0 14959	-0 73385	168 0	0 18184	-7 40316	-8 28660
80 0	1 02022	0 08695	-0 79649	170 0	0.12892	-8 89682	-9 78026
82 0	1 00726	0 03183	-0 85161	172 0	0 08392	-10 76317	-11 64661
84 0	0 99666	0 01453	-0 89797	174 0	0 04784	-13 20234	-14 08579
86 0	0 98871	-0 05407	-0 93451	176 0	0 02146	-16 68294	-17 56638
88 0	0 98393	-0 07699	-0 96044	178 0	0 00530	-22 67877	-23 56222
90 0	0 97910	-0 09175	-0 97519	180	0 00000	-INFINITY	-INFINITY

$h/\lambda = 0.10,\ 0 \leq ka \leq 3.0.$

TABLE A1-25

INTEGRAL EQUATION METHOD
EPSILON= 2 7500(NORMALIZED GROUNDPLANE RADIUS)
MONOPOLE LENGTH= 0 100000(WAVELENGTH)
INFINITELY THIN MONOPOLE RADIUS
RADIATION RESISTANCE = 3 832907 (OHMS)

ELEVATION ANGLE (DEG)	DIRECTIVITY (NUMERIC)	DIRECTIVITY (DBI)	RELATIVE POWER (DB)	ELEVATION ANGLE (DEG)	DIRECTIVITY (NUMERIC)	DIRECTIVITY (DBI)	RELATIVE POWER (DB)
0	0 00000	-INFINITY	-INFINITY				
2 0	0 33458	-4 75496	-6 01229	92 0	0.82263	-0 84689	-2 10422
4 0	0.08184	-10.87035	-12 12768	94 0	0 82389	-0 84132	-2 09866
6 0	0.03555	-14 48803	-15 74836	96 0	0 82886	-0 81521	-2 07254
8 0	0 01953	-17 09339	-18 35072	98 0	0 83765	-0 76940	-2.02673
10 0	0 01219	-19.14066	-20 39799	100 0	0 85011	-0 70525	-1 96258
12 0	0 00824	-20 83972	-22.09705	102 0	0.86606	-0 62453	-1.88186
14 0	0.00589	-22.30144	-23 55878	104 0	0.88524	-0.52937	-1.78671
16 0	0.00437	-23.59260	-24.84993	106.0	0 90737	-0.42217	-1.67950
18 0	0 00334	-24 75685	-26 01418	108 0	0 93207	-0 30550	-1.56283
20 0	0 00262	-25 82470	-27 08203	110 0	0 95895	-0 18206	-1.43939
22.0	0 00208	-26.81867	-28 07601	112 0	0 98751	-0 05460	-1.31193
24 0	0 00168	-27 75632	-29.01366	114 0	1 01722	0.07415	-1.18318
26 0	0.00136	-28.65205	-29 90938	116 0	1 04749	0.20148	-1.05585
28 0	0 00112	-29 51836	-30 77569	118 0	1 07764	0 32475	-0 93259
30 0	0 00092	-30.36685	-31.62418	120.0	1.10698	0.44139	-0.81595
32 0	0 00076	-31 20889	-32 46623	122 0	1 13473	0.54891	-0 70842
34 0	0 00062	-32 05707	-33.31441	124 0	1.16008	0.64491	-0 61242
36 0	0 00051	-32.92525	-34.18258	126 0	1 18223	0.72702	-0 53031
38 0	0 00041	-33 83118	-35 08851	128 0	1 20031	0.79293	-0.46440
40 0	0 00033	-34 79874	-36.05607	130.0	1 21348	0 84034	-0 41699
42 0	0 00026	-35 86305	-37 12038	132 0	1 22094	0.86696	-0 39038
44 0	0 00020	-37 08103	-38 33836	134 0	1 22192	0 87044	-0 38688
46 0	0.00014	-38 55739	-39.81472	136 0	1.21574	0.84838	-0.40894
48 0	0 00009	-40 52488	-41 78221	138 0	1 20180	0.79830	-0 45903
50 0	0 00004	-43 72276	-44.98009	140 0	1.17965	0 71752	-0.53982
52 0	1 33577	1 25733	0 0	142 0	1 14899	0.60317	-0.65417
54 0	1.31585	1 19205	-0 06528	144 0	1 10972	0.45212	-0.80521
56 0	1 29097	1.10916	-0.14817	146.0	1.06192	0.26091	-0.99642
58 0	1.26203	1.01071	-0 24662	148 0	1.00591	0.02560	-1.23173
60 0	1 22992	0.89877	-0.35856	150 0	0.94225	-0 25832	-1 51565
62 0	1 19549	0.77545	-0 48189	152 0	0 87174	-0.59613	-1 85346
64 0	1 15955	0.64289	-0.61444	154.0	0.79541	-0 99408	-2.25142
66 0	1 12288	0.50334	-0.75399	156.0	0.71452	-1.45984	-2.71717
68 0	1 08620	0.35911	-0.89822	158 0	0 63055	-2 00280	-3 26013
70 0	1 05017	0 21259	-1.04474	160 0	0 54514	-2.63494	-3.89227
72 0	1 01537	0.06626	-1 19108	162 0	0.46006	-3 37187	-4 62920
74 0	0 98235	-0 07734	-1.33468	164 0	0 37718	-4.23454	-5 49187
76 0	0 95156	-0 21562	-1.47295	166 0	0 29839	-5 25213	-6 50947
78 0	0 92342	-0 34599	-1.60332	168 0	0 22557	-6 46724	-7 72457
80 0	0 89828	-0 46580	-1 72323	170 0	0.16048	-7 94569	-9.20302
82 0	0 87641	-0 57291	-1 83035	172 0	0 10477	-9 79756	-11.05489
84 0	0 85807	-0 66479	-1 92213	174 0	0 05985	-12 22902	-13 48635
86 0	0 84342	-0 73654	-1 99387	176 0	0 02690	-15 70267	-16 96000
88 0	0 83262	-0 79553	-2 05286	178.0	0.00677	-21 69433	-22.95166
90 0	0 82574	-0 83146	-2 08889	180	0 00000	-INFINITY	-INFINITY

$h/\lambda = 0.10$, $0 \leq ka \leq 3.0$.

TABLE A1-26

INTEGRAL EQUATION METHOD
EPSILON= 0.0 (NORMALIZED GROUNDPLANE RADIUS)
MONOPOLE LENGTH= 0.025000(WAVELENGTH)
INFINITELY THIN MONOPOLE RADIUS
RADIATION RESISTANCE = 0.123760 (OHMS)

ELEVATION ANGLE (DEG)	DIRECTIVITY (NUMERIC)	DIRECTIVITY (DBI)	RELATIVE POWER (DB)	ELEVATION ANGLE (DEG)	DIRECTIVITY (NUMERIC)	DIRECTIVITY (DBI)	RELATIVE POWER (DB)
0	0.00000	-INFINITY	-INFINITY				
2.0	0.00182	-27.38746	-29.14957	92.0	1.49858	1.75680	-0.00530
4.0	0.00729	-21.37213	-23.13424	94.0	1.49310	1.74089	-0.02121
6.0	0.01637	-17.85910	-19.62120	96.0	1.48400	1.71433	-0.04778
8.0	0.02902	-15.37263	-17.13473	98.0	1.47131	1.67704	-0.08506
10.0	0.04518	-13.45027	-15.21237	100.0	1.45511	1.62895	-0.13315
12.0	0.06477	-11.88602	-13.64812	102.0	1.43547	1.56993	-0.19217
14.0	0.08770	-10.57000	-12.33210	104.0	1.41248	1.49984	-0.26227
16.0	0.11385	-9.43664	-11.19874	106.0	1.38627	1.41848	-0.34362
18.0	0.14310	-8.44364	-10.20574	108.0	1.35696	1.32566	-0.43644
20.0	0.17530	-7.56212	-9.32423	110.0	1.32468	1.22112	-0.54098
22.0	0.21030	-6.77151	-8.53361	112.0	1.28961	1.10458	-0.65752
24.0	0.24784	-6.05660	-7.81870	114.0	1.25191	0.97572	-0.78638
26.0	0.28801	-5.40587	-7.16797	116.0	1.21176	0.83416	-0.92794
28.0	0.33034	-4.81035	-6.57246	118.0	1.16936	0.67949	-1.08261
30.0	0.37472	-4.26296	-6.02507	120.0	1.12492	0.51123	-1.25088
32.0	0.42092	-3.75799	-5.52009	122.0	1.07866	0.32884	-1.43326
34.0	0.46873	-3.29076	-5.05286	124.0	1.03080	0.13173	-1.63038
36.0	0.51791	-2.85742	-4.61952	126.0	0.98157	-0.08060	-1.84290
38.0	0.56829	-2.45476	-4.21686	128.0	0.93121	-0.30951	-2.07161
40.0	0.61944	-2.08004	-3.84215	130.0	0.87998	-0.55528	-2.31738
42.0	0.67178	-1.73097	-3.49307	132.0	0.82811	-0.81909	-2.58120
44.0	0.72351	-1.40555	-3.16766	134.0	0.77587	-1.10208	-2.86419
46.0	0.77587	-1.10209	-2.86419	136.0	0.72351	-1.40555	-3.16766
48.0	0.82811	-0.81909	-2.58120	138.0	0.67128	-1.73097	-3.49307
50.0	0.87998	-0.55528	-2.31738	140.0	0.61944	-2.08004	-3.84215
52.0	0.93121	-0.30951	-2.07161	142.0	0.56823	-2.45476	-4.21686
54.0	0.98157	-0.08060	-1.84290	144.0	0.51791	-2.85742	-4.61952
56.0	1.03080	0.13173	-1.63038	146.0	0.46873	-3.29076	-5.05286
58.0	1.07866	0.32884	-1.43326	148.0	0.42092	-3.75799	-5.52009
60.0	1.12492	0.51123	-1.25088	150.0	0.37472	-4.26296	-6.02507
62.0	1.16936	0.67949	-1.08261	152.0	0.33034	-4.81035	-6.57246
64.0	1.21176	0.83416	-0.92794	154.0	0.28801	-5.40587	-7.16797
66.0	1.25191	0.97572	-0.78638	156.0	0.24794	-6.05660	-7.81870
68.0	1.28961	1.10458	-0.65752	158.0	0.21030	-6.77151	-8.53361
70.0	1.32468	1.22112	-0.54098	160.0	0.17530	-7.56212	-9.32423
72.0	1.35696	1.32566	-0.43644	162.0	0.14310	-8.44364	-10.20574
74.0	1.38627	1.41848	-0.34362	164.0	0.11385	-9.43664	-11.19874
76.0	1.41248	1.49984	-0.26227	166.0	0.08770	-10.57000	-12.33210
78.0	1.43547	1.56993	-0.19217	168.0	0.06477	-11.88602	-13.64812
80.0	1.45511	1.62895	-0.13315	170.0	0.04518	-13.45027	-15.21237
82.0	1.47131	1.67704	-0.08506	172.0	0.02902	-15.37263	-17.13473
84.0	1.48400	1.71433	-0.04778	174.0	0.01637	-17.85910	-19.62120
86.0	1.49310	1.74089	-0.02121	176.0	0.00729	-21.37213	-23.13424
88.0	1.49858	1.75680	-0.00530	178.0	0.00182	-27.38746	-29.14957
90.0	1.50041	1.76210	0.0	180	0.00000	-INFINITY	-INFINITY

$h/\lambda = 0.025$, $0 \leq ka \leq 3.0$.

TABLE A1-27

INTEGRAL EQUATION METHOD
EPSILON= 0.25000(NORMALIZED GROUNDPLANE RADIUS)
MONOPOLE LENGTH= 0.025000(WAVELENGTH)
INFINITELY THIN MONOPOLE RADIUS
RADIATION RESISTANCE = 0.124039 (OHMS)

ELEVATION ANGLE (DEG)	DIRECTIVITY (NUMERIC)	DIRECTIVITY (DBI)	RELATIVE POWER (DB)	ELEVATION ANGLE (DEG)	DIRECTIVITY (NUMERIC)	DIRECTIVITY (DBI)	RELATIVE POWER (DB)
0	0.00000	-INFINITY	-INFINITY				
2.0	0.00184	-27.34979	-29.10244	92.0	1.49534	1.74741	-0.00524
4.0	0.00735	-21.33463	-23.08729	94.0	1.48993	1.73167	-0.02098
6.0	0.01651	-17.82188	-19.57454	96.0	1.48095	1.70539	-0.04726
8.0	0.02927	-15.33581	-17.08847	98.0	1.46842	1.66851	-0.08414
10.0	0.04556	-13.41396	-15.16661	100.0	1.45242	1.62093	-0.13173
12.0	0.06531	-11.85032	-13.60298	102.0	1.43302	1.56252	-0.19013
14.0	0.08841	-10.53503	-12.28768	104.0	1.41031	1.49315	-0.25950
16.0	0.11475	-9.40249	-11.15514	106.0	1.38440	1.41262	-0.34003
18.0	0.14420	-8.41041	-10.16306	108.0	1.35541	1.32072	-0.43193
20.0	0.17661	-7.52891	-9.28256	110.0	1.32349	1.21720	-0.53546
22.0	0.21182	-6.74039	-8.49305	112.0	1.28877	1.10176	-0.65089
24.0	0.24965	-6.02667	-7.77932	114.0	1.25143	0.97408	-0.77857
26.0	0.28992	-5.37720	-7.12985	116.0	1.21165	0.83379	-0.91887
28.0	0.33243	-4.78301	-6.53567	118.0	1.16962	0.68045	-1.07221
30.0	0.37696	-4.23702	-5.98967	120.0	1.12553	0.51358	-1.23907
32.0	0.42330	-3.73949	-5.48615	122.0	1.07961	0.33265	-1.42000
34.0	0.47122	-3.28777	-5.02042	124.0	1.03206	0.13704	-1.61561
36.0	0.52048	-2.83598	-4.58863	126.0	0.98312	-0.07394	-1.82659
38.0	0.57083	-2.43490	-4.18755	128.0	0.93303	-0.30107	-2.05372
40.0	0.62204	-2.06179	-3.81445	130.0	0.88202	-0.54522	-2.29788
42.0	0.67385	-1.71435	-3.46700	132.0	0.83035	-0.80741	-2.56006
44.0	0.72601	-1.39058	-3.14323	134.0	0.77826	-1.08876	-2.84141
46.0	0.77826	-1.08876	-2.84141	136.0	0.72601	-1.39058	-3.14323
48.0	0.83035	-0.80741	-2.56006	138.0	0.67385	-1.71435	-3.46700
50.0	0.88202	-0.54522	-2.29788	140.0	0.62204	-2.06179	-3.81445
52.0	0.93303	-0.30107	-2.05372	142.0	0.57083	-2.43490	-4.18755
54.0	0.98312	-0.07394	-1.82659	144.0	0.52048	-2.83598	-4.58863
56.0	1.03206	0.13704	-1.61561	146.0	0.47122	-3.28777	-5.02042
58.0	1.07961	0.33265	-1.42000	148.0	0.42330	-3.73950	-5.48615
60.0	1.12553	0.51358	-1.23907	150.0	0.37696	-4.23702	-5.98967
62.0	1.16962	0.68045	-1.07221	152.0	0.33243	-4.78302	-6.53567
64.0	1.21165	0.83379	-0.91887	154.0	0.28992	-5.37720	-7.12985
66.0	1.25144	0.97408	-0.77857	156.0	0.24965	-6.02667	-7.77932
68.0	1.28877	1.10176	-0.65089	158.0	0.21182	-6.74039	-8.49305
70.0	1.32349	1.21720	-0.53546	160.0	0.17661	-7.52891	-9.28256
72.0	1.35541	1.32072	-0.43193	162.0	0.14420	-8.41041	-10.16306
74.0	1.38440	1.41262	-0.34003	164.0	0.11475	-9.40249	-11.15514
76.0	1.41031	1.49315	-0.25950	166.0	0.08841	-10.53503	-12.28768
78.0	1.43302	1.56252	-0.19013	168.0	0.06531	-11.85033	-13.60298
80.0	1.45242	1.62093	-0.13173	170.0	0.04556	-13.41396	-15.16661
82.0	1.46842	1.66851	-0.08414	172.0	0.02927	-15.33582	-17.08847
84.0	1.48095	1.70539	-0.04726	174.0	0.01651	-17.82188	-19.57454
86.0	1.48993	1.73167	-0.02098	176.0	0.00735	-21.33463	-23.08729
88.0	1.49534	1.74741	-0.00524	178.0	0.00184	-27.34979	-29.10244
90.0	1.49718	1.75265	0.0	180	0.00000	-INFINITY	-INFINITY

$h/\lambda = 0.025$, $0 \leq ka \leq 3.0$.

TABLE A1-28

INTEGRAL EQUATION METHOD
EPSILON= 0.5000(NORMALIZED GROUNDPLANE RADIUS)
MONOPOLE LENGTH= 0.025000(WAVELENGTH)
INFINITELY THIN MONOPOLE RADIUS
RADIATION RESISTANCE = 0.124796 (OHMS)

ELEVATION ANGLE (DEG)	DIRECTIVITY (NUMERIC)	DIRECTIVITY (DBI)	RELATIVE POWER (DB)	ELEVATION ANGLE (DEG)	DIRECTIVITY (NUMERIC)	DIRECTIVITY (DBI)	RELATIVE POWER (DB)
0	0.00000	-INFINITY	+INFINITY				
2.0	0.00189	-27.24403	+28.96992	92.0	1.48621	1.72081	-0.00508
4.0	0.00753	-21.22935	+22.95524	94.0	1.48100	1.70555	-0.02034
6.0	0.01691	-17.71740	+19.44329	96.0	1.47234	1.68008	-0.04581
8.0	0.02987	-15.25245	+16.95834	98.0	1.46027	1.64432	-0.08157
10.0	0.04663	+13.31202	+15.03791	100.0	1.44483	1.59818	-0.12771
12.0	0.06683	+11.75011	+13.47600	102.0	1.42611	1.54152	-0.18437
14.0	0.09043	+10.43683	+12.16272	104.0	1.40417	1.47418	-0.25171
16.0	0.11731	+9.30660	+11.03249	106.0	1.37911	1.39598	-0.32991
18.0	0.14733	+8.31709	+10.04298	108.0	1.35104	1.30668	-0.41921
20.0	0.18033	+7.43943	+9.16532	110.0	1.32008	1.20602	-0.51987
22.0	0.21612	+6.65301	+8.37890	112.0	1.28638	1.09369	+0.63220
24.0	0.25453	+5.93260	+7.65849	114.0	1.25007	0.96935	-0.75654
26.0	0.29535	+5.27668	+7.00255	116.0	1.21133	0.83261	-0.89328
28.0	0.33836	+4.67621	+6.40210	118.0	1.17022	0.68303	+1.04286
30.0	0.38334	+4.12414	+5.85003	120.0	1.12722	0.52010	-1.20579
32.0	0.43006	+3.66468	+5.38058	122.0	1.08225	0.34327	+1.38262
34.0	0.47828	+3.20318	+4.91907	124.0	1.03559	0.15189	-1.57400
36.0	0.52775	+2.77574	+4.50163	126.0	0.98746	-0.05473	-1.78062
38.0	0.57822	+2.37840	+4.10429	128.0	0.93812	-0.27740	+2.00329
40.0	0.62943	+2.01052	+3.73641	130.0	0.88776	-0.51702	-2.24291
42.0	0.68114	+1.66766	+3.39355	132.0	0.83664	-0.77462	-2.50051
44.0	0.73308	+1.34850	+3.07439	134.0	0.78499	-1.05135	-2.77724
46.0	0.78500	+1.05132	+2.77721	136.0	0.73307	-1.34854	-3.07443
48.0	0.83665	+0.77458	+2.50048	138.0	0.68113	-1.66770	+3.39359
50.0	0.88777	+0.51699	+2.24288	140.0	0.62942	-2.01056	-3.73645
52.0	0.93813	+0.27737	+2.00326	142.0	0.57821	-2.37914	+4.10503
54.0	0.98748	+0.05470	+1.78059	144.0	0.52774	-2.77578	+4.50167
56.0	1.03560	0.15192	+1.57397	146.0	0.47827	-3.20323	+4.92912
58.0	1.08225	0.34329	+1.38260	148.0	0.43006	+3.66473	-5.39062
60.0	1.12723	0.52013	+1.20576	150.0	0.38334	+4.16418	-5.89007
62.0	1.17032	0.68305	+1.04284	152.0	0.33836	+4.70626	+6.43215
64.0	1.21133	0.83264	+0.89325	154.0	0.29534	+5.29671	-7.02260
66.0	1.25008	0.96937	+0.75652	156.0	0.25453	+5.94265	-7.66854
68.0	1.28638	1.09371	+0.63218	158.0	0.21612	+6.65305	-8.37894
70.0	1.32009	1.20603	+0.51986	160.0	0.18032	+7.43948	9.16537
72.0	1.35104	1.30669	+0.41920	162.0	0.14733	+8.31714	+10.04303
74.0	1.37911	1.39598	+0.32990	164.0	0.11731	+9.30665	+11.03254
76.0	1.40417	1.47420	+0.25169	166.0	0.09043	+10.43688	+12.16277
78.0	1.42611	1.54153	+0.18436	168.0	0.06683	+11.75016	+13.47605
80.0	1.44484	1.59819	+0.12770	170.0	0.04664	+13.31207	+15.03796
82.0	1.46027	1.64433	+0.08156	172.0	0.02997	+15.23250	+16.95839
84.0	1.47234	1.68009	+0.04580	174.0	0.01691	+17.71745	+19.44334
86.0	1.48100	1.70556	+0.02033	176.0	0.00753	+21.22840	+22.95429
88.0	1.48621	1.72081	+0.00508	178.0	0.00189	27.24408	+28.96997
90.0	1.48795	1.72583	0.0	180	0.00000	-INFINITY	+INFINITY

$h/\lambda = 0.025$, $0 \leq ka \leq 3.0$.

TABLE A1-29

INTEGRAL EQUATION METHOD
EPSILON= 0.7500(NORMALIZED GROUNDPLANE RADIUS)
MONOPOLE LENGTH= 0.025000(WAVELENGTH)
INFINITELY THIN MONOPOLE RADIUS
RADIATION RESISTANCE = 0.326059 (OHMS)

ELEVATION ANGLE (DEG)	DIRECTIVITY (NUMERIC)	DIRECTIVITY (DBI)	RELATIVE POWER (DB)	ELEVATION ANGLE (DEG)	DIRECTIVITY (NUMERIC)	DIRECTIVITY (DBI)	RELATIVE POWER (DB)
0	0.00000	-INFINITY	-INFINITY				
2.0	0.00186	-27.07383	-28.75599	92.0	1.47141	1.67733	-0.00482
4.0	0.00783	-21.05993	-22.74208	94.0	1.46651	1.66286	-0.01929
6.0	0.01758	-17.54926	-19.23141	96.0	1.45838	1.63869	-0.04346
8.0	0.03115	-15.06609	-16.74825	98.0	1.44702	1.60476	-0.07740
10.0	0.04844	-13.14785	-14.83010	100.0	1.43250	1.56094	-0.12121
12.0	0.06936	-11.58881	-13.27096	102.0	1.41485	1.50711	-0.17505
14.0	0.09378	-10.27877	-11.96093	104.0	1.39414	1.44307	-0.23908
16.0	0.12156	-9.15224	-10.83439	106.0	1.37045	1.36864	-0.31352
18.0	0.15252	-8.16687	-9.84903	108.0	1.34386	1.28355	-0.39861
20.0	0.18648	-7.29377	-8.97592	110.0	1.31447	1.18752	-0.49463
22.0	0.22324	-6.51230	-8.19445	112.0	1.28240	1.08023	-0.60192
24.0	0.26259	-5.80722	-7.48938	114.0	1.24776	0.96130	-0.72085
26.0	0.30430	-5.16697	-6.84912	116.0	1.21069	0.83033	-0.85183
28.0	0.34814	-4.58252	-6.26468	118.0	1.17134	0.68682	-0.99533
30.0	0.39385	-4.04674	-5.72889	120.0	1.12986	0.53026	-1.15189
32.0	0.44118	-3.55386	-5.23601	122.0	1.08644	0.36005	-1.32210
34.0	0.48988	-3.09915	-4.78130	124.0	1.04125	0.17553	-1.50662
36.0	0.53967	-2.67869	-4.36085	126.0	0.99448	-0.02405	-1.70620
38.0	0.59031	-2.28931	-3.97147	128.0	0.94634	-0.22952	-1.91167
40.0	0.64152	-1.92793	-3.61008	130.0	0.89705	-0.47182	-2.15398
42.0	0.69303	-1.59245	-3.27461	132.0	0.84683	-0.72202	-2.40417
44.0	0.74460	-1.28075	-2.96290	134.0	0.79592	-0.99130	-2.67345
46.0	0.79587	-0.99103	-2.67318	136.0	0.74456	-1.28102	-2.96317
48.0	0.84688	-0.72176	-2.40391	138.0	0.69299	-1.59274	-3.27489
50.0	0.89710	-0.47158	-2.15373	140.0	0.64147	-1.92822	-3.61037
52.0	0.94639	-0.23928	-1.92144	142.0	0.59027	-2.28951	-3.97167
54.0	0.99453	-0.02382	-1.70597	144.0	0.53963	-2.67900	-4.36115
56.0	1.04130	0.17575	-1.50641	146.0	0.48984	-3.09946	-4.78161
58.0	1.08649	0.36026	-1.32190	148.0	0.44115	-3.55418	-5.23633
60.0	1.12991	0.53046	-1.15170	150.0	0.39382	-4.04707	-5.72922
62.0	1.17139	0.68700	-0.99515	152.0	0.34811	-4.58286	-6.26501
64.0	1.21074	0.83050	-0.85166	154.0	0.30428	-5.16731	-6.84946
66.0	1.24780	0.96146	-0.72069	156.0	0.26257	-5.80757	-7.48972
68.0	1.28244	1.08038	-0.60178	158.0	0.22322	-6.51265	-8.19480
70.0	1.31451	1.18765	-0.49450	160.0	0.18646	-7.29412	-8.97627
72.0	1.34390	1.28367	-0.39849	162.0	0.15250	-8.16723	-9.84938
74.0	1.37049	1.36874	-0.31341	164.0	0.12155	-9.15260	-10.83475
76.0	1.39417	1.44317	-0.23899	166.0	0.09377	-10.27914	-11.96129
78.0	1.41488	1.50719	-0.17497	168.0	0.06936	-11.58917	-13.27133
80.0	1.43252	1.56101	-0.12114	170.0	0.04844	-13.14832	-14.83047
82.0	1.44704	1.60481	-0.07734	172.0	0.03114	-15.06646	-16.74862
84.0	1.45839	1.63874	-0.04342	174.0	0.01758	-17.54963	-19.23179
86.0	1.46652	1.66288	-0.01927	176.0	0.00783	-21.06035	-22.74246
88.0	1.47141	1.67734	-0.00481	178.0	0.00196	-27.07420	-28.75636
90.0	1.47304	1.68215	0.0	180.0	0.00000	-INFINITY	-INFINITY

$h/\lambda = 0.025$, $0 \leq ka \leq 3.0$.

TABLE A1-30

INTEGRAL EQUATION METHOD
EPSILON= 1.0000(NORMALIZED GROUNDPLANE RADIUS)
MONOPOLE LENGTH= 0.025000(WAVELENGTH)
INFINITELY THIN MONOPOLE RADIUS
RADIATION RESISTANCE = 0.127868 (OHMS)

ELEVATION ANGLE (DEG)	DIRECTIVITY (NUMERIC)	DIRECTIVITY (DBI)	RELATIVE POWER (DB)	ELEVATION ANGLE (DEG)	DIRECTIVITY (NUMERIC)	DIRECTIVITY (DBI)	RELATIVE POWER (DB)
0	0.00000	-INFINITY	+INFINITY				
2.0	0.00207	-26.83564	-28.45522	92.0	1.45048	1.61512	-0.00447
4.0	0.00827	-20.82281	-22.44239	94.0	1.44602	1.60174	+0.01784
6.0	0.01856	-17.31393	-18.93351	96.0	1.43960	1.57941	-0.04017
8.0	0.03286	-14.83325	+16.45284	98.0	1.42825	1.54805	+0.07154
10.0	0.05107	-12.91829	-14.53787	100.0	1.41498	1.50751	+0.11207
12.0	0.07306	-11.36301	-12.98259	102.0	1.39883	1.45786	-0.16192
14.0	0.09868	-10.05749	+11.67708	104.0	1.37984	1.39829	+0.22129
16.0	0.12776	-8.93611	-10.55570	106.0	1.35805	1.32917	-0.29041
18.0	0.16008	-7.95652	+9.57611	108.0	1.33353	1.25003	+0.36956
20.0	0.19544	-7.08978	-8.70936	110.0	1.30634	1.16055	-0.45904
22.0	0.23360	-6.31523	-7.93481	112.0	1.27655	1.06036	+0.55922
24.0	0.27431	-5.61760	+7.23718	114.0	1.24425	0.94907	+0.67051
26.0	0.31730	+4.98528	-6.60487	116.0	1.20954	0.82622	-0.79337
28.0	0.36231	-4.40923	-6.02881	118.0	1.17254	0.69128	+0.92830
30.0	0.40905	-3.88225	-5.50184	120.0	1.13336	0.54370	-1.07589
32.0	0.45724	-3.39855	-5.01814	122.0	1.09215	0.38282	+1.23677
34.0	0.50660	-2.95335	-4.57294	124.0	1.04905	0.20794	-1.41164
36.0	0.55684	-2.54270	-4.16228	126.0	1.00422	0.01827	-1.60131
38.0	0.60768	-2.16325	-3.78284	128.0	0.95784	-0.18708	-1.80666
40.0	0.65884	+1.81219	-3.43178	130.0	0.91010	-0.40909	-2.02868
42.0	0.71005	-1.48709	-3.10667	132.0	0.86121	+0.64868	+2.26847
44.0	0.76105	+1.18584	-2.80543	134.0	0.81139	-0.90770	-2.52729
46.0	0.81159	-0.90663	+2.52621	136.0	0.76086	-1.18695	-2.80654
48.0	0.86142	-0.64785	-2.26743	138.0	0.70987	-1.48823	+3.10782
50.0	0.91031	-0.40809	+2.02768	140.0	0.65866	-1.81037	-3.43295
52.0	0.95805	-0.18611	+1.80570	142.0	0.60751	-2.16446	-3.78405
54.0	1.00443	0.01919	-1.60039	144.0	0.55668	-2.54393	-4.16352
56.0	1.04926	0.20882	+1.41076	146.0	0.50645	-2.95461	+4.57420
58.0	1.09236	0.38366	-1.23593	148.0	0.45711	-3.39884	-5.01942
60.0	1.13357	0.54449	-1.07510	150.0	0.40892	-3.88356	-5.50315
62.0	1.17274	0.69203	-0.92756	152.0	0.36220	-4.41056	+6.03015
64.0	1.20974	0.82691	-0.79267	154.0	0.31720	-4.98663	-6.60622
66.0	1.24443	0.94972	-0.66987	156.0	0.27422	+5.61897	-7.23856
68.0	1.27672	1.06096	-0.55862	158.0	0.23353	-6.31661	-7.93620
70.0	1.30650	1.16109	-0.45849	160.0	0.19538	-7.09148	+8.71077
72.0	1.33368	1.25052	-0.36906	162.0	0.16003	-7.95794	-9.57752
74.0	1.35819	1.32962	-0.28997	164.0	0.12772	-8.93754	-10.55713
76.0	1.37987	1.39868	-0.22090	166.0	0.09865	+10.05893	+11.67852
78.0	1.39854	1.45800	-0.16159	168.0	0.07304	-11.36446	-12.98404
80.0	1.41407	1.50779	-0.11179	170.0	0.05105	-12.91975	-14.53933
82.0	1.42632	1.54827	-0.07132	172.0	0.03285	-14.83472	-16.45430
84.0	1.43466	1.57958	-0.04000	174.0	0.01855	-17.31540	-18.93498
86.0	1.44606	1.60185	-0.01773	176.0	0.00827	-20.82428	-22.44387
88.0	1.45050	1.61517	-0.00441	178.0	0.00207	-26.83711	-28.45670
90.0	1.45197	1.61959	0.0	180.0	0.00000	-INFINITY	INFINITY

$h/\lambda = 0.025$, $0 \leq ka \leq 3.0$.

TABLE A1-31

INTEGRAL EQUATION METHOD
EPSILON= 1.2500(NORMALIZED GROUNDPLANE RADIUS)
MONOPOLE LENGTH= 0.025000(WAVELENGTHS)
INFINITELY THIN MONOPOLE RADIUS
RADIATION RESISTANCE = 0.130457 (OHMS)

ELEVATION ANGLE θ (DEG)	DIRECTIVITY (NUMERIC)	DIRECTIVITY (DBI)	RELATIVE POWER (DB)	ELEVATION ANGLE (DEG)	DIRECTIVITY (NUMERIC)	DIRECTIVITY (DBI)	RELATIVE POWER (DB)
0	0.00000	-INFINITY	+INFINITY				
2.0	0.00223	-26.51682	-28.05005	92.0	1.42207	1.52920	-0.00402
4.0	0.00890	-20.50543	-22.03865	94.0	1.41818	1.51730	-0.01592
6.0	0.01996	-16.99892	-18.53214	96.0	1.41171	1.49745	-0.03577
8.0	0.03531	-14.52156	-16.05478	98.0	1.40267	1.46955	-0.06367
10.0	0.05482	-12.61002	-14.14324	100.0	1.39106	1.43347	-0.09975
12.0	0.07833	-11.06068	-12.59390	102.0	1.37690	1.38901	-0.14421
14.0	0.10565	-9.76118	-11.29440	104.0	1.36018	1.33597	-0.19726
16.0	0.13656	-8.64667	-10.17989	106.0	1.34093	1.27406	-0.25917
18.0	0.17081	-7.67476	-9.20798	108.0	1.31916	1.20297	-0.33025
20.0	0.20814	-6.81649	-8.34971	110.0	1.29490	1.12236	-0.41086
22.0	0.24825	-6.05117	-7.58439	112.0	1.26818	1.03180	-0.50142
24.0	0.29084	-5.36347	-6.89670	114.0	1.23904	0.93085	-0.60237
26.0	0.33560	-4.74175	-6.27487	116.0	1.20753	0.81899	-0.71423
28.0	0.38222	-4.17691	-5.71013	118.0	1.17372	0.69564	-0.83758
30.0	0.43036	-3.66171	-5.19493	120.0	1.13768	0.56019	-0.97303
32.0	0.47970	-3.19029	-4.72351	122.0	1.09949	0.41192	-1.12130
34.0	0.52993	-2.75783	-4.29105	124.0	1.05927	0.25007	-1.28315
36.0	0.58072	-2.36030	-3.89352	126.0	1.01713	0.07376	-1.45946
38.0	0.63178	-1.99432	-3.52754	128.0	0.97321	-0.11794	-1.65116
40.0	0.68281	-1.65698	-3.19020	130.0	0.92766	-0.32610	-1.85932
42.0	0.73353	-1.34580	-2.87902	132.0	0.88066	-0.55190	-2.08512
44.0	0.78368	-1.05862	-2.59184	134.0	0.83241	-0.79664	-2.32986
46.0	0.83300	-0.79354	-2.32676	136.0	0.78310	-1.06182	-2.59504
48.0	0.88127	-0.54889	-2.08211	138.0	0.73298	-1.34909	-2.88231
50.0	0.92828	-0.32320	-1.85642	140.0	0.68228	-1.66035	-3.19357
52.0	0.97383	-0.11515	-1.64837	142.0	0.63128	-1.99777	-3.53099
54.0	1.01776	0.07644	-1.45678	144.0	0.58025	-2.36383	-3.89705
56.0	1.05989	0.25263	-1.28060	146.0	0.52949	-2.76143	-4.29465
58.0	1.10011	0.41436	-1.11886	148.0	0.47930	-3.19395	-4.72718
60.0	1.13828	0.56250	-0.97072	150.0	0.42999	-3.66544	-5.19866
62.0	1.17431	0.69782	-0.83540	152.0	0.38188	-4.18068	-5.71391
64.0	1.20810	0.82103	-0.71219	154.0	0.33531	-4.74559	-6.27881
66.0	1.23958	0.93275	-0.60047	156.0	0.29058	-5.36736	-6.90058
68.0	1.26869	1.03356	-0.49966	158.0	0.24802	-6.05510	-7.58832
70.0	1.29538	1.12397	-0.40925	160.0	0.20795	-6.82046	-8.35368
72.0	1.31960	1.20443	-0.32879	162.0	0.17066	-7.67877	-9.21199
74.0	1.34133	1.27536	-0.25786	164.0	0.13644	-8.65070	-10.18392
76.0	1.36054	1.33711	-0.19611	166.0	0.10555	-9.76524	-11.29846
78.0	1.37721	1.39000	-0.14322	168.0	0.07826	-11.06477	-12.59799
80.0	1.39133	1.43430	-0.09893	170.0	0.05477	-12.61493	-14.14815
82.0	1.40288	1.47022	-0.06300	172.0	0.03527	-14.52568	-16.05893
84.0	1.41187	1.49795	-0.03527	174.0	0.01994	-17.00306	-18.53628
86.0	1.41828	1.51763	-0.01559	176.0	0.00889	-20.50957	-22.04279
88.0	1.42212	1.52937	-0.00385	178.0	0.00223	-26.52098	-28.05420
90.0	1.42338	1.53322	0.0	180.0	0.00000	-INFINITY	-INFINITY

$h/\lambda = 0.025$, $0 \leq ka \leq 3.0$.

TABLE A1-32

INTEGRAL EQUATION METHOD
EPSILON= 1.5000(NORMALIZED GROUNDPLANE RADIUS)
MONOPOLE LENGTH= 0.025000(WAVELENGTH)
INFINITELY THIN MONOPOLE RADIUS
RADIATION RESISTANCE = 0.134091 (OHMS)

ELEVATION ANGLE (DEG)	DIRECTIVITY (NUMERIC)	DIRECTIVITY (DBI)	RELATIVE POWER (DB)	ELEVATION ANGLE (DEG)	DIRECTIVITY (NUMERIC)	DIRECTIVITY (DBI)	RELATIVE POWER (DB)
0	0.00000	-INFINITY	-INFINITY				
2.0	0.00246	-26.09575	-27.50963	92.0	1.38371	1.41044	+0.00344
4.0	0.00980	-20.08621	-21.50010	94.0	1.38054	1.40050	-0.01339
6.0	0.02196	-16.58281	-17.99669	96.0	1.37530	1.38398	+0.02991
8.0	0.03882	-14.10977	-15.52365	98.0	1.36797	1.36076	-0.05313
10.0	0.06019	-12.20456	-13.61845	100.0	1.35853	1.33068	+0.08321
12.0	0.08588	-10.66113	-12.07501	102.0	1.34695	1.29352	+0.12037
14.0	0.11562	-9.36949	-10.78337	104.0	1.33322	1.24901	-0.16487
16.0	0.14914	-8.26386	-9.67785	106.0	1.31730	1.19685	+0.21704
18.0	0.18612	-7.30212	-8.71601	108.0	1.29917	1.13665	-0.27723
20.0	0.22621	-6.45496	-7.86885	110.0	1.27879	1.06801	-0.34588
22.0	0.26905	-5.70173	-7.11562	112.0	1.25616	0.99044	-0.42344
24.0	0.31426	-5.02708	-6.44096	114.0	1.23124	0.90343	-0.51046
26.0	0.36147	-4.41928	-5.83317	116.0	1.20403	0.80638	+0.60751
28.0	0.41028	-3.86919	-5.28307	118.0	1.17453	0.69863	-0.71525
30.0	0.46031	-3.36949	-4.78338	120.0	1.14274	0.57948	-0.83440
32.0	0.51118	-2.91427	-4.32815	122.0	1.10870	0.44814	-0.96574
34.0	0.56252	-2.49862	-3.91250	124.0	1.07244	0.30374	+1.11014
36.0	0.61398	-2.11864	-3.53233	126.0	1.03403	0.14534	+1.26855
38.0	0.66523	-1.77028	-3.18416	128.0	0.99355	-0.02812	+1.44200
40.0	0.71596	-1.45114	-2.86502	130.0	0.95109	-0.21778	+1.63166
42.0	0.76587	-1.15846	-2.57234	132.0	0.90680	-0.42491	+1.83879
44.0	0.81471	-0.88998	-2.30386	134.0	0.86081	-0.65091	+2.06480
46.0	0.86224	-0.64372	-2.05760	136.0	0.81332	-0.89737	+2.31126
48.0	0.90826	-0.41792	-1.83180	138.0	0.76453	-1.16604	+2.57993
50.0	0.95257	-0.21102	-1.62490	140.0	0.71468	-1.45890	+2.87278
52.0	0.99504	-0.02160	-1.43548	142.0	0.66402	-1.77820	+3.19209
54.0	1.03553	0.15161	+1.26227	144.0	0.61284	-2.12652	+3.54041
56.0	1.07393	0.30975	+1.10413	146.0	0.56146	-2.50684	+3.92072
58.0	1.11017	0.45388	+0.96001	148.0	0.51020	-2.92262	+4.33650
60.0	1.14418	0.58493	+0.82895	150.0	0.45941	-3.37796	+4.78185
62.0	1.17592	0.70378	+0.71010	152.0	0.40947	-3.87777	+5.29165
64.0	1.20537	0.81122	+0.60267	154.0	0.36075	-4.42797	+5.84185
66.0	1.23252	0.90795	+0.50594	156.0	0.31363	-5.03586	+6.44974
68.0	1.25737	0.99463	+0.41926	158.0	0.26850	-5.71060	+7.12448
70.0	1.27993	1.07185	+0.34204	160.0	0.22574	-6.46390	+7.87778
72.0	1.30021	1.14014	+0.27375	162.0	0.18573	-7.31113	+8.72501
74.0	1.31825	1.19997	+0.21391	164.0	0.14883	-8.27303	+9.68691
76.0	1.33406	1.25177	+0.16212	166.0	0.11538	-9.37861	+10.79249
78.0	1.34768	1.29588	+0.11798	168.0	0.08570	-10.67029	+12.08417
80.0	1.35915	1.33267	+0.08122	170.0	0.06007	-12.21376	+13.62765
82.0	1.36847	1.36236	+0.05153	172.0	0.03873	-14.11900	+15.53288
84.0	1.37568	1.38518	+0.02871	174.0	0.02192	-16.59206	+18.00595
86.0	1.38080	1.40130	+0.01258	176.0	0.00978	-20.09548	+21.50937
88.0	1.38384	1.41085	+0.00304	178.0	0.00245	-26.10503	+27.51891
90.0	1.38480	1.41388	0.0	180	0.00000	-INFINITY	-INFINITY

$h/\lambda = 0.025$, $0 \leq ka \leq 3.0$.

TABLE A1-33

INTEGRAL EQUATION METHOD
EPSILON= 1.7500(NORMALIZED GROUNDPLANE RADIUS)
MONOPOLE LENGTH= 0.025000(WAVELENGTH)
INFINITELY THIN MONOPOLE RADIUS
RADIATION RESISTANCE = 0.139354 (OHMS)

ELEVATION ANGLE (DEG)	DIRECTIVITY (NUMERIC)	DIRECTIVITY (DBI)	RELATIVE POWER (DB)	ELEVATION ANGLE (DEG)	DIRECTIVITY (NUMERIC)	DIRECTIVITY (DBI)	RELATIVE POWER (DB)
0	0.00000	-INFINITY	-INFINITY				
2.0	0.00279	-25.54439	-26.79107	92.0	1.33167	1.24398	-0.00270
4.0	0.01112	-19.53725	-20.78394	94.0	1.32944	1.23668	+0.01001
6.0	0.02490	-16.03782	-17.28451	96.0	1.32577	1.22469	-0.02200
8.0	0.04395	-13.57033	-14.81702	98.0	1.32065	1.20787	+0.03882
10.0	0.06804	-11.67223	-12.91892	100.0	1.31401	1.18600	-0.06069
12.0	0.09689	-10.13742	-11.38410	102.0	1.30582	1.15882	-0.08787
14.0	0.13014	-8.85589	-10.10258	104.0	1.29598	1.12600	+0.12069
16.0	0.16742	-7.76193	-9.00862	106.0	1.28444	1.08715	-0.15854
18.0	0.20830	-6.81307	+8.05976	108.0	1.27111	1.04182	+0.20487
20.0	0.25233	-5.98024	-7.22693	110.0	1.25589	0.98950	-0.25718
22.0	0.29904	-5.24766	-6.48934	112.0	1.23869	0.92963	-0.31706
24.0	0.34795	-4.58488	-5.83157	114.0	1.21943	0.86155	+0.38513
26.0	0.39855	-3.99514	-5.24182	116.0	1.19801	0.78459	-0.46210
28.0	0.45038	-3.46420	-4.71088	118.0	1.17435	0.69796	+0.54872
30.0	0.50296	-2.98468	-4.23137	120.0	1.14838	0.60084	+0.64584
32.0	0.55583	-2.55058	-3.79726	122.0	1.12004	0.49232	-0.75437
34.0	0.60857	-2.15690	-3.40358	124.0	1.08928	0.37140	+0.87529
36.0	0.66078	-1.79945	-3.04614	126.0	1.05609	0.23700	+1.00968
38.0	0.71209	-1.47467	-2.72136	128.0	1.02046	0.08797	+1.15871
40.0	0.76217	-1.17948	-2.42617	130.0	0.98243	-0.07698	-1.32366
42.0	0.81074	-0.91119	-2.15788	132.0	0.94205	-0.25924	+1.50593
44.0	0.85754	-0.66744	+1.91412	134.0	0.89942	-0.46035	-1.70704
46.0	0.90238	-0.44613	-1.69281	136.0	0.85467	-0.68200	+1.92869
48.0	0.94507	-0.24538	+1.49207	138.0	0.80797	-0.92607	-2.17276
50.0	0.98548	-0.06351	-1.31020	140.0	0.75951	-1.19465	+2.44134
52.0	1.02353	0.10101	+1.14567	142.0	0.70956	-1.49011	+2.73680
54.0	1.05915	0.24959	-0.99709	144.0	0.65839	-1.81514	-3.06182
56.0	1.09232	0.38350	+0.86319	146.0	0.60634	-2.17280	+3.41948
58.0	1.12303	0.50391	-0.74278	148.0	0.55377	-2.56669	-3.81337
60.0	1.15130	0.61189	-0.63479	150.0	0.50107	-3.00098	+4.24766
62.0	1.17718	0.70844	+0.53824	152.0	0.44868	-3.48066	-4.72734
64.0	1.20073	0.79447	-0.45222	154.0	0.39703	-4.01174	+5.25840
66.0	1.22203	0.87080	+0.37588	156.0	0.34681	+4.60162	-5.84831
68.0	1.24114	0.93822	-0.30847	158.0	0.29788	-5.25952	+6.50620
70.0	1.25817	0.99741	+0.24928	160.0	0.25135	-5.99721	-7.24390
72.0	1.27321	1.04902	-0.19767	162.0	0.20749	-6.83013	+8.07681
74.0	1.28636	1.09361	+0.15308	164.0	0.16676	+7.77907	-9.02576
76.0	1.29769	1.13170	-0.11498	166.0	0.12963	-8.87310	+10.11979
78.0	1.30730	1.16375	+0.08294	168.0	0.09650	-10.15468	-11.40137
80.0	1.31527	1.19013	-0.05655	170.0	0.06777	+11.68954	+12.93623
82.0	1.32166	1.21119	+0.03549	172.0	0.04378	-13.58769	-14.83437
84.0	1.32654	1.22720	-0.01849	174.0	0.02480	+16.05521	+17.30189
86.0	1.32995	1.23836	+0.00833	176.0	0.01108	-19.55465	+20.80134
88.0	1.33193	1.24482	-0.00187	178.0	0.00278	+25.56180	-26.80849
90.0	1.33250	1.24669	0.0 '	180.	0.00000	-INFINITY	+INFINITY

$h/\lambda = 0.025$, $0 \leq ka \leq 3.0$.

TABLE A1-34

INTEGRAL EQUATION METHOD
EPSILON= 2.0000(NORMALIZED GROUNDPLANE RADIUS)
MONOPOLE LENGTH= 0.025000(WAVELENGTH)
INFINITELY THIN MONOPOLE RADIUS
RADIATION RESISTANCE = 0.147191 (OHMS)

ELEVATION ANGLE (DEG)	DIRECTIVITY (NUMERIC)	DIRECTIVITY (DBI)	RELATIVE POWER (DB)	ELEVATION ANGLE (DEG)	DIRECTIVITY (NUMERIC)	DIRECTIVITY (DBI)	RELATIVE POWER (DB)
0	0.00000	-INFINITY	-INFINITY				
2.0	0.00328	-24.83551	-25.84458	92.0	1.26105	1.00733	-0.00170
4.0	0.01309	-18.83135	-19.84042	94.0	1.25999	1.00368	-0.00539
6.0	0.02926	-15.33688	-16.34595	96.0	1.25834	0.99798	-0.01108
8.0	0.05157	-12.87631	-13.88538	98.0	1.25604	0.99005	-0.01902
10.0	0.07967	-10.98706	-11.99613	100.0	1.25303	0.97960	-0.02946
12.0	0.11316	-9.46302	-10.47209	102.0	1.24919	0.96629	-0.04277
14.0	0.15156	-8.19414	-9.20321	104.0	1.24443	0.94969	-0.05938
16.0	0.19433	-7.11466	-8.12373	106.0	1.23859	0.92929	-0.07978
18.0	0.24088	-6.18207	-7.19114	108.0	1.23155	0.90451	-0.10456
20.0	0.29059	-5.36726	-6.37633	110.0	1.22312	0.87469	-0.13438
22.0	0.34282	-4.64936	-5.65842	112.0	1.21314	0.83912	-0.16995
24.0	0.39693	-4.01288	-5.02195	114.0	1.20143	0.79699	-0.21208
26.0	0.45228	-3.44597	-4.45504	116.0	1.18780	0.74744	-0.26163
28.0	0.50824	-2.93932	-3.94839	118.0	1.17207	0.68953	-0.31953
30.0	0.56423	-2.48547	-3.49454	120.0	1.15405	0.62225	-0.38682
32.0	0.61968	-2.07830	-3.08737	122.0	1.13358	0.54451	-0.46456
34.0	0.67410	-1.71273	-2.72180	124.0	1.11049	0.45514	-0.55393
36.0	0.72703	-1.38447	-2.39354	126.0	1.08465	0.35288	-0.65618
38.0	0.77807	-1.08982	-2.09889	128.0	1.05594	0.23640	-0.77267
40.0	0.82688	-0.82559	-1.83466	130.0	1.02429	0.10424	-0.90483
42.0	0.87318	-0.58896	-1.59802	132.0	0.98966	-0.04516	-1.05423
44.0	0.91676	-0.37743	-1.38650	134.0	0.95203	-0.21350	-1.22257
46.0	0.95747	-0.18677	-1.19783	136.0	0.91146	-0.40262	-1.41169
48.0	0.99519	-0.02094	-1.03001	138.0	0.86805	-0.61457	-1.62363
50.0	1.02989	0.12789	-0.88117	140.0	0.82195	-0.85157	-1.86063
52.0	1.06156	0.25943	-0.74964	142.0	0.77337	-1.11613	-2.12520
54.0	1.09024	0.37529	-0.63384	144.0	0.72259	-1.41107	-2.42013
56.0	1.11603	0.47674	-0.53233	146.0	0.66995	-1.73959	-2.74865
58.0	1.13902	0.56630	-0.44376	148.0	0.61583	-2.10538	-3.11444
60.0	1.15936	0.64217	-0.36689	150.0	0.56069	-2.51274	-3.52181
62.0	1.17720	0.70852	-0.30055	152.0	0.50504	-2.96676	-3.97583
64.0	1.19273	0.76542	-0.24365	154.0	0.44941	-3.47355	-4.48262
66.0	1.20612	0.81390	-0.19517	156.0	0.39440	-4.04059	-5.04965
68.0	1.21756	0.85469	-0.15418	158.0	0.34063	-4.67717	-5.68624
70.0	1.22723	0.88926	-0.11960	160.0	0.28872	-5.39516	-6.40423
72.0	1.23533	0.91782	-0.09125	162.0	0.23933	-6.21005	-7.21912
74.0	1.24202	0.94129	-0.06778	164.0	0.19308	-7.14270	-8.15177
76.0	1.24747	0.96032	-0.04875	166.0	0.15058	-8.22223	-9.23130
78.0	1.25184	0.97550	-0.03357	168.0	0.11243	-9.49115	-10.50021
80.0	1.25526	0.98734	-0.02172	170.0	0.07915	-11.01522	-12.02429
82.0	1.25785	0.99629	-0.01276	172.0	0.05123	-12.90450	-13.91356
84.0	1.25970	1.00269	-0.00638	174.0	0.02907	-15.36509	-16.37415
86.0	1.26091	1.00683	-0.00224	176.0	0.01300	-18.85957	-19.86864
88.0	1.26151	1.00891	-0.00015	178.0	0.00326	-24.86374	-25.87280
90.0	1.26156	1.00907	0.0	180.	0.00000	-INFINITY	-INFINITY

$h/\lambda = 0.025$, $0 \leq ka \leq 3.0$.

TABLE A1-35

INTEGRAL EQUATION METHOD
EPSILON= 2.2500(NORMALIZED GROUNDPLANE RADIUS)
MONOPOLE LENGTH= 0.025000(WAVELENGTH)
INFINITELY THIN MONOPOLE RADIUS
RADIATION RESISTANCE = 0.159189 (OHMS)

ELEVATION ANGLE (DEG)	DIRECTIVITY (NUMERIC)	DIRECTIVITY (DBI)	RELATIVE POWER (DB)	ELEVATION ANGLE (DEG)	DIRECTIVITY (NUMERIC)	DIRECTIVITY (DBI)	RELATIVE POWER (DB)
0	0.00000	-INFINITY	-INFINITY				
2.0	0.00402	-23.95498	-24.68588	92.0	1.16837	0.66835	-0.06255
4.0	0.01602	-17.95436	-18.68527	94.0	1.16676	0.66983	-0.06107
6.0	0.03576	-14.46579	-15.19669	96.0	1.16762	0.67303	-0.05787
8.0	0.06290	-12.01346	-12.74436	98.0	1.16887	0.67767	-0.05323
10.0	0.09694	-10.13477	-10.86567	100.0	1.17040	0.68336	-0.04754
12.0	0.13729	-8.62357	-9.35447	102.0	1.17208	0.68959	-0.04131
14.0	0.18324	-7.36981	-8.10071	104.0	1.17375	0.69575	-0.03515
16.0	0.23401	-6.30767	-7.03857	106.0	1.17521	0.70114	-0.02976
18.0	0.28876	-5.39461	-6.12551	108.0	1.17624	0.70496	-0.02594
20.0	0.34662	-4.60145	-5.33235	110.0	1.17660	0.70631	-0.02459
22.0	0.40670	-3.90729	-4.63819	112.0	1.17604	0.70423	-0.02669
24.0	0.46811	-3.29656	-4.02746	114.0	1.17425	0.69762	-0.03328
26.0	0.52999	-2.75735	-3.48825	116.0	1.17095	0.68539	-0.04551
28.0	0.59152	-2.28027	-3.01118	118.0	1.16582	0.66633	-0.06457
30.0	0.65196	-1.85777	-2.58867	120.0	1.15855	0.63915	-0.09175
32.0	0.71062	-1.48365	-2.21455	122.0	1.14882	0.60251	-0.12839
34.0	0.76688	-1.15272	-1.88362	124.0	1.13631	0.55499	-0.17592
36.0	0.82024	-0.86057	-1.59147	126.0	1.12075	0.48508	-0.23582
38.0	0.87028	-0.60339	-1.33429	128.0	1.10184	0.42120	-0.30970
40.0	0.91667	-0.37786	-1.10876	130.0	1.07937	0.33169	-0.39921
42.0	0.95918	-0.18102	-0.91192	132.0	1.05311	0.22475	-0.50615
44.0	0.99765	-0.01022	-0.74112	134.0	1.02294	0.09850	-0.63240
46.0	1.03203	0.13694	-0.59396	136.0	0.98876	-0.04910	-0.78000
48.0	1.06235	0.26266	-0.46824	138.0	0.95054	-0.22028	-0.95118
50.0	1.08867	0.36897	-0.36193	140.0	0.90836	-0.41742	-1.14832
52.0	1.11115	0.45776	-0.27314	142.0	0.86234	-0.64320	-1.37410
54.0	1.13001	0.53081	-0.20009	144.0	0.81272	-0.90057	-1.63147
56.0	1.14546	0.58978	-0.14112	146.0	0.75982	-1.19287	-1.92377
58.0	1.15778	0.63625	-0.09465	148.0	0.70406	-1.52391	-2.25481
60.0	1.16727	0.67170	-0.05920	150.0	0.64594	-1.89810	-2.62900
62.0	1.17424	0.69756	-0.03334	152.0	0.58605	-2.32065	-3.05155
64.0	1.17901	0.71517	-0.01573	154.0	0.52508	-2.79775	-3.52865
66.0	1.18190	0.72581	-0.00509	156.0	0.46377	-3.33696	-4.06786
68.0	1.18322	0.73067	-0.00023	158.0	0.40293	-3.94767	-4.67857
70.0	1.18329	0.73090	0.0	160.0	0.34341	-4.64181	-5.37271
72.0	1.18237	0.72755	-0.00335	162.0	0.28609	-5.43493	-6.16583
74.0	1.18076	0.72160	-0.00930	164.0	0.23185	-6.34796	-7.07886
76.0	1.17868	0.71396	-0.01694	166.0	0.18155	-7.41006	-8.14096
78.0	1.17637	0.70542	-0.02548	168.0	0.13603	-8.66378	-9.39468
80.0	1.17401	0.69672	-0.03418	170.0	0.09605	-10.17494	-10.90584
82.0	1.17178	0.68848	-0.04242	172.0	0.06232	-12.05360	-12.78450
84.0	1.16982	0.68120	-0.04970	174.0	0.03543	-14.50591	-15.23681
86.0	1.16824	0.67531	-0.05559	176.0	0.01587	-17.99447	-18.72537
88.0	1.16711	0.67110	-0.05980	178.0	0.00399	-23.99507	-24.72597
90.0	1.16648	0.66876	-0.06214	180	0.00000	-INFINITY	-INFINITY

$h/\lambda = 0.025$, $0 \leq ka \leq 3.0$.

TABLE A1-36

INTEGRAL EQUATION METHOD
EPSILON= 2.5000(NORMALIZED GROUNDPLANE RADIUS)
MONOPOLE LENGTH= 0.025000(WAVELENGTH)
INFINITELY THIN MONOPOLE RADIUS
RADIATION RESISTANCE = 0.178038 (OHMS)

ELEVATION ANGLE (DEG)	DIRECTIVITY (NUMERIC)	DIRECTIVITY (DBI)	RELATIVE POWER (DB)	ELEVATION ANGLE (DEG)	DIRECTIVITY (NUMERIC)	DIRECTIVITY (DBI)	RELATIVE POWER (DB)
0	0.00000	-INFINITY	-INFINITY				
2.0	0.00511	-22.91583	-23.63294	92.0	1.04333	0.18423	-0.53286
4.0	0.02033	-16.91920	-17.63631	94.0	1.04546	0.19309	-0.52402
6.0	0.04532	-13.43726	-14.15437	96.0	1.04932	0.20907	-0.50805
8.0	0.07954	-10.99419	-11.71130	98.0	1.05480	0.23171	-0.48540
10.0	0.12225	-9.12739	-9.84450	100.0	1.06180	0.26041	-0.45670
12.0	0.17256	-7.63068	-8.34780	102.0	1.07013	0.29437	-0.42274
14.0	0.22940	-6.39400	-7.11111	104.0	1.07960	0.33265	-0.38447
16.0	0.29164	-5.35148	-6.06859	106.0	1.08997	0.37416	-0.34295
18.0	0.35805	-4.46056	-5.17767	108.0	1.10095	0.41772	-0.29939
20.0	0.42736	-3.69203	-4.40914	110.0	1.11225	0.46202	-0.25509
22.0	0.49832	-3.02493	-3.74204	112.0	1.12348	0.50564	-0.21147
24.0	0.56868	-2.44365	-3.16077	114.0	1.13426	0.54712	-0.16999
26.0	0.64029	-1.93623	-2.65334	116.0	1.14417	0.58490	-0.13221
28.0	0.70805	-1.49321	-2.21033	118.0	1.15276	0.61738	-0.09974
30.0	0.77500	-1.10698	-1.82409	120.0	1.15955	0.64288	-0.07423
32.0	0.83729	-0.77126	-1.48837	122.0	1.16404	0.65970	-0.05742
34.0	0.88520	-0.48078	-1.19789	124.0	1.16575	0.66606	-0.05105
36.0	0.94819	-0.23103	-0.94814	126.0	1.16417	0.66017	-0.05695
38.0	0.99584	-0.01811	-0.73522	128.0	1.15881	0.64013	-0.07699
40.0	1.03787	0.16142	-0.55569	130.0	1.14921	0.60400	-0.11311
42.0	1.07415	0.31066	-0.40645	132.0	1.13495	0.54977	-0.16734
44.0	1.10460	0.43238	-0.28473	134.0	1.11566	0.47531	-0.24180
46.0	1.12957	0.52915	-0.18797	136.0	1.09104	0.37839	-0.33872
48.0	1.14904	0.60334	-0.11378	138.0	1.06087	0.25660	-0.46051
50.0	1.16337	0.65717	-0.05994	140.0	1.02504	0.10738	-0.60972
52.0	1.17294	0.69276	-0.02436	142.0	0.98354	-0.07206	-0.78917
54.0	1.17817	0.71208	-0.00502	144.0	0.93652	-0.28484	-1.00195
56.0	1.17954	0.71711	0.0	146.0	0.88422	-0.53440	-1.25151
58.0	1.17752	0.70967	-0.00745	148.0	0.82705	-0.82466	-1.54178
60.0	1.17262	0.69156	-0.02556	150.0	0.76557	-1.16014	-1.87726
62.0	1.16534	0.66453	-0.05258	152.0	0.70047	-1.54611	-2.26323
64.0	1.15619	0.63029	-0.08682	154.0	0.63258	-1.98886	-2.70598
66.0	1.14564	0.59048	-0.12663	156.0	0.56286	-2.49601	-3.21313
68.0	1.13415	0.54671	-0.17041	158.0	0.49238	-3.07702	-3.79413
70.0	1.12215	0.50051	-0.21660	160.0	0.42229	-3.74386	-4.46097
72.0	1.11003	0.45337	-0.26375	162.0	0.35382	-4.51215	-5.22926
74.0	1.09817	0.40668	-0.31043	164.0	0.28821	-5.40284	-6.11995
76.0	1.08687	0.36178	-0.35533	166.0	0.22672	-6.44514	-7.16225
78.0	1.07643	0.31987	-0.39725	168.0	0.17054	-7.68164	-8.39875
80.0	1.06710	0.28204	-0.43507	170.0	0.12083	-9.17818	-9.89529
82.0	1.05908	0.24928	-0.46783	172.0	0.07862	-11.04484	-11.76196
84.0	1.05254	0.22240	-0.49472	174.0	0.04479	-13.48781	-14.20492
86.0	1.04762	0.20205	-0.51506	176.0	0.02009	-16.96967	-17.68678
88.0	1.04443	0.18874	-0.52837	178.0	0.00505	-22.96626	-23.68337
90.0	1.04298	0.18276	-0.53435	180	0.00000	-INFINITY	-INFINITY

$h/\lambda = 0.025$, $0 \leq ka \leq 3.0$.

TABLE A1-37

INTEGRAL EQUATION METHOD
EPSILON= 2.7500(NORMALIZED GROUNDPLANE RADIUS)
MONOPOLE LENGTH= 0.025000(WAVELENGTH)
INFINITELY THIN MONOPOLE RADIUS
RADIATION RESISTANCE = 0.208486 (OHMS)

Method gives poor results for $\epsilon > 2.5$.

ELEVATION ANGLE θ (DEG)	DIRECTIVITY (NUMERIC)	DIRECTIVITY (DBI)	RELATIVE POWER (DB)	ELEVATION ANGLE (DEG)	DIRECTIVITY (NUMERIC)	DIRECTIVITY (DBI)	RELATIVE POWER (DB)
0.	0.00000	-INFINITY	-INFINITY				
2.0	1.39465	1.44466	0.0	92.0	0.88914	-0.51032	-1.95497
4.0	0.34114	-4.67071	-6.11536	94.0	0.89079	-0.50225	-1.94691
6.0	0.14821	-8.29135	-9.73601	96.0	0.89557	-0.47900	-1.92365
8.0	0.08140	-10.89359	-12.33824	98.0	0.90340	-0.44119	-1.88584
10.0	0.05080	-12.94094	-14.38559	100.0	0.91415	-0.38980	-1.83446
12.0	0.03436	-14.63996	-16.08462	102.0	0.92766	-0.32610	-1.77075
14.0	0.02454	-16.10166	-17.54632	104.0	0.94372	-0.25158	-1.69624
16.0	0.01823	-17.39279	-18.83744	106.0	0.96206	-0.16798	-1.61263
18.0	0.01394	-18.55701	-20.00167	108.0	0.98239	-0.07717	-1.52183
20.0	0.01090	-19.62483	-21.06949	110.0	1.00434	0.01880	-1.42586
22.0	0.00867	-20.61878	-22.06344	112.0	1.02751	0.11784	-1.32681
24.0	0.00699	-21.55640	-23.00106	114.0	1.05142	0.21776	-1.22688
26.0	0.00569	-22.45210	-23.89675	116.0	1.07556	0.31635	-1.12830
28.0	0.00466	-23.31838	-24.76304	118.0	1.09936	0.41138	-1.03327
30.0	0.00383	-24.16684	-25.61150	120.0	1.12218	0.50062	-0.94403
32.0	0.00316	-25.00886	-26.45362	122.0	1.14336	0.58183	-0.86282
34.0	0.00260	-25.85701	-27.30167	124.0	1.16220	0.65280	-0.79186
36.0	0.00213	-26.72516	-28.16981	126.0	1.17795	0.71128	-0.73338
38.0	0.00173	-27.63106	-29.07572	128.0	1.18988	0.75504	-0.68962
40.0	0.00138	-28.59860	-30.04325	130.0	1.19724	0.78182	-0.66283
42.0	0.00108	-29.66287	-31.10753	132.0	1.19931	0.78933	-0.65533
44.0	0.00082	-30.88082	-32.32548	134.0	1.19542	0.77520	-0.66945
46.0	0.00058	-32.35716	-33.80181	136.0	1.18495	0.73698	-0.70766
48.0	0.00037	-34.32462	-35.76927	138.0	1.16736	0.67213	-0.77252
50.0	0.00018	-37.52247	-38.96713	140.0	1.14232	0.57790	-0.86676
52.0	1.27923	1.06948	-0.37518	142.0	1.10952	0.45134	-0.99331
54.0	1.26582	1.02373	-0.42092	144.0	1.06887	0.28926	-1.15539
56.0	1.24803	0.96224	-0.48242	146.0	1.02049	0.08810	-1.35655
58.0	1.22662	0.88709	-0.55757	148.0	0.96468	-0.15615	-1.60081
60.0	1.20236	0.80035	-0.64431	150.0	0.90197	-0.44808	-1.89274
62.0	1.17601	0.70411	-0.74055	152.0	0.83310	-0.79304	-2.23770
64.0	1.14827	0.60044	-0.84422	154.0	0.75904	-1.19738	-2.64203
66.0	1.11981	0.49143	-0.95322	156.0	0.68096	-1.66876	-3.11342
68.0	1.09124	0.37919	-1.06547	158.0	0.60025	-2.21670	-3.66135
70.0	1.06312	0.26581	-1.17886	160.0	0.51842	-2.85321	-4.29787
72.0	1.03595	0.15340	-1.29126	162.0	0.43712	-3.59395	-5.03860
74.0	1.01019	0.04402	-1.40063	164.0	0.35810	-4.45990	-5.90456
76.0	0.98622	-0.06028	-1.50494	166.0	0.28312	-5.48031	-6.92496
78.0	0.96437	-0.15756	-1.60222	168.0	0.21391	-6.69778	-8.14244
80.0	0.94494	-0.24598	-1.69063	170.0	0.15219	-8.17818	-9.62284
82.0	0.92815	-0.32381	-1.76847	172.0	0.09927	-10.03162	-11.47628
84.0	0.91420	-0.38957	-1.83422	174.0	0.05670	-12.46428	-13.90894
86.0	0.90321	-0.44195	-1.88661	176.0	0.02548	-15.93878	-17.38343
88.0	0.89532	-0.47956	-1.92421	178.0	0.00641	-21.93094	-23.37560
90.0	0.89066	-0.50287	-1.94753	180.	0.00000	-INFINITY	-INFINITY

$h/\lambda = 0.025$, $0 \leq ka \leq 3.0$.

TABLE A1-38

INTEGRAL EQUATION METHOD
EPSILON= 0.0 (NORMALIZED GROUNDPLANE RADIUS)
MONOPOLE LENGTH= 0.010000(WAVELENGTHS)
INFINITELY THIN MONOPOLE RADIUS
RADIATION RESISTANCE = 0.019738 (OHMS)

ELEVATION ANGLE (DEG)	DIRECTIVITY (NUMERIC)	DIRECTIVITY (DBI)	RELATIVE POWER (DB)	ELEVATION ANGLE (DEG)	DIRECTIVITY (NUMERIC)	DIRECTIVITY (DBI)	RELATIVE POWER (DB)
0.	0.00000	-INFINITY	-INFINITY				
2.0	0.00183	-27.38347	-29.14457	92.0	1.49824	1.75581	-0.00529
4.0	0.00730	-21.36815	-23.12926	94.0	1.49276	1.73991	-0.02119
6.0	0.01639	-17.85515	-19.61625	96.0	1.48367	1.71338	-0.04772
8.0	0.02905	-15.36873	-17.12983	98.0	1.47100	1.67614	-0.08496
10.0	0.04522	-13.44642	-15.20752	100.0	1.45482	1.62810	-0.13300
12.0	0.06483	-11.88223	-13.64333	102.0	1.43521	1.56915	-0.19195
14.0	0.08778	-10.56629	-12.32739	104.0	1.41225	1.49913	-0.26197
16.0	0.11395	-9.43302	-11.19412	106.0	1.38607	1.41786	-0.34324
18.0	0.14322	-8.44011	-10.20121	108.0	1.35679	1.32514	-0.43596
20.0	0.17544	-7.55870	-9.31981	110.0	1.32456	1.22071	-0.54040
22.0	0.21046	-6.76821	-8.52931	112.0	1.28952	1.10429	-0.65682
24.0	0.24812	-6.05343	-7.81453	114.0	1.25186	0.97555	-0.78555
26.0	0.28822	-5.40283	-7.16393	116.0	1.21175	0.83412	-0.92698
28.0	0.33056	-4.80745	-6.56856	118.0	1.16939	0.67959	-1.08151
30.0	0.37495	-4.26021	-6.02131	120.0	1.12498	0.51148	-1.24963
32.0	0.42117	-3.75539	-5.51649	122.0	1.07876	0.32925	-1.43186
34.0	0.46899	-3.28832	-5.04942	124.0	1.03093	0.13229	-1.62881
36.0	0.51819	-2.85515	-4.61625	126.0	0.98173	-0.08007	-1.84118
38.0	0.56851	-2.45265	-4.21375	128.0	0.93140	-0.30862	-2.06972
40.0	0.61971	-2.07811	-3.83921	130.0	0.88019	-0.55421	-2.31531
42.0	0.67155	-1.72921	-3.49031	132.0	0.82835	-0.81785	-2.57896
44.0	0.72377	-1.40396	-3.16507	134.0	0.77613	-1.10067	-2.86178
46.0	0.77613	-1.10067	-2.86178	136.0	0.72377	-1.40396	-3.16507
48.0	0.82835	-0.81785	-2.57896	138.0	0.67155	-1.72921	-3.49031
50.0	0.88019	-0.55421	-2.31531	140.0	0.61971	-2.07811	-3.83921
52.0	0.93140	-0.30862	-2.06972	142.0	0.56851	-2.45265	-4.21375
54.0	0.98173	-0.08007	-1.84118	144.0	0.51819	-2.85515	-4.61625
56.0	1.03093	0.13229	-1.62881	146.0	0.46899	-3.28832	-5.04942
58.0	1.07876	0.32925	-1.43186	148.0	0.42117	-3.75539	-5.51649
60.0	1.12498	0.51148	-1.24963	150.0	0.37495	-4.26021	-6.02131
62.0	1.16939	0.67959	-1.08151	152.0	0.33056	-4.80745	-6.56856
64.0	1.21175	0.83412	-0.92698	154.0	0.28822	-5.40283	-7.16393
66.0	1.25186	0.97555	-0.78555	156.0	0.24812	-6.05343	-7.81453
68.0	1.28952	1.10429	-0.65682	158.0	0.21046	-6.76821	-8.52931
70.0	1.32456	1.22071	-0.54040	160.0	0.17544	-7.55870	-9.31981
72.0	1.35679	1.32514	-0.43596	162.0	0.14322	-8.44011	-10.20121
74.0	1.38607	1.41786	-0.34324	164.0	0.11395	-9.43302	-11.19412
76.0	1.41225	1.49913	-0.26197	166.0	0.08778	-10.56629	-12.32739
78.0	1.43521	1.56915	-0.19195	168.0	0.06483	-11.88223	-13.64333
80.0	1.45482	1.62810	-0.13300	170.0	0.04522	-13.44642	-15.20752
82.0	1.47100	1.67614	-0.08496	172.0	0.02905	-15.36873	-17.12983
84.0	1.48367	1.71338	-0.04772	174.0	0.01639	-17.85515	-19.61625
86.0	1.49276	1.73991	-0.02119	176.0	0.00730	-21.36815	-23.12926
88.0	1.49824	1.75581	-0.00529	178.0	0.00183	-27.38347	-29.14457
90.0	1.50007	1.76110	0.0	180.	0.00000	-INFINITY	-INFINITY

$h/\lambda = 0.01$, $0 \leq ka \leq 3.0$.

TABLE A1-39

INTEGRAL EQUATION METHOD
EPSILON= 0.2500(NORMALIZED GROUNDPLANE RADIUS)
MONOPOLE LENGTH= 0.010000(WAVELENGTH)
INFINITELY THIN MONOPOLE RADIUS
RADIATION RESISTANCE = 0.019769 (OHMS)

ELEVATION ANGLE (DEG)	DIRECTIVITY (NUMERIC)	DIRECTIVITY (DBI)	RELATIVE POWER (DB)	ELEVATION ANGLE (DEG)	DIRECTIVITY (NUMERIC)	DIRECTIVITY (DBI)	RELATIVE POWER (DB)
0	0.00000	-INFINITY	-INFINITY				
2.0	0.00184	-27.35570	-29.10984	92.0	1.49585	1.74889	-0.00525
4.0	0.00734	-21.34052	-23.09466	94.0	1.48043	1.73312	-0.02102
6.0	0.01649	-17.82772	-19.58186	96.0	1.46888	1.70680	-0.04734
8.0	0.02923	-15.34159	-17.09574	98.0	1.46284	1.66985	-0.08429
10.0	0.04550	-13.41966	-15.17380	100.0	1.46284	1.62219	-0.13195
12.0	0.06522	-11.85593	-13.61007	102.0	1.47341	1.56369	-0.19045
14.0	0.08830	-10.54052	-12.29466	104.0	1.49420	1.49420	-0.25994
16.0	0.11461	-9.40785	-11.16199	106.0	1.52470	1.41355	-0.34060
18.0	0.14402	-8.41563	-10.16977	108.0	1.56566	1.32150	-0.43264
20.0	0.17640	-7.53496	-9.28911	110.0	1.62368	1.21782	-0.53633
22.0	0.21158	-6.74528	-8.49942	112.0	1.68890	1.10221	-0.65194
24.0	0.24938	-6.03137	-7.78551	114.0	1.75151	0.97434	-0.77980
26.0	0.28962	-5.38170	-7.13584	116.0	1.81167	0.83385	-0.92030
28.0	0.33210	-4.78731	-6.54145	118.0	1.86959	0.68030	-1.07385
30.0	0.37661	-4.24110	-5.99524	120.0	1.92544	0.51321	-1.24093
32.0	0.42293	-3.73734	-5.49149	122.0	1.97946	0.33205	-1.42209
34.0	0.47083	-3.27138	-5.02553	124.0	2.03186	0.13620	-1.61794
36.0	0.52007	-2.83935	-4.59349	126.0	0.98287	-0.07502	-1.82916
38.0	0.57042	-2.43802	-4.19216	128.0	0.93274	-0.30240	-2.05654
40.0	0.62163	-2.06466	-3.81881	130.0	0.88170	-0.54681	-2.30095
42.0	0.67345	-1.71696	-3.47111	132.0	0.82999	-0.80925	-2.56339
44.0	0.72562	-1.39293	-3.14708	134.0	0.77788	-1.08086	-2.84500
46.0	0.77788	-1.09086	-2.84500	136.0	0.72562	-1.39293	-3.14708
48.0	0.82999	-0.80925	-2.56339	138.0	0.67345	-1.71696	-3.47111
50.0	0.88170	-0.54680	-2.30095	140.0	0.62163	-2.06466	-3.81881
52.0	0.93274	-0.30240	-2.05654	142.0	0.57042	-2.43802	-4.19216
54.0	0.98287	-0.07502	-1.82916	144.0	0.52007	-2.83935	-4.59349
56.0	1.03186	0.13620	-1.61794	146.0	0.47083	-3.27138	-5.02553
58.0	1.07946	0.33205	-1.42209	148.0	0.42293	-3.73734	-5.49149
60.0	1.12544	0.51321	-1.24093	150.0	0.37661	-4.24110	-5.99524
62.0	1.16958	0.68030	-1.07385	152.0	0.33210	-4.78731	-6.54145
64.0	1.21167	0.83385	-0.92030	154.0	0.28962	-5.38170	-7.13584
66.0	1.25151	0.97434	-0.77980	156.0	0.24938	-6.03137	-7.78551
68.0	1.28890	1.10221	-0.65194	158.0	0.21158	-6.74528	-8.49942
70.0	1.32368	1.21782	-0.53633	160.0	0.17640	-7.53497	-9.28911
72.0	1.35566	1.32150	-0.43264	162.0	0.14402	-8.41563	-10.16977
74.0	1.38470	1.41355	-0.34060	164.0	0.11461	-9.40785	-11.16199
76.0	1.41065	1.49420	-0.25994	166.0	0.08830	-10.54052	-12.29466
78.0	1.43341	1.56369	-0.19045	168.0	0.06522	-11.85593	-13.61007
80.0	1.45284	1.62219	-0.13195	170.0	0.04550	-13.41966	-15.17380
82.0	1.46888	1.66985	-0.08429	172.0	0.02923	-15.34159	-17.09574
84.0	1.48143	1.70680	-0.04734	174.0	0.01649	-17.82772	-19.58187
86.0	1.49043	1.73312	-0.02102	176.0	0.00734	-21.34052	-23.09466
88.0	1.49585	1.74889	-0.00525	178.0	0.00184	-27.35570	-29.10985
90.0	1.49765	1.75414	0.0	180	0.00000	INFINITY	-INFINITY

$h/\lambda = 0.01,\ 0 \le ka \le 3.0.$

TABLE A1-40

INTEGRAL EQUATION METHOD
EPSILON= 0.5000(NORMALIZED GROUNDPLANE RADIUS)
MONOPOLE LENGTH= 0.25000(WAVELENGTH)
INFINITELY THIN MONOPOLE RADIUS
RADIATION RESISTANCE = 0.019825 (OHMS)

ELEVATION ANGLE (DEG)	DIRECTIVITY (NUMERIC)	DIRECTIVITY (DBI)	RELATIVE POWER (DB)	ELEVATION ANGLE (DEG)	DIRECTIVITY (NUMERIC)	DIRECTIVITY (DBI)	RELATIVE POWER (DB)
0	0.00000	-INFINITY	-INFINITY				
2.0	0.00186	-27.30677	-29.04865	92.0	1.49168	1.73670	-0.00518
4.0	0.00743	-21.29182	-23.03369	94.0	1.48633	1.72115	-0.02072
6.0	0.01667	-17.77939	-19.52127	96.0	1.47747	1.69520	-0.04668
8.0	0.02955	-15.29378	-17.03566	98.0	1.46513	1.65877	-0.08311
10.0	0.04600	-13.37251	-15.11439	100.0	1.44936	1.61176	-0.13011
12.0	0.06592	-11.80958	-13.55146	102.0	1.43023	1.55406	-0.18781
14.0	0.08923	-10.49513	-12.23699	104.0	1.40783	1.48551	-0.25637
16.0	0.11578	-9.36352	-11.10539	106.0	1.38226	1.40591	-0.33596
18.0	0.14546	-8.37249	-10.11437	108.0	1.35365	1.31506	-0.42682
20.0	0.17811	-7.49315	-9.23503	110.0	1.32211	1.21269	-0.52919
22.0	0.21356	-6.70490	-8.44678	112.0	1.28781	1.09850	-0.64337
24.0	0.25162	-5.99253	-7.73441	114.0	1.25088	0.97217	-0.76970
26.0	0.29211	-5.34451	-7.08638	116.0	1.21152	0.83331	-0.90856
28.0	0.33482	-4.75185	-6.49372	118.0	1.16990	0.68149	-1.06039
30.0	0.37954	-4.20745	-5.94933	120.0	1.12621	0.51621	-1.22567
32.0	0.42603	-3.70559	-5.44747	122.0	1.08057	0.33693	-1.40494
34.0	0.47407	-3.24159	-4.98346	124.0	1.03348	0.14304	-1.59884
36.0	0.52341	-2.81157	-4.55344	126.0	0.98488	-0.06618	-1.80806
38.0	0.57381	-2.41229	-4.15417	128.0	0.93505	-0.29150	-2.03338
40.0	0.62502	-2.04103	-3.78290	130.0	0.88434	-0.53382	-2.27570
42.0	0.67679	-1.69545	-3.43732	132.0	0.83289	-0.79415	-2.53602
44.0	0.72886	-1.37355	-3.11542	134.0	0.78098	-1.07363	-2.81550
46.0	0.78098	-1.07361	-2.81549	136.0	0.72886	-1.37357	-3.11544
48.0	0.83289	-0.79414	-2.53601	138.0	0.67679	-1.69546	-3.43734
50.0	0.88434	-0.53381	-2.27569	140.0	0.62502	-2.04104	-3.78292
52.0	0.93508	-0.29149	-2.03337	142.0	0.57381	-2.41231	-4.15418
54.0	0.98488	-0.06617	-1.80804	144.0	0.52341	-2.81158	-4.55346
56.0	1.03349	0.14305	-1.59883	146.0	0.47407	-3.24160	-4.98348
58.0	1.08067	0.33694	-1.40493	148.0	0.42603	-3.70561	-5.44748
60.0	1.12622	0.51622	-1.22565	150.0	0.37954	-4.20747	-5.94935
62.0	1.16990	0.68150	-1.06038	152.0	0.33482	-4.75187	-6.49374
64.0	1.21152	0.83332	-0.90856	154.0	0.29211	-5.34453	-7.08640
66.0	1.25089	0.97218	-0.76968	156.0	0.25162	-5.99255	-7.73443
68.0	1.28781	1.09851	-0.64335	158.0	0.21355	-6.70492	-8.44680
70.0	1.32212	1.21269	-0.52918	160.0	0.17811	-7.49317	-9.23505
72.0	1.35365	1.31506	-0.42681	162.0	0.14546	-8.37251	-10.11439
74.0	1.38227	1.40582	-0.33596	164.0	0.11578	-9.36354	-11.10541
76.0	1.40783	1.48551	-0.25638	166.0	0.08922	-10.49514	-12.23701
78.0	1.43023	1.55407	-0.18781	168.0	0.06592	-11.80960	-13.55148
80.0	1.44936	1.61177	-0.13011	170.0	0.04600	-13.37253	-15.11441
82.0	1.46513	1.65877	-0.08311	172.0	0.02955	-15.29380	-17.03568
84.0	1.47747	1.69520	-0.04668	174.0	0.01667	-17.77941	-19.52129
86.0	1.48633	1.72115	-0.02072	176.0	0.00743	-21.29184	-23.03371
88.0	1.49166	1.73670	-0.00518	178.0	0.00186	-27.30680	-29.04867
90.0	1.49344	1.74188	0.0	180.0	0.00000	-INFINITY	-INFINITY

$h/\lambda = 0.01$, $0 \leq ka \leq 3.0$.

TABLE A1-41

INTEGRAL EQUATION METHOD
EPSILON= 0.7500(NORMALIZED GROUNDPLANE RADIUS)
MONOPOLE LENGTH= 0.010000(WAVELENGTH)
INFINITELY THIN MONOPOLE RADIUS
RADIATION RESISTANCE = 0.019871 (OHMS)

ELEVATION ANGLE (DEG)	DIRECTIVITY (NUMERIC)	DIRECTIVITY (DBI)	RELATIVE POWER (DB)	ELEVATION ANGLE (DEG)	DIRECTIVITY (NUMERIC)	DIRECTIVITY (DBI)	RELATIVE POWER (DB)
0	0.00000	-INFINITY	-INFINITY				
2.0	0.00188	-27.26650	-28.99837	92.0	1.48825	1.72675	-0.00512
4.0	0.00750	-21.25172	-22.98360	94.0	1.48298	1.71138	-0.02048
6.0	0.01683	-17.73961	-19.47148	96.0	1.47425	1.68572	-0.04615
8.0	0.02982	-15.25443	-16.98631	98.0	1.46208	1.64971	-0.08216
10.0	0.04641	-13.33372	-15.06559	100.0	1.44652	1.60323	-0.12864
12.0	0.06650	-11.77146	-13.50333	102.0	1.42764	1.54618	-0.18570
14.0	0.09000	-10.45777	-12.18965	104.0	1.40552	1.47837	-0.25350
16.0	0.11676	-9.32707	-11.05894	106.0	1.38027	1.39964	-0.33223
18.0	0.14666	-8.33704	-10.06891	108.0	1.35199	1.30975	-0.42212
20.0	0.17952	-7.45880	-9.19067	110.0	1.32082	1.20844	-0.52343
22.0	0.21519	-6.67174	-8.40361	112.0	1.28689	1.09541	-0.63646
24.0	0.25347	-5.96066	-7.69253	114.0	1.25035	0.97032	-0.76155
26.0	0.29417	-5.31099	-7.04586	116.0	1.21137	0.83278	-0.89909
28.0	0.33707	-4.72277	-6.45464	118.0	1.17013	0.68236	-1.04951
30.0	0.38196	-4.17988	-5.91175	120.0	1.12682	0.51855	-1.21332
32.0	0.42859	-3.67958	-5.41145	122.0	1.08164	0.34081	-1.39106
34.0	0.47674	-3.21719	-4.94906	124.0	1.03478	0.14850	-1.58337
36.0	0.52616	-2.78883	-4.52071	126.0	0.98649	-0.05908	-1.79095
38.0	0.57660	-2.39126	-4.12313	128.0	0.93697	-0.28273	-2.01460
40.0	0.62781	-2.02172	-3.75359	130.0	0.88647	-0.52334	-2.25521
42.0	0.67953	-1.67788	-3.40975	132.0	0.83523	-0.78194	-2.51381
44.0	0.73152	-1.35774	-3.08961	134.0	0.78349	-1.05967	-2.79154
46.0	0.78351	-1.05956	-2.79143	136.0	0.73150	-1.35765	-3.08972
48.0	0.83525	-0.78183	-2.51370	138.0	0.67952	-1.67800	-3.40987
50.0	0.88649	-0.52324	-2.25511	140.0	0.62779	-2.02184	-3.75371
52.0	0.93699	-0.28263	-2.01450	142.0	0.57658	-2.39138	-4.12325
54.0	0.98651	-0.05899	-1.79086	144.0	0.52614	-2.78896	-4.52083
56.0	1.03481	0.14859	-1.58328	146.0	0.47672	-3.21732	-4.94920
58.0	1.08166	0.34089	-1.39098	148.0	0.42858	-3.67971	-5.41159
60.0	1.12684	0.51863	-1.21324	150.0	0.38194	-4.18001	-5.91188
62.0	1.17015	0.68243	-1.04944	152.0	0.33706	-4.72291	-6.45478
64.0	1.21139	0.83285	-0.89902	154.0	0.29416	-5.31413	-7.04600
66.0	1.25037	0.97038	-0.76149	156.0	0.25347	-5.96080	-7.69267
68.0	1.28691	1.09547	-0.63640	158.0	0.21518	-6.67189	-8.40376
70.0	1.32084	1.20849	-0.52338	160.0	0.17952	-7.45895	-9.19082
72.0	1.35201	1.30980	-0.42207	162.0	0.14665	-8.33719	-10.06906
74.0	1.38028	1.39968	-0.33219	164.0	0.11676	-9.32722	-11.05909
76.0	1.40553	1.47841	-0.25346	166.0	0.08998	-10.45793	-12.18980
78.0	1.42765	1.54621	-0.18566	168.0	0.06650	-11.77161	-13.50348
80.0	1.44653	1.60326	-0.12861	170.0	0.04641	-13.33387	-15.06574
82.0	1.46209	1.64973	-0.08214	172.0	0.02982	-15.25459	-16.98646
84.0	1.47426	1.68574	-0.04613	174.0	0.01683	-17.73977	-19.47164
86.0	1.48299	1.71139	-0.02048	176.0	0.00750	-21.25188	-22.98375
88.0	1.48825	1.72676	-0.00511	178.0	0.00188	-27.26665	-28.99853
90.0	1.49000	1.73187	0.0	180.	0.00000	-INFINITY	-INFINITY

$h/\lambda = 0.01$, $0 \leq ka \leq 3.0$.

TABLE A1-42

INTEGRAL EQUATION METHOD
EPSILON= 1.0000(NORMALIZED GROUNDPLANE RADIUS)
MONOPOLE LENGTH= 0.010000(WAVELENGTH)
INFINITELY THIN MONOPOLE RADIUS
RADIATION RESISTANCE = 0.019898 (OHMS)

ELEVATION ANGLE (DEG)	DIRECTIVITY (NUMERIC)	DIRECTIVITY (DBI)	RELATIVE POWER (DB)	ELEVATION ANGLE (DEG)	DIRECTIVITY (NUMERIC)	DIRECTIVITY (DBI)	RELATIVE POWER (DB)
0.	0.00000	-INFINITY	-INFINITY				
2.0	0.00189	-27.24179	-28.96770	92.0	1.48622	1.72082	-0.00509
4.0	0.00754	-21.22714	-22.95305	94.0	1.48100	1.70555	-0.02036
6.0	0.01692	-17.71522	-19.44113	96.0	1.47233	1.68005	-0.04586
8.0	0.02998	-15.23031	-16.95622	98.0	1.46025	1.64427	-0.08164
10.0	0.04667	-13.30994	-15.03585	100.0	1.44481	1.59810	-0.12781
12.0	0.06686	-11.74810	-13.47401	102.0	1.42607	1.54141	-0.18450
14.0	0.09047	-10.43491	-12.16082	104.0	1.40412	1.47405	-0.25186
16.0	0.11736	-9.30476	-11.03067	106.0	1.37905	1.39581	-0.33010
18.0	0.14739	-8.31536	-10.04127	108.0	1.35098	1.30648	-0.41943
20.0	0.18039	-7.43780	-9.16371	110.0	1.32002	1.20579	-0.52012
22.0	0.21620	-6.65148	-8.37739	112.0	1.28630	1.09344	-0.63247
24.0	0.25461	-5.94119	-7.66710	114.0	1.24999	0.96908	-0.75683
26.0	0.29544	-5.29537	-7.02128	116.0	1.21125	0.83232	-0.89359
28.0	0.33845	-4.70504	-6.43095	118.0	1.17023	0.68272	-1.04319
30.0	0.38344	-4.16308	-5.88899	120.0	1.12714	0.51979	-1.20612
32.0	0.43016	-3.66375	-5.38966	122.0	1.08217	0.34285	-1.38296
34.0	0.47837	-3.20236	-4.92827	124.0	1.03552	0.15158	-1.57423
36.0	0.52782	-2.77502	-4.50093	126.0	0.98741	-0.05502	-1.78093
38.0	0.57830	-2.37848	-4.10439	128.0	0.93806	-0.27767	-2.00358
40.0	0.62951	-2.01000	-3.73591	130.0	0.88772	-0.51726	-2.24317
42.0	0.68120	-1.66723	-3.39314	132.0	0.83660	-0.77482	-2.50073
44.0	0.73314	-1.34816	-3.07407	134.0	0.78496	-1.05150	-2.77741
46.0	0.78505	-1.05105	-2.77696	136.0	0.73306	-1.34863	-3.07454
48.0	0.83668	-0.77438	-2.50029	138.0	0.68113	-1.66772	-3.39363
50.0	0.88780	-0.51684	-2.24275	140.0	0.62943	-2.01051	-3.73642
52.0	0.93815	-0.27727	-2.00318	142.0	0.57823	-2.37900	-4.10491
54.0	0.98750	-0.05464	-1.78055	144.0	0.52777	-2.77555	-4.50146
56.0	1.03561	0.15195	-1.57396	146.0	0.47831	-3.20290	-4.92881
58.0	1.08225	0.34330	-1.38261	148.0	0.43010	-3.66431	-5.39022
60.0	1.12723	0.52011	-1.20580	150.0	0.38338	-4.16365	-5.88956
62.0	1.17032	0.68303	-1.04286	152.0	0.33841	-4.70562	-6.43153
64.0	1.21132	0.83261	-0.89330	154.0	0.29540	-5.29597	-7.02188
66.0	1.25007	0.96934	-0.75657	156.0	0.25458	-5.94180	-7.66771
68.0	1.28638	1.09358	-0.63223	158.0	0.21617	-6.65210	-8.37801
70.0	1.32008	1.20601	-0.51990	160.0	0.18037	-7.43842	-9.16433
72.0	1.35104	1.30668	-0.41923	162.0	0.14737	-8.31599	-10.04190
74.0	1.37911	1.39599	-0.32992	164.0	0.11734	-9.30540	-11.03131
76.0	1.40417	1.47421	-0.25170	166.0	0.09046	-10.43555	-12.16146
78.0	1.42612	1.54155	-0.18436	168.0	0.06685	-11.74875	-13.47466
80.0	1.44485	1.59822	-0.12770	170.0	0.04666	-13.31060	-15.03651
82.0	1.46028	1.64436	-0.08155	172.0	0.02998	-15.23097	-16.95688
84.0	1.47235	1.68012	-0.04579	174.0	0.01692	-17.71588	-19.44179
86.0	1.48101	1.70559	-0.02032	176.0	0.00754	-21.22780	-22.95371
88.0	1.48622	1.72084	-0.00507	178.0	0.00189	-27.24246	-28.96837
90.0	1.48796	1.72591	0.0	180.	0.00000	-INFINITY	-INFINITY

$h/\lambda = 0.01$, $0 \leq ka \leq 3.0$.

TABLE A1-43

INTEGRAL EQUATION METHOD
EPSILON= 1.25001(NORMALIZED GROUNDPLANE RADIUS)
MONOPOLE LENGTH= 0.010000(WAVELENGTH)
INFINITELY THIN MONOPOLE RADIUS
RADIATION RESISTANCE = 0.019916 (OHMS)

ELEVATION ANGLE (DEG)	DIRECTIVITY (NUMERIC)	DIRECTIVITY (DBI)	RELATIVE POWER (DB)	ELEVATION ANGLE (DEG)	DIRECTIVITY (NUMERIC)	DIRECTIVITY (DBI)	RELATIVE POWER (DB)
0	0.00000	-INFINITY	-INFINITY				
2.0	0.00189	-27.22511	-28.94725	92.0	1.48493	1.71705	-0.00509
4.0	0.00757	-21.21054	-22.93268	94.0	1.47973	1.70182	-0.02032
6.0	0.01699	-17.69875	-19.42089	96.0	1.47110	1.67641	-0.04573
8.0	0.03010	-15.21403	-16.93617	98.0	1.45907	1.64076	-0.08138
10.0	0.04684	-13.29390	-15.01604	100.0	1.44370	1.59476	-0.12738
12.0	0.06711	-11.73235	-13.45449	102.0	1.42505	1.53829	-0.18385
14.0	0.09078	-10.41949	-12.14163	104.0	1.40319	1.47118	-0.25097
16.0	0.11777	-9.28973	-11.01187	106.0	1.37824	1.39323	-0.32891
18.0	0.14789	-8.30075	-10.02289	108.0	1.35028	1.30424	-0.41791
20.0	0.18098	-7.42366	-9.14580	110.0	1.31945	1.20392	-0.51823
22.0	0.21688	-6.63785	-8.35999	112.0	1.28587	1.09197	-0.63017
24.0	0.25538	-5.92810	-7.65024	114.0	1.24970	0.96805	-0.75409
26.0	0.29629	-5.28285	-7.00500	116.0	1.21109	0.83177	-0.89038
28.0	0.33938	-4.69313	-6.41527	118.0	1.17022	0.68267	-1.03947
30.0	0.38443	-4.15179	-5.87394	120.0	1.12727	0.52027	-1.20187
32.0	0.43121	-3.65312	-5.37526	122.0	1.08243	0.34399	-1.37815
34.0	0.47947	-3.19240	-4.91454	124.0	1.03591	0.15321	-1.56893
36.0	0.52896	-2.76574	-4.48789	126.0	0.98792	-0.05279	-1.77493
38.0	0.57944	-2.36991	-4.09205	128.0	0.93868	-0.27481	-1.99695
40.0	0.63065	-2.00213	-3.72427	130.0	0.88843	-0.51376	-2.23590
42.0	0.68233	-1.66007	-3.38221	132.0	0.83740	-0.77066	-2.49280
44.0	0.73423	-1.34171	-3.06385	134.0	0.78584	-1.04668	-2.76882
46.0	0.78609	-1.04530	-2.76744	136.0	0.73398	-1.34313	-3.06528
48.0	0.83766	-0.76934	-2.49148	138.0	0.68210	-1.66155	-3.38369
50.0	0.88869	-0.51249	-2.23463	140.0	0.63043	-2.00366	-3.72580
52.0	0.93894	-0.27360	-1.99574	142.0	0.57923	-2.37148	-4.09362
54.0	0.98818	-0.05164	-1.77378	144.0	0.52877	-2.76736	-4.48951
56.0	1.03617	0.15431	-1.56784	146.0	0.47929	-3.19406	-4.91620
58.0	1.08269	0.34503	-1.37711	148.0	0.43104	-3.65482	-5.37696
60.0	1.12752	0.52124	-1.20090	150.0	0.38428	-4.15354	-5.87568
62.0	1.17047	0.68358	-1.03856	152.0	0.33924	-4.69491	-6.41705
64.0	1.21133	0.83262	-0.88953	154.0	0.29616	-5.28467	-7.00681
66.0	1.24992	0.96884	-0.75330	156.0	0.25527	-5.92895	-7.65209
68.0	1.28608	1.09269	-0.62945	158.0	0.21678	-6.63873	-8.36187
70.0	1.31965	1.20458	-0.51757	160.0	0.18090	-7.42557	-9.14871
72.0	1.35046	1.30483	-0.41731	162.0	0.14782	-8.30268	-10.02582
74.0	1.37840	1.39377	-0.32838	164.0	0.11771	-9.29169	-11.01383
76.0	1.40334	1.47164	-0.25050	166.0	0.09075	-10.42147	-12.14361
78.0	1.42518	1.53869	-0.18345	168.0	0.06708	-11.73434	-13.45649
80.0	1.44381	1.59510	-0.12705	170.0	0.04682	-13.29581	-15.01805
82.0	1.45916	1.64103	-0.08111	172.0	0.03009	-15.21606	-16.93830
84.0	1.47117	1.67661	-0.04553	174.0	0.01698	-17.70079	-19.42293
86.0	1.47977	1.70195	-0.02019	176.0	0.00756	-21.21258	-22.93472
88.0	1.48495	1.71711	-0.00503	178.0	0.00189	-27.22715	-28.94930
90.0	1.48667	1.72214	0.0	180.0	0.00000	-INFINITY	-INFINITY

$h/\lambda = 0.01$, $0 \leq ka \leq 3.0$.

TABLE A1-44

INTEGRAL EQUATION METHOD
EPSILON= 1 5000(NORMALIZED GROUNDPLANE RADIUS)
MONOPOLE LENGTH= 0.010000(WAVELENGTH)
INFINITELY THIN MONOPOLE RADIUS
RADIATION RESISTANCE = 0 019840 (OHMS)

ELEVATION ANGLE (DEG)	DIRECTIVITY (NUMERIC)	DIRECTIVITY (DBI)	RELATIVE POWER (DB)	ELEVATION ANGLE (DEG)	DIRECTIVITY (NUMERIC)	DIRECTIVITY (DBI)	RELATIVE POWER (DB)
0	0 00000	-INFINITY	-INFINITY				
2 0	0 00191	-27 19992	-28 91674	92.0	1 48310	1 71171	-0.00511
4 0	0 00761	-21 18547	-22 90229	94.0	1 47792	1 69652	-0.02030
6 0	0 01708	-17 67390	-19 39072	96 0	1 46934	1 67122	-0.04560
8 0	0 03027	-15 18947	-16 90629	98.0	1 45738	1 63573	-0.08109
10 0	0 04710	-13 26871	-14 98553	100 0	1 44210	1 58994	-0 12688
12 0	0 06747	-11 70861	-13 42543	102.0	1 42356	1 53375	-0 18307
14 0	0 09128	-10 39628	-12 11310	104 0	1 40183	1 46697	-0.24985
16 0	0 11838	-9 26711	-10.98393	106 0	1 37702	1 38941	-0.32741
18.0	0 14863	-8 27880	-9 99562	108.0	1 34923	1 30085	-0.41595
20 0	0 18187	-7 40243	-9 11925	110 0	1 31857	1 20103	-0.51579
22 0	0 21790	-6 61741	-8 33423	112 0	1 28518	1 08964	-0.62718
24 0	0 25654	-5 90850	-7 62532	114 0	1 24920	0 96632	-0.75050
26 0	0 29757	-5 26414	-6.98096	116 0	1 21079	0 83068	-0.88614
28 0	0 34077	-4 67534	-6 39216	118.0	1 17011	0 68228	-1.03454
30 0	0 38593	-4 13497	-5.85179	120.0	1 12736	0 52062	-1.19620
32 0	0 43278	-3 63728	-5.35410	122 0	1 08271	0 34512	-1.37170
34.0	0 48111	-3.17758	-4.89440	124.0	1 03637	0 15516	-1.56166
36 0	0 53064	-2 75197	-4 46879	126 0	0 98856	-0 04989	-1.76681
38.0	0 58114	-2.35719	-4.07401	128.0	0 93948	-0 27113	-1.98795
40 0	0 63234	-1.99047	-3 70729	130 0	0 88937	-0 50915	-2.22598
42 0	0 68400	-1.64947	-3.36629	132 0	0 83847	-0 76513	-2.48195
44 0	0 73584	-1.33217	-3.04899	134 0	0 78701	-1.04019	-2.75701
46.0	0 78762	-1.03681	-2.75363	136 0	0 73524	-1.33568	-3.05250
48 0	0 83910	-0 76189	-2.47871	138 0	0 68342	-1.65311	-3.36993
50 0	0.89001	-0.50606	-2.22288	140 0	0.63179	-1.99424	-3.71106
52.0	0.94012	-0.26817	-1.98499	142.0	0.58062	-2.36108	-4.07790
54 0	0.98920	-0.04717	-1 76399	144 0	0.53015	-2.75598	-4.47280
56 0	1.03701	0.15783	-1.55899	146 0	0.48065	-3.18171	-4.89853
58 0	1 08334	0 34764	-1.36918	148.0	0.43236	-3.64152	-5.35834
60 0	1.12797	0.52299	-1.19383	150 0	0 38554	-4.13931	-5.85613
62.0	1.17071	0.68450	-1 03232	152 0	0.34043	-4.67977	-6.39659
64 0	1 21136	0.83275	-0 88407	154 0	0.29726	-5.26867	-6.98549
66.0	1.24975	0.96823	-0.74859	156.0	0 25626	-5.91311	-7.62993
68.0	1.28570	1 09139	-0.62543	158 0	0.21767	-6.62211	-8.33893
70.0	1.31906	1.20263	-0.51419	160 0	0.18167	-7.40721	-9.12403
72 0	1 34968	1 30230	-0.41452	162 0	0 14847	-8.28364	-10.00046
74.0	1.37743	1.39070	-0.32612	164.0	0 11825	-9.27202	-10.98884
76 0	1.40220	1.46809	-0 24873	166 0	0.09118	-10.40124	-12.11806
78 0	1.42387	1 53471	-0.18211	168 0	0 06740	-11.71362	-13.43044
80 0	1 44236	1 59075	-0.12607	170.0	0.04705	-13 27476	-14.99158
82 0	1 45759	1.63637	-0.08045	172 0	0.03024	-15.19455	-16.91137
84 0	1 46950	1 67170	-0 04512	174 0	0.01706	-17.67900	-19.39582
86 0	1 47803	1 69684	-0.01998	176 0	0.00760	-21.19059	-22 90741
88.0	1 48316	1 71187	-0.00495	178 0	0 00190	-27.20505	-28.92187
90 0	1 48485	1 71682	0 0	180	0 00000	-INFINITY	-INFINITY

$h/\lambda = 0.01$, $0 \leq ka \leq 3.0$.

TABLE A1-45

INTEGRAL EQUATION METHOD
EPSILON= 1.7500(NORMALIZED GROUNDPLANE RADIUS)
MONOPOLE LENGTH= 0.010000(WAVELENGTH)
INFINITELY THIN MONOPOLE RADIUS
RADIATION RESISTANCE = 0.019997 (OHMS)

ELEVATION ANGLE (DEG)	DIRECTIVITY (NUMERIC)	DIRECTIVITY (DBI)	RELATIVE POWER (DB)	ELEVATION ANGLE (DEG)	DIRECTIVITY (NUMERIC)	DIRECTIVITY (DBI)	RELATIVE POWER (DB)
0	0.00000	-INFINITY	-INFINITY				
2.0	0.00193	-27.13917	-28.84367	92.0	1.47889	1.69937	-0.00519
4.0	0.00772	-21.12505	-22.82955	94.0	1.47377	1.68429	-0.02021
6.0	0.01732	-17.61402	-19.31852	96.0	1.46529	1.65923	-0.04527
8.0	0.03069	-15.13034	-16.83484	98.0	1.45349	1.62411	-0.08039
10.0	0.04774	-13.21154	-14.91604	100.0	1.43841	1.57883	-0.12567
12.0	0.06837	-11.65159	-13.35609	102.0	1.42012	1.52327	-0.18123
14.0	0.09246	-10.34060	-12.04510	104.0	1.39870	1.45725	-0.24725
16.0	0.11987	-9.21295	-10.91745	106.0	1.37423	1.38059	-0.32391
18.0	0.15044	-8.22632	-9.93082	108.0	1.34681	1.29305	-0.41145
20.0	0.18400	-7.35180	-9.05630	110.0	1.31655	1.19437	-0.51013
22.0	0.22036	-6.56876	-8.27326	112.0	1.28358	1.08424	-0.62026
24.0	0.25930	-5.86195	-7.56645	114.0	1.24805	0.96230	-0.74220
26.0	0.30062	-5.21981	-6.92431	116.0	1.21009	0.82817	-0.87633
28.0	0.34409	-4.63333	-6.33783	118.0	1.16987	0.68139	-1.02311
30.0	0.38946	-4.09536	-5.79986	120.0	1.12757	0.52145	-1.18305
32.0	0.43650	-3.60014	-5.30464	122.0	1.08337	0.34778	-1.35672
34.0	0.48496	-3.14296	-4.84746	124.0	1.03749	0.15974	-1.54476
36.0	0.53458	-2.71930	-4.42440	126.0	0.99006	-0.04338	-1.74788
38.0	0.58510	-2.32788	-4.03218	128.0	0.94137	-0.26742	-1.96692
40.0	0.63628	-1.96355	-3.66805	130.0	0.89161	-0.49827	-2.20277
42.0	0.68784	-1.62512	-3.32962	132.0	0.84101	-0.73199	-2.45649
44.0	0.73954	-1.31037	-3.01487	134.0	0.78982	-1.02474	-2.72924
46.0	0.79113	-1.01753	-2.72203	136.0	0.73827	-1.31787	-3.02237
48.0	0.84235	-0.74508	-2.44958	138.0	0.68661	-1.63292	-3.33742
50.0	0.89296	-0.49167	-2.19617	140.0	0.63509	-1.97162	-3.67612
52.0	0.94273	-0.25613	-1.96063	142.0	0.58398	-2.33604	-4.04054
54.0	0.99142	-0.03741	-1.74191	144.0	0.53352	-2.72851	-4.43301
56.0	1.03882	0.16540	-1.53910	146.0	0.48397	-3.15183	-4.85633
58.0	1.08470	0.35311	-1.35139	148.0	0.43559	-3.60926	-5.31376
60.0	1.12887	0.52645	-1.17805	150.0	0.38862	-4.10472	-5.80922
62.0	1.17113	0.68607	-1.01843	152.0	0.34333	-4.64291	-6.34741
64.0	1.21130	0.83252	-0.87198	154.0	0.29994	-5.22960	-6.93410
66.0	1.24920	0.96632	-0.73818	156.0	0.25871	-5.87194	-7.57644
68.0	1.28467	1.08792	-0.61658	158.0	0.21984	-6.57093	-8.28343
70.0	1.31757	1.19772	-0.50678	160.0	0.18356	-7.36215	-9.06665
72.0	1.34774	1.29607	-0.40843	162.0	0.15008	-8.23683	-9.94133
74.0	1.37508	1.38327	-0.32123	164.0	0.11957	-9.22360	-10.92810
76.0	1.39946	1.45960	-0.24490	166.0	0.09223	-10.35137	-12.05587
78.0	1.42078	1.52528	-0.17922	168.0	0.06829	-11.66247	-13.36697
80.0	1.43897	1.58051	-0.12399	170.0	0.04762	-13.22252	-14.92702
82.0	1.45394	1.62545	-0.07905	172.0	0.03061	-15.14140	-16.84590
84.0	1.46563	1.66024	-0.04426	174.0	0.01728	-17.62513	-19.32963
86.0	1.47400	1.68496	-0.01954	176.0	0.00770	-21.13621	-22.84071
88.0	1.47901	1.69970	-0.00480	178.0	0.00193	-27.15036	-28.85486
90.0	1.48064	1.70450	0.0	180	0.00000	-INFINITY	-INFINITY

$h/\lambda = 0.01$, $0 \leq ka \leq 3.0$.

TABLE A1-46

INTEGRAL EQUATION METHOD
EPSILON= ? 0000(NORMALIZED GROUNDPLANE RADIUS)
MONOPOLE LENGTH= 0.010000(WAVELENGTH)
INFINITELY THIN MONOPOLE RADIUS
RADIATION RESISTANCE = 0.020129 (OHMS)

ELEVATION ANGLE (DEG)	DIRECTIVITY (NUMERIC)	DIRECTIVITY (DBI)	RELATIVE POWER (DB)	ELEVATION ANGLE (DEG)	DIRECTIVITY (NUMERIC)	DIRECTIVITY (DBI)	RELATIVE POWER (DB)
0	0.00000	-INFINITY	-INFINITY				
2.0	0.00200	-26.99127	-28.66703	92.0	1.46914	1.67062	-0.00514
4.0	0.00798	-20.97800	-22.65376	94.0	1.46414	1.65584	-0.01992
6.0	0.01791	-17.46837	-19.14413	96.0	1.45591	1.63135	-0.04441
8.0	0.03172	-14.98665	-16.66241	98.0	1.44448	1.59711	-0.07865
10.0	0.04931	-13.07033	-14.74609	100.0	1.42986	1.55299	-0.12277
12.0	0.07058	-11.51337	-13.18913	102.0	1.41217	1.49888	-0.17688
14.0	0.09537	-10.20584	-11.88160	104.0	1.39143	1.43462	-0.24114
16.0	0.12353	-9.08212	-10.75788	106.0	1.36773	1.36000	-0.31575
18.0	0.15489	-8.09883	-9.77559	108.0	1.34116	1.27480	-0.40096
20.0	0.18923	-7.23003	-8.90579	110.0	1.31182	1.17875	-0.49701
22.0	0.22636	-6.45206	-8.12782	112.0	1.27983	1.07154	-0.60422
24.0	0.26603	-5.75063	-7.42639	114.0	1.24532	0.95282	-0.72294
26.0	0.30803	-5.11413	-6.78989	116.0	1.20842	0.82218	-0.85358
28.0	0.35209	-4.53352	-6.20928	118.0	1.16926	0.67918	-0.99658
30.0	0.39786	-4.00180	-5.67756	120.0	1.12805	0.52330	-1.15246
32.0	0.44539	-3.51256	-5.18832	122.0	1.08492	0.35396	-1.32180
34.0	0.49412	-3.06167	-4.73743	124.0	1.04004	0.17051	-1.50525
36.0	0.54386	-2.64498	-4.32071	126.0	0.99352	-0.02779	-1.70355
38.0	0.59442	-2.25910	-3.93486	128.0	0.94585	-0.24176	-1.91752
40.0	0.64546	-1.90130	-3.57706	130.0	0.89695	-0.47233	-2.14809
42.0	0.69676	-1.56917	-3.24493	132.0	0.84712	-0.72057	-2.39633
44.0	0.74806	-1.26062	-2.93638	134.0	0.79659	-0.98768	-2.66344
46.0	0.79912	-0.97387	-2.64963	136.0	0.74559	-1.27501	-2.95077
48.0	0.84970	-0.70735	-2.38311	138.0	0.69436	-1.58413	-3.25989
50.0	0.89956	-0.45971	-2.13547	140.0	0.64316	-1.91682	-3.59258
52.0	0.94847	-0.22975	-1.90551	142.0	0.59222	-2.27515	-3.95091
54.0	0.99623	-0.01639	-1.69215	144.0	0.54181	-2.66153	-4.33729
56.0	1.04263	0.18128	-1.49448	146.0	0.49218	-3.07875	-4.75451
58.0	1.08745	0.36411	-1.31165	148.0	0.44360	-3.53013	-5.20589
60.0	1.13053	0.53282	-1.14294	150.0	0.39631	-4.01963	-5.69539
62.0	1.17167	0.68807	-0.98769	152.0	0.35059	-4.55199	-6.22775
64.0	1.21072	0.83044	-0.84532	154.0	0.30669	-5.13302	-6.80878
66.0	1.24751	0.96043	-0.71533	156.0	0.26486	-5.76991	-7.44567
68.0	1.28189	1.07852	-0.59724	158.0	0.22534	-6.47171	-8.14747
70.0	1.31374	1.18509	-0.49067	160.0	0.18836	-7.25002	-8.92578
72.0	1.34292	1.28050	-0.39526	162.0	0.15417	-8.12013	-9.79589
74.0	1.36933	1.36507	-0.31069	164.0	0.12295	-9.10270	-10.77846
76.0	1.39285	1.43905	-0.23671	166.0	0.09491	-10.22667	-11.90243
78.0	1.41341	1.50268	-0.17308	168.0	0.07024	-11.53441	-13.21017
80.0	1.43092	1.55616	-0.11960	170.0	0.04907	-13.09156	-14.76732
82.0	1.44532	1.59964	-0.07612	172.0	0.03156	-15.00804	-16.68380
84.0	1.45655	1.63325	-0.04251	174.0	0.01782	-17.48988	-19.16564
86.0	1.46457	1.65710	-0.01866	176.0	0.00794	-20.99959	-22.67535
88.0	1.46935	1.67126	-0.00450	178.0	0.00199	-27.01281	-28.68857
90.0	1.47088	1.67576	0.0	180	0.00000	-INFINITY	-INFINITY

$h/\lambda = 0.01$, $0 \leq ka \leq 3.0$.

TABLE A1-47

INTEGRAL EQUATION METHOD
EPSILON= 2.2500(NORMALIZED GROUNDPLANE RADIUS)
MONOPOLE LENGTH= 0.010000(WAVELENGTH)
INFINITELY THIN MONOPOLE RADIUS
RADIATION RESISTANCE = 0.020430 (OHMS)

ELEVATION ANGLE (DEG)	DIRECTIVITY (NUMERIC)	DIRECTIVITY (DBI)	RELATIVE POWER (DB)	ELEVATION ANGLE (DEG)	DIRECTIVITY (NUMERIC)	DIRECTIVITY (DBI)	RELATIVE POWER (DB)
0.	0.00000	-INFINITY	-INFINITY				
2.0	0.00216	-26.65019	+28.26161	92.0	1.44757	1.60641	-0.00507
4.0	0.00863	-20.63892	+22.25040	94.0	1.44288	1.59230	-0.01918
6.0	0.01935	-17.13271	+18.74418	96.0	1.43519	1.56910	-0.04237
8.0	0.03423	-14.65572	+16.26719	98.0	1.42454	1.53675	-0.07472
10.0	0.05314	-12.74540	+14.35688	100.0	1.41096	1.49516	-0.11631
12.0	0.07593	+11.19568	+12.80715	102.0	1.39450	1.44420	-0.16728
14.0	0.10241	-9.89654	+11.50802	104.0	1.37522	1.38371	-0.22776
16.0	0.13235	+8.78229	+10.39376	106.0	1.35317	1.31352	-0.29796
18.0	0.16556	-7.81047	+9.42194	108.0	1.32843	1.23339	-0.37809
20.0	0.20174	-6.95205	+8.56352	110.0	1.30109	1.14306	-0.46841
22.0	0.24064	+6.18627	+7.79774	112.0	1.27123	1.04225	-0.56923
24.0	0.28198	-5.49774	+7.10921	114.0	1.23896	0.93058	-0.68089
26.0	0.32548	+4.87475	+6.48622	116.0	1.20439	0.80768	-0.80380
28.0	0.37084	+4.30813	+5.91961	118.0	1.16764	0.67308	-0.93840
30.0	0.41777	+3.79060	+5.40208	120.0	1.12882	0.52625	+1.08522
32.0	0.46599	+3.31625	+4.92772	122.0	1.08809	0.36664	+1.24484
34.0	0.51520	+2.88021	+4.49168	124.0	1.04557	0.19355	+1.41793
36.0	0.56514	+2.47842	+4.08990	126.0	1.00144	0.00624	+1.60524
38.0	0.61553	+2.10749	+3.71896	128.0	0.95584	-0.19615	+1.80763
40.0	0.66612	+1.76450	+3.37597	130.0	0.90895	-0.41458	+2.02606
42.0	0.71664	+1.44697	+3.05845	132.0	0.86096	+0.65015	+2.26163
44.0	0.76687	+1.15276	+2.76423	134.0	0.81206	-0.90411	+2.51559
46.0	0.81658	+0.88000	+2.49147	136.0	0.76245	-1.17787	+2.78935
48.0	0.86555	+0.62706	+2.23853	138.0	0.71235	-1.47306	+3.08454
50.0	0.91358	+0.39253	+2.00401	140.0	0.66198	-1.79154	+3.40301
52.0	0.96047	+0.17516	+1.78663	142.0	0.61156	-2.13545	+3.74692
54.0	1.00604	0.02615	+1.58532	144.0	0.56140	-2.50727	+4.11874
56.0	1.05012	0.21238	+1.39908	146.0	0.51169	-2.90990	+4.52137
58.0	1.09254	0.38437	+1.22710	148.0	0.46273	-3.34676	+4.95823
60.0	1.13316	0.54289	+1.06858	150.0	0.41477	-3.82188	+5.43336
62.0	1.17182	0.68860	+0.92287	152.0	0.36812	-4.34014	+5.95162
64.0	1.20840	0.82209	+0.78938	154.0	0.32304	+4.90744	+6.51892
66.0	1.24276	0.94388	+0.66759	156.0	0.27983	-5.53108	+7.14255
68.0	1.27480	1.05449	+0.55704	158.0	0.23877	+6.22020	+7.83167
70.0	1.30441	1.15413	+0.45734	160.0	0.20015	-6.98653	+8.59800
72.0	1.33148	1.24334	+0.36819	162.0	0.16423	+7.84545	+9.45692
74.0	1.35593	1.32236	+0.28912	164.0	0.13129	-8.81771	+10.42919
76.0	1.37767	1.39144	+0.22003	166.0	0.10157	-9.93236	+11.54384
78.0	1.39663	1.45082	+0.16066	168.0	0.07530	+11.23184	+12.84332
80.0	1.41275	1.50067	+0.11080	170.0	0.05270	+12.78186	+14.39334
82.0	1.42599	1.54116	+0.07031	172.0	0.03394	+14.69242	+16.30389
84.0	1.43628	1.57241	+0.03907	174.0	0.01919	+17.16959	+18.78107
86.0	1.44361	1.59450	+0.01698	176.0	0.00856	+20.67594	+22.28742
88.0	1.44794	1.60751	+0.00397	178.0	0.00214	+26.68723	+28.29871
90.0	1.44926	1.61147	0.0	180	0.00000	-INFINITY	-INFINITY

$h/\lambda = 0.01$, $0 \leq ka \leq 3.0$.

TABLE A1-48

INTEGRAL EQUATION METHOD
EPS(LOW= 2 5000 NORMALIZED GROUNDPLANE RADIUS)
MONOPOLE LENGTH= 0.010000(WAVELENGTH)
INFINITELY THIN MONOPOLE RADIUS
RADIATION RESISTANCE = 0.021093 (OHMS)

ELEVATION ANGLE (DEG)	DIRECTIVITY (NUMERIC)	DIRECTIVITY (DBI)	RELATIVE POWER (DB)	ELEVATION ANGLE (DEG)	DIRECTIVITY (NUMERIC)	DIRECTIVITY (DBI)	RELATIVE POWER (DB)
0	0 00000	-INFINITY	-INFINITY				
2 0	0 00255	-25 93310	-27 40572	92 0	1 40210	1 46780	-0 00481
4 0	0 01017	-19 92621	-21 39883	94 0	1 39803	1 45517	-0 01745
6 0	0 02277	-16 42717	-17 89978	96 0	1 39145	1 43467	-0 03795
8 0	0 04018	-13 96013	-15 43274	98 0	1 38237	1 40626	-0 06636
10 0	0 06219	-12 06246	-13 53507	100 0	1 37084	1 36986	-0 10275
12 0	0 08855	-10 52797	-12 00059	102 0	1 35687	1 32538	-0 14724
14 0	0 11894	-9 24654	-10 71916	104 0	1 34050	1 27268	-0 19993
16 0	0 15303	-8 15231	-9 62492	106 0	1 32179	1 21162	-0 26100
18 0	0 19043	-7 20265	-8 67527	108 0	1 30077	1 14199	-0 33062
20 0	0 23076	-6 36837	-7 84098	110 0	1 27748	1 06357	-0 40904
22 0	0 27362	-5 62849	-7 10110	112 0	1 25201	0 97609	-0 49653
24 0	0 31861	-4 96742	-6 44004	114 0	1 22439	0 87921	-0 59340
26 0	0 36532	-4 37323	-5 84584	116 0	1 19469	0 77257	-0 70005
28 0	0 41338	-3 83652	-5 30914	118 0	1 16298	0 65571	-0 81690
30 0	0 46240	-3 34978	-4 82240	120 0	1 12931	0 52813	-0 94449
32 0	0 51205	-2 90686	-4 37948	122 0	1 09376	0 38922	-1 08340
34 0	0 56200	-2 50267	-3 97528	124 0	1 05640	0 23830	-1 23432
36 0	0 61194	-2 13293	-3 60554	126 0	1 01732	0 07457	-1 39804
38 0	0 66161	-1 79400	-3 26662	128 0	0 97659	-0 10287	-1 57548
40 0	0 71076	-1 48278	-2 95540	130 0	0 93432	-0 29506	-1 76767
42 0	0 75917	-1 19659	-2 66921	132 0	0 89060	-0 50318	-1 97580
44 0	0 80666	-0 93310	-2 40571	134 0	0 84555	-0 72860	-2 20122
46 0	0 85305	-0 69027	-2 16289	136 0	0 79931	-0 97286	-2 44548
48 0	0 89818	-0 46634	-1 93896	138 0	0 75202	-1 23773	-2 71035
50 0	0 94194	-0 25976	-1 73238	140 0	0 70384	-1 52524	-2 99785
52 0	0 98420	-0 06916	-1 54178	142 0	0 65498	-1 83770	-3 31031
54 0	1 02486	0 10665	-1 36597	144 0	0 60565	-2 17780	-3 65042
56 0	1 06383	0 26870	-1 20391	146 0	0 55608	-2 54865	-4 02127
58 0	1 10101	0 41793	-1 05469	148 0	0 50654	-2 95388	-4 42650
60 0	1 13635	0 55511	-0 91751	150 0	0 45732	-3 39777	-4 87038
62 0	1 16975	0 68094	-0 79167	152 0	0 40875	-3 88540	-5 35801
64 0	1 20117	0 79603	-0 67659	154 0	0 36117	-4 42293	-5 89554
66 0	1 23052	0 90089	-0 57173	156 0	0 31493	-5 01787	-6 49049
68 0	1 25776	0 99597	-0 47664	158 0	0 27042	-5 67962	-7 15223
70 0	1 28282	1 08165	-0 39086	160 0	0 22803	-6 42011	-7 89273
72 0	1 30565	1 15827	-0 31435	162 0	0 18815	-7 25494	-8 72756
74 0	1 32620	1 22608	-0 24653	164 0	0 15118	-8 20507	-9 67769
76 0	1 34442	1 28534	-0 18728	166 0	0 11750	-9 29973	-10 77234
78 0	1 36026	1 33622	-0 13639	168 0	0 08747	-10 58152	-12 05413
80 0	1 37369	1 37889	-0 09372	170 0	0 06143	-12 11630	-13 58892
82 0	1 38468	1 41349	-0 05913	172 0	0 03968	-14 01421	-15 48683
84 0	1 39318	1 44008	-0 03253	174 0	0 02248	-16 48144	-17 95406
86 0	1 39919	1 45877	-0 01384	176 0	0 01004	-19 98062	-21 45323
88 0	1 40269	1 46961	-0 00301	178 0	0 00252	-25 98759	-27 46020
90 0	1 40386	1 47262	0 0	180	0 00000	-INFINITY	-INFINITY

$h/\lambda = 0.01$, $0 \leq ka \leq 3.0$.

TABLE A1-49

INTEGRAL EQUATION METHOD
EPSILON= 2.7500(NORMALIZED GROUNDPLANE RADIUS)
MONOPOLE LENGTH= 0.010000(WAVELENGTH)
INFINITELY THIN MONOPOLE RADIUS
RADIATION RESISTANCE = 0.022546 (OHMS)

Method gives poor results for $\epsilon > 2.5$.

ELEVATION ANGLE (DEG)	DIRECTIVITY (NUMERIC)	DIRECTIVITY (DBI)	RELATIVE POWER (DB)	ELEVATION ANGLE (DEG)	DIRECTIVITY (NUMERIC)	DIRECTIVITY (DBI)	RELATIVE POWER (DB)
0	0.00000	-INFINITY	-INFINITY				
2.0	5.13099	7.10202	0.0	92.0	1.30845	1.16759	-5.93443
4.0	1.25506	0.98666	-6.11536	94.0	1.30203	1.14622	-5.95580
6.0	0.54526	-2.63398	-9.73601	96.0	1.29399	1.11932	-5.98269
8.0	0.29948	-5.23632	-12.33834	98.0	1.28436	1.08687	-6.01514
10.0	0.18691	-7.28357	-14.38559	100.0	1.27316	1.04884	-6.05318
12.0	0.12640	-8.98260	-16.08461	102.0	1.26043	1.00517	-6.09684
14.0	0.09028	-10.44428	-17.54631	104.0	1.24618	0.95582	-6.14619
16.0	0.06706	-11.73542	-18.83743	106.0	1.23047	0.90071	-6.20131
18.0	0.05129	-12.89964	-20.00165	108.0	1.21331	0.83973	-6.26229
20.0	0.04011	-13.96746	-21.06947	110.0	1.19474	0.77274	-6.32928
22.0	0.03191	-14.96141	-22.06342	112.0	1.17478	0.69955	-6.40247
24.0	0.02571	-15.89903	-23.00104	114.0	1.15343	0.61983	-6.48209
26.0	0.02092	-16.79472	-23.89674	116.0	1.13072	0.53356	-6.56846
28.0	0.01714	-17.66100	-24.76302	118.0	1.10664	0.44005	-6.66197
30.0	0.01409	-18.50946	-25.61147	120.0	1.08116	0.33892	-6.76310
32.0	0.01161	-19.35158	-26.45359	122.0	1.05428	0.22958	-6.87244
34.0	0.00955	-20.19963	-27.30164	124.0	1.02596	0.11130	-6.99072
36.0	0.00782	-21.06777	-28.16979	126.0	0.99615	-0.01677	-7.11878
38.0	0.00635	-21.97367	-29.07569	128.0	0.96480	-0.15564	-7.25766
40.0	0.00508	-22.94121	-30.04322	130.0	0.93186	-0.30651	-7.40853
42.0	0.00398	-24.00548	-31.10750	132.0	0.89727	-0.47076	-7.57277
44.0	0.00300	-25.22343	-32.32545	134.0	0.86100	-0.64997	-7.75198
46.0	0.00214	-26.69876	-33.80078	136.0	0.82300	-0.84599	-7.94800
48.0	0.00136	-28.66722	-35.76924	138.0	0.78327	-1.06088	-8.16290
50.0	0.00065	-31.86507	-38.96709	140.0	0.74182	-1.29704	-8.39905
52.0	1.07833	0.33153	-6.77048	142.0	0.69869	-1.55716	-8.65918
54.0	1.10870	0.44816	-6.65386	144.0	0.65398	-1.84433	-8.94635
56.0	1.13582	0.55309	-6.54892	146.0	0.60764	-2.16208	-9.26410
58.0	1.16077	0.64746	-6.45456	148.0	0.56047	-2.51447	-9.61649
60.0	1.18365	0.73222	-6.36979	150.0	0.51213	-2.90621	-10.00822
62.0	1.20454	0.80821	-6.29381	152.0	0.46315	-3.34261	-10.44483
64.0	1.22352	0.87612	-6.22590	154.0	0.41392	-3.83085	-10.93286
66.0	1.24066	0.93653	-6.16548	156.0	0.36490	-4.37825	-11.48026
68.0	1.25601	0.98995	-6.11207	158.0	0.31661	-4.99478	-12.09679
70.0	1.26962	1.03674	-6.06527	160.0	0.26960	-5.69274	-12.79476
72.0	1.28151	1.07724	-6.02478	162.0	0.22448	-6.48807	-13.59009
74.0	1.29172	1.11168	-5.99034	164.0	0.18189	-7.40203	-14.50404
76.0	1.30024	1.14024	-5.96177	166.0	0.14243	-8.46411	-15.56613
78.0	1.30710	1.16308	-5.93893	168.0	0.10673	-9.71718	-16.81920
80.0	1.31229	1.18029	-5.92173	170.0	0.07538	-11.22731	-18.32933
82.0	1.31581	1.19193	-5.91009	172.0	0.04892	-13.10481	-20.20682
84.0	1.31766	1.19805	-5.90397	174.0	0.02792	-15.55600	-22.65802
86.0	1.31785	1.19867	-5.90335	176.0	0.01246	-19.04365	-26.14567
88.0	1.31638	1.19380	-5.90821	178.0	0.00313	-25.04367	-32.14568
90.0	1.31324	1.18344	-5.91857	180	0.00000	-INFINITY	-INFINITY

$h/\lambda = 0.01$, $0 \leq ka \leq 3.0$.

A.2 METHOD OF MOMENTS—FREE SPACE

$0 < ka \leq 14.0$, $h/\lambda = 0.25$, $b/\lambda = 10^{-6}$, $N = 1$ (Tables A2-1–A2-57).
Experimental Monopole Antennas: $h/\lambda \approx 0.25$, $b = 0.25$ in., $N = 4$ (Tables A2-58–A2-66).

TABLE A2-1 $2\pi a/\lambda = 0.25$

EFFECT (.25000=NUMBERIZED GROUNDPLANE RADIUS)
MONOPOLE LENGTH= 0 250000(WAVELENGTH)
MONOPOLE RADIUS= 0 1000E-03(WAVELENGTH)
NUMBER OF MONOPOLE SEGMENTS= 1
NUMBER OF DISK SEGMENTS= 1
RADIATION RESISTANCE DETERMINED BY PATTERN= 0 194895E+02 OHMS

ELEVATION ANGLE (DEG)	DIRECTIVITY (NUMERIC)	DIRECTIVITY (DBI)	RELATIVE POWER (DB)	ELEVATION ANGLE (DEG)	DIRECTIVITY (NUMERIC)	DIRECTIVITY (DBI)	RELATIVE POWER (DB)
0	0 00000	-INFINITY	INFINITY				
2 0	0 00164	-27 84266	-29 71598	92 0	1 53717	1 86723	-0 00598
4 0	0 00657	-21 82525	-23 69846	94 0	1 53083	1 84927	-0 02395
6 0	0 01476	-18 30874	-20 18196	96 0	1 52030	1 81930	-0 05392
8 0	0 02620	-15 81745	-17 69066	98 0	1 50566	1 77727	-0 09594
10 0	0 04084	-13 88892	-15 76213	100 0	1 48700	1 72312	-0 15010
12 0	0 05865	-12 31719	-14 19040	102 0	1 46445	1 65675	-0 21647
14 0	0 07957	-10 99243	-12 86564	104 0	1 43815	1 57805	-0 29517
16 0	0 10354	-9 84909	-11 72230	106. 0	1. 40828	1 48688	-0 38634
18 0	0 13047	-8 84494	-10 71815	108 0	1 37502	1 38307	-0 49014
20 0	0 16028	-7. 95115	-9 82437	110 0	1 33838	1 26644	-0. 60677
22 0	0 19288	-7 14721	-9 02042	112 0	1 29920	1 13675	-0 73646
24 0	0 22814	-6 41797	-8 29119	114 0	1. 25711	0 99374	-0. 87947
26 0	0 26595	-5 75199	-7 62521	116. 0	1. 21258	0 83712	-1 03610
28 0	0 30617	-5. 14038	-7 01360	118. 0	1. 16587	0 66652	-1. 20669
30 0	0 34865	-4. 57613	-6. 44934	120 0	1. 11726	0 48156	-1 39166
32 0	0 39322	-4 05361	-5. 92682	122 0	1. 06703	0 28177	-1 59144
34 0	0 43972	-3 56823	-5 44145	124 0	1 01546	0 06665	-1 80657
36 0	0 48795	-3 11624	-4. 98946	126 0	0 96285	-0 16441	-2 03763
38 0	0. 53771	-2. 69451	-4. 56772	128. 0	0. 90947	-0. 41210	-2. 28531
40. 0	0 58879	-2. 30040	-4. 17361	130 0	0. 85562	-0. 67718	-2. 55040
42 0	0. 64096	-1 93171	-3. 80492	132. 0	0. 80157	-0. 96057	-2 83378
44 0	0 69398	-1 58654	-3. 45975	134 0	0. 74760	-1. 26329	-3. 13651
46. 0	0 74760	-1 26329	-3. 13650	136 0	0. 69398	-1. 58655	-3. 45976
48 0	0 80157	-0 96036	-2 83378	138 0	0. 64096	-1. 93171	-3. 80493
50 0	0 85562	-0 67718	-2 55039	140. 0	0. 58879	-2. 30041	-4. 17362
52 0	0 90948	-0 41209	-2. 28531	142 0	0. 53771	-2. 69451	-4. 56773
54 0	0 96285	-0 16441	-2 03762	144. 0	0. 48795	-3. 11625	-4. 98946
56 0	1 01547	0 06665	-1. 80656	146 0	0 43972	-3 56824	-5 44145
58 0	1. 06703	0 28178	-1 59144	148. 0	0. 39322	-4. 05361	-5. 92683
60 0	1 11727	0 48156	-1 39165	150. 0	0. 34865	-4. 57614	-6 44935
62 0	1 16588	0 66652	-1 20669	152 0	0. 30617	-5. 14039	-7. 01361
64 0	1 21258	0 83712	-1. 03609	154 0	0. 26595	-5. 75200	-7 62522
66 0	1 25711	0 99375	-0 87947	156 0	0. 22814	-6. 41798	-8 29120
68 0	1 29920	1 13676	-0. 73646	158 0	0. 19288	-7. 14722	-9 02043
70 0	1 33838	1 26644	-0. 60677	160 0	0. 16029	-7. 95116	-9 82438
72 0	1 37502	1 38308	-0 49014	162 0	0. 13047	-8 84495	-10 71816
74 0	1 40828	1 48688	-0. 38633	164 0	0. 10354	-9. 84910	-11. 72231
76 0	1 43815	1 57805	-0 29516	166. 0	0. 07957	-10 99243	-12 86565
78 0	1 46445	1 65675	-0. 21646	168 0	0. 05865	-12. 31720	-14 19041
80 0	1 48700	1 72312	-0. 15010	170. 0	0. 04084	-13 88892	-15 76214
82. 0	1 50566	1 77727	-0. 09594	172 0	0. 02620	-15. 81746	-17 69067
84 0	1 52030	1 81930	-0 05392	174 0	0. 01476	-18 30875	-20 18197
86 0	1 53083	1 84927	-0 02395	176. 0	0 00657	-21. 82526	-23 69847
88 0	1 53717	1 86723	-0 00598	178. 0	0. 00164	-27 84267	-29 71599
90 0	1 53929	1 87321	0 00000	180.	0. 00000	-INFINITY	-INFINITY

TABLE A2-2 $2\pi a/\lambda = 0.50$

```
EPSLNE = 5000(NORMALIZED GROUNDPLANE RADIUS)
MONOPOLE LENGTH= 0 250000(WAVELENGTH)
MONOPOLE RADIUS=  0 1000E-05(WAVELENGTH)
NUMBER OF MONOPOLE SEGMENTS=  1
NUMBER OF DISK SEGMENTS=  7
RADIATION RESISTANCE DETERMINED BY PATTERN= 0 196224E+02 OHMS
```

ELEVATION ANGLE (DEG)	DIRECTIVITY (NUMERIC)	DIRECTIVITY (DBI)	RELATIVE POWER (DB)	ELEVATION ANGLE (DEG)	DIRECTIVITY (NUMERIC)	DIRECTIVITY (DBI)	RELATIVE POWER (DB)
0	0 00000	-INFINITY	-INFINITY				
2 0	0 00169	-27 72040	-29 56410	92 0	1 52682	1 83789	-0 00581
4 0	0 00676	-21 70354	-23 54724	94 0	1 52071	1 82047	-0 02323
6 0	0 01518	-18 18796	-20 03166	96 0	1 51057	1 79141	-0 05229
8 0	0 02693	-15 69795	-17 54165	98 0	1 49646	1 75065	-0 09304
10 0	0 04197	-13 77107	-15 61476	100 0	1 47847	1 69812	-0 14557
12 0	0 06024	-12 20133	-14 04503	102 0	1 45671	1 63373	-0 20997
14 0	0 08168	-10 87890	-12 72260	104 0	1 43131	1 55733	-0 28636
16 0	0 10621	-9 73822	-11 58192	106 0	1 40243	1 46880	-0 37490
18 0	0 13375	-8 73704	-10 58074	108 0	1 37023	1 36794	-0 47576
20 0	0 16419	-7 84653	-9 69023	110 0	1 33492	1 25455	-0 58915
22 0	0 19742	-7 04614	-8 88984	112 0	1 29670	1 12839	-0 71531
24 0	0 23331	-6 32073	-8 16442	114 0	1 25579	0 98918	-0 85452
26 0	0 27172	-5 66892	-7 50251	116 0	1 21244	0 83659	-1 00711
28 0	0 31250	-5 05150	-6 88520	118 0	1 16688	0 67027	-1 17343
30 0	0 35549	-4 49175	-6 32545	120 0	1 11938	0 48978	-1 35392
32 0	0 40051	-3 97391	-5 80761	122 0	1 07020	0 29466	-1 54904
34 0	0 44736	-3 49339	-5 32708	124 0	1 01961	0 08436	-1 73924
36 0	0 49586	-3 04638	-4 88008	126 0	0 96789	-0 14174	-1 98544
38 0	0 54579	-2 62975	-4 47344	128 0	0 91530	-0 38434	-2 22804
40 0	0 59692	-2 24083	-4 08453	130 0	0 86213	-0 64426	-2 48795
42 0	0 64903	-1 87736	-3 72108	132 0	0 80865	-0 92241	-2 76610
44 0	0 70186	-1 53751	-3 38120	134 0	0 75512	-1 21985	-3 06355
46 0	0 75517	-1 21955	-3 06325	136 0	0 70181	-1 53781	-3 38151
48 0	0 80870	-0 92212	-2 76581	138 0	0 64898	-1 87770	-3 72140
50 0	0 86219	-0 64398	-2 48767	140 0	0 59688	-2 24113	-4 08485
52 0	0 91536	-0 38407	-2 22777	142 0	0 54575	-2 63008	-4 47378
54 0	0 96795	-0 14148	-1 98518	144 0	0 49582	-3 04672	-4 89042
56 0	1 01967	0 08461	-1 75909	146 0	0 44733	-3 49373	-5 33743
58 0	1 07026	0 29489	-1 54880	148 0	0 40047	-3 97427	-5 81796
60 0	1 11944	0 49000	-1 35370	150 0	0 35546	-4 49211	-6 33581
62 0	1 16694	0 67047	-1 17322	152 0	0 31247	-5 05187	-6 89557
64 0	1 21249	0 83679	-1 00691	154 0	0 27169	-5 65919	-7 50288
66 0	1 25585	0 98936	-0 85434	156 0	0 23329	-6 32110	-8 16480
68 0	1 29675	1 12856	-0 71514	158 0	0 19740	-7 04652	-8 89022
70 0	1 33497	1 25471	-0 58899	160 0	0 16418	-7 84691	-9 69061
72 0	1 37028	1 36808	-0 47562	162 0	0 13374	-8 73743	-10 58113
74 0	1 40247	1 46892	-0 37477	164 0	0 10620	-9 73861	-11 58231
76 0	1 43135	1 55744	-0 28625	166 0	0 08167	-10 87929	-12 72299
78 0	1 45674	1 63382	-0 20988	168 0	0 06023	-12 20173	-14 04542
80 0	1 47850	1 69820	-0 14549	170 0	0 04196	-13 77146	-15 61516
82 0	1 49648	1 75072	-0 09298	172 0	0 02693	-15 69835	-17 54205
84 0	1 51059	1 79146	-0 05224	174 0	0 01518	-18 18836	-20 03206
86 0	1 52072	1 82050	-0 02319	176 0	0 00675	-21 70394	-23 54764
88 0	1 52683	1 83791	-0 00579	178 0	0 00169	-27 72080	-29 56450
90 0	1 52887	1 84370	0 00000	180.	0. 00000	-INFINITY	-INFINITY

TABLE A2-3 $2\pi a/\lambda = 0.75$

```
FPSLN= 0. 7500<NORMALIZED GROUNDPLANE RADIUS)
MONOPOLE LENGTH= 0 250000(WAVELENGTH)
MONOPOLE RADIUS=   0 1000E-05(WAVELENGTH)
NUMBER OF MONOPOLE SEGMENTS=  1
NUMBER OF DISK SEGMENTS= 16
RADIATION RESISTANCE DETERMINED BY PATTERN= 0 198576E+02 OHMS
```

ELEVATION ANGLE (DEG)	DIRECTIVITY (NUMERIC)	DIRECTIVITY (DBI)	RELATIVE POWER (DB)	ELEVATION ANGLE (DEG)	DIRECTIVITY (NUMERIC)	DIRECTIVITY (DBI)	RELATIVE POWER (DB)
0	0 00000	-INFINITY	-INFINITY				
2 0	0 00177	-27. 50945	-29 30139	92. 0	1 50882	1 78638	-0. 00556
4 0	0 00709	-21 49354	-23 28548	94 0	1 50309	1 76985	-0 02208
6 0	0. 01592	-17 97953	-19. 77147	96. 0	1. 49359	1. 74232	-0. 04961
8 0	0 02824	-15 49172	-17 28365	98 0	1 48038	1 70372	-0 08821
10 0	0 04398	-13 56763	-15 35957	100. 0	1 46351	1 65397	-0. 13797
12 0	0 06308	-12. 00129	-13 79323	102. 0	1 44310	1 59295	-0. 19898
14 0	0 08545	-10. 68284	-12. 47477	104. 0	1. 41923	1 52053	-0. 27141
16 0	0 11100	-9 54670	-11 33863	106. 0	1 39204	1 43652	-0. 35541
18 0	0 13962	-8. 55059	-10 34253	108. 0	1. 36168	1. 34074	-0. 45119
20 0	0 17117	-7 66567	-9 45760	110 0	1 32830	1 23295	-0. 55899
22. 0	0 20552	-6 87135	-8 66329	112. 0	1. 29207	1 11287	-0. 67906
24 0	0 24252	-6. 15248	-7 94442	114 0	1 25320	0 98020	-0. 81173
26 0	0 28200	-5. 49753	-7 28947	116. 0	1 21188	0 83459	-0. 95735
28 0	0 32377	-4 89758	-6 68951	118. 0	1 16832	0 67562	-1. 11631
30 0	0 36766	-4. 34354	-6 13748	120. 0	1. 12276	0. 50286	-1. 28908
32 0	0 41345	-3 83575	-5 62768	122. 0	1 07542	0 31577	-1. 47617
34 0	0. 46094	-3. 36354	-5 15548	124. 0	1. 02654	0. 11378	-1. 67816
36 0	0 50990	-2 92511	-4 71705	126. 0	0. 97639	-0. 10377	-1. 89571
38 0	0 56011	-2 51724	-4 30918	128. 0	0. 92520	-0. 33764	-2. 12957
40 0	0. 61133	-2. 13726	-3 92920	130. 0	0. 87324	-0. 58866	-2 39060
42 0	0. 66331	-1 78287	-3 57480	132. 0	0. 82076	-0. 85781	-2. 64975
44 0	0 71580	-1 45211	-3 24405	134. 0	0. 76803	-1. 14620	-2. 93814
46 0	0 76854	-1. 14331	-2 93525	136. 0	0. 71531	-1. 45508	-3. 24702
48 0	0 82129	-0 85302	-2 64693	138. 0	0. 66284	-1. 78592	-3. 57785
50 0	0 87378	-0 58596	-2 37790	140. 0	0. 61089	-2. 14039	-3. 93232
52 0	0 92576	-0 33503	-2 12697	142. 0	0. 55970	-2. 52044	-4. 31238
54 0	0 97695	-0 10128	-1. 89321	144. 0	0. 50952	-2. 92838	-4. 72031
56. 0	1 02711	0 11617	-1. 67577	146. 0	0. 46059	-3. 36687	-5 15881
58 0	1 07598	0. 31804	-1 47389	148. 0	0. 41313	-3. 83913	-5. 63107
60. 0	1 12331	0 50501	-1 28692	150. 0	0. 36737	-4. 34698	-6. 14092
62 0	1 16887	0. 67766	-1 11428	152. 0	0. 32351	-4. 90107	-6. 69300
64 0	1 21241	0. 83650	-0 95544	154. 0	0. 28177	-5. 50107	-7. 29300
66 0	1 25371	0 98198	-0 80995	156. 0	0. 24232	-6. 15606	-7 94799
68 0	1 29256	1. 11452	-0 67742	158. 0	0. 20535	-6. 87497	-8 66691
70. 0	1 32876	1 23446	-0 55748	160. 0	0. 17103	-7. 66932	-9. 46125
72 0	1 36211	1 34211	-0 44983	162. 0	0. 13950	-8. 55427	-10 34621
74 0	1 39243	1 43775	-0 35419	164. 0	0. 11091	-9. 55040	-11. 34234
76 0	1 41958	1. 52160	-0 27033	166. 0	0. 08538	-10. 68657	-12 47850
78 0	1 44340	1 59388	-0 19806	168. 0	0. 06302	-12 00504	-13 79698
80 0	1 46378	1. 65475	-0 13719	170. 0	0. 04394	-13. 57140	-15. 36334
82 0	1 48059	1. 70435	-0 08759	172. 0	0. 02821	-15 49550	-17 28744
84 0	1 49375	1 74279	-0 04915	174. 0	0. 01591	-17. 98303	-19. 77526
86 0	1 50320	1. 77017	-0 02177	176. 0	0. 00709	-21. 49734	-23 28928
88 0	1 50888	1 78654	-0 00540	178. 0	0. 00177	-27. 51326	-29. 30519
90 0	1 51075	1 79194	0 00000	180	0 00000	-INFINITY	-INFINITY

TABLE A2-4 $2\pi a/\lambda = 1.00$

```
EPSLN= 1.0000(NORMALIZED GROUNDPLANE RADIUS)
MONOPOLE LENGTH= 0.250000(WAVELENGTH)
MONOPOLE RADIUS=  0.1000E-05(WAVELENGTH)
NUMBER OF MONOPOLE SEGMENTS=  1
NUMBER OF DISK SEGMENTS= 16
RADIATION RESISTANCE DETERMINED BY PATTERN= 0.202093E+02 OHMS
```

ELEVATION ANGLE (DEG)	DIRECTIVITY (NUMERIC)	DIRECTIVITY (DBI)	RELATIVE POWER (DB)	ELEVATION ANGLE (DEG)	DIRECTIVITY (NUMERIC)	DIRECTIVITY (DBI)	RELATIVE POWER (DB)
0	0.00000	-INFINITY	-INFINITY				
2.0	0.00190	-27.20604	-28.92170	92.0	1.46262	1.71031	-0.00534
4.0	0.00760	-21.19146	-22.90712	94.0	1.47739	1.69494	-0.02072
6.0	0.01706	-17.67967	-19.39533	96.0	1.46875	1.66949	-0.04616
8.0	0.03023	-15.19495	-16.91060	98.0	1.45677	1.63390	-0.08176
10.0	0.04705	-13.27481	-14.99046	100.0	1.44147	1.58805	-0.12760
12.0	0.06740	-11.71326	-13.42891	102.0	1.42293	1.53182	-0.18383
14.0	0.09119	-10.40041	-12.11607	104.0	1.40121	1.46504	-0.25061
16.0	0.11829	-9.27068	-10.98633	106.0	1.37642	1.38751	-0.32814
18.0	0.14853	-8.28174	-9.99739	108.0	1.34865	1.29899	-0.41666
20.0	0.18177	-7.40472	-9.12037	110.0	1.31802	1.19921	-0.51644
22.0	0.21782	-6.61901	-8.33466	112.0	1.28465	1.08785	-0.62780
24.0	0.25648	-5.90939	-7.62505	114.0	1.24870	0.96457	-0.75109
26.0	0.29756	-5.26432	-6.97997	116.0	1.21030	0.82895	-0.88671
28.0	0.34082	-4.67481	-6.39047	118.0	1.16964	0.68054	-1.03512
30.0	0.38603	-4.13375	-5.84941	120.0	1.12689	0.51893	-1.19682
32.0	0.43297	-3.63540	-5.35105	122.0	1.08224	0.34325	-1.37240
34.0	0.48139	-3.17506	-4.89072	124.0	1.03590	0.15316	-1.56249
36.0	0.53102	-2.74886	-4.46451	126.0	0.98806	-0.05216	-1.76781
38.0	0.58163	-2.35353	-4.06919	128.0	0.93896	-0.27353	-1.98918
40.0	0.63295	-1.98634	-3.70199	130.0	0.88882	-0.51185	-2.22751
42.0	0.68471	-1.64492	-3.36058	132.0	0.83788	-0.76817	-2.48382
44.0	0.73667	-1.32728	-3.04293	134.0	0.78639	-1.04364	-2.75929
46.0	0.78856	-1.03166	-2.74731	136.0	0.73458	-1.33959	-3.05524
48.0	0.84013	-0.75634	-2.47219	138.0	0.68272	-1.65754	-3.37320
50.0	0.89113	-0.50060	-2.21625	140.0	0.63107	-1.99925	-3.71490
52.0	0.94131	-0.26267	-1.97832	142.0	0.57997	-2.36671	-4.08237
54.0	0.99044	-0.04171	-1.75737	144.0	0.52938	-2.76229	-4.47794
56.0	1.03829	0.16218	-1.55348	146.0	0.47987	-3.18872	-4.90438
58.0	1.08463	0.35281	-1.36285	148.0	0.43159	-3.64927	-5.36493
60.0	1.12925	0.52791	-1.18775	150.0	0.38478	-4.14782	-5.86348
62.0	1.17196	0.68911	-1.02654	152.0	0.33970	-4.68906	-6.40472
64.0	1.21253	0.83700	-0.87865	154.0	0.29657	-5.27874	-6.99439
66.0	1.25086	0.97209	-0.74357	156.0	0.25569	-5.92396	-7.63961
68.0	1.28671	1.09482	-0.62084	158.0	0.21708	-6.63371	-8.34936
70.0	1.31996	1.20560	-0.51005	160.0	0.18115	-7.41934	-9.13519
72.0	1.35045	1.30479	-0.41086	162.0	0.14802	-8.29667	-10.01232
74.0	1.37807	1.39271	-0.32295	164.0	0.11788	-9.28569	-11.00135
76.0	1.40269	1.46962	-0.24603	166.0	0.09088	-10.41551	-12.13117
78.0	1.42422	1.53577	-0.17988	168.0	0.06717	-11.72943	-13.44508
80.0	1.44257	1.59136	-0.12429	170.0	0.04688	-13.29004	-15.00569
82.0	1.45766	1.63655	-0.07910	172.0	0.03013	-15.21022	-16.92588
84.0	1.46942	1.67149	-0.04416	174.0	0.01700	-17.69499	-19.41064
86.0	1.47784	1.69627	-0.01938	176.0	0.00757	-21.20680	-22.92246
88.0	1.48285	1.71098	-0.00467	178.0	0.00190	-27.22140	-28.93705
90.0	1.48443	1.71565	0.00000	180.	0.00000	-INFINITY	-INFINITY

TABLE A2-5 $2\pi a/\lambda = 1.25$

EPSLN= 1 2500(NORMALIZED GROUNDPLANE RADIUS)
MONOPOLE LENGTH= 0 250000(WAVELENGTH)
MONOPOLE RADIUS= 0 10000E-03(WAVELENGTH)
NUMBER OF MONOPOLE SEGMENTS= 1
NUMBER OF DISK SEGMENTS= 16
RADIATION RESISTANCE DETERMINED BY PATTERN= 0 207151E+02 OHMS

ELEVATION ANGLE (DEG)	DIRECTIVITY (NUMERIC)	DIRECTIVITY (DBI)	RELATIVE POWER (DB)	ELEVATION ANGLE (DEG)	DIRECTIVITY (NUMERIC)	DIRECTIVITY (DBI)	RELATIVE POWER (DB)
0	0 00000	-INFINITY	-INFINITY				
2 0	0 00209	-26 79196	-28 40031	92 0	1 44640	1 60287	-0 00548
4 0	0 00836	-20 77914	-22 38749	94 0	1 44168	1 58867	-0 01967
6 0	0 01873	-17 27027	-18 87862	96 0	1 43407	1 56571	-0 04264
8 0	0 03319	-14 78961	-16 39796	98 0	1 42360	1 53387	-0 07447
10 0	0 05159	-12 87468	-14 48302	100 0	1 41028	1 49305	-0 11529
12 0	0 07380	-11 31944	-12 92779	102 0	1 39414	1 44308	-0 16527
14 0	0 09968	-10 01400	-11 62235	104 0	1 37523	1 38374	-0 22460
16 0	0 12904	-8 89272	-10 50107	106 0	1 35357	1 31460	-0 29354
18 0	0 16169	-7 91327	-9 52161	108 0	1 32922	1 23597	-0 37238
20 0	0 19739	-7 04671	-8 65506	110 0	1 30224	1 14891	-0 45143
22 0	0 23592	-6 27240	-7 88075	112 0	1 27270	1 04726	-0 56109
24 0	0 27701	-5 57508	-7 18343	114 0	1 24068	0 93658	-0 67177
26 0	0 32039	-4 94314	-6 55149	116 0	1 20626	0 81441	-0 79394
28 0	0 36580	-4 36755	-5 97590	118 0	1 16956	0 68021	-0 92814
30 0	0 41294	-3 84114	-5 44948	120 0	1 13068	0 53339	-1 07495
32 0	0 46152	-3 35809	-4 96644	122 0	1 08976	0 37331	-1 23504
34 0	0 51125	-2 91366	-4 52201	124 0	1 04694	0 19923	-1 40912
36 0	0 56184	-2 50388	-4 11223	126 0	1 00239	0 01035	-1 59800
38 0	0 61299	-2 12544	-3 73379	128 0	0 95626	-0 19423	-1 80258
40 0	0 66443	-1 77551	-3 38385	130 0	0 90876	-0 41552	-2 02386
42 0	0 71587	-1 45186	-3 06020	132 0	0 86008	-0 65461	-2 26296
44 0	0 76704	-1 15179	-2 76014	134 0	0 81044	-0 91278	-2 52113
46 0	0 81769	-0 87409	-2 48244	136 0	0 76007	-1 19144	-2 79979
48 0	0 86757	-0 61696	-2 22530	138 0	0 70922	-1 49219	-3 10054
50 0	0 91644	-0 37896	-1 98731	140 0	0 65813	-1 81687	-3 42521
52 0	0 96408	-0 15887	-1 76721	142 0	0 60708	-2 16755	-3 77590
54 0	1 01029	0 04443	-1 56389	144 0	0 55633	-2 54669	-4 15303
56 0	1 05487	0 23200	-1 37633	146 0	0 50618	-2 95709	-4 56544
58 0	1 09766	0 40466	-1 20369	148 0	0 45687	-3 40210	-5 01045
60 0	1 13848	0 56325	-1 04510	150 0	0 40873	-3 88367	-5 49402
62 0	1 17720	0 70849	-0 89983	152 0	0 36203	-4 41256	-6 02091
64 0	1 21368	0 84104	-0 76730	154 0	0 31706	-4 98857	-6 59692
66 0	1 24781	0 96149	-0 64685	156 0	0 27410	-5 62089	-7 22923
68 0	1 27949	1 07038	-0 53797	158 0	0 23342	-6 31854	-7 92689
70 0	1 30863	1 16817	-0 44018	160 0	0 19529	-7 09315	-8 70150
72 0	1 33515	1 25530	-0 35305	162 0	0 15996	-7 95997	-9 56832
74 0	1 35898	1 33218	-0 27620	164 0	0 12765	-8 93965	-10 54800
76 0	1 38008	1 39905	-0 20930	166 0	0 09860	-10 06112	-11 66947
78 0	1 39839	1 45629	-0 15206	168 0	0 07300	-11 36673	-12 97508
80 0	1 41386	1 50413	-0 10422	170 0	0 05103	-12 92210	-14 53045
82 0	1 42652	1 54278	-0 06557	172 0	0 03283	-14 83715	-16 44549
84 0	1 43629	1 57241	-0 03593	174 0	0 01854	-17 31789	-18 92623
86 0	1 44316	1 59316	-0 01519	176 0	0 00827	-20 82682	-22 43517
88 0	1 44714	1 60512	-0 00323	178 0	0 00207	-26 83968	-28 44802
90 0	1 44822	1 60835	0 00000	180	0 00000	-INFINITY	-INFINITY

TABLE A2-6 $2\pi a/\lambda = 1.50$

EPSLN= 1.5000(NORMALIZED GROUNDPLANE RADIUS)
MONOPOLE LENGTH= 0.250000(WAVELENGTH)
MONOPOLE RADIUS= 0.1000E-05(WAVELENGTH)
NUMBER OF MONOPOLE SEGMENTS= 1
NUMBER OF DISK SEGMENTS= 16
RADIATION RESISTANCE DETERMINED BY PATTERN= 0.212521E+02 OHMS

ELEVATION ANGLE (DEG)	DIRECTIVITY (NUMERIC)	DIRECTIVITY (DBI)	RELATIVE POWER (DB)	ELEVATION ANGLE (DEG)	DIRECTIVITY (NUMERIC)	DIRECTIVITY (DBI)	RELATIVE POWER (DB)
0.	0.00000	-INFINITY	-INFINITY				
2.0	0.00235	-26.29046	-27.79070	92.0	1.40824	1.48675	-0.01349
4.0	0.00938	-20.27942	-21.77966	94.0	1.40247	1.46893	-0.03131
6.0	0.02102	-16.77352	-18.27376	96.0	1.39434	1.44368	-0.05656
8.0	0.03718	-14.29701	-15.79725	98.0	1.38386	1.41093	-0.08931
10.0	0.05771	-12.38738	-13.88761	100.0	1.37105	1.37053	-0.12971
12.0	0.08244	-10.83859	-12.33882	102.0	1.35591	1.32232	-0.17792
14.0	0.11116	-9.54071	-11.04094	104.0	1.33846	1.26605	-0.23419
16.0	0.14361	-8.42808	-9.92832	106.0	1.31870	1.20147	-0.29877
18.0	0.17954	-7.45835	-8.95859	108.0	1.29665	1.12824	-0.37200
20.0	0.21865	-6.60254	-8.10278	110.0	1.27233	1.04599	-0.45425
22.0	0.26062	-5.83997	-7.34021	112.0	1.24574	0.95428	-0.54595
24.0	0.30512	-5.15534	-6.65557	114.0	1.21693	0.85265	-0.64759
26.0	0.35180	-4.53699	-6.03723	116.0	1.18592	0.74054	-0.75970
28.0	0.40033	-3.97586	-5.47610	118.0	1.15275	0.61735	-0.88289
30.0	0.45033	-3.46470	-4.96494	120.0	1.11749	0.48243	-1.01781
32.0	0.50146	-2.99767	-4.49791	122.0	1.08020	0.33503	-1.16521
34.0	0.55336	-2.56995	-4.07018	124.0	1.04096	0.17434	-1.32590
36.0	0.60569	-2.17752	-3.67776	126.0	0.99988	-0.00052	-1.50076
38.0	0.65811	-1.81699	-3.31723	128.0	0.95707	-0.19056	-1.69080
40.0	0.71032	-1.48548	-2.98572	130.0	0.91267	-0.39685	-1.89709
42.0	0.76199	-1.18049	-2.68073	132.0	0.86684	-0.62062	-2.12085
44.0	0.81286	-0.89986	-2.40010	134.0	0.81975	-0.86320	-2.36344
46.0	0.86264	-0.64169	-2.14193	136.0	0.77159	-1.12612	-2.62635
48.0	0.91111	-0.40429	-1.90453	138.0	0.72259	-1.41106	-2.91130
50.0	0.95803	-0.18619	-1.68643	140.0	0.67298	-1.71995	-3.22019
52.0	1.00322	0.01396	-1.48628	142.0	0.62302	-2.05497	-3.55521
54.0	1.04649	0.19735	-1.30289	144.0	0.57297	-2.41866	-3.91889
56.0	1.08769	0.36505	-1.13518	146.0	0.52313	-2.81390	-4.31414
58.0	1.12670	0.51806	-0.98217	148.0	0.47379	-3.24413	-4.74437
60.0	1.16339	0.65726	-0.84298	150.0	0.42527	-3.71338	-5.21362
62.0	1.19770	0.78346	-0.71677	152.0	0.37788	-4.22649	-5.72673
64.0	1.22953	0.89741	-0.60283	154.0	0.33195	-4.78933	-6.28957
66.0	1.25886	0.99976	-0.50048	156.0	0.28780	-5.40916	-6.90940
68.0	1.28563	1.09115	-0.40909	158.0	0.24575	-6.09508	-7.59532
70.0	1.30982	1.17213	-0.32811	160.0	0.20612	-6.85876	-8.35899
72.0	1.33143	1.24320	-0.25704	162.0	0.16922	-7.71551	-9.21575
74.0	1.35046	1.30482	-0.19542	164.0	0.13533	-8.68604	-10.18628
76.0	1.36691	1.35740	-0.14284	166.0	0.10473	-9.79933	-11.29957
78.0	1.38080	1.40131	-0.09893	168.0	0.07766	-11.09776	-12.59800
80.0	1.39215	1.43686	-0.06338	170.0	0.05436	-12.64700	-14.14724
82.0	1.40098	1.46432	-0.03592	172.0	0.03502	-14.55698	-16.05722
84.0	1.40732	1.48392	-0.01632	174.0	0.01980	-17.03376	-18.53400
86.0	1.41119	1.49585	-0.00439	176.0	0.00883	-20.53985	-22.04008
88.0	1.41262	1.50024	0.00000	178.0	0.00221	-26.55099	-28.05123
90.0	1.41162	1.49719	-0.00305	180.	0.00000	-INFINITY	-INFINITY

TABLE A2-7

EPSLN= 1.7500(NORMALIZED GROUNDPLANE RADIUS)
MONOPOLE LENGTH= 0.250000(WAVELENGTH)
MONOPOLE RADIUS= 0.1000E-05(WAVELENGTH)
NUMBER OF MONOPOLE SEGMENTS= 1
NUMBER OF DISK SEGMENTS= 16
RADIATION RESISTANCE DETERMINED BY PATTERN= 0.224457E+02 OHMS

ELEVATION ANGLE (DEG)	DIRECTIVITY (NUMERIC)	DIRECTIVITY (DBI)	RELATIVE POWER (DB)	ELEVATION ANGLE (DEG)	DIRECTIVITY (NUMERIC)	DIRECTIVITY (DBI)	RELATIVE POWER (DB)
0.	0.00000	-INFINITY	-INFINITY				
2.0	0.00279	-25.55117	-26.81661	92.0	1.33361	1.25028	-0.01516
4.0	0.01111	-19.54315	-20.80860	94.0	1.32928	1.23617	-0.02928
6.0	0.02488	-16.04227	-17.30771	96.0	1.32357	1.21747	-0.04797
8.0	0.04393	-13.57276	-14.83821	98.0	1.31646	1.19408	-0.07137
10.0	0.06804	-11.67211	-12.93755	100.0	1.30791	1.16577	-0.09967
12.0	0.09696	-10.13423	-11.39967	102.0	1.29786	1.13229	-0.13316
14.0	0.13034	-8.84916	-10.11460	104.0	1.28626	1.09330	-0.17215
16.0	0.16783	-7.75121	-9.01665	106.0	1.27303	1.04839	-0.21705
18.0	0.20903	-6.79797	-8.06341	108.0	1.25809	0.99710	-0.26834
20.0	0.25349	-5.96041	-7.22586	110.0	1.24134	0.93890	-0.32654
22.0	0.30076	-5.21780	-6.48325	112.0	1.22270	0.87318	-0.39226
24.0	0.35037	-4.55477	-5.82022	114.0	1.20207	0.79929	-0.46615
26.0	0.40183	-3.95960	-5.22504	116.0	1.17937	0.71650	-0.54895
28.0	0.45466	-3.42312	-4.68856	118.0	1.15452	0.62401	-0.64144
30.0	0.50839	-2.93802	-4.20346	120.0	1.12745	0.52096	-0.74448
32.0	0.56255	-2.49836	-3.76380	122.0	1.09810	0.40643	-0.85901
34.0	0.61671	-2.09922	-3.36466	124.0	1.06645	0.27941	-0.98604
36.0	0.67043	-1.73648	-3.00192	126.0	1.03248	0.13880	-1.12665
38.0	0.72333	-1.40665	-2.67209	128.0	0.99619	-0.01657	-1.28201
40.0	0.77505	-1.10670	-2.37214	130.0	0.95764	-0.18798	-1.45342
42.0	0.82527	-0.83403	-2.09947	132.0	0.91689	-0.37681	-1.64225
44.0	0.87371	-0.58633	-1.85177	134.0	0.87406	-0.58460	-1.85004
46.0	0.92012	-0.36157	-1.62701	136.0	0.82928	-0.81301	-2.07845
48.0	0.96429	-0.15791	-1.42336	138.0	0.78272	-1.06391	-2.32935
50.0	1.00607	0.02627	-1.23917	140.0	0.73462	-1.33937	-2.60481
52.0	1.04532	0.19249	-1.07296	142.0	0.68522	-1.64172	-2.90716
54.0	1.08195	0.34209	-0.92335	144.0	0.63480	-1.97362	-3.23906
56.0	1.11592	0.47633	-0.78911	146.0	0.58370	-2.33810	-3.60354
58.0	1.14720	0.59638	-0.66907	148.0	0.53227	-2.73870	-4.00414
60.0	1.17579	0.70329	-0.56215	150.0	0.48089	-3.17957	-4.44502
62.0	1.20173	0.79807	-0.46738	152.0	0.42997	-3.66566	-4.93110
64.0	1.22508	0.88163	-0.38381	154.0	0.37993	-4.20294	-5.46838
66.0	1.24591	0.95485	-0.31059	156.0	0.33123	-4.79874	-6.06419
68.0	1.26431	1.01852	-0.24692	158.0	0.28430	-5.46226	-6.72771
70.0	1.28038	1.07338	-0.19206	160.0	0.23959	-6.20524	-7.47069
72.0	1.29423	1.12012	-0.14532	162.0	0.19756	-7.04307	-8.30851
74.0	1.30598	1.15937	-0.10608	164.0	0.15862	-7.99650	-9.26195
76.0	1.31574	1.19169	-0.07375	166.0	0.12318	-9.09458	-10.36002
78.0	1.32361	1.21761	-0.04783	168.0	0.09163	-10.37973	-11.64517
80.0	1.32971	1.23758	-0.02787	170.0	0.06430	-11.91766	-13.18310
82.0	1.33413	1.25199	-0.01345	172.0	0.04151	-13.81834	-15.08378
84.0	1.33696	1.26119	-0.00425	174.0	0.02351	-16.28786	-17.55330
86.0	1.33827	1.26544	0.00000	176.0	0.01050	-19.78874	-21.05418
88.0	1.33812	1.26496	-0.00048	178.0	0.00263	-25.79676	-27.06220
90.0	1.33656	1.25988	-0.00556	180.	0.00000	-INFINITY	-INFINITY

TABLE A2-8 $2\pi a/\lambda = 2.00$

EPSLN = 0.000 (NORMALIZED GROUNDPLANE RADIUS)
MONOPOLE LENGTH= 0.250000 (WAVELENGTH)
MONOPOLE RADIUS= 0.10000E-05 (WAVELENGTH)
NUMBER OF MONOPOLE SEGMENTS= 1
NUMBER OF DISK SEGMENTS= 16
RADIATION RESISTANCE DETERMINED BY PATTERN= 0.238990E+02 OHMS

ELEVATION ANGLE (DEG)	DIRECTIVITY (NUMERIC)	DIRECTIVITY (DBI)	RELATIVE POWER (DB)	ELEVATION ANGLE (DEG)	DIRECTIVITY (NUMERIC)	DIRECTIVITY (DBI)	RELATIVE POWER (DB)
0.	0.00000	-INFINITY	-INFINITY				
2.0	0.00340	-24.69016	-25.74217	92.0	1.25046	0.97070	-0.08131
4.0	0.01354	-18.68510	-19.73712	94.0	1.24530	0.95273	-0.09929
6.0	0.03026	-15.18715	-16.24116	96.0	1.23979	0.93347	-0.11854
8.0	0.05338	-12.72653	-13.77854	98.0	1.23390	0.91280	-0.13921
10.0	0.08251	-10.83469	-11.88670	100.0	1.22757	0.89048	-0.16153
12.0	0.11729	-9.30755	-10.35956	102.0	1.22072	0.86616	-0.18585
14.0	0.15731	-8.03512	-9.08713	104.0	1.21322	0.83941	-0.21260
16.0	0.20176	-6.95167	-8.00368	106.0	1.20495	0.80970	-0.24231
18.0	0.25004	-6.01475	-7.06676	108.0	1.19575	0.77640	-0.27561
20.0	0.30232	-5.19531	-6.24732	110.0	1.18544	0.73880	-0.31321
22.0	0.35706	-4.47257	-5.52458	112.0	1.17385	0.69612	-0.35589
24.0	0.41390	-3.83110	-4.88311	114.0	1.16077	0.64748	-0.40454
26.0	0.47216	-3.25913	-4.31114	116.0	1.14602	0.59192	-0.46009
28.0	0.53120	-2.74744	-3.79946	118.0	1.12939	0.52843	-0.52358
30.0	0.59038	-2.28867	-3.34068	120.0	1.11069	0.45591	-0.59610
32.0	0.64911	-1.87679	-2.92880	122.0	1.08973	0.37320	-0.67881
34.0	0.70683	-1.50683	-2.55884	124.0	1.06637	0.27906	-0.77295
36.0	0.76303	-1.17457	-2.22658	126.0	1.04044	0.17217	-0.87984
38.0	0.81725	-0.87645	-1.92846	128.0	1.01184	0.05113	-1.00088
40.0	0.86909	-0.60936	-1.66137	130.0	0.98049	-0.08556	-1.13757
42.0	0.91821	-0.37058	-1.42259	132.0	0.94635	-0.23950	-1.29151
44.0	0.96434	-0.15771	-1.20972	134.0	0.90941	-0.41240	-1.46441
46.0	1.00725	0.03139	-1.02063	136.0	0.86973	-0.60614	-1.65815
48.0	1.04681	0.19866	-0.85335	138.0	0.82742	-0.82275	-1.87476
50.0	1.08290	0.34588	-0.70613	140.0	0.78262	-1.06447	-2.11648
52.0	1.11550	0.47468	-0.57733	142.0	0.73556	-1.33380	-2.38581
54.0	1.14461	0.58656	-0.46545	144.0	0.68651	-1.63353	-2.68554
56.0	1.17029	0.68293	-0.36908	146.0	0.63579	-1.96685	-3.01886
58.0	1.19265	0.76512	-0.28690	148.0	0.58379	-2.33742	-3.38943
60.0	1.21181	0.83436	-0.21766	150.0	0.53094	-2.74951	-3.80152
62.0	1.22796	0.89183	-0.16018	152.0	0.47773	-3.20818	-4.26019
64.0	1.24127	0.93866	-0.11335	154.0	0.42467	-3.71950	-4.77151
66.0	1.25196	0.97591	-0.07610	156.0	0.37231	-4.29091	-5.34292
68.0	1.26026	1.00460	-0.04742	158.0	0.32124	-4.93168	-5.98369
70.0	1.26639	1.02567	-0.02634	160.0	0.27204	-5.65363	-6.70564
72.0	1.27058	1.04003	-0.01198	162.0	0.22531	-6.47222	-7.52423
74.0	1.27308	1.04855	-0.00346	164.0	0.18162	-7.40828	-8.46029
76.0	1.27409	1.05201	0.00000	166.0	0.14155	-8.49089	-9.54290
78.0	1.27384	1.05113	-0.00088	168.0	0.10562	-9.76254	-10.81455
80.0	1.27252	1.04664	-0.00537	170.0	0.07432	-11.28897	-12.34099
82.0	1.27030	1.03907	-0.01294	172.0	0.04808	-13.18020	-14.23222
84.0	1.26735	1.02897	-0.02304	174.0	0.02728	-15.64234	-16.69435
86.0	1.26380	1.01677	-0.03524	176.0	0.01220	-19.13793	-20.18994
88.0	1.25975	1.00284	-0.04917	178.0	0.00306	-25.14277	-26.19478
90.0	1.25529	0.98742	-0.06459	180.	0.00000	-INFINITY	-INFINITY

TABLE A2-9 $2\pi a/\lambda = 2.25$

EPSLN= 2 2500(NORMALIZED GROUNDPLANE RADIUS)
MONOPOLE LENGTH= 0 250000(WAVELENGTH)
MONOPOLE RADIUS= 0 1000E-05(WAVELENGTH)
NUMBER OF MONOPOLE SEGMENTS= 1
NUMBER OF DISK SEGMENTS= 16
RADIATION RESISTANCE DETERMINED BY PATTERN= 0 259969E+02 OHMS

ELEVATION ANGLE (DEG)	DIRECTIVITY (NUMERIC)	DIRECTIVITY (DBI)	RELATIVE POWER (DB)	ELEVATION ANGLE (DEG)	DIRECTIVITY (NUMERIC)	DIRECTIVITY (DBI)	RELATIVE POWER (DB)
0	0 00000	-INFINITY	-INFINITY				
2 0	0 00429	-23 67209	-24 71056	92 0	1 14569	0 59069	-0 44778
4 0	0 01710	-17 67022	-18 70869	94 0	1 13828	0 56249	-0 47598
6 0	0 03820	-14 17957	-15 21804	96 0	1 13175	0 53749	-0 50098
8 0	0 06723	-11 72436	-12 76283	98 0	1 12606	0 51560	-0 52286
10 0	0 10370	-9 84203	-10 88050	100 0	1 12114	0 49660	-0 54186
12 0	0 14701	-8 32648	-9 36494	102 0	1 11689	0 48009	-0 55838
14 0	0 19644	-7 06768	-8 10614	104 0	1 11314	0 46550	-0 57297
16 0	0 25120	-5 99989	-7 03835	106 0	1 10972	0 45214	-0 58633
18 0	0 31041	-5 08063	-6 11910	108 0	1 10641	0 43916	-0 59930
20 0	0 37318	-4 28082	-5 31928	110 0	1 10296	0 42560	-0 61287
22 0	0 43857	-3 57962	-4 61809	112 0	1 09910	0 41036	-0 62811
24 0	0 50564	-2 96160	-4 00006	114 0	1 09452	0 39225	-0 64622
26 0	0 57347	-2 41492	-3 45339	116 0	1 08892	0 37018	-0 66849
28 0	0 64116	-1 93033	-2 96879	118 0	1 08198	0 34218	-0 69629
30 0	0 70788	-1 50040	-2 53886	120 0	1 07335	0 30740	-0 73107
32 0	0 77285	-1 11906	-2 15753	122 0	1 06271	0 26413	-0 77433
34 0	0 83536	-0 78128	-1 81975	124 0	1 04973	0 21079	-0 82768
36 0	0 89479	-0 48280	-1 52127	126 0	1 03412	0 14572	-0 89274
38 0	0 95061	-0 21997	-1 25844	128 0	1 01560	0 06722	-0 97125
40 0	1 00239	0 01038	-1 02809	130 0	0 99391	-0 02652	-1 06499
42 0	1 04979	0 21103	-0 82744	132 0	0 96886	-0 13738	-1 17585
44 0	1 09256	0 38446	-0 65400	134 0	0 94030	-0 26734	-1 30581
46 0	1 13055	0 53291	-0 50555	136 0	0 90813	-0 41851	-1 45698
48 0	1 16370	0 65841	-0 38005	138 0	0 87234	-0 59315	-1 63162
50 0	1 19202	0 76284	-0 27563	140 0	0 83297	-0 79371	-1 83218
52 0	1 21561	0 84793	-0 19054	142 0	0 79015	-1 02288	-2 06135
54 0	1 23461	0 91531	-0 12316	144 0	0 74411	-1 28363	-2 32209
56 0	1 24926	0 96653	-0 07193	146 0	0 69514	-1 57929	-2 61776
58 0	1 25981	1 00307	-0 03540	148 0	0 64362	-1 91268	-2 95115
60 0	1 26658	1 02633	-0 01214	150 0	0 59004	-2 29120	-3 32967
62 0	1 26990	1 03769	-0 00078	152 0	0 53493	-2 71702	-3 75549
64 0	1 27013	1 03847	0 00000	154 0	0 47892	-3 19734	-4 23580
66 0	1 26764	1 02998	-0 00851	156 0	0 42270	-3 73967	-4 77813
68 0	1 26282	1 01342	-0 02505	158 0	0 36700	-4 35338	-5 39185
70 0	1 25605	0 99008	-0 04839	160 0	0 31258	-5 05038	-6 08885
72 0	1 24771	0 96114	-0 07733	162 0	0 26024	-5 84619	-6 88465
74 0	1 23816	0 92776	-0 11071	164 0	0 21078	-6 76170	-7 80016
76 0	1 22774	0 89106	-0 14741	166 0	0 16497	-7 82605	-8 86452
78 0	1 21677	0 85210	-0 18636	168 0	0 12354	-9 08179	-10 12025
80 0	1 20557	0 81191	-0 22656	170 0	0 08720	-10 59468	-11 63313
82 0	1 19438	0 77141	-0 26705	172 0	0 05656	-12 47479	-13 51325
84 0	1 18344	0 73147	-0 30699	174 0	0 03215	-14 92824	-15 96671
86 0	1 17296	0 69284	-0 34562	176 0	0 01440	-18 41762	-19 45608
88 0	1 16310	0 65618	-0 38229	178 0	0 00362	-24 41872	-25 45719
90 0	1 15398	0 62200	-0 41647	180.	0 00000	-INFINITY	-INFINITY

TABLE A2-10 $2\pi a/\lambda = 2.50$

EPSLN= 2.500(NORMALIZED GROUNDPLANE RADIUS)
MONOPOLE LENGTH= 0.250000(WAVELENGTH)
MONOPOLE RADIUS= 0.10000E-05(WAVELENGTH)
NUMBER OF MONOPOLE SEGMENTS= 8
NUMBER OF DISK SEGMENTS= 16
RADIATION RESISTANCE DETERMINED BY PATTERN= 0.29019E+02 OHMS

ELEVATION ANGLE (DEG)	DIRECTIVITY (NUMERIC)	DIRECTIVITY (DBI)	RELATIVE POWER (DB)	ELEVATION ANGLE (DEG)	DIRECTIVITY (NUMERIC)	DIRECTIVITY (DBI)	RELATIVE POWER (DB)
0	0.00000	-INFINITY	-INFINITY				
2.0	0.00558	-22.53282	-23.86563	92.0	1.01981	0.08519	-1.24763
4.0	0.02221	-16.53422	-17.86704	94.0	1.00804	0.03476	-1.29805
6.0	0.04956	-13.04902	-14.38183	96.0	0.99849	-0.00655	-1.33937
8.0	0.08707	-10.60142	-11.93423	98.0	0.99116	-0.03856	-1.37138
10.0	0.13400	-8.72885	-10.06166	100.0	0.98597	-0.06135	-1.39417
12.0	0.18944	-7.22518	-8.55800	102.0	0.98282	-0.07525	-1.40807
14.0	0.25233	-5.98038	-7.31320	104.0	0.98154	-0.08090	-1.41372
16.0	0.32146	-4.92868	-6.26150	106.0	0.98193	-0.07919	-1.41200
18.0	0.39559	-4.02757	-5.36039	108.0	0.98373	-0.07123	-1.40405
20.0	0.47338	-3.24793	-4.58074	110.0	0.98665	-0.05838	-1.39120
22.0	0.55349	-2.56890	-3.90172	112.0	0.99033	-0.04219	-1.37500
24.0	0.63460	-1.97499	-3.30781	114.0	0.99441	-0.02433	-1.35713
26.0	0.71542	-1.45436	-2.78718	116.0	0.99847	-0.00665	-1.33946
28.0	0.79475	-0.99770	-2.33051	118.0	1.00206	0.00894	-1.32388
30.0	0.87146	-0.59754	-1.93036	120.0	1.00471	0.02043	-1.31239
32.0	0.94454	-0.24779	-1.58060	122.0	1.00595	0.02575	-1.30707
34.0	1.01319	0.05665	-1.27617	124.0	1.00526	0.02280	-1.31002
36.0	1.07648	0.32005	-1.01276	126.0	1.00217	0.00942	-1.32340
38.0	1.13400	0.54612	-0.78669	128.0	0.99620	-0.01656	-1.34937
40.0	1.18524	0.73806	-0.59476	130.0	0.98688	-0.05736	-1.39017
42.0	1.22990	0.89869	-0.43412	132.0	0.97381	-0.11525	-1.44807
44.0	1.26781	1.03054	-0.30228	134.0	0.95663	-0.19258	-1.52540
46.0	1.29894	1.13588	-0.19694	136.0	0.93502	-0.29177	-1.62459
48.0	1.32336	1.21679	-0.11603	138.0	0.90879	-0.41536	-1.74819
50.0	1.34128	1.27520	-0.05762	140.0	0.87780	-0.56603	-1.89887
52.0	1.35297	1.31288	-0.01993	142.0	0.84203	-0.74675	-2.07957
54.0	1.35880	1.33155	-0.00127	144.0	0.80156	-0.96062	-2.29344
56.0	1.35920	1.33282	0.00000	146.0	0.75662	-1.21120	-2.54401
58.0	1.35464	1.31824	-0.01458	148.0	0.70755	-1.50242	-2.83524
60.0	1.34565	1.28933	-0.04348	150.0	0.65481	-1.83884	-3.17166
62.0	1.33278	1.24759	-0.08522	152.0	0.59900	-2.22575	-3.55857
64.0	1.31659	1.19449	-0.13832	154.0	0.54082	-2.66944	-4.00226
66.0	1.29763	1.13151	-0.20131	156.0	0.48111	-3.17734	-4.51036
68.0	1.27647	1.06011	-0.27271	158.0	0.42078	-3.75948	-5.09230
70.0	1.25365	0.98178	-0.35104	160.0	0.36081	-4.42725	-5.76007
72.0	1.22971	0.89802	-0.43480	162.0	0.30224	-5.19643	-6.52925
74.0	1.20513	0.81033	-0.52249	164.0	0.24615	-6.08798	-7.42080
76.0	1.18038	0.72022	-0.61259	166.0	0.19359	-7.13108	-8.46390
78.0	1.15590	0.62922	-0.70360	168.0	0.14560	-8.36831	-9.70113
80.0	1.13209	0.53880	-0.79402	170.0	0.10315	-9.86549	-11.19831
82.0	1.10929	0.45044	-0.88238	172.0	0.06710	-11.73270	-13.06552
84.0	1.08781	0.36554	-0.96728	174.0	0.03923	-14.17610	-15.50891
86.0	1.06793	0.28542	-1.04740	176.0	0.01715	-17.65628	-18.99110
88.0	1.04986	0.21131	-1.12151	178.0	0.00431	-23.65506	-24.98988
90.0	1.03378	0.14426	-1.18855	180	0.00000	-INFINITY	-INFINITY

TABLE A2-11 $2\pi a/\lambda = 2.75$

EPSLN= 2. 7500(NORMALIZED GROUNDPLANE RADIUS)
MONOPOLE LENGTH= 0 250000(WAVELENGTH)
MONOPOLE RADIUS= 0 1000E-05(WAVELENGTH)
NUMBER OF MONOPOLE SEGMENTS= 1
NUMBER OF DISK SEGMENTS= 16
RADIATION RESISTANCE DETERMINED BY PATTERN= 0 3324076+02 OHMS

ELEVATION ANGLE (DEG)	DIRECTIVITY (NUMERIC)	DIRECTIVITY (DBI)	RELATIVE POWER (DB)	ELEVATION ANGLE (DEG)	DIRECTIVITY (NUMERIC)	DIRECTIVITY (DBI)	RELATIVE POWER (DB)
0	0 00000	-INFINITY	-INFINITY				
2 0	0 00734	-21. 34301	-23 19298	92 0	0 88037	-0 55334	-2 40331
4 0	0 02919	-15 34767	-17. 19764	94 0	0. 86170	-0 64644	-2 49641
6 0	0 06504	-11. 86788	-13. 71785	96 0	0. 84657	-0 72340	-2 57337
8 0	0 11408	-9. 42784	-11. 27781	98. 0	0. 83499	-0. 78318	-2 63315
10 0	0. 17519	-7. 56495	-9 41492	100 0	0 82695	-0. 82521	-2 67518
12 0	0. 24700	-6. 07308	-7. 92305	102 0	0 82236	-0 84936	-2 69932
14. 0	0 32793	-4 84215	-6 69212	104 0	0 82110	-0. 85603	-2 70600
16 0	0 41626	-3 80637	-5 65634	106. 0	0 82298	-0. 84613	-2 69610
18 0	0 51013	-2. 92319	-4. 77316	108 0	0 82774	-0 82105	-2 67102
20. 0	0. 60765	-2. 16346	-4 01343	110. 0	0. 83510	-0. 78260	-2. 63257
22 0	0. 70692	-1 50628	-3 35625	112. 0	0. 84470	-0. 73298	-2. 58295
24. 0	0. 80610	-0. 93611	-2 78608	114 0	0 85612	-0 67467	-2. 52464
26 0	0. 90343	-0. 44107	-2 29104	116. 0	0. 86888	-0 61038	-2. 46035
28. 0	0. 99728	-0 01181	-1 86178	118. 0	0 88248	-0. 54296	-2. 39293
30 0	1 08622	0 33917	-1 49080	120. 0	0 89632	-0 47536	-2 32532
32 0	1 16897	0. 67802	-1 17194	122. 0	0 90980	-0 41053	-2. 26050
34 0	1. 24448	0 94987	-0. 90010	124 0	0 92226	-0 35146	-2. 20143
36 0	1 31191	1 17903	-0 67094	126. 0	0. 93302	-0 30108	-2. 15105
38 0	1. 37064	1. 36923	-0. 48074	128. 0	0 94139	-0 26229	-2 11226
40 0	1. 42027	1. 52370	-0. 32627	130. 0	0. 94668	-0 23795	-2. 08792
42. 0	1 46059	1. 64529	-0 20468	132. 0	0 94823	-0. 23088	-2. 08085
44 0	1. 49160	1. 73652	-0. 11345	134. 0	0 94539	-0 24391	-2. 09387
46. 0	1 51345	1. 79969	-0. 05028	136. 0	0. 93759	-0 27987	-2. 12984
48. 0	1 52646	1. 83687	-0 01310	138. 0	0. 92434	-0. 34167	-2. 19164
50. 0	1 53108	1. 84997	0. 00000	140 0	0 90525	-0 43230	-2. 28227
52 0	1 52784	1. 84078	-0 00919	142. 0	0. 88005	-0 55493	-2. 40490
54 0	1 51739	1. 81097	-0 03900	144. 0	0. 84861	-0. 71294	-2. 56290
56 0	1 50042	1. 76214	-0 08783	146. 0	0. 81096	-0 91001	-2 75998
58. 0	1 47769	1 69593	-0 15414	148. 0	0. 76731	-1 15027	-3. 00024
60 0	1. 44995	1. 61352	-0 23644	150 0	0. 71806	-1. 43837	-3. 28834
62 0	1 41799	1. 51672	-0 33325	152. 0	0. 66379	-1. 77972	-3. 62969
64 0	1 38257	1 40689	-0. 44308	154. 0	0. 60524	-2. 18070	-4. 03067
66. 0	1 34447	1 28552	-0 56445	156. 0	0. 54337	-2 64901	-4. 49898
68 0	1 30442	1. 15416	-0 69581	158. 0	0. 47927	-3. 19415	-5 04412
70 0	1 26310	1. 01438	-0 83559	160. 0	0. 41417	-3. 82816	-5. 67813
72 0	1 22119	0 86782	-0 98215	162. 0	0. 34941	-4. 56669	-6. 41665
74 0	1 17929	0 71620	-1 13376	164. 0	0. 28637	-5. 43070	-7 28067
76. 0	1 13798	0 56134	-1 28863	166. 0	0. 22649	-6. 44944	-8. 29940
78 0	1 09777	0 40512	-1 44484	168 0	0 17118	-7. 66549	-9 51546
80 0	1 05914	0 24954	-1 60043	170. 0	0. 12177	-9. 14472	-10. 99469
82 0	1 02250	0 09665	-1 75332	172. 0	0. 07948	-10. 99721	-12. 84718
84 0	0 98823	-0 05143	-1 90140	174. 0	0. 04540	-13 42915	-15 27913
86 0	0 95663	-0. 19256	-2 04253	176. 0	0. 02040	-16. 90314	-18. 75311
88 0	0 92798	-0 32459	-2 17456	178. 0	0 00513	-22. 89500	-24. 74496
90 0	0 90231	-0 44549	-2 29546	180.	0. 00000	-INFINITY	-INFINITY

TABLE A2-12

EPSLN= 3.0000 (NORMALIZED GROUNDPLANE RADIUS)
MONOPOLE LENGTH= 0.250000 (WAVELENGTHS)
MONOPOLE RADIUS= 0.10000E-05 (WAVELENGTHS)
NUMBER OF MONOPOLE SEGMENTS= 1
NUMBER OF DISK SEGMENTS= 16
RADIATION RESISTANCE DETERMINED BY PATTERN= 0.386185E+02 OHMS

ELEVATION ANGLE (DEG)	DIRECTIVITY (NUMERIC)	DIRECTIVITY (DBI)	RELATIVE POWER (DB)	ELEVATION ANGLE (DEG)	DIRECTIVITY (NUMERIC)	DIRECTIVITY (DBI)	RELATIVE POWER (DB)
0	0.00000	-INFINITY	-INFINITY				
2.0	0.00957	-20.18869	-22.64786	92.0	0.74435	-1.28224	-3.74142
4.0	0.03805	-14.19634	-16.65571	94.0	0.71630	-1.44904	-3.90822
6.0	0.08468	-10.72206	-13.18143	96.0	0.69281	-1.59384	-4.05301
8.0	0.14827	-8.28943	-10.74881	98.0	0.67397	-1.71362	-4.17279
10.0	0.22719	-6.43604	-8.89521	100.0	0.65980	-1.80588	-4.26506
12.0	0.31947	-4.95570	-7.41487	102.0	0.65030	-1.86884	-4.32801
14.0	0.42283	-3.73631	-6.19748	104.0	0.64543	-1.90154	-4.36071
16.0	0.53481	-2.71803	-5.17720	106.0	0.64505	-1.90404	-4.36321
18.0	0.65270	-1.85225	-4.31143	108.0	0.64902	-1.87740	-4.33657
20.0	0.77414	-1.11179	-3.57096	110.0	0.65710	-1.82367	-4.28284
22.0	0.89626	-0.47367	-2.93284	112.0	0.66900	-1.74576	-4.20493
24.0	1.01665	0.07170	-2.38748	114.0	0.68433	-1.64732	-4.10649
26.0	1.13299	0.54226	-1.91691	116.0	0.70267	-1.53248	-3.99165
28.0	1.24321	0.94544	-1.51373	118.0	0.72348	-1.40571	-3.86488
30.0	1.34549	1.28880	-1.17038	120.0	0.74617	-1.27161	-3.73078
32.0	1.43832	1.57854	-0.88063	122.0	0.77035	-1.13479	-3.59396
34.0	1.52050	1.81985	-0.63932	124.0	0.79438	-0.99973	-3.45890
36.0	1.59115	2.01712	-0.44205	126.0	0.81832	-0.87075	-3.32993
38.0	1.64972	2.17410	-0.28307	128.0	0.84102	-0.75196	-3.21113
40.0	1.69593	2.29408	-0.16310	130.0	0.86155	-0.64722	-3.10639
42.0	1.72979	2.37992	-0.07725	132.0	0.87898	-0.56022	-3.01940
44.0	1.75154	2.43419	-0.02298	134.0	0.89238	-0.49450	-2.95367
46.0	1.76164	2.45917	0.00000	136.0	0.90085	-0.45346	-2.91263
48.0	1.76073	2.45694	-0.00224	138.0	0.90356	-0.44044	-2.89961
50.0	1.74959	2.42937	-0.02980	140.0	0.89974	-0.45881	-2.91798
52.0	1.72910	2.37821	-0.08096	142.0	0.88879	-0.51199	-2.97116
54.0	1.70022	2.30506	-0.15411	144.0	0.87024	-0.60359	-3.06277
56.0	1.66396	2.21144	-0.24774	146.0	0.84383	-0.73747	-3.19664
58.0	1.62135	2.09876	-0.36041	148.0	0.80950	-0.91786	-3.37703
60.0	1.57340	1.96840	-0.49077	150.0	0.76745	-1.14951	-3.60868
62.0	1.52114	1.82169	-0.63748	152.0	0.71814	-1.43790	-3.89707
64.0	1.46552	1.65992	-0.79925	154.0	0.66230	-1.78946	-4.24863
66.0	1.40748	1.48442	-0.97475	156.0	0.60091	-2.21193	-4.67110
68.0	1.34788	1.29652	-1.16265	158.0	0.53520	-2.71485	-5.17402
70.0	1.28754	1.09760	-1.36157	160.0	0.46663	-3.31026	-5.76943
72.0	1.22719	0.88913	-1.57004	162.0	0.39684	-4.01383	-6.47300
74.0	1.16753	0.67269	-1.78648	164.0	0.32760	-4.84655	-7.30573
76.0	1.10918	0.45000	-2.00917	166.0	0.26076	-5.83766	-8.29683
78.0	1.05268	0.22295	-2.23622	168.0	0.19816	-7.02977	-9.48894
80.0	0.99853	-0.00637	-2.46554	170.0	0.14162	-8.48872	-10.94789
82.0	0.94719	-0.23563	-2.69480	172.0	0.09280	-10.32462	-12.78379
84.0	0.89903	-0.46225	-2.92142	174.0	0.05317	-12.74369	-15.20286
86.0	0.85440	-0.68340	-3.14257	176.0	0.02394	-16.20841	-18.66758
88.0	0.81358	-0.89599	-3.35517	178.0	0.00603	-22.19474	-24.65391
90.0	0.77683	-1.09673	-3.55592	180	0.00000	-INFINITY	-INFINITY

TABLE A2-13 $2\pi a/\lambda = 3.25$

```
EPSLN= 3.7500(NORMALIZED GROUNDPLANE RADIUS)
MONOPOLE LENGTH= 0 250000(WAVELENGTH)
MONOPOLE RADIUS=   0 1000E-05(WAVELENGTH)
NUMBER OF MONOPOLE SEGMENTS=  1
NUMBER OF DISK SEGMENTS= 16
RADIATION RESISTANCE DETERMINED BY PATTERN= 0 441233E+02 OHMS
```

ELEVATION ANGLE (DEG)	DIRECTIVITY (NUMERIC)	DIRECTIVITY (DBI)	RELATIVE POWER (DB)	ELEVATION ANGLE (DEG)	DIRECTIVITY (NUMERIC)	DIRECTIVITY (DBI)	RELATIVE POWER (DB)
0	0 00000	-INFINITY	-INFINITY				
2 0	0 01213	-19 16045	-22 19734	92.0	0. 63630	-1. 96205	-4. 99894
4 0	0. 04818	-13 17147	-16 20837	94.0	0. 59793	-2 23349	-5. 27039
6.0	0 10710	-9 70228	-12 73918	96.0	0. 56439	-2. 48423	-5. 52113
8.0	0 18720	-7 27701	-10 31391	98.0	0 53601	-2. 70830	-5. 74520
10 0	0 28622	-5 43301	-8 46991	100. 0	0. 51291	-2. 89962	-5. 93651
12. 0	0 40142	-3. 96406	-7 00096	102. 0	0. 49518	-3. 05238	-6. 08927
14 0	0 52966	-2 76001	-5 79691	104. 0	0. 48288	-3. 16160	-6. 19850
16. 0	0 66758	-1. 75494	-4. 79184	106. 0	0 47603	-3. 22368	-6. 26057
18 0	0 81167	-0 90619	-3 94308	108. 0	0. 47459	-3. 23679	-6. 27369
20. 0	0 95842	-0 18446	-3 22136	110. 0	0 47849	-3. 20128	-6. 23818
22 0	1. 10440	0 43127	-2 60563	112. 0	0. 48757	-3. 11966	-6. 15656
24. 0	1. 24644	0. 95670	-2. 08020	114. 0	0. 50160	-2. 99444	-6. 03334
26 0	1 38162	1 40389	-1 63301	116. 0	0. 52027	-2. 83771	-5. 87660
28. 0	1. 50742	1. 78203	-1. 25486	118. 0	0. 54317	-2. 65060	-5. 68750
30. 0	1 62170	2 09972	-0 93718	120. 0	0. 56980	-2. 44280	-5. 47970
32. 0	1. 72280	2. 36235	-0. 67455	122. 0	0. 59951	-2 22203	-5. 25893
34. 0	1 80947	2 57551	-0 46138	124. 0	0. 63158	-1. 99570	-5. 03263
36. 0	1 88092	2. 74370	-0. 29320	126. 0	0. 66515	-1. 77083	-4. 80773
38. 0	1 93676	2. 87076	-0. 16614	128. 0	0. 69925	-1. 55366	-4. 59056
40. 0	1 97700	2. 96007	-0. 07683	130. 0	0. 73284	-1. 34993	-4. 38682
42 0	2. 00197	3. 01457	-0. 02233	132. 0	0. 76476	-1. 16474	-4. 20164
44. 0	2. 01229	3. 03690	0. 00000	134. 0	0. 79383	-1. 00273	-4. 03963
46. 0	2. 00881	3. 02939	-0. 00751	136. 0	0. 81882	-0. 86812	-3. 90502
48 0	1. 99257	2. 99414	-0. 04276	138. 0	0. 83852	-0. 76486	-3. 80176
50. 0	1. 96474	2. 93303	-0. 10385	140. 0	0. 85178	-0. 69670	-3. 73363
52. 0	1. 92657	2. 84784	-0. 18905	142. 0	0. 85754	-0. 66744	-3. 70434
54. 0	1. 87936	2. 74009	-0. 29681	144. 0	0. 85491	-0. 68078	-3. 71768
56 0	1. 82441	2 61122	-0. 42567	146. 0	0. 84320	-0. 74071	-3. 77761
58. 0	1. 76301	2. 46256	-0. 57434	148. 0	0. 82195	-0. 85153	-3. 88843
60 0	1. 69641	2 29530	-0. 74160	150. 0	0. 79104	-1. 01802	-4. 05492
62. 0	1. 62577	2. 11059	-0. 92630	152. 0	0. 75065	-1. 24564	-4. 28254
64. 0	1. 55220	1. 90949	-1. 12741	154. 0	0. 70132	-1. 54081	-4. 57771
66 0	1 47673	1. 69300	-1. 34389	156. 0	0. 64398	-1. 91124	-4. 94814
68. 0	1. 40027	1. 46211	-1. 57478	158. 0	0. 57990	-2. 36644	-5. 40334
70. 0	1. 32367	1. 21780	-1. 81910	160. 0	0. 51069	-2. 91842	-5. 95532
72 0	1. 24769	0 96106	-2. 07584	162. 0	0. 43825	-3. 58280	-6. 61970
74. 0	1 17299	0 69294	-2 34396	164. 0	0. 36471	-4. 38053	-7. 41744
76. 0	1 10017	0 41460	-2. 62229	166. 0	0. 29236	-5. 34087	-8. 37778
78. 0	1 02976	0 12735	-2. 90955	168. 0	0. 22355	-6. 50634	-9. 54324
80. 0	0. 96221	-0 16732	-3. 20422	170. 0	0. 16059	-7. 94280	-10. 97970
82. 0	0. 89792	-0 46762	-3. 50451	172. 0	0. 10567	-9. 76032	-12. 79722
84 0	0 83726	-0 77141	-3. 80831	174. 0	0. 06074	-12 16507	-15. 20197
86. 0	0 78052	-1 07614	-4. 11304	176. 0	0. 02742	-15. 61965	-18. 65655
88. 0	0 72799	-1 37872	-4. 41562	178. 0	0. 00692	-21. 99986	-24. 63676
90 0	0 67991	-1 67346	-4 71236	180.	0. 00000	-INFINITY	-INFINITY

TABLE A2-14 $2\pi a/\lambda = 3.50$

```
EPSLN= 3 5000(NORMALIZED GROUNDPLANE RADIUS)
MONOPOLE LENGTH= 0 250000(WAVELENGTH)
MONOPOLE RADIUS=  0 10000E-03(WAVELENGTH)
NUMBER OF MONOPOLE SEGMENTS=  9
NUMBER OF DISK SEGMENTS= 16
RADIATION RESISTANCE DETERMINED BY PATTERN= 0 475769E+02 OHMS
```

ELEVATION ANGLE (DEG)	DIRECTIVITY (NUMERIC)	DIRECTIVITY (DBI)	RELATIVE POWER (DB)	ELEVATION ANGLE (DEG)	DIRECTIVITY (NUMERIC)	DIRECTIVITY (DBI)	RELATIVE POWER (DB)
0	0.00000	-INFINITY	-INFINITY				
2.0	0.01475	-18.31222	-21.80048	92.0	0.57769	-2.38302	-5.97128
4.0	0.05853	-12.32650	-15.81476	94.0	0.52944	-2.76186	-6.25013
6.0	0.12994	-8.86269	-12.35095	96.0	0.48597	-3.13392	-6.62218
8.0	0.22673	-6.44492	-9.93318	98.0	0.44748	-3.49228	-6.98055
10.0	0.34590	-4.61048	-8.09874	100.0	0.41415	-3.82942	-7.31668
12.0	0.48383	-3.15309	-6.64135	102.0	0.38617	-4.13222	-7.62048
14.0	0.63643	-1.96231	-5.45078	104.0	0.36371	-4.39240	-7.88066
16.0	0.79933	-0.97276	-4.46103	106.0	0.34695	-4.59737	-8.08563
18.0	0.96804	-0.14107	-3.62933	108.0	0.33601	-4.73649	-8.22475
20.0	1.13814	0.56196	-2.92630	110.0	0.33101	-4.80163	-8.28989
22.0	1.30542	1.15750	-2.33076	112.0	0.33200	-4.78863	-8.27690
24.0	1.46601	1.66136	-1.82690	114.0	0.33898	-4.69824	-8.18652
26.0	1.61649	2.08574	-1.40252	116.0	0.35186	-4.53624	-8.02451
28.0	1.75400	2.44030	-1.04797	118.0	0.37047	-4.31248	-7.80074
30.0	1.87623	2.73286	-0.75540	120.0	0.39449	-4.03960	-7.52787
32.0	1.98148	2.96990	-0.51836	122.0	0.42351	-3.73141	-7.21967
34.0	2.06863	3.15687	-0.33139	124.0	0.45692	-3.40155	-6.88981
36.0	2.13718	3.29841	-0.18986	126.0	0.49401	-3.06260	-6.55087
38.0	2.18703	3.39854	-0.08972	128.0	0.53387	-2.72563	-6.21389
40.0	2.21860	3.46079	-0.02747	130.0	0.57543	-2.40006	-5.88832
42.0	2.23268	3.48826	0.00000	132.0	0.61748	-2.09379	-5.58205
44.0	2.23034	3.48371	-0.00455	134.0	0.65865	-1.81343	-5.30170
46.0	2.21269	3.44960	-0.03867	136.0	0.69750	-1.56457	-5.05283
48.0	2.18179	3.38814	-0.10013	138.0	0.73248	-1.35201	-4.84028
50.0	2.13861	3.30131	-0.18696	140.0	0.76207	-1.18006	-4.66833
52.0	2.08492	3.19090	-0.29737	142.0	0.78475	-1.05271	-4.54098
54.0	2.02232	3.05850	-0.42977	144.0	0.79913	-0.97385	-4.46212
56.0	1.95234	2.90555	-0.58272	146.0	0.80400	-0.94743	-4.43571
58.0	1.87643	2.73332	-0.75494	148.0	0.79841	-0.97772	-4.46599
60.0	1.79595	2.54295	-0.94532	150.0	0.78173	-1.06935	-4.55761
62.0	1.71216	2.33543	-1.15283	152.0	0.75376	-1.22766	-4.71592
64.0	1.62617	2.11165	-1.37661	154.0	0.71467	-1.45893	-4.94719
66.0	1.53899	1.87236	-1.61590	156.0	0.66516	-1.77074	-5.25901
68.0	1.45152	1.61822	-1.87004	158.0	0.60639	-2.17247	-5.66073
70.0	1.36452	1.34981	-2.13845	160.0	0.54001	-2.67601	-6.16427
72.0	1.27868	1.06762	-2.42064	162.0	0.46807	-3.29687	-6.78513
74.0	1.19457	0.77210	-2.71616	164.0	0.39301	-4.05592	-7.54418
76.0	1.11268	0.46368	-3.02458	166.0	0.31752	-4.98228	-8.47055
78.0	1.03343	0.14280	-3.34547	168.0	0.24443	-6.11847	-9.60673
80.0	0.95718	-0.19006	-3.67832	170.0	0.17659	-7.53025	-11.01851
82.0	0.88425	-0.53426	-4.02253	172.0	0.11674	-9.32764	-12.81591
84.0	0.81489	-0.88900	-4.37727	174.0	0.06735	-11.71678	-15.20504
86.0	0.74935	-1.25315	-4.74141	176.0	0.03048	-15.16022	-18.64849
88.0	0.68784	-1.62513	-5.11339	178.0	0.00770	-21.13077	-24.62203
90.0	0.63056	-2.00275	-5.49102	180.	0.00000	-INFINITY	-INFINITY

TABLE A2-15 $2\pi a/\lambda = 3.75$

```
EPSILON= 3 7500(NORMALIZED GROUNDPLANE RADIUS)
MONOPOLE LENGTH= 0 250000(WAVELENGTH)
MONOPOLE RADIUS=  0 1000E-03(WAVELENGTH)
NUMBER OF MONOPOLE SEGMENTS=  1
NUMBER OF DISK SEGMENTS= 11
RADIATION RESISTANCE DETERMINED BY PATTERN= 0 473479E+02 OHMS
```

ELEVATION ANGLE (DEG)	DIRECTIVITY (NUMERIC)	DIRECTIVITY (DBI)	RELATIVE POWER (DB)	ELEVATION ANGLE (DEG)	DIRECTIVITY (NUMERIC)	DIRECTIVITY (DBI)	RELATIVE POWER (DB)
0	0 00000	-INFINITY	-INFINITY				
2 0	0 01708	-17.67612	-21. 44083	92.0	0. 57493	-2. 40383	-6. 16854
4 0	0 06771	-11 69375	-15. 45846	94. 0	0. 52008	-2 83930	-6. 60401
6 0	0 13012	-8. 23551	-12. 00022	96. 0	0. 46921	-3 28629	-7. 05100
8 0	0 26149	-5. 82547	-9. 59018	98 0	0. 42253	-3 74144	-7. 50615
10 0	0 39803	-4 00087	-7. 76558	100. 0	0. 38024	-4. 19944	-7. 96415
12 0	0 55522	-2. 55535	-6. 32006	102 0	0. 34238	-4 65232	-8 41703
14 0	0 72802	-1. 37858	-5. 14329	104 0	0. 30983	-5. 08876	-8 85347
16 0	0 91108	-0. 40445	-4. 16916	106 0	0. 28226	-5 49355	-9 25826
18 0	1 09899	0. 40992	-3. 35479	108. 0	0. 26016	-5. 84767	-9. 61238
20. 0	1 28649	1 09408	-2. 67063	110 0	0. 24381	-6 12940	-9 89411
22. 0	1 46871	1. 66936	-2. 09535	112. 0	0. 23351	-6 31700	-10. 08171
24 0	1 64125	2. 15174	-1. 61297	114. 0	0. 22947	-6 39274	-10. 15744
26. 0	1 80037	2. 55361	-1. 21110	116. 0	0. 23189	-6 34721	-10. 11192
28 0	1 94308	2. 88484	-0. 87987	118. 0	0. 24086	-6. 18229	-9. 94700
30. 0	2 06702	3 15345	-0. 61126	120. 0	0. 25640	-5. 91090	-9. 67561
32 0	2 17077	3. 36615	-0. 39856	122. 0	0. 27835	-5. 55412	-9. 31883
34. 0	2 25351	3 52859	-0. 23612	124. 0	0. 30643	-5. 13672	-8. 90142
36 0	2 31508	3. 64567	-0. 11904	126. 0	0. 34016	-4. 68821	-8. 44792
38 0	2 35593	3. 72162	-0 04309	128. 0	0. 37885	-4 21532	-7. 98003
40. 0	2 37695	3. 76019	-0. 00452	130. 0	0. 42161	-3. 75091	-7. 51561
42. 0	2 37942	3 76471	0. 00000	132. 0	0. 46730	-3. 30402	-7. 06872
44 0	2. 36490	3. 73813	-0 02657	134. 0	0. 51458	-2. 88543	-6. 65014
46 0	2 33514	3. 68312	-0. 08159	136. 0	0. 56191	-2. 50335	-6. 26806
48 0	2 29195	3. 60206	-0. 16265	138. 0	0. 60756	-2. 16411	-5. 92882
50. 0	2 23722	3. 49708	-0. 26763	140. 0	0 64971	-1. 87281	-5. 63752
52 0	2 17275	3. 37009	-0. 39462	142. 0	0. 68647	-1. 63376	-5. 39847
54 0	2 10030	3. 22280	-0. 54191	144. 0	0. 71600	-1. 45087	-5. 21558
56. 0	2 02149	3. 05671	-0. 70800	146. 0	0. 73636	-1. 32794	-5. 09265
58. 0	1 93782	2. 87314	-0. 89157	148. 0	0. 74663	-1. 26894	-5. 03365
60. 0	1 85064	2. 67322	-1. 09149	150. 0	0. 74503	-1. 27826	-5. 04297
62. 0	1. 76113	2. 45791	-1. 30680	152. 0	0. 73098	-1. 36093	-5. 12564
64. 0	1. 67033	2. 22802	-1. 53669	154. 0	0. 70422	-1. 52294	-5. 28765
66. 0	1 57913	1 98418	-1. 78053	156. 0	0. 66503	-1. 77159	-5. 53630
68. 0	1. 48829	1. 72688	-2 03783	158. 0	0. 61431	-2. 11600	-5. 88071
70. 0	1 39845	1. 45646	-2. 30825	160. 0	0. 55362	-2. 56786	-6. 33257
72 0	1 31012	1. 17311	-2. 59160	162. 0	0. 48501	-3. 14248	-6. 90719
74. 0	1 22374	0 87688	-2. 88783	164. 0	0. 41110	-3. 86057	-7. 62528
76. 0	1 13965	0. 56771	-3. 19700	166. 0	0 33488	-4. 75110	-8. 51581
78. 0	1 05814	0. 24541	-3. 51930	168. 0	0. 25963	-5. 85645	-9. 62116
80. 0	0 97943	-0 09028	-3. 85499	170. 0	0. 18870	-7. 24230	-11. 00701
82. 0	0 90371	-0. 43973	-4. 20444	172. 0	0. 12535	-9. 01860	-12. 78331
84 0	0 83113	-0. 80331	-4. 56802	174. 0	0. 07259	-11. 39138	-15. 15609
86 0	0 76184	-1 18138	-4. 94609	176. 0	0. 03294	-14. 82319	-18. 58790
88. 0	0 69595	-1. 57420	-5. 33891	178. 0	0. 00834	-20. 78976	-24. 55447
90 0	0 63361	-1 98180	-5. 74651	180.	0. 00000	-INFINITY	-INFINITY

TABLE A2-16 $2\pi a/\lambda = 4.00$

```
EPSLN= 4.000(NORMALIZED GROUNDPLANE RADIUS)
MONOPOLE LENGTH= 0.250000(WAVELENGTH)
MONOPOLE RADIUS=  0.1000E-05(WAVELENGTH)
NUMBER OF MONOPOLE SEGMENTS=  1
NUMBER OF DISK SEGMENTS= 16
RADIATION RESISTANCE DETERMINED BY PATTERN= 0.444339E+02 OHMS
```

ELEVATION ANGLE (DEG)	DIRECTIVITY (NUMERIC)	DIRECTIVITY (DBI)	RELATIVE POWER (DB)	ELEVATION ANGLE (DEG)	DIRECTIVITY (NUMERIC)	DIRECTIVITY (DBI)	RELATIVE POWER (DB)
0	0.00000	-INFINITY	-INFINITY				
2.0	0.01922	-17.16234	-21.07366	92.0	0.61408	-2.11778	-6.02910
4.0	0.07614	-11.18380	-15.09512	94.0	0.55574	-2.55127	-6.46259
6.0	0.16858	-7.73189	-11.64321	96.0	0.50027	-3.00795	-6.91927
8.0	0.29305	-5.33064	-9.24196	98.0	0.44781	-3.48905	-7.40037
10.0	0.44492	-3.51720	-7.42852	100.0	0.39856	-3.99503	-7.90637
12.0	0.61871	-2.08513	-5.99645	102.0	0.35276	-4.52520	-8.43652
14.0	0.80836	-0.92396	-4.83528	104.0	0.31070	-5.07654	-8.98786
16.0	1.00753	0.03256	-3.87876	106.0	0.27273	-5.64265	-9.55397
18.0	1.20990	0.82748	-3.08384	108.0	0.23923	-6.21179	-10.12311
20.0	1.40947	1.49055	-2.42077	110.0	0.21063	-6.76471	-10.67603
22.0	1.60077	2.04330	-1.86802	112.0	0.18739	-7.27253	-11.18385
24.0	1.77908	2.50193	-1.40927	114.0	0.16996	-7.69642	-11.60774
26.0	1.94051	2.87916	-1.03216	116.0	0.15881	-7.99120	-11.90252
28.0	2.08212	3.18505	-0.72627	118.0	0.15434	-8.11509	-12.02641
30.0	2.20189	3.42796	-0.48336	120.0	0.15691	-8.04244	-11.95477
32.0	2.29873	3.61487	-0.29645	122.0	0.16675	-7.77927	-11.69059
34.0	2.37234	3.75178	-0.15954	124.0	0.18396	-7.35270	-11.26402
36.0	2.42318	3.84386	-0.06746	126.0	0.20845	-6.80992	-10.72124
38.0	2.45228	3.89570	-0.01563	128.0	0.23991	-6.19952	-10.11084
40.0	2.46112	3.91132	0.00000	130.0	0.27776	-5.56326	-9.47458
42.0	2.45152	3.89435	-0.01697	132.0	0.32115	-4.93287	-8.84420
44.0	2.42551	3.84803	-0.06329	134.0	0.36892	-4.33063	-8.24196
46.0	2.38521	3.77527	-0.13606	136.0	0.41961	-3.77151	-7.68284
48.0	2.33273	3.67865	-0.23267	138.0	0.47148	-3.26541	-7.17673
50.0	2.27014	3.56032	-0.35080	140.0	0.52252	-2.81894	-6.73026
52.0	2.19935	3.42294	-0.48838	142.0	0.57059	-2.43679	-6.34811
54.0	2.12213	3.26771	-0.64361	144.0	0.61340	-2.12260	-6.03392
56.0	2.04006	3.09443	-0.81689	146.0	0.64870	-1.87958	-5.79090
58.0	1.95454	2.91044	-1.00088	148.0	0.67437	-1.71102	-5.62234
60.0	1.86677	2.71090	-1.20042	150.0	0.68856	-1.62057	-5.53189
62.0	1.77776	2.49874	-1.41258	152.0	0.68983	-1.61256	-5.52389
64.0	1.68838	2.27471	-1.63661	154.0	0.67727	-1.69236	-5.60369
66.0	1.59932	2.03935	-1.87197	156.0	0.65062	-1.86671	-5.77803
68.0	1.51114	1.79305	-2.11827	158.0	0.61035	-2.14424	-6.05557
70.0	1.42429	1.53600	-2.37533	160.0	0.55767	-2.53621	-6.44753
72.0	1.33913	1.26822	-2.64310	162.0	0.49459	-3.05757	-6.96889
74.0	1.25591	0.98958	-2.92174	164.0	0.42377	-3.72872	-7.64004
76.0	1.17483	0.69975	-3.21157	166.0	0.34847	-4.57837	-8.48969
78.0	1.09604	0.39825	-3.51307	168.0	0.27235	-5.64869	-9.56001
80.0	1.01962	0.08440	-3.82692	170.0	0.19929	-7.00517	-10.91649
82.0	0.94566	-0.24263	-4.15395	172.0	0.13312	-8.75762	-12.66894
84.0	0.87420	-0.58389	-4.49521	174.0	0.07741	-11.11197	-15.02329
86.0	0.80527	-0.94058	-4.85190	176.0	0.03523	-14.53067	-18.44199
88.0	0.73891	-1.31408	-5.22540	178.0	0.00893	-20.48940	-24.40072
90.0	0.67516	-1.70594	-5.61726	180.	0.00000	-INFINITY	-INFINITY

TABLE A2-17 $2\pi a/\lambda = 4.25$

```
EPSLN= 4 ,SIG=(NORMALIZED GROUNDPLANE RADIUS)
MONOPOLE LENGTH= 0 250000(WAVELENGTH)
MONOPOLE RADIUS=  0 10000E-05(WAVELENGTH)
NUMBER OF MONOPOLE SEGMENTS=  1
NUMBER OF DISK SEGMENTS= 16
RADIATION RESISTANCE DETERMINED BY PATTERN= 0 405777E+02 OHMS
```

ELEVATION ANGLE (DEG)	DIRECTIVITY (NUMERIC)	DIRECTIVITY (DBI)	RELATIVE POWER (DB)	ELEVATION ANGLE (DEG)	DIRECTIVITY (NUMERIC)	DIRECTIVITY (DBI)	RELATIVE POWER (DB)
0	0 00000	-INFINITY	-INFINITY				
2 0	0 02096	-16 78670	-20 70236	92.0	0 67953	-1 67794	-5.59359
4 0	0 08294	-10 81236	-14 72802	94 0	0.62146	-2 06586	-5.98152
6 0	0 18334	-7.36741	-11 28307	96.0	0 56516	-2 47829	-6.39395
8 0	0 31799	-4 97582	-8 89148	98.0	0.51069	-2.91842	-6.83407
10. 0	0 48143	-3.17464	-7 09030	100. 0	0.45818	-3 38965	-7.30531
12 0	0 66722	-1 75729	-5.67295	102. 0	0.40780	-3 89551	-7.81117
14. 0	0 86833	-0 61317	-4.52883	104. 0	0.35981	-4 43932	-8.35498
16 0	1 07749	0. 32415	-3.59151	106. 0	0.31451	-5 02366	-8.93932
18. 0	1 28764	1. 09794	-2.81771	108. 0	0.27231	-5 64937	-9.56503
20. 0	1 49218	1 73920	-2.17746	110. 0	0.23368	-6.31385	-10.22951
22. 0	1 68528	2. 26672	-1.64894	112. 0	0.19915	-7 00811	-10.92377
24. 0	1 86210	2. 70004	-1 21562	114 0	0.16935	-7.71225	-11.62791
26. 0	2 01889	3. 05113	-0 86452	116. 0	0.14490	-8 38925	-12.30491
28. 0	2 15302	3 33049	-0. 58517	118. 0	0 12649	-8.97939	-12.89505
30. 0	2 26298	3. 54681	-0. 36885	120. 0	0. 11477	-9 40169	-13.31735
32. 0	2 34827	3 70749	-0. 20817	122. 0	0. 11034	-9. 57249	-13. 48815
34. 0	2 40929	3. 81890	-0. 09676	124. 0	0. 11372	-9. 44168	-13. 35734
36. 0	2 44717	3 88664	-0. 02902	126. 0	0 12525	-9 02234	-12. 93800
38. 0	2 46357	3. 91566	0. 00000	128. 0	0. 14507	-8 38413	-12. 29979
40. 0	2 46058	3 91038	-0. 00528	130. 0	0 17308	-7 61759	-11. 53324
42 0	2 44049	3 87476	-0. 04089	132. 0	0. 20882	-6. 80221	-10. 71787
44 0	2 40566	3. 81235	-0. 10331	134. 0	0 25151	-5 99443	-9. 91008
46 0	2 35847	3 72631	-0. 18935	136. 0	0. 29995	-5. 22945	-9. 14510
48 0	2 30115	3. 61944	-0. 29621	138. 0	0. 35257	-4. 52757	-8. 44323
50 0	2. 23575	3 49423	-0 42142	140. 0	0 40739	-3 89991	-7. 81557
52 0	2 16413	3 35283	-0. 56282	142. 0	0. 46212	-3. 35244	-7. 26810
54 0	2. 08790	3 19710	-0. 71856	144. 0	0. 51422	-2 88853	-6. 80419
56. 0	2 00845	3 02860	-0. 88706	146 0	0 56099	-2. 51041	-6. 42607
58. 0	1 92692	2. 84864	-1. 06702	148. 0	0 59977	-2. 22015	-6. 13581
60 0	1 84428	2 65827	-1. 25739	150. 0	0. 62804	-2 02016	-5. 93581
62 0	1. 76129	2 45832	-1. 45734	152. 0	0 64363	-1 91365	-5. 82931
64 0	1 67857	2 24941	-1. 66625	154. 0	0. 64492	-1. 90497	-5. 82063
66. 0	1 59660	2 03197	-1. 88369	156. 0	0. 63096	-2 00000	-5. 91566
68 0	1. 51574	1 80625	-2 10941	158. 0	0. 60164	-2. 20864	-6. 12230
70 0	1 43627	1 57236	-2. 34330	160. 0	0. 55776	-2. 53551	-6. 45116
72 0	1 35836	1. 33022	-2 58544	162. 0	0 50107	-3. 00104	-6. 91670
74. 0	1 28222	1 07980	-2. 83603	164. 0	0. 43419	-3. 62321	-7. 53887
76 0	1 20787	0 82022	-3 09544	166 0	0. 36035	-4. 43036	-8. 34602
78 0	1 13539	0. 55145	-3. 36421	168. 0	0. 28416	-5. 46438	-9. 38003
80 0	1 06479	0 27263	-3 64303	170. 0	0. 20939	-6. 79030	-10 70616
82. 0	0. 99606	-0 01715	-3 93281	172. 0	0. 14066	-8. 51836	-12. 43402
84 0	0 92918	-0 31899	-4 23465	174 0	0. 08215	-10. 85273	-14 76939
86. 0	0 86412	-0 63424	-4 54989	176. 0	0. 03751	-14. 25894	-18 17460
88 0	0 80088	-0. 96430	-4 88015	178 0	0 00953	-20 20962	-24 12527
90 0	0 73932	-1 31166	-5 22732	180.	0. 00000	-INFINITY	-INFINITY

TABLE A2-18 $2\pi a/\lambda = 4.50$

```
EPSILN= 4.5000(NORMALIZED GROUNDPLANE RADIUS)
MONOPOLE LENGTH= 0.25000(WAVELENGTH)
MONOPOLE RADIUS=  0.10000E-03(WAVELENGTH)
NUMBER OF MONOPOLE SEGMENTS=  1
NUMBER OF DISK SEGMENTS= 16
RADIATION RESISTANCE DETERMINED BY PATTERN= 0.371323E+02 OHMS
```

ELEVATION ANGLE (DEG)	DIRECTIVITY (NUMERIC)	DIRECTIVITY (DBI)	RELATIVE POWER (DB)	ELEVATION ANGLE (DEG)	DIRECTIVITY (NUMERIC)	DIRECTIVITY (DBI)	RELATIVE POWER (DB)
0	0.00000	-INFINITY	-INFINITY				
2.0	0.03248	-14.88123	-20.31094	92.0	0.75173	-1.23939	-5.06911
4.0	0.08889	-10.51173	-14.34144	94.0	0.69652	-1.57066	-5.40037
6.0	0.19612	-7.07480	-10.90451	96.0	0.64224	-1.92304	-5.75275
8.0	0.33929	-4.69422	-8.52403	98.0	0.58985	-2.29999	-6.12970
10.0	0.51201	-2.90722	-6.73694	100.0	0.53638	-2.70554	-6.53525
12.0	0.70684	-1.50679	-5.33651	102.0	0.48481	-3.14433	-6.97404
14.0	0.91375	-0.38223	-4.21194	104.0	0.43435	-3.62162	-7.45133
16.0	1.13061	0.53312	-3.29659	106.0	0.38519	-4.14325	-7.97296
18.0	1.34364	1.28282	-2.54689	108.0	0.33764	-4.71546	-8.54518
20.0	1.54780	1.89715	-1.93256	110.0	0.29211	-5.34449	-9.17420
22.0	1.73711	2.39827	-1.43144	112.0	0.24914	-6.03564	-9.86535
24.0	1.90683	2.80313	-1.02659	114.0	0.20935	-6.79136	-10.62107
26.0	2.05338	3.12512	-0.70459	116.0	0.17349	-7.60736	-11.43707
28.0	2.17531	3.37522	-0.45450	118.0	0.14239	-8.46530	-12.29501
30.0	2.27124	3.56263	-0.26708	120.0	0.11674	-9.32028	-13.14999
32.0	2.34167	3.69527	-0.13445	122.0	0.09807	-10.08465	-13.91436
34.0	2.38783	3.78003	-0.04968	124.0	0.08666	-10.62175	-14.45146
36.0	2.41159	3.82303	-0.00668	126.0	0.08352	-10.78194	-14.61165
38.0	2.41530	3.82971	0.00000	128.0	0.08930	-10.49129	-14.32100
40.0	2.40156	3.80494	-0.02477	130.0	0.10442	-9.81220	-13.64191
42.0	2.37304	3.75306	-0.07666	132.0	0.12897	-8.89514	-12.72485
44.0	2.33233	3.67790	-0.15181	134.0	0.16267	-7.88704	-11.71675
46.0	2.28184	3.58285	-0.24686	136.0	0.20477	-6.88743	-10.71715
48.0	2.22373	3.47083	-0.35889	138.0	0.25403	-5.95120	-9.78091
50.0	2.15990	3.34430	-0.48539	140.0	0.30969	-5.10473	-8.93444
52.0	2.09191	3.20543	-0.62429	142.0	0.36651	-4.39913	-8.18885
54.0	2.02107	3.05582	-0.77389	144.0	0.42479	-3.71825	-7.50797
56.0	1.94844	2.89686	-0.93285	146.0	0.48052	-3.18292	-7.01263
58.0	1.87482	2.72959	-1.10013	148.0	0.53050	-2.75318	-6.58289
60.0	1.80085	2.55476	-1.27495	150.0	0.57156	-2.42942	-6.25913
62.0	1.72701	2.37294	-1.45677	152.0	0.60076	-2.21301	-6.04272
64.0	1.65366	2.18447	-1.64524	154.0	0.61564	-2.10670	-5.93641
66.0	1.58109	1.98936	-1.84035	156.0	0.61446	-2.11304	-5.94275
68.0	1.50949	1.78829	-2.04142	158.0	0.59637	-2.24882	-6.07853
70.0	1.43901	1.58065	-2.24907	160.0	0.56160	-2.50576	-6.33548
72.0	1.36978	1.36651	-2.46320	162.0	0.51130	-2.91157	-6.74128
74.0	1.30187	1.14568	-2.68403	164.0	0.44838	-3.48138	-7.31130
76.0	1.23534	0.91786	-2.91185	166.0	0.37638	-4.24360	-8.07339
78.0	1.17022	0.68266	-3.14705	168.0	0.29927	-5.23934	-9.06905
80.0	1.10651	0.43954	-3.39017	170.0	0.22215	-6.53348	-10.36320
82.0	1.04420	0.18782	-3.64189	172.0	0.15012	-8.23549	-12.06520
84.0	0.98325	-0.07338	-3.90210	174.0	0.08809	-10.55094	-14.38066
86.0	0.92360	-0.34517	-4.17488	176.0	0.04033	-13.94203	-17.77174
88.0	0.86518	-0.62891	-4.45862	178.0	0.01027	-19.88426	-23.71398
90.0	0.80792	-0.92630	-4.75602	180.	0.00000	-INFINITY	-INFINITY

TABLE A2-19 $2\pi a/\lambda = 4.75$

EPSILON= 4.750 CONDUCTIVITY= 0.000 GROUNDPLANE RADIUS=
MONOPOLE LENGTH= 0.25000 (WAVELENGTH)
MONOPOLE RADIUS= 0.10000E-03 (WAVELENGTH)
NUMBER OF MONOPOLE SEGMENTS= 1
NUMBER OF DISK SEGMENTS= 18
RADIATION RESISTANCE DETERMINED BY PATTERN= 0.344626E+02 OHMS

ELEVATION ANGLE (DEG)	DIRECTIVITY (NUMERIC)	DIRECTIVITY (DBI)	RELATIVE POWER (DB)	ELEVATION ANGLE (DEG)	DIRECTIVITY (NUMERIC)	DIRECTIVITY (DBI)	RELATIVE POWER (DB)
0	0.00000	-INFINITY	-INFINITY				
2.0	0.02388	-16.21896	-19.89249	92.0	0.81904	-0.86694	-4.54047
4.0	0.09430	-10.25509	-13.92862	94.0	0.74822	-1.14513	-4.81867
6.0	0.20761	-6.82747	-10.50101	96.0	0.71789	-1.43943	-5.11296
8.0	0.35811	-4.45989	-8.13343	98.0	0.66789	-1.75296	-5.42649
10.0	0.53837	-2.68916	-6.36270	100.0	0.61808	-2.08952	-5.76306
12.0	0.73988	-1.30836	-4.98189	102.0	0.56838	-2.45364	-6.12717
14.0	0.95357	-0.20646	-3.87999	104.0	0.51872	-2.85065	-6.52418
16.0	1.17044	0.68349	-2.99005	106.0	0.46916	-3.28680	-6.96033
18.0	1.38209	1.40537	-2.26816	108.0	0.41982	-3.76934	-7.44287
20.0	1.58121	1.98989	-1.68365	110.0	0.37097	-4.30657	-7.98011
22.0	1.76185	2.45968	-1.21385	112.0	0.32301	-4.90788	-8.58141
24.0	1.91944	2.83221	-0.84132	114.0	0.27648	-5.58341	-9.25694
26.0	2.05186	3.12149	-0.55205	116.0	0.23210	-6.34332	-10.01686
28.0	2.15731	3.33912	-0.33441	118.0	0.19074	-7.19564	-10.86917
30.0	2.23615	3.49302	-0.17852	120.0	0.15342	-8.14117	-11.81470
32.0	2.28970	3.59778	-0.07575	122.0	0.12128	-9.16204	-12.83558
34.0	2.32008	3.65503	-0.01851	124.0	0.09553	-10.19849	-13.87202
36.0	2.32999	3.67353	0.00000	126.0	0.07740	-11.11287	-14.78640
38.0	2.32239	3.65935	-0.01418	128.0	0.06803	-11.67327	-15.34680
40.0	2.30030	3.61784	-0.05569	130.0	0.06842	-11.64825	-15.32179
42.0	2.26659	3.55373	-0.11981	132.0	0.07930	-11.00718	-14.68071
44.0	2.22386	3.47107	-0.20247	134.0	0.10102	-9.95574	-13.62927
46.0	2.17435	3.37329	-0.30024	136.0	0.13345	-8.74674	-12.42028
48.0	2.11993	3.26321	-0.41032	138.0	0.17587	-7.54799	-11.22152
50.0	2.06207	3.14304	-0.53049	140.0	0.22694	-6.44096	-10.11450
52.0	2.00192	3.01446	-0.65907	142.0	0.28462	-5.45737	-9.13090
54.0	1.94030	2.87868	-0.79485	144.0	0.34626	-4.60601	-8.27954
56.0	1.87780	2.73649	-0.93704	146.0	0.40863	-3.88666	-7.56019
58.0	1.81484	2.58838	-1.08516	148.0	0.46812	-3.29645	-6.96998
60.0	1.75169	2.43457	-1.23896	150.0	0.52089	-2.83257	-6.50610
62.0	1.68855	2.27514	-1.39840	152.0	0.56318	-2.49352	-6.16706
64.0	1.62557	2.11005	-1.56349	154.0	0.59161	-2.27964	-5.95317
66.0	1.56287	1.93922	-1.73431	156.0	0.60346	-2.19349	-5.86702
68.0	1.50057	1.76256	-1.91097	158.0	0.59700	-2.24026	-5.91380
70.0	1.43879	1.57999	-2.09353	160.0	0.57169	-2.42841	-6.10195
72.0	1.37766	1.39142	-2.28211	162.0	0.52837	-2.77062	-6.44415
74.0	1.31729	1.19682	-2.47672	164.0	0.46931	-3.28541	-6.95894
76.0	1.25780	0.99610	-2.67743	166.0	0.39811	-4.00000	-7.67353
78.0	1.19928	0.78919	-2.88434	168.0	0.31949	-4.95337	-8.62690
80.0	1.14180	0.57591	-3.09762	170.0	0.23900	-6.21403	-9.88756
82.0	1.08542	0.35598	-3.31755	172.0	0.16252	-7.89102	-11.56455
84.0	1.03015	0.12899	-3.54455	174.0	0.09581	-10.18571	-13.85924
86.0	0.97595	-0.10573	-3.77926	176.0	0.04403	-13.56208	-17.23561
88.0	0.92277	-0.34907	-4.02260	178.0	0.01123	-19.49553	-23.16907
90.0	0.87051	-0.60227	-4.27580	180	0.00000	-INFINITY	-INFINITY

TABLE A2-20 $2\pi a/\lambda = 5.00$

```
EPSLN= 5.0000(NORMALIZED GROUNDPLANE RADIUS)
MONOPOLE LENGTH= 0.250000(WAVELENGTH)
MONOPOLE RADIUS=  0.10006E-05(WAVELENGTH)
NUMBER OF MONOPOLE SEGMENTS=  1
NUMBER OF DISK SEGMENTS= 16
RADIATION RESISTANCE DETERMINED BY PATTERN= 0.326839E+02 OHMS
```

ELEVATION ANGLE (DEG)	DIRECTIVITY (NUMERIC)	DIRECTIVITY (DBI)	RELATIVE POWER (DB)	ELEVATION ANGLE (DEG)	DIRECTIVITY (NUMERIC)	DIRECTIVITY (DBI)	RELATIVE POWER (DB)
0	0.00000	-INFINITY	-INFINITY				
2.0	0.02533	-15.96361	-19.41636	92.0	0.87123	-0.59866	-4.03141
4.0	0.09985	-10.00660	-13.45935	94.0	0.82541	-0.83330	-4.28606
6.0	0.21926	-6.59037	-10.04312	96.0	0.78017	-1.07812	-4.53087
8.0	0.37683	-4.23855	-7.69130	98.0	0.73523	-1.33579	-4.78854
10.0	0.56392	-2.48781	-5.94056	100.0	0.69029	-1.60966	-5.06241
12.0	0.77073	-1.13099	-4.58375	102.0	0.64508	-1.90390	-5.35665
14.0	0.98701	-0.05678	-3.50954	104.0	0.59931	-2.22349	-5.67624
16.0	1.20286	0.80214	-2.65061	106.0	0.55279	-2.57440	-6.02715
18.0	1.40933	1.49014	-1.96262	108.0	0.50540	-2.96367	-6.41642
20.0	1.59899	2.03845	-1.41430	110.0	0.45713	-3.39959	-6.85234
22.0	1.76620	2.47039	-0.98236	112.0	0.40814	-3.89187	-7.34462
24.0	1.90730	2.80418	-0.64857	114.0	0.35877	-4.45188	-7.90463
26.0	2.02053	3.05467	-0.39806	116.0	0.30954	-5.09277	-8.54552
28.0	2.10596	3.23450	-0.21825	118.0	0.26125	-5.82948	-9.28223
30.0	2.16497	3.35452	-0.09823	120.0	0.21488	-6.67805	-10.13080
32.0	2.20008	3.42439	-0.02836	122.0	0.17167	-7.65299	-11.10574
34.0	2.21450	3.45275	0.00000	124.0	0.13305	-8.75972	-12.21247
36.0	2.21172	3.44730	-0.00346	126.0	0.10060	-9.97418	-13.42693
38.0	2.19525	3.41483	-0.03792	128.0	0.07594	-11.19539	-14.64814
40.0	2.16834	3.36128	-0.09147	130.0	0.06068	-12.16948	-15.62223
42.0	2.13384	3.29161	-0.16114	132.0	0.05626	-12.49812	-15.95087
44.0	2.09404	3.20986	-0.24289	134.0	0.06379	-11.95233	-15.40508
46.0	2.05074	3.11911	-0.33364	136.0	0.08393	-10.76061	-14.21336
48.0	2.00519	3.02156	-0.43120	138.0	0.11672	-9.32869	-12.78144
50.0	1.95820	2.91808	-0.53417	140.0	0.16142	-7.92048	-11.37323
52.0	1.91024	2.81089	-0.64187	142.0	0.21648	-6.64590	-10.09865
54.0	1.86150	2.69863	-0.75412	144.0	0.27945	-5.53498	-8.98774
56.0	1.81200	2.58139	-0.87117	146.0	0.34705	-4.59602	-8.04877
58.0	1.76169	2.45930	-0.99345	148.0	0.41531	-3.81633	-7.26908
60.0	1.71049	2.33121	-1.12154	150.0	0.47972	-3.19016	-6.64291
62.0	1.65835	2.19677	-1.25598	152.0	0.53561	-2.71148	-6.16423
64.0	1.60529	2.05553	-1.39722	154.0	0.57851	-2.37690	-5.82965
66.0	1.55137	1.90715	-1.54560	156.0	0.60450	-2.18603	-5.63878
68.0	1.49675	1.75150	-1.70126	158.0	0.61069	-2.14177	-5.59452
70.0	1.44164	1.58858	-1.86417	160.0	0.59556	-2.25077	-5.70352
72.0	1.38630	1.41858	-2.03417	162.0	0.55920	-2.52430	-5.97705
74.0	1.33101	1.24182	-2.21093	164.0	0.50352	-2.97981	-6.43257
76.0	1.27606	1.05870	-2.39405	166.0	0.43215	-3.64367	-7.09642
78.0	1.22171	0.86968	-2.58307	168.0	0.35025	-4.55617	-8.00892
80.0	1.16821	0.67520	-2.77755	170.0	0.26416	-5.78130	-9.23405
82.0	1.11574	0.47564	-2.97711	172.0	0.18081	-7.42772	-10.88047
84.0	1.06445	0.27123	-3.18152	174.0	0.10714	-9.70047	-13.15322
86.0	1.01438	0.06202	-3.39073	176.0	0.04942	-13.06139	-16.51407
88.0	0.96555	-0.15224	-3.60499	178.0	0.01263	-18.98553	-22.43828
90.0	0.91788	-0.37213	-3.82488	180	0.00000	-INFINITY	-INFINITY

TABLE A2-21 $2\pi a/\lambda = 5.25$

```
EPSLN= 5.2500(NORMALIZED GROUNDPLANE RADIUS)
MONOPOLE LENGTH= 0.250000(WAVELENGTH)
MONOPOLE RADIUS=  0.10000E-05(WAVELENGTH)
NUMBER OF MONOPOLE SEGMENTS= 1
NUMBER OF DISK SEGMENTS= 16
RADIATION RESISTANCE DETERMINED BY PATTERN= 0.31705E+02 OHMS
```

ELEVATION ANGLE (DEG)	DIRECTIVITY (NUMERIC)	DIRECTIVITY (DBI)	RELATIVE POWER (DB)	ELEVATION ANGLE (DEG)	DIRECTIVITY (NUMERIC)	DIRECTIVITY (DBI)	RELATIVE POWER (DB)
0	0.00000	-INFINITY	-INFINITY				
2.0	0.02678	-15.72116	-18.98373	92.0	0.90345	-0.44093	-3.60351
4.0	0.10538	-9.77247	-12.93504	94.0	0.86224	-0.64370	-3.80628
6.0	0.23067	-6.37000	-9.53258	96.0	0.82227	-0.84984	-4.01241
8.0	0.39470	-4.03730	-7.19987	98.0	0.78316	-1.06150	-4.22408
10.0	0.58738	-2.31081	-5.47338	100.0	0.74445	-1.28163	-4.44421
12.0	0.79742	-0.98312	-4.14569	102.0	0.70566	-1.51402	-4.67659
14.0	1.01332	0.05743	-3.10513	104.0	0.66629	-1.76335	-4.92592
16.0	1.22425	0.87869	-2.28388	106.0	0.62585	-2.03530	-5.19788
18.0	1.42088	1.52557	-1.63701	108.0	0.58390	-2.33662	-5.49920
20.0	1.59592	2.03010	-1.13247	110.0	0.54010	-2.67526	-5.83783
22.0	1.74443	2.41652	-0.74605	112.0	0.49425	-3.06053	-6.22311
24.0	1.86388	2.70419	-0.45838	114.0	0.44633	-3.50341	-6.66598
26.0	1.95401	2.90927	-0.25330	116.0	0.39657	-4.01681	-7.17938
28.0	2.01641	3.04380	-0.11878	118.0	0.34546	-4.61606	-7.77864
30.0	2.05410	3.12622	-0.03635	120.0	0.29381	-5.31935	-8.48192
32.0	2.07099	3.16178	-0.00079	122.0	0.24277	-6.14797	-9.31054
34.0	2.07137	3.16257	0.00000	124.0	0.19384	-7.12566	-10.28823
36.0	2.05947	3.13755	-0.02503	126.0	0.14878	-8.27454	-11.43711
38.0	2.03910	3.09439	-0.06818	128.0	0.10964	-9.60034	-12.76292
40.0	2.01346	3.03942	-0.12315	130.0	0.07858	-11.04672	-14.20929
42.0	1.98493	2.97746	-0.18511	132.0	0.05778	-12.38202	-15.54459
44.0	1.95516	2.91182	-0.25076	134.0	0.04923	-13.07751	-16.24009
46.0	1.92503	2.84438	-0.31819	136.0	0.05454	-12.63283	-15.79540
48.0	1.89486	2.77577	-0.38681	138.0	0.07471	-11.26611	-14.42868
50.0	1.86448	2.70559	-0.45698	140.0	0.10993	-9.58874	-12.75132
52.0	1.83347	2.63274	-0.52984	142.0	0.15939	-7.97552	-11.13809
54.0	1.80123	2.55569	-0.60688	144.0	0.22113	-6.55359	-9.71616
56.0	1.76716	2.47276	-0.68981	146.0	0.29205	-5.34543	-8.50800
58.0	1.73075	2.38234	-0.78024	148.0	0.36796	-4.34201	-7.50458
60.0	1.69162	2.28303	-0.87954	150.0	0.44377	-3.52843	-6.69100
62.0	1.64960	2.17379	-0.98879	152.0	0.51384	-2.89171	-6.05429
64.0	1.60469	2.05391	-1.10866	154.0	0.57242	-2.42286	-5.58544
66.0	1.55708	1.92311	-1.23946	156.0	0.61416	-2.11716	-5.27974
68.0	1.50712	1.78148	-1.38109	158.0	0.63471	-1.97423	-5.13681
70.0	1.45527	1.62944	-1.53314	160.0	0.63121	-1.99826	-5.16084
72.0	1.40207	1.46771	-1.69487	162.0	0.60275	-2.19865	-5.36123
74.0	1.34811	1.29725	-1.86533	164.0	0.55063	-2.59143	-5.75400
76.0	1.29396	1.11920	-2.04338	166.0	0.47843	-3.20185	-6.36443
78.0	1.24017	0.93481	-2.22777	168.0	0.39180	-4.06939	-7.23197
80.0	1.18723	0.74536	-2.41722	170.0	0.29803	-5.25740	-8.41997
82.0	1.13556	0.55210	-2.61048	172.0	0.20540	-6.87402	-10.03660
84.0	1.08546	0.35618	-2.80642	174.0	0.12235	-9.12395	-12.28652
86.0	1.03716	0.15846	-3.00411	176.0	0.05664	-12.46868	-15.63125
88.0	0.99075	-0.04037	-3.20294	178.0	0.01451	-18.38327	-21.54583
90.0	0.94622	-0.24009	-3.40266	180	0.00000	-INFINITY	-INFINITY

TABLE A2-22 $2\pi a/\lambda = 5.50$

```
EPSLN= 5 5000(NORMALIZED GROUNDPLANE RADIUS)
MONOPOLE LENGTH= 0 250000(WAVELENGTH)
MONOPOLE RADIUS=   0 1000E-05(WAVELENGTH)
NUMBER OF MONOPOLE SEGMENTS=  1
NUMBER OF DISK SEGMENTS= 16
RADIATION RESISTANCE DETERMINED BY PATTERN= 0 315339E+02 OHMS
```

ELEVATION ANGLE (DEG)	DIRECTIVITY (NUMERIC)	DIRECTIVITY (DBI)	RELATIVE POWER (DB)	ELEVATION ANGLE (DEG)	DIRECTIVITY (NUMERIC)	DIRECTIVITY (DBI)	RELATIVE POWER (DB)
0	0.00000	-INFINITY	-INFINITY				
2.0	0.02821	-15.49576	-18.27460	92.0	0.91052	-0.40711	-3.18396
4.0	0.11073	-9.55737	-12.33622	94.0	0.87253	-0.59218	-3.37103
6.0	0.24143	-6.17201	-8.93085	96.0	0.83706	-0.77243	-3.55128
8.0	0.41086	-3.86307	-6.64191	98.0	0.80364	-0.94938	-3.72823
10.0	0.60718	-2.16681	-4.94566	100.0	0.77170	-1.12552	-3.90437
12.0	0.81743	-0.87552	-3.65437	102.0	0.74057	-1.30433	-4.08318
14.0	1.02871	0.12291	-2.65593	104.0	0.70952	-1.49026	-4.26920
16.0	1.22939	0.89689	-1.88196	106.0	0.67777	-1.68920	-4.46804
18.0	1.41000	1.49219	-1.28665	108.0	0.64453	-1.90757	-4.68642
20.0	1.56385	1.94194	-0.83691	110.0	0.60906	-2.15337	-4.93221
22.0	1.68724	2.27176	-0.50708	112.0	0.57072	-2.43374	-5.21458
24.0	1.77942	2.50278	-0.27607	114.0	0.52902	-2.76528	-5.54613
26.0	1.84215	2.65325	-0.12559	116.0	0.48369	-3.15436	-5.93521
28.0	1.87915	2.73961	-0.03924	118.0	0.43476	-3.61749	-6.39834
30.0	1.89534	2.77688	-0.00197	120.0	0.38265	-4.17197	-6.95082
32.0	1.89620	2.77885	0.00000	122.0	0.32819	-4.83873	-7.61757
34.0	1.88706	2.75785	-0.02100	124.0	0.27269	-5.64327	-8.42211
36.0	1.87261	2.72448	-0.05437	126.0	0.21795	-6.61646	-9.39531
38.0	1.85659	2.68716	-0.09169	128.0	0.16621	-7.79338	-10.57222
40.0	1.84157	2.65187	-0.12698	130.0	0.12012	-9.20401	-11.98286
42.0	1.82895	2.62201	-0.15684	132.0	0.08254	-10.83354	-13.61238
44.0	1.81908	2.59852	-0.18032	134.0	0.05640	-12.48701	-15.26586
46.0	1.81147	2.58032	-0.19853	136.0	0.04444	-13.52234	-16.30119
48.0	1.80501	2.56479	-0.21405	138.0	0.04868	-13.10906	-15.88790
50.0	1.79823	2.54846	-0.23039	140.0	0.07113	-11.47939	-14.25824
52.0	1.78958	2.52751	-0.25134	142.0	0.11151	-9.52691	-12.30575
54.0	1.77757	2.49828	-0.28057	144.0	0.16894	-7.72257	-10.50142
56.0	1.76099	2.45758	-0.32127	146.0	0.24084	-6.18264	-8.96148
58.0	1.73894	2.40285	-0.37599	148.0	0.32307	-4.90708	-7.68593
60.0	1.71092	2.33229	-0.44656	150.0	0.41006	-3.87133	-6.65037
62.0	1.67679	2.24479	-0.53405	152.0	0.49520	-3.05220	-5.83104
64.0	1.63680	2.13995	-0.63889	154.0	0.57130	-2.43138	-5.21023
66.0	1.59147	2.01798	-0.76087	156.0	0.63126	-1.99791	-4.77675
68.0	1.54156	1.87960	-0.89925	158.0	0.66883	-1.74669	-4.52554
70.0	1.48799	1.72600	-1.05285	160.0	0.67944	-1.67849	-4.45734
72.0	1.43177	1.55872	-1.22013	162.0	0.66066	-1.80020	-4.57904
74.0	1.37392	1.37962	-1.39923	164.0	0.61292	-2.12593	-4.90479
76.0	1.31546	1.19077	-1.58808	166.0	0.53956	-2.67962	-5.45847
78.0	1.25730	0.99441	-1.78444	168.0	0.44672	-3.49962	-6.27847
80.0	1.20029	0.79285	-1.98600	170.0	0.34298	-4.64851	-7.42736
82.0	1.14510	0.58842	-2.19043	172.0	0.23802	-6.23383	-9.01268
84.0	1.09229	0.38337	-2.39548	174.0	0.14257	-8.45982	-11.23867
86.0	1.04226	0.17975	-2.59910	176.0	0.06626	-11.78767	-14.56651
88.0	0.99523	-0.02068	-2.79953	178.0	0.01701	-17.69222	-20.47107
90.0	0.95136	-0.21657	-2.99541	180	0.00000	-INFINITY	-INFINITY

TABLE A2-23 $2\pi a/\lambda = 5.75$

```
EPSLN= 5.7500(NORMALIZED GROUNDPLANE RADIUS)
MONOPOLE LENGTH= 0.250000(WAVELENGTH)
MONOPOLE RADIUS=  0.1000E-03(WAVELENGTH)
NUMBER OF MONOPOLE SEGMENTS=  1
NUMBER OF DISK SEGMENTS= 16
RADIATION RESISTANCE DETERMINED BY PATTERN= 0.322632E+02 OHMS
```

ELEVATION ANGLE (DEG)	DIRECTIVITY (NUMERIC)	DIRECTIVITY (DBI)	RELATIVE POWER (DB)	ELEVATION ANGLE (DEG)	DIRECTIVITY (NUMERIC)	DIRECTIVITY (DBI)	RELATIVE POWER (DB)
0	0.00000	-INFINITY	-INFINITY				
2.0	0.02943	-15.30901	-17.89665	92.0	0.88786	-0.51638	-3.10422
4.0	0.11525	-9.38061	-11.97125	94.0	0.85054	-0.70303	-3.29067
6.0	0.25004	-6.01983	-8.60747	96.0	0.81760	-0.87481	-3.46225
8.0	0.42257	-3.74099	-6.32863	98.0	0.78853	-1.03182	-3.61946
10.0	0.61899	-2.08319	-4.67083	100.0	0.76270	-1.17643	-3.76407
12.0	0.82444	-0.83842	-3.42606	102.0	0.73934	-1.31158	-3.89922
14.0	1.02469	0.10592	-2.48172	104.0	0.71751	-1.44174	-4.02938
16.0	1.20752	0.81895	-1.76869	106.0	0.69619	-1.57272	-4.16036
18.0	1.36382	1.34758	-1.24006	108.0	0.67428	-1.71163	-4.29927
20.0	1.48818	1.72634	-0.86110	110.0	0.65061	-1.86679	-4.45443
22.0	1.57896	1.98371	-0.60393	112.0	0.62406	-2.04776	-4.63540
24.0	1.63800	2.14314	-0.44450	114.0	0.59356	-2.26536	-4.85300
26.0	1.66985	2.22677	-0.36087	116.0	0.55823	-2.53187	-5.11951
28.0	1.68087	2.25534	-0.33230	118.0	0.51745	-2.86130	-5.44894
30.0	1.67922	2.24849	-0.33915	120.0	0.47099	-3.26998	-5.85762
32.0	1.66891	2.22433	-0.36331	122.0	0.41906	-3.77728	-6.36492
34.0	1.65903	2.19855	-0.38909	124.0	0.36251	-4.40681	-6.99445
36.0	1.65024	2.18036	-0.40728	126.0	0.30283	-5.18808	-7.77572
38.0	1.65445	2.18655	-0.40109	128.0	0.24219	-6.15845	-8.74609
40.0	1.66383	2.21109	-0.37655	130.0	0.18346	-7.36466	-9.95230
42.0	1.68093	2.25353	-0.33209	132.0	0.13006	-8.85865	-11.44629
44.0	1.70412	2.31301	-0.27263	134.0	0.08581	-10.66465	-13.25229
46.0	1.73079	2.38244	-0.20320	136.0	0.05464	-12.62461	-15.21225
48.0	1.75793	2.45001	-0.13763	138.0	0.04024	-13.95346	-16.54110
50.0	1.78246	2.51019	-0.07745	140.0	0.04560	-13.41010	-15.99774
52.0	1.80153	2.55642	-0.03122	142.0	0.07261	-11.39002	-13.97766
54.0	1.81280	2.58349	-0.00415	144.0	0.12158	-9.15121	-11.73885
56.0	1.81453	2.58764	0.00000	146.0	0.19095	-7.19078	-9.77842
58.0	1.80569	2.56644	-0.02120	148.0	0.27705	-5.57442	-8.16206
60.0	1.78593	2.51884	-0.06900	150.0	0.37416	-4.26942	-6.85706
62.0	1.75550	2.44400	-0.14364	152.0	0.47478	-3.23504	-5.82268
64.0	1.71518	2.34309	-0.24455	154.0	0.57019	-2.43977	-5.02741
66.0	1.66614	2.21712	-0.37052	156.0	0.65124	-1.86258	-4.45022
68.0	1.60984	2.06783	-0.51981	158.0	0.70933	-1.49153	-4.07917
70.0	1.54788	1.89738	-0.69026	160.0	0.73747	-1.32255	-3.91019
72.0	1.48193	1.70828	-0.87936	162.0	0.73129	-1.35912	-3.94676
74.0	1.41361	1.50331	-1.08433	164.0	0.68977	-1.61295	-4.20059
76.0	1.34447	1.28350	-1.30214	166.0	0.61573	-2.10609	-4.69373
78.0	1.27588	1.05810	-1.52754	168.0	0.51575	-2.87563	-5.46327
80.0	1.20906	0.82449	-1.76115	170.0	0.39965	-3.98315	-6.57079
82.0	1.14503	0.58816	-1.99748	172.0	0.27955	-5.53347	-8.12111
84.0	1.08458	0.35263	-2.23301	174.0	0.16841	-7.73628	-10.32392
86.0	1.02834	0.12135	-2.46429	176.0	0.07859	-11.04640	-13.63404
88.0	0.97669	-0.10244	-2.69008	178.0	0.02023	-16.94042	-19.52806
90.0	0.92985	-0.31586	-2.90350	180.	0.00000	-INFINITY	-INFINITY

TABLE A2-24 $2\pi a/\lambda = 6.00$

```
LENGTH = 1.000 (NORMALIZED GROUNDPLANE RADIUS
MONOPOLE LENGTH= 0.250000(WAVELENGTH)
MONOPOLE RADIUS=  0.10000E-05(WAVELENGTH)
NUMBER OF MONOPOLE SEGMENTS= 1
NUMBER OF DISK SEGMENTS= 16
RADIATION RESISTANCE DETERMINED BY PATTERN= 0.340436E+02 OHMS
```

ELEVATION ANGLE (DEG)	DIRECTIVITY (NUMERIC)	DIRECTIVITY (DBI)	RELATIVE POWER (DB)	ELEVATION ANGLE (DEG)	DIRECTIVITY (NUMERIC)	DIRECTIVITY (DBI)	RELATIVE POWER (DB)
0	0.00000	-INFINITY	-INFINITY				
2.0	0.03020	-15.19936	-18.09671	92.0	0.80394	-0.78863	-3.69598
4.0	0.11775	-9.29050	-12.18785	94.0	0.79352	-1.00440	-3.90175
6.0	0.25384	-5.95434	-8.85169	96.0	0.75971	-1.19353	-4.09088
8.0	0.42518	-3.71423	-6.61158	98.0	0.73207	-1.35449	-4.25185
10.0	0.61571	-2.10624	-5.00360	100.0	0.70999	-1.48750	-4.38486
12.0	0.80868	-0.92223	-3.81959	102.0	0.69267	-1.59473	-4.49208
14.0	0.98873	-0.04921	-2.94657	104.0	0.67914	-1.68039	-4.57774
16.0	1.14361	0.58278	-2.31458	106.0	0.66824	-1.75067	-4.64803
18.0	1.26335	1.02212	-1.87523	108.0	0.65863	-1.81357	-4.71092
20.0	1.35083	1.30680	-1.59136	110.0	0.64884	-1.87861	-4.77596
22.0	1.40154	1.46605	-1.43131	112.0	0.63729	-1.95663	-4.85399
24.0	1.42289	1.53171	-1.36564	114.0	0.62235	-2.05966	-4.95702
26.0	1.42101	1.53208	-1.36527	116.0	0.60244	-2.20083	-5.09818
28.0	1.41137	1.49642	-1.40094	118.0	0.57616	-2.39455	-5.29191
30.0	1.39742	1.45327	-1.44408	120.0	0.54239	-2.65689	-5.55425
32.0	1.38940	1.42826	-1.46910	122.0	0.50047	-3.00621	-5.90356
34.0	1.39348	1.44102	-1.45634	124.0	0.45039	-3.46416	-6.36151
36.0	1.41333	1.50244	-1.39492	126.0	0.39289	-4.05726	-6.95462
38.0	1.44996	1.61356	-1.28380	128.0	0.32967	-4.81925	-7.71660
40.0	1.50198	1.76666	-1.13070	130.0	0.26337	-5.79441	-8.69176
42.0	1.56610	1.94819	-0.94916	132.0	0.19761	-7.04181	-9.93917
44.0	1.63768	2.14228	-0.75507	134.0	0.13688	-8.63672	-11.53407
46.0	1.71142	2.33358	-0.56378	136.0	0.08619	-10.64532	-13.54268
48.0	1.78199	2.50906	-0.38830	138.0	0.05078	-12.94283	-15.84019
50.0	1.84449	2.65876	-0.23860	140.0	0.03352	-14.49485	-17.39221
52.0	1.89485	2.77574	-0.12162	142.0	0.04433	-13.53310	-16.43045
54.0	1.93005	2.85569	-0.04167	144.0	0.07951	-10.99570	-13.89305
56.0	1.94824	2.89642	-0.00094	146.0	0.14119	-8.50207	-11.39942
58.0	1.94866	2.89735	0.00000	148.0	0.22684	-6.44287	-9.34023
60.0	1.93157	2.85910	-0.03825	150.0	0.33112	-4.80015	-7.69750
62.0	1.89807	2.78313	-0.11423	152.0	0.44602	-3.50647	-6.40382
64.0	1.84990	2.67149	-0.22587	154.0	0.56137	-2.50750	-5.40486
66.0	1.78924	2.52668	-0.37067	156.0	0.66578	-1.76669	-4.66404
68.0	1.71851	2.35152	-0.54584	158.0	0.74786	-1.26181	-4.15917
70.0	1.64023	2.14906	-0.74830	160.0	0.79763	-0.98197	-3.87933
72.0	1.55688	1.92236	-0.97479	162.0	0.80798	-0.92598	-3.82334
74.0	1.47079	1.67551	-1.22185	164.0	0.77584	-1.10228	-3.99964
76.0	1.38406	1.41136	-1.48579	166.0	0.70297	-1.53064	-4.42800
78.0	1.29857	1.13965	-1.75771	168.0	0.59614	-2.24648	-5.14384
80.0	1.21589	0.84893	-2.04843	170.0	0.46664	-3.31016	-6.20751
82.0	1.13732	0.55883	-2.33853	172.0	0.32903	-4.82761	-7.72497
84.0	1.06391	0.26904	-2.62832	174.0	0.19944	-7.00189	-9.89925
86.0	0.99643	-0.01554	-2.91290	176.0	0.09347	-10.29336	-13.19071
88.0	0.93542	-0.28992	-3.18727	178.0	0.02412	-16.17629	-19.07364
90.0	0.88122	-0.54915	-3.44650	180	0.00000	-INFINITY	-INFINITY

TABLE A2-25 $2\pi a/\lambda = 6.25$

EPSLN= 0 (SQUARE-NORMALIZED GROUNDPLANE RADIUS)
MONOPOLE LENGTH= 0 250000(WAVELENGTH)
MONOPOLE RADIUS= 0 10000E-05(WAVELENGTH)
NUMBER OF MONOPOLE SEGMENTS= 1
NUMBER OF DISK SEGMENTS= 14
RADIATION RESISTANCE DETERMINED BY PATTERN= 0 3694236+02 OHMS

ELEVATION ANGLE (DEG)	DIRECTIVITY (NUMERIC)	DIRECTIVITY (DBI)	RELATIVE POWER (DB)	ELEVATION ANGLE (DEG)	DIRECTIVITY (NUMERIC)	DIRECTIVITY (DBI)	RELATIVE POWER (DB)
0	0.00000	-INFINITY	-INFINITY				
2.0	0.03004	-15.22289	-18.58903	92.0	0.75521	-1.21934	-4.58548
4.0	0.11654	-9.33518	-12.70132	94.0	0.70726	-1.50420	-4.87034
6.0	0.24920	-6.03452	-9.40066	96.0	0.66911	-1.73153	-5.11767
8.0	0.41261	-3.84460	-7.21074	98.0	0.63745	-1.95336	-5.32170
10.0	0.58858	-2.30192	-5.66806	100.0	0.61481	-2.11259	-5.47874
12.0	0.75882	-1.19863	-4.56477	102.0	0.59954	-2.22180	-5.58794
14.0	0.90744	-0.42193	-3.78797	104.0	0.59078	-2.28572	-5.65186
16.0	1.02306	0.09902	-3.26712	106.0	0.58744	-2.31035	-5.67649
18.0	1.10003	0.41406	-2.95208	108.0	0.58819	-2.30486	-5.67100
20.0	1.13872	0.56418	-2.80196	110.0	0.59143	-2.28100	-5.64714
22.0	1.14494	0.58782	-2.77832	112.0	0.59534	-2.25238	-5.61852
24.0	1.12860	0.52538	-2.84076	114.0	0.59798	-2.23284	-5.59898
26.0	1.10193	0.42134	-2.94460	116.0	0.59689	-2.24102	-5.60716
28.0	1.07759	0.32453	-3.04161	118.0	0.59017	-2.29020	-5.65634
30.0	1.06687	0.28112	-3.08502	120.0	0.57564	-2.39846	-5.76460
32.0	1.07838	0.32770	-3.03844	122.0	0.55154	-2.58421	-5.95035
34.0	1.11715	0.48113	-2.88501	124.0	0.51665	-2.86800	-6.23415
36.0	1.18445	0.73517	-2.63097	126.0	0.47055	-3.27392	-6.64006
38.0	1.27795	1.06513	-2.30101	128.0	0.41385	-3.83159	-7.19773
40.0	1.39240	1.43764	-1.92850	130.0	0.34838	-4.57941	-7.94555
42.0	1.52053	1.81996	-1.54618	132.0	0.27736	-5.56951	-8.93565
44.0	1.65402	2.18542	-1.18072	134.0	0.20533	-6.87539	-10.24153
46.0	1.78443	2.51499	-0.85115	136.0	0.13602	-8.66044	-11.96658
48.0	1.90399	2.79664	-0.56950	138.0	0.08197	-10.86353	-14.22967
50.0	2.00621	3.02376	-0.34238	140.0	0.04393	-13.57221	-16.93835
52.0	2.08624	3.19364	-0.17250	142.0	0.02016	-15.95791	-19.32406
54.0	2.14099	3.30814	-0.05800	144.0	0.00550	-17.59630	-20.96245
56.0	2.16910	3.36279	-0.00335	146.0	0.00251	-18.00817	-21.37431
58.0	2.17077	3.36614	0.00000	148.0	0.01069	-17.67799	-21.04413
60.0	2.14749	3.31932	-0.04682	150.0	0.02594	-15.89187	-19.25801
62.0	2.10173	3.22576	-0.14038	152.0	0.04047	-13.97428	-17.34043
64.0	2.03659	3.08903	-0.27711	154.0	0.05319	-12.73121	-16.09735
66.0	1.95557	2.91274	-0.45340	156.0	0.06063	-11.80042	-15.16656
68.0	1.86229	2.70048	-0.66566	158.0	0.06845	-11.14383	-14.50997
70.0	1.76026	2.45582	-0.91032	160.0	0.08323	-10.74054	-14.10668
72.0	1.65285	2.18203	-1.18391	162.0	0.07441	-10.98267	-13.94901
74.0	1.54298	1.88359	-1.48255	164.0	0.05607	-10.67490	-14.04104
76.0	1.43928	1.56933	-1.80282	166.0	0.06824	-11.03340	-14.39954
78.0	1.32599	1.22542	-2.14672	168.0	0.07736	-11.69168	-15.05782
80.0	1.22294	0.87405	-2.49809	170.0	0.03597	-12.70859	-16.07473
82.0	1.12559	0.51381	-2.85233	172.0	0.03113	-14.18899	-17.55513
84.0	1.03510	0.14982	-3.21632	174.0	0.03252	-16.33515	-19.70129
86.0	0.95232	-0.21219	-3.57833	176.0	0.10947	-19.60888	-22.97502
88.0	0.87785	-0.56582	-3.93196	178.0	0.02833	-15.47611	-18.84425
90.0	0.81208	-0.90403	-4.27017	180.	0.00000	-INFINITY	-INFINITY

TABLE A2-26 $2\pi a/\lambda = 6.50$

```
EPSLN= 6.5000(NORMALIZED GROUNDPLANE RADIUS)
MONOPOLE LENGTH= 0.250000(WAVELENGTH)
MONOPOLE RADIUS=   0.1000E-03(WAVELENGTH)
NUMBER OF MONOPOLE SEGMENTS=  1
NUMBER OF DISK SEGMENTS= 16
RADIATION RESISTANCE DETERMINED BY PATTERN= 0.405661E+02 OHMS
```

ELEVATION ANGLE (DEG)	DIRECTIVITY (NUMERIC)	DIRECTIVITY (DBI)	RELATIVE POWER (DB)	ELEVATION ANGLE (DEG)	DIRECTIVITY (NUMERIC)	DIRECTIVITY (DBI)	RELATIVE POWER (DB)
0	0.00000	-INFINITY	-INFINITY				
2.0	0.02867	-15.42621	-19.32198	92.0	0.67013	-1.73840	-5.63417
4.0	0.11053	-9.56530	-13.46107	94.0	0.61098	-2.13974	-6.03551
6.0	0.23388	-6.31000	-10.20577	96.0	0.56207	-2.50209	-6.39786
8.0	0.38150	-4.18504	-8.08081	98.0	0.52330	-2.81231	-6.70828
10.0	0.53355	-2.72827	-6.62404	100.0	0.49444	-3.05886	-6.95483
12.0	0.67089	-1.73350	-5.62927	102.0	0.47514	-3.23181	-7.12778
14.0	0.77815	-1.08936	-4.98513	104.0	0.46485	-3.32690	-7.22287
16.0	0.84601	-0.72622	-4.62199	106.0	0.46281	-3.34600	-7.24177
18.0	0.87239	-0.59292	-4.48869	108.0	0.46798	-3.29775	-7.19352
20.0	0.86231	-0.64335	-4.53912	110.0	0.47900	-3.19663	-7.09240
22.0	0.82678	-0.82609	-4.72186	112.0	0.49416	-3.06129	-6.95705
24.0	0.78064	-1.07547	-4.97124	114.0	0.51138	-2.91255	-6.80832
26.0	0.74014	-1.30685	-5.20261	116.0	0.52822	-2.77184	-6.66761
28.0	0.72044	-1.42403	-5.31980	118.0	0.54197	-2.66024	-6.55601
30.0	0.73354	-1.34573	-5.24152	120.0	0.54976	-2.59825	-6.49402
32.0	0.78689	-1.04083	-4.93660	122.0	0.54876	-2.60615	-6.50192
34.0	0.88276	-0.54159	-4.43736	124.0	0.53644	-2.70482	-6.60059
36.0	1.01833	0.07889	-3.81688	126.0	0.51086	-2.91701	-6.81278
38.0	1.18635	0.74284	-3.15293	128.0	0.47106	-3.26923	-7.16500
40.0	1.37723	1.39006	-2.50571	130.0	0.41740	-3.79443	-7.69020
42.0	1.57851	1.98246	-1.91331	132.0	0.35186	-4.53634	-8.43211
44.0	1.77818	2.49975	-1.39602	134.0	0.27819	-5.55660	-9.45237
46.0	1.96489	2.92338	-0.96239	136.0	0.20198	-6.94697	-10.84274
48.0	2.12904	3.28184	-0.61393	138.0	0.13036	-8.84851	-12.74428
50.0	2.26336	3.54753	-0.34824	140.0	0.07152	-11.45572	-15.35149
52.0	2.36311	3.73485	-0.16092	142.0	0.03386	-14.70290	-18.59867
54.0	2.42609	3.84907	-0.04670	144.0	0.02497	-16.02609	-19.92186
56.0	2.45232	3.89577	0.00000	146.0	0.05040	-12.97553	-16.87130
58.0	2.44370	3.88047	-0.01529	148.0	0.11253	-9.48734	-13.38311
60.0	2.40352	3.80847	-0.08729	150.0	0.20957	-6.78671	-10.68248
62.0	2.33601	3.68475	-0.21102	152.0	0.33507	-4.74860	-8.64437
64.0	2.24591	3.51393	-0.38184	154.0	0.47802	-3.20555	-7.10132
66.0	2.13811	3.30030	-0.59547	156.0	0.62366	-2.05054	-5.94631
68.0	2.01735	3.04781	-0.84796	158.0	0.75508	-1.22008	-5.11585
70.0	1.88803	2.76010	-1.13567	160.0	0.85540	-0.67832	-4.57409
72.0	1.75411	2.44057	-1.45520	162.0	0.91025	-0.40839	-4.30416
74.0	1.61898	2.09242	-1.80335	164.0	0.91023	-0.40848	-4.30425
76.0	1.48550	1.71873	-2.17704	166.0	0.85281	-0.69146	-4.58723
78.0	1.35600	1.32258	-2.57319	168.0	0.74337	-1.28793	-5.18370
80.0	1.23231	0.90719	-2.98858	170.0	0.59499	-2.25489	-6.15066
82.0	1.11585	0.47607	-3.41970	172.0	0.42699	-3.69586	-7.59163
84.0	1.00769	0.03328	-3.86249	174.0	0.26229	-5.81218	-9.70795
86.0	0.90859	-0.41630	-4.31207	176.0	0.12408	-9.06301	-12.95878
88.0	0.81909	-0.86668	-4.76245	178.0	0.03220	-14.92186	-18.81763
90.0	0.73953	-1.31042	-5.20619	180	0.00000	-INFINITY	-INFINITY

TABLE A2-27 $2\pi a/\lambda = 6.75$

```
EPSLN= 5  SQU(NORMALIZED GROUNDPLANE RADIUS)
MONOPOLE LENGTH= 0 250000(WAVELENGTH)
MONOPOLE RADIUS=  0 1000E-05(WAVELENGTH)
NUMBER OF MONOPOLE SEGMENTS=  1
NUMBER OF DISK SEGMENTS= 16
RADIATION RESISTANCE DETERMINED BY PATTERN= 0 435313E+02 OHMS
```

ELEVATION ANGLE (DEG)	DIRECTIVITY (NUMERIC)	DIRECTIVITY (DBI)	RELATIVE POWER (DB)	ELEVATION ANGLE (DEG)	DIRECTIVITY (NUMERIC)	DIRECTIVITY (DBI)	RELATIVE POWER (DB)
0	0 00000	-INFINITY	-INFINITY				
2 0	0 02612	-15 82993	-20 19410	92. 0	0. 60775	-2 16278	-6 52695
4 0	0 09996	-10 00186	-14. 36603	94. 0	0. 53659	-2 70357	-7 06774
6 0	0 20080	-6 97277	-11 16694	96 0	0 47578	-3 22597	-7 59014
8. 0	0 33422	-4. 75965	-9 12382	98. 0	0. 42537	-3 71230	-8. 07647
10 0	0 45564	-3 41375	-7 77792	100 0	0 38544	-4 14048	-8 50465
12 0	0 55419	-2 56341	-6 92758	102. D	0 35597	-4 48585	-8. 85002
14 0	0 61618	-2 10293	-6 46710	104. 0	0 33689	-4 72508	-9 08925
16. 0	0 63551	-1 96877	-6. 33294	106. D	0. 32796	-4 84177	-9. 20594
18 0	0 61460	-2 11405	-6 47822	108 0	0 32871	-4 83186	-9. 19603
20 0	0 56375	-2 48913	-6 85330	110. D	0 33836	-4. 70620	-9. 07037
22 0	0 49916	-3 01758	-7 38175	112. 0	0 35574	-4. 48873	-8. 85290
24 0	0 44010	-3 56447	-7 92864	114 0	0 37919	-4 21142	-8. 57560
26 0	0 40572	-3 91773	-8 28190	116. D	0. 40656	-3 90975	-8. 27292
28 0	0 41215	-3 84950	-8 21367	118. 0	0 43516	-3. 61353	-7. 97770
30 0	0 47027	-3 27649	-7 64066	120. 0	0 46183	-3. 35521	-7. 71938
32 0	0 58454	-2 33184	-6 69601	122 0	0 48308	-3 15984	-7. 52401
34 0	0 75275	-1 23352	-5 59769	124 0	0. 49532	-3. 05114	-7. 41531
36 0	0 96677	-0 14673	-4 31092	126 0	0 49520	-3 03222	-7 41639
38. 0	1 21404	0 84232	-3 52185	128 0	0. 47999	-3. 18764	-7. 55181
40 0	1 47927	1. 70049	-2 66368	130. 0	0. 44812	-3. 48604	-7. 85021
42 0	1 74640	2 42143	-1 94274	132 0	0 39960	-3 98380	-8. 34797
44. 0	2 00018	3 01068	-1. 35349	134 0	0. 33645	-4. 73080	-9. 09497
46 0	2 22754	3. 47825	-0. 88592	136 0	0. 26300	-5. 80048	-10. 16465
48 0	2 41841	3 83530	-0 52887	138 0	0 18583	-7. 30888	-11 67305
50 0	2. 56610	4 09274	-0. 27143	140 0	0. 11347	-9 45113	-13. 81532
52 0	2. 66730	4 26072	-0. 10345	142. 0	0. 05567	-12. 54378	-16 90795
54. 0	2 72172	4. 34844	-0 01573	144 0	0. 02228	-16. 52122	-20. 88539
56 0	2 73160	4 36417	0 00000	146. 0	0 02185	-16 60538	-20 96955
58. 0	2 70103	4 31530	-0 04887	148 0	0. 06011	-12 21066	-16. 57483
60 0	2 63538	4 20842	-0. 15575	150. 0	0. 13851	-8 58529	-12. 94946
62 0	2 54063	4 04941	-0 31476	152 0	0 25320	-5 96541	-10. 32958
64 0	2 42296	3 86345	-0. 50272	154 0	0. 39466	-4. 03774	-8. 40191
66 0	2 28831	3 59316	-0 76901	156 0	0 54824	-2 61031	-6 97448
68. 0	2 14217	3 30955	-1 05562	158 0	0. 69561	-1 57635	-5. 94052
70. 0	1 98937	2 98713	-1 37702	160 0	0. 81719	-0. 87677	-5 24094
72. 0	1 83401	2 63401	-1 73016	162 0	0 89509	-0 48133	-4. 84550
74 0	1 67947	2 25173	-2 11244	164 0	0 91620	-0 38008	-4. 74425
76. 0	1 52846	1 84255	-2 52162	166 0	0 87485	-0 58067	-4 94484
78 0	1 38306	1 40840	-2. 95577	168 0	0. 77441	-1. 11026	-5 47443
80. 0	1 24480	0 95099	-3 41318	170 0	0 62755	-2 02349	-6 38766
82 0	1 11480	0 47196	-3 89221	172 0	0 43475	-3. 42223	-7. 78640
84 0	0 99382	-0 02694	-4 38111	174 0	0. 20140	-5 90470	-9 87087
86 0	0 88236	-0 54356	-4 90773	176 0	0. 13380	-8. 73529	-13 09946
88 0	0 78074	-1 07494	-5 43911	178 0	0. 03483	-14. 58098	-18. 94515
90 0	0 68916	-1 61681	-5 98098	180	0 00000	-INFINITY	-INFINITY

TABLE A2-28 $2\pi a/\lambda = 7.00$

```
EPSLN= 7 0000(NORMALIZED GROUNDPLANE RADIUS)
MONOPOLE LENGTH= 0 250000(WAVELENGTH)
MONOPOLE RADIUS=  0 1000E-05(WAVELENGTH)
NUMBER OF MONOPOLE SEGMENTS=  1
NUMBER OF DISK SEGMENTS= 16
RADIATION RESISTANCE DETERMINED BY PATTERN= 0 441969E+02 OHMS
```

ELEVATION ANGLE (DEG)	DIRECTIVITY (NUMERIC)	DIRECTIVITY (DBI)	RELATIVE POWER (DB)	ELEVATION ANGLE (DEG)	DIRECTIVITY (NUMERIC)	DIRECTIVITY (DBI)	RELATIVE POWER (DB)
0	0 00000	-INFINITY	-INFINITY				
2 0	0 02306	-16 37058	-21 06374	92 0	0 58973	-2 29345	-6 98661
4 0	0 08750	-10 58008	-15.27324	94 0	0 50961	-2. 92761	-7 62077
6 0	0 18005	-7 44608	-12 13924	96 0	0 43849	-3 58037	-8 27353
8 0	0 28186	-5 49973	-10.19289	98 0	0. 37654	-4. 24189	-8. 93505
10 0	0 37249	-4 28885	-8 98201	100 0	0 32400	-4 89461	-9 58777
12 0	0 43433	-3 62181	-8 31497	102 0	0. 28117	-5 51023	-10 20341
14 0	0 45627	-3 40779	-8 10095	104 0	0 24842	-6 04816	-10 74132
16 0	0 43606	-3 60449	-8 29765	106 0	0 22604	-6 45810	-11 15126
18 0	0 38065	-4 19249	-8.88565	108 0	0 21425	-6 69079	-11 38395
20 0	0 30582	-5 14533	-9 83849	110 0	0. 21303	-6 71551	-11. 40867
22 0	0 23150	-6 35452	-11 04768	112. 0	0. 22206	-6. 53535	-11. 22851
24 0	0 18010	-7 44487	-12 13803	114 0	0 24052	-6 18941	-10 88157
26 0	0 17185	-7 64851	-12 34167	116 0	0. 26707	-5 73382	-10 42598
28 0	0 22184	-6 53952	-11.23268	118 0	0. 29964	-5 23402	-9. 92718
30 0	0 33797	-4 71122	-9 40438	120 0	0 33548	-4 74327	-9 43643
32 0	0 52011	-2 83903	-7 53219	122 0	0. 37116	-4 30437	-8 99753
34 0	0 76061	-1 18836	-5 88152	124 0	0 40269	-3 95034	-8. 64350
36 0	1 04574	0 19423	-4 49893	126 0	0 42379	-3 70805	-8 40121
38 0	1 35779	1 32833	-3 36483	128 0	0 43634	-3 60179	-8 29495
40 0	1 67743	2 24644	-2 44672	130 0	0. 43083	-3 65691	-8 35007
42 0	1 98587	2 97950	-1 71366	132. 0	0. 40705	-3 90352	-8 59668
44 0	2 26665	3 55385	-1 13931	134 0	0 36464	-4 38131	-9. 07447
46 0	2 50686	3 99130	-0 70186	136 0	0. 30568	-5 14726	-9 84042
48. 0	2 69770	4 30994	-0 38322	138 0	0 23498	-6 28964	-10 98280
50 0	2 83459	4 52490	-0 16826	140 0	0. 16006	-7 95722	-12 65038
52 0	2 91673	4 64899	-0 04417	142 0	0 09067	-10 42542	-15 11858
54 0	2 94656	4 69316	0. 00000	144 0	0 03783	-14. 22139	-18 91455
56 0	2 92879	4 66689	-0. 02627	146 0	0 01238	-19 07226	-23 76542
58 0	2 86973	4 57841	-0 11475	148 0	0. 02319	-16. 34623	-21 03939
60 0	2 77646	4. 43491	-0. 25825	150 0	0 07534	-11 22955	-15 92271
62 0	2 65625	4 24268	-0 45048	152. 0	0. 16851	-7 73365	-12 42681
64 0	2 51605	4. 00719	-0. 68597	154 0	0 29603	-5 28633	-9 97949
66 0	2. 36220	3. 73317	-0. 95999	156 0	0 44498	-3 51661	-8 20977
68 0	2 20022	3 42467	-1 26849	158 0	0 59718	-2 23897	-6. 93213
70 0	2 03473	3 08507	-1. 60809	160 0	0 73173	-1 35651	-6 04967
72 0	1 86946	2 71716	-1 97600	162 0	0. 82814	-0 81896	-5 51212
74 0	1 70731	2 32312	-2 37004	164 0	0 86999	-0 60487	-5 29803
76 0	1 55044	1 90454	-2 78862	166 0	0 84923	-0 71485	-5 40801
78 0	1 40039	1 46248	-3 23068	168 0	0 76356	-1 17134	-5 86470
80 0	1 25819	0 99746	-3 69570	170 0	0 62710	-2 02660	-6 71976
82 0	1 12448	0 50950	-4 18366	172 0	0 45921	-3 37987	-8 07303
84 0	0 99959	-0 00178	-4 69494	174 0	0 28641	-5 43017	-10 12333
86 0	0 88367	-0 53708	-5 23024	176 0	0 13693	-8 63495	-13 32811
88 0	0 77675	-1 09719	-5 79035	178 0	0 03576	-14 46658	-19 15974
90 0	0 67878	-1 68271	-6 37587	180	0 00000	-INFINITY	-INFINITY

TABLE A2-29 $2\pi a/\lambda = 7.25$

EPSLN= 7.2500 (NORMALIZED GROUNDPLANE RADIUS)
MONOPOLE LENGTH= 0.250000 (WAVELENGTH)
MONOPOLE RADIUS= 0.100000E-05 (WAVELENGTH)
NUMBER OF MONOPOLE SEGMENTS= 1
NUMBER OF DISK SEGMENTS= 16
RADIATION RESISTANCE DETERMINED BY PATTERN= 0.422974E+02 OHMS

ELEVATION ANGLE (DEG)	DIRECTIVITY (NUMERIC)	DIRECTIVITY (DBI)	RELATIVE POWER (DB)	ELEVATION ANGLE (DEG)	DIRECTIVITY (NUMERIC)	DIRECTIVITY (DBI)	RELATIVE POWER (DB)
0	0.00000	-INFINITY	-INFINITY				
2.0	0.02033	-16.91763	-21.76379	92.0	0.61882	-2.08439	-6.93054
4.0	0.07647	-11.16526	-16.01142	94.0	0.53518	-2.71502	-7.56117
6.0	0.15495	-8.09817	-12.94432	96.0	0.45892	-3.38830	-8.23445
8.0	0.23676	-6.25324	-11.09940	98.0	0.38836	-4.10762	-8.95378
10.0	0.30282	-5.18821	-10.03436	100.0	0.32558	-4.87345	-9.71961
12.0	0.33665	-4.72624	-9.57440	102.0	0.27041	-5.67981	-10.52596
14.0	0.33024	-4.81168	-9.65784	104.0	0.22344	-6.50834	-11.35449
16.0	0.28516	-5.44911	-10.29526	106.0	0.18539	-7.31924	-12.16540
18.0	0.21274	-6.72144	-11.56759	108.0	0.15699	-8.04135	-12.88750
20.0	0.13209	-8.79132	-13.63748	110.0	0.13696	-8.57121	-13.41737
22.0	0.06654	-11.76938	-16.61554	112.0	0.13183	-8.79984	-13.64600
24.0	0.03946	-14.03870	-18.88485	114.0	0.13983	-8.67013	-13.51629
26.0	0.07023	-11.53452	-16.38068	116.0	0.15067	-8.21966	-13.06582
28.0	0.17116	-7.66586	-12.51202	118.0	0.17543	-7.55905	-12.40521
30.0	0.34577	-4.61213	-9.45828	120.0	0.20833	-6.81239	-11.65855
32.0	0.58864	-2.30148	-7.14764	122.0	0.24673	-6.07776	-10.92391
34.0	0.88667	-0.52237	-5.36853	124.0	0.28704	-5.42056	-10.26672
36.0	1.22124	0.86802	-3.97813	126.0	0.32491	-4.88240	-9.72855
38.0	1.57094	1.96160	-2.88456	128.0	0.35550	-4.49165	-9.33781
40.0	1.91422	2.81793	-2.02623	130.0	0.37396	-4.27170	-9.11785
42.0	2.23172	3.48640	-1.35976	132.0	0.37611	-4.24687	-9.09303
44.0	2.50786	3.99303	-0.85313	134.0	0.35911	-4.44767	-9.29382
46.0	2.73176	4.36443	-0.48173	136.0	0.32233	-4.91699	-9.76314
48.0	2.89746	4.62018	-0.22598	138.0	0.26791	-5.72013	-10.56628
50.0	3.00351	4.77629	-0.06987	140.0	0.20117	-6.96438	-11.81054
52.0	3.05222	4.84616	0.00000	142.0	0.13050	-8.84381	-13.68996
54.0	3.04873	4.84119	-0.00497	144.0	0.06671	-11.75831	-16.60447
56.0	2.99999	4.77120	-0.07495	146.0	0.02170	-16.63487	-21.48103
58.0	2.91370	4.64474	-0.20141	148.0	0.00672	-21.72495	-26.57110
60.0	2.79848	4.46923	-0.37693	150.0	0.03019	-15.20206	-20.04821
62.0	2.66140	4.25111	-0.59505	152.0	0.09563	-10.19390	-15.04006
64.0	2.50954	3.99595	-0.85021	154.0	0.20016	-6.98623	-11.83238
66.0	2.34892	3.70851	-1.13765	156.0	0.33379	-4.76532	-9.61148
68.0	2.18413	3.39278	-1.45338	158.0	0.48011	-3.18656	-8.03271
70.0	2.01932	3.05205	-1.79411	160.0	0.61838	-2.08742	-6.93357
72.0	1.85733	2.68868	-2.15728	162.0	0.72673	-1.38625	-6.23241
74.0	1.70028	2.30520	-2.54076	164.0	0.78617	-1.04483	-5.89099
76.0	1.54962	1.90226	-2.94370	166.0	0.78451	-1.05404	-5.90020
78.0	1.40626	1.48066	-3.36530	168.0	0.71936	-1.43055	-6.27671
80.0	1.27068	1.04035	-3.80561	170.0	0.59950	-2.22213	-7.06829
82.0	1.14303	0.58059	-4.26536	172.0	0.44401	-3.52607	-8.37223
84.0	1.02329	0.09999	-4.74617	174.0	0.27929	-5.53946	-10.38562
86.0	0.91125	-0.40361	-5.24977	176.0	0.13432	-8.71859	-13.56475
88.0	0.80667	-0.93306	-5.77922	178.0	0.03520	-14.53512	-19.38127
90.0	0.70926	-1.49193	-6.33808	180.	0.00000	-INFINITY	-INFINITY

TABLE A2-30 $2\pi a/\lambda = 7.50$

```
EPSLN= 7 5000(NORMALIZED GROUNDPLANE RADIUS)
MONOPOLE LENGTH= 0 250000(WAVELENGTH)
MONOPOLE RADIUS=  0 1000E-05(WAVELENGTH)
NUMBER OF MONOPOLE SEGMENTS=  1
NUMBER OF DISK SEGMENTS= 16
RADIATION RESISTANCE DETERMINED BY PATTERN= 0 391003E+02 OHMS
```

ELEVATION ANGLE (DEG)	DIRECTIVITY (NUMERIC)	DIRECTIVITY (DBI)	RELATIVE POWER (DB)	ELEVATION ANGLE (DEG)	DIRECTIVITY (NUMERIC)	DIRECTIVITY (DBI)	RELATIVE POWER (DB)
0	0 00000	-INFINITY	-INFINITY				
2 0	0 01853	-17 32209	-22 18205	92 0	0 68087	-1 66937	-6 52933
4 0	0 06915	-11 60200	-16 46196	94 0	0 59916	-2 22460	-7 08457
6 0	0 15830	-8 59176	-13 45173	96 0	0 52191	-2 82400	-7 69397
8 0	0 20731	-6 83376	-11 69372	98 0	0 44909	-3 47663	-8 33659
10 0	0 25730	-5 89555	-10 75551	100 0	0 38083	-4 19272	-9 05269
12 0	0 27414	-5 62029	-10 48025	102 0	0 31746	-4 98308	-9 84304
14 0	0 25228	-5 98118	-10 84115	104 0	0 25958	-5 85728	-10 71724
16 0	0 19660	-7 06426	-11 92423	106 0	0 20799	-6 81953	-11 67950
18 0	0 12180	-9 14346	-14 00342	108 0	0 16371	-7 85920	-12 71917
20 0	0 04971	-13 03524	-17 89521	110 0	0 12790	-8 93134	-13 79131
22 0	0 00506	-22 96253	-27 82249	112 0	0 10176	-9 92433	-14 78430
24 0	0 01080	-19 66616	-24 52612	114 0	0 08640	-10 63504	-15 49500
26 0	0 08403	-10 75546	-15 61543	116 0	0 08264	-10 82807	-15 68803
28 0	0 23314	-6 32382	-11 18378	118 0	0 09081	-10 41853	-15 27849
30 0	0 43669	-3 60379	-8 46375	120 0	0 11050	-9 56631	-14 42627
32 0	0 74406	-1 28293	-6 14289	122 0	0 14034	-8 52807	-13 38804
34 0	1 07745	0 32399	-4 53597	124 0	0 17787	-7 49904	-12 35900
36 0	1 43478	1 56785	-3 29211	126 0	0 21945	-6 58665	-11 44661
38 0	1 79274	2 53516	-2 32480	128 0	0 26044	-5 84297	-10 70293
40 0	2 12965	3 28307	-1 57689	130 0	0 29548	-5 29476	-10 15473
42 0	2 42758	3 85173	-1 00823	132 0	0 31908	-4 96102	-9 82099
44 0	2 67363	4 27101	-0 58895	134 0	0 32639	-4 86268	-9 72264
46 0	2 86035	4 56419	-0 29577	136 0	0 31409	-5 02942	-9 88938
48 0	2 98343	4 75007	-0 10990	138 0	0 28136	-5 50741	-10 36737
50 0	3 05087	4 84424	-0 01572	140 0	0 23056	-6 37225	-11 23221
52 0	3 06194	4 85996	0 00000	142 0	0 16764	-7 75635	-12 61631
54 0	3 02596	4 80863	-0 05134	144 0	0 10190	-9 91820	-14 77816
56 0	2 95128	4 70011	-0 15986	146 0	0 04308	-13 65642	-18 51638
58 0	2 84642	4 54298	-0 31698	148 0	0 00965	-20 15405	-25 01401
60 0	2 71938	4 34469	-0 51527	150 0	0 00667	-21 76071	-26 62067
62 0	2 57728	4 11162	-0 74834	152 0	0 04330	-13 63556	-18 49553
64 0	2 42616	3 84920	-1 01076	154 0	0 12069	-9 18339	-14 04335
66 0	2 27090	3 56198	-1 29798	156 0	0 23264	-6 33310	-11 19307
68 0	2 11528	3 25367	-1 60629	158 0	0 36559	-4 37001	-9 22997
70 0	1 96211	2 92724	-1 93272	160 0	0 50016	-3 00893	-7 86889
72 0	1 81340	2 58494	-2 27503	162 0	0 61421	-2 11686	-6 97682
74 0	1 67046	2 22837	-2 63159	164 0	0 68700	-1 63045	-6 49041
76 0	1 53409	1 85852	-3 00144	166 0	0 70358	-1 52688	-6 38685
78 0	1 40468	1 47578	-3 38418	168 0	0 65845	-1 81475	-6 67472
80 0	1 28231	1 07993	-3 78003	170 0	0 55760	-2 53680	-7 39677
82 0	1 16685	0 67014	-4 18982	172 0	0 41811	-3 78707	-8 64704
84 0	1 05801	0 24490	-4 61507	174 0	0 26542	-5 76050	-10 62047
86 0	0 95542	-0 19807	-5 05804	176 0	0 12847	-8 91196	-13 77193
88 0	0 85864	-0 66188	-5 52184	178 0	0 03379	-14 71221	-19 57217
90 0	0 76726	-1 15059	-6 01055	180	0 00000	-INFINITY	-INFINITY

TABLE A2-31 $2\pi a/\lambda = 7.75$

```
EPSLN= 1 (DIELECTRIC CONSTANT)
SIG= 0 (CONDUCTIVITY)
RADIAL WIRE GROUND SYSTEM
  NUMBER OF RADIALS= 16
  RADIAL WIRE LENGTH= 0.250000 (WAVELENGTH)
  HEIGHT OF RADIAL WIRES ABOVE GROUND= 0.000000 (WAVELENGTH)
  RADIAL WIRE RADIUS= 0.100000E-05 (WAVELENGTH)
  CONDUCTIVITY OF RADIAL WIRE MEDIUM= 0.100000E+09 (MHOS/METER)
  PERMITTIVITY OF RADIAL WIRE MEDIUM= 1.000000
  NUMBER OF RADIAL WIRE SEGMENTS= 16
  NUMBER OF DISK SEGMENTS= 16
  RADIATION RESISTANCE DETERMINED BY PATTERN= 0.357610E+02 OHMS
```

ELEVATION ANGLE (DEG)	DIRECTIVITY (NUMERIC)	DIRECTIVITY (DBI)	RELATIVE POWER (DB)	ELEVATION ANGLE (DEG)	DIRECTIVITY (NUMERIC)	DIRECTIVITY (DBI)	RELATIVE POWER (DB)
0	0.00000	-INFINITY	-INFINITY				
2.0	0.01784	-17.48706	-32.24659	92.0	0.75517	-1.21953	-5.97906
4.0	0.06625	-11.78837	-16.54789	94.0	0.67926	-1.67962	-6.43915
6.0	0.13136	-8.81524	-13.57477	96.0	0.60609	-2.17460	-6.93413
8.0	0.19442	-7.11251	-11.87204	98.0	0.53537	-2.71350	-7.47303
10.0	0.23703	-6.25193	-11.01146	100.0	0.46693	-3.30745	-8.06697
12.0	0.24640	-6.08351	-10.84304	102.0	0.40086	-3.97003	-8.72955
14.0	0.21920	-6.59151	-11.35104	104.0	0.33748	-4.71754	-9.47707
16.0	0.16301	-7.87779	-12.63732	106.0	0.27740	-5.56900	-10.32853
18.0	0.09515	-10.21591	-14.97544	108.0	0.22155	-6.54521	-11.30474
20.0	0.03921	-14.06578	-18.82531	110.0	0.17120	-7.66496	-12.42449
22.0	0.02026	-16.93328	-21.69280	112.0	0.12785	-8.93307	-13.69260
24.0	0.05983	-12.23063	-16.99016	114.0	0.09317	-10.30714	-15.06667
26.0	0.17186	-7.64820	-12.40773	116.0	0.06885	-11.62068	-16.38021
28.0	0.36032	-4.43317	-9.19270	118.0	0.05636	-12.49043	-17.24996
30.0	0.61881	-2.08440	-6.84393	120.0	0.05665	-12.46764	-17.22717
32.0	0.93210	-0.30536	-5.06489	122.0	0.06992	-11.55413	-16.31366
34.0	1.27884	1.06817	-3.69136	124.0	0.09523	-10.21247	-14.97200
36.0	1.63500	2.13518	-2.62434	126.0	0.13033	-8.84953	-13.60906
38.0	1.97721	2.96052	-1.79901	128.0	0.17156	-7.65572	-12.41525
40.0	2.28542	3.58967	-1.16986	130.0	0.21395	-6.69692	-11.45645
42.0	2.54474	4.05644	-0.70309	132.0	0.25157	-5.99340	-10.75293
44.0	2.74611	4.38718	-0.37235	134.0	0.27826	-5.55542	-10.31495
46.0	2.88616	4.60320	-0.15633	136.0	0.28854	-5.39799	-10.15752
48.0	2.96638	4.72227	-0.03725	138.0	0.27867	-5.54905	-10.30858
50.0	2.99194	4.75953	0.00000	140.0	0.24782	-6.05866	-10.81819
52.0	2.97030	4.72800	-0.03153	142.0	0.19881	-7.01560	-11.77513
54.0	2.91005	4.63900	-0.12053	144.0	0.13848	-8.58600	-13.34553
56.0	2.81987	4.50230	-0.25723	146.0	0.07723	-11.12196	-15.88149
58.0	2.70787	4.32628	-0.43325	148.0	0.02770	-15.57486	-20.33439
60.0	2.58110	4.11806	-0.64147	150.0	0.00267	-25.72946	-30.48899
62.0	2.44542	3.88354	-0.87599	152.0	0.01243	-19.05387	-23.81340
64.0	2.30545	3.62756	-1.13197	154.0	0.06212	-12.06758	-16.82711
66.0	2.16469	3.35395	-1.40558	156.0	0.14968	-8.24840	-13.00793
68.0	2.02568	3.06571	-1.69382	158.0	0.26505	-5.76666	-10.52619
70.0	1.89021	2.76509	-1.99443	160.0	0.39109	-4.07721	-8.83674
72.0	1.75945	2.45376	-2.30577	162.0	0.50623	-2.95635	-7.71608
74.0	1.63412	2.13284	-2.62669	164.0	0.58861	-2.30175	-7.06128
76.0	1.51462	1.80303	-2.95649	166.0	0.62088	-2.06995	-6.82946
78.0	1.40108	1.46464	-3.29487	168.0	0.59449	-2.25855	-7.01808
80.0	1.29347	1.11755	-3.64198	170.0	0.51244	-2.90359	-7.66311
82.0	1.19158	0.76120	-3.99830	172.0	0.38950	-4.09488	-8.85441
84.0	1.09513	0.39465	-4.36488	174.0	0.24977	-6.02465	-10.78418
86.0	1.00372	0.01614	-4.74339	176.0	0.12173	-9.14600	-13.90553
88.0	0.91692	-0.37668	-5.13621	178.0	0.03215	-14.92858	-19.68811
90.0	0.83424	-0.78711	-5.54664	180	0.00000	-INFINITY	-INFINITY

TABLE A2-32 $2\pi a/\lambda = 8.00$

```
EPSLN= 3.000(NORMALIZED GROUNDPLANE RADIUS)
MONOPOLE LENGTH= 0.250000(WAVELENGTHS)
MONOPOLE RADIUS=  0.10000E-05(WAVELENGTHS)
NUMBER OF MONOPOLE SEGMENTS=  1
NUMBER OF DISK SEGMENTS= 12
RADIATION RESISTANCE DETERMINED BY PATTERN= 0.334954E+02 OHMS
```

ELEVATION ANGLE (DEG)	DIRECTIVITY (NUMERIC)	DIRECTIVITY (DBI)	RELATIVE POWER (DB)	ELEVATION ANGLE (DEG)	DIRECTIVITY (NUMERIC)	DIRECTIVITY (DBI)	RELATIVE POWER (DB)
0	0.00000	-INFINITY	-INFINITY				
2.0	0.01822	-17.39420	-21.95972	92.0	0.82468	-0.83717	-5.40269
4.0	0.06752	-11.70576	-16.27128	94.0	0.75628	-1.21315	-5.77867
6.0	0.13338	-8.74916	-13.31468	96.0	0.68987	-1.61231	-6.17783
8.0	0.19643	-7.06787	-11.63338	98.0	0.62486	-2.04215	-6.60767
10.0	0.23822	-6.23020	-10.79572	100.0	0.56076	-2.51222	-7.07774
12.0	0.24677	-6.07715	-10.64267	102.0	0.49722	-3.03454	-7.60006
14.0	0.22042	-6.56744	-11.13296	104.0	0.43411	-3.62403	-8.18955
16.0	0.16899	-7.72144	-12.28695	106.0	0.37160	-4.29919	-8.86470
18.0	0.11186	-9.51318	-14.07870	108.0	0.31025	-5.08284	-9.64835
20.0	0.07383	-11.31738	-15.88290	110.0	0.25102	-6.00297	-10.56849
22.0	0.07968	-10.98636	-15.55188	112.0	0.19530	-7.09293	-11.65845
24.0	0.14892	-8.27038	-12.83590	114.0	0.14493	-8.38846	-12.95398
26.0	0.29194	-5.34707	-9.91259	116.0	0.10203	-9.91258	-14.47810
28.0	0.50820	-2.93963	-7.50515	118.0	0.06889	-11.61826	-16.18378
30.0	0.78675	-1.04166	-5.60718	120.0	0.04766	-13.21859	-17.78411
32.0	1.10851	0.44741	-4.11811	122.0	0.04001	-13.97816	-18.54368
34.0	1.44987	1.61328	-2.95224	124.0	0.04676	-13.30092	-17.86643
36.0	1.78637	2.51972	-2.04580	126.0	0.06746	-11.70953	-16.27505
38.0	2.09616	3.21424	-1.35128	128.0	0.10005	-9.99765	-14.56317
40.0	2.36227	3.73329	-0.83223	130.0	0.14075	-8.51344	-13.07896
42.0	2.57388	4.10589	-0.45963	132.0	0.18413	-7.34885	-11.91437
44.0	2.72638	4.35586	-0.20966	134.0	0.22356	-6.50598	-11.07149
46.0	2.82053	4.50331	-0.06220	136.0	0.25211	-5.98417	-10.54968
48.0	2.86122	4.56552	0.00000	138.0	0.26359	-5.79068	-10.35620
50.0	2.85590	4.55743	-0.00809	140.0	0.25400	-5.95170	-10.51722
52.0	2.81318	4.49198	-0.07354	142.0	0.22270	-6.52277	-11.08829
54.0	2.74174	4.38026	-0.18526	144.0	0.17336	-7.61049	-12.17600
56.0	2.64947	4.23159	-0.33393	146.0	0.11409	-9.42763	-13.99315
58.0	2.54309	4.05361	-0.51191	148.0	0.05663	-12.46805	-17.03357
60.0	2.42795	3.85239	-0.71312	150.0	0.01465	-18.34102	-22.90654
62.0	2.30813	3.63261	-0.93291	152.0	0.00086	-30.67217	-35.23769
64.0	2.18660	3.39769	-1.16783	154.0	0.02413	-16.17406	-20.73958
66.0	2.06344	3.15012	-1.41540	156.0	0.08669	-10.62006	-15.18558
68.0	1.94608	2.89160	-1.67392	158.0	0.18243	-7.38849	-11.95401
70.0	1.82951	2.62336	-1.94216	160.0	0.29709	-5.27114	-9.83666
72.0	1.71643	2.34628	-2.21926	162.0	0.41020	-3.87004	-8.43556
74.0	1.60731	2.06099	-2.50452	164.0	0.49929	-3.01644	-7.58196
76.0	1.50250	1.76814	-2.79738	166.0	0.54486	-2.63714	-7.20266
78.0	1.40223	1.46818	-3.09733	168.0	0.53535	-2.71361	-7.27913
80.0	1.30663	1.16153	-3.40399	170.0	0.47068	-3.27278	-7.83830
82.0	1.21573	0.84837	-3.71714	172.0	0.36317	-4.39893	-8.96445
84.0	1.12944	0.52864	-4.03688	174.0	0.23546	-6.28080	-10.84631
86.0	1.04756	0.20179	-4.36372	176.0	0.11563	-9.36926	-13.93478
88.0	0.96977	-0.13331	-4.69883	178.0	0.03067	-15.13261	-19.69813
90.0	0.89565	-0.47863	-5.04415	180	0.00000	-INFINITY	-INFINITY

TABLE A2-33 $2\pi a/\lambda = 8.25$

```
EPSLN= 0 2500(NORMALIZED GROUNDPLANE RADIUS)
MONOPOLE LENGTH= 0 250000(WAVELENGTH)
MONOPOLE RADIUS=  0 1000E-05(WAVELENGTH)
NUMBER OF MONOPOLE SEGMENTS=  1
NUMBER OF DISK SEGMENTS= 16
RADIATION RESISTANCE DETERMINED BY PATTERN= 0 318841E+02 OHMS
```

ELEVATION ANGLE (DEG)	DIRECTIVITY (NUMERIC)	DIRECTIVITY (DBI)	RELATIVE POWER (DB)	ELEVATION ANGLE (DEG)	DIRECTIVITY (NUMERIC)	DIRECTIVITY (DBI)	RELATIVE POWER (DB)
0	0 00000	-INFINITY	-INFINITY				
2 0	0 01931	-17 09849	-21 40430	92 0	0 87662	-0 57187	-4 87768
4 0	0 07222	-11 41326	-15 71906	94 0	0 81344	-0 88608	-5 19189
6 0	0 14255	-8 46026	-12 76606	96 0	0 75461	-1 21126	-5 51707
8 0	0 20992	-6 77947	-11 08528	98 0	0 69932	-1 55326	-5 85907
10 0	0 25516	-5 93182	-10 23763	100 0	0 64269	-1 91996	-6 22577
12 0	0 26656	-5 74202	-10 04783	102 0	0 58594	-2 32150	-6 62731
14 0	0 24374	-6 13081	-10 43662	104 0	0 52836	-2 77069	-7 07650
16 0	0 19837	-7 02533	-11 33114	106 0	0 46953	-3 28339	-7 58920
18 0	0 13163	-8 19216	-12 49797	108 0	0 40930	-3 87925	-8 18506
20 0	0 12919	-8 88770	-13 19351	110 0	0 34812	-4 58267	-8 88848
22 0	0 15519	-8 09141	-12 39722	112 0	0 28680	-5 42425	-9 73006
24 0	0 24682	-6 07612	-10 38193	114 0	0 22685	-6 44259	-10 74840
26 0	0 41080	-3 86369	-8 16950	116 0	0 17038	-7 68571	-11 99152
28 0	0 64229	-1 92276	-6 22856	118 0	0 12001	-9 20786	-13 51367
30 0	0 92630	-0 33246	-4 63827	120 0	0 07865	-11 04298	-15 34879
32 0	1 24104	0 93786	-3 36795	122 0	0 04923	-13 07732	-17 38313
34 0	1 56190	1 93654	-2 36926	124 0	0 03423	-14 65581	-18 96162
36 0	1 86556	2 70809	-1 59772	126 0	0 03516	-14 54011	-18 84592
38 0	2 13304	3 29060	-1 01581	128 0	0 05203	-12 83783	-17 14364
40 0	2 35160	3 71364	-0 59217	130 0	0 08293	-10 81305	-15 11886
42 0	2 51511	4 00558	-0 30023	132 0	0 12379	-9 07317	-13 37898
44 0	2 62344	4 18872	-0 11709	134 0	0 16852	-7 73348	-12 03929
46 0	2 68102	4 28301	-0 02280	136 0	0 20958	-6 78642	-11 09223
48 0	2 69518	4 30581	0 00000	138 0	0 23906	-6 21490	-10 52071
50 0	2 67430	4 27209	-0 03372	140 0	0 25010	-6 01885	-10 32466
52 0	2 62691	4 19445	-0 11136	142 0	0 23954	-6 20438	-10 53019
54 0	2 56041	4 08309	-0 22272	144 0	0 20436	-6 89597	-11 20178
56 0	2 48079	3 94590	-0 35991	146 0	0 15256	-8 16554	-12 47135
58 0	2 39255	3 78861	-0 51720	148 0	0 09303	-10 31400	-14 61981
60 0	2 29882	3 61505	-0 69076	150 0	0 03920	-14 06663	-18 37244
62 0	2 20167	3 42753	-0 87828	152 0	0 00560	-22 52162	-26 82743
64 0	2 10246	3 22727	-1 07854	154 0	0 00441	-23 55649	-27 86230
66 0	2 00207	3 01480	-1 29101	156 0	0 04216	-13 75131	-18 05712
68 0	1 90123	2 79035	-1 51546	158 0	0 11706	-9 31583	-13 62164
70 0	1 80038	2 55413	-1 75168	160 0	0 21819	-6 61167	-10 91748
72 0	1 70079	2 30651	-1 99930	162 0	0 32686	-4 85642	-9 16222
74 0	1 60255	2 04812	-2 25769	164 0	0 42035	-3 76394	-8 06975
76 0	1 50659	1 77994	-2 52587	166 0	0 47719	-3 21305	-7 51886
78 0	1 41357	1 50318	-2 80262	168 0	0 48284	-3 16194	-7 46775
80 0	1 32412	1 21927	-3 08654	170 0	0 43402	-3 62492	-7 93073
82 0	1 23870	0 92966	-3 37615	172 0	0 34049	-4 67891	-8 98471
84 0	1 15764	0 63572	-3 67009	174 0	0 22345	-6 50812	-10 81392
86 0	1 08106	0 33850	-3 96731	176 0	0 11065	-9 56063	-13 86643
88 0	1 00890	0 03850	-4 26731	178 0	0 02949	-15 30301	-19 60882
90 0	0 94091	-0 26453	-4 57034	180.	0 00000	-INFINITY	-INFINITY

TABLE A2-34 $2\pi a/\lambda = 8.50$

```
EPSLN= 8.5000(NORMALIZED GROUNDPLANE RADIUS)
MONOPOLE LENGTH= 0.250000(WAVELENGTH)
MONOPOLE RADIUS=   0.1000E-05(WAVELENGTH)
NUMBER OF MONOPOLE SEGMENTS=  1
NUMBER OF DISK SEGMENTS= 16
RADIATION RESISTANCE DETERMINED BY PATTERN= 0.3:1644E+02 OHMS
```

ELEVATION ANGLE (DEG)	DIRECTIVITY (NUMERIC)	DIRECTIVITY (DBI)	RELATIVE POWER (DB)	ELEVATION ANGLE (DEG)	DIRECTIVITY (NUMERIC)	DIRECTIVITY (DBI)	RELATIVE POWER (DB)
0	0.00000	-INFINITY	-INFINITY				
2.0	0.02145	-16.68529	-20.65873	92.0	0.90179	-0.44893	-4.42238
4.0	0.07941	-11.00120	-14.97465	94.0	0.84562	-0.72826	-4.70170
6.0	0.15674	-8.04830	-12.02175	96.0	0.79330	-1.00560	-4.97905
8.0	0.23104	-6.36307	-10.33652	98.0	0.74385	-1.28517	-5.25862
10.0	0.28187	-5.49946	-9.47291	100.0	0.69609	-1.57334	-5.54679
12.0	0.29729	-5.26823	-9.24168	102.0	0.64881	-1.87883	-5.85228
14.0	0.27786	-5.56175	-9.53519	104.0	0.60077	-2.21295	-6.18640
16.0	0.23696	-6.25330	-10.22675	106.0	0.55084	-2.58978	-6.56322
18.0	0.19737	-7.04715	-11.02060	108.0	0.49813	-3.02654	-6.99999
20.0	0.18545	-7.31784	-11.29128	110.0	0.44216	-3.54423	-7.51768
22.0	0.22447	-6.48844	-10.46189	112.0	0.38295	-4.16960	-8.14305
24.0	0.32918	-4.82571	-8.79916	114.0	0.32124	-4.93174	-8.90519
26.0	0.50266	-2.98728	-6.96073	116.0	0.25886	-5.87443	-9.84788
28.0	0.73619	-1.33009	-5.30354	118.0	0.19728	-7.04927	-11.02272
30.0	1.01169	0.05048	-3.92297	120.0	0.14052	-8.52265	-12.49610
32.0	1.30581	1.15880	-2.81464	122.0	0.09195	-10.36455	-14.33800
34.0	1.59452	2.02634	-1.94711	124.0	0.05536	-12.56775	-16.54120
36.0	1.85714	2.68845	-1.28500	126.0	0.03414	-14.66738	-18.64083
38.0	2.07886	3.17826	-0.79519	128.0	0.03055	-15.14986	-19.12331
40.0	2.25189	3.52547	-0.44798	130.0	0.04506	-13.46181	-17.43526
42.0	2.37493	3.75635	-0.21690	132.0	0.07576	-11.20554	-15.17899
44.0	2.45189	3.89500	-0.07843	134.0	0.11806	-9.27891	-13.25236
46.0	2.48968	3.96144	-0.01201	136.0	0.16491	-7.82760	-11.80105
48.0	2.49638	3.97345	0.00000	138.0	0.20755	-6.82870	-10.80215
50.0	2.48050	3.94540	-0.02805	140.0	0.23696	-6.25320	-10.22665
52.0	2.44807	3.88824	-0.08521	142.0	0.24565	-6.09688	-10.07033
54.0	2.40414	3.80960	-0.16385	144.0	0.22984	-6.38952	-10.36297
56.0	2.35180	3.71400	-0.25945	146.0	0.19010	-7.21019	-11.18364
58.0	2.29270	3.60347	-0.36998	148.0	0.13402	-8.72815	-12.70160
60.0	2.22754	3.47825	-0.49520	150.0	0.07364	-11.32915	-15.30260
62.0	2.15650	3.33749	-0.63596	152.0	0.02424	-16.15425	-20.12770
64.0	2.07966	3.17992	-0.79353	154.0	0.00085	-30.70211	-34.67556
66.0	1.99728	3.00438	-0.96907	156.0	0.01416	-18.48817	-22.46162
68.0	1.90993	2.81017	-1.16328	158.0	0.06703	-11.73701	-15.71046
70.0	1.81853	2.59719	-1.37626	160.0	0.15249	-8.16760	-12.14105
72.0	1.72428	2.36608	-1.60737	162.0	0.25421	-5.94805	-9.92149
74.0	1.62861	2.11816	-1.85529	164.0	0.34976	-4.56231	-8.53576
76.0	1.53298	1.85538	-2.11807	166.0	0.41599	-3.80922	-7.78267
78.0	1.43867	1.58022	-2.39323	168.0	0.43533	-3.61181	-7.58526
80.0	1.34758	1.29554	-2.67791	170.0	0.40119	-3.96654	-7.93999
82.0	1.26022	1.00448	-2.96900	172.0	0.32060	-4.94036	-8.91381
84.0	1.17763	0.71009	-3.26336	174.0	0.21323	-6.71161	-10.68506
86.0	1.10038	0.41542	-3.55802	176.0	0.10654	-9.72478	-13.69823
88.0	1.02873	0.12300	-3.85045	178.0	0.02855	-15.44433	-19.41778
90.0	0.96264	-0.16537	-4.13882	180	0.00000	-INFINITY	-INFINITY

TABLE A2-35 $2\pi a/\lambda = 8.50$

```
EPSLN=  5.0000(NORMALIZED GROUNDPLANE RADIUS)
MONOPOLE LENGTH= 0.250000(WAVELENGTH)
MONOPOLE RADIUS=  0.1000E-03(WAVELENGTH)
NUMBER OF MONOPOLE SEGMENTS=  1
NUMBER OF DISK SEGMENTS= 20
NUMBER OF ANNULAR ZONES PER DISK SEGEMENT=  1
RADIATION RESISTANCE DETERMINED BY PATTERN= 0.315105E+02 OHMS
```

ELEVATION ANGLE (DEG)	DIRECTIVITY (NUMERIC)	DIRECTIVITY (dBi)	RELATIVE POWER (dB)	ELEVATION ANGLE (DEG)	DIRECTIVITY (NUMERIC)	DIRECTIVITY (dBi)	RELATIVE POWER (dB)
0	0.00000	-INFINITY	-INFINITY				
2.0	0.02167	-16.64156	-20.62027	92.0	0.09041	-0.50412	-4.48282
4.0	0.08021	-10.95788	-14.93659	94.0	0.83972	-0.78980	-4.76850
6.0	0.15829	-8.00572	-11.98442	96.0	0.78119	-1.07242	-5.05112
8.0	0.23326	-6.32167	-10.30037	98.0	0.73181	-1.35600	-5.33470
10.0	0.28445	-5.45988	-9.43859	100.0	0.68441	-1.64684	-5.62555
12.0	0.29981	-5.23156	-9.21027	102.0	0.63772	-1.95371	-5.93241
14.0	0.27991	-5.52989	-9.50859	104.0	0.59047	-2.28799	-6.26669
16.0	0.23825	-6.22962	-10.20833	106.0	0.54151	-2.66394	-6.64265
18.0	0.19786	-7.03632	-11.01502	108.0	0.48989	-3.09905	-7.07773
20.0	0.18532	-7.32088	-11.29958	110.0	0.43505	-3.61456	-7.59326
22.0	0.22407	-6.49615	-10.47486	112.0	0.37701	-4.23651	-8.21521
24.0	0.32893	-4.82895	-8.80766	114.0	0.31643	-4.99718	-8.97589
26.0	0.50293	-2.98489	-6.96359	116.0	0.25483	-5.93742	-9.91613
28.0	0.73721	-1.32407	-5.30277	118.0	0.19457	-7.10933	-11.08803
30.0	1.01349	0.05819	-3.92051	120.0	0.13876	-8.57722	-12.55593
32.0	1.30823	1.16685	-2.81185	122.0	0.09112	-10.40385	-14.38255
34.0	1.59731	2.03389	-1.94481	124.0	0.05548	-12.55835	-16.53705
36.0	1.85998	2.69507	-1.28363	126.0	0.03529	-14.52323	-18.50193
38.0	2.08151	3.18379	-0.79491	128.0	0.03288	-14.83076	-18.80946
40.0	2.25424	3.53001	-0.44869	130.0	0.04876	-13.11967	-17.09838
42.0	2.37707	3.76042	-0.21828	132.0	0.08101	-10.91430	-14.89321
44.0	2.45397	3.89870	-0.08001	134.0	0.12501	-9.03038	-13.00909
46.0	2.49205	3.96557	-0.01313	136.0	0.17360	-7.60458	-11.58329
48.0	2.49960	3.97870	0.00000	138.0	0.21784	-6.61857	-10.59727
50.0	2.48451	3.95241	-0.02629	140.0	0.24850	-6.04674	-10.02544
52.0	2.45332	3.89755	-0.08115	142.0	0.25786	-5.88621	-9.86492
54.0	2.41075	3.82152	-0.15719	144.0	0.24176	-6.16624	-10.14494
56.0	2.35973	3.72862	-0.25009	146.0	0.20124	-6.96275	-10.94146
58.0	2.30177	3.62062	-0.35809	148.0	0.14333	-8.43650	-12.41521
60.0	2.23743	3.49749	-0.48121	150.0	0.08039	-10.94786	-14.92656
62.0	2.16680	3.35818	-0.62052	152.0	0.02801	-15.52684	-19.50554
64.0	2.08990	3.20126	-0.77744	154.0	0.00156	-28.07083	-32.04954
66.0	2.00700	3.02546	-0.95324	156.0	0.01213	-19.16061	-23.13931
68.0	1.91867	2.82999	-1.14871	158.0	0.06291	-12.01246	-15.99116
70.0	1.82589	2.61474	-1.36397	160.0	0.14714	-8.32262	-12.30132
72.0	1.72994	2.38036	-1.59838	162.0	0.24854	-6.04605	-10.02476
74.0	1.63233	2.12805	-1.85068	164.0	0.34454	-4.62763	-8.60634
76.0	1.53464	1.86005	-2.11865	166.0	0.41174	-3.85376	-7.83246
78.0	1.43839	1.57876	-2.39994	168.0	0.43228	-3.64232	-7.62102
80.0	1.34499	1.28719	-2.69151	170.0	0.39928	-3.98724	-7.96593
82.0	1.25568	0.98856	-2.99014	172.0	0.31958	-4.95415	-8.93285
84.0	1.17119	0.68607	-3.29263	174.0	0.21279	-6.72059	-10.69929
86.0	1.09210	0.38342	-3.59527	176.0	0.10646	-9.73060	-13.70930
88.0	1.01876	0.08157	-3.89984	178.0	0.02852	-15.44933	-19.42804
90.0	0.95115	-0.21353	-4.19494	180	0.00000	-INFINITY	-INFINITY

TABLE A2-36 $2\pi a/\lambda = 8.75$

```
EPSLN=  8.7500(NORMALIZED GROUNDPLANE RADIUS)
MONOPOLE LENGTH= 0.250000(WAVELENGTH)
MONOPOLE RADIUS=  0.1000E-05(WAVELENGTH)
NUMBER OF MONOPOLE SEGMENTS=  1
NUMBER OF DISK SEGMENTS= 24
NUMBER OF ANNULAR ZONES PER DISK SEGEMENT=  1
RADIATION RESISTANCE DETERMINED BY PATTERN= 0.317823E+02 OHMS
```

ELEVATION ANGLE (DEG)	DIRECTIVITY (NUMERIC)	DIRECTIVITY (dBi)	RELATIVE POWER (dB)	ELEVATION ANGLE (DEG)	DIRECTIVITY (NUMERIC)	DIRECTIVITY (dBi)	RELATIVE POWER (dB)
0	0.00000	-INFINITY	-INFINITY				
2.0	0.02410	-16.18012	-19.84221	92.0	0.88059	-0.55228	-4.21437
4.0	0.08915	-10.49883	-14.16092	94.0	0.82469	-0.83711	-4.49920
6.0	0.17382	-7.59944	-11.21153	96.0	0.77544	-1.10453	-4.76661
8.0	0.25904	-5.86625	-9.52834	98.0	0.73177	-1.35623	-5.01832
10.0	0.31629	-5.99921	-8.66130	100.0	0.69237	-1.59663	-5.25872
12.0	0.33483	-4.75177	-8.41386	102.0	0.65568	-1.83309	-5.49518
14.0	0.31596	-5.00364	-8.66573	104.0	0.62001	-2.07601	-5.73810
16.0	0.27474	-5.61073	-9.27282	106.0	0.58360	-2.33886	-6.00095
18.0	0.23569	-6.27666	-9.93875	108.0	0.54473	-2.63819	-6.30028
20.0	0.22590	-6.46081	-10.12290	110.0	0.50191	-2.99374	-6.65583
22.0	0.26787	-5.72070	-9.38279	112.0	0.45406	-3.42890	-7.09099
24.0	0.37395	-4.27185	-7.93394	114.0	0.40072	-3.97156	-7.63365
26.0	0.54389	-2.64488	-6.30697	116.0	0.34232	-4.65566	-8.31775
28.0	0.76574	-1.15919	-4.82128	118.0	0.29031	-5.52354	-9.18563
30.0	1.01938	0.08335	-3.57874	120.0	0.21730	-6.62931	-10.29140
32.0	1.28143	1.07696	-2.58513	122.0	0.15698	-8.04130	-11.70339
34.0	1.53013	1.84729	-1.81480	124.0	0.10387	-9.83524	-13.49733
36.0	1.74894	2.42776	-1.23433	126.0	0.06281	-12.01968	-15.68177
38.0	1.92841	2.85199	-0.81010	128.0	0.03825	-14.17390	-17.83599
40.0	2.06612	3.15156	-0.51053	130.0	0.03332	-14.77316	-18.43525
42.0	2.16533	3.35523	-0.30686	132.0	0.04890	-13.10707	-16.76916
44.0	2.23270	3.48830	-0.17379	134.0	0.08266	-10.81678	-14.47887
46.0	2.27608	3.57187	-0.09022	136.0	0.12971	-8.87031	-12.53240
48.0	2.30261	3.62221	-0.03988	138.0	0.18095	-7.42450	-11.08659
50.0	2.31755	3.65030	-0.01179	140.0	0.22615	-6.45497	-10.11706
52.0	2.32393	3.66209	0.00000	142.0	0.25467	-5.93681	-9.59890
54.0	2.32231	3.63921	-0.00288	144.0	0.25903	-5.86650	-9.52859
56.0	2.31217	3.64020	+0.02109	146.0	0.23528	-6.28408	-9.94616
58.0	2.29184	3.60185	+0.06024	148.0	0.18672	-7.28801	-10.93010
60.0	2.25963	3.54036	-0.12172	150.0	0.12322	-9.09304	-12.73513
62.0	2.21425	3.45227	-0.20982	152.0	0.06000	-12.21820	-15.86029
64.0	2.15524	3.33497	+0.32712	154.0	0.01438	-18.42110	-22.06319
66.0	2.08303	3.18695	+0.47514	156.0	0.00133	-28.75558	-32.41767
68.0	1.99890	3.00791	+0.65418	158.0	0.02889	-15.39267	-19.05476
70.0	1.90485	2.79862	-0.86347	160.0	0.09489	-10.22778	-13.88987
72.0	1.80336	2.56081	-1.10128	162.0	0.18623	-7.29953	-10.96161
74.0	1.69711	2.29709	-1.36500	164.0	0.28134	-5.50776	-9.16985
76.0	1.58882	2.01075	-1.65134	166.0	0.33356	-4.49081	-8.15290
78.0	1.48105	1.70570	-1.95639	168.0	0.38817	-4.10980	-7.77189
80.0	1.37605	1.38635	-2.27574	170.0	0.36878	-4.33228	-7.99437
82.0	1.27571	1.05750	-2.60459	172.0	0.30130	-5.21002	-8.87210
84.0	1.18145	0.72437	-2.93772	174.0	0.20358	-6.91272	-10.57481
86.0	1.09442	0.39186	-3.27024	176.0	0.10281	-9.87981	-13.54190
88.0	1.01516	0.06533	-3.59676	178.0	0.02772	-15.57274	-19.23483
90.0	0.94332	-0.25764	-3.91973	180	0.00000	-INFINITY	-INFINITY

TABLE A2-37 $2\pi a/\lambda = 9.00$

```
EPSLN=  9.0000(NORMALIZED GROUNDPLANE RADIUS)
MONOPOLE LENGTH= 0 2500001(WAVELENGTH)
MONOPOLE RADIUS=  0 1000E-051(WAVELENGTH)
NUMBER OF MONOPOLE SEGMENTS=  1
NUMBER OF DISK SEGMENTS= 37
NUMBER OF ANNULAR ZONES PER DISK SEGEMENT=  1
RADIATION RESISTANCE DETERMINED BY PATTERN= 0 328995E+02 OHMS
```

ELEVATION ANGLE (DEG)	DIRECTIVITY (NUMERIC)	DIRECTIVITY (dBi)	RELATIVE POWER (dB)	ELEVATION ANGLE (DEG)	DIRECTIVITY (NUMERIC)	DIRECTIVITY (dBi)	RELATIVE POWER (dB)
0.	0 00000	-INFINITY	-INFINITY				
2 0	0 02659	-15.75210	-19.32164	92.0	0.84199	-0 74694	-4 51648
4.0	0 09828	-10 07542	-13.84495	94 0	0. 78223	-1 06666	-4 83620
6 0	0.19350	-7. 13315	-10.90269	96 0	0.73193	-1 35553	-5 12487
8.0	0 28453	-5 45871	-9 22825	98 0	0.69010	-1 61088	-5 38042
10. 0	0.36669	-4 60035	-8 37009	100 0	0 65547	-1 83449	-5 60402
12. 0	0 43643	-4 36007	-8 12961	102 0	0. 62645	-2 03116	-5 80070
14. 0	0. 49555	-4. 61494	-8. 38448	104. 0	0. 60117	-2 21000	-5 97954
16. 0	0. 50041	-5 22268	-8 99242	106 0	0. 57755	-2. 38409	-6 15363
18. 0	0. 25673	-5 90518	-9. 67472	108 0	0. 55333	-2. 57018	-6 33972
20. 0	0. 24185	-6 16453	-9 93406	110 0	0. 52622	-2 78830	-6 55783
22. 0	0. 27708	-5 57391	-9. 34345	112 0	0 49413	-3 06157	-6 83111
24. 0	0 37248	-4 28897	-8 05851	114 0	0. 45536	-3. 41642	-7. 18595
26. 0	0. 52519	-2. 79683	-6. 56637	116 0	0. 40895	-3 88032	-7 65286
28. 0	0. 72143	-1 41808	-5 18762	118 0	0. 35493	-4. 49839	-8 26792
30. 0	0. 94096	-0. 26427	-4 03381	120 0	0. 29472	-5. 30586	-9. 07340
32. 0	1. 16254	0. 65406	-3. 11348	122. 0	0. 23112	-6 36164	-10 13117
34. 0	1 36052	1 36252	-2. 40701	124. 0	0. 16841	-7. 73633	-11. 50586
36. 0	1. 54786	1. 89731	-1. 87222	126 0	0. 11200	-9 50783	-13 27737
38. 0	1. 69675	2. 29618	-1. 47335	128 0	0. 06779	-11. 68855	-15 45788
40. 0	1. 81735	2. 59466	-1 17468	130 0	0 04123	-13. 84916	-17. 61770
42. 0	1. 91640	2 82486	-0. 94448	132 0	0 03614	-14. 42059	-18 19012
44. 0	2. 00063	3. 01166	-0. 75788	134. 0	0 05353	-12. 71362	-16. 48316
46. 0	2 07646	3. 17329	-0 59631	136. 0	0. 09072	-10 42276	-14 19229
48 0	2 14758	3 31950	-0 45004	138 0	0 14098	-8. 50838	-12. 27792
50. 0	2 21468	3. 45311	-0. 31643	140. 0	0. 19415	-7 11873	-10 88827
52. 0	2 27575	3 57125	-0 19829	142 0	0 23823	-6. 23012	-9 99966
54. 0	2. 32698	3 66793	-0 10161	144 0	0. 26190	-5 81867	-9 58820
56. 0	2 36383	3 73616	-0 03337	146. 0	0 25744	-5. 89322	-9. 66276
58. 0	2 38207	3 76954	0 00000	148. 0	0. 22336	-6. 51001	-10 27955
60 0	2 37850	3 76309	-0 00645	150 0	0 16583	-7 80331	-11 57284
62. 0	2 35161	3 71366	-0. 05588	152 0	0 09828	-10. 07518	-13 84471
64 0	2 30136	3. 61984	-0 14970	154 0	0 03867	-14 12583	-17 89537
66. 0	2 22935	3 48178	-0. 28776	156. 0	0. 00497	-23 03919	-26 80872
68 0	2 13839	3 30087	-0 46886	158 0	0 00980	-20 08930	-23 85884
70. 0	2 03214	3 07953	-0 69001	160 0	0 03593	-12 52319	-16 29273
72 0	1 91466	2 82091	-0 94862	162 0	0 13421	-8 72219	-12 49173
74 0	1 79012	2 52882	-1 24072	164 0	0 22496	-6 47890	-10 24844
76 0	1 66247	2 20753	-1 56201	166 0	0. 30310	-5 18417	-8 95371
78 0	1 53626	1 86182	-1 90772	168 0	0 34547	-4 61595	-8 38549
80 0	1 41153	1 49690	-2 27264	170 0	0 33836	-4 70621	-8 47574
82 0	1 29074	1 11846	-2 65108	172 0	0 28055	-5 48906	-9 25860
84 0	1 18077	0 73267	-3 03687	174 0	0 19388	-7 12461	-10 89415
86 0	1 08247	0 34618	-3 40336	176 0	0 09893	-10 04676	-13 81630
88 0	0 99220	-0 03409	-3 80364	178 0	0 02683	-15 71382	-19 48336
90 0	0 91187	-0 40468	-4 17422	180	0 00000	-INFINITY	-INFINITY

TABLE A2-38 $2\pi a/\lambda = 9.25$

```
EPSLN=  9.2500(NORMALIZED GROUNDPLANE RADIUS)
MONOPOLE LENGTH= 0.250000(WAVELENGTH)
MONOPOLE RADIUS=  0.10000E-03(WAVELENGTH)
NUMBER OF MONOPOLE SEGMENTS=  5
NUMBER OF DISK SEGMENTS= 27
NUMBER OF ANNULAR ZONES PER DISK SEGEMENT=  1
RADIATION RESISTANCE DETERMINED BY PATTERN= 0.346397E+02 OHMS
```

ELEVATION ANGLE (DEG)	DIRECTIVITY (NUMERIC)	DIRECTIVITY (dBi)	RELATIVE POWER (dB)	ELEVATION ANGLE (DEG)	DIRECTIVITY (NUMERIC)	DIRECTIVITY (dBi)	RELATIVE (dB)
0	0.00000	-INFINITY	-INFINITY				
2.0	0.02890	-15.39035	-19.49540	92.0	0.78629	-1.04419	-5.14925
4.0	0.10666	-9.72003	-13.82509	94.0	0.71882	-1.43380	-5.53886
6.0	0.20949	-6.78837	-10.89343	96.0	0.66216	-1.78381	-5.88887
8.0	0.30698	-5.12893	-9.23399	98.0	0.61854	-2.08632	-6.19138
10.0	0.37232	-4.29080	-8.39586	100.0	0.58390	-2.33638	-6.44144
12.0	0.39107	-4.07748	-8.18254	102.0	0.55789	-2.53431	-6.63937
14.0	0.36536	-4.37280	-8.47786	104.0	0.53880	-2.68572	-6.79078
16.0	0.31238	-5.05034	-9.15540	106.0	0.52458	-2.80186	-6.90692
18.0	0.25925	-5.86278	-9.96784	108.0	0.51285	-2.90010	-7.00516
20.0	0.23255	-6.33475	-10.43981	110.0	0.50094	-3.00214	-7.10719
22.0	0.25253	-5.97653	-10.08159	112.0	0.48606	-3.13308	-7.23814
24.0	0.32737	-4.84952	-8.95463	114.0	0.46551	-3.32074	-7.42580
26.0	0.43255	-3.64336	-7.74847	116.0	0.43696	-3.59558	-7.70063
28.0	0.61400	-2.11831	-6.22337	118.0	0.39890	-3.99137	-8.09643
30.0	0.79328	-1.00571	-5.11077	120.0	0.35100	-4.54697	-8.65203
32.0	0.97306	-0.11861	-4.22367	122.0	0.29451	-5.30901	-9.41407
34.0	1.14120	0.57362	-3.53144	124.0	0.23251	-6.33553	-10.44059
36.0	1.29261	1.11468	-2.99038	126.0	0.16988	-7.69846	-11.80351
38.0	1.42868	1.54934	-2.55572	128.0	0.11292	-9.47229	-13.57735
40.0	1.55503	1.91738	-2.18768	130.0	0.06852	-11.64182	-15.74688
42.0	1.67857	2.24940	-1.85566	132.0	0.04298	-13.66719	-17.77225
44.0	1.80478	2.56424	-1.54082	134.0	0.04053	-13.92190	-18.02696
46.0	1.93584	2.86870	-1.23636	136.0	0.06191	-12.08227	-16.18733
48.0	2.07006	3.15983	-0.94523	138.0	0.10337	-9.85607	-13.96113
50.0	2.20225	3.42867	-0.67639	140.0	0.15654	-8.05377	-12.15882
52.0	2.32497	3.66417	-0.44088	142.0	0.20947	-6.78882	-10.89388
54.0	2.43001	3.85608	-0.24898	144.0	0.24889	-6.03996	-10.14502
56.0	2.50984	3.99646	-0.10860	146.0	0.26340	-5.79378	-9.89884
58.0	2.55874	4.08026	-0.02480	148.0	0.24698	-6.07520	-10.18025
60.0	2.57339	4.10506	0.00000	150.0	0.20100	-6.96794	-11.07300
62.0	2.55310	4.07068	-0.03438	152.0	0.13606	-8.66283	-12.76789
64.0	2.49953	3.97859	-0.12647	154.0	0.06910	-11.60501	-15.71007
66.0	2.41628	3.83147	-0.27359	156.0	0.01979	-17.03657	-21.14163
68.0	2.30822	3.63278	-0.47228	158.0	0.00452	-23.44414	-27.54920
70.0	2.18098	3.38651	-0.71855	160.0	0.03090	-15.10029	-19.20535
72.0	2.04031	3.09696	-1.00809	162.0	0.09416	-10.26148	-14.36654
74.0	1.89176	2.76866	-1.33640	164.0	0.17742	-7.51009	-11.61515
76.0	1.74032	2.40628	-1.69878	166.0	0.25607	-5.91640	-10.02145
78.0	1.59027	2.01470	-2.09036	168.0	0.30523	-5.15227	-9.25733
80.0	1.44512	1.59924	-2.50582	170.0	0.30856	-5.10661	-9.21167
82.0	1.30763	1.16482	-2.94024	172.0	0.26345	-5.79306	-9.89812
84.0	1.17901	0.71811	-3.38695	174.0	0.18362	-7.36069	-11.46575
86.0	1.06307	0.26547	-3.83959	176.0	0.09467	-10.23795	-14.34301
88.0	0.96225	-0.13414	-4.23920	178.0	0.02583	-15.87912	-19.98418
90.0	0.87496	-0.57431	-4.67937	180	0.00000	-INFINITY	-INFINITY

TABLE A2-39 $2\pi a/\lambda = 9.50$

```
EPSLN=  9.5000(NORMALIZED GROUNDPLANE RADIUS)
MONOPOLE LENGTH= 0.250000(WAVELENGTH)
MONOPOLE RADIUS=   0.1000E-03(WAVELENGTH)
NUMBER OF MONOPOLE SEGMENTS=  1
NUMBER OF DISK SEGMENTS= 28
NUMBER OF ANNULAR ZONES PER DISK SEGMENT=  1
RADIATION RESISTANCE DETERMINED BY PATTERN= 0.365792E+02 OHMS
```

ELEVATION ANGLE (DEG)	DIRECTIVITY (NUMERIC)	DIRECTIVITY (dBi)	RELATIVE POWER (dB)	ELEVATION ANGLE (DEG)	DIRECTIVITY (NUMERIC)	DIRECTIVITY (dBi)	RELATIVE POWER (dB)
0	0.00000	-INFINITY	-INFINITY				
2.0	0.03092	-15.09731	-19.56780	92.0	0.72979	-1.36804	-5.83853
4.0	0.11392	-9.43396	-13.90444	94.0	0.65287	-1.85173	-6.32221
6.0	0.22314	-6.51417	-10.98466	96.0	0.58905	-2.29850	-6.76899
8.0	0.32368	-4.87215	-9.34264	98.0	0.53780	-2.69379	-7.16427
10.0	0.39276	-4.05873	-8.52922	100.0	0.49843	-3.02399	-7.49448
12.0	0.40909	-3.88178	-8.35226	102.0	0.46997	-3.27926	-7.74974
14.0	0.37705	-4.23606	-8.70655	104.0	0.45119	-3.45640	-7.92689
16.0	0.31470	-5.02109	-9.49157	106.0	0.44044	-3.56114	-8.03162
18.0	0.24894	-6.03913	-10.50962	108.0	0.43565	-3.60862	-8.07911
20.0	0.20650	-6.85087	-11.32136	110.0	0.43429	-3.62217	-8.09265
22.0	0.20619	-6.85724	-11.32772	112.0	0.43343	-3.63086	-8.10135
24.0	0.25479	-5.93820	-10.40868	114.0	0.42982	-3.66709	-8.13758
26.0	0.34729	-4.59308	-9.06357	116.0	0.42024	-3.76499	-8.23548
28.0	0.47086	-3.27108	-7.74156	118.0	0.40179	-3.96001	-8.43050
30.0	0.61042	-2.14368	-6.61417	120.0	0.37241	-4.28984	-8.76033
32.0	0.75382	-1.22730	-5.69778	122.0	0.33140	-4.79643	-9.26691
34.0	0.89496	-0.48196	-4.95245	124.0	0.27996	-5.52904	-9.99953
36.0	1.03427	0.14636	-4.32413	126.0	0.22142	-6.54786	-11.01834
38.0	1.17693	0.70758	-3.76291	128.0	0.16127	-7.92451	-12.39500
40.0	1.32980	1.23787	-3.23261	130.0	0.10664	-9.72085	-14.19133
42.0	1.49807	1.75532	-2.71516	132.0	0.06526	-11.85324	-16.32372
44.0	1.68305	2.26097	-2.20952	134.0	0.04397	-13.56878	-18.03927
46.0	1.88111	2.74415	-1.72634	136.0	0.04689	-13.28906	-17.75955
48.0	2.08412	3.18929	-1.28120	138.0	0.07391	-11.31311	-15.78359
50.0	2.28087	3.58100	-0.88948	140.0	0.11968	-9.21992	-13.69041
52.0	2.45907	3.90771	-0.56278	142.0	0.17389	-7.59717	-12.06765
54.0	2.60730	4.16192	-0.30857	144.0	0.22299	-6.51706	-10.98755
56.0	2.71658	4.34022	-0.13027	146.0	0.25322	-5.96505	-10.43554
58.0	2.78124	4.44239	-0.02810	148.0	0.25444	-5.94422	-10.41471
60.0	2.79929	4.47049	0.00000	150.0	0.22369	-6.50357	-10.97406
62.0	2.77210	4.42808	-0.04240	152.0	0.16718	-7.76819	-12.23868
64.0	2.70375	4.31966	-0.15083	154.0	0.09968	-10.01403	-14.48452
66.0	2.60027	4.15018	-0.32031	156.0	0.04098	-13.87390	-18.34439
68.0	2.46876	3.92478	-0.54570	158.0	0.01010	-19.95706	-24.42755
70.0	2.31664	3.64859	-0.82190	160.0	0.01879	-17.26167	-21.73216
72.0	2.15109	3.32658	-1.14390	162.0	0.06675	-11.75580	-16.22629
74.0	1.97858	2.96054	-1.50994	164.0	0.14047	-8.52417	-12.99466
76.0	1.80470	2.56426	-1.90643	166.0	0.21672	-6.64099	-11.11148
78.0	1.63401	2.13256	-2.33793	168.0	0.26992	-5.68762	-10.15811
80.0	1.47008	1.67742	-2.79307	170.0	0.28111	-5.51124	-9.98173
82.0	1.31537	1.19113	-3.27936	172.0	0.24517	-6.10527	-10.57576
84.0	1.17239	0.68075	-3.78974	174.0	0.17245	-7.63832	-12.10881
86.0	1.04160	0.17351	-4.29698	176.0	0.09032	-10.44231	-14.91279
88.0	0.92469	-0.34285	-4.81334	178.0	0.02478	-16.05877	-20.52925
90.0	0.82214	-0.86115	-5.33162	180	0.00000	-INFINITY	-INFINITY

TABLE A2-40 $2\pi a/\lambda = 9.75$

EPSLN= 9.7500(NORMALIZED GROUNDPLANE RADIUS)
MONOPOLE LENGTH= 0.250000(WAVELENGTH)
MONOPOLE RADIUS= 0.10606E-05(WAVELENGTH)
NUMBER OF MONOPOLE SEGMENTS= 1
NUMBER OF DISK SEGMENTS= 29
NUMBER OF ANNULAR ZONES PER DISK SEGEMENT= 1
RADIATION RESISTANCE DETERMINED BY PATTERN= 0.380863E+02 OHMS

ELEVATION ANGLE (DEG)	DIRECTIVITY (NUMERIC)	DIRECTIVITY (dBi)	RELATIVE POWER (dB)	ELEVATION ANGLE (DEG)	DIRECTIVITY (NUMERIC)	DIRECTIVITY (dBi)	RELATIVE POWER (dB)
0	0.00000	-INFINITY	-INFINITY				
2.0	0.03276	-14.84643	-19.61948	92.0	0.68892	-1.61803	-6.39138
4.0	0.12052	-9.18932	-13.96236	94.0	0.60348	-2.19341	-6.96645
6.0	0.23550	-6.28011	-11.05316	96.0	0.53110	-2.74820	-7.52124
8.0	0.34249	-4.65357	-9.42662	98.0	0.47151	-3.26511	-8.03815
10.0	0.41095	-3.86209	-8.63514	100.0	0.42420	-3.72301	-8.49605
12.0	0.42483	-3.71783	-8.49087	102.0	0.38908	-4.09960	-8.87264
14.0	0.38664	-4.12692	-8.89997	104.0	0.36510	-4.37393	-9.14697
16.0	0.31492	-5.01795	-9.79099	106.0	0.35138	-4.54219	-9.31524
18.0	0.23667	-6.25840	-11.03145	108.0	0.34653	-4.60262	-9.37567
20.0	0.17799	-7.49607	-12.26912	110.0	0.34859	-4.57691	-9.34995
22.0	0.15661	-8.05193	-12.82498	112.0	0.35502	-4.49748	-9.27052
24.0	0.17847	-7.48427	-12.25731	114.0	0.36272	-4.40431	-9.17735
26.0	0.23903	-6.21344	-10.98649	116.0	0.36813	-4.33993	-9.11298
28.0	0.32779	-4.84408	-9.61713	118.0	0.36737	-4.34657	-9.11962
30.0	0.43396	-3.62552	-8.39857	120.0	0.35764	-4.46359	-9.23664
32.0	0.55096	-2.58882	-7.36187	122.0	0.33582	-4.73698	-9.51192
34.0	0.67831	-1.68573	-6.45877	124.0	0.30119	-5.21139	-9.98464
36.0	0.82077	-0.85778	-5.63082	126.0	0.25493	-5.93573	-10.70878
38.0	0.98544	-0.06368	-4.83673	128.0	0.20076	-6.97321	-11.74626
40.0	1.17815	0.71201	-4.06103	130.0	0.14480	-8.39225	-13.16530
42.0	1.40043	1.46260	-3.31045	132.0	0.09493	-10.22583	-14.99888
44.0	1.64790	2.16932	-2.60372	134.0	0.05945	-12.25883	-17.03187
46.0	1.91045	2.81136	-1.96168	136.0	0.04520	-13.44685	-18.22190
48.0	2.17370	3.37199	-1.40106	138.0	0.05539	-12.56980	-17.32285
50.0	2.42139	3.84066	-0.93239	140.0	0.08893	-10.50938	-15.28243
52.0	2.63797	4.21270	-0.56035	142.0	0.13778	-8.60818	-13.38123
54.0	2.81061	4.48801	-0.28504	144.0	0.18984	-7.21609	-11.98913
56.0	2.93065	4.66964	-0.10341	146.0	0.23057	-6.37206	-11.14511
58.0	2.99406	4.76260	-0.01044	148.0	0.24701	-6.07283	-10.84588
60.0	3.00127	4.77305	0.00000	150.0	0.23207	-6.34380	-11.11685
62.0	2.95638	4.70761	-0.06544	152.0	0.18760	-7.26773	-12.04078
64.0	2.86618	4.57303	-0.20002	154.0	0.12510	-9.02734	-13.80039
66.0	2.73899	4.37590	-0.39715	156.0	0.06321	-11.99197	-16.76501
68.0	2.58373	4.12247	-0.65058	158.0	0.02219	-16.53925	-21.31229
70.0	2.40911	3.81856	-0.95447	160.0	0.01700	-17.69639	-22.46943
72.0	2.22305	3.46950	-1.30355	162.0	0.05139	-12.89147	-17.66451
74.0	2.03241	3.08011	-1.69294	164.0	0.11536	-9.37934	-14.15239
76.0	1.84276	2.65469	-2.11836	166.0	0.18759	-7.26796	-12.04101
78.0	1.65847	2.19705	-2.57598	168.0	0.24239	-6.15482	-10.92786
80.0	1.48277	1.71074	-3.06230	170.0	0.25911	-5.86305	-10.63613
82.0	1.31791	1.19823	-3.57480	172.0	0.23026	-6.37787	-11.15092
84.0	1.16513	0.65851	-4.11452	174.0	0.16506	-7.82351	-12.59656
86.0	1.02589	0.11102	-4.66201	176.0	0.08671	-10.61912	-15.39217
88.0	0.90148	-0.43762	-5.20072	178.0	0.02391	-16.21350	-20.98655
90.0	0.79345	-1.00648	-5.76957	180	0.00000	-INFINITY	-INFINITY

TABLE A2-41 $2\pi a/\lambda = 10.00$

```
EPSLN= 10 0000(NORMALIZED GROUNDPLANE RADIUS)
MONOPOLE LENGTH= 0.250000(WAVELENGTH)
MONOPOLE RADIUS=   0 1000E-05(WAVELENGTH)
NUMBER OF MONOPOLE SEGMENTS=  1
NUMBER OF DISK SEGMENTS= 30
NUMBER OF ANNULAR ZONES PER DISK SEGEMENT=  1
RADIATION RESISTANCE DETERMINED BY PATTERN= 0 387759E+02 OHMS
```

ELEVATION ANGLE (DEG)	DIRECTIVITY (NUMERIC)	DIRECTIVITY (dBi)	RELATIVE POWER (dB)	ELEVATION ANGLE (DEG)	DIRECTIVITY (NUMERIC)	DIRECTIVITY (dBi)	RELATIVE POWER (dB)
0.	0 00000	-INFINITY	-INFINITY				
2.0	0. 03473	-14. 59347	-19. 58491	92. 0	0. 67036	-1 73695	-6. 72838
4.0	0. 12761	-8. 94129	-13. 93272	94. 0	0. 57930	-2. 37097	-7. 36241
6.0	0. 24887	-6. 04019	-11. 03163	96. 0	0. 50025	-3 00816	-7. 99960
8.0	0. 36100	-4. 42494	-9. 41638	98. 0	0. 43301	-3 63500	-8 62643
10.0	0 43167	-3. 64846	-8. 63989	100. 0	0. 37749	-4. 23100	-9 22243
12. 0	0. 44410	-3. 52517	-8. 51661	102. 0	0. 33358	-4 76801	-9 75944
14. 0	0. 40098	-3. 96879	-8. 96023	104. 0	0. 30116	-5. 21207	-10 20351
16. 0	0. 32132	-4 93065	-9. 92208	106. 0	0. 27991	-5. 52982	-10. 52125
18. 0	0. 23221	-6. 34119	-11. 33262	108. 0	0. 26921	-5 69903	-10 69047
20. 0	0. 15922	-7. 98002	-12. 97146	110. 0	0. 26796	-5. 71927	-10. 71071
22. 0	0 11920	-9. 23742	-14. 22885	112. 0	0. 27442	-5. 61589	-10. 60733
24. 0	0. 11770	-9 29233	-14. 28377	114 0	0. 28610	-5. 43478	-10 42621
26. 0	0 15113	-8. 20640	-13. 19784	116. 0	0. 29980	-5. 23165	-10. 22309
28. 0	0. 21183	-6 74021	-11. 73165	118. 0	0. 31169	-5 06272	-10. 05415
30. 0	0 29346	-5. 32453	-10 31596	120. 0	0. 31769	-4. 97995	-9. 97139
32. 0	0. 39466	-4. 03780	-9 02923	122. 0	0. 31398	-5. 03102	-10. 02245
34. 0	0. 51959	-2 84038	-7. 83482	124 0	0 29772	-5 26185	-10 25328
36. 0	0 67582	-1. 70169	-6. 69312	126. 0	0. 26788	-5. 72057	-10. 71200
38. 0	0. 87058	-0. 60193	-5. 59337	128 0	0 22586	-6. 46156	-11. 45299
40. 0	1 10702	0 44154	-4. 54989	130 0	0. 17591	-7. 54711	-12. 53854
42. 0	1. 38176	1. 40432	-3. 58712	132 0	0 12489	-9 03487	-14. 02631
44. 0	1 69431	2 26422	-2. 72722	134 0	0. 08133	-10 89736	-15 88899
46. 0	1 99839	3. 00681	-1. 98463	136. 0	0 05376	-12 69535	-17. 68678
48. 0	2 30453	3. 62582	-1 36562	138 0	0. 04849	-13 14338	-18 13481
50. 0	2 58310	4. 12142	-0. 87002	140 0	0. 06743	-11 71162	-16 70305
52. 0	2 81713	4 49810	-0 49334	142 0	0. 10660	-9. 72240	-14. 71383
54. 0	2. 99429	4 76294	-0 22849	144 0	0 13612	-8 65540	-13 65687
56. 0	3 10770	4 92439	-0. 06704	146 0	0 20200	-6 94639	-11 93782
58 0	3. 15605	4 99143	0 00000	148 0	0 22979	-6 38664	-11 37807
60 0	3 14274	4 97308	-0 01835	150 0	0 22909	-6 39993	-11 39137
62 0	3. 07472	4 87806	-0 11338	152. 0	0. 19765	-7 04093	-12 03236
64. 0	2 96113	4 71458	-0 27685	154 0	0 14335	-8 43591	-13 42734
66 0	2 81208	4 49028	-0 50116	156 0	0. 08279	-10. 82008	-15 81152
68 0	2 63760	4 21209	-0 77934	158 0	0. 03645	-14 38318	-19 37461
70 0	2 44696	3 88626	-1 10517	160 0	0 02158	-16 65960	-21 65103
72 0	2 24818	3 51830	-1 47313	162 0	0. 04536	-13 43369	-18 42513
74 0	2 04786	3 11299	-1 87844	164 0	0 10105	-9 95448	-14 94591
76 0	1 85114	2 67439	-2 31704	166 0	0 16933	-7 71278	-12 70421
78 0	1 66184	2 20588	-2 78555	168 0	0 22469	-6 48416	-11 47560
80 0	1 48256	1 71017	-3 28126	170 0	0 24515	-6 10574	-11 09717
82 0	1 31504	1 18929	-3 80214	172 0	0 22118	-6 55246	-11 54390
84 0	1 16016	0 64519	-4 34625	174 0	0 16031	-7 95040	-12 94184
86 0	1 01803	0 07069	-4 91254	176 0	0 08485	-10 71372	-15 70515
88 0	0 88957	-0 50521	-5 49944	178 0	0 02350	-16 28937	-21. 28080
90 0	0 77368	-1 11441	-6 10.d5	180	0 00000	-INFINITY	-INFINITY

TABLE A2-42 $2\pi a/\lambda = 10.25$

```
EPSLN= 10 2500(NORMALIZED GROUNDPLANE RADIUS)
MONOPOLE LENGTH= 0 250000(WAVELENGTH)
MONOPOLE RADIUS=  0 10006-03(WAVELENGTH)
NUMBER OF MONOPOLE SEGMENTS=  1
NUMBER OF DISK SEGMENTS= 30
NUMBER OF ANNULAR ZONES PER DISK SEGEMENT=  I
RADIATION RESISTANCE DETERMINED BY PATTERN= 0.385880E+02 OHMS
```

ELEVATION ANGLE (DEG)	DIRECTIVITY (NUMERIC)	DIRECTIVITY (dBi)	RELATIVE POWER (dB)	ELEVATION ANGLE (DEG)	DIRECTIVITY (NUMERIC)	DIRECTIVITY (dBi)	RELATIVE POWER (dB)
0	0. 00000	-INFINITY	-INFINITY				
2. 0	0. 03708	-14. 30827	-19. 42820	92. 0	0. 67349	-1 71669	-6. 83662
4. 0	0. 13615	-8. 65979	-13. 77972	94. 0	0. 58025	-2. 36383	-7 48376
6. 0	0. 26319	-5. 79440	-10. 88433	96. 0	0. 49737	-3 03319	-8. 15312
8. 0	0. 38404	-4. 15618	-9 27611	98 0	0. 42466	-3 71956	-8 83949
10. 0	0 45844	-3. 38719	-8 50712	100 0	0. 36211	-4 41164	-9 53157
12. 0	0. 47083	-3. 27139	-8 39132	102 0	0. 30984	-5 08857	-10. 20850
14. 0	0. 42421	-3. 72418	-8 84411	104 0	0. 26812	-5. 71673	-10 83666
16. 0	0 33829	-4. 70707	-9. 82700	106 0	0 23718	-6 24926	-11. 36918
18. 0	0. 24048	-6. 18921	-11 30914	108 0	0. 21712	-6. 63290	-11. 75283
20. 0	0 15599	-8 06902	-13. 18894	110 0	0 20773	-6. 82496	-11. 94489
22. 0	0 10100	-9. 95700	-15 07693	112 0	0. 20823	-6. 81456	-11 93448
24. 0	0 08086	-10 92236	-16 04249	114 0	0. 21710	-6. 63331	-11. 75324
26. 0	0 09313	-10. 30931	-15 42924	116 0	0. 23195	-6 34614	-11 46606
28. 0	0. 13294	-8. 76360	-13 88353	118 0	0. 24942	-6. 03062	-11. 15054
30. 0	0 19815	-7 03016	-12. 15009	120 0	0. 26545	-5 76022	-10. 88015
32. 0	0. 29188	-5. 34791	-10. 46784	122. 0	0. 27536	-5 59768	-10 71760
34. 0	0 42184	-3. 74850	-8 86843	124 0	0. 27559	-5. 59734	-10. 71727
36. 0	0. 59700	-2. 24028	-7 36020	126 0	0 26254	-5 80812	-10 92804
38. 0	0 82334	-0. 84422	-5. 96414	128 0	0 23545	-6 28096	-11. 40089
40. 0	1 10031	0 41516	-4. 70477	130 0	0. 19624	-7. 07218	-12 19211
42. 0	1. 41918	1 52038	-3. 59955	132. 0	0 14991	-8. 24159	-13. 36152
44. 0	1. 76360	2 46407	-2. 65586	134 0	0 10419	-9. 82134	-14 94147
46 0	2 11321	3 24745	-1. 87247	136. 0	0 06816	-11. 66478	-16 78471
48. 0	2. 44201	3 87748	-1. 24245	138 0	0 03012	-12 99990	-18 11983
50. 0	2. 73172	4 36436	-0. 75556	140. 0	0 05512	-12 58719	-17 70712
52 0	2 96477	4 71990	-0. 40003	142. 0	0 08273	-10 82345	-15 94337
54. 0	3. 13066	4 95636	-0 16357	144 0	0 12609	-8 99320	-14 11313
56. 0	3 22540	5 08569	+0. 03409	146 0	0 17281	-7. 62492	-12 74484
58. 0	3 25082	5 11993	0. 00000	148 0	0 20802	-6 81892	-11 93884
60 0	3 21028	5 06949	-0 05044	150 0	0 21899	-6. 59302	-11 71375
62 0	3 12217	4 94457	-0 17536	152. 0	0. 19989	-6. 99211	-12 11204
64. 0	2. 98835	4 75431	-0 36562	154 0	0 15498	-8. 09736	-13 21729
66 0	2 82291	4 50697	-0. 61296	156. 0	0 09842	-10. 06923	-15 18916
68 0	2 63628	4 20991	-0 91002	158. 0	0 03025	-12 98836	-18 10829
70 0	2 43757	3 86938	-1 25035	160 0	0 02932	-15 32831	-20 44824
72 0	2 23437	3 49155	-1 62898	162 0	0 04564	-13 40691	-18 52684
74 0	2 03261	3 08083	-2 03940	164 0	0 09536	-10 20648	-15 32641
76 0	1 83671	2 64042	-2 47951	166 0	0 16090	-7. 93403	-13 05426
78 0	1 64978	2 17426	-2 94566	168 0	0 21691	-6 63762	-11 75715
80 0	1 47379	1 68435	-3 43558	170. 0	0 24009	-6 19624	-11 31617
82 0	1 30984	1 17210	-3 94775	172 0	0 21913	-6 59291	-11 71284
84 0	1 15938	0 63851	-4 48140	174 0	0 16020	-7 95331	-13 07324
86 0	1 01940	0 08345	-5 03646	176 0	0 08530	-10 69064	-15 81057
88 0	0 89257	-0 49356	-5 61349	178 0	0 02571	-16 25104	-21 37097
90 0	0 [illegible]	-1 08931	-6 21324	180	0 00000	-INFINITY	-INFINITY

TABLE A2-43 $2\pi a/\lambda = 10.50$

EPSLN= 10.5000(NORMALIZED GROUNDPLANE RADIUS)
MONOPOLE LENGTH= 0.250000(WAVELENGTH)
MONOPOLE RADIUS= 0.1000E-03(WAVELENGTH)
NUMBER OF MONOPOLE SEGMENTS= 1
NUMBER OF DISK SEGMENTS= 31
NUMBER OF ANNULAR ZONES PER DISK SEGEMENT= 1
RADIATION RESISTANCE DETERMINED BY PATTERN= 0.378627E+02 OHMS

ELEVATION ANGLE (DEG)	DIRECTIVITY (NUMERIC)	DIRECTIVITY (dBi)	RELATIVE POWER (dB)	ELEVATION ANGLE (DEG)	DIRECTIVITY (NUMERIC)	DIRECTIVITY (dBi)	RELATIVE POWER (dB)
0.	0.00000	-INFINITY	-INFINITY				
2.0	0.04012	-13.96648	-19.13043	92.0	0.69076	-1.60675	-6.77069
4.0	0.14719	-8.32129	-13.48524	94.0	0.59832	-2.23066	-7.39460
6.0	0.28638	-5.43065	-10.59459	96.0	0.51452	-2.88594	-8.04988
8.0	0.41425	-3.82737	-8.99132	98.0	0.43906	-3.57477	-8.73872
10.0	0.49413	-3.06157	-8.22551	100.0	0.37185	-4.29633	-9.46027
12.0	0.50766	-2.94431	-8.10825	102.0	0.31307	-5.04352	-10.20746
14.0	0.45841	-3.38748	-8.55143	104.0	0.26315	-5.79798	-10.96193
16.0	0.36723	-4.35060	-9.51454	106.0	0.22266	-6.52360	-11.68754
18.0	0.26230	-5.81201	-10.97596	108.0	0.19225	-7.16134	-12.32529
20.0	0.16877	-7.72697	-12.89092	110.0	0.17245	-7.63343	-12.79738
22.0	0.10225	-9.90342	-15.06737	112.0	0.16343	-7.86674	-13.03069
24.0	0.06786	-11.68378	-16.84773	114.0	0.16475	-7.83179	-12.99574
26.0	0.06412	-11.93006	-17.09401	116.0	0.17509	-7.56751	-12.73145
28.0	0.08872	-10.51967	-15.68362	118.0	0.19204	-7.16610	-12.33004
30.0	0.14323	-8.43964	-13.60359	120.0	0.21209	-6.73471	-11.89866
32.0	0.23457	-6.29724	-11.46119	122.0	0.23081	-6.36745	-11.53139
34.0	0.37304	-4.28244	-9.44638	124.0	0.24333	-6.13812	-11.30207
36.0	0.56802	-2.45637	-7.62032	126.0	0.24516	-6.10542	-11.26937
38.0	0.82338	-0.84402	-6.00796	128.0	0.23328	-6.32126	-11.48520
40.0	1.13435	0.54745	-4.61649	130.0	0.20711	-6.83909	-12.00204
42.0	1.48689	1.72278	-3.44116	132.0	0.16935	-7.71218	-12.87513
44.0	1.85954	2.69406	-2.46989	134.0	0.12611	-8.99260	-14.15555
46.0	2.22697	3.47714	-1.68681	136.0	0.08606	-10.65202	-15.81597
48.0	2.56408	4.08931	-1.07464	138.0	0.05862	-12.31976	-17.48371
50.0	2.84964	4.54791	-0.61604	140.0	0.05131	-12.89804	-18.06199
52.0	3.06874	4.86960	-0.29435	142.0	0.06705	-11.73584	-16.89979
54.0	3.21369	5.07004	-0.09390	144.0	0.10227	-9.90271	-15.06665
56.0	3.28377	5.16373	-0.00021	146.0	0.14679	-8.33296	-13.49690
58.0	3.28394	5.16395	0.00000	148.0	0.18620	-7.30027	-12.46422
60.0	3.22311	5.08276	-0.08119	150.0	0.20618	-6.85762	-12.02156
62.0	3.11246	4.93104	-0.23291	152.0	0.19787	-7.03615	-12.20010
64.0	2.96381	4.71850	-0.44545	154.0	0.16211	-7.90185	-13.06579
66.0	2.78851	4.45373	-0.71022	156.0	0.11054	-9.56498	-14.72893
68.0	2.59669	4.14421	-1.01974	158.0	0.06246	-12.04431	-17.20825
70.0	2.39685	3.79640	-1.36755	160.0	0.03795	-14.20798	-19.37193
72.0	2.19573	3.41579	-1.74816	162.0	0.04953	-13.05140	-18.21535
74.0	1.99845	3.00693	-2.15702	164.0	0.09587	-10.18318	-15.34713
76.0	1.80863	2.57351	-2.59044	166.0	0.16076	-7.93809	-13.10204
78.0	1.62869	2.11838	-3.04557	168.0	0.21855	-6.60453	-11.76848
80.0	1.46002	1.64359	-3.52035	170.0	0.24434	-6.12001	-11.28395
82.0	1.30328	1.15039	-4.01356	172.0	0.22498	-6.47859	-11.64254
84.0	1.15856	0.63918	-4.52476	174.0	0.16561	-7.80917	-12.97312
86.0	1.02555	0.10956	-5.05438	176.0	0.08861	-10.52536	-15.68931
88.0	0.90370	-0.43976	-5.60370	178.0	0.02470	-16.07319	-21.23713
90.0	0.79234	-1.01090	-6.17485	180.	0.00000	-INFINITY	-INFINITY

TABLE A2-44 $2\pi a/\lambda = 10.75$

```
EPSLN= 10 7500(NORMALIZED GROUNDPLANE RADIUS)
MONOPOLE LENGTH= 0 250000(WAVELENGTH)
MONOPOLE RADIUS=  0 10000E-03(WAVELENGTH)
NUMBER OF MONOPOLE SEGMENTS=  1
NUMBER OF DISK SEGMENTS= 32
NUMBER OF ANNULAR ZONES PER DISK SEGEMENT=  1
RADIATION RESISTANCE DETERMINED BY PATTERN= 0 368938E+02 OHMS
```

ELEVATION ANGLE (DEG)	DIRECTIVITY (NUMERIC)	DIRECTIVITY (dBi)	RELATIVE POWER (dB)	ELEVATION ANGLE (DEG)	DIRECTIVITY (NUMERIC)	DIRECTIVITY (dBi)	RELATIVE POWER (dB)
0.	0.00000	-INFINITY	-INFINITY				
2.0	0.04402	-13.56330	-18.73479	92.0	0.71581	-1.45200	-6.62348
4.0	0.16136	-7.92193	-13.09344	94.0	0.62636	-2.03174	-7.20323
6.0	0.31356	-5.03682	-10.20831	96.0	0.54410	-2.64322	-7.81470
8.0	0.45298	-3.43917	-8.61065	98.0	0.46851	-3.29277	-8.46425
10.0	0.55996	-2.67639	-7.84788	100.0	0.39925	-3.98649	-9.15798
12.0	0.63525	-2.25514	-7.72662	102.0	0.33664	-4.72840	-9.89988
14.0	0.68347	-2.98029	-8.15177	104.0	0.28074	-5.51691	-10.68840
16.0	0.40728	-3.90108	-9.07256	106.0	0.23235	-6.33838	-11.51007
18.0	0.29619	-5.28424	-10.45572	108.0	0.19239	-7.15823	-12.32972
20.0	0.19539	-7.08656	-12.25805	110.0	0.16191	-7.90733	-13.07881
22.0	0.12043	-9.19254	-14.36402	112.0	0.14187	-8.48120	-13.65268
24.0	0.07534	-11.22959	-16.40108	114.0	0.13284	-8.76675	-13.93824
26.0	0.03942	-12.26043	-17.43192	116.0	0.13468	-8.70705	-13.87854
28.0	0.07252	-11.39356	-16.56505	118.0	0.14618	-8.35107	-13.52256
30.0	0.11945	-9.22807	-14.39956	120.0	0.16485	-7.82903	-13.00052
32.0	0.21042	-6.76915	-11.94063	122.0	0.18683	-7.28501	-12.45650
34.0	0.35768	-4.46500	-9.63648	124.0	0.20727	-6.83469	-12.00618
36.0	0.57039	-2.43825	-7.60973	126.0	0.22076	-6.56071	-11.73219
38.0	0.84981	-0.70676	-5.87825	128.0	0.22261	-6.52447	-11.69596
40.0	1.18683	0.74390	-4.42759	130.0	0.20994	-6.77896	-11.95044
42.0	1.56246	1.93810	-3.23339	132.0	0.18293	-7.37711	-12.54860
44.0	1.95092	2.90240	-2.26909	134.0	0.14551	-8.37105	-13.54254
46.0	2.32414	3.66263	-1.50886	136.0	0.10518	-9.78084	-14.95233
48.0	2.65632	4.24280	-0.92868	138.0	0.07159	-11.45117	-16.62266
50.0	2.92742	4.66486	-0.50663	140.0	0.05410	-12.66816	-17.83965
52.0	3.12512	4.94847	-0.22282	142.0	0.05658	-12.47267	-17.64416
54.0	3.24501	5.11216	-0.05932	144.0	0.08478	-10.71689	-15.88838
56.0	3.28964	5.17149	0.00000	146.0	0.12520	-9.02397	-14.19545
58.0	3.26669	5.14108	-0.03040	148.0	0.16683	-7.78778	-12.95927
60.0	3.18700	5.03382	-0.13767	150.0	0.19320	-7.13995	-12.31144
62.0	3.06270	4.86103	-0.31044	152.0	0.19406	-7.12065	-12.29214
64.0	2.90384	4.63271	-0.53878	154.0	0.16663	-7.78259	-12.95407
66.0	2.72734	4.35739	-0.81410	156.0	0.12009	-9.20681	-14.37830
68.0	2.53654	4.04241	-1.12908	158.0	0.07284	-11.37630	-16.54778
70.0	2.34098	3.69398	-1.47751	160.0	0.04629	-13.34343	-18.51494
72.0	2.14647	3.31726	-1.85423	162.0	0.03529	-14.52349	-19.69497
74.0	1.95726	2.91649	-2.25499	164.0	0.10082	-9.96454	-15.13602
76.0	1.77628	2.49312	-2.67836	166.0	0.16760	-7.75730	-12.92878
78.0	1.60340	2.05383	-3.11765	168.0	0.22904	-6.40093	-11.57242
80.0	1.44564	1.60060	-3.57088	170.0	0.25805	-5.88295	-11.05443
82.0	1.29739	1.13070	-4.04078	172.0	0.23930	-6.21049	-11.38198
84.0	1.16055	0.64665	-4.52484	174.0	0.17717	-7.51605	-12.68753
86.0	1.03470	0.14814	-5.02335	176.0	0.09319	-10.21421	-15.38569
88.0	0.91916	-0.36609	-5.53757	178.0	0.02660	-15.75121	-20.92270
90.0	0.81315	-0.89832	-6.06980	180	0.00000	-INFINITY	-INFINITY

TABLE A2-45 $2\pi a/\lambda = 11.00$

```
EPSLN= [[ 0000(NORMALIZED GROUNDPLANE RADIUS)
MONOPOLE LENGTH= 0 250000(WAVELENGTH)
MONOPOLE RADIUS=   0.1000E-03(WAVELENGTH)
NUMBER OF MONOPOLE SEGMENTS=  1
NUMBER OF DISK SEGMENTS= 30
NUMBER OF ANNULAR ZONES PER DISK SEGMENT=  1
RADIATION RESISTANCE DETERMINED BY PATTERN= 0 359200E+02 OHMS
```

ELEVATION ANGLE (DEG)	DIRECTIVITY (NUMERIC)	DIRECTIVITY (dBi)	RELATIVE POWER (dB)	ELEVATION ANGLE (DEG)	DIRECTIVITY (NUMERIC)	DIRECTIVITY (dBi)	RELATIVE POWER (dB)
0.	0.00000	-INFINITY	-INFINITY				
2.0	0.04884	-13.11211	-18.23369	92.0	0.74289	-1.29073	-6.41431
4.0	0.17881	-7.47614	-12.59771	94.0	0.65773	-1.81955	-6.94312
6.0	0.34691	-4.59903	-9.72061	96.0	0.57980	-2.37475	-7.49832
8.0	0.49999	-3.01038	-8.13196	98.0	0.50534	-2.96413	-8.08770
10.0	0.59303	-2.25458	-7.37613	100.0	0.43682	-3.59693	-8.72050
12.0	0.61193	-2.13301	-7.25458	102.0	0.37299	-4.28308	-9.40665
14.0	0.55698	-2.54161	-7.66318	104.0	0.31394	-5.03152	-10.15509
16.0	0.45551	-3.41498	-8.53655	106.0	0.26022	-5.84664	-10.97022
18.0	0.33899	-4.69814	-9.82172	108.0	0.21275	-6.72123	-11.84480
20.0	0.23313	-6.32406	-11.44763	110.0	0.17284	-7.62358	-12.74715
22.0	0.15196	-8.18275	-13.30632	112.0	0.14195	-8.47856	-13.60214
24.0	0.09903	-10.04214	-15.16572	114.0	0.12150	-9.15415	-14.27772
26.0	0.07352	-11.33577	-16.45934	116.0	0.11246	-9.48998	-14.61356
28.0	0.07701	-11.13468	-16.25825	118.0	0.11493	-9.39548	-14.51906
30.0	0.11728	-9.30761	-14.43118	120.0	0.12775	-8.93654	-14.06011
32.0	0.20733	-6.82913	-11.95270	122.0	0.14814	-8.29333	-13.41691
34.0	0.36166	-4.41700	-9.54058	124.0	0.17176	-7.65070	-12.77428
36.0	0.58823	-2.30454	-7.42811	126.0	0.19307	-7.14276	-12.26633
38.0	0.88569	-0.52720	-5.65077	128.0	0.20621	-6.85690	-11.98047
40.0	1.24086	0.93652	-4.18704	130.0	0.20631	-6.85483	-11.97840
42.0	1.62769	2.12103	-2.99252	132.0	0.19101	-7.18945	-12.31302
44.0	2.02358	3.06120	-2.06238	134.0	0.16172	-7.91236	-13.03593
46.0	2.39264	3.78878	-1.33479	136.0	0.12410	-9.06222	-14.18580
48.0	2.71153	4.33214	-0.79143	138.0	0.08730	-10.58963	-15.71322
50.0	2.96235	4.71636	-0.40722	140.0	0.06177	-12.09230	-17.21587
52.0	3.13389	4.96361	-0.15996	142.0	0.05595	-12.52222	-17.64579
54.0	3.23114	5.09356	-0.03001	144.0	0.07288	-11.37408	-16.49765
56.0	3.25355	5.12357	0.00000	146.0	0.10798	-9.66655	-14.79012
58.0	3.21286	5.06892	-0.05465	148.0	0.14938	-8.25714	-13.38071
60.0	3.12098	4.94291	-0.18066	150.0	0.18132	-7.41538	-12.53895
62.0	2.99022	4.75702	-0.36655	152.0	0.19005	-7.21131	-12.33488
64.0	2.83205	4.52100	-0.60257	154.0	0.17009	-7.69310	-12.81667
66.0	2.65646	4.24304	-0.88054	156.0	0.12810	-8.92462	-14.04820
68.0	2.47167	3.92991	-1.19366	158.0	0.08186	-10.86921	-15.99278
70.0	2.28414	3.58722	-1.53635	160.0	0.05395	-12.67992	-17.80349
72.0	2.09873	3.21956	-1.90401	162.0	0.06184	-12.08738	-17.21095
74.0	1.91899	2.83072	-2.29286	164.0	0.10877	-9.63473	-14.75830
76.0	1.74736	2.42381	-2.69976	166.0	0.18006	-7.44383	-12.56741
78.0	1.58542	2.00144	-3.12216	168.0	0.24747	-6.06477	-11.18834
80.0	1.43406	1.56366	-3.55791	170.0	0.28098	-5.51487	-10.63844
82.0	1.29362	1.11937	-4.00220	172.0	0.26202	-5.81303	-10.93661
84.0	1.16403	0.65796	-4.46362	174.0	0.19319	-7.09352	-12.21710
86.0	1.04489	0.18972	-4.93186	176.0	0.10527	-9.77685	-14.90042
88.0	0.93535	-0.28493	-5.41650	178.0	0.02949	-15.30374	-20.42731
90.0	0.83519	-0.78016	-5.91173	180	0.00000	-INFINITY	-INFINITY

TABLE A2-46 $2\pi a/\lambda = 11.25$

```
EPSLN= 11 2500(NORMALIZED GROUNDPLANE RADIUS)
MONOPOLE LENGTH= 0 250000(WAVELENGTH)
MONOPOLE RADIUS=   0.1000E-03(WAVELENGTH)
NUMBER OF MONOPOLE SEGMENTS=  1
NUMBER OF DISK SEGMENTS= 30
NUMBER OF ANNULAR ZONES PER DISK SEGEMENT=  1
RADIATION RESISTANCE DETERMINED BY PATTERN= 0 350770E+02 OHMS
```

ELEVATION ANGLE (DEG)	DIRECTIVITY (NUMERIC)	DIRECTIVITY (dBi)	RELATIVE POWER (dB)	ELEVATION ANGLE (DEG)	DIRECTIVITY (NUMERIC)	DIRECTIVITY (dBi)	RELATIVE POWER (dB)
0.	0 00000	-INFINITY	-INFINITY				
2.0	0 05434	-12 63293	-17. 66518	92.0	0. 76774	-1. 14787	-6. 18012
4.0	0. 19932	-7. 00456	-12. 03681	94.0	0. 68721	-1. 62911	-6 66136
6.0	0. 38554	-4. 13927	-9. 17151	96.0	0. 61260	-2. 12820	-7. 16045
8.0	0 55399	-2 56499	-7. 59724	98.0	0. 54290	-2 65281	-7 68506
10.0	0 65720	-1 82302	-6. 85527	100.0	0. 47721	-3. 21294	-8. 24519
12.0	0 67467	-1. 70906	-6. 74131	102.0	0 41488	-3. 82076	-8. 85301
14.0	0. 61533	-2. 10891	-7. 14116	104.0	0. 35563	-4. 49004	-9. 52229
16.0	0 50815	-2 94012	-7. 97237	106.0	0. 29960	-5. 23464	-10. 26689
18.0	0. 38709	-4. 12192	-9. 15417	108.0	0. 24746	-6. 06500	-11. 09724
20.0	0 27813	-5. 55750	-10. 58975	110.0	0. 20042	-6. 98054	-12. 01279
22.0	0 19374	-7. 12781	-12. 16006	112 0	0. 16017	-7 95420	-12 98645
24.0	0. 13339	-8. 67770	-13. 70995	114. 0	0. 12866	-8. 90573	-13. 93798
26.0	0. 10225	-9. 90340	-14. 93565	116 0	0. 10778	-9. 67468	-14 70692
28.0	0 09667	-10. 14694	-15 17919	118 0	0. 09892	-10 04737	-15. 07962
30.0	0. 12930	-8. 87719	-13. 90944	120 0	0. 10237	-9. 89846	-14. 93071
32.0	0. 21686	-6 63830	-11. 67055	122 0	0. 11683	-9. 32434	-14. 35659
34.0	0 37418	-4 26922	-9. 30147	124 0	0 13910	-8 56684	-13 59909
36.0	0. 60933	-2 15148	-7. 18372	126 0	0. 16407	-7. 84978	-12. 88203
38.0	0 91792	-0. 37196	-5. 40421	128 0	0. 18540	-7. 31883	-12 35107
40 0	1 28236	1. 08079	-3 95146	130 0	0. 19673	-7 06133	-12. 09358
42.0	1 67600	2 24273	-2. 78952	132 0	0 19331	-7. 13725	-12. 16960
44.0	2 06654	3 15244	-1. 87980	134 0	0 17383	-7 59870	-12. 63093
46.0	2 42406	3 84543	-1. 18682	136 0	0 14156	-8 49071	-13. 52294
48.0	2 72465	4 35310	-0 67915	138 0	0 10436	-9 81449	-14 84674
50.0	2 95324	4 70299	-0. 32926	140 0	0 07307	-11. 36240	-16 39465
52.0	3 10400	4 91922	-0. 11303	142 0	0 05820	-12 25071	-17. 28296
54.0	3 17897	5 02287	-0. 00938	144 0	0. 06595	-11 80756	-16 83981
56.0	3 18585	5 03225	0 00000	146 0	0 09494	-10 22549	-15 25774
58 0	3 13532	4 96309	-0 06916	148 0	0 13526	-8 68834	-13 72059
60 0	3 03998	4 82070	-0 20155	150 0	0 17111	-7 66712	-12 69937
62 0	2 91082	4 64015	-0 38210	152 0	0 18671	-7 28826	-12 32051
64 0	2 76833	4 40646	-0. 62579	154 0	0 17350	-7 60707	-12 63932
66 0	2 59112	4 13488	-0 89737	156 0	0 13554	-8 67922	-13 71147
68.0	2 41613	3 83121	-1 20104	158 0	0 08993	-10 46080	-15 49305
70 0	2 23877	3 50009	-1 53216	160 0	0 06076	-12 16363	-17 19588
72 0	2 06316	3 14533	-1 88692	162 0	0 06841	-11 64903	-16 68128
74 0	1 89246	2 77017	-2 26208	164 0	0 11861	-9 25891	-14 29116
76 0	1 72851	2 37756	-2 65468	166 0	0 19702	-7 05494	-12 08719
78 0	1 57352	1 96982	-3 06242	168 0	0 27204	-5 65771	-10 66996
80 0	1 42878	1 54966	-3 48258	170 0	0 31249	-5 05161	-10 06386
82 0	1 29564	1 11911	-3 91313	172 0	0 29581	-5 31933	-10 33158
84 0	1 16552	0 69016	-4 34213	174 0	0 21991	-6 57751	-11 60975
86 0	1 03932	0 25383	-4 77846	176 0	0 11708	-9 31176	-14 27401
88 0	0 91801	-0 18931	-5 21139	178 0	0 03343	-14 75846	-19 72071
90 0	0 80247	-0 62543	-5 64751	180	0 00000	-INFINITY	-INFINITY

TABLE A2-47 $2\pi a/\lambda = 11.50$

```
EPSLN= 15.5000(NORMALIZED GROUNDPLANE RADIUS)
MONOPOLE LENGTH= 0.2500000(WAVELENGTH)
MONOPOLE RADIUS=  0.1000E-05(WAVELENGTH)
NUMBER OF MONOPOLE SEGMENTS=  1
NUMBER OF DISK SEGMENTS= 34
NUMBER OF ANNULAR ZONES PER DISK SEGEMENT=  1
RADIATION RESISTANCE DETERMINED BY PATTERN= 0.345396E+02 OHMS
```

ELEVATION ANGLE (DEG)	DIRECTIVITY (NUMERIC)	DIRECTIVITY (dBi)	RELATIVE POWER (dB)	ELEVATION ANGLE (DEG)	DIRECTIVITY (NUMERIC)	DIRECTIVITY (dBi)	RELATIVE POWER (dB)
0.	0.00000	-INFINITY	-INFINITY				
2.0	0.06109	-12.14065	-17.05348	92.0	0.78459	-1.05356	-5.96640
4.0	0.22270	-6.52286	-11.43570	94.0	0.70818	-1.49859	-6.41142
6.0	0.42909	-3.67450	-8.58733	96.0	0.63811	-1.95106	-6.86389
8.0	0.61348	-2.12201	-7.03484	98.0	0.57312	-2.41756	-7.33040
10.0	0.72383	-1.40363	-6.31646	100.0	0.51197	-2.90735	-7.82039
12.0	0.73976	-1.30909	-6.22192	102.0	0.45358	-3.43350	-8.34633
14.0	0.67407	-1.71297	-6.62580	104.0	0.39712	-4.01078	-8.92361
16.0	0.56061	-2.51349	-7.42626	106.0	0.34220	-4.65715	-9.56998
18.0	0.43639	-3.60124	-8.51408	108.0	0.28898	-5.39132	-10.30415
20.0	0.32728	-4.85084	-9.76368	110.0	0.23926	-6.22941	-11.14224
22.0	0.24312	-6.14173	-11.05457	112.0	0.19157	-7.17674	-12.08957
24.0	0.18257	-7.38576	-12.29859	114.0	0.15103	-8.20946	-13.12229
26.0	0.14273	-8.45473	-13.36757	116.0	0.11914	-9.23933	-14.15217
28.0	0.12762	-8.94081	-13.85365	118.0	0.09836	-10.07184	-14.98468
30.0	0.13077	-8.83686	-13.74969	120.0	0.09045	-10.43612	-15.34896
32.0	0.14144	-8.49369	-13.40652	122.0	0.09579	-10.18688	-15.09971
34.0	0.38677	-4.12548	-9.03831	124.0	0.11276	-9.47861	-14.39144
36.0	0.62402	-2.04799	-6.96082	126.0	0.13736	-8.62126	-13.53410
38.0	0.93616	-0.28652	-5.19935	128.0	0.16350	-7.86484	-12.77767
40.0	1.30229	1.14687	-3.76596	130.0	0.18388	-7.35467	-12.26750
42.0	1.69194	2.28383	-2.62899	132.0	0.19175	-7.17271	-12.08553
44.0	2.07220	3.16432	-1.74851	134.0	0.18299	-7.37574	-12.28857
46.0	2.41349	3.82646	-1.08638	136.0	0.15806	-8.01187	-12.92470
48.0	2.69422	4.30432	-0.60851	138.0	0.12284	-9.10649	-14.01932
50.0	2.90254	4.62778	-0.28506	140.0	0.08779	-10.56566	-15.47850
52.0	3.03560	4.82273	-0.09010	142.0	0.06493	-11.87573	-16.78856
54.0	3.09846	4.91146	-0.00137	144.0	0.06348	-11.97304	-16.88617
56.0	3.09944	4.91283	0.00000	146.0	0.08350	-10.68059	-15.59342
58.0	3.04963	4.84247	-0.07036	148.0	0.12352	-9.08250	-13.99533
60.0	2.96006	4.71300	-0.19983	150.0	0.16219	-7.89980	-12.81263
62.0	2.84075	4.53433	-0.37851	152.0	0.18386	-7.35506	-12.26790
64.0	2.70025	4.31405	-0.59879	154.0	0.17684	-7.52417	-12.43700
66.0	2.54560	4.05790	-0.85494	156.0	0.14243	-8.46402	-13.37686
68.0	2.38246	3.77026	-1.14258	158.0	0.09694	-10.13479	-15.04762
70.0	2.21544	3.45460	-1.45823	160.0	0.06630	-11.78511	-16.69795
72.0	2.04829	3.11381	-1.79893	162.0	0.07429	-11.29080	-16.20363
74.0	1.88405	2.75695	-2.15579	164.0	0.12957	-8.87510	-13.78794
76.0	1.72522	2.38845	-2.52429	166.0	0.21802	-6.61495	-11.52779
78.0	1.57274	2.00934	-2.90339	168.0	0.30588	-5.14453	-10.05737
80.0	1.43106	1.70659	-3.20614	170.0	0.35362	-4.51458	-9.42741
82.0	1.29815	1.12574	-3.78699	172.0	0.33514	-4.74775	-9.66059
84.0	1.17514	0.70235	-4.21038	174.0	0.25635	-5.91292	-10.82575
86.0	1.06042	0.25456	-4.65816	176.0	0.13721	-8.62603	-13.53887
88.0	0.95214	-0.21194	-5.12466	178.0	0.03862	-14.13209	-19.04493
90.0	0.84957	-0.61176	-5.52448	180.	0.00000	-INFINITY	-INFINITY

TABLE A2-48 $2\pi a/\lambda = 11.75$

```
EPSLN= 11.7500(NORMALIZED GROUNDPLANE RADIUS)
MONOPOLE LENGTH= 0.250000(WAVELENGTH)
MONOPOLE RADIUS=   0.1000E-03(WAVELENGTH)
NUMBER OF MONOPOLE SEGMENTS= 1
NUMBER OF DISK SEGMENTS= 35
NUMBER OF ANNULAR ZONES PER DISK SEGMENT= 1
RADIATION RESISTANCE DETERMINED BY PATTERN= 0.350588E+02 OHMS
```

ELEVATION ANGLE (DEG)	DIRECTIVITY (NUMERIC)	DIRECTIVITY (dBi)	RELATIVE POWER (dB)	ELEVATION ANGLE (DEG)	DIRECTIVITY (NUMERIC)	DIRECTIVITY (dBi)	RELATIVE POWER (dB)
0.	0.00000	-INFINITY	-INFINITY				
2.0	0.06752	-11.70358	-16.50360	92.0	0.77281	-1.11929	-5.91731
4.0	0.24558	-6.09808	-10.89610	94.0	0.69896	-1.55549	-6.35351
6.0	0.47143	-3.26579	-8.06381	96.0	0.63290	-1.98663	-6.78465
8.0	0.67096	-1.73303	-6.53105	98.0	0.57323	-2.41674	-7.21476
10.0	0.78620	-1.03345	-5.83147	100.0	0.51849	-2.85307	-7.65110
12.0	0.80374	-0.94883	-5.74687	102.0	0.46704	-3.30642	-8.10445
14.0	0.73492	-1.32757	-6.12560	104.0	0.41772	-3.79113	-8.58917
16.0	0.62051	-2.07234	-6.87036	106.0	0.36942	-4.32483	-9.12285
18.0	0.49979	-3.01216	-7.81018	108.0	0.32156	-4.92735	-9.72537
20.0	0.39721	-4.00974	-8.80777	110.0	0.27423	-5.61883	-10.41685
22.0	0.31876	-4.96332	-9.76334	112.0	0.22830	-6.41497	-11.21299
24.0	0.25919	-5.86378	-10.66178	114.0	0.18549	-7.31679	-12.11481
26.0	0.21397	-6.69654	-11.49456	116.0	0.14829	-8.28899	-13.08701
28.0	0.18834	-7.25093	-12.04855	118.0	0.11960	-9.22259	-14.02061
30.0	0.19908	-7.00970	-11.80772	120.0	0.10223	-9.90439	-14.70242
32.0	0.26872	-5.70707	-10.50509	122.0	0.09803	-10.08644	-14.88446
34.0	0.41604	-3.80863	-8.60666	124.0	0.10711	-9.70170	-14.49972
36.0	0.64767	-1.88645	-6.68447	126.0	0.12708	-8.95939	-13.75742
38.0	0.95419	-0.20363	-5.00165	128.0	0.15280	-8.15868	-12.95670
40.0	1.31192	1.17909	-3.61894	130.0	0.17698	-7.52064	-12.31866
42.0	1.68890	2.27579	-2.52224	132.0	0.19160	-7.17593	-11.97395
44.0	2.05181	3.12138	-1.67665	134.0	0.19021	-7.20761	-12.00563
46.0	2.37330	3.75357	-1.04446	136.0	0.17042	-7.68479	-12.48281
48.0	2.63481	4.20750	-0.59052	138.0	0.13570	-8.67409	-13.47211
50.0	2.82765	4.51425	-0.28377	140.0	0.09547	-10.20191	-14.99994
52.0	2.95166	4.70063	-0.09739	142.0	0.06271	-12.02638	-16.82440
54.0	3.01240	4.78912	-0.00890	144.0	0.04955	-13.04961	-17.84763
56.0	3.01838	4.79802	0.00000	146.0	0.06187	-12.08495	-16.88297
58.0	2.97965	4.74166	-0.05637	148.0	0.09560	-10.19559	-14.99362
60.0	2.90493	4.63079	-0.16723	150.0	0.13672	-8.64168	-13.43970
62.0	2.80103	4.47318	-0.32484	152.0	0.16639	-7.78874	-12.58676
64.0	2.67563	4.27426	-0.52376	154.0	0.16966	-7.70412	-12.50214
66.0	2.53387	4.03784	-0.76018	156.0	0.14429	-8.40758	-13.20560
68.0	2.38054	3.76676	-1.03126	158.0	0.10466	-9.80216	-14.60018
70.0	2.21994	3.46341	-1.33462	160.0	0.07742	-11.11103	-15.90905
72.0	2.05596	3.13014	-1.66788	162.0	0.08924	-10.49463	-15.29265
74.0	1.89214	2.76953	-2.02849	164.0	0.15159	-8.19318	-12.99120
76.0	1.73161	2.38450	-2.41353	166.0	0.25092	-6.00465	-10.80267
78.0	1.57702	1.97838	-2.81964	168.0	0.35049	-4.55321	-9.35123
80.0	1.43031	1.55492	-3.24310	170.0	0.40555	-3.91956	-8.71758
82.0	1.29366	1.11619	-3.67983	172.0	0.38534	-4.14153	-8.93955
84.0	1.16748	0.67249	-4.12353	174.0	0.29096	-5.36165	-10.15967
86.0	1.05248	0.22110	-4.57589	176.0	0.15857	-7.99787	-12.79589
88.0	0.94868	-0.22879	-5.02681	178.0	0.04469	-13.49750	-18.29552
90.0	0.85571	-0.67676	-5.47478	180.	0.00000	-INFINITY	-INFINITY

TABLE A2-49 $2\pi a/\lambda = 12.00$

TABLE A2-49 $2\pi a/\lambda$ = 12.00

EPSLN= 13 0000(NORMALIZED GROUNDPLANE RADIUS)
MONOPOLE LENGTH= 0 250000(WAVELENGTH)
MONOPOLE RADIUS= 0 1000E-05(WAVELENGTH)
NUMBER OF MONOPOLE SEGMENTS= 1
NUMBER OF DISK SEGMENTS= 36
NUMBER OF ANNULAR ZONES PER DISK SEGMENT= 1
RADIATION RESISTANCE DETERMINED BY PATTERN= 0 344984E+02 OHMS

ELEVATION ANGLE (DEG)	DIRECTIVITY (NUMERIC)	DIRECTIVITY (dBi)	RELATIVE POWER (dB)	ELEVATION ANGLE (DEG)	DIRECTIVITY (NUMERIC)	DIRECTIVITY (dBi)	RELATIVE POWER (dB)
0.	0.00000	-INFINITY	-INFINITY				
2.0	0.07468	-11.26769	-15.92317	92.0	0.78616	-1.04490	-5.70038
4.0	0.27028	-5.68194	-10.33742	94.0	0.71317	-1.46808	-6.12356
6.0	0.51449	-2.88821	-7.54169	96.0	0.64933	-1.87534	-6.53082
8.0	0.72060	-1.40482	-6.06031	98.0	0.59310	-2.26875	-6.92423
10.0	0.80747	-0.77030	-5.42578	100.0	0.54273	-2.65413	-7.30963
12.0	0.80969	-0.73879	-5.41428	102.0	0.49640	-3.04171	-7.69719
14.0	0.75378	-1.21607	-5.87155	104.0	0.45226	-3.44615	-8.10163
16.0	0.69270	-1.98778	-6.64327	106.0	0.40863	-3.88674	-8.54222
18.0	0.61370	-2.89268	-7.54816	108.0	0.36417	-4.38691	-9.04239
20.0	0.42103	-3.75690	-8.41238	110.0	0.31817	-4.97346	-9.62894
22.0	0.35421	-4.50743	-9.16291	112.0	0.27072	-5.67484	-10.33032
24.0	0.30116	-5.21205	-9.86753	114.0	0.22300	-6.51698	-11.17246
26.0	0.25339	-5.96210	-10.61758	116.0	0.17732	-7.51231	-12.16779
28.0	0.21643	-6.64682	-11.30230	118.0	0.13701	-8.63261	-13.28809
30.0	0.21046	-6.76835	-11.42383	120.0	0.10390	-9.75091	-14.40639
32.0	0.26218	-5.81401	-10.46949	122.0	0.08763	-10.57936	-15.23484
34.0	0.39312	-4.05490	-8.71038	124.0	0.08431	-10.73116	-15.38664
36.0	0.61023	-2.14508	-6.80057	126.0	0.09642	-10.15843	-14.81391
38.0	0.90263	-0.44483	-5.10031	128.0	0.12005	-9.20652	-13.86201
40.0	1.24486	0.95121	-3.70427	130.0	0.14879	-8.27420	-12.92968
42.0	1.60408	2.05223	-2.60323	132.0	0.17384	-7.59853	-12.25402
44.0	1.94833	2.89663	-1.75883	134.0	0.18638	-7.29595	-11.95143
46.0	2.25265	3.52693	-1.12853	136.0	0.18063	-7.43221	-12.08769
48.0	2.50181	3.98233	-0.67293	138.0	0.15656	-8.05317	-12.70865
50.0	2.69209	4.29766	-0.35760	140.0	0.12123	-9.16973	-13.81921
52.0	2.81884	4.50070	-0.15478	142.0	0.08735	-10.58722	-15.24270
54.0	2.89353	4.61428	-0.04120	144.0	0.06895	-11.61450	-16.26998
56.0	2.92111	4.65548	0.00000	146.0	0.07527	-11.23360	-15.88909
58.0	2.90833	4.63643	-0.01905	148.0	0.10537	-9.77280	-14.42828
60.0	2.86099	4.56517	-0.09031	150.0	0.14654	-8.34037	-12.99586
62.0	2.78401	4.44670	-0.20878	152.0	0.17859	-7.48139	-12.13681
64.0	2.68168	4.28407	-0.37141	154.0	0.18334	-7.36733	-12.02281
66.0	2.55817	4.07930	-0.57618	156.0	0.15547	-8.08340	-12.73888
68.0	2.41774	3.83409	-0.82139	158.0	0.10883	-9.63248	-14.28796
70.0	2.26483	3.55036	-1.10512	160.0	0.07319	-11.35556	-16.01104
72.0	2.10400	3.23046	-1.42502	162.0	0.06083	-12.92438	-17.57986
74.0	1.93971	2.87736	-1.77812	164.0	0.14826	-8.28983	-12.94531
76.0	1.77608	2.49462	-2.16086	166.0	0.26275	-5.80460	-10.46008
78.0	1.61675	2.08644	-2.56904	168.0	0.38272	-4.17123	-8.82671
80.0	1.46471	1.65750	-2.99798	170.0	0.45459	-3.42380	-8.07928
82.0	1.32223	1.21338	-3.44210	172.0	0.43943	-3.57107	-8.22655
84.0	1.19037	0.75845	-3.89703	174.0	0.33564	-4.74126	-9.39674
86.0	1.07153	0.30076	-4.35472	176.0	0.19428	-7.11523	-11.77071
88.0	0.96451	-0.15691	-4.81239	178.0	0.05216	-12.82667	-17.48215
90.0	0.86760	-0.62475	-5.28056	180	0.00000	-INFINITY	-INFINITY

TABLE A2-50 $2\pi a/\lambda = 12.25$

```
EPSLN= 12.2500(NORMALIZED GROUNDPLANE RADIUS)
MONOPOLE LENGTH= 0.250000(WAVELENGTH)
MONOPOLE RADIUS=  0.1000E-05(WAVELENGTH)
NUMBER OF MONOPOLE SEGMENTS=  1
NUMBER OF DISK SEGMENTS= 36
NUMBER OF ANNULAR ZONES PER DISK SEGEMENT=  1
RADIATION RESISTANCE DETERMINED BY PATTERN= 0.330038E+02 OHMS
```

ELEVATION ANGLE (DEG)	DIRECTIVITY (NUMERIC)	DIRECTIVITY (dBi)	RELATIVE POWER (dB)	ELEVATION ANGLE (DEG)	DIRECTIVITY (NUMERIC)	DIRECTIVITY (dBi)	RELATIVE POWER (dB)
0.	0.00000	-INFINITY	-INFINITY				
2.0	0.08047	-10.94356	-15.54015	92.0	0.76992	-1.13553	-5.73212
4.0	0.28973	-5.38000	-9.97658	94.0	0.69516	-1.57916	-6.17573
6.0	0.54683	-2.62147	-7.21805	96.0	0.63147	-1.99649	-6.59307
8.0	0.73999	-1.19192	-5.78850	98.0	0.57733	-2.38578	-6.98237
10.0	0.86667	-0.62144	-5.21802	100.0	0.53096	-2.74939	-7.34597
12.0	0.95544	-0.47811	-5.27469	102.0	0.49038	-3.09468	-7.69126
14.0	0.76077	-1.18745	-5.78404	104.0	0.45345	-3.43469	-8.03127
16.0	0.63743	-1.95568	-6.55227	106.0	0.41801	-3.78818	-8.38476
18.0	0.53063	-2.75206	-7.34865	108.0	0.38201	-4.17924	-8.77582
20.0	0.45815	-3.38996	-7.98655	110.0	0.34383	-4.63651	-9.23309
22.0	0.41116	-3.85994	-8.45632	112.0	0.30235	-5.19202	-9.78860
24.0	0.38986	-4.32193	-8.91851	114.0	0.25628	-5.87904	-10.47562
26.0	0.32120	-4.93221	-9.52879	116.0	0.21247	-6.72693	-11.32351
28.0	0.27208	-5.65297	-10.24956	118.0	0.16798	-7.74733	-12.34391
30.0	0.24641	-6.08344	-10.68002	120.0	0.12886	-8.89867	-13.49526
32.0	0.27526	-5.60259	-10.19917	122.0	0.09973	-10.01181	-14.60840
34.0	0.38290	-4.16916	-8.76574	124.0	0.08467	-10.72259	-15.31917
36.0	0.57688	-2.38912	-6.98570	126.0	0.08591	-10.65932	-15.25591
38.0	0.84570	-0.72783	-5.32441	128.0	0.10249	-9.89217	-14.48976
40.0	1.16349	0.65764	-3.93894	130.0	0.12952	-8.87668	-13.47327
42.0	1.49833	1.75670	-2.83988	132.0	0.15860	-7.99700	-12.59358
44.0	1.82159	2.60452	-1.99207	134.0	0.17967	-7.45525	-12.05184
46.0	2.11123	3.24536	-1.35122	136.0	0.18416	-7.34810	-11.94468
48.0	2.35551	3.72085	-0.87573	138.0	0.16856	-7.73257	-12.32915
50.0	2.55049	4.06623	-0.53035	140.0	0.13694	-8.63466	-13.23124
52.0	2.69732	4.30932	-0.28726	142.0	0.10085	-9.96238	-14.55996
54.0	2.79931	4.47050	-0.12608	144.0	0.07559	-11.21538	-15.81196
56.0	2.85989	4.56349	-0.03310	146.0	0.07373	-11.32335	-15.91993
58.0	2.88176	4.59658	0.00000	148.0	0.09821	-10.07859	-14.67517
60.0	2.86700	4.57428	-0.02230	150.0	0.13876	-8.57724	-13.17382
62.0	2.81760	4.49879	-0.09779	152.0	0.17487	-7.57291	-12.16949
64.0	2.73611	4.37134	-0.22524	154.0	0.18531	-7.32096	-11.91755
66.0	2.62606	4.19305	-0.40353	156.0	0.16090	-7.93432	-12.53090
68.0	2.49202	3.96351	-0.63308	158.0	0.11341	-9.45354	-14.05012
70.0	2.33937	3.69098	-0.90560	160.0	0.07414	-11.29939	-15.89597
72.0	2.17396	3.37251	-1.22407	162.0	0.08011	-10.96240	-15.55899
74.0	2.00163	3.01384	-1.58274	164.0	0.15291	-8.15377	-12.75036
76.0	1.82783	2.61935	-1.97723	166.0	0.28151	-5.50513	-10.10171
78.0	1.65729	2.19399	-2.40259	168.0	0.42044	-3.76297	-8.35955
80.0	1.49389	1.74318	-2.85340	170.0	0.50790	-2.94216	-7.53877
82.0	1.34055	1.27284	-3.32374	172.0	0.49681	-3.03808	-7.63466
84.0	1.19932	0.78935	-3.80723	174.0	0.38263	-4.17224	-8.76882
86.0	1.07140	0.29453	-4.30205	176.0	0.21125	-6.75213	-11.34871
88.0	0.95752	-0.18944	-4.78602	178.0	0.05898	-12.29169	-16.88827
90.0	0.85720	-0.67018	-5.26677	180.	0.00000	-INFINITY	-INFINITY

TABLE A2-51 $2\pi a/\lambda = 12.50$

EPSLN= 12 3000(NORMALIZED GROUNDPLANE RADIUS)
MONOPOLE LENGTH= 0 2500000(WAVELENGTH)
MONOPOLE RADIUS= 0 1000E-05(WAVELENGTH)
NUMBER OF MONOPOLE SEGMENTS= 1
NUMBER OF DISK SEGMENTS= 37
NUMBER OF ANNULAR ZONES PER DISK SEGEMENT= 1
RADIATION RESISTANCE DETERMINED BY PATTERN= 0 357880E+02 OHMS

ELEVATION ANGLE (DEG)	DIRECTIVITY (NUMERIC)	DIRECTIVITY (dBi)	RELATIVE POWER (dB)	ELEVATION ANGLE (DEG)	DIRECTIVITY (NUMERIC)	DIRECTIVITY (dBi)	RELATIVE POWER (dB)
0	0 00000	-INFINITY	-INFINITY				
2.0	0. 08453	-10 73005	-15. 37846	92. 0	0 74565	-1. 27467	-5. 92308
4.0	0. 30246	-5 19325	-9. 84166	94 0	0. 66700	-1. 75877	-6. 40718
6.0	0. 56492	-2 48016	-7. 12837	96 0	0 60119	-2 20988	-6. 85829
8 0	0 77354	-1 11518	-5. 76359	98. 0	0. 54683	-2. 62145	-7 26986
10. 0	0. 86566	-0 62655	-5 27496	100 0	0. 50227	-2. 99061	-7. 63902
12. 0	0. 83693	-0 77009	-5 42150	102. 0	0. 46558	-3 32001	-7. 96842
14 0	0. 73229	-1. 35017	-6. 00158	104. 0	0. 43459	-3 61919	-8 26760
16. 0	0. 61413	-2 11737	-6. 76578	106. 0	0. 40690	-3. 90315	-8. 55356
18. 0	0. 52818	-2 77221	-7. 42062	108 0	0 38001	-4 20201	-8. 85042
20. 0	0 48529	-3 13994	-7. 78835	110. 0	0. 35157	-4. 53992	-9 18833
22. 0	0. 46612	-3 31504	-7. 96345	112. 0	0. 31962	-4 95360	-9 60201
24. 0	0. 44149	-3 55084	-8. 19925	114. 0	0 28310	-5. 48060	-10. 12901
26. 0	0. 39469	-4 03745	-8. 68586	116 0	0. 24219	-6. 15837	-10 80678
28. 0	0. 33318	-4 77321	-9. 42162	118 0	0. 19872	-7. 01750	-11. 66591
30. 0	0. 28543	-5 44496	-10. 09337	120. 0	0. 15621	-8 06288	-12. 71129
32. 0	0. 26719	-5 41824	-10. 06665	122. 0	0. 11932	-9 22560	-13 87401
34. 0	0 26372	-4. 36846	-9 01687	124 0	0. 09395	-10 27108	-14. 91949
36. 0	0 52970	-2. 75969	-7. 40810	126. 0	0. 08380	-10 76742	-15 41583
38. 0	0 76804	-1 14615	-5 79456	128 0	0. 09071	-10. 42333	-15. 07174
40. 0	1 03606	0. 23690	-4 41151	130 0	0. 11224	-9 49850	-14. 14691
42. 0	1 36473	1. 35045	-3. 29796	132. 0	0 14147	-8 49340	-13. 14184
44. 0	1 66861	2 22356	-2. 42485	134. 0	0. 16817	-7. 74243	-12 39084
46. 0	1 93017	2 90073	-1. 74768	136 0	0. 18178	-7. 40453	-12. 05294
48. 0	2. 19997	3. 42417	-1. 22424	138 0	0. 17542	-7 55903	-12 20744
50. 0	2. 41434	3 82798	-0. 82043	140 0	0 14967	-8 24860	-12 89701
52. 0	2. 59229	4 13683	-0. 51158	142 0	0. 11384	-9. 43708	-14 08549
54. 0	2. 73312	4 36659	-0 28182	144 0	0. 08347	-10. 78493	-15. 43334
56. 0	2. 83539	4. 52613	-0 12228	146. 0	0. 07383	-11. 31743	-15. 96584
58. 0	2 89704	4 61955	-0 02886	148 0	0 09187	-10 36830	-15 01671
60 0	2 91636	4 64961	0 00000	150. 0	0 13052	-8 84337	-13 49178
62. 0	2 89293	4 61338	-0 03503	152 0	0 16976	-7 70161	-12 35002
64 0	2 82836	4 51534	-0 13307	154. 0	0 18383	-7 30891	-11 95732
66 0	2 72644	4 35896	-0 29245	156 0	0 16538	-7 81513	-12 46354
68. 0	2 59288	4 13782	-0 51059	158 0	0 11731	-9 30654	-13 95495
70 0	2 43468	3 86443	-0 78398	160 0	0 07372	-11 32421	-15 97262
72 0	2 25943	3 53999	-1 10842	162 0	0 07621	-11 17975	-15 82816
74 0	2 07458	3 16930	-1. 47911	164 0	0 15214	-8 17754	-12 82595
76 0	1 88693	2 75755	-1 89086	166 0	0 29325	-5 32759	-9 97600
78 0	1 70226	2 31027	-2. 33814	168 0	0 45101	-3 45811	-8 10652
80 0	1 52520	1 83387	-2 81514	170 0	0 55542	-2 55375	-7 20216
82 0	1 39915	1 43258	-3 21643	172 0	0 59252	-2 27224	-7 24067
84 0	1 26544	1 01505	-3 63396	174 0	0 62789	-2 02070	-6 98913
86 0	1 16842	0 67423	-4 37478	176 0	0 23767	-6 24029	-10 88870
88 0	0 94570	-0 24249	-4 89086	178 0	0 06772	-11 69277	-16 34118
90 0	1 80827	-0 76416	-5 41457	180	0 00000	-INFINITY	-INFINITY

TABLE A2-52 $2\pi a/\lambda = 12.75$

```
EPSLN= 12 7500(NORMALIZED GROUNDPLANE RADIUS)
MONOPOLE LENGTH= 0 250000(WAVELENGTH)
MONOPOLE RADIUS=  0 1000E-05(WAVELENGTH)
NUMBER OF MONOPOLE SEGMENTS=  1
NUMBER OF DISK SEGMENTS= 38
NUMBER OF ANNULAR ZONES PER DISK SEGEMENT=  1
RADIATION RESISTANCE DETERMINED BY PATTERN= 0 386734E+02 OHMS
```

ELEVATION ANGLE (DEG)	DIRECTIVITY (NUMERIC)	DIRECTIVITY (dBi)	RELATIVE POWER (dB)	ELEVATION ANGLE (DEG)	DIRECTIVITY (NUMERIC)	DIRECTIVITY (dBi)	RELATIVE POWER (dB)
0.	0.00000	-INFINITY	-INFINITY				
2.0	0.08672	-10.61894	-15.38977	92.0	0.71920	-1.43153	-6.20237
4.0	0.30807	-5.11352	-9.88436	94.0	0.63544	-1.96924	-6.74007
6.0	0.56827	-2.45444	-7.22527	96.0	0.54577	-2.63061	-7.40143
8.0	0.76421	-1.16795	-5.93868	98.0	0.46898	-3.29303	-8.06387
10.0	0.88592	-0.52969	-5.30228	100.0	0.40366	-3.93804	-8.70888
12.0	0.78636	-1.04377	-5.81460	102.0	0.42815	-3.68406	-8.45489
14.0	0.67358	-1.71613	-6.48697	104.0	0.40049	-3.97411	-8.74495
16.0	0.56641	-2.46872	-7.23956	106.0	0.37837	-4.22082	-8.99165
18.0	0.50921	-2.92106	-7.70190	108.0	0.35919	-4.44670	-9.21754
20.0	0.50276	-2.97777	-7.74861	110.0	0.34018	-4.68296	-9.45380
22.0	0.51849	-2.85260	-7.62344	112.0	0.31863	-4.96719	-9.73803
24.0	0.51447	-2.88639	-7.65722	114.0	0.29235	-5.34093	-10.11176
26.0	0.47102	-3.26958	-8.04042	116.0	0.26019	-5.84706	-10.61790
28.0	0.39730	-4.00883	-8.77967	118.0	0.22254	-6.52588	-11.29672
30.0	0.32652	-4.86089	-9.63173	120.0	0.18175	-7.40520	-12.17604
32.0	0.29917	-5.24084	-10.01168	122.0	0.14213	-8.47316	-13.24400
34.0	0.34554	-4.61499	-9.38582	124.0	0.10935	-9.61178	-14.38261
36.0	0.47588	-3.22505	-7.99589	126.0	0.08918	-10.49717	-15.26800
38.0	0.68050	-1.67172	-6.44256	128.0	0.08564	-10.67307	-15.44391
40.0	0.93725	-0.28144	-5.05227	130.0	0.09907	-10.04065	-14.81149
42.0	1.22099	0.86713	-3.90371	132.0	0.12487	-9.03553	-13.80636
44.0	1.51072	1.79185	-2.97899	134.0	0.15380	-8.13031	-12.90114
46.0	1.79238	2.53429	-2.23654	136.0	0.17437	-7.58596	-12.35680
48.0	2.05779	3.13401	-1.63682	138.0	0.17693	-7.52196	-12.29280
50.0	2.30180	3.62068	-1.15016	140.0	0.15840	-8.00233	-12.77316
52.0	2.51951	4.01315	-0.75768	142.0	0.12510	-9.02730	-13.79813
54.0	2.70483	4.32144	-0.44940	144.0	0.09168	-10.37743	-15.14826
56.0	2.85084	4.54972	-0.22111	146.0	0.07525	-11.23510	-16.00593
58.0	2.95075	4.69933	-0.07151	148.0	0.08652	-10.62870	-15.39954
60.0	2.99974	4.77084	0.00000	150.0	0.12216	-9.13079	-13.90162
62.0	2.99599	4.76540	-0.00544	152.0	0.16356	-7.86329	-12.63413
64.0	2.94122	4.68528	-0.08556	154.0	0.18503	-7.32760	-12.09844
66.0	2.84046	4.53089	-0.23994	156.0	0.16906	-7.71949	-12.49033
68.0	2.70126	4.31367	-0.45717	158.0	0.12094	-9.17433	-13.94517
70.0	2.53264	4.03573	-0.73510	160.0	0.07260	-11.39064	-16.16147
72.0	2.34405	3.69967	-1.07116	162.0	0.06981	-11.56094	-16.33178
74.0	2.14452	3.31031	-1.45753	164.0	0.14610	-8.35363	-13.12447
76.0	1.94201	2.88252	-1.88832	166.0	0.29711	-5.27090	-10.04164
78.0	1.74308	2.41317	-2.35767	168.0	0.47241	-3.25678	-8.02762
80.0	1.55278	1.91110	-2.85970	170.0	0.59431	-2.25986	-7.03069
82.0	1.37474	1.38221	-3.38860	172.0	0.59760	-2.23586	-7.00670
84.0	1.21191	0.83251	-3.93829	174.0	0.46908	-3.28750	-8.05837
86.0	1.06380	0.26861	-4.50219	176.0	0.29224	-5.34301	-10.11388
88.0	0.93274	-0.30241	-5.07325	178.0	0.07500	-11.24944	-16.02028
90.0	0.81800	-0.87360	-5.64444	180	0.00000	-INFINITY	-INFINITY

TABLE A2-53 $2\pi a/\lambda = 13.00$

```
EPSLN= 13 0000(NORMALIZED GROUNDPLANE RADIUS)
MONOPOLE LENGTH= 0 250000(WAVELENGTH)
MONOPOLE RADIUS=   0.1000E-03(WAVELENGTH)
NUMBER OF MONOPOLE SEGMENTS=  1
NUMBER OF DISK SEGMENTS= 39
NUMBER OF ANNULAR ZONES PER DISK SEGEMENT=  1
RADIATION RESISTANCE DETERMINED BY PATTERN= 0 374754E+02 OHMS
```

ELEVATION ANGLE (DEG)	DIRECTIVITY (NUMERIC)	DIRECTIVITY (dBi)	RELATIVE POWER (dB)	ELEVATION ANGLE (DEG)	DIRECTIVITY (NUMERIC)	DIRECTIVITY (dBi)	RELATIVE POWER (dB)
0	0 00000	-INFINITY	-INFINITY				
2 0	0 08752	-10 57877	-15 50015	92 0	0 69633	-1 57184	-6 49322
4 0	0 30839	-5 10901	-10 03039	94 0	0 60762	-2 16271	-7 08509
6 0	0 36076	-4 51220	-7 43358	96 0	0 53347	-2 72889	-7 65027
8 0	0 73821	-1 31818	-6 23956	98 0	0 47290	-3 25229	-8 17367
10 0	0 78407	-1 05446	-5 97784	100 0	0 42480	-3 71815	-8 63953
12 0	0 71367	-1 46500	-6 38838	102 0	0 38788	-4 11304	-9 03442
14 0	0 59507	-2 25403	-7 17371	104 0	0 36057	-4 43008	-9 35146
16 0	0 50388	-2 97674	-7 89812	106 0	0 34094	-4 67319	-9 59457
18 0	0 48133	-3 17536	-8 09694	108 0	0 32662	-4 85963	-9 78101
20 0	0 51832	-2 85398	-7 77536	110 0	0 31480	-5 01967	-9 94105
22 0	0 57009	-2 44060	-7 36198	112 0	0 30244	-5 19360	-10 11498
24 0	0 58800	-2 30625	-7 22763	114 0	0 28657	-5 42770	-10 34908
26 0	0 54817	-2 61085	-7 53223	116 0	0 26482	-5 77051	-10 69189
28 0	0 46226	-3 35114	-8 27253	118 0	0 23608	-6 26932	-11 19070
30 0	0 36859	-4 33454	-9 25592	120 0	0 20117	-6 96441	-11 88579
32 0	0 31230	-5 05431	-9 97569	122 0	0 16316	-7 87396	-12 79534
34 0	0 32657	-4 86027	-9 78165	124 0	0 12726	-8 95292	-13 87430
36 0	0 42338	-3 73269	-8 65407	126 0	0 09989	-10 00489	-14 92627
38 0	0 59513	-2 25392	-7 17530	128 0	0 08684	-10 61262	-15 53400
40 0	0 82302	-0 84592	-5 76730	130 0	0 09113	-10 40342	-15 32480
42 0	1 08638	0 35982	-4 56156	132 0	0 11093	-9 54937	-14 47075
44 0	1 36854	1 36257	-3 55881	134 0	0 13894	-8 57177	-13 49315
46 0	1 65801	2 19586	-2 72552	136 0	0 16380	-7 85679	-12 77817
48 0	1 94642	2 89236	-2 02902	138 0	0 17402	-7 59299	-12 51437
50 0	2 22554	3 47435	-1 44703	140 0	0 16314	-7 87452	-12 79590
52 0	2 48531	3 95080	-0 96758	142 0	0 13402	-8 72816	-13 64954
54 0	2 71078	4 33374	-0 58564	144 0	0 09952	-10 02093	-14 94231
56 0	2 89860	4 62188	-0 29950	146 0	0 07764	-11 09891	-16 02029
58 0	3 02923	4 81332	-0 10806	148 0	0 08243	-10 83923	-15 76061
60 0	3 09887	4 91203	-0 00935	150 0	0 11449	-9 41246	-14 33384
62 0	3 10555	4 92138	0 00000	152 0	0 15738	-8 03061	-12 95199
64 0	3 05218	4 84611	-0 07527	154 0	0 18417	-7 34791	-12 26929
66 0	2 94578	4 69201	-0 22938	156 0	0 17326	-7 61310	-12 53448
68 0	2 79611	4 46554	-0 45584	158 0	0 12568	-9 00726	-13 92864
70 0	2 61428	4 17353	-0 74785	160 0	0 07230	-11 40887	-16 33025
72 0	2 41146	3 82280	-1 09858	162 0	0 06245	-12 04469	-16 96607
74 0	2 19789	3 42006	-1 50132	164 0	0 13617	-8 65916	-13 58054
76 0	1 98236	2 97170	-1 94968	166 0	0 29411	-5 31497	-10 23635
78 0	1 77163	2 48374	-2 43764	168 0	0 48515	-3 14123	-8 06261
80 0	1 57104	1 96186	-2 95952	170 0	0 62461	-2 04388	-6 96526
82 0	1 38403	1 41145	-3 50993	172 0	0 63783	-1 95295	-6 87433
84 0	1 21276	0 83776	-4 08362	174 0	0 50592	-2 96922	-7 89060
86 0	1 05823	0 24617	-4 67521	176 0	0 28477	-5 45503	-10 37641
88 0	0 92699	-0 33744	-5 25882	178 0	0 08176	-10 87459	-15 79597
90 0	0 82059	-0 85625	-5 [illegible]	180	0 00000	-INFINITY	-INFINITY

TABLE A2-54 $2\pi a/\lambda = 13.25$

```
EPSLN= 13.2500(NORMALIZED GROUNDPLANE RADIUS)
MONOPOLE LENGTH= 0 250000(WAVELENGTH)
MONOPOLE RADIUS=  0 1000E-03(WAVELENGTH)
NUMBER OF MONOPOLE SEGMENTS=  1
NUMBER OF DISK SEGMENTS= 39
NUMBER OF ANNULAR ZONES PER DISK SEGEMENT=  1
RADIATION RESISTANCE DETERMINED BY PATTERN= 0 380403E+02 OHMS
```

ELEVATION ANGLE (DEG)	DIRECTIVITY (NUMERIC)	DIRECTIVITY (dBi)	RELATIVE POWER (dB)	ELEVATION ANGLE (DEG)	DIRECTIVITY (NUMERIC)	DIRECTIVITY (dBi)	RELATIVE POWER (dB)
0.	0. 00000	-INFINITY	-INFINITY				
2. 0	0 08791	-10 55976	-15. 61588	92. 0	0. 68078	-1. 66996	-6. 72608
4. 0	0. 30696	-5. 12914	-10. 18526	94. 0	0 58814	-2. 30520	-7 36132
6. 0	0. 54930	-2. 60190	-7 65802	96 0	0 50986	-2 92948	-7. 98160
8 0	0 70564	-1 51419	-6 57031	98 0	0. 44511	-3 51537	-8 57150
10. 0	0. 72419	-1. 40147	-6 45759	100. 0	0. 39304	-4 05367	-9 11179
12. 0	0. 63196	-1 99311	-7 04923	102 0	0 35276	-4 52522	-9. 58134
14 0	0. 50920	-2 93115	-7. 98727	104. 0	0. 32319	-4 90541	-9. 96153
16. 0	0. 40713	-3. 89394	-8 85006	106. 0	0. 30292	-5 18670	-10 24282
18. 0	0. 45251	-3 44368	-8 49980	108 0	0. 29006	-5 37503	-10 43117
20. 0	0. 53407	-2. 72405	-7 78017	110 0	0. 28217	-5 49488	-10 55100
22. 0	0 62029	-2 05313	-7 10925	112. 0	0. 27625	-5 58699	-10 64311
24. 0	0 66230	-1 78942	-6 84554	114 0	0. 26898	-5. 70277	-10. 75889
26. 0	0. 62503	-2. 04097	-7. 09709	116. 0	0. 25717	-5 89787	-10 95399
28 0	0 52654	-2. 78572	-7 84184	118. 0	0 23939	-6 22712	-11. 28324
30. 0	0. 41061	-3. 86575	-8. 92187	120 0	0 21184	-6 73999	-11. 79611
32. 0	0 32688	-4 85613	-9 91225	122. 0	0. 17899	-7. 47164	-12. 52776
34. 0	0 31116	-5 07011	-10 12623	124 0	0 14394	-8 41822	-13 47434
36. 0	0. 37714	-4. 23497	-9 29110	126 0	0 11287	-9 47435	-14 53047
38. 0	0 51952	-2 84396	-7 90009	128. 0	0. 09262	-10. 33309	-15. 38921
40 0	0. 72321	-1. 40734	-6 46346	130. 0	0 08837	-10 53690	-15 39302
42. 0	0. 97200	-0 12332	-5 17944	132 0	0. 10112	-9 95157	-15. 00770
44 0	1. 25292	0. 97924	-4 07689	134. 0	0 12602	-8 99553	-14 05165
46. 0	1. 55592	1. 91907	-3 13625	136 0	0 15282	-8 15812	-13. 21424
48. 0	1 87108	2. 72092	-2 33520	138. 0	0 18906	-7 27950	-12. 77562
50. 0	2. 18595	3. 39640	-1. 65973	140 0	0 16547	-7 81283	-12. 86895
52. 0	2. 48479	3 95288	-1 10325	142. 0	0 14141	-8 49522	-13. 55134
54. 0	2 74991	4. 39319	-0. 66293	144 0	0 10728	-9 69496	-14 75109
56. 0	2 96453	4. 71956	-0 33656	146 0	0 08118	-10 90548	-15. 96160
58. 0	3. 11551	4. 93530	-0 12083	148 0	0 07995	-10 97205	-16. 02817
60. 0	3 19546	5. 04533	-0 01079	150 0	0. 10819	-9 65804	-14 71417
62. 0	3. 20341	5. 05612	0 00000	152 0	0 15216	-8 17693	-13 23305
64 0	3 14427	4 97520	-0 08092	154 0	0 18426	-7 34577	-12 40189
66 0	3 02741	4 81072	-0 24540	156 0	0 17890	-7. 47380	-12 52992
68 0	2 86487	4 57105	-0 48507	158. 0	0 13240	-8 78102	-13 83714
70 0	2 66958	4 26443	-0 79169	160 0	0 07074	-11. 32277	-16. 37889
72 0	2 45401	3 89876	-1 15737	162 0	0 05543	-12 56242	-17 61854
74 0	2 22914	3 48138	-1 57474	164 0	0 12432	-9. 05467	-14 11079
76 0	2 00404	3 01926	-2. 03706	166 0	0 28702	-5 42068	-10 47701
78 0	1 78562	2 51789	-2 53843	168 0	0. 49277	-3 07351	-8 12964
80 0	1 57862	1 98332	-3 07280	170 0	0. 65025	-1 86921	-6 92533
82 0	1 38692	1 42020	-3 63592	172 0	0 67495	-1 70794	-6 76406
84 0	1 21142	0 83294	-4 22318	174 0	0 54114	-2 66691	-7 72303
86 0	1 05304	0 22569	-4 83043	176 0	0 30676	-5 13197	-10 18810
88 0	0 91258	-0 39731	-5 45343	178 0	0 08843	-10 53411	-15 59023
90 0	0 78964	-1 03139	-6 08735	180	0 00000	-INFINITY	-INFINITY

TABLE A2-55 $2\pi a/\lambda = 13.50$

```
EPSLN= 13 5000(NORMALIZED GROUNDPLANE RADIUS)
MONOPOLE LENGTH= 0 250000(WAVELENGTH)
MONOPOLE RADIUS=   0.1000E-03(WAVELENGTH)
NUMBER OF MONOPOLE SEGMENTS=  1
NUMBER OF DISK SEGMENTS= 40
NUMBER OF ANNULAR RINGS PER DISK SEGEMENT=  1
RADIATION RESISTANCE DETERMINED BY PATTERN= 0 383927E+02 OHMS
```

ELEVATION ANGLE (DEG)	DIRECTIVITY (NUMERIC)	DIRECTIVITY (dBi)	RELATIVE POWER (dB)	ELEVATION ANGLE (DEG)	DIRECTIVITY (NUMERIC)	DIRECTIVITY (dBi)	RELATIVE POWER (dB)
0.	0.00000	-INFINITY	-INFINITY				
2.0	0.08912	-10.50009	-15.65753	92.0	0.67197	-1.72652	-6.88097
4.0	0.30827	-5.11062	-10.26807	94.0	0.57709	-2.38759	-7.54504
6.0	0.54226	-2.65789	-7.81533	96.0	0.49587	-3.04632	-8.20377
8.0	0.67801	-1.68766	-6.84510	98.0	0.42756	-3.69003	-8.84748
10.0	0.66871	-1.74762	-6.90506	100.0	0.37152	-4.30017	-9.45762
12.0	0.59398	-2.26306	-7.72251	102.0	0.32718	-4.85211	-10.00956
14.0	0.48723	-3.69336	-8.85081	104.0	0.29392	-5.31776	-10.47520
16.0	0.37539	-4.25312	-9.41237	106.0	0.27068	-5.67227	-10.82971
18.0	0.42995	-3.66583	-8.82327	108.0	0.25679	-5.90415	-11.06159
20.0	0.53632	-2.54676	-7.70421	110.0	0.24979	-6.02428	-11.18172
22.0	0.68175	-1.66375	-6.82120	112.0	0.24727	-6.06834	-11.22579
24.0	0.73953	-1.31046	-6.46790	114.0	0.24598	-6.09108	-11.24852
26.0	0.70241	-1.53408	-6.69152	116.0	0.24230	-6.15638	-11.31383
28.0	0.58992	-2.29204	-7.44949	118.0	0.23289	-6.32856	-11.48601
30.0	0.45186	-3.44991	-8.60736	120.0	0.21546	-6.66639	-11.82383
32.0	0.34236	-4.65321	-9.81266	122.0	0.18980	-7.21693	-12.37438
34.0	0.29952	-5.23575	-10.39519	124.0	0.15847	-8.00050	-13.15795
36.0	0.33848	-4.70470	-9.86215	126.0	0.12679	-8.96912	-14.12657
38.0	0.43616	-3.60885	-8.76630	128.0	0.10188	-9.91917	-15.07662
40.0	0.64101	-1.93134	-7.08879	130.0	0.09048	-10.43448	-15.59192
42.0	0.88086	-0.55094	-5.70838	132.0	0.09613	-10.17152	-15.32897
44.0	1.16559	0.66547	-4.49197	134.0	0.11666	-9.33076	-14.48821
46.0	1.48551	1.71875	-3.43870	136.0	0.14355	-8.43008	-13.58753
48.0	1.82806	2.61992	-2.53753	138.0	0.16416	-7.84729	-13.00473
50.0	2.17598	3.37655	-1.78090	140.0	0.16703	-7.77218	-12.92963
52.0	2.50783	3.99299	-1.16446	142.0	0.14816	-8.29268	-13.45013
54.0	2.80096	4.47307	-0.68437	144.0	0.11520	-9.38541	-14.54286
56.0	3.03521	4.82189	-0.33555	146.0	0.08579	-10.66581	-15.82326
58.0	3.19622	5.04636	-0.11108	148.0	0.07911	-11.01764	-16.17509
60.0	3.27718	5.15501	-0.00244	150.0	0.10078	-9.93895	-14.99640
62.0	3.27902	5.15745	0.00000	152.0	0.14903	-8.26719	-13.42464
64.0	3.20910	5.06383	-0.09362	154.0	0.18692	-7.28354	-12.44098
66.0	3.07921	4.88439	-0.27306	156.0	0.18782	-7.26263	-12.42008
68.0	2.90339	4.62905	-0.52840	158.0	0.14280	-8.45262	-13.61006
70.0	2.69600	4.30720	-0.85025	160.0	0.07844	-11.05442	-16.21187
72.0	2.47031	3.92752	-1.22993	162.0	0.05034	-12.98121	-18.13866
74.0	2.23762	3.49785	-1.65959	164.0	0.11282	-9.47618	-14.63363
76.0	2.00688	3.02521	-2.13224	166.0	0.27951	-5.53608	-10.69353
78.0	1.78472	2.51569	-2.64176	168.0	0.50059	-3.00521	-8.16265
80.0	1.57564	1.97457	-3.18288	170.0	0.67771	-1.68955	-6.84699
82.0	1.38238	1.40628	-3.75117	172.0	0.71519	-1.45578	-6.61322
84.0	1.20629	0.81453	-4.34291	174.0	0.57992	-2.36632	-7.52376
86.0	1.04773	0.20248	-4.95497	176.0	0.33113	-4.80004	-9.95748
88.0	0.90634	-0.42709	-5.58453	178.0	0.09584	-10.18445	-15.34189
90.0	0.78140	-1.07128	-6.22872	180	0.00000	-INFINITY	-INFINITY

TABLE A2-56 $2\pi a/\lambda = 13.75$

```
EPSLN= 13 7500(NORMALIZED GROUNDPLANE RADIUS)
MONOPOLE LENGTH= 0 250000(WAVELENGTH)
MONOPOLE RADIUS=  0 10000E-05(WAVELENGTH)
NUMBER OF MONOPOLE SEGMENTS=  1
NUMBER OF DISK SEGMENTS= 41
NUMBER OF ANNULAR ZONES PER DISK SEGEMENT=  1
RADIATION RESISTANCE DETERMINED BY PATTERN= 0 385409E+02 OHMS
```

ELEVATION ANGLE (DEG)	DIRECTIVITY (NUMERIC)	DIRECTIVITY (dBi)	RELATIVE POWER (dB)	ELEVATION ANGLE (DEG)	DIRECTIVITY (NUMERIC)	DIRECTIVITY (dBi)	RELATIVE POWER (dB)
0.	0.00000	-INFINITY	-INFINITY				
2.0	0.09237	-10.34473	-15.57915	92.0	0.66921	-1.74436	-6.97878
4.0	0.31648	-4.99654	-10.23096	94.0	0.57371	-2.41309	-7.64751
6.0	0.54702	-2.62000	-7.85442	96.0	0.49092	-3.08988	-8.32430
8.0	0.64464	-1.77414	-7.00856	98.0	0.42009	-3.76654	-9.00096
10.0	0.62696	-2.02761	-7.26203	100.0	0.36069	-4.42866	-9.66308
12.0	0.48731	-3.12021	-8.35463	102.0	0.31236	-5.05346	-10.28788
14.0	0.33479	-4.50027	-9.73469	104.0	0.27484	-5.60925	-10.84367
16.0	0.32251	-4.91459	-10.14901	106.0	0.24778	-6.03930	-11.29372
18.0	0.41647	-3.80414	-9.03856	108.0	0.23055	-6.37233	-11.60675
20.0	0.58759	-2.30923	-7.54365	110.0	0.22195	-6.53753	-11.77195
22.0	0.74769	-1.26164	-6.49606	112.0	0.21999	-6.57597	-11.81039
24.0	0.82181	-0.85226	-6.08668	114.0	0.22182	-6.53990	-11.77432
26.0	0.78190	-1.06830	-6.30272	116.0	0.22394	-6.50069	-11.73511
28.0	0.65327	-1.84908	-7.08350	118.0	0.22211	-6.53429	-11.76871
30.0	0.49250	-3.07597	-8.31039	120.0	0.21326	-6.71095	-11.94537
32.0	0.35831	-4.45744	-9.69186	122.0	0.19549	-7.08896	-12.32338
34.0	0.29084	-5.36349	-10.59791	124.0	0.16963	-7.70492	-12.93934
36.0	0.30626	-5.13913	-10.37353	126.0	0.13976	-8.54630	-13.78072
38.0	0.40336	-3.94307	-9.17749	128.0	0.11262	-9.48381	-14.71823
40.0	0.57378	-2.41252	-7.64694	130.0	0.09591	-10.18126	-15.41568
42.0	0.80882	-0.92149	-6.15590	132.0	0.09328	-10.29982	-15.53424
44.0	1.10045	0.41569	-4.81872	134.0	0.11121	-9.53858	-14.77300
46.0	1.43841	1.57881	-3.65561	136.0	0.13721	-8.62603	-13.86045
48.0	1.80687	2.56927	-2.66515	138.0	0.16108	-7.92970	-13.16412
50.0	2.18349	3.39152	-1.84290	140.0	0.16963	-7.70492	-12.93941
52.0	2.54157	4.05102	-1.18340	142.0	0.15578	-8.07479	-13.30921
54.0	2.85429	4.55498	-0.67944	144.0	0.12429	-9.05569	-14.29011
56.0	3.09934	4.91269	-0.32173	146.0	0.09200	-10.36235	-15.59677
58.0	3.26223	5.13514	-0.09928	148.0	0.08025	-10.95360	-16.18802
60.0	3.33766	5.23442	0.00000	150.0	0.10169	-9.92732	-15.16174
62.0	3.32893	5.22304	-0.01138	152.0	0.14878	-8.27446	-13.50888
64.0	3.24596	5.11343	-0.12099	154.0	0.19330	-7.13767	-12.37209
66.0	3.10279	4.91752	-0.31690	156.0	0.20127	-6.96229	-12.19671
68.0	2.91506	4.64647	-0.58794	158.0	0.15796	-8.01618	-13.25060
70.0	2.69608	4.31053	-0.92387	160.0	0.08698	-10.60600	-15.84042
72.0	2.46546	3.91898	-1.31544	162.0	0.04758	-13.22551	-18.45993
74.0	2.22841	3.47995	-1.75446	164.0	0.10274	-9.88260	-15.11702
76.0	1.99554	3.00061	-2.23381	166.0	0.27430	-5.61774	-10.85216
78.0	1.77299	2.48707	-2.74735	168.0	0.51361	-2.89362	-8.12804
80.0	1.56475	1.94445	-3.28997	170.0	0.71399	-1.46310	-6.69752
82.0	1.37307	1.37691	-3.85749	172.0	0.76639	-1.15550	-6.38992
84.0	1.19866	0.78777	-4.44665	174.0	0.62848	-2.01711	-7.25153
86.0	1.04218	0.17945	-5.05497	176.0	0.36147	-4.41930	-9.65372
88.0	0.90235	-0.44627	-5.68069	178.0	0.10505	-9.78594	-15.02036
90.0	0.77839	-1.08801	-6.32244	180	0.00000	-INFINITY	-INFINITY

TABLE A2-57 $2\pi a/\lambda = 14.00$

EPSLN= 14 0000(NORMALIZED GROUNDPLANE RADIUS)
MONOPOLE LENGTH= 0 250000(WAVELENGTH)
MONOPOLE RADIUS= 0.1000E-03(WAVELENGTH)
NUMBER OF MONOPOLE SEGMENTS= 1
NUMBER OF DISK SEGMENTS= 42
NUMBER OF ANNULAR ZONES PER DISK SEGEMENT= 1
RADIATION RESISTANCE DETERMINED BY PATTERN= 0.3862?6E+02 OHMS

ELEVATION ANGLE (DEG)	DIRECTIVITY (NUMERIC)	DIRECTIVITY (dBi)	RELATIVE POWER (dB)	ELEVATION ANGLE (DEG)	DIRECTIVITY (NUMERIC)	DIRECTIVITY (dBi)	RELATIVE P (dB)
0.	0.00000	-INFINITY	-INFINITY				
2.0	0.09904	-10.04177	-13.32676	92.0	0.66917	-1.74464	-7.02963
4.0	0.33635	-4.73209	-10.01707	94.0	0.57449	-2.40715	-7.69214
6.0	0.37175	-2.42794	-7.71292	96.0	0.49136	-3.08429	-8.36924
8.0	0.42539	-1.70443	-6.98942	98.0	0.41954	-3.77230	-9.05729
10.0	0.60808	-2.16043	-7.44541	100.0	0.35790	-4.46243	-9.74742
12.0	0.43931	-3.57227	-8.85726	102.0	0.30639	-5.13724	-10.42223
14.0	0.29609	-5.28378	-10.57077	104.0	0.26500	-5.76761	-11.05260
16.0	0.28110	-5.51143	-10.79842	106.0	0.23377	-6.31220	-11.59719
18.0	0.41442	-3.82560	-9.11059	108.0	0.21261	-6.72413	-12.00912
20.0	0.63072	-2.00166	-7.28665	110.0	0.20102	-6.96769	-12.25268
22.0	0.82501	-0.83540	-6.12039	112.0	0.19772	-7.03958	-12.32457
24.0	0.91240	-0.39813	-5.68312	114.0	0.20046	-6.97981	-12.26480
26.0	0.96601	-0.62476	-5.90975	116.0	0.20593	-6.86287	-12.14786
28.0	0.71800	-1.43873	-6.72371	118.0	0.21003	-6.77709	-12.06208
30.0	0.53280	-2.73493	-8.01992	120.0	0.20860	-6.80685	-12.09183
32.0	0.37406	-4.27055	-9.55554	122.0	0.19847	-7.02297	-12.30796
34.0	0.28361	-5.47273	-10.75772	124.0	0.17883	-7.47336	-12.75834
36.0	0.27811	-5.55785	-10.84283	126.0	0.15220	-8.17581	-13.46080
38.0	0.35770	-4.46485	-9.74983	128.0	0.12437	-9.04572	-14.33071
40.0	0.51679	-2.86721	-8.15219	130.0	0.10407	-9.82684	-15.11182
42.0	0.74954	-1.25202	-6.53701	132.0	0.09806	-10.08522	-15.37020
44.0	1.04958	0.21003	-5.07495	134.0	0.10951	-9.60542	-14.89041
46.0	1.40535	1.47785	-3.80714	136.0	0.12417	-9.12033	-14.40532
48.0	1.79743	2.54653	-2.73846	138.0	0.14059	-8.52274	-13.80772
50.0	2.19841	3.42108	-1.86390	140.0	0.17428	-7.58764	-12.87262
52.0	2.57674	4.11070	-1.17428	142.0	0.16518	-7.82049	-13.10547
54.0	2.90231	4.62744	-0.65755	144.0	0.13510	-8.69335	-13.97834
56.0	3.15158	4.98329	-0.29970	146.0	0.09998	-10.00096	-15.28595
58.0	3.31081	5.19934	-0.08363	148.0	0.08332	-10.79262	-16.07760
60.0	3.37673	5.28499	0.00000	150.0	0.10204	-9.91244	-15.19743
62.0	3.35530	5.25731	-0.02768	152.0	0.15208	-8.17923	-13.46422
64.0	3.25886	5.13065	-0.15433	154.0	0.20480	-6.88661	-12.17160
66.0	3.10337	4.91834	-0.36665	156.0	0.22117	-6.55282	-11.83780
68.0	2.90569	4.63250	-0.65249	158.0	0.17962	-7.45648	-12.74146
70.0	2.68164	4.28401	-1.00098	160.0	0.10081	-9.96499	-15.24997
72.0	2.44482	3.88247	-1.40251	162.0	0.04824	-13.16597	-18.45096
74.0	2.20611	3.43626	-1.84872	164.0	0.09338	-10.19639	-15.48137
76.0	1.97360	2.95258	-2.33240	166.0	0.27464	-5.61229	-10.89728
78.0	1.75288	2.43752	-2.84746	168.0	0.53785	-2.69041	-7.97539
80.0	1.54744	1.89613	-3.38886	170.0	0.76761	-1.14857	-6.43356
82.0	1.35908	1.33084	-3.95255	172.0	0.83789	-0.76812	-6.05311
84.0	1.18937	0.74952	-4.53546	174.0	0.89476	-0.48167	-5.76665
86.0	1.03507	0.14951	-5.13548	176.0	0.40244	-3.95300	-9.23799
88.0	0.89817	-0.46840	-5.75139	178.0	0.11743	-9.30226	-14.58725
90.0	0.77665	-1.09776	-6.38075	180	0.00000	-INFINITY	-INFINITY

TABLE A2-58 $2\pi a/\lambda = 0.7660$

EPSLN= 0 7660(NORMALIZED GROUNDPLANE RADIUS)
MONOPOLE LENGTH= 0 239600(WAVELENGTH)
MONOPOLE RADIUS= 0 6350E-03(WAVELENGTH)
NUMBER OF MONOPOLE SEGMENTS= 4
NUMBER OF DISK SEGMENTS= 12
RADIATION RESISTANCE DETERMINED BY PATTERN= 0 177438E+02 OHMS

ELEVATION ANGLE (DEG)	DIRECTIVITY (NUMERIC)	DIRECTIVITY (DBI)	RELATIVE POWER (DB)	ELEVATION ANGLE (DEG)	DIRECTIVITY (NUMERIC)	DIRECTIVITY (DBI)	RELATIVE POWER (DB)
0	0 00000	-INFINITY	-INFINITY				
2 0	0 00181	-27.41896	-29.19799	92.0	1 50391	1 77221	-0 00683
4.0	0 00724	-21.40335	-23 18238	94.0	1.49781	1 75457	-0.02446
6.0	0 01626	-17.88983	-19.66889	96.0	1.48802	1.72609	-0.05295
8.0	0 02882	-15.40275	-17 18178	98.0	1.47458	1.68670	-0 09234
10.0	0 04488	-13.47957	-15.25860	100.0	1.45758	1 63631	-0.14272
12.0	0 06435	-11.91433	-13.69337	102.0	1.43708	1 57481	-0 20422
14.0	0 08715	-10.59717	-12 37621	104 0	1.41321	1.50206	-0 27697
16.0	0. 11317	-9.46231	-11.24154	106.0	1.38608	1.41789	-0.36113
18.0	0. 14230	-8.46806	-10.24710	108.0	1.35584	1 32208	-0 45696
20.0	0 17438	-7.58497	-9.36400	110.0	1.32263	1.21440	-0 56464
22.0	0. 20928	-6.79265	-8.57168	112.0	1.28664	1.09457	-0 68446
24.0	0. 24684	-6.07593	-7.85496	114.0	1.24804	0 96228	-0 81675
26.0	0. 28686	-5 42328	-7.20232	116.0	1.20703	0.81717	-0.96186
28.0	0. 32917	-4 82577	-6 60480	118.0	1.16381	0.65883	-1 12021
30.0	0 37357	-4 27630	-6 05534	120.0	1.11861	0.48679	-1 29223
32.0	0. 41984	-3.76920	-5 54823	122.0	1.07163	0.30033	-1.47850
34 0	0 46776	-3 29980	-5 07883	124 0	1 02317	0.09947	-1 67957
36.0	0. 51710	-2.86426	-4.64330	126.0	0.97340	-0.11708	-1.89611
38.0	0 56763	-2 45938	-4 23842	128.0	0 92260	-0 34986	-2 12889
40.0	0 61909	-2.08246	-3 86149	130.0	0.87102	-0.59973	-2.37877
42 0	0. 67124	-1.73119	-3 51023	132.0	0.81890	-0 86768	-2.64672
44.0	0 72383	-1.40361	-3 18265	134.0	0.76651	-1.15481	-2.93385
46.0	0. 77660	-1.09803	-2 87707	136.0	0 71410	-1.46241	-3.24144
48.0	0 82928	-0.81298	-2.59202	138.0	0.66192	-1.79193	-3.57096
50.0	0 88162	-0.54719	-2 32622	140.0	0 61023	-2 14506	-3 92409
52.0	0. 93336	-0.29953	-2.07856	142.0	0.55927	-2.52377	-4.30281
54 0	0 98423	-0.06902	-1 84806	144.0	0.50929	-2.93036	-4 70940
56.0	1.03400	0.14519	-1.63385	146.0	0.46052	-3.36753	-5 14657
58 0	1.08240	0.34386	-1.43517	148.0	0.41319	-3.83848	-5 61752
60 0	1.12919	0.52768	-1 25136	150.0	0.36753	-4.34705	-6 12609
62 0	1.17415	0.69722	-1.08182	152.0	0.32375	-4.89789	-6.67693
64 0	1.21703	0.85302	-0.92601	154.0	0.28205	-5.49670	-7 27573
66 0	1 25764	0.99555	-0 78349	156.0	0.24263	-6 13054	-7 92958
68 0	1.29575	1.12521	-0.65382	158.0	0.20567	-6.86837	-8 64741
70.0	1 33118	1.24237	-0.53666	160.0	0.17133	-7.66171	-9.44074
72 0	1 36375	1.34736	-0 43168	162.0	0.13977	-8 54573	-10 32476
74 0	1 39330	1.44043	-0.33860	164.0	0.11115	-9.54101	-11 32004
76 0	1 41966	1.52185	-0.25718	166.0	0.08558	-10.67640	-12 45544
78.0	1 44272	1 59182	-0 18721	168.0	0 06318	-11.99420	-13.77324
80.0	1 46235	1.65052	-0 12852	170.0	0.04406	-13 53998	-15 31901
82 0	1 47846	1 69808	-0 08095	172 0	0 02829	-15 48360	-17 26264
84 0	1 49095	1.73464	-0.04440	174.0	0.01595	-17.97105	-19 75009
86 0	1 49978	1 76028	-0.01876	176.0	0 00710	-21 48480	-23 26383
88 0	1 50490	1 77506	-0 00397	178 0	0 00178	-27 50055	-29 27959
90 0	1.50627	1.77903	0.00000	180.	0 00000	-INFINITY	-INFINITY

TABLE A2-59 $2\pi a/\lambda = 0.9190$

```
EPSLN= 0 9190(NORMALIZED GROUNDPLANE RADIUS)
MONOPOLE LENGTH= 0.239600(WAVELENGTH)
MONOPOLE RADIUS=   0 7630E-03(WAVELENGTH)
NUMBER OF MONOPOLE SEGMENTS= 4
NUMBER OF DISK SEGMENTS= 11
RADIATION RESISTANCE DETERMINED BY PATTERN= 0.183449E+02 OHMS
```

ELEVATION ANGLE (DEG)	DIRECTIVITY (NUMERIC)	DIRECTIVITY (DBI)	RELATIVE POWER (DB)	ELEVATION ANGLE (DEG)	DIRECTIVITY (NUMERIC)	DIRECTIVITY (DBI)	RELATIVE POWER (DB)
0	0 00000	-INFINITY	-INFINITY				
2 0	0 00189	-27 24413	-28 97891	92 0	1 49872	1 72812	-0 00665
4 0	0 00753	-21 22930	-22 96407	94 0	1 48293	1 71121	-0 02357
6 0	0 01692	-17 71708	-19 45186	96 0	1 47366	1 68398	-0 05079
8 0	0 02998	-15 23177	-16 96655	98 0	1 46096	1 64639	-0 08839
10 0	0 04666	-13 31088	-15 04566	100 0	1 44488	1 59832	-0 13646
12 0	0 06686	-11 74842	-13 48320	102 0	1 42549	1 53965	-0 19512
14 0	0 09048	-10 43451	-12 16928	104 0	1 40289	1 47023	-0 26455
16 0	0 11739	-9 30336	-11 03813	106 0	1 37716	1 38985	-0 34492
18 0	0 14746	-8 31326	-10 04804	108 0	1 34844	1 29831	-0 43647
20 0	0 18052	-7 43475	-9 16952	110 0	1 31684	1 19533	-0 53945
22 0	0 21640	-6 64741	-8 38219	112 0	1 28251	1 08061	-0 65416
24 0	0 25491	-5 93605	-7 67083	114 0	1 24561	0 95382	-0 78096
26 0	0 29586	-5 28913	-7 02390	116 0	1 20630	0 81456	-0 92022
28 0	0 33903	-4 69766	-6 43244	118 0	1 16477	0 66239	-1 07239
30 0	0 38419	-4 15456	-5 88933	120 0	1 12120	0 49682	-1 23795
32 0	0 43111	-3 65408	-5 38885	122 0	1 07580	0 31730	-1 41748
34 0	0 47956	-3 19154	-4 92632	124 0	1 02877	0 12319	-1 61159
36 0	0 52929	-2 76309	-4 49786	126 0	0 98035	-0 08620	-1 82098
38 0	0 58003	-2 36547	-4 10024	128 0	0 93075	-0 31168	-2 04645
40 0	0 63155	-1 99594	-3 73072	130 0	0 88021	-0 55413	-2 28890
42 0	0 68357	-1 65218	-3 38696	132 0	0 82898	-0 81457	-2 54935
44 0	0 73584	-1 33219	-3 06697	134 0	0 77729	-1 09415	-2 82893
46 0	0 78809	-1 03423	-2 76900	136 0	0 72541	-1 39419	-3 12896
48 0	0 84008	-0 75679	-2 49157	138 0	0 67357	-1 71617	-3 45095
50 0	0 89154	-0 49858	-2 23335	140 0	0 62204	-2 06184	-3 79662
52 0	0 94223	-0 25842	-1 99320	142 0	0 57106	-2 43320	-4 16797
54 0	0 99190	-0 03531	-1 77009	144 0	0 52089	-2 83256	-4 56734
56 0	1 04031	0 17165	-1 56313	146 0	0 47177	-3 26268	-4 99745
58 0	1 08724	0 36326	-1 37152	148 0	0 42396	-3 72678	-5 46155
60 0	1 13246	0 54022	-1 19455	150 0	0 37768	-4 22874	-5 96351
62 0	1 17576	0 70317	-1 03160	152 0	0 33318	-4 77324	-6 50801
64 0	1 21693	0 85267	-0 88211	154 0	0 29067	-5 36600	-7 10078
66 0	1 25580	0 98920	-0 74557	156 0	0 25037	-6 01413	-7 74891
68 0	1 29218	1 11322	-0 62155	158 0	0 21249	-6 72660	-8 46138
70 0	1 32590	1 22512	-0 50965	160 0	0 17722	-7 51496	-9 24973
72 0	1 35683	1 32524	-0 40953	162 0	0 14473	-8 39440	-10 12917
74 0	1 38481	1 41389	-0 32088	164 0	0 11520	-9 38552	-11 12030
76 0	1 40972	1 49133	-0 24344	166 0	0 08877	-10 51720	-12 25198
78 0	1 43146	1 55780	-0 17698	168 0	0 06559	-11 83175	-13 56653
80 0	1 44993	1 61348	-0 12129	170 0	0 04576	-13 39475	-15 12953
82 0	1 46506	1 65854	-0 07623	172 0	0 02940	-15 31608	-17 05086
84 0	1 47677	1 69312	-0 04166	174 0	0 01659	-17 80174	-19 53652
86 0	1 48501	1 71730	-0 01747	176 0	0 00739	-21 31420	-23 04897
88 0	1 48976	1 73117	-0 00360	178 0	0 00185	-27 32918	-29 06396
90 0	1 49100	1 73478	0 00000	180	0 00000	-INFINITY	-INFINITY

TABLE A2-60 $2\pi a/\lambda = 1.0970$

```
EPSLN= 1 0970(NORMALIZED GROUNDPLANE RADIUS)
MONOPOLE LENGTH= 0 238500(WAVELENGTH)
MONOPOLE RADIUS=   0 9110E-03(WAVELENGTH)
NUMBER OF MONOPOLE SEGMENTS=  4
NUMBER OF DISK SEGMENTS= 13
RADIATION RESISTANCE DETERMINED BY PATTERN= 0 187752E+02 OHMS
```

ELEVATION ANGLE (DEG)	DIRECTIVITY (NUMERIC)	DIRECTIVITY (DBI)	RELATIVE POWER (DB)	ELEVATION ANGLE (DEG)	DIRECTIVITY (NUMERIC)	DIRECTIVITY (DBI)	RELATIVE (DB)
0	0 00000	-INFINITY	-INFINITY				
2 0	0 00200	-26 98412	-28 65160	92 0	1. 46388	1 66098	-0 00630
4 0	0. 00800	-20 97041	-22 63790	94. 0	1. 46051	1 64504	-0 02245
6 0	0 01795	-17. 46008	-19. 12756	96. 0	1 45198	1 61960	-0 04788
8 0	0. 03179	-14 97738	-16 64486	98. 0	1. 44032	1 58460	-0 08288
10. 0	0. 04943	-13 03983	-14 72732	100. 0	1 42558	1 53992	-0 12756
12 0	0. 07077	-11 50143	-13 16892	102. 0	1 40780	1 48541	-0. 18207
14. 0	0. 09567	-10 19227	-11. 85976	104. 0	1. 38704	1 42090	-0. 24659
16. 0	0. 12397	-9. 06675	-10. 73424	106. 0	1. 36338	1 34615	-0 32133
18. 0	0 15551	-8 08254	-9 75003	108 0	1 33688	1 26093	-0. 40656
20. 0	0 19008	-7. 21073	-8. 87822	110. 0	1. 30765	1 16492	-0. 50257
22. 0	0. 22747	-6. 43071	-8. 09819	112. 0	1. 27579	1 05779	-0. 60969
24. 0	0. 26747	-5. 72722	-7. 39471	114. 0	1 24141	0 93916	-0. 72832
26 0	0 30983	-5. 08870	-6. 75619	116. 0	1. 20463	0 80860	-0. 85889
28. 0	0. 35431	-4. 50613	-6. 17362	118. 0	1. 16563	0 66561	-1. 00188
30 0	0. 40065	-3 97238	-5 63987	120 0	1. 12452	0 50966	-1. 15783
32 0	0. 44857	-3. 48167	-5. 14915	122. 0	1. 08147	0 34013	-1. 32736
34 0	0. 49782	-3. 02927	-4. 69676	124. 0	1. 03666	0 15635	-1. 51114
36. 0	0. 54812	-2. 61127	-4. 27876	126. 0	0. 99028	-0. 04244	-1. 70992
38 0	0. 59919	-2 22439	-3. 89187	128. 0	0 94252	-0 25708	-1 92457
40 0	0 65075	-1 86593	-3 53331	130. 0	0. 89361	-0. 48853	-2. 15602
42 0	0. 70255	-1. 53321	-3. 20069	132. 0	0. 84375	-0. 73786	-2. 40535
44 0	0 75431	-1. 22447	-2 89196	134. 0	0 79318	-1 00628	-2 67376
46 0	0 80578	-0 93785	-2 60533	136. 0	0 74214	-1 29514	-2. 96263
48. 0	0. 85669	-0 67176	-2. 33925	138. 0	0. 69087	-1. 60601	-3. 27349
50. 0	0. 90680	-0. 42486	-2. 09235	140. 0	0. 63964	-1. 94067	-3. 60815
52 0	0. 95589	-0 19593	-1 86341	142. 0	0 58869	-2 30117	-3. 96865
54. 0	1. 00372	0. 01610	-1 65138	144. 0	0. 53828	-2. 68989	-4. 35738
56 0	1 05007	0. 21219	-1. 45529	146. 0	0. 48869	-3 10963	-4. 77711
58 0	1 09476	0 39318	-1 27430	148. 0	0. 44018	-3 56366	-5. 23115
60 0	1. 13759	0. 55984	-1 10764	150. 0	0. 39301	-4 05391	-5. 72340
62 0	1 17838	0. 71285	-0 95464	152. 0	0. 34745	-4 59110	-6. 25859
64. 0	1 21697	0. 85281	-0. 81468	154. 0	0. 30374	-5 17500	-6. 84249
66 0	1. 25322	0. 98027	-0 68721	156. 0	0. 26213	-5 81476	-7. 48225
68. 0	1. 28698	1. 09573	-0 57175	158. 0	0. 22288	-6 51938	-8 18687
70 0	1. 31814	1. 19963	-0 46786	160. 0	0 18619	-7 30044	-8. 96793
72 0	1 34659	1. 29234	-0. 37515	162. 0	0. 15229	-8 17318	-9. 84067
74 0	1. 37221	1. 37422	-0 29327	164. 0	0. 12139	-9 15823	-10. 82571
76 0	1 39494	1 44557	-0 22192	166. 0	0 09366	-10 28448	-11. 95197
78 0	1 41470	1 50664	-0. 16085	168. 0	0. 06927	-11. 59428	-13. 26177
80 0	1 43142	1 55767	-0 10982	170. 0	0 04838	-13 15322	-14 82071
82 0	1 44505	1 59884	-0 06865	172. 0	0. 03111	-15. 07121	-16 73869
84. 0	1. 45556	1. 63030	-0. 03718	174. 0	0. 01756	-17 55425	-19. 22173
86 0	1 46291	1 65218	-0 01530	176 0	0 00783	-21. 06483	-22. 73231
88 0	1 46709	1. 66456	-0. 00293	178 0	0 00196	-27. 07868	-28 74617
90 0	1 46808	1. 66749	0. 00000	180.	0. 00000	-INFINITY	-INFINITY

TABLE A2-61 $2\pi a/\lambda = 1.3790$

```
EPSLN= 1 3790(NORMALIZED GROUNDPLANE RADIUS)
MONOPOLE LENGTH= 0 238200(WAVELENGTH)
MONOPOLE RADIUS=   0.1143E-02(WAVELENGTH)
NUMBER OF MONOPOLE SEGMENTS=  4
NUMBER OF DISK SEGMENTS= 20
RADIATION RESISTANCE DETERMINED BY PATTERN= 0 198933E+02 OHMS
```

ELEVATION ANGLE (DEG)	DIRECTIVITY (NUMERIC)	DIRECTIVITY (DBI)	RELATIVE POWER (DB)	ELEVATION ANGLE (DEG)	DIRECTIVITY (NUMERIC)	DIRECTIVITY (DBI)	RELATIVE POWER (DB)
0	0 00000	-INFINITY	-INFINITY				
2 0	0. 00227	-26. 44481	-27. 96848	92 0	1 41797	1 51666	-0 00700
4 0	0. 00903	-20. 43334	-21. 95701	94. 0	1. 41318	1. 50196	-0. 02170
6 0	0. 02029	-16. 92672	-18. 45039	96. 0	1 40589	1 47951	-0. 04416
8 0	0. 03590	-14. 44920	-15. 97287	98. 0	1 39611	1. 44920	-0. 07447
10 0	0 05574	-12. 53928	-14. 06195	100. 0	1 38385	1. 41090	-0. 11277
12 0	0 07963	-10. 98793	-12. 51159	102. 0	1. 36912	1 36441	-0 15926
14. 0	0. 10744	-9. 68820	-11. 21187	104. 0	1 35192	1 30950	-0. 21417
16 0	0 13888	-8. 57347	-10. 09714	106. 0	1. 33226	1. 24588	-0. 27778
18 0	0. 17373	-7. 60137	-9 12503	108. 0	1 31016	1. 17325	-0. 35042
20 0	0. 21169	-6. 74293	-8. 26660	110. 0	1. 28564	1 09120	-0. 43246
22 0	0. 25249	-5. 97748	-7. 50115	112. 0	1. 25873	0. 99933	-0. 52433
24 0	0. 29582	-5. 28974	-6. 81340	114. 0	1 22946	0. 89716	-0 62651
26 0	0 34135	-4. 66805	-6. 19171	116. 0	1. 19789	0. 78415	-0. 73951
28 0	0. 38875	-4. 10034	-5. 62701	118. 0	1. 16405	0. 65972	-0. 86395
30. 0	0 43768	-3. 58840	-5. 11207	120. 0	1. 12803	0. 52321	-1 00045
32 0	0. 48782	-3. 13738	-4. 64104	122 0	1 08991	0 37392	-1 14975
34. 0	0. 53883	-2. 68547	-4. 20913	124. 0	1. 04979	0. 21103	-1. 31263
36 0	0. 59038	-2. 28867	-3. 81234	126 0	1. 00779	0 00369	-1. 48997
38 0	0. 64215	-1. 92360	-3. 44727	128. 0	0. 96404	-0. 15907	-1. 68273
40 0	0. 69384	-1. 58739	-3. 11106	130. 0	0. 91869	-0. 36831	-1. 89198
42 0	0. 74513	-1. 27755	-2. 80121	132. 0	0. 87192	-0 59523	-2. 11890
44 0	0. 79581	-0. 99192	-2. 51559	134. 0	0. 82392	-0. 84114	-2. 36481
46. 0	0. 84555	-0. 72862	-2. 25229	136. 0	0. 77490	-1. 10753	-2. 63120
48 0	0 89413	-0. 48399	-2. 00966	138. 0	0. 72509	-1. 39606	-2. 91972
50. 0	0. 94134	-0. 26255	-1. 78822	140. 0	0. 67474	-1. 70862	-3. 23229
52 0	0 98697	-0. 05698	-1. 58065	142. 0	0. 62411	-2. 04737	-3. 57104
54. 0	1. 03084	0. 13191	-1. 39176	144. 0	0. 57348	-2. 41480	-3. 93847
56. 0	1. 07280	0. 30517	-1. 21849	146. 0	0. 52314	-2. 81380	-4. 33747
58. 0	1. 11270	0. 46379	-1. 05988	148. 0	0. 47340	-3. 24774	-4. 77141
60. 0	1 15043	0. 60862	-0. 91505	150. 0	0. 42456	-3. 72064	-5. 24430
62. 0	1. 18590	0. 74046	-0. 78320	152. 0	0. 37694	-4. 23730	-5. 76097
64. 0	1 21900	0. 86005	-0. 66362	154. 0	0. 33086	-4. 80358	-6. 32725
66. 0	1. 24969	0. 96802	-0. 55565	156. 0	0. 28663	-5. 42671	-6. 95038
68. 0	1. 27790	1. 06498	-0. 45868	158. 0	0. 24458	-6. 11576	-7. 63942
70. 0	1 30361	1. 15148	-0. 37219	160. 0	0. 20500	-6. 88237	-8. 40604
72. 0	1. 32678	1. 22798	-0. 29569	162. 0	0. 16820	-7. 74185	-9. 26552
74. 0	1 34739	1. 29493	-0. 22873	164. 0	0. 13444	-8. 71487	-10. 23854
76. 0	1. 36544	1. 35273	-0. 17094	166. 0	0. 10398	-9. 83041	-11. 35407
78. 0	1 38092	1. 40170	-0. 12197	168. 0	0. 07708	-11. 13081	-12 65448
80. 0	1. 39384	1. 44214	-0. 08153	170. 0	0. 05393	-12. 68175	-14 20541
82. 0	1 40421	1. 47431	-0. 04936	172. 0	0. 03473	-14. 59313	-16. 11680
84. 0	1. 41202	1. 49840	-0. 02526	174. 0	0. 01962	-17. 07101	-18. 59468
86. 0	1. 41729	1. 51459	-0. 00908	176. 0	0. 00875	-20. 57789	-22. 10156
88. 0	1 42003	1. 52299	-0. 00068	178. 0	0. 00219	-26. 58952	-28. 11319
90 0	1. 42026	1. 52367	0. 00000	180.	0. 00000	-INFINITY	-INFINITY

TABLE A2-62 $2\pi a/\lambda = 1.5930$

EPSLN= 1.5930(NORMALIZED GROUNDPLANE RADIUS)
MONOPOLE LENGTH= 0.237900(WAVELENGTH)
MONOPOLE RADIUS= 0.1321E-02(WAVELENGTH)
NUMBER OF MONOPOLE SEGMENTS= 4
NUMBER OF DISK SEGMENTS= 26
RADIATION RESISTANCE DETERMINED BY PATTERN= 0.209239E+02 OHMS

ELEVATION ANGLE (DEG)	DIRECTIVITY (NUMERIC)	DIRECTIVITY (DBI)	RELATIVE POWER (DB)	ELEVATION ANGLE (DEG)	DIRECTIVITY (NUMERIC)	DIRECTIVITY (DBI)	RELATIVE I (DB)
0.	0.00000	-INFINITY	-INFINITY				
2.0	0.00256	-25.91172	-27.28861	92.0	1.36949	1.36359	-0.01131
4.0	0.01023	-19.90232	-21.27922	94.0	1.36493	1.35109	-0.02580
6.0	0.02291	-16.39915	-17.77605	96.0	1.35852	1.33064	-0.04625
8.0	0.04049	-13.92645	-15.30334	98.0	1.35024	1.30412	-0.07277
10.0	0.06278	-12.02170	-13.39859	100.0	1.34009	1.27134	-0.10555
12.0	0.08956	-10.47884	-11.85573	102.0	1.32803	1.23208	-0.14481
14.0	0.12056	-9.18792	-10.56481	104.0	1.31403	1.18604	-0.19085
16.0	0.15548	-8.08326	-9.46016	106.0	1.29804	1.13289	-0.24401
18.0	0.19398	-7.12248	-8.49937	108.0	1.28003	1.07220	-0.30469
20.0	0.23569	-6.27657	-7.65346	110.0	1.25995	1.00353	-0.37336
22.0	0.28023	-5.52482	-6.90171	112.0	1.23776	0.92635	-0.45054
24.0	0.32720	-4.85189	-6.22877	114.0	1.21341	0.84008	-0.53681
26.0	0.37618	-4.24606	-5.62296	116.0	1.18689	0.74409	-0.63280
28.0	0.42675	-3.69825	-5.07514	118.0	1.15816	0.63768	-0.73921
30.0	0.47850	-3.20115	-4.57804	120.0	1.12722	0.52008	-0.85681
32.0	0.53102	-2.74886	-4.12575	122.0	1.09407	0.39045	-0.98644
34.0	0.58391	-2.33651	-3.71340	124.0	1.05874	0.24788	-1.12901
36.0	0.63679	-1.96001	-3.33690	126.0	1.02126	0.09138	-1.28551
38.0	0.68930	-1.61592	-2.99282	128.0	0.98172	-0.08014	-1.45703
40.0	0.74109	-1.30128	-2.67817	130.0	0.94019	-0.26785	-1.64474
42.0	0.79186	-1.01351	-2.39041	132.0	0.89679	-0.47307	-1.84996
44.0	0.84132	-0.75038	-2.12728	134.0	0.85168	-0.69723	-2.07412
46.0	0.88922	-0.50991	-1.88680	136.0	0.80502	-0.94193	-2.31882
48.0	0.93533	-0.29033	-1.66722	138.0	0.75702	-1.20893	-2.58582
50.0	0.97948	-0.09006	-1.46696	140.0	0.70791	-1.50024	-2.87713
52.0	1.02148	0.09231	-1.28458	142.0	0.65794	-1.81812	-3.19501
54.0	1.06123	0.25808	-1.11881	144.0	0.60742	-2.16514	-3.54203
56.0	1.09861	0.40843	-0.96846	146.0	0.55663	-2.54430	-3.92119
58.0	1.13356	0.54443	-0.83246	148.0	0.50593	-2.95906	-4.33595
60.0	1.16602	0.66707	-0.70982	150.0	0.45567	-3.41331	-4.79040
62.0	1.19599	0.77727	-0.59963	152.0	0.40621	-3.91255	-5.28944
64.0	1.22345	0.87585	-0.50104	154.0	0.35792	-4.46209	-5.83898
66.0	1.24842	0.96360	-0.41330	156.0	0.31121	-5.06944	-6.44633
68.0	1.27093	1.04122	-0.33568	158.0	0.26646	-5.74273	-7.12062
70.0	1.29103	1.10936	-0.26753	160.0	0.22404	-6.49668	-7.87357
72.0	1.30877	1.16863	-0.20826	162.0	0.18435	-7.34362	-8.72052
74.0	1.32421	1.21956	-0.15733	164.0	0.14773	-8.30531	-9.68220
76.0	1.33741	1.26264	-0.11425	166.0	0.11453	-9.41073	-10.78762
78.0	1.34844	1.29831	-0.07858	168.0	0.08507	-10.70229	-12.07918
80.0	1.35736	1.32695	-0.04994	170.0	0.05963	-12.24568	-13.62257
82.0	1.36423	1.34888	-0.02801	172.0	0.03845	-14.15086	-15.52775
84.0	1.36911	1.36437	-0.01252	174.0	0.02176	-16.62389	-18.00078
86.0	1.37204	1.37366	-0.00323	176.0	0.00971	-20.12729	-21.50418
88.0	1.37306	1.37689	0.00000	178.0	0.00243	-26.13682	-27.51371
90.0	1.37220	1.37418	-0.00271	180.	0.00000	-INFINITY	-INFINITY

TABLE A2-63 $2\pi a/\lambda = 1.9150$

```
EPSLN= 1 9150(NORMALIZED GROUNDPLANE RADIUS)
MONOPOLE LENGTH= 0 237400(WAVELENGTH)
MONOPOLE RADIUS=   0 1589E-02(WAVELENGTH)
NUMBER OF MONOPOLE SEGMENTS= 4
NUMBER OF DISK SEGMENTS= 27
RADIATION RESISTANCE DETERMINED BY PATTERN= 0 229245E+02 OHMS
```

ELEVATION ANGLE (DEG)	DIRECTIVITY (NUMERIC)	DIRECTIVITY (DBI)	RELATIVE POWER (DB)	ELEVATION ANGLE (DEG)	DIRECTIVITY (NUMERIC)	DIRECTIVITY (DBI)	RELATIVE POWER (DB)
0	0 00000	-INFINITY	-INFINITY				
2.0	0 00324	-24 88942	-25 99127	92 0	1 27250	1.04659	-0.03327
4 0	0.01293	-18 88366	-19.98551	94 0	1 26738	1.02906	-0.07279
6 0	0 02893	-15 38634	-16 48840	96 0	1 26184	1.00935	-0.09251
8 0	0 05102	-12 92230	-14.02415	98 0	1.25525	0.98729	-0 11456
10 0	0 07892	-11 02838	-12 13023	100. 0	1.24815	0.96268	-0.13917
12 0	0 11224	-9 49871	-10 60056	102 0	1.24026	0 93519	-0 16667
14 0	0 15055	-8 22329	-9 32514	104. 0	1.23152	0 90440	-0 19745
16 0	0 19336	-7.13642	-8 23828	106 0	1.22175	0.86984	-0.23201
18 0	0 24012	-6.19565	-7 29750	108 0	1.21085	0.83092	-0.27094
20 0	0. 29027	-5 37193	-6 47379	110 0	1.19867	0.78698	-0.31487
22 0	0 34320	-4.64450	-5 74635	112. 0	1.18503	0 73730	-0.36456
24 0	0 39830	-3 99793	-5 09979	114. 0	1.16978	0.68105	-0.42080
26 0	0 45494	-3.42048	-4 52233	116. 0	1.15275	0 61737	-0 48449
28 0	0 51252	-2. 90293	-4 00478	118. 0	1.13378	0. 54529	-0 55657
30. 0	0. 57044	-2. 43792	-3. 53978	120 0	1 11270	0 46379	-0. 63807
32. 0	0. 62814	-2. 01946	-3. 12132	122. 0	1.08937	0 37177	-0 73009
34. 0	0. 68508	-1. 64257	-2 74443	124 0	1 06367	0. 26806	-0. 83379
36 0	0. 74079	-1. 30308	-2. 40493	126. 0	1 03548	0 15141	-0 95044
38. 0	0. 79480	-0. 99741	-2. 09926	128. 0	1 00473	0. 02049	-1. 08137
40. 0	0. 84674	-0. 72248	-1. 82434	130. 0	0 97137	-0. 12615	-1. 22800
42 0	0. 89627	-0. 47561	-1. 57746	132. 0	0. 93540	-0. 29004	-1. 39189
44. 0	0. 94310	-0. 25441	-1. 35626	134. 0	0. 89684	-0. 47283	-1. 57471
46. 0	0. 98702	-0. 05675	-1. 15860	136. 0	0 85577	-0 67641	-1. 77826
48 0	1. 02784	0. 11928	-0. 98258	138. 0	0. 81233	-0. 90268	-2. 00453
50 0	1. 06547	0. 27542	-0. 82644	140 0	0 76668	-1 15388	-2 25573
52 0	1 09983	0. 41326	-0. 68859	142. 0	0. 71904	-1. 43245	-2. 53430
54 0	1. 13092	0. 53430	-0. 56755	144 0	0. 66971	-1. 74116	-2. 84301
56 0	1 15875	0. 63989	-0. 46196	146. 0	0. 61899	-2 08315	-3. 18500
58 0	1. 18340	0. 73132	-0. 37053	148 0	0. 56728	-2. 46205	-3. 56390
60 0	1 20498	0. 80979	-0. 29206	150. 0	0. 51498	-2. 88211	-3. 98396
62. 0	1. 22361	0. 87644	-0. 22541	152 0	0. 46256	-3. 34834	-4. 45020
64 0	1. 23946	0. 93233	-0. 16952	154 0	0. 41051	-3. 86681	-4 96867
66. 0	1 25270	0. 97848	-0. 12338	156. 0	0. 35934	-4. 44493	-5. 54678
68. 0	1. 26352	1. 01583	-0. 08602	158 0	0. 30960	-5 09194	-6. 19379
70 0	1. 27213	1. 04530	-0. 05655	160. 0	0. 26184	-5 81965	-6. 92150
72 0	1. 27871	1. 06772	-0. 03413	162 0	0. 21660	-6. 64250	-7. 74435
74 0	1 28348	1. 08389	-0. 01796	164. 0	0. 17441	-7 58430	-8. 68616
76. 0	1. 28663	1 09453	-0. 00732	166. 0	0. 13580	-8 67113	-9 77298
78 0	1. 28834	1 10032	-0. 00154	168. 0	0. 10124	-9 94646	-11 04831
80. 0	1. 28880	1 10185	0 00000	170 0	0. 07119	-11 47602	-12 57787
82. 0	1. 28815	1. 09968	-0 00218	172 0	0. 04603	-13 36982	-14 47167
84. 0	1 28655	1 09425	-0. 00760	174. 0	0. 02610	-15 83396	-16. 93581
86. 0	1. 28409	1 08597	-0 01589	176. 0	0. 01167	-19 33099	-20. 43284
88. 0	1. 28089	1 07513	-0 02673	178 0	0. 00293	-25 33669	-26 43855
90. 0	1 27701	1 06196	-0. 03990	180.	0. 00000	-INFINITY	-INFINITY

TABLE A2-64 $2\pi a/\lambda = 2.1970$

```
EPSLN= 2 1970(NORMALIZED GROUNDPLANE RADIUS)
MONOPOLE LENGTH= 0 236600(WAVELENGTH)
MONOPOLE RADIUS=  0 1822E-02(WAVELENGTH)
NUMBER OF MONOPOLE SEGMENTS= 4
NUMBER OF DISK SEGMENTS= 27
RADIATION RESISTANCE DETERMINED BY PATTERN= 0 253505E+00 OHMS
```

ELEVATION ANGLE (DEG)	DIRECTIVITY (NUMERIC)	DIRECTIVITY (DBI)	RELATIVE POWER (DB)	ELEVATION ANGLE (DEG)	DIRECTIVITY (NUMERIC)	DIRECTIVITY (DBI)	RELATIVI (DB)
0	0 00000	-INFINITY	-INFINITY				
2 0	0 00420	-23 76991	-24 80549	92 0	1 15871	0 63976	-0 39583
4 0	0 01672	-17 76771	-18 80329	94 0	1 15139	0 61221	-0 42337
6 0	0 03735	-14 27651	-15 31210	96 0	1 14479	0 58725	-0 44833
8 0	0 06576	-11 82034	-12 85612	98 0	1 13888	0 56479	-0 47079
10 0	0 10146	-9 93723	-10 97281	100 0	1 13359	0 54458	-0 49101
12 0	0 14386	-8 42048	-9 45607	102 0	1 12882	0 52623	-0 50935
14 0	0 19230	-7 16029	-8 19587	104 0	1 12440	0 50921	-0 52637
16 0	0 24599	-6 09089	-7 12648	106 0	1 12017	0 49284	-0 54274
18 0	0 30410	-5 16983	-6 20541	108 0	1 11592	0 47632	-0 55926
20 0	0 36576	-4 36801	-5 40359	110 0	1 11140	0 45871	-0 57688
22 0	0 43007	-3 66462	-4 70020	112 0	1 10636	0 43897	-0 59662
24 0	0 49611	-3 04420	-4 07978	114 0	1 10051	0 41595	-0 61963
26 0	0 56300	-2 49495	-3 53053	116 0	1 09356	0 38843	-0 64715
28 0	0 62985	-2 00760	-3 04318	118 0	1 08520	0 35509	-0 68049
30 0	0 69587	-1 57474	-2 61032	120 0	1 07511	0 31453	-0 72105
32 0	0 76027	-1 19030	-2 22588	122 0	1 06299	0 26529	-0 77030
34 0	0 82236	-0 84925	-1 88483	124 0	1 04854	0 20584	-0 82975
36 0	0 88159	-0 54734	-1 58292	126 0	1 03147	0 13457	-0 90101
38 0	0 93736	-0 28092	-1 31650	128 0	1 01134	0 04982	-0 98576
40 0	0 98928	-0 04683	-1 08241	130 0	0 98851	-0 05017	-1 08575
42 0	1 03698	0 15771	-0 87787	132 0	0 96222	-0 16724	-1 20282
44 0	1 08023	0 33318	-0 70041	134 0	0 93234	-0 30304	-1 33892
46 0	1 11887	0 48779	-0 54779	136 0	0 89938	-0 46055	-1 49614
48 0	1 15281	0 61759	-0 41799	138 0	0 86276	-0 64111	-1 67669
50 0	1 18207	0 72644	-0 30915	140 0	0 82273	-0 84743	-1 88302
52 0	1 20672	0 81606	-0 21952	142 0	0 77944	-1 08219	-2 11777
54 0	1 22690	0 88809	-0 14750	144 0	0 73311	-1 34832	-2 38391
56 0	1 24281	0 94405	-0 09154	146 0	0 68404	-1 64916	-2 68475
58 0	1 25470	0 98540	-0 05018	148 0	0 63263	-1 98850	-3 02409
60 0	1 26286	1 01355	-0 02203	150 0	0 57939	-2 37073	-3 40631
62 0	1 26761	1 02984	-0 00574	152 0	0 52469	-2 80101	-3 83659
64 0	1 26928	1 03558	0 00000	154 0	0 46930	-3 28550	-4 32109
66 0	1 26825	1 03204	-0 00355	156 0	0 41383	-3 83175	-4 86733
68 0	1 26486	1 02044	-0 01515	158 0	0 35900	-4 44909	-5 48467
70 0	1 25950	1 00198	-0 03361	160 0	0 30553	-5 14942	-6 18500
72 0	1 25251	0 97782	-0 05776	162 0	0 25420	-5 94826	-6 98385
74 0	1 24425	0 94909	-0 08650	164 0	0 20575	-6 86650	-7 90209
76 0	1 23509	0 91685	-0 11873	166 0	0 16094	-7 93328	-8 96886
78 0	1 22522	0 88213	-0 15345	168 0	0 12047	-9 19112	-10 22670
80 0	1 21504	0 84590	-0 18969	170 0	0 08500	-10 70581	-11 74139
82 0	1 20477	0 80903	-0 22655	172 0	0 05511	-12 58738	-13 62296
84 0	1 19463	0 77233	-0 26325	174 0	0 03132	-15 04198	-16 07756
86 0	1 18482	0 73632	-0 29906	176 0	0 01402	-18 53218	-19 56776
88 0	1 17549	0 70219	-0 33339	178 0	0 00352	-24 53377	-25 56935
90 0	1 16676	0 66982	-0 36576	180	0 00000	-INFINITY	-INFINITY

TABLE A2-65 $2\pi a/\lambda = 3.0000$

```
EPSLN= 3 0000(NORMALIZED GROUNDPLANE RADIUS)
MONOPOLE LENGTH= 0 235500(WAVELENGTH)
MONOPOLE RADIUS=   0 2478E-02(WAVELENGTH)
NUMBER OF MONOPOLE SEGMENTS=  4
NUMBER OF DISK SEGMENTS= 27
RADIATION RESISTANCE DETERMINED BY PATTERN= 0 3934276+02 OHMS
```

ELEVATION ANGLE (DEG)	DIRECTIVITY (NUMERIC)	DIRECTIVITY (DBI)	RELATIVE POWER (DB)	ELEVATION ANGLE (DEG)	DIRECTIVITY (NUMERIC)	DIRECTIVITY (DBI)	RELATIVE POWER (DB)
0.	0.00000	-INFINITY	-INFINITY				
2.0	0.00987	-20.05844	-22.60144	92.0	0.73392	-1.34351	-3.88652
4.0	0.03921	-14.06638	-16.60958	94.0	0.70441	-1.52173	-4.06474
6.0	0.08725	-10.59258	-13.13559	96.0	0.67950	-1.67809	-4.22109
8.0	0.15273	-8.16063	-10.70364	98.0	0.65928	-1.80932	-4.35233
10.0	0.23399	-6.30811	-8.85111	100.0	0.64376	-1.91265	-4.45566
12.0	0.32894	-4.82882	-7.37183	102.0	0.63300	-1.98594	-4.52895
14.0	0.43524	-3.61267	-6.15568	104.0	0.62691	-2.02796	-4.57096
16.0	0.55032	-2.59281	-5.13682	106.0	0.62540	-2.03845	-4.58146
18.0	0.67148	-1.72965	-4.27365	108.0	0.62831	-2.01826	-4.56127
20.0	0.79598	-0.99096	-3.53497	110.0	0.63544	-1.96928	-4.51229
22.0	0.92113	-0.35679	-2.89980	112.0	0.64649	-1.89436	-4.43737
24.0	1.04435	0.18845	-2.35456	114.0	0.66113	-1.79713	-4.34016
26.0	1.16325	0.65673	-1.88627	116.0	0.67891	-1.68186	-4.22489
28.0	1.27570	1.05747	-1.48554	118.0	0.69933	-1.55516	-4.09817
30.0	1.37982	1.39823	-1.14477	120.0	0.72181	-1.41578	-3.95879
32.0	1.47409	1.68324	-0.85777	122.0	0.74567	-1.27455	-3.81756
34.0	1.55728	1.92367	-0.61934	124.0	0.77017	-1.13416	-3.67717
36.0	1.62851	2.11791	-0.42510	126.0	0.79449	-0.99912	-3.54213
38.0	1.68723	2.27175	-0.27126	128.0	0.81777	-0.87371	-3.41672
40.0	1.73318	2.38845	-0.15456	130.0	0.83908	-0.76198	-3.30499
42.0	1.76640	2.47090	-0.07211	132.0	0.85748	-0.66775	-3.21076
44.0	1.78717	2.52165	-0.02136	134.0	0.87203	-0.59467	-3.13768
46.0	1.79598	2.54301	0.00000	136.0	0.88181	-0.54625	-3.08926
48.0	1.79351	2.53703	-0.00597	138.0	0.88595	-0.52592	-3.06893
50.0	1.78058	2.50562	-0.03739	140.0	0.88367	-0.53710	-3.08011
52.0	1.75812	2.45049	-0.09251	142.0	0.87432	-0.58328	-3.12629
54.0	1.72714	2.37327	-0.16974	144.0	0.85741	-0.66811	-3.21112
56.0	1.68867	2.27545	-0.26756	146.0	0.83263	-0.79548	-3.33849
58.0	1.64378	2.15848	-0.38456	148.0	0.79990	-0.96965	-3.51265
60.0	1.59354	2.02362	-0.51939	150.0	0.75938	-1.19540	-3.73840
62.0	1.53896	1.87228	-0.67073	152.0	0.71151	-1.47822	-4.02122
64.0	1.48105	1.70571	-0.83730	154.0	0.65697	-1.82455	-4.36756
66.0	1.42076	1.52520	-1.01781	156.0	0.59674	-2.24216	-4.78517
68.0	1.35895	1.33205	-1.21096	158.0	0.53204	-2.74058	-5.28359
70.0	1.29647	1.12761	-1.41539	160.0	0.46431	-3.33188	-5.87488
72.0	1.23405	0.91332	-1.62969	162.0	0.39521	-4.03171	-6.57471
74.0	1.17238	0.69069	-1.85232	164.0	0.32651	-4.86107	-7.40408
76.0	1.11209	0.46139	-2.08162	166.0	0.26006	-5.84921	-8.39222
78.0	1.05372	0.22726	-2.31575	168.0	0.19775	-7.03874	-9.58175
80.0	0.99778	-0.00965	-2.55266	170.0	0.14140	-8.49551	-11.03852
82.0	0.94470	-0.24707	-2.79008	172.0	0.09269	-10.32963	-12.87263
84.0	0.89486	-0.48246	-3.02547	174.0	0.05312	-12.74726	-15.29027
86.0	0.84859	-0.71300	-3.25601	176.0	0.02393	-16.21103	-18.75404
88.0	0.80619	-0.93561	-3.47861	178.0	0.00603	-22.19676	-24.73977
90.0	0.76790	-1.14695	-3.68995	180	0.00000	-INFINITY	-INFINITY

TABLE A2-66 $2\pi a/\lambda = 4.000$

```
EPSLN= 4 0000(NORMALIZED GROUNDPLANE RADIUS)
MONOPOLE LENGTH= 0 2346UD(WAVELENGTH)
MONOPOLE RADIUS=  0 5304E-02(WAVELENGTH)
NUMBER OF MONOPOLE SEGMENTS=  4
NUMBER OF DISK SEGMENTS= 27
RADIATION RESISTANCE DETERMINED BY PATTERN= 0 405539E+02 OHMS
```

ELEVATION ANGLE (DEG)	DIRECTIVITY (NUMERIC)	DIRECTIVITY (DBI)	RELATIVE POWER (DB)	ELEVATION ANGLE (DEG)	DIRECTIVITY (NUMERIC)	DIRECTIVITY (DBI)	RELATIVE PO (DB)
0	0 00000	-INFINITY	-INFINITY				
2 0	0. 01927	-17 15085	-21 08158	92 0	0. 62892	-2 01408	-5 92481
4. 0	0. 07634	-11 17250	-15. 08323	94 0	0. 57077	-2. 43538	-6 34611
6. 0	0 16901	-7 72092	-11 63165	96. 0	0. 51534	-2 87905	-6. 78978
8. 0	0 29376	-5. 32011	-9. 23085	98 0	0. 46275	-3 34651	-7 25724
10 0	0 44594	-3 50724	-7 41798	100 0	0. 41318	-3 83864	-7. 74937
12. 0	0. 62004	-2. 07583	-5 98656	102. 0	0. 36683	-4. 35533	-8. 26606
14. 0	0. 80995	-0. 91541	-4. 82614	104 0	0. 32399	-4. 89471	-8. 80544
16 0	1 00932	0 04038	-3 87046	106 0	0. 28497	-5 45205	-9 36279
18. 0	1. 21180	0. 83432	-3. 07642	108. 0	0. 25014	-6. 01613	-9. 92689
20 0	1 41139	1 49646	-2 41428	110 0	0 21992	-6 57726	-10 48799
22. 0	1 60260	2 04826	-1 86247	112 0	0. 19477	-7 10484	-11. 01557
24. 0	1. 78073	2. 50598	-1 40475	114. 0	0. 17514	-7. 56626	-11. 47700
26. 0	1 94191	2. 88220	-1 02845	116 0	0. 16149	-7. 91847	-11. 82920
28. 0	2 08320	3 18731	-0 72342	118 0	0. 15428	-8. 11702	-12. 02775
30 0	2 20264	3 42943	-0 48130	120 0	0. 15386	-8 12870	-12. 03944
32 0	2 29914	3. 61566	-0 29507	122 0	0. 16053	-7. 94440	-11. 85513
34 0	2 37246	3 75200	-0 15874	124 0	0. 17443	-7 58369	-11 49442
36. 0	2. 42306	3. 84365	-0 06708	126 0	0. 19554	-7. 08758	-10. 99831
38 0	2 45200	3 89521	-0 01553	128 0	0. 22362	-6 50496	-10 41569
40 0	2 46078	3. 91073	0 00000	130 0	0. 25816	-5. 88107	-9. 79180
42 0	2 45124	3. 89366	-0. 01688	132. 0	0. 29841	-5. 25192	-9. 16266
44 0	2 42539	3 84782	-0 06291	134 0	0. 34327	-4. 64358	-8. 55432
46 0	2 38537	3 77555	-0 13519	136 0	0. 39139	-4. 07391	-7. 98464
48 0	2 33327	3 67965	-0 23109	138 0	0. 44108	-3. 55479	-7 46553
50 0	2 27114	3 56244	-0 34829	140 0	0. 49044	-3 09418	-7. 00491
52. 0	2 20090	3 42600	-0 48473	142. 0	0. 53733	-2. 69758	-6. 60832
54 0	2. 12430	3 27215	-0. 63858	144. 0	0. 57934	-2 36917	-6. 27991
56. 0	2 04290	3 10247	-0 80826	146 0	0. 61482	-2. 11249	-6. 02322
58 0	1. 95809	2. 91832	-0 99241	148. 0	0. 64107	-1. 93098	-5. 84171
60 0	1. 87105	2 72096	-1 18987	150 0	0. 65639	-1. 82839	-5. 73912
62. 0	1. 78280	2. 51104	-1. 39970	152 0	0. 65931	-1. 80911	-5. 71985
64 0	1. 69419	2 28961	-1 62112	154 0	0. 64885	-1 87852	-5 78926
66. 0	1. 60589	2 05716	-1 85357	156 0	0. 62469	-2. 04336	-5. 95409
68. 0	1 51848	1 81409	-2. 09664	158 0	0. 58719	-2. 31223	-6. 22297
70. 0	1. 43240	1 56064	-2 35010	160 0	0 53748	-2 69638	-6. 60712
72 0	1. 34799	1 29686	-2. 61387	162. 0	0. 47745	-3. 21075	-7. 12148
74 0	1. 26552	1 02267	-2 88806	164 0	0. 40967	-3 87570	-7 78644
76 0	1 18517	0 73781	-3 17292	166 0	0 33729	-4. 71993	-8. 63067
78 0	1. 10709	0 44185	-3. 46889	168. 0	0 26390	-5 78560	-9. 69633
80 0	1 03138	0 13417	-3 77656	170 0	D 19328	-7 13817	-11 04890
82. 0	0. 95808	-0 18599	-4 09673	172. 0	0. 12920	-8. 88743	-12 79817
84 0	0 88724	-0 51940	-4 43034	174 0	0 07317	-11 23933	-15 15006
86 0	0. 81888	-0 86781	-4 77855	176. 0	0. 03423	-14 65627	-18 56700
88 0	0 75302	-1 23195	-5 14268	178 0	0. 00868	-20 61395	-24 52469
90 0	0 68968	-1 61349	-5 52423	180	0. 00000	-INFINITY	-INFINITY

A.3 OBLATE SPHEROIDAL WAVE FUNCTIONS

TABLE A3-1 Directivity and Radiation Resistance of Quarter-wave Monopole Mounted on Circular Ground Plane of Finite Extent, $2\pi a/\lambda = 3.0$

2Pi*A = 3.00 radiation resistance = 37.4765 ohms

ELEVATION ANGLE, Φ (DEG)	DIRECTIVITY D(Φ) (ABSOLUTE)	DIRECTIVITY D(Φ) (dBi)	RELATIVE POWER (dB)	ELEVATION ANGLE, Φ (DEG)	DIRECTIVITY D(Φ) (ABSOLUTE)	DIRECTIVITY D(Φ) (dBi)	RELATIVE POWER (dB)
0 00000	0 00000	-INFINITY	-INFINITY	92 00000	0 76429	-1 16744	-3 68994
2 00000	0 00993	-20 03232	-22 55502	94 00000	0 73249	-1 35197	-3 87447
4 00000	0 03943	-14 04121	-16 56371	96 00000	0 70472	-1 51980	-4 04230
6 00000	0 08774	-10 56811	-13 09061	98 00000	0 68111	-1 66780	-4 19030
8 00000	0 15355	-8 13740	-10 65990	100 00000	0 66176	-1 79299	-4 31549
10 00000	0 23516	-6 28645	-8 80895	102 00000	0 64674	-1 89273	-4 41523
12 00000	0 33044	-4 80905	-7 33155	104 00000	0 63607	-1 96494	-4 48744
14 00000	0 43701	-3 59307	-6 11757	106 00000	0 62976	-2 00827	-4 53077
16 00000	0 55225	-2 57866	-5 10316	108 00000	0 62774	-2 02223	-4 54473
18 00000	0 67342	-1 71716	-4 23966	110 00000	0 62989	-2 00735	-4 52985
20 00000	0 79775	-0 98135	-3 50385	112 00000	0 63604	-1 96515	-4 48765
22 00000	0 92253	-0 35021	-2 87271	114 00000	0 64593	-1 89711	-4 41961
24 00000	1 04517	0 19189	-2 33061	116 00000	0 65924	-1 80957	-4 33207
26 00000	1 16331	0 65696	-1 86554	118 00000	0 67554	-1 70350	-4 22600
28 00000	1 27482	1 05449	-1 46801	120 00000	0 69433	-1 58436	-4 10686
30 00000	1 37787	1 39209	-1 13041	122 00000	0 71501	-1 45689	-3 97939
32 00000	1 47098	1 67606	-0 84644	124 00000	0 73690	-1 32593	-3 84843
34 00000	1 55297	1 91164	-0 61086	126 00000	0 75922	-1 19631	-3 71881
36 00000	1 62305	2 10331	-0 41919	128 00000	0 78114	-1 07272	-3 59522
38 00000	1 68071	2 25492	-0 26758	130 00000	0 80174	-0 95966	-3 48216
40 00000	1 72577	2 36983	-0 15267	132 00000	0 82007	-0 86147	-3 38397
42 00000	1 75833	2 45100	-0 07150	134 00000	0 83517	-0 78226	-3 30476
44 00000	1 77873	2 50110	-0 02140	136 00000	0 84606	-0 72598	-3 24848
46 00000	1 78752	2 52250	0 00000	138 00000	0 85183	-0 69648	-3 21898
48 00000	1 78541	2 51738	+0 00512	140 00000	0 85162	-0 69755	-3 22005
50 00000	1 77325	2 48769	+0 03481	142 00000	0 84470	-0 73298	-3 25548
52 00000	1 75198	2 43528	+0 08722	144 00000	0 83048	-0 80570	-3 32820
54 00000	1 72259	2 36182	+0 16068	146 00000	0 80857	-0 92282	-3 44532
56 00000	1 68612	2 26889	+0 25361	148 00000	0 77879	-1 08580	-3 60830
58 00000	1 64360	2 15797	+0 36453	150 00000	0 74121	-1 30059	-3 82309
60 00000	1 59604	2 03045	+0 49205	152 00000	0 69618	-1 57279	-4 09529
62 00000	1 54442	1 88766	+0 63484	154 00000	0 64432	-1 90897	-4 43147
64 00000	1 48967	1 73089	+0 79161	156 00000	0 58655	-2 31696	-4 83946
66 00000	1 43264	1 56138	+0 96112	158 00000	0 52404	-2 80637	-5 32887
68 00000	1 37416	1 38037	+1 14213	160 00000	0 45821	-3 38933	-5 91183
70 00000	1 31494	1 18908	+1 33342	162 00000	0 39070	-4 08152	-6 60402
72 00000	1 25567	0 98876	+1 53374	164 00000	0 32330	-4 90400	-7 42650
74 00000	1 19694	0 78071	+1 74179	166 00000	0 25787	-5 88601	-8 40851
76 00000	1 13928	0 56630	+1 95620	168 00000	0 19633	-7 07020	-9 59270
78 00000	1 08318	0 34700	+2 17550	170 00000	0 14053	-8 52244	-11 04494
80 00000	1 02906	0 12440	+2 39810	172 00000	0 09220	-10 35283	-12 87533
82 00000	0 97729	-0 09975	+2 62225	174 00000	0 05287	-12 76756	-15 29006
84 00000	0 92822	-0 32048	+2 84298	176 00000	0 02383	-16 22925	-18 75175
86 00000	0 88214	-0 54464	+3 06714	178 00000	0 00601	-22 21373	-24 73623
88 00000	0 83930	-0 76082	+3 28332	180 00000	0 00000	+INFINITY	+INFINITY
90 00000	0 79995	-0 96938	+3 49188				

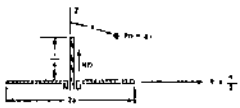

$ka = 3, 4, 5, \sqrt{42},\ h/\lambda = 0.25.$

TABLE A3-2 Directivity and Radiation Resistance of Quarter-wave Monopole Mounted on Circular Ground Plane of Finite Extent, $2\pi a/\lambda = 4.0$

ELEVATION ANGLE (DEG)	DIRECTIVITY (NUMERIC)	DIRECTIVITY (DBI)	RELATIVE LEVEL (DB)	ELEVATION ANGLE (DEG)	DIRECTIVITY (NUMERIC)	DIRECTIVITY (DBI)	RELATIVE LEVEL (DB)
0.00000	0.00000	-INFINITY	-INFINITY	92.00000	0.64167	-1.92691	-5.82634
2.00000	0.01944	-17.11225	-21.01168	94.00000	0.58310	-2.34255	-6.24198
4.00000	0.07701	-11.13439	-15.03382	96.00000	0.52695	-2.78228	-6.68171
6.00000	0.17047	-7.68361	-11.58304	98.00000	0.47336	-3.24811	-7.14754
8.00000	0.29622	-5.28393	-9.18336	100.00000	0.42251	-3.74161	-7.64104
10.00000	0.44952	-3.47249	-7.37192	102.00000	0.37466	-4.26361	-8.16304
12.00000	0.62477	-2.04281	-5.94224	104.00000	0.33011	-4.81337	-8.71280
14.00000	0.81575	-0.88441	-4.78384	106.00000	0.28923	-5.38758	-9.28701
16.00000	1.01601	0.06897	-3.83046	108.00000	0.25243	-5.97863	-9.87806
18.00000	1.21911	0.86044	-3.03899	110.00000	0.22017	-6.57234	-10.47177
20.00000	1.41899	1.51978	-2.37965	112.00000	0.19297	-7.14509	-11.04452
22.00000	1.61011	2.06856	-1.83087	114.00000	0.17134	-7.66144	-11.56087
24.00000	1.78774	2.52305	-1.37638	116.00000	0.15580	-8.07432	-11.97375
26.00000	1.94803	2.89593	-1.00349	118.00000	0.14685	-8.33133	-12.23076
28.00000	2.08808	3.19746	-0.70197	120.00000	0.14491	-8.38898	-12.28841
30.00000	2.20595	3.43597	-0.46346	122.00000	0.15032	-8.22971	-12.12914
32.00000	2.30066	3.61852	-0.28091	124.00000	0.16328	-7.87069	-11.77012
34.00000	2.37202	3.75119	-0.14824	126.00000	0.18379	-7.35684	-11.25627
36.00000	2.42059	3.83922	-0.06021	128.00000	0.21164	-6.74413	-10.64356
38.00000	2.44752	3.88726	-0.01217	130.00000	0.24635	-6.08456	-9.98399
40.00000	2.45439	3.89943	0.00000	132.00000	0.28715	-5.41895	-9.31838
42.00000	2.44311	3.87943	-0.02000	134.00000	0.33296	-4.77613	-8.67556
44.00000	2.41578	3.83057	-0.06886	136.00000	0.38237	-4.17521	-8.07464
46.00000	2.37456	3.75583	-0.14360	138.00000	0.43367	-3.62844	-7.52787
48.00000	2.32161	3.65789	-0.24154	140.00000	0.48488	-3.14367	-7.04310
50.00000	2.25899	3.53915	-0.36028	142.00000	0.53381	-2.72610	-6.62553
52.00000	2.18863	3.40170	-0.49770	144.00000	0.57816	-2.37953	-6.27896
54.00000	2.11226	3.24752	-0.65191	146.00000	0.61559	-2.10711	-6.00654
56.00000	2.03149	3.07816	-0.82127	148.00000	0.64388	-1.91197	-5.81140
58.00000	1.94762	2.89504	-1.00439	150.00000	0.66107	-1.79754	-5.69697
60.00000	1.86182	2.69937	-1.20006	152.00000	0.66558	-1.76798	-5.66741
62.00000	1.77506	2.49212	-1.40731	154.00000	0.65638	-1.82840	-5.72786
64.00000	1.68813	2.27407	-1.62536	156.00000	0.63307	-1.98547	-5.88493
66.00000	1.60170	2.04580	-1.85363	158.00000	0.59600	-2.24757	-6.14703
68.00000	1.51625	1.80770	-2.09173	160.00000	0.54628	-2.62584	-6.52527
70.00000	1.43218	1.55998	-2.33945	162.00000	0.48583	-3.13511	-7.03454
72.00000	1.34979	1.30267	-2.59676	164.00000	0.41728	-3.79569	-7.69512
74.00000	1.26929	1.03562	-2.86381	166.00000	0.34366	-4.63619	-8.53562
76.00000	1.19082	0.75847	-3.14096	168.00000	0.26923	-5.69872	-9.59815
78.00000	1.11448	0.47071	-3.42872	170.00000	0.19730	-7.04870	-10.94813
80.00000	1.04031	0.17182	-3.72761	172.00000	0.13195	-8.79590	-12.69533
82.00000	0.96834	-0.13972	-4.03915	174.00000	0.07680	-11.14620	-15.04563
84.00000	0.89858	-0.46444	-4.36387	176.00000	0.03498	-14.56203	-18.46146
86.00000	0.83102	-0.80397	-4.70330	178.00000	0.00987	-20.05403	-23.95346
88.00000	0.76567	-1.15936	-5.05899	180.00000	0.00000	-INFINITY	-INFINITY
90.00000	0.70254	-1.53327	-5.43270				

$ka = 3, 4, 5, \sqrt{42},\ h/\lambda = 0.25.$

TABLE A3-3 Directivity and Radiation Resistance of Quarter-wave Monopole Mounted on Circular Ground Plane of Finite Extent, $2\pi a/\lambda = 5.0$

2*a/λ = 5.00 — Radiation resistance = 32.5653 ohms

ELEVATION ANGLE, ° (DEG)	DIRECTIVITY d( ) (NUMERIC)	DIRECTIVITY D(=) (dBi)	RELATIVE POWER (dB)	ELEVATION ANGLE, ° (DEG)	DIRECTIVITY d(=) (NUMERIC)	DIRECTIVITY D(=) (dBi)	RELATIVE POWER (dB)
0.00000	0.00000	-INFINITY	-INFINITY	92.00000	0.87449	-0.58246	-3.95421
2.00000	0.02482	-16.05208	-19.42383	94.00000	0.82949	-0.81188	-4.18363
4.00000	0.09782	-10.09571	-13.46746	96.00000	0.78534	-1.04941	-4.42116
6.00000	0.21476	-6.68050	-10.05225	98.00000	0.74175	-1.29741	-4.66916
8.00000	0.36897	-4.33006	-7.70181	100.00000	0.69841	-1.55692	-4.93067
10.00000	0.55196	-2.58096	-5.95271	102.00000	0.65499	-1.83766	-5.20941
12.00000	0.75406	-1.22596	-4.59771	104.00000	0.61120	-2.13818	-5.50993
14.00000	0.96524	-0.15364	-3.52539	106.00000	0.56678	-2.46383	-5.83758
16.00000	1.17584	0.70348	-2.66827	108.00000	0.52156	-2.82695	-6.19870
18.00000	1.37717	1.38988	-1.98187	110.00000	0.47546	-3.22886	-6.60061
20.00000	1.56207	1.93701	-1.43474	112.00000	0.42854	-3.68005	-7.05180
22.00000	1.72518	2.36835	-1.00340	114.00000	0.38105	-4.19022	-7.56197
24.00000	1.86308	2.70232	-0.66943	116.00000	0.33340	-4.77031	-8.14206
26.00000	1.97423	2.93399	-0.41776	118.00000	0.28627	-5.43226	-8.80401
28.00000	2.05878	3.13610	-0.23565	120.00000	0.24054	-6.18819	-9.55994
30.00000	2.11823	3.25972	-0.11203	122.00000	0.19733	-7.04807	-10.41982
32.00000	2.15306	3.33460	-0.03715	124.00000	0.15798	-8.01386	-11.38561
34.00000	2.17240	3.36939	-0.00236	126.00000	0.12400	-9.06566	-12.43741
36.00000	2.17358	3.37175	0.00000	128.00000	0.09699	-10.13273	-13.50448
38.00000	2.16190	3.34835	-0.02340	130.00000	0.07855	-11.04864	-14.42039
40.00000	2.14037	3.30488	-0.06687	132.00000	0.07016	-11.53903	-14.91078
42.00000	2.11155	3.24602	-0.12573	134.00000	0.07305	-11.36388	-14.73562
44.00000	2.07752	3.17544	-0.19631	136.00000	0.08801	-10.55472	-13.92647
46.00000	2.03979	3.09585	-0.27590	138.00000	0.11527	-9.38302	-12.75477
48.00000	1.99943	3.00905	-0.36270	140.00000	0.15432	-8.11571	-11.48746
50.00000	1.95708	2.91608	-0.45567	142.00000	0.20386	-6.90657	-10.27832
52.00000	1.91308	2.81734	-0.55441	144.00000	0.26171	-5.82188	-9.19363
54.00000	1.86757	2.71277	-0.65898	146.00000	0.32480	-4.88378	-8.25553
56.00000	1.82054	2.60201	-0.76974	148.00000	0.38938	-4.09623	-7.46798
58.00000	1.77196	2.48434	-0.88721	150.00000	0.45112	-3.45707	-6.82882
60.00000	1.72180	2.35982	-1.01173	152.00000	0.50545	-2.96325	-6.33500
62.00000	1.67008	2.22739	-1.14436	154.00000	0.54790	-2.61299	-5.98474
64.00000	1.61692	2.08689	-1.28486	156.00000	0.57459	-2.40478	-5.77653
66.00000	1.56249	1.93818	-1.43357	158.00000	0.58237	-2.34797	-5.71972
68.00000	1.50705	1.78127	-1.59048	160.00000	0.56971	-2.44330	-5.81525
70.00000	1.45090	1.61639	-1.75536	162.00000	0.53644	-2.70476	-6.07671
72.00000	1.39441	1.44396	-1.92785	164.00000	0.48425	-3.14928	-6.52123
74.00000	1.33793	1.26434	-2.10741	166.00000	0.41654	-3.80345	-7.17540
76.00000	1.28183	1.07831	-2.29344	168.00000	0.33825	-4.70757	-8.07952
78.00000	1.22644	0.88647	-2.48528	170.00000	0.25552	-5.92564	-9.29759
80.00000	1.17204	0.68944	-2.68231	172.00000	0.17513	-7.56629	-10.93824
82.00000	1.11887	0.48782	-2.88393	174.00000	0.10388	-9.83457	-13.20652
84.00000	1.06709	0.28202	-3.08973	176.00000	0.04795	-13.19224	-16.56419
86.00000	1.01679	0.07231	-3.29944	178.00000	0.01226	-19.11454	-22.48649
88.00000	0.96797	-0.14137	-3.51312	180.00000	0.00000	-INFINITY	-INFINITY
90.00000	0.92058	-0.35937	-3.73112				

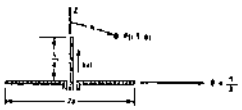

$ka = 3, 4, 5, \sqrt{42},\ h/\lambda = 0.25.$

TABLE A3-4 Directivity and Radiation Resistance of Quarter-wave Monopole Mounted on Circular Ground plane of Finite Extent, $2\pi a/\lambda = \sqrt{42}$

ELEVATION ANGLE, ϕ (DEG)	2-a/λ = 6.48 DIRECTIVITY d(φ) (NUMERIC)	DIRECTIVITY D(φ) (dBi)	RELATIVE PATTERN (dB)	radiation resistance = 40.1666 ohms ELEVATION ANGLE, ϕ (DEG)	DIRECTIVITY d(φ) (NUMERIC)	DIRECTIVITY D(φ) (dBi)	RELATIVE PATTERN (dB)
0.00000	0.00000	-INFINITY	-INFINITY	92.00000	0.67231	-1.72428	-5.79331
2.00000	0.02090	-16.79764	-20.86667	94.00000	0.60756	-2.16409	-6.23312
4.00000	0.08056	-10.93877	-15.00780	96.00000	0.55213	-2.57960	-6.64863
6.00000	0.17036	-7.68624	-11.75527	98.00000	0.50596	-2.95882	-7.02785
8.00000	0.27774	-5.56365	-9.63268	100.00000	0.46895	-3.28869	-7.35772
10.00000	0.38842	-4.10697	-8.17600	102.00000	0.44091	-3.55647	-7.62550
12.00000	0.48900	-3.10694	-7.17597	104.00000	0.42153	-3.75175	-7.82078
14.00000	0.56920	-2.44734	-6.51637	106.00000	0.41033	-3.86868	-7.93771
16.00000	0.62359	-2.05104	-6.12007	108.00000	0.40664	-3.90789	-7.97692
18.00000	0.65226	-1.85579	-5.92482	110.00000	0.40953	-3.87714	-7.94617
20.00000	0.66065	-1.80030	-5.86933	112.00000	0.41776	-3.79075	-7.85978
22.00000	0.65893	-1.81553	-5.88456	114.00000	0.42975	-3.66784	-7.73687
24.00000	0.65732	-1.82220	-5.89123	116.00000	0.44359	-3.53020	-7.59923
26.00000	0.66999	-1.73930	-5.80833	118.00000	0.45704	-3.40044	-7.46947
28.00000	0.70715	-1.50491	-5.57394	120.00000	0.46764	-3.30084	-7.36987
30.00000	0.77647	-1.09876	-5.16779	122.00000	0.47283	-3.25299	-7.32202
32.00000	0.88155	-0.54752	-4.61655	124.00000	0.47011	-3.27797	-7.34700
34.00000	1.02161	0.09285	-3.97618	126.00000	0.45739	-3.39717	-7.46620
36.00000	1.19179	0.76201	-3.30702	128.00000	0.43317	-3.63342	-7.70245
38.00000	1.38401	1.41140	-2.65763	130.00000	0.39696	-4.01254	-8.08157
40.00000	1.58806	2.00867	-2.06036	132.00000	0.34951	-4.56539	-8.63442
42.00000	1.79284	2.53541	-1.53362	134.00000	0.29306	-5.33046	-9.39949
44.00000	1.98751	2.98310	-1.08593	136.00000	0.23140	-6.35645	-10.42548
46.00000	2.16247	3.34950	-0.71953	138.00000	0.16977	-7.70145	-11.77048
48.00000	2.31001	3.63614	-0.43289	140.00000	0.11453	-9.41087	-13.47990
50.00000	2.42471	3.84660	-0.22243	142.00000	0.07254	-11.39394	-15.46297
52.00000	2.50351	3.98550	-0.08353	144.00000	0.05038	-12.97752	-17.04655
54.00000	2.54561	4.05792	-0.01111	146.00000	0.05332	-12.73134	-16.80037
56.00000	2.55213	4.06903	0.00000	148.00000	0.08437	-10.73804	-14.80707
58.00000	2.52571	4.02384	-0.04519	150.00000	0.14342	-8.43399	-12.50302
60.00000	2.47012	3.92718	-0.14185	152.00000	0.22664	-6.44658	-10.51561
62.00000	2.38976	3.78355	-0.28548	154.00000	0.32649	-4.86135	-8.93038
64.00000	2.28936	3.59714	-0.47189	156.00000	0.43216	-3.64353	-7.71256
66.00000	2.17362	3.37184	-0.69719	158.00000	0.53081	-2.75063	-6.81966
68.00000	2.04701	3.11119	-0.95784	160.00000	0.60915	-2.15273	-6.22176
70.00000	1.91337	2.81843	-1.25058	162.00000	0.65552	-1.83417	-5.90320
72.00000	1.77689	2.49660	-1.57243	164.00000	0.66177	-1.79291	-5.86194
74.00000	1.63998	2.14840	-1.92063	166.00000	0.62500	-2.04117	-6.11020
76.00000	1.50536	1.77639	-2.29264	168.00000	0.54842	-2.60887	-6.67790
78.00000	1.37500	1.38304	-2.68599	170.00000	0.44133	-3.55241	-7.62144
80.00000	1.25048	0.97077	-3.09826	172.00000	0.31807	-4.97483	-9.04386
82.00000	1.13296	0.54214	-3.52689	174.00000	0.19602	-7.07709	-11.14612
84.00000	1.02328	0.09996	-3.96907	176.00000	0.09294	-10.31807	-14.38710
86.00000	0.92205	-0.35244	-4.42147	178.00000	0.02415	-16.17109	-20.24012
88.00000	0.82967	-0.81097	-4.88000	180.00000	0.00000	-INFINITY	-INFINITY
90.00000	0.74637	-1.27046	-5.33949				

$ka = 3, 4, 5, \sqrt{42},\ h/\lambda = 0.25.$

A.4 VARIATIONAL METHOD

TABLE A4-1 $28.0 < ka < \infty$, $h/\lambda = 0.25$

$2\pi a/\lambda$	$R - R_\infty$ (OHMS)	$X - X_\infty$ (OHMS)	R (OHMS)	X (OHMS)	$d(\pi/2)$ (NUMERIC)	$D(\pi/2)$ (dBi)
28.2743340	-0.0428709	-1.0999534	36.4966393	20.1576080	0.8214043	-0.8544304
29.0597324	1.0697033	0.0411037	37.6092110	21.2986641	0.7971051	-0.9848440
29.8451309	-0.0340973	0.9679080	36.5054131	22.2254696	0.8212068	-0.8554745
30.6305294	-0.9435477	0.0328219	35.5959625	21.2903824	0.8421881	-0.7459092
31.4159279	-0.0364609	-0.9881375	36.5030479	20.2694225	0.8212600	-0.8551931
32.2013245	0.9636334	0.0351067	37.5031433	21.2926674	0.7993595	-0.9725786
32.9867249	-0.0294509	0.8773347	36.5100594	22.1348953	0.8211023	-0.8560272
33.7721214	-0.8572898	0.0284486	35.6822205	21.2860088	0.8401521	-0.7564207
34.5575218	-0.0314970	-0.8968816	36.5080109	20.3606796	0.8211484	-0.8557835
35.3429184	0.8766313	0.0304365	37.4161415	21.2879963	0.8012182	-0.9624919
36.1283150	-0.0257698	0.8023182	36.5137405	22.0598793	0.8210195	-0.8564651
36.9137154	-0.7855343	0.0249676	35.7539749	21.2825279	0.8384660	-0.7651453
37.6991119	-0.0275676	-0.8210008	36.5119400	20.4365597	0.8210601	-0.8562508
38.4845123	0.8039876	0.0267142	37.3434982	21.2842751	0.8027768	-0.9540519
39.2699089	-0.0228035	0.7391611	36.5167046	21.9967213	0.8209529	-0.8568177
40.0553093	-0.7249014	0.0221447	35.8146057	21.2797030	0.8370466	-0.7725036
40.8407059	-0.0243846	-0.7569175	36.5151253	20.5006428	0.8209884	-0.8566298
41.6261024	0.7424243	0.0236855	37.2819328	21.2812462	0.8041025	-0.9468860
42.4115028	-0.0203678	0.6852531	36.5191422	21.9428139	0.8208981	-0.8571074
43.1968994	-0.6729873	0.0198227	35.8665199	21.2773838	0.8358350	-0.7787943
43.9822998	-0.0217679	-0.7020830	36.5177422	20.5554771	0.8209296	-0.8569410
44.7676964	0.6895890	0.0211916	37.2290993	21.2787514	0.8052436	-0.9407272
45.5530930	-0.0183338	0.6386985	36.5211754	21.8962593	0.8208524	-0.8573493
46.3384933	-0.6280351	0.0178772	35.9114723	21.2754383	0.8347888	-0.7842339
47.1238899	-0.0195912	-0.6546321	36.5199165	20.6029282	0.8208807	-0.8571995
47.9092903	0.6437514	0.0191055	37.1832619	21.2766666	0.8062363	-0.9353768
48.6946869	-0.0166221	0.5980861	36.5228882	21.8556461	0.8208139	-0.8575531
49.4800873	-0.5887301	0.0162310	35.9507790	21.2737923	0.8338761	-0.7889849
50.2654839	-0.0177491	-0.6131703	36.5217590	20.6443901	0.8208393	-0.8574187
51.0508804	0.6036100	0.0173351	37.1431198	21.2748966	0.8071076	-0.9306855
51.8362808	-0.0151622	0.5623448	36.5243454	21.8199062	0.8207812	-0.8577261
52.6216774	-0.5540695	0.0148274	35.9854393	21.2729885	0.8330729	-0.7931700
53.4070778	-0.0161776	-0.5766323	36.5233307	20.6809292	0.8208039	-0.8576057
54.1924744	0.5681658	0.0158252	37.1076736	21.2733860	0.8078786	-0.9265392
54.9778748	-0.0139050	0.5306469	36.5256042	21.7882080	0.8207529	-0.8578759
55.7632713	-0.5232750	0.0136123	36.0162354	21.2711735	0.8323606	-0.7968851
56.5486679	-0.0148283	-0.5441912	36.5246811	20.7133694	0.8207736	-0.8577662
57.3340683	0.5366415	0.0145221	37.0761490	21.2720833	0.8085655	-0.9228480
58.1194649	-0.0128094	0.5023422	36.5266991	21.7599030	0.8207283	-0.8580059
58.9048653	-0.4957332	0.0125548	36.0437775	21.2701149	0.8317245	-0.8002049
59.6902618	-0.0136525	-0.5151959	36.5258560	20.7423649	0.8207472	-0.8579059
60.4756584	0.5084220	0.0133842	37.0479317	21.2709446	0.8091813	-0.9195414
61.2610588	-0.0118541	0.4769124	36.5276566	21.7344723	0.8207068	-0.8581198
62.0464554	-0.4709536	0.0116311	36.0685539	21.2691917	0.8311532	-0.8031892

98.1747742	0.3115083	0.0064025	36.8510170	21.2639637	0.8135052	-0.8963966
98.9601746	-0.0058392	0.2968726	36.5336685	21.5544338	0.8205717	-0.8588346
99.7455673	-0.2945590	0.0057676	36.2449493	21.2633286	0.8271082	-0.8243767
100.5309677	-0.0061717	-0.3041370	36.5333366	20.9534245	0.8205792	-0.8587951
101.3163681	0.3017562	0.0061040	36.8412666	21.2636642	0.8137205	-0.8952473
102.1017609	-0.0055717	0.2878293	36.5339355	21.5453892	0.8205657	-0.8588665
102.8871613	-0.2856542	0.0055081	36.2538528	21.2630692	0.8269051	-0.8254435
103.6725616	-0.0058889	-0.2948331	36.5336189	20.9627285	0.8205728	-0.8588289
104.4579620	0.2925949	0.0058280	36.8321037	21.2633896	0.8139229	-0.8941671
105.2433548	-0.0053280	0.2793218	36.5341797	21.5368824	0.8205602	-0.8588954
106.0287552	-0.2772731	0.0052675	36.2622375	21.2628288	0.8267139	-0.8264478
106.8141556	-0.0056270	-0.2860803	36.5338821	20.9714813	0.8205669	-0.8588602
107.5995483	0.2839723	0.0055678	36.8234825	21.2631283	0.8141135	-0.8931505
108.3849487	-0.0051016	0.2713037	36.5344086	21.5288639	0.8205551	-0.8589226
109.1703491	-0.2693710	0.0050439	36.2701378	21.2626038	0.8265338	-0.8273939
109.9557495	-0.0053838	-0.2778310	36.5341263	20.9797306	0.8205614	-0.8588892
110.7411423	0.2758422	0.0053304	36.8153496	21.2628918	0.8142934	-0.8921910
111.5265427	-0.0048909	0.2637343	36.5346184	21.5212955	0.8205504	-0.8589475
112.3119431	-0.2619078	0.0048357	36.2775993	21.2623959	0.8263638	-0.8282872
113.0973358	-0.0051617	-0.2700431	36.5343475	20.9875183	0.8205565	-0.8589154
113.8827362	0.2681635	0.0051093	36.8076706	21.2626705	0.8144633	-0.8912850
114.6681366	-0.0046944	0.2565766	36.5348129	21.5141373	0.8205460	-0.8589709
115.4535370	-0.2548479	0.0046414	36.2846603	21.2622013	0.8262030	-0.8291324
116.2389297	-0.0049507	-0.2626789	36.5345573	20.9948826	0.8205518	-0.8589402
117.0243301	0.2608999	0.0049032	36.8004074	21.2624645	0.8146240	-0.8904280
117.8097305	-0.0045108	0.2497980	36.5349998	21.5073586	0.8205418	-0.8589929
118.5951233	-0.2481594	0.0044634	36.2913513	21.2620239	0.8260506	-0.8299333
119.3805237	-0.0047535	-0.2557049	36.5347557	21.0018559	0.8205473	-0.8589639
120.1659241	0.2540186	0.0047106	36.7935257	21.2622719	0.8147764	-0.8896159
120.9513168	-0.0043353	0.2433694	36.5351753	21.5009308	0.8205379	-0.8590138
121.7367172	-0.2418137	0.0042932	36.2976952	21.2618542	0.8259063	-0.8306924
122.5221176	-0.0045691	-0.2490909	36.5349388	21.0084705	0.8205432	-0.8589857
123.3075180	0.2474902	0.0045303	36.7869987	21.2620907	0.8149209	-0.8888455
124.0929108	-0.0041742	0.2372638	36.5353355	21.4948254	0.8205343	-0.8590326
124.8783112	-0.2357852	0.0041335	36.3037224	21.2616940	0.8257692	-0.8314133
125.6637115	-0.0043961	-0.2428097	36.5351143	21.0147514	0.8205392	-0.8590065
126.4491043	0.2412883	0.0043575	36.7807961	21.2619190	0.8150584	-0.8881130
127.2345047	-0.0040230	0.2314578	36.5354843	21.4890194	0.8205310	-0.8590504
128.0198975	-0.2300505	0.0039869	36.3094597	21.2615471	0.8256387	-0.8320996
128.8052979	-0.0042375	-0.2368367	36.5352707	21.0207233	0.8205357	-0.8590251
129.5906982	0.2353889	0.0041988	36.7748985	21.2617588	0.8151891	-0.8874166
130.3760986	-0.0038806	0.2259296	36.5356293	21.4834900	0.8205277	-0.8590677
131.1614990	-0.2245889	0.0038422	36.3149185	21.2614021	0.8255146	-0.8327526
131.9468994	-0.0040811	-0.2311501	36.5354271	21.0264111	0.8205322	-0.8590438
132.7322998	0.2297704	0.0040531	36.7692795	21.2616138	0.8153136	-0.8867530

TABLE A4-1 (Continued)

$2\pi a/\lambda$	$R - R_\infty$ (OHMS)	$X - X_\infty$ (OHMS)	R (OHMS)	X (OHMS)	d(π/2) (NUMERIC)	D(π/2) (dBi)
62.8318558	-0.0126236	-0.4891256	36.5268860	20.7684345	0.8207241	-0.8580283
63.6172523	0.4830137	0.0123905	37.0225220	21.2699509	0.8097367	-0.9165620
64.4026489	-0.0110089	0.4539403	36.5284996	21.7115002	0.8206878	-0.8582201
65.1880493	-0.4485402	0.0108128	36.0909691	21.2683735	0.8306370	-0.8058872
65.9734497	-0.0117172	-0.4655595	36.5277901	20.7920017	0.8207037	-0.8581358
66.7588425	0.4600173	0.0115103	36.9995270	21.2690716	0.8102400	-0.9138634
67.5442429	-0.0102629	0.4330855	36.5292473	21.6906471	0.8206710	-0.8583090
68.3296432	-0.4281690	0.0100862	36.1113396	21.2676468	0.8301684	-0.8083379
69.1150436	-0.0109139	-0.4441538	36.5285950	20.8134079	0.8206857	-0.8582314
69.9004364	0.4391052	0.0107323	36.9786148	21.2682934	0.8106982	-0.9114082
70.6858368	-0.0095979	0.4140679	36.5299110	21.6716290	0.8206561	-0.8583879
71.4712372	-0.4095726	0.0094376	36.1299362	21.2669983	0.8297411	-0.8105739
72.2566299	-0.0102046	-0.4246245	36.5293045	20.8329353	0.8206697	-0.8583160
73.0420303	0.4200068	0.0100381	36.9595146	21.2675991	0.8111171	-0.9091644
73.8274307	-0.0090070	0.3966545	36.5305061	21.6542149	0.8206428	-0.8584585
74.6128311	-0.3925286	0.0088557	36.1469803	21.2664165	0.8293499	-0.8126222
75.3982239	-0.0095630	-0.4067361	36.5299454	20.8508244	0.8206553	-0.8583920
76.1836243	0.4024961	0.0094156	36.9420052	21.2669754	0.8115016	-0.9071064
76.9690247	-0.0084656	0.3806503	36.5310440	21.6382103	0.8206307	-0.8585226
77.7544174	-0.3768499	0.0083369	36.1626587	21.2658978	0.8289903	-0.8145053
78.5398178	-0.0089857	-0.3902901	36.5305214	20.8672714	0.8206424	-0.8584604
79.3252182	0.3863834	0.0088547	36.9258919	21.2664146	0.8118557	-0.9052117
80.1106186	-0.0079807	0.3658908	36.5315285	21.6234512	0.8206198	-0.8585804
80.8960114	-0.3623789	0.0078620	36.1771317	21.2654228	0.8286587	-0.8162431
81.6814117	-0.0084639	-0.3751190	36.5310440	20.8824425	0.8206307	-0.8585226
82.4668121	0.3715079	0.0083475	36.9110184	21.2659073	0.8121828	-0.9034622
83.2522049	-0.0075354	0.3522363	36.5319748	21.6097965	0.8206097	-0.8586333
84.0376053	-0.3489809	0.0074307	36.1905289	21.2649918	0.8283519	-0.8178512
84.8230057	-0.0079905	-0.3610804	36.5315170	20.8964806	0.8206201	-0.8585787
85.6083984	0.3577328	0.0078812	36.8972435	21.2654419	0.8124861	-0.9018409
86.3937988	-0.0071347	0.3395666	36.5323753	21.5971279	0.8206007	-0.8586810
87.1791992	-0.3365408	0.0070373	36.2029686	21.2645988	0.8280673	-0.8193436
87.9645996	-0.0075594	-0.3480521	36.5319481	20.9095078	0.8206103	-0.8586302
88.7499924	0.3449399	0.0074616	36.8844490	21.2650223	0.8127679	-0.9003348
89.5353928	-0.0067684	0.3277787	36.5327415	21.5853386	0.8205925	-0.8587244
90.3207932	-0.3249591	0.0066775	36.2145500	21.2642384	0.8278025	-0.8207328
91.1061859	-0.0071708	-0.3359287	36.5323372	20.9216328	0.8206016	-0.8586765
91.8915863	0.3330283	0.0070780	36.8725357	21.2646389	0.8130305	-0.8989318
92.6769867	-0.0064327	0.3167838	36.5330772	21.5743446	0.8205850	-0.8587642
93.4623871	-0.3141500	0.0063474	36.2253571	21.2639084	0.8275555	-0.8220285
94.2477798	-0.0068096	-0.3246197	36.5326996	20.9329414	0.8205935	-0.8587194
95.0331802	0.3219100	0.0067261	36.8614197	21.2642860	0.8132756	-0.8976224
95.8185806	-0.0061239	0.3065044	36.5333862	21.5640659	0.8205780	-0.8588012
96.6039734	-0.3040383	0.0060481	36.2354698	21.2636089	0.8273246	-0.8232408
97.3893738	-0.0064776	-0.3140456	36.5330315	20.9435158	0.8205860	-0.8587589

133.5176849	-0.0037433	0.2206601	36.5357666	21.4782200	0.8205246	-0.8590841
134.3030853	-0.2193809	0.0037124	36.3201294	21.2612724	0.8253961	-0.8333758
135.0884857	-0.0039409	-0.2257294	36.5355682	21.0318317	0.8205290	-0.8590605
135.8738861	0.2244135	0.0039089	36.7639236	21.2614689	0.8154324	-0.8861202
136.6592865	-0.0036202	0.2156310	36.5358887	21.4731922	0.8205218	-0.8590986
137.4446869	-0.2144097	0.0035835	36.3250999	21.2611446	0.8252832	-0.8339702
138.2300873	-0.0038018	-0.2205569	36.5357056	21.0370045	0.8205259	-0.8590769
139.0154724	0.2193003	0.0037729	36.7588081	21.2613335	0.8155459	-0.8855162
139.8008728	-0.0034976	0.2108267	36.5360107	21.4683876	0.8205191	-0.8591131
140.5862732	-0.2096590	0.0034680	36.3298492	21.2610283	0.8251753	-0.8345379
141.3716736	-0.0036771	-0.2156154	36.5358315	21.0419445	0.8205231	-0.8590918
142.1570740	0.2144142	0.0036510	36.7539215	21.2612114	0.8156543	-0.8849385
142.9424744	-0.0033878	0.2062321	36.5361214	21.4637928	0.8205166	-0.8591264
143.7278748	-0.2051150	0.0033526	36.3343925	21.2609138	0.8250721	-0.8350810
144.5132599	-0.0035593	-0.2108901	36.5359497	21.0466709	0.8205205	-0.8591059
145.2986603	0.2097409	0.0035293	36.7492485	21.2610893	0.8157580	-0.8843864
314.1591797	-0.0011151	-0.0965002	36.5383949	21.1610603	0.8204656	-0.8593965
314.9445801	0.0962590	0.0010780	36.6357689	21.2586384	0.8182849	-0.8709548
471.2387695	-0.0006121	-0.0642021	36.5388985	21.1933594	0.8204542	-0.8594564
472.0241699	0.0640954	0.0005776	36.6036034	21.2581387	0.8190039	-0.8671401
628.3183594	-0.0004024	-0.0480928	36.5391083	21.2094669	0.8204495	-0.8594813
629.1037598	0.0480331	0.0003687	36.5875435	21.2579288	0.8193634	-0.8652343
785.3981934	-0.0002733	-0.0384425	36.5392342	21.2191181	0.8204467	-0.8594962
786.1835938	0.0384038	0.0002777	36.5779114	21.2578392	0.8195792	-0.8640909
942.4777832	-0.0002102	-0.0320156	36.5392990	21.2255459	0.8204452	-0.8595040
943.2631836	0.0319889	0.0002084	36.5714989	21.2577686	0.8197229	-0.8633294
10**99	0.0000000	0.0000000	36.5395090	21.2575610	0.8204405	-0.85952902
INFINITY	0.0000000	0.0000000	36.5395090	21.2575610	3.2818500	5.16118730

A.5 METHOD OF MOMENTS COMBINED WITH GEOMETRICAL THEORY OF DIFFRACTION

TABLE A5-1 $2\pi a/\lambda = 20.0$, $h/\lambda = 0.25$, $b/\lambda = 10^{-6}$

AWADALLA RESULT
EPSLN= 20.00000000 (NORMALIZED GROUNDPLANE RADIUS)
MONOPLE LENGTH= 0.25000000 (WAVELENGTH)
MONOPLE RADIUS= 0.00000100 (WAVELENGTH)
INPUT IMPEDANCE= 0.39301902BE+02 +j 0.20170610 4E+02 (OHMS)

ELEVATION ANGLE (DEG)	DIRECTIVITY (NUMERIC)	DIRECTIVITY (dBi)	RELATIVE POWER (dB)	ELEVATION ANGLE (DEG)	DIRECTIVITY (NUMERIC)	DIRECTIVITY (dBi)	RELATIVE POWER (dB)
0	0.00000	-INFINITE	-INFINITE				
1	0.06796	-11.67747	-17.72616	45	0.47273	-3.25390	-9.30259
2	0.24612	-6.08851	-12.13720	46	0.41968	-3.77077	-9.81946
3	0.46721	-3.30488	-9.35356	47	0.39627	-4.02008	-10.06877
4	0.64815	-1.88322	-7.93190	48	0.39948	-3.98501	-10.03370
5	0.72163	-1.41685	-7.46554	49	0.42857	-3.67973	-9.72844
6	0.66119	-1.79673	-7.84542	50	0.48542	-3.13881	-9.18750
7	0.49049	-3.09366	-9.14235	51	0.57395	-2.41129	-8.45998
8	0.27338	-5.62909	-11.67778	52	0.69883	-1.55627	-7.60496
9	0.09030	-10.43371	-16.48240	53	0.86399	-0.63489	-6.68358
10	0.00793	-21.00809	-27.05678	54	1.07116	0.29833	-5.75014
11	0.05607	-12.51250	-18.56119	55	1.31888	1.20206	-4.84663
12	0.21974	-6.58088	-12.62956	56	1.60211	2.04691	-4.00177
13	0.44608	-3.50587	-9.55456	57	1.91237	2.81572	-3.23297
14	0.66481	-1.77302	-7.82170	58	2.23848	3.49953	-2.54916
15	0.81272	-0.90058	-6.94927	59	2.56756	4.09521	-1.95348
16	0.85329	-0.68901	-6.73770	60	2.88624	4.60332	-1.44536
17	0.78509	-1.05078	-7.09947	61	3.18178	5.02670	-1.02198
18	0.63734	-1.95629	-8.00498	62	3.44309	5.36949	-0.67920
19	0.45585	-3.41174	-9.46043	63	3.66141	5.63649	-0.41220
20	0.28575	-5.44013	-11.48882	64	3.83072	5.83280	-0.21588
21	0.15747	-8.02805	-14.07674	65	3.94784	5.96359	-0.08509
22	0.08068	-10.93260	-16.98129	66	4.01229	6.03393	-0.01476
23	0.04696	-13.28296	-19.33165	67	4.02595	6.04869	0.00000
24	0.03888	-14.10309	-20.15178	68	3.99261	6.01257	-0.03612
25	0.04090	-13.88312	-19.93181	69	3.91742	5.93000	-0.11869
26	0.04763	-13.22128	-19.26997	70	3.80641	5.80516	-0.24353
27	0.06646	-11.77436	-17.82305	71	3.66605	5.64198	-0.40671
28	0.11410	-9.42717	-15.47585	72	3.50277	5.44411	-0.60458
29	0.20892	-6.80028	-12.84897	73	3.32974	5.21496	-0.83373
30	0.36230	-4.40930	-10.45799	74	3.13158	4.95763	-1.09105
31	0.57232	-2.42364	-8.47233	75	2.93426	4.67499	-1.37370
32	0.82178	-0.85246	-6.90115	76	2.73502	4.38961	-1.67908
33	1.08125	0.33926	-5.70940	77	2.53733	4.09378	-2.00491
34	1.31575	1.19172	-4.85697	78	2.34386	3.69949	-2.34919
35	1.49288	1.74024	-4.30845	79	2.15698	3.33846	-2.71023
36	1.59002	2.01404	-4.03465	80	1.97791	2.96206	-3.08663
37	1.59865	2.03752	-4.01116	81	1.80774	2.57137	-3.47732
38	1.52488	1.83236	-4.21632	82	1.64707	2.16712	-3.88157
39	1.38678	1.42007	-4.62862	83	1.49615	1.74774	-4.30095
40	1.20929	0.82529	-5.22339	84	1.35497	1.31929	-4.72940
41	1.01860	0.08005	-5.96864	85	1.22335	0.87551	-5.17318
42	0.83732	-0.77101	-6.81980	86	1.10099	0.41782	-5.63087
43	0.68137	-1.66615	-7.71494	87	0.98749	-0.05468	-6.10335
44	0.55920	-2.52435	-8.57304	88	0.88248	-0.54301	-6.59172

89	0.78549	-1.04857	-7.09726	134	0.20692	-6.84207	-12.89075
90	0.69622	-1.57253	-7.62122	135	0.14450	-8.40143	-14.45012
91	0.61434	-2.11591	-8.16460	136	0.08112	-10.90860	-16.95728
92	0.53962	-2.67910	-8.72779	137	0.03067	-15.13315	-21.18184
93	0.47193	-3.26121	-9.30990	138	0.00458	-23.39319	-29.44189
94	0.41123	-3.85919	-9.90788	139	0.00877	-20.57190	-26.62059
95	0.35756	-4.46647	-10.51516	140	0.04160	-13.80860	-19.85729
96	0.31109	-5.07113	-11.11982	141	0.09375	-10.28045	-16.32914
97	0.27203	-5.65377	-11.70246	142	0.15012	-8.23576	-14.28444
98	0.24068	-6.18564	-12.23433	143	0.19379	-7.12669	-13.17537
99	0.21733	-6.62873	-12.67742	144	0.21090	-6.75930	-12.80799
100	0.20230	-6.94002	-12.98871	145	0.19311	-7.09717	-13.14586
101	0.19581	-7.08158	-13.13027	146	0.15030	-8.23055	-14.27923
102	0.19798	-7.03073	-13.07942	147	0.09012	-10.45171	-16.50040
103	0.20873	-6.80419	-12.85288	148	0.03442	-14.63222	-20.68091
104	0.22770	-6.42630	-12.47499	149	0.00300	-25.23113	-31.27982
105	0.25423	-5.94781	-11.99650	150	0.00881	-20.54938	-26.59806
106	0.28720	-5.41809	-11.46678	151	0.05272	-12.77989	-18.82858
107	0.32510	-4.87985	-10.92854	152	0.12206	-9.13432	-15.18301
108	0.36589	-4.36650	-10.41519	153	0.19391	-7.12389	-13.17258
109	0.40710	-3.90301	-9.95170	154	0.24268	-6.14973	-12.19842
110	0.44588	-3.50811	-9.55680	155	0.24939	-6.03114	-12.07983
111	0.47901	-3.19654	-9.24523	156	0.20970	-6.78402	-12.83271
112	0.50337	-2.98112	-9.02980	157	0.13696	-8.63419	-14.68288
113	0.51591	-2.87424	-8.92293	158	0.05879	-12.30668	-18.35537
114	0.51411	-2.88940	-8.93809	159	0.00737	-21.20760	-27.25629
115	0.49631	-3.04248	-9.09117	160	0.00782	-21.06523	-27.11391
116	0.46200	-3.35354	-9.40223	161	0.06544	-11.84184	-17.89052
117	0.41219	-3.84904	-9.89773	162	0.16323	-7.87204	-13.92073
118	0.34949	-4.56565	-10.61434	163	0.26562	-5.75747	-11.80616
119	0.27820	-5.55648	-11.60517	164	0.33154	-4.79458	-10.84327
120	0.20404	-6.90292	-12.95161	165	0.33138	-4.79670	-10.84539
121	0.13372	-8.73790	-14.78659	166	0.26114	-5.83118	-11.87987
122	0.07426	-11.29272	-17.34140	167	0.14774	-8.30502	-14.35371
123	0.03201	-14.94763	-20.99632	168	0.04190	-13.77805	-19.82674
124	0.01174	-19.30150	-25.35019	169	0.00020	-37.02296	-43.07164
125	0.01569	-18.04321	-24.09189	170	0.06237	-12.03005	-18.09874
126	0.04282	-13.68314	-19.73183	171	0.25273	-6.33144	-12.38013
127	0.08860	-10.52583	-16.57452	172	0.47380	-3.24409	-9.29278
128	0.14525	-8.37898	-14.42767	173	0.71599	-1.45095	-7.49964
129	0.20273	-6.93074	-12.97943	174	0.88100	-0.55025	-6.59894
130	0.25029	-6.01552	-12.06420	175	0.91069	-0.40631	-6.45500
131	0.27836	-5.55393	-11.60261	176	0.79043	-1.02138	-7.07007
132	0.28057	-5.51954	-11.56823	177	0.55740	-2.53857	-8.58726
133	0.25539	-5.92786	-11.97657	178	0.28966	-5.38113	-11.42982
134	0.20692	-6.84207	-12.89075	179	0.07440	-11.00158	-17.05026
135	0.14450	-8.40143	-14.45012	180	0.00000	-81.87164	-87.92033

A.6 METHOD OF MOMENTS (RICHMOND)—PROXIMITY TO EARTH

A.6.1 QUARTER-WAVE ELEMENTS WITH DISK GROUND PLANES ON FLAT EARTH: ATLAS OF DIRECTIVITY, RADIATION EFFICIENCY, RADIATION RESISTANCE, AND INPUT IMPEDANCE

The computer plots are grouped in subsections corresponding to Cases 2–l0 of Earth classifications in Table 16 of Sec. 8.2 and in an additional subsection Case 12 that compares the computer plots of Case 2 Sea Water with those of Case 5 Medium Dry Ground. Each of the computer plots are compared with the corresponding plots for Table 16 Case 1 Perfect ground and Case 11 free space.

Case	Earth classification	A.6 figure nos.
1	Perfect ground	1–160
2	Sea water (Average Salinity, 20°C)	1–16
3	Fresh water	17–32
4	Wet ground	33–48
5	Medium dry ground	49–64
6	Very dry ground	65–80
7	Pure water, 20°C	81–96
8	Ice (fresh water, −1°C)	97–112
9	Ice (fresh water, −10°C)	112–128
10	Average land (TCI)	129–144
11	Free space	1–160
12	Sea water compared with Medium dry ground	145–160

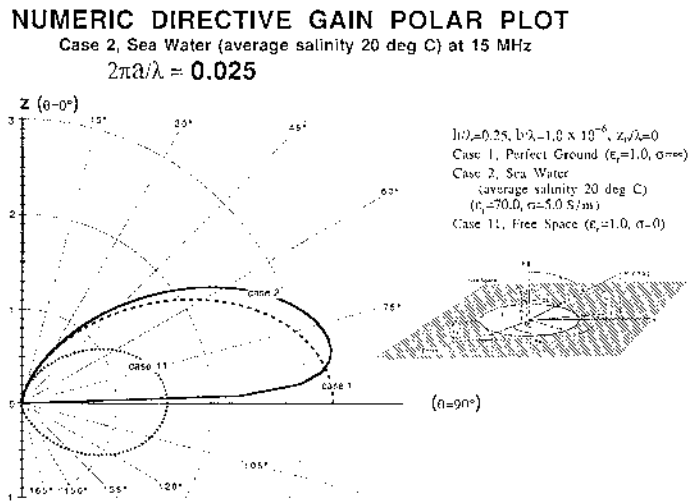
NUMERIC DIRECTIVE GAIN POLAR PLOT
Case 2, Sea Water (average salinity 20 deg C) at 15 MHz
2πa/λ = 0.025
z (θ=0°)
h/λ=0.25, b/λ=1.0 x 10⁻⁶, z_p/λ=0
Case 1, Perfect Ground (ε_r=1.0, σ=∞)
Case 2, Sea Water
(average salinity 20 deg C)
(ε_r=70.0, σ=5.0 S/m)
Case 11, Free Space (ε_r=1.0, σ=0)
case 2
case 11
case 1
(θ=90°)

FIGURE A6-1 Directivity pattern, $2\pi a/\lambda = 0.025$, sea water (average salinity, 20°C).

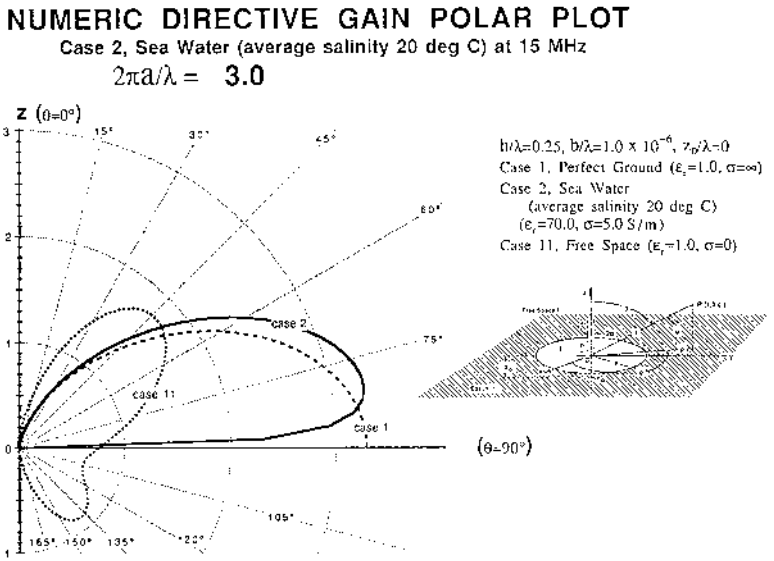
NUMERIC DIRECTIVE GAIN POLAR PLOT
Case 2, Sea Water (average salinity 20 deg C) at 15 MHz
2πa/λ = 3.0
z (θ=0°)
h/λ=0.25, b/λ=1.0 x 10⁻⁶, z_p/λ=0
Case 1, Perfect Ground (ε_r=1.0, σ=∞)
Case 2, Sea Water
(average salinity 20 deg C)
(ε_r=70.0, σ=5.0 S/m)
Case 11, Free Space (ε_r=1.0, σ=0)
case 2
case 11
case 1
(θ=90°)

FIGURE A6-2 Directivity pattern, $2\pi a/\lambda = 3.0$, sea water (average salinity, 20°C).

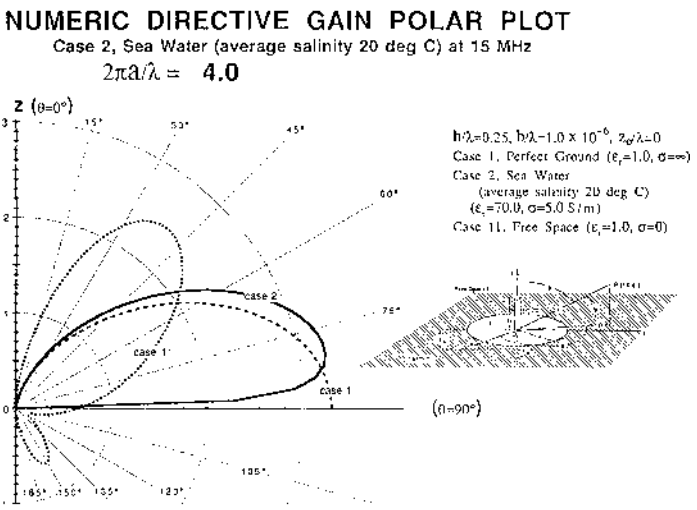
NUMERIC DIRECTIVE GAIN POLAR PLOT
Case 2, Sea Water (average salinity 20 deg C) at 15 MHz
2πa/λ = 4.0
z (θ=0°)
h/λ=0.25, b/λ=1.0 x 10⁻⁶, z₀/λ=0
Case 1. Perfect Ground (εr=1.0, σ=∞)
Case 2. Sea Water
(average salinity 20 deg C)
(εr=70.0, σ=5.0 S/m)
Case 11. Free Space (εr=1.0, σ=0)
case 2
case 1
case 1
(θ=90°)

FIGURE A6-3 Directivity pattern, $2\pi a/\lambda = 4.0$, sea water (average salinity, 20°C).

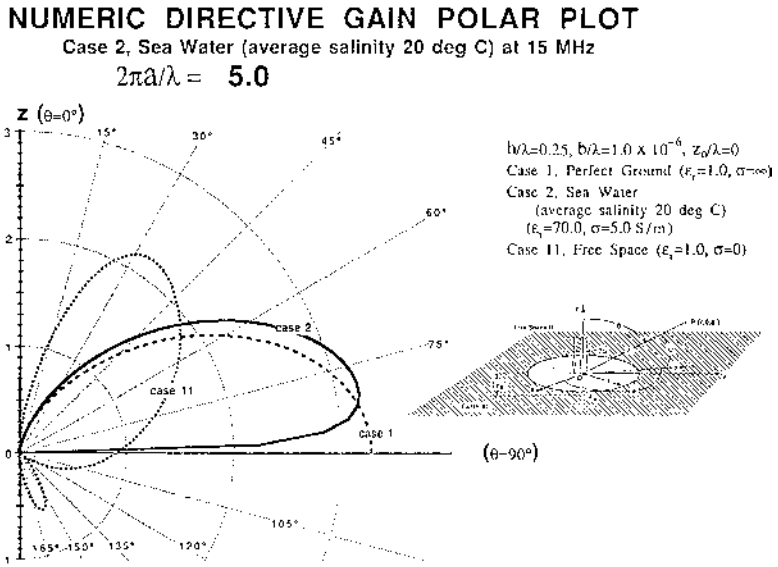
NUMERIC DIRECTIVE GAIN POLAR PLOT
Case 2, Sea Water (average salinity 20 deg C) at 15 MHz
2πa/λ = 5.0
z (θ=0°)
h/λ=0.25, b/λ=1.0 x 10⁻⁶, z₀/λ=0
Case 1. Perfect Ground (εr=1.0, σ=∞)
Case 2. Sea Water
(average salinity 20 deg C)
(εr=70.0, σ=5.0 S/m)
Case 11. Free Space (εr=1.0, σ=0)
case 2
case 11
case 1
(θ=90°)

FIGURE A6-4 Directivity pattern, $2\pi a/\lambda = 5.0$, sea water (average salinity, 20°C).

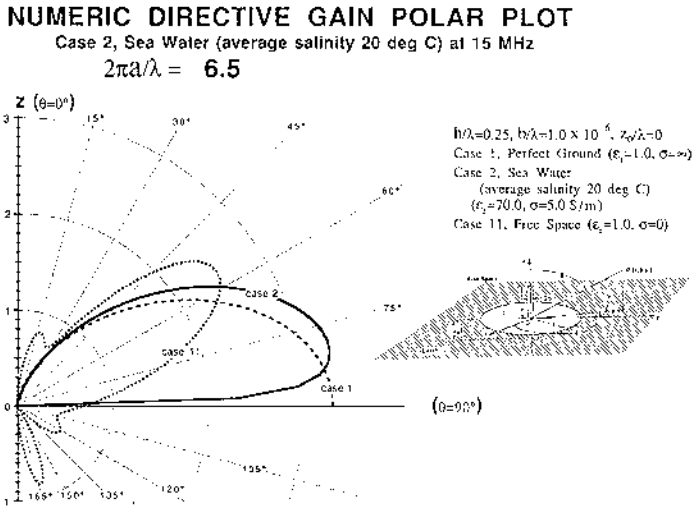
NUMERIC DIRECTIVE GAIN POLAR PLOT
Case 2, Sea Water (average salinity 20 deg C) at 15 MHz
2πa/λ = 6.5
z (θ=0°)
h/λ=0.25, b/λ=1.0 x 10⁻⁶, z₀/λ=0
Case 1, Perfect Ground (ε_r=1.0, σ=∞)
Case 2, Sea Water
(average salinity 20 deg C)
(ε_r=70.0, σ=5.0 S/m)
Case 11, Free Space (ε_r=1.0, σ=0)
case 2
case 11
case 1
(θ=90°)

FIGURE A6-5 Directivity pattern, $2\pi a/\lambda = 6.5$, sea water (average salinity, 20°C).

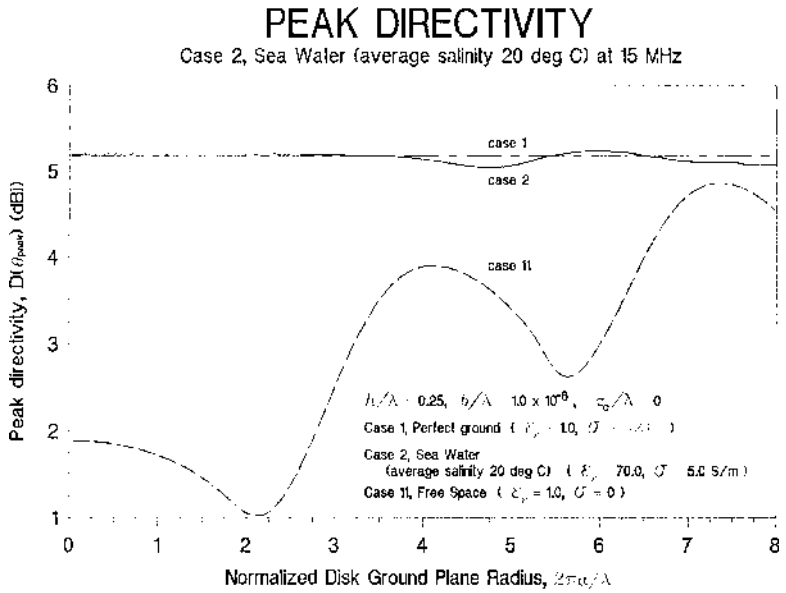
PEAK DIRECTIVITY
Case 2, Sea Water (average salinity 20 deg C) at 15 MHz
Peak directivity, D(θpeak) (dBi)
Normalized Disk Ground Plane Radius, 2πa/λ
case 1
case 2
case 11
h/λ = 0.25, b/λ = 1.0 x 10⁻⁶, z₀/λ = 0
Case 1, Perfect ground (ε_r = 1.0, σ = ∞)
Case 2, Sea Water
(average salinity 20 deg C) (ε_r = 70.0, σ = 5.0 S/m)
Case 11, Free Space (ε_r = 1.0, σ = 0)

FIGURE A6-6 Peak directivity, sea water (average salinity, 20°C).

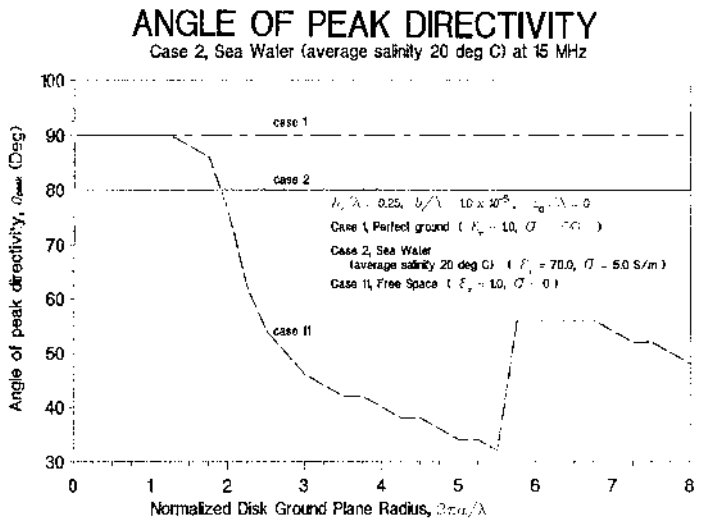
ANGLE OF PEAK DIRECTIVITY
Case 2, Sea Water (average salinity 20 deg C) at 15 MHz
Angle of peak directivity, θ_{max} (Deg)
Normalized Disk Ground Plane Radius, $2\pi a/\lambda$
case 1
case 2
case II
Case 1, Perfect ground
Case 2, Sea Water
(average salinity 20 deg C)
Case II, Free Space

FIGURE A6-7 Angle of incidence of peak directivity, sea water (average salinity, 20°C).

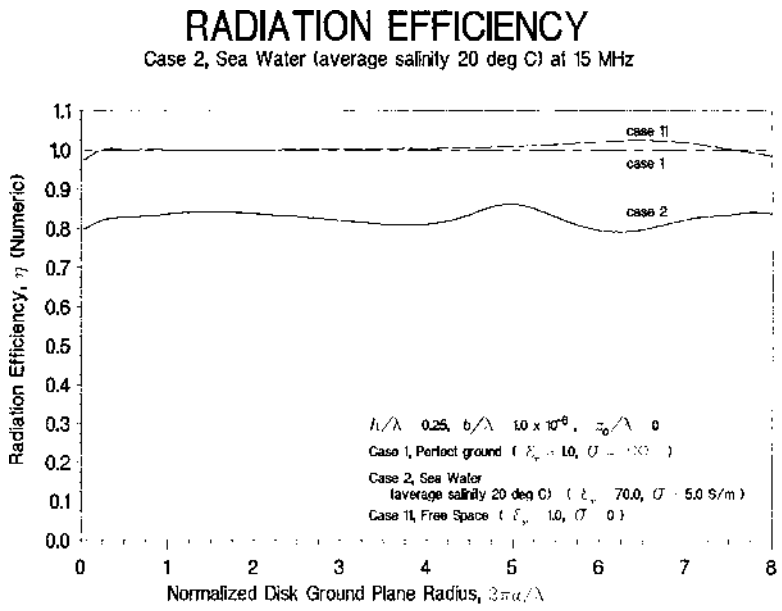
RADIATION EFFICIENCY
Case 2, Sea Water (average salinity 20 deg C) at 15 MHz
Radiation Efficiency, η (Numeric)
Normalized Disk Ground Plane Radius, $2\pi a/\lambda$
case II
case 1
case 2
Case 1, Perfect ground
Case 2, Sea Water
(average salinity 20 deg C)
Case II, Free Space

FIGURE A6-8 Radiation efficiency, sea water (average salinity, 20°C).

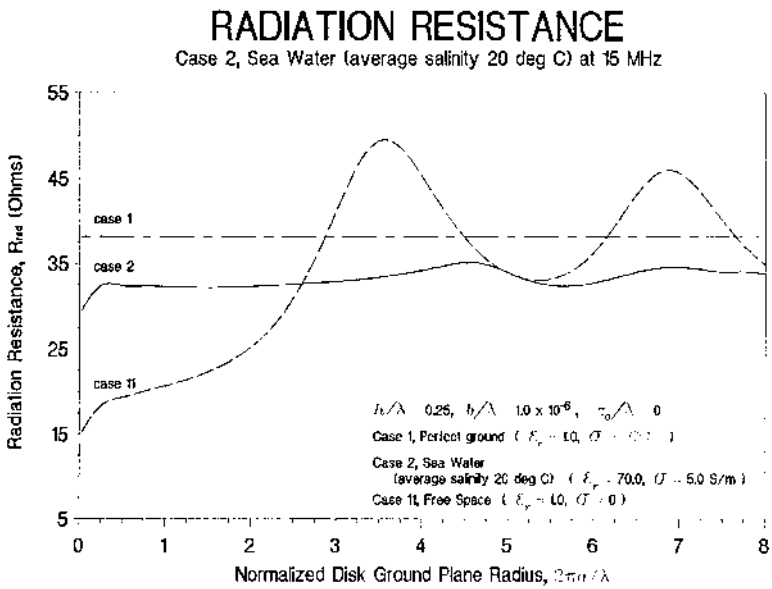

FIGURE A6-9 Radiation resistance, sea water (average salinity, 20°C).

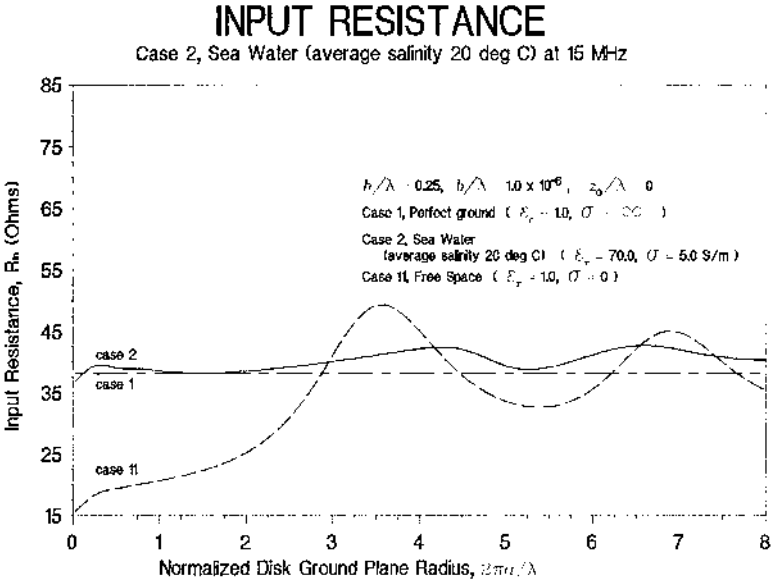

FIGURE A6-10 Input resistance, sea water (average salinity, 20°C).

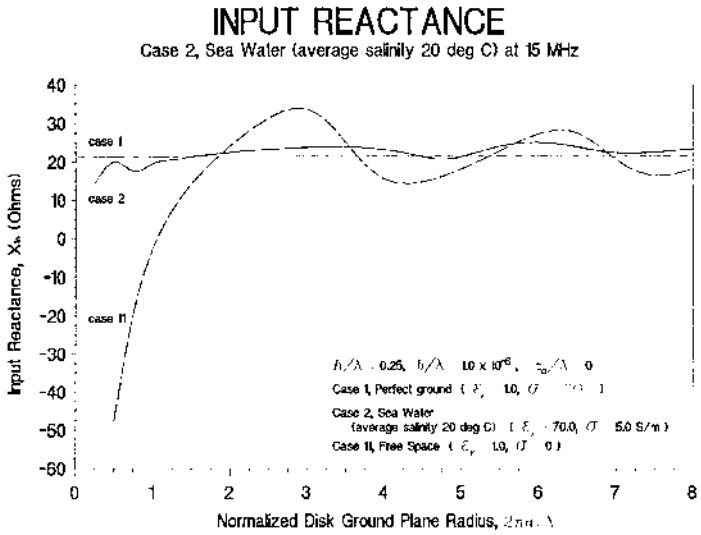
INPUT REACTANCE
Case 2, Sea Water (average salinity 20 deg C) at 15 MHz
Input Reactance, X_{in} (Ohms)
Normalized Disk Ground Plane Radius, $2\pi a/\lambda$
case I
case 2
case II
h/λ = 0.25, b/λ = 1.0 x 10^{-6}, z_o/λ = 0
Case 1, Perfect ground (ε_r = 1.0, σ = ∞)
Case 2, Sea Water
(average salinity 20 deg C) (ε_r = 70.0, σ = 5.0 S/m)
Case II, Free Space (ε_r = 1.0, σ = 0)

FIGURE A6-11 Input reactance, sea water (average salinity, 20°C).

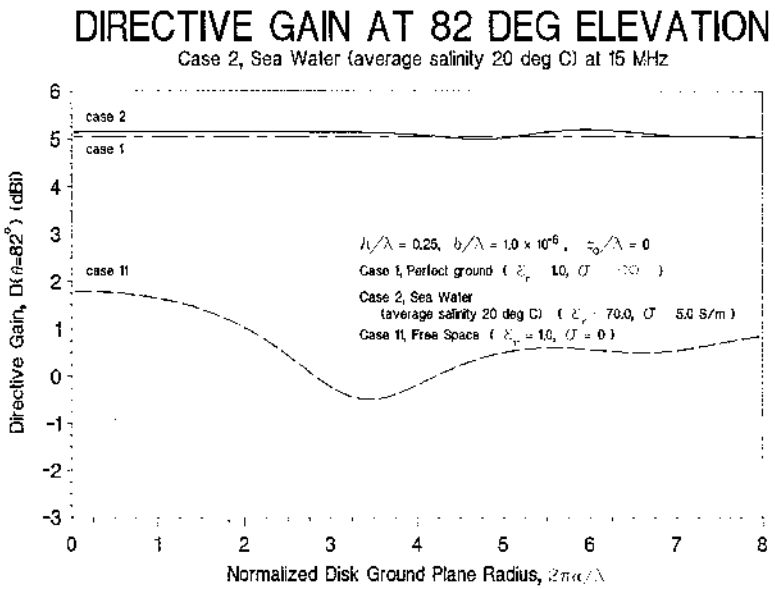
DIRECTIVE GAIN AT 82 DEG ELEVATION
Case 2, Sea Water (average salinity 20 deg C) at 15 MHz
Directive Gain, Dirθ=82°) (dBi)
Normalized Disk Ground Plane Radius, $2\pi a/\lambda$
case 2
case 1
case II
h/λ = 0.25, b/λ = 1.0 x 10^{-6}, z_o/λ = 0
Case 1, Perfect ground (ε_r = 1.0, σ = ∞)
Case 2, Sea Water
(average salinity 20 deg C) (ε_r = 70.0, σ = 5.0 S/m)
Case II, Free Space (ε_r = 1.0, σ = 0)

FIGURE A6-12 Directivity at 8° above the horizon, sea water (average salinity, 20°C).

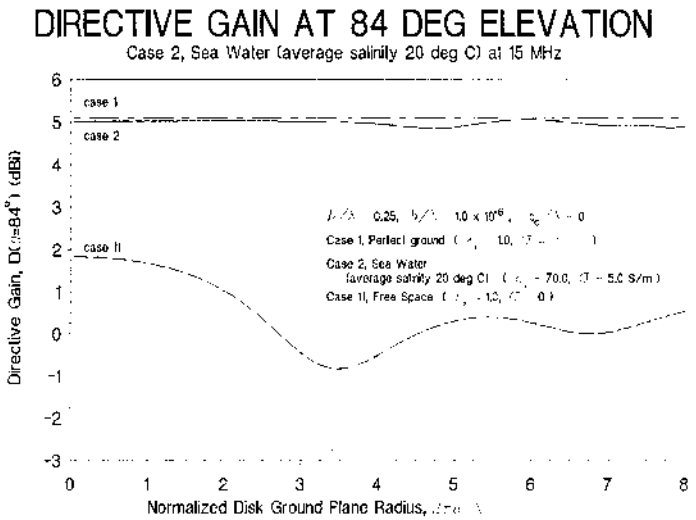
DIRECTIVE GAIN AT 84 DEG ELEVATION
Case 2, Sea Water (average salinity 20 deg C) at 15 MHz
case 1
case 2
case II
Case 1, Perfect ground
Case 2, Sea Water
(average salinity 20 deg C)
Case II, Free Space
Directive Gain, D(θ=84°) (dBi)
Normalized Disk Ground Plane Radius,

FIGURE A6-13 Directivity at 6° above the horizon, sea water (average salinity, 20°C).

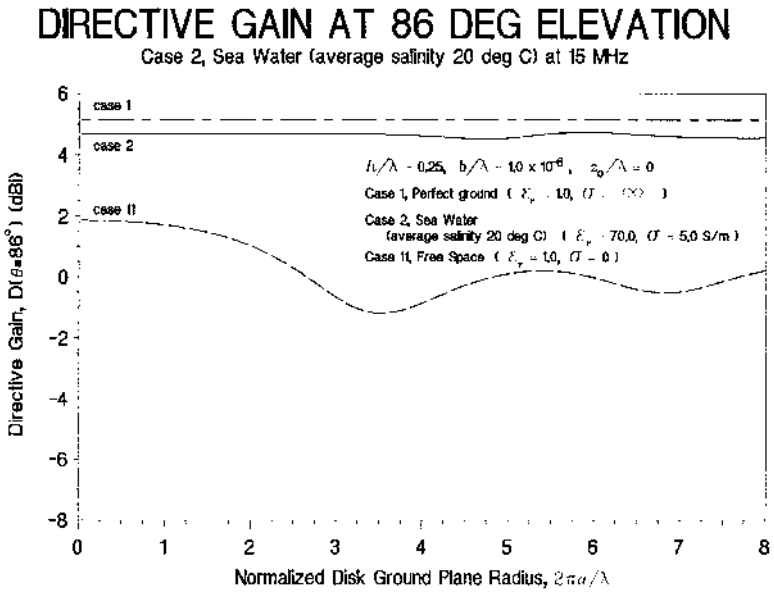
DIRECTIVE GAIN AT 86 DEG ELEVATION
Case 2, Sea Water (average salinity 20 deg C) at 15 MHz
case 1
case 2
case II
Case 1, Perfect ground
Case 2, Sea Water
(average salinity 20 deg C)
Case II, Free Space
Directive Gain, D(θ=86°) (dBi)
Normalized Disk Ground Plane Radius, 2πa/λ

FIGURE A6-14 Directivity at 4° above the horizon, sea water (average salinity, 20°C).

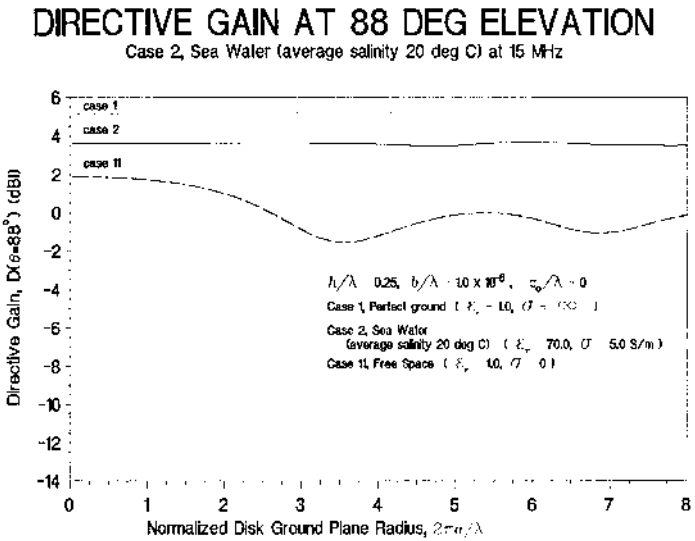
DIRECTIVE GAIN AT 88 DEG ELEVATION
Case 2, Sea Water (average salinity 20 deg C) at 15 MHz
case 1
case 2
case 11
Directive Gain, D(θ=88°) (dBi)
h/λ 0.25, b/λ 1.0 x 10⁻⁶, z₀/λ 0
Case 1, Perfect ground (ε_r 1.0, σ ∞)
Case 2, Sea Water
(average salinity 20 deg C) (ε_r 70.0, σ 5.0 S/m)
Case 11, Free Space (ε_r 1.0, σ 0)
Normalized Disk Ground Plane Radius, 2πa/λ

FIGURE A6-15 Directivity at 2° above the horizon, sea water (average salinity, 20°C).

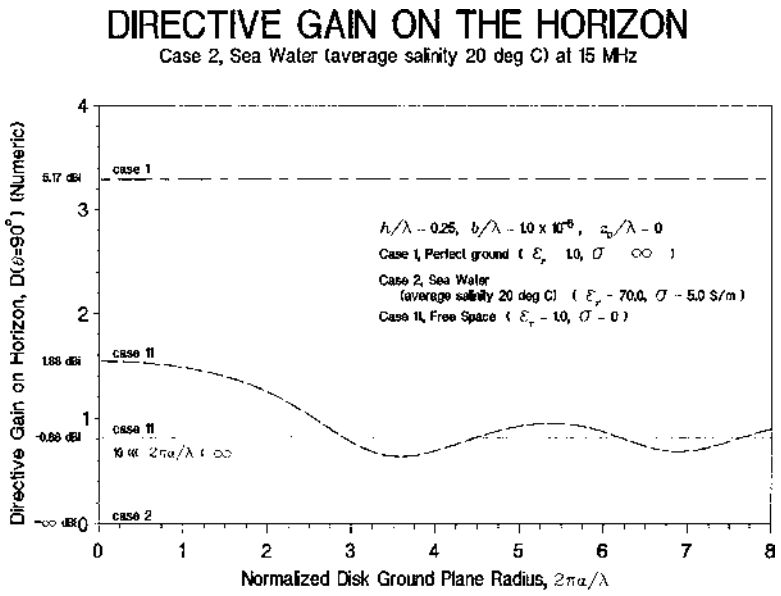
DIRECTIVE GAIN ON THE HORIZON
Case 2, Sea Water (average salinity 20 deg C) at 15 MHz
Directive Gain on Horizon, D(θ=90°) (Numeric)
5.17 dBi
case 1
1.88 dBi
case 11
-0.88 dBi
case 11
10 ≪ 2πa/λ ≪ ∞
-∞ dBi
case 2
h/λ 0.25, b/λ 1.0 x 10⁻⁶, z₀/λ 0
Case 1, Perfect ground (ε_r 1.0, σ ∞)
Case 2, Sea Water
(average salinity 20 deg C) (ε_r 70.0, σ 5.0 S/m)
Case 11, Free Space (ε_r 1.0, σ 0)
Normalized Disk Ground Plane Radius, 2πa/λ

FIGURE A6-16 Directivity on the horizon, sea water (average salinity, 20°C).

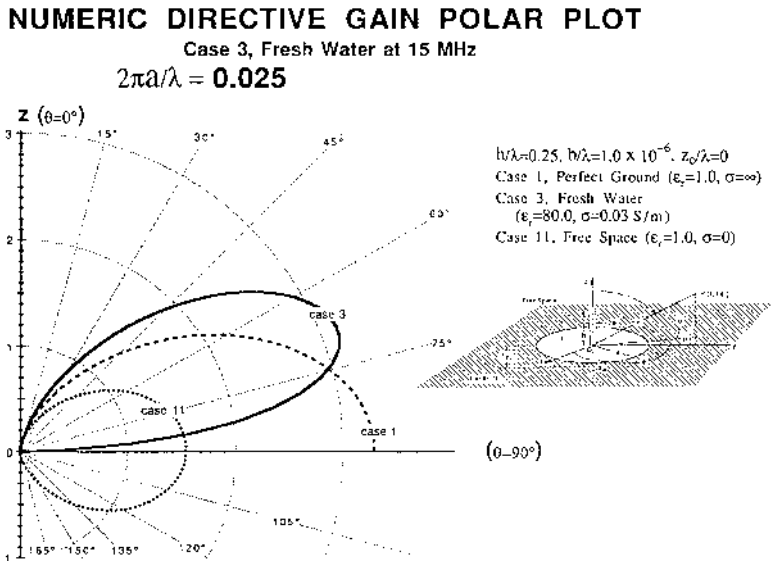

FIGURE A6-17 Directivity pattern, $2\pi a/\lambda = 0.025$, fresh water.

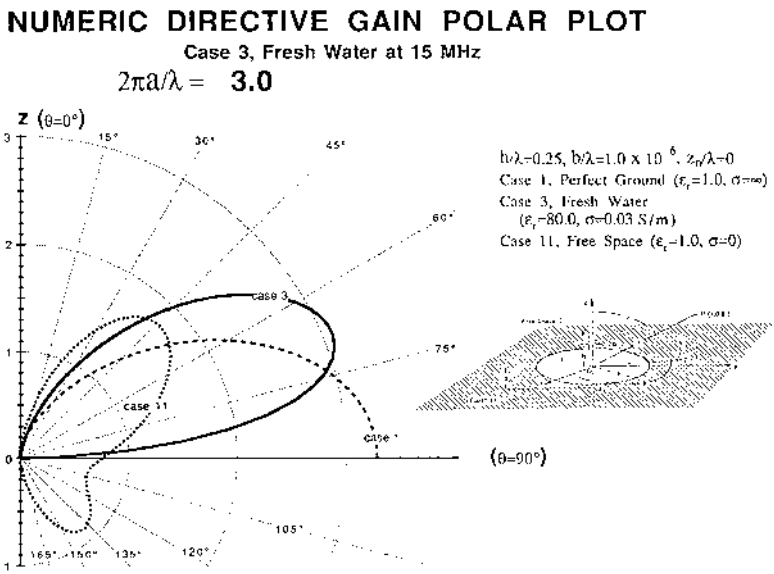

FIGURE A6-18 Directivity pattern, $2\pi a/\lambda = 3.0$, fresh water.

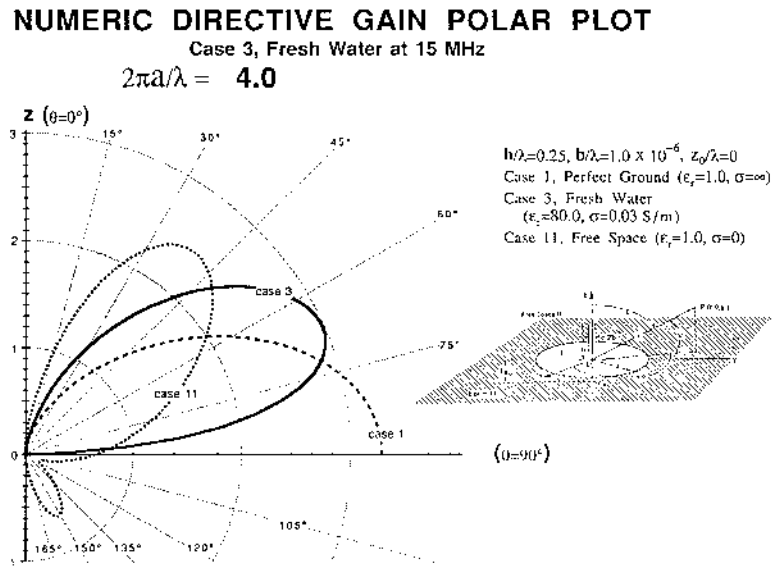

FIGURE A6-19 Directivity pattern, $2\pi a/\lambda = 4.0$, fresh water.

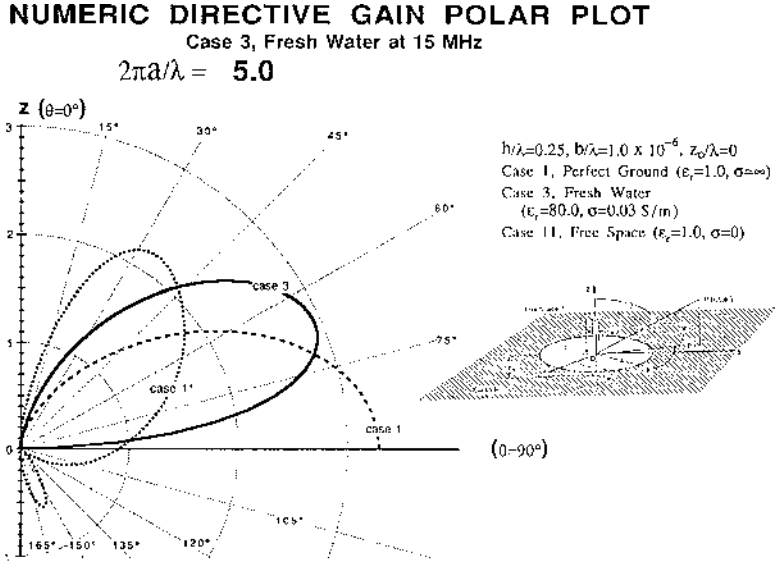

FIGURE A6-20 Directivity pattern, $2\pi a/\lambda = 5.0$, fresh water.

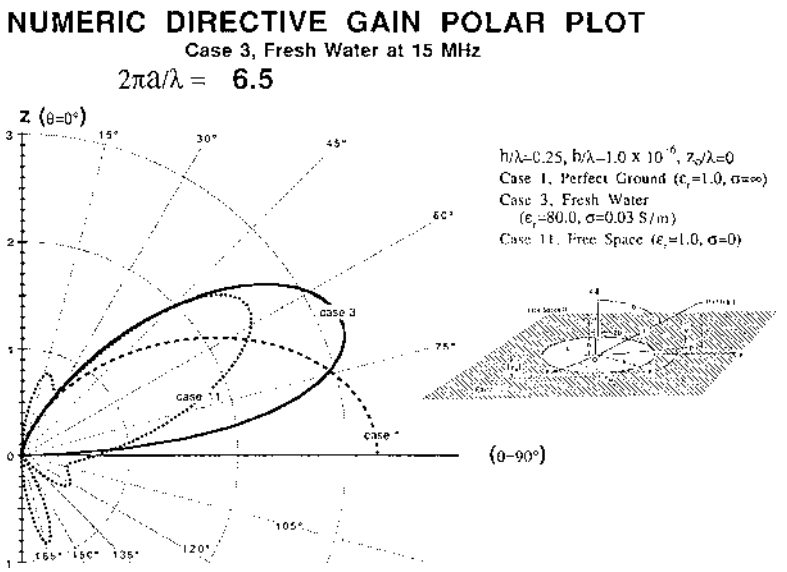

FIGURE A6-21 Directivity pattern, $2\pi a/\lambda = 6.5$, fresh water.

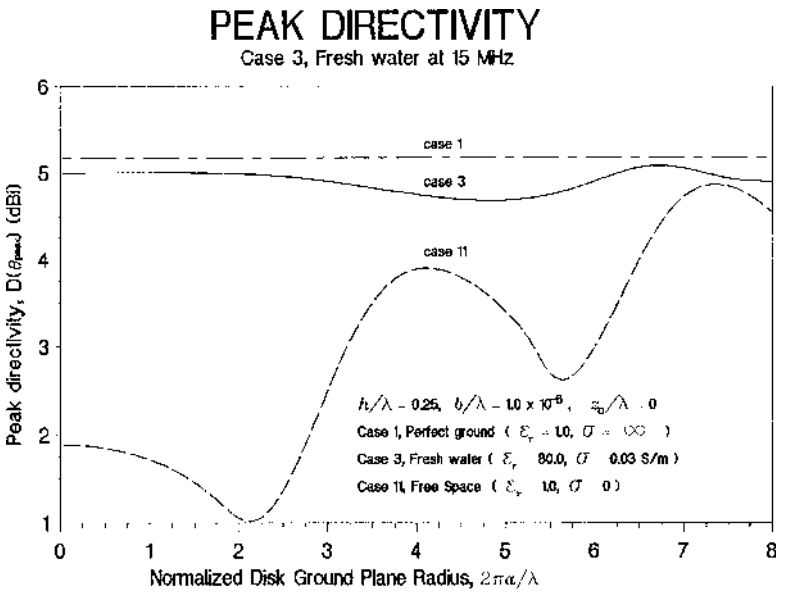
PEAK DIRECTIVITY
Case 3, Fresh water at 15 MHz
Peak directivity, D(θpeak) (dBi)
Normalized Disk Ground Plane Radius, 2πa/λ
case 1
case 3
case 11
h/λ = 0.25, b/λ = 1.0 x 10⁻⁶, z₀/λ = 0
Case 1, Perfect ground (εr = 1.0, σ = ∞)
Case 3, Fresh water (εr = 80.0, σ = 0.03 S/m)
Case 11, Free Space (εr = 1.0, σ = 0)

FIGURE A6-22 Peak directivity, fresh water.

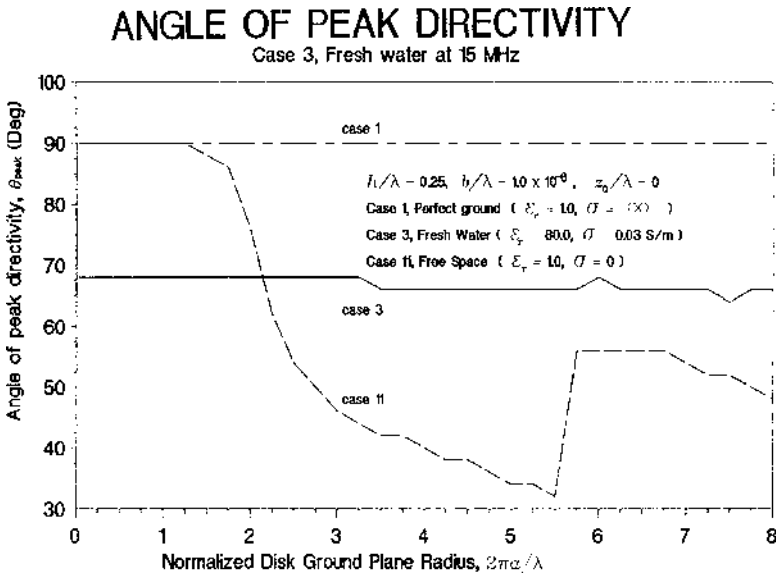
ANGLE OF PEAK DIRECTIVITY
Case 3, Fresh water at 15 MHz
Angle of peak directivity, θ_{max} (Deg)
Normalized Disk Ground Plane Radius, $2\pi a/\lambda$
case 1
case 3
case 11
h/λ = 0.25, b/λ = 1.0 x 10^{-6}, z_0/λ = 0
Case 1, Perfect ground (ε_r = 1.0, σ = ∞)
Case 3, Fresh Water (ε_r = 80.0, σ = 0.03 S/m)
Case 11, Free Space (ε_r = 1.0, σ = 0)

FIGURE A6-23 Angle of incidence of peak directivity, fresh water.

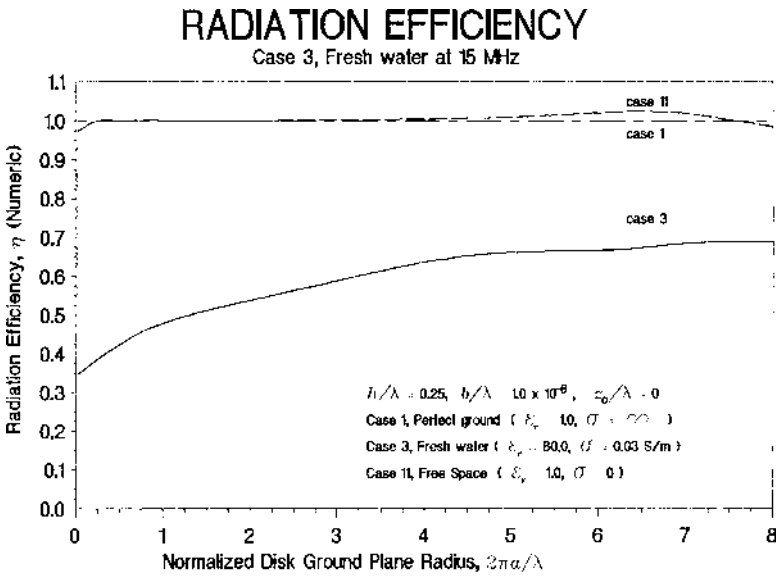
RADIATION EFFICIENCY
Case 3, Fresh water at 15 MHz
Radiation Efficiency, η (Numeric)
Normalized Disk Ground Plane Radius, $2\pi a/\lambda$
case 11
case 1
case 3
h/λ = 0.25, b/λ = 1.0 x 10^{-6}, z_0/λ = 0
Case 1, Perfect ground (ε_r = 1.0, σ = ∞)
Case 3, Fresh water (ε_r = 80.0, σ = 0.03 S/m)
Case 11, Free Space (ε_r = 1.0, σ = 0)

FIGURE A6-24 Radiation efficiency, fresh water.

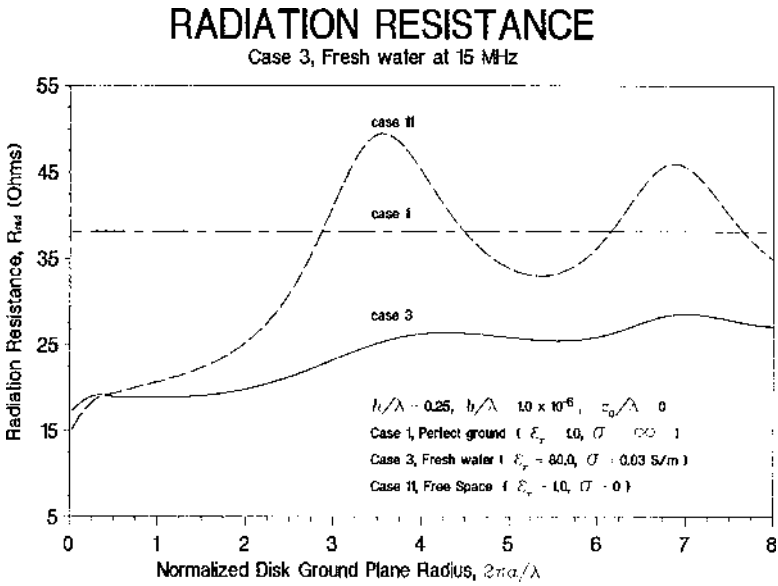
RADIATION RESISTANCE
Case 3, Fresh water at 15 MHz
Radiation Resistance, R_{rad} (Ohms)
Normalized Disk Ground Plane Radius, $2\pi a/\lambda$
case II
case I
case 3
h/λ = 0.25, b/λ = 1.0 x 10^{-6}, z_0/λ = 0
Case 1, Perfect ground (ε_r = 1.0, σ = ∞)
Case 3, Fresh water (ε_r = 80.0, σ = 0.03 S/m)
Case II, Free Space (ε_r = 1.0, σ = 0)

FIGURE A6-25 Radiation resistance, fresh water.

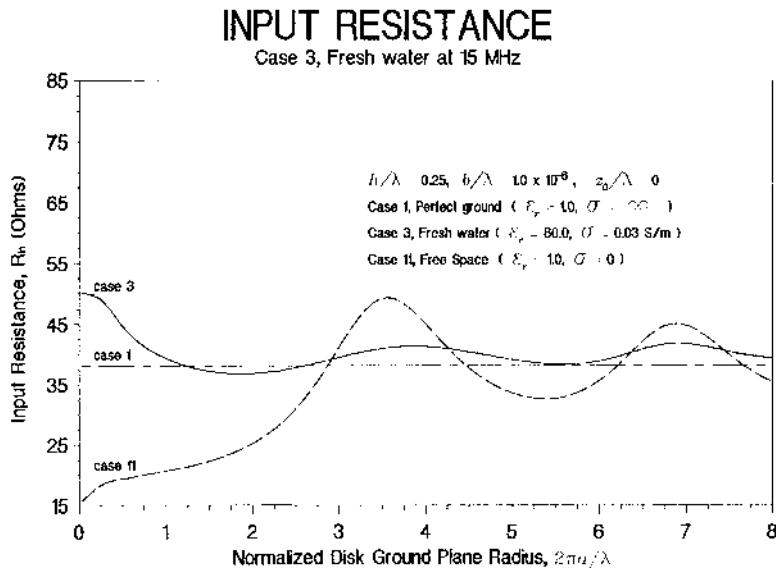
INPUT RESISTANCE
Case 3, Fresh water at 15 MHz
Input Resistance, R_{in} (Ohms)
Normalized Disk Ground Plane Radius, $2\pi a/\lambda$
case 3
case I
case II
h/λ = 0.25, b/λ = 1.0 x 10^{-6}, z_0/λ = 0
Case 1, Perfect ground (ε_r = 1.0, σ = ∞)
Case 3, Fresh water (ε_r = 80.0, σ = 0.03 S/m)
Case II, Free Space (ε_r = 1.0, σ = 0)

FIGURE A6-26 Input resistance, fresh water.

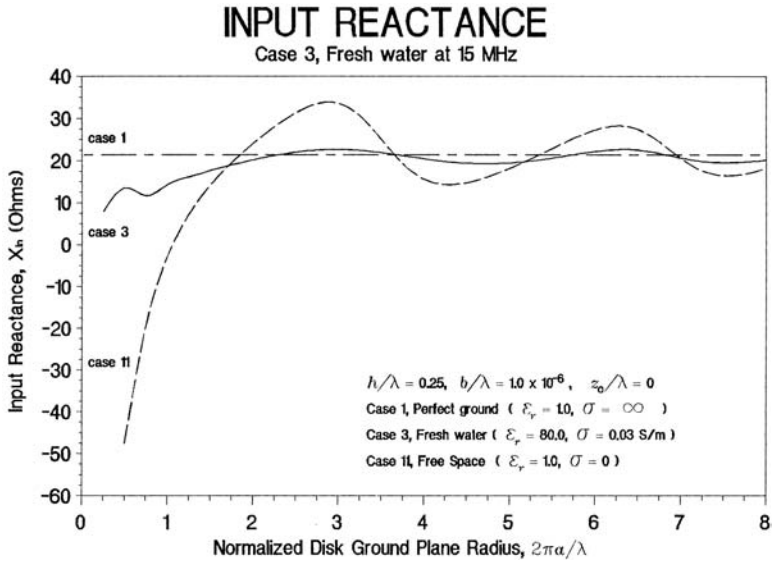
INPUT REACTANCE
Case 3, Fresh water at 15 MHz
Input Reactance, Xin (Ohms)
Normalized Disk Ground Plane Radius, 2πa/λ
case 1
case 3
case 11
h/λ = 0.25, b/λ = 1.0 x 10⁻⁶, z0/λ = 0
Case 1, Perfect ground (εr = 1.0, σ = ∞)
Case 3, Fresh water (εr = 80.0, σ = 0.03 S/m)
Case 11, Free Space (εr = 1.0, σ = 0)

FIGURE A6-27 Input reactance, fresh water.

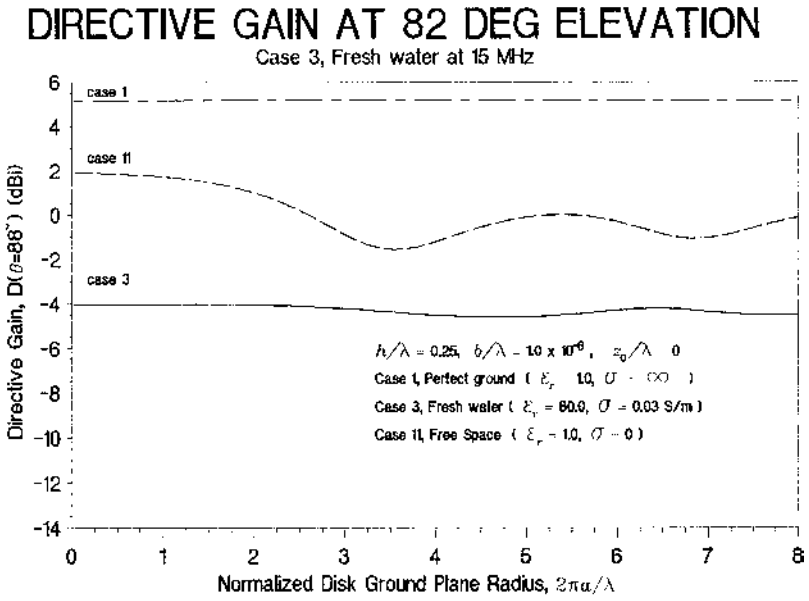
DIRECTIVE GAIN AT 82 DEG ELEVATION
Case 3, Fresh water at 15 MHz
Directive Gain, D(θ=88°) (dBi)
Normalized Disk Ground Plane Radius, 2πa/λ
case 1
case 11
case 3
h/λ = 0.25, b/λ = 1.0 x 10⁻⁶, z0/λ = 0
Case 1, Perfect ground (εr = 1.0, σ = ∞)
Case 3, Fresh water (εr = 80.0, σ = 0.03 S/m)
Case 11, Free Space (εr = 1.0, σ = 0)

FIGURE A6-28 Directivity at 8° above the horizon, fresh water.

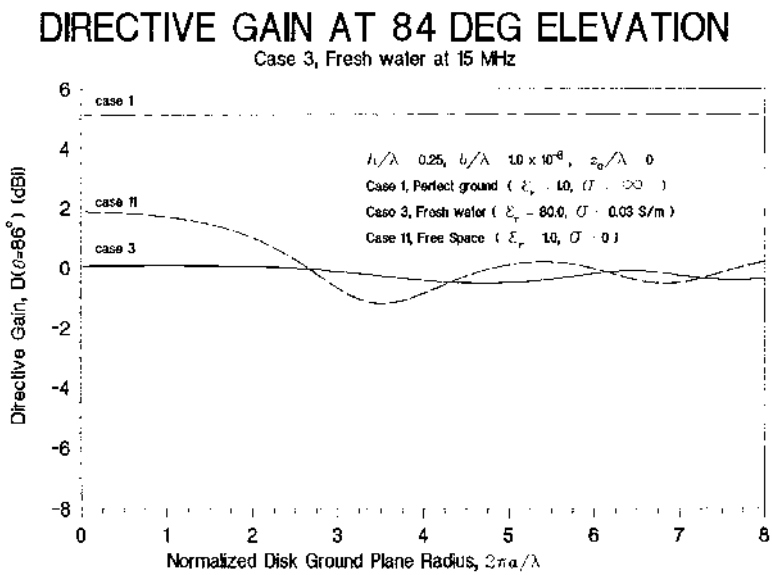
DIRECTIVE GAIN AT 84 DEG ELEVATION
Case 3, Fresh water at 15 MHz
case 1
case II
case 3
Directive Gain, D(θ=86°) (dBi)
Normalized Disk Ground Plane Radius, 2πa/λ

FIGURE A6-29 Directivity at 6° above the horizon, fresh water.

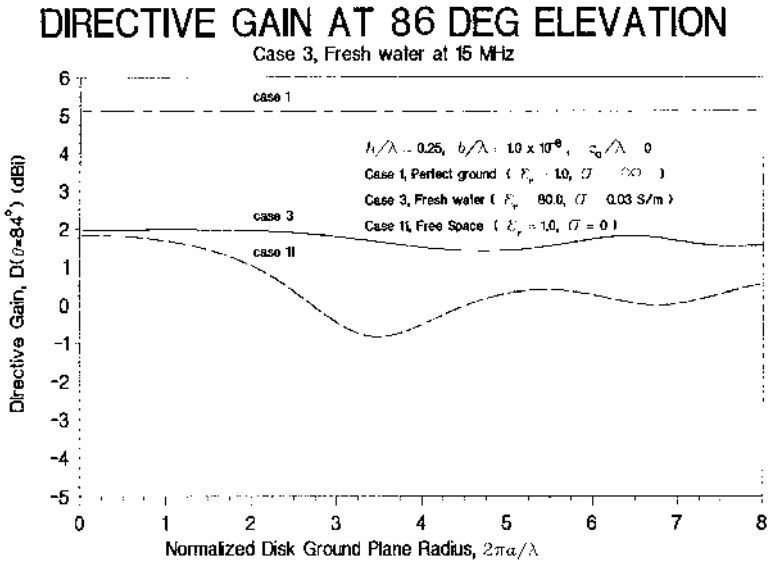
DIRECTIVE GAIN AT 86 DEG ELEVATION
Case 3, Fresh water at 15 MHz
case 1
case 3
case II
Directive Gain, D(θ=84°) (dBi)
Normalized Disk Ground Plane Radius, 2πa/λ

FIGURE A6-30 Directivity at 4° above the horizon, fresh water.

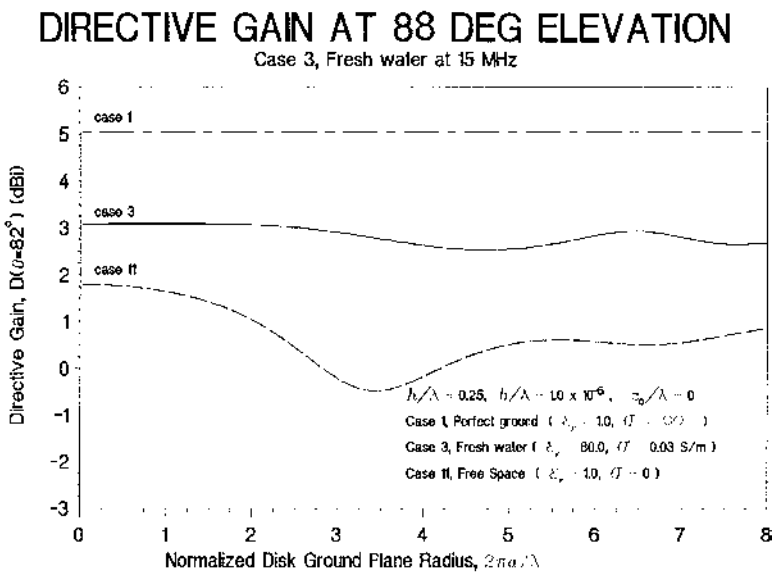
DIRECTIVE GAIN AT 88 DEG ELEVATION
Case 3, Fresh water at 15 MHz
Directive Gain, D(θ=82°) (dBi)
Normalized Disk Ground Plane Radius, 2πa/λ
case I
case 3
case II
h/λ = 0.25, b/λ = 1.0 x 10⁻⁶, σ₀/λ = 0
Case I, Perfect ground (ε_r = 1.0, σ = ∞)
Case 3, Fresh water (ε_r = 80.0, σ = 0.03 S/m)
Case II, Free Space (ε_r = 1.0, σ = 0)

FIGURE A6-31 Directivity at 2° above the horizon, fresh water.

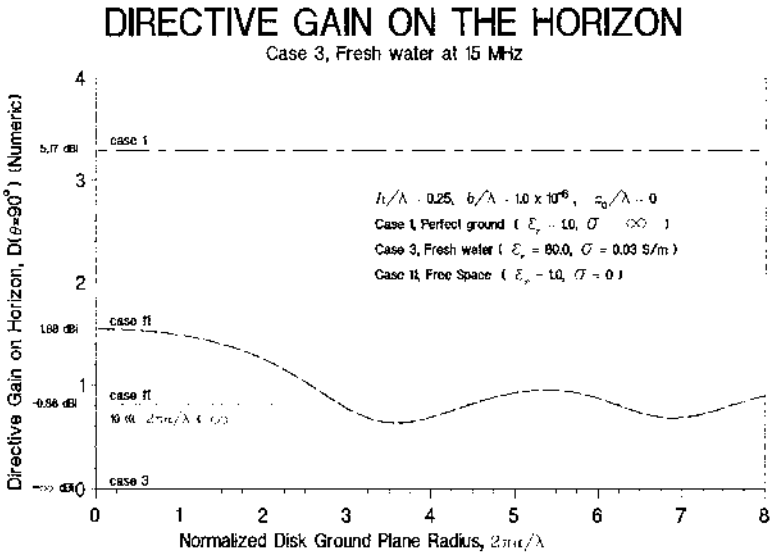
DIRECTIVE GAIN ON THE HORIZON
Case 3, Fresh water at 15 MHz
Directive Gain on Horizon, D(θ=90°) (Numeric)
Normalized Disk Ground Plane Radius, 2πa/λ
5.77 dBi
case I
1.88 dBi
case II
-0.56 dBi
case III
case 3
h/λ = 0.25, b/λ = 1.0 x 10⁻⁶, σ₀/λ = 0
Case I, Perfect ground (ε_r = 1.0, σ = ∞)
Case 3, Fresh water (ε_r = 80.0, σ = 0.03 S/m)
Case II, Free Space (ε_r = 1.0, σ = 0)

FIGURE A6-32 Directivity on the horizon, fresh water.

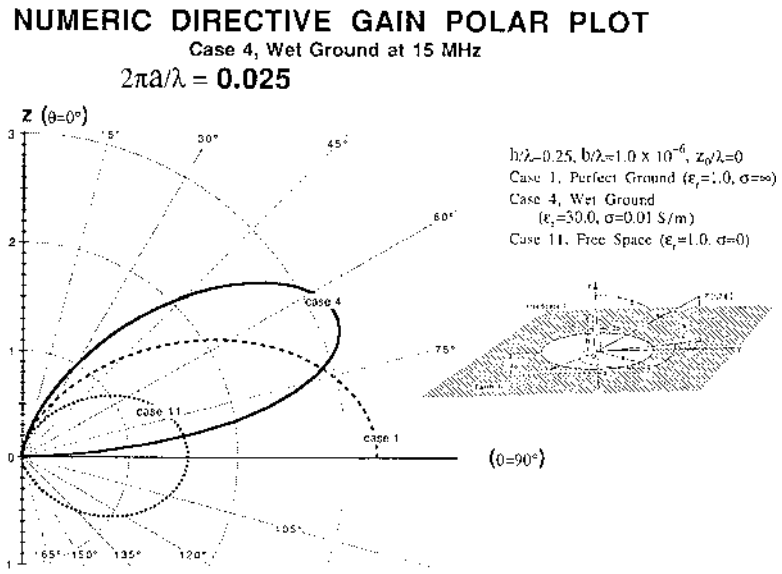

FIGURE A6-33 Directivity pattern, $2\pi a/\lambda = 0.025$, wet ground.

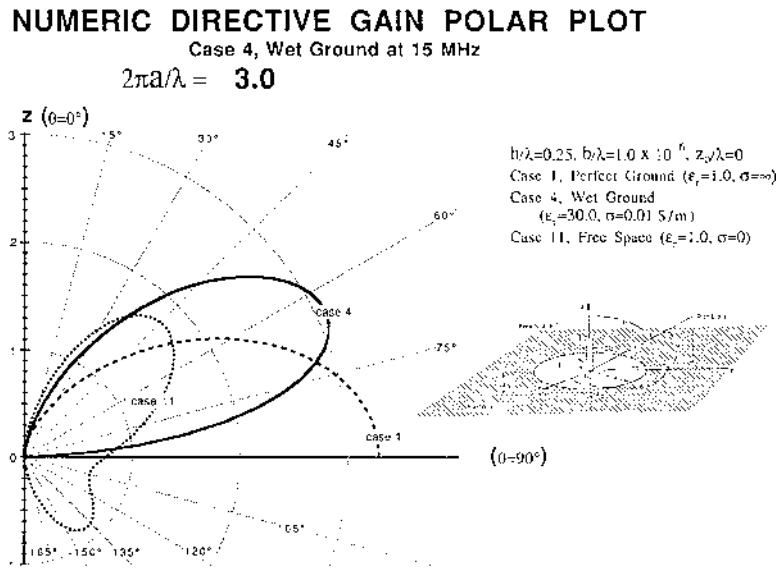

FIGURE A6-34 Directivity pattern, $2\pi a/\lambda = 3.0$, wet ground.

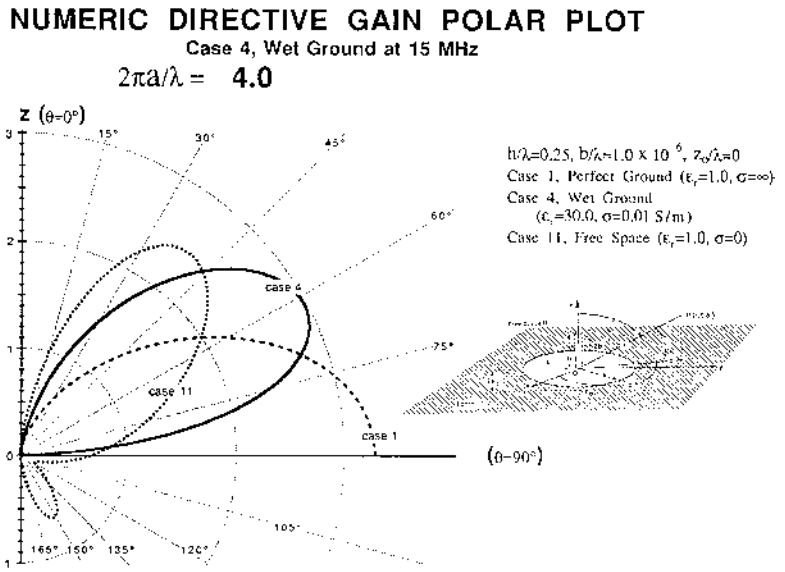

FIGURE A6-35 Directivity pattern, $2\pi a/\lambda = 4.0$, wet ground.

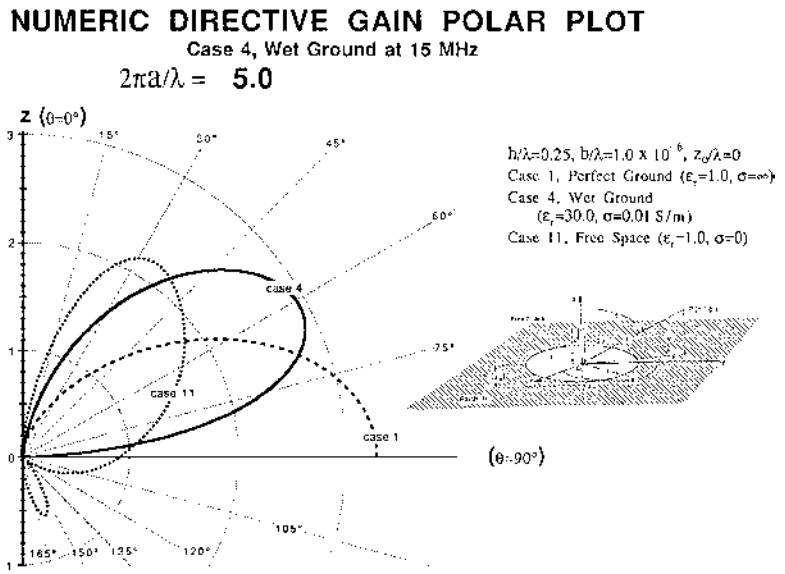

FIGURE A6-36 Directivity pattern, $2\pi a/\lambda = 5.0$, wet ground.

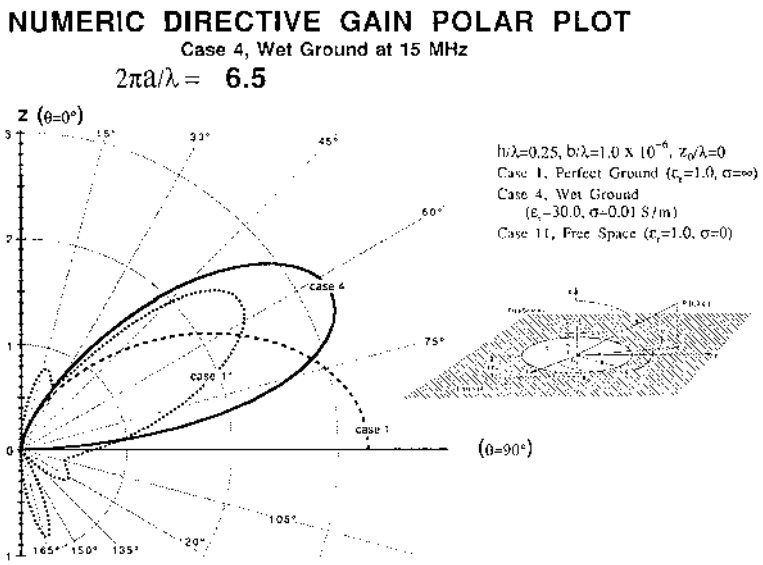

FIGURE A6-37 Directivity pattern, $2\pi a/\lambda = 6.5$, wet ground.

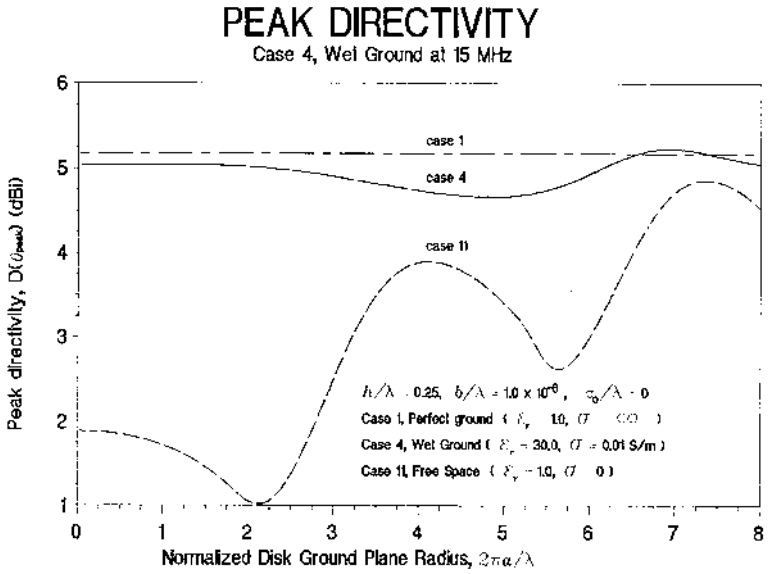
PEAK DIRECTIVITY
Case 4, Wet Ground at 15 MHz
Peak directivity, D(θmax) (dBi)
Normalized Disk Ground Plane Radius, 2πa/λ
case 1
case 4
case 11
h/λ = 0.25, b/λ = 1.0 x 10⁻⁶, z₀/λ = 0
Case 1, Perfect ground (εr = 1.0, σ = ∞)
Case 4, Wet Ground (εr = 30.0, σ = 0.01 S/m)
Case 11, Free Space (εr = 1.0, σ = 0)

FIGURE A6-38 Peak directivity, wet ground.

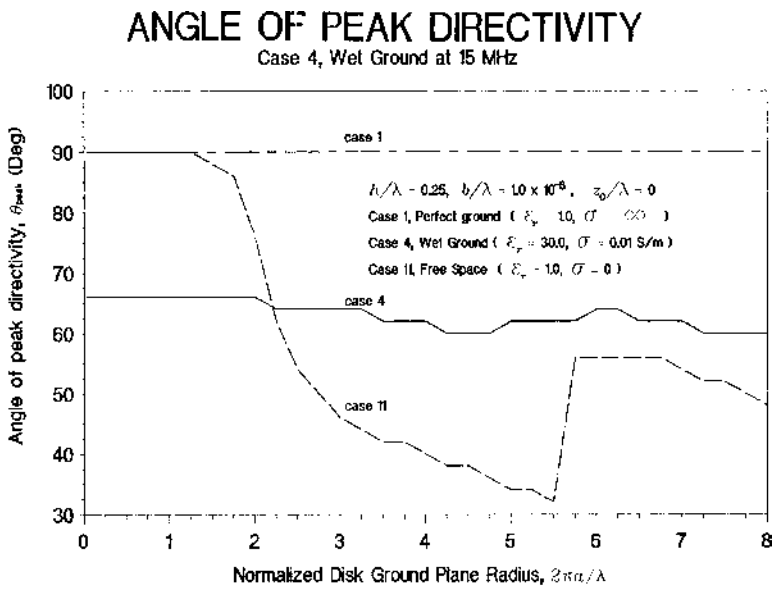
ANGLE OF PEAK DIRECTIVITY
Case 4, Wet Ground at 15 MHz
Angle of peak directivity, θ_{peak} (Deg)
Normalized Disk Ground Plane Radius, $2\pi a/\lambda$
case 1
case 4
case 11
h/λ = 0.25, b/λ = 1.0 x 10^{-6}, z_0/λ = 0
Case 1, Perfect ground (ε_r 1.0, σ)
Case 4, Wet Ground (ε_r = 30.0, σ = 0.01 S/m)
Case 11, Free Space (ε_r = 1.0, σ = 0)

FIGURE A6-39 Angle of incidence of peak directivity, wet ground.

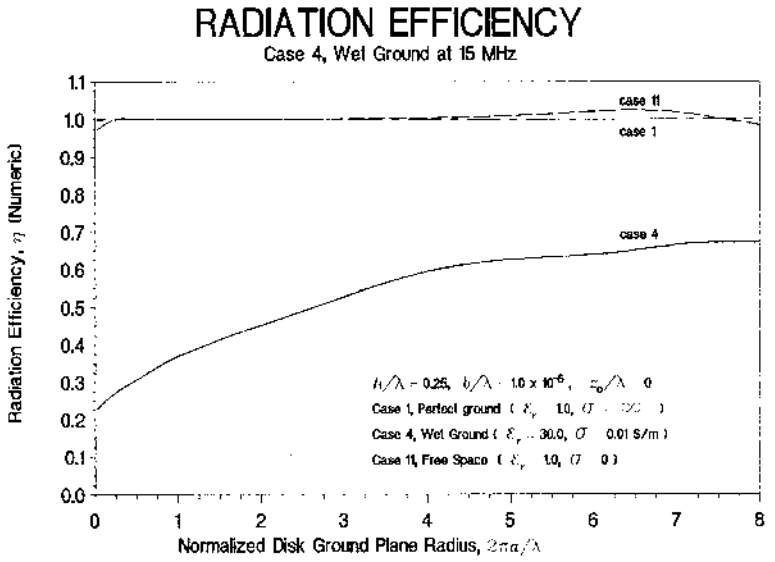
RADIATION EFFICIENCY
Case 4, Wet Ground at 15 MHz
Radiation Efficiency, η (Numeric)
Normalized Disk Ground Plane Radius, $2\pi a/\lambda$
case 11
case 1
case 4
h/λ = 0.25, b/λ = 1.0 x 10^{-6}, z_0/λ = 0
Case 1, Perfect ground (ε_r 1.0, σ)
Case 4, Wet Ground (ε_r = 30.0, σ 0.01 S/m)
Case 11, Free Space (ε_r 1.0, σ 0)

FIGURE A6-40 Radiation efficiency, wet ground.

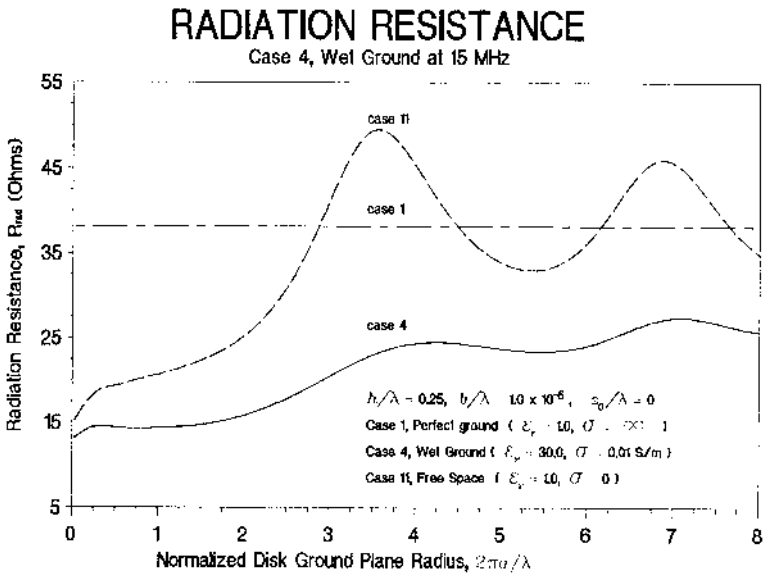
RADIATION RESISTANCE
Case 4, Wet Ground at 15 MHz
Radiation Resistance, R_{rad} (Ohms)
Normalized Disk Ground Plane Radius, $2\pi a/\lambda$
case II
case I
case 4
h/λ = 0.25, b/λ = 1.0 x 10^{-6}, z_0/λ = 0
Case 1, Perfect ground (ε_r = 1.0, σ = ∞)
Case 4, Wet Ground (ε_r = 30.0, σ = 0.01 S/m)
Case II, Free Space (ε_r = 1.0, σ = 0)

FIGURE A6-41 Radiation resistance, wet ground.

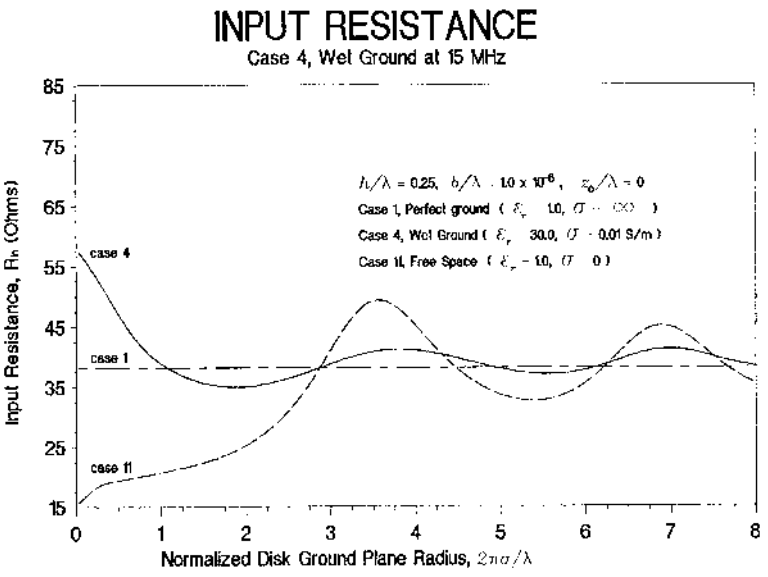
INPUT RESISTANCE
Case 4, Wet Ground at 15 MHz
Input Resistance, R_{in} (Ohms)
Normalized Disk Ground Plane Radius, $2\pi a/\lambda$
case 4
case I
case II
h/λ = 0.25, b/λ = 1.0 x 10^{-6}, z_0/λ = 0
Case 1, Perfect ground (ε_r = 1.0, σ = ∞)
Case 4, Wet Ground (ε_r = 30.0, σ = 0.01 S/m)
Case II, Free Space (ε_r = 1.0, σ = 0)

FIGURE A6-42 Input resistance, wet ground.

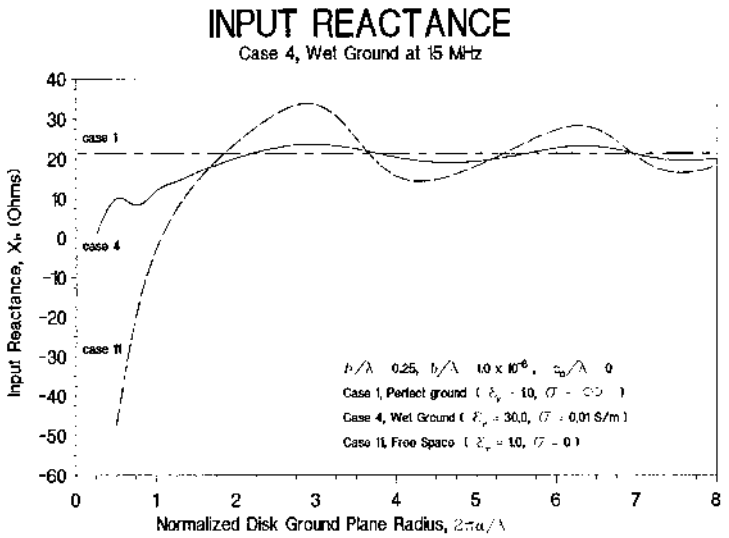
INPUT REACTANCE
Case 4, Wet Ground at 15 MHz
Input Reactance, X_{in} (Ohms)
Normalized Disk Ground Plane Radius, $2\pi a/\lambda$
case 1
case 4
case 11
h/λ = 0.25, b/λ = 1.0 x 10^{-6}, z_0/λ = 0
Case 1, Perfect ground (ε_r = 1.0, σ = ∞)
Case 4, Wet Ground (ε_r = 30.0, σ = 0.01 S/m)
Case 11, Free Space (ε_r = 1.0, σ = 0)

FIGURE A6-43 Input reactance, wet ground.

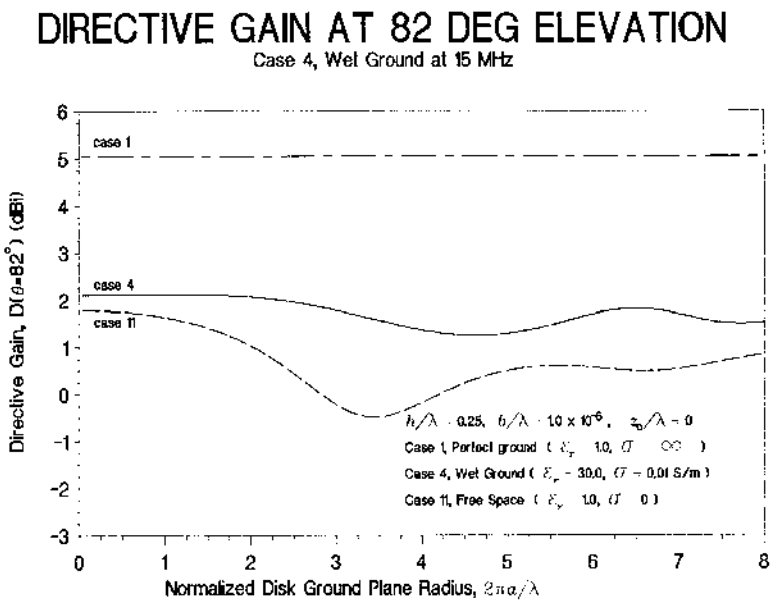
DIRECTIVE GAIN AT 82 DEG ELEVATION
Case 4, Wet Ground at 15 MHz
Directive Gain, D(α=82°) (dBi)
Normalized Disk Ground Plane Radius, $2\pi a/\lambda$
case 1
case 4
case 11
h/λ = 0.25, b/λ = 1.0 x 10^{-6}, z_0/λ = 0
Case 1, Perfect ground (ε_r = 1.0, σ = ∞)
Case 4, Wet Ground (ε_r = 30.0, σ = 0.01 S/m)
Case 11, Free Space (ε_r = 1.0, σ = 0)

FIGURE A6-44 Directivity at 8° above the horizon, wet ground.

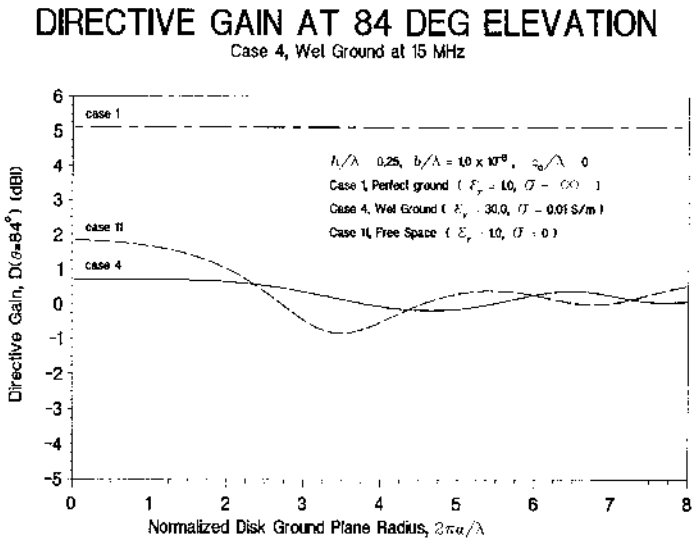
DIRECTIVE GAIN AT 84 DEG ELEVATION
Case 4, Wet Ground at 15 MHz
case I
case II
case 4
Directive Gain, D(θ=84°) (dBi)
Normalized Disk Ground Plane Radius, 2πa/λ

FIGURE A6-45 Directivity at 6° above the horizon, wet ground.

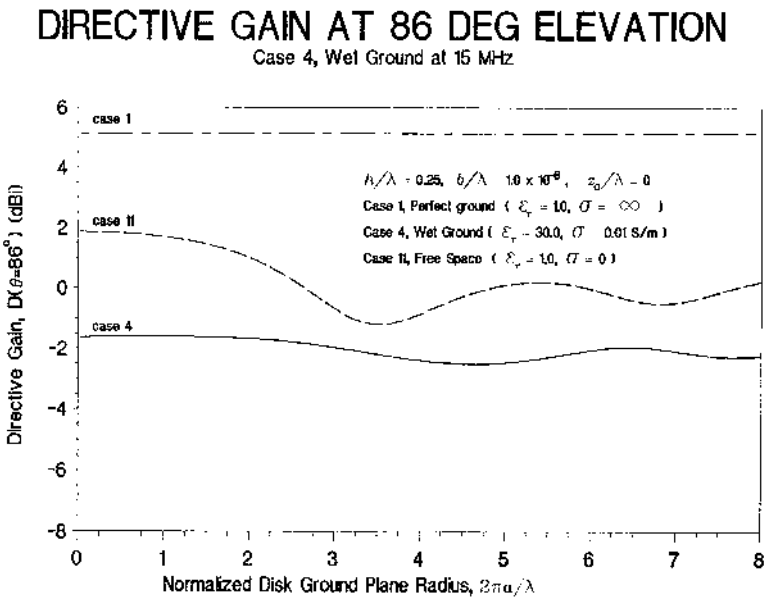
DIRECTIVE GAIN AT 86 DEG ELEVATION
Case 4, Wet Ground at 15 MHz
case I
case II
case 4
Directive Gain, D(θ=86°) (dBi)
Normalized Disk Ground Plane Radius, 2πa/λ

FIGURE A6-46 Directivity at 4° above the horizon, wet ground.

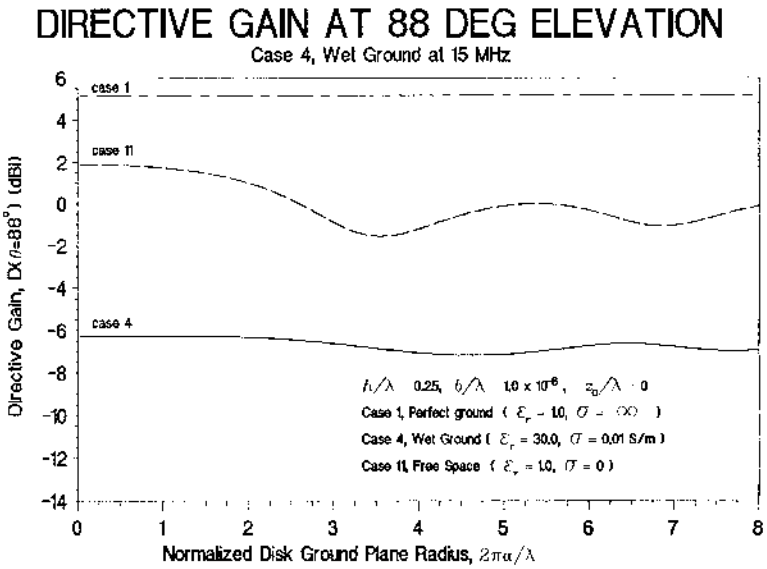

FIGURE A6-47 Directivity at 2° above the horizon, wet ground.

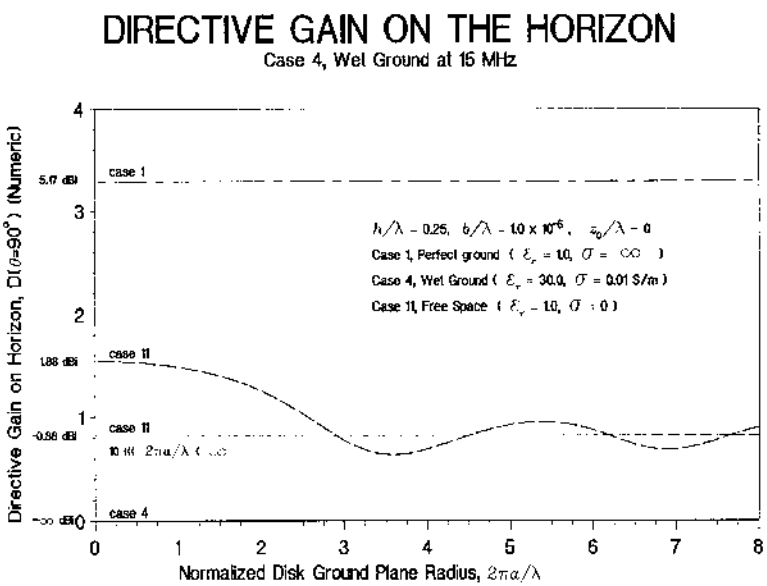

FIGURE A6-48 Directivity on the horizon, wet ground.

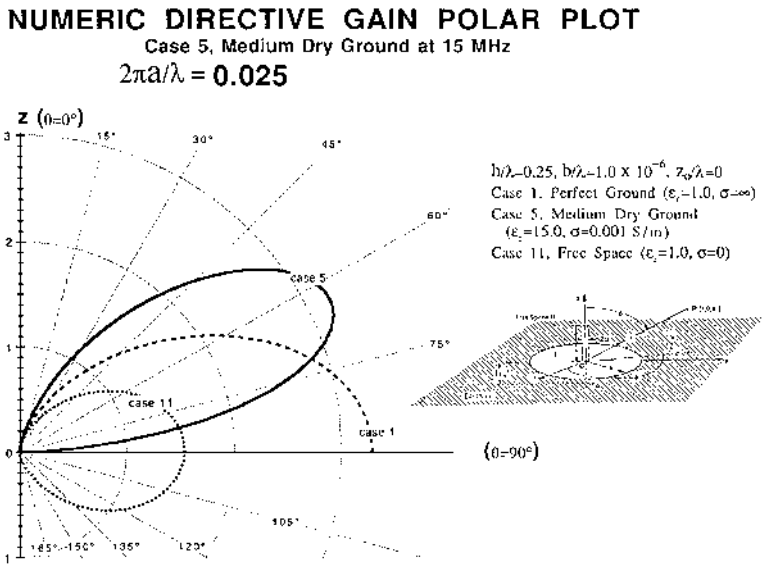
NUMERIC DIRECTIVE GAIN POLAR PLOT
Case 5, Medium Dry Ground at 15 MHz
2πa/λ = 0.025
z (θ=0°)
h/λ=0.25, b/λ=1.0 x 10⁻⁶, z₀/λ=0
Case 1, Perfect Ground (εr=1.0, σ=∞)
Case 5, Medium Dry Ground (εr=15.0, σ=0.001 S/m)
Case 11, Free Space (εr=1.0, σ=0)
case 5
case 11
case 1
(θ=90°)

FIGURE A6-49 Directivity pattern, $2\pi a/\lambda = 0.025$, medium dry ground.

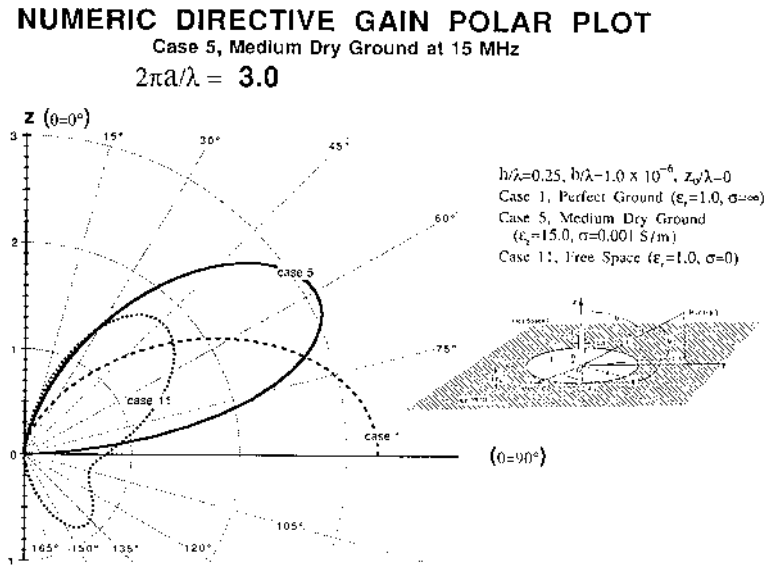
NUMERIC DIRECTIVE GAIN POLAR PLOT
Case 5, Medium Dry Ground at 15 MHz
2πa/λ = 3.0
z (θ=0°)
h/λ=0.25, b/λ=1.0 x 10⁻⁶, z₀/λ=0
Case 1, Perfect Ground (εr=1.0, σ=∞)
Case 5, Medium Dry Ground (εr=15.0, σ=0.001 S/m)
Case 11, Free Space (εr=1.0, σ=0)
case 5
case 11
(θ=90°)

FIGURE A6-50 Directivity pattern, $2\pi a/\lambda = 3.0$, medium dry ground.

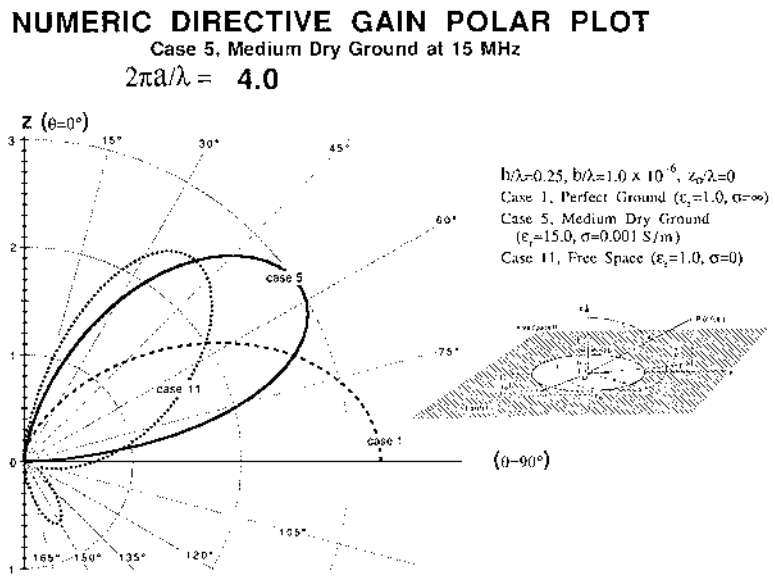

FIGURE A6-51 Directivity pattern, $2\pi a/\lambda = 4.0$, medium dry ground.

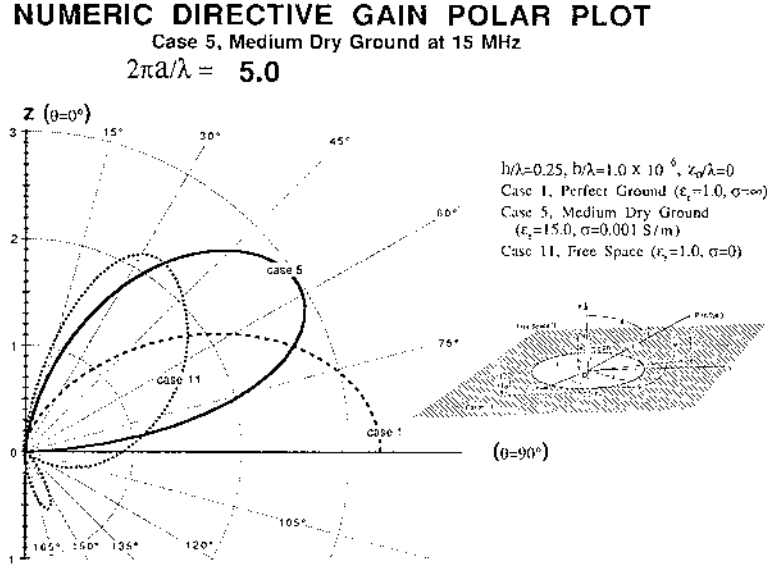

FIGURE A6-52 Directivity pattern, $2\pi a/\lambda = 5.0$, medium dry ground.

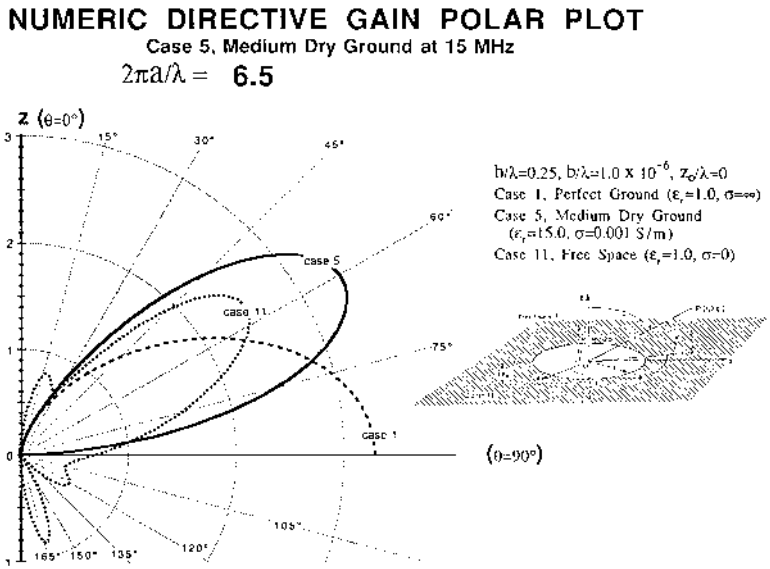

FIGURE A6-53 Directivity pattern, $2\pi a/\lambda = 6.5$, medium dry ground.

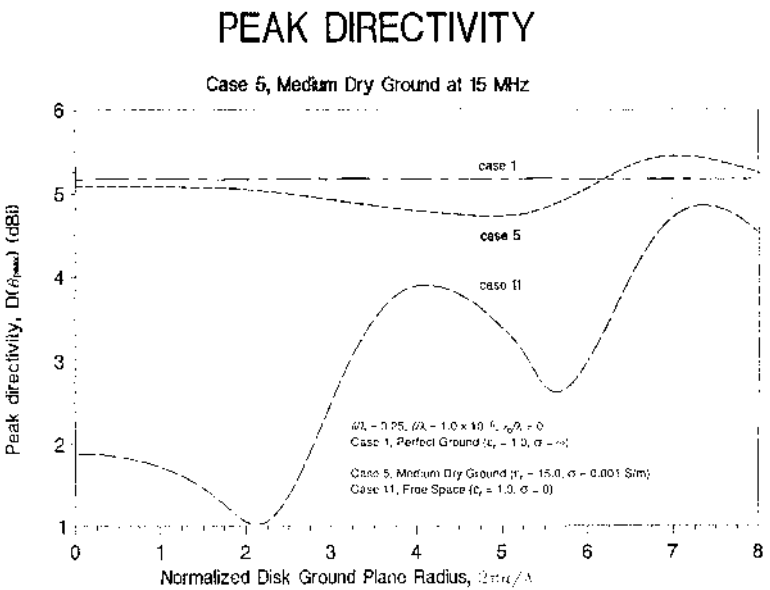
PEAK DIRECTIVITY
Case 5, Medium Dry Ground at 15 MHz
Peak directivity, D(θ_max) (dBi)
Normalized Disk Ground Plane Radius, 2πa/λ
case 1
case 5
case 11
Case 1, Perfect Ground (ε_r = 1.0, σ = ∞)
Case 5, Medium Dry Ground (ε_r = 15.0, σ = 0.001 S/m)
Case 11, Free Space (ε_r = 1.0, σ = 0)

FIGURE A6-54 Peak directivity, medium dry ground.

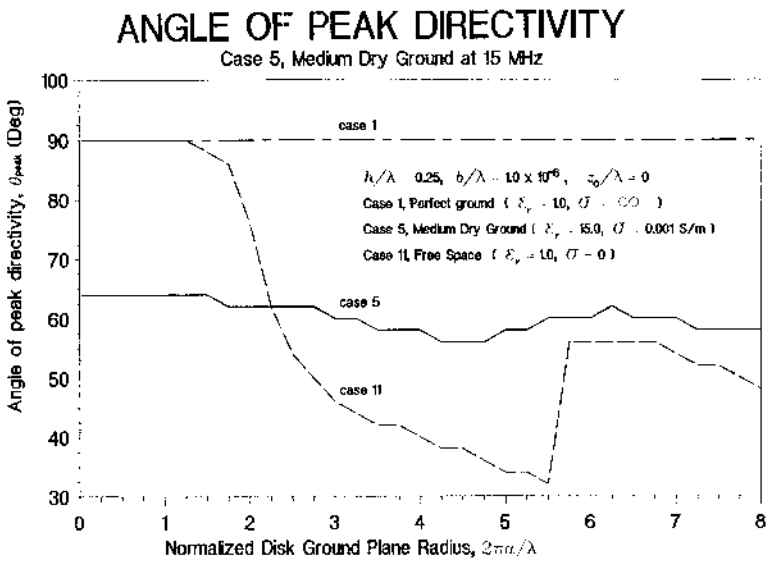
ANGLE OF PEAK DIRECTIVITY
Case 5, Medium Dry Ground at 15 MHz
Angle of peak directivity, θ_{peak} (Deg)
Normalized Disk Ground Plane Radius, $2\pi a/\lambda$
case 1
case 5
case 11
h/λ = 0.25, b/λ = 1.0 x 10^{-6}, z_0/λ = 0
Case 1, Perfect ground (ε_r = 1.0, σ = ∞)
Case 5, Medium Dry Ground (ε_r = 15.0, σ = 0.001 S/m)
Case 11, Free Space (ε_r = 1.0, σ = 0)

FIGURE A6-55 Angle of incidence of peak directivity, medium dry ground.

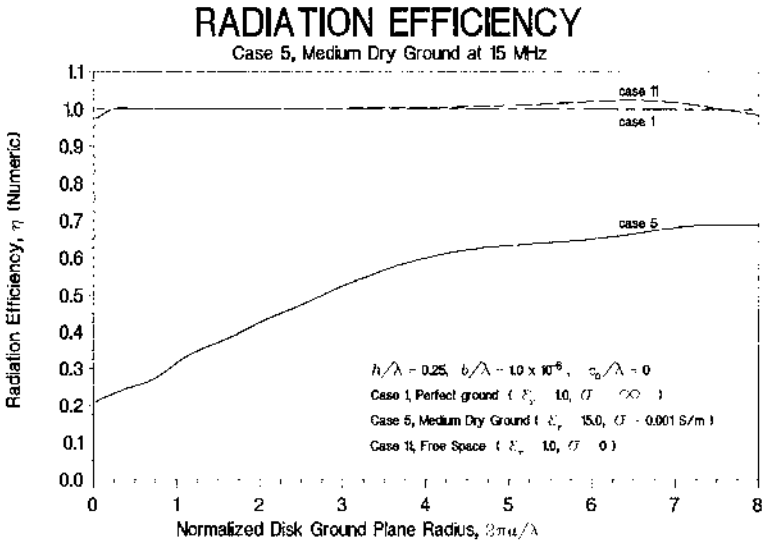
RADIATION EFFICIENCY
Case 5, Medium Dry Ground at 15 MHz
Radiation Efficiency, η (Numeric)
Normalized Disk Ground Plane Radius, $2\pi a/\lambda$
case 11
case 1
case 5
h/λ = 0.25, b/λ = 1.0 x 10^{-6}, z_0/λ = 0
Case 1, Perfect ground (ε_r = 1.0, σ = ∞)
Case 5, Medium Dry Ground (ε_r = 15.0, σ = 0.001 S/m)
Case 11, Free Space (ε_r = 1.0, σ = 0)

FIGURE A6-56 Radiation efficiency, medium dry ground.

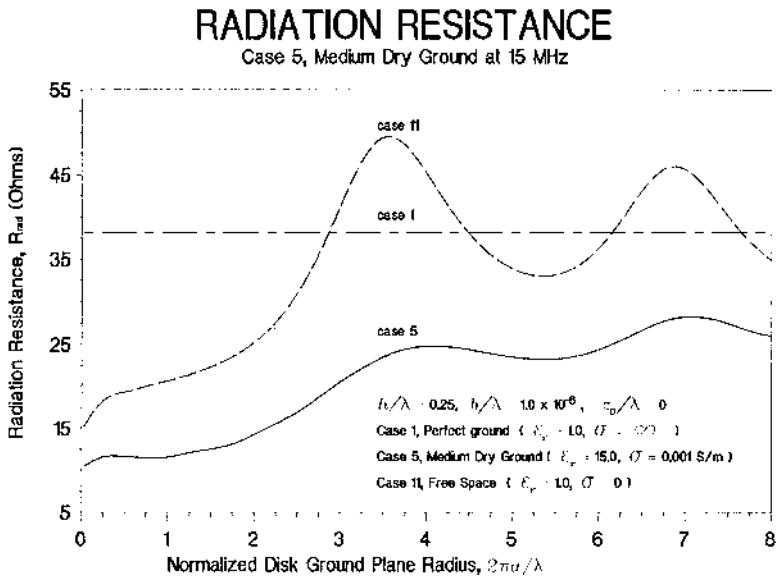

FIGURE A6-57 Radiation resistance, medium dry ground.

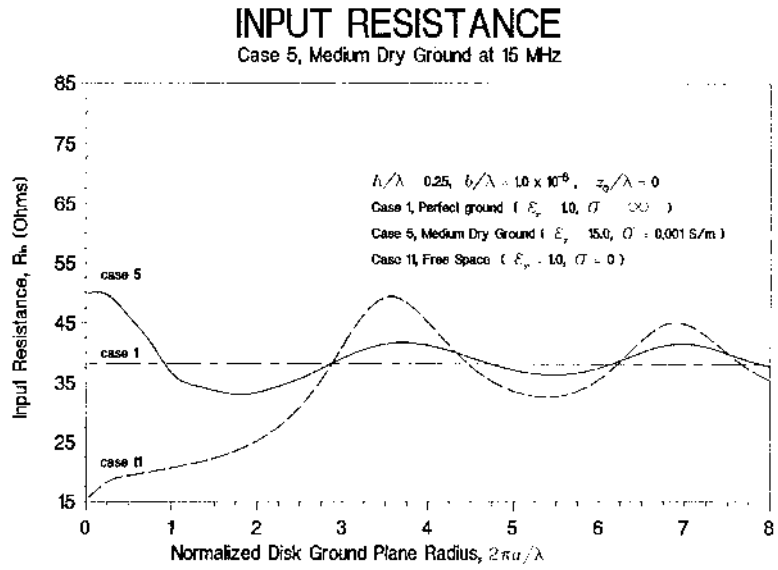

FIGURE A6-58 Input resistance, medium dry ground.

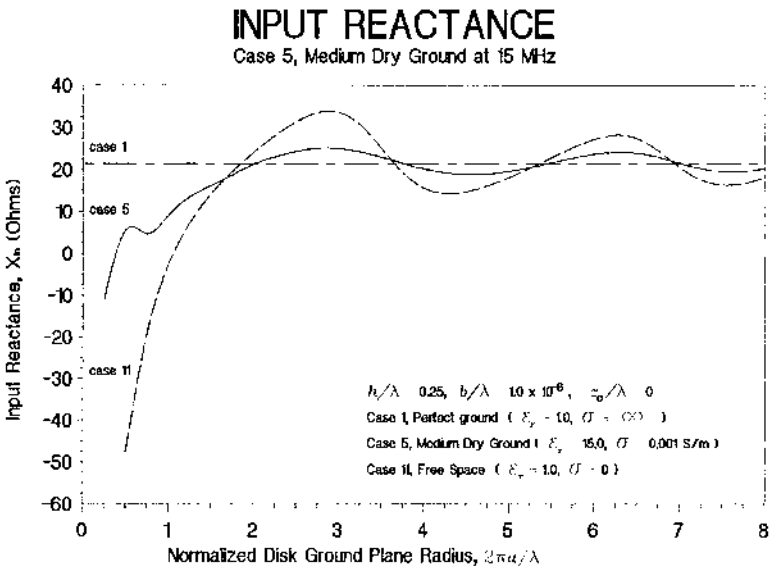
INPUT REACTANCE
Case 5, Medium Dry Ground at 15 MHz
Input Reactance, Xin (Ohms)
Normalized Disk Ground Plane Radius, 2πa/λ
case 1
case 5
case 11
h/λ 0.25, b/λ 1.0 x 10⁻⁶, z0/λ 0
Case 1, Perfect ground (εr = 1.0, σ = ∞)
Case 5, Medium Dry Ground (εr 15.0, σ 0.001 S/m)
Case 11, Free Space (εr = 1.0, σ = 0)

FIGURE A6-59 Input reactance, medium dry ground.

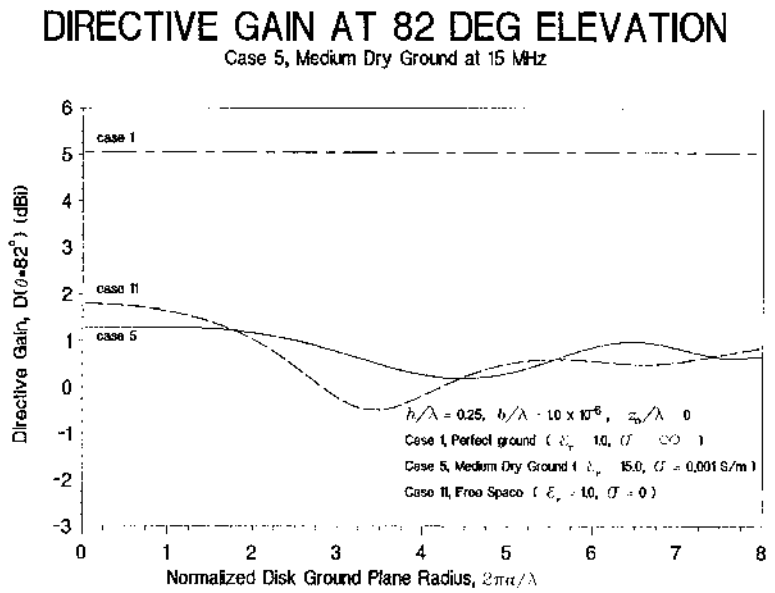
DIRECTIVE GAIN AT 82 DEG ELEVATION
Case 5, Medium Dry Ground at 15 MHz
Directive Gain, D(θ=82°) (dBi)
Normalized Disk Ground Plane Radius, 2πa/λ
case 1
case 11
case 5
h/λ = 0.25, b/λ = 1.0 x 10⁻⁶, z0/λ 0
Case 1, Perfect ground (εr 1.0, σ ∞)
Case 5, Medium Dry Ground (εr 15.0, σ = 0.001 S/m)
Case 11, Free Space (εr = 1.0, σ = 0)

FIGURE A6-60 Directivity at 8° above the horizon, medium dry ground.

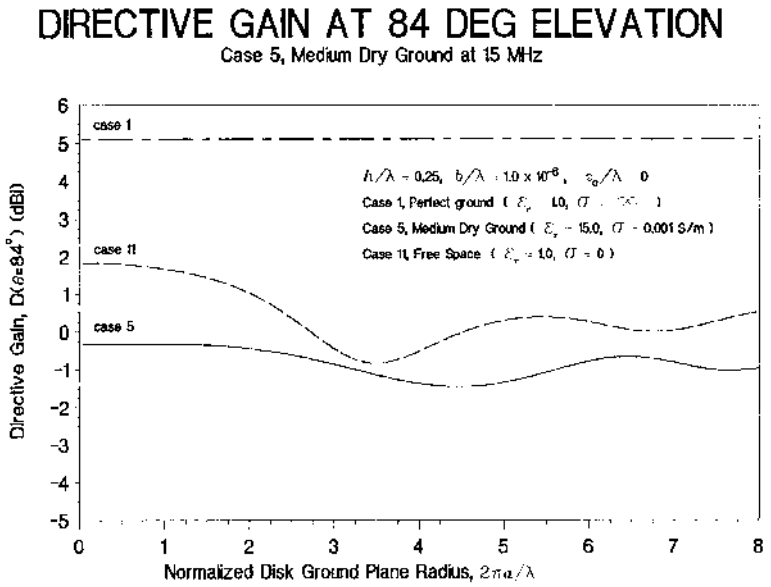
DIRECTIVE GAIN AT 84 DEG ELEVATION
Case 5, Medium Dry Ground at 15 MHz
case 1
case 11
case 5
Case 1, Perfect ground (ε_r 1.0, σ ∞)
Case 5, Medium Dry Ground (ε_r = 15.0, σ = 0.001 S/m)
Case 11, Free Space (ε_r = 1.0, σ = 0)
Directive Gain, D(θ=84°) (dBi)
Normalized Disk Ground Plane Radius, $2\pi a/\lambda$

FIGURE A6-61 Directivity at 6° above the horizon, medium dry ground.

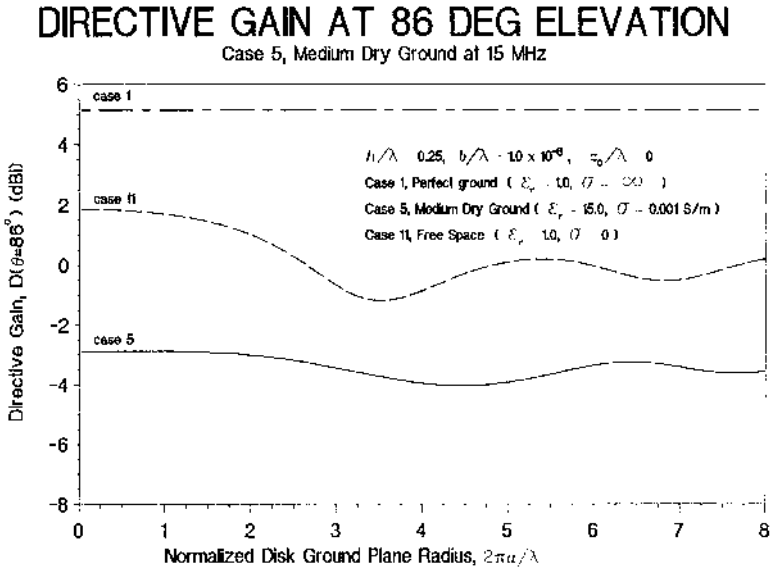
DIRECTIVE GAIN AT 86 DEG ELEVATION
Case 5, Medium Dry Ground at 15 MHz
case 1
case 11
case 5
Case 1, Perfect ground (ε_r 1.0, σ ∞)
Case 5, Medium Dry Ground (ε_r = 15.0, σ = 0.001 S/m)
Case 11, Free Space (ε_r 1.0, σ 0)
Directive Gain, D(θ=86°) (dBi)
Normalized Disk Ground Plane Radius, $2\pi a/\lambda$

FIGURE A6-62 Directivity at 4° above the horizon, medium dry ground.

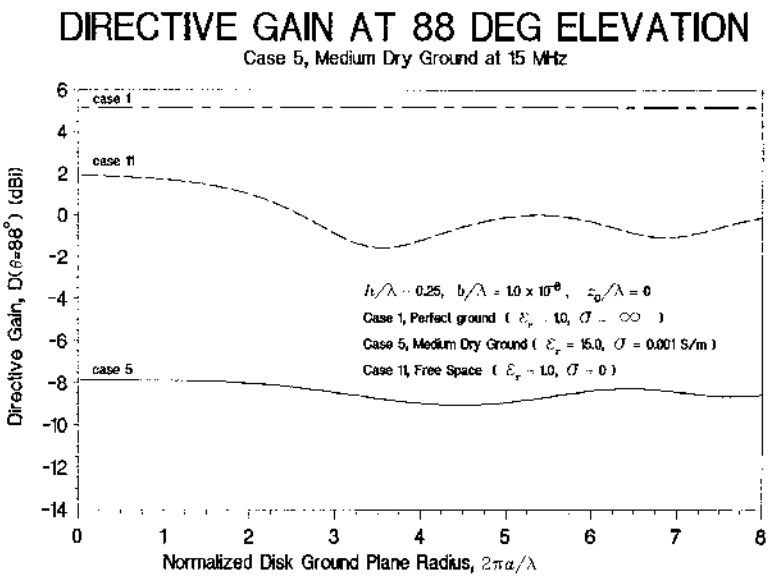
DIRECTIVE GAIN AT 88 DEG ELEVATION
Case 5, Medium Dry Ground at 15 MHz
case 1
case II
case 5
h/λ = 0.25, b/λ = 1.0 x 10^{-6}, z_0/λ = 0
Case 1, Perfect ground (ε_r = 1.0, σ = ∞)
Case 5, Medium Dry Ground (ε_r = 15.0, σ = 0.001 S/m)
Case II, Free Space (ε_r = 1.0, σ = 0)
Directive Gain, D(θ=88°) (dBi)
Normalized Disk Ground Plane Radius, $2\pi a/\lambda$

FIGURE A6-63 Directivity at 2° above the horizon, medium dryground.

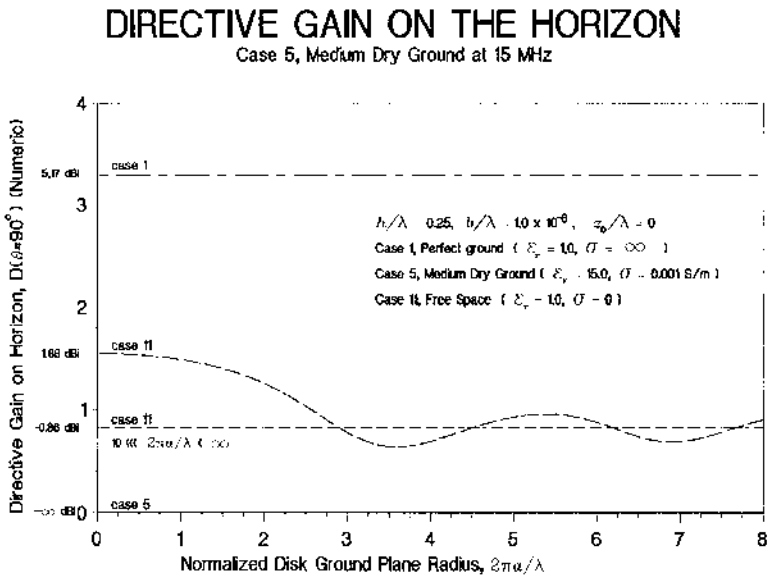
DIRECTIVE GAIN ON THE HORIZON
Case 5, Medium Dry Ground at 15 MHz
case 1
5.17 dBi
case II
1.68 dBi
case III
-0.86 dBi
case 5
h/λ = 0.25, b/λ = 1.0 x 10^{-6}, z_0/λ = 0
Case 1, Perfect ground (ε_r = 1.0, σ = ∞)
Case 5, Medium Dry Ground (ε_r = 15.0, σ = 0.001 S/m)
Case II, Free Space (ε_r = 1.0, σ = 0)
Directive Gain on Horizon, D(θ=90°) (Numeric)
Normalized Disk Ground Plane Radius, $2\pi a/\lambda$

FIGURE A6-64 Directivity on the horizon, medium dry ground.

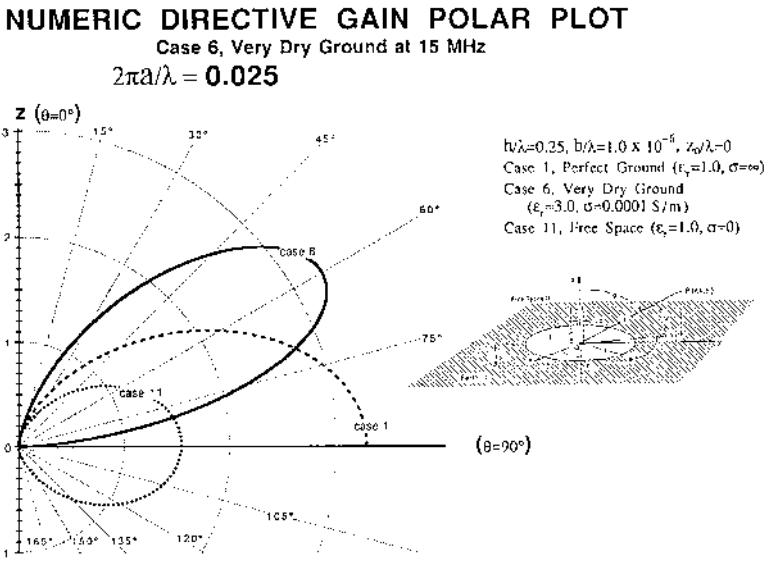

FIGURE A6-65 Directivity pattern, $2\pi a/\lambda = 0.025$, very dry ground.

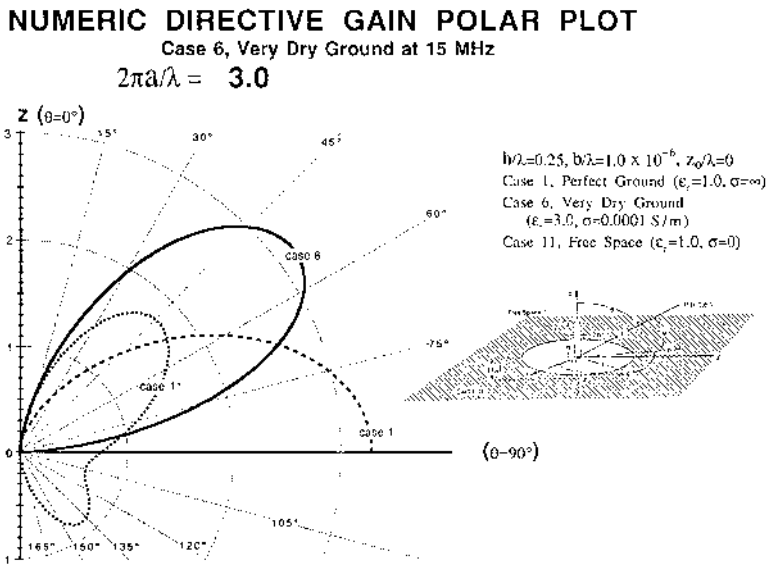

FIGURE A6-66 Directivity pattern, $2\pi a/\lambda = 3.0$, very dry ground.

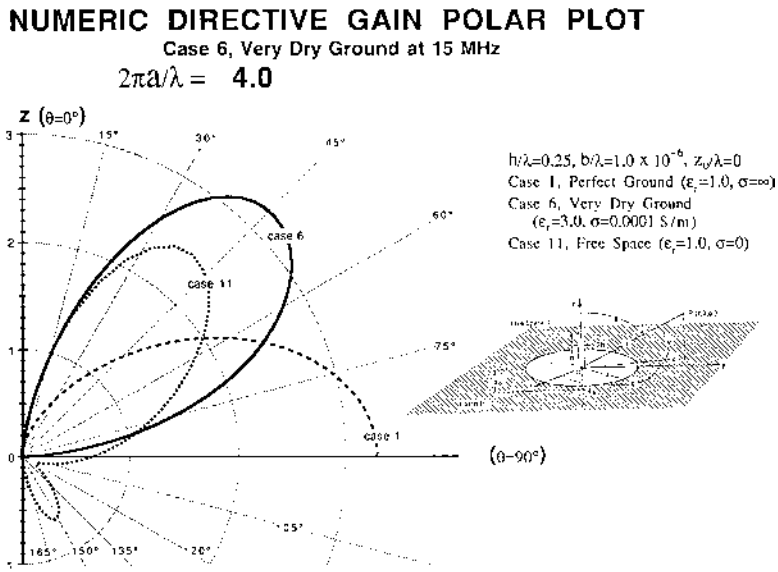

FIGURE A6-67 Directivity pattern, $2\pi a/\lambda = 4.0$, very dry ground.

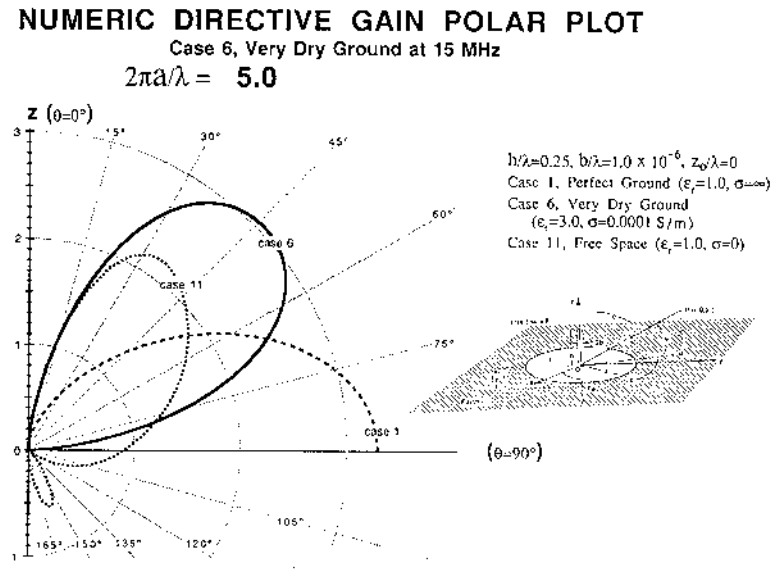

FIGURE A6-68 Directivity Pattern, $2\pi a/\lambda = 5.0$, very dry ground.

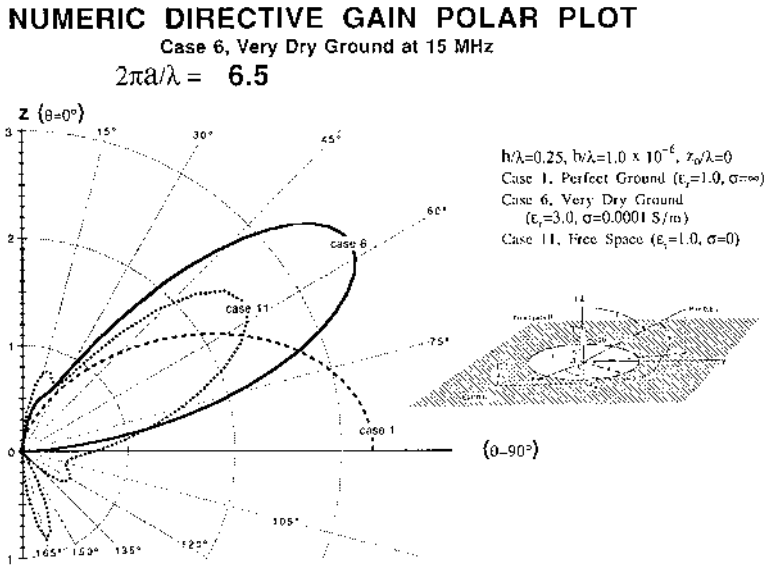

FIGURE A6-69 Directivity pattern, $2\pi a/\lambda = 6.5$, very dry ground.

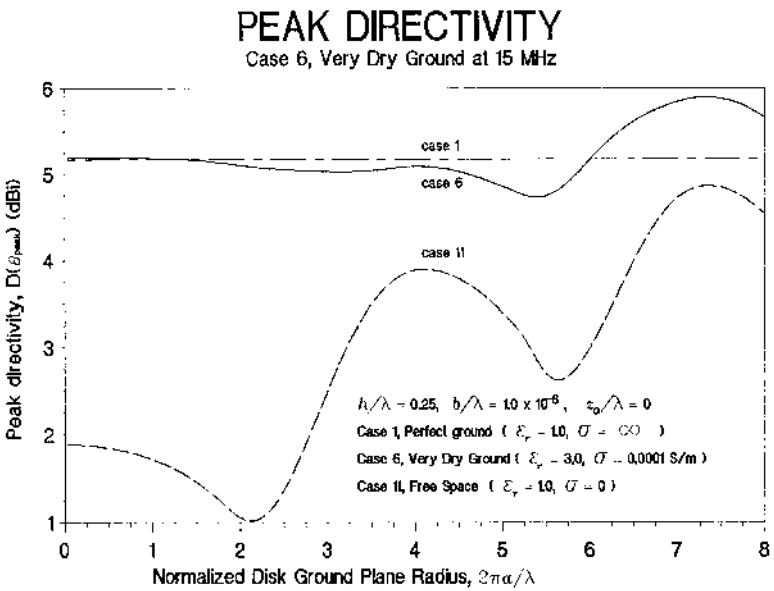
PEAK DIRECTIVITY
Case 6, Very Dry Ground at 15 MHz
Peak directivity, D(θ_peak) (dBi)
Normalized Disk Ground Plane Radius, 2πa/λ
case 1
case 6
case 11
h/λ = 0.25, b/λ = 1.0 x 10⁻⁶, r₀/λ = 0
Case 1, Perfect ground (ε_r = 1.0, σ = ∞)
Case 6, Very Dry Ground (ε_r = 3.0, σ = 0.0001 S/m)
Case 11, Free Space (ε_r = 1.0, σ = 0)

FIGURE A6-70 Directivity pattern, very dry ground.

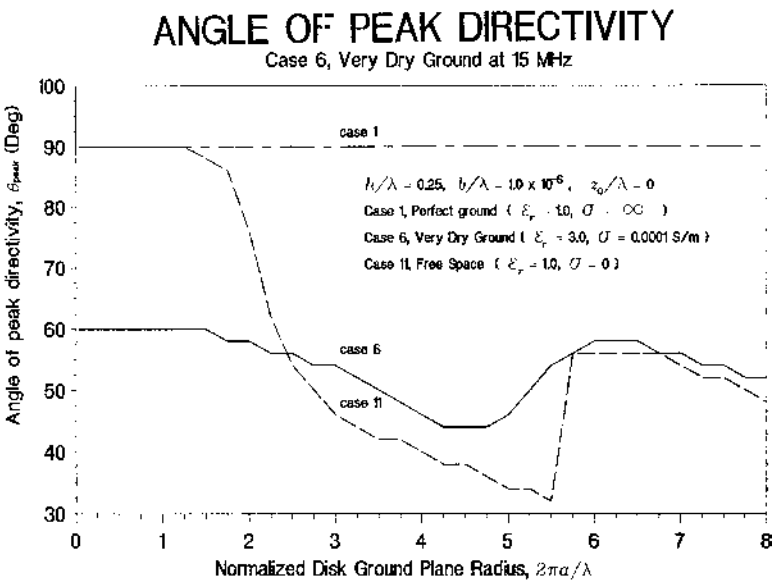
ANGLE OF PEAK DIRECTIVITY
Case 6, Very Dry Ground at 15 MHz
Angle of peak directivity, θ_{peak} (Deg)
Normalized Disk Ground Plane Radius, $2\pi a/\lambda$
case 1
case 6
case 11
h/λ = 0.25, b/λ = 1.0 x 10^{-6}, z_0/λ = 0
Case 1, Perfect ground (ε_r = 1.0, σ = ∞)
Case 6, Very Dry Ground (ε_r = 3.0, σ = 0.0001 S/m)
Case 11, Free Space (ε_r = 1.0, σ = 0)

FIGURE A6-71 Angle of incidence of peak directivity, very dry ground.

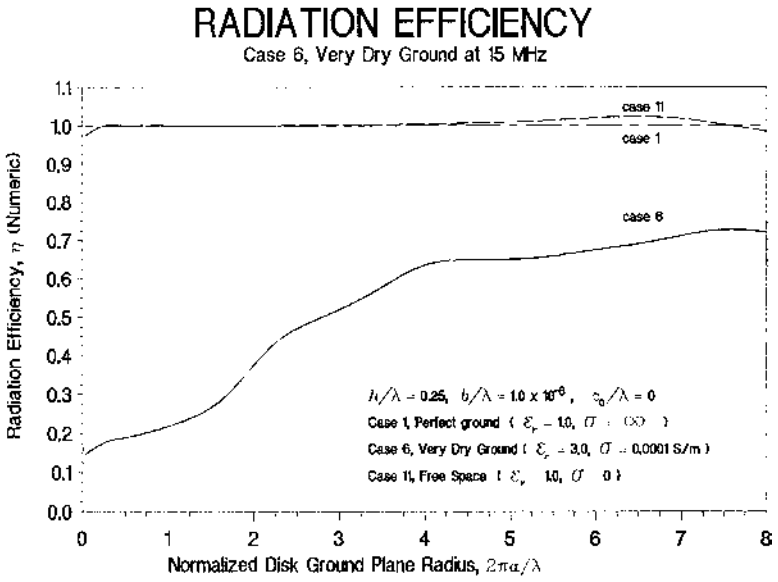
RADIATION EFFICIENCY
Case 6, Very Dry Ground at 15 MHz
Radiation Efficiency, η (Numeric)
Normalized Disk Ground Plane Radius, $2\pi a/\lambda$
case 11
case 1
case 6
h/λ = 0.25, b/λ = 1.0 x 10^{-6}, z_0/λ = 0
Case 1, Perfect ground (ε_r = 1.0, σ = ∞)
Case 6, Very Dry Ground (ε_r = 3.0, σ = 0.0001 S/m)
Case 11, Free Space (ε_r = 1.0, σ = 0)

FIGURE A6-72 Radiation efficiency, very dry ground.

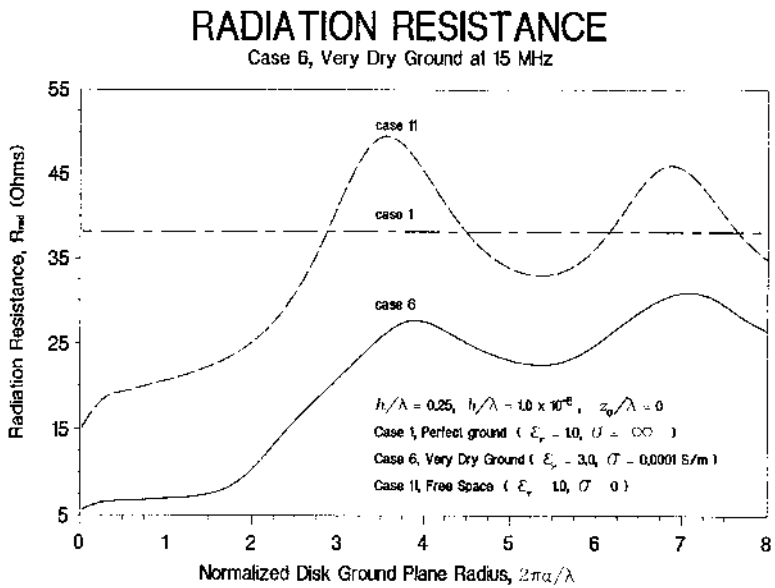
RADIATION RESISTANCE
Case 6, Very Dry Ground at 15 MHz
Radiation Resistance, R_{rad} (Ohms)
Normalized Disk Ground Plane Radius, $2\pi a/\lambda$
case 11
case 1
case 6
$h/\lambda = 0.25$, $b/\lambda = 1.0 \times 10^{-6}$, $z_0/\lambda = 0$
Case 1, Perfect ground ($\varepsilon_r = 1.0$, $\sigma = \infty$)
Case 6, Very Dry Ground ($\varepsilon_r = 3.0$, $\sigma = 0.0001$ S/m)
Case 11, Free Space ($\varepsilon_r = 1.0$, $\sigma = 0$)

FIGURE A6-73 Radiation resistance, very dry ground.

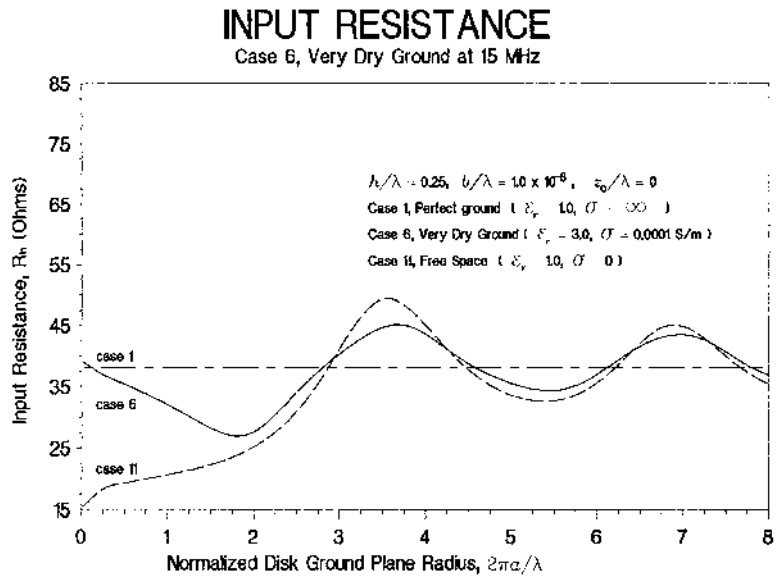
INPUT RESISTANCE
Case 6, Very Dry Ground at 15 MHz
Input Resistance, R_{in} (Ohms)
Normalized Disk Ground Plane Radius, $2\pi a/\lambda$
case 1
case 6
case 11
$h/\lambda = 0.25$, $b/\lambda = 1.0 \times 10^{-6}$, $z_0/\lambda = 0$
Case 1, Perfect ground ($\varepsilon_r = 1.0$, $\sigma = \infty$)
Case 6, Very Dry Ground ($\varepsilon_r = 3.0$, $\sigma = 0.0001$ S/m)
Case 11, Free Space ($\varepsilon_r = 1.0$, $\sigma = 0$)

FIGURE A6-74 Input resistance, very dry ground.

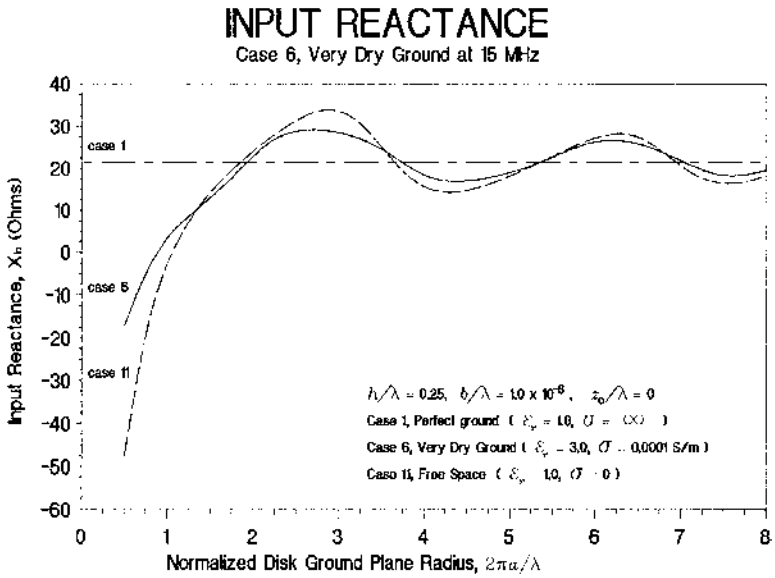
INPUT REACTANCE
Case 6, Very Dry Ground at 15 MHz
Input Reactance, X_{in} (Ohms)
Normalized Disk Ground Plane Radius, $2\pi a/\lambda$
case 1
case 6
case 11
h/λ = 0.25, b/λ = 1.0 x 10^{-6}, z_0/λ = 0
Case 1, Perfect ground (ε_r = 1.0, σ = ∞)
Case 6, Very Dry Ground (ε_r = 3.0, σ = 0.0001 S/m)
Case 11, Free Space (ε_r = 1.0, σ = 0)

FIGURE A6-75 Input reactance, very dry ground.

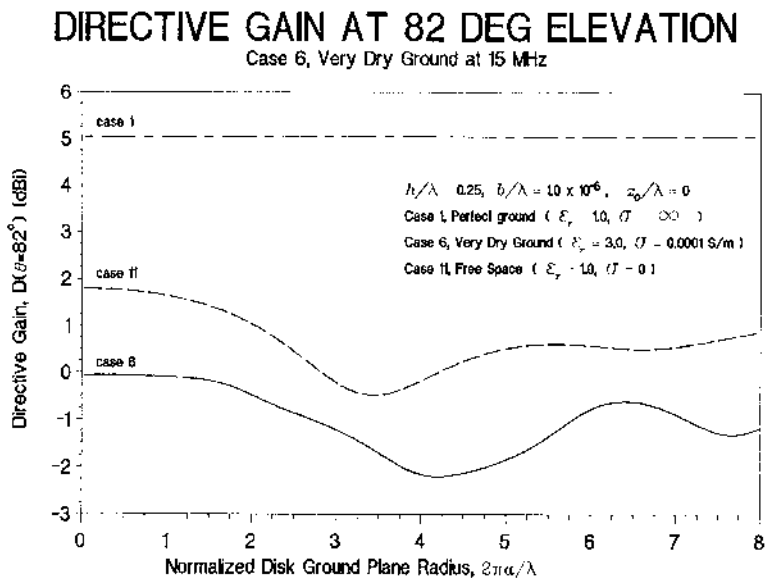
DIRECTIVE GAIN AT 82 DEG ELEVATION
Case 6, Very Dry Ground at 15 MHz
Directive Gain, D(θ=82°) (dBi)
Normalized Disk Ground Plane Radius, $2\pi a/\lambda$
case 1
case 11
case 6
h/λ = 0.25, b/λ = 1.0 x 10^{-6}, z_0/λ = 0
Case 1, Perfect ground (ε_r = 1.0, σ = ∞)
Case 6, Very Dry Ground (ε_r = 3.0, σ = 0.0001 S/m)
Case 11, Free Space (ε_r = 1.0, σ = 0)

FIGURE A6-76 Directivity at 8° above the horizon, very dry ground.

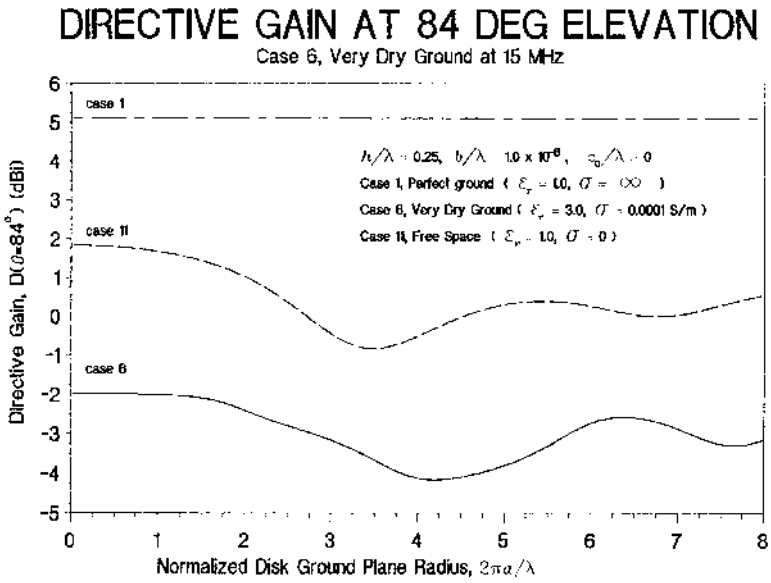
DIRECTIVE GAIN AT 84 DEG ELEVATION
Case 6, Very Dry Ground at 15 MHz
case I
case II
case 6
h/λ = 0.25, b/λ = 1.0 x 10⁻⁶, z₀/λ = 0
Case 1, Perfect ground (ε_r = 1.0, σ = ∞)
Case 6, Very Dry Ground (ε_r = 3.0, σ = 0.0001 S/m)
Case II, Free Space (ε_r = 1.0, σ = 0)
Directive Gain, D(θ=84°) (dBi)
Normalized Disk Ground Plane Radius, 2πa/λ

FIGURE A6-77 Directivity at 6° above the horizon, very dry ground.

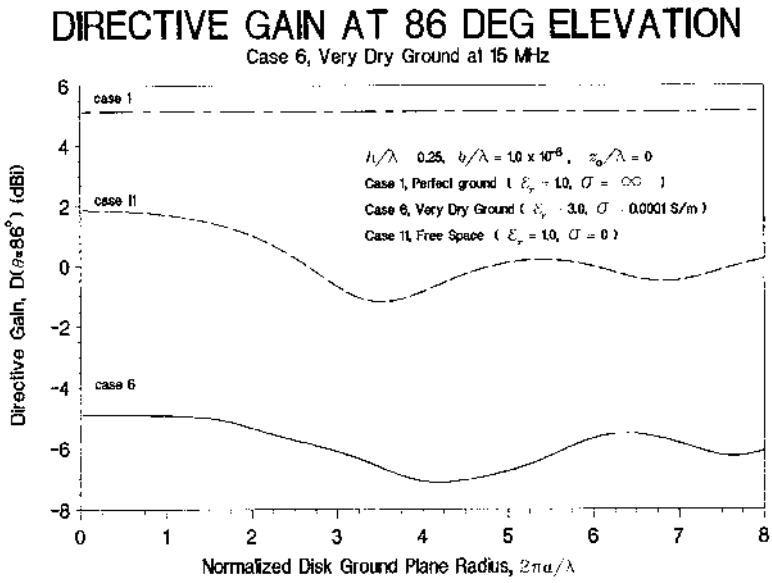
DIRECTIVE GAIN AT 86 DEG ELEVATION
Case 6, Very Dry Ground at 15 MHz
case I
case II
case 6
h/λ = 0.25, b/λ = 1.0 x 10⁻⁶, z₀/λ = 0
Case 1, Perfect ground (ε_r = 1.0, σ = ∞)
Case 6, Very Dry Ground (ε_r = 3.0, σ = 0.0001 S/m)
Case II, Free Space (ε_r = 1.0, σ = 0)
Directive Gain, D(θ=86°) (dBi)
Normalized Disk Ground Plane Radius, 2πa/λ

FIGURE A6-78 Directivity at 4° above the horizon, very dry ground.

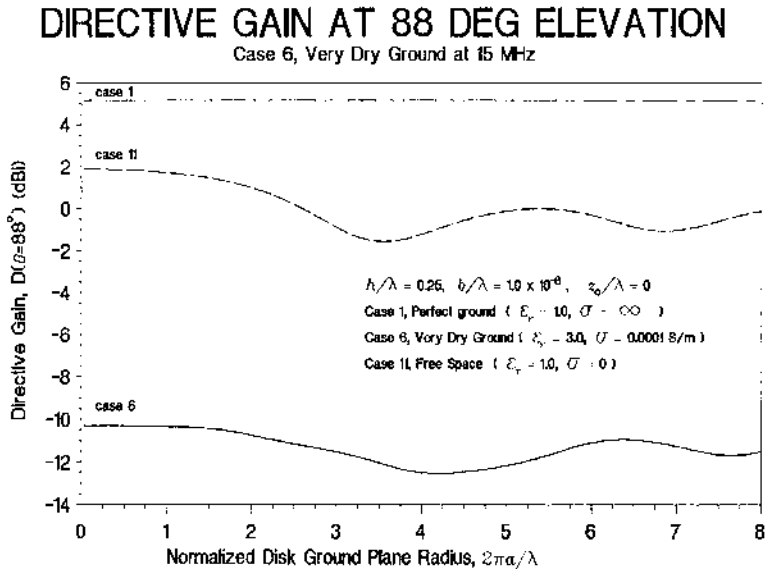
DIRECTIVE GAIN AT 88 DEG ELEVATION
Case 6, Very Dry Ground at 15 MHz
Directive Gain, D(θ=88°) (dBi)
Normalized Disk Ground Plane Radius, 2πa/λ
case I
case II
case 6
h/λ = 0.25, b/λ = 1.0 x 10⁻⁶, z₀/λ = 0
Case 1, Perfect ground (ε_r = 1.0, σ = ∞)
Case 6, Very Dry Ground (ε_r = 3.0, σ = 0.0001 S/m)
Case 11, Free Space (ε_r = 1.0, σ = 0)

FIGURE A6-79 Directivity at 2° above the horizon, very dry ground.

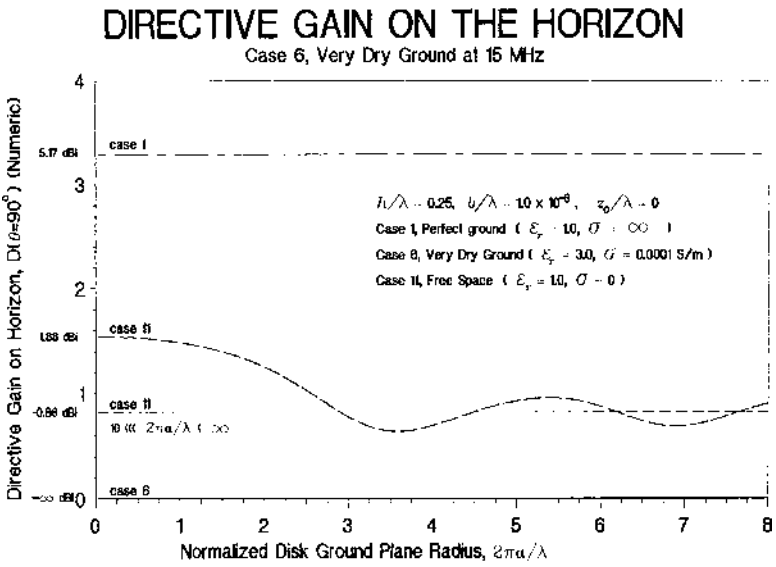
DIRECTIVE GAIN ON THE HORIZON
Case 6, Very Dry Ground at 15 MHz
Directive Gain on Horizon, D(θ=90°) (Numeric)
Normalized Disk Ground Plane Radius, 2πa/λ
5.17 dBi
case I
case II
case 6
h/λ = 0.25, b/λ = 1.0 x 10⁻⁶, z₀/λ = 0
Case 1, Perfect ground (ε_r = 1.0, σ = ∞)
Case 6, Very Dry Ground (ε_r = 3.0, σ = 0.0001 S/m)
Case 11, Free Space (ε_r = 1.0, σ = 0)

FIGURE A6-80 Directivity on the horizon, very dry ground.

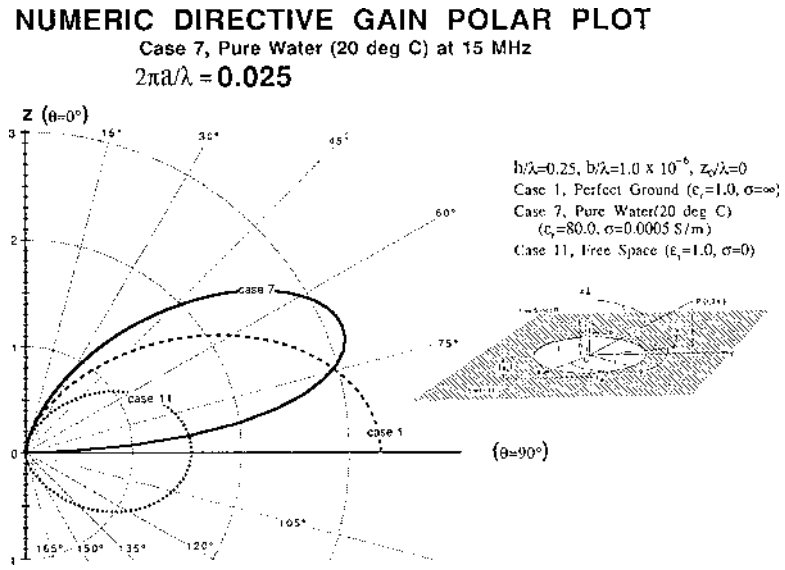
NUMERIC DIRECTIVE GAIN POLAR PLOT
Case 7, Pure Water (20 deg C) at 15 MHz
2πa/λ = 0.025
z (θ=0°)
h/λ=0.25, b/λ=1.0 x 10⁻⁶, z_w/λ=0
Case 1, Perfect Ground (ε_r=1.0, σ=∞)
Case 7, Pure Water(20 deg C)
(ε_r=80.0, σ=0.0005 S/m)
Case 11, Free Space (ε_r=1.0, σ=0)
case 7
case 11
case 1
(θ=90°)

FIGURE A6-81 Directivity pattern, $2\pi a/\lambda = 0.025$, pure water (20°C).

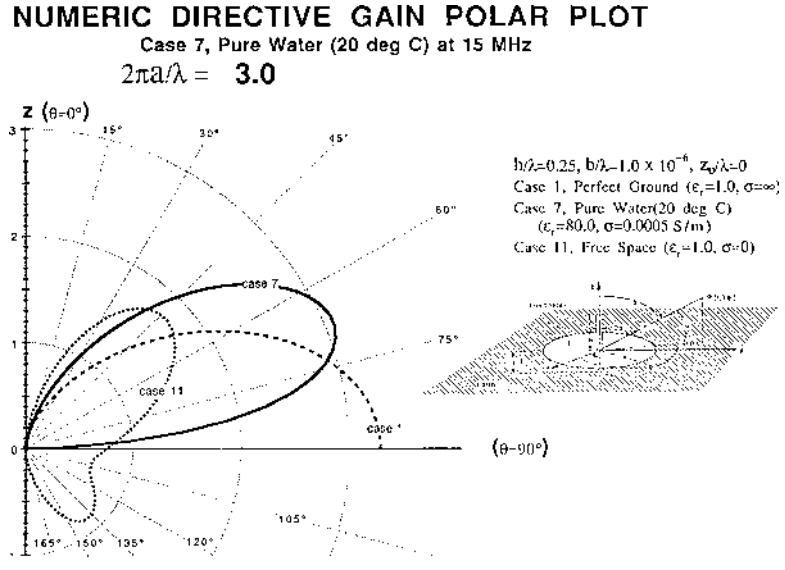
NUMERIC DIRECTIVE GAIN POLAR PLOT
Case 7, Pure Water (20 deg C) at 15 MHz
2πa/λ = 3.0
z (θ=0°)
h/λ=0.25, b/λ=1.0 x 10⁻⁶, z_w/λ=0
Case 1, Perfect Ground (ε_r=1.0, σ=∞)
Case 7, Pure Water(20 deg C)
(ε_r=80.0, σ=0.0005 S/m)
Case 11, Free Space (ε_r=1.0, σ=0)
case 7
case 11
case 1
(θ=90°)

FIGURE A6-82 Directivity pattern, $2\pi a/\lambda = 3.0$, pure water (20°C).

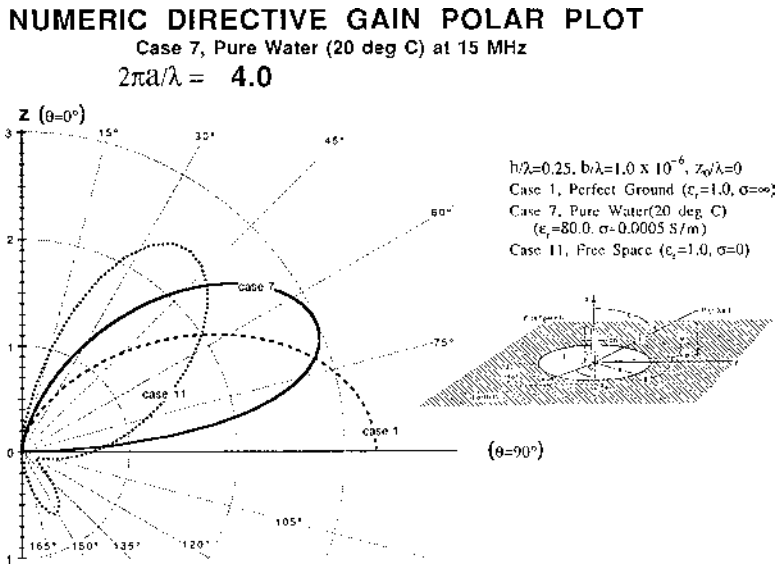

FIGURE A6-83 Directivity pattern, $2\pi a/\lambda = 4.0$, pure water (20°C).

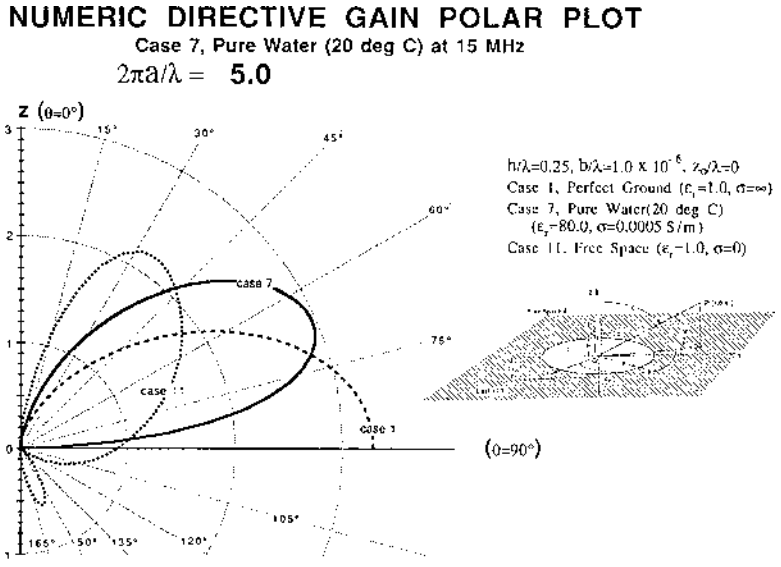

FIGURE A6-84 Directivity pattern, $2\pi a/\lambda = 5.0$, pure water (20°C).

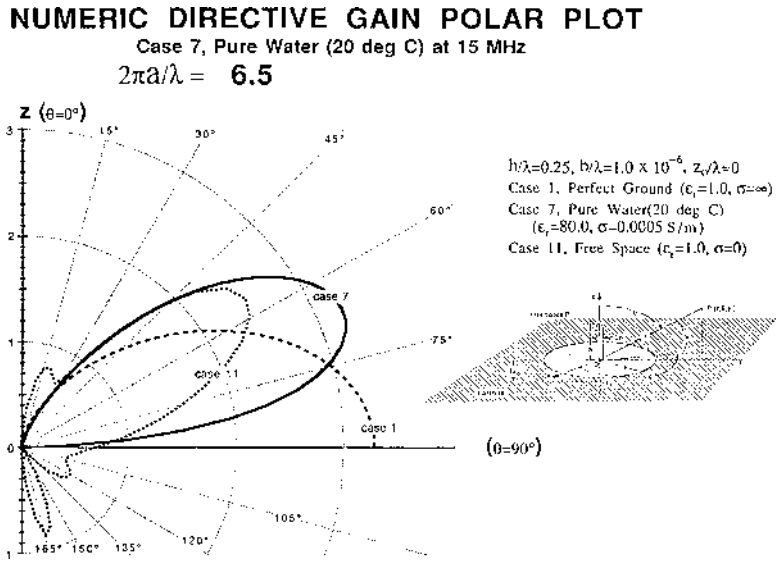
NUMERIC DIRECTIVE GAIN POLAR PLOT
Case 7, Pure Water (20 deg C) at 15 MHz
2πa/λ = 6.5
z (θ=0°)
h/λ=0.25, b/λ=1.0 x 10⁻⁶, z₀/λ=0
Case 1, Perfect Ground (εr=1.0, σ=∞)
Case 7, Pure Water(20 deg C)
(εr=80.0, σ=0.0005 S/m)
Case 11, Free Space (εr=1.0, σ=0)
case 7
case 11
case 1
(θ=90°)

FIGURE A6-85 Directivity pattern, $2\pi a/\lambda = 6.5$, pure water (20°C).

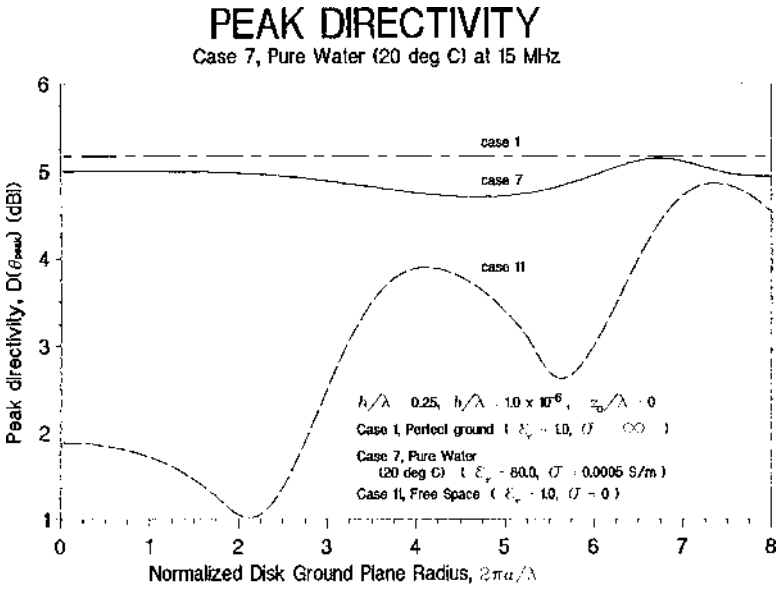
PEAK DIRECTIVITY
Case 7, Pure Water (20 deg C) at 15 MHz
Peak directivity, D(θmax) (dBi)
Normalized Disk Ground Plane Radius, 2πa/λ
case 1
case 7
case 11
h/λ 0.25, h/λ 1.0 x 10⁻⁶, z₀/λ 0
Case 1, Perfect ground (εr 1.0, σ ∞)
Case 7, Pure Water
(20 deg C) (εr 80.0, σ 0.0005 S/m)
Case 11, Free Space (εr 1.0, σ 0)

FIGURE A6-86 Peak directivity, pure water (20°C).

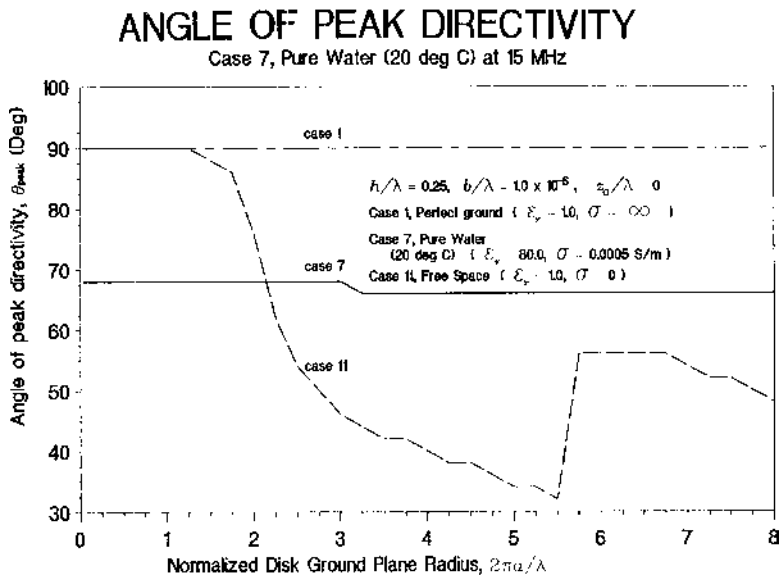
ANGLE OF PEAK DIRECTIVITY
Case 7, Pure Water (20 deg C) at 15 MHz
Angle of peak directivity, θ_{peak} (Deg)
Normalized Disk Ground Plane Radius, $2\pi a/\lambda$
case I
case 7
case II
h/λ = 0.25, b/λ = 1.0 x 10^{-6}, z_0/λ 0
Case 1, Perfect ground (ε_r = 1.0, σ = ∞)
Case 7, Pure Water
(20 deg C) (ε_r 80.0, σ = 0.0005 S/m)
Case 11, Free Space (ε_r = 1.0, σ 0)

FIGURE A6-87 Angle of incidence of peak directivity, pure water (20°C).

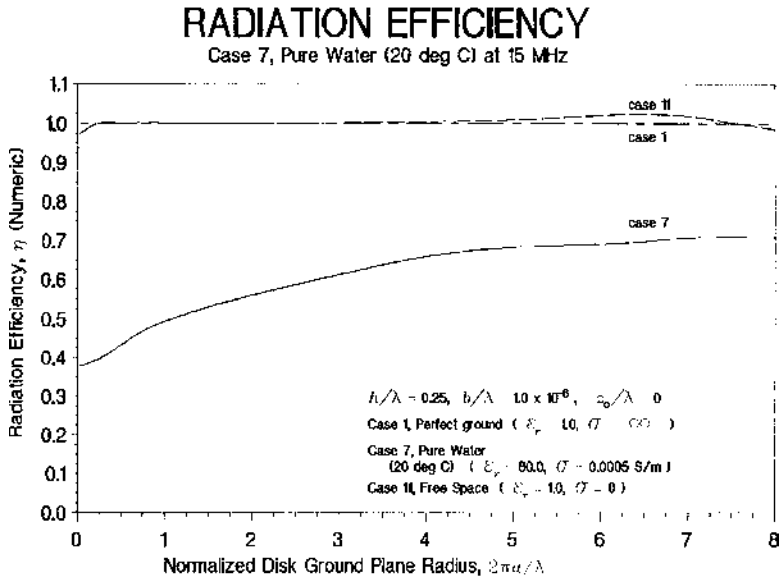
RADIATION EFFICIENCY
Case 7, Pure Water (20 deg C) at 15 MHz
Radiation Efficiency, η (Numeric)
Normalized Disk Ground Plane Radius, $2\pi a/\lambda$
case II
case 1
case 7
h/λ = 0.25, b/λ 1.0 x 10^{-6}, z_0/λ 0
Case 1, Perfect ground (ε_r 1.0, σ ∞)
Case 7, Pure Water
(20 deg C) (ε_r 80.0, σ = 0.0005 S/m)
Case 11, Free Space (ε_r = 1.0, σ = 0)

FIGURE A6-88 Radiation efficiency, pure water (20°C).

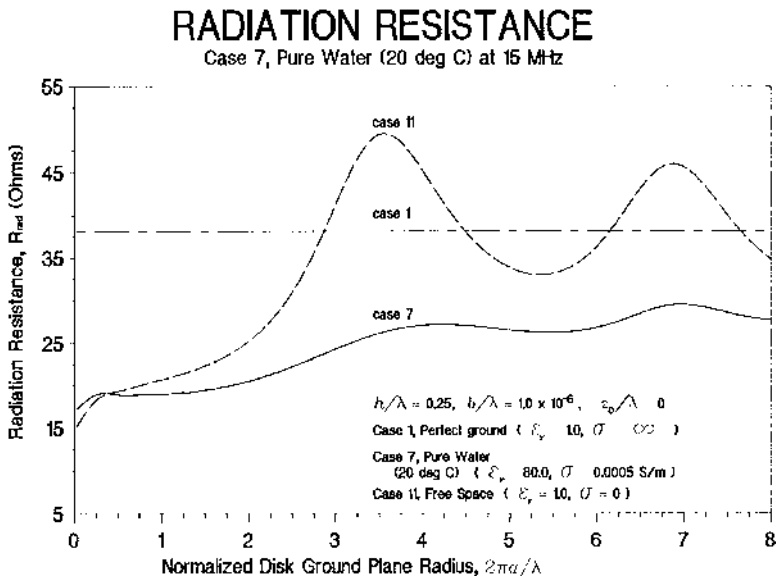
RADIATION RESISTANCE
Case 7, Pure Water (20 deg C) at 15 MHz
Radiation Resistance, R_{rad} (Ohms)
Normalized Disk Ground Plane Radius, $2\pi a/\lambda$
case II
case I
case 7
h/λ = 0.25, b/λ = 1.0 x 10^{-6}, z_0/λ = 0
Case I, Perfect ground (ε_r = 1.0, σ = ∞)
Case 7, Pure Water
(20 deg C) (ε_r = 80.0, σ = 0.0005 S/m)
Case II, Free Space (ε_r = 1.0, σ = 0)

FIGURE A6-89 Radiation resistance, pure water (20°C).

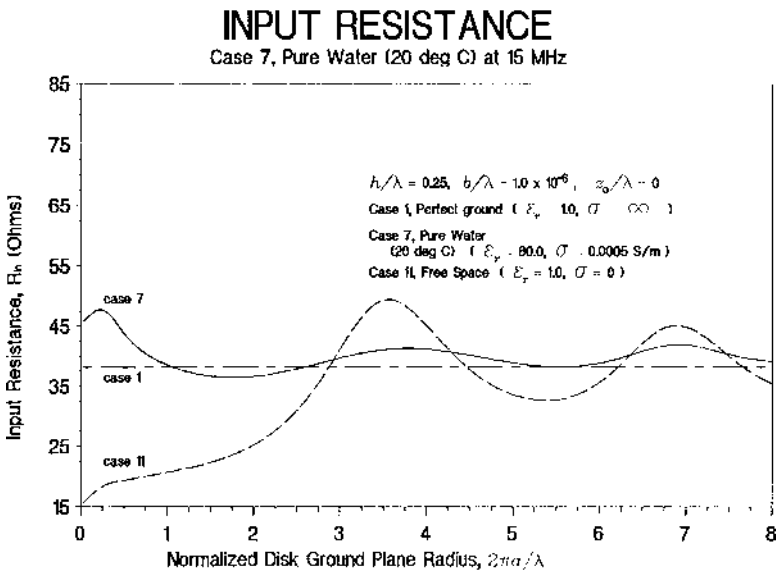
INPUT RESISTANCE
Case 7, Pure Water (20 deg C) at 15 MHz
Input Resistance, R_{in} (Ohms)
Normalized Disk Ground Plane Radius, $2\pi a/\lambda$
case 7
case I
case II
h/λ = 0.25, b/λ = 1.0 x 10^{-6}, z_0/λ = 0
Case I, Perfect ground (ε_r = 1.0, σ = ∞)
Case 7, Pure Water
(20 deg C) (ε_r = 80.0, σ = 0.0005 S/m)
Case II, Free Space (ε_r = 1.0, σ = 0)

FIGURE A6-90 Input resistance, pure water (20°C).

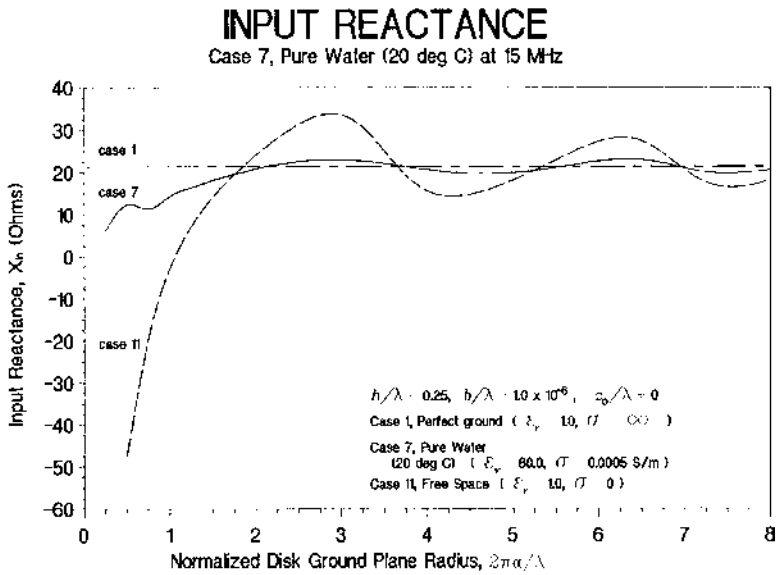
INPUT REACTANCE
Case 7, Pure Water (20 deg C) at 15 MHz
Input Reactance, X_{in} (Ohms)
Normalized Disk Ground Plane Radius, $2\pi a/\lambda$
case I
case 7
case II
h/λ = 0.25, b/λ = 1.0 x 10^{-6}, z_0/λ = 0
Case I, Perfect ground (ε_r 1.0, σ ∞)
Case 7, Pure Water
(20 deg C) (ε_r 80.0, σ 0.0005 S/m)
Case II, Free Space (ε_r 1.0, σ 0)

FIGURE A6-91 Input reactance, pure water (20°C).

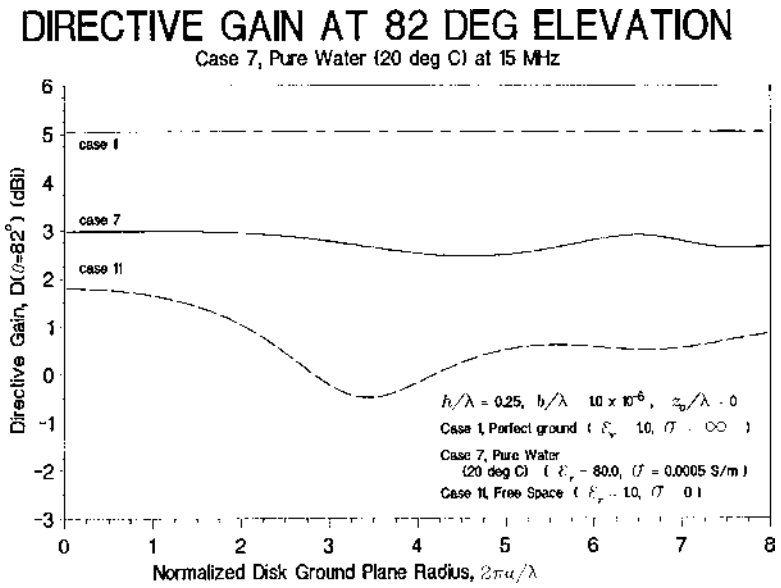
DIRECTIVE GAIN AT 82 DEG ELEVATION
Case 7, Pure Water (20 deg C) at 15 MHz
Directive Gain, D(θ=82°) (dBi)
Normalized Disk Ground Plane Radius, $2\pi a/\lambda$
case I
case 7
case II
h/λ = 0.25, b/λ 1.0 x 10^{-6}, z_0/λ = 0
Case I, Perfect ground (ε_r 1.0, σ ∞)
Case 7, Pure Water
(20 deg C) (ε_r = 80.0, σ = 0.0005 S/m)
Case II, Free Space (ε_r = 1.0, σ 0)

FIGURE A6-92 Directivity at 8° above the horizon, pure water (20°C).

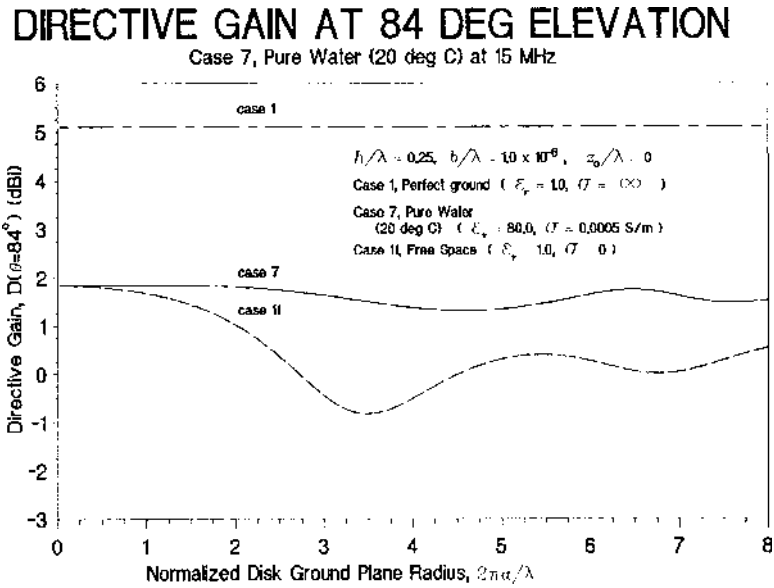
DIRECTIVE GAIN AT 84 DEG ELEVATION
Case 7, Pure Water (20 deg C) at 15 MHz
case 1
case 7
case 11
Directive Gain, D(θ=84°) (dBi)
Normalized Disk Ground Plane Radius, 2πa/λ

FIGURE A6-93 Directivity at 6° above the horizon, pure water (20°C).

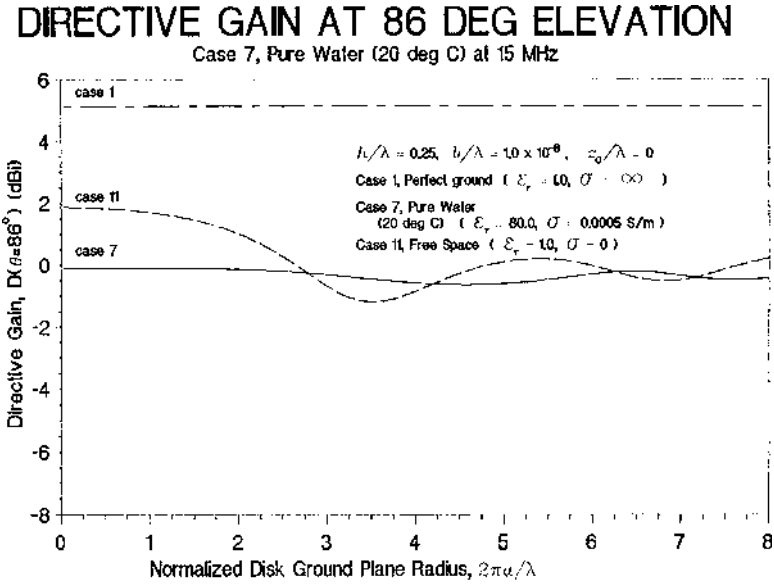
DIRECTIVE GAIN AT 86 DEG ELEVATION
Case 7, Pure Water (20 deg C) at 15 MHz
case 1
case 11
case 7
Directive Gain, D(θ=86°) (dBi)
Normalized Disk Ground Plane Radius, 2πa/λ

FIGURE A6-94 Directivity at 4° above the horizon, pure water (20°C).

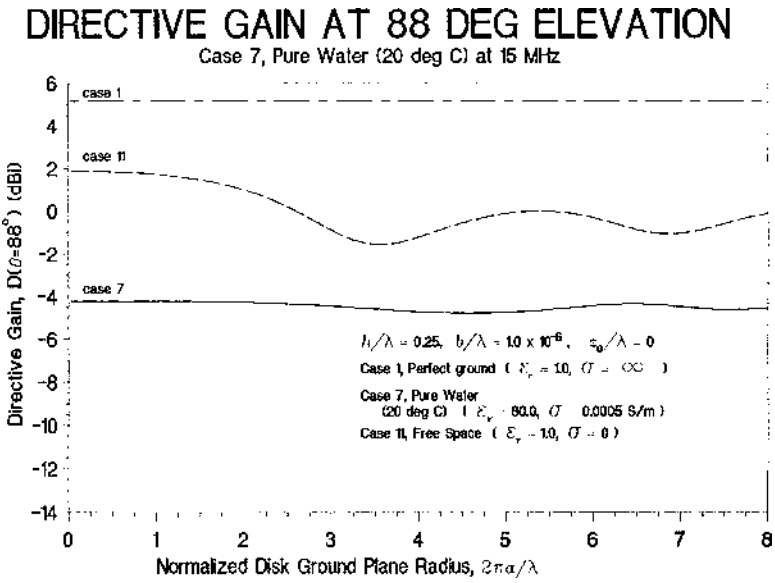
DIRECTIVE GAIN AT 88 DEG ELEVATION
Case 7, Pure Water (20 deg C) at 15 MHz
case 1
case 11
case 7
Directive Gain, D(θ=88°) (dBi)
Normalized Disk Ground Plane Radius, 2πa/λ
h/λ = 0.25, b/λ = 1.0 x 10⁻⁶, z₀/λ = 0
Case 1, Perfect ground (ε_r = 1.0, σ = ∞)
Case 7, Pure Water
(20 deg C) (ε_r = 80.0, σ = 0.0005 S/m)
Case 11, Free Space (ε_r = 1.0, σ = 0)

FIGURE A6-95 Directivity at 2° above the horizon, pure water (20°C).

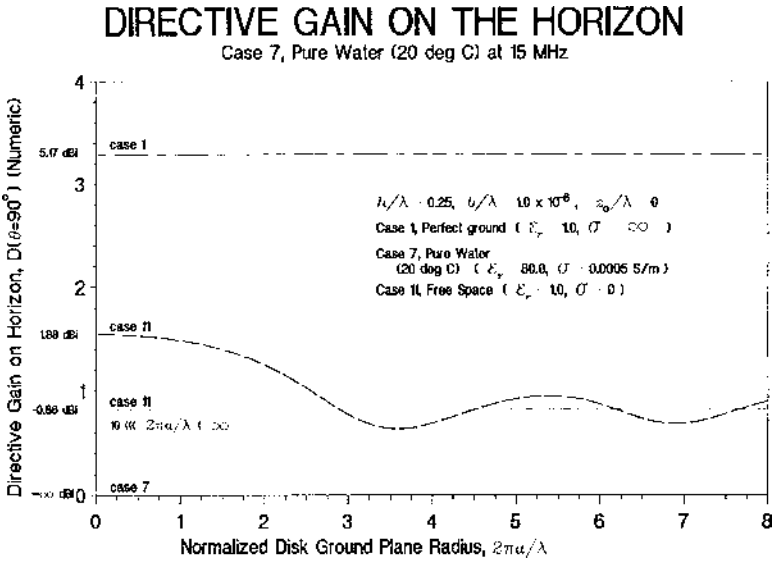
DIRECTIVE GAIN ON THE HORIZON
Case 7, Pure Water (20 deg C) at 15 MHz
case 1
5.07 dBi
case 11
1.88 dBi
case 11
-0.86 dBi
10 ≪ 2πa/λ ≪ ∞
case 7
-∞ dBi
Directive Gain on Horizon, D(θ=90°) (Numeric)
Normalized Disk Ground Plane Radius, 2πa/λ
h/λ = 0.25, b/λ = 1.0 x 10⁻⁶, z₀/λ = 0
Case 1, Perfect ground (ε_r = 1.0, σ = ∞)
Case 7, Pure Water
(20 deg C) (ε_r = 80.0, σ = 0.0005 S/m)
Case 11, Free Space (ε_r = 1.0, σ = 0)

FIGURE A6-96 Directivity on the horizon, pure water (20°C).

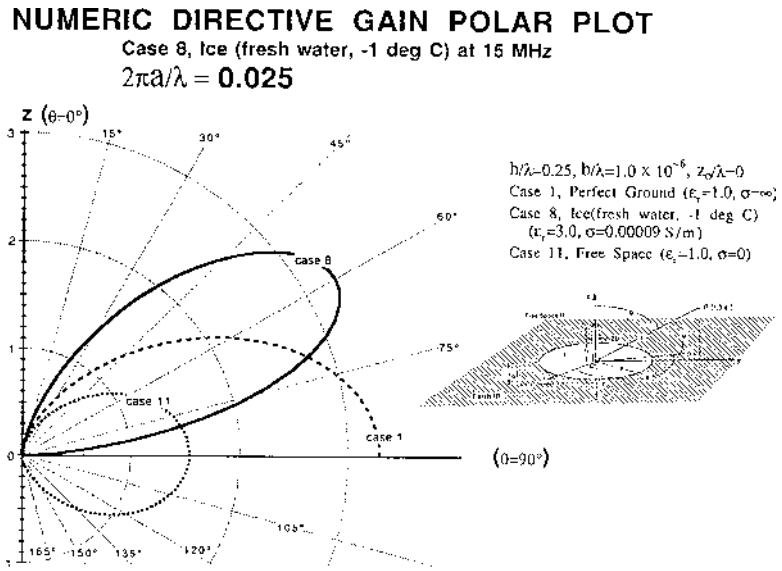
NUMERIC DIRECTIVE GAIN POLAR PLOT
Case 8, Ice (fresh water, -1 deg C) at 15 MHz
2πa/λ = 0.025
z (θ=0°)
h/λ=0.25, b/λ=1.0 x 10⁻⁶, z₀/λ=0
Case 1, Perfect Ground (εr=1.0, σ=∞)
Case 8, Ice(fresh water, -1 deg C)
(εr=3.0, σ=0.00009 S/m)
Case 11, Free Space (εr=1.0, σ=0)
case 8
case 11
case 1
(θ=90°)

FIGURE A6-97 Directivity pattern, $2\pi a/\lambda = 0.025$, ice (fresh water, $-1°$C).

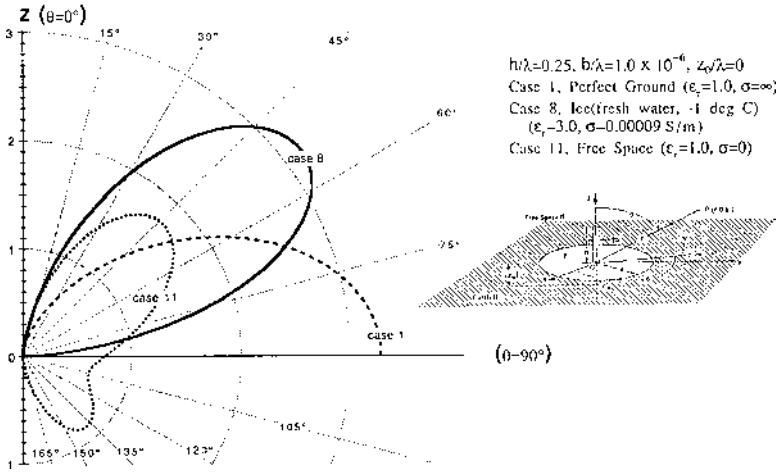
NUMERIC DIRECTIVE GAIN POLAR PLOT
Case 8, Ice (fresh water, -1 deg C) at 15 MHz
2πa/λ = 3.0
z (θ=0°)
h/λ=0.25, b/λ=1.0 x 10⁻⁶, z₀/λ=0
Case 1, Perfect Ground (εr=1.0, σ=∞)
Case 8, Ice(fresh water, -1 deg C)
(εr=3.0, σ=0.00009 S/m)
Case 11, Free Space (εr=1.0, σ=0)
case 8
case 11
case 1
(θ=90°)

FIGURE A6-98 Directivity pattern, $2\pi a/\lambda = 3.0$, ice (fresh water, $-1°$C).

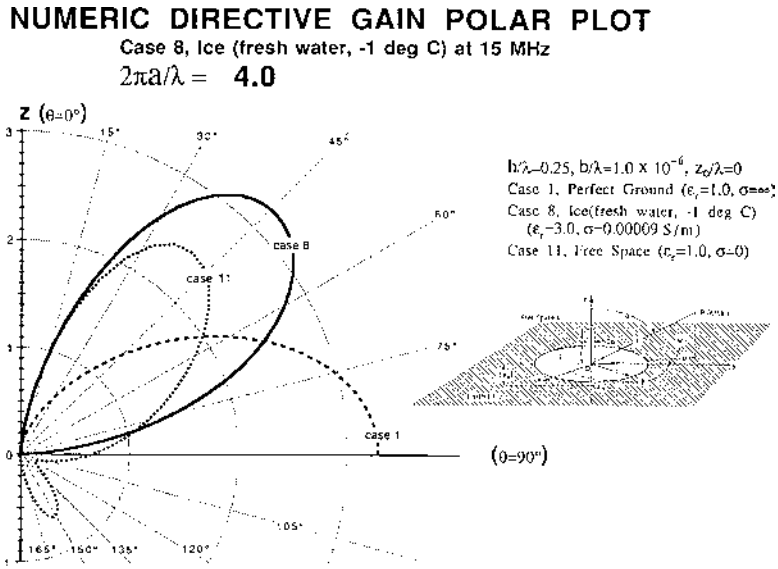

FIGURE A6-99 Directivity pattern, $2\pi a/\lambda = 4.0$, ice (fresh water, $-1°$C).

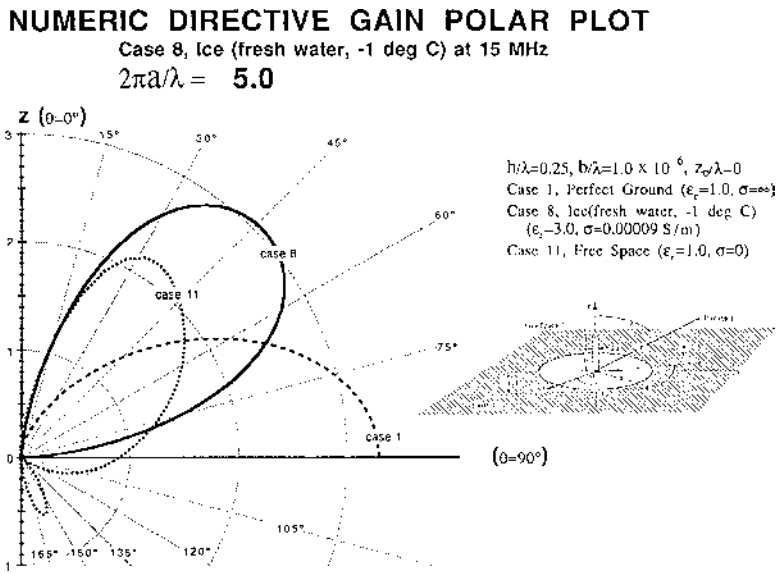

FIGURE A6-100 Directivity pattern, $2\pi a/\lambda = 5.0$, ice (fresh water, $-1°$C).

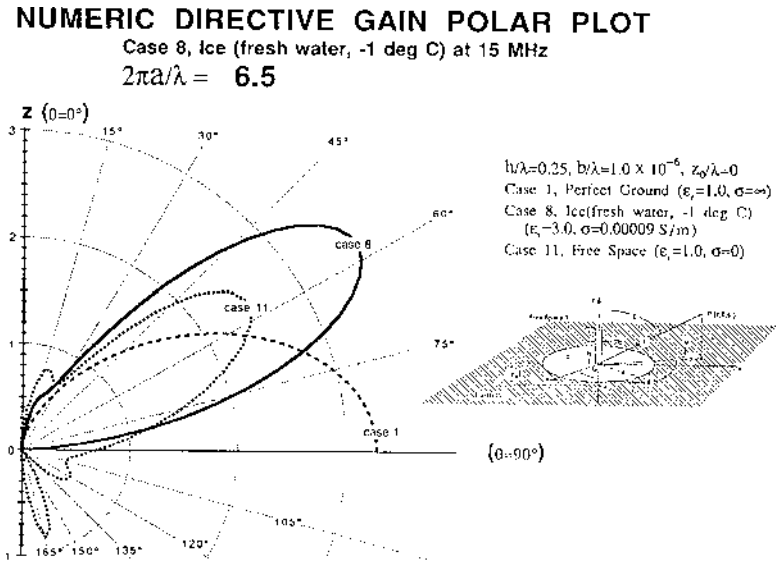

FIGURE A6-101 Directivity pattern, $2\pi a/\lambda = 6.5$, ice (fresh water, $-1°$C).

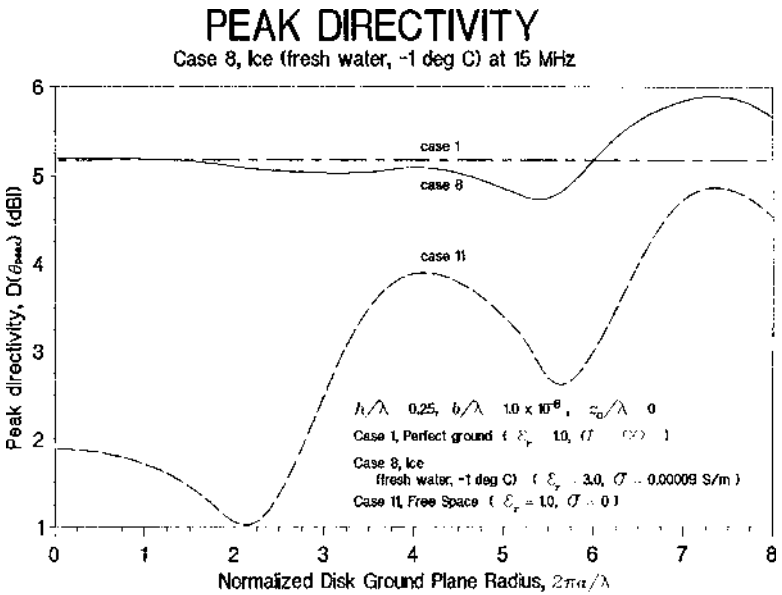
PEAK DIRECTIVITY
Case 8, Ice (fresh water, -1 deg C) at 15 MHz
Peak directivity, D(θpeak) (dBi)
Normalized Disk Ground Plane Radius, 2πa/λ
case 1
case 8
case 11
h/λ 0.25, b/λ 1.0 x 10⁻⁶, z₀/λ 0
Case 1, Perfect ground (εr 1.0, σ (∞))
Case 8, Ice
(fresh water, -1 deg C) (εr 3.0, σ 0.00009 S/m)
Case 11, Free Space (εr = 1.0, σ 0)

FIGURE A6-102 Peak directivity, ice (fresh water, $-1°$C).

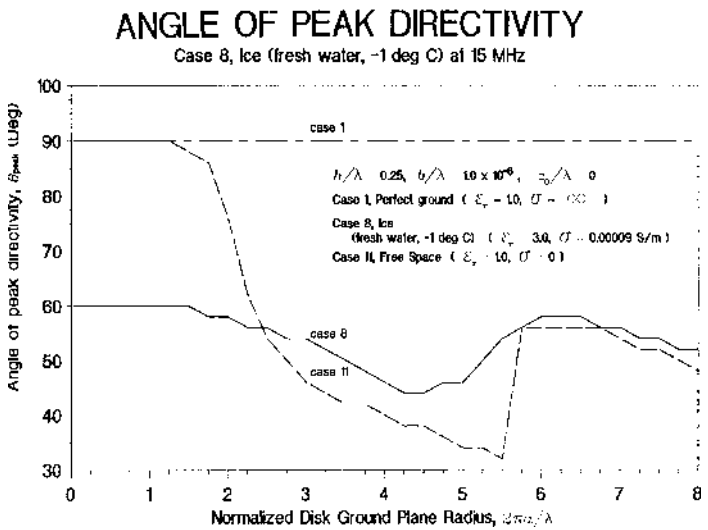
ANGLE OF PEAK DIRECTIVITY
Case 8, Ice (fresh water, -1 deg C) at 15 MHz
Angle of peak directivity, θ_{max} (Deg)
Normalized Disk Ground Plane Radius, $2\pi a/\lambda$
case 1
case 8
case 11
h/λ 0.25, b/λ 1.0 x 10^{-6}, z_0/λ 0
Case 1, Perfect ground (ε_r = 1.0, σ = ∞)
Case 8, Ice
(fresh water, -1 deg C) (ε_r 3.0, σ = 0.00009 S/m)
Case 11, Free Space (ε_r = 1.0, σ = 0)

FIGURE A6-103 Angle of incidence of peak directivity, ice (fresh water, −1°C).

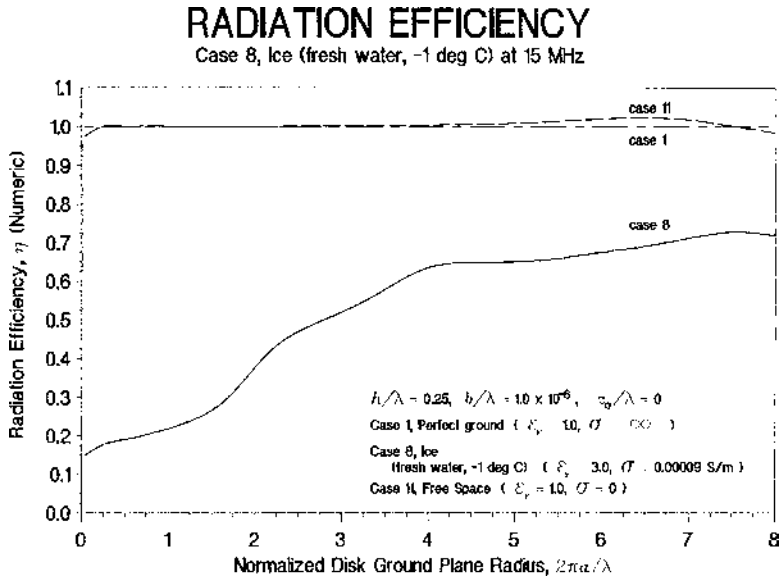
RADIATION EFFICIENCY
Case 8, Ice (fresh water, -1 deg C) at 15 MHz
Radiation Efficiency, η (Numeric)
Normalized Disk Ground Plane Radius, $2\pi a/\lambda$
case 11
case 1
case 8
h/λ = 0.25, b/λ = 1.0 x 10^{-6}, z_0/λ = 0
Case 1, Perfect ground (ε_r 1.0, σ ∞)
Case 8, Ice
(fresh water, -1 deg C) (ε_r 3.0, σ 0.00009 S/m)
Case 11, Free Space (ε_r = 1.0, σ = 0)

FIGURE A6-104 Radiation efficiency, ice (fresh water, −1°C).

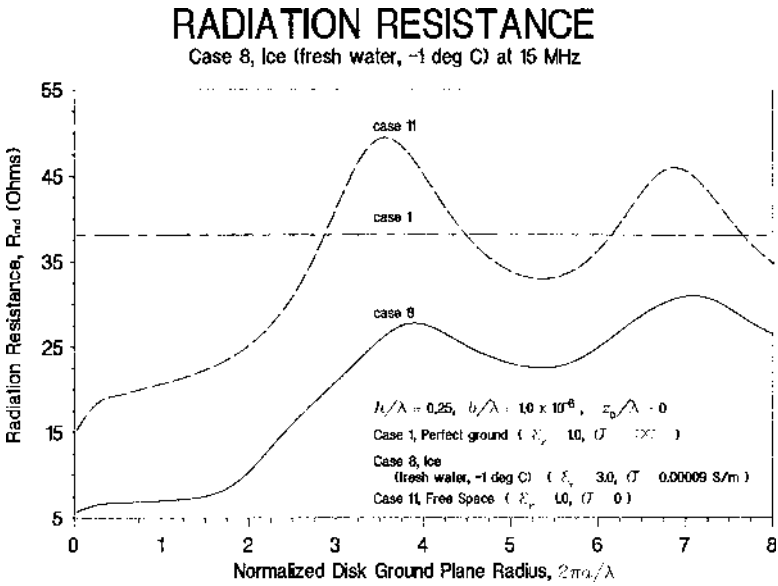
RADIATION RESISTANCE
Case 8, Ice (fresh water, -1 deg C) at 15 MHz
Radiation Resistance, R_{rad} (Ohms)
Normalized Disk Ground Plane Radius, $2\pi a/\lambda$
case 11
case 1
case 8
h/λ = 0.25, b/λ = 1.0 x 10^{-6}, z_0/λ = 0
Case 1, Perfect ground (ε_r 1.0, σ ∞)
Case 8, Ice
(fresh water, -1 deg C) (ε_r 3.0, σ 0.00009 S/m)
Case 11, Free Space (ε_r 1.0, σ 0)

FIGURE A6-105 Radiation resistance, ice (fresh water, −1°C).

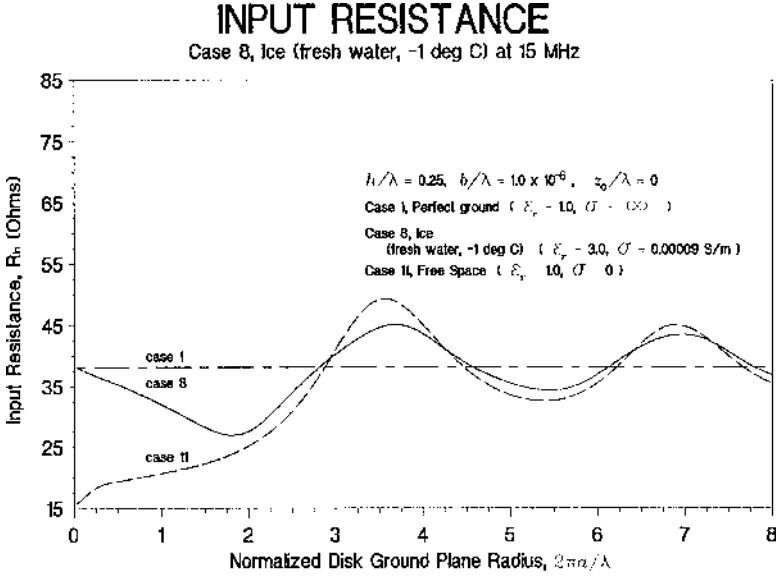
INPUT RESISTANCE
Case 8, Ice (fresh water, -1 deg C) at 15 MHz
Input Resistance, R_{in} (Ohms)
Normalized Disk Ground Plane Radius, $2\pi a/\lambda$
case 1
case 8
case 11
h/λ = 0.25, b/λ = 1.0 x 10^{-6}, z_0/λ = 0
Case 1, Perfect ground (ε_r = 1.0, σ = ∞)
Case 8, Ice
(fresh water, -1 deg C) (ε_r = 3.0, σ = 0.00009 S/m)
Case 11, Free Space (ε_r 1.0, σ 0)

FIGURE A6-106 Input resistance, ice (fresh water, −1°C).

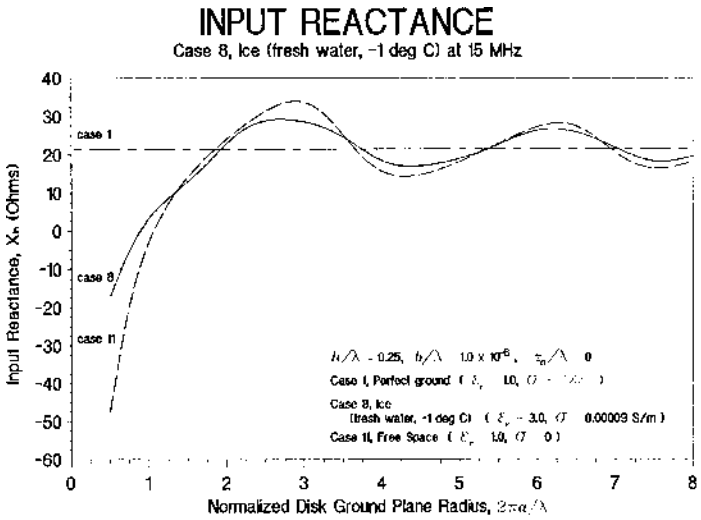
INPUT REACTANCE
Case 8, Ice (fresh water, -1 deg C) at 15 MHz
Input Reactance, X_A (Ohms)
Normalized Disk Ground Plane Radius, $2\pi a/\lambda$
case 1
case 8
case 11
h/λ = 0.25, b/λ = 1.0 x 10^{-6}, τ_a/λ = 0
Case 1, Perfect ground (ε_r = 1.0, σ = ∞)
Case 8, Ice
(fresh water, -1 deg C) (ε_r = 3.0, σ = 0.00009 S/m)
Case 11, Free Space (ε_r = 1.0, σ = 0)

FIGURE A6-107 Input reactance, ice (fresh water, −1°C).

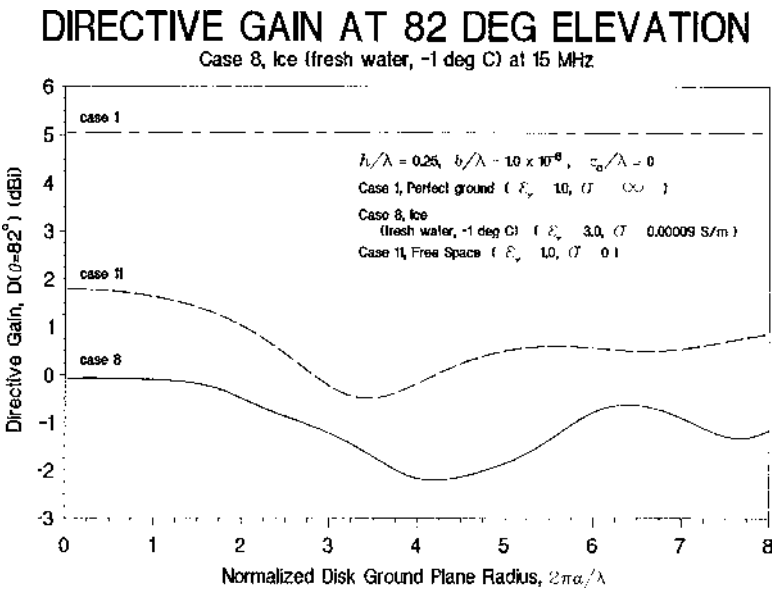
DIRECTIVE GAIN AT 82 DEG ELEVATION
Case 8, Ice (fresh water, -1 deg C) at 15 MHz
Directive Gain, D(θ=82°) (dBi)
Normalized Disk Ground Plane Radius, $2\pi a/\lambda$
case 1
case 11
case 8
h/λ = 0.25, b/λ = 1.0 x 10^{-6}, τ_a/λ = 0
Case 1, Perfect ground (ε_r = 1.0, σ = ∞)
Case 8, Ice
(fresh water, -1 deg C) (ε_r = 3.0, σ = 0.00009 S/m)
Case 11, Free Space (ε_r = 1.0, σ = 0)

FIGURE A6-108 Directivity at 8° above the horizon, ice (fresh water, −1°C).

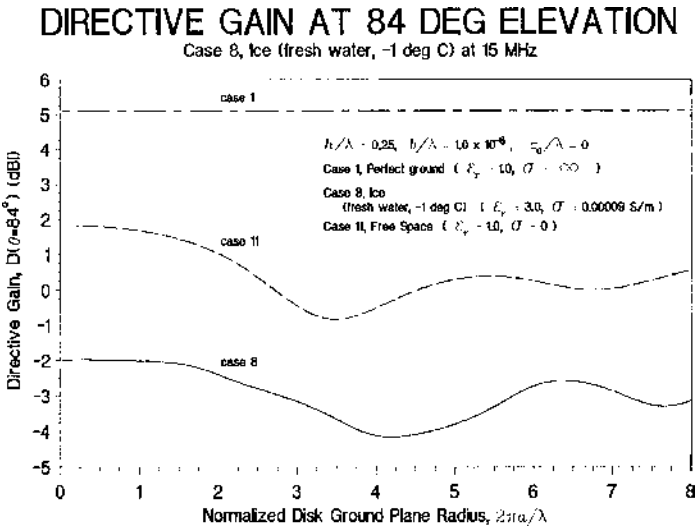
DIRECTIVE GAIN AT 84 DEG ELEVATION
Case 8, Ice (fresh water, -1 deg C) at 15 MHz
case 1
case 11
case 8
h/λ = 0.25, b/λ = 1.0 x 10⁻⁸, z₀/λ = 0
Case 1, Perfect ground (ε_r = 1.0, σ = ∞)
Case 8, Ice
(fresh water, -1 deg C) (ε_r = 3.0, σ = 0.00009 S/m)
Case 11, Free Space (ε_r = 1.0, σ = 0)
Directive Gain, D(θ=84°) (dBi)
Normalized Disk Ground Plane Radius, 2πa/λ

FIGURE A6-109 Directivity at 6° above the horizon, ice (fresh water, −1°C).

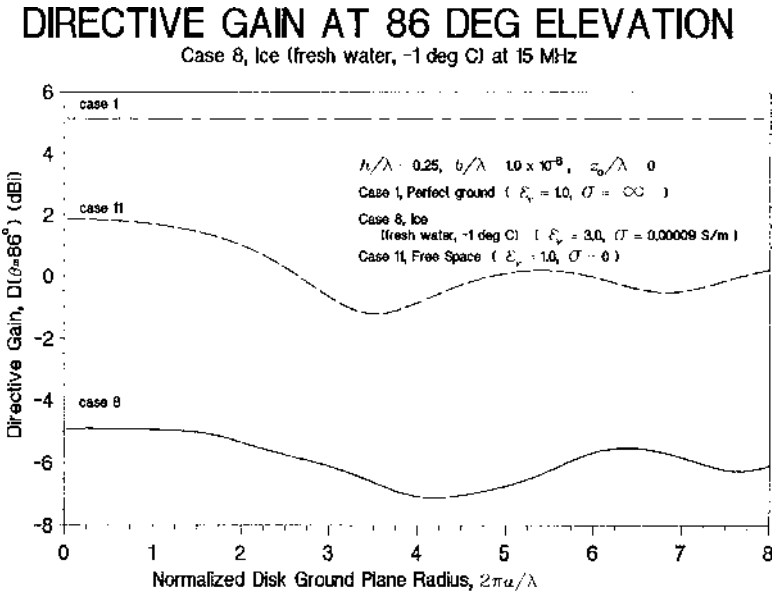
DIRECTIVE GAIN AT 86 DEG ELEVATION
Case 8, Ice (fresh water, -1 deg C) at 15 MHz
case 1
case 11
case 8
h/λ = 0.25, b/λ = 1.0 x 10⁻⁸, z₀/λ = 0
Case 1, Perfect ground (ε_r = 1.0, σ = ∞)
Case 8, Ice
(fresh water, -1 deg C) (ε_r = 3.0, σ = 0.00009 S/m)
Case 11, Free Space (ε_r = 1.0, σ = 0)
Directive Gain, D(θ=86°) (dBi)
Normalized Disk Ground Plane Radius, 2πa/λ

FIGURE A6-110 Directivity at 4° above the horizon, ice (fresh water, −1°C).

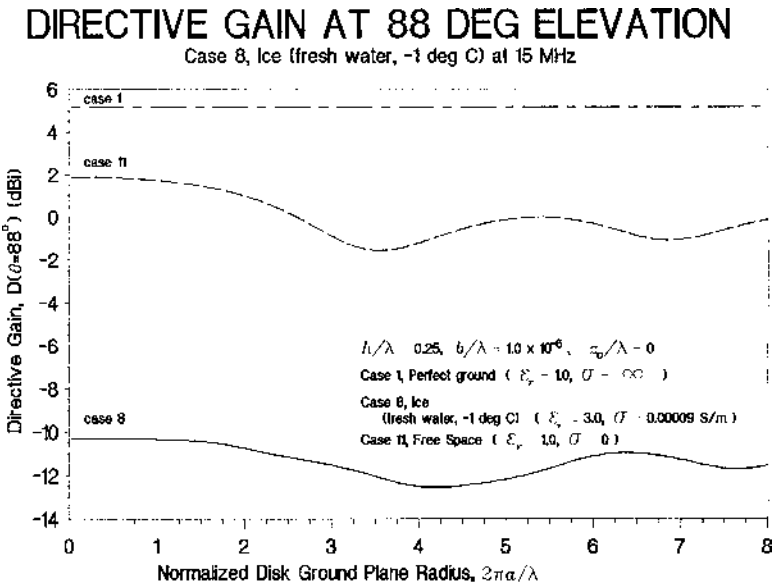
DIRECTIVE GAIN AT 88 DEG ELEVATION
Case 8, Ice (fresh water, -1 deg C) at 15 MHz
Directive Gain, D(θ=88°) (dBi)
Normalized Disk Ground Plane Radius, 2πa/λ
case 1
case 11
case 8
h/λ 0.25, b/λ = 1.0 x 10⁻⁶, r₀/λ = 0
Case 1, Perfect ground (εr = 1.0, σ = ∞)
Case 8, Ice
(fresh water, -1 deg C) (εr = 3.0, σ = 0.00009 S/m)
Case 11, Free Space (εr = 1.0, σ = 0)

FIGURE A6-111 Directivity at 2° above the horizon, ice (fresh water, −1°C).

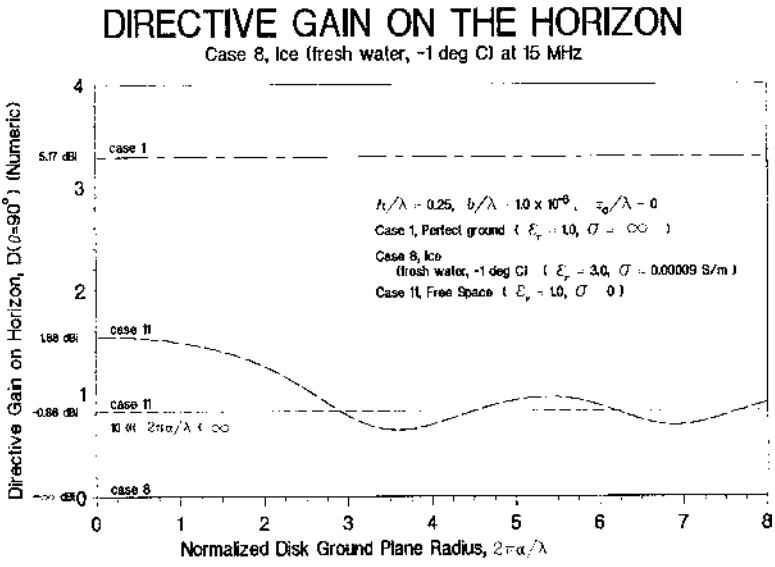
DIRECTIVE GAIN ON THE HORIZON
Case 8, Ice (fresh water, -1 deg C) at 15 MHz
Directive Gain on Horizon, D(θ=90°) (Numeric)
Normalized Disk Ground Plane Radius, 2πa/λ
5.17 dBi
1.88 dBi
-0.88 dBi
-∞ dBi
case 1
case 11
case 11
case 8
10 at 2πa/λ = ∞
h/λ = 0.25, b/λ = 1.0 x 10⁻⁶, r₀/λ = 0
Case 1, Perfect ground (εr = 1.0, σ = ∞)
Case 8, Ice
(fresh water, -1 deg C) (εr = 3.0, σ = 0.00009 S/m)
Case 11, Free Space (εr = 1.0, σ = 0)

FIGURE A6-112 Directivity on the horizon, ice (fresh water, −1°C).

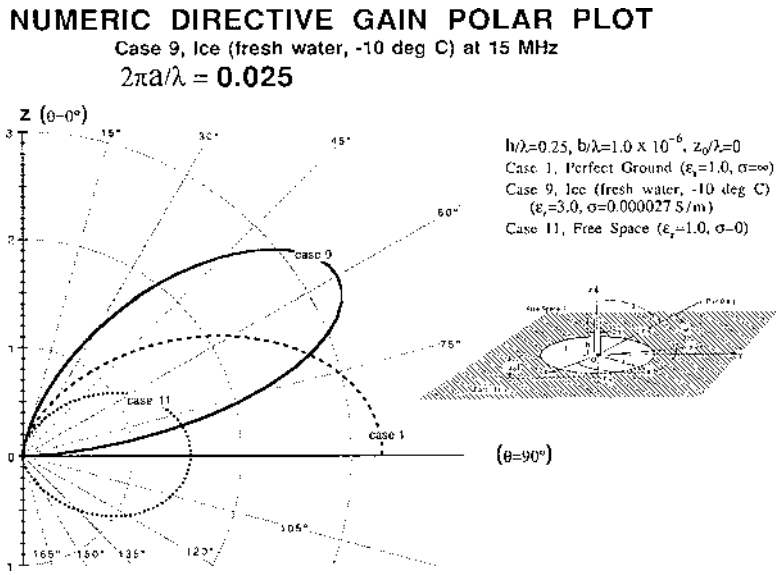
NUMERIC DIRECTIVE GAIN POLAR PLOT
Case 9, Ice (fresh water, -10 deg C) at 15 MHz
2πa/λ = 0.025
Z (θ=0°)
h/λ=0.25, b/λ=1.0 x 10⁻⁶, z₀/λ=0
Case 1, Perfect Ground (εr=1.0, σ=∞)
Case 9, Ice (fresh water, -10 deg C)
(εr=3.0, σ=0.000027 S/m)
Case 11, Free Space (εr=1.0, σ=0)
case 9
case 11
case 1
(θ=90°)

FIGURE A6-113 Directivity pattern, $2\pi a/\lambda = 0.025$, ice (fresh water, $-10°C$).

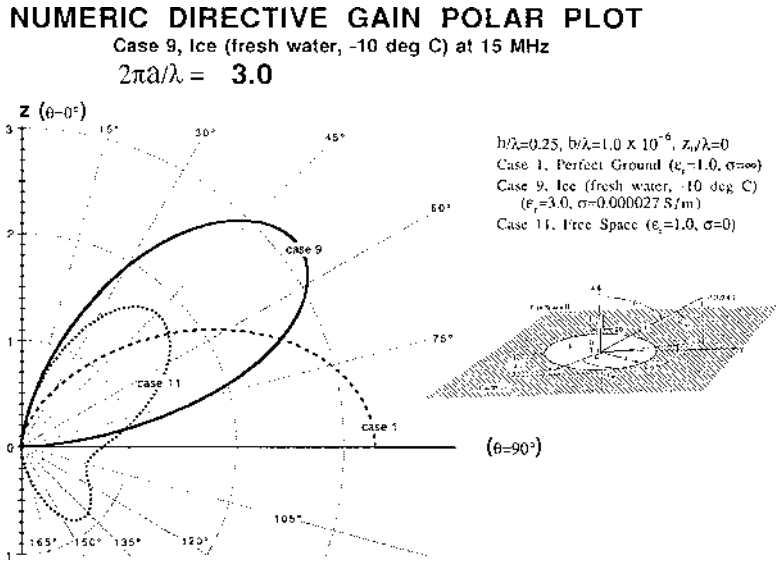
NUMERIC DIRECTIVE GAIN POLAR PLOT
Case 9, Ice (fresh water, -10 deg C) at 15 MHz
2πa/λ = 3.0
Z (θ=0°)
h/λ=0.25, b/λ=1.0 x 10⁻⁶, z₀/λ=0
Case 1, Perfect Ground (εr=1.0, σ=∞)
Case 9, Ice (fresh water, -10 deg C)
(εr=3.0, σ=0.000027 S/m)
Case 11, Free Space (εr=1.0, σ=0)
case 9
case 11
case 1
(θ=90°)

FIGURE A6-114 Directivity pattern, $2\pi a/\lambda = 3.0$, ice (fresh water, $-10°C$).

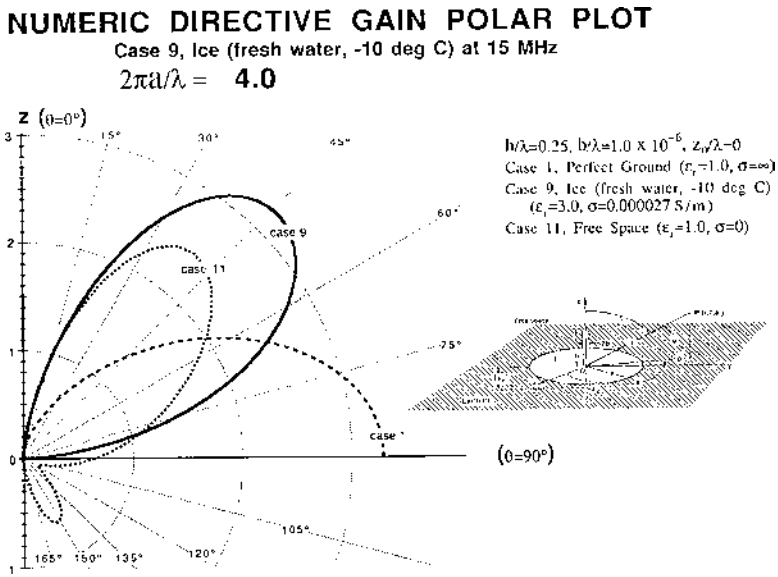
NUMERIC DIRECTIVE GAIN POLAR PLOT
Case 9, Ice (fresh water, -10 deg C) at 15 MHz
2πa/λ = 4.0
z (θ=0°)
h/λ=0.25, b/λ=1.0 x 10⁻⁶, z₀/λ=0
Case 1, Perfect Ground (εr=1.0, σ=∞)
Case 9, Ice (fresh water, -10 deg C)
(εr=3.0, σ=0.000027 S/m)
Case 11, Free Space (εr=1.0, σ=0)
case 9
case 11
case 1
(θ=90°)

FIGURE A6-115 Directivity pattern, $2\pi a/\lambda = 4.0$, ice (fresh water, $-10°$C).

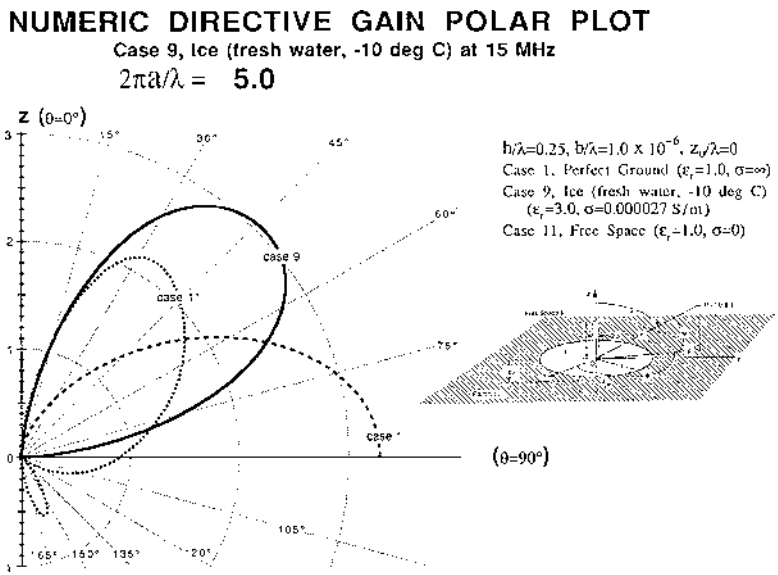
NUMERIC DIRECTIVE GAIN POLAR PLOT
Case 9, Ice (fresh water, -10 deg C) at 15 MHz
2πa/λ = 5.0
z (θ=0°)
h/λ=0.25, b/λ=1.0 x 10⁻⁶, z₀/λ=0
Case 1, Perfect Ground (εr=1.0, σ=∞)
Case 9, Ice (fresh water, -10 deg C)
(εr=3.0, σ=0.000027 S/m)
Case 11, Free Space (εr=1.0, σ=0)
case 9
case 11
case 1
(θ=90°)

FIGURE A6-116 Directivity pattern, $2\pi a/\lambda = 5.0$, ice (fresh water, $-10°$C).

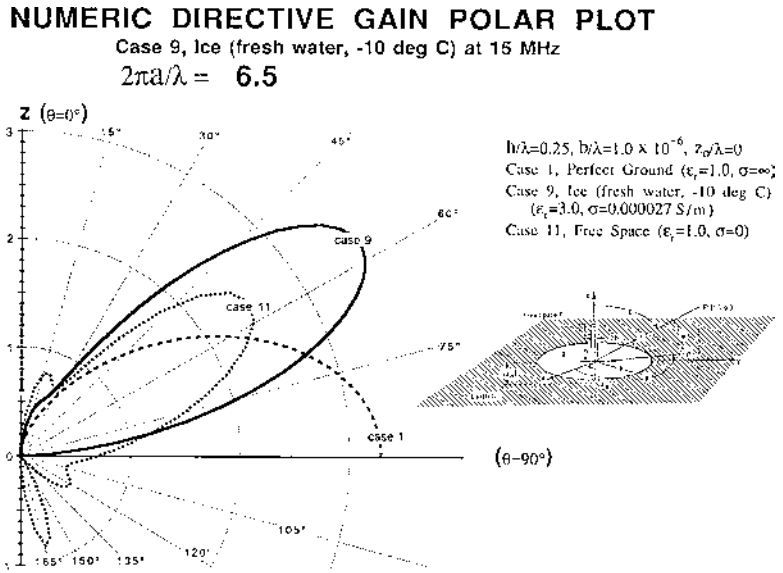
NUMERIC DIRECTIVE GAIN POLAR PLOT
Case 9, Ice (fresh water, -10 deg C) at 15 MHz
2πa/λ = 6.5
z (θ=0°)
h/λ=0.25, b/λ=1.0 x 10⁻⁶, z₀/λ=0
Case 1, Perfect Ground (εr=1.0, σ=∞)
Case 9, Ice (fresh water, -10 deg C)
(εr=3.0, σ=0.000027 S/m)
Case 11, Free Space (εr=1.0, σ=0)
case 9
case 11
case 1
(θ=90°)

FIGURE A6-117 Directivity pattern, $2\pi a/\lambda = 6.5$, ice (fresh water, $-10°C$).

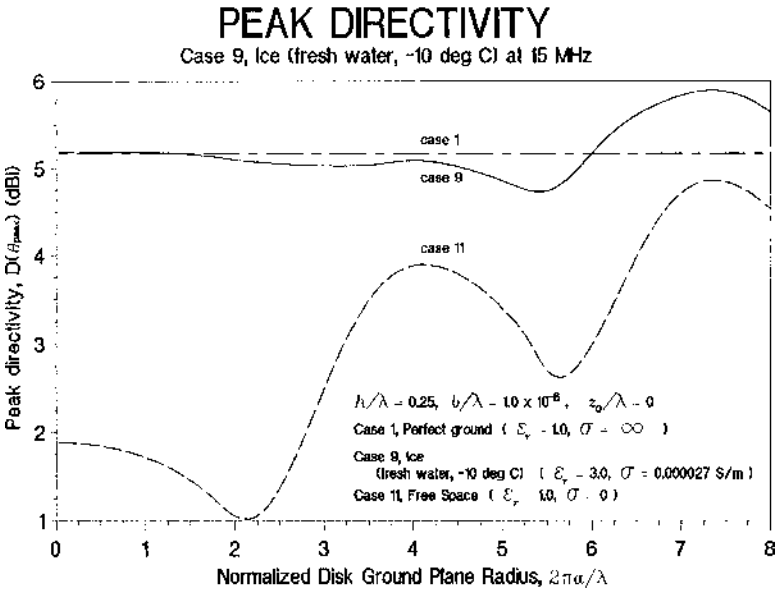
PEAK DIRECTIVITY
Case 9, Ice (fresh water, -10 deg C) at 15 MHz
Peak directivity, D(θpeak) (dBi)
Normalized Disk Ground Plane Radius, 2πa/λ
case 1
case 9
case 11
h/λ = 0.25, b/λ = 1.0 x 10⁻⁶, z₀/λ = 0
Case 1, Perfect ground (εr = 1.0, σ = ∞)
Case 9, Ice
(fresh water, -10 deg C) (εr = 3.0, σ = 0.000027 S/m)
Case 11, Free Space (εr = 1.0, σ = 0)

FIGURE A6-118 Peak directivity, ice (fresh water, $-10°C$).

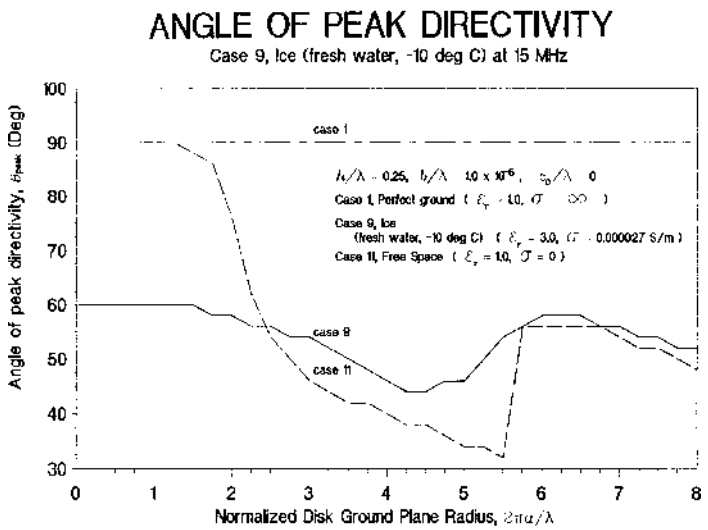
ANGLE OF PEAK DIRECTIVITY
Case 9, Ice (fresh water, -10 deg C) at 15 MHz
Angle of peak directivity, θ_{peak} (Deg)
Normalized Disk Ground Plane Radius, $2\pi a/\lambda$
case 1
case 9
case 11
h/λ = 0.25, b/λ = 1.0 x 10^{-6}, z_0/λ = 0
Case 1, Perfect ground (ε_r = 1.0, σ = ∞)
Case 9, Ice
(fresh water, -10 deg C) (ε_r = 3.0, σ = 0.000027 S/m)
Case 11, Free Space (ε_r = 1.0, σ = 0)

FIGURE A6-119 Angle of incidence of peak directivity, ice (fresh water, −10°C).

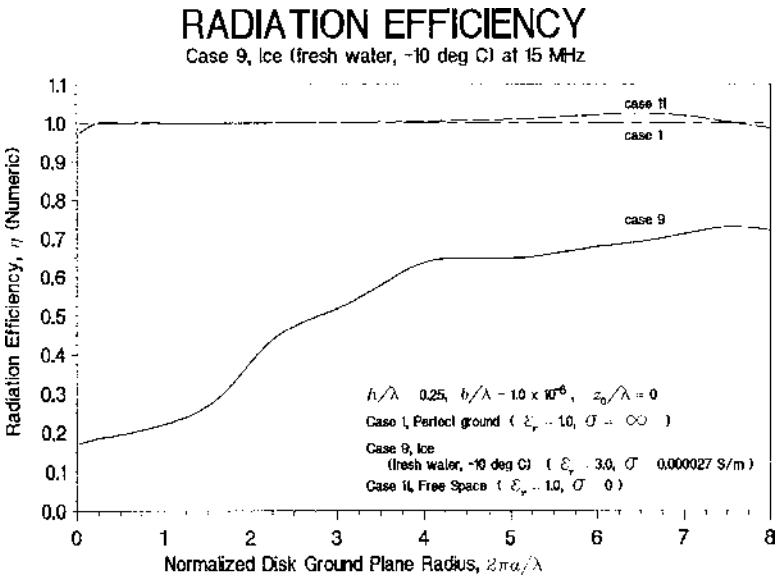
RADIATION EFFICIENCY
Case 9, Ice (fresh water, -10 deg C) at 15 MHz
Radiation Efficiency, η (Numeric)
Normalized Disk Ground Plane Radius, $2\pi a/\lambda$
case 11
case 1
case 9
h/λ = 0.25, b/λ = 1.0 x 10^{-6}, z_0/λ = 0
Case 1, Perfect ground (ε_r = 1.0, σ = ∞)
Case 9, Ice
(fresh water, -10 deg C) (ε_r = 3.0, σ = 0.000027 S/m)
Case 11, Free Space (ε_r = 1.0, σ = 0)

FIGURE A6-120 Radiation efficiency, ice (fresh water, −10°C).

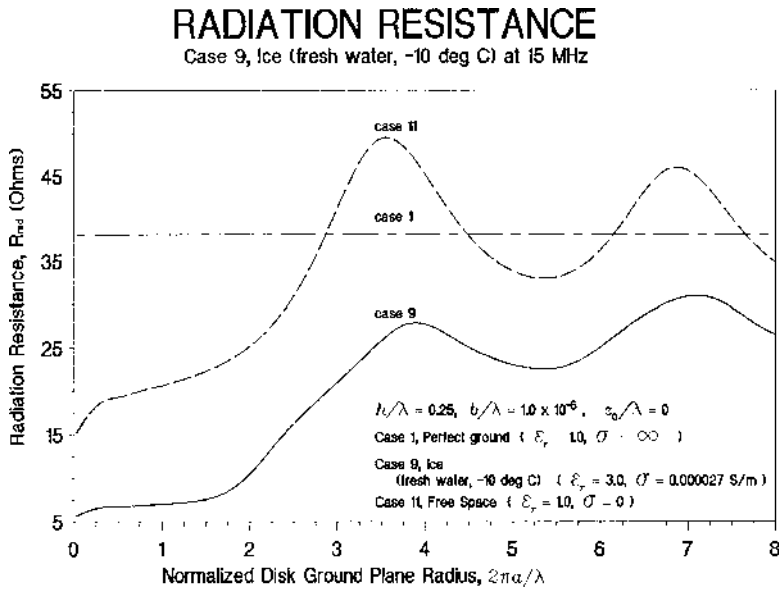
RADIATION RESISTANCE
Case 9, Ice (fresh water, -10 deg C) at 15 MHz
Radiation Resistance, R_{rad} (Ohms)
Normalized Disk Ground Plane Radius, $2\pi a/\lambda$
case 11
case 1
case 9
h/λ = 0.25, b/λ = 1.0 x 10^{-6}, z_0/λ = 0
Case 1, Perfect ground (ε_r 1.0, σ · ∞)
Case 9, Ice
(fresh water, -10 deg C) (ε_r = 3.0, σ = 0.000027 S/m)
Case 11, Free Space (ε_r = 1.0, σ = 0)

FIGURE A6-121 Radiation resistance, ice (fresh water, −10°C).

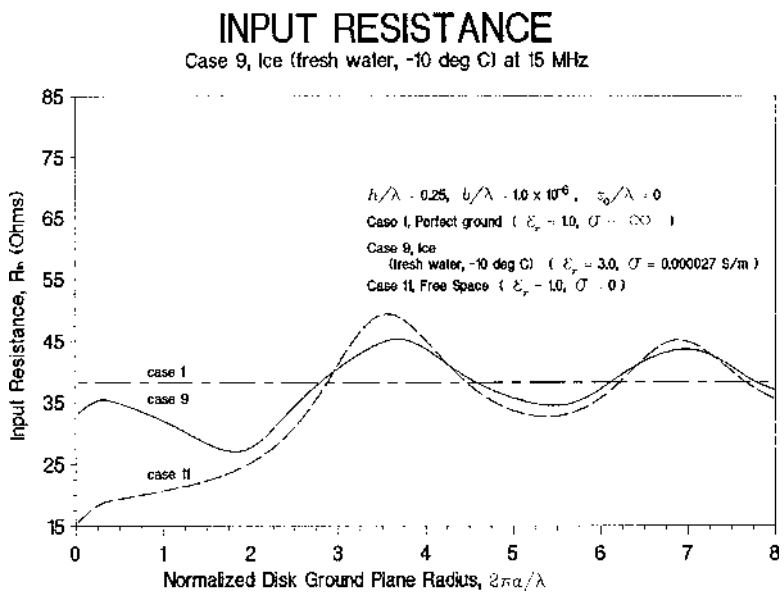
INPUT RESISTANCE
Case 9, Ice (fresh water, -10 deg C) at 15 MHz
Input Resistance, R_{in} (Ohms)
Normalized Disk Ground Plane Radius, $2\pi a/\lambda$
case 1
case 9
case 11
h/λ = 0.25, b/λ = 1.0 x 10^{-6}, z_0/λ = 0
Case 1, Perfect ground (ε_r = 1.0, σ = ∞)
Case 9, Ice
(fresh water, -10 deg C) (ε_r = 3.0, σ = 0.000027 S/m)
Case 11, Free Space (ε_r = 1.0, σ = 0)

FIGURE A6-122 Input resistance, ice (fresh water, −10°C).

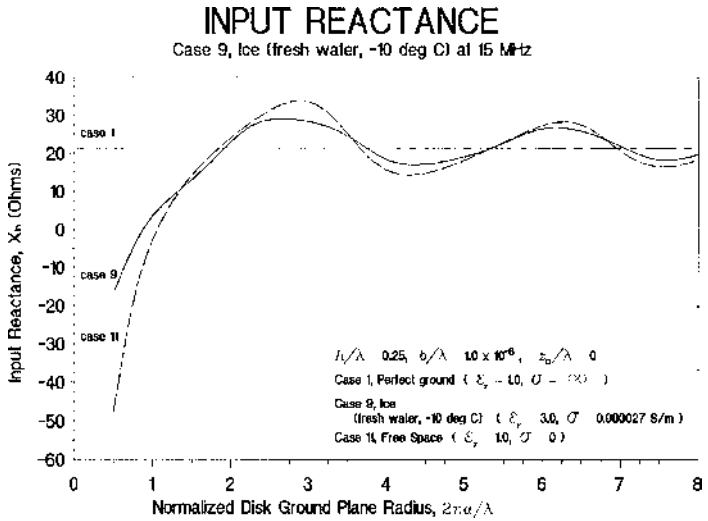
INPUT REACTANCE
Case 9, Ice (fresh water, -10 deg C) at 15 MHz
Input Reactance, X_{in} (Ohms)
Normalized Disk Ground Plane Radius, $2\pi a/\lambda$
case 1
case 9
case 11
h/λ 0.25, b/λ 1.0 x 10^{-6}, z_0/λ 0
Case 1, Perfect ground (ε_r = 1.0, σ = ∞)
Case 9, Ice
(fresh water, -10 deg C) (ε_r 3.0, σ 0.000027 S/m)
Case 11, Free Space (ε_r 1.0, σ 0)

FIGURE A6-123 Input reactance, ice (fresh water, −10°C).

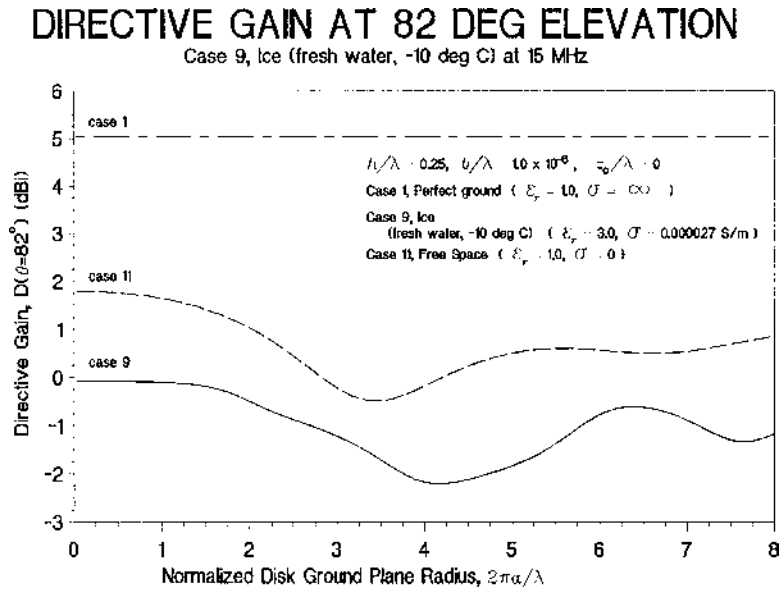
DIRECTIVE GAIN AT 82 DEG ELEVATION
Case 9, Ice (fresh water, -10 deg C) at 15 MHz
Directive Gain, D(θ=82°) (dBi)
Normalized Disk Ground Plane Radius, $2\pi a/\lambda$
case 1
case 11
case 9
h/λ = 0.25, b/λ 1.0 x 10^{-6}, z_0/λ = 0
Case 1, Perfect ground (ε_r = 1.0, σ = ∞)
Case 9, Ice
(fresh water, -10 deg C) (ε_r = 3.0, σ = 0.000027 S/m)
Case 11, Free Space (ε_r = 1.0, σ = 0)

FIGURE A6-124 Directivity at 8° above the horizon, ice (fresh water, −10°C).

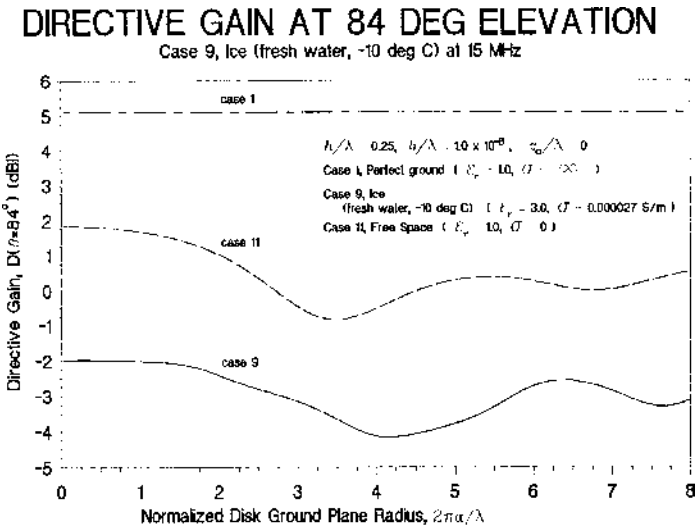
DIRECTIVE GAIN AT 84 DEG ELEVATION
Case 9, Ice (fresh water, -10 deg C) at 15 MHz
case 1
case 11
case 9
Directive Gain, D(θ=84°) (dBi)
Normalized Disk Ground Plane Radius, 2πa/λ

FIGURE A6-125 Directivity at 6° above the horizon, ice (fresh water, −10°C).

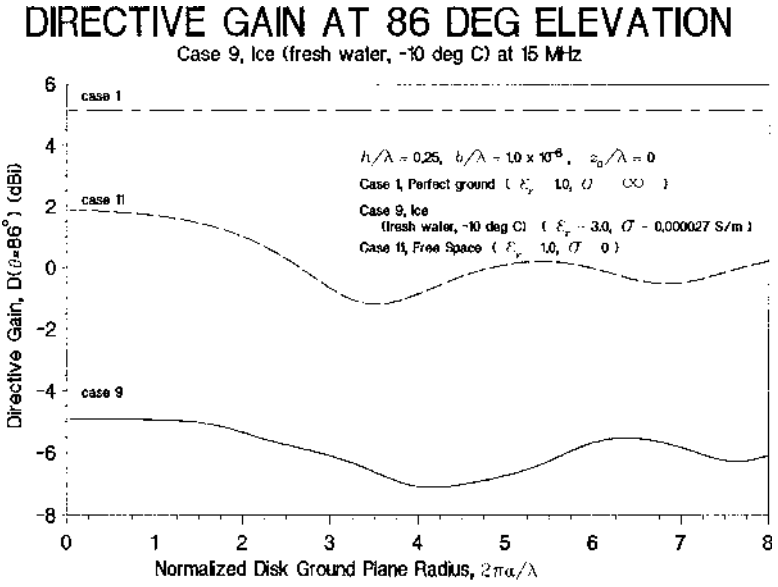
DIRECTIVE GAIN AT 86 DEG ELEVATION
Case 9, Ice (fresh water, -10 deg C) at 15 MHz
case 1
case 11
case 9
Directive Gain, D(θ=86°) (dBi)
Normalized Disk Ground Plane Radius, 2πa/λ

FIGURE A6-126 Directivity at 4° above the horizon, ice (fresh water, −10°C).

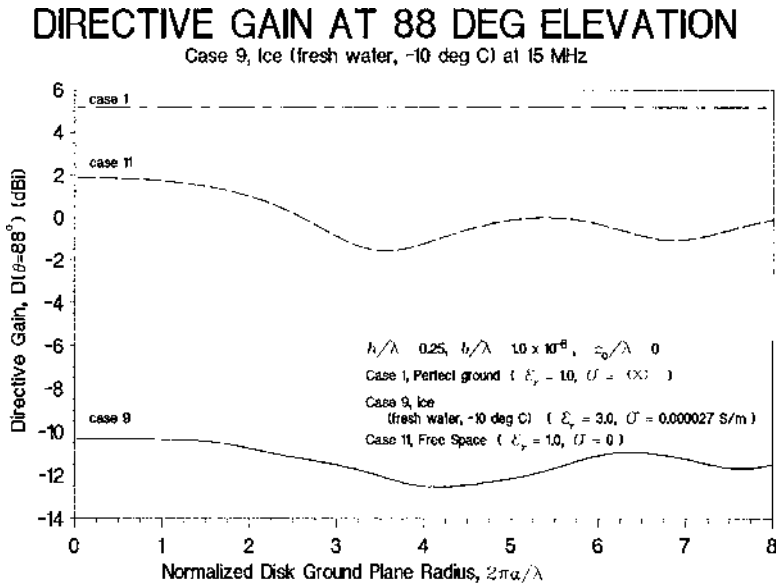
DIRECTIVE GAIN AT 88 DEG ELEVATION
Case 9, Ice (fresh water, -10 deg C) at 15 MHz
Directive Gain, Dl(θ=88°) (dBi)
Normalized Disk Ground Plane Radius, 2πa/λ
case 1
case 11
case 9
h/λ 0.25, b/λ 1.0 x 10^6, z0/λ 0
Case 1, Perfect ground (εr = 1.0, σ = ∞)
Case 9, Ice
(fresh water, -10 deg C) (εr = 3.0, σ = 0.000027 S/m)
Case 11, Free Space (εr = 1.0, σ = 0)

FIGURE A6-127 Directivity at 2° above the horizon, ice (fresh water, −10°C).

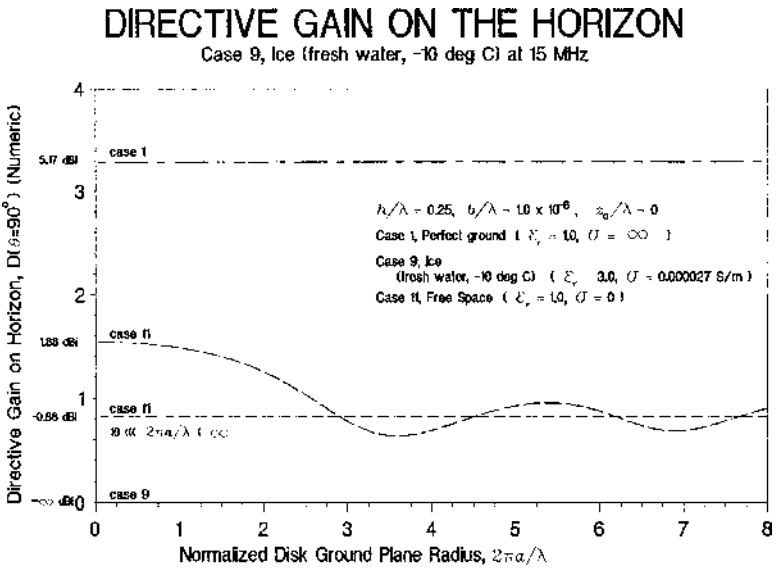
DIRECTIVE GAIN ON THE HORIZON
Case 9, Ice (fresh water, -10 deg C) at 15 MHz
Directive Gain on Horizon, Dl(θ=90°) (Numeric)
Normalized Disk Ground Plane Radius, 2πa/λ
5.17 dBi
1.88 dBi
-0.58 dBi
-∞ dBi
case 1
case 11
case 9
θ ≪ 2πa/λ (∞)
h/λ = 0.25, b/λ = 1.0 x 10^6, z0/λ = 0
Case 1, Perfect ground (εr = 1.0, σ = ∞)
Case 9, Ice
(fresh water, -10 deg C) (εr = 3.0, σ = 0.000027 S/m)
Case 11, Free Space (εr = 1.0, σ = 0)

FIGURE A6-128 Directivity on the horizon, ice (fresh water, −10°C).

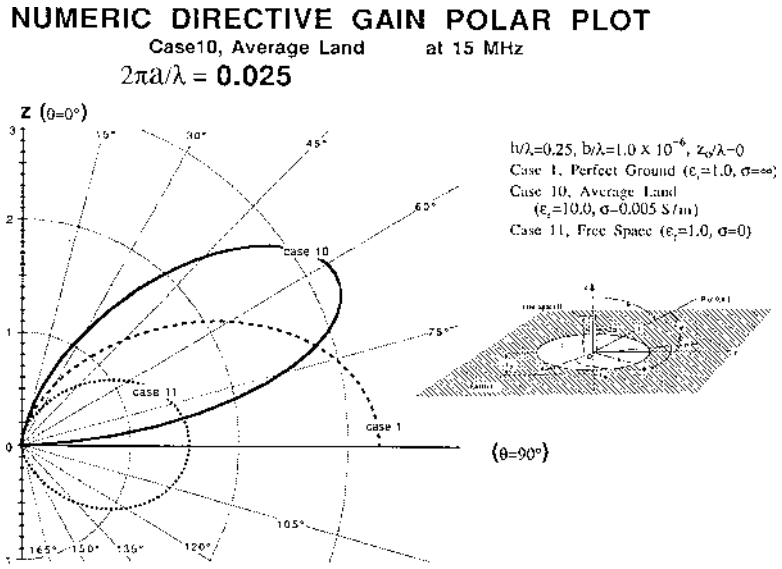

FIGURE A6-129 Directivity pattern $2\pi a/\lambda = 0.025$, average land.

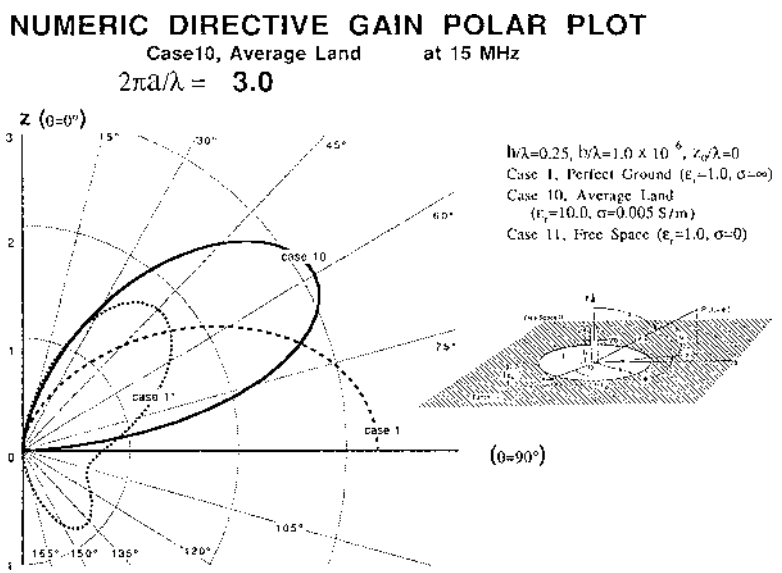

FIGURE A6-130 Directivity pattern $2\pi a/\lambda = 3.0$, average land.

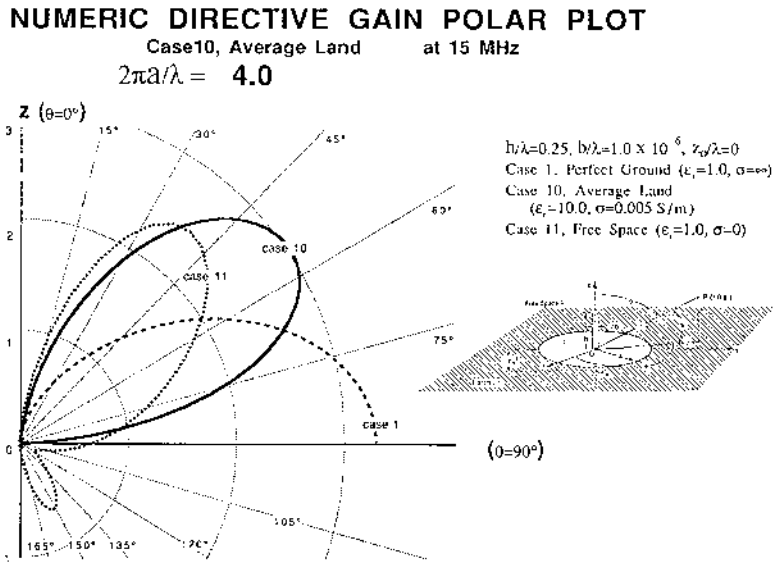

FIGURE A6-131 Directivity pattern $2\pi a/\lambda = 4.0$, average land.

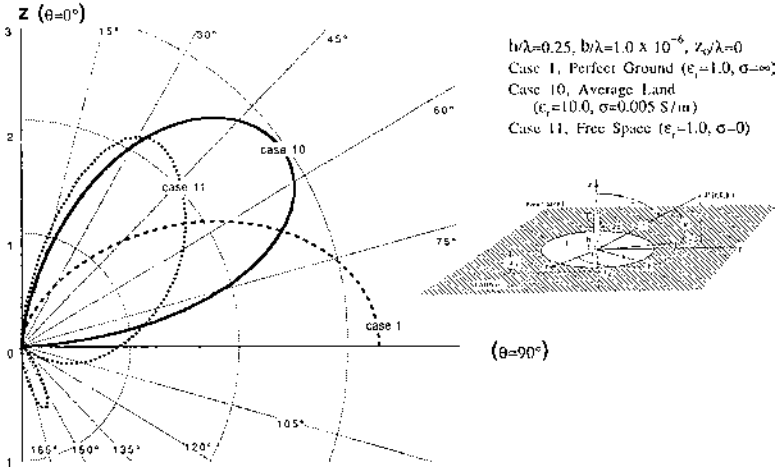

FIGURE A6-132 Directivity pattern $2\pi a/\lambda = 5.0$, average land.

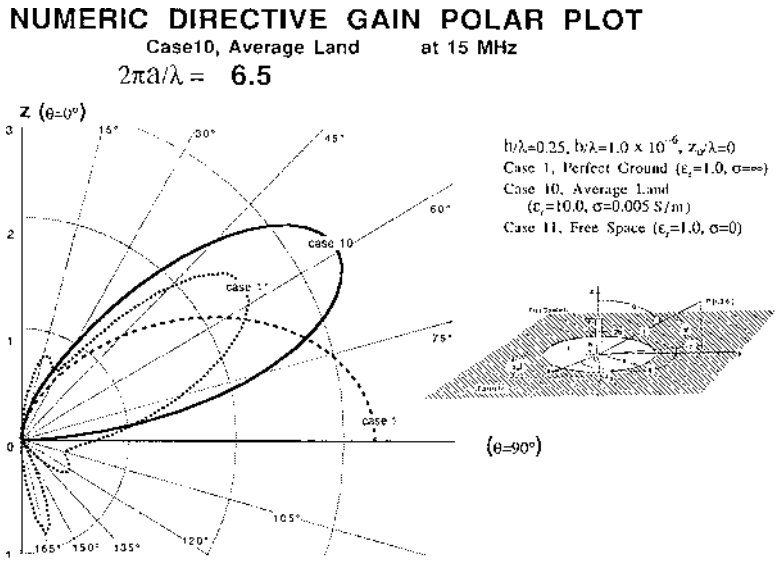

FIGURE A6-133 Directivity pattern $2\pi a/\lambda = 6.5$, average land.

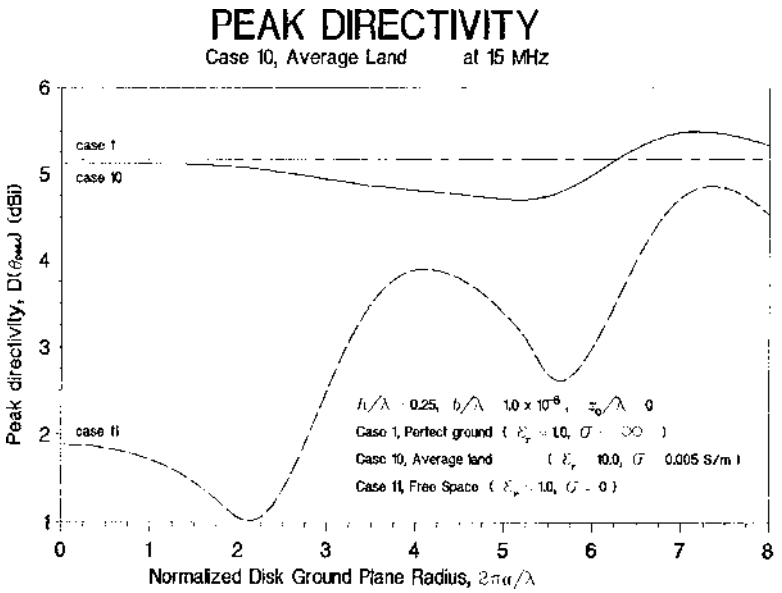
PEAK DIRECTIVITY
Case 10, Average Land at 15 MHz
Peak directivity, D(θmax) (dBi)
Normalized Disk Ground Plane Radius, 2πa/λ
case 1
case 10
case 11
h/λ = 0.25, b/λ = 1.0 x 10⁻⁶, z₀/λ = 0
Case 1, Perfect ground (εr = 1.0, σ = ∞)
Case 10, Average land (εr = 10.0, σ = 0.005 S/m)
Case 11, Free Space (εr = 1.0, σ = 0)

FIGURE A6-134 Peak directivity, average land.

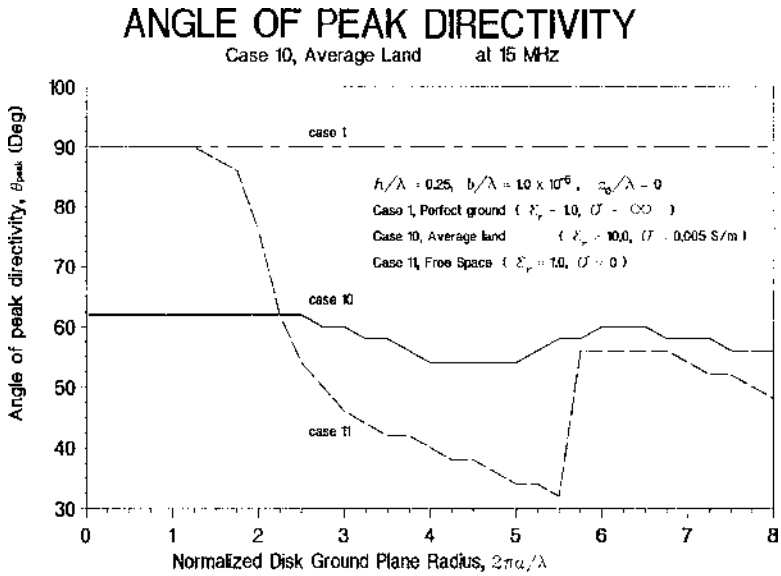
ANGLE OF PEAK DIRECTIVITY
Case 10, Average Land at 15 MHz
Angle of peak directivity, θ_{peak} (Deg)
Normalized Disk Ground Plane Radius, $2\pi a/\lambda$
case 1
case 10
case 11
h/λ = 0.25, b/λ = 1.0 x 10^{-6}, z_0/λ = 0
Case 1, Perfect ground (ε_r = 1.0, σ = ∞)
Case 10, Average land (ε_r = 10.0, σ = 0.005 S/m)
Case 11, Free Space (ε_r = 1.0, σ = 0)

FIGURE A6-135 Angle of incidence of peak directivity, average land.

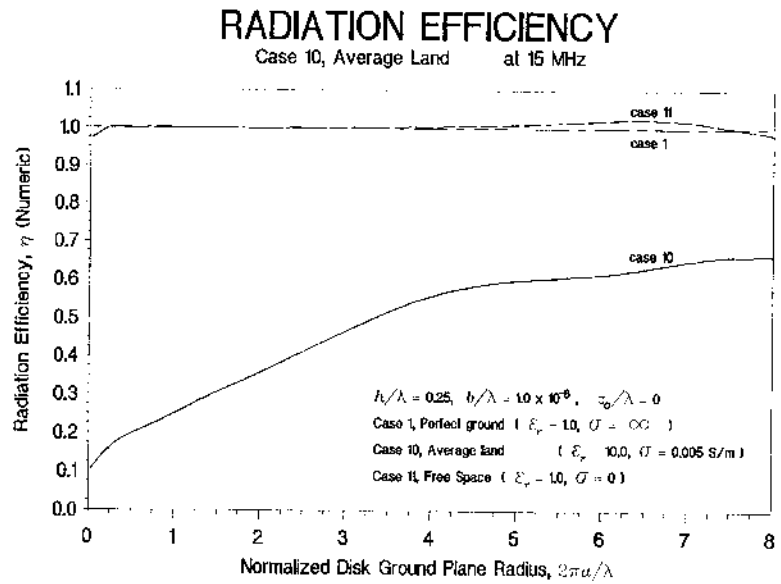
RADIATION EFFICIENCY
Case 10, Average Land at 15 MHz
Radiation Efficiency, η (Numeric)
Normalized Disk Ground Plane Radius, $2\pi a/\lambda$
case 11
case 1
case 10
h/λ = 0.25, b/λ = 1.0 x 10^{-6}, z_0/λ = 0
Case 1, Perfect ground (ε_r = 1.0, σ = ∞)
Case 10, Average land (ε_r 10.0, σ = 0.005 S/m)
Case 11, Free Space (ε_r = 1.0, σ = 0)

FIGURE A6-136 Radiation efficiency, average land.

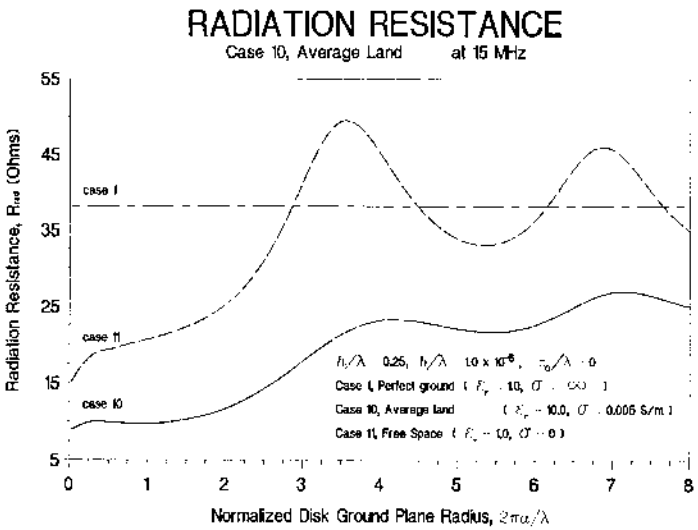
RADIATION RESISTANCE
Case 10, Average Land at 15 MHz
Radiation Resistance, R_{rad} (Ohms)
55
45
35
25
15
5
case I
case II
case 10
h/λ 0.25, b/λ 1.0 x 10^{-6}, z_0/λ = 0
Case I, Perfect ground (ε_r = 1.0, σ = ∞)
Case 10, Average land (ε_r = 10.0, σ = 0.005 S/m)
Case 11, Free Space (ε_r = 1.0, σ = 0)
0 1 2 3 4 5 6 7 8
Normalized Disk Ground Plane Radius, $2\pi a/\lambda$

FIGURE A6-137 Radiation resistance, average land.

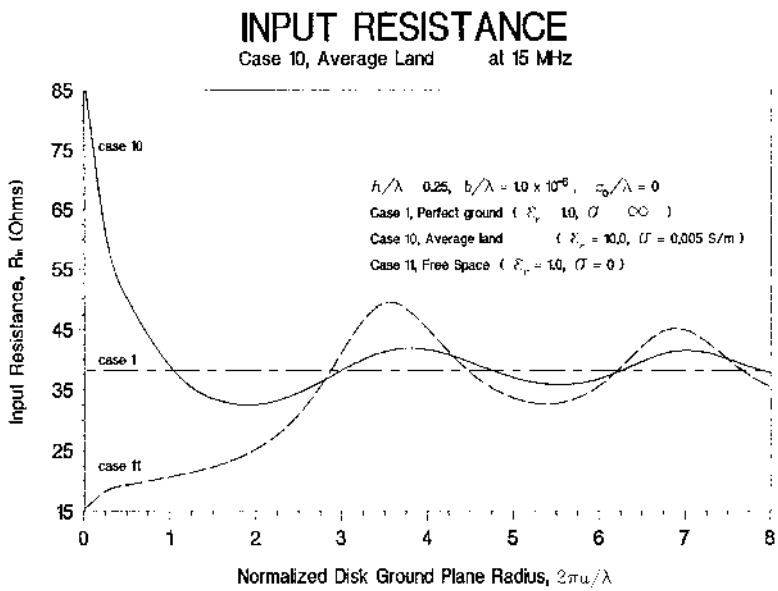
INPUT RESISTANCE
Case 10, Average Land at 15 MHz
Input Resistance, R_{in} (Ohms)
85
75
65
55
45
35
25
15
case 10
case 1
case II
h/λ 0.25, b/λ = 1.0 x 10^{-6}, z_0/λ = 0
Case 1, Perfect ground (ε_r 1.0, σ ∞)
Case 10, Average land (ε_r = 10.0, σ = 0.005 S/m)
Case 11, Free Space (ε_r = 1.0, σ = 0)
0 1 2 3 4 5 6 7 8
Normalized Disk Ground Plane Radius, $2\pi a/\lambda$

FIGURE A6-138 Input resistance, average land.

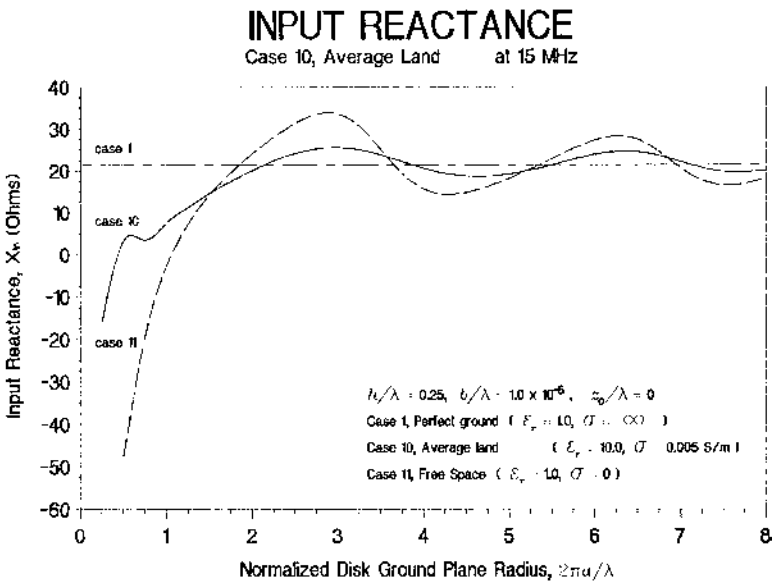
INPUT REACTANCE
Case 10, Average Land at 15 MHz
Input Reactance, X_{in} (Ohms)
Normalized Disk Ground Plane Radius, $2\pi a/\lambda$
case I
case IC
case II
h/λ = 0.25, b/λ = 1.0 x 10^{-6}, z_o/λ = 0
Case 1, Perfect ground (ε_r = 1.0, σ = ∞)
Case 10, Average land (ε_r = 10.0, σ = 0.005 S/m)
Case 11, Free Space (ε_r = 1.0, σ = 0)

FIGURE A6-139 Input reactance, average land.

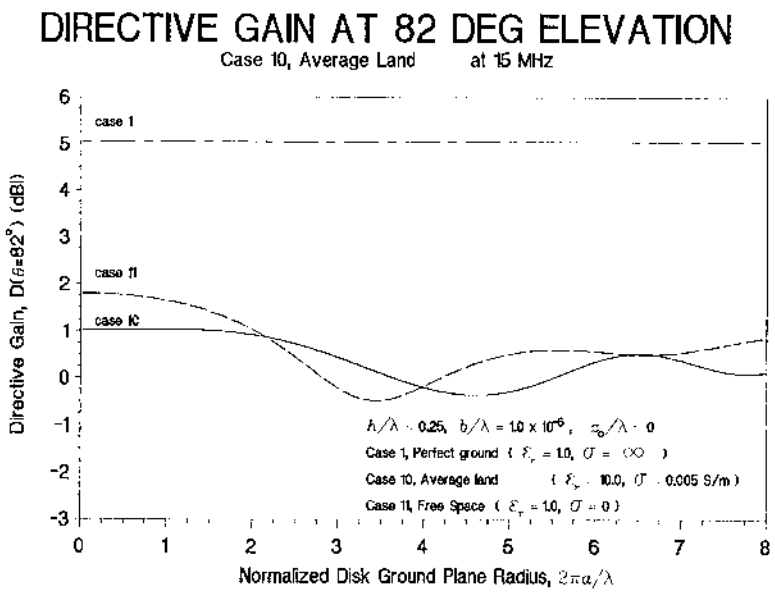
DIRECTIVE GAIN AT 82 DEG ELEVATION
Case 10, Average Land at 15 MHz
Directive Gain, $D(\theta=82^\circ)$ (dBi)
Normalized Disk Ground Plane Radius, $2\pi a/\lambda$
case I
case II
case IC
h/λ = 0.25, b/λ = 1.0 x 10^{-6}, z_o/λ = 0
Case 1, Perfect ground (ε_r = 1.0, σ = ∞)
Case 10, Average land (ε_r = 10.0, σ = 0.005 S/m)
Case 11, Free Space (ε_r = 1.0, σ = 0)

FIGURE A6-140 Directivity at 8° above the horizon, average land.

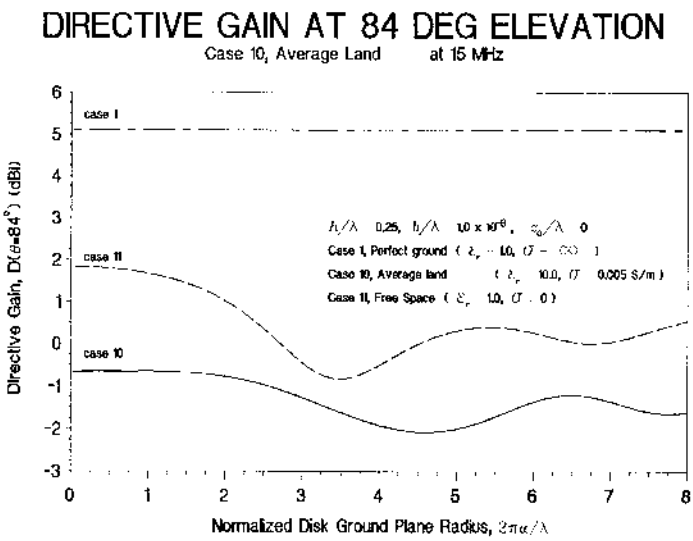
DIRECTIVE GAIN AT 84 DEG ELEVATION
Case 10, Average Land at 15 MHz
Directive Gain, D(θ=84°) (dBi)
Normalized Disk Ground Plane Radius, 2πa/λ
case I
case II
case 10
Case 1, Perfect ground
Case 10, Average land
Case 11, Free Space

FIGURE A6-141 Directivity at 6° above the horizon, average land.

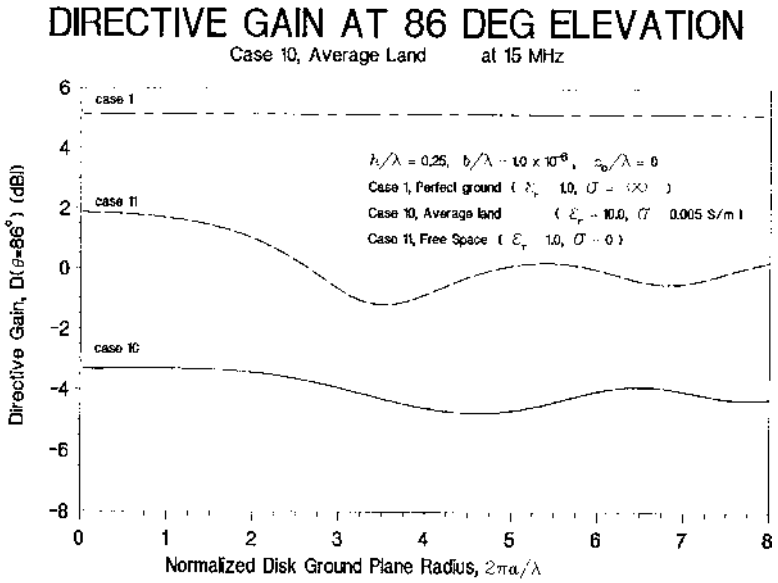
DIRECTIVE GAIN AT 86 DEG ELEVATION
Case 10, Average Land at 15 MHz
Directive Gain, D(θ=86°) (dBi)
Normalized Disk Ground Plane Radius, 2πa/λ
case I
case II
case 10
Case 1, Perfect ground
Case 10, Average land
Case 11, Free Space

FIGURE A6-142 Directivity at 4° above the horizon, average land.

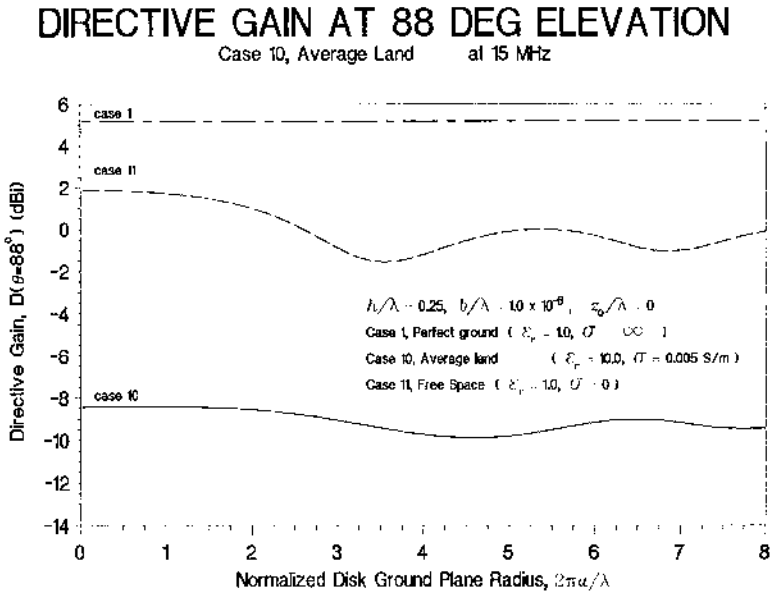
DIRECTIVE GAIN AT 88 DEG ELEVATION
Case 10, Average Land
at 15 MHz
Directive Gain, D(θ=88°) (dBi)
Normalized Disk Ground Plane Radius, 2πa/λ
case 1
case 11
case 10
h/λ = 0.25, b/λ = 1.0 x 10⁻⁶, z₀/λ = 0
Case 1, Perfect ground (ε_r = 1.0, σ = ∞)
Case 10, Average land (ε_r = 10.0, σ = 0.005 S/m)
Case 11, Free Space (ε_r = 1.0, σ = 0)

FIGURE A6-143 Directivity at 2° above the horizon, average land.

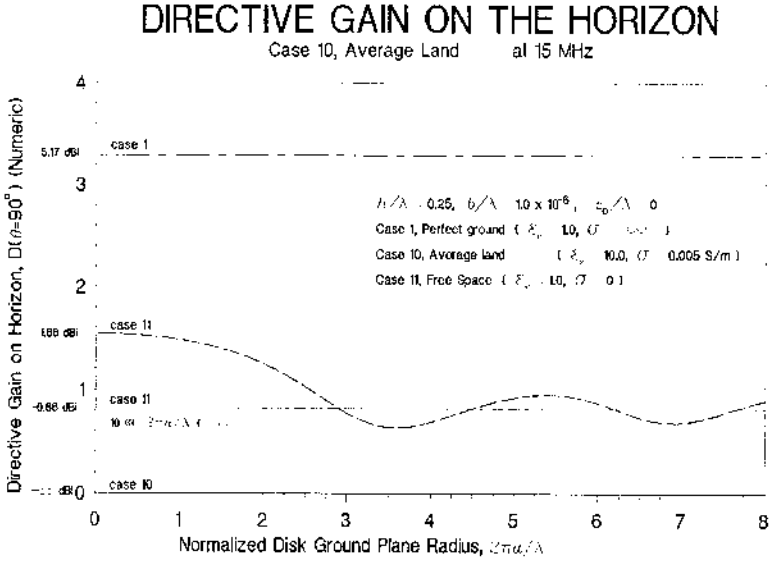
DIRECTIVE GAIN ON THE HORIZON
Case 10, Average Land
at 15 MHz
Directive Gain on Horizon, D(θ=90°) (Numeric)
Normalized Disk Ground Plane Radius, 2πa/λ
5.17 dBi
case 1
case 11
case 11
case 10
h/λ = 0.25, b/λ = 1.0 x 10⁻⁶, z₀/λ = 0
Case 1, Perfect ground (ε_r = 1.0, σ = ∞)
Case 10, Average land (ε_r = 10.0, σ = 0.005 S/m)
Case 11, Free Space (ε_r = 1.0, σ = 0)

FIGURE A6-144 Directivity on the horizon, average land.

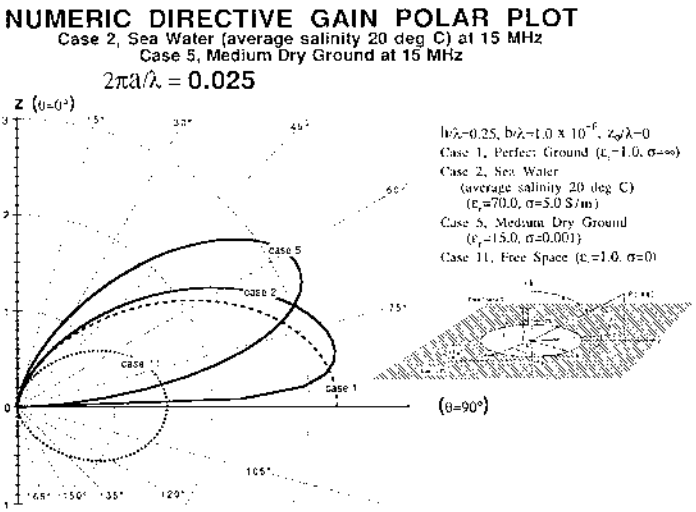

FIGURE A6-145 Directivity pattern, $2\pi a/\lambda = 0.025$, sea water compared with medium dry ground.

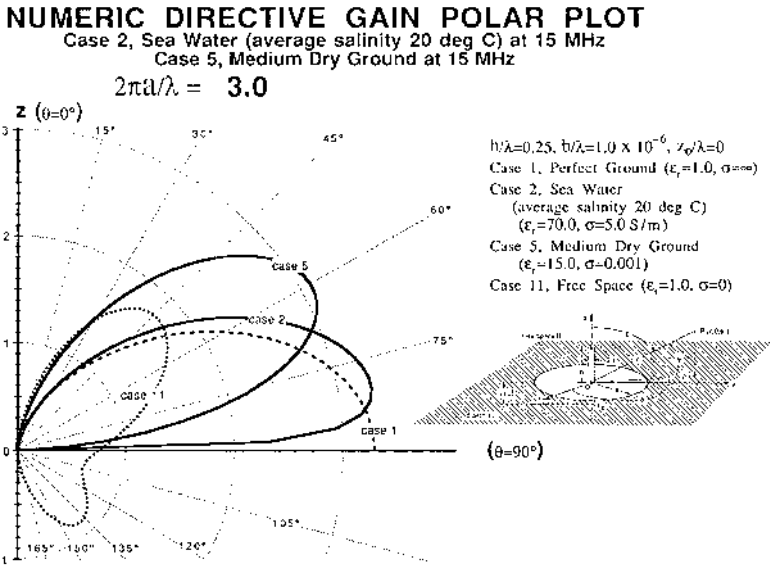

FIGURE A6-146 Directivity pattern, $2\pi a/\lambda = 3.0$, sea water compared with medium dry ground.

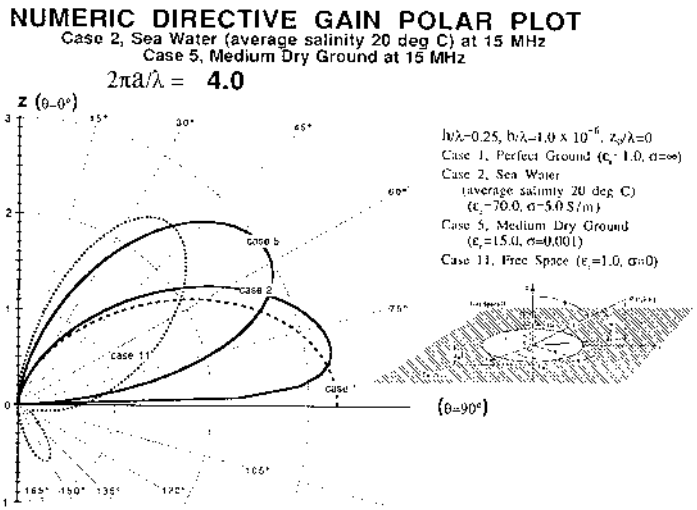
NUMERIC DIRECTIVE GAIN POLAR PLOT
Case 2, Sea Water (average salinity 20 deg C) at 15 MHz
Case 5, Medium Dry Ground at 15 MHz
2πa/λ = 4.0
z (θ=0°)
h/λ=0.25, b/λ=1.0 x 10⁻⁶, z₀/λ=0
Case 1, Perfect Ground (εr=1.0, σ=∞)
Case 2, Sea Water
(average salinity 20 deg C)
(εr=70.0, σ=5.0 S/m)
Case 5, Medium Dry Ground
(εr=15.0, σ=0.001)
Case 11, Free Space (εr=1.0, σ=0)
case 5
case 2
case 11
case 1
(θ=90°)

FIGURE A6-147 Directivity pattern, $2\pi a/\lambda = 4.0$, sea water compared with medium dry ground.

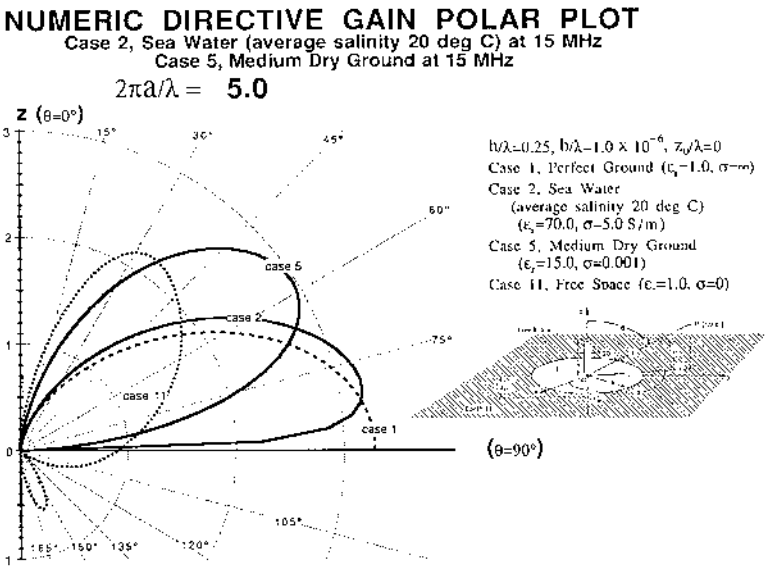
NUMERIC DIRECTIVE GAIN POLAR PLOT
Case 2, Sea Water (average salinity 20 deg C) at 15 MHz
Case 5, Medium Dry Ground at 15 MHz
2πa/λ = 5.0
z (θ=0°)
h/λ=0.25, b/λ=1.0 x 10⁻⁶, z₀/λ=0
Case 1, Perfect Ground (εr=1.0, σ=∞)
Case 2, Sea Water
(average salinity 20 deg C)
(εr=70.0, σ=5.0 S/m)
Case 5, Medium Dry Ground
(εr=15.0, σ=0.001)
Case 11, Free Space (εr=1.0, σ=0)
case 5
case 2
case 11
case 1
(θ=90°)

FIGURE A6-148 Directivity pattern, $2\pi a/\lambda = 5.0$, sea water compared with medium dry ground.

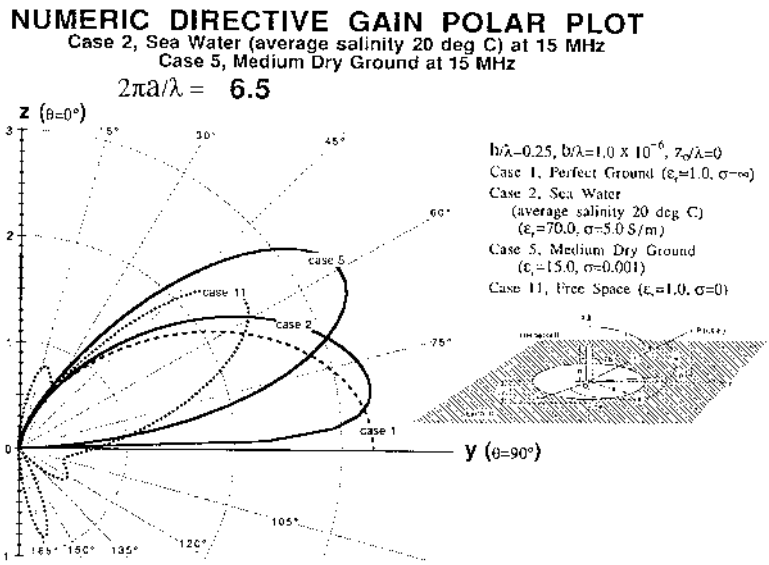
NUMERIC DIRECTIVE GAIN POLAR PLOT
Case 2, Sea Water (average salinity 20 deg C) at 15 MHz
Case 5, Medium Dry Ground at 15 MHz
2πa/λ = 6.5
z (θ=0°)
y (θ=90°)
case 1
case 2
case 5
case 11
b/λ=0.25, b/λ=1.0 x 10⁻⁶, z₀/λ=0
Case 1, Perfect Ground (εr=1.0, σ=∞)
Case 2, Sea Water
(average salinity 20 deg C)
(εr=70.0, σ=5.0 S/m)
Case 5, Medium Dry Ground
(εr=15.0, σ=0.001)
Case 11, Free Space (εr=1.0, σ=0)

FIGURE A6-149 Directivity pattern, $2\pi a/\lambda = 6.5$, sea water compared with medium dry ground.

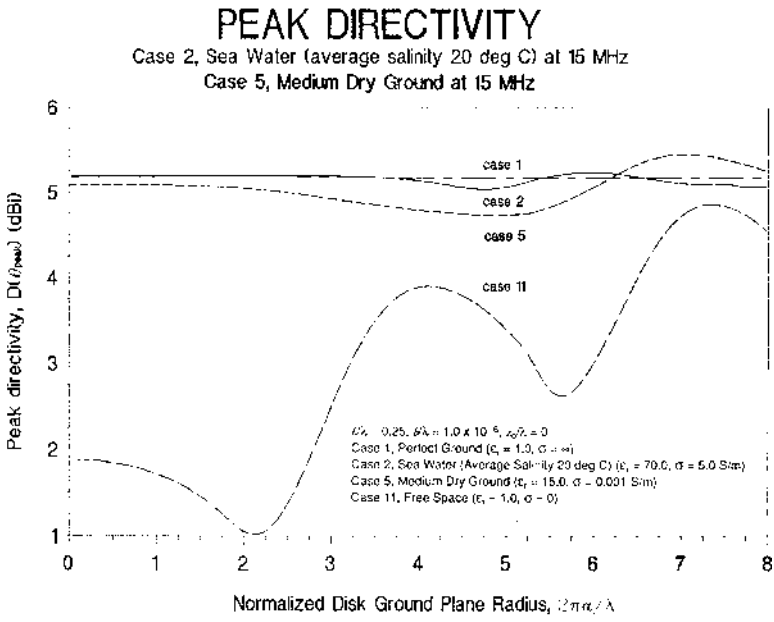
PEAK DIRECTIVITY
Case 2, Sea Water (average salinity 20 deg C) at 15 MHz
Case 5, Medium Dry Ground at 15 MHz
Peak directivity, D(θpeak) (dBi)
Normalized Disk Ground Plane Radius, 2πa/λ
case 1
case 2
case 5
case 11
Case 1, Perfect Ground (εr = 1.0, σ = ∞)
Case 2, Sea Water (Average Salinity 20 deg C) (εr = 70.0, σ = 5.0 S/m)
Case 5, Medium Dry Ground (εr = 15.0, σ = 0.001 S/m)
Case 11, Free Space (εr = 1.0, σ = 0)

FIGURE A6-150 Peak directivity, sea water compared with medium dry ground.

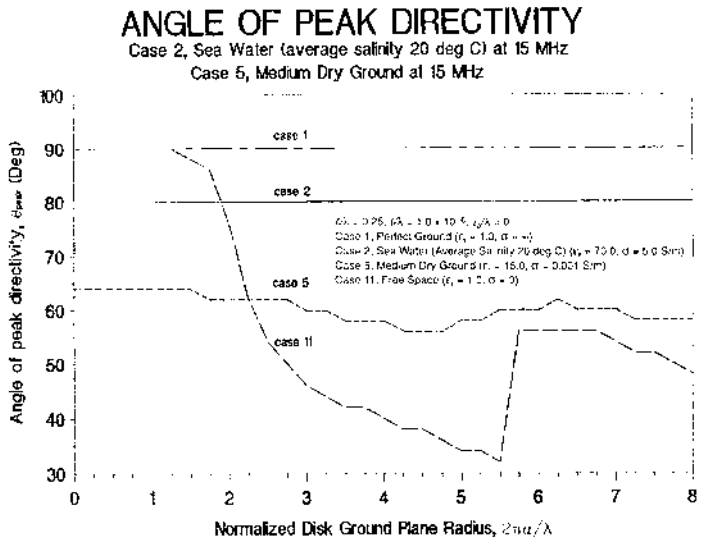

FIGURE A6-151 Angle of incidence of peak directivity, sea water compared with medium dry ground.

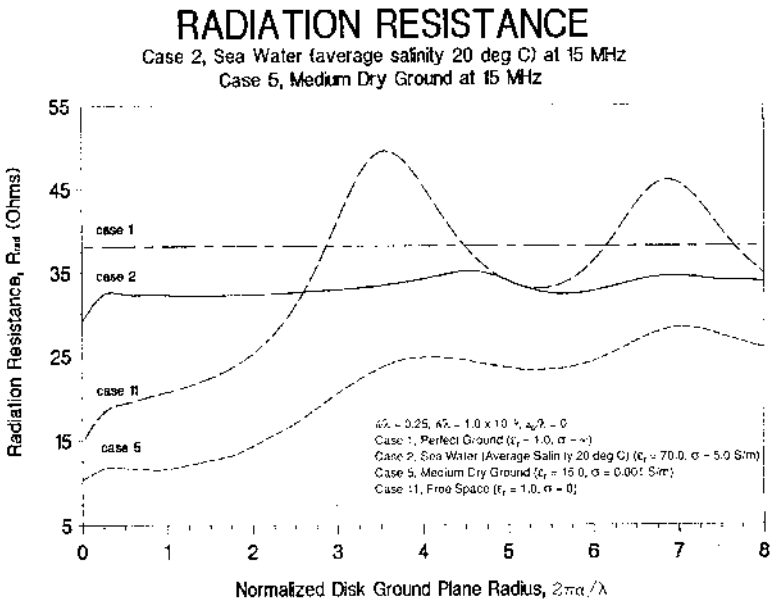

FIGURE A6-152 Radiation efficiency, sea water compared with medium dry ground.

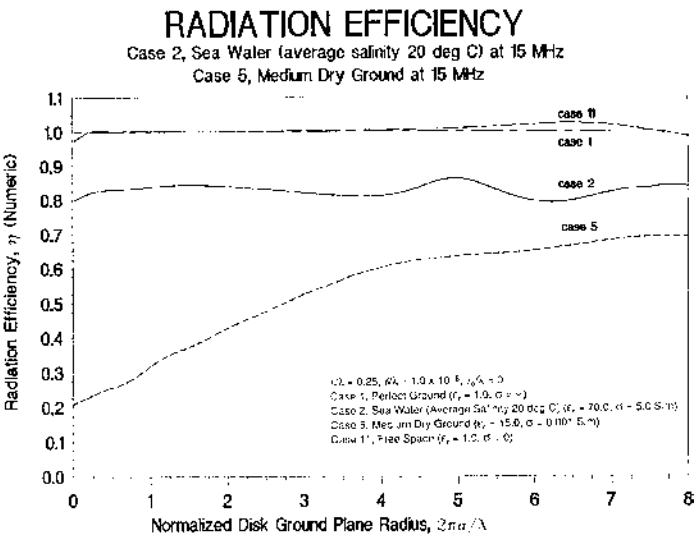

FIGURE A6-153 Radiation resistance, sea water compared with medium dry ground.

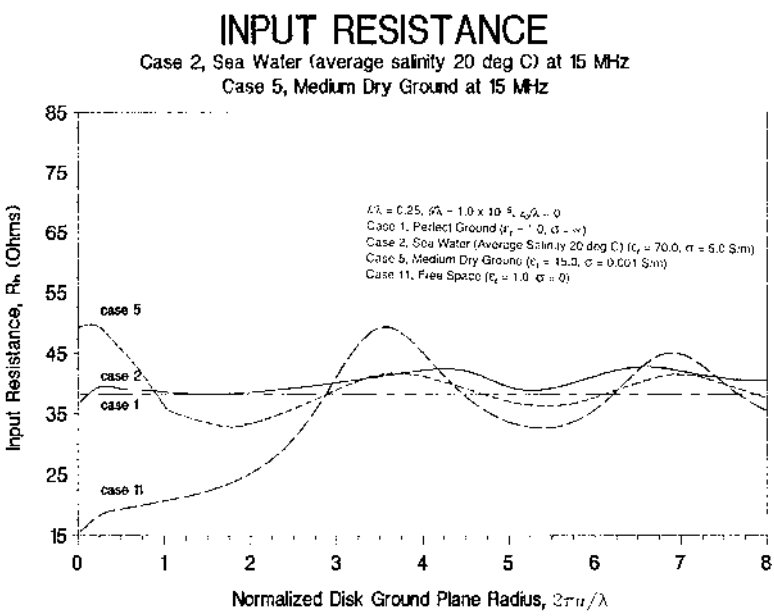

FIGURE A6-154 Input resistance, sea water compared with medium dry ground.

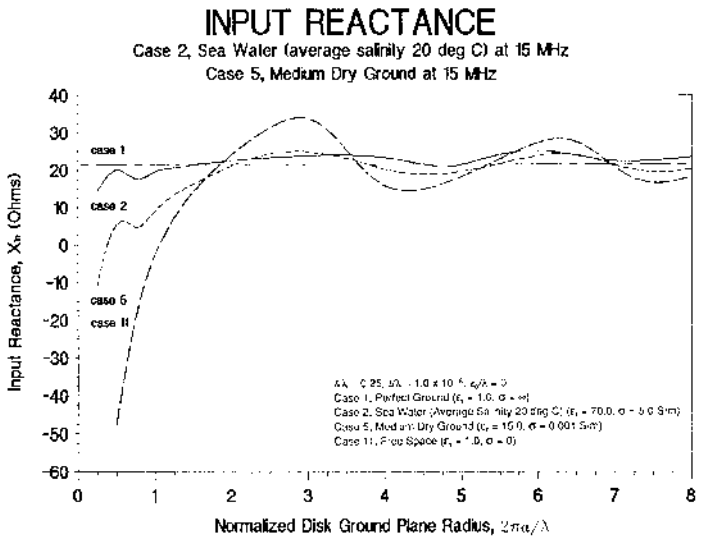
INPUT REACTANCE
Case 2, Sea Water (average salinity 20 deg C) at 15 MHz
Case 5, Medium Dry Ground at 15 MHz
Input Reactance, X_a (Ohms)
Normalized Disk Ground Plane Radius, $2\pi a/\lambda$
case 1
case 2
case 5
case 11
Case 1, Perfect Ground (ε_r = 1.0, σ = ∞)
Case 2, Sea Water (Average Salinity 20 deg C) (ε_r = 70.0, σ = 5.0 S/m)
Case 5, Medium Dry Ground (ε_r = 15.0, σ = 0.001 S/m)
Case 11, Free Space (ε_r = 1.0, σ = 0)

FIGURE A6-155 Input reactance, sea water compared with medium dry ground.

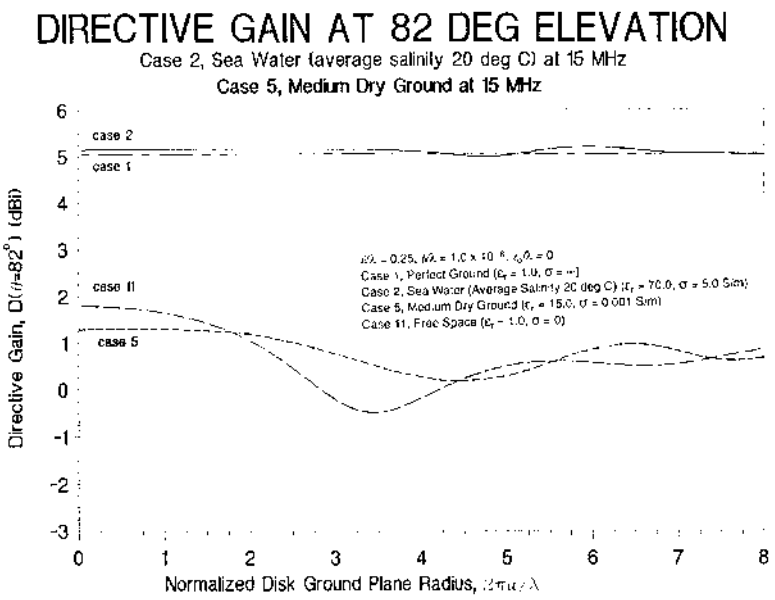
DIRECTIVE GAIN AT 82 DEG ELEVATION
Case 2, Sea Water (average salinity 20 deg C) at 15 MHz
Case 5, Medium Dry Ground at 15 MHz
Directive Gain, D(θ=82°) (dBi)
Normalized Disk Ground Plane Radius, $2\pi a/\lambda$
case 2
case 1
case 11
case 5
Case 1, Perfect Ground (ε_r = 1.0, σ = ∞)
Case 2, Sea Water (Average Salinity 20 deg C) (ε_r = 70.0, σ = 5.0 S/m)
Case 5, Medium Dry Ground (ε_r = 15.0, σ = 0.001 S/m)
Case 11, Free Space (ε_r = 1.0, σ = 0)

FIGURE A6-156 Directivity at 8° above the horizon, sea water compared with medium dry ground.

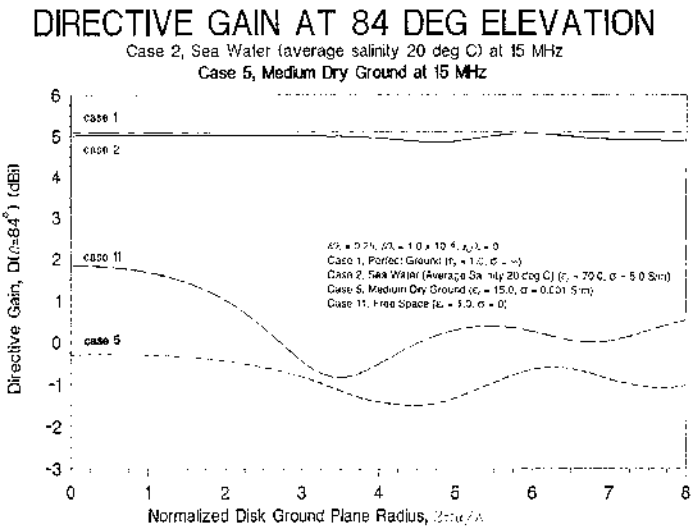
DIRECTIVE GAIN AT 84 DEG ELEVATION
Case 2, Sea Water (average salinity 20 deg C) at 15 MHz
Case 5, Medium Dry Ground at 15 MHz
case 1
case 2
case 11
case 5
Directive Gain, D(θ=84°) (dBi)
Normalized Disk Ground Plane Radius, 2πa/λ

FIGURE A6-157 Directivity at 6° above the horizon, sea water compared with medium dry ground.

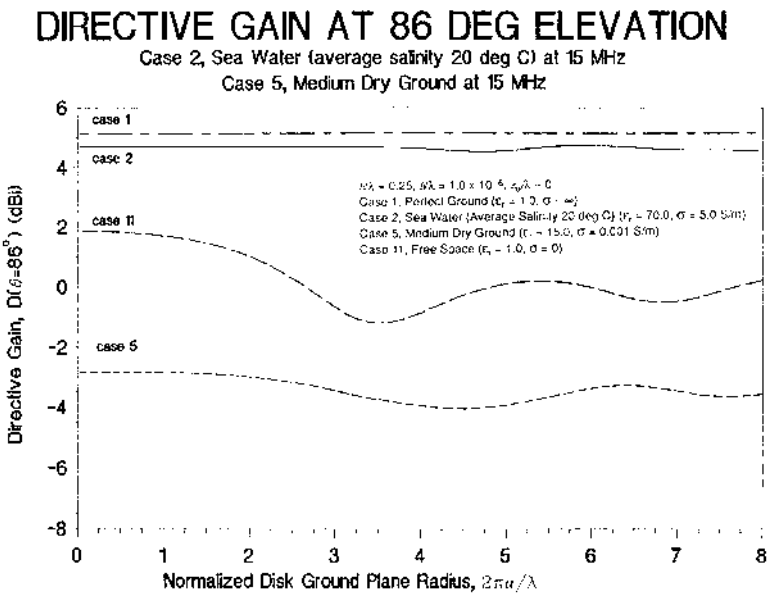
DIRECTIVE GAIN AT 86 DEG ELEVATION
Case 2, Sea Water (average salinity 20 deg C) at 15 MHz
Case 5, Medium Dry Ground at 15 MHz
case 1
case 2
case 11
case 5
Directive Gain, D(θ=86°) (dBi)
Normalized Disk Ground Plane Radius, 2πa/λ

FIGURE A6-158 Directivity at 4° above the horizon, sea water compared with medium dry ground.

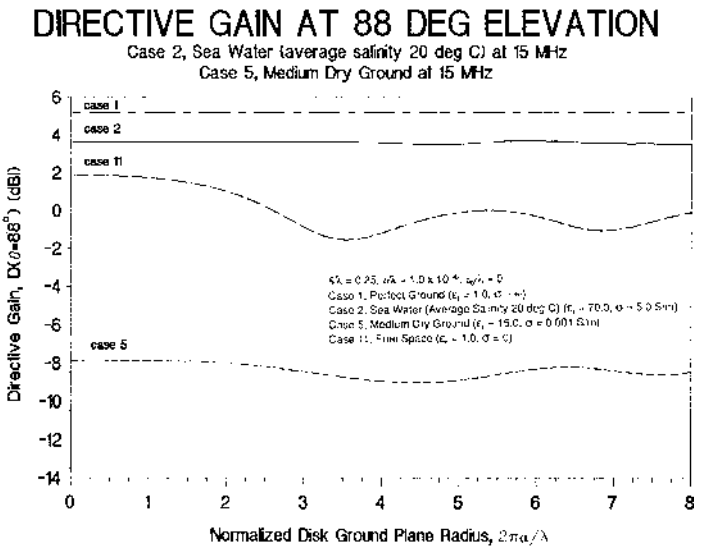
DIRECTIVE GAIN AT 88 DEG ELEVATION
Case 2, Sea Water (average salinity 20 deg C) at 15 MHz
Case 5, Medium Dry Ground at 15 MHz
case 1
case 2
case 11
case 5
Directive Gain, D(θ=88°) (dBi)
Normalized Disk Ground Plane Radius, 2πa/λ

FIGURE A6-159 Directivity at 2° above the horizon, sea water compared with medium dry ground.

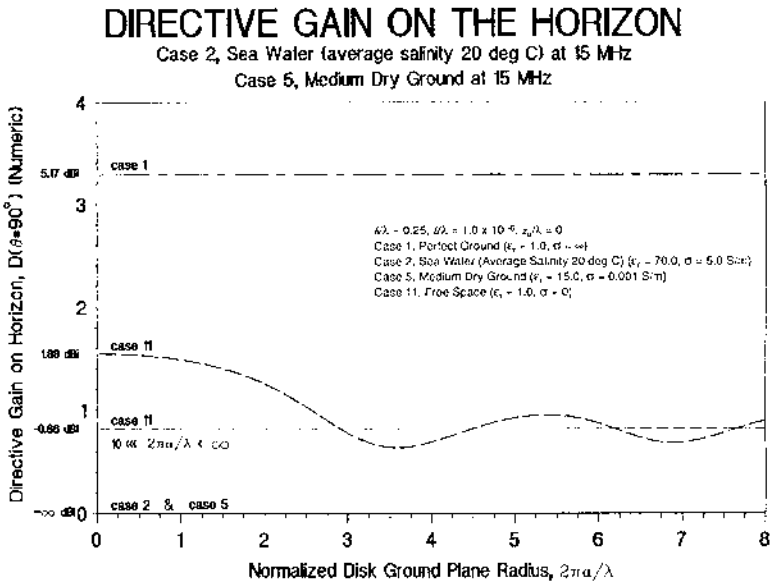
DIRECTIVE GAIN ON THE HORIZON
Case 2, Sea Water (average salinity 20 deg C) at 15 MHz
Case 5, Medium Dry Ground at 15 MHz
case 1
5.17 dBi
case 11
1.88 dBi
case 11
-0.68 dBi
case 2 & case 5
Directive Gain on Horizon, D(θ=90°) (Numeric)
Normalized Disk Ground Plane Radius, 2πa/λ

FIGURE A6-160 Directivity on the horizon, sea water compared with medium dry ground.

A.7 METHOD OF MOMENTS (NEC-GS): QUARTER-WAVE ELEMENTS WITH RADIAL-WIRE GROUND PLANES NEAR FLAT EARTH: RADIATION EFFICIENCY AND INPUT IMPEDANCE

The computer plots of radiation efficiency, input resistance, and input reactance, for earth of complex relative permittivities $15 - j\,1.5$, $15 - j\,15$, $15 - j\,150$, and $15 - j\,1500$, are grouped in App. A.7 subsections corresponding to the following radial-wire ground-plane normalized depths z_0/λ :

1. Ground-plane normalized depth $z_0/\lambda = 10^{-4}$ (below earth).
2. Ground-plane normalized depth $z_0/\lambda = -10^{-4}$ (above earth).
3. Ground-plane normalized depth $z_0/\lambda = -10^{-2}$ (above earth).

Subsection	Normalized depth, z_0/λ	A7 table nos.
A.7.1	10^{-4} (below earth)	1–12
A.7.2	-10^{-4} (above earth)	13–24
A.7.3	-10^{-2} (above earth)	25–36

A.7.1 Radial-Wire Ground Plane at Depth $|z_0/\lambda| = 10^{-4}$ Below Earth

Radial-wire ground-plane at depth $|z_0/\lambda| = 10^{-4}$ below earth are shown in Figs. A7-1–A7-12.

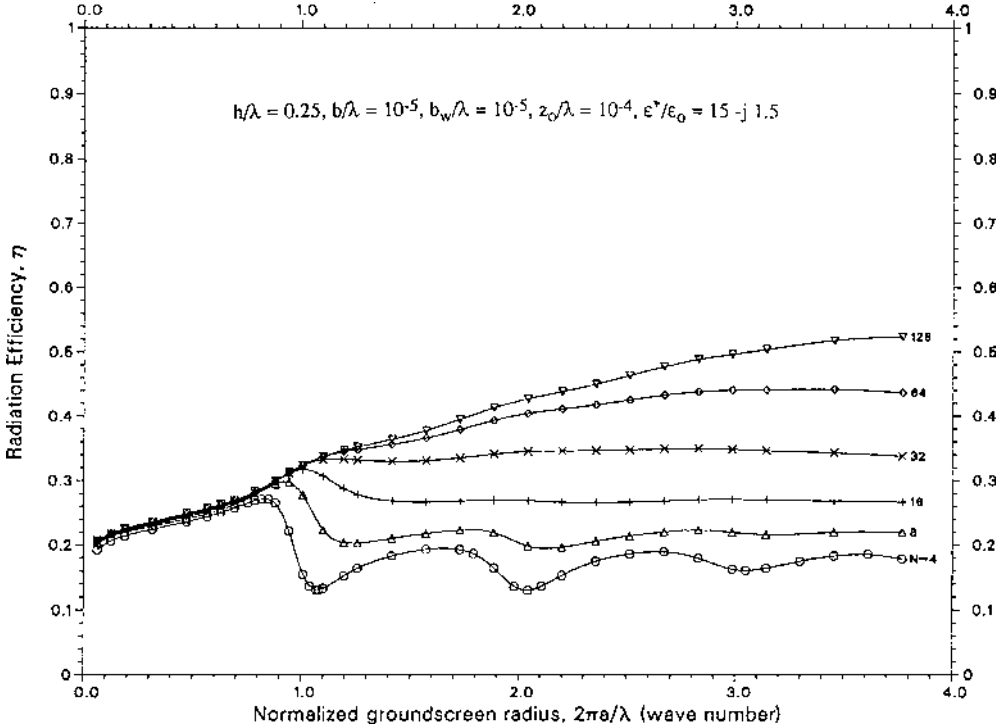

FIGURE A7-1 Radiation efficiency of quarter-wave monopole element with a radial-wire ground plane at a depth $|z_0/\lambda| = 10^{-4}$ below earth of relative permittivity $\varepsilon^*/\varepsilon_0 = 15 - j\,1.5$.

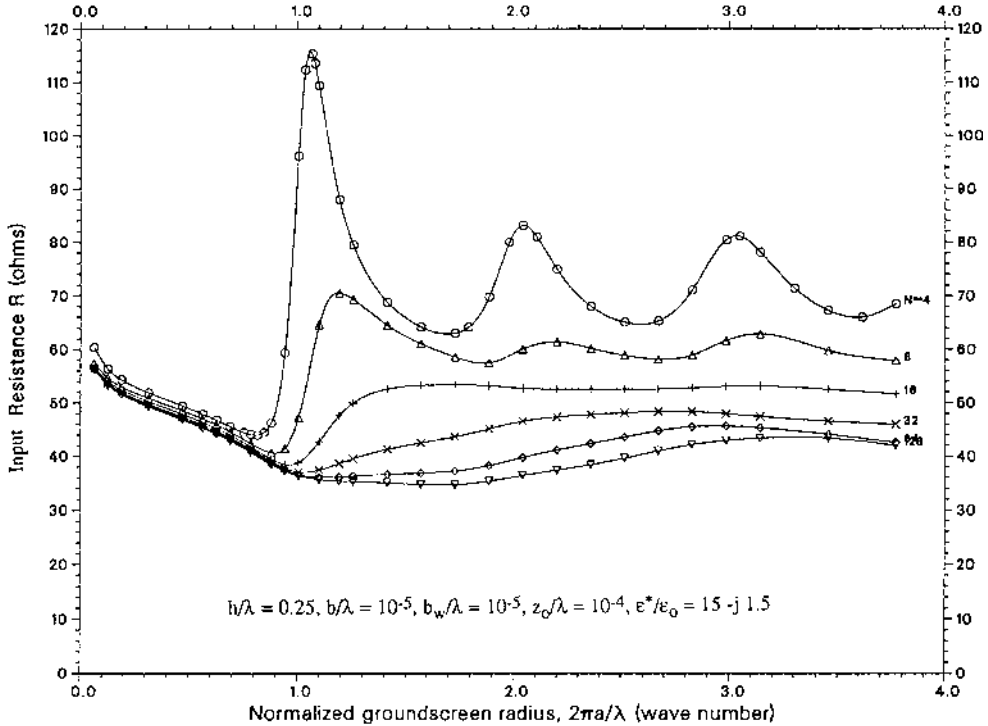
Input Resistance R (ohms)
Normalized groundscreen radius, 2πa/λ (wave number)
h/λ = 0.25, b/λ = 10-5, bw/λ = 10-5, z0/λ = 10-4, ε*/ε0 = 15 -j 1.5
N=4
8
16
32
64

FIGURE A7-2 Input resistance of a quarter-wave monopole element with a radial-wire ground plane at a depth $|z_0/\lambda| = 10^{-4}$ below earth of relative permittivity $\varepsilon^*/\varepsilon_0 = 15 - j\,1.5$.

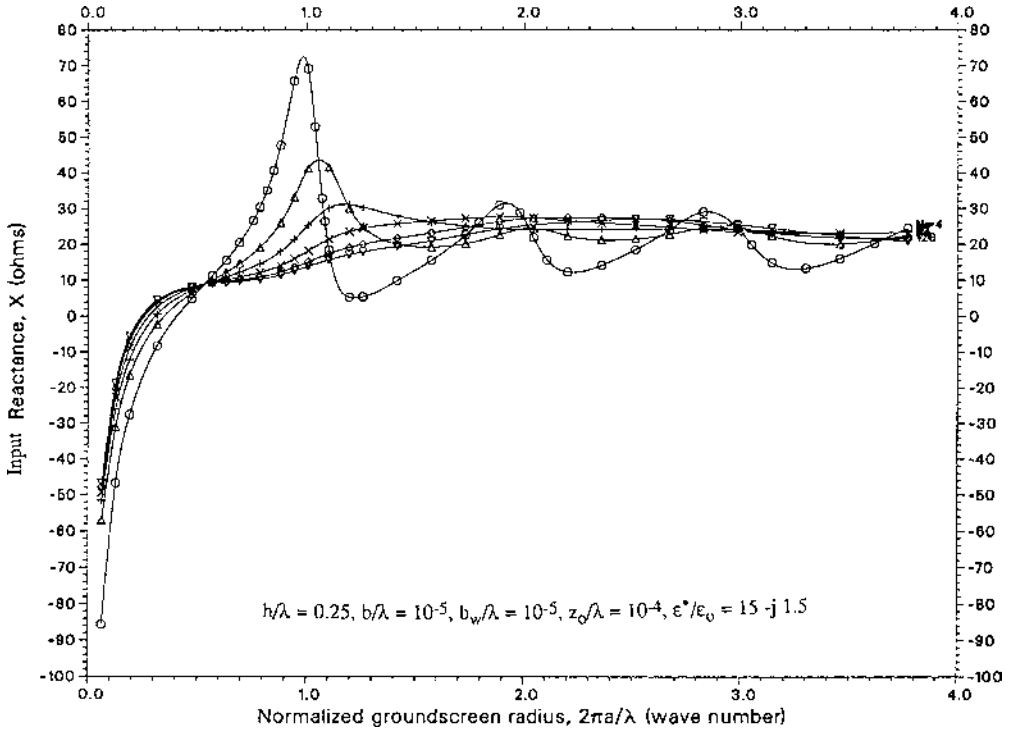

FIGURE A7-3 Input reactance of a quarter-wave monopole element with a radial-wire ground plane at a depth $|z_0/\lambda| = 10^{-4}$ below earth of relative permittivity $\varepsilon^*/\varepsilon_0 = 15 - j\,1.5$.

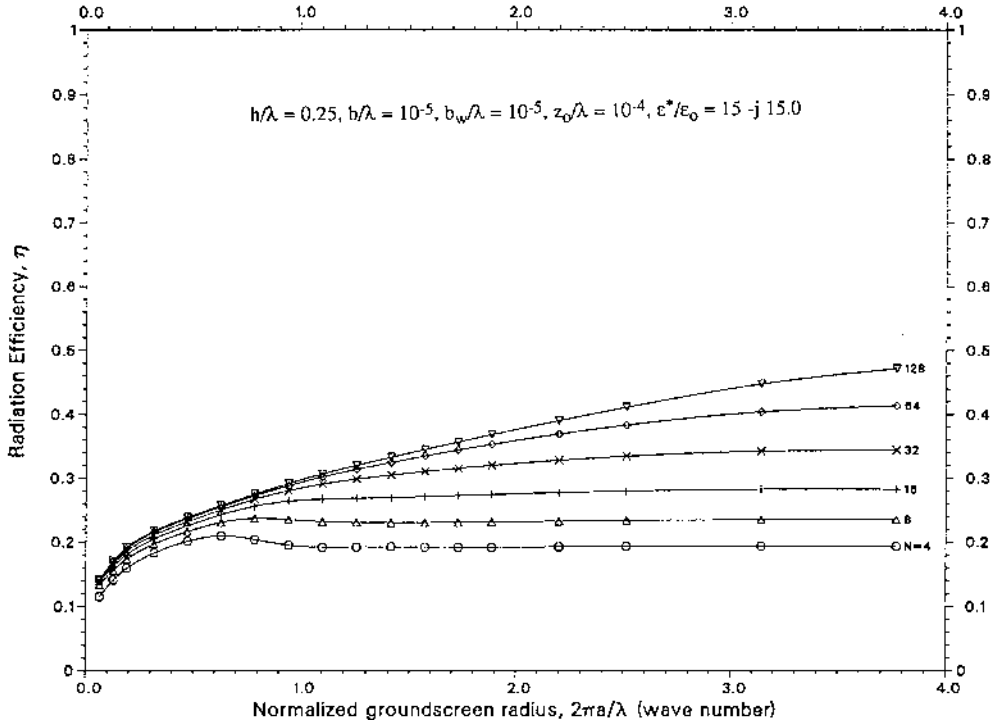

FIGURE A7-4 Radiation efficiency of a quarter-wave monopole element with a radial-wire ground plane at a depth $|z_0/\lambda| = 10^{-4}$ below earth of relative permittivity $\varepsilon^*/\varepsilon_0 = 15 - j\,15.0$.

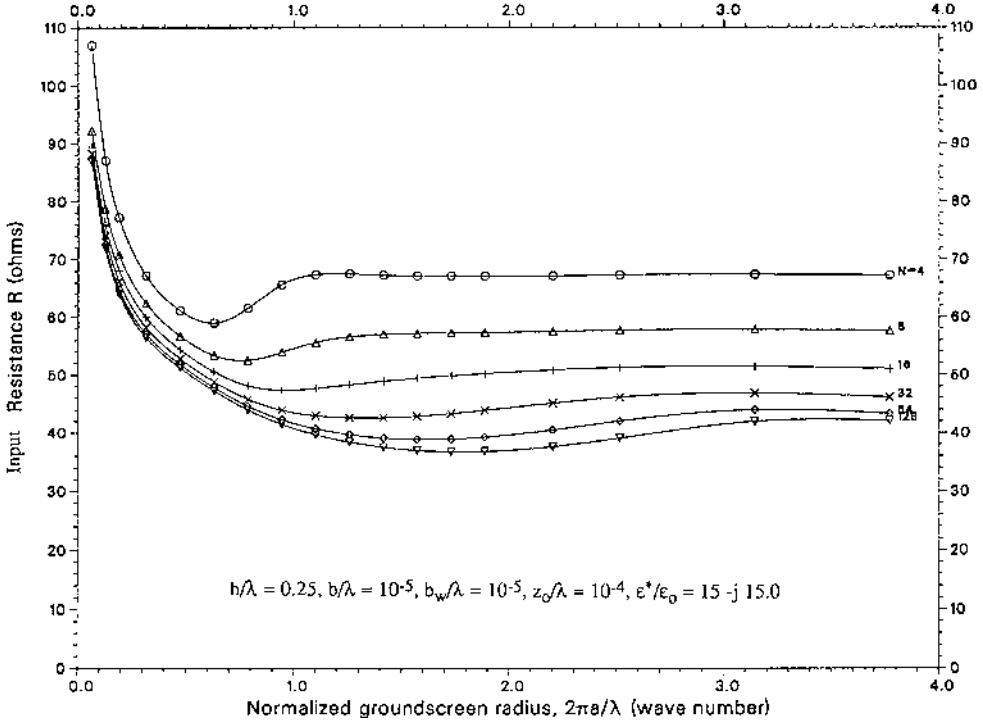

FIGURE A7-5 Input resistance of a quarter-wave monopole element with a radial-wire ground plane at a depth $|z_0/\lambda| = 10^{-4}$ below earth of relative permittivity $\varepsilon^*/\varepsilon_0 = 15 - j\,15.0$.

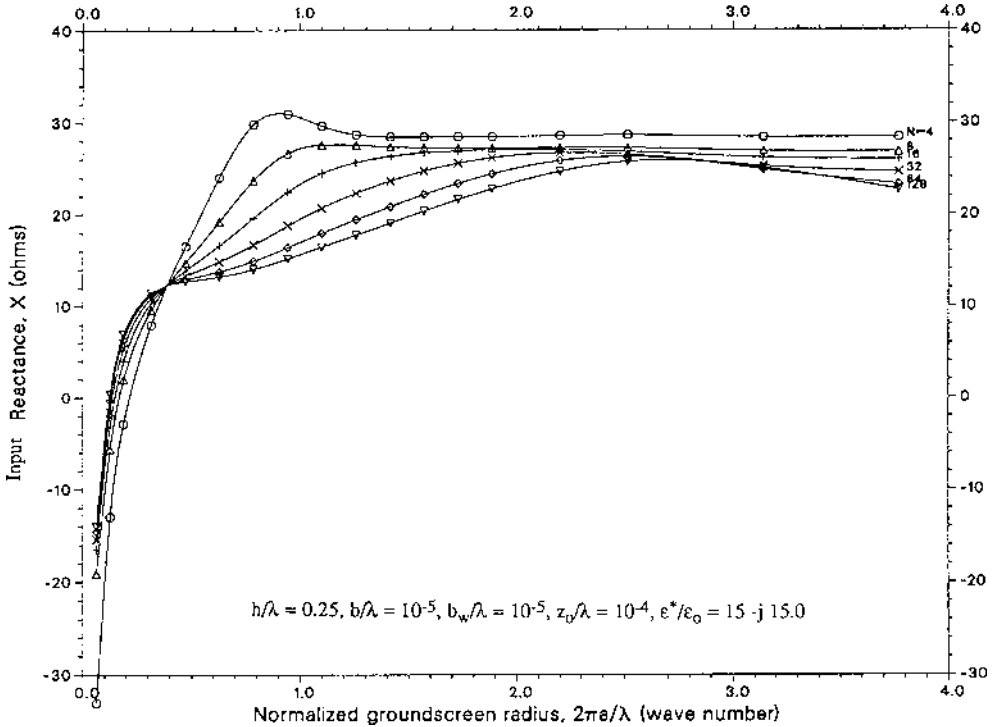

FIGURE A7-6 Input reactance of a quarter-wave monopole element with a radial-wire ground plane at a depth $|z_0/\lambda| = 10^{-4}$ below earth of relative permittivity $\varepsilon^*/\varepsilon_0 = 15 - j\,15.0$.

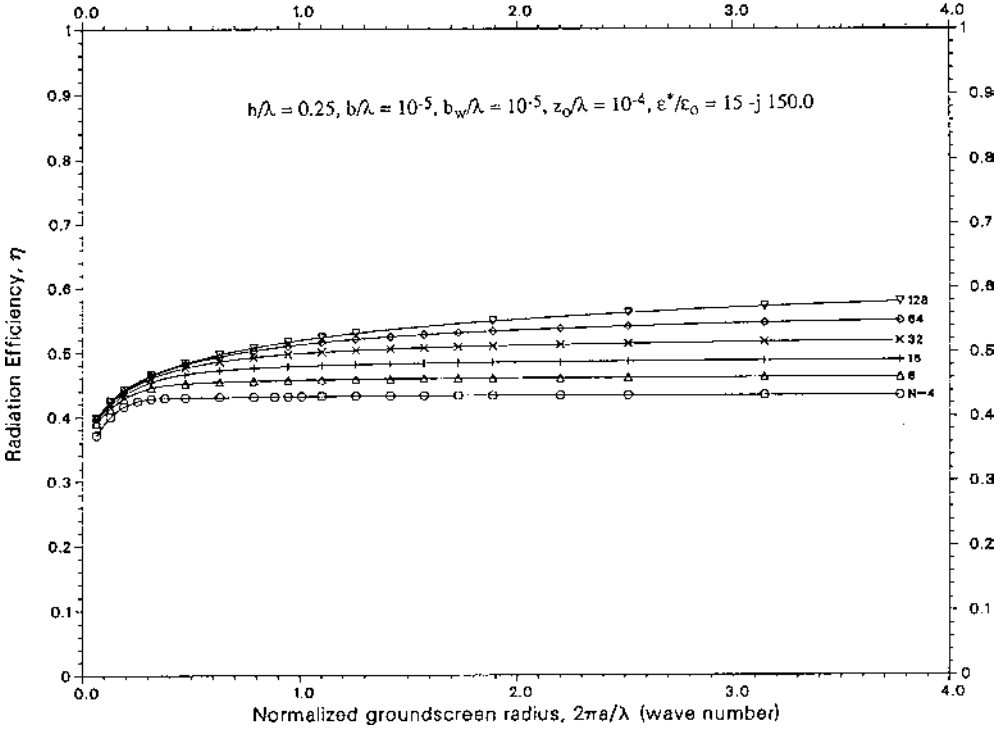

FIGURE A7-7 Radiation efficiency of a quarter-wave monopole element with a radial-wire ground plane at a depth $|z_0/\lambda| = 10^{-4}$ below earth of relative permittivity $\varepsilon^*/\varepsilon_0 = 15 - j\,150.0$.

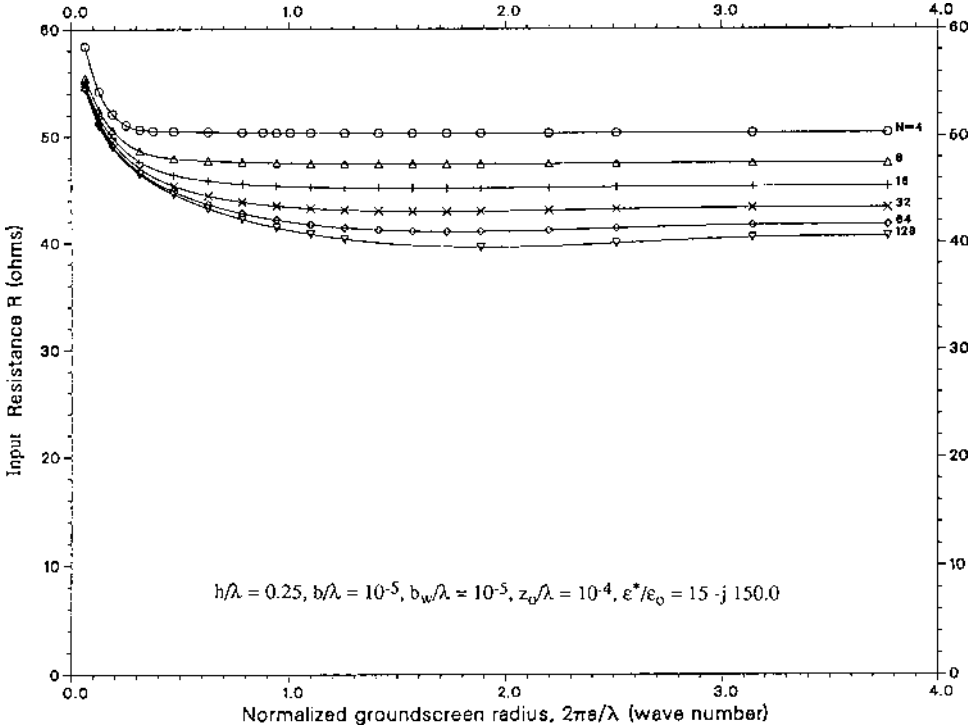

FIGURE A7-8 Input resistance of a quarter-wave monopole element with a radial-wire ground plane at a depth $|z_0/\lambda| = 10^{-4}$ below earth of relative permittivity $\varepsilon^*/\varepsilon_0 = 15 - j\,150.0$.

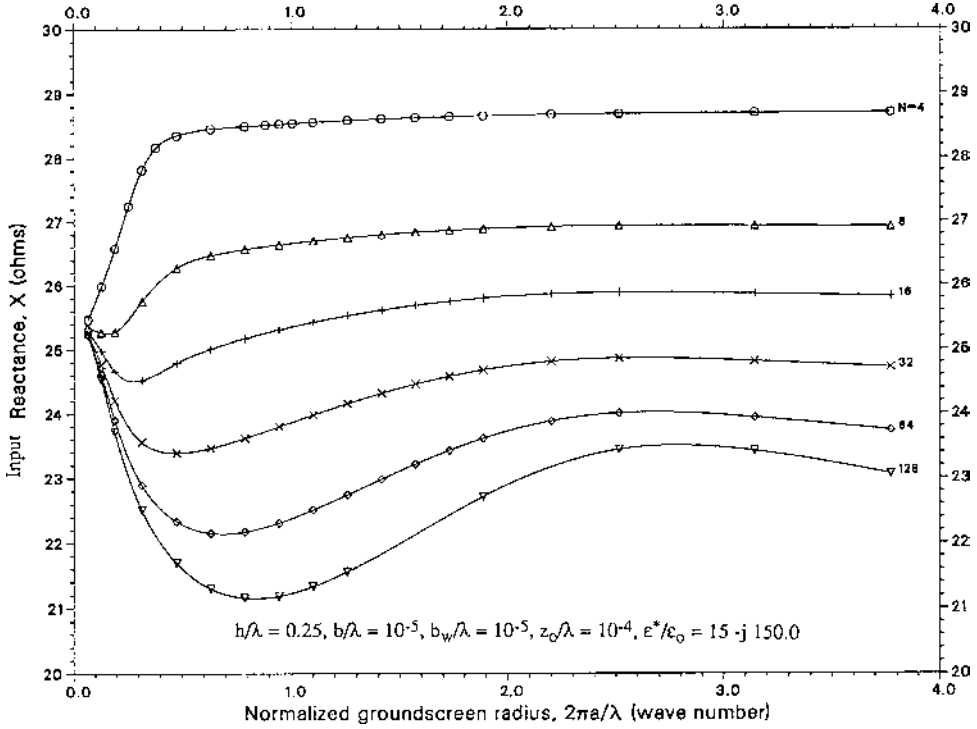

FIGURE A7-9 Input reactance of a quarter-wave monopole element with a radial-wire ground plane at a depth $|z_0/\lambda| = 10^{-4}$ below earth of relative permittivity $\varepsilon^*/\varepsilon_0 = 15 - j\,150.0$.

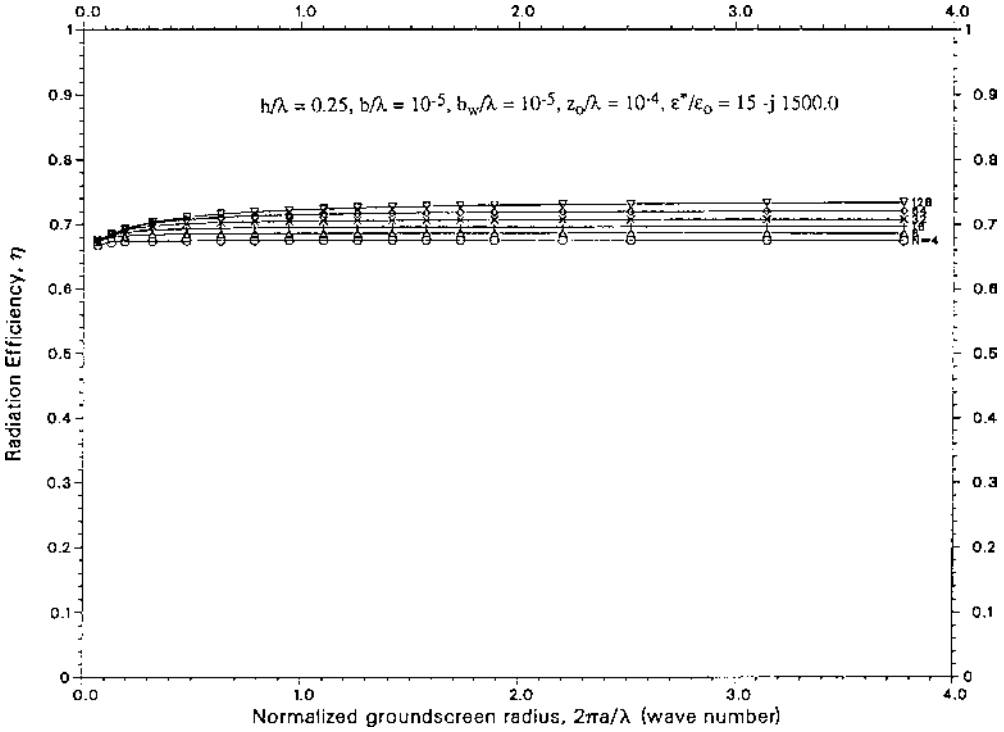

FIGURE A7-10 Radiation efficiency of a quarter-wave monopole element with a radial-wire ground plane at a depth $|z_0/\lambda| = 10^{-4}$ below earth of relative permittivity $\varepsilon^*/\varepsilon_0 = 15 - j\,1500.0$.

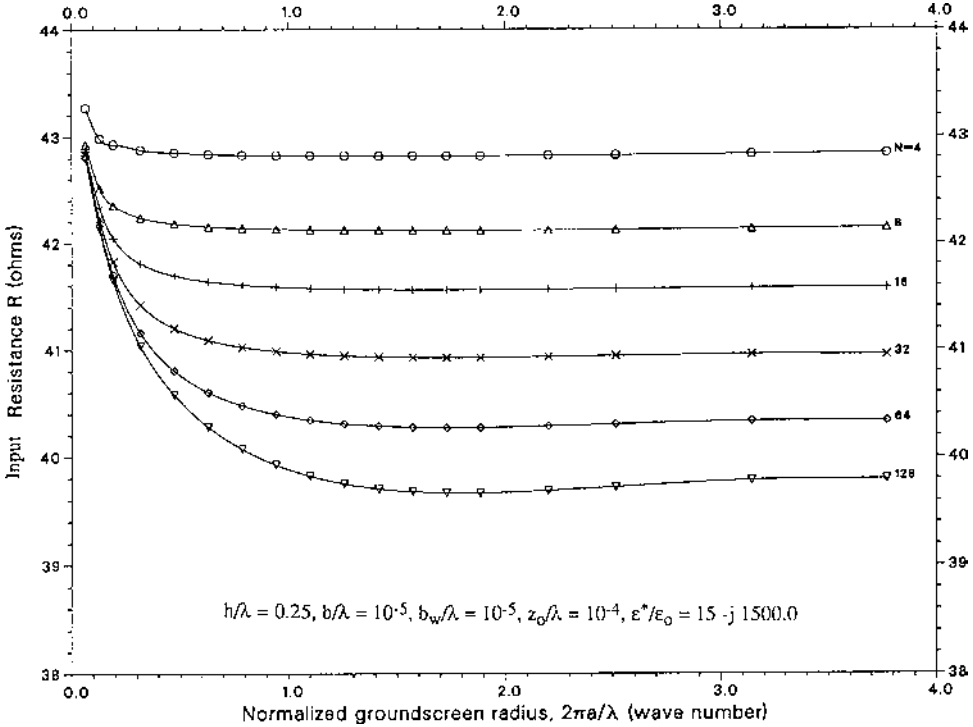

FIGURE A7-11 Input resistance of a quarter-wave monopole element with a radial-wire ground plane at a depth $|z_0/\lambda| = 10^{-4}$ below earth of relative permittivity $\varepsilon^*/\varepsilon_0 = 15 - j\,1500.0$.

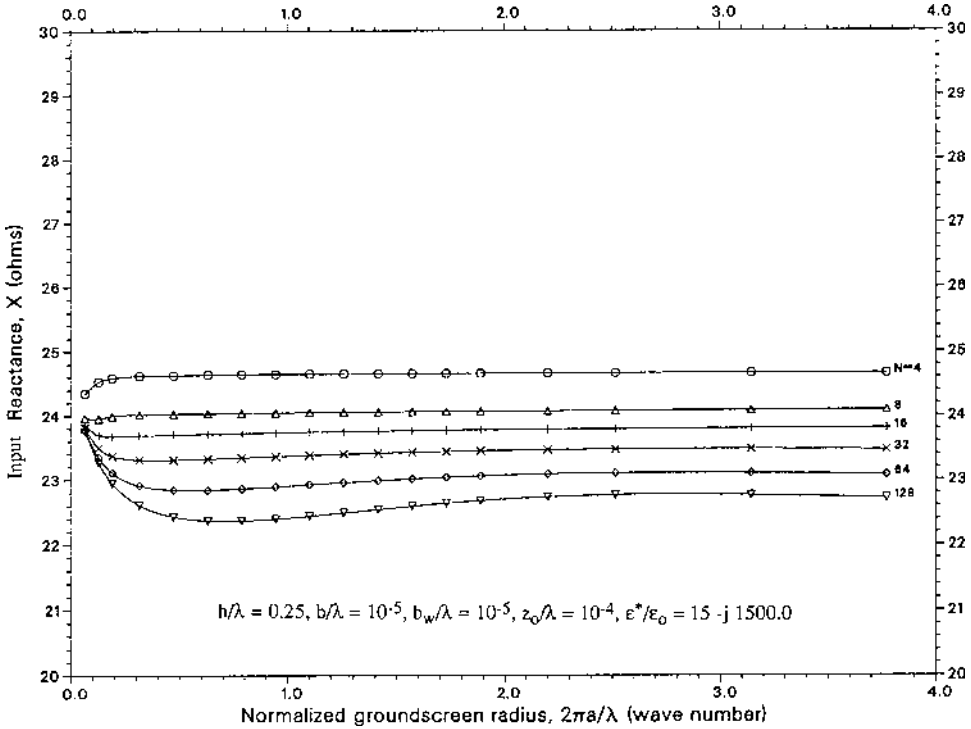

FIGURE A7-12 Input reactance of a quarter-wave monopole element with a radial-wire ground plane at a depth $|z_0/\lambda| = 10^{-4}$ below earth of relative permittivity $\varepsilon^*/\varepsilon_0 = 15 - j\,1500.0$.

A.7.2 Radial-Wire Ground Plane at Height $|z_0/\lambda| = 10^{-4}$ Above Earth

Radial-wire ground-plane at height $|z_0/\lambda| = 10^{-4}$ above earth are shown in Figs. A7-13–A7-24.

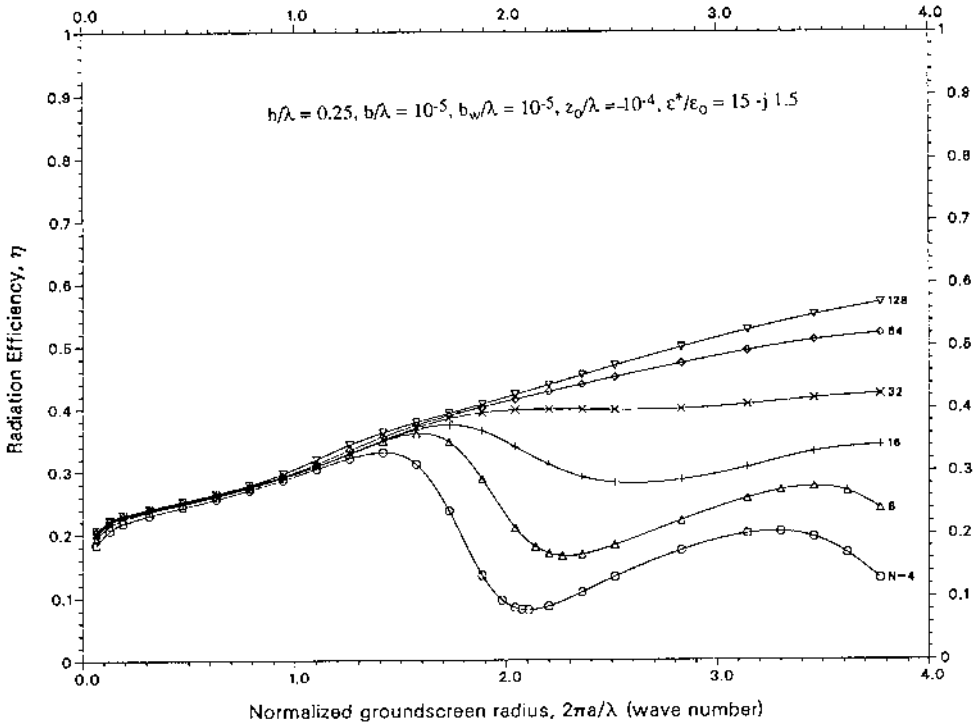

FIGURE A7-13 Radiation efficiency of a quarter-wave monopole element with a radial-wire ground plane at a height $|z_0/\lambda| = 10^{-4}$ above.

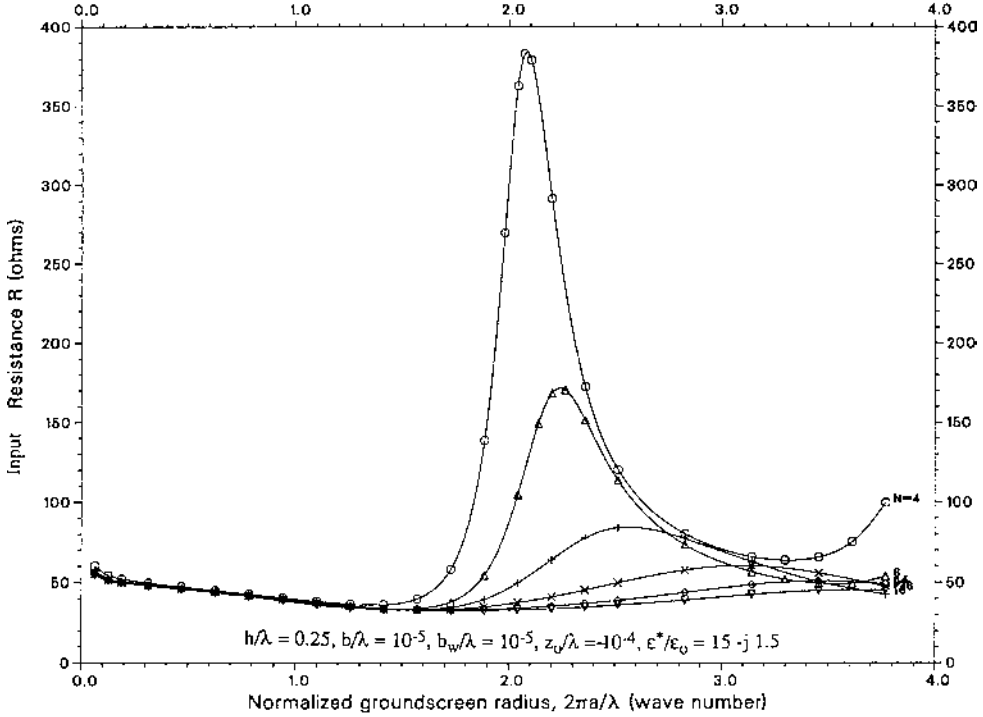

FIGURE A7-14 Input resistance of a quarter-wave monopole element with a radial-wire ground plane at a height $|z_0/\lambda| = 10^{-4}$ above earth of relative permittivity $\varepsilon^*/\varepsilon_0 = 15 - j\,1.5$.

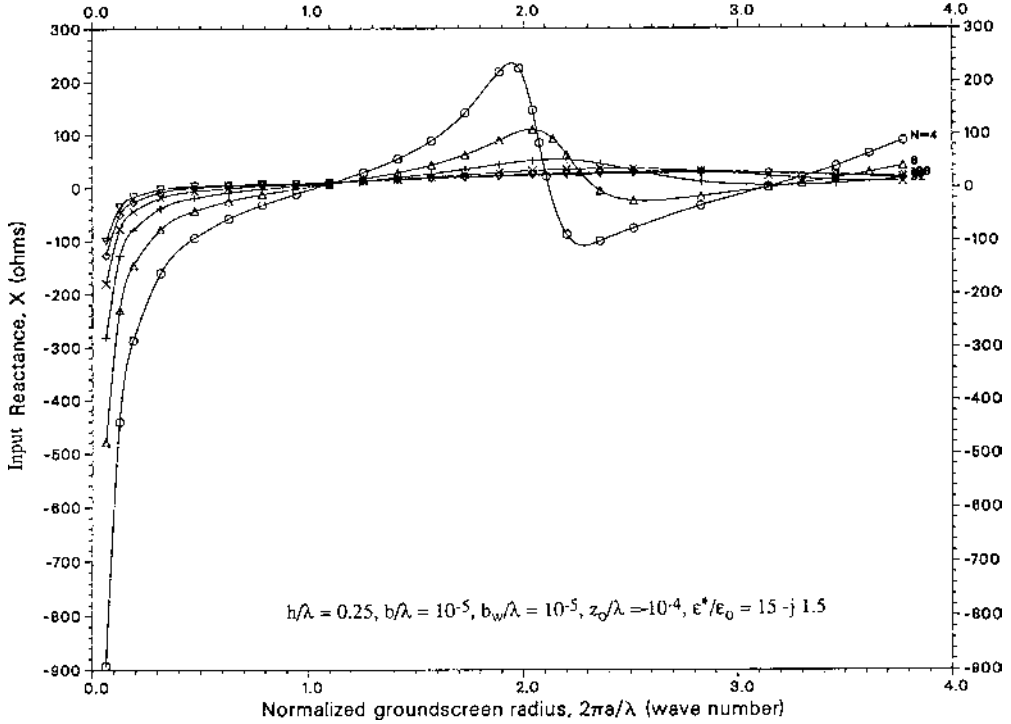

FIGURE A7-15 Input reactance of a quarter-wave monopole element with a radial-wire ground plane at a height $|z_0/\lambda| = 10^{-4}$ above earth of relative permittivity $\varepsilon^*/\varepsilon_0 = 15 - j\,1.5$.

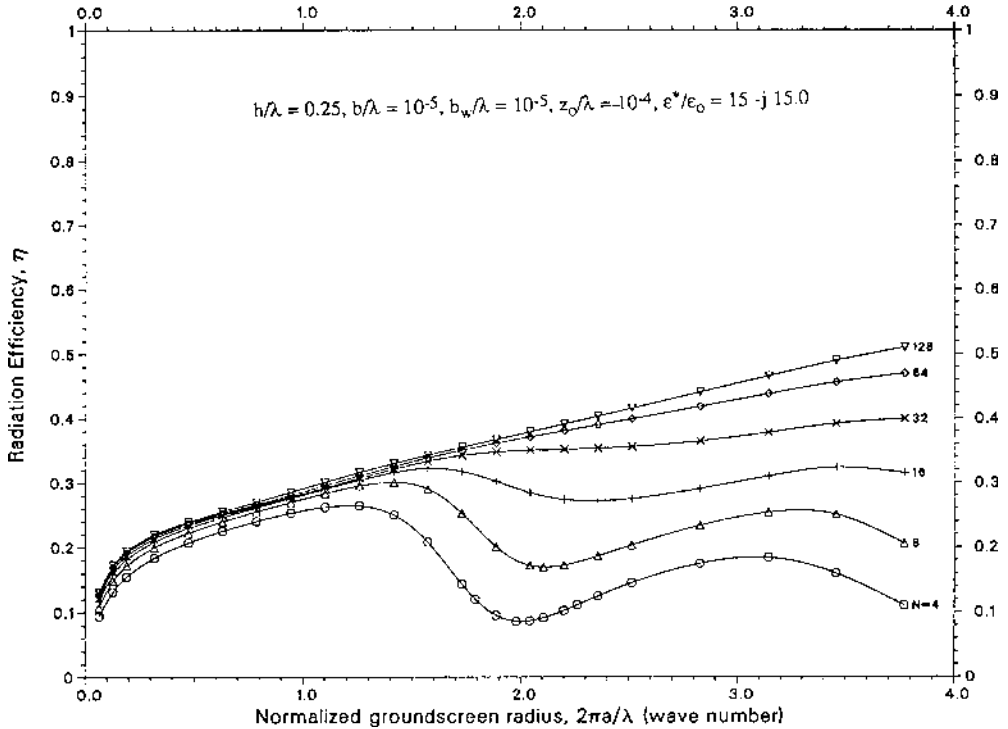

FIGURE A7-16 Radiation efficiency of a quarter-wave monopole element with a radial-wire ground plane at a height $|z_0/\lambda| = 10^{-4}$ above earth of relative permittivity $\varepsilon^*/\varepsilon_0 = 15 - j\,15.0$.

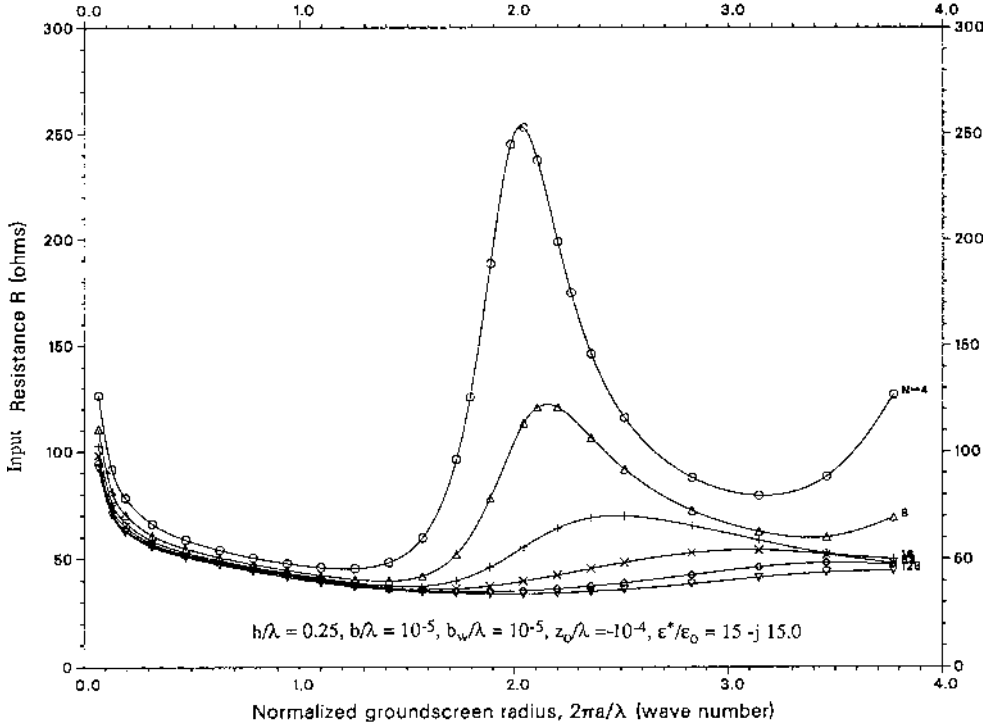

FIGURE A7-17 Input resistance of a quarter-wave monopole element with a radial-wire ground plane at a height $|z_0/\lambda| = 10^{-4}$ above earth of relative permittivity $\varepsilon^*/\varepsilon_0 = 15 - j\,15.0$.

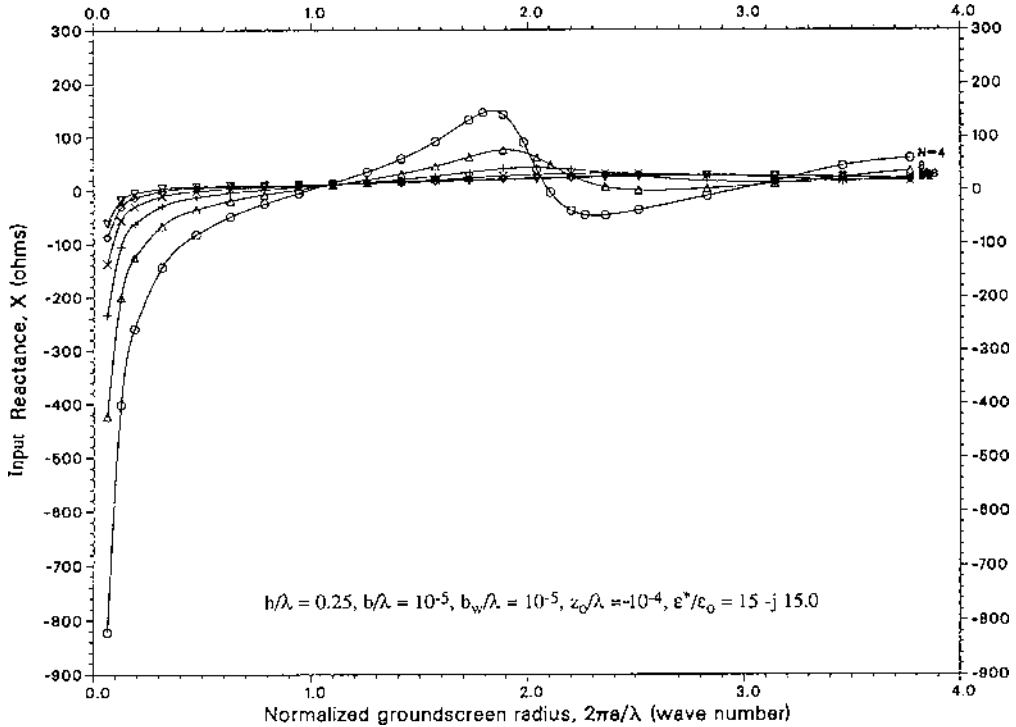

FIGURE A7-18 Input reactance of a quarter-wave monopole element with a radial-wire ground plane at a height $|z_0/\lambda| = 10^{-4}$ above earth of relative permittivity $\varepsilon^*/\varepsilon_0 = 15 - j\,15.0$.

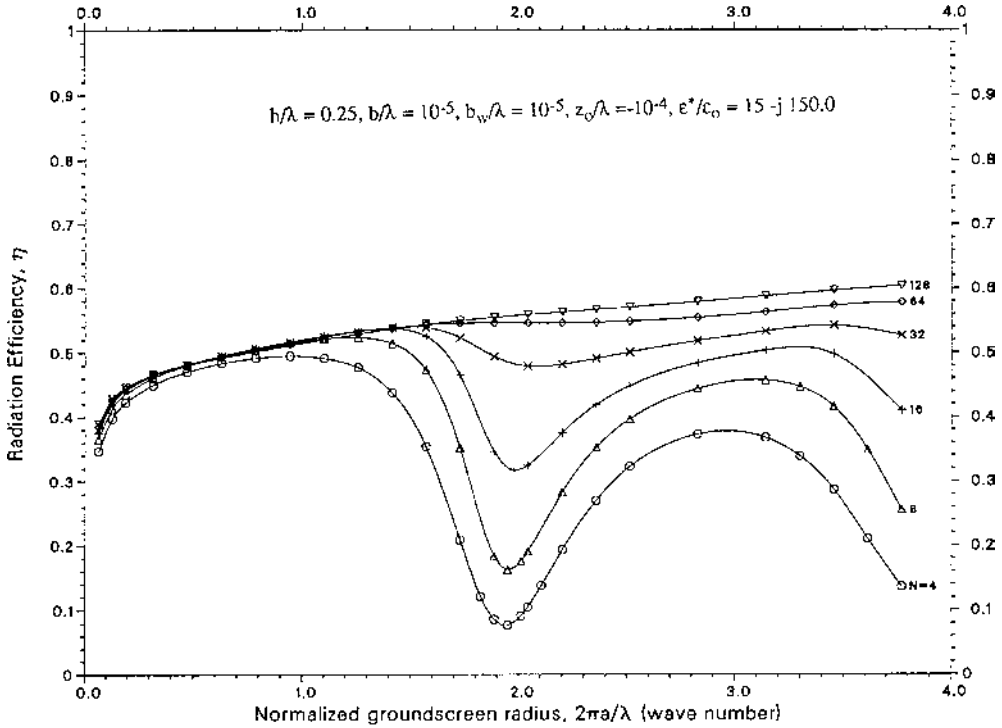

FIGURE A7-19 Radiation efficiency of a quarter-wave monopole element with a radial-wire ground plane at a height $|z_0/\lambda| = 10^{-4}$ above earth of relative permittivity $\varepsilon^*/\varepsilon_0 = 15 - j\,150.0$.

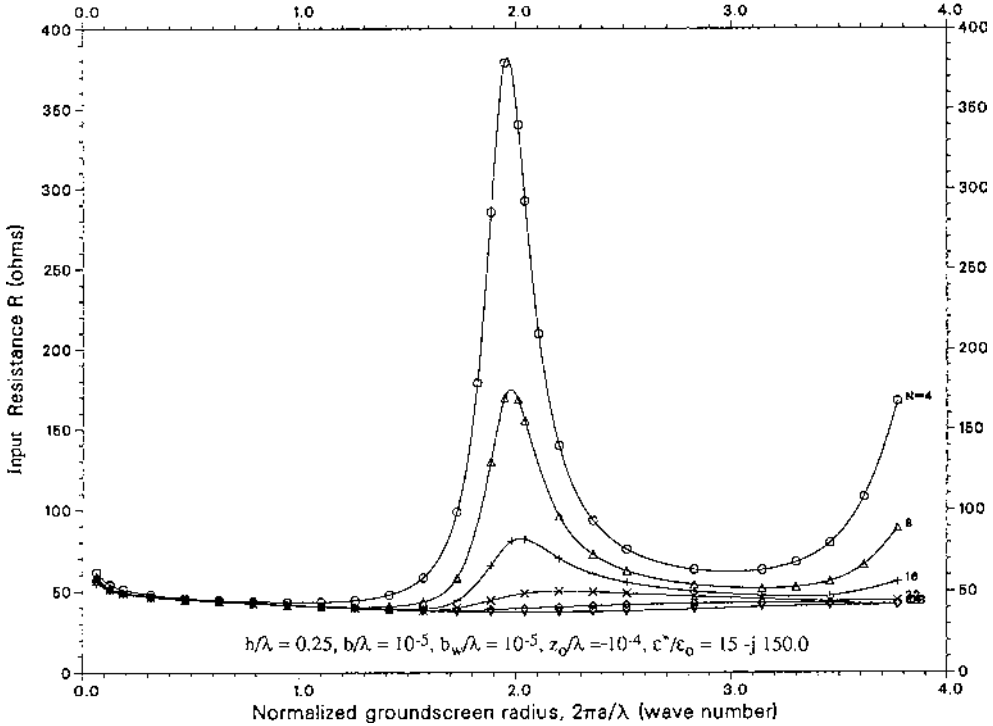

FIGURE A7-20 Input resistance of a quarter-wave monopole element with a radial-wire ground plane at a height $|z_0/\lambda| = 10^{-4}$ above earth of relative permittivity $\varepsilon^*/\varepsilon_0 = 15 - j\,150.0$.

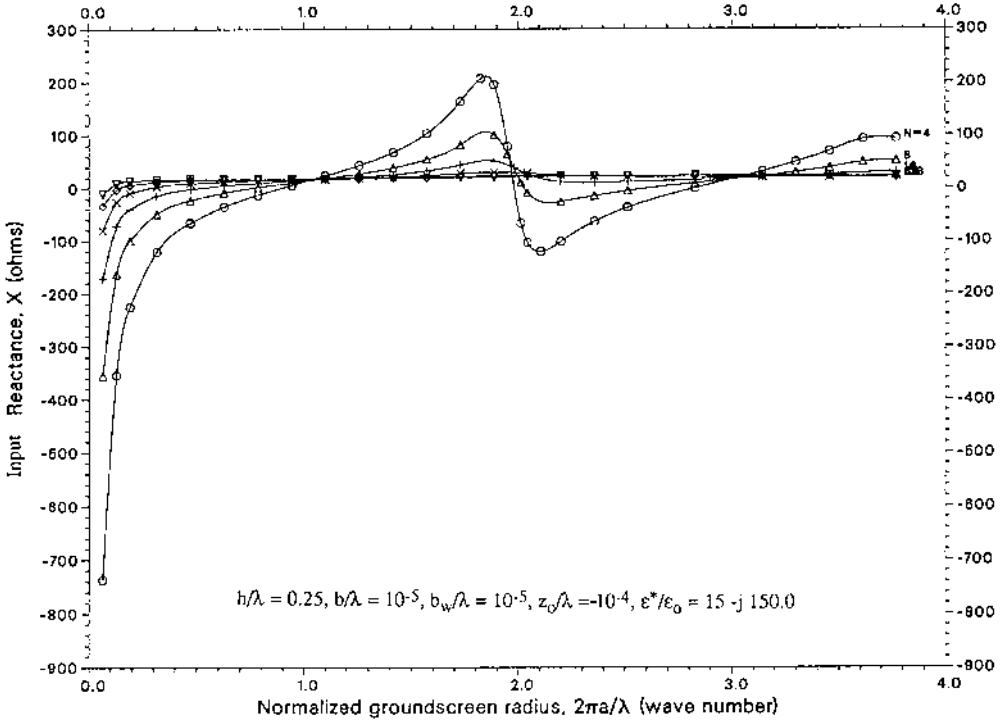

FIGURE A7-21 Input reactance of a quarter-wave monopole element with a radial-wire ground plane at a height $|z_0/\lambda| = 10^{-4}$ above earth of relative permittivity $\varepsilon^*/\varepsilon_0 = 15 - j\,150.0$.

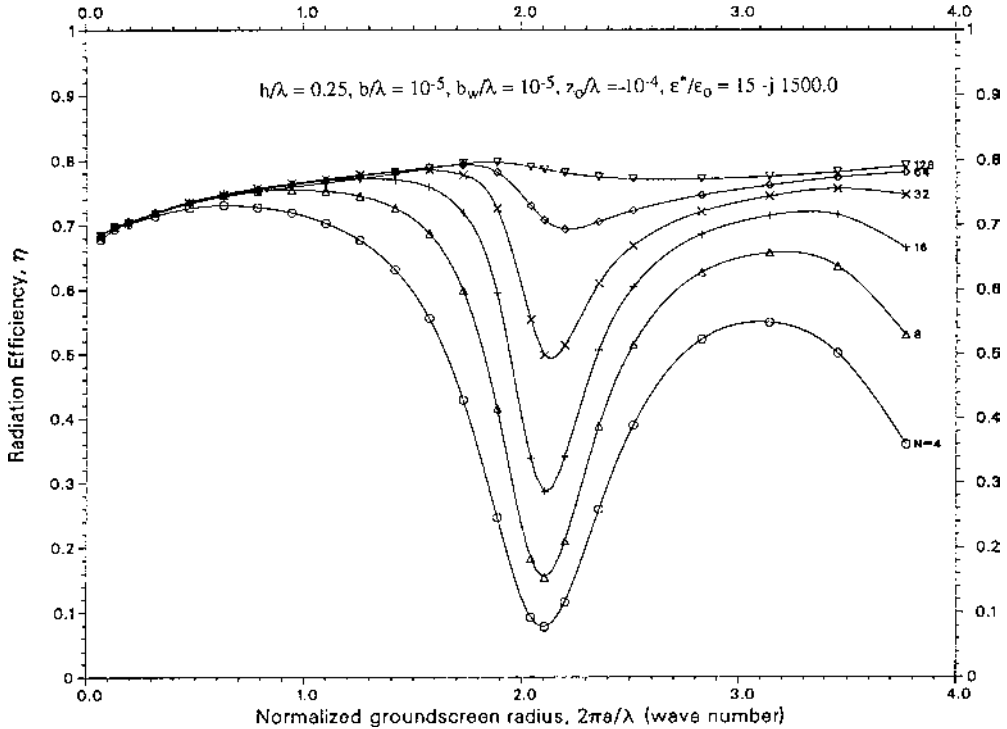

FIGURE A7-22 Radiation efficiency of a quarter-wave monopole element with a radial-wire ground plane at a height $|z_0/\lambda| = 10^{-4}$ above earth of relative permittivity $\varepsilon^*/\varepsilon_0 = 15 - j\,1500.0$.

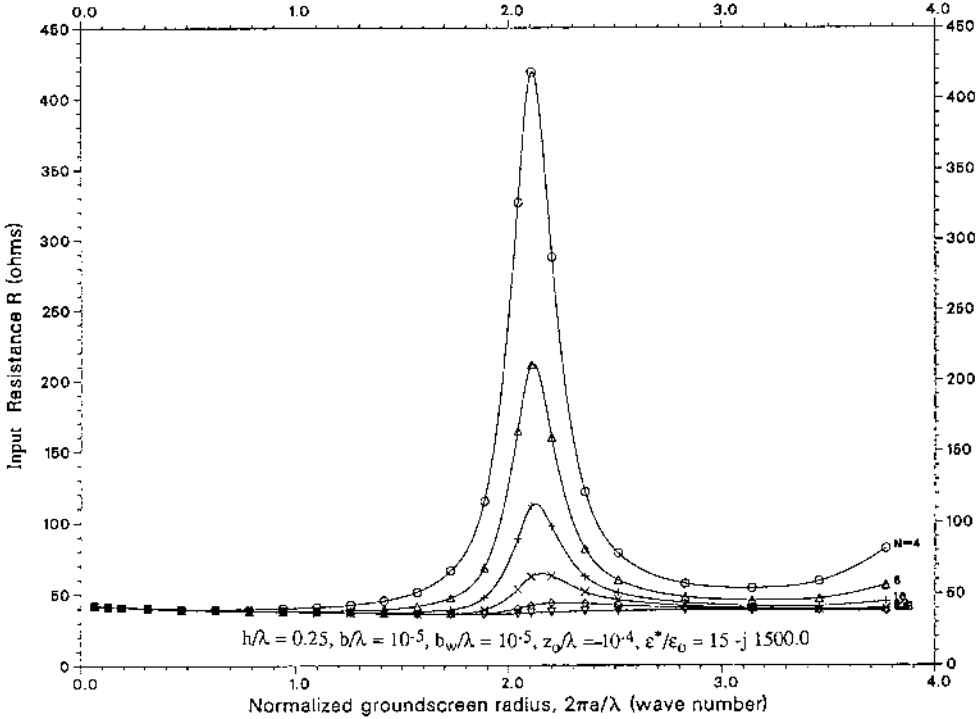

FIGURE A7-23 Input resistance of a quarter-wave monopole element with a radial-wire ground plane at a height $|z_0/\lambda| = 10^{-4}$ above earth of relative permittivity $\varepsilon^*/\varepsilon_0 = 15 - j\,1500.0$.

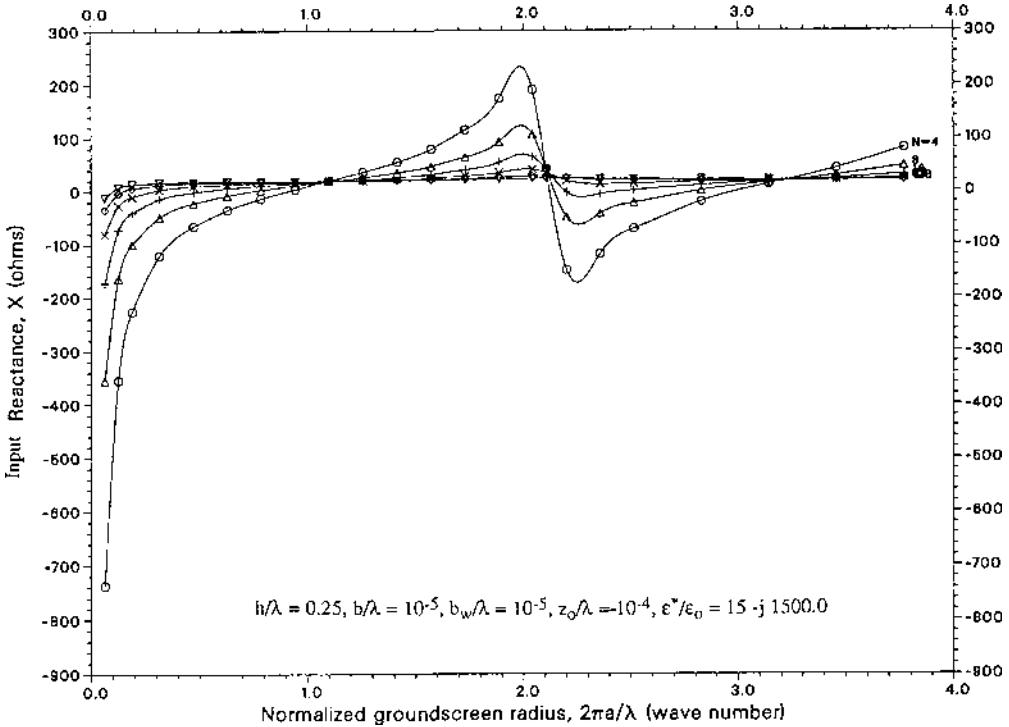

FIGURE A7-24 Input reactance of a quarter-wave monopole element with a radial-wire ground plane at a height $|z_0/\lambda| = 10^{-4}$ above earth of relative permittivity $\varepsilon^*/\varepsilon_0 = 15 - j\,1500.0$.

A.7.3 Radial-Wire Ground Plane at Height $|z_0/\lambda| = 10^{-2}$ Above Earth

Radial-wire ground-plane at height $|z_0/\lambda| = 10^{-2}$ above earth are shown in Figs. A7-25–A7-36.

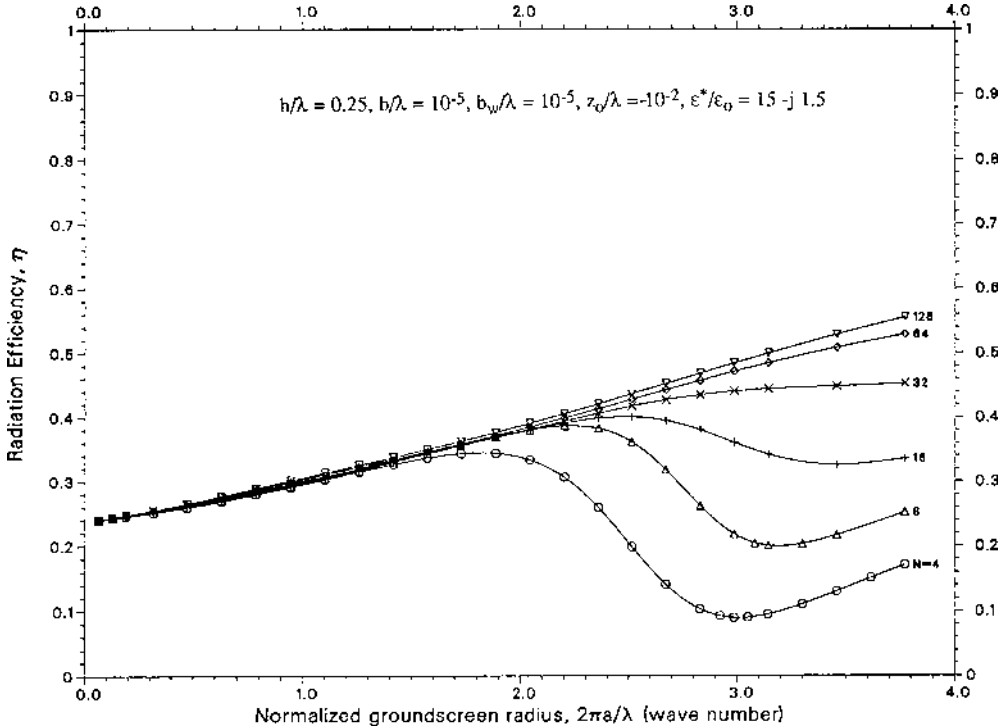

FIGURE A7-25 Radiation efficiency of a quarter-wave monopole element with a radial-wire ground plane at a height $|z_0/\lambda| = 10^{-4}$ above earth of relative permittivity $\varepsilon^*/\varepsilon_0 = 15 - j\,1.5$.

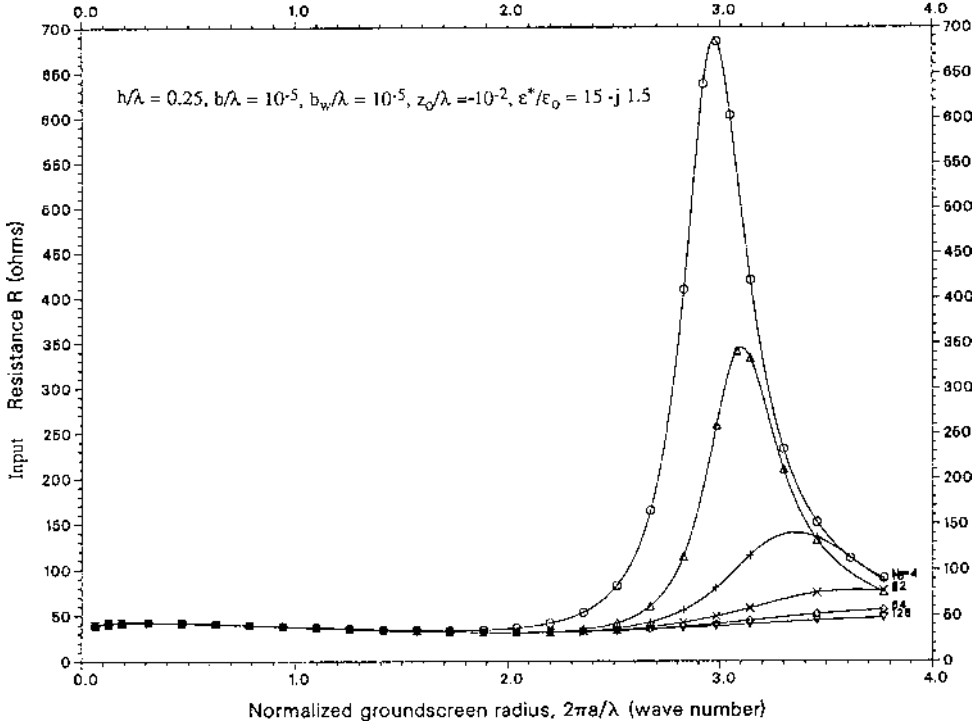

FIGURE A7-26 Input resistance of a quarter-wave monopole element with a radial-wire ground plane at a height $|z_0/\lambda| = 10^{-2}$ above earth of relative permittivity $\varepsilon^*/\varepsilon_0 = 15 - j\,1.5$.

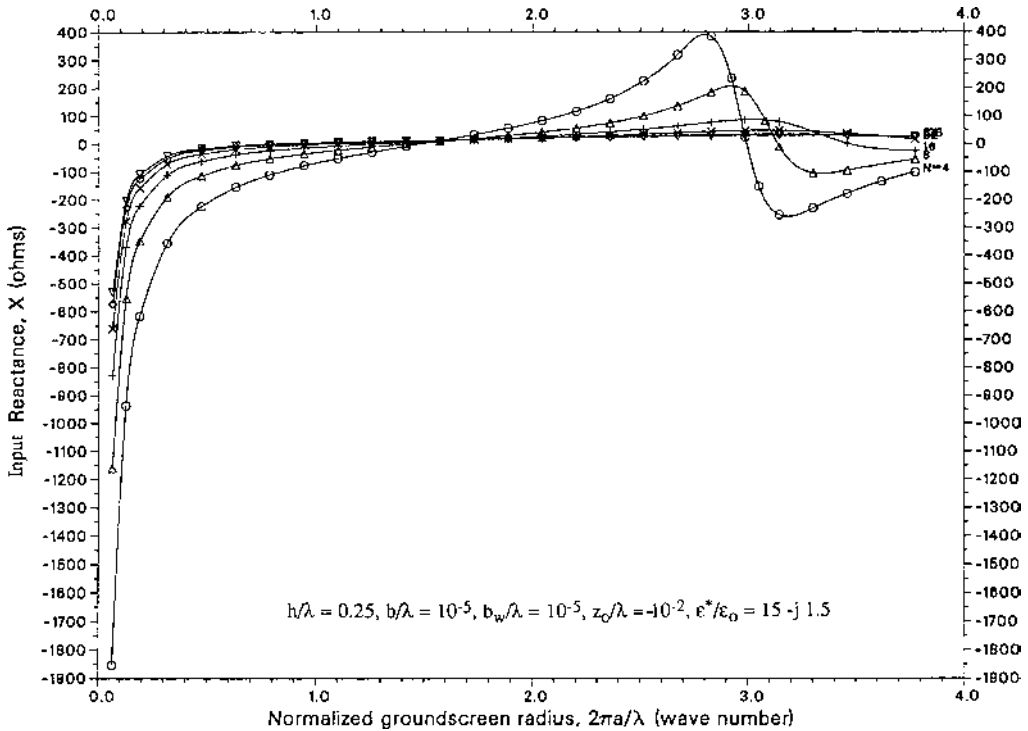

FIGURE A7-27 Input reactance of a quarter-wave monopole element with a radial-wire ground plane at a height $|z_0/\lambda| = 10^{-2}$ above earth of relative permittivity $\varepsilon^*/\varepsilon_0 = 15 - j\,1.5$.

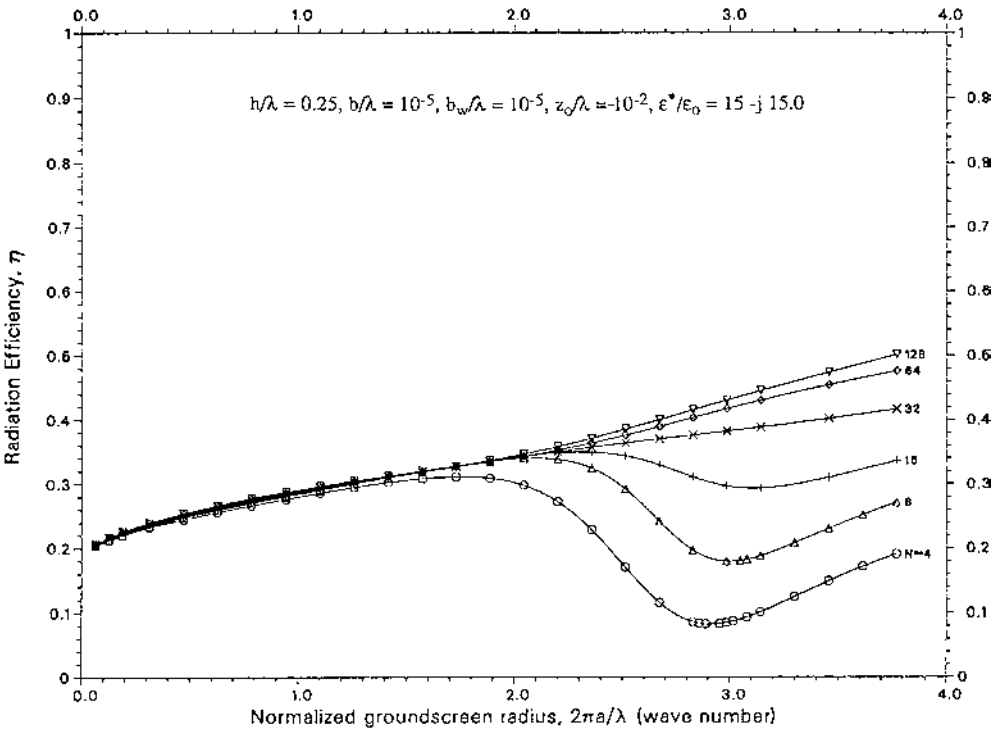

FIGURE A7-28 Radiation efficiency of a quarter-wave monopole element with a radial-wire ground plane at a height $|z_0/\lambda| = 10^{-2}$ above earth of relative permittivity $\varepsilon^*/\varepsilon_0 = 15 - j\,15.0$.

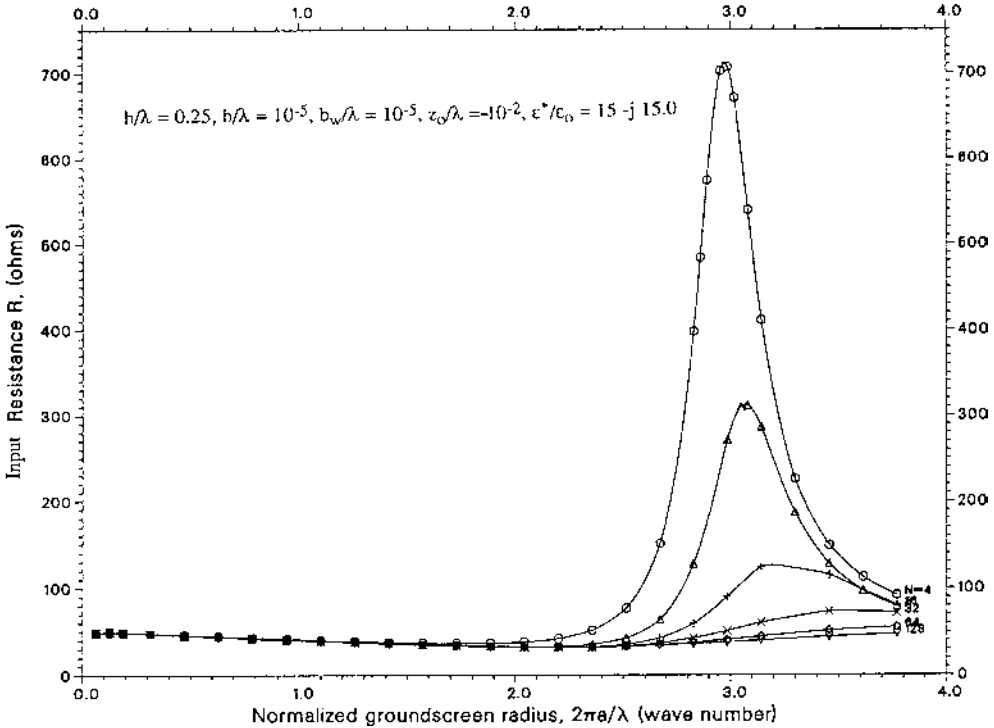

FIGURE A7-29 Input resistance of a quarter-wave monopole element with a radial-wire ground plane at a height $|z_0/\lambda| = 10^{-2}$ above earth of relative permittivity $\varepsilon^*/\varepsilon_0 = 15 - j\,15.0$.

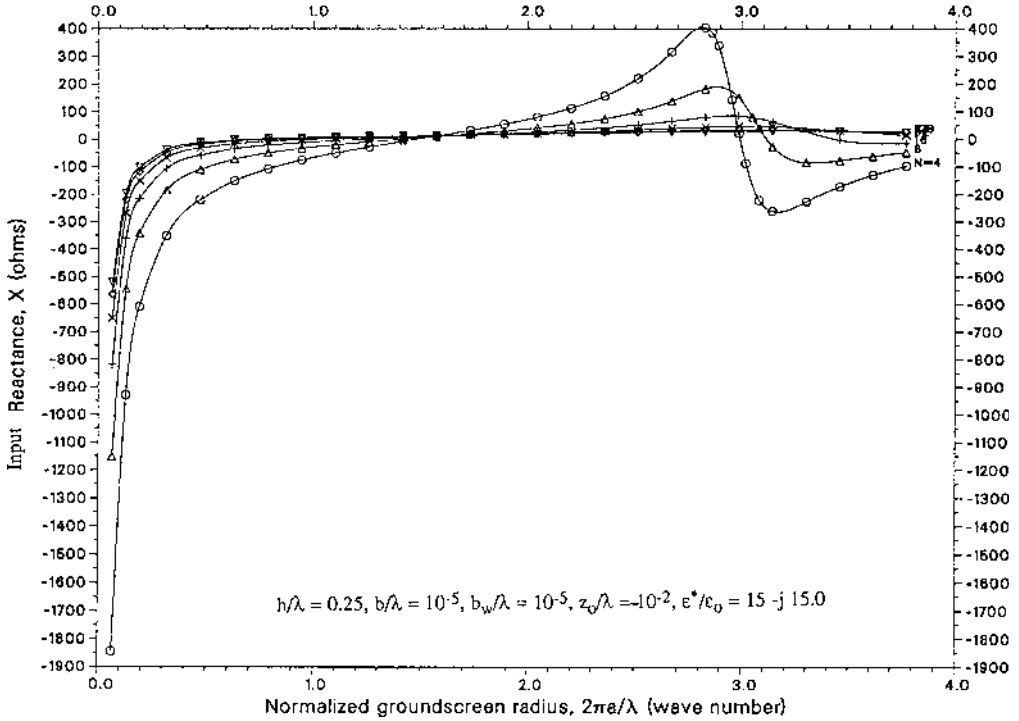

FIGURE A7-30 Input reactance of a quarter-wave monopole element with a radial-wire ground plane at a height $|z_0/\lambda| = 10^{-2}$ above earth of relative permittivity $\varepsilon^*/\varepsilon_0 = 15 - j\,15.0$.

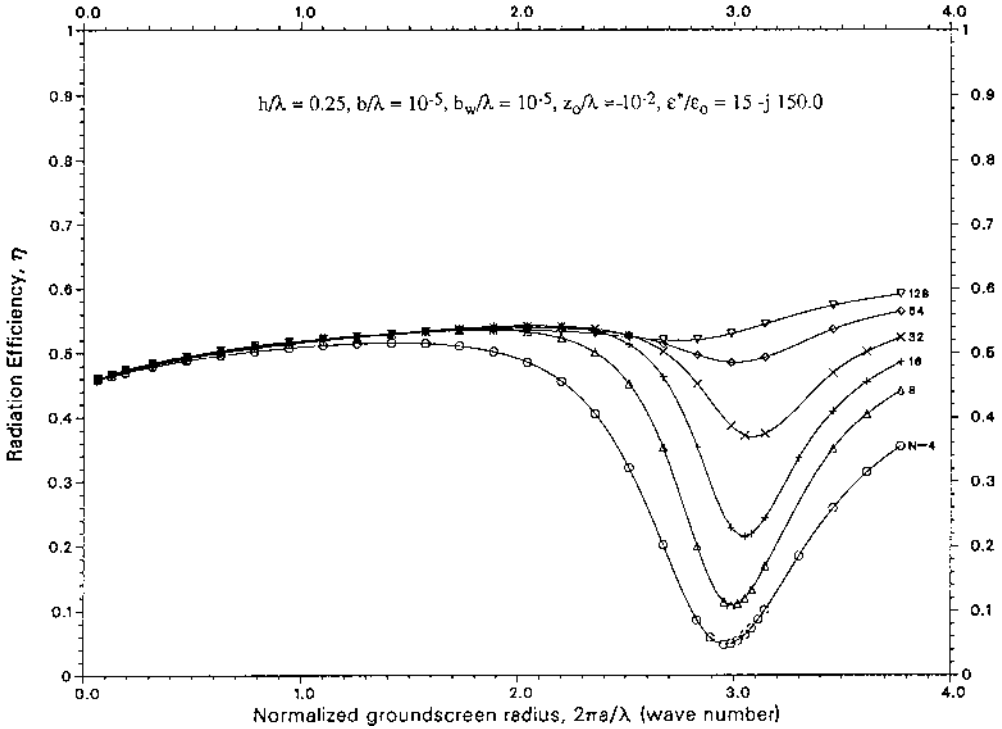

FIGURE A7-31 Radiation efficiency of a quarter-wave monopole element with a radial-wire ground plane at a height $|z_0/\lambda| = 10^{-2}$ above earth of relative permittivity $\varepsilon^*/\varepsilon_0 = 15 - j\,150.0$.

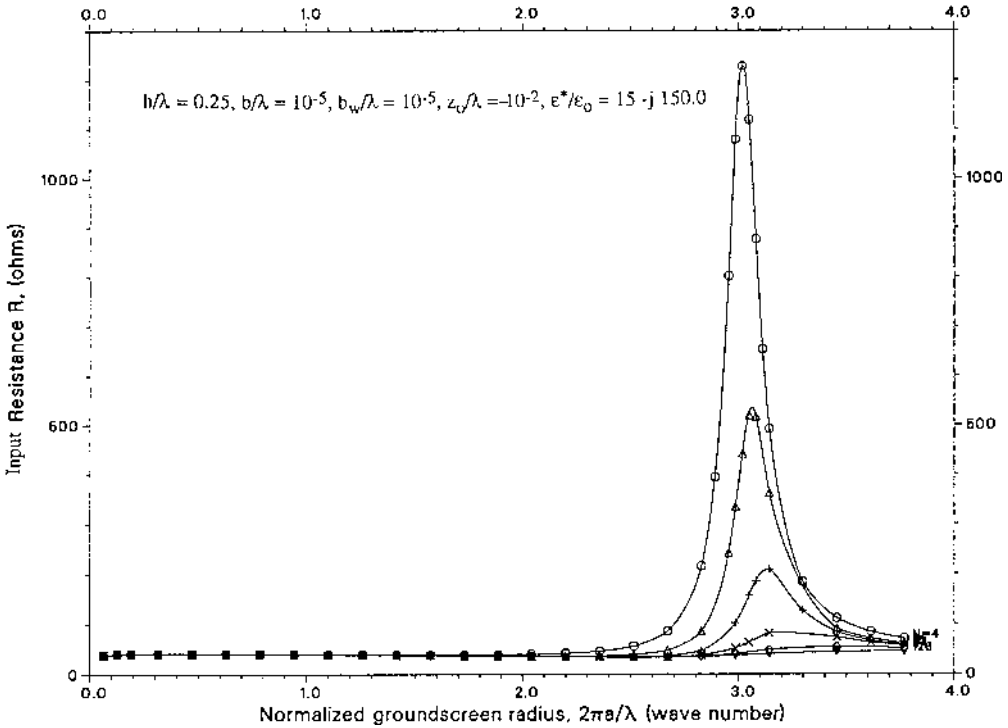

FIGURE A7-32 Input resistance of a quarter-wave monopole element with a radial-wire ground plane at a height $|z_0/\lambda| = 10^{-2}$ above earth of relative permittivity $\varepsilon^*/\varepsilon_0 = 15 - j\,150.0$.

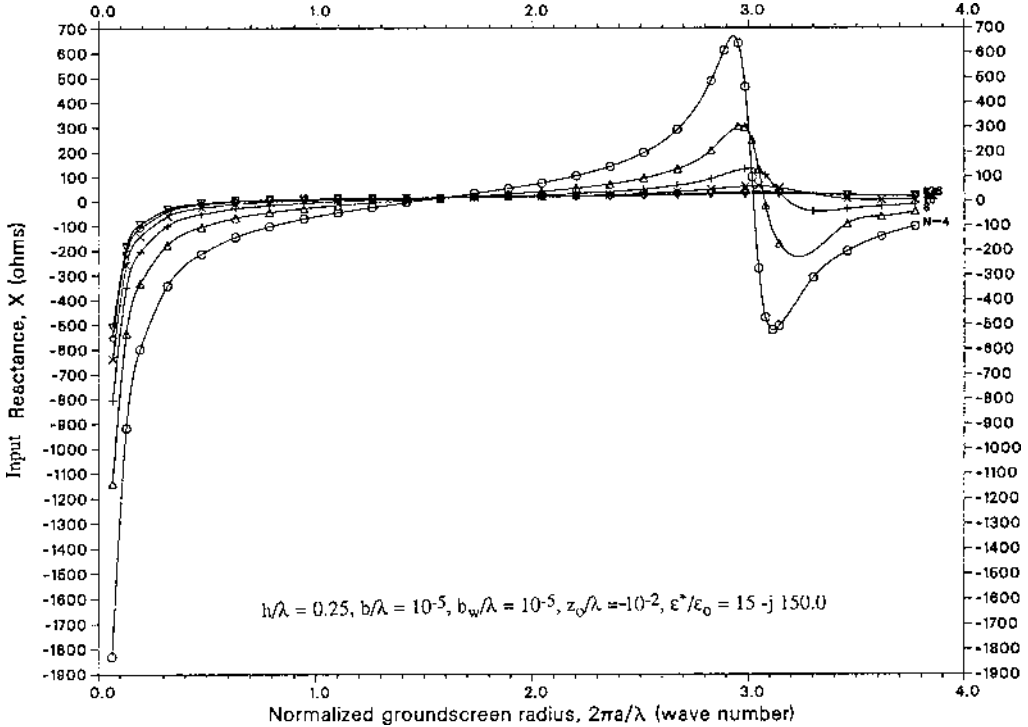

FIGURE A7-33 Input reactance of a quarter-wave monopole element with a radial-wire ground plane at a height $|z_0/\lambda| = 10^{-2}$ above earth of relative permittivity $\varepsilon^*/\varepsilon_0 = 15 - j\,150.0$.

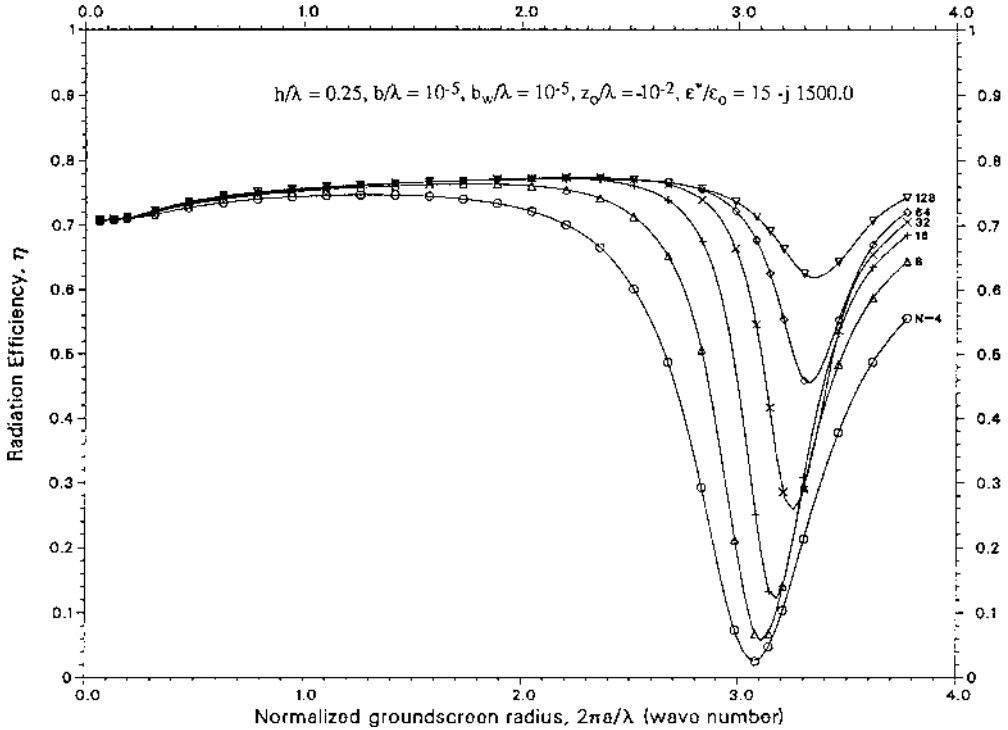

FIGURE A7-34 Radiation efficiency of a quarter-wave monopole element with a radial-wire ground plane at a height $|z_0/\lambda| = 10^{-2}$ above earth of relative permittivity $\varepsilon^*/\varepsilon_0 = 15 - j\,1500.0$.

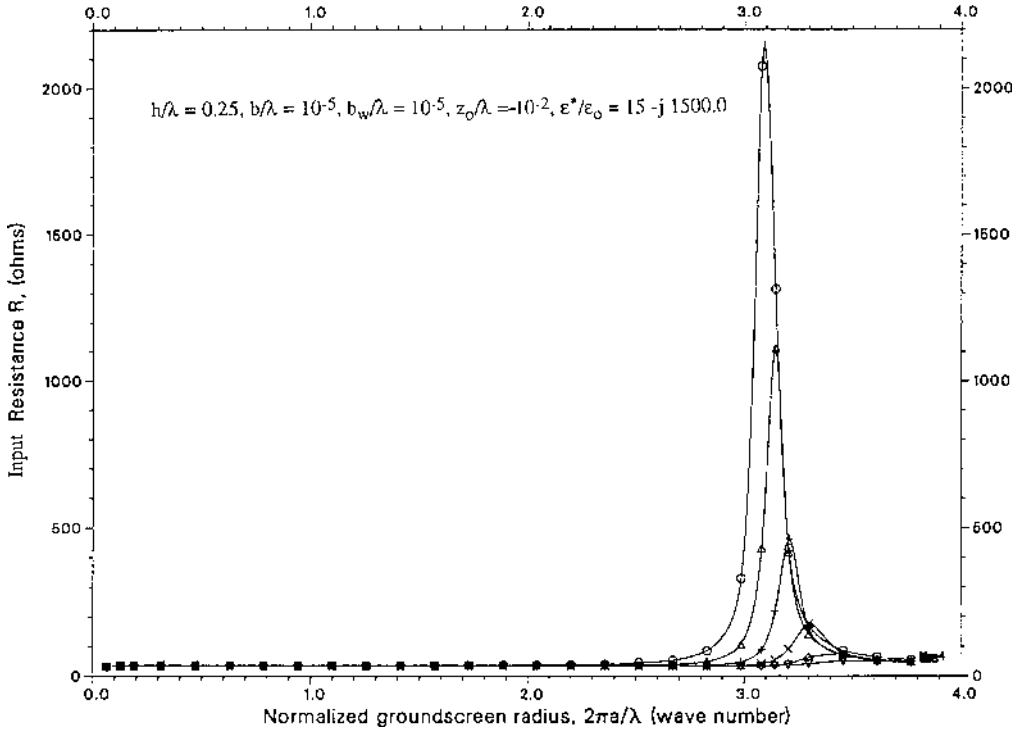

FIGURE A7-35 Input resistance of a quarter-wave monopole element with a radial-wire ground plane at a height $|z_0/\lambda| = 10^{-2}$ above earth of relative permittivity $\varepsilon^*/\varepsilon_0 = 15 - j\,1500.0$.

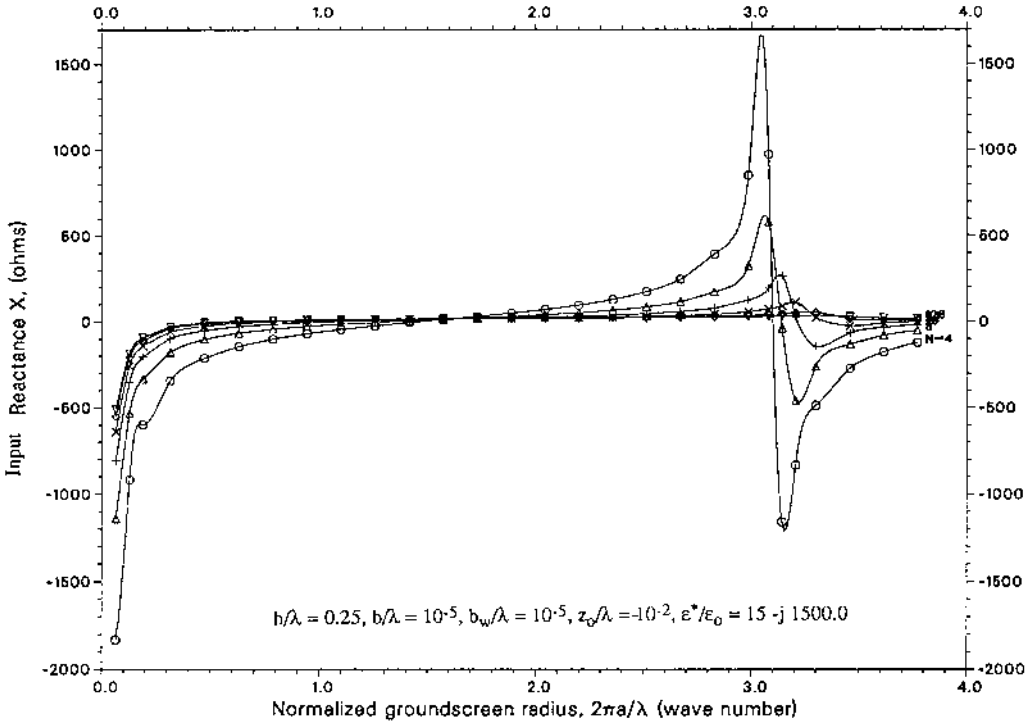

FIGURE A7-36 Input reactance of a quarter-wave monopole element with a radial-wire ground plane at a height $|z_0/\lambda| = 10^{-2}$ above earth of relative permittivity $\varepsilon^*/\varepsilon_0 = 15 - j\,1500.0$.

A.8 METHOD OF IMAGES WITH FRESNEL REFLECTION: MONOPOLE ELEMENTS ON FLAT EARTH: DIRECTIVITY AND RADIATION EFFICIENCY

The tables of directivity and radiation efficiency at 6.0, 15, and 30 MHz for thin elements of length h and normalized lengths $N = (h/0.05\lambda) = 0, 1, 2, 3, 4, 5$ are grouped in subsections corresponding to Cases 1–10 of earth classifications in Table 16 of Sec. 8.2.

The values of radiation efficiency obtained by the method of images with Fresnel reflection are not as accurate as those obtained by method-of-moments programs (see Sec. 9.2.3, Table 20). The plane wave Fresnel reflection method neglects the surface-wave near field that can significantly reduce the energy radiated into the half-space above the Earth.

Case	Earth classification	A8 Table nos.
1	Perfect ground	1–6
2	Sea water (Average salinity, 20°C)	7–12
3	Fresh water	13–18
4	Wet ground	19–24
5	Medium dry ground	25–30
6	Very dry ground	31–36
7	Pure water, 20°C	37–42
8	Ice (fresh water, −1°C)	43–48
9	Ice (fresh water, −10°C)	49–54
10	Average land (TCI)	55–60

Table A8-1 Case 1: Perfect Ground, $N = 0$ ($h = 0 \times 0.05\lambda$)

N=0, CASE(1): Perfect Ground (Relative Dielectric Constant = 1.0, Conductivity = INFINITY S/m)

Grazing ang. deg	FREQUENCY = 8.0 MHz. Fresnel Reflect Coef		Directive gain	FREQUENCY = 15.0 MHz. Fresnel Reflect Coef		Directive gain	FREQUENCY = 30.0 MHz. Fresnel Reflect Coef		Directive gain
PSI(deg)	|Rv|	ang Rv(deg)	G(dBi)	|Rv|	ang Rv(deg)	D(dBi)	|Rv|	ang Rv(deg)	D(dBi)
0.00	1.00000	0.00000	4.7712	1.00000	0.00000	4.7712	1.00000	0.00000	4.7712
0.50	1.00000	0.00000	4.7709	1.00000	0.00000	4.7709	1.00000	0.00000	4.7709
1.00	1.00000	0.00000	4.7699	1.00000	0.00000	4.7699	1.00000	0.00000	4.7698
1.50	1.00000	0.00000	4.7682	1.00000	0.00000	4.7682	1.00000	0.00000	4.7682
2.00	1.00000	0.00000	4.7659	1.00000	0.00000	4.7659	1.00000	0.00000	4.7659
2.50	1.00000	0.00000	4.7629	1.00000	0.00000	4.7629	1.00000	0.00000	4.7629
3.00	1.00000	0.00000	4.7593	1.00000	0.00000	4.7593	1.00000	0.00000	4.7593
3.50	1.00000	0.00000	4.7550	1.00000	0.00000	4.7550	1.00000	0.00000	4.7550
4.00	1.00000	0.00000	4.7500	1.00000	0.00000	4.7500	1.00000	0.00000	4.7500
5.00	1.00000	0.00000	4.7381	1.00000	0.00000	4.7381	1.00000	0.00000	4.7381
6.00	1.00000	0.00000	4.7235	1.00000	0.00000	4.7235	1.00000	0.00000	4.7235
7.00	1.00000	0.00000	4.7062	1.00000	0.00000	4.7062	1.00000	0.00000	4.7062
8.00	1.00000	0.00000	4.6863	1.00000	0.00000	4.6863	1.00000	0.00000	4.6863
9.00	1.00000	0.00000	4.6636	1.00000	0.00000	4.6636	1.00000	0.00000	4.6636
10.00	1.00000	0.00000	4.6382	1.00000	0.00000	4.6382	1.00000	0.00000	4.6382
12.00	1.00000	0.00000	4.5793	1.00000	0.00000	4.5793	1.00000	0.00000	4.5793
14.00	1.00000	0.00000	4.5093	1.00000	0.00000	4.5093	1.00000	0.00000	4.5093
16.00	1.00000	0.00000	4.4280	1.00000	0.00000	4.4280	1.00000	0.00000	4.4280
18.00	1.00000	0.00000	4.3353	1.00000	0.00000	4.3353	1.00000	0.00000	4.3353
20.00	1.00000	0.00000	4.2309	1.00000	0.00000	4.2309	1.00000	0.00000	4.2309
22.00	1.00000	0.00000	4.1145	1.00000	0.00000	4.1145	1.00000	0.00000	4.1145
24.00	1.00000	0.00000	3.9858	1.00000	0.00000	3.9858	1.00000	0.00000	3.9858
26.00	1.00000	0.00000	3.8444	1.00000	0.00000	3.8444	1.00000	0.00000	3.8444
28.00	1.00000	0.00000	3.6899	1.00000	0.00000	3.6899	1.00000	0.00000	3.6899
30.00	1.00000	0.00000	3.5218	1.00000	0.00000	3.5218	1.00000	0.00000	3.5218
32.00	1.00000	0.00000	3.3396	1.00000	0.00000	3.3396	1.00000	0.00000	3.3396
34.00	1.00000	0.00000	3.1427	1.00000	0.00000	3.1427	1.00000	0.00000	3.1427
36.00	1.00000	0.00000	2.9304	1.00000	0.00000	2.9304	1.00000	0.00000	2.9304
38.00	1.00000	0.00000	2.7019	1.00000	0.00000	2.7019	1.00000	0.00000	2.7019
40.00	1.00000	0.00000	2.4563	1.00000	0.00000	2.4563	1.00000	0.00000	2.4563
42.00	1.00000	0.00000	2.1927	1.00000	0.00000	2.1927	1.00000	0.00000	2.1927
44.00	1.00000	0.00000	1.9099	1.00000	0.00000	1.9099	1.00000	0.00000	1.9099
46.00	1.00000	0.00000	1.6066	1.00000	0.00000	1.6066	1.00000	0.00000	1.6066
48.00	1.00000	0.00000	1.2814	1.00000	0.00000	1.2814	1.00000	0.00000	1.2814
50.00	1.00000	0.00000	0.9326	1.00000	0.00000	0.9326	1.00000	0.00000	0.9326
52.00	1.00000	0.00000	0.5581	1.00000	0.00000	0.5581	1.00000	0.00000	0.5581
54.00	1.00000	0.00000	0.1556	1.00000	0.00000	0.1556	1.00000	0.00000	0.1556
56.00	1.00000	0.00000	-0.2776	1.00000	0.00000	-0.2776	1.00000	0.00000	-0.2776
58.00	1.00000	0.00000	-0.7446	1.00000	0.00000	-0.7446	1.00000	0.00000	-0.7446
60.00	1.00000	0.00000	-1.2494	1.00000	0.00000	-1.2494	1.00000	0.00000	-1.2494
62.00	1.00000	0.00000	-1.7966	1.00000	0.00000	-1.7966	1.00000	0.00000	-1.7966
64.00	1.00000	0.00000	-2.3919	1.00000	0.00000	-2.3919	1.00000	0.00000	-2.3919
66.00	1.00000	0.00000	-3.0425	1.00000	0.00000	-3.0425	1.00000	0.00000	-3.0425
68.00	1.00000	0.00000	-3.7573	1.00000	0.00000	-3.7573	1.00000	0.00000	-3.7573
70.00	1.00000	0.00000	-4.5478	1.00000	0.00000	-4.5478	1.00000	0.00000	-4.5478
72.00	1.00000	0.00000	-5.4291	1.00000	0.00000	-5.4291	1.00000	0.00000	-5.4291
74.00	1.00000	0.00000	-6.4220	1.00000	0.00000	-6.4220	1.00000	0.00000	-6.4220
76.00	1.00000	0.00000	-7.5553	1.00000	0.00000	-7.5553	1.00000	0.00000	-7.5553
78.00	1.00000	0.00000	-8.8712	1.00000	0.00000	-8.8712	1.00000	0.00000	-8.8712
80.00	1.00000	0.00000	-10.4354	1.00000	0.00000	-10.4354	1.00000	0.00000	-10.4354
82.00	1.00000	0.00000	-12.3577	1.00000	0.00000	-12.3577	1.00000	0.00000	-12.3577
84.00	1.00000	0.00000	-14.8441	1.00000	0.00000	-14.8441	1.00000	0.00000	-14.8441
86.00	1.00000	0.00000	-18.3571	1.00000	0.00000	-18.3571	1.00000	0.00000	-18.3571
88.00	1.00000	0.00000	-24.3724	1.00000	0.00000	-24.3724	1.00000	0.00000	-24.3724
90.00	1.00000	0.00000	-142.4169	1.00000	0.00000	-142.4169	1.00000	0.00000	-142.4169
	Radiation Efficiency			Radiation Efficiency			Radiation Efficiency		
	ETA = 1.0000, H = 0.000E+00 (dB)			ETA = 1.0000, H = 0.000E+00 (dB)			ETA = 1.0000, H = 0.000E+00 (dB)		

Table A8-2 Case 1: Perfect Ground, $N = 1$ ($h = 1 \times 0.05\lambda$)

N=1, CASE(1): Perfect Ground (Relative Dielectric Constant = 1.0, Conductivity = INFINITY S/m)

Grazing ang. deg	FREQUENCY = 6.0 MHz. Fresnel Reflect Coef		Directive gain	FREQUENCY = 15.0 MHz. Fresnel Reflect Coef		Directive gain	FREQUENCY = 30.0 MHz. Fresnel Reflect Coef		Directive gain
PSI(deg)	|Rv|	ang Rv(deg)	D(dBi)	|Rv|	ang Rv(deg)	D(dBi)	|Rv|	ang Rv(deg)	D(dBi)
0.00	1.00000	0.00000	4.7926	1.00000	0.00000	4.7926	1.00000	0.00000	4.7926
0.50	1.00000	0.00000	4.7923	1.00000	0.00000	4.7923	1.00000	0.00000	4.7923
1.00	1.00000	0.00000	4.7913	1.00000	0.00000	4.7913	1.00000	0.00000	4.7913
1.50	1.00000	0.00000	4.7896	1.00000	0.00000	4.7895	1.00000	0.00000	4.7896
2.00	1.00000	0.00000	4.7872	1.00000	0.00000	4.7872	1.00000	0.00000	4.7872
2.50	1.00000	0.00000	4.7841	1.00000	0.00000	4.7841	1.00000	0.00000	4.7841
3.00	1.00000	0.00000	4.7804	1.00000	0.00000	4.7804	1.00000	0.00000	4.7804
3.50	1.00000	0.00000	4.7760	1.00000	0.00000	4.7760	1.00000	0.00000	4.7760
4.00	1.00000	0.00000	4.7709	1.00000	0.00000	4.7709	1.00000	0.00000	4.7709
5.00	1.00000	0.00000	4.7587	1.00000	0.00000	4.7587	1.00000	0.00000	4.7587
6.00	1.00000	0.00000	4.7437	1.00000	0.00000	4.7437	1.00000	0.00000	4.7437
7.00	1.00000	0.00000	4.7260	1.00000	0.00000	4.7260	1.00000	0.00000	4.7260
8.00	1.00000	0.00000	4.7056	1.00000	0.00000	4.7056	1.00000	0.00000	4.7056
9.00	1.00000	0.00000	4.6824	1.00000	0.00000	4.6824	1.00000	0.00000	4.6824
10.00	1.00000	0.00000	4.6564	1.00000	0.00000	4.6564	1.00000	0.00000	4.6564
12.00	1.00000	0.00000	4.5961	1.00000	0.00000	4.5961	1.00000	0.00000	4.5961
14.00	1.00000	0.00000	4.5244	1.00000	0.00000	4.5244	1.00000	0.00000	4.5244
16.00	1.00000	0.00000	4.4413	1.00000	0.00000	4.4413	1.00000	0.00000	4.4413
18.00	1.00000	0.00000	4.3465	1.00000	0.00000	4.3465	1.00000	0.00000	4.3465
20.00	1.00000	0.00000	4.2398	1.00000	0.00000	4.2398	1.00000	0.00000	4.2398
22.00	1.00000	0.00000	4.1209	1.00000	0.00000	4.1209	1.00000	0.00000	4.1209
24.00	1.00000	0.00000	3.9895	1.00000	0.00000	3.9895	1.00000	0.00000	3.9895
26.00	1.00000	0.00000	3.8452	1.00000	0.00000	3.8452	1.00000	0.00000	3.8452
28.00	1.00000	0.00000	3.6877	1.00000	0.00000	3.6877	1.00000	0.00000	3.6877
30.00	1.00000	0.00000	3.5164	1.00000	0.00000	3.5164	1.00000	0.00000	3.5164
32.00	1.00000	0.00000	3.3309	1.00000	0.00000	3.3309	1.00000	0.00000	3.3309
34.00	1.00000	0.00000	3.1306	1.00000	0.00000	3.1306	1.00000	0.00000	3.1306
36.00	1.00000	0.00000	2.9147	1.00000	0.00000	2.9147	1.00000	0.00000	2.9147
38.00	1.00000	0.00000	2.6826	1.00000	0.00000	2.6826	1.00000	0.00000	2.6826
40.00	1.00000	0.00000	2.4334	1.00000	0.00000	2.4334	1.00000	0.00000	2.4334
42.00	1.00000	0.00000	2.1660	1.00000	0.00000	2.1660	1.00000	0.00000	2.1660
44.00	1.00000	0.00000	1.8795	1.00000	0.00000	1.8795	1.00000	0.00000	1.8795
46.00	1.00000	0.00000	1.5725	1.00000	0.00000	1.5725	1.00000	0.00000	1.5725
48.00	1.00000	0.00000	1.2435	1.00000	0.00000	1.2435	1.00000	0.00000	1.2435
50.00	1.00000	0.00000	0.8909	1.00000	0.00000	0.8909	1.00000	0.00000	0.8909
52.00	1.00000	0.00000	0.5127	1.00000	0.00000	0.5127	1.00000	0.00000	0.5127
54.00	1.00000	0.00000	0.1067	1.00000	0.00000	0.1067	1.00000	0.00000	0.1067
56.00	1.00000	0.00000	-0.3300	1.00000	0.00000	-0.3300	1.00000	0.00000	-0.3300
58.00	1.00000	0.00000	-0.8005	1.00000	0.00000	-0.8005	1.00000	0.00000	-0.8005
60.00	1.00000	0.00000	-1.3086	1.00000	0.00000	-1.3086	1.00000	0.00000	-1.3086
62.00	1.00000	0.00000	-1.8590	1.00000	0.00000	-1.8590	1.00000	0.00000	-1.8590
64.00	1.00000	0.00000	-2.4574	1.00000	0.00000	-2.4574	1.00000	0.00000	-2.4574
66.00	1.00000	0.00000	-3.1109	1.00000	0.00000	-3.1109	1.00000	0.00000	-3.1108
68.00	1.00000	0.00000	-3.8283	1.00000	0.00000	-3.8283	1.00000	0.00000	-3.8283
70.00	1.00000	0.00000	-4.6213	1.00000	0.00000	-4.6213	1.00000	0.00000	-4.6213
72.00	1.00000	0.00000	-5.5050	1.00000	0.00000	-5.5050	1.00000	0.00000	-5.5050
74.00	1.00000	0.00000	-6.5000	1.00000	0.00000	-6.5000	1.00000	0.00000	-6.5000
76.00	1.00000	0.00000	-7.6352	1.00000	0.00000	-7.6352	1.00000	0.00000	-7.6352
78.00	1.00000	0.00000	-8.9527	1.00000	0.00000	-8.9527	1.00000	0.00000	-8.9527
80.00	1.00000	0.00000	-10.5183	1.00000	0.00000	-10.5183	1.00000	0.00000	-10.5183
82.00	1.00000	0.00000	-12.4418	1.00000	0.00000	-12.4418	1.00000	0.00000	-12.4418
84.00	1.00000	0.00000	-14.9291	1.00000	0.00000	-14.9291	1.00000	0.00000	-14.9291
86.00	1.00000	0.00000	-18.4428	1.00000	0.00000	-18.4428	1.00000	0.00000	-18.4428
88.00	1.00000	0.00000	-24.4585	1.00000	0.00000	-24.4585	1.00000	0.00000	-24.4585
90.00	1.00000	0.00000	-142.5031	1.00000	0.00000	-142.5031	1.00000	0.00000	-142.5031
	Radiation Efficiency			Radiation Efficiency			Radiation Efficiency		
	ETA = 1.0000, M = 0.000E+00 (dB)			ETA = 1.0000, M = 0.000E+00 (dB)			ETA = 1.0000, M = 0.000E+00 (dB)		

Table A8-3 Case 1: Perfect Ground, $N = 2$ ($h = 2 \times 0.05\lambda$)

N=2, CASE(1): Perfect Ground (Relative Dielectric Constant = 1.0, Conductivity = INFINITY S/m)

Grazing ang. deg	FREQUENCY = 6.0 MHz. Fresnel Reflect Coef		Directive gain	FREQUENCY = 15.0 MHz. Fresnel Reflect Coef		Directive gain	FREQUENCY = 30.0 MHz. Fresnel Reflect Coef		Directive gain
PSI(deg)	|Rv|	ang Rv(deg)	D(dBi)	|Rv|	ang Rv(deg)	D(dBi)	|Rv|	ang Rv(deg)	D(dBi)
0.00	1.00000	0.00000	4.8361	1.00000	0.00000	4.8361	1.00000	0.00000	4.8361
0.50	1.00000	0.00000	4.8358	1.00000	0.00000	4.8358	1.00000	0.00000	4.8358
1.00	1.00000	0.00000	4.8347	1.00000	0.00000	4.8347	1.00000	0.00000	4.8347
1.50	1.00000	0.00000	4.8329	1.00000	0.00000	4.8329	1.00000	0.00000	4.8329
2.00	1.00000	0.00000	4.8305	1.00000	0.00000	4.8305	1.00000	0.00000	4.8305
2.50	1.00000	0.00000	4.8272	1.00000	0.00000	4.8272	1.00000	0.00000	4.8272
3.00	1.00000	0.00000	4.8233	1.00000	0.00000	4.8233	1.00000	0.00000	4.8233
3.50	1.00000	0.00000	4.8187	1.00000	0.00000	4.8187	1.00000	0.00000	4.8187
4.00	1.00000	0.00000	4.8134	1.00000	0.00000	4.8134	1.00000	0.00000	4.8134
5.00	1.00000	0.00000	4.8005	1.00000	0.00000	4.8005	1.00000	0.00000	4.8005
6.00	1.00000	0.00000	4.7849	1.00000	0.00000	4.7849	1.00000	0.00000	4.7849
7.00	1.00000	0.00000	4.7663	1.00000	0.00000	4.7663	1.00000	0.00000	4.7663
8.00	1.00000	0.00000	4.7449	1.00000	0.00000	4.7449	1.00000	0.00000	4.7449
9.00	1.00000	0.00000	4.7205	1.00000	0.00000	4.7205	1.00000	0.00000	4.7205
10.00	1.00000	0.00000	4.6933	1.00000	0.00000	4.6933	1.00000	0.00000	4.6933
12.00	1.00000	0.00000	4.6301	1.00000	0.00000	4.6301	1.00000	0.00000	4.6301
14.00	1.00000	0.00000	4.5551	1.00000	0.00000	4.5551	1.00000	0.00000	4.5551
16.00	1.00000	0.00000	4.4681	1.00000	0.00000	4.4681	1.00000	0.00000	4.4681
18.00	1.00000	0.00000	4.3690	1.00000	0.00000	4.3690	1.00000	0.00000	4.3690
20.00	1.00000	0.00000	4.2576	1.00000	0.00000	4.2576	1.00000	0.00000	4.2576
22.00	1.00000	0.00000	4.1336	1.00000	0.00000	4.1336	1.00000	0.00000	4.1336
24.00	1.00000	0.00000	3.9966	1.00000	0.00000	3.9966	1.00000	0.00000	3.9966
26.00	1.00000	0.00000	3.8465	1.00000	0.00000	3.8465	1.00000	0.00000	3.8465
28.00	1.00000	0.00000	3.6827	1.00000	0.00000	3.6827	1.00000	0.00000	3.6827
30.00	1.00000	0.00000	3.5050	1.00000	0.00000	3.5050	1.00000	0.00000	3.5050
32.00	1.00000	0.00000	3.3127	1.00000	0.00000	3.3127	1.00000	0.00000	3.3127
34.00	1.00000	0.00000	3.1053	1.00000	0.00000	3.1053	1.00000	0.00000	3.1053
36.00	1.00000	0.00000	2.8822	1.00000	0.00000	2.8822	1.00000	0.00000	2.8822
38.00	1.00000	0.00000	2.6427	1.00000	0.00000	2.6427	1.00000	0.00000	2.6427
40.00	1.00000	0.00000	2.3859	1.00000	0.00000	2.3859	1.00000	0.00000	2.3859
42.00	1.00000	0.00000	2.1110	1.00000	0.00000	2.1110	1.00000	0.00000	2.1110
44.00	1.00000	0.00000	1.8168	1.00000	0.00000	1.8168	1.00000	0.00000	1.8168
46.00	1.00000	0.00000	1.5021	1.00000	0.00000	1.5021	1.00000	0.00000	1.5021
48.00	1.00000	0.00000	1.1654	1.00000	0.00000	1.1654	1.00000	0.00000	1.1654
50.00	1.00000	0.00000	0.8052	1.00000	0.00000	0.8052	1.00000	0.00000	0.8052
52.00	1.00000	0.00000	0.4195	1.00000	0.00000	0.4195	1.00000	0.00000	0.4195
54.00	1.00000	0.00000	0.0060	1.00000	0.00000	0.0060	1.00000	0.00000	0.0060
56.00	1.00000	0.00000	-0.4379	1.00000	0.00000	-0.4379	1.00000	0.00000	-0.4379
58.00	1.00000	0.00000	-0.9155	1.00000	0.00000	-0.9155	1.00000	0.00000	-0.9155
60.00	1.00000	0.00000	-1.4304	1.00000	0.00000	-1.4304	1.00000	0.00000	-1.4304
62.00	1.00000	0.00000	-1.9873	1.00000	0.00000	-1.9873	1.00000	0.00000	-1.9873
64.00	1.00000	0.00000	-2.5920	1.00000	0.00000	-2.5920	1.00000	0.00000	-2.5920
66.00	1.00000	0.00000	-3.2514	1.00000	0.00000	-3.2514	1.00000	0.00000	-3.2514
68.00	1.00000	0.00000	-3.9744	1.00000	0.00000	-3.9744	1.00000	0.00000	-3.9744
70.00	1.00000	0.00000	-4.7725	1.00000	0.00000	-4.7725	1.00000	0.00000	-4.7725
72.00	1.00000	0.00000	-5.6610	1.00000	0.00000	-5.6610	1.00000	0.00000	-5.6610
74.00	1.00000	0.00000	-6.6603	1.00000	0.00000	-6.6603	1.00000	0.00000	-6.6603
76.00	1.00000	0.00000	-7.7993	1.00000	0.00000	-7.7993	1.00000	0.00000	-7.7993
78.00	1.00000	0.00000	-9.1203	1.00000	0.00000	-9.1203	1.00000	0.00000	-9.1203
80.00	1.00000	0.00000	-10.6888	1.00000	0.00000	-10.6888	1.00000	0.00000	-10.6888
82.00	1.00000	0.00000	-12.6146	1.00000	0.00000	-12.6146	1.00000	0.00000	-12.6146
84.00	1.00000	0.00000	-15.1038	1.00000	0.00000	-15.1038	1.00000	0.00000	-15.1038
86.00	1.00000	0.00000	-18.6188	1.00000	0.00000	-18.6188	1.00000	0.00000	-18.6188
88.00	1.00000	0.00000	-24.6353	1.00000	0.00000	-24.6353	1.00000	0.00000	-24.6353
90.00	1.00000	0.00000	-142.6803	1.00000	0.00000	-142.6803	1.00000	0.00000	-142.6803
	Radiation Efficiency			Radiation Efficiency			Radiation Efficiency		
	ETA = 1.0000, H = 0.000E+00 (dB)			ETA = 1.0000, H = 0.000E+00 (dB)			ETA = 1.0000, H = 0.000E+00 (dB)		

Table A8-4 Case 1: Perfect Ground, $N = 3$ ($h = 3 \times 0.05\lambda$)

N=3, CASE(1): Perfect Ground (Relative Dielectric Constant = 1.0, Conductivity = INFINITY S/m)

Grazing ang. deg	FREQUENCY = 6.0 MHz. Fresnel Reflect Coef		Directive gain	FREQUENCY = 15.0 MHz. Fresnel Reflect Coef		Directive gain	FREQUENCY = 30.0 MHz. Fresnel Reflect Coef		Directive gain
PSI(deg)	|Rv|	ang Rv(deg)	D(dBi)	|Rv|	ang Rv(deg)	D(dBi)	|Rv|	ang Rv(deg)	D(dBi)
0.00	1.00000	0.00000	4.9107	1.00000	0.00000	4.9107	1.00000	0.00000	4.9107
0.50	1.00000	0.00000	4.9103	1.00000	0.00000	4.9103	1.00000	0.00000	4.9103
1.00	1.00000	0.00000	4.9092	1.00000	0.00000	4.9092	1.00000	0.00000	4.9092
1.50	1.00000	0.00000	4.9072	1.00000	0.00000	4.9072	1.00000	0.00000	4.9072
2.00	1.00000	0.00000	4.9045	1.00000	0.00000	4.9045	1.00000	0.00000	4.9045
2.50	1.00000	0.00000	4.9011	1.00000	0.00000	4.9011	1.00000	0.00000	4.9011
3.00	1.00000	0.00000	4.8969	1.00000	0.00000	4.8969	1.00000	0.00000	4.8969
3.50	1.00000	0.00000	4.8918	1.00000	0.00000	4.8918	1.00000	0.00000	4.8918
4.00	1.00000	0.00000	4.8861	1.00000	0.00000	4.8861	1.00000	0.00000	4.8861
5.00	1.00000	0.00000	4.8722	1.00000	0.00000	4.8722	1.00000	0.00000	4.8722
6.00	1.00000	0.00000	4.8553	1.00000	0.00000	4.8553	1.00000	0.00000	4.8553
7.00	1.00000	0.00000	4.8352	1.00000	0.00000	4.8352	1.00000	0.00000	4.8352
8.00	1.00000	0.00000	4.8120	1.00000	0.00000	4.8120	1.00000	0.00000	4.8120
9.00	1.00000	0.00000	4.7858	1.00000	0.00000	4.7858	1.00000	0.00000	4.7858
10.00	1.00000	0.00000	4.7564	1.00000	0.00000	4.7564	1.00000	0.00000	4.7564
12.00	1.00000	0.00000	4.6882	1.00000	0.00000	4.6882	1.00000	0.00000	4.6882
14.00	1.00000	0.00000	4.6073	1.00000	0.00000	4.6073	1.00000	0.00000	4.6073
16.00	1.00000	0.00000	4.5137	1.00000	0.00000	4.5137	1.00000	0.00000	4.5137
18.00	1.00000	0.00000	4.4072	1.00000	0.00000	4.4072	1.00000	0.00000	4.4072
20.00	1.00000	0.00000	4.2875	1.00000	0.00000	4.2875	1.00000	0.00000	4.2875
22.00	1.00000	0.00000	4.1546	1.00000	0.00000	4.1546	1.00000	0.00000	4.1546
24.00	1.00000	0.00000	4.0080	1.00000	0.00000	4.0080	1.00000	0.00000	4.0080
26.00	1.00000	0.00000	3.8476	1.00000	0.00000	3.8476	1.00000	0.00000	3.8476
28.00	1.00000	0.00000	3.6731	1.00000	0.00000	3.6731	1.00000	0.00000	3.6731
30.00	1.00000	0.00000	3.4839	1.00000	0.00000	3.4839	1.00000	0.00000	3.4839
32.00	1.00000	0.00000	3.2798	1.00000	0.00000	3.2798	1.00000	0.00000	3.2798
34.00	1.00000	0.00000	3.0602	1.00000	0.00000	3.0602	1.00000	0.00000	3.0602
36.00	1.00000	0.00000	2.8245	1.00000	0.00000	2.8245	1.00000	0.00000	2.8245
38.00	1.00000	0.00000	2.5721	1.00000	0.00000	2.5721	1.00000	0.00000	2.5721
40.00	1.00000	0.00000	2.3022	1.00000	0.00000	2.3022	1.00000	0.00000	2.3022
42.00	1.00000	0.00000	2.0140	1.00000	0.00000	2.0140	1.00000	0.00000	2.0140
44.00	1.00000	0.00000	1.7063	1.00000	0.00000	1.7063	1.00000	0.00000	1.7063
46.00	1.00000	0.00000	1.3781	1.00000	0.00000	1.3781	1.00000	0.00000	1.3781
48.00	1.00000	0.00000	1.0281	1.00000	0.00000	1.0281	1.00000	0.00000	1.0281
50.00	1.00000	0.00000	0.6545	1.00000	0.00000	0.6545	1.00000	0.00000	0.6545
52.00	1.00000	0.00000	0.2555	1.00000	0.00000	0.2555	1.00000	0.00000	0.2555
54.00	1.00000	0.00000	-0.1710	1.00000	0.00000	-0.1710	1.00000	0.00000	-0.1710
56.00	1.00000	0.00000	-0.6276	1.00000	0.00000	-0.6276	1.00000	0.00000	-0.6276
58.00	1.00000	0.00000	-1.1175	1.00000	0.00000	-1.1175	1.00000	0.00000	-1.1175
60.00	1.00000	0.00000	-1.6444	1.00000	0.00000	-1.6444	1.00000	0.00000	-1.6444
62.00	1.00000	0.00000	-2.2128	1.00000	0.00000	-2.2128	1.00000	0.00000	-2.2128
64.00	1.00000	0.00000	-2.8284	1.00000	0.00000	-2.8284	1.00000	0.00000	-2.8284
66.00	1.00000	0.00000	-3.4982	1.00000	0.00000	-3.4982	1.00000	0.00000	-3.4982
68.00	1.00000	0.00000	-4.2310	1.00000	0.00000	-4.2310	1.00000	0.00000	-4.2310
70.00	1.00000	0.00000	-5.0383	1.00000	0.00000	-5.0383	1.00000	0.00000	-5.0383
72.00	1.00000	0.00000	-5.9351	1.00000	0.00000	-5.9351	1.00000	0.00000	-5.9351
74.00	1.00000	0.00000	-6.9421	1.00000	0.00000	-6.9421	1.00000	0.00000	-6.9421
76.00	1.00000	0.00000	-8.0879	1.00000	0.00000	-8.0879	1.00000	0.00000	-8.0879
78.00	1.00000	0.00000	-9.4148	1.00000	0.00000	-9.4148	1.00000	0.00000	-9.4148
80.00	1.00000	0.00000	-10.9884	1.00000	0.00000	-10.9884	1.00000	0.00000	-10.9884
82.00	1.00000	0.00000	-12.9185	1.00000	0.00000	-12.9185	1.00000	0.00000	-12.9185
84.00	1.00000	0.00000	-15.4110	1.00000	0.00000	-15.4110	1.00000	0.00000	-15.4110
86.00	1.00000	0.00000	-18.9283	1.00000	0.00000	-18.9283	1.00000	0.00000	-18.9283
88.00	1.00000	0.00000	-24.9463	1.00000	0.00000	-24.9463	1.00000	0.00000	-24.9463
90.00	1.00000	0.00000	-142.9917	1.00000	0.00000	-142.9917	1.00000	0.00000	-142.9917
	Radiation Efficiency			Radiation Efficiency			Radiation Efficiency		
	ETA = 1.0000, H = 0.000E+00 (dB)			ETA = 1.0000, H = 0.000E+00 (dB)			ETA = 1.0000, H = 0.000E+00 (dB)		

Table A8-5 Case 1: Perfect Ground, $N = 4$ ($h = 4 \times 0.05\lambda$)

N=4, CASE(1): Perfect Ground (Relative Dielectric Constant = 1.0, Conductivity = INFINITY S/m)

Grazing Ang, deg	FREQUENCY = 6.0 MHz. Fresnel Reflect Coef		Directive gain	FREQUENCY = 15.0 MHz. Fresnel Reflect Coef		Directive gain	FREQUENCY = 30.0 MHz. Fresnel Reflect Coef		Directive gain
PSI(deg)	|Rv|	ang Rv(deg)	D(dBi)	|Rv|	ang Rv(deg)	D(dBi)	|Rv|	ang Rv(deg)	D(dBi)
0.00	1.00000	0.00000	5.0195	1.00000	0.00000	5.0195	1.00000	0.00000	5.0195
0.50	1.00000	0.00000	5.0191	1.00000	0.00000	5.0191	1.00000	0.00000	5.0191
1.00	1.00000	0.00000	5.0178	1.00000	0.00000	5.0178	1.00000	0.00000	5.0178
1.50	1.00000	0.00000	5.0157	1.00000	0.00000	5.0157	1.00000	0.00000	5.0157
2.00	1.00000	0.00000	5.0127	1.00000	0.00000	5.0127	1.00000	0.00000	5.0127
2.50	1.00000	0.00000	5.0088	1.00000	0.00000	5.0088	1.00000	0.00000	5.0088
3.00	1.00000	0.00000	5.0041	1.00000	0.00000	5.0041	1.00000	0.00000	5.0041
3.50	1.00000	0.00000	4.9986	1.00000	0.00000	4.9986	1.00000	0.00000	4.9986
4.00	1.00000	0.00000	4.9921	1.00000	0.00000	4.9921	1.00000	0.00000	4.9921
5.00	1.00000	0.00000	4.9767	1.00000	0.00000	4.9767	1.00000	0.00000	4.9767
6.00	1.00000	0.00000	4.9579	1.00000	0.00000	4.9579	1.00000	0.00000	4.9579
7.00	1.00000	0.00000	4.9356	1.00000	0.00000	4.9356	1.00000	0.00000	4.9356
8.00	1.00000	0.00000	4.9099	1.00000	0.00000	4.9099	1.00000	0.00000	4.9099
9.00	1.00000	0.00000	4.8807	1.00000	0.00000	4.8807	1.00000	0.00000	4.8807
10.00	1.00000	0.00000	4.8481	1.00000	0.00000	4.8481	1.00000	0.00000	4.8481
12.00	1.00000	0.00000	4.7725	1.00000	0.00000	4.7725	1.00000	0.00000	4.7725
14.00	1.00000	0.00000	4.6829	1.00000	0.00000	4.6829	1.00000	0.00000	4.6829
16.00	1.00000	0.00000	4.5794	1.00000	0.00000	4.5794	1.00000	0.00000	4.5794
18.00	1.00000	0.00000	4.4617	1.00000	0.00000	4.4617	1.00000	0.00000	4.4617
20.00	1.00000	0.00000	4.3298	1.00000	0.00000	4.3298	1.00000	0.00000	4.3298
22.00	1.00000	0.00000	4.1835	1.00000	0.00000	4.1835	1.00000	0.00000	4.1835
24.00	1.00000	0.00000	4.0227	1.00000	0.00000	4.0227	1.00000	0.00000	4.0227
26.00	1.00000	0.00000	3.8470	1.00000	0.00000	3.8470	1.00000	0.00000	3.8470
28.00	1.00000	0.00000	3.6562	1.00000	0.00000	3.6562	1.00000	0.00000	3.6562
30.00	1.00000	0.00000	3.4501	1.00000	0.00000	3.4501	1.00000	0.00000	3.4501
32.00	1.00000	0.00000	3.2283	1.00000	0.00000	3.2283	1.00000	0.00000	3.2263
34.00	1.00000	0.00000	2.9903	1.00000	0.00000	2.9903	1.00000	0.00000	2.9903
36.00	1.00000	0.00000	2.7357	1.00000	0.00000	2.7357	1.00000	0.00000	2.7357
38.00	1.00000	0.00000	2.4639	1.00000	0.00000	2.4639	1.00000	0.00000	2.4639
40.00	1.00000	0.00000	2.1742	1.00000	0.00000	2.1742	1.00000	0.00000	2.1742
42.00	1.00000	0.00000	1.8658	1.00000	0.00000	1.8658	1.00000	0.00000	1.8659
44.00	1.00000	0.00000	1.5379	1.00000	0.00000	1.5379	1.00000	0.00000	1.5379
46.00	1.00000	0.00000	1.1894	1.00000	0.00000	1.1894	1.00000	0.00000	1.1894
48.00	1.00000	0.00000	0.8190	1.00000	0.00000	0.8190	1.00000	0.00000	0.8190
50.00	1.00000	0.00000	0.4252	1.00000	0.00000	0.4252	1.00000	0.00000	0.4252
52.00	1.00000	0.00000	0.0062	1.00000	0.00000	0.0062	1.00000	0.00000	0.0062
54.00	1.00000	0.00000	-0.4400	1.00000	0.00000	-0.4400	1.00000	0.00000	-0.4400
56.00	1.00000	0.00000	-0.9159	1.00000	0.00000	-0.9159	1.00000	0.00000	-0.9159
58.00	1.00000	0.00000	-1.4246	1.00000	0.00000	-1.4246	1.00000	0.00000	-1.4246
60.00	1.00000	0.00000	-1.9697	1.00000	0.00000	-1.9697	1.00000	0.00000	-1.9697
62.00	1.00000	0.00000	-2.5557	1.00000	0.00000	-2.5557	1.00000	0.00000	-2.5557
64.00	1.00000	0.00000	-3.1880	1.00000	0.00000	-3.1880	1.00000	0.00000	-3.1880
66.00	1.00000	0.00000	-3.8737	1.00000	0.00000	-3.8737	1.00000	0.00000	-3.8737
68.00	1.00000	0.00000	-4.6214	1.00000	0.00000	-4.6214	1.00000	0.00000	-4.6214
70.00	1.00000	0.00000	-5.4426	1.00000	0.00000	-5.4426	1.00000	0.00000	-5.4426
72.00	1.00000	0.00000	-6.3523	1.00000	0.00000	-6.3523	1.00000	0.00000	-6.3523
74.00	1.00000	0.00000	-7.3709	1.00000	0.00000	-7.3709	1.00000	0.00000	-7.3709
76.00	1.00000	0.00000	-8.5271	1.00000	0.00000	-8.5271	1.00000	0.00000	-8.5271
78.00	1.00000	0.00000	-9.8632	1.00000	0.00000	-9.8632	1.00000	0.00000	-9.8632
80.00	1.00000	0.00000	-11.4446	1.00000	0.00000	-11.4446	1.00000	0.00000	-11.4446
82.00	1.00000	0.00000	-13.3812	1.00000	0.00000	-13.3812	1.00000	0.00000	-13.3812
84.00	1.00000	0.00000	-15.8787	1.00000	0.00000	-15.8787	1.00000	0.00000	-15.8787
86.00	1.00000	0.00000	-19.3997	1.00000	0.00000	-19.3997	1.00000	0.00000	-19.3997
88.00	1.00000	0.00000	-25.4198	1.00000	0.00000	-25.4198	1.00000	0.00000	-25.4198
90.00	1.00000	0.00000	-143.4660	1.00000	0.00000	-143.4660	1.00000	0.00000	-143.4660
	Radiation Efficiency			Radiation Efficiency			Radiation Efficiency		
	ETA = 1.0000, M = 0.000E+00 (dB)			ETA = 1.0000, M = 0.000E+00 (dB)			ETA = 1.0000, M = 0.000E+00 (dB)		

Table A8-6 Case 1: Perfect Ground, $N = 5$ ($h = 5 \times 0.05\lambda$)

N=5, CASE(1): Perfect Ground (Relative Dielectric Constant = 1.0, Conductivity = INFINITY S/m)

Grazing ang. deg	FREQUENCY = 6.0 MHz. Fresnel Reflect Coef		Directive gain	FREQUENCY = 15.0 MHz. Fresnel Reflect Coef		Directive gain	FREQUENCY = 30.0 MHz. Fresnel Reflect Coef		Directive gain
PSI(deg)	|Rv|	ang Rv(deg)	D(dBi)	|Rv|	ang Rv(deg)	D(dBi)	|Rv|	ang Rv(deg)	D(dBi)
0.00	1.00000	0.00000	5.1676	1.00000	0.00000	5.1676	1.00000	0.00000	5.1676
0.50	1.00000	0.00000	5.1671	1.00000	0.00000	5.1671	1.00000	0.00000	5.1671
1.00	1.00000	0.00000	5.1656	1.00000	0.00000	5.1656	1.00000	0.00000	5.1656
1.50	1.00000	0.00000	5.1632	1.00000	0.00000	5.1632	1.00000	0.00000	5.1632
2.00	1.00000	0.00000	5.1597	1.00000	0.00000	5.1597	1.00000	0.00000	5.1597
2.50	1.00000	0.00000	5.1554	1.00000	0.00000	5.1554	1.00000	0.00000	5.1554
3.00	1.00000	0.00000	5.1500	1.00000	0.00000	5.1500	1.00000	0.00000	5.1500
3.50	1.00000	0.00000	5.1436	1.00000	0.00000	5.1436	1.00000	0.00000	5.1436
4.00	1.00000	0.00000	5.1363	1.00000	0.00000	5.1363	1.00000	0.00000	5.1363
5.00	1.00000	0.00000	5.1187	1.00000	0.00000	5.1187	1.00000	0.00000	5.1187
6.00	1.00000	0.00000	5.0973	1.00000	0.00000	5.0973	1.00000	0.00000	5.0973
7.00	1.00000	0.00000	5.0719	1.00000	0.00000	5.0719	1.00000	0.00000	5.0719
8.00	1.00000	0.00000	5.0426	1.00000	0.00000	5.0426	1.00000	0.00000	5.0426
9.00	1.00000	0.00000	5.0094	1.00000	0.00000	5.0094	1.00000	0.00000	5.0094
10.00	1.00000	0.00000	4.9722	1.00000	0.00000	4.9722	1.00000	0.00000	4.9722
12.00	1.00000	0.00000	4.8862	1.00000	0.00000	4.8862	1.00000	0.00000	4.8862
14.00	1.00000	0.00000	4.7845	1.00000	0.00000	4.7845	1.00000	0.00000	4.7845
16.00	1.00000	0.00000	4.6671	1.00000	0.00000	4.6671	1.00000	0.00000	4.6671
18.00	1.00000	0.00000	4.5339	1.00000	0.00000	4.5339	1.00000	0.00000	4.5339
20.00	1.00000	0.00000	4.3848	1.00000	0.00000	4.3848	1.00000	0.00000	4.3848
22.00	1.00000	0.00000	4.2198	1.00000	0.00000	4.2198	1.00000	0.00000	4.2198
24.00	1.00000	0.00000	4.0387	1.00000	0.00000	4.0387	1.00000	0.00000	4.0387
26.00	1.00000	0.00000	3.8415	1.00000	0.00000	3.8415	1.00000	0.00000	3.8415
28.00	1.00000	0.00000	3.6279	1.00000	0.00000	3.6279	1.00000	0.00000	3.6279
30.00	1.00000	0.00000	3.3978	1.00000	0.00000	3.3978	1.00000	0.00000	3.3978
32.00	1.00000	0.00000	3.1509	1.00000	0.00000	3.1509	1.00000	0.00000	3.1509
34.00	1.00000	0.00000	2.8868	1.00000	0.00000	2.8868	1.00000	0.00000	2.8868
36.00	1.00000	0.00000	2.6053	1.00000	0.00000	2.6053	1.00000	0.00000	2.6053
38.00	1.00000	0.00000	2.3059	1.00000	0.00000	2.3059	1.00000	0.00000	2.3059
40.00	1.00000	0.00000	1.9881	1.00000	0.00000	1.9881	1.00000	0.00000	1.9881
42.00	1.00000	0.00000	1.6511	1.00000	0.00000	1.6511	1.00000	0.00000	1.6511
44.00	1.00000	0.00000	1.2942	1.00000	0.00000	1.2942	1.00000	0.00000	1.2942
46.00	1.00000	0.00000	0.9165	1.00000	0.00000	0.9165	1.00000	0.00000	0.9165
48.00	1.00000	0.00000	0.5169	1.00000	0.00000	0.5169	1.00000	0.00000	0.5169
50.00	1.00000	0.00000	0.0940	1.00000	0.00000	0.0940	1.00000	0.00000	0.0940
52.00	1.00000	0.00000	-0.3538	1.00000	0.00000	-0.3538	1.00000	0.00000	-0.3538
54.00	1.00000	0.00000	-0.8285	1.00000	0.00000	-0.8285	1.00000	0.00000	-0.8285
56.00	1.00000	0.00000	-1.3324	1.00000	0.00000	-1.3324	1.00000	0.00000	-1.3324
58.00	1.00000	0.00000	-1.8684	1.00000	0.00000	-1.8684	1.00000	0.00000	-1.8684
60.00	1.00000	0.00000	-2.4400	1.00000	0.00000	-2.4400	1.00000	0.00000	-2.4400
62.00	1.00000	0.00000	-3.0514	1.00000	0.00000	-3.0514	1.00000	0.00000	-3.0514
64.00	1.00000	0.00000	-3.7082	1.00000	0.00000	-3.7082	1.00000	0.00000	-3.7082
66.00	1.00000	0.00000	-4.4171	1.00000	0.00000	-4.4171	1.00000	0.00000	-4.4171
68.00	1.00000	0.00000	-5.1866	1.00000	0.00000	-5.1866	1.00000	0.00000	-5.1866
70.00	1.00000	0.00000	-6.0282	1.00000	0.00000	-6.0282	1.00000	0.00000	-6.0282
72.00	1.00000	0.00000	-6.9567	1.00000	0.00000	-6.9567	1.00000	0.00000	-6.9567
74.00	1.00000	0.00000	-7.9924	1.00000	0.00000	-7.9924	1.00000	0.00000	-7.9924
76.00	1.00000	0.00000	-9.1640	1.00000	0.00000	-9.1640	1.00000	0.00000	-9.1640
78.00	1.00000	0.00000	-10.5135	1.00000	0.00000	-10.5135	1.00000	0.00000	-10.5135
80.00	1.00000	0.00000	-12.1065	1.00000	0.00000	-12.1065	1.00000	0.00000	-12.1065
82.00	1.00000	0.00000	-14.0526	1.00000	0.00000	-14.0526	1.00000	0.00000	-14.0526
84.00	1.00000	0.00000	-16.5576	1.00000	0.00000	-16.5576	1.00000	0.00000	-16.5576
86.00	1.00000	0.00000	-20.0840	1.00000	0.00000	-20.0840	1.00000	0.00000	-20.0840
88.00	1.00000	0.00000	-26.1073	1.00000	0.00000	-26.1073	1.00000	0.00000	-26.1073
90.00	1.00000	0.00000	-144.1545	1.00000	0.00000	-144.1545	1.00000	0.00000	-144.1545
	Radiation Efficiency			Radiation Efficiency			Radiation Efficiency		
	ETA = 1.0000, H = 0.000E+00 (dB)			ETA = 1.0000, H = 0.000E+00 (dB)			ETA = 1.0000, H = 0.000E+00 (dB)		

Table A8-7 Case 2: Sea Water, $N = 0$ ($h = 0 \times 0.05\lambda$)

N=0, CASE(2): Sea Water (av salinity 20 deg C) (Relative Dielectric Constant = 70.0, Conductivity = 5.000000 S/m)

Grazing ang. deg	FREQUENCY = 6.0 MHz. Fresnel Reflect Coef		Directive gain	FREQUENCY = 15.0 MHz. Fresnel Reflect Coef		Directive gain	FREQUENCY = 30.0 MHz. Fresnel Reflect Coef		Directive gain
PSI(deg)	|Rv|	ang Rv(deg)	D(dBi)	|Rv|	ang Rv(deg)	D(dBi)	|Rv|	ang Rv(deg)	D(dBi)
0.00	1.00000	-180.00000	-999.9999	1.00000	-180.00000	-999.9999	1.00000	-180.00000	-999.9999
0.50	0.41413	-84.80905	0.0552	0.45255	-119.74591	-1.9779	0.53359	-139.11167	-3.8131
1.00	0.54337	-40.19803	2.3618	0.43633	-66.46782	1.1092	0.40790	-93.68260	-0.1391
1.50	0.65235	-25.98895	3.2328	0.52775	-42.49292	2.3677	0.44345	-62.20481	1.4593
2.00	0.72220	-19.24878	3.6853	0.60595	-31.08702	3.0450	0.50963	-45.17813	2.3508
2.50	0.76935	-15.30605	3.9605	0.66472	-24.51328	3.4653	0.56999	-35.33808	2.9183
3.00	0.80304	-12.71306	4.1441	0.70915	-20.26586	3.7498	0.61978	-29.02690	3.3049
3.50	0.82673	-10.87583	4.2744	0.74355	-17.28586	3.9541	0.66032	-24.64940	3.5872
4.00	0.84775	-9.50509	4.3708	0.77084	-15.07728	4.1070	0.69354	-21.43360	3.8004
5.00	0.87598	-7.59517	4.5013	0.81125	-12.01889	4.3178	0.74423	-17.02003	4.0983
6.00	0.89538	-6.32721	4.5819	0.83962	-9.99814	4.4527	0.78082	-14.12879	4.2929
7.00	0.90953	-5.42399	4.6327	0.86059	-8.58480	4.5426	0.80834	-12.08565	4.4261
8.00	0.92029	-4.74795	4.6638	0.87671	-7.48332	4.6032	0.82874	-10.56426	4.5196
9.00	0.92874	-4.22303	4.6808	0.88947	-6.66746	4.6433	0.84684	-9.38708	4.5854
10.00	0.93556	-3.80375	4.6873	0.89982	-5.99941	4.6681	0.86081	-8.44911	4.6310
12.00	0.94588	-3.17619	4.6759	0.91558	-5.00789	4.6844	0.88221	-7.04861	4.6785
14.00	0.95330	-2.72930	4.6399	0.92695	-4.30239	4.6681	0.89783	-6.05349	4.6846
16.00	0.95889	-2.39525	4.5840	0.93559	-3.77530	4.6271	0.90971	-5.31065	4.6603
18.00	0.96325	-2.13639	4.5110	0.94234	-3.36699	4.5856	0.91904	-4.73554	4.6118
20.00	0.96673	-1.93016	4.4222	0.94775	-3.04176	4.4860	0.92654	-4.27765	4.5426
22.00	0.96958	-1.76220	4.3166	0.95218	-2.77695	4.3899	0.93270	-3.90491	4.4550
24.00	0.97195	-1.62298	4.2005	0.95587	-2.55743	4.2779	0.93784	-3.59601	4.3501
26.00	0.97395	-1.50581	4.0680	0.95898	-2.37277	4.1507	0.94219	-3.33620	4.2288
28.00	0.97565	-1.40604	3.9211	0.96165	-2.21551	4.0082	0.94591	-3.11496	4.0913
30.00	0.97712	-1.32018	3.7596	0.96395	-2.08018	3.8505	0.94912	-2.92461	3.9380
32.00	0.97840	-1.24563	3.5830	0.96595	-1.96269	3.6773	0.95192	-2.75936	3.7686
34.00	0.97952	-1.18041	3.3911	0.96770	-1.85991	3.4882	0.95438	-2.61481	3.5828
36.00	0.98050	-1.12298	3.1831	0.96925	-1.76941	3.2828	0.95655	-2.48754	3.3803
38.00	0.98138	-1.07213	2.9585	0.97062	-1.68927	3.0604	0.95848	-2.37485	3.1605
40.00	0.98216	-1.02688	2.7163	0.97184	-1.61797	2.8203	0.96019	-2.27459	2.9227
42.00	0.98285	-0.98645	2.4558	0.97293	-1.55426	2.5616	0.96173	-2.18501	2.6661
44.00	0.98348	-0.95020	2.1758	0.97391	-1.49713	2.2832	0.96311	-2.10468	2.3895
46.00	0.98404	-0.91760	1.8750	0.97480	-1.44576	1.9839	0.96435	-2.03245	2.0918
48.00	0.98455	-0.88820	1.5520	0.97559	-1.39944	1.6622	0.96547	-1.96733	1.7717
50.00	0.98501	-0.86165	1.2052	0.97632	-1.35760	1.3166	0.96649	-1.90851	1.4274
52.00	0.98542	-0.83763	0.8325	0.97697	-1.31975	0.9450	0.96741	-1.85530	1.0570
54.00	0.98580	-0.81588	0.4317	0.97756	-1.28548	0.5451	0.96824	-1.80712	0.6582
56.00	0.98614	-0.79618	0.0001	0.97809	-1.25444	0.1144	0.96899	-1.76347	0.2285
58.00	0.98645	-0.77833	-0.4656	0.97858	-1.22632	-0.3505	0.96968	-1.72394	-0.2355
60.00	0.98672	-0.76217	-0.9692	0.97902	-1.20086	-0.8534	0.97030	-1.68815	-0.7375
62.00	0.98698	-0.74756	-1.5153	0.97942	-1.17784	-1.3988	0.97086	-1.65579	-1.2822
64.00	0.98721	-0.73438	-2.1096	0.97978	-1.15708	-1.9926	0.97136	-1.62660	-1.8753
66.00	0.98741	-0.72253	-2.7593	0.98010	-1.13839	-2.6417	0.97182	-1.60033	-2.5238
68.00	0.98759	-0.71190	-3.4732	0.98039	-1.12165	-3.3552	0.97223	-1.57679	-3.2368
70.00	0.98776	-0.70242	-4.2630	0.98065	-1.10672	-4.1445	0.97259	-1.55580	-4.0256
72.00	0.98790	-0.69403	-5.1437	0.98088	-1.09349	-5.0249	0.97292	-1.53722	-4.9056
74.00	0.98803	-0.68665	-6.1361	0.98108	-1.08189	-6.0189	0.97320	-1.52090	-5.8972
76.00	0.98814	-0.68027	-7.2686	0.98125	-1.07181	-7.1494	0.97345	-1.50674	-7.0293
78.00	0.98824	-0.67481	-8.5844	0.98140	-1.06321	-8.4646	0.97366	-1.49464	-8.3443
80.00	0.98832	-0.67024	-10.1482	0.98153	-1.05602	-10.0283	0.97383	-1.48454	-9.9077
82.00	0.98838	-0.66655	-12.0702	0.98163	-1.05020	-11.9501	0.97398	-1.47635	-11.8294
84.00	0.98843	-0.66370	-14.5584	0.98171	-1.04571	-14.4362	0.97408	-1.47004	-14.3153
86.00	0.98847	-0.66167	-18.0692	0.98176	-1.04252	-17.9469	0.97416	-1.46555	-17.8280
88.00	0.98849	-0.66046	-24.0845	0.98179	-1.04061	-23.9641	0.97421	-1.46288	-23.8431
90.00	0.98849	-0.66006	-142.1289	0.98181	-1.03998	-142.0085	0.97423	-1.46199	-141.8875

Radiation Efficiency	Radiation Efficiency	Radiation Efficiency
ETA = 0.9250, H =-0.339E+00 (dB)	ETA = 0.8938, H =-0.469E+00 (dB)	ETA = 0.8624, H =-0.643E+00 (dB)

Table A8-8 Case 2: Sea Water, $N = 1$ ($h = 1 \times 0.05\lambda$)

N=1, CASE(2): Sea Water (av salinity 70 deg C) (Relative Dielectric Constant = 70.0, Conductivity = 5.000000 S/m)

Grazing ang. deg	FREQUENCY = 6.0 MHz. Fresnel Reflect Coef |Rv|	Fresnel Reflect Coef ang Rv(deg)	Directive gain D(dBi)	FREQUENCY = 15.0 MHz. Fresnel Reflect Coef |Rv|	Fresnel Reflect Coef ang Rv(deg)	Directive gain D(dBi)	FREQUENCY = 30.0 MHz. Fresnel Reflect Coef |Rv|	Fresnel Reflect Coef ang Rv(deg)	Directive gain D(dBi)
PSI(deg)	|Rv|	ang Rv(deg)	D(dBi)	|Rv|	ang Rv(deg)	D(dBi)	|Rv|	ang Rv(deg)	D(dBi)
0.00	1.00000	-180.00000	-999.9999	1.00000	-180.00000	-999.9999	1.00000	-180.00000	-999.9999
0.50	0.41413	-84.60905	0.0779	0.45255	-118.74591	-1.9548	0.53359	-139.11157	-3.7894
1.00	0.54337	-40.19803	2.3844	0.43633	-66.46782	1.1324	0.40790	-93.68280	-0.1155
1.50	0.65235	-25.98895	3.2554	0.52775	-42.49292	2.3908	0.44345	-62.20481	1.4829
2.00	0.72220	-19.24878	3.7079	0.60595	-31.06702	3.0680	0.50963	-46.17813	2.3744
2.50	0.76935	-15.30605	3.9829	0.66472	-24.51326	3.4662	0.56999	-35.33608	2.9398
3.00	0.80304	-12.71306	4.1665	0.70915	-20.26586	3.7727	0.61978	-28.02890	3.3283
3.50	0.82823	-10.87583	4.2967	0.74355	-17.28586	3.9769	0.66032	-24.64940	3.6314
4.00	0.84775	-9.50509	4.3930	0.77084	-15.07728	4.1297	0.69354	-21.43360	3.8235
4.50	0.87588	-7.59517	4.5231	0.81125	-12.01889	4.3402	0.74423	-17.02003	4.1212
6.00	0.89538	-6.32721	4.6034	0.83962	-9.99914	4.4747	0.78082	-14.12979	4.3154
7.00	0.90953	-5.42399	4.6537	0.86059	-8.56480	4.5642	0.80834	-12.08565	4.4482
8.00	0.92029	-4.74795	4.6844	0.87671	-7.49332	4.6243	0.82974	-10.56428	4.5412
9.00	0.92874	-4.22303	4.7009	0.88947	-6.66246	4.6638	0.84684	-9.38708	4.6065
10.00	0.93556	-3.80375	4.7067	0.89982	-5.99941	4.6880	0.86081	-8.44911	4.6514
12.00	0.94588	-3.17619	4.6940	0.91556	-5.00789	4.7030	0.88221	-7.04861	4.6975
14.00	0.95330	-2.72930	4.6562	0.92696	-4.30259	4.6850	0.89783	-6.05349	4.7020
16.00	0.95880	-2.39525	4.5985	0.93559	-3.77530	4.6421	0.90971	-5.31065	4.6758
18.00	0.96325	-2.13639	4.5234	0.94234	-3.36699	4.5785	0.91904	-4.73554	4.6252
20.00	0.96673	-1.93016	4.4324	0.94775	-3.04176	4.4968	0.92654	-4.27765	4.5538
22.00	0.96958	-1.76220	4.3262	0.95218	-2.77695	4.3980	0.93270	-3.90491	4.4636
24.00	0.97195	-1.62296	4.2054	0.95587	-2.55743	4.2834	0.93784	-3.59801	4.3560
26.00	0.97395	-1.50581	4.0701	0.95898	-2.37277	4.1532	0.94219	-3.33620	4.2318
28.00	0.97565	-1.40604	3.9201	0.96165	-2.21551	4.0077	0.94591	-3.11496	4.0914
30.00	0.97717	-1.32018	3.7554	0.96395	-2.08018	3.8468	0.94912	-2.92461	3.9348
32.00	0.97840	-1.24563	3.5755	0.96595	-1.96289	3.6703	0.95192	-2.75936	3.7621
34.00	0.97952	-1.18041	3.3802	0.96770	-1.85991	3.4778	0.95438	-2.61481	3.5729
36.00	0.98050	-1.12298	3.1687	0.96925	-1.76941	3.2688	0.95655	-2.48754	3.3669
38.00	0.98138	-1.07213	2.9404	0.97062	-1.68927	3.0429	0.95846	-2.37485	3.1435
40.00	0.98216	-1.02688	2.6946	0.97184	-1.61797	2.7991	0.96019	-2.27459	2.9020
42.00	0.98285	-0.98645	2.4304	0.97293	-1.55426	2.5367	0.96173	-2.18501	2.6416
44.00	0.98348	-0.95020	2.1466	0.97391	-1.49713	2.2545	0.96311	-2.10468	2.3613
46.00	0.98404	-0.91760	1.8421	0.97480	-1.44575	1.9514	0.96435	-2.03245	2.0599
48.00	0.98455	-0.88820	1.5154	0.97559	-1.39944	1.6260	0.96547	-1.96733	1.7360
50.00	0.98501	-0.86165	1.1648	0.97632	-1.35760	1.2767	0.96649	-1.90851	1.3879
52.00	0.98542	-0.83763	0.7884	0.97697	-1.31975	0.9014	0.96741	-1.85530	1.0139
54.00	0.98580	-0.81588	0.3840	0.97756	-1.28548	0.4979	0.96824	-1.80712	0.6115
56.00	0.98614	-0.79618	-0.0512	0.97809	-1.25444	0.0636	0.96899	-1.76347	0.1782
58.00	0.98645	-0.77833	-0.5203	0.97858	-1.22632	-0.4047	0.96968	-1.72394	-0.2892
60.00	0.98672	-0.76217	-1.0272	0.97902	-1.20086	-0.9109	0.97030	-1.68815	-0.7945
62.00	0.98698	-0.74756	-1.5785	0.97942	-1.17784	-1.4595	0.97086	-1.65579	-1.3424
64.00	0.98721	-0.73438	-2.1739	0.97978	-1.15708	-2.0563	0.97138	-1.62660	-1.9386
66.00	0.98741	-0.72253	-2.8264	0.98010	-1.13839	-2.7084	0.97182	-1.60033	-2.5900
68.00	0.98759	-0.71190	-3.5431	0.98039	-1.12165	-3.4245	0.97223	-1.57679	-3.3057
70.00	0.98776	-0.70242	-4.3354	0.98065	-1.10672	-4.2164	0.97259	-1.55580	-4.0970
72.00	0.98790	-0.69403	-5.2184	0.98088	-1.09349	-5.0991	0.97292	-1.53722	-4.9793
74.00	0.98803	-0.68666	-6.2129	0.98108	-1.08189	-6.0932	0.97320	-1.52090	-5.9730
76.00	0.98814	-0.68027	-7.3475	0.98125	-1.07181	-7.2276	0.97345	-1.50674	-7.1071
78.00	0.98824	-0.67481	-8.6647	0.98140	-1.06321	-8.5445	0.97366	-1.49464	-8.4237
80.00	0.98832	-0.67024	-10.2299	0.98153	-1.05602	-10.1095	0.97383	-1.48454	-9.9885
82.00	0.98838	-0.66655	-12.1531	0.98163	-1.05020	-12.0325	0.97398	-1.47635	-11.9113
84.00	0.98843	-0.66370	-14.6402	0.98171	-1.04571	-14.5195	0.97408	-1.47004	-14.3982
86.00	0.98847	-0.66167	-18.1537	0.98176	-1.04252	-18.0329	0.97416	-1.46555	-17.9115
88.00	0.98849	-0.66048	-24.1693	0.98179	-1.04061	-24.0485	0.97421	-1.46288	-23.9270
90.00	0.98849	-0.66006	-142.2139	0.98181	-1.03998	-142.0931	0.97423	-1.46199	-141.9715
	Radiation Efficiency ETA = 0.9231, H =-0.348E+00 (dB)			Radiation Efficiency ETA = 0.8907, H =-0.503E+00 (dB)			Radiation Efficiency ETA = 0.8585, H =-0.663E+00 (dB)		

Table A8-9 Case 2: Sea Water, $N = 2$ ($h = 2 \times 0.05\lambda$)

N=2, CASE(2): Sea Water (av salinity 20 deg C) (Relative Dielectric Constant = 70.0, Conductivity = 5.000000 S/m)

Grazing ang. deg	FREQUENCY = 6.0 MHz. Fresnel Reflect Coef		Directive gain	FREQUENCY = 15.0 MHz. Fresnel Reflect Coef		Directive gain	FREQUENCY = 30.0 MHz. Fresnel Reflect Coef		Directive gain
PSI(deg)	|Rv|	ang Rv(deg)	D(dBi)	|Rv|	ang Rv(deg)	D(dBi)	|Rv|	ang Rv(deg)	D(dBi)
0.00	1.00000	-180.00000	-999.9999	1.00000	-180.00000	-999.9999	1.00000	-180.00000	-999.9999
0.50	0.41413	-84.60905	0.1240	0.45255	-119.74591	-1.9077	0.53359	-139.11157	-3.7413
1.00	0.54337	-40.19803	2.4304	0.42633	-66.46782	1.1794	0.40790	-93.68260	-0.0674
1.50	0.65235	-25.98895	3.3014	0.52775	-42.49292	2.4378	0.44345	-62.20481	1.5309
2.00	0.72220	-19.24878	3.7537	0.60595	-31.06702	3.1149	0.50963	-45.17813	2.4223
2.50	0.78335	-15.30605	4.0286	0.66472	-24.51326	3.5350	0.56999	-35.33508	2.9875
3.00	0.80304	-12.71306	4.2120	0.70915	-20.26586	3.8193	0.61978	-29.02690	3.3759
3.50	0.82823	-10.87583	4.3420	0.74365	-17.28586	4.0232	0.66032	-24.64940	3.6578
4.00	0.84775	-9.50509	4.4380	0.77084	-15.07728	4.1757	0.69354	-21.43360	3.8706
5.00	0.87598	-7.59517	4.5676	0.81125	-12.01809	4.3856	0.74423	-17.02003	4.1677
6.00	0.89538	-6.32721	4.6471	0.83962	-9.99914	4.5194	0.78082	-14.12879	4.3612
7.00	0.90953	-5.42399	4.6966	0.86059	-8.56480	4.6080	0.80834	-12.08565	4.4932
8.00	0.92029	-4.74795	4.7262	0.87671	-7.49332	4.6672	0.82974	-10.56426	4.5851
9.00	0.92874	-4.22303	4.7416	0.88947	-6.66246	4.7056	0.84684	-9.38706	4.6493
10.00	0.93556	-3.80375	4.7462	0.89982	-5.99941	4.7265	0.86081	-8.44911	4.6930
12.00	0.94588	-3.17619	4.7305	0.91558	-5.00789	4.7406	0.88221	-7.04861	4.7362
14.00	0.95330	-2.72930	4.6895	0.92696	-4.30239	4.7193	0.89783	-6.05349	4.7373
16.00	0.95889	-2.39525	4.6279	0.93559	-3.77530	4.6725	0.90971	-5.31065	4.7079
18.00	0.96325	-2.13639	4.5485	0.94234	-3.36699	4.6046	0.91904	-4.73554	4.6524
20.00	0.96673	-1.93016	4.4527	0.94775	-3.04178	4.5180	0.92654	-4.27765	4.5762
22.00	0.96958	-1.76220	4.3415	0.95218	-2.77895	4.4142	0.93270	-3.90491	4.4809
24.00	0.97195	-1.62298	4.2151	0.95587	-2.55743	4.2941	0.93784	-3.59601	4.3678
26.00	0.97395	-1.50581	4.0739	0.95898	-2.37277	4.1581	0.94219	-3.33820	4.2377
28.00	0.97565	-1.40604	3.9177	0.96165	-2.21551	4.0063	0.94591	-3.11496	4.0910
30.00	0.97712	-1.32018	3.7465	0.96395	-2.08018	3.8389	0.94912	-2.92481	3.9279
32.00	0.97840	-1.24563	3.5598	0.96595	-1.96709	3.6556	0.95192	-2.75936	3.7484
34.00	0.97952	-1.18041	3.3574	0.96770	-1.85991	3.4561	0.95438	-2.61481	3.5522
36.00	0.98050	-1.12298	3.1387	0.96925	-1.76941	3.2399	0.95655	-2.48754	3.3390
38.00	0.98138	-1.07213	2.9031	0.97062	-1.68927	3.0066	0.95848	-2.37485	3.1081
40.00	0.98218	-1.02688	2.6497	0.97184	-1.61797	2.7552	0.96018	-2.27459	2.8591
42.00	0.98285	-0.98645	2.3779	0.97293	-1.55426	2.4852	0.96173	-2.18501	2.5911
44.00	0.98348	-0.95020	2.0864	0.97381	-1.49713	2.1953	0.96311	-2.10468	2.3031
46.00	0.98404	-0.91760	1.7742	0.97480	-1.44576	1.8845	0.96435	-2.03245	1.9940
48.00	0.98455	-0.88820	1.4397	0.97559	-1.39944	1.5514	0.96547	-1.96733	1.6624
50.00	0.98501	-0.86165	1.0815	0.97632	-1.35760	1.1944	0.96649	-1.90851	1.3087
52.00	0.98542	-0.83763	0.6976	0.97697	-1.31975	0.8116	0.96741	-1.85530	0.9251
54.00	0.98580	-0.81586	0.2858	0.97756	-1.28548	0.4007	0.96824	-1.80712	0.5153
56.00	0.98614	-0.79616	-0.1586	0.97809	-1.25444	-0.0409	0.96899	-1.76347	0.0747
58.00	0.98645	-0.77833	-0.6328	0.97858	-1.22632	-0.5162	0.96968	-1.72394	-0.3997
60.00	0.98672	-0.76217	-1.1455	0.97902	-1.20086	-1.0292	0.97030	-1.68815	-0.9119
62.00	0.98698	-0.74756	-1.7024	0.97942	-1.17784	-1.5844	0.97086	-1.65579	-1.4664
64.00	0.98721	-0.73438	-2.3060	0.97978	-1.15708	-2.1875	0.97136	-1.62660	-2.0688
66.00	0.98741	-0.72253	-2.9645	0.98010	-1.13839	-2.8454	0.97182	-1.60033	-2.7261
68.00	0.98759	-0.71190	-3.6867	0.98039	-1.12165	-3.5672	0.97223	-1.57679	-3.4473
70.00	0.98776	-0.70242	-4.4841	0.98065	-1.10672	-4.3642	0.97259	-1.55580	-4.2439
72.00	0.98790	-0.69403	-5.3720	0.98088	-1.09349	-5.2517	0.97292	-1.53722	-5.1309
74.00	0.98803	-0.68666	-6.3707	0.98108	-1.08189	-6.2504	0.97320	-1.52090	-6.1290
76.00	0.98814	-0.68027	-7.5093	0.98125	-1.07181	-7.3883	0.97345	-1.50674	-7.2669
78.00	0.98824	-0.67481	-8.8298	0.98140	-1.06321	-8.7087	0.97365	-1.49464	-8.5869
80.00	0.98832	-0.67024	-10.3979	0.98153	-1.05602	-10.2766	0.97383	-1.48454	-10.1546
82.00	0.98838	-0.66655	-12.3235	0.98163	-1.05020	-12.2020	0.97398	-1.47635	-12.0798
84.00	0.98843	-0.66370	-14.8125	0.98171	-1.04571	-14.6909	0.97408	-1.47004	-14.5686
86.00	0.98847	-0.66167	-18.3273	0.98176	-1.04252	-18.2056	0.97416	-1.46555	-18.0832
88.00	0.98849	-0.66046	-24.3438	0.98179	-1.04061	-24.2220	0.97421	-1.46288	-24.0995
90.00	0.98849	-0.66006	-142.3886	0.98181	-1.03998	-142.2868	0.97423	-1.46199	-142.1448
	Radiation Efficiency			Radiation Efficiency			Radiation Efficiency		
	ETA = 0.9217, M =-0.354E+00 (dB)			ETA = 0.8887, M =-0.512E+00 (dB)			ETA = 0.8558, M =-0.676E+00 (dB)		

Table A8-10 Case 2: Sea Water, $N = 3$ ($h = 3 \times 0.05\lambda$)

N=3, CASE(2): Sea Water (av salinity 20 deg C) (Relative Dielectric Constant = 70.0, Conductivity = 5.000000 S/m)

Grazing ang. deg	FREQUENCY = 6.0 MHz. Fresnel Reflect Coef		Directive gain	FREQUENCY = 15.0 MHz. Fresnel Reflect Coef		Directive gain	FREQUENCY = 30.0 MHz. Fresnel Reflect Coef		Directive gain
PSI(deg)	|Rv|	ang Rv(deg)	D(dBi)	|Rv|	ang Rv(deg)	D(dBi)	|Rv|	ang Rv(deg)	D(dBi)
0.00	1.00000	-180.00000	-999.9999	1.00000	-180.00000	-999.9999	1.00000	-180.00000	-999.9999
0.50	0.41413	-84.60905	0.2030	0.45255	-118.74591	-1.8268	0.53359	-139.11157	-3.6586
1.00	0.54337	-40.19803	2.5094	0.43633	-66.46782	1.2602	0.40790	-93.68260	0.0152
1.50	0.65235	-25.98895	3.3802	0.52775	-42.49292	2.5184	0.44345	-62.20481	1.6134
2.00	0.72220	-19.24878	3.8323	0.60595	-31.06702	3.1953	0.50963	-45.17813	2.5045
2.50	0.76935	-15.30505	4.1069	0.66472	-24.51326	3.6151	0.58998	-35.33606	3.0895
3.00	0.80304	-12.71308	4.2900	0.70915	-20.26586	3.8991	0.61978	-29.02690	3.4578
3.50	0.82823	-10.87583	4.4196	0.74355	-17.28686	4.1027	0.66032	-24.64940	3.7391
4.00	0.84775	-9.50509	4.5152	0.77084	-15.07728	4.2547	0.68354	-21.43360	3.9515
5.00	0.87598	-7.59517	4.6437	0.81125	-12.01689	4.4636	0.74423	-17.02003	4.2475
6.00	0.89538	-6.32721	4.7219	0.83962	-9.99914	4.5961	0.78082	-14.17879	4.4397
7.00	0.90953	-5.42399	4.7700	0.86059	-8.56480	4.6833	0.80834	-12.08565	4.5702
8.00	0.92029	-4.74795	4.7979	0.87671	-7.49332	4.7407	0.82974	-10.56426	4.6605
9.00	0.92874	-4.22303	4.8113	0.88947	-6.66746	4.7771	0.84864	-9.38708	4.7226
10.00	0.93556	-3.80375	4.8137	0.89982	-5.99941	4.7979	0.86081	-8.44911	4.7641
12.00	0.94588	-3.17619	4.7931	0.91556	-5.00789	4.8050	0.88221	-7.04861	4.8024
14.00	0.95330	-2.72930	4.7462	0.92696	-4.30239	4.7778	0.89763	-6.05349	4.7976
16.00	0.95889	-2.39525	4.6779	0.93559	-3.77530	4.7244	0.90971	-5.31085	4.7609
18.00	0.96325	-2.13639	4.5911	0.94234	-3.36699	4.6490	0.91904	-4.73554	4.6966
20.00	0.96673	-1.93018	4.4871	0.94775	-3.04176	4.5542	0.92654	-4.27785	4.6142
22.00	0.96958	-1.76220	4.3669	0.95218	-2.77695	4.4415	0.93270	-3.90491	4.5099
24.00	0.97195	-1.62298	4.2309	0.95587	-2.55743	4.3117	0.93784	-3.59601	4.3872
26.00	0.97395	-1.50581	4.0794	0.95898	-2.37277	4.1654	0.94219	-3.33620	4.2468
28.00	0.97565	-1.40604	3.9124	0.96165	-2.21551	4.0029	0.94591	-3.11496	4.0893
30.00	0.97712	-1.32018	3.7298	0.96395	-2.08018	3.8241	0.94912	-2.92461	3.9149
32.00	0.97840	-1.24563	3.5314	0.96595	-1.96259	3.6289	0.95192	-2.75938	3.7235
34.00	0.97952	-1.18041	3.3167	0.96770	-1.85991	3.4172	0.95438	-2.61481	3.5150
36.00	0.98050	-1.12298	3.0854	0.96925	-1.76941	3.1884	0.95655	-2.48754	3.2891
38.00	0.98138	-1.07213	2.8368	0.97062	-1.68927	2.9421	0.95848	-2.37485	3.0454
40.00	0.98218	-1.02688	2.5703	0.97184	-1.61797	2.6776	0.96019	-2.27459	2.7832
42.00	0.98285	-0.98645	2.2851	0.97293	-1.55426	2.3942	0.96173	-2.18501	2.5018
44.00	0.98348	-0.95020	1.9802	0.97391	-1.49713	2.0909	0.96311	-2.10468	2.2004
46.00	0.98404	-0.91760	1.6545	0.97480	-1.44576	1.7666	0.96435	-2.03245	1.8777
48.00	0.98455	-0.88820	1.3068	0.97559	-1.39944	1.4200	0.96547	-1.96733	1.5327
50.00	0.98501	-0.86165	0.9351	0.97632	-1.35760	1.0496	0.96649	-1.90851	1.1636
52.00	0.98542	-0.83763	0.5378	0.97697	-1.31975	0.6536	0.96741	-1.85530	0.7687
54.00	0.98580	-0.81586	0.1131	0.97756	-1.28548	0.2297	0.96824	-1.80712	0.3459
56.00	0.98614	-0.79618	-0.3421	0.97809	-1.25444	-0.2246	0.96899	-1.76347	-0.1074
58.00	0.98645	-0.77833	-0.8366	0.97858	-1.22632	-0.7124	0.96968	-1.72394	-0.5942
60.00	0.98672	-0.76217	-1.3563	0.97902	-1.20086	-1.2374	0.97030	-1.68815	-1.1184
62.00	0.98698	-0.74756	-1.9237	0.97942	-1.17784	-1.8041	0.97086	-1.65579	-1.6844
64.00	0.98721	-0.73438	-2.5383	0.97978	-1.15708	-2.4181	0.97136	-1.62660	-2.2978
66.00	0.98741	-0.72253	-3.2072	0.98010	-1.13839	-3.0865	0.97182	-1.60033	-2.9656
68.00	0.98759	-0.71190	-3.9392	0.98039	-1.12165	-3.8180	0.97223	-1.57679	-3.6966
70.00	0.98776	-0.70242	-4.7458	0.98065	-1.10672	-4.6242	0.97259	-1.55580	-4.5022
72.00	0.98790	-0.69403	-5.6420	0.98088	-1.09349	-5.5200	0.97292	-1.53722	-5.3977
74.00	0.98803	-0.68666	-6.6484	0.98108	-1.08189	-6.5261	0.97320	-1.52090	-6.4034
76.00	0.98814	-0.68027	-7.7937	0.98125	-1.07181	-7.6712	0.97345	-1.50674	-7.5481
78.00	0.98824	-0.67481	-9.1202	0.98140	-1.06321	-8.9975	0.97366	-1.49464	-8.8741
80.00	0.98832	-0.67024	-10.6935	0.98153	-1.05602	-10.5705	0.97383	-1.48458	-10.4470
82.00	0.98838	-0.66655	-12.8233	0.98163	-1.05020	-12.5001	0.97398	-1.47635	-12.3764
84.00	0.98843	-0.66370	-15.1156	0.98171	-1.04571	-14.9823	0.97408	-1.47004	-14.6684
86.00	0.98847	-0.66167	-18.6328	0.98176	-1.04252	-18.5094	0.97416	-1.46555	-18.3855
88.00	0.98849	-0.66046	-24.6506	0.98179	-1.04061	-24.5272	0.97421	-1.46288	-24.4032
90.00	0.98849	-0.66006	-142.6960	0.98181	-1.03998	-142.5725	0.97423	-1.46199	-142.4485

Radiation Efficiency	Radiation Efficiency	Radiation Efficiency
ETA = 0.9196, H =-0.364E+00 (dB)	ETA = 0.8858, H =-0.527E+00 (dB)	ETA = 0.8520, H =-0.696E+00 (dB)

Table A8-11 Case 2: Sea Water, $N = 4$ ($h = 4 \times 0.05\lambda$)

N=4, CASE(2): Sea Water (av salinity 20 deg C) (Relative Dielectric Constant = 70.0, Conductivity = 5.000000 S/m)

Grazing ang, deg	FREQUENCY = 6.0 MHz. Fresnel Reflect Coef		Directive gain	FREQUENCY = 15.0 MHz. Fresnel Reflect Coef		Directive gain	FREQUENCY = 30.0 MHz. Fresnel Reflect Coef		Directive gain
PSI(deg)	|Rv|	ang Rv(deg)	D(dBi)	|Rv|	ang Rv(deg)	D(dBi)	|Rv|	ang Rv(deg)	D(dBi)
0.00	1.00000	-180.00000	-999.9999	1.00000	-180.00000	-999.9999	1.00000	-180.00000	-999.9999
0.50	0.41413	-84.60905	0.3185	0.45255	-119.74591	-1.7085	0.53359	-139.11157	-3.5376
1.00	0.54337	-40.19803	2.6248	0.43633	-88.46782	1.3784	0.40790	-93.68260	0.1362
1.50	0.65235	-25.98895	3.4953	0.52775	-42.49292	2.6363	0.44345	-62.20481	1.7341
2.00	0.72220	-19.24878	3.9471	0.60595	-31.08702	3.3129	0.50963	-45.17813	2.6249
2.50	0.76835	-15.90505	4.2214	0.66472	-24.51326	3.7324	0.56999	-35.33608	3.1895
3.00	0.80304	-12.71305	4.4040	0.70915	-20.26586	4.0159	0.61978	-29.02690	3.5771
3.50	0.82823	-10.87583	4.5330	0.74355	-17.28586	4.2189	0.66032	-24.64940	3.8581
4.00	0.84775	-9.50509	4.6280	0.77084	-15.07728	4.3703	0.69354	-21.43360	4.0698
5.00	0.87598	-7.59517	4.7550	0.81125	-12.01889	4.5776	0.74423	-17.02003	4.3643
6.00	0.89538	-6.32721	4.8313	0.83962	-9.99914	4.7082	0.78082	-14.12879	4.5546
7.00	0.90953	-5.42399	4.8771	0.86059	-8.56480	4.7931	0.80834	-12.08565	4.6628
8.00	0.92029	-4.74795	4.9024	0.87671	-7.49332	4.8480	0.82974	-10.56426	4.7705
9.00	0.92874	-4.22303	4.9130	0.88947	-6.66246	4.8815	0.84684	-9.38706	4.8298
10.00	0.93556	-3.80375	4.9121	0.89982	-5.99941	4.8991	0.86081	-8.44911	4.8681
12.00	0.94588	-3.17619	4.8841	0.91556	-5.00789	4.8987	0.88221	-7.04861	4.8989
14.00	0.95330	-2.72930	4.8265	0.92696	-4.30239	4.8629	0.89783	-6.05349	4.8854
16.00	0.95889	-2.39525	4.7503	0.93559	-3.77530	4.7995	0.90971	-5.31065	4.8387
18.00	0.96325	-2.13639	4.6523	0.94234	-3.36699	4.7130	0.91904	-4.73554	4.7652
20.00	0.96673	-1.93016	4.5360	0.94775	-3.04176	4.6059	0.92654	-4.27765	4.6685
22.00	0.96958	-1.76220	4.4025	0.95218	-2.77695	4.4798	0.93270	-3.90491	4.5509
24.00	0.97195	-1.62256	4.2522	0.95587	-2.55743	4.3358	0.93784	-3.59601	4.4138
26.00	0.97395	-1.50581	4.0853	0.95898	-2.37277	4.1740	0.94218	-3.32620	4.2581
28.00	0.97565	-1.40604	3.9021	0.96165	-2.21551	3.9952	0.94591	-3.11496	4.0843
30.00	0.97712	-1.32018	3.7025	0.96395	-2.08018	3.7994	0.94912	-2.92461	3.8928
32.00	0.97840	-1.24563	3.4863	0.96595	-1.96269	3.5865	0.95192	-2.75936	3.6836
34.00	0.97952	-1.18041	3.2532	0.96770	-1.85991	3.3563	0.95438	-2.61481	3.4587
36.00	0.98050	-1.12298	3.0029	0.96925	-1.76941	3.1085	0.95655	-2.48754	3.2119
38.00	0.98138	-1.07213	2.7349	0.97062	-1.68927	2.8428	0.95848	-2.37485	2.9487
40.00	0.98216	-1.02688	2.4487	0.97184	-1.61797	2.5585	0.96019	-2.27459	2.6666
42.00	0.98285	-0.98645	2.1434	0.97293	-1.55426	2.2545	0.96173	-2.18501	2.3651
44.00	0.98348	-0.95020	1.8182	0.97391	-1.49713	1.9313	0.96311	-2.10468	2.0433
46.00	0.98404	-0.91760	1.4721	0.97480	-1.44576	1.5867	0.96435	-2.03245	1.7003
48.00	0.98455	-0.88820	1.1038	0.97559	-1.39944	1.2197	0.96547	-1.96733	1.3348
50.00	0.98501	-0.86165	0.7120	0.97632	-1.35760	0.8280	0.96649	-1.90851	0.9454
52.00	0.98542	-0.83763	0.2948	0.97697	-1.31975	0.4129	0.96741	-1.85530	0.5305
54.00	0.98580	-0.81588	-0.1498	0.97756	-1.28548	-0.0308	0.96824	-1.80712	0.0879
56.00	0.98614	-0.79618	-0.6243	0.97809	-1.25444	-0.5044	0.96899	-1.76347	-0.3848
58.00	0.98645	-0.77833	-1.1317	0.97858	-1.22632	-1.0110	0.96968	-1.72394	-0.8805
60.00	0.98672	-0.76217	-1.6756	0.97902	-1.20086	-1.5543	0.97030	-1.68815	-1.4330
62.00	0.98698	-0.74756	-2.2605	0.97942	-1.17784	-2.1386	0.97086	-1.65579	-2.0165
64.00	0.98721	-0.73438	-2.8819	0.97978	-1.15708	-2.7694	0.97136	-1.62660	-2.6467
66.00	0.98741	-0.72253	-3.5767	0.98010	-1.13839	-3.4537	0.97182	-1.60033	-3.3305
68.00	0.98759	-0.71190	-4.3237	0.98039	-1.12165	-4.2002	0.97223	-1.57679	-4.0765
70.00	0.98776	-0.70242	-5.1442	0.98065	-1.10672	-5.0203	0.97259	-1.55580	-4.8961
72.00	0.98790	-0.69403	-6.0532	0.98088	-1.09349	-5.9290	0.97292	-1.53722	-5.8044
74.00	0.98803	-0.68666	-7.0713	0.98108	-1.08189	-6.9467	0.97320	-1.52090	-6.8218
76.00	0.98814	-0.68027	-8.2271	0.98125	-1.07181	-8.1023	0.97345	-1.50674	-7.9770
78.00	0.98824	-0.67481	-9.5628	0.98140	-1.06321	-9.4377	0.97366	-1.49464	-9.3122
80.00	0.98832	-0.67024	-11.1439	0.98153	-1.05602	-11.0186	0.97383	-1.48464	-10.8929
82.00	0.98838	-0.66655	-13.0801	0.98163	-1.05020	-12.9547	0.97398	-1.47635	-12.8288
84.00	0.98843	-0.66370	-15.5775	0.98171	-1.04571	-15.4520	0.97408	-1.47004	-15.3259
86.00	0.98847	-0.66167	-19.0983	0.98176	-1.04252	-18.9728	0.97416	-1.46555	-18.8466
88.00	0.98849	-0.66046	-25.1184	0.98179	-1.04061	-24.9928	0.97421	-1.46288	-24.8665
90.00	0.98849	-0.66006	-143.1645	0.98181	-1.03998	-143.0388	0.97423	-1.46199	-142.9128
	Radiation Efficiency			Radiation Efficiency			Radiation Efficiency		
	ETA = 0.9170, H =-0.376E+00 (dB)			ETA = 0.8820, H =-0.545E+00 (dB)			ETA = 0.8471, H =-0.721E+00 (dB)		

Table A8-12 Case 2: Sea Water, $N = 5$ ($h = 5 \times 0.05\lambda$)

N=5, CASE(2): Sea Water (av salinity 20 deg C) (Relative Dielectric Constant = 70.0, Conductivity = 5.000000 S/m)

Grazing ang. deg	FREQUENCY = 6.0 MHz. Fresnel Reflect Coef		Directive gain	FREQUENCY = 15.0 MHz. Fresnel Reflect Coef		Directive gain	FREQUENCY = 30.0 MHz. Fresnel Reflect Coef		Directive gain
PSI(deg)	|Rv|	ang Rv(deg)	D(dBi)	|Rv|	ang Rv(deg)	D(dBi)	|Rv|	ang Rv(deg)	D(dBi)
0.00	1.00000	-180.00000	-999.9999	1.00000	-180.00000	-999.9999	1.00000	-180.00000	-999.9999
0.50	0.41413	-84.60905	0.4759	0.45265	-119.74591	-1.5472	0.53359	-139.11157	-3.3723
1.00	0.54337	-40.19803	2.7820	0.43633	-66.46782	1.5395	0.40790	-93.68260	0.3012
1.50	0.65235	-25.98895	3.6523	0.52775	-42.49292	2.7972	0.44345	-62.20481	1.8588
2.00	0.72220	-19.24878	4.1037	0.60585	-31.06702	3.4734	0.50963	-45.17813	2.7893
2.50	0.76935	-15.30605	4.3774	0.66472	-24.53328	3.8922	0.56999	-35.33608	3.3533
3.00	0.80304	-12.71306	4.5593	0.70915	-20.26586	4.1751	0.61978	-29.02690	3.7402
3.50	0.82823	-10.87583	4.6876	0.74358	-17.28586	4.3773	0.66032	-24.64940	4.0204
4.00	0.84775	-9.50509	4.7816	0.77084	-15.07728	4.5278	0.69354	-21.43360	4.2313
5.00	0.87598	-7.59517	4.9064	0.81125	-12.01689	4.7330	0.74423	-17.02003	4.5235
6.00	0.89538	-6.32721	4.9801	0.83962	-9.99914	4.8610	0.78082	-14.12879	4.7112
7.00	0.90963	-5.42399	5.0228	0.86059	-8.56480	4.9427	0.80834	-12.08585	4.8363
8.00	0.92029	-4.74795	5.0446	0.87671	-7.49332	4.9940	0.82974	-10.58425	4.9204
9.00	0.92874	-4.22303	5.0511	0.88947	-6.66246	5.0235	0.84684	-9.38708	4.9756
10.00	0.93556	-3.80375	5.0457	0.89982	-5.99941	5.0365	0.86081	-8.44911	5.0094
12.00	0.94588	-3.17619	5.0072	0.91556	-5.00789	5.0257	0.88221	-7.04861	5.0298
14.00	0.95230	-2.72930	4.9394	0.92696	-4.30239	4.9777	0.89783	-6.05349	5.0040
16.00	0.95889	-2.39525	4.8479	0.93559	-3.77530	4.9004	0.90971	-5.31065	4.9435
18.00	0.96325	-2.13639	4.7337	0.94234	-3.36899	4.7982	0.91904	-4.73554	4.8543
20.00	0.96673	-1.93016	4.6003	0.94775	-3.04176	4.6739	0.92654	-4.27765	4.7403
22.00	0.96958	-1.76220	4.4479	0.95218	-2.77695	4.5290	0.93270	-3.90491	4.6039
24.00	0.97195	-1.62286	4.2774	0.95587	-2.55743	4.3646	0.93784	-3.59601	4.4465
26.00	0.97395	-1.50561	4.0890	0.95898	-2.37277	4.1814	0.94219	-3.33620	4.2691
28.00	0.97565	-1.40604	3.8829	0.96165	-2.21551	3.9797	0.94591	-3.11496	4.0725
30.00	0.97712	-1.32018	3.6592	0.96395	-2.08018	3.7598	0.94912	-2.92461	3.8568
32.00	0.97840	-1.24563	3.4179	0.96595	-1.96269	3.5217	0.95192	-2.75936	3.6225
34.00	0.97952	-1.18041	3.1587	0.96770	-1.85991	3.2654	0.95438	-2.61481	3.3694
36.00	0.98050	-1.12298	2.8815	0.96925	-1.76941	2.9907	0.95655	-2.48754	3.0975
38.00	0.98138	-1.07213	2.5859	0.97062	-1.68927	2.6972	0.95848	-2.37485	2.8066
40.00	0.98216	-1.02686	2.2713	0.97184	-1.61797	2.3846	0.96019	-2.27459	2.4982
42.00	0.98285	-0.98645	1.9373	0.97293	-1.55426	2.0523	0.96173	-2.18501	2.1659
44.00	0.98348	-0.95020	1.5831	0.97391	-1.49713	1.6997	0.96311	-2.10466	1.8150
46.00	0.98404	-0.91760	1.2078	0.97480	-1.44576	1.3257	0.96435	-2.03245	1.4427
48.00	0.98455	-0.88820	0.8102	0.97559	-1.39944	0.9295	0.96547	-1.96733	1.0478
50.00	0.98501	-0.86165	0.3892	0.97632	-1.35760	0.5096	0.96649	-1.90851	0.8292
52.00	0.98542	-0.83763	-0.0569	0.97697	-1.31975	0.0645	0.96741	-1.85530	0.1852
54.00	0.98580	-0.81588	-0.5300	0.97756	-1.28548	-0.4078	0.96824	-1.80712	-0.2860
56.00	0.98614	-0.79618	-1.0325	0.97809	-1.25444	-0.9095	0.96899	-1.76347	-0.7867
58.00	0.98645	-0.77833	-1.5673	0.97858	-1.22632	-1.4435	0.96968	-1.72394	-1.3199
60.00	0.98672	-0.76217	-2.1377	0.97902	-1.20086	-2.0133	0.97030	-1.68815	-1.8889
62.00	0.98698	-0.74756	-2.7482	0.97942	-1.17784	-2.6231	0.97086	-1.65579	-2.4981
64.00	0.98721	-0.73438	-3.4041	0.97978	-1.15708	-3.2785	0.97136	-1.62660	-3.1529
66.00	0.98741	-0.72253	-4.1121	0.98010	-1.13839	-3.9861	0.97182	-1.60033	-3.8599
68.00	0.98759	-0.71180	-4.8810	0.98039	-1.12165	-4.7545	0.97223	-1.57879	-4.6279
70.00	0.98776	-0.70242	-5.7219	0.98065	-1.10672	-5.5951	0.97259	-1.55580	-5.4680
72.00	0.98790	-0.69403	-6.6496	0.98088	-1.09349	-6.5226	0.97292	-1.53722	-6.3952
74.00	0.98803	-0.68666	-7.6850	0.98108	-1.08189	-7.5576	0.97320	-1.52090	-7.4296
76.00	0.98814	-0.68027	-8.8562	0.98125	-1.07181	-8.7285	0.97345	-1.50674	-8.6004
78.00	0.98824	-0.67481	-10.2054	0.98140	-1.06321	-10.0775	0.97366	-1.49464	-9.9492
80.00	0.98832	-0.67024	-11.7981	0.98153	-1.05602	-11.6700	0.97383	-1.48454	-11.5415
82.00	0.98838	-0.66655	-13.7439	0.98163	-1.05020	-13.6157	0.97398	-1.47635	-13.4870
84.00	0.98843	-0.66370	-16.2488	0.98171	-1.04571	-16.1204	0.97408	-1.47004	-15.9916
86.00	0.98847	-0.66167	-19.7750	0.98178	-1.04252	-19.6466	0.97416	-1.46555	-19.5177
88.00	0.98849	-0.66046	-25.7983	0.98179	-1.04061	-25.6698	0.97421	-1.46288	-25.5409
90.00	0.98849	-0.66006	-143.8454	0.98181	-1.03998	-143.7170	0.97423	-1.46199	-143.5980

Radiation Efficiency	Radiation Efficiency	Radiation Efficiency
ETA = 0.9137, M =-0.392E+00 (dB)	ETA = 0.8773, M =-0.569E+00 (dB)	ETA = 0.8410, M =-0.752E+00 (dB)

Table A8-13 Case 3: Fresh Water, $N = 0$ ($h = 0 \times 0.05\lambda$)

N=0, CASE(3): Fresh Water (Relative Dielectric Constant = 80.0, Conductivity = 0.030000 S/m)

Grazing ang. deg	FREQUENCY = 5.0 MHz. Fresnel Reflect Coef		Directive gain	FREQUENCY = 15.0 MHz. Fresnel Reflect Coef		Directive gain	FREQUENCY = 30.0 MHz. Fresnel Reflect Coef		Directive gain
PSI(deg)	|Rv|	ang Rv(deg)	D(dBi)	|Rv|	ang Rv(deg)	D(dBi)	|Rv|	ang Rv(deg)	D(dBi)
0.00	1.00000	-180.00000	-999.9999	1.00000	-180.00000	-999.9999	1.00000	-180.00000	-999.9999
0.50	0.83894	-175.49135	-13.8869	0.85125	-178.03345	-14.8065	0.85354	-179.00006	-14.9947
1.00	0.70309	-170.78518	-8.5548	0.72332	-175.99016	-9.4131	0.72713	-177.96196	-9.5900
1.50	0.58617	-165.66431	-5.8783	0.61235	-173.78383	-6.4785	0.61898	-176.84261	-6.6446
2.00	0.49104	-159.87224	-3.7860	0.51541	-171.30666	-4.5318	0.52021	-175.58774	-4.6876
2.50	0.40955	-153.09521	-2.4194	0.43031	-168.41162	-3.1146	0.43481	-174.12224	-3.2607
3.00	0.34241	-144.98724	-1.3761	0.35541	-164.88354	-2.0242	0.35845	-172.33318	-2.1612
3.50	0.28915	-135.11427	-0.5493	0.28957	-160.38675	-1.1536	0.29041	-170.03693	-1.2622
4.00	0.24989	-123.33838	0.1240	0.23217	-154.38623	-0.4398	0.22951	-166.90907	-0.5605
5.00	0.21363	-95.87459	1.1563	0.14395	-133.80182	0.6850	0.12723	-154.89259	0.5588
6.00	0.22377	-70.96504	1.9109	0.10523	-94.41348	1.4823	0.05895	-114.20327	1.3887
7.00	0.25760	-53.81433	2.4851	0.12537	-56.40618	2.1111	0.07561	-46.19757	2.0287
8.00	0.29849	-42.81383	2.9346	0.17040	-37.19947	2.6085	0.13010	-24.50036	2.5380
9.00	0.33926	-35.51364	3.2929	0.21805	-27.61649	3.0100	0.18355	-16.79543	2.9463
10.00	0.37745	-30.38718	3.5855	0.26268	-22.09290	3.3389	0.23182	-12.94742	3.2831
12.00	0.44412	-23.74165	4.0219	0.34006	-16.02251	3.8385	0.31357	-9.08301	3.7963
14.00	0.49885	-19.58853	4.3212	0.40325	-12.73478	4.1892	0.37949	-7.11487	4.1580
16.00	0.54395	-16.78267	4.5256	0.45531	-10.65257	4.4360	0.43252	-5.90497	4.4141
18.00	0.58152	-14.69151	4.6603	0.49875	-9.20508	4.6061	0.47852	-5.07824	4.5922
20.00	0.61318	-13.10976	4.7409	0.53544	-8.13541	4.7168	0.51651	-4.47403	4.7096
22.00	0.64014	-11.86098	4.7778	0.56679	-7.31043	4.7795	0.54895	-4.01156	4.7781
24.00	0.66333	-10.84573	4.7780	0.59383	-6.65377	4.8021	0.57693	-3.64546	4.8057
26.00	0.68345	-10.01432	4.7463	0.61736	-6.11834	4.7899	0.60128	-3.34817	4.7980
28.00	0.70103	-9.31297	4.6863	0.63797	-5.67340	4.7470	0.62263	-3.10191	4.7590
30.00	0.71650	-8.71638	4.8002	0.65616	-5.29799	4.6761	0.64147	-2.89465	4.6916
32.00	0.73019	-8.20329	4.4897	0.67229	-4.97726	4.5791	0.65818	-2.71794	4.5977
34.00	0.74237	-7.75797	4.3560	0.68666	-4.70039	4.4573	0.67308	-2.56564	4.4787
36.00	0.75326	-7.36843	4.1996	0.69954	-4.45931	4.3117	0.68643	-2.43321	4.3356
38.00	0.76302	-7.02543	4.0209	0.71111	-4.24784	4.1427	0.69843	-2.31716	4.1688
40.00	0.77181	-6.72168	3.8199	0.72153	-4.06120	3.9504	0.70825	-2.21488	3.9785
42.00	0.77974	-6.45144	3.5962	0.73096	-3.89560	3.7347	0.71903	-2.12418	3.7646
44.00	0.78692	-6.20999	3.3494	0.73951	-3.74801	3.4950	0.72790	-2.04342	3.5266
46.00	0.79343	-5.99353	3.0786	0.74726	-3.61599	3.2307	0.73595	-1.97122	3.2639
48.00	0.79935	-5.79883	2.7827	0.75432	-3.49753	2.9407	0.74327	-1.90647	2.9753
50.00	0.80473	-5.62360	2.4604	0.76074	-3.39097	2.8238	0.74994	-1.84825	2.8597
52.00	0.80982	-5.46533	2.1100	0.76658	-3.29494	2.2783	0.75601	-1.79581	2.3153
54.00	0.81408	-5.32233	1.7294	0.77191	-3.20828	1.9022	0.76155	-1.74851	1.9402
56.00	0.81813	-5.19300	1.3161	0.77677	-3.13001	1.4930	0.76660	-1.70580	1.5320
58.00	0.82183	-5.07605	0.8671	0.78119	-3.05930	1.0477	0.77119	-1.66723	1.0875
60.00	0.82518	-4.97033	0.3786	0.78521	-2.99544	0.5626	0.77537	-1.63241	0.6033
62.00	0.82823	-4.87468	-0.1538	0.78886	-2.93784	0.0332	0.77916	-1.60100	0.0746
64.00	0.83098	-4.78886	-0.7358	0.79217	-2.88597	-0.5460	0.78260	-1.57273	-0.5039
66.00	0.83347	-4.71154	-1.3744	0.79516	-2.83938	-1.1820	0.78570	-1.54735	-1.1394
68.00	0.83571	-4.64232	-2.0783	0.79784	-2.79770	-1.8837	0.78849	-1.52464	-1.8405
70.00	0.83771	-4.58065	-2.8592	0.80024	-2.76058	-2.6625	0.79099	-1.50442	-2.6189
72.00	0.83948	-4.52607	-3.7320	0.80237	-2.72776	-3.5336	0.79321	-1.48654	-3.4896
74.00	0.84104	-4.47819	-4.7174	0.80424	-2.69897	-4.5174	0.79515	-1.47086	-4.4730
76.00	0.84240	-4.43667	-5.8441	0.80587	-2.67401	-5.6428	0.79685	-1.45728	-5.5980
78.00	0.84356	-4.40123	-7.1545	0.80727	-2.65272	-6.9519	0.79830	-1.44568	-6.9089
80.00	0.84453	-4.37162	-8.7140	0.80843	-2.63494	-8.5105	0.79951	-1.43600	-8.4652
82.00	0.84531	-4.34765	-10.6325	0.80938	-2.62054	-10.4282	0.80050	-1.42816	-10.3828
84.00	0.84592	-4.32916	-13.1160	0.81011	-2.60945	-12.9111	0.80126	-1.42212	-12.8655
86.00	0.84635	-4.31604	-16.8270	0.81063	-2.60157	-16.4216	0.80179	-1.41783	-16.3758
88.00	0.84661	-4.30820	-22.6410	0.81094	-2.59687	-22.4354	0.80212	-1.41527	-22.3897
90.00	0.84670	-4.30559	-140.8851	0.81104	-2.59530	-140.4784	0.80222	-1.41442	-140.4336
	Radiation Efficiency ETA = 0.5714, H =-0.243E+01 (dB)			Radiation Efficiency ETA = 0.5246, H =-0.280E+01 (dB)			Radiation Efficiency ETA = 0.5142, H =-0.289E+01 (dB)		

Table A8-14 Case 3: Fresh Water, $N = 1$ ($h = 1 \times 0.05\lambda$)

No1, CASE(3): Fresh Water (Relative Dielectric Constant = 80.0, Conductivity = 0.000000 S/m)

Grazing ang. deg	FREQUENCY = 6.0 MHz. Fresnel Reflect Coef |Rv|	Fresnel Reflect Coef ang Rv(deg)	Directive gain D(dBi)	FREQUENCY = 15.0 MHz. Fresnel Reflect Coef |Rv|	Fresnel Reflect Coef ang Rv(deg)	Directive gain D(dBi)	FREQUENCY = 30.0 MHz. Fresnel Reflect Coef |Rv|	Fresnel Reflect Coef ang Rv(deg)	Directive gain D(dBi)
PS1(deg)									
0.00	1.00000	-180.00000	-999.9999	1.00000	+180.00000	-999.9999	1.00000	-180.00000	-999.9999
0.50	0.83894	-175.49135	+13.8583	0.85125	-178.03345	-14.7772	0.85354	-179.00008	+14.9653
1.00	0.70309	-170.78516	-8.5262	0.72332	-175.99016	-9.3838	0.72713	-177.96196	-9.5607
1.50	0.58817	-165.66431	-5.6497	0.61235	-173.78383	-6.4493	0.61698	-176.84261	-6.6153
2.00	0.49104	-159.87224	-3.7575	0.51541	-171.30666	-4.5027	0.52021	-175.56774	-4.6584
2.50	0.40955	-153.09621	-2.3310	0.43031	-168.41182	-3.0855	0.43483	-174.12224	-3.2315
3.00	0.34241	-144.96724	-1.3478	0.35944	-164.88054	-1.9952	0.36545	-172.33318	-2.1321
3.50	0.28815	-135.11427	-0.5211	0.28967	+160.38875	+1.1247	0.29041	+170.03693	+1.2532
4.00	0.24889	-123.33838	0.1521	0.23217	-154.38623	-0.4110	0.23951	-166.90907	-0.5316
5.00	0.21363	-85.87459	1.1841	0.14395	+133.80182	0.6935	0.12723	-154.89259	0.5873
6.00	0.22377	-70.96504	1.9383	0.10523	-94.41348	1.5104	0.05995	-114.20327	1.4169
7.00	0.25760	-53.81433	2.5121	0.12537	-56.40618	2.1388	0.07561	-46.19757	2.0585
8.00	0.28849	-42.81393	2.9611	0.17040	-37.19942	2.6357	0.13010	-24.50036	2.5633
9.00	0.33926	-35.51354	3.3159	0.21803	-27.61849	3.0366	0.18355	-16.79543	2.9730
10.00	0.37745	-30.39718	3.6106	0.26268	-22.09290	3.3643	0.23182	-12.94742	3.3092
12.00	0.44412	-23.74165	4.0458	0.34006	-16.02251	3.8632	0.31357	-9.08301	3.8210
14.00	0.49885	-19.59953	4.3434	0.40325	+12.73478	4.2121	0.37949	-7.11487	4.1811
16.00	0.54395	-16.78267	4.5660	0.45531	-10.65257	4.4571	0.43352	-5.90497	4.4354
18.00	0.58152	+14.69151	4.6785	0.49875	-9.20506	4.6251	0.47852	-5.07824	4.6113
20.00	0.61318	-13.10975	4.7568	0.53544	-8.13541	4.7335	0.51651	-4.47403	4.7264
22.00	0.64014	-11.86098	4.7912	0.56579	-7.31043	4.7937	0.54895	-4.01156	4.7924
24.00	0.66333	-10.84973	4.7887	0.59383	+6.65377	4.8135	0.57693	-3.64546	4.8173
26.00	0.68345	-10.01432	4.7541	0.61736	-6.11834	4.7985	0.60128	-3.34817	4.8067
28.00	0.70103	-9.31297	4.6910	0.63797	+5.67340	4.7525	0.62263	-3.10191	4.7647
30.00	0.71650	-8.71638	4.6017	0.65516	-5.29799	4.6784	0.64147	-2.89465	4.6940
32.00	0.73019	-8.20329	4.4879	0.67229	+4.97726	4.5780	0.65818	-2.71794	4.5968
34.00	0.74237	-7.75797	4.3507	0.68666	-4.70039	4.4529	0.67308	+2.56564	4.4744
36.00	0.75326	+7.36843	4.1908	0.69954	-4.45931	4.3037	0.68643	-2.43321	4.3278
38.00	0.76302	-7.02543	4.0085	0.71111	-4.24784	4.1311	0.69843	+2.31716	4.1574
40.00	0.77181	-6.72169	3.8038	0.72153	-4.06120	3.9351	0.70925	-2.21488	3.9634
42.00	0.77974	-6.45144	3.5763	0.73096	+3.89560	3.7156	0.71903	-2.12418	3.7458
44.00	0.78692	-6.20999	3.3257	0.73951	-3.74801	3.4721	0.72790	-2.04342	3.5040
46.00	0.79343	-5.99353	3.0511	0.74726	-3.61599	3.2041	0.73595	-1.97122	3.2375
48.00	0.79935	-5.79893	2.7515	0.75432	+3.49753	2.9103	0.74327	-1.90647	2.9451
50.00	0.80473	-5.62360	2.4254	0.76074	-3.38097	2.5897	0.74994	-1.84825	2.6258
52.00	0.80962	-5.46533	2.0713	0.76658	+3.29494	2.2405	0.75601	+1.79581	2.2777
54.00	0.81408	-5.32233	1.6871	0.77191	-3.20828	1.8607	0.76155	-1.74851	1.8990
56.00	0.81813	-5.19300	1.2702	0.77677	-3.13001	1.4479	0.76660	+1.70580	1.4872
58.00	0.82183	-5.07805	0.8177	0.78119	-3.05930	0.9992	0.77119	-1.66723	1.0393
60.00	0.82518	-4.97033	0.3259	0.78521	-2.99544	0.5107	0.77537	+1.63241	0.5517
62.00	0.82823	-4.87488	-0.2098	0.78886	-2.83784	-0.0218	0.77916	-1.60100	0.0199
64.00	0.83098	-4.78886	-0.7948	0.79217	-2.88597	-0.6041	0.78260	+1.57273	-0.5617
66.00	0.83347	-4.71154	-1.4363	0.79516	-2.83939	-1.2430	0.78570	-1.54735	-1.2001
68.00	0.83571	+4.64232	-2.1430	0.79784	-2.79770	+1.9475	0.78849	-1.52464	+1.9040
70.00	0.83771	-4.58065	-2.9263	0.80024	+2.76058	+2.7288	0.79099	-1.50442	+2.6848
72.00	0.83948	-4.52607	-3.8015	0.80237	-2.72776	-3.6022	0.79321	-1.48654	-3.5578
74.00	0.84104	-4.47819	-4.7890	0.80424	+2.69897	-4.5881	0.79515	-1.47086	-4.5433
76.00	0.84240	-4.43667	-5.9177	0.80587	-2.67401	-5.7154	0.79685	-1.45728	-5.6703
78.00	0.84356	-4.40123	-7.2297	0.80727	-2.65272	-7.0263	0.79830	+1.44566	-6.9809
80.00	0.84453	-4.37162	-8.7906	0.80843	+2.63494	-8.5862	0.79951	-1.43600	-8.5406
82.00	0.84531	-4.34765	-10.7103	0.80938	-2.62054	-10.5051	0.80050	-1.42816	+10.4593
84.00	0.84592	-4.32916	-13.1948	0.81011	-2.60945	-12.9889	0.80126	-1.42212	+12.9430
86.00	0.84635	-4.31604	-16.7064	0.81063	-2.60157	-16.5001	0.80179	-1.41783	-16.4940
88.00	0.84661	-4.30820	-22.7208	0.81094	+2.59687	-22.5143	0.80212	-1.41527	-22.4681
90.00	0.84670	-4.30559	-140.7650	0.81104	-2.59530	-140.5584	0.80222	-1.41442	+140.5123
	Radiation Efficiency ETA = 0.5839, H =-0.249E+01 (dB)			Radiation Efficiency ETA = 0.5201, H =-0.284E+01 (dB)			Radiation Efficiency ETA = 0.5115, H =-0.291E+01 (dB)		

Table A8-15 Case 3: Fresh Water, $N = 2$ ($h = 2 \times 0.05\lambda$)

N=2, CASE(3): Fresh Water (Relative Dielectric Constant = 80.0, Conductivity = 0.030000 S/m)

Grazing ang. deg	FREQUENCY = 6.0 MHz. Fresnel Reflect Coef		Directive gain	FREQUENCY = 15.0 MHz. Fresnel Reflect Coef		Directive gain	FREQUENCY = 30.0 MHz. Fresnel Reflect Coef		Directive gain
PSI(deg)	|Rv|	ang Rv(deg)	D(dBi)	|Rv|	ang Rv(deg)	D(dBi)	|Rv|	ang Rv(deg)	D(dBi)
0.00	1.00000	-180.00000	-999.9999	1.00000	-180.00000	-999.9999	1.00000	-180.00000	-999.9999
0.50	0.83894	-175.49135	-13.8003	0.85126	-178.03345	-14.7177	0.85354	-179.00006	-14.9057
1.00	0.70309	-170.76516	-8.4682	0.72332	-175.99016	-9.3244	0.72713	-177.96196	-9.5010
1.50	0.58017	-165.66431	-5.5919	0.61235	-173.78383	-6.3900	0.61698	-176.84261	-6.5557
2.00	0.49104	-159.87224	-3.6998	0.51541	-171.30886	-4.4435	0.52021	-175.58774	-4.5969
2.50	0.40955	-153.09621	-2.3334	0.43031	-168.41162	-3.0764	0.43481	-174.12224	-3.1722
3.00	0.34241	-144.96724	-1.2804	0.35541	-164.88284	-1.9363	0.35845	-172.33318	-2.0730
3.50	0.28815	-135.11427	-0.4639	0.28957	-160.38875	-1.0661	0.29041	-170.03693	-1.1943
4.00	0.24988	-123.33838	0.2090	0.23217	-154.38623	-0.3527	0.27951	-166.90907	-0.4730
5.00	0.21363	-85.87459	1.2405	0.14395	-133.80187	0.7513	0.12723	-154.69259	0.6454
6.00	0.22377	-70.96504	1.9939	0.10523	-94.41348	1.5675	0.05995	-114.20327	1.4742
7.00	0.25760	-53.81433	2.5668	0.12537	-56.40618	2.1950	0.07561	-46.19757	2.1129
8.00	0.29649	-42.81393	3.0149	0.17040	-37.19942	2.6909	0.13010	-24.50038	2.5187
9.00	0.33926	-35.51364	3.3725	0.21803	-27.61649	3.0907	0.18356	-16.79543	3.0273
10.00	0.37745	-30.39718	3.6622	0.26268	-22.09290	3.4177	0.23182	-12.94742	3.3823
12.00	0.44412	-23.74165	4.0943	0.34006	-16.02251	3.9131	0.31357	-8.08301	3.8712
14.00	0.49886	-19.59953	4.3885	0.40325	-12.73478	4.2587	0.37949	-7.11487	4.2279
16.00	0.54395	-16.76767	4.5873	0.45531	-10.85257	4.4988	0.43352	-5.80497	4.4783
18.00	0.58152	-14.69151	4.7159	0.49875	-9.20506	4.6635	0.47852	-5.07824	4.6500
20.00	0.61318	-13.10976	4.7890	0.53544	-8.13541	4.7672	0.51051	-4.47403	4.7604
22.00	0.64014	-11.86098	4.8182	0.56679	-7.31043	4.8222	0.54895	-4.01156	4.8212
24.00	0.66333	-10.84973	4.8101	0.59383	-6.65377	4.8365	0.57693	-3.64546	4.8406
26.00	0.68345	-10.01432	4.7697	0.61736	-6.11834	4.8156	0.60128	-3.34817	4.8241
28.00	0.70103	-9.31297	4.7004	0.63797	-5.67340	4.7634	0.62263	-3.10191	4.7759
30.00	0.71650	-8.71638	4.6045	0.65616	-5.29799	4.6827	0.64147	-2.89465	4.6987
32.00	0.73019	-8.20229	4.4839	0.67229	-4.97726	4.5755	0.65818	-2.71794	4.5946
34.00	0.74237	-7.75797	4.3396	0.68666	-4.70039	4.4433	0.67308	-2.56564	4.4652
36.00	0.75326	-7.36843	4.1725	0.69954	-4.45931	4.2869	0.68643	-2.43321	4.3113
38.00	0.76302	-7.02543	3.9827	0.71111	-4.24789	4.1068	0.69843	-2.31718	4.1335
40.00	0.77181	-6.72169	3.7704	0.72153	-4.06120	3.9033	0.70925	-2.21488	3.9320
42.00	0.77974	-6.45144	3.5353	0.73096	-3.89560	3.6762	0.71903	-2.12418	3.7066
44.00	0.78692	-6.20999	3.2770	0.73951	-3.74801	3.4250	0.72790	-2.04342	3.4573
46.00	0.79343	-5.99353	2.9946	0.74726	-3.61599	3.1492	0.73595	-1.97122	3.1831
48.00	0.79935	-5.79893	2.6873	0.75432	-3.49753	2.8478	0.74327	-1.90647	2.8830
50.00	0.80473	-5.62360	2.3536	0.76074	-3.39097	2.5195	0.74994	-1.84825	2.5560
52.00	0.80962	-5.46533	1.9918	0.76658	-3.29494	2.1627	0.75601	-1.79581	2.2004
54.00	0.81406	-5.32233	1.6002	0.77191	-3.20828	1.7755	0.76155	-1.74851	1.8143
56.00	0.81812	-5.19300	1.1760	0.77677	-3.13001	1.3555	0.76660	-1.70560	1.3953
58.00	0.82183	-5.07605	0.7164	0.78119	-3.05930	0.8996	0.77119	-1.66723	0.9403
60.00	0.82518	-4.97033	0.2178	0.78521	-2.99544	0.4044	0.77537	-1.63241	0.4459
62.00	0.82823	-4.87488	-0.3245	0.78886	-2.93784	-0.1348	0.77916	-1.60100	-0.0925
64.00	0.83098	-4.78886	-0.9158	0.79217	-2.88597	-0.7233	0.78260	-1.57279	-0.6804
66.00	0.83347	-4.71154	-1.5632	0.79516	-2.83939	-1.3682	0.78570	-1.54735	-1.3247
68.00	0.83571	-4.64232	-2.2755	0.79784	-2.79770	-2.0782	0.78849	-1.52464	-2.0341
70.00	0.83771	-4.58065	-3.0640	0.80024	-2.76058	-2.8647	0.79099	-1.50442	-2.8202
72.00	0.83948	-4.52607	-3.9440	0.80237	-2.72776	-3.7429	0.79321	-1.48654	-3.6979
74.00	0.84104	-4.47819	-4.9359	0.80424	-2.69897	-4.7332	0.79515	-1.47086	-4.6878
76.00	0.84240	-4.43667	-6.0664	0.80587	-2.67401	-5.8643	0.79685	-1.45726	-5.8186
78.00	0.84356	-4.40123	-7.3638	0.80727	-2.65272	-7.1786	0.79830	-1.44568	-7.1326
80.00	0.84453	-4.37162	-8.9477	0.80843	-2.63494	-8.7414	0.79951	-1.43600	-8.6952
82.00	0.84531	-4.34765	-10.8698	0.80938	-2.62054	-10.6627	0.80050	-1.42818	-10.6163
84.00	0.84592	-4.32916	-13.3561	0.81011	-2.60945	-13.1484	0.80126	-1.42212	-13.1018
86.00	0.84635	-4.31604	-16.8690	0.81063	-2.60157	-16.6609	0.80179	-1.41783	-16.6142
88.00	0.84661	-4.30820	-22.8643	0.81094	-2.59687	-22.6759	0.80212	-1.41527	-22.6292
90.00	0.84670	-4.30559	-140.9288	0.81104	-2.59530	-140.7203	0.80222	-1.41442	-140.6736
	Radiation Efficiency ETA = 0.5588, M =-0.253E+01 (dB)			Radiation Efficiency ETA = 0.5165, M =-0.287E+01 (dB)			Radiation Efficiency ETA = 0.5088, M =-0.293E+01 (dB)		

Table A8-16 Case 3: Fresh Water, $N = 3$ ($h = 3 \times 0.05\lambda$)

N=3, CASE(3): Fresh Water (Relative Dielectric Constant = 80.0, Conductivity = 0.030000 S/m)

Grazing ang. deg	FREQUENCY = 6.0 MHz, Fresnel Reflect Coef		Directive gain	FREQUENCY = 15.0 MHz, Fresnel Reflect Coef		Directive gain	FREQUENCY = 30.0 MHz, Fresnel Reflect Coef		Directive gain
PSI(deg)	|Rv|	ang Rv(deg)	D(dBi)	|Rv|	ang Rv(deg)	D(dBi)	|Rv|	ang Rv(deg)	D(dBi)
0.00	1.00000	-180.00000	-999.9999	1.00000	-180.00000	-999.9999	1.00000	-180.00000	-999.9999
0.50	0.83894	-175.49135	-13.7004	0.85125	-178.03345	-14.6155	0.85354	-179.00008	-14.8030
1.00	0.70309	-170.78516	-8.3684	0.72332	-175.99016	-9.2222	0.72713	-177.96198	-9.3985
1.50	0.58817	-165.86431	-5.4922	0.61235	-173.78383	-6.2879	0.61698	-176.84251	-6.4533
2.00	0.49104	-159.87224	-3.6003	0.51591	-171.30686	-4.3416	0.52021	-175.58774	-4.4967
2.50	0.40955	-153.08621	-2.2342	0.43031	-168.41162	-2.9246	0.43461	-174.12224	-3.0703
3.00	0.34241	-144.55724	-1.1915	0.35941	-164.98354	-1.8350	0.36845	-172.33318	-1.9714
3.50	0.28915	-135.11427	-0.3654	0.28957	-160.38875	-0.9652	0.29041	-170.03693	-1.0931
4.00	0.24989	-123.33838	0.3071	0.23217	-154.38623	-0.2527	0.22951	-166.90907	-0.3722
4.50	0.21369	-95.87459	1.3375	0.14395	-133.80182	0.8507	0.12723	-154.89259	0.7451
5.00	0.22377	-70.96504	2.0696	0.10523	-84.41348	1.6656	0.05995	-114.20327	1.5727
5.50	0.25760	-53.81433	2.6610	0.12537	-56.40618	2.2916	0.07561	-46.19757	2.2099
6.00	0.29849	-42.81393	3.1074	0.17040	-37.19947	2.7858	0.13010	-24.50036	2.7140
6.50	0.33926	-35.51364	3.4630	0.21803	-27.61649	3.1836	0.18255	-16.75543	3.1207
7.00	0.37745	-30.39716	3.7605	0.26268	-22.09290	3.5085	0.23182	-12.84742	3.4534
7.50	0.41412	-26.74165	4.1776	0.34006	-16.02751	3.9989	0.31357	-9.08301	3.9574
8.00	0.44885	-18.59953	4.4660	0.40325	-12.73478	4.3388	0.37949	-7.11487	4.3083
8.50	0.54395	-16.76267	4.6580	0.45531	-10.65257	4.5730	0.43352	-5.90497	4.5520
9.00	0.58152	-14.69151	4.7787	0.49875	-9.20506	4.7292	0.47852	-5.07824	4.7161
9.50	0.61318	-13.10976	4.8440	0.53544	-8.13541	4.8247	0.51651	-4.47403	4.8183
10.00	0.64014	-11.86096	4.8642	0.56679	-7.31043	4.8707	0.54895	-4.01156	4.8702
10.50	0.66333	-10.84973	4.8484	0.59383	-6.65377	4.8754	0.57693	-3.64546	4.8800
11.00	0.68345	-10.01432	4.7957	0.61736	-6.11834	4.8442	0.60126	-3.34817	4.8533
11.50	0.70103	-9.31297	4.7155	0.63797	-5.67340	4.7811	0.62263	-3.10191	4.7942
12.00	0.71650	-8.71638	4.6082	0.65616	-5.29799	4.6890	0.64147	-2.89455	4.7056
12.50	0.73019	-8.20329	4.4757	0.67229	-4.97726	4.5700	0.65819	-2.71794	4.5887
13.00	0.74237	-7.75797	4.3191	0.68666	-4.70039	4.4255	0.67308	-2.56564	4.4480
13.50	0.75326	-7.36843	4.1392	0.69954	-4.45931	4.2565	0.68643	-2.43321	4.2815
14.00	0.76302	-7.02343	3.9364	0.71111	-4.24784	4.0634	0.69843	-2.31718	4.0908
14.50	0.77181	-6.72169	3.7109	0.72153	-4.06120	3.8467	0.70925	-2.21488	3.8762
15.00	0.77974	-6.45144	3.4624	0.73098	-3.89560	3.6062	0.71903	-2.12418	3.6376
15.50	0.78692	-6.20999	3.1906	0.73951	-3.74801	3.3416	0.72790	-2.04342	3.3747
16.00	0.79343	-5.99353	2.8947	0.74726	-3.61599	3.0522	0.73595	-1.97127	3.0869
16.50	0.79935	-5.79893	2.5737	0.75432	-3.49753	2.7373	0.74327	-1.90647	2.7734
17.00	0.80473	-5.62360	2.2266	0.76074	-3.39097	2.3956	0.74994	-1.84825	2.4330
17.50	0.80982	-5.46533	1.8516	0.76658	-3.29494	2.0255	0.75601	-1.79581	2.0642
18.00	0.81408	-5.32233	1.4468	0.77191	-3.20828	1.6253	0.76155	-1.74851	1.6650
18.50	0.81813	-5.19300	1.0098	0.77677	-3.13001	1.1925	0.76660	-1.70580	1.2332
19.00	0.82183	-5.07605	0.5378	0.78119	-3.05930	0.7242	0.77119	-1.66723	0.7659
19.50	0.82518	-4.97033	0.0271	0.78521	-2.99544	0.2170	0.77537	-1.63241	0.2595
20.00	0.82823	-4.87488	-0.5267	0.78886	-2.93784	-0.3337	0.77916	-1.60100	-0.2804
20.50	0.83098	-4.78886	-1.1291	0.79217	-2.88597	-0.9333	0.78260	-1.57273	-0.8893
21.00	0.83347	-4.71154	-1.7870	0.79516	-2.83939	-1.5886	0.78570	-1.54735	-1.5440
21.50	0.83571	-4.64232	-2.5091	0.79784	-2.79770	-2.3084	0.78849	-1.52464	-2.2632
22.00	0.83771	-4.58065	-3.3069	0.80024	-2.76058	-3.1041	0.79099	-1.50442	-3.0584
22.50	0.83948	-4.52607	-4.1953	0.80237	-2.72776	-3.9907	0.79321	-1.48654	-3.9445
23.00	0.84104	-4.47818	-5.1948	0.80424	-2.69897	-4.9866	0.79515	-1.47086	-4.9420
23.50	0.84240	-4.43667	-6.3342	0.80587	-2.67401	-6.1266	0.79685	-1.45728	-6.0797
24.00	0.84358	-4.40123	-7.6557	0.80727	-2.65272	-7.4468	0.79830	-1.44568	-7.3996
24.50	0.84458	-4.37162	-9.2247	0.80843	-2.63494	-9.0148	0.79951	-1.43600	-8.9674
25.00	0.84531	-4.34765	-11.1510	0.80938	-2.62054	-10.9404	0.80050	-1.42816	-10.8927
25.50	0.84592	-4.32916	-13.5406	0.81011	-2.60945	-13.4294	0.80126	-1.42212	-13.3815
26.00	0.84635	-4.31604	-17.1560	0.81063	-2.60157	-16.9443	0.80179	-1.41783	-16.8963
26.50	0.84661	-4.30820	-23.1727	0.81094	-2.59687	-22.9607	0.80212	-1.41527	-22.9127
27.00	0.84670	-4.30559	-141.2176	0.81104	-2.59530	-141.0056	0.80222	-1.41442	-140.9576

Radiation Efficiency	Radiation Efficiency	Radiation Efficiency
ETA = 0.5515, H =-0.258E+01 (dB)	ETA = 0.5113, H =-0.291E+01 (dB)	ETA = 0.5046, H =-0.297E+01 (dB)

Table A8-17 Case 3: Fresh Water, $N = 4$ ($h = 4 \times 0.05\lambda$)

N=4, CASE(3): Fresh Water [Relative Dielectric Constant = 80.0, Conductivity = 0.030000 S/m)

Grazing ang. deg	FREQUENCY = 5.0 MHz. Fresnel Reflect Coef		Directive gain	FREQUENCY = 15.0 MHz. Fresnel Reflect Coef		Directive gain	FREQUENCY = 30.0 MHz. Fresnel Reflect Coef		Directive gain
PSI(deg)	|Rv|	ang Rv(deg)	D(dBi)	|Rv|	ang Rv(deg)	D(dBi)	|Rv|	ang Rv(deg)	D(dBi)
0.00	1.00000	-180.00000	-999.9999	1.00000	-180.00000	-999.9999	1.00000	-180.00000	-999.9999
0.50	0.83894	-175.49135	-13.5536	0.85125	-178.03345	-14.4653	0.85354	-179.00008	-14.6524
1.00	0.70309	-170.78516	-8.2217	0.72332	-175.99016	-9.0722	0.72713	-177.96196	-9.2480
1.50	0.58817	-165.66431	-5.3457	0.61235	-173.78383	-6.1381	0.61698	-176.84261	-6.3030
2.00	0.49104	-159.87224	-3.4541	0.51541	-171.30686	-4.1921	0.52021	-175.58774	-4.3468
2.50	0.40955	-153.09621	-2.0884	0.43031	-168.41162	-2.7757	0.43461	-174.12224	-2.9207
3.00	0.34241	-144.96724	-1.0462	0.35941	-164.98354	-1.6864	0.36845	-172.33318	-1.8223
3.50	0.28915	-135.11427	-0.2206	0.30957	-160.88875	-0.8171	0.29041	-170.03693	-0.9445
4.00	0.24989	-123.33838	0.4512	0.27217	-155.98623	-0.1047	0.22951	-166.90907	-0.2243
5.00	0.21063	-95.87459	1.4800	0.14395	-133.80182	0.9966	0.12723	-154.69259	0.8915
6.00	0.22377	-70.96504	2.2303	0.10523	-94.41348	1.8098	0.05995	-114.20327	1.7172
7.00	0.25760	-53.81433	2.7994	0.12537	-56.40618	2.4334	0.07561	-46.19757	2.3521
8.00	0.29849	-42.81393	3.2432	0.17040	-37.19942	2.9250	0.13010	-24.50036	2.8536
9.00	0.33976	-35.51364	3.5959	0.21803	-27.61649	3.3199	0.18355	-16.79543	3.2574
10.00	0.37745	-30.39718	3.8801	0.26766	-22.09280	3.6415	0.23182	-12.94742	3.5870
12.00	0.44412	-22.74165	4.2997	0.34006	-16.02251	4.1245	0.31357	-9.08301	4.0834
14.00	0.49885	-19.59953	4.5793	0.40325	-12.73478	4.4555	0.37949	-7.11487	4.4256
16.00	0.54395	-16.76267	4.7613	0.45531	-10.65257	4.6799	0.43352	-5.90497	4.6594
18.00	0.58152	-14.69151	4.8706	0.49875	-9.20506	4.8250	0.47852	-5.07824	4.8124
20.00	0.61318	-13.10976	4.9237	0.53544	-8.13541	4.9081	0.51651	-4.47403	4.9023
22.00	0.64014	-11.86098	4.9305	0.56679	-7.31043	4.9407	0.54885	-4.01156	4.9409
24.00	0.66313	-10.84973	4.8983	0.59383	-6.65377	4.9310	0.57693	-3.64548	4.9363
26.00	0.68345	-10.01432	4.8321	0.61736	-6.11834	4.8844	0.60178	-3.34817	4.8942
28.00	0.70103	-9.31297	4.7355	0.63797	-5.67340	4.8051	0.62363	-3.10191	4.8189
30.00	0.71650	-8.71638	4.6111	0.65616	-5.28799	4.6959	0.64347	-2.89465	4.7133
32.00	0.73019	-8.20329	4.4607	0.67229	-4.97726	4.5591	0.66818	-2.71794	4.5797
34.00	0.74237	-7.75797	4.2855	0.68666	-4.70039	4.3961	0.67308	-2.56564	4.4196
36.00	0.75326	-7.36843	4.0865	0.69954	-4.45931	4.2080	0.68643	-2.43321	4.2341
38.00	0.76302	-7.02543	3.8642	0.71111	-4.24784	3.9955	0.69843	-2.31718	4.0240
40.00	0.77181	-6.72169	3.6187	0.72153	-4.06120	3.7589	0.70925	-2.21488	3.7895
42.00	0.77974	-6.45144	3.3499	0.73096	-3.89560	3.4982	0.71903	-2.12418	3.5308
44.00	0.78692	-6.20999	3.0576	0.73951	-3.74801	3.2132	0.72790	-2.04342	3.2476
46.00	0.79343	-5.99353	2.7412	0.74726	-3.61599	2.9035	0.73595	-1.97122	2.9395
48.00	0.79935	-5.79893	2.3997	0.75432	-3.49753	2.5681	0.74327	-1.90647	2.6056
50.00	0.80473	-5.62360	2.0321	0.76074	-3.39097	2.2060	0.74994	-1.84825	2.2450
52.00	0.80962	-5.46533	1.6368	0.76658	-3.29494	1.8159	0.75601	-1.79581	1.8561
54.00	0.81408	-5.32233	1.2122	0.77191	-3.20828	1.3958	0.76155	-1.74851	1.4372
56.00	0.81813	-5.19300	0.7557	0.77677	-3.13001	0.9436	0.76660	-1.70580	0.9861
58.00	0.82183	-5.07605	0.2647	0.78119	-3.05930	0.4564	0.77119	-1.66723	0.4999
60.00	0.82518	-4.97033	-0.2644	0.78521	-2.99544	0.0691	0.77537	-1.63241	-0.0248
62.00	0.82823	-4.87488	-0.8359	0.78885	-2.93784	-0.6374	0.77916	-1.60100	-0.5923
64.00	0.83098	-4.78886	-1.4553	0.79217	-2.88597	-1.2538	0.78260	-1.57273	-1.2079
66.00	0.83347	-4.71154	-2.1292	0.79518	-2.83939	-1.9251	0.78570	-1.54735	-1.8785
68.00	0.83571	-4.64232	-2.8664	0.79784	-2.79770	-2.6599	0.78849	-1.52464	-2.6127
70.00	0.83771	-4.58065	-3.6782	0.80024	-2.76058	-3.4696	0.79099	-1.50442	-3.4218
72.00	0.83948	-4.52607	-4.5796	0.80237	-2.72778	-4.3691	0.79321	-1.48654	-4.3208
74.00	0.84104	-4.47819	-5.5909	0.80424	-2.69897	-5.3767	0.79515	-1.47086	-5.3300
76.00	0.84240	-4.43667	-6.7406	0.80587	-2.67401	-6.5272	0.79685	-1.45728	-6.4781
78.00	0.84356	-4.40123	-8.0715	0.80727	-2.65272	-7.8566	0.79830	-1.44568	-7.8072
80.00	0.84453	-4.37162	-9.6484	0.80843	-2.63494	-9.4325	0.79951	-1.43600	-9.3828
82.00	0.84531	-4.34765	-11.5813	0.80938	-2.62054	-11.3645	0.80050	-1.42816	-11.3146
84.00	0.84592	-4.32916	-14.0760	0.81011	-2.60945	-13.8586	0.80126	-1.42212	-13.8085
86.00	0.84635	-4.31604	-17.5950	0.81063	-2.60157	-17.3772	0.80179	-1.41783	-17.3269
88.00	0.84661	-4.30820	-23.6140	0.81094	-2.59687	-23.3958	0.80212	-1.41527	-23.3455
90.00	0.84670	-4.30559	-141.6597	0.81104	-2.59530	-141.4414	0.80222	-1.41442	-141.3911

Radiation Efficiency	Radiation Efficiency	Radiation Efficiency
ETA = 0.5424, H =-0.266E+01 [dB]	ETA = 0.5044, H =-0.297E+01 [dB]	ETA = 0.4989, H =-0.302E+01 [dB]

Table A8-18 Case 3: Fresh Water, $N = 5$ ($h = 5 \times 0.05\lambda$)

N=5, CASE(3): Fresh Water (Relative Dielectric Constant = 80.0, Conductivity = 0.330000 S/m)

Grazing ang, deg	FREQUENCY = 6.0 MHz. Fresnel Reflect Coef		Directive gain	FREQUENCY = 15.0 MHz. Fresnel Reflect Coef		Directive gain	FREQUENCY = 30.0 MHz. Fresnel Reflect Coef		Directive gain
PSI(deg)	|Rv|	ang Rv(deg)	D(dBi)	|Rv|	ang Rv(deg)	D(dBi)	|Rv|	ang Rv(deg)	D(dBi)
0.00	1.00000	-180.00000	-999.9999	1.00000	-180.00000	-999.9999	1.00000	-180.00000	-999.9999
0.50	0.83894	-175.49135	-13.3519	0.85125	-178.03345	-14.2593	0.85354	-179.00006	-14.4480
1.00	0.70309	-170.78516	-8.0203	0.72332	-175.89016	-8.6664	0.72713	-177.96196	-8.8418
1.50	0.58817	-165.68431	-5.1445	0.61235	-173.78383	-5.9326	0.61698	-176.84261	-6.0971
2.00	0.49104	-159.87224	-3.2534	0.51541	-171.30666	-3.9870	0.52021	-175.58774	-4.1413
2.50	0.40955	-153.09821	-1.8882	0.43031	-168.41162	-2.5772	0.43481	-174.13224	-2.7158
3.00	0.34241	-144.56724	-0.8467	0.35541	-164.88355	-1.4625	0.35845	-172.33318	-1.6180
3.50	0.28915	-135.11427	-0.0219	0.28957	-160.38875	-0.6140	0.29041	-170.03693	-0.7411
4.00	0.24989	-123.33838	0.6490	0.23217	-154.38623	0.0974	0.22951	-166.90907	-0.0217
5.00	0.21363	-95.87459	1.6756	0.14395	-133.80182	1.1966	0.12723	-154.89259	1.0919
6.00	0.22377	-70.86504	2.4232	0.10523	-94.41348	2.0070	0.05995	-114.20327	1.9150
7.00	0.25760	-53.81433	2.9893	0.12537	-56.40618	2.6276	0.07561	-46.19757	2.5468
8.00	0.29849	-42.81383	3.4294	0.17040	-37.19942	3.1156	0.13010	-24.50036	3.0447
9.00	0.33928	-35.51364	3.7760	0.21803	-27.61649	3.5065	0.18355	-16.78543	3.4445
10.00	0.37745	-30.39718	4.0577	0.26288	-22.09290	3.8238	0.23182	-12.84742	3.7895
12.00	0.44412	-23.74165	4.4668	0.34006	-16.02251	4.2961	0.31357	-9.08301	4.2556
14.00	0.49885	-19.59953	4.7341	0.40325	-12.73478	4.6148	0.37949	-7.11487	4.5856
16.00	0.54395	-16.76267	4.9020	0.45531	-10.65757	4.8253	0.43352	-5.90497	4.8055
18.00	0.58152	-14.69151	4.9957	0.49875	-9.20506	4.9547	0.47852	-5.07824	4.9429
20.00	0.61318	-13.10976	5.0313	0.53544	-8.13541	5.0205	0.51551	-4.47403	5.0156
22.00	0.64014	-11.86098	5.0191	0.56679	-7.31043	5.0344	0.54885	-4.01156	5.0354
24.00	0.66333	-10.84973	4.9664	0.59383	-6.65377	5.0043	0.57693	-3.64546	5.0106
26.00	0.68345	-10.01432	4.8784	0.61736	-6.11834	4.9361	0.60128	-3.34817	4.9469
28.00	0.70103	-9.31297	4.7587	0.63797	-5.67340	4.8338	0.62263	-3.10191	4.8488
30.00	0.71650	-8.71638	4.6100	0.65616	-5.29799	4.7005	0.64147	-2.89465	4.7191
32.00	0.73019	-8.20329	4.4342	0.67229	-4.97726	4.5384	0.65818	-2.71794	4.5604
34.00	0.74237	-7.75797	4.2327	0.68666	-4.70039	4.3493	0.67308	-2.56564	4.3742
36.00	0.75326	-7.36843	4.0084	0.69954	-4.45931	4.1341	0.68643	-2.43321	4.1618
38.00	0.76302	-7.02543	3.7561	0.71111	-4.24784	3.8939	0.69843	-2.31716	3.9240
40.00	0.77181	-6.72159	3.4821	0.72153	-4.06120	3.6289	0.70925	-2.21488	3.6613
42.00	0.77974	-6.45144	3.1843	0.73096	-3.89560	3.3394	0.71903	-2.12418	3.3739
44.00	0.78692	-6.20999	2.8626	0.73951	-3.74801	3.0253	0.72790	-2.04342	3.0617
46.00	0.79343	-5.99353	2.5166	0.74726	-3.61599	2.6862	0.73595	-1.97122	2.7244
48.00	0.79935	-5.79893	2.1456	0.75432	-3.49753	2.3214	0.74327	-1.90647	2.3613
50.00	0.80473	-5.62360	1.7485	0.76074	-3.39087	1.9301	0.74994	-1.84825	1.9715
52.00	0.80962	-5.46533	1.3240	0.76658	-3.29484	1.5109	0.75601	-1.79581	1.5537
54.00	0.81408	-5.32233	0.8704	0.77191	-3.20828	1.0621	0.76155	-1.74851	1.1063
56.00	0.81813	-5.19300	0.3856	0.77677	-3.13001	0.5816	0.76660	-1.70580	0.6271
58.00	0.82183	-5.07605	-0.1331	0.78119	-3.05930	0.0672	0.77119	-1.66723	0.1136
60.00	0.82518	-4.97033	-0.6890	0.78521	-2.99544	-0.4850	0.77537	-1.63241	-0.4375
62.00	0.82823	-4.87488	-1.2864	0.78886	-2.93784	-1.0790	0.77916	-1.60100	-1.0306
64.00	0.83098	-4.78886	-1.9304	0.79217	-2.88597	-1.7200	0.78260	-1.57273	-1.6707
66.00	0.83347	-4.71154	-2.6279	0.79516	-2.83939	-2.4146	0.78570	-1.54735	-2.3645
68.00	0.83571	-4.64232	-3.3873	0.79784	-2.79770	-3.1714	0.78849	-1.52464	-3.1206
70.00	0.83771	-4.58065	-4.2197	0.80024	-2.76058	-4.0016	0.79099	-1.50442	-3.9501
72.00	0.83948	-4.52607	-5.1402	0.80237	-2.72776	-4.9200	0.79321	-1.48654	-4.8679
74.00	0.84104	-4.47819	-6.1688	0.80424	-2.69857	-5.9468	0.79515	-1.47086	-5.8942
76.00	0.84240	-4.43667	-7.3343	0.80587	-2.67401	-7.1108	0.79685	-1.45726	-7.0577
78.00	0.84356	-4.40123	-8.6787	0.80727	-2.65272	-8.4538	0.79830	-1.44568	-8.4003
80.00	0.84453	-4.37162	-10.2673	0.80843	-2.63494	-10.0413	0.79951	-1.43600	-9.9874
82.00	0.84531	-4.34765	-12.2099	0.80938	-2.62054	-11.9829	0.80050	-1.42816	-11.9288
84.00	0.84592	-4.32916	-14.7122	0.81011	-2.60945	-14.4845	0.80126	-1.42212	-14.4302
86.00	0.84635	-4.31604	-18.2367	0.81063	-2.60157	-18.0084	0.80179	-1.41783	-17.9540
88.00	0.84661	-4.30820	-24.2589	0.81094	-2.59687	-24.0303	0.80212	-1.41527	-23.9758
90.00	0.84670	-4.30559	-142.3097	0.81104	-2.59530	-142.0770	0.80222	-1.41442	-142.0225
	Radiation Efficiency			Radiation Efficiency			Radiation Efficiency		
	ETA = 0.5312, H =-0.275E+01 (dB)			ETA = 0.4956, H =-0.305E+01 (dB)			ETA = 0.4916, H =-0.308E+01 (dB)		

Table A8-19 Case 4: Wet Ground, $N = 0$ ($h = 0 \times 0.05\lambda$)

N=0, CASE(4): Wet Ground (Relative Dielectric Constant = 30.0, Conductivity = 0.010000 S/m)

Grazing ang. deg	FREQUENCY = 5.0 MHz. Fresnel Reflect Coef		Directive gain	FREQUENCY = 15.0 MHz. Fresnel Reflect Coef		Directive gain	FREQUENCY = 30.0 MHz. Fresnel Reflect Coef		Directive gain
PSI(deg)	|Rv|	ang Rv(deg)	D(dBi)	|Rv|	ang Rv(deg)	D(dBi)	|Rv|	ang Rv(deg)	D(dBi)
0.00	1.00000	-180.00000	-999.9999	1.00000	-180.00000	-999.9999	1.00000	-180.00000	-999.9999
0.50	0.89913	-177.53148	-17.0270	0.90572	-178.94031	-17.7075	0.90888	-179.46329	-17.8355
1.00	0.80820	-175.02328	-11.4400	0.81997	-177.86513	-12.0093	0.82206	-178.91888	-12.2117
1.50	0.72605	-172.43419	-8.3347	0.74170	-176.75835	-8.9534	0.74449	-178.35872	-9.0705
2.00	0.65170	-169.71970	-6.2364	0.67007	-175.60228	-6.8256	0.67331	-177.77399	-6.9375
2.50	0.58435	-166.83031	-4.6839	0.60417	-174.37687	-5.2445	0.60777	-177.15462	-5.3513
3.00	0.52334	-163.70963	-3.4721	0.54353	-173.05827	-4.0053	0.54724	-176.48869	-4.1072
3.50	0.46815	-160.29240	-2.4921	0.48756	-171.61778	-2.9990	0.49116	-175.76157	-3.0962
4.00	0.41835	-156.50290	-1.6792	0.43581	-170.01923	-2.1609	0.43915	-174.95476	-2.2536
5.00	0.33389	-147.44798	-0.4018	0.34352	-166.14746	-0.8364	0.34582	-172.88739	-0.9206
6.00	0.26892	-135.76707	0.5602	0.26445	-160.85295	0.1686	0.26413	-170.29880	0.0924
7.00	0.22391	-120.91679	1.3121	0.19754	-153.01488	0.9597	0.19295	-166.18292	0.8907
8.00	0.19972	-103.51068	1.9153	0.14340	-140.41918	1.5987	0.13122	-158.98991	1.5364
9.00	0.19508	-85.89762	2.4085	0.10591	-119.41214	2.1240	0.08013	-143.57930	2.0886
10.00	0.20536	-70.66362	2.8178	0.09252	-89.66296	2.5641	0.04933	-104.43576	2.5135
12.00	0.24836	-49.87074	3.4513	0.12927	-45.24990	3.2506	0.09106	-31.45758	3.2102
14.00	0.29901	-38.06417	3.9067	0.18885	-28.48850	3.7532	0.15944	-17.03982	3.7215
16.00	0.34723	-30.86202	4.2475	0.24531	-20.98231	4.1257	0.22022	-11.96165	4.1015
18.00	0.39063	-26.07735	4.4847	0.29534	-16.80100	4.4014	0.27283	-9.37218	4.3839
20.00	0.42906	-22.67734	4.6560	0.33920	-14.13327	4.6020	0.31845	-7.79073	4.5902
22.00	0.46297	-20.13859	4.7703	0.37768	-12.27667	4.7419	0.35825	-6.71791	4.7352
24.00	0.49259	-18.18470	4.8372	0.41157	-10.90581	4.8315	0.39320	-5.93881	4.8293
26.00	0.51846	-16.58914	4.8636	0.44156	-9.84978	4.8779	0.42406	-5.34553	4.8798
28.00	0.54307	-15.30126	4.8543	0.46822	-9.01013	4.8866	0.45147	-4.87779	4.8920
30.00	0.56415	-14.22921	4.8130	0.49203	-8.32616	4.8613	0.47582	-4.49921	4.8689
32.00	0.58305	-13.32351	4.7422	0.51338	-7.75822	4.8049	0.49784	-4.18642	4.8165
34.00	0.60004	-12.54901	4.6438	0.53259	-7.27932	4.7195	0.51755	-3.92373	4.7337
36.00	0.61536	-11.87998	4.5191	0.54993	-6.87042	4.6065	0.53535	-3.70017	4.6231
38.00	0.62922	-11.29714	4.3688	0.56563	-6.51768	4.4668	0.55145	-3.50782	4.4856
40.00	0.64179	-10.78574	4.1936	0.57987	-6.21069	4.3010	0.56607	-3.34083	4.3218
42.00	0.65321	-10.33432	3.9929	0.59283	-5.94164	4.1093	0.57935	-3.19476	4.1318
44.00	0.66361	-9.93383	3.7670	0.60462	-5.70440	3.8914	0.59146	-3.06617	3.9158
46.00	0.67308	-9.57689	3.5152	0.61539	-5.49416	3.6469	0.60250	-2.95239	3.6726
48.00	0.68173	-9.25793	3.2367	0.62522	-5.30707	3.3750	0.61258	-2.85126	3.4020
50.00	0.68963	-8.97183	2.9301	0.63420	-5.14000	3.0745	0.62179	-2.76106	3.1028
52.00	0.69684	-8.71472	2.5940	0.64241	-4.99043	2.7440	0.63032	-2.68034	2.7734
54.00	0.70343	-8.48326	2.2264	0.64991	-4.85622	2.3815	0.63791	-2.60806	2.4120
56.00	0.70945	-8.27470	1.8250	0.65677	-4.73565	1.9847	0.64495	-2.54314	2.0161
58.00	0.71495	-8.08569	1.3868	0.66303	-4.62724	1.5508	0.65137	-2.48481	1.5830
60.00	0.71995	-7.91719	0.9082	0.66873	-4.52977	1.0760	0.65722	-2.43239	1.1090
62.00	0.72450	-7.76456	0.3847	0.67393	-4.44217	0.5560	0.66255	-2.38532	0.5898
64.00	0.72863	-7.62733	-0.1892	0.67864	-4.36358	-0.0147	0.66738	-2.34310	0.0197
66.00	0.73237	-7.50424	-0.8704	0.68290	-4.29319	-0.6431	0.67175	-2.30531	-0.6081
68.00	0.73573	-7.39425	-1.5479	0.68673	-4.23040	-1.3379	0.67569	-2.27161	-1.3024
70.00	0.73874	-7.29642	-2.2928	0.69017	-4.17463	-2.1106	0.67921	-2.24170	-2.0746
72.00	0.74141	-7.20997	-3.1605	0.69322	-4.12541	-2.9762	0.68234	-2.21531	-2.9397
74.00	0.74377	-7.13423	-4.1413	0.69591	-4.08234	-3.9552	0.68510	-2.19221	-3.9184
76.00	0.74582	-7.06863	-5.2640	0.69825	-4.04508	-5.0763	0.68750	-2.17224	-5.0392
78.00	0.74757	-7.01268	-6.5710	0.70025	-4.01331	-6.3820	0.68955	-2.15522	-6.3446
80.00	0.74904	-6.96598	-8.1277	0.70193	-3.98681	-7.9375	0.69127	-2.14103	-7.8999
82.00	0.75023	-6.92821	-10.0439	0.70329	-3.96540	-9.8528	0.69267	-2.12955	-9.8150
84.00	0.75115	-6.89909	-12.5256	0.70434	-3.94890	-12.3338	0.69375	-2.12072	-12.2959
86.00	0.75180	-6.87843	-16.0353	0.70509	-3.93720	-15.8430	0.69451	-2.11445	-15.8049
88.00	0.75219	-6.86609	-22.0486	0.70553	-3.93021	-21.8560	0.69497	-2.11071	-21.8179
90.00	0.75232	-6.86198	-140.0924	0.70568	-3.92788	-139.8997	0.69513	-2.10946	-139.8616
	Radiation Efficiency			Radiation Efficiency			Radiation Efficiency		
	ETA = 0.4479, H =-0.349E+01 (dB)			ETA = 0.4069, H =-0.391E+01 (dB)			ETA = 0.3987, H =-0.399E+01 (dB)		

Table A8-20 Case 4: Wet Ground, $N = 1$ ($h = 1 \times 0.05\lambda$)

N=1, CASE(4): Wet Ground (Relative Dielectric Constant = 30.0, Conductivity = 0.010000 S/m)

Grazing ang, deg	FREQUENCY = 5.0 MHz. Fresnel Reflect Coef		Directive gain	FREQUENCY = 15.0 MHz. Fresnel Reflect Coef		Directive gain	FREQUENCY = 30.0 MHz. Fresnel Reflect Coef		Directive gain
PSI(deg)	|Rv|	ang Rv(deg)	D(dBi)	|Rv|	ang Rv(deg)	D(dBi)	|Rv|	ang Rv(deg)	D(dBi)
0.00	1.00000	-180.00000	-999.9999	1.00000	-180.00000	-999.9999	1.00000	-180.00000	-999.9999
0.50	0.89913	-177.53148	-16.9956	0.90572	-178.94031	-17.6756	0.90688	-179.46329	-17.8037
1.00	0.80820	-175.02328	-11.4086	0.81997	-177.86513	-12.0574	0.82206	-178.91888	-12.1800
1.50	0.72605	-172.43419	-8.3033	0.74170	-176.75836	-8.9215	0.74449	-178.35872	-9.0388
2.00	0.65170	-169.71970	-6.2052	0.67002	-175.60228	-6.7936	0.67331	-177.77399	-6.9059
2.50	0.58435	-166.83031	-4.6527	0.60417	-174.37682	-5.2128	0.60777	-177.15462	-5.3198
3.00	0.52334	-163.70983	-3.4410	0.54353	-173.05827	-3.9737	0.54724	-176.48869	-4.0758
3.50	0.46815	-160.29240	-2.4611	0.48756	-171.61778	-2.9675	0.49118	-175.76157	-3.0649
4.00	0.41835	-156.50290	-1.6483	0.43581	-170.01923	-2.1295	0.43915	-174.95476	-2.2223
5.00	0.33389	-147.44798	-0.3713	0.34352	-166.14746	-0.8053	0.34562	-172.99738	-0.8896
6.00	0.26882	-135.76707	0.5904	0.26445	-160.85295	0.1994	0.26413	-170.29680	0.1229
7.00	0.22391	-120.91679	1.3419	0.19754	-153.01488	0.9900	0.19295	-165.18292	0.9209
8.00	0.19972	-103.51065	1.9445	0.14340	-140.41916	1.6285	0.13122	-158.98991	1.5680
9.00	0.19508	-85.89782	2.4372	0.10591	-119.41214	2.1540	0.08813	-143.57930	2.0977
10.00	0.20536	-70.56352	2.8459	0.09252	-89.66296	2.5927	0.04933	-104.43576	2.5421
12.00	0.24836	-49.87074	3.4779	0.12927	-45.24930	3.2778	0.09106	-31.45258	3.2373
14.00	0.29901	-38.08417	3.9336	0.18885	-28.48850	3.7787	0.15944	-12.03982	3.7469
16.00	0.34723	-30.86202	4.2655	0.24631	-20.98231	4.1493	0.22022	-11.96165	4.1251
18.00	0.39063	-26.07735	4.5056	0.29534	-16.80100	4.4229	0.27283	-9.37218	4.4053
20.00	0.42906	-22.67734	4.6745	0.33920	-14.13327	4.6211	0.31845	-7.79073	4.6093
22.00	0.46297	-20.13659	4.7862	0.37768	-12.27667	4.7585	0.35825	-6.71791	4.7518
24.00	0.49292	-18.16470	4.8504	0.41157	-10.90581	4.8453	0.39320	-5.93681	4.8431
26.00	0.51946	-16.58814	4.8738	0.44156	-9.84976	4.8888	0.42406	-5.34553	4.8907
28.00	0.54307	-15.30126	4.8614	0.46822	-9.01013	4.8943	0.45147	-4.87779	4.8898
30.00	0.56415	-14.22821	4.8169	0.49203	-8.32616	4.8658	0.47592	-4.49921	4.8748
32.00	0.58305	-13.32351	4.7427	0.51338	-7.75822	4.8080	0.49784	-4.18642	4.8178
34.00	0.60004	-12.54901	4.6408	0.53259	-7.27932	4.7171	0.51755	-3.92373	4.7315
36.00	0.61536	-11.87998	4.5124	0.54993	-6.87042	4.6005	0.53535	-3.70017	4.6173
38.00	0.62922	-11.29714	4.3585	0.56563	-6.51756	4.4572	0.55145	-3.50782	4.4782
40.00	0.64179	-10.78574	4.1793	0.57987	-6.21089	4.2877	0.56607	-3.33483	4.3087
42.00	0.65321	-10.33432	3.9749	0.59283	-5.94164	4.0921	0.57935	-3.19478	4.1150
44.00	0.66361	-9.93383	3.7452	0.60462	-5.70440	3.8704	0.59146	-3.06617	3.8949
46.00	0.67308	-9.57699	3.4898	0.61539	-5.49416	3.6221	0.60250	-2.95239	3.6481
48.00	0.68173	-9.25793	3.2071	0.62522	-5.30707	3.3464	0.61258	-2.85126	3.3738
50.00	0.68963	-8.97183	2.8967	0.63420	-5.14000	3.0421	0.62179	-2.76106	3.0708
52.00	0.69684	-8.71472	2.5569	0.64241	-4.99043	2.7078	0.63022	-2.68038	2.7377
54.00	0.70343	-8.48326	2.1856	0.64991	-4.85622	2.3416	0.63791	-2.60806	2.3726
56.00	0.70945	-8.27470	1.7806	0.65677	-4.73565	1.9412	0.64495	-2.54314	1.9732
58.00	0.71496	-8.08658	1.3388	0.66302	-4.62724	1.5036	0.65137	-2.48481	1.5366
60.00	0.71995	-7.91719	0.8568	0.66873	-4.52977	1.0256	0.65722	-2.43239	1.0593
62.00	0.72450	-7.76456	0.3300	0.67393	-4.44217	0.5023	0.66255	-2.38532	0.5368
64.00	0.72863	-7.62733	-0.2470	0.67864	-4.36356	-0.0715	0.66738	-2.34310	-0.0384
66.00	0.73237	-7.50424	-0.8812	0.68290	-4.29319	-0.7028	0.67175	-2.30531	-0.6671
68.00	0.73573	-7.39425	-1.5614	0.68673	-4.23040	-1.4004	0.67569	-2.27161	-1.3641
70.00	0.73874	-7.29642	-2.3590	0.69017	-4.17463	-2.1756	0.67921	-2.24170	-2.1389
72.00	0.74141	-7.20987	-3.2290	0.69322	-4.12541	-3.0436	0.68234	-2.21531	-3.0064
74.00	0.74377	-7.13423	-4.2120	0.69591	-4.08234	-4.0247	0.68510	-2.19221	-3.9871
76.00	0.74582	-7.06863	-5.3367	0.69825	-4.04506	-5.1478	0.68750	-2.17224	-5.1099
78.00	0.74757	-7.01268	-6.8453	0.70025	-4.01331	-6.4551	0.68956	-2.15522	-6.4169
80.00	0.74904	-6.96598	-8.2034	0.70193	-3.98681	-8.0121	0.69127	-2.14103	-7.9736
82.00	0.75023	-6.92821	-10.1209	0.70329	-3.96540	-9.9286	0.69267	-2.12955	-9.8899
84.00	0.75115	-6.89909	-12.6035	0.70434	-3.94890	-12.4106	0.69375	-2.12072	-12.3717
86.00	0.75180	-6.87843	-16.1139	0.70509	-3.93720	-15.9204	0.69451	-2.11445	-15.8815
88.00	0.75219	-6.86609	-22.1276	0.70553	-3.93021	-21.9338	0.69497	-2.11071	-21.8948
90.00	0.75232	-6.86198	-140.1715	0.70568	-3.92788	-139.9777	0.69513	-2.10946	-139.9387
	Radiation Efficiency			Radiation Efficiency			Radiation Efficiency		
	ETA = 0.4391, H =-0.357E+01 (dB)			ETA = 0.4021, H =-0.396E+01 (dB)			ETA = 0.3959, H =-0.402E+01 (dB)		

Table A8-21 Case 4: Wet Ground, $N = 2$ ($h = 2 \times 0.05\lambda$)

N=2, CASE(4): Wet Ground (Relative Dielectric Constant = 30.0, Conductivity = 0.010000 S/m)

Grazing ang. deg	FREQUENCY = 6.0 MHz. Fresnel Reflect Coef		Directive gain	FREQUENCY = 15.0 MHz. Fresnel Reflect Coef		Directive gain	FREQUENCY = 30.0 MHz. Fresnel Reflect Coef		Directive gain
PSI(deg)	|Rv|	ang Rv(deg)	D(dBi)	|Rv|	ang Rv(deg)	D(dBi)	|Rv|	ang Rv(deg)	D(dBi)
0.00	1.00000	-180.00000	-999.9999	1.00000	-180.00000	-999.9999	1.00000	-180.00000	-999.9999
0.50	0.89913	-177.53148	-16.9327	0.90572	-178.94031	-17.6115	0.90888	-179.46329	-17.7396
1.00	0.80820	-175.02328	-11.3457	0.81997	-177.86513	-11.9933	0.82206	-178.91888	-12.1159
1.50	0.72605	-172.43419	-8.2405	0.74170	-176.75836	-8.8576	0.74449	-178.35872	-8.9748
2.00	0.65170	-169.71970	-6.1425	0.67002	-175.60228	-6.7299	0.67331	-177.77398	-6.8420
2.50	0.58435	-166.83031	-4.5902	0.60417	-174.37682	-5.1491	0.60777	-177.15462	-5.2581
3.00	0.52324	-163.70959	-3.3786	0.54353	-173.05827	-3.9102	0.54724	-176.48868	-4.0122
3.50	0.46815	-160.29240	-2.3990	0.48756	-171.61778	-2.9042	0.49118	-175.76157	-3.0015
4.00	0.41835	-156.50290	-1.5864	0.43581	-170.01923	-2.0664	0.43915	-174.95476	-2.1593
5.00	0.33389	-147.44798	-0.3100	0.34352	-166.14746	-0.7429	0.34562	-172.99739	-0.8272
6.00	0.26892	-135.76707	0.6510	0.26445	-160.85295	0.2611	0.26413	-170.29680	0.1847
7.00	0.22391	-120.91879	1.4015	0.19754	-153.01488	1.0509	0.19285	-166.18292	0.9817
8.00	0.19972	-103.51066	2.0032	0.14340	-140.41916	1.6884	0.13122	-158.98991	1.6259
9.00	0.19508	-85.88762	2.4948	0.10551	-119.41214	2.2127	0.08013	-143.57930	2.1565
10.00	0.20536	-70.66362	2.9021	0.08752	-89.66296	2.6502	0.04533	-104.43576	2.5996
12.00	0.24836	-48.87074	3.5313	0.12927	-45.24990	3.3324	0.09106	-31.45258	3.2919
14.00	0.29901	-38.06417	3.9836	0.18885	-28.48650	3.8298	0.15944	-17.03962	3.7981
16.00	0.34723	-30.86202	4.3116	0.24531	-20.98231	4.1966	0.22022	-11.96165	4.1725
18.00	0.39063	-26.07735	4.5473	0.29534	-16.80100	4.4659	0.27283	-9.37216	4.4484
20.00	0.42906	-22.67734	4.7115	0.33920	-14.13327	4.6593	0.31845	-7.79073	4.6476
22.00	0.46297	-20.13659	4.8180	0.37768	-12.27667	4.7916	0.35825	-6.71791	4.7850
24.00	0.49292	-18.16470	4.8766	0.41157	-10.90581	4.8728	0.39320	-5.93881	4.8708
26.00	0.51946	-16.58914	4.8941	0.44156	-9.85876	4.9104	0.42406	-5.34553	4.9135
28.00	0.54307	-15.30126	4.8754	0.46822	-9.01013	4.9097	0.45147	-4.87779	4.9154
30.00	0.56415	-14.22921	4.8242	0.49203	-8.32616	4.8746	0.47592	-4.49921	4.8836
32.00	0.58305	-13.32351	4.7432	0.51338	-7.75822	4.8090	0.49784	-4.18642	4.8200
34.00	0.60004	-12.54901	4.6342	0.53259	-7.27932	4.7120	0.51755	-3.92373	4.7267
36.00	0.61536	-11.87998	4.4985	0.54993	-6.87042	4.5891	0.53535	-3.70017	4.6052
38.00	0.62922	-11.29714	4.3371	0.56563	-6.51786	4.4373	0.55145	-3.50783	4.4567
40.00	0.64179	-10.78574	4.1503	0.57987	-6.21069	4.2602	0.56607	-3.34003	4.2816
42.00	0.65321	-10.33432	3.9383	0.59283	-5.94164	4.0570	0.57935	-3.19476	4.0803
44.00	0.66361	-9.93383	3.7008	0.60462	-5.70440	3.8276	0.59148	-3.08817	3.8525
46.00	0.67308	-9.57699	3.4373	0.61539	-5.49416	3.5715	0.60250	-2.95239	3.5980
48.00	0.68173	-9.25793	3.1471	0.62522	-5.30707	3.2880	0.61258	-2.85128	3.3159
50.00	0.68963	-8.97183	2.8290	0.63420	-5.14000	2.9760	0.62179	-2.76106	3.0053
52.00	0.69684	-8.71422	2.4815	0.64241	-4.99043	2.6342	0.63022	-2.68038	2.6646
54.00	0.70343	-8.48326	2.1026	0.64991	-4.85622	2.2605	0.63791	-2.60806	2.2921
56.00	0.70945	-8.27470	1.6904	0.65677	-4.73565	1.8529	0.64495	-2.54214	1.8854
58.00	0.71495	-8.08668	1.2415	0.66303	-4.62724	1.4083	0.65137	-2.48481	1.4418
60.00	0.71995	-7.91710	0.7526	0.66873	-4.52977	0.9232	0.65722	-2.43239	0.9576
62.00	0.72450	-7.76456	0.2197	0.67393	-4.44217	0.3934	0.66255	-2.38532	0.4285
64.00	0.72863	-7.62733	-0.3641	0.67864	-4.36356	-0.1867	0.66738	-2.34310	-0.1509
66.00	0.73237	-7.50424	-1.0043	0.68290	-4.29319	-0.8240	0.67175	-2.30531	-0.7875
68.00	0.73573	-7.39425	-1.7101	0.68673	-4.23040	-1.5272	0.67568	-2.27161	-1.4901
70.00	0.73874	-7.29642	-2.4929	0.69017	-4.17463	-2.3076	0.67921	-2.24170	-2.2701
72.00	0.74141	-7.20997	-3.3678	0.69322	-4.12541	-3.1804	0.68234	-2.21531	-3.1423
74.00	0.74377	-7.13423	-4.3551	0.69591	-4.08234	-4.1659	0.68510	-2.19221	-4.1274
76.00	0.74582	-7.06863	-5.4837	0.69825	-4.04508	-5.2929	0.68750	-2.17224	-5.2541
78.00	0.74757	-7.01268	-6.7958	0.70025	-4.01331	-6.6036	0.68955	-2.15522	-6.5645
80.00	0.74904	-6.98598	-8.3568	0.70193	-3.98681	-8.1635	0.69127	-2.14103	-8.1241
82.00	0.75023	-6.92821	-10.2767	0.70329	-3.96540	-10.0824	0.69267	-2.12955	-10.0428
84.00	0.75115	-6.89909	-12.7612	0.70434	-3.94890	-12.5662	0.69375	-2.12072	-12.5265
86.00	0.75180	-6.87843	-16.2729	0.70509	-3.93720	-16.0774	0.69451	-2.11445	-16.0376
88.00	0.75219	-6.86609	-22.2875	0.70553	-3.93021	-22.0916	0.69497	-2.11071	-22.0518
90.00	0.75232	-6.86198	-140.3317	0.70568	-3.92768	-140.1358	0.69513	-2.10946	-140.0959
	Radiation Efficiency			Radiation Efficiency			Radiation Efficiency		
	ETA = 0.4334, H =-0.363E+01 (dB)			ETA = 0.3986, H =-0.399E+01 (dB)			ETA = 0.3934, H =-0.405E+01 (dB)		

Table A8-22 Case 4: Wet Ground, $N = 3$ ($h = 3 \times 0.05\lambda$)

N=3, CASE[4]: Wet Ground (Relative Dielectric Constant = 30.0, Conductivity = 0.010000 S/m)

Grazing ang. deg	FREQUENCY = 6.0 MHz. Fresnel Reflect Coef		Directive gain	FREQUENCY = 15.0 MHz. Fresnel Reflect Coef		Directive gain	FREQUENCY = 30.0 MHz. Fresnel Reflect Coef		Directive gain
PSI(deg)	|Rv|	ang Rv(deg)	D(dBi)	|Rv|	ang Rv(deg)	D(dBi)	|Rv|	ang Rv(deg)	D(dBi)
0.00	1.00000	-180.00000	-999.9999	1.00000	-180.00000	-999.9999	1.00000	-180.00000	-999.9999
0.50	0.89913	-177.53146	-16.8242	0.90572	-178.94031	-17.5012	0.90688	-179.46329	-17.6294
1.00	0.80820	-175.02326	-11.2374	0.81997	-177.86513	-11.8832	0.82206	-178.91888	-12.0058
1.50	0.72605	-172.43419	-8.1323	0.74170	-176.75836	-8.7475	0.74449	-178.35872	-8.8648
2.00	0.65170	-169.71970	-6.0345	0.67002	-175.60228	-6.6201	0.67331	-177.77399	-6.7322
2.50	0.58435	-166.83031	-4.4824	0.60417	-174.37682	-5.0386	0.60777	-177.15462	-5.1465
3.00	0.52334	-163.70963	-3.2717	0.54353	-173.05827	-3.8009	0.54724	-176.48859	-3.9030
3.50	0.46815	-160.29240	-2.2919	0.48756	-171.61778	-2.7953	0.49118	-175.76157	-2.8927
4.00	0.41835	-156.50290	-1.4796	0.43581	-170.01923	-1.9580	0.43915	-174.95476	-2.0508
5.00	0.33389	-147.44798	-0.2044	0.34352	-165.14746	-0.6356	0.34562	-172.99739	-0.7198
6.00	0.26892	-135.76707	0.7552	0.26445	-160.85295	0.3671	0.26413	-170.29680	0.2908
7.00	0.22391	-120.91679	1.5043	0.19754	-153.01488	1.1554	0.19295	-166.18292	1.0863
8.00	0.19972	-103.51066	2.1042	0.14340	-140.41918	1.7912	0.13122	-158.98991	1.7288
9.00	0.19508	-85.89782	2.5938	0.10551	-119.41214	2.3136	0.08913	-143.57930	2.2574
10.00	0.20536	-70.66362	2.9990	0.09252	-89.56206	2.7489	0.04933	-104.43576	2.6963
12.00	0.24836	-49.87074	3.6231	0.12927	-45.24990	3.4261	0.09106	-31.45258	3.3857
14.00	0.29901	-38.06417	4.0695	0.18885	-28.48850	3.9177	0.15944	-17.03987	3.8660
16.00	0.34723	-30.86202	4.3907	0.24531	-20.98231	4.2727	0.22022	-11.96165	4.2537
18.00	0.39063	-26.07735	4.6189	0.29534	-16.80100	4.5395	0.27283	-9.37216	4.5221
20.00	0.42906	-22.67734	4.7748	0.33920	-14.13327	4.7247	0.31845	-7.79073	4.7132
22.00	0.46297	-20.13659	4.8722	0.37768	-12.27667	4.8479	0.35825	-6.71791	4.8416
24.00	0.49292	-18.10470	4.9211	0.41157	-10.90581	4.9195	0.39320	-5.93881	4.9177
26.00	0.51946	-16.58914	4.9282	0.44156	-9.84976	4.9467	0.42406	-5.34553	4.9491
28.00	0.54307	-15.30126	4.8988	0.46822	-9.01013	4.9351	0.45147	-4.87779	4.9412
30.00	0.56415	-14.22921	4.8359	0.49203	-8.32616	4.8866	0.47592	-4.49921	4.8881
32.00	0.58305	-13.32351	4.7479	0.51338	-7.75822	4.8101	0.49784	-4.18642	4.8226
34.00	0.60004	-12.54901	4.6215	0.53259	-7.77937	4.7018	0.51755	-3.92373	4.7170
36.00	0.61536	-11.87998	4.4731	0.54993	-6.87042	4.5653	0.53535	-3.70017	4.5830
38.00	0.62922	-11.29714	4.2986	0.56563	-6.51766	4.4015	0.55145	-3.50782	4.4215
40.00	0.64179	-10.78574	4.0984	0.57987	-6.21069	4.2112	0.56607	-3.34003	4.2333
42.00	0.65321	-10.33432	3.8729	0.59283	-5.94164	3.9945	0.57935	-3.19478	4.0186
44.00	0.66361	-9.93383	3.6218	0.60462	-5.70440	3.7516	0.59146	-3.06817	3.7774
46.00	0.67308	-9.57699	3.3447	0.61539	-5.49416	3.4819	0.60250	-2.95239	3.5093
48.00	0.68173	-9.25793	3.0409	0.62522	-5.30707	3.1849	0.61258	-2.85126	3.2138
50.00	0.68963	-8.97183	2.7083	0.63420	-5.14000	2.8595	0.62179	-2.76106	2.8898
52.00	0.69684	-8.71472	2.3464	0.64241	-4.99043	2.5043	0.63022	-2.68038	2.5358
54.00	0.70343	-8.48328	1.9565	0.64989	-4.85622	2.1176	0.63791	-2.60808	2.1509
56.00	0.70945	-8.27470	1.5312	0.65677	-4.73585	1.6971	0.64495	-2.54314	1.7309
58.00	0.71495	-8.08688	1.0698	0.66309	-4.62724	1.2401	0.65137	-2.48481	1.2748
60.00	0.71995	-7.91719	0.5687	0.66873	-4.52977	0.7430	0.65722	-2.43239	0.7787
62.00	0.72450	-7.76456	0.0237	0.67393	-4.44217	0.2016	0.66255	-2.38532	0.2381
64.00	0.72863	-7.62733	-0.5708	0.67864	-4.36356	-0.3895	0.66738	-2.34310	-0.3523
66.00	0.73237	-7.50424	-1.2215	0.68290	-4.29319	-1.0373	0.67175	-2.30531	-0.9994
68.00	0.73573	-7.39425	-1.9373	0.68673	-4.23040	-1.7504	0.67569	-2.27161	-1.7118
70.00	0.73874	-7.29642	-2.7293	0.69017	-4.17463	-2.5400	0.67921	-2.24170	-2.5009
72.00	0.74141	-7.20997	-3.6126	0.69322	-4.12541	-3.4212	0.68234	-2.21531	-3.3815
74.00	0.74377	-7.13423	-4.6077	0.69591	-4.08234	-4.4143	0.68510	-2.19221	-4.3743
76.00	0.74582	-7.06863	-5.7432	0.69825	-4.04506	-5.5482	0.68750	-2.17224	-5.5077
78.00	0.74757	-7.01268	-7.0613	0.70025	-4.01331	-6.8649	0.68955	-2.15522	-6.8241
80.00	0.74904	-6.96598	-8.6275	0.70193	-3.98681	-8.4300	0.69127	-2.14103	-8.3889
82.00	0.75023	-6.92821	-10.5516	0.70329	-3.96540	-10.3531	0.69267	-2.12955	-10.3118
84.00	0.75115	-6.89909	-13.0395	0.70434	-3.94890	-12.8403	0.69375	-2.12072	-12.7988
86.00	0.75180	-6.87843	-16.5536	0.70509	-3.93720	-16.3538	0.69451	-2.11445	-16.3122
88.00	0.75219	-6.86609	-22.5696	0.70553	-3.93021	-22.3695	0.69497	-2.11071	-22.3278
90.00	0.75232	-6.86198	-140.6143	0.70566	-3.92788	-140.4141	0.69513	-2.10948	-140.3724
	Radiation Efficiency			Radiation Efficiency			Radiation Efficiency		
	ETA = 0.4254, H =-0.371E+01 (dB)			ETA = 0.3934, H =-0.405E+01 (dB)			ETA = 0.3895, H =-0.409E+01 (dB)		

Table A8-23 Case 4: Wet Ground, $N = 4$ ($h = 4 \times 0.05\lambda$)

N=4, CASE(4): Wet Ground (Relative Dielectric Constant = 30.0, Conductivity = 0.010000 S/m)

Grazing ang, deg	FREQUENCY = 6.0 MHz. Fresnel Reflect Coef		Directive gain	FREQUENCY = 15.0 MHz. Fresnel Reflect Coef		Directive gain	FREQUENCY = 30.0 MHz. Fresnel Reflect Coef		Directive gain
PSI(deg)	|Rv|	ang Rv(deg)	D(dBi)	|Rv|	ang Rv(deg)	D(dBi)	|Rv|	ang Rv(deg)	D(dBi)
0.00	1.00000	-180.00000	-999.9999	1.00000	-180.00000	-999.9999	1.00000	-180.00000	-999.9999
0.50	0.99913	+177.53148	-16.6646	0.90572	-178.94031	-17.3394	0.90588	-179.46329	-17.4678
1.00	0.80820	-175.02376	-11.0779	0.81997	-177.86513	-11.7214	0.82206	-178.91888	-11.8442
1.50	0.72605	+172.43419	-7.9731	0.74170	-176.75835	-8.5861	0.74449	-178.35872	-8.7035
2.00	0.65170	-169.71970	-5.8755	0.67002	-175.60228	-6.4589	0.67331	-177.77399	-6.5711
2.50	0.58435	+166.63031	-4.3239	0.60417	-174.37882	-4.8787	0.60777	-177.15482	-4.9858
3.00	0.52334	-163.70963	-3.1132	0.54353	-173.05827	-3.6408	0.54724	-176.48889	-3.7428
3.50	0.46815	+160.29240	-2.1344	0.48758	-171.61778	-2.6356	0.49118	-175.76157	-2.7330
4.00	0.41835	-156.50790	-1.3730	0.43581	+170.01923	-1.7989	0.43915	-174.95478	-1.8918
4.50	0.37369	+147.44798	-0.8492	0.38852	-165.14745	-0.4780	0.34582	-172.99739	-0.5823
5.00	0.33389	-135.76707	0.9088	0.28445	+180.85295	0.5228	0.26413	-170.29680	0.4463
5.50	0.29871	+120.91679	1.6554	0.19754	-153.01488	1.3089	0.18795	-166.18792	1.2397
6.00	0.26792	-103.51066	2.2527	0.14340	-140.41916	1.9421	0.13122	-158.98991	1.8796
6.50	0.24130	-85.89762	2.7394	0.10591	-119.41214	2.4616	0.08913	-143.57930	2.4053
7.00	0.21866	-70.68362	3.1413	0.09252	-88.66286	2.8938	0.04933	-104.43676	2.8430
7.50	0.19983	-59.87074	3.4579	0.12927	+45.24980	3.5633	0.09106	-31.45256	3.5228
8.00	0.18465	-52.06417	3.7154	0.18885	-28.48850	4.0461	0.15944	-17.03982	4.0145
8.50	0.17299	-46.86202	3.9266	0.24531	+20.98231	4.3962	0.22022	-11.96165	4.3723
9.00	0.16472	-43.72735	4.0966	0.28534	+16.80100	4.6468	0.27283	-9.37218	4.6296
9.50	0.15966	-41.98235	4.2335	0.31820	-14.13327	4.8197	0.31845	-7.79073	4.8084
10.00	0.15760	-41.16470	4.3451	0.34758	-12.27667	4.9295	0.35825	-6.71791	4.9234
10.50	0.15830	-41.00000	4.4351	0.37457	-10.90581	4.9866	0.39320	-5.93681	4.9852
11.00	0.16153	-41.32892	4.5064	0.39992	-9.84976	4.9985	0.42406	-5.34553	5.0013
12.00	0.17299	-42.72735	4.6106	0.44822	-9.01013	4.9705	0.45147	-4.87779	4.9772
13.00	0.19983	-46.86202	4.6999	0.49203	-8.32616	4.9070	0.47592	-4.49921	4.9170
14.00	0.24130	-52.06417	4.7923	0.53138	-7.75822	4.8106	0.49784	-4.18642	4.8238
15.00	0.29871	-59.87074	4.8999	0.53259	+7.27932	4.6838	0.51755	-3.92373	4.6999
16.00	0.37369	-72.06417	5.0260	0.54993	-6.87047	4.5262	0.53535	-3.70017	4.5469
17.00	0.46815	-89.87074	5.1750	0.56563	-6.51766	4.3449	0.55145	-3.50782	4.3660
18.00	0.58435	-116.70963	5.3523	0.57987	-6.21069	4.1347	0.56607	-3.34083	4.1579
19.00	0.72605	-152.43419	5.5650	0.59283	-5.94184	3.8979	0.57935	-3.19476	3.9232
20.00	0.90000	+180.00000	5.8225	0.60462	-5.70440	3.6345	0.59146	-3.06617	3.6617
21.00	0.80820	+175.02376	6.1373	0.61539	-5.49416	3.3444	0.60250	-2.95239	3.3733
22.00	0.72605	+172.43419	6.5294	0.62522	-5.30707	3.0269	0.61258	-2.85126	3.0574
23.00	0.65170	+169.71970	7.0255	0.63420	+5.14000	2.6811	0.62179	-2.76106	2.7132
24.00	0.58435	+166.63031	7.6619	0.64241	-4.99043	2.3058	0.63022	-2.68038	2.3392
25.00	0.52334	+163.70963	8.4887	0.64991	-4.85622	1.8992	0.63791	-2.60806	1.9339
26.00	0.46815	+160.29240	9.5744	0.65677	-4.73565	1.4593	0.64495	-2.54314	1.4952
27.00	0.41835	+156.50790	11.0270	0.66303	-4.62724	0.9834	0.65137	-2.48481	1.0203
28.00	0.37369	+147.44798	13.0085	0.66873	-4.52977	0.4680	0.65722	-2.43239	0.5059
29.00	0.33389	+135.76707	15.7491	0.67393	-4.44217	-0.0911	0.66255	-2.38532	-0.0522
30.00	0.29871	+120.91679	19.5650	0.67864	-4.36356	-0.6991	0.66738	-2.34310	-0.6594
31.00	0.26792	+103.51066	24.8225	0.68290	-4.29319	-1.3629	0.67175	-2.30531	-1.3223
32.00	0.24130	+85.89762	31.8373	0.68673	-4.23040	-2.0909	0.67589	-2.27151	-2.0497
33.00	0.21866	+70.68362	40.3451	0.69017	-4.17463	-2.8946	0.67921	-2.24170	-2.8526
34.00	0.19983	+59.87074	49.4579	0.69322	-4.12541	-3.7886	0.68234	-2.21531	-3.7461
35.00	0.18465	+52.06417	58.4154	0.69591	-4.08234	-4.7935	0.68510	-2.19221	-4.7505
36.00	0.17299	+46.86202	66.7154	0.69825	-4.04506	-5.9379	0.68750	-2.17224	-5.8844
37.00	0.16472	+43.72735	73.9266	0.70025	-4.01331	-7.2639	0.68955	-2.15522	-7.2200
38.00	0.15966	+41.98235	79.8373	0.70193	-3.98681	-8.8368	0.69127	-2.14103	-8.7926
39.00	0.15760	+41.16470	84.4351	0.70329	-3.96540	-10.7664	0.69267	-2.12955	-10.7270
40.00	0.15830	+41.00000	87.9064	0.70434	-3.94890	-13.2587	0.69375	-2.12072	-13.2140
41.00	0.16153	+41.32892	90.4225	0.70509	-3.93720	-16.7759	0.69451	-2.11446	-16.7311
42.00	0.16707	+42.12735	92.1373	0.70553	-3.93021	-22.7938	0.69497	-2.11074	-22.7489
43.00	0.17485	+43.30000	93.1750	0.70568	-3.92788	-140.8392	0.69513	-2.10946	-140.7942
44.00	0.18465	+44.83597	93.6154						
45.00	0.19630	+46.70000	93.5225						
46.00	0.20962	+48.85597	93.0300						
47.00	0.22441	+51.25000	92.2337						
48.00	0.24045	+53.83597	91.2900						
49.00	0.25750	+56.56000	90.3225						
50.00	0.27532	+59.36597	89.4150						
51.00	0.29365	+62.19000	88.6154						
52.00	0.31220	+64.96597	87.9350						
53.00	0.33070	+67.62000	87.3600						
54.00	0.34885	+70.08597	86.8500						
55.00	0.36635	+72.29000	86.3350						
56.00	0.38290	+74.16597	85.7450						
57.00	0.39820	+75.65000	85.0000						
58.00	0.41195	+76.68597	84.0200						
59.00	0.42385	+77.22000	82.7350						
60.00	0.43360	+77.20597	81.0950						
61.00	0.44090	+76.59000	79.0000						
62.00	0.44545	+75.32597	76.4000						
63.00	0.44695	+73.36000	73.2450						
64.00	0.44513	+70.63597	69.4650						
65.00	0.43970	+67.09000	65.0000						
66.00	0.43040	+62.66597	59.7850						
67.00	0.41695	+57.30000	53.7200						
68.00	0.39910	+50.93597	46.7500						
69.00	0.37650	+43.51000	38.8000						
70.00	0.34885	+35.04597	30.0000						
71.00	0.31585	+25.64000	20.5000						
72.00	0.27732	+15.48597	10.5000						
73.00	0.23330	+4.85000	0.3000						
74.00	0.18465	-5.92403	-9.3000						
75.00	0.13330	-16.13000	-18.5000						
76.00	0.08290	-24.93403	-26.5000						
77.00	0.04000	-31.30000	-33.0000						
78.00	0.01470	-34.07403	-38.0000						
79.00	0.01000	-33.00000	-41.0000						
80.00	0.02530	-28.07403	-42.0000						
81.00	0.05710	-20.70000	-41.0000						
82.00	0.09850	-12.32403	-38.0000						
83.00	0.14000	-5.70000	-33.0000						
84.00	0.17180	-2.47403	-26.5000						
85.00	0.18710	-2.00000	-18.5000						
86.00	0.18710	-2.47403	-9.3000						
87.00	0.17180	-5.70000	0.3000						
88.00	0.14000	-12.32403	10.5000						
89.00	0.09850	-20.70000	20.5000						
90.00	0.05710	-31.30000	30.0000						

Radiation Efficiency	Radiation Efficiency	Radiation Efficiency
ETA = 0.4157, M =-0.381E+01 (dB)	ETA = 0.3868, M =-0.413E+01 (dB)	ETA = 0.3844, M =-0.415E+01 (dB)

Table A8-24 Case 4: Wet Ground, $N = 5$ ($h = 5 \times 0.05\lambda$)

N=5, CASE(4): Wet Ground (Relative Dielectric Constant = 30.0, Conductivity = 0.010000 S/m)

Grazing ang. deg	FREQUENCY = 6.0 MHz. Fresnel Reflect Coef		Directive gain	FREQUENCY = 15.0 MHz. Fresnel Reflect Coef		Directive gain	FREQUENCY = 30.0 MHz. Fresnel Reflect Coef		Directive gain
PSI(deg)	|Rv|	ang Rv(deg)	D(dBi)	|Rv|	ang Rv(deg)	D(dBi)	|Rv|	ang Rv(deg)	D(dBi)
0.00	1.00000	+180.00000	-999.9999	1.00000	-180.00000	-999.9999	1.00000	-180.00000	-999.9999
0.50	0.89913	-177.53148	-16.4451	0.90572	-178.94031	-17.1174	0.90688	-179.48329	-17.2461
1.00	0.80820	-175.02328	-10.8585	0.81997	-177.88513	-11.4996	0.82206	-178.91888	-11.6228
1.50	0.72605	-172.43419	-7.7540	0.74170	-176.75836	-8.3645	0.74449	-178.35872	-8.4824
2.00	0.65170	-169.71970	-5.6569	0.67002	-175.60228	-6.2378	0.67331	-177.77399	-6.3505
2.50	0.58435	-166.83031	-4.1058	0.60417	-174.37682	-4.6582	0.60777	-177.15462	-4.7658
3.00	0.52334	-163.70953	-2.8957	0.54353	-173.05827	-3.4207	0.54724	-176.48059	-3.5234
3.50	0.46815	-160.29240	-1.9178	0.48758	-171.61778	-2.4164	0.49118	-175.78157	-2.5144
4.00	0.41835	-156.50290	-1.1073	0.43581	-170.01823	-1.5807	0.43915	-174.95476	-1.6741
5.00	0.33389	-147.44798	0.1643	0.34352	-166.14746	-0.2619	0.34562	-172.99739	-0.3468
6.00	0.26892	-135.76707	1.1194	0.26445	-160.85295	0.7362	0.26413	-170.29680	0.6593
7.00	0.22391	-120.91679	1.8630	0.19754	-153.01488	1.5191	0.19295	-166.18292	1.4495
8.00	0.19972	-103.51066	2.4567	0.14340	-140.41916	2.1487	0.13122	-158.98991	2.0858
9.00	0.19508	-85.89762	2.9393	0.10591	-119.41214	2.6642	0.08013	-143.57930	2.6075
10.00	0.20536	-70.66362	3.3366	0.08252	-88.66296	3.0917	0.04933	-104.43576	3.0407
12.00	0.24836	-49.87074	3.9426	0.12927	-45.24990	3.7509	0.09108	-31.45258	3.7103
14.00	0.29901	-38.06417	4.3678	0.18885	-28.48850	4.2215	0.15944	-17.03962	4.1896
16.00	0.34723	-30.86202	4.6648	0.24531	-20.98231	4.5576	0.22022	-11.96165	4.5336
18.00	0.39063	-25.87735	4.8656	0.29534	-16.80100	4.7926	0.27283	-9.37218	4.7754
20.00	0.42906	-22.67734	4.9918	0.33820	-14.13327	4.9482	0.31845	-7.79073	4.9370
22.00	0.46297	-20.13659	5.0567	0.37768	-12.27667	5.0391	0.35825	-6.71781	5.0334
24.00	0.49292	-18.18470	5.0704	0.41157	-10.90561	5.0760	0.39320	-5.93681	5.0750
26.00	0.51948	-16.58914	5.0400	0.44156	-9.84976	5.0662	0.42406	-5.34553	5.0696
28.00	0.54307	-15.30126	4.9707	0.46822	-9.01013	5.0193	0.45147	-4.87779	5.0227
30.00	0.56415	-14.22921	4.8663	0.49203	-8.32618	4.9276	0.47592	-4.49921	4.9386
32.00	0.58305	-13.32351	4.7298	0.51338	-7.75822	4.8060	0.49784	-4.18642	4.8203
34.00	0.60004	-12.54901	4.5632	0.53259	-7.27932	4.6531	0.51755	-3.92373	4.6704
36.00	0.61536	-11.87996	4.3682	0.54993	-6.87042	4.4704	0.53535	-3.70017	4.4905
38.00	0.62922	-11.29714	4.1458	0.56563	-6.51766	4.2593	0.55145	-3.50782	4.2821
40.00	0.64179	-10.78574	3.8969	0.57987	-6.21069	4.0208	0.56607	-3.34083	4.0459
42.00	0.65321	-10.33432	3.6217	0.59283	-5.94164	3.7551	0.57935	-3.19476	3.7825
44.00	0.66361	-9.93383	3.3205	0.60462	-5.70440	3.4627	0.59146	-3.06617	3.4922
46.00	0.67308	-9.57699	2.9931	0.61539	-5.49416	3.1432	0.60250	-2.95239	3.1747
48.00	0.68173	-9.25793	2.6388	0.62522	-5.30707	2.7963	0.61259	-2.85126	2.8296
50.00	0.68963	-8.97183	2.2569	0.63420	-5.14000	2.4213	0.62179	-2.76106	2.4563
52.00	0.69684	-8.71472	1.8462	0.64241	-4.99043	2.0169	0.63022	-2.68038	2.0535
54.00	0.70343	-8.48326	1.4052	0.64991	-4.85622	1.5817	0.63791	-2.60806	1.6186
56.00	0.70945	-8.27470	0.9318	0.65677	-4.73565	1.1137	0.64495	-2.54314	1.1532
58.00	0.71495	-8.08568	0.4234	0.66303	-4.62724	0.6103	0.65137	-2.48481	0.6511
60.00	0.71995	-7.91719	-0.1231	0.66873	-4.52977	0.0663	0.65722	-2.43239	0.1104
62.00	0.72450	-7.76456	-0.7120	0.67393	-4.44217	-0.5165	0.66255	-2.38532	-0.4732
64.00	0.72863	-7.62733	-1.3485	0.67864	-4.36356	-1.1491	0.66738	-2.34310	-1.1046
66.00	0.73237	-7.50424	-2.0390	0.68290	-4.29319	-1.8361	0.67175	-2.30531	-1.7908
68.00	0.73573	-7.39425	-2.7922	0.68673	-4.23040	-2.5862	0.67569	-2.27161	-2.5400
70.00	0.73874	-7.29642	-3.6192	0.69017	-4.17463	-3.4103	0.67921	-2.24170	-3.3633
72.00	0.74141	-7.20997	-4.5348	0.69322	-4.12541	-4.3233	0.68234	-2.21531	-4.2755
74.00	0.74377	-7.13423	-5.5597	0.69591	-4.08234	-5.3454	0.68510	-2.19221	-5.2970
76.00	0.74582	-7.06863	-6.7210	0.69825	-4.04506	-6.5052	0.68750	-2.17224	-6.4562
78.00	0.74757	-7.01266	-8.0622	0.70025	-4.01331	-7.8447	0.68955	-2.15522	-7.7952
80.00	0.74904	-6.96598	-9.5482	0.70193	-3.98681	-9.4292	0.69127	-2.14103	-9.3793
82.00	0.75023	-6.92821	-11.5886	0.70329	-3.96540	-11.3685	0.69267	-2.12955	-11.3182
84.00	0.75115	-6.89909	-14.0893	0.70434	-3.94890	-13.8683	0.69375	-2.12072	-13.8177
86.00	0.75180	-6.87843	-17.6126	0.70509	-3.93720	-17.3909	0.69451	-2.11445	-17.3402
88.00	0.75219	-6.86609	-23.6341	0.70553	-3.93021	-23.4130	0.69497	-2.11071	-23.3612
90.00	0.75232	-6.86198	-141.6806	0.70568	-3.92788	-141.4585	0.69513	-2.10948	-141.4076
	Radiation Efficiency			Radiation Efficiency			Radiation Efficiency		
	ETA = 0.4041, M =-0.394E+01 (dB)			ETA = 0.3787, M =-0.422E+01 (dB)			ETA = 0.3779, M =-0.423E+01 (dB)		

Table A8-25 Case 5: Medium Dry Ground, $N = 0$ ($h = 0 \times 0.05\lambda$)

N=0, CASE(5): Medium Dry Ground (Relative Dielectric Constant = 15.0, Conductivity = 0.001000 S/m)

Grazing ang. deg	FREQUENCY = 8.0 MHz. Fresnel Reflect Coef [Rv]	ang Rv(deg)	Directive gain D(dBi)	FREQUENCY = 15.0 MHz. Fresnel Reflect Coef [Rv]	ang Rv(deg)	Directive gain D(dBi)	FREQUENCY = 30.0 MHz. Fresnel Reflect Coef [Rv]	ang Rv(deg)	Directive gain D(dBi)
PSI(deg)									
0.00	1.00000	-180.00000	-999.9999	1.00000	-180.00000	-999.9999	1.00000	-180.00000	-999.9999
0.50	0.93213	-179.82875	-19.6298	0.93235	-179.85101	-19.6599	0.93239	-179.92548	-19.6642
1.00	0.86872	-179.25478	-13.9006	0.86914	-179.70094	-13.9296	0.86920	-179.85040	-13.9338
1.50	0.80935	-178.87526	-10.6617	0.80894	-179.54885	-10.6897	0.81003	-179.77422	-10.6937
2.00	0.75367	-178.48729	-8.4380	0.75440	-179.39256	-8.4649	0.75450	-179.69635	-8.4688
2.50	0.70135	-178.08771	-6.7675	0.70218	-179.23265	-6.7934	0.70230	-179.61615	-6.7972
3.00	0.65210	-177.67305	-5.4447	0.65300	-179.06831	-5.4696	0.65314	-179.53296	-5.4732
3.50	0.60566	-177.23953	-4.3601	0.60662	-178.89244	-4.3841	0.60678	-179.44598	-4.3875
4.00	0.56181	-176.78278	-3.4485	0.56280	-178.70926	-3.4715	0.56294	-179.35435	-3.4749
5.00	0.48110	-175.77838	-1.9899	0.48206	-178.30853	-2.0111	0.48220	-179.15292	-2.0142
6.00	0.40858	-174.60728	-0.8655	0.40940	-177.83684	-0.8851	0.40952	-178.91803	-0.8879
7.00	0.34315	-173.19183	0.0324	0.34370	-177.28906	0.0144	0.34378	-178.63999	0.0118
8.00	0.28393	-171.41025	0.7674	0.28405	-176.55312	0.7510	0.28406	-178.27577	0.7485
9.00	0.23021	-169.05791	1.3804	0.22967	-175.60406	1.3693	0.22960	-177.80066	1.3682
10.00	0.18152	-165.76236	1.8985	0.17997	-174.26274	1.8848	0.17974	-177.12831	1.8829
12.00	0.09680	-152.40818	2.7227	0.09278	-168.52808	2.7114	0.09188	-174.22993	2.7098
14.00	0.04773	-104.73233	3.3411	0.02434	-130.07385	3.3320	0.01867	-150.04589	3.3307
16.00	0.07016	-41.07962	3.8124	0.05264	-20.70421	3.8052	0.04959	-10.82862	3.8042
18.00	0.11862	-22.68665	4.1732	0.10732	-8.91372	4.1678	0.10558	-5.02667	4.1670
20.00	0.16531	-15.87302	4.4476	0.15629	-5.71162	4.4437	0.15494	-3.38414	4.4431
22.00	0.20756	-12.39734	4.6522	0.19972	-5.17379	4.6498	0.19856	-2.80329	4.6492
24.00	0.24545	-10.29028	4.7986	0.23834	-4.26571	4.7972	0.23729	-2.31414	4.7970
26.00	0.27944	-8.87327	4.8954	0.27282	-3.66376	4.8951	0.27185	-1.84045	4.8951
28.00	0.30998	-7.85288	4.9489	0.30374	-3.23416	4.9496	0.30282	-1.62402	4.9497
30.00	0.33791	-7.08192	4.9637	0.33155	-2.91154	4.9652	0.33068	-1.46163	4.9655
32.00	0.36240	-6.47844	4.9433	0.35667	-2.66031	4.9456	0.35583	-1.33516	4.9460
34.00	0.38495	-5.99314	4.8902	0.37941	-2.45859	4.8933	0.37860	-1.23384	4.8938
36.00	0.40543	-5.59457	4.8065	0.40006	-2.29350	4.8102	0.39927	-1.15067	4.8108
38.00	0.42408	-5.26169	4.6933	0.41886	-2.15581	4.6976	0.41808	-1.08174	4.6983
40.00	0.44108	-4.97985	4.5515	0.43598	-2.03951	4.5564	0.43523	-1.02333	4.5571
42.00	0.45662	-4.73858	4.3816	0.45162	-1.94018	4.3870	0.45088	-0.97340	4.3878
44.00	0.47087	-4.53010	4.1836	0.46592	-1.85437	4.1894	0.46520	-0.93031	4.1903
46.00	0.48383	-4.34859	3.9572	0.47901	-1.77974	3.9635	0.47830	-0.89284	3.9644
48.00	0.49574	-4.18956	3.7018	0.49100	-1.71440	3.7085	0.49031	-0.86005	3.7094
50.00	0.50666	-4.04950	3.4155	0.50199	-1.65691	3.4234	0.50130	-0.83119	3.4244
52.00	0.51667	-3.92562	3.0997	0.51208	-1.60609	3.1070	0.51136	-0.80589	3.1080
54.00	0.52584	-3.81569	2.7498	0.52128	-1.56102	2.7574	0.52061	-0.78308	2.7585
56.00	0.53423	-3.71790	2.3645	0.52972	-1.52095	2.3723	0.52906	-0.76297	2.3735
58.00	0.54191	-3.63075	1.9410	0.53744	-1.48525	1.9491	0.53679	-0.74506	1.9502
60.00	0.54892	-3.55300	1.4758	0.54449	-1.45343	1.4840	0.54385	-0.72909	1.4852
62.00	0.55531	-3.48364	0.9645	0.55092	-1.42504	0.9729	0.55028	-0.71485	0.9741
64.00	0.56111	-3.42181	0.4016	0.55676	-1.39974	0.4102	0.55612	-0.70216	0.4115
66.00	0.56636	-3.36676	-0.2197	0.56204	-1.37723	-0.2109	0.56141	-0.69087	-0.2097
68.00	0.57110	-3.31791	-0.9081	0.56680	-1.35725	-0.8992	0.56617	-0.68085	-0.8979
70.00	0.57534	-3.27473	-1.6751	0.57107	-1.33960	-1.6661	0.57044	-0.67199	-1.6647
72.00	0.57912	-3.23677	-2.5358	0.57487	-1.32409	-2.5265	0.57424	-0.66421	-2.5251
74.00	0.58245	-3.20368	-3.5102	0.57821	-1.31057	-3.5009	0.57759	-0.65743	-3.4996
76.00	0.58535	-3.17514	-4.6275	0.58112	-1.29891	-4.6181	0.58051	-0.65158	-4.6168
78.00	0.58783	-3.15089	-5.9298	0.58362	-1.28900	-5.9204	0.58300	-0.64662	-5.9190
80.00	0.58991	-3.13071	-7.4826	0.58571	-1.28078	-7.4731	0.58509	-0.64248	-7.4717
82.00	0.59159	-3.11442	-9.3956	0.58741	-1.27411	-9.3851	0.58679	-0.63915	-9.3847
84.00	0.59290	-3.10190	-11.8749	0.58872	-1.26900	-11.8653	0.58810	-0.63658	-11.8639
86.00	0.59382	-3.09303	-15.3828	0.58965	-1.26537	-15.3732	0.58904	-0.63477	-15.3718
88.00	0.59438	-3.08773	-21.3961	0.59021	-1.26321	-21.3855	0.58959	-0.63368	-21.3841
90.00	0.59456	-3.08597	-139.4386	0.59039	-1.26249	-139.4290	0.58978	-0.63332	-139.4278
	Radiation Efficiency			Radiation Efficiency			Radiation Efficiency		
	ETA = 0.3199, H =-0.495E+01 (dB)			ETA = 0.3177, H =-0.498E+01 (dB)			ETA = 0.3174, H =-0.498E+01 (dB)		

Table A8-26 Case 5: Medium Dry Ground, $N = 1$ ($h = 1 \times 0.05\lambda$)

NEC, CASE(5): Medium Dry Ground (Relative Dielectric Constant = 15.0, Conductivity = 0.001000 S/m)

Grazing ang. deg	FREQUENCY = 0.0 MHz, Fresnel Reflect Coef		Directive gain	FREQUENCY = 15.0 MHz, Fresnel Reflect Coef		Directive gain	FREQUENCY = 30.0 MHz, Fresnel Reflect Coef		Directive gain
PST(deg)	|Rv|	ang Rv(deg)	D(dBi)	|Rv|	ang Rv(deg)	D(dBi)	|Rv|	ang Rv(deg)	D(dBi)
0.00	1.00000	-180.00000	-999.9999	1.00000	-180.00000	-999.9999	1.00000	-180.00000	-999.9999
0.50	0.93213	-179.62625	-19.5959	0.93235	-179.85101	-19.6266	0.93239	-179.92548	-19.6312
1.00	0.86872	-179.25476	-13.8667	0.86914	-179.70094	-13.8963	0.86920	-179.85040	-13.9008
1.50	0.80935	-178.87526	-10.6279	0.80994	-179.54865	-10.6565	0.81003	-179.77422	-10.6607
2.00	0.75387	-178.48729	-8.4042	0.75440	-179.39298	-8.4318	0.75450	-179.69635	-8.4359
2.50	0.70135	-178.08771	-6.7338	0.70218	-179.23265	-6.7604	0.70230	-179.61615	-6.7643
3.00	0.65210	-177.67305	-5.4111	0.65300	-179.06831	-5.4367	0.65314	-179.53296	-5.4405
3.50	0.60566	-177.23953	-4.3266	0.60662	-178.89244	-4.3512	0.60678	-179.44598	-4.3549
4.00	0.56181	-176.78276	-3.4151	0.56280	-178.70926	-3.4386	0.56294	-179.35435	-3.4423
5.00	0.48110	-175.77838	-1.8568	0.48205	-178.30653	-1.9787	0.48220	-179.15292	-1.9820
6.00	0.40858	-174.60728	-0.8328	0.40940	-177.83694	-0.8530	0.40952	-178.91803	-0.8560
7.00	0.34315	-173.19183	0.0647	0.34370	-177.26906	0.0461	0.34378	-178.63399	0.0433
8.00	0.28393	-171.41025	0.7992	0.28405	-176.55312	0.7822	0.28405	-178.27577	0.7796
9.00	0.23021	-169.05791	1.4116	0.22967	-175.60406	1.3950	0.22960	-177.80066	1.3926
10.00	0.18152	-165.76236	1.9291	0.17997	-174.26274	1.9149	0.17974	-177.12831	1.8127
12.00	0.09880	-152.40816	2.7518	0.09278	-168.52808	2.7400	0.09188	-174.22993	2.7382
14.00	0.04773	-104.73233	3.3686	0.02434	-130.07385	3.3590	0.01867	-150.04689	3.3575
16.00	0.07016	-41.07962	3.8380	0.05264	-20.70421	3.8303	0.04959	-10.82862	3.8291
18.00	0.11862	-22.88665	4.1965	0.10732	-9.91372	4.1902	0.10558	-5.02667	4.1897
20.00	0.16531	-15.87302	4.4686	0.15629	-6.71162	4.4643	0.15494	-3.38414	4.4636
22.00	0.20756	-12.39734	4.6708	0.19972	-5.17379	4.6677	0.19856	-2.60329	4.6672
24.00	0.24545	-10.29028	4.8143	0.23834	-4.26571	4.8126	0.23729	-2.14414	4.8123
26.00	0.27944	-8.87227	4.9081	0.27282	-3.66376	4.9076	0.27185	-1.84045	4.9075
28.00	0.30998	-7.85286	4.9585	0.30374	-3.23416	4.9590	0.30282	-1.62402	4.9590
30.00	0.33751	-7.08192	4.9700	0.33155	-2.91154	4.9715	0.33068	-1.46163	4.9716
32.00	0.36240	-6.47844	4.9462	0.35667	-2.66011	4.9485	0.35583	-1.33516	4.9488
34.00	0.38495	-5.99314	4.8896	0.37941	-2.45859	4.8927	0.37860	-1.23384	4.8932
36.00	0.40543	-5.59457	4.8022	0.40006	-2.29350	4.8061	0.39927	-1.15087	4.8087
38.00	0.42408	-5.26169	4.6853	0.41885	-2.15593	4.6899	0.41808	-1.08174	4.6905
40.00	0.44108	-4.97986	4.5398	0.43598	-2.03961	4.5449	0.43523	-1.02333	4.5457
42.00	0.45662	-4.73858	4.3660	0.45162	-1.94018	4.3718	0.45088	-0.97340	4.3727
44.00	0.47082	-4.53010	4.1642	0.46592	-1.85437	4.1704	0.46520	-0.93031	4.1714
46.00	0.48383	-4.34859	3.9339	0.47901	-1.77974	3.9407	0.47830	-0.89284	3.9418
48.00	0.49574	-4.18956	3.6747	0.49100	-1.71440	3.6819	0.49031	-0.86005	3.6830
50.00	0.50666	-4.04950	3.3855	0.50199	-1.65691	3.3931	0.50130	-0.83119	3.3943
52.00	0.51667	-3.92562	3.0649	0.51206	-1.60609	3.0729	0.51138	-0.80569	3.0742
54.00	0.52584	-3.81569	2.7113	0.52128	-1.56102	2.7197	0.52061	-0.78308	2.7211
56.00	0.53423	-3.71780	2.3224	0.52972	-1.52095	2.3311	0.52906	-0.76297	2.3325
58.00	0.54191	-3.63075	1.8954	0.53744	-1.48526	1.9044	0.53679	-0.74506	1.9058
60.00	0.54892	-3.55300	1.4267	0.54449	-1.45343	1.4360	0.54385	-0.72909	1.4375
62.00	0.55531	-3.48364	0.9121	0.55092	-1.42504	0.9216	0.55028	-0.71485	0.9232
64.00	0.56111	-3.42181	0.3461	0.55678	-1.39974	0.3568	0.55612	-0.70216	0.3575
66.00	0.56636	-3.36676	-0.2682	0.56204	-1.37723	-0.2582	0.56141	-0.69087	-0.2665
68.00	0.57110	-3.31791	-0.9694	0.56680	-1.35726	-0.9592	0.56617	-0.68085	-0.9575
70.00	0.57534	-3.27473	-1.7389	0.57107	-1.33960	-1.7286	0.57044	-0.67199	-1.7268
72.00	0.57912	-3.23677	-2.6019	0.57487	-1.32409	-2.5913	0.57424	-0.66421	-2.5896
74.00	0.58245	-3.20368	-3.5786	0.57821	-1.31057	-3.5679	0.57759	-0.65743	-3.5661
76.00	0.58535	-3.17514	-4.6978	0.58112	-1.29891	-4.6871	0.58051	-0.65158	-4.6852
78.00	0.58783	-3.15088	-6.0018	0.58362	-1.28900	-5.9909	0.58300	-0.64662	-5.9891
80.00	0.58991	-3.13071	-7.5560	0.58571	-1.28076	-7.5451	0.58509	-0.64248	-7.5432
82.00	0.59159	-3.11442	-9.4703	0.58741	-1.27411	-9.4583	0.58679	-0.63915	-9.4574
84.00	0.59290	-3.10190	-11.9505	0.58872	-1.26900	-11.9394	0.58810	-0.63658	-11.9375
86.00	0.59382	-3.09303	-15.4591	0.58965	-1.26537	-15.4480	0.58904	-0.63477	-15.4461
88.00	0.59436	-3.08773	-21.4718	0.59021	-1.26321	-21.4606	0.58959	-0.63368	-21.4587
90.00	0.59456	-3.08597	-139.5154	0.59039	-1.26249	-139.5043	0.58978	-0.63332	-139.5023
Radiation Efficiency	ETA = 0.3172, H =-0.499E+01 (dB)			ETA = 0.3164, H =-0.500E+01 (dB)			ETA = 0.3166, H =-0.499E+01 (dB)		

Table A8-27 Case 5: Medium Dry Ground, $N = 2$ ($h = 2 \times 0.05\lambda$)

N=2, CASE(5): Medium Dry Ground (Relative Dielectric Constant = 15.0, Conductivity = 0.001000 S/m)

	FREQUENCY = 6.0 MHz.			FREQUENCY = 15.0 MHz.			FREQUENCY = 30.0 MHz.		
Grazing ang. deg	Fresnel Reflect Coef		Directive gain	Fresnel Reflect Coef		Directive gain	Fresnel Reflect Coef		Directive gain
PSI(deg)	|Rv|	ang Rv(deg)	D(dBi)	|Rv|	ang Rv(deg)	D(dBi)	|Rv|	ang Rv(deg)	D(dBi)
0.00	1.00000	-180.00000	-999.9999	1.00000	-180.00000	-999.9999	1.00000	-180.00000	-999.9999
0.50	0.93213	-179.62875	-19.5284	0.93235	-179.85101	-19.5595	0.93239	-179.92548	-19.5641
1.00	0.86872	-179.25478	-13.7992	0.86914	-179.70094	-13.8292	0.86920	-179.85040	-13.8338
1.50	0.80935	-178.87525	-10.5605	0.80994	-179.54865	-10.5894	0.81003	-179.77422	-10.5938
2.00	0.75367	-178.48729	-8.3370	0.75440	-179.39298	-8.3649	0.75450	-179.69835	-8.3691
2.50	0.70135	-178.08771	-6.6667	0.70218	-179.23265	-6.6936	0.70230	-179.61615	-6.6977
3.00	0.65210	-177.67305	-5.3441	0.65300	-179.06631	-5.3701	0.65314	-179.53298	-5.3740
3.50	0.60566	-177.23953	-4.2599	0.60662	-178.89244	-4.2846	0.60676	-179.44598	-4.2887
4.00	0.56181	-176.78276	-3.3486	0.56280	-178.70926	-3.3727	0.56294	-179.35435	-3.3764
5.00	0.48110	-175.77838	-1.8910	0.48206	-178.30653	-1.9132	0.48220	-179.15292	-1.9166
6.00	0.40858	-174.60728	-0.7677	0.40940	-177.83694	-0.7882	0.40952	-178.91803	-0.7914
7.00	0.34315	-173.19183	0.1288	0.34370	-177.26906	0.1100	0.34378	-178.63389	0.1071
8.00	0.28393	-171.41025	0.8625	0.28405	-176.55312	0.8451	0.28408	-178.27577	0.8424
9.00	0.23021	-169.05791	1.4737	0.22967	-175.60406	1.4578	0.22960	-177.80066	1.4553
10.00	0.18152	-165.76236	1.9900	0.17997	-174.26274	1.9754	0.17974	-177.12831	1.9731
12.00	0.09880	-152.40816	2.8098	0.09278	-168.52808	2.7977	0.09188	-174.22893	2.7958
14.00	0.04773	-104.73233	3.4232	0.02434	-130.07385	3.4133	0.01867	-150.04689	3.4117
16.00	0.07016	-41.07962	3.8887	0.05264	-20.70421	3.8808	0.04950	-10.82862	3.8795
18.00	0.11862	-22.68665	4.2430	0.10732	-9.91372	4.2369	0.10558	-5.02667	4.2359
20.00	0.16531	-15.87302	4.5103	0.15629	-6.71162	4.5058	0.15494	-3.38414	4.5050
22.00	0.20756	-12.39734	4.7071	0.19972	-5.17379	4.7040	0.19856	-2.60329	4.7034
24.00	0.24545	-10.29028	4.8452	0.23834	-4.26571	4.8434	0.23729	-2.11414	4.8430
26.00	0.27944	-8.87327	4.9322	0.27282	-3.66376	4.9325	0.27185	-1.84045	4.9324
28.00	0.30998	-7.85288	4.9773	0.30374	-3.23416	4.9777	0.30282	-1.62402	4.9777
30.00	0.33751	-7.08192	4.9822	0.33155	-2.91154	4.9837	0.33068	-1.46163	4.9838
32.00	0.36240	-6.47844	4.9516	0.35667	-2.66011	4.9539	0.35583	-1.33518	4.9543
34.00	0.38495	-5.99314	4.8879	0.37941	-2.45859	4.8911	0.37860	-1.23384	4.8916
36.00	0.40543	-5.59457	4.7933	0.40006	-2.29350	4.7973	0.39927	-1.15087	4.7979
38.00	0.42408	-5.26169	4.6689	0.41885	-2.15591	4.6736	0.41808	-1.08114	4.6744
40.00	0.44106	-4.97986	4.5158	0.43598	-2.03961	4.5212	0.43523	-1.02333	4.5221
42.00	0.45662	-4.73858	4.3344	0.45162	-1.84018	4.3404	0.45088	-0.97340	4.3414
44.00	0.47082	-4.53010	4.1248	0.46592	-1.85437	4.1314	0.46520	-0.93031	4.1325
46.00	0.48383	-4.34859	3.8868	0.47901	-1.77924	3.8940	0.47830	-0.89284	3.8951
48.00	0.49574	-4.18956	3.6199	0.49100	-1.71440	3.6275	0.49031	-0.86005	3.6288
50.00	0.50666	-4.04950	3.3230	0.50199	-1.65691	3.3310	0.50130	-0.83119	3.3324
52.00	0.51667	-3.92562	2.9948	0.51206	-1.60609	3.0034	0.51138	-0.80569	3.0048
54.00	0.52584	-3.81569	2.6338	0.52128	-1.56102	2.6427	0.52061	-0.78308	2.6443
56.00	0.53423	-3.71790	2.2376	0.52972	-1.52095	2.2469	0.52906	-0.76297	2.2485
58.00	0.54191	-3.63075	1.8034	0.53744	-1.48525	1.8131	0.53679	-0.74506	1.8148
60.00	0.54892	-3.55300	1.3279	0.54449	-1.45343	1.3379	0.54385	-0.72909	1.3397
62.00	0.55531	-3.48364	0.8067	0.55092	-1.42504	0.8170	0.55028	-0.71485	0.8188
64.00	0.56111	-3.42181	0.2344	0.55676	-1.39974	0.2450	0.55612	-0.70216	0.2469
66.00	0.56636	-3.36676	-0.3958	0.56204	-1.37723	-0.3650	0.56141	-0.69087	-0.3830
68.00	0.57110	-3.31791	-1.0925	0.56680	-1.35726	-1.0816	0.56617	-0.68085	-1.0796
70.00	0.57534	-3.27473	-1.8674	0.57107	-1.33960	-1.8561	0.57044	-0.67199	-1.8541
72.00	0.57912	-3.23672	-2.7351	0.57487	-1.32409	-2.7236	0.57424	-0.66421	-2.7215
74.00	0.58245	-3.20368	-3.7161	0.57821	-1.31057	-3.7045	0.57759	-0.65743	-3.7024
76.00	0.58535	-3.17514	-4.8393	0.58112	-1.29891	-4.8275	0.58051	-0.65158	-4.8253
78.00	0.58783	-3.15089	-6.1467	0.58362	-1.28900	-6.1348	0.58300	-0.64662	-6.1326
80.00	0.58991	-3.13071	-7.7038	0.58571	-1.28076	-7.6918	0.58509	-0.64248	-7.6896
82.00	0.59159	-3.11442	-9.6205	0.58741	-1.27411	-9.6084	0.58679	-0.63915	-9.6061
84.00	0.59290	-3.10190	-12.1026	0.58872	-1.26900	-12.0904	0.58810	-0.63658	-12.0882
86.00	0.59382	-3.09303	-15.6125	0.58965	-1.26537	-15.6003	0.58904	-0.63477	-15.5980
88.00	0.59436	-3.08773	-21.6260	0.59021	-1.26321	-21.6136	0.58959	-0.63368	-21.6115
90.00	0.59456	-3.08597	-139.6699	0.59039	-1.26249	-139.6677	0.58978	-0.63332	-139.6654
	Radiation Efficiency			Radiation Efficiency			Radiation Efficiency		
	ETA = 0.3149, H =-0.502E+01 (dB)			ETA = 0.3148, H =-0.502E+01 (dB)			ETA = 0.3152, H =-0.501E+01 (dB)		

Table A8-28 Case 5: Medium Dry Ground, $N = 3$ ($h = 3 \times 0.05\lambda$)

N=3, CASE(5): Medium Dry Ground (Relative Dielectric Constant = 15.0, Conductivity = 0.001000 S/m)

Grazing	FREQUENCY = 6.0 MHz.			FREQUENCY = 15.0 MHz.			FREQUENCY = 30.0 MHz.		
ang, deg	Fresnel Reflect Coef		Directive gain	Fresnel Reflect Coef		Directive gain	Fresnel Reflect Coef		Directive gain
PSI(deg)	|Rv|	ang Rv(deg)	D(dBi)	|Rv|	ang Rv(deg)	D(dBi)	|Rv|	ang Rv(deg)	D(dBi)
0.00	1.00000	-180.00000	-999.9999	1.00000	-180.00000	-999.9999	1.00000	-180.00000	-999.9999
0.50	0.93213	-179.62875	-19.4126	0.93235	-179.65101	-19.4442	0.93239	-179.92546	-19.4491
1.00	0.86872	-179.25478	-13.6835	0.86814	-179.70094	-13.7141	0.86920	-179.85040	-13.7189
1.50	0.80935	-178.87526	-10.4449	0.80994	-179.54865	-10.4744	0.81003	-179.77422	-10.4790
2.00	0.75367	-178.48729	-8.2216	0.75440	-179.39296	-8.2501	0.75450	-179.69635	-8.2545
2.50	0.70135	-178.08771	-6.5516	0.70218	-179.23265	-6.5790	0.70230	-179.61615	-6.5834
3.00	0.65210	-177.67505	-5.2293	0.65300	-179.06531	-5.2558	0.65314	-179.53296	-5.2600
3.50	0.60566	-177.23953	-4.1454	0.60662	-178.89244	-4.1710	0.60676	-179.44598	-4.1750
4.00	0.56181	-176.78278	-3.2348	0.56280	-178.70926	-3.2592	0.56294	-179.35435	-3.2631
5.00	0.48110	-175.77838	-1.7780	0.48206	-178.30653	-1.8008	0.48220	-179.15292	-1.8044
6.00	0.40858	-174.60728	-0.6560	0.40940	-177.83694	-0.6770	0.40952	-178.91803	-0.6804
7.00	0.34315	-173.19183	0.2391	0.34370	-177.26906	0.2197	0.34378	-178.63399	0.2165
8.00	0.28393	-171.41025	0.9709	0.28405	-176.55312	0.9537	0.28408	-178.27577	0.9501
9.00	0.23021	-169.05791	1.5802	0.22967	-175.60406	1.5638	0.22960	-177.80066	1.5810
10.00	0.18152	-165.76236	2.0943	0.17997	-174.26274	2.0782	0.17974	-177.12831	2.0767
12.00	0.09880	-152.40618	2.9051	0.09278	-168.52808	2.8966	0.09188	-174.22993	2.8944
14.00	0.04773	-104.73233	3.5156	0.02434	-130.07385	3.5063	0.01867	-150.04689	3.5045
16.00	0.07016	-41.07962	3.9755	0.05284	-20.70421	3.9672	0.04959	-10.82862	3.9657
18.00	0.11862	-22.68665	4.3224	0.10732	-9.91372	4.3159	0.10558	-5.02667	4.3147
20.00	0.16531	-15.87302	4.5814	0.15629	-6.71162	4.5765	0.15484	-3.38414	4.5758
22.00	0.20756	-12.39734	4.7692	0.19972	-5.17379	4.7659	0.19858	-2.60329	4.7652
24.00	0.24545	-10.29028	4.8977	0.23834	-4.26571	4.8967	0.23729	-2.14414	4.8953
26.00	0.27944	-8.87327	4.9764	0.27282	-3.66376	4.9747	0.27185	-1.84045	4.9744
28.00	0.30998	-7.85208	5.0086	0.30374	-3.23416	5.0091	0.30282	-1.62402	5.0090
30.00	0.33751	-7.08192	5.0022	0.33155	-2.91154	5.0037	0.33066	-1.46153	5.0038
32.00	0.36240	-6.47844	4.9597	0.35667	-2.66011	4.9622	0.35583	-1.33516	4.9625
34.00	0.38485	-5.99314	4.8838	0.37941	-2.45859	4.8872	0.37860	-1.23384	4.8877
36.00	0.40543	-5.59457	4.7765	0.40006	-2.29350	4.7807	0.39927	-1.15087	4.7814
38.00	0.42408	-5.25169	4.6392	0.41885	-2.15591	4.6443	0.41808	-1.08174	4.6451
40.00	0.44108	-4.97988	4.4729	0.43596	-2.03961	4.4787	0.43523	-1.02333	4.4797
42.00	0.45662	-4.73858	4.2787	0.45162	-1.94018	4.2847	0.45088	-0.97340	4.2858
44.00	0.47082	-4.53010	4.0551	0.46592	-1.85437	4.0623	0.46520	-0.93031	4.0635
46.00	0.48383	-4.34859	3.8036	0.47901	-1.77974	3.8114	0.47830	-0.89284	3.8128
48.00	0.49574	-4.18966	3.5232	0.49100	-1.71440	3.5315	0.49031	-0.86005	3.5330
50.00	0.50666	-4.04950	3.2129	0.50199	-1.65691	3.2218	0.50130	-0.83119	3.2234
52.00	0.51667	-3.92562	2.8715	0.51206	-1.60609	2.8809	0.51138	-0.80569	2.8827
54.00	0.52584	-3.81569	2.4974	0.52128	-1.56102	2.5073	0.52061	-0.78308	2.5092
56.00	0.53423	-3.71790	2.0884	0.52972	-1.52095	2.0988	0.52906	-0.76297	2.1008
58.00	0.54181	-3.63075	1.6419	0.53744	-1.48525	1.6527	0.53679	-0.74506	1.6548
60.00	0.54892	-3.55300	1.1544	0.54449	-1.45343	1.1656	0.54385	-0.72909	1.1678
62.00	0.55531	-3.48364	0.6216	0.55092	-1.42508	0.6332	0.55028	-0.71485	0.6355
64.00	0.56111	-3.42181	0.0383	0.55676	-1.39974	0.0503	0.55612	-0.70216	0.0526
66.00	0.56636	-3.36676	-0.6023	0.56204	-1.37723	-0.5900	0.56141	-0.69087	-0.5876
68.00	0.57110	-3.31791	-1.3089	0.56680	-1.35726	-1.2964	0.56617	-0.68085	-1.2939
70.00	0.57534	-3.27423	-2.0928	0.57107	-1.33960	-2.0800	0.57044	-0.67199	-2.0774
72.00	0.57912	-3.23677	-2.9889	0.57487	-1.32409	-2.9558	0.57424	-0.66421	-2.9532
74.00	0.58245	-3.20368	-3.9576	0.57821	-1.31067	-3.9449	0.57759	-0.65743	-3.9416
76.00	0.58535	-3.17514	-5.0876	0.58112	-1.29891	-5.0741	0.58051	-0.65156	-5.0713
78.00	0.58783	-3.15089	-6.4010	0.58362	-1.28900	-6.3873	0.58300	-0.64662	-6.3845
80.00	0.58991	-3.13071	-7.9632	0.58571	-1.28076	-7.9494	0.58509	-0.64248	-7.9466
82.00	0.59159	-3.11442	-9.8641	0.58741	-1.27411	-9.8702	0.58679	-0.63915	-9.8673
84.00	0.59290	-3.10190	-12.3695	0.58872	-1.26900	-12.3555	0.58810	-0.63658	-12.3526
86.00	0.59382	-3.09303	-15.8818	0.58965	-1.26537	-15.8678	0.58904	-0.63477	-15.8648
88.00	0.59438	-3.08773	-21.8958	0.59021	-1.26321	-21.8827	0.58959	-0.63368	-21.8798
90.00	0.59456	-3.08597	-139.9411	0.59039	-1.26248	-139.9270	0.58978	-0.63332	-139.9241
	Radiation Efficiency			Radiation Efficiency			Radiation Efficiency		
	ETA = 0.3118, H =-0.506E+01 (dB)			ETA = 0.3126, H =-0.505E+01 (dB)			ETA = 0.3132, H =-0.504E+01 (dB)		

Table A8-29 Case 5: Medium Dry Ground, $N = 4$ ($h = 4 \times 0.05\lambda$)

N=4, CASE(5): Medium Dry Ground (Relative Dielectric Constant = 15.0, Conductivity = 0.001000 S/m)

Grazing ang. deg	FREQUENCY = 6.0 MHz. Fresnel Reflect Coef		Directive gain	FREQUENCY = 15.0 MHz. Fresnel Reflect Coef		Directive gain	FREQUENCY = 30.0 MHz. Fresnel Reflect Coef		Directive gain
PSI(deg)	|Rv|	ang Rv(deg)	D(dBi)	|Rv|	ang Rv(deg)	D(dBi)	|Rv|	ang Rv(deg)	D(dBi)
0.00	1.00000	-180.00000	-999.9999	1.00000	-180.00000	-999.9999	1.00000	-180.00000	-999.9999
0.50	0.93213	+179.62875	-19.2430	0.93235	-179.85101	-19.2755	0.93239	-179.92548	-19.2807
1.00	0.86872	-179.25478	-13.5140	0.86914	-179.70094	-13.5455	0.86920	-179.85040	-13.5506
1.50	0.80935	-178.87526	-10.2756	0.80994	+179.54865	-10.3060	0.81003	-179.77422	-10.3110
2.00	0.75367	-178.48729	-8.0526	0.75440	-179.39296	-8.0820	0.75450	-179.69635	-8.0868
2.50	0.70135	-178.08771	-6.3630	0.70218	-179.23265	-6.4113	0.70230	-179.61615	-8.4160
3.00	0.65210	+177.67305	-5.0612	0.65300	-179.06631	-5.0885	0.65314	-179.53286	-5.0921
3.50	0.60566	-177.23955	-3.9779	0.60662	-178.89244	-4.0043	0.60676	-179.44598	-4.0086
4.00	0.56181	+176.78276	-3.0677	0.56280	-178.70926	-3.0932	0.56294	-179.35435	-3.0974
5.00	0.48110	-175.77838	-1.6127	0.48206	-178.30653	-1.6383	0.48220	-179.15292	-1.6402
6.00	0.40858	-174.60728	-0.4925	0.40940	+177.83894	-0.5144	0.40952	-178.91803	-0.5161
7.00	0.34315	-173.19183	0.4003	0.34370	+177.26906	0.3801	0.34378	-178.63399	0.3766
8.00	0.28393	-171.41025	1.1296	0.28405	+176.55312	1.1109	0.28406	-178.27577	1.1077
9.00	0.23021	-169.05741	1.7360	0.22967	+175.60406	1.7188	0.22960	-177.80066	1.7156
10.00	0.18152	-165.76236	2.2469	0.17997	-174.26274	2.2310	0.17974	-177.12831	2.2282
12.00	0.09840	-152.40616	3.0543	0.09278	-168.52808	3.0410	0.09188	-174.22993	3.0386
14.00	0.04773	-104.73233	3.6531	0.02434	+130.07385	3.6421	0.01867	-150.04689	3.8401
16.00	0.07016	+41.07962	4.1020	0.05264	-20.70421	4.0931	0.04959	-10.82862	4.0914
18.00	0.11852	-22.68665	4.4378	0.10737	-9.91372	4.4308	0.10558	-5.02607	4.4294
20.00	0.16531	-15.87302	4.6846	0.15629	-6.71162	4.6793	0.15494	-3.38414	4.6782
22.00	0.20756	-12.39734	4.8591	0.19972	-5.17379	4.8554	0.19856	-2.60329	4.8546
24.00	0.24545	+10.29028	4.9733	0.23834	-4.26571	4.9710	0.23729	-2.14414	4.9704
26.00	0.27944	-8.87327	5.0357	0.27282	-3.66376	5.0347	0.27185	-1.84045	5.0344
28.00	0.30998	-7.85288	5.0522	0.30374	-3.23416	5.0531	0.30282	-1.62402	5.0530
30.00	0.33751	-7.08192	5.0293	0.33155	+2.91154	5.0309	0.33068	-1.46163	5.0310
32.00	0.36240	-6.47844	4.9691	0.35667	-2.66011	4.9718	0.35583	-1.33516	4.9721
34.00	0.38495	-5.99314	4.8749	0.37941	+2.45859	4.8785	0.37860	-1.23384	4.8791
36.00	0.40543	-5.59457	4.7487	0.40006	-2.29350	4.7533	0.39927	-1.15087	4.7541
38.00	0.42408	-5.26169	4.5920	0.41885	-2.15591	4.5976	0.41808	-1.08174	4.5986
40.00	0.44108	-4.97986	4.4080	0.43598	-2.03961	4.4124	0.43523	-1.02333	4.4138
42.00	0.45662	-4.73858	4.1912	0.45162	-1.94018	4.1985	0.45086	-0.97340	4.1998
44.00	0.47082	-4.53010	3.9479	0.46592	-1.85437	3.9560	0.46520	-0.93031	3.9575
46.00	0.48383	-4.34859	3.6761	0.47901	-1.77974	3.6849	0.47830	-0.89284	3.6867
48.00	0.49574	-4.18956	3.3763	0.49100	-1.71440	3.3849	0.49031	-0.86005	3.3868
50.00	0.50666	-4.04950	3.0448	0.50199	-1.65691	3.0551	0.50130	-0.83119	3.0571
52.00	0.51687	-3.92562	2.6835	0.51206	-1.60609	2.6944	0.51138	-0.80569	2.6966
54.00	0.52584	-3.81569	2.2897	0.52128	-1.56102	2.3013	0.52061	-0.78308	2.3036
56.00	0.53423	-3.71790	1.8615	0.52972	-1.52095	1.8736	0.52906	-0.76297	1.8761
58.00	0.54181	-3.63075	1.3961	0.53744	-1.48525	1.4089	0.53679	-0.74506	1.4115
60.00	0.54892	-3.55300	0.8905	0.54449	-1.45343	0.9037	0.54385	-0.72909	0.9065
62.00	0.55531	-3.48364	0.3402	0.55092	-1.42504	0.3540	0.55028	-0.71485	0.3569
64.00	0.56111	-3.42181	-0.2598	0.55676	-1.39974	-0.2456	0.55612	-0.70216	-0.2425
66.00	0.56636	-3.36676	-0.9183	0.56204	-1.37723	-0.9016	0.56141	-0.69087	-0.8985
68.00	0.57110	-3.31791	-1.6378	0.56680	-1.35726	-1.6228	0.56617	-0.68085	-1.6195
70.00	0.57534	-3.27473	-2.4056	0.57107	-1.33950	-2.4202	0.57044	-0.67199	-2.4168
72.00	0.57912	-3.23677	-3.3244	0.57487	-1.32409	-3.3087	0.57424	-0.66421	-3.3052
74.00	0.58245	-3.20368	-4.3248	0.57821	-1.31067	-4.3087	0.57759	-0.65743	-4.3052
76.00	0.58535	-3.17514	-5.4652	0.58112	-1.29891	-5.4488	0.58051	-0.65158	-5.4452
78.00	0.58783	-3.15089	-6.7677	0.58362	-1.28900	-6.7711	0.58300	-0.64662	-6.7674
80.00	0.58991	-3.13071	-8.3578	0.58571	-1.28076	-8.3410	0.58509	-0.64248	-8.3373
82.00	0.59159	-3.11442	-10.2851	0.58741	-1.27411	-10.2582	0.58679	-0.63915	-10.2544
84.00	0.59290	-3.10190	-12.7756	0.58872	-1.26900	-12.7585	0.58810	-0.63658	-12.7547
86.00	0.59382	-3.09303	-16.2915	0.58965	-1.26537	-16.2744	0.58904	-0.63477	-16.2705
88.00	0.59438	-3.08773	-22.3086	0.59021	-1.26321	-22.2915	0.58959	-0.63368	-22.2876
90.00	0.59456	-3.08597	-140.3537	0.59039	-1.26249	-140.3365	0.58978	-0.63332	-140.3327
	Radiation Efficiency			Radiation Efficiency			Radiation Efficiency		
	ETA = 0.3024, H =-0.512E+01 (dB)			ETA = 0.3083, H =-0.510E+01 (dB)			ETA = 0.3103, H =-0.508E+01 (dB)		

Table A8-30 Case 5: Medium Dry Ground, $N = 5$ ($h = 5 \times 0.05\lambda$)

N=5, CASE(5): Medium Dry Ground (Relative Dielectric Constant = 15.0, Conductivity = 0.001000 S/m)

Grazing ang, deg	FREQUENCY = 6.0 MHz. Fresnel Reflect Coef		Directive gain	FREQUENCY = 15.0 MHz. Fresnel Reflect Coef		Directive gain	FREQUENCY = 30.0 MHz. Fresnel Reflect Coef		Directive gain
PSI(deg)	|Rv|	ang Rv(deg)	D(dBi)	|Rv|	ang Rv(deg)	D(dBi)	|Rv|	ang Rv(deg)	D(dBi)
0.00	1.00000	-180.00000	-999.9999	1.00000	-180.00000	-999.9999	1.00000	-180.00000	-999.9999
0.50	0.93213	-179.82875	-19.0112	0.93235	-179.85101	-19.0451	0.93239	-179.92546	-19.0508
1.00	0.86872	-179.25478	-13.2824	0.86914	-179.70094	-13.3152	0.86920	-179.85040	-13.3208
1.50	0.80935	-178.87526	-10.0444	0.80994	-179.54865	-10.0761	0.81003	-179.77422	-10.0815
2.00	0.75367	-178.48729	-7.8217	0.75440	-179.39286	-7.8524	0.75450	-179.69635	-7.8577
2.50	0.70135	-178.08771	-6.1527	0.70218	-179.23265	-6.1824	0.70230	-179.61615	-6.1875
3.00	0.65210	-177.67305	-4.8316	0.65300	-179.06631	-4.8603	0.65314	-179.53296	-4.8652
3.50	0.60566	-177.23953	-3.7490	0.60667	-178.89244	-3.7767	0.60676	-179.44598	-3.7816
4.00	0.56181	-176.78276	-2.8358	0.56280	-178.70926	-2.8665	0.56294	-179.35435	-2.8712
5.00	0.48110	-175.77638	-1.3868	0.48206	-178.30653	-1.4117	0.48220	-179.15292	-1.4162
6.00	0.40858	-174.60728	-0.2693	0.40940	-177.83694	-0.2925	0.40952	-178.91803	-0.2966
7.00	0.34315	-173.19183	0.6205	0.34370	-177.28908	0.5990	0.34378	-178.63399	0.5950
8.00	0.28393	-171.41025	1.3462	0.28405	-176.55312	1.3263	0.28406	-178.27577	1.3228
9.00	0.23021	-169.05791	1.9485	0.22967	-175.60406	1.9301	0.22960	-177.80066	1.9267
10.00	0.18152	-165.76236	2.4550	0.17997	-174.26274	2.4379	0.17974	-177.12831	2.4347
12.00	0.09880	-152.40618	3.2521	0.09278	-168.52808	3.2477	0.09188	-174.22993	3.2448
14.00	0.04773	-104.73233	3.8388	0.02434	-130.07385	3.8268	0.01867	-150.04683	3.8244
16.00	0.07016	-41.07962	4.2739	0.05264	-20.70421	4.2641	0.04959	-10.82862	4.2621
18.00	0.11862	-22.68665	4.5942	0.10732	-9.91372	4.5864	0.10558	-5.02667	4.5847
20.00	0.16531	-15.87302	4.8240	0.15679	-6.71162	4.8180	0.15494	-3.38414	4.8166
22.00	0.20756	-12.39734	4.9799	0.19972	-5.17379	4.9756	0.19856	-2.60329	4.9748
24.00	0.24545	-10.29028	5.0740	0.23834	-4.26571	5.0713	0.23729	-2.14414	5.0706
26.00	0.27944	-8.87327	5.1150	0.27282	-3.66376	5.1138	0.27185	-1.84045	5.1134
28.00	0.30998	-7.85788	5.1094	0.30374	-3.23416	5.1097	0.30282	-1.62402	5.1095
30.00	0.33751	-7.08192	5.0622	0.33155	-2.91154	5.0638	0.33068	-1.46162	5.0639
32.00	0.36240	-6.47844	4.9771	0.35667	-2.66011	4.9800	0.35583	-1.33516	4.9803
34.00	0.38495	-5.99314	4.8570	0.37941	-2.45859	4.8611	0.37860	-1.23384	4.8618
36.00	0.40543	-5.59457	4.7041	0.40006	-2.29350	4.7094	0.39927	-1.15087	4.7103
38.00	0.42408	-5.26169	4.5200	0.41885	-2.15591	4.5265	0.41808	-1.08174	4.5277
40.00	0.44108	-4.97986	4.3060	0.43598	-2.03861	4.3136	0.43523	-1.02333	4.3150
42.00	0.45662	-4.73858	4.0628	0.45162	-1.94018	4.0714	0.45088	-0.97340	4.0732
44.00	0.47082	-4.53019	3.7908	0.46592	-1.85437	3.8004	0.46520	-0.93031	3.8024
46.00	0.48383	-4.34659	3.4901	0.47901	-1.77974	3.5007	0.47830	-0.89284	3.5029
48.00	0.49574	-4.18956	3.1603	0.49100	-1.71440	3.1719	0.49031	-0.86005	3.1744
50.00	0.50666	-4.04950	2.8010	0.50199	-1.65691	2.8135	0.50130	-0.83119	2.8162
52.00	0.51667	-3.92562	2.4110	0.51206	-1.60609	2.4244	0.51138	-0.80569	2.4274
54.00	0.52584	-3.81569	1.9880	0.52128	-1.56102	2.0033	0.52061	-0.78308	2.0065
56.00	0.53423	-3.71790	1.5331	0.52972	-1.52085	1.5481	0.52906	-0.76297	1.5516
58.00	0.54191	-3.63075	1.0408	0.53744	-1.48525	1.0566	0.53679	-0.74506	1.0602
60.00	0.54892	-3.55300	0.5089	0.54449	-1.45343	0.5264	0.54385	-0.72909	0.5293
62.00	0.55531	-3.48364	-0.0666	0.55092	-1.42504	-0.0493	0.55028	-0.71485	-0.0453
64.00	0.56111	-3.42181	-0.6908	0.55676	-1.39974	-0.6728	0.55612	-0.70216	-0.6886
66.00	0.56636	-3.36676	-1.3703	0.56204	-1.37723	-1.3517	0.56141	-0.69087	-1.3472
68.00	0.57110	-3.31791	-2.1134	0.56680	-1.35726	-2.0942	0.56617	-0.68085	-2.0896
70.00	0.57534	-3.27473	-2.9314	0.57107	-1.33960	-2.9116	0.57044	-0.67199	-2.9069
72.00	0.57912	-3.23677	-3.8389	0.57487	-1.32409	-3.8186	0.57424	-0.66421	-3.8137
74.00	0.58245	-3.20368	-4.8561	0.57821	-1.31057	-4.8355	0.57759	-0.65743	-4.8304
76.00	0.58535	-3.17514	-6.0117	0.58112	-1.29893	-5.9806	0.58051	-0.65158	-5.9855
78.00	0.58783	-3.15088	-7.3476	0.58362	-1.28900	-7.3261	0.58300	-0.64662	-7.3209
80.00	0.58991	-3.13071	-8.9291	0.58571	-1.28076	-8.9073	0.58509	-0.64248	-8.9020
82.00	0.59159	-3.11442	-10.8658	0.58741	-1.27411	-10.8438	0.58679	-0.63915	-10.8384
84.00	0.59290	-3.10190	-13.3637	0.58872	-1.26900	-13.3415	0.58810	-0.63658	-13.3360
86.00	0.59382	-3.09303	-16.8850	0.58965	-1.26537	-16.8626	0.58904	-0.63477	-16.8571
88.00	0.59438	-3.08773	-22.9053	0.59021	-1.26321	-22.8829	0.58959	-0.63368	-22.8773
90.00	0.59456	-3.08597	-140.9514	0.59039	-1.26249	-140.9290	0.58978	-0.63337	-140.9235
	Radiation Efficiency			Radiation Efficiency			Radiation Efficiency		
	ETA = 0.3022, H =-0.520E+01 (dB)			ETA = 0.3052, H =-0.515E+01 (dB)			ETA = 0.3066, H =-0.513E+01 (dB)		

Table A8-31 Case 6: Very Dry Ground, $N = 0$ ($h = 0 \times 0.05\lambda$)

N=0, CASE(6): Very Dry Ground (Relative Dielectric Constant = 3.0, Conductivity = 0.000100 S/m)

Grazing Ang, deg	FREQUENCY = 6.0 MHz. Fresnel Reflect Coef		Directive gain	FREQUENCY = 15.0 MHz. Fresnel Reflect Coef		Directive gain	FREQUENCY = 30.0 MHz. Fresnel Reflect Coef		Directive gain
PSI(deg)	|Rv|	ang Rv(deg)	D(dBi)	|Rv|	ang Rv(deg)	D(dBi)	|Rv|	ang Rv(deg)	D(dBi)
0.00	1.00000	-180.00000	-999.9999	1.00000	-180.00000	-999.9999	1.00000	-180.00000	-999.9999
0.50	0.96368	-179.94652	-22.4733	0.96366	-179.97874	-22.4658	0.96365	-179.98940	-22.4647
1.00	0.92867	-179.89288	-16.6108	0.92861	-179.95746	-16.6034	0.92861	-179.97874	-16.6023
1.50	0.89489	-179.83899	-13.2454	0.89482	-179.93604	-13.2381	0.89480	-179.96805	-13.2371
2.00	0.86229	-179.78468	-10.9016	0.86220	-179.91446	-10.8944	0.86218	-179.95728	-10.8934
2.50	0.83083	-179.72981	-9.1168	0.83071	-179.89267	-9.1098	0.83069	-179.94640	-9.1088
3.00	0.80043	-179.67427	-7.6853	0.80030	-179.87068	-7.6784	0.80028	-179.93536	-7.6774
3.50	0.77106	-179.61789	-6.4979	0.77091	-179.84819	-6.4909	0.77089	-179.92416	-6.4899
4.00	0.74267	-179.56052	-5.4866	0.74250	-179.82538	-5.4800	0.74248	-179.91277	-5.4790
5.00	0.68866	-179.44214	-3.8436	0.68846	-179.77832	-3.8372	0.68844	-179.88928	-3.8362
6.00	0.63808	-179.31784	-2.5506	0.63786	-179.72888	-2.5445	0.63783	-179.86458	-2.5436
7.00	0.59066	-179.18614	-1.4962	0.59042	-179.67650	-1.4923	0.59038	-179.83841	-1.4915
8.00	0.54613	-179.04533	-0.6712	0.54587	-179.62045	-0.6155	0.54583	-179.81039	-0.6147
9.00	0.50427	-178.89354	0.1225	0.50400	-179.56004	0.1279	0.50396	-179.78020	0.1287
10.00	0.46488	-178.72862	0.7614	0.46460	-179.49428	0.7666	0.46455	-179.74736	0.7673
12.00	0.39279	-178.34776	1.8007	0.39247	-179.34251	1.8053	0.39243	-179.67151	1.8060
14.00	0.32856	-177.87482	2.6095	0.32822	-179.15382	2.6086	0.32817	-179.57721	2.6092
16.00	0.27116	-177.26640	3.2364	0.27079	-178.91084	3.2400	0.27073	-179.45573	3.2406
18.00	0.21971	-176.45151	3.7371	0.21929	-178.58498	3.7402	0.21923	-179.29282	3.7407
20.00	0.17350	-175.30396	4.1339	0.17298	-178.12523	4.1365	0.17291	-179.08290	4.1369
22.00	0.13192	-173.57455	4.4480	0.13124	-177.43015	4.4481	0.13115	-178.71512	4.4484
24.00	0.09459	-170.69418	4.6872	0.09355	-176.28411	4.6888	0.09342	-178.13107	4.6891
26.00	0.06111	-165.03671	4.8678	0.05950	-173.92628	4.8690	0.05927	-176.95580	4.8691
28.00	0.03234	-148.84061	4.9955	0.02889	-167.02364	4.9962	0.02836	-170.43538	4.9963
30.00	0.01670	-89.02242	5.0762	0.00667	-89.61656	5.0765	0.00333	-89.80935	5.0766
32.00	0.03114	-33.37439	5.1145	0.02660	-14.90757	5.1144	0.02589	-7.59295	5.1144
34.00	0.05247	-19.53377	5.1139	0.04960	-8.12801	5.1133	0.04917	-4.08820	5.1133
36.00	0.07309	-14.21117	5.0769	0.07081	-5.81511	5.0760	0.07048	-2.91726	5.0758
38.00	0.09224	-11.45934	5.0065	0.09024	-4.65907	5.0043	0.08996	-2.33506	5.0041
40.00	0.10988	-9.79510	4.9013	0.10804	-3.97016	4.8997	0.10777	-1.98888	4.8994
42.00	0.12609	-8.68640	4.7650	0.12433	-3.51568	4.7630	0.12407	-1.76077	4.7628
44.00	0.14097	-7.90459	4.5971	0.13924	-3.19538	4.5949	0.13900	-1.60012	4.5946
46.00	0.15461	-7.32409	4.3979	0.15291	-2.95895	4.3953	0.15268	-1.48160	4.3950
48.00	0.16713	-6.87971	4.1668	0.16543	-2.77839	4.1640	0.16519	-1.39111	4.1636
50.00	0.17860	-6.53081	3.9033	0.17690	-2.63688	3.9003	0.17665	-1.32022	3.8998
52.00	0.18911	-6.25140	3.6063	0.18740	-2.52371	3.6030	0.18715	-1.26353	3.6025
54.00	0.19873	-6.02407	3.2741	0.19701	-2.43174	3.2706	0.19675	-1.21747	3.2701
56.00	0.20753	-5.83675	2.9047	0.20578	-2.35602	2.9010	0.20554	-1.17956	2.9004
58.00	0.21557	-5.68081	2.4955	0.21382	-2.29304	2.4916	0.21356	-1.14802	2.4910
60.00	0.22290	-5.54992	2.0431	0.22113	-2.24022	2.0390	0.22087	-1.12158	2.0384
62.00	0.22957	-5.43935	1.5432	0.22778	-2.19562	1.5390	0.22752	-1.09925	1.5383
64.00	0.23562	-5.34550	0.9906	0.23381	-2.15778	0.9862	0.23355	-1.08031	0.9856
66.00	0.24109	-5.26556	0.3785	0.23927	-2.12557	0.3740	0.23900	-1.06418	0.3733
68.00	0.24601	-5.19737	0.3018	0.24417	-2.09810	-0.3065	0.24390	-1.05043	-0.3072
70.00	0.25041	-5.13919	-1.0616	0.24856	-2.07467	-1.0684	0.24829	-1.03871	-1.0671
72.00	0.25432	-5.08985	-1.9158	0.25249	-2.05472	-1.9207	0.25219	-1.02873	-1.9214
74.00	0.25775	-5.04764	-2.8848	0.25588	-2.03782	-2.8898	0.25561	-1.02027	-2.8905
76.00	0.26076	-5.01229	-3.9974	0.25886	-2.02369	-4.0025	0.25859	-1.01315	-4.0032
78.00	0.26332	-4.98288	-5.2957	0.26141	-2.01176	-5.3008	0.26114	-1.00723	-5.3016
80.00	0.26546	-4.95885	-6.8451	0.26355	-2.00209	-6.8503	0.26327	-1.00239	-6.8510
82.00	0.26720	-4.93974	-8.7555	0.26528	-1.99440	-8.7607	0.26500	-0.99854	-8.7615
84.00	0.26854	-4.92521	-11.2327	0.26662	-1.98856	-11.2380	0.26634	-0.99562	-11.2387
86.00	0.26949	-4.91504	-14.7391	0.26756	-1.98446	-14.7444	0.26729	-0.99357	-14.7452
88.00	0.27006	-4.90896	-20.7505	0.26813	-1.98203	-20.7559	0.26785	-0.99235	-20.7566
90.00	0.27025	-4.90695	-138.7937	0.26832	-1.98122	-138.7991	0.26804	-0.99195	-138.7999
	Radiation Efficiency			Radiation Efficiency			Radiation Efficiency		
	ETA = 0.1748, M =-0.757E+01 (dB)			ETA = 0.1747, M =-0.758E+01 (dB)			ETA = 0.1747, M =-0.758E+01 (dB)		

Table A8-32 Case 6: Very Dry Ground, $N = 1$ ($h = 1 \times 0.05\lambda$)

N=1, CASE(6): Very Dry Ground (Relative Dielectric Constant = 3.0, Conductivity = 0.000100 S/m)

Grazing ang. deg	FREQUENCY = 8.0 MHz. Fresnel Reflect Coef		Directive gain	FREQUENCY = 15.0 MHz. Fresnel Reflect Coef		Directive gain	FREQUENCY = 30.0 MHz. Fresnel Reflect Coef		Directive gain
PSI(deg)	|Rv|	ang Rv(deg)	D(dBi)	|Rv|	ang Rv(deg)	D(dBi)	|Rv|	ang Rv(deg)	D(dBi)
0.00	1.00000	-180.00000	-999.9999	1.00000	-180.00000	-999.9999	1.00000	-180.00000	-999.9999
0.50	0.96368	-179.94652	-22.4335	0.96366	-179.97874	-22.4310	0.96365	-179.98840	-22.4316
1.00	0.92867	-179.89288	-16.5710	0.92861	-179.95745	-16.5686	0.92861	-179.97874	-16.5692
1.50	0.89489	-179.83899	-13.2057	0.89482	-179.93604	-13.2035	0.89480	-179.96805	-13.2041
2.00	0.86229	-179.78468	-10.8619	0.86220	-179.91446	-10.8598	0.86218	-179.95728	-10.8604
2.50	0.83083	-179.72981	-9.0773	0.83071	-179.89267	-9.0752	0.83069	-179.94640	-9.0759
3.00	0.80043	-179.67427	-7.6458	0.80030	-179.87059	-7.6439	0.80028	-179.93536	-7.6445
3.50	0.77106	-179.61789	-6.4577	0.77091	-179.84819	-6.4559	0.77088	-179.92416	-6.4565
4.00	0.74267	-179.56052	-5.4474	0.74250	-179.82538	-5.4457	0.74248	-179.91227	-5.4464
5.00	0.68886	-179.44214	-3.8047	0.68846	-179.77832	-3.8032	0.68844	-179.88928	-3.8039
6.00	0.63808	-179.31784	-2.5122	0.63786	-179.72888	-2.5109	0.63783	-179.86458	-2.5116
7.00	0.59086	-179.18614	-1.4603	0.59042	-179.67650	-1.4591	0.59038	-179.83841	-1.4599
8.00	0.54613	-179.04533	-0.5838	0.54587	-179.62045	-0.5828	0.54583	-179.81039	-0.5836
9.00	0.50427	-178.89354	0.1593	0.50400	-179.56001	0.1601	0.50396	-179.78020	0.1593
10.00	0.46488	-178.72852	0.7975	0.46460	-179.49428	0.7981	0.46455	-179.74736	0.7974
12.00	0.39279	-178.34776	1.8352	0.39247	-179.34251	1.8355	0.39243	-179.67151	1.8348
14.00	0.32856	-177.87482	2.6371	0.32822	-179.15382	2.6372	0.32817	-179.57721	2.6364
16.00	0.27116	-177.26640	3.2669	0.27079	-178.91084	3.2667	0.27073	-179.45573	3.2660
18.00	0.21971	-176.45151	3.7652	0.21929	-178.58498	3.7649	0.21923	-179.29282	3.7642
20.00	0.17350	-175.30386	4.1594	0.17298	-178.12623	4.1588	0.17291	-179.06290	4.1583
22.00	0.13192	-173.57455	4.4687	0.13124	-177.43015	4.4680	0.13115	-178.71512	4.4674
24.00	0.09453	-170.69418	4.7068	0.09356	-176.76411	4.7061	0.09342	-178.13107	4.7056
26.00	0.06111	-165.03611	4.8842	0.05950	-173.92628	4.8834	0.05927	-176.95660	4.8829
28.00	0.03234	-145.84061	5.0085	0.02849	-167.02364	5.0077	0.02836	-173.43638	5.0073
30.00	0.01670	-89.02242	5.0856	0.00667	-89.61656	5.0849	0.00333	-89.80935	5.0846
32.00	0.03114	-33.37439	5.1202	0.02660	-14.90757	5.1195	0.02589	-7.59295	5.1193
34.00	0.05247	-19.53377	5.1158	0.04980	-8.12801	5.1151	0.04917	-4.08820	5.1150
36.00	0.07309	-14.21117	5.0748	0.07081	-5.81511	5.0743	0.07048	-2.91726	5.0743
38.00	0.09224	-11.45934	4.9995	0.09024	-4.65907	4.9991	0.08996	-2.33506	4.9992
40.00	0.10988	-9.79510	4.8912	0.10804	-3.97016	4.8909	0.10777	-1.98888	4.8911
42.00	0.12609	-8.68840	4.7508	0.12433	-3.51568	4.7506	0.12407	-1.76077	4.7510
44.00	0.14097	-7.90459	4.5788	0.13924	-3.19548	4.5789	0.13900	-1.60012	4.5793
46.00	0.15461	-7.32409	4.3754	0.15291	-2.95895	4.3757	0.15266	-1.48160	4.3762
48.00	0.16713	-6.87971	4.1403	0.16543	-2.77839	4.1407	0.16519	-1.39111	4.1414
50.00	0.17860	-6.53081	3.8727	0.17690	-2.63688	3.8734	0.17665	-1.32022	3.8742
52.00	0.18911	-6.25140	3.5716	0.18740	-2.52371	3.5725	0.18715	-1.26353	3.5734
54.00	0.19873	-6.02407	3.2355	0.19701	-2.43174	3.2366	0.19676	-1.21747	3.2377
56.00	0.20753	-5.83675	2.8623	0.20579	-2.35602	2.8636	0.20554	-1.17956	2.8648
58.00	0.21557	-5.68081	2.4494	0.21382	-2.29304	2.4509	0.21356	-1.14802	2.4522
60.00	0.22290	-5.54992	1.9933	0.22113	-2.24022	1.9951	0.22087	-1.12158	1.9965
62.00	0.22957	-5.43935	1.4900	0.22778	-2.19562	1.4920	0.22752	-1.09925	1.4935
64.00	0.23562	-5.34550	0.9347	0.23381	-2.15778	0.9369	0.23355	-1.08031	0.9378
66.00	0.24109	-5.26556	0.3189	0.23927	-2.12557	0.3213	0.23900	-1.06418	0.3230
68.00	0.24601	-5.19737	-0.3643	0.24417	-2.09810	-0.3618	0.24390	-1.05043	-0.3600
70.00	0.25041	-5.13919	-1.1268	0.24856	-2.07467	-1.1241	0.24829	-1.03871	-1.1222
72.00	0.25432	-5.08965	-1.9835	0.25245	-2.05472	-1.9806	0.25219	-1.02873	-1.9787
74.00	0.25776	-5.04764	-2.9548	0.25588	-2.03782	-2.9518	0.25561	-1.02027	-2.9498
76.00	0.26078	-5.01229	-4.0694	0.25886	-2.02359	-4.0662	0.25859	-1.01315	-4.0642
78.00	0.26332	-4.98288	-5.3694	0.26141	-2.01176	-5.3661	0.26114	-1.00723	-5.3641
80.00	0.26546	-4.95885	-6.9204	0.26355	-2.00209	-6.9170	0.26327	-1.00239	-6.9148
82.00	0.26720	-4.93974	-8.8320	0.26528	-1.99440	-8.8285	0.26500	-0.99854	-8.8263
84.00	0.26854	-4.92521	-11.3102	0.26662	-1.98858	-11.3066	0.26634	-0.99562	-11.3044
86.00	0.26949	-4.91504	-14.8173	0.26758	-1.98446	-14.8137	0.26729	-0.99363	-14.8115
88.00	0.27006	-4.90896	-20.8292	0.26813	-1.98203	-20.8255	0.26785	-0.99235	-20.8233
90.00	0.27026	-4.90695	-138.8725	0.26832	-1.98122	-138.8689	0.26804	-0.99195	-138.8666
	Radiation Efficiency			Radiation Efficiency			Radiation Efficiency		
	ETA = 0.1744, M =-0.758E+01 (dB)			ETA = 0.1749, M =-0.757E+01 (dB)			ETA = 0.1751, M =-0.757E+01 (dB)		

Table A8-33 Case 6: Very Dry Ground, $N = 2$ ($h = 2 \times 0.05\lambda$)

N=2, CASE(6): Very Dry Ground (Relative Dielectric Constant = 3.0, Conductivity = 0.000100 S/m)

Grazing ang. deg	FREQUENCY = 8.0 MHz. Fresnel Reflect Coef |Rv|	Fresnel Reflect Coef ang Rv(deg)	Directive gain D(dBi)	FREQUENCY = 15.0 MHz. Fresnel Reflect Coef |Rv|	Fresnel Reflect Coef ang Rv(deg)	Directive gain D(dBi)	FREQUENCY = 30.0 MHz. Fresnel Reflect Coef |Rv|	Fresnel Reflect Coef ang Rv(deg)	Directive gain D(dBi)
PSI(deg)									
0.00	1.00000	-180.00000	-999.9999	1.00000	-180.00000	-999.9999	1.00000	-180.00000	-999.9999
0.50	0.98368	-179.94652	-22.3624	0.98368	-179.97874	-22.3625	0.98365	-179.98940	-22.3640
1.00	0.92867	-179.89288	-16.5000	0.92861	-179.95746	-16.5002	0.92861	-179.97874	-16.5017
1.50	0.89489	-179.83899	-13.1348	0.89482	-179.93604	-13.1351	0.89480	-179.96805	-13.1366
2.00	0.86229	-179.78466	-10.7911	0.86220	-179.91446	-10.7915	0.86218	-179.95728	-10.7930
2.50	0.83083	-179.72981	-9.0066	0.83071	-179.89267	-9.0071	0.83069	-179.94640	-9.0086
3.00	0.80043	-179.67422	-7.5753	0.80030	-179.87059	-7.5759	0.80028	-179.93536	-7.5775
3.50	0.77106	-179.61769	-6.3874	0.77091	-179.84819	-6.3881	0.77089	-179.92416	-6.3897
4.00	0.74267	-179.56052	-5.3774	0.74250	-179.82538	-5.3782	0.74248	-179.91277	-5.3797
5.00	0.68866	-179.44214	-3.7353	0.68846	-179.77832	-3.7363	0.68844	-179.88928	-3.7378
6.00	0.63808	-179.31784	-2.4435	0.63786	-179.72886	-2.4446	0.63783	-179.86458	-2.4462
7.00	0.59066	-179.18614	-1.3924	0.59042	-179.67650	-1.3937	0.59038	-179.83841	-1.3953
8.00	0.54613	-179.04533	-0.5188	0.54587	-179.62045	-0.5184	0.54583	-179.81039	-0.5199
9.00	0.50427	178.89354	0.2251	0.50400	-179.56001	0.2235	0.50396	-179.78020	0.2219
10.00	0.46488	-178.72852	0.8620	0.46460	-179.49428	0.8603	0.46455	-179.74736	0.8588
12.00	0.39279	-178.34776	1.8968	0.39247	-179.34251	1.8950	0.39243	-179.67151	1.8935
14.00	0.32856	-177.87482	2.6855	0.32822	-179.15382	2.6934	0.32817	-179.57724	2.6920
16.00	0.27116	-177.20040	3.3215	0.27079	-178.91084	3.3194	0.27073	-179.45573	3.3180
18.00	0.21971	-176.45151	3.8156	0.21929	-178.58498	3.8134	0.21923	-179.29282	3.8122
20.00	0.17350	-175.30396	4.2051	0.17298	-178.12523	4.2030	0.17291	-179.08290	4.2018
22.00	0.13192	-173.57455	4.5093	0.13124	-177.43015	4.5072	0.13115	-178.71512	4.5062
24.00	0.09453	-170.69418	4.7420	0.09356	-176.26411	4.7401	0.09342	-178.13107	4.7391
26.00	0.06111	-165.03671	4.9136	0.05950	-173.92628	4.9118	0.05927	-176.95660	4.9110
28.00	0.03234	-149.84061	5.0317	0.02889	-167.02364	5.0302	0.02836	-173.43538	5.0295
30.00	0.01670	+89.02242	5.1025	0.00667	-89.81656	5.1012	0.00333	-89.80935	5.1007
32.00	0.03114	-33.37439	5.1304	0.02880	+14.90757	5.1294	0.02589	-2.59295	5.1291
34.00	0.05247	-19.53327	5.1190	0.04960	-8.17801	5.1183	0.04917	-4.06820	5.1182
36.00	0.07309	-14.21117	5.0710	0.07081	+5.81511	5.0707	0.07048	-2.91726	5.0708
38.00	0.09224	-11.45834	4.9885	0.09024	-4.65907	4.9885	0.08996	-2.33506	4.9888
40.00	0.10988	-9.79510	4.8727	0.10804	-3.87016	4.8732	0.10777	-1.98688	4.8736
42.00	0.12609	-8.68840	4.7249	0.12433	-3.31568	4.7257	0.12407	-1.76077	4.7264
44.00	0.14097	-7.90459	4.5456	0.13924	-3.19538	4.5467	0.13900	-1.60012	4.5476
46.00	0.15461	-7.32409	4.3345	0.15291	-2.95895	4.3362	0.15266	-1.48180	4.3373
48.00	0.16713	-6.87971	4.0918	0.16543	-2.77639	4.0940	0.16519	-1.39111	4.0953
50.00	0.17860	-6.53081	3.8188	0.17690	-2.63688	3.8195	0.17665	-1.32022	3.8210
52.00	0.18911	-6.25140	3.5084	0.18740	-2.52371	3.5115	0.18715	-1.26353	3.5132
54.00	0.19873	-6.02407	3.1651	0.19701	-2.43174	3.1686	0.19676	-1.21747	3.1705
56.00	0.20753	-5.83675	2.7848	0.20579	-2.35602	2.7888	0.20554	-1.17956	2.7909
58.00	0.21557	-5.68081	2.3650	0.21382	-2.29304	2.3695	0.21356	-1.14802	2.3717
60.00	0.22290	-5.54992	1.9074	0.22113	-2.24022	1.9072	0.22087	-1.12158	1.9087
62.00	0.22957	-5.43935	1.3927	0.22778	-2.19562	1.3980	0.22752	-1.09925	1.4006
64.00	0.23562	-5.34550	0.8307	0.23381	-2.15778	0.8364	0.23355	-1.08031	0.8392
66.00	0.24109	-5.26556	0.2098	0.23927	-2.12557	0.2156	0.23900	-1.06418	0.2187
68.00	0.24601	-5.19737	-0.4789	0.24417	-2.09810	-0.4724	0.24390	-1.05043	-0.4694
70.00	0.25041	-5.13919	-1.2484	0.24856	-2.07467	-1.2396	0.24829	-1.03871	-1.2384
72.00	0.25432	-5.08965	-2.1077	0.25245	-2.05472	-2.1006	0.25219	-1.02873	-2.0973
74.00	0.25776	-5.04764	-3.0832	0.25588	-2.03782	-3.0758	0.25561	-1.02027	-3.0724
76.00	0.26076	-5.01229	-4.2015	0.25886	-2.02359	-4.1939	0.25859	-1.01315	-4.1904
78.00	0.26332	-4.98288	-5.5048	0.26141	-2.01176	-5.4970	0.26114	-1.00723	-5.4934
80.00	0.26546	-4.95885	-7.0586	0.26355	-2.00209	-7.0506	0.26327	-1.00239	-7.0469
82.00	0.26720	-4.93974	+8.9725	0.26528	-1.99440	-8.9643	0.26500	-0.99854	+8.9606
84.00	0.26854	-4.92521	-11.4525	0.26662	-1.98856	-11.4442	0.26634	-0.99562	-11.4405
86.00	0.26949	-4.91501	-14.9610	0.26758	-1.98446	-14.9576	0.26729	-0.99357	-14.9488
88.00	0.27006	-4.90896	+20.9736	0.26813	-1.98203	+20.9652	0.26785	-0.99235	-20.9613
90.00	0.27025	-4.90695	-139.0172	0.26832	-1.98122	-139.0087	0.26804	-0.99195	+139.0049
	Radiation Efficiency ETA = 0.1742, H =-0.759E+01 (dB)			Radiation Efficiency ETA = 0.1750, H =-0.757E+01 (dB)			Radiation Efficiency ETA = 0.1753, H =-0.756E+01 (dB)		

Table A8-34 Case 6: Very Dry Ground, $N = 3$ ($h = 3 \times 0.05\lambda$)

N=3, CASE(6): Very Dry Ground (Relative Dielectric Constant = 3.0, Conductivity = 0.000100 S/m)

Grazing ang, deg	FREQUENCY = 6.0 MHz. Fresnel Reflect Coef |Rv|	Fresnel Reflect Coef ang Rv(deg)	Directive gain D(dBi)	FREQUENCY = 15.0 MHz. Fresnel Reflect Coef |Rv|	Fresnel Reflect Coef ang Rv(deg)	Directive gain D(dBi)	FREQUENCY = 30.0 MHz. Fresnel Reflect Coef |Rv|	Fresnel Reflect Coef ang Rv(deg)	Directive gain D(dBi)
PSI(deg)									
0.00	1.00000	-180.00000	-999.9999	1.00000	-180.00000	-999.9999	1.00000	-180.00000	-999.9999
0.50	0.96368	-179.94652	-22.2436	0.96366	-179.97874	-22.2470	0.96365	-179.98940	-22.2495
1.00	0.92867	-179.89288	-16.3812	0.92861	-179.95746	-16.3847	0.92861	-179.97874	-16.3873
1.50	0.89489	-179.83699	-13.0162	0.89482	-179.93604	-13.0198	0.89480	-179.96805	-13.0223
2.00	0.86228	-179.78468	-10.6727	0.86220	-179.91446	-10.6764	0.86218	-179.95728	-10.6790
2.50	0.83083	-179.72981	-8.8884	0.83071	-179.89267	-8.8923	0.83069	-179.94640	-8.8948
3.00	0.80049	-179.67427	-7.4575	0.80030	-179.87059	-7.4614	0.80028	-179.93536	-7.4639
3.50	0.77106	-179.61789	-6.2599	0.77091	-179.84819	-6.2739	0.77089	-179.92416	-6.2765
4.00	0.74287	-179.56052	-5.2603	0.74250	-179.82538	-5.2644	0.74248	-179.91277	-5.2670
5.00	0.68855	-179.44214	-3.6192	0.68846	-179.77832	-3.6234	0.68844	-179.88928	-3.6260
6.00	0.63808	-179.31764	-2.3286	0.63786	-179.72688	-2.3330	0.63783	-179.86458	-2.3355
7.00	0.59086	-179.18614	-1.2790	0.59042	-179.67650	-1.2834	0.59038	-179.83841	-1.2860
8.00	0.54613	-179.04533	-0.4051	0.54587	-179.62045	-0.4097	0.54583	-179.81039	-0.4122
9.00	0.50427	-178.89354	0.3350	0.50400	-179.56001	0.3303	0.50396	-179.78020	0.3276
10.00	0.46588	-178.72852	0.9699	0.46460	-179.49426	0.9652	0.46455	-179.74736	0.9627
12.00	0.39279	-178.34776	1.9996	0.39247	-179.34251	1.9952	0.39243	-179.67151	1.9928
14.00	0.32856	-177.87482	2.7929	0.32822	-179.15382	2.7882	0.32817	-179.57721	2.7859
16.00	0.27116	-177.26640	3.4125	0.27079	-178.91084	3.4080	0.27073	-179.45573	3.4058
18.00	0.21971	-176.45151	3.8995	0.21929	-178.58498	3.8951	0.21923	-179.28282	3.8931
20.00	0.17350	-175.30396	4.2812	0.17298	-178.12523	4.2770	0.17291	-179.06290	4.2752
22.00	0.13192	-173.57455	4.5768	0.13124	-177.43015	4.5730	0.13115	-178.71512	4.5713
24.00	0.09453	-170.68418	4.8008	0.09358	-176.26411	4.7989	0.09342	-178.13107	4.7954
26.00	0.06111	-165.03671	4.9621	0.05950	-173.92628	4.9591	0.05927	-176.95660	4.9579
28.00	0.03234	-149.84061	5.0699	0.02889	-167.07364	5.0674	0.02836	-173.43538	5.0665
30.00	0.01670	-89.02242	5.1299	0.00667	-89.61656	5.1279	0.00333	-89.80935	5.1273
32.00	0.03114	-33.37439	5.1465	0.02660	-14.90757	5.1452	0.02589	-7.59295	5.1448
34.00	0.05247	-19.53377	5.1235	0.04980	-8.12801	5.1228	0.04817	-4.08820	5.1227
36.00	0.07309	-14.21117	5.0635	0.07081	-5.81511	5.0635	0.07048	-2.91726	5.0637
38.00	0.09224	-11.45934	4.9686	0.09024	-4.65907	4.9693	0.08996	-2.33506	4.9698
40.00	0.10988	-9.79510	4.8405	0.10804	-3.97016	4.8419	0.10777	-1.98888	4.8427
42.00	0.12609	-8.68840	4.6800	0.12433	-3.51568	4.6822	0.12407	-1.76077	4.6833
44.00	0.14097	-7.90459	4.4878	0.13924	-3.19538	4.4907	0.13900	-1.60012	4.4922
46.00	0.15461	-7.32409	4.2641	0.15291	-2.95895	4.2678	0.15268	-1.48160	4.2696
48.00	0.16713	-6.87971	4.0087	0.16543	-2.77839	4.0132	0.16519	-1.39111	4.0153
50.00	0.17860	-6.53081	3.7210	0.17690	-2.63688	3.7264	0.17665	-1.32022	3.7287
52.00	0.18911	-6.25140	3.4001	0.18740	-2.52371	3.4063	0.18715	-1.26353	3.4089
54.00	0.19873	-6.02407	3.0445	0.19701	-2.43174	3.0514	0.19676	-1.21747	3.0544
56.00	0.20753	-5.83675	2.6522	0.20578	-2.35602	2.6599	0.20554	-1.17956	2.6631
58.00	0.21557	-5.68081	2.2208	0.21382	-2.29304	2.2292	0.21356	-1.14802	2.2327
60.00	0.22290	-5.54892	1.7469	0.22113	-2.24022	1.7580	0.22087	-1.12158	1.7598
62.00	0.22957	-5.43935	1.2264	0.22778	-2.19562	1.2362	0.22752	-1.09925	1.2402
64.00	0.23562	-5.34550	0.6541	0.23381	-2.15778	0.6645	0.23355	-1.08031	0.6688
66.00	0.24109	-5.26556	0.0233	0.23927	-2.12557	0.0344	0.23900	-1.06418	0.0389
68.00	0.24601	-5.19737	-0.6745	0.24417	-2.09840	-0.6628	0.24390	-1.05043	-0.6581
70.00	0.25041	-5.13919	-1.4505	0.24856	-2.07467	-1.4393	0.24829	-1.03871	-1.4334
72.00	0.25432	-5.08965	-2.3197	0.25245	-2.05472	-2.3070	0.25219	-1.02873	-2.3019
74.00	0.25778	-5.04764	-3.3023	0.25588	-2.03782	-3.2892	0.25561	-1.02027	-3.2839
76.00	0.26078	-5.01229	-4.4271	0.25886	-2.02359	-4.4135	0.25859	-1.01315	-4.4081
78.00	0.26332	-4.98286	-5.7350	0.26141	-2.01176	-5.7221	0.26114	-1.00723	-5.7165
80.00	0.26548	-4.95885	-7.2945	0.26355	-2.00209	-7.2803	0.26327	-1.00239	-7.2746
82.00	0.26720	-4.93974	-9.2124	0.26528	-1.99440	-9.1979	0.26500	-0.99854	-9.1922
84.00	0.26854	-4.92521	-11.6955	0.26662	-1.98856	-11.6808	0.26634	-0.99562	-11.6750
86.00	0.26949	-4.91501	-15.2062	0.26756	-1.98446	-15.1914	0.26729	-0.99357	-15.1855
88.00	0.27006	-4.90898	-21.2201	0.26813	-1.98203	-21.2052	0.26785	-0.99235	-21.1993
90.00	0.27025	-4.90695	-139.2642	0.26832	-1.98122	-139.2493	0.26804	-0.99195	-139.2433
	Radiation Efficiency			Radiation Efficiency			Radiation Efficiency		
	ETA = 0.1743, H =-0.759E+01 (dB)			ETA = 0.1754, H =-0.758E+01 (dB)			ETA = 0.1756, H =-0.755E+01 (dB)		

Table A8-35 Case 6: Very Dry Ground, $N = 4$ ($h = 4 \times 0.05\lambda$)

N=4, CASE(6): Very Dry Ground (Relative Dielectric Constant = 3.0, Conductivity = 0.000100 S/m)

Grazing ang. deg	FREQUENCY = 6.0 MHz. Fresnel Reflect Coef		Directive gain	FREQUENCY = 15.0 MHz. Fresnel Reflect Coef		Directive gain	FREQUENCY = 30.0 MHz. Fresnel Reflect Coef		Directive gain
PSI(deg)	|Rv|	ang Rv(deg)	D(dBi)	|Rv|	ang Rv(deg)	D(dBi)	|Rv|	ang Rv(deg)	D(dBi)
0.00	1.00000	-180.00000	-999.9999	1.00000	-180.00000	-999.9999	1.00000	-180.00000	-999.9999
0.50	0.96368	-178.84652	-22.0735	0.96366	-179.97874	-22.0805	0.96365	-179.98940	-22.0842
1.00	0.92867	-178.89288	-16.2113	0.92861	-179.95745	-16.2184	0.92861	-179.97874	-16.2220
1.50	0.89489	-178.83899	-12.8464	0.89482	-179.93604	-12.8536	0.89480	-179.96805	-12.8572
2.00	0.86229	-178.78468	-10.5032	0.86220	-179.91446	-10.5105	0.86218	-179.95728	-10.5142
2.50	0.83083	-178.72981	-8.7193	0.83071	-179.89267	-8.7267	0.83069	-179.94640	-8.7304
3.00	0.80043	-178.67427	-7.2888	0.80030	-179.87059	-7.2962	0.80028	-179.93538	-7.3000
3.50	0.77106	-178.61799	-6.1018	0.77091	-179.84819	-6.1093	0.77089	-179.92418	-6.1130
4.00	0.74267	-178.56052	-5.0928	0.74250	-179.82538	-5.1004	0.74248	-179.91277	-5.1041
5.00	0.68866	-178.44214	-3.4531	0.68846	-179.77832	-3.4608	0.68844	-179.88928	-3.4645
6.00	0.63808	-178.31784	-2.1643	0.63786	-179.72888	-2.1721	0.63783	-179.86458	-2.1758
7.00	0.59066	-178.18614	-1.1167	0.59042	-179.67650	-1.1246	0.59038	-179.83841	-1.1283
8.00	0.54613	-178.04533	-0.2453	0.54587	-179.62045	-0.2532	0.54583	-179.81039	-0.2568
9.00	0.50427	-177.89354	0.4821	0.50400	-179.56001	0.4842	0.50396	-179.78020	0.4806
10.00	0.46468	-177.72852	1.1240	0.46460	-179.49428	1.1161	0.46455	-179.74736	1.1126
12.00	0.39279	-178.34776	2.1471	0.39247	-179.34251	2.1394	0.39243	-179.67151	2.1360
14.00	0.32856	-177.87482	2.9320	0.32822	-179.15382	2.9244	0.32817	-179.57721	2.9212
16.00	0.27116	-177.26640	3.5424	0.27079	-178.91084	3.5351	0.27073	-179.45573	3.5321
18.00	0.21971	-176.45151	4.0190	0.21929	-178.58498	4.0121	0.21923	-179.29282	4.0093
20.00	0.17350	-175.30386	4.3892	0.17298	-178.12523	4.3829	0.17291	-179.08290	4.3804
22.00	0.13192	-173.57455	4.6725	0.13124	-177.43015	4.6667	0.13115	-178.71512	4.6645
24.00	0.09453	-170.69418	4.8826	0.09356	-176.25411	4.8776	0.09342	-178.13107	4.8757
26.00	0.06111	-165.03871	5.0302	0.05950	-173.92678	5.0259	0.05927	-176.95660	5.0243
28.00	0.03234	-149.84081	5.1230	0.02889	-167.02054	5.1186	0.02838	-173.43538	5.1184
30.00	0.01670	-89.02242	5.1672	0.00667	-89.61656	5.1647	0.00333	-89.80935	5.1638
32.00	0.03114	-33.37439	5.1675	0.02660	-14.90757	5.1659	0.02589	-7.59295	5.1654
34.00	0.05247	-19.53377	5.1275	0.04980	-8.12801	5.1269	0.04917	-4.08820	5.1288
36.00	0.07309	-14.21117	5.0500	0.07081	-5.81511	5.0505	0.07048	-2.91728	5.0508
38.00	0.08224	-11.45934	4.9372	0.08024	-4.65907	4.9388	0.08996	-2.33508	4.9396
40.00	0.10988	-9.79510	4.7908	0.10804	-3.97016	4.7935	0.10777	-1.98888	4.7947
42.00	0.12809	-8.68840	4.6119	0.12433	-3.51558	4.6157	0.12407	-1.75077	4.6174
44.00	0.14097	-7.90459	4.4031	0.13924	-3.19538	4.4061	0.13900	-1.60012	4.4082
46.00	0.15461	-7.32408	4.1587	0.15291	-2.95895	4.1649	0.15268	-1.48160	4.1674
48.00	0.16713	-6.87971	3.8847	0.16543	-2.77839	3.8921	0.16519	-1.39111	3.8950
50.00	0.17860	-6.53081	3.5785	0.17690	-2.63688	3.5871	0.17665	-1.32022	3.5905
52.00	0.18911	-6.25140	3.2393	0.18740	-2.52371	3.2491	0.18715	-1.26353	3.2529
54.00	0.19873	-6.02407	2.8657	0.19701	-2.43174	2.8766	0.19676	-1.21747	2.8808
56.00	0.20753	-5.83675	2.4559	0.20579	-2.35502	2.4678	0.20554	-1.17956	2.4725
58.00	0.21557	-5.68081	2.0073	0.21382	-2.29304	2.0203	0.21356	-1.14802	2.0254
60.00	0.22290	-5.54982	1.5168	0.22113	-2.24022	1.5309	0.22087	-1.12158	1.5363
62.00	0.22957	-5.43935	0.9804	0.22778	-2.19562	0.9955	0.22752	-1.09925	1.0013
64.00	0.23562	-5.34550	0.3929	0.23381	-2.15778	0.4090	0.23355	-1.08031	0.4152
66.00	0.24109	-5.26556	-0.2522	0.23927	-2.12557	-0.2352	0.23900	-1.06410	-0.2288
68.00	0.24601	-5.19737	-0.9635	0.24417	-2.09810	-0.9457	0.24390	-1.05043	-0.9389
70.00	0.25041	-5.13919	-1.7521	0.24856	-2.07467	-1.7335	0.24829	-1.03871	-1.7265
72.00	0.25432	-5.08865	-2.6329	0.25245	-2.05472	-2.6135	0.25219	-1.02873	-2.6062
74.00	0.25776	-5.04764	-3.6261	0.25588	-2.03782	-3.6060	0.25561	-1.02027	-3.5985
76.00	0.26076	-5.01229	-4.7602	0.25886	-2.02359	-4.7396	0.25859	-1.01315	-4.7318
78.00	0.26332	-4.98286	-6.0774	0.26141	-2.01176	-6.0562	0.25114	-1.00723	-6.0483
80.00	0.26546	-4.95865	-7.6430	0.26355	-2.00209	-7.6214	0.26327	-1.00239	-7.6133
82.00	0.26720	-4.93974	-9.5667	0.26528	-1.99440	-9.5447	0.26500	-0.99854	-9.5365
84.00	0.26854	-4.92521	-12.0543	0.26662	-1.98856	-12.0321	0.26634	-0.99562	-12.0238
86.00	0.26949	-4.91501	-15.5683	0.26756	-1.98446	-15.5458	0.26729	-0.99357	-15.5375
88.00	0.27006	-4.90896	-21.5942	0.26813	-1.98203	-21.5616	0.26785	-0.99235	-21.5532
90.00	0.27025	-4.90695	-139.6289	0.26832	-1.98122	-139.6063	0.26804	-0.99195	-139.5979
	Radiation Efficiency ETA = 0.1748, H =-0.757E+01 (dB)			Radiation Efficiency ETA = 0.1763, H =-0.754E+01 (dB)			Radiation Efficiency ETA = 0.1769, H =-0.752E+01 (dB)		

Appendix B

Computer Programs

B.01 BARDEEN (INTEGRAL EQUATION)*

Program BARDEEN computes the relative power radiation pattern, directivity, and radiation resistance of a vertical electrically thin monopole element of length h at the center of a horizontal electrically small disk ground plane of radius a, at an excitation free-space wavelength λ. A description of the program is given in Sec. 3.3. The program utilizes the integral equation method of Bardeen as modified in Sec. 3.3.

The input parameters and range of values for reasonably accurate values of the output parameters are:

$2\pi h/\lambda$ = normalized element length in radians (0–6)
$\varepsilon = 2\pi a/\lambda$ = normalized ground plane radius in radians (0–2.75).

The output parameters are:

θ = elevation angle from zenith (deg)
R_{rad} = radiation resistance (ohm)
$d(\theta)$ = directivity (numeric)
$D(\theta)$ = directivity (dBi).

The program runs on an IBM compatible personal computer (PC) with a Windows 32-bit operating system (see enclosed software disk). The program is written in FORTRAN. A listing of the program is found in M. M. Weiner, et al.,

---

*Section numbers correspond to the files on the disk that accompanies this book.

Monopole Elements on Circular Ground Planes, Norwood, MA: Artech House, 1987, Appendix B.1, pp. 241–243.

B.02 RICHMOND1, RICHMOND2 (METHOD OF MOMENTS—FREE SPACE)

RICHMOND1

Program RICHMOND1 computes the input impedance and current distributions, on the element and ground plane, of a vertical monopole element of length h and radius b at the center of a horizontal disk ground plane of radius a, at an excitation free-space wavelength λ, and fed by a coaxial line with conductors of outer to inner radius ratio b_1/b. The program uses a sinusoidal-Galerkin method of moments and was written by Prof. Jack Richmond (deceased) of Ohio State University. A description of the program is given in Secs. 3.4 and 4.2.

The input parameters and range of values for reasonably accurate values of the output parameters are:

b/λ = normalized element radius in wavelengths (10^{-10} – 0.25)
h/λ = normalized element length in wavelengths (0–10)
$\varepsilon = 2\pi a/\lambda$ = normalized ground plane radius in radians (0.25–14)
b_1/b = ratio of outer to inner radii of the coaxial feed (>1)
N = number of element segments ($12h/\lambda$ − $18h/\lambda$)
M = number of ground plane concentric annular zones (12ε–18ε)
X = IX = number of subdivisions per disk annular zone (1–10).

The input parameter X is not used in RICHMOND1 but is required for RICHMOND2.

The output parameters are:

Z_{in} = input impedance (ohm)
I_n = current amplitude at beginning of nth element segment (A)
I_m = current amplitude at beginning of mth ground plane annular zone (A).

The program runs on an IBM compatible personal computer (PC) with a Windows 32-bit operating system (see enclosed software disk). The program is written in FORTRAN. A listing of the program is found in M. M. Weiner, et al., *Monopole Elements on Circular Ground Planes*, Norwood, MA: Artech House, 1987, Appendix B.2, pp. 244–273.

RICHMOND2

Program RICHMOND2 computes the radiation resistance, numeric directivity, directivity (dBi), and far-field radiated power relative to the peak power of

a vertical monopole element of length h and radius b at the center of a horizontal disk ground plane of radius a, at an excitation free-space wavelength λ, and fed by a coaxial line with conductors of outer to inner radius ratio b_1/b. The program RICHMOND2 was written by MITRE and is described in Sec. 4.2.

The input parameters and range of values for reasonably accurate values of the output parameters are the same as RICHMOND1.

The output parameters are:

R_{rad} = radiation resistance (ohm)
$d(\theta)$ = numeric directivity (numeric)
$D(\theta)$ = directivity (dBi)
$P(\theta)$ = relative power (dB).

Program RICHMOND2 runs on an IBM compatible personal computer (PC) with a Windows 32-bit operating system (see enclosed software disc). The programs are written in FORTRAN. A listing of the program is found in M. M. Weiner, et al., *Monopole Elements on Circular Ground Planes*, Norwood, MA: Artech House, 1987, Appendix B.2, pp. 274–277.

B.03 LEITNER–SPENCE (OBLATE SPHEROIDAL WAVE FUNCTIONS)

Program LEITNER–SPENCE computes the relative power radiation pattern, directivity, and radiation resistance of a vertical electrically thin *quarter-wave* monopole element at the center of a horizontal disk ground plane of radius a, at an excitation free-space wavelength λ. A description of the program is given in Sec. 3.5. The program utilizes the oblate spheroidal wave function method of Leitner and Spence as modified in Sec. 3.5.

The only input parameter and the range of values for reasonably accurate values of the output parameters are:

$\varepsilon = 2\pi a/\lambda$ = normalized ground plane radius in radians (3.0–6.5).

The output parameters are:

R_{rad} = radiation resistance (ohm)
$d(\theta)$ = directivity (numeric)
$D(\theta)$ = directivity (dBi)
θ = elevation angle measured from zenith (deg).

The program runs on an IBM personal computer (PC) with a Windows 32-bit operating system (see enclosed software disc). The program is written in FORTRAN. A listing of the program is found in M. M. Weiner, et al., *Monopole Elements on Circular Ground Planes*, Norwood, MA: Artech House, 1987, Appendix B.3, pp. 278–295.

B.04 STORER (VARIATIONAL METHOD—FREE SPACE)

Program STORER computes the input impedance $Z_{in} = R_{in} + jX_{in}$ of a vertical electrically thin monopole element of length h at the center of a horizontal electrically large disk ground plane of radius a, at an excitation free-space wavelength λ. Program STORER also computes the directivity $d(\pi/2)$ on the horizon of a vertical electrically thin element at the center of a horizontal electrically large disk ground plane of radius a. A description of the program is given in Sec. 3.7. The program utilizes the variational method of Storer as described in Sec. 3.7.

The input parameters and range of values for reasonably accurate values of the output parameters are:

$kh = 2\pi h/\lambda =$ normalized element length in radians (0–6, not $\pi, 2\pi, \ldots, n\pi$)
$\varepsilon = 2\pi a/\lambda =$ normalized ground plane radius in radians (≥ 30)
$h/b =$ element length to radius ratio ($1–10^6$).

The output variables are:

$R_{in} =$ input resistance (ohm)
$X_{in} =$ input reactance (ohm)
$d(\pi/2) =$ directivity on horizon (numeric)
$D(\pi/2) =$ directivity on horizon (dBi).

The program runs on an IBM compatible personal computer (PC) with a Windows 32-bit operating system (see enclosed software disk). The program is written in FORTRAN. A listing of the program is found in M. M. Weiner, et al., *Monopole Elements on Circular Ground Planes*, Norwood, MA: Artech House, 1987, Appendix B.4, p. 296.

B.05 AWADALLA (METHOD OF MOMENTS WITH GEOMETRICAL THEORY OF DIFFRACTION)

Program AWADALLA computes the input impedance, directivity, and relative power radiation pattern of a vertical monopole element of radius b and length h at the center of a horizontal electrically large ground plane of radius a, at an excitation free-space wavelength λ. A description of the program is given in Sec. 4.3. The program utilizes Awadalla's method of moments combined with the geometrical theory of diffraction as described in Sec. 4.3.

The input parameters and range of values for reasonably accurate values of the output parameters are:

b/λ = normalized element radius in wavelengths (10^{-10}–0.25)
h/λ = normalized element length in wavelengths (0–3)
$\varepsilon = 2\pi a/\lambda$ = normalized ground plane radius in radians (>8, finite).

The output parameters are:

Z_{in} = input impedance (ohm)
$d(\theta)$ = numeric directivity (numeric)
$D(\theta)$ = directivity (dBi)
$P(\theta)$ = relative power (dB).

Please note that the output values for peak directivity are inaccurate (too large) because the program model assumes a ground plane current distribution, identical to that for an infinite ground plane, but truncated to correspond to the finite extent of the ground plane.

The program runs on an IBM compatible personal computer (PC) with a Windows 32-bit operating system (see enclosed software disc). The program is written in FORTRAN. A listing of the program is found in M. M. Weiner, et al., *Monopole Elements on Circular Ground Planes*, Norwood, MA: Artech House, 1987, Appendix B.5, pp. 297–304.

B.06 RICHMOND5, RICHMOND6 (METHOD OF IMAGES WITH MOMENTS—FREE SPACE)

RICHMOND5

Program RICHMOND5 computes the input impedance and element current distribution of a vertical monopole element of radius b and length h at the center of a horizontal ground plane of infinite extent, at an excitation free-space wavelength λ. The program uses the method of images and the method of moments and was written by Prof. Jack Richmond (deceased) of Ohio State University. A description of the program is given in Sec. 4.4.

The input parameters and range of values for reasonably accurate values of the output parameters are:

b/λ = normalized element radius in wavelengths (10^{-10}–0.25)
h/λ = normalized element length in wavelengths (0–10)
b_1/b = ratio of outer to inner radii of the coaxial feed (>1)
σ_w = conductivity of element in megamhos/m (>0, finite) = −1 for perfectly conducting element
IFLAG = elementcurrent distribution
= 0, element current distribution computed by method of moments
= −1, element current distribution is sinusoidal and element conductivity is infinite
f = frequency in MHz (>0)

Note: If $\sigma_w = -1$, it is not necessary to specify an input value for frequency.

The output parameters are:

Z_{in} = input impedance (ohm)
I_n = current amplitude at beginning of nth element segment (A).

Program RICHMOND5 runs on an IBM compatible personal computer (PC) with a Windows 32-bit operating system (see enclosed software disc). The programs are written in FORTRAN. A listing of RICHMOND5 is within RICHMOND6 in M. M. Weiner, "Far-Zone Field of a Monopole Element on a Disk Ground Plane above Flat Earth," MITRE Technical Report MTR 92B0000090, June 1992, NTIS AD-A253580.

RICHMOND6

Program RICHMOND6 computes the input impedance, element current distribution, radiation resistance, radiation efficiency, directivity, and relative power radiation pattern of a vertical monopole element of radius b and length h at the center of a horizontal ground plane of infinite extent, at an excitation free-space wavelength λ. The program RICHMOND6 was written by J. Richmond and is described in Sec. 4.4.

The input parameters are identical to those of RICHMOND5.

The output parameters include those of RICHMOND5 with the following additional output parameters:

R_{rad} = radiation resistance (ohm)
η = radiation efficiency (numeric)
$d(\theta)$ = numeric directivity (numeric)
$D(\theta)$ = directivity (dBi)
$P(\theta)$ = relative power (dB).

The program runs on an IBM compatible personal computer (PC) with a Windows 32-bit operating system (see enclosed software disk). A listing of the program is found in M. M. Weiner, "Far-Zone Field of a Monopole Element on a Disk Ground Plane above Flat Earth," MITRE Technical Report MTR 92B0000090, June 1992, NTIS AD-A253580.

B.07 LONGLEY–RICE (TROPOSPHERIC PROPAGATION—PROGRAM ITM)

Program LONGLEY–RICE computes the basic transmission loss and excess propagation loss over that of free-space for low-altitude propagation paths over irregular terrain in the frequency range 0.02–20 GHz. The enclosed disk contains

the Institute for Telecommunication Sciences Irregular Terrain Model (ITM) of the Longley–Rice program, version 1.2.2. Ionospheric and ground wave propagation paths, which can be dominant at frequencies below 20 MHz, are not considered. Absorption and refractivity of the atmosphere at frequencies above 20 GHz are also not considered. A description of the program is given in Sec. 6.5.

The input parameters are described in Sec. 6.5.3. The output variables are statistical values of basic transmission loss, including the expected value (50% confidence level), standard deviation, and values at other confidence levels.

The program runs on an IBM compatible personal computer (PC) with a Windows 32-bit operating system (see enclosed software disk). The program is written in FORTRAN.

The enclosed disk contains the following files:

Adobe Acrobat formatted files (.pdf)

1. *itm_alg.pdf*: The ITS Irregular Terrain Model, version 1.2.2 Algorithm.
2. *itm.pdf*: The "definitive" representation of the ITS Irregular Terrain Model. It contains both the source code and a rather extensive documentation.

TeX formatted files (.tex) (If unfamiliar with TeX, use above .pdf files)

3. *itm_alg.tex*: The ITS Irregular Terrain Model, version 1.2.2 Algorithm, written in the TeX language. It is a stand-alone file, prepared for Plain TeX. It might be almost readable as is.
4. *itm.tex tm.cts itm.mds itm.ndx fwebmac.sty*: The documentation files for the programming of the ITM. This is written in the TeX language and should have the program TEX applied to it, as it is not very readable.

FORTRAN source code and sample results

5. *itm.for*: The source code for the ITM subroutines.
6. *itm_man.txt*: A manual for ITM. A straight ASCII file intended to aid the programmer in preparing a main program for ITM.
7. *uarea.for*: "Users Area model," to illustrate one way to use ITM in the *area prediction* mode. It is interactive with output directed to a file of the user's choice. This is the source code for the main program.
8. *uarea.exe*: An executable file for UAREA. Runs on an IBM compatible personal computer (PC) with a DOS operating system. Using the software that accompanies this book, enter new input values directly below sample input values. Enter "yes" to override prompt. New output values will then appear.
9. *urea_man.txt*: A manual for UAREA. A straight ASCII file.
10. *qkpfl.for*: "Quick Profile," to illustrate one way to use the ITM in the *point-to point* mode. It was written for batch processing on

a mainframe computer, but may be run on a PC by redirecting input and output. This is the source code for the main program.

11. *qkpflman.txt*: A manual for QKPFL. A straight ASCII file.
12. *qkpfl.exe*: An executable file for QKPFL. Runs on an PC with a DOS operating system.
13. *qkpfl32.exe*: An executable file for QKPFL. Runs on a PC with a DOS operating system (in 32-bit mode). You will need to put *salflibc.dll* into your c:WINDOWSSYSTEM directory for it to work.
14. *qkpflbat.txt qkpfldat.txt qkpflanx.txt*: A sample showing how to run QKPFL on a PC—a batch file which runs the program using QKPFL.DAT as input and writing output to QKPFL.ANS. When run, the latter may be compared with QKPFL.ANX. Files should be renamed to QKPFL.BAT, QKPFL.DAT, and QKPFL.ANX. The.txt suffix was used to easily view the files with your browser.

B.08 JOHNSON–GIERHART (TROPOSPHERIC PROPAGATION—PROGRAM IF-77)

Program JOHNSON–GIERHART computes the basic transmission loss and excess propagation loss over that of free-space for high-altitude propagation paths over irregular terrain in the frequency range 0.02–20 GHz. The enclosed disk contains the Institute for Telecommunication Sciences IF-77 Electromagnetic Wave Propagation Model of the Johnson–Gierhart program. Ionospheric and ground wave propagation paths, which can be dominant at frequencies below 20 MHz, are not considered. Absorption and refractivity of the atmosphere at frequencies above 20 GHz are also not considered. A description of the program is given in Sec. 6.5.

The input parameters are described in Sec. 6.5.4. The output variables are statistical values of basic transmission loss, including the expected value (50% confidence level), standard deviation, and values at other confidence levels.

The program description runs on an IBM compatible personal computer (PC) with a Windows 32-bit operating system (see enclosed software disk). The program is written in FORTRAN.

The enclosed disk contains the following files:

1. *ata.exe.*: An executable file for ATA. Runs on a, PC under DOS operating system. (Does not include change by ITS on Sept. 8, 2000.)
2. *atoa.in*: Sample input file for ITA. Run with *ata atoa.in atoa.out.*
3. *atoa.out*: Sample output file for ATA.
4. *cards.txt*: Text description of data input cards.
5. *ata.for*: Source file for ATA.
6. *aalos. for*: Source file.

7. *amsc.for*: Source file. (Does not include change by ITS on Sept. 8, 2000.)
8. *asorp.for*: Source file.

B.09 RICHMOND3, RICHMOND4 (METHOD OF MOMENTS—PROXIMITY TO EARTH)

RICHMOND3

Program RICHMOND3 computes the input impedance and current distributions, on the element and ground plane, of a vertical monopole element of length h and radius b at the center of a horizontal disk ground plane of radius a at a height z_o above flat earth of relative dielectric constant ε_r and conductivity σ, at an excitation free-space wavelength λ. The program uses a sinusoidal-Galerkin method of moments and was written by Prof. Jack Richmond (deceased) of Ohio State University. A description of the program is given in Sec. 10.1.

The input parameters and range of values for reasonably accurate values of the output parameters are:

b/λ = normalized element radius in wavelengths (10^{-10}–0.25)
h/λ = normalized element length in wavelengths (0–10)
f = frequency in MHz (>0, finite)
b_1/b = ratio of outer to inner radii of coaxial feed (>1)
$\varepsilon = 2\pi a/\lambda$ = normalized ground plane radius in radians (0.25–14)
M = number of ground plane concentric annular zones (12ε–18ε)
N = number of element segments ($12h/\lambda$–$18h/\lambda$)
z_0/λ = normalized height above earth of ground plane in wavelengths (0–0.5)
$= -1$, in absence of earth
ε_r = relative dielectric constant of earth (≥ 1)
σ = conductivity of earth in S/m (≥ 0).

The output parameters are:

Z_{in} = input impedance (ohm)
I_n = current amplitude at beginning of nth element segment (A)
I'_m = current amplitude at beginning of mth ground plane annular zone (A).

The program runs on an IBM compatible personal computer (PC) with a Windows 32-bit operating system (see enclosed software disk). The program is written in FORTRAN. A listing of the program is found in M. M. Weiner, "Far-Zone Field of a Monopole Element on a Disk Ground Plane above Flat Earth," MITRE Technical Report MTR-93B0000090, Appendix A, June 1992, NTIS, AD-A253580.

RICHMOND4

Program RICHMOND4 computes the input impedance, element and ground plane current distributions, radiation resistance, and directivity, of a vertical monopole element of length h and radius b at the center of a horizontal disk ground plane of radius a at a height z_o above flat earth of relative dielectric constant ε_r and conductivity σ, at an excitation free-space wavelength λ. Program RICHMOND 4 was written by Richmond and is described in Sec. 10.1.

The input parameters are identical to those of RICHMOND3.

The output parameters of RICHMOND4 are identical to those of RICHMOND3 with the following additional parameters:

R_{rad} = radiation resistance (ohm)
$d(\theta)$ = numeric directivity (numeric)
$D(\theta)$ = directivity (dBi)
$P(\theta)$ = relative power (dB).

The program runs on a IBM personal computer (PC) with a Windows 32-bit operating system (see enclosed software disk). The program is written in FORTRAN. A listing of the program is found in M. M. Weiner, "Far-Zone Field of a Monopole Element on a Disk Ground Plane above Flat Earth," MITRE Technical Report MTR-93B0000090, Appendix B, June 1992, NTIS, AD-A253580.

B.10 RICHMOND7 (VARIATIONAL METHOD—PROXIMITY TO EARTH)

Program RICHMOND7 computes the input impedance of a vertical monopole element of length h and radius b at the center of a horizontal disk ground plane of radius a at a height z_0 above flat earth of relative dielectric constant ε_r and conductivity σ, at an excitation free-space wavelength λ. The program combines the method of moments program RICHMOND5 of J. Richmond with the variational method of J. R. Wait and W. J. Surtees. The program was written by Prof. Jack Richmond of Ohio State University. A description of the program is given in Sec. 10.3.

The input parameters and range of values for reasonably accurate values of the output parameters are:

b/λ = normalized element radius in wavelengths (10^{-10}–0.25)
b_1/b = ratio of outer to inner radii of the coaxial feed (>1)
$\varepsilon = 2\pi a/\lambda$ = normalized ground plane radius in radians (>2)
σ = conductivity of element in megamhos/meter (>0, finite)
$= -1$, perfectly conducting element

ε_r = relative dielectric constant of earth (≥ 1)
f = frequency in MHz (>0)
z_o/λ = normalized height above earth of ground plane in wavelengths (0–0.5)
= -1, in the absence of the earth
h/λ = normalized element length in wavelengths (0–0.5)
σ = conductivity of earth in S/m (≥ 0).

The output parameters are:

Z_{inf} = input impedance for a perfect ground plane (ohms)
$Z_{in} - Z_{inf}$ = difference in input impedance from that of a perfect ground plane (ohm).

The program runs on an IBM compatible personal computer (PC) with a Windows 32-bit operating system (see enclosed software disk). The program is written in FORTRAN. A listing of the program is found in M. M. Weiner, "Far-Zone Field of a Monopole Element on a Disk Ground Plane above Flat Earth," MITRE Technical Report MTR-93B0000090, Appendix D, June 1992, NTIS, AD-A253580.

B.11 MODIFIED IMAGES (METHOD OF IMAGES WITH FRESNEL REFLECTION)

The program MODIFIED IMAGES computes the directivity and radiation efficiency of a vertical electrically thin monopole element of length h on a horizontal flat earth of relative dielectric constant ε_r and conductivity σ, at an excitation free-space wavelength λ. *Although the program computes radiation efficiency, the resulting values of radiation efficiency are inaccurate (too large) because the surface wave is not considered.* A description of the program is given in Sec. 9.2. The program was developed at MITRE and utilizes the method of images modified by Fresnel reflection.

The input parameters and range of values for reasonably accurate values of the output parameters are:

N = number of element segments, each of length 0.05λ (1–10)
ε_r = relative dielectric constant of earth (≥ 1)
σ = conductivity of earth in S/m (>0)
f = excitation frequency in MHz (>0).

The output parameters are:

$D(\psi)$ = directivity at a grazing angle ψ (dBi)
η = radiation efficiency (numeric)
H = radiation efficiency (dB)

R_v = Fresnel reflection coefficient for parallel polarization.

The program runs on an IBM compatible personal computer (PC) with a Windows 32-bit operating system (see enclosed software disk). The program is written in FORTRAN.

B.12 IONCAP (HF IONOSPHERIC PROPAGATION—PROGRAM HFWIN32)

Program IONCAP computes the basic transmission loss for space wave propagation paths through the ionosphere in the HF band (3–30 MHz). Program HFWIN32 contains the programs ICEPAC, VOACAP, and REC533. These programs are propagation programs of the Institute for Telecommunication Sciences (ITS), a research and engineering arm of the National Telecommunications and Information Administration (NTIA) of the U.S. Dept. of Commerce. These programs are written in FORTRAN and are available free to the public by downloading from the ITS Internet site at the address http://elbert.its.bldrdoc.gov/hf.html. User assistance, if required, is available for a nominal fee.

HFWIN32 utilizes several accepted HF propagation prediction models. One of the more accepted and widely used models for HF propagation predictions is Ionospheric Communications Analysis and Prediction Program (IONCAP), developed by ITS and its predecessor organizations, and first released in 1983. ICEPAC and VOACAP are direct descendents of IONCAP. VOACAP was modified by the Voice of America (VOA) to meet the demands of the HF broadcaster community. The resulting program is used by VOA to develop and coordinate broadcast schedules with other international broadcasters. The Ionospheric Communications Enhanced Profile Analysis and Circuit (ICEPAC) prediction program was developed by adding to IONCAP the Ionospheric Conductivity and Electron Density (ICED) profile model. ICED is a statistical model of the large-scale features of the northern hemisphere and contains distinct algorithms for the sub-auroral trough, aurora1 zone, and polar cap. REC533 is an implementation of Recommendation 533, Plenary Session, International Telecommunication Union, Geneva 1987, WARC HFBC-87. It was developed specifically for the planning of HF bands allocated to the broadcasting service.

The software allows color or black/white plots of any output parameter (including basic transmission loss) from any of the propagation models to be displayed and printed. Additionally, a powerful *combine* function allows area coverage maps to be mathematically combined to produce maps that represent worst or best cases for many combinations of month, sunspot number, frequencies, hours, or transmitters.

A description of IONCAP Version 78.03 (third version of IONCAP developed in 1978) is given in L. R. Teters, J. L. Lloyd, G. W. Haydon, and D. L.

Lucas, "Estimating the Performance of Telecommunication Systems Using the Ionospheric Transmission Channel: IONCAP User's Manual," NTIA Report 83-127, July 1983. This report may be downloaded at the above ITS Internet site address by clicking *here* on *Original User's Manual*. The technical manual for ICEPAC, VOACAP, and REC533 may be downloaded at the ITS site by clicking *here* on *Technical Manual*. Both of those manuals are in PKZIPed self-exploding Word Perfect 5.1 format. The input and output parameters and their various options for point-to-point models and area coverage models are described in the user's manuals.

Basic transmission loss is among the output parameters for system performance in Methods 20–22 of output options described in IONCAP User's Manual, pp. 39–40, 97–99. The median value (50% confidence level) is designated LOSS expressed in dB for the most reliable mode and consists of the free-space loss, ionospheric absorption loss, and, for multiple hops, earth reflection loss. The lower decile (10% confidence level) is designated SIG LW expressed in dB increment from the median value. The upper decile (90% confidence level) is designated SIG UP expressed in dB increment from the median value.

The transmitting and receiving antenna patterns are required input parameters for determining basic transmission loss because they determine the most reliable mode, operating frequency, and slant path. There are options for specifying one's own antenna patterns or antenna types with nominal patterns based on antenna models prior to 1983.

The present versions of the programs run on an IBM compatible personal computer (PC) with a Windows 32-bit operating system and require approximately 5.0 MB to download. The execution of these programs requires an additional 20 MB. The programs can be downloaded and installed on the PC hard drive by clicking *here* on *install from your hard drive* that links to the install file at ftp://elbert.its.bldrdoc.gov/hf.prop/Windows/pcinstall/itshfbc.exe. Program HFWIN32 on the enclosed software disk was obtained by downloading from the above website address.

Appendix C

Evaluation of Sommerfeld–King Integrals for Surface-Wave Fields

C.1 EXACT INTEGRAL EXPRESSIONS FOR PSEUDO-SURFACE WAVE FIELDS

King [85] defines the following parameters:

$$\gamma_0 = (k_0^2 - \lambda^2)^{1/2} = k_0[1 - (\lambda/k_0)^2]^{1/2} \tag{C-1}$$

$$\gamma_1 = (k_1^2 - \lambda^2)^{1/2} = (n^2 k_0^2 - \lambda^2)^{1/2} = k_0 n[1 - (\lambda/nk_0)^2]^{1/2} \tag{C-2}$$

$$N_0 = n^2 k_0^2 \gamma_0 \tag{C-3}$$

$$N = n^2 k_0^2 \gamma_0 + k_0^2 \gamma_1 = N_0 + k_0^2 \gamma_1 \tag{C-4}$$

where k_0, k_1 are the wave numbers in air and earth, respectively; γ_0, γ_1 are parameters identical to those defined in Eqs. (9.3.4) and (9.3.6); λ is identical to the eigenvalue defined in Eq. (9.3.4); and n is the earth index of refraction. The notation of Eqs. (C-1)–(C-4) differs from the notation of [85]. The difference in notation in [85] from that of this Appendix is summarized in Table C-1.

The pseudo-surface wave fields $H_{\text{pseudo-surface}} = u_\phi H_{\phi\text{pseudo-surface}}$ and $E_{\text{pseudo-surface}} = u_\rho E_{\rho\,\text{pseudo-surface}} + u_z E_{z\,\text{pseudo-surface}}$ have cylindrical coordinate components whose expressions from Eqs. 20(a)–(c) of [85] are given by

$$H_{\phi\,\text{pseudo-surface}} = [(-jn^2 k_0^2 p)/(2\pi)]\, G_\phi(\rho, z_d) \tag{C-5}$$

$$E_{\rho\,\text{pseudo-surface}} = [(-j\omega\mu_0 n^2 p)/(2\pi)] G_\rho(\rho, z_d) \tag{C-6}$$

TABLE C-1 Comparison of Notations in Appendix C and King [85]

No.	Parameter	Appendix C	King [85]
1	Time dependence	$\exp(j\omega t)$	$\exp(i\omega t) = \exp(-j\omega t)$
2	Imaginary unit	j	$-i$
3	Air half-space	Subscript o	Subscript 2
4	Earth half-space	Subscript 1	Subscript 1
5	Height of field point	z	z'
6	Height of dipole	z_0	d
7	Distance from dipole	r_0	r_1
8	Distance from dipole image	r_1	r_2
9	Distance from origin	r	r_0
10	Dipole moment	p	1
11	Trigometric identity	$\sin\theta_0 = \rho/r_0$	ρ/r_1
12	Trigometric identity	$\cos\theta_0 = (z - z_0)/r_0$	$(z' - d)/r_1$
13	Trigometric identity	$\sin\theta_1 = \rho/r_1$	ρ/r_2
14	Trigometric identity	$\cos\theta_1 = (z + z_0)/r_1$	$(z' + d)/r_2$
15	Argument, Fresnel integral	s_0	$P = (\pi/2)s_0^2$
16	Conjugate Fresnel integral	$F^*(s_0) = \int_0^{s_0} \exp[-j(\pi/2)s^2]\mathrm{d}s$	$F_2^*(P)$, subscript 2 added $= \int_0^P s^{-1/2}\exp(-js)\mathrm{d}s$
17	Complimentary conjugate Fresnel integral	$\mathscr{F}^*(s_0) = F^*(\infty) - F^*(s_0)$ $= \int_{s_0}^{\infty} \exp[-\mathrm{j}(\pi/2)s^2]\mathrm{d}s$	$\mathscr{F}_2^*(P)$, subscript 2 added $= F_2^*(\infty) - F_2^*(P)$ $= \int_P^{\infty} s^{-1/2}\exp(-js)\mathrm{d}s$
18	Positive direction of H_ϕ	$+\mathbf{u}_\phi$ unit vector	$-\mathbf{u}_\phi$ unit vector (consequence of nos. 1,2)
19	Positive direction of E_z	$+\mathbf{u}_z$ unit vector	$+\mathbf{u}_z$ unit vector
20	Positive direction of E_ρ	$+\mathbf{u}_\rho$ unit vector	$+\mathbf{u}_\rho$ unit vector

[85] R. W. P. King, *Radio Science*, Vol. 25, No. 2, March–April, 1990, pp. 149–160.

$$E_{z\,\text{pseudo-surface}} = [(-\omega\mu_0 n^2 p)/(2\pi)]G_z(\rho, z_d) \tag{C-7}$$

where p is the dipole moment and $z_d = z + z_0$.

From Eqs. 21(a)–(c) of [85],

$$G_\phi(\rho, z_d) = \int_0^\infty (N^{-1} - N_0^{-1})\exp(-j\gamma_0 z_d) J_1(\lambda\rho)\lambda^2\,\mathrm{d}\lambda \tag{C-8}$$

$$G_\rho(\rho, z_d) = \int_0^\infty \gamma_0(N^{-1} - N_0^{-1})\exp(-j\gamma_0 z_d) J_1(\lambda\rho)\lambda^2\,\mathrm{d}\lambda \tag{C-9}$$

$$G_z(\rho, z_d) = \int_0^\infty (N^{-1} - N_0^{-1})\exp(-j\gamma_0 z_d) J_0(\lambda\rho)\lambda^3\,\mathrm{d}\lambda \tag{C-10}$$

where $J_0(x)$ and $J_1(x)$ are Bessel functions of the first kind of order 0 and 1, respectively.

Equations (C-8)–(C-10) may be rewritten as

$$G_\phi(\rho, z_d) = I_\phi(\rho, z_d) - I_1(\rho, z_d) \tag{C-11}$$

$$G_\rho(\rho, z_d) = I_\rho(\rho, z_d) - I_0(\rho, z_d) \tag{C-12}$$

$$G_z(\rho, z_d) = I_z(\rho, z_d) - I_2(\rho, z_d) \tag{C-13}$$

where

$$I_\phi(\rho, z_d) = \int_0^\infty (1/N)\exp(-j\gamma_0 z_d) J_1(\lambda\rho)\lambda^2 \, d\lambda \tag{C-14a}$$

$$I_\rho(\rho, z_d) = \int_0^\infty (\gamma_0/N)\exp(-j\gamma_0 z_d) J_1(\lambda\rho)\lambda^2 \, d\lambda \tag{C-14b}$$

$$I_z(\rho, z_d) = \int_0^\infty (1/N)\exp(-j\gamma_0 z_d) J_0(\lambda\rho)\lambda^3 \, d\lambda \tag{C-14c}$$

From Eqs. (A5), (A6), and (19) of [85],

$$\begin{aligned} I_1(\rho, z_d) &= \int_0^\infty (1/N_0)\exp(-j\gamma_0 z_d) J_1(\lambda\rho)\lambda^2 \, d\lambda \\ &= -(1/n^2)(\sin\theta_1)(1/k_0 r_1)\exp(-jk_0 r_1)[1 + (jk_0 r_1)^{-1}] \end{aligned} \tag{C-15}$$

$$\begin{aligned} I_0(\rho, z_d) &= \int_0^\infty (\gamma_0/\mathrm{N}_0)\exp(-j\gamma_0 z_d) J_1(\lambda\rho)\lambda^2 \, d\lambda \\ &= -(k_0/n^2)(\sin\theta_1)(\cos\theta_1)(k_0 r_1)^{-1}\exp(-jk_0 r_1) \\ &\quad \times [1 + 3(jk_0 r_1)^{-1} + 3(jk_0 \mathrm{r}_1)^{-2}] \end{aligned} \tag{C-16}$$

$$\begin{aligned} I_2(\rho, z_d) &= \int_0^\infty (1/N_0)\exp(-j\gamma_0 z_d) J_0(\lambda\rho)\lambda^3 \, d\lambda \\ &= -(k_0/n^2)(\sin^2\theta_1)(jk_0 r_1)^{-1}\exp(-jk_0 r_1) \\ &\quad \times \{1 + (\sin^2\theta_1)^{-1}(1 - 3(\cos^2\theta_1)[(jk_0 r_1)^{-1} + (jk_0 r_1)^{-2}]\} \end{aligned} \tag{C-17}$$

where $r_1 = (\rho^2 + z_d^2)^{1/2}$. The above definite integrals and other related definite integrals of King [85] are summarized in Table C-2.

TABLE C-2 King's Definite Integrals for the Surface-Wave Fields $N_0 = n^2 k_0^2 \gamma_0$, $N = N_0 + k_0^2 \gamma_1$

No.	Symbol	Integral [85]	Exact closed-form expression
1	I_ϕ	$\int_0^\infty (1/N)\exp(-j\gamma_0 z_d) J_1(\lambda\rho)\,\lambda^2\,d\lambda$	Unknown
2	I_ρ	$\int_0^\infty (\gamma_0/N)\exp(-j\gamma_0 z_d) J_1(\lambda\rho)\lambda^2\,d\lambda$	Unknown
3	I_z	$\int_0^\infty (1/N)\exp(-j\gamma_0 z_d) J_0(\lambda\rho)\lambda^3\,d\lambda$	Unknown
4	I_1	$\int_0^\infty (1/N_0)\exp(-j\gamma_0 z_d) J_1(\lambda\rho)\lambda^2\,d\lambda$	Eq. (C-15)
5	I_0	$\int_0^\infty (\gamma_0/N_0)\exp(-j\gamma_0 z_d) J_1(\lambda\rho)\lambda^2\,d\lambda$	Eq. (C-16)
6	I_2	$\int_0^\infty (1/N_0)\exp(-j\gamma_0 z_d) J_0(\lambda\rho)\lambda^3\,d\lambda$	Eq. (C-17)
7	I_4	$-j\int_0^\infty (1/\gamma_0)\exp(-j\gamma_0 z_d) J_0(\lambda\rho)\lambda\,d\lambda$	$(1/r_1)\exp(-jk_0 r_1)$
8	$\partial I_\phi/\partial z_d$	$-j\int_0^\infty (\gamma_0/N)\exp(-j\gamma_0 z_d) J_1(\lambda\rho)\lambda^2\,d\lambda$	$-jI_\rho$
9	$\partial I_\rho/\partial z_d$	$-j\int_0^\infty (\gamma_0^2/N)\exp(-j\gamma_0 z_d) J_1(\lambda\rho)\lambda^2\,d\lambda$	Unknown
10	$\partial I_z/\partial z_d$	$-j\int_0^\infty (\gamma_0/N)\exp(-j\gamma_0 z_d) J_0(\lambda\rho)\lambda^3\,d\lambda$	Unknown
11	$\partial I_1/\partial z_d$	$-j\int_0^\infty (\gamma_0/N_0)\exp(-j\gamma_0 z_d) J_1(\lambda\rho)\lambda^2\,d\lambda$	$-jI_0$
12	$\partial I_0/\partial z_d$	$-j\int_0^\infty (\gamma_0^2/N_0)\exp(-j\gamma_0 z_d) J_1(\lambda\rho)\lambda^2\,d\lambda$	∂[Eq. (C-16)]$/\partial z_d$
13	$\partial I_2/\partial z_d$	$-j\int_0^\infty (\gamma_0/N_0)\exp(-j\gamma_0 z_d) J_0(\lambda\rho)\,\lambda^3\,d\lambda$	∂[Eq. (C-17)]$/\partial z_d$
14	$\partial I_4/\partial z_d$	$-\int_0^\infty \exp(-j\gamma_0 z_d) J_0(\lambda\rho)\lambda\,d\lambda$	$\partial[(1/r_1)\exp(-jk_0 r_1)]/\partial z_d$

[85] R. W. P. King, *Radio Science*, Vol. 25, No. 2, March–April, 1990, pp. 149–160.

Substituting Eq. (C-2) into Eq. (C-4),

$$N = n^2 k_0^{\,2}\,\gamma_0 + k_0^{\,3}\,n[1 - (\lambda/nk_0)^2]^{1/2} \tag{C-18}$$

$$n^2 k_0^{\,2}\,\gamma_0/N = 1 - (k_0^{\,3} n/N)[1 - (\lambda/nk_0)^2]^{1/2} \tag{C-19}$$

Dividing Eq. (C-19) by $n^2 k_0^{\,2}$,

$$\begin{aligned}\gamma_0/N &= (1/n^2 k_0^{\,2}) - (k_0/Nn)[1 - (\lambda/nk_0)^2]^{1/2} \\ &= (1/n^2 k_0^{\,2}) - (k_0/N)\varepsilon\end{aligned} \tag{C-20}$$

where

$$\varepsilon = (1/n)[1 - (\lambda/nk_0)^2]^{1/2} = \gamma_1/(k_0 n^2) \tag{C-21}$$

$$k_0\varepsilon = (N/n^2 k_0^{\,2}) - \gamma_0 = \gamma_1/n^2 \tag{C-22}$$

Differentiating Eq. (C-14a) with respect to z_d and substituting Eq. (C-20) into Eq. (C-14b),

$$\begin{aligned}\partial I_\phi(\rho, z_d)/\partial z_d &= -jI_\rho(\rho, z_d) = -jI_0(\rho, z_d) \\ &\quad + j\int_0^\infty (k_0\varepsilon/N)\exp(-\mathrm{j}\gamma_0 z_d) J_1(\lambda\rho)\lambda^2\,\mathrm{d}\lambda\end{aligned} \tag{C-23}$$

Differentiating Eq. (C-15) with respect to z_d,

$$\partial I_1(\rho, z_d)/\partial z_d = -jI_0(\rho, z_d) \tag{C-24}$$

Substituting Eq. (C-24) into Eq. (C-23),

$$\begin{aligned}\partial I_\phi(\rho, z_d)/\partial z_d &= \partial I_1(\rho, z_d)/\partial z_d \\ &\quad + j\int_0^\infty (k_0\varepsilon/N)\exp(-j\gamma_0 z_d) J_1(\lambda\rho)\lambda^2\,\mathrm{d}\lambda\end{aligned} \tag{C-25}$$

Differentiating Eq. (C-14b) with respect to z_d and then substituting Eqs. (C-16) and (C-20),

$$\begin{aligned}\partial I_\rho(\rho, z_d)/\partial z_d &= -j\int_0^\infty (\gamma_0^2/N)\exp(-j\gamma_0 z_d) J_1(\lambda\rho)\lambda^2\,\mathrm{d}\lambda \\ &= -j\int_0^\infty (\gamma_0^2/N_0)\exp(-j\gamma_0 z_d) J_1(\lambda\rho)\lambda^2\,\mathrm{d}\lambda \\ &\quad + j\int_0^\infty (k_0\varepsilon\gamma_0/N)\exp(-j\gamma_0 z_d) J_1(\lambda\rho)\lambda^2\,\mathrm{d}\lambda\end{aligned} \tag{C-26}$$

Differentiating Eq. (C-16) with respect to z_d,

$$\partial I_0(\rho, z_d)/\partial z_d = -j\int_0^\infty (\gamma_0^2/N_0)\exp(-j\gamma_0 z_d) J_1(\lambda\rho)\lambda^2\,\mathrm{d}\lambda \tag{C-27}$$

Substituting Eq. (C-27) into Eq. (C-26),

$$\begin{aligned}\partial I_\rho(\rho, z_d)/\partial z_d &= \partial I_0(\rho, z_d)/\partial z_d \\ &\quad + j\int_0^\infty (k_0\varepsilon\gamma_0/N)\exp(-j\gamma_0 z_d) J_1(\lambda\rho)\lambda^2\,\mathrm{d}\lambda\end{aligned} \tag{C-28}$$

Differentiating Eq. (C-14c) with respect to z_d and substituting Eq. (C-20),

$$\begin{aligned}\partial I_z(\rho, z_d)/\partial z_d &= -j\int_0^\infty (\gamma_0/N)\exp(-j\gamma_0 z_d) J_0(\lambda\rho)\lambda^3\,\mathrm{d}\lambda \\ &= -j\int_0^\infty (\gamma_0/N_0)\exp(-j\gamma_0 z_d) J_0(\lambda\rho)\lambda^3\,\mathrm{d}\lambda \\ &\quad + j\int_0^\infty (\mathrm{k}_0\varepsilon/\mathrm{N})\exp(-j\gamma_0 z_d) J_0(\lambda\rho)\lambda^3\,\mathrm{d}\lambda\end{aligned} \tag{C-29}$$

Differentiating Eq. (C-17) with respect to z_d,

$$\partial I_2(\rho, z_d)/\partial z_d = -j\int_0^\infty (\gamma_0/N_0)\exp(-j\gamma_0 z_d) J_0(\lambda\rho)\lambda^3\,\mathrm{d}\lambda \tag{C-30}$$

Substituting Eq. (C-30) into Eq. (C-29),

$$\begin{aligned}\partial I_z(\rho, z_d)/\partial z_d = \partial I_2(\rho, z_d)/\partial z_d + j\int_0^\infty (k_0\varepsilon/N)\exp \\ \times(-j\gamma_0 z_d) J_0(\lambda\rho)\lambda^3\,\mathrm{d}\lambda\end{aligned} \tag{C-31}$$

Equations (C-25), (C-28), and (C-31) are exact but not readily solveable for I_ϕ, I_ρ, and I_z, respectively. In the following development, approximate solutions are obtained for the cases $|n^2| \gg 1$ and $|n^2| \approx 1$. The parameters ε for the former case or $\varepsilon' = \varepsilon - (\gamma_0/k_0)$ for the latter case are approximately constant over the range of integration $\lambda = 0$ to $\lambda = \infty$. Furthermore, $\varepsilon = 0$ and $\varepsilon' = 0$ correspond to the cases $|n^2| = \infty$ and $|n^2| = 1$, respectively, for which exact solutions are known. Consequently, in the following development, ε or ε' is brought outside the respective integrand to obtain solveable approximate first-order differential equations. Therefore, the following development may be interpreted as a *variational* method [119] for reducing nonreadily-solveable *exact* integral equations to more-readily-solveable *approximate* equations.

C.2 $|n^2| \gg 1$, APPROXIMATE CLOSED-FORM EXPRESSIONS FOR FIELDS

Before obtaining approximate solutions for the case $|n^2| \gg 1$, consider exact results for the case $|n^2| = \infty$ corresponding to the Fresnel reflection coefficient $R_v(\theta_1) = +1$ for earth of infinite conductivity. For $|n^2| = \infty$, the Hertz potential $\Pi_{z\,\text{pseudo-surface}} = 0$ [see Eq. (9.3.16)].

Consequently,

$$H_{\phi\text{pseudo-surface}} = E_{\rho\text{pseudo-surface}} = E_{z\text{pseudo-surface}} = 0, |n^2| = \infty \tag{C-32}$$

Equation (C-32) follows also from the definitions of *pseudo-space* and *pseudo-surface* waves. Substituting Eq. (C-32) into Eqs. (C-5)–(C-7),

$$G_\phi(\rho, z_d) = G_\rho(\rho, z_d) = G_z(\rho, z_d) = 0, |n^2| = \infty \tag{C-33}$$

Substituting Eq. (C-33) into Eqs. (C-11)–(C-13),

$$I_\phi(\rho, z_d) = I_1(\rho, z_d) = 0, |n^2| = \infty \tag{C-34a}$$

$$I_\rho(\rho, z_d) = I_0(\rho, z_d) = 0, |n^2| = \infty \tag{C-34b}$$

$$I_z(\rho, z_d) = I_2(\rho, z_d) = 0, |n^2| = \infty \tag{C-34c}$$

The pseudo-surface fields are proportional to the integrals G_ϕ, G_ρ, G_z given by Eqs. (C-8)–(C-10) whose integrands contain the factor $(N^{-1} - N_0^{-1}) = -N^{-1}[(N/N_0) - 1] = -N^{-1}\xi$ where

$$\xi = (N/N_0) - 1 \tag{C-35}$$

Substituting Eqs. (C-1)–(C-4) into Eq. (C-35),

$$\begin{aligned} \xi &= {k_0}^2 \gamma_1 N_0^{-1} = \gamma_1 (n^2 \gamma_0)^{-1} \\ &= n^{-1}[1 - (\lambda/nk_0)^2]^{1/2}[1 - (\lambda/k_0)^2]^{-1/2} \end{aligned} \tag{C-36}$$

Since the pseudo-surface fields are zero for $|n^2| = \infty$ [see Eq. (C-32)], it follows from Eq. (C-36)

$$\xi = 0, |n^2| = \infty \tag{C-37}$$

$$N/N_0 = 1, |n^2| = \infty \tag{C-38}$$

An approximate solution to Eqs. (C-11)–(C-13) for the case $|n^2| \gg 1$ can be obtained by a variational method that maximizes $|\xi|$ because $|\xi|$ is proportional to the difference between the functions I_ϕ, I_ρ, I_z for $|n^2| \gg 1$ and the functions I_1, I_0, I_2 for $|n^2| = \infty$. The approximation that follows is modified from the variational method of Storer who obtained an approximate solution for the impedance of an antenna with a large ground plane by finding the variation from the exact known solution for a perfect ground plane (see Part 1, Sec. 3.7 of [119]). In Storer's variational method, an integral I is integrated by parts under conditions that allow the part containing the new integral to be neglected ($I = \int_a^b U\,\mathrm{d}V = UV|_a^b - \int_a^b V\,\mathrm{d}U \approx UV|_a^b$). In the modified variational method,

a far-field constraint is employed to approximate the previously neglected part of integration.

For $|n^2| \gg 1$, the magnitude $|\xi|$ of Eq. (C-36) is maximized the most when $\lambda/k_0 = O(1)$, second most when $\lambda/k_0 = O(\ll 1)$, and least when $\lambda/k_0 = O(n)$ where $y = O(x)$ denotes y is of the order of magnitude x. For purposes of comparison, consider (a) $\lambda/k_0 = O(0 \leq 1)$; (b) $\lambda/k_0 = O(n)$; and (c) $\lambda/k_0 = O(\ll 1)$ for $|n^2| \gg 1$.

(a)

$$|\xi| = n^{-1}|\{1 - n^{-2}[O(0 \leq 1)]^2\}^{1/2}\{1 - [O(0 \leq 1)]^2\}^{-1/2}| \approx \mathrm{n}^{-1}|\{1 - [O(0 \leq 1)]^2\}^{-1/2}|; \lambda/k_0 = O(0 \leq 1), |n^2| \gg 1 \tag{C-39a}$$

(b)

$$|\xi| = n^{-1}|\{1 - n^{-2}[O(n)]^2\}^{1/2}\{1 - [O(n)]^2\}^{-1/2}| \approx n^{-1}|[O(\ll 1)](jn)^{-1}| \approx n^{-2}[O(\ll 1)]; \lambda/k_0 = O(n), |n^2| \gg 1 \tag{C-39b}$$

(c)

$$|\xi| = n^{-1}|\{1 - n^{-2}[O(\ll 1)]^2\}^{1/2}\{1 - [O(\ll 1)]^2\}^{-1/2}| \approx n^{-1}; \lambda/k_0 = O(\ll 1)], |n^2| \gg 1 \tag{C-39c}$$

It is clear from Eqs. (C-39a–c) that $|\xi|$ is approximately an order of magnitude larger for (a) than for (c) and approximately two orders of magnitude larger for (c) than for (b). We shall assume for present purposes that

$$\lambda/k_0 = O(1), |n^2| \gg 1 \tag{C-40}$$

Equation (C-40) agrees with the requirement given by King [85] (see discussion at the beginning of the Appendix in [85]).
Substituting Eq. (C-40) into Eq. (C-21),

$$\varepsilon = n^{-1}[1 - (\lambda/nk_0)^2]^{1/2} = n^{-1}\{1 - n^{-2}[O(1)]^2\}^{1/2}; \quad \lambda/k_0 = O(1), |n^2| \gg 1 \tag{C-41a}$$

A more precise value of λ/k_0 and ε for $|n^2| \gg 1$ will be determined later from a constraint on the lowest-order term in the far-field.

For $\lambda/k_0 = O(1)$ and assuming that λ is approximately independent of n for $|n^2| \gg 1$,

$$\begin{aligned}\partial(k_0\varepsilon)/\partial\lambda &= -n^{-3}(\lambda/k_0)[1-(\lambda/nk_0)^2]^{-1/2} \\ &= -n^{-3}O(1)\{1-n^{-2}[O(1)]^2\}^{-1/2};\ \lambda/k_0 = O(1),\ |n^2| \gg 1\end{aligned} \tag{C-41b}$$

Approximate solutions to Eqs. (C-25), (C-28), and (C-31) can be obtained for $|n^2| \gg 1$ by utilization of Eqs. (C-41a and b). Integrating by parts the integral contained within Eq. (C-25),

$$\begin{aligned}&\int_0^\infty (k_0\,\varepsilon)\,N^{-1}\exp(-j\gamma_0 z_d)\,J_1(\lambda\rho)\lambda^2\,\mathrm{d}\lambda \\ &\quad = \int_0^\infty U\,\mathrm{d}V = [k_0\,\varepsilon(\lambda)V(\lambda)]\Big|_0^\infty - \int_0^\infty V(\lambda)\,[\partial(k_0\varepsilon)/\partial\lambda]\mathrm{d}\lambda \\ &\quad = \left[-k_0\varepsilon(\lambda)\int_\lambda^\infty N^{-1}\exp(-j\gamma_0 z_d)\,J_1(t\rho)t^2\,\mathrm{d}t\right]\Big|_0^\infty \\ &\qquad + \int_0^\infty\left[\int_\lambda^\infty \mathrm{N}^{-1}\exp(-j\gamma_0 z_d)\,J_1(t\rho)t^2\,\mathrm{d}t\right]\mathrm{s}[\partial(k_0\varepsilon)/\partial\lambda]\mathrm{d}\lambda \\ &\quad = k_0\varepsilon(0)\int_0^\infty N^{-1}\exp(-j\gamma_0 z_d)\,J_1(t\rho)t^2\,\mathrm{d}t \\ &\qquad + \int_0^\infty\left[\int_\lambda^\infty N^{-1}\exp(-j\gamma_0 z_d)\,J_1(t\rho)t^2\,\mathrm{d}t\right][\partial(k_0\varepsilon)/\partial\lambda]\mathrm{d}\lambda \\ &\quad \approx \left\{k_0\varepsilon(0)\int_0^\infty N^{-1}\exp(-j\gamma_0 z_d)\,J_1(\lambda\rho)\lambda^2\,\mathrm{d}\lambda\right\} \\ &\qquad \times\left\{1+[k_0\varepsilon(0)]^{-1}[\partial(k_0\varepsilon)/\partial\lambda]\Delta\lambda\right\}\end{aligned} \tag{C-42a}$$

where

$$U = k_0\varepsilon, \quad \mathrm{d}V = N^{-1}\exp(-j\gamma_0 z_d)\,J_1(t\rho)\,t^2\,\mathrm{d}t$$

$$\begin{aligned} V(\lambda) &= \int_{\infty}^{\lambda} N^{-1}\exp(-j\gamma_0 z_d)\,J_1(t\rho)t^2\,\mathrm{d}t \\ &= -\int_{\lambda}^{\infty} N^{-1}\exp(-j\gamma_0 z_d)\,J_1(t\rho)t^2\,\mathrm{d}t \end{aligned}$$

$$\varepsilon(0) = n^{-1}[1-(\lambda/nk_0)^2]^{1/2}|_{\lambda=\mathrm{o}} = n^{-1}$$

$$\begin{aligned} \Delta\lambda &= k_0\{[O(1)] - [O(\ll 1)]\} \approx k_0[O(1)] \ \text{ for } \ \lambda/k_0 \\ &= O(1) \ \text{ and } \ |n^2| \gg 1 \end{aligned} \qquad \text{(C-42b)}$$

Substituting Eq. (C-41a) into Eq. (C-42a),

$$\begin{aligned} &\int_0^{\infty} (k_0\varepsilon)N^{-1}\exp(-j\gamma_0 z_d)\,J_1(\lambda\rho)\lambda^2\,\mathrm{d}\lambda \\ &\quad\approx \left\{(k_0\varepsilon)\int_0^{\infty} N^{-1}\exp(-j\gamma_0 z_d)\,J_1(\lambda\rho)\lambda^2\,\mathrm{d}\lambda\right\} \\ &\qquad\times\left\{1-\{n^{-2}[O(1)]^2\}\{1-n^{-2}[O(1)]^2\}^{-1/2}\right\} \\ &\quad= \left\{k_0\varepsilon(0)\int_0^{\infty} \mathrm{N}^{-1}\exp(-j\gamma_0 z_d)\,J_1(\lambda\rho)\lambda^2\,\mathrm{d}t\right\} \\ &\qquad\times\left\{1-\{1-[\varepsilon/\varepsilon(0)]^2\}[\varepsilon(0)/\varepsilon\,]\right\} \\ &\quad= \left\{k_0\varepsilon(0)\int_0^{\infty} N^{-1}\exp(-j\gamma_0 z_d)\,J_1(\lambda\rho)\lambda^2\,\mathrm{d}\lambda\right\} \\ &\qquad\times\left\{1-[\varepsilon(0)/\varepsilon\,]+[\varepsilon/\varepsilon(0)]\right\} \end{aligned} \qquad \text{(C-42c)}$$

where ε and $\varepsilon(0)$ are given by Eqs. (C-41a) and (C-42b), respectively.

$$[\varepsilon/\varepsilon(0)] = 1 - x, \quad [\varepsilon(0)/\varepsilon] \approx 1 + x, \quad x \ll 1 \tag{C-42d}$$

$$\begin{aligned} 1 - [\varepsilon(0)/\varepsilon] + [\varepsilon/\varepsilon(0)] &\approx 1 - (1 + x) + (1 - x) = 1 - 2x \\ &= (1 - x) - x = [\varepsilon/\varepsilon(0)] - x \\ &\approx [\varepsilon/\varepsilon(0)], \quad |n^2| \gg 1 \end{aligned} \tag{C-42e}$$

Substituting Eq. (C-42e) into Eq. (C-42c),

$$\begin{aligned} &\int_0^\infty (k_0\varepsilon) N^{-1} \exp(-j\gamma_0 z_d) J_1(\lambda\rho)\lambda^2 \, d\lambda \\ &\quad \approx k_0\varepsilon \int_0^\infty N^{-1} \exp(-j\gamma_0 z_d) J_1(\lambda\rho)\lambda^2 \, d\lambda, \quad |n^2| \gg 1 \end{aligned} \tag{C-42f}$$

The approximation of the two integrals of Eq. (C-42a) by a single integral in Eq. (C-42f), is precisely the approximation made by Storer in his variational method [see [119], discussion following Eq. (18)] except that $\varepsilon(0)$ has been replaced by ε. *This change is found to yield more accurate results provided that the approximation of Eq. (C-42d) remains valid.* The parameter ε will be explicitly determined later from a far-field constraint, unlike King [85] who assumed that $\varepsilon = \varepsilon(0)$.

In effect then, for $|n^2| \gg 1$, the factor $(k_0\,\varepsilon)$ within the integrands of Eqs. (C-25), (C-28), and (C-31) may be treated as a constant and be brought outside the integrand without introducing appreciable error. Accordingly, Eqs. (C-25), (C-28), and (C-31) reduce to

$$\begin{aligned} \partial I_\phi(\rho, z_d)/\partial z_d &\approx \partial I_1(\rho, z_d)/\partial z_d + jk_0\varepsilon \int_0^\infty (1/N) \exp(-j\gamma_0 z_d) J_1(\lambda\rho)\lambda^2 \, d\lambda \\ &= \partial I_1(\rho, z_d)/\partial z_d + jk_0\varepsilon I_\phi(\rho, z_d), |n^2| \gg 1 \end{aligned} \tag{C-43}$$

$$\begin{aligned} \partial I_\rho(\rho, z_d)/\partial z_d &\approx \partial I_0(\rho, z_d)/\partial z_d + jk_0\varepsilon \int_0^\infty (\gamma_0/N) \exp(-j\gamma_0 z_d) J_1(\lambda\rho)\lambda^2 \, d\lambda \\ &= \partial I_0(\rho, z_d)/\partial z_d + jk_0\varepsilon I_\rho(\rho, z_d), |n^2| \gg 1 \end{aligned} \tag{C-44}$$

$$\begin{aligned} \partial I_z(\rho, z_d)/\partial z_d &\approx \partial I_2(\rho, z_d)/\partial z_d + jk_0\varepsilon \int_0^\infty (1/N) \exp(-j\gamma_0 z_d) J_0(\lambda\rho)\lambda^3 \, d\lambda \\ &= \partial I_2(\rho, z_d)/\partial z_d + jk_0\varepsilon I_z(\rho, z_d), |n^2| \gg 1 \end{aligned} \tag{C-45}$$

Eqs. (C-43)–(C-45) may be treated as first-order linear *ordinary* differential equations because differentiation is with respect to only a single variable z_d. Therefore, Eqs. (C-43)–(C-45) have the general solutions (compare with [120])

$$I_\phi(\rho, z_d) = \exp(j\varepsilon k_0 z_d)\left\{ \int \left[\partial I_1(\rho, z_d)/\partial z_d\right] \times \exp(-j\varepsilon k_0 z_d)\, \mathrm{d}z_d + F_1(\rho) \right\} \tag{C-46}$$

$$I_\rho(\rho, z_d) = \exp(j\varepsilon k_0 z_d)\left\{ \int \left[\partial I_0(\rho, z_d)/\partial z_d\right] \times \exp(-j\varepsilon k_0 z_d)\, \mathrm{d}z_d + F_2(\rho) \right\} \tag{C-47}$$

$$I_z(\rho, z_d) = \exp(j\varepsilon k_0 z_d)\left\{ \int \left[\partial I_2(\rho, z_d)/\partial z_d\right] \times \exp(-j\varepsilon k_0 z_d)\, \mathrm{d}z_d + F_3(\rho) \right\} \tag{C-48}$$

Substituting a dummy variable of integration z_3 for the variable of integration z_d and replacing the indefinite integrals with definite integrals, the particular solutions are given by

$$I_\phi(\rho, z_d) = -\int_{z_d}^{\infty} \left[\partial I_1(\rho, z_3)/\partial z_3\right] \exp\left[-j\varepsilon k_0 (z_3 - z_d)\right] \mathrm{d}z_3 \tag{C-49}$$

$$I_\rho(\rho, z_d) = -\int_{z_d}^{\infty} \left[\partial I_0(\rho, z_3)/\partial z_3\right] \exp\left[-j\varepsilon k_0 (z_3 - z_d)\right] \mathrm{d}z_3 \tag{C-50}$$

$$I_z(\rho, z_d) = -\int_{z_d}^{\infty} \left[\partial I_2(\rho, z_3)/\partial z_3\right] \exp\left[-j\varepsilon k_0 (z_3 - z_d)\right] \mathrm{d}z_3 \tag{C-51}$$

The variable z_3 is generally a complex variable. Therefore, the integration in Eqs. (C-49)–(C-51) is generally performed in the complex plane. However, for the case when z_3 is real, the limits of integration between $z_3 = \infty$ and $z_3 = z_d$ (or, with the introduction of a minus sign in front of the integral, between $z_3 = z_d$ and $z_3 = \infty$) correspond to the line source ($z_3 = \infty$ to $z_3 = z_d$) shown in Fig. 79. This line source is suggested by and identical to the line source ($z = -\infty$ to $z = -z_0$)

of Booker and Clemmow [86,87]. The line source interpretation is akin to integration along a line of *stationary* (constant) phase in the complex plane. Integrating Eqs. (C-49)–(C-51) by parts,

$$\begin{aligned} I_\phi(\rho, z_d) &= -I_1(\rho, z_3)\exp[-j\varepsilon k_0(z_3 - z_d)]\big|_{z_3=\infty} \\ &\quad + I_1(\rho, z_3)\exp[-j\varepsilon k_0(z_3 - z_d)]\big|_{z_3=z_d} \\ &\quad - j\varepsilon k_0\int_{z_d}^{\infty} I_1(\rho, z_3)\exp[-j\varepsilon k_0(z_3 - z_d)]\mathrm{d}z_3 \\ &= I_1(\rho, z_d) - j\varepsilon k_0\int_{z_d}^{\infty} A_\phi(\rho, z_3)\exp[-j\vartheta(z_3)]\mathrm{d}z_3 \end{aligned} \tag{C-52}$$

$$\begin{aligned} I_\rho(\rho, z_d) &= -I_0(\rho, z_3)\exp[-j\varepsilon k_0(z_3 - z_d)]\big|_{z_3=\infty} \\ &\quad + I_0(\rho, z_3)\exp[-j\varepsilon k_0(z_3 - z_d)]\big|_{z_3=z_d} \\ &\quad - j\varepsilon k_0\int_{z_d}^{\infty} I_0(\rho, z_3)\exp[-j\varepsilon k_0(z_3 - z_d)]\mathrm{d}z_3 \\ &= I_0(\rho, z_d) - (j\varepsilon k_0)\int_{z_d}^{\infty} j[\partial I_1(\rho, z_3)/\partial z_3]\exp[-j\vartheta(z_3)]\mathrm{d}z_3 \\ &= I_0(\rho, z_d) - \varepsilon k_0 I_\phi(\rho, z_d) \end{aligned} \tag{C-53}$$

$$\begin{aligned} I_z(\rho, z_d) &= -I_2(\rho, z_3)\exp[-j\varepsilon k_0(z_3 - z_d)]\big|_{z_3=\infty} \\ &\quad + I_2(\rho, z_3)\exp[-j\varepsilon k_0(z_3 - z_d)]\big|_{z_3=z_d} \\ &\quad - j\varepsilon k_0\int_{z_d}^{\infty} I_2(\rho, z_3)\exp[-j\varepsilon k_0(z_3 - z_d)]\mathrm{d}z_3 \\ &= I_2(\rho, z_d) - j\varepsilon k_0\int_{z_d}^{\infty} A_z(\rho, z_3)\exp[-j\vartheta(z_3)]\mathrm{d}z_3 \end{aligned} \tag{C-54}$$

where from Eqs. (C-15)–(C-17) and (C-24),

$$I_1(\rho, z_3) = -(1/n^2)(\sin\theta_3)(k_0 r_3)^{-1}\exp(-jk_0 r_3)[1 + (jk_0 r_3)^{-1}] \tag{C-55}$$

$$\begin{aligned} I_0(\rho, z_3) &= -(k_0/n^2)(\sin\theta_3)(\cos\theta_3)(k_0 r_3)^{-1}\exp(-jk_0 r_3) \\ &\quad \times [1 + 3(jk_0 r_3)^{-1} + 3(jk_0 r_3)^{-2}] \\ &= j[\partial I_1(\rho, z_3)/\partial z_3] \end{aligned} \tag{C-56}$$

$$I_2(\rho, z_3) = -(k_0/n^2)(\sin^2\theta_3)(jk_0r_3)^{-1}\exp(-jk_0r_3) \times \{1 + (\sin^2\theta_3)^{-1}(1 - 3\cos^2\theta_3)[(jk_0r_3)^{-1} + (jk_0r_3)^{-2}]\} \tag{C-57}$$

$$A_\phi(\rho, z_3) = I_1(\rho, z_3)\exp(jk_0r_3) \tag{C-58}$$

$$A_z(\rho, z_3) = I_2(\rho, z_3)\exp(jk_0r_3) \tag{C-59}$$

$$\vartheta(z_3) = k_0r_3 + \varepsilon k_0(z_3 - z_d) = k_0(\rho^2 + z_3^2)^{1/2} + \varepsilon k_0(z_3 - z_d) \tag{C-60}$$

$$r_3 = (\rho^2 + z_3^2)^{1/2}, \sin\theta_3 = \rho/r_3, \cos\theta_3 = z_3/r_3 \tag{C-61}$$

The method of *stationary phase* may be utilized to obtain approximate closed-form expressions for the integrals of Eqs. (C-52) and (C-54). The following description of the method is from Jackson [121] with additions enclosed in brackets.

> "The method of *stationary* phase addresses itself to the problem of evaluating integrals of the general type, $I = \int_{\omega_1}^{\omega_2} A(\omega)\exp[i\vartheta(\omega)]\mathrm{d}\omega$ where $A(\omega)$ is a function that varies relatively slowly with ω and $\vartheta(\omega)$ is a phase that is generally large and rapidly varying. The rapid oscillations of $\exp[i\vartheta(\omega)]$ over most of the range of integration means that the integrand averages to almost zero.Exceptions to this cancellation occur only when $\vartheta(\omega)$ is 'stationary', that is, when $\vartheta(\omega)$ has an extremum [provided that $A(\omega)$ is not zero at the extremum]. The integral can therefore be estimated by finding the place where $\vartheta(\omega)$ has a vanishing derivative [or other extremum], evaluating approximately the integral in the neighborhood of each of these [extremum] points, and summing the contributions. Let $\vartheta(\omega)$ have a vanishing first derivative [or other extremum] at $\omega = \omega_S$. In the neighborhood of this point, $\vartheta(\omega)$ can be expanded in a Taylor series $\vartheta(\omega) = \vartheta_S + \vartheta'_S(\omega - \omega_S) + (1/2)\vartheta''_S(\omega - \omega_S)^2 + \cdots$. Here the subscript s is used to indicate that ϑ, ϑ', or ϑ'' are evaluated at $\omega = \omega_S$. Since $A(\omega)$ is slowly varying, the contribution to the integral from this stationary phase point is approximately
>
> $$I_S \approx A(\omega_S)\exp[i\vartheta(\omega_S)]\int_{\omega_1}^{\omega_2}\exp\{i[\vartheta'_S(\omega - \omega_S) + (1/2)\vartheta''_S(\omega - \omega_S)^2)]\}\mathrm{d}\omega$$
>
> If the extremum is a vanishing first derivative then the remaining integral can be recognized as a Fresnel integral." [If the extremum is

a minimum or maximum of $\vartheta(\omega)$, then the remaining integral can also be arranged as a Fresnel integral by adding a constant phase to the integrand so that the resulting phase varies only as $(\omega - \omega_S)^2$ (see A. Papoulis, *Signal Analysis*, New York: McGraw-Hill, 1977, pp. 271–273)].

The phase $\vartheta(z_3)$ in the integrands of Eqs. (C-52) and (C-54) is a monotonic increasing function over the range of integration and has a minimum value at the extremum point $z_3 = z_d$. There are no other extremum points within the range of integration except at $z_3 = \infty$ where the amplitudes $A_\phi(\infty) = A_z(\infty) = 0$. The corresponding integrals are of a form suitable for evaluation by the method of stationary phase. The amplitudes $A_\phi(z_3)A_z(z_3)$ vary slowly and the phase $\vartheta(z_3)$ varies rapidly over the range of integration *except for small values of* $k_0 z_3$ *when* $k_0\rho$ *is also small*. The method of stationary phase should therefore produce reasonably accurate evaluations of the integrals, except for small values of $k_0 r_1$. In Eq. (C-53), the amplitude function $I_0(\rho, z_3)$ is zero at the extremum $z_3 = z_d$ when $z_d = 0$. Since the method of stationary phase can fail for such a condition, Eq. (C-53) is integrated by parts *before* applying the method of stationary phase. For the same reason, Eq. (C-49) is integrated by parts before applying the method of stationary phase.

In accordance with the method of stationary phase, the respective amplitudes within the integrands may be approximated by

$$A_\phi(\rho, z_3) \approx A_\phi(\rho, z_d) = I_1(\rho, z_d)\exp(jk_0 r_1) \tag{C-62a}$$

$$A_z(\rho, z_3) \approx A_z(\rho, z_d) = I_2(\rho, z_d)\exp(jk_0 r_1) \tag{C-62b}$$

Furthermore, rapid variation of $A_\phi(\rho, z_3)$ and $A_z(\rho, z_3)$ is reduced for small values of $k_0 r_3$ by ignoring higher-order terms $(jk_0 r_3)^{-2}$ and $(jk_0 r_3)^{-3}$. Consequently, the method of stationary phase is more accurate (as confirmed later by numerical integration) if Eqs. (C-62a and b) are approximated by

$$A_\phi(\rho, z_3) \approx I_{11}(\rho, z_d)\exp(jk_0 r_1) = -(1/n^2)(\sin\theta_1)(k_0 r_1)^{-1} \tag{C-62c}$$

$$A_z(\rho, z_3) \approx I_{21}(\rho, z_d)\exp(jk_0 r_1) = -(k_0/n^2)(\sin^2\theta_1)(jk_0 r_1)^{-1} \tag{C-62d}$$

Substituting Eq. (C-62a–d) into Eqs. (C-52)–(C-54),

$$I_\phi(\rho, z_d) \approx I_1(\rho, z_d) - j\varepsilon k_0 I_{11}(\rho, z_d)\exp(jk_0 r_1)\int_{z_d}^{\infty}\exp[-j\vartheta(z_3)]\mathrm{d}z_3 \tag{C-63a}$$

$$I_\rho(\rho, z_d) \approx I_0(\rho, z_d) - \varepsilon k_0 I_\phi(\rho, z_d) \tag{C-63b}$$

$$I_z(\rho, z_d) \approx I_2(\rho, z_d) - j\varepsilon k_0 I_{21}(\rho, z_d)\exp(jk_0 r_1)\int_{z_d}^{\infty}\exp[-j\vartheta(z_3)]\mathrm{d}z_3 \tag{C-63c}$$

Expanding $\vartheta(z_3)$ in a Taylor series about $z_3 = z_d$ and retaining the first three terms,

$$\begin{aligned}\vartheta(z_3) &= \vartheta(z_3)|_{z_3=z_d} + [\mathrm{d}\vartheta(z_3)/\mathrm{d}z_3]|_{z_3=z_d}(z_3 - z_d) \\ &\quad + (1/2)[d^2\vartheta(z_3)/\mathrm{d}z_3^2]|_{z_3=z_d}(z_3 - z_d)^2 \\ &= k_0 r_1 + [(z_d/r_1) + \varepsilon]k_0(z_3 - z_d) + (1/2)(1/k_0 r_1)[1 - (z_d/r_1)^2]k_0^2(z_3 - z_d)^2 \\ &= k_0 r_1 + (\varepsilon + \cos\theta_1)k_0(z_3 - z_d) + (1/2k_0 r_1)k_0^2(z_3 - z_d)^2\sin^2\theta_1\end{aligned} \tag{C-64}$$

where

$z_d/r_1 = \cos\theta_1$ (see Table C-1 and Fig. 79)

$$\begin{aligned}\vartheta(z_3)|_{z_3=z_d} &= k_0 r_1[\mathrm{d}\vartheta(z_3)/\mathrm{d}z_3]|_{z_3=z_d} = k_0^2[(z_d/r_1) + \varepsilon] \\ &= k_0[\cos\theta_1 + \varepsilon][\mathrm{d}^2\vartheta(z_3)/\mathrm{d}z_3^2]|_{z_3=z_d} = k_0^2(1/k_0 r_1)[1 - (z_d/r_1)^2] \\ &= k_0^2(1/k_0 r_1)\sin^2\theta_1\end{aligned}$$

Now let $f(a)$ be some unknown function that satisfies the identity

$$\vartheta(z_3) + [f(a)]^2 - k_0 r_1 = [f(a) + (1/2k_0 r_1)^{1/2}k_0^2(z_3 - z_d)\sin\theta_1]^2 \tag{C-65}$$

Substituting $\vartheta(z_3)$ from Eq. (C-64) into Eq. (C-65) and solving for $f(a)$,

$$f(a) = (\varepsilon + \cos\theta_1)(1/\sin\theta_1)(k_0 r_1/2)^{1/2} \tag{C-66}$$

Substituting Eq. (C-66) into Eq. (C-65),

$$\begin{aligned}\vartheta(z_3) &= -[(\varepsilon + \cos\theta_1)(1/\sin\theta_1)]^2(k_0 r_1/2) + k_0 r_1 \\ &\quad + [(\varepsilon + \cos\theta_1)(1/\sin\theta_1)(k_0 r_1/2)^{1/2} + (2k_0 r_1)^{-1/2}k_0(z_3 - z_d)\sin\theta_1]^2\end{aligned} \tag{C-67}$$

Substituting Eq. (C-67) into Eq. (C-63a and c),

$$I_\phi(\rho,z_d)=I_1(\rho,z_d)-j\varepsilon k_0 I_{11}(\rho,z_d)\exp\{jk_0[(\varepsilon+\cos\theta_1)(1/\sin\theta_1)]^2(r_1/2)\}$$
$$\times\int_{z_d}^{\infty}\exp\{-j[(\varepsilon+\cos\theta_1)(1/\sin\theta_1)(k_0r_1/2)^{1/2} \tag{C-68}$$
$$+(2k_0r_1)^{-1/2}k_0(z_3-z_d)\sin\theta_1]^2\}\mathrm{d}z_3$$

$$I_z(\rho,z_d)=I_2(\rho,z_d)-j\varepsilon k_0 I_{21}(\rho,z_d)\exp\{jk_0[(\varepsilon+\cos\theta_1)(1/\sin\theta_1)]^2(r_1/2)\}$$
$$\times\int_{z_d}^{\infty}\exp\{-j[(\varepsilon+\cos\theta_1)(1/\sin\theta_1)(k_0r_1/2)^{1/2} \tag{C-69}$$
$$+(2k_0r_1)^{-1/2}k_0(z_3-z_d)\sin\theta_1]^2\}\mathrm{d}z_3$$

Introducing the variable s defined by

$$\begin{aligned} s &= s_0+(2/\pi)^{1/2}(2k_0r_1)^{-1/2}k_0(z_3-z_d)\sin\theta_1 \\ &= s_0+(\pi k_0r_1)^{-1/2}k_0(z_3-z_d)\sin\theta_1 \end{aligned} \tag{C-70}$$

$$\begin{aligned} s_0 &= s|_{z_3=z_d}=(2/\pi)^{1/2}(\varepsilon+\cos\theta_1)(1/\sin\theta_1)(k_0r_1/2)^{1/2} \\ &= (\varepsilon+\cos\theta_1)(1/\sin\theta_1)(k_0r_1/\pi)^{1/2} \end{aligned} \tag{C-71}$$

it follows that

$$\mathrm{d}s=\sin\theta_1(\pi k_0r_1)^{-1/2}k_0\,\mathrm{d}z_3 \tag{C-72}$$

$$\mathrm{d}z_3=(1/k_0\sin\theta_1)(\pi k_0r_1)^{1/2}\,\mathrm{d}s \tag{C-73}$$

$$(\pi k_0r_1)^{1/2}=\pi s_0\sin\theta_1(\varepsilon+\cos\theta_1)^{-1} \tag{C-74}$$

Substituting Eqs. (C-70)–(C-74) into Eqs. (C-68) and (C-69),

$$I_\phi(\rho,z_d)=I_1(\rho,z_d)-I_{11}(\rho,z_d)j\pi s_0\varepsilon(\varepsilon+\cos\theta_1)^{-1}$$
$$\times\exp[j(\pi/2)s_0^2]\int_{s_0}^{\infty}\exp[-j(\pi/2)s^2]\mathrm{d}s \tag{C-75}$$
$$=I_1(\rho,z_d)-I_{11}(\rho,z_d)j\pi s_0\varepsilon(\varepsilon+\cos\theta_1)^{-1}\times\exp[j(\pi/2)s_0^2]\mathscr{F}^*(s_0)\}$$

$$I_z(\rho,z_d) = I_2(\rho,z_d) - I_{21}(\rho,z_d) j\pi s_0 \varepsilon(\varepsilon+\cos\theta_1)^{-1} \times \exp[j(\pi/2)s_0^2]\int_{s_0}^{\infty} \exp[-j(\pi/2)s^2]\mathrm{d}s \quad \text{(C-76)}$$
$$= I_2(\rho,z_d) - I_{21}(\rho,z_d) j\pi s_0 \varepsilon(\varepsilon+\cos\theta_1)^{-1} \times \exp[j(\pi/2)s_0^2]\mathscr{F}^*(s_0)\}$$

where

$$\mathscr{F}^*(s_0) = \text{complimentary conjugate Fresnel integral} = \int_{s_0}^{\infty} \exp[-j(\pi/2)s^2]\mathrm{d}s = F^*(\infty) - F^*(s_0) \quad \text{(C-77)}$$

$$F^*(\infty) = \int_0^{\infty} \exp[-j(\pi/2)s^2]\mathrm{d}s [= (1-j)/2, s \text{ real}] \quad \text{(C-78)}$$

$$F^*(s_0) = \text{conjugate Fresnel integral} = \int_0^{s_0} \exp[-j(\pi/2)s^2]\mathrm{d}s \quad \text{(C-79)}$$

Substituting Eqs. (C-63b), (C-75), and (C-76) into Eqs. (C-11)–(C-13),

$$G_\phi(\rho, z_d) - j\varepsilon\pi s_0 I_{11}(\rho, z_d)(\varepsilon + \cos\theta_1)^{-1} \exp[j(\pi/2)s_0^2]\mathscr{F}^*(s_0) \quad \text{(C-80)}$$

$$G_\rho(\rho, z_d) = -\varepsilon k_0 I_{11}(\rho, z_d)\{1 - j\varepsilon\pi s_0(\varepsilon + \cos\theta_1)^{-1} \times \exp[j(\pi/2)s_0^2]\mathscr{F}^*(s_0)\} \quad \text{(C-81)}$$

$$G_z(\rho,z_d) = -j\varepsilon\pi s_0 I_{21}(\rho,z_d)(\varepsilon+\cos\theta_1)^{-1} \exp[j(\pi/2)s_0^2]\mathscr{F}^*(s_0) \quad \text{(C-82)}$$

Substituting Eqs. (C-80)–(C-82) into Eqs. (C-5)–(C-7),

$$H_{\phi\,\text{pseudo-surface}} = [(-jn^2k_0^2p)/(2\pi)][-j\varepsilon\pi s_0 I_{11}(\rho, z_d)(\varepsilon + \cos\theta_1)^{-1} \times \exp[j(\pi/2)s_0^2]\mathscr{F}^*(s_0)] \quad \text{(C-83)}$$
$$= -2jH_{\phi 1\,\text{image}}\varepsilon\pi s_0(\varepsilon + \cos\theta_1)^{-1} \exp[j(\pi/2)s_0^2]\mathscr{F}^*(s_0)$$

$$
\begin{aligned}
E_{\rho\,\text{pseudo-surface}} &= [(-j\omega\mu_0 n^2\text{p})/(2\pi)][-\varepsilon k_0 I_{11}(\rho, z_d)] \\
&\quad \{1 - j\varepsilon\pi s_0(\varepsilon + \cos\theta_1)^{-1}\exp[j(\pi/2)s_0^2]\mathscr{F}^*(s_0)\} \\
&= -2\varepsilon Z_0 H_{\phi 1\,\text{image}}\{1 - j\varepsilon\pi s_0 \\
&\quad (\varepsilon + \cos\theta_1)^{-1}\exp[j(\pi/2)s_0^2]\mathscr{F}^*(s_0)\}
\end{aligned}
\tag{C-84}
$$

$$
\begin{aligned}
E_{z\,\text{pseudo-surface}} &= [(-j\omega\mu_0 n^2 p)/(2\pi)][-j\varepsilon\pi s_0 I_{21}(\rho, z_d) \\
&\quad (\varepsilon + \cos\theta_1)^{-1} \times \exp[j(\pi/2)s_0^2]\mathscr{F}^*(s_0)] \\
&= -2jE_{z1\,\text{image}}\varepsilon\pi s_0 \\
&\quad (\varepsilon + \cos\theta_1)^{-1}\exp[j(\pi/2)s_0^2]\mathscr{F}^*(s_0)
\end{aligned}
\tag{C-85}
$$

where

$$
H_{\phi 1\,\text{image}} = [(-jn^2 k_0^2 p)/(2\pi)](1/2)\, I_{11}(\rho, z_d) = (1/Z_0)A_1 \sin\theta_1 \tag{C-86}
$$

$$
\begin{aligned}
E_{\rho 1\,\text{image}} &= [(-j\omega\mu_0 n^2 p)/(2\pi)](1/2)\, I_{\text{o}1}(\rho, z_d) \\
&= A_1 \sin\theta_1 \cos\theta_1
\end{aligned}
\tag{C-87}
$$

$$
E_{z1\,\text{image}} = [(-j\omega\mu_0 n^2 p)/(2\pi)](1/2)\, I_{21}(\rho, z_d) = -A_1 \sin^2\theta_1 \tag{C-88}
$$

$$
A_1 = j[(Z_0 k_0 p)/(4\pi r_1)]\exp(-jk_0 r_1) \tag{C-89}
$$

$$
Z_0 = (\mu_0/\varepsilon_0)^{1/2} \tag{C-90}
$$

It should be noted that Eqs. (C-86)–(C-88) are identical to the lowest-order term of the image fields given by Eqs. (9.3.24)–(9.3.27) and are identical to the lowest-order term of the indirect space-wave fields given by Eqs. (9.2.31)–(9.2.33).

From Eqs. (9.3.20) and (9.3.21),

$$H_{\phi\,\text{surface}} = H_{\phi\,\text{pseudo-surface}} + [1 - R_v(\theta_1)]H_{\phi\,\text{image}} \tag{C-91}$$

$$E_{\rho\,\text{surface}} = E_{\rho\,\text{pseudo-surface}} + [1 - R_v(\theta_1)]E_{\rho\,\text{image}} \tag{C-92}$$

$$E_{z\,\text{surface}} = E_{z\,\text{pseudo-surface}} + [1 - R_v(\theta_1)]E_{z\,\text{image}} \tag{C-93}$$

where $R_v(\theta_1)$ is the Fresnel reflection coefficient given by Eq. (9.2.5) and $H_{\phi\ \text{image}}$, $E_{\rho\ \text{image}}$, $E_{z\ \text{image}}$ are the total image fields given by Eqs. (9.3.24)–(9.3.27). Substituting Eqs. (C-83)–(C-85) into Eqs. (C-91)–(C-93),

$$\begin{aligned} H_{\phi\,\text{surface}} &= H_{\phi\,\text{image}}[1 - R_v(\theta_1)] \\ &\quad - 2j\varepsilon H_{\phi 1\,\text{image}}\pi s_0(\varepsilon + \cos\theta_1)^{-1}\exp[j(\pi/2)s_0^2]\mathscr{F}^*(s_0) \end{aligned} \tag{C-94}$$

$$\begin{aligned} E_{\rho\,\text{surface}} &= E_{\rho\,\text{image}}[1 - R_v(\theta_1)] \\ &\quad - 2\varepsilon Z_0 H_{\phi 1\,\text{image}}\{1 - j\varepsilon\pi s_0(\varepsilon + \cos\theta_1)^{-1}\exp[j(\pi/2)s_0^2]\mathscr{F}^*(s_0)\} \end{aligned} \tag{C-95}$$

$$\begin{aligned} E_{z\,\text{surface}} &= E_{z\,\text{image}}[1 - R_v(\theta_1)] \\ &\quad - 2j\varepsilon E_{z1\,\text{image}}\pi s_0(\varepsilon + \cos\theta_1)^{-1}\exp[j(\pi/2)s_0^2]\mathscr{F}^*(s_0) \end{aligned} \tag{C-96}$$

The parameter ε in Eqs. (C-94)–(C-96) is determined by expanding $\mathscr{F}^*(s_0)$ for $s_0 \gg 1$ in an asymptotic series and then requiring that the lowest-order term (the $1/r_1$ field) of the surface-wave fields vanish in the far-field, but not the higher-order terms, because the $1/r_1$ field is accounted for completely by the lowest-order term of the space-wave field. Expanding $\mathscr{F}^*(s_0)$ for $s_0 \gg 1$, $\mathscr{F}^*(s_0)$ is given by [122] as

$$\begin{aligned} \mathscr{F}^*(s_0) = &(j\pi s_0)^{-1}\exp[-j(\pi/2)s_0^2]\{1 - [(1\cdot 3)/(\pi s_0^2)^2] \\ &+ [(1\cdot 3\cdot 5\cdot 7)/(\pi s_0^2)^4] - \cdots\} \\ &+ (\pi s_0)^{-1}(\pi s_0^2)^{-1}\exp[-j(\pi/2)s_0^2] \\ &\{[1 - [(1\cdot 3\cdot 5)/(\pi s_0^2)^2] + \cdots\},\ s_0 \gg 1 \end{aligned} \tag{C-97}$$

Approximating $\mathscr{F}^*(s_0)$ by its lowest-order term, Eq. (C-97) reduces to

$$\mathscr{F}^*(s_0) \approx (j\pi s_0)^{-1}\exp[-j(\pi/2)s_0^2],\ \text{lowest-order term},\ s_0 \gg 1 \quad \text{(C-98)}$$

Substituting Eq. (C-98) into Eqs. (C-94)–(C-96) and requiring that the surface-wave fields vanish in the far-field for the lowest-order term,

$$H_{\phi 1\,\text{image}}\{[1 - R_v(\theta_1)] - 2\varepsilon(\varepsilon + \cos\theta_1)^{-1}\} = 0 \quad \text{(C-99)}$$

$$\begin{aligned} &E_{\rho 1\,\text{image}}[1 - R_v(\theta_1)] - 2\varepsilon Z_0 H_{\phi 1\,\text{image}}[1 - \varepsilon(\varepsilon + \cos\theta_1)^{-1}] = 0 \\ &= \mathrm{E}_{\rho 1\,\text{image}}\{[1 - R_v(\theta_1)] - 2\varepsilon(\cos\theta_1)^{-1}[1 - \varepsilon(\varepsilon + \cos\theta_1)^{-1}\} \quad \text{(C-100)} \\ &= 0 = \mathrm{E}_{\rho 1\,\text{image}}\{[1 - R_v(\theta_1)] - 2\varepsilon(\varepsilon + \cos\theta_1)^{-1}\} = 0 \end{aligned}$$

$$E_{z1\,\text{image}}\{[1 - R_v(\theta_1)] - 2\varepsilon(\varepsilon + \cos\theta_1)^{-1}\} = 0 \quad \text{(C-101)}$$

where in the second line of Eq. (C-100), $H_{\phi 1\,\text{image}} = (Z_0\cos\theta_1)^{-1}\,E_{\rho 1\,\text{image}}$.

Since the lowest-order image fields are nonzero, Eqs. (C-99)–(C-101) are satisfied if and only if

$$1 - R_v(\theta_1) = (2\varepsilon)/(\varepsilon + \cos\theta_1) = 2/(1 + \varepsilon^{-1}\cos\theta_1) \quad \text{(C-102)}$$

Solving for ε in Eq. (C-102),

$$\begin{aligned} \varepsilon &= [1 - R_v(\theta_1)]/[1 + R_v(\theta_1)]\cos\theta_1 \\ &= n^{-1}[1 - n^{-2}\sin^2\theta_1]^{1/2}, |n^2| \gg 1 \end{aligned} \quad \text{(C-103)}$$

where ε follows exactly from Eq. (C-102) which in turn follows from the variational method employed earlier subject to the condition $|n^2| \gg 1$. Equation (C-103) is an approximation to the exact expression for ε defined by Eq. (C-21) and is consistent with Eq. (C-42d) associated with the variational method provided that $|n^2| \gg 1$. Substituting Eq. (C-103) into Eq. (C-71),

$$s_0 = 2[1 + R_v(\theta_1)]^{-1}(\cot\theta_1)(k_0 r_1/\pi)^{1/2}, |n^2| \gg 1 \quad \text{(C-104)}$$

Substituting Eqs. (C-103) and (C-104) into Eqs. (C-83)–(C-85) and Eqs. (C-94)–(C-96),

$$\begin{aligned} H_{\phi\,\text{pseudo-surface}} = &- H_{\phi 1\,\text{image}}[1 - R_v(\theta_1)] \\ &\times (j\pi s_0)\exp[j(\pi/2)s_0^2]\mathscr{F}^*(s_0), |n^2| \gg 1 \end{aligned} \quad \text{(C-105)}$$

$$
\begin{aligned}
E_{\rho\,\text{pseudo-surface}} &= -2\,Z_0 H_{\phi 1\,\text{image}}[1 - R_\text{v}(\theta_1)][1 + R_\text{v}(\theta_1)]^{-1}\cos\theta_1 \\
&\quad \times \{1 - (1/2)[1 - R_\text{v}(\theta_1)](j\pi s_0)\exp[j(\pi/2)\text{s}_0^2]\mathscr{F}^*(s_0)\} \\
&= -2E_{\rho 1\,\text{image}}[1 - R_\text{v}(\theta_1)][1 + R_\text{v}(\theta_1)]^{-1} \\
&\quad \times \{1 - (1/2)[1 - R_\text{v}(\theta_1)] \\
&\quad \times (j\pi s_0)\exp[j(\pi/2)s_0^2]\mathscr{F}^*(s_0)\},\ |n^2| \gg 1
\end{aligned}
\tag{C-106}
$$

$$
\begin{aligned}
E_{z\,\text{pseudo-surface}} &= -E_{z1\,\text{image}}[1 - R_\text{v}(\theta_1)] \\
&\quad \times (j\pi s_0)\exp[j(\pi/2)s_0^2]\mathscr{F}^*(s_0),\ |n^2| \gg 1
\end{aligned}
\tag{C-107}
$$

$$
\begin{aligned}
H_{\phi\,\text{surface}} &= \text{H}_{\phi 2\,\text{image}}[1 - R_\text{v}(\theta_1)] + H_{\phi 1}[1 - R_\text{v}(\theta_1)] \\
&\quad \times \{1 - (j\pi s_0)\exp[j(\pi/2)s_0^2]\mathscr{F}^*(s_0)\},\ |n^2| \gg 1
\end{aligned}
\tag{C-108}
$$

$$
\begin{aligned}
E_{\rho\,\text{surface}} &= (E_{\rho 2\,\text{image}} + E_{\rho 3\,\text{image}}[1 - R_\text{v}(\theta_1)] \\
&\quad - 2E_{\rho 1\,\text{image}}[1 - R_\text{v}(\theta_1)][1 + R_\text{v}(\theta_1)]^{-1} \\
&\quad \times \{1 - (1/2)[1 - R_\text{v}(\theta_1)](j\pi s_0)\exp[j(\pi/2)s_0^2]\mathscr{F}^*(s_0)\} \\
&= (E_{\rho 2\,\text{image}} + E_{\rho 3\,\text{image}})[1 - R_\text{v}(\theta_1)] \\
&\quad - E_{\rho 1\,\text{image}}[1 - R_\text{v}(\theta_1)]^2 \times [1 + R_\text{v}(\theta_1)]^{-1} \\
&\quad \{1 - (j\pi s_0)\exp[j(\pi/2)s_0^2]\mathscr{F}^*(s_0)\},\ |n^2| \gg 1
\end{aligned}
\tag{C-109}
$$

$$
\begin{aligned}
E_{z\,\text{surface}} &= (E_{z2\,\text{image}} + E_{z3\,\text{image}})[1 - R_\text{v}(\theta_1)] \\
&\quad + E_{z1\,\text{image}}[1 - R_\text{v}(\theta_1)]\{1 - (j\pi s_0)\exp[j(\pi/2)s_0^2]\mathscr{F}^*(s_0)\}, \\
&\quad |n^2| \gg 1
\end{aligned}
\tag{C-110}
$$

where

$$H_{\phi 2\,\text{image}} = H_{\phi 1\,\text{image}}(jk_0r_1)^{-1} = (1/Z_0)A_1 \sin\theta_1(jk_0r_1)^{-1}$$

$$E_{\rho 2\,\text{image}} = E_{\rho 1\,\text{image}}\, 3(jk_0r_1)^{-1} = 3A_1 \sin\theta_1 \cos\theta_1\,(jk_0r_1)^{-1}$$

$$E_{\rho 3\,\text{image}} = E_{\rho 1\,\text{image}}\, 3(jk_0r_1)^{-2} = 3A_1 \sin\theta_1 \cos\theta_1(jk_0r_1)^{-2}$$

$$E_{z2\,\text{image}} = E_{z1\,\text{image}}(1/\sin^2\theta_1)(1 - 3\cos^2\theta_1)(jk_0r_1)^{-1}$$

$$= -A_1(1 - 3\cos^2\theta_1)(jk_0r_1)^{-1}$$

$$E_{z3\,\text{image}} = E_{z1\,\text{image}}(1/\sin^2\theta_1)(1 - 3\cos^2\theta_1)(jk_0r_1)^{-2}$$

$$= -A_1(1 - 3\cos^2\theta_1)(jk_0r_1)^{-2}$$

Equations. (C-103)–(C-110) were derived subject to three approximations:

1. A modified variational method, realized in Eqs. (C-43)–(C-45), subject to the condition $|n^2| \gg 1$. Unlike Storer, who utilized a variational method that neglects entirely one of the parts of integration, a far-field constraint is employed to approximate the part of integration that was previously neglected.
2. Method of stationary phase that approximates the integrals in Eqs. (C-52)–(C-54) by their asymptotic behavior.
3. Neglect of the higher-order $(jk_0r_1)^{-2}$ and $(jk_0r_1)^{-3}$ amplitude terms in Eq. (C-62c and d).

Substituting ε given by Eq. (C-103) into Eq. (C-21), the eigenvalue λ is given by

$$\lambda = k_0 \sin\theta_1,\ |n^2| \gg 1 \tag{C-111}$$

Substituting Eq. (C-111) into Eqs. (C-1)–(C-4),

$$\gamma_0 = (k_0^2 - \lambda^2)^{1/2} = k_0 \cos\theta_1, |n^2| \gg 1 \tag{C-112}$$

$$\gamma_1 = (n^2k_0^2 - \lambda^2)^{1/2} = k_0(n^2 - \sin^2\theta_1)^{1/2}$$

$$= k_0 n^2 \cos\theta_1[1 - R_v(\theta_1)][1 + R_v(\theta_1)]^{-1},\ |n^2| \gg 1 \tag{C-113}$$

$$N_0 = n^2k_0^2\gamma_0 = n^2k_0^3 \cos\theta_1,\ |n^2| \gg 1 \tag{C-114}$$

$$
\begin{aligned}
N &= N_0 + k_0^2\gamma_1 \\
&= n^2 k_0^3 \cos\theta_1 + k_0^3 n^2 \cos\theta_1 [1 - R_{\mathrm{v}}(\theta_1)][1 + R_{\mathrm{v}}(\theta_1)]^{-1} \\
&= 2n^2 k_0^3 \cos\theta_1 [1 + R_{\mathrm{v}}(\theta_1)]^{-1},\ |n^2| \gg 1
\end{aligned} \tag{C-115}
$$

$$
\gamma_0/N = [2n^2 k_0^2]^{-1}[1 + R_{\mathrm{v}}(\theta_1)],\ |n^2| \gg 1 \tag{C-116}
$$

$$
\begin{aligned}
\varepsilon/N = {} & \cos\theta_1 [1 - R_{\mathrm{v}}(\theta_1)][1 + R_{\mathrm{v}}(\theta_1)]^{-1}\}/\{2n^2 k_0^3 \cos\theta_1 \\
& [1 + R_{\mathrm{v}}(\theta_1)]^{-1}\} = [1 - R_{\mathrm{v}}(\theta_1)][2n^2 k_0^3]^{-1},\ \ |n^2| \gg 1
\end{aligned} \tag{C-117}
$$

C.3 $|n^2| \approx 1$, APPROXIMATE CLOSED-FORM EXPRESSIONS FOR FIELDS

Before obtaining approximate solutions for the case $|n^2| \approx 1$, consider exact results for the case $n = 1$ corresponding to the Fresnel reflection coefficient $R_{\mathrm{v}}(\theta_1) = 0$ for earth identical to that of free space. For $n = 1$, Eqs. (C-2)–(C-5) reduce to

$$
\gamma_1 = \gamma_0, n = 1 \tag{C-118a}
$$

$$
N_0 = k_0^2 \gamma_0, n = 1 \tag{C-118b}
$$

$$
N = k_0^2\gamma_0 + k_0^2\gamma_0 = 2k_0^2\gamma_0 = 2N_0, n = 1 \tag{C-118c}
$$

$$
\begin{aligned}
N^{-1} - N_0^{-1} &= (2k_0^2\gamma_0)^{-1} - (k_0^2\gamma_0)^{-1} = (2k_0^2\gamma_0)^{-1} \\
&= -(2N_0)^{-1}, n = 1
\end{aligned} \tag{C-118d}
$$

Substituting Eq. (C-118c) into Eqs. (C-11)–(C-13), (C-14a–c), and (C-22),

$$
\varepsilon = \gamma_1/(k_0 n^2) = \gamma_0/k_0, n = 1 \tag{C-119a}
$$

$$
\partial(k_0\varepsilon)/\partial\lambda = -(\lambda/n^2\gamma_1) = -\lambda/\gamma_0, n = 1 \tag{C-119b}
$$

$$
I_\phi(\rho, z_d) = (1/2) I_1(\rho, z_d), n = 1 \tag{C-120a}
$$

$$
I_\rho(\rho, z_d) = (1/2) I_0(\rho, z_d), n = 1 \tag{C-120b}
$$

$$I_z(\rho, z_d) = (1/2)\, I_2(\rho,\ z_d), n = 1 \tag{C-120c}$$

$$G_\phi(\rho, z_d) = -(1/2)\, I_1(\rho, z_d), n = 1 \tag{C-121a}$$

$$G_\rho(\rho, z_d) = -(1/2)\, I_0(\rho, z_d), n = 1 \tag{C-121b}$$

$$G_z(\rho, z_d) = -(1/2)\, I_2(\rho, z_d), n = 1 \tag{C-121c}$$

Substituting Eq. (C-121a–c) into Eqs. (C-5)–(C-7),

$$H_{\phi\,\text{pseudo-surface}} = -H_{\phi\,\text{image}}, n = 1 \tag{C-122a}$$

$$H_{\rho\,\text{pseudo-surface}} = -E_{\rho\,\text{image}}, n = 1 \tag{C-122b}$$

$$H_{z\,\text{pseudo-surface}} = -E_z\,\text{image}, n = 1 \tag{C-122c}$$

where $H_{\phi\,\text{image}}, E_{\rho\,\text{image}}$, and E_z are given by Eqs. (C-86)–(C-88).

It is seen from Eq. (C-119a and b) that for $n = 1$, the parameters $\varepsilon = \gamma_0/k_0$ and $\partial(k_0\varepsilon)/\partial\lambda = -\lambda/\gamma_0$ unlike the case $|n^2| = \infty$ for which $\varepsilon = 0$ and $\partial(k_0\varepsilon)/\partial\lambda = 0$. Therefore, consider a new parameter ε' defined by

$$\varepsilon' = \varepsilon - (\gamma_0/k_0) \tag{C-123}$$

where ε and γ_0 are defined by Eqs. (C-1) and (C-41a), respectively, and ε' is defined such that $\varepsilon' = 0$ and $\partial(k_0\varepsilon')/\partial\lambda = 0$ for $n = 1$. The motivation for doing so is to obtain an approximate solution of Eqs. (C-25), (C-28), and (C-31) for the case $|n^2|1$ using a variational method similar to that used for the case $|n^2| \gg 1$. Substituting Eq. (C-123) into Eqs. (C-25), (C-28), and (C-31),

$$\begin{aligned}\partial I_\phi(\rho,z_d)/\partial z_d &= \partial I_1(\rho,z_d)/\partial z_d + j\int_0^\infty (\gamma_0/N)\exp(-j\gamma_0 z_d) J_1(\lambda\rho)\lambda^2\,\mathrm{d}\lambda \\ &\quad + j\int_0^\infty (k_0\varepsilon')N^{-1}\exp(-j\gamma_0 z_d) J_1(\lambda\rho)\lambda^2\,\mathrm{d}\lambda \\ &= \partial I_1(\rho,z_d)/\partial z_d - \partial I_\phi(\rho,z_d)/\partial z_d + j\int_0^\infty (k_0\varepsilon')\mathrm{N}^{-1} \\ &\quad \times\exp(-j\gamma_0 z_d)\mathrm{J}_1(\lambda\rho)\lambda^2\,\mathrm{d}\lambda = (1/2)\partial I_1(\rho, z_d)/\partial z_d \\ &\quad + (j/2)\int_0^\infty (k_0\varepsilon')N^{-1}\exp(-j\gamma_0 z_d) J_1(\lambda\rho)\lambda^2\,\mathrm{d}\lambda,\ |n^2| \approx 1\end{aligned} \tag{C-124a}$$

$$\partial I_\rho(\rho,z_d)/\partial z_d = \partial I_0(\rho,z_d)/\partial z_d$$
$$+j\int_0^\infty (\gamma_0^2/N)\exp(-j\gamma_0 z_d)J_1(\lambda\rho)\lambda^2\,\mathrm{d}\lambda$$
$$+j\int_0^\infty (k_0\varepsilon')(\gamma_0/N)\exp(-j\gamma_0 z_d)J_1(\lambda\rho)\lambda^2\,\mathrm{d}\lambda$$
$$= \partial I_0(\rho,z_d)/\partial z_d - \partial I_\rho(\rho,z_d)/\partial z_d \qquad \text{(C-124b)}$$
$$+j\int_0^\infty (k_0\varepsilon')(\gamma_0/N)\exp(-j\gamma_0 z_d)J_1(\lambda\rho)\lambda^2\,\mathrm{d}\lambda$$
$$= (1/2)\partial I_0(\rho,z_d)/\partial z_d$$
$$+(j/2)\int_0^\infty (k_0\varepsilon')(\gamma_0/N)\exp(-j\gamma_0 z_d)J_1(\lambda\rho)\lambda^2\,\mathrm{d}\lambda, |n^2| \approx 1$$

$$\partial I_z(\rho,z_d)/\partial z_d = \partial I_2(\rho,z_d)/\partial z_d$$
$$+j\int_0^\infty (\gamma_0/N)\exp(-j\gamma_0 z_d)J_0(\lambda\rho)\lambda^3\,\mathrm{d}\lambda$$
$$+j\int_0^\infty (k_0\varepsilon')N^{-1}\exp(-j\gamma_0 z_d)J_0(\lambda\rho)\lambda^3\,\mathrm{d}\lambda$$
$$= \partial I_2(\rho,z_d)/\partial z_d - \partial I_z(\rho,z_d)/\partial z_d \qquad \text{(C-124c)}$$
$$+j\int_0^\infty (k_0\varepsilon')N^{-1}\exp(-j\gamma_0 z_d)J_0(\lambda\rho)\lambda^3\,\mathrm{d}\lambda$$
$$= (1/2)\partial I_2(\rho,z_d)/\partial z_d$$
$$+(j/2)\int_0^\infty (k_0\varepsilon')N^{-1}\exp(-j\gamma_0 z_d)J_0(\lambda\rho)\lambda^3\,\mathrm{d}\lambda, |n^2| \approx 1$$

In each of Eqs. (C-124a–c), the first integral in the first line is replaced by the identity in Tables C-2, nos. (8)–(10), respectively. The final line follows from grouping of terms (adding the left-hand side of the equation to both sides of the equation and dividing by 2).

The integral in the last line of Eq. (C-124a) may be approximated using the variational method of Eq. (C-42a). Accordingly,

$$\begin{aligned}
&\int_0^\infty (k_0\varepsilon')N^{-1}\exp(-j\gamma_0 z_d)\,J_1(\lambda\rho)\lambda^2\,\mathrm{d}\lambda \\
&\quad = k_0\varepsilon'(0)\int_0^\infty N^{-1}\exp(-j\gamma_0 z_d)\,J_1(t\rho)t^2\,\mathrm{d}t \\
&\qquad + \int_0^\infty \left[\int_\lambda^\infty N^{-1}\exp(-j\gamma_0 z_d)\,J_1(t\rho)t^2\,\mathrm{d}t\right][\partial(k_0\varepsilon')/\partial\lambda\,]\mathrm{d}\lambda \\
&\quad = \left[k_0\varepsilon'(0)\int_0^\infty N^{-1}\exp(-j\gamma_0 z_d)\,J_1(\lambda\rho)\lambda^2\,\mathrm{d}\lambda\right][1+F\,]
\end{aligned} \tag{C-125}$$

where

$$\begin{aligned}
F &= [k_0\varepsilon'(0)]^{-1}[\int_0^\infty N^{-1}\exp(-j\gamma_0 z_d)\,J_1(\lambda\rho)\lambda^2\,\mathrm{d}\lambda\,]^{-1} \\
&\quad \times\{\int_0^\infty [\int_\lambda^\infty N^{-1}\exp(-j\gamma_0 z_d)\,J_1(t\rho)t^2\,\mathrm{d}t\,][\partial(k_0\varepsilon')/\partial\lambda\,]\mathrm{d}\lambda\} \\
&\approx [k_0\varepsilon'(0)]^{-1}[\partial(k_0\varepsilon')/\partial\lambda\,]\Delta\lambda = [k_0\varepsilon'(0)]^{-1}\lambda[-(n^4\varepsilon\,)^{-1} + (k_0\gamma_0^{-1}]
\end{aligned} \tag{C-126}$$

$$\begin{aligned}
\varepsilon'(0) &= n^{-1}[1-(\lambda/nk_0)^2]^{1/2}|_{\lambda=0} - [1-(\lambda/k_0)^2]^{1/2}|_{\lambda=0} \\
&= n^{-1} - 1
\end{aligned} \tag{C-127}$$

$$\begin{aligned}
\partial(k_0\varepsilon')/\partial\lambda &= -n^{-3}[\lambda/k_0)[1-(\lambda/nk_0)^2]^{-1/2} + (\lambda/k_0)[1-(\lambda/k_0)^2]^{-1/2} \\
&= (\lambda/k_0)[-(n^4\varepsilon\,)^{-1} + k_0\gamma_0^{-1}]
\end{aligned} \tag{C-128}$$

$$\Delta\lambda \approx k_0(\lambda/k_0)|_0^1 = k_0 \tag{C-129}$$

[see Eq. (C-42b) where the principal contribution to the variation is for $\lambda/k_0 = O(0 \leq 1)$]

If the function F in Eq. (C-125) is neglected, as in the conventional variational method of Storer [119], then Eq. (C-125) reduces to

$$\begin{aligned}\int_0^\infty (k_0\varepsilon')N^{-1}\exp(-j\gamma_0 z_d)\,J_1(\lambda\rho)\lambda^2\,\mathrm{d}\lambda \\ \approx k_0\varepsilon'(0)\int_0^\infty N^{-1}\exp(-j\gamma_0 z_d)\,J_1(\lambda\rho)\lambda^2\,\mathrm{d}\lambda,\ \mathrm{F\ neglected}\end{aligned} \tag{C-130}$$

where $\varepsilon'(0)$ is given by Eq. (C-127).

However, if F is not neglected but is small quantity $|F| \ll 1$, then the modified variational method of Eq. (C-42f) is applicable. Accordingly,

$$\begin{aligned}\int_0^\infty (k_0\varepsilon')N^{-1}\exp(-j\gamma_0 z_d)\,J_1(\lambda\rho)\lambda^2\,\mathrm{d}\lambda \\ \approx k_0\varepsilon'\int_0^\infty N^{-1}\exp(-j\gamma_0 z_d)\,J_1(\lambda\rho)\lambda^2\,\mathrm{d}\lambda,\ |F| \ll 1\end{aligned} \tag{C-131}$$

where the parameter ε' will be explicitly determined later from a far-field constraint.

If $|F| \ll 1$ and $|n^2| \approx 1$, it will be shown later that ε, λ, γ_0 are given by Eqs. (C-103), (C-111), and (C-112), respectively, provided that those equations are restricted to the conditions for which $|F| \ll 1$. Those conditions are determined by substituting Eqs. (C-103), (C-111), (C-112), and (C-127) into Eq. (C-126). Accordingly,

$$\begin{aligned}F &\approx (n^{-1}-1)^{-1}\tan\theta_1[(1-n^{-4})-(1+n^{-4})R_\mathrm{v}(\theta_1)][1-R_\mathrm{v}(\theta_1)]^{-1} \\ &\approx (n^{-1}-1)^{-1}\tan\theta_1(1-n^{-3}) \approx -3\tan\theta_1 \approx -3\,\theta_1,\ |F| \ll 1\end{aligned} \tag{C-132}$$

$$R_\mathrm{v}(\theta_1) \approx (n-1)(n+1)^{-1};\ \theta_1 \ll 1\,\mathrm{rad},\ |n^2| \approx 1 \tag{C-133a}$$

$$1 - R_\mathrm{v}(\theta_1) \approx 2n(n+1)^{-1};\ \theta_1 \ll 1\,\mathrm{rad},\ |n^2| \approx 1 \tag{C-133b}$$

From Eq. (C-132),

$$|F| \ll 1;\ 0 \le \theta_1 \ll (1/3)\,\mathrm{rad},\ |n^2| \approx 1 \tag{C-134a}$$

$$|F|\ \mathrm{undetermined};\ (\ll 1/3) \le \theta_1 \le (\pi/2)\,\mathrm{rad},\ |n^2| \approx 1 \tag{C-134b}$$

ε, λ, γ_0 are given by Eqs. (C-103), (C-111), and (C-112), respectively;

$$0 \le \theta_1 \ll (1/3)\,\mathrm{rad},\ |n^2| \approx 1 \tag{C-135a}$$

$$\varepsilon,\ \lambda,\ \gamma_0\ \mathrm{undetermined};\ (\ll 1/3) \le \theta_1 \le (\pi/2)\,\mathrm{rad},\ |n^2| \approx 1 \tag{C-135b}$$

For $|n^2| \approx 1$, the problem remains of how to treat the case when $|F|$ is not a small quantity or equivalently when θ_1 is not a small angle [see Eq. (C-134a)]. For $|n^2| \gg 1$, $\varepsilon = \varepsilon|_{\text{far-field constraint}} =$ value of ε determined by satisfying a far-field constraint. Furthermore, for $|n^2| \gg 1$, $|F|$ is a small quantity for all values of θ_1 [see Eq. (C-42e)] and consequently $\varepsilon = \varepsilon|_{\text{far-field constraint}} \approx \varepsilon(0)\,[= n^{-1}]$ for all values of θ_1 [compare Eq. (C-103) with Eq. (C-21). The use of $\varepsilon|_{\text{far-field constraint}}$ to determine the functional form of the fields insures that the lowest-order term (the $1/r_1$ field) of the surface-wave fields vanishes in the far-field, but not the higher-order terms, because the $1/r_1$ field is accounted for completely by the lowest-order term of the space-wave field. This suggests for $|n^2| \approx 1$ that a modified variational method be utilized to determine the functional form of the fields provided that $\varepsilon'(0)$ is substituted for $\varepsilon'|_{\text{far-field constraint}}$ in the argument of the functional form whenever $\varepsilon'|_{\text{far-field constraint}}$ differs appreciably from $\varepsilon'(0)$.The requirement—that $\varepsilon'(0)$ replace $\varepsilon'|_{\text{far-field constraint}}$ in the argument of the functional form whenever $\varepsilon'|_{\text{far-field constraint}}$ differs appreciably from $\varepsilon'(0)$—insures the integrity of the variational method. Therefore, as a compromise between Eqs. (C-130) and (C-131), Eq. (C-125) may be approximated as

$$\begin{aligned}\int_0^\infty (k_0\varepsilon')N^{-1}\exp(-j\gamma_0 z_d)\,J_1(\lambda\rho)\lambda^2\,\mathrm{d}\lambda \\ \approx k_0\varepsilon'\int_0^\infty N^{-1}\exp(-j\gamma_0 z_d)\,J_1(\lambda\rho)\lambda^2\,\mathrm{d}\lambda\end{aligned} \tag{C-136}$$

where

$$\varepsilon' = \varepsilon'|_{\text{far-field constraint}}; \quad |\varepsilon'|_{\text{far-field constraint}}/\varepsilon'(0)| \approx 1 \tag{C-137a}$$

$$\varepsilon' = \varepsilon'(0) = n^{-1} - 1; \quad |\varepsilon'|_{\text{far-field constraint}}/\varepsilon'(0)| \gg 1. \tag{C-137b}$$

In effect then, for $|n^2| \approx 1$, the factor $(k_0\varepsilon')$ within the integrands of Eq. (C-124a–c) may be treated as a constant and brought outside the integrand. Equation (C-137a) *when applicable* yields the most accurate results over a wider range of values of n because the modified variational method is fully implemented. Equation (C-137b) *when applicable* yields more accurate results over a wider range of angles θ_1 than the modified variational method.

Accordingly, Eq. (C-124a–c) reduce to

$$\partial I_\phi(\rho, z_d)/\partial z_d \approx (1/2)\partial I_1(\rho, z_d)/\partial z_d + (jk_0\varepsilon'/2)\int_0^\infty N^{-1}\exp(-j\gamma_0 z_d)\,J_1(\lambda\rho)\lambda^2\,\mathrm{d}\lambda \quad \text{(C-138)}$$
$$= (1/2)\partial I_1(\rho, z_d)/\partial z_d + (jk_0\varepsilon'/2)\,I_\phi(\rho, z_d), |n^2| \approx 1$$

$$\partial I_\rho(\rho, z_d)/\partial z_d \approx (1/2)\partial I_0(\rho, z_d)/\partial z_d + (jk_0\varepsilon'/2)\int_0^\infty (\gamma_0/N)\exp(-j\gamma_0 z_d)J_1(\lambda\rho)\lambda^2\,\mathrm{d}\lambda \quad \text{(C-139)}$$
$$= (1/2) \approx \partial I_0(\rho, z_d)/\partial z_d + (jk_0\varepsilon'/2)I_\rho(\rho, z_d), |n^2| \approx 1$$

$$\partial I_z(\rho, z_d)/\partial z_d \approx (1/2)\partial I_2(\rho, z_d)/\partial z_d + (jk_0\varepsilon'/2)\int_0^\infty N^{-1}\exp(-j\gamma_0 z_d)J_0(\lambda\rho)\lambda^3\,\mathrm{d}\lambda \quad \text{(C-140)}$$
$$= (1/2) \approx \partial I_2(\rho, z_d)/\partial z_d + (jk_0\varepsilon'/2)I_z(\rho, z_d), |n^2| \approx 1$$

where the identities of Table C-2, nos. 1–3 have been utilized.

Equations. (C-138)–(C-140) are identical to Eqs. (C-43)–(C-45) except that $(1/2)\,I_1(\rho, z_d)$, $(1/2)\,I_0(\rho, z_d)$, $(1/2)\,I_2(\rho, z_d)$, and $\varepsilon'/2$ in Eqs. (C-138)–(C-140) have replaced $I_1(\rho, z_d)$, $I_0(\rho, z_d)$, $I_2(\rho, z_d)$, and ε, respectively, in Eqs. (C-43)–(C-45). It therefore follows that the solutions of Eqs. (C-138)–(C-140) are given by the solutions of Eqs. (C-43)–(C-45) if $(1/2)\,I_1(\rho, z_d)$, $(1/2)\,I_0(\rho, z_d)$, $(1/2)\,I_2(\rho, z_d)$, and $\varepsilon'/2$ are substituted for $I_1(\rho, z_d)$, $I_0(\rho, z_d)$, $I_2(\rho, z_d)$, and ε, respectively, in the solutions of Eqs. (C-43)–(C-45). Please note that the substitution of a factor of (1/2) does not apply to the functions $I_\phi(\rho, z_d)$, $I_\rho(\rho, z_d)$, or $I_z(\rho, z_d)$.

With these substitutions, Eqs. (C-53), (C-70), (C-71), (C-75), and (C-76) reduce respectively to

$$s = s_1 + (\pi k_0 r_1)^{-1/2} k_0(z_3 - z_d)\sin\theta_1 \quad \text{(C-141)}$$

$$s_1 = s|_{z_3 = z_d} = [(\varepsilon'/2) + \cos\theta_1](1/\sin\theta_1)(k_0 r_1/\pi)^{1/2} \quad \text{(C-142)}$$

$$I_\phi(\rho, z_d) = (1/2)\,I_1(\rho, z_d) - j(\varepsilon'/2)\pi s_1(1/2)\,I_{11}(\rho, z_d) \times [(\varepsilon'/2) + \cos\theta_1]^{-1}\exp[j(\pi/2)s_1^2]\mathscr{F}^*(s_1) \quad \text{(C-143)}$$

$$I_\rho(\rho, z_d) = (1/2)\,I_0(\rho, z_d) - (\varepsilon'/2)k_0 I_\phi(\rho, z_d) \quad \text{(C-144)}$$

$$I_z(\rho, z_d) = (1/2)\, I_2(\rho, z_d) - j(\varepsilon'/2)\pi s_1 (1/2)\, I_{21}(\rho, z_d) \times [(\varepsilon'/2) + \cos s\theta_1]^{-1} \exp[j(\pi/2)s_0^2]\mathscr{F}^*(s_1) \tag{C-145}$$

where $\mathscr{F}^*(s_1)$ = complimentary conjugate Fresnel integral

$$= \int_{s_1}^{\infty} \exp[-j(\pi/2)s^2]\, ds = F^*(\infty) - F^*(s_1) \tag{C-146}$$

$$F^*(\infty) = \int_0^{\infty} \exp[-j(\pi/2)s^2]\, ds \,[= (1-j)/2,\ s \text{ real}] \tag{C-147}$$

$F^*(s_1)$ = conjugate Fresnel integral

$$= \int_0^{s_1} \exp[-j(\pi/2)s^2]\, ds \tag{C-148}$$

Substituting Eqs. (C-143)–(C-145) into Eqs. (C-11)–(C-13),

$$G_\phi(\rho, z_d) = -(1/2)\, I_1(\rho, z_d) - j(\varepsilon'/2)\pi s_1 (1/2)\, I_{11}(\rho, z_d) \times [(\varepsilon'/2) + \cos\theta_1]^{-1} \exp[j(\pi/2)s_1^2]\mathscr{F}^*(s_1) \tag{C-149}$$

$$G_\rho(\rho, z_d) = -(1/2)\, I_0(\rho, z_d) - (\varepsilon'/2)k_0 I_\phi(\rho, z_d) \tag{C-150}$$

$$G_z(\rho, z_d) = -(1/2)\, I_2(\rho, z_d) - j(\varepsilon'/2)\pi s_1 (1/2)\, I_{21}(\rho, z_d) \times [(\varepsilon'/2) + \cos\theta_1]^{-1} \exp[j(\pi/2)s_1^2]\mathscr{F}^*(s_1) \tag{C-151}$$

Substituting Eqs. (C-149)–(C-151) into Eqs. (C-5)–(C-7),

$$H_{\phi\,\text{pseudo-surface}} = -H_{\phi 1\,\text{image}}\{1 + j(\varepsilon'/2)\pi s_1[(\varepsilon'/2) + \cos\theta_1]^{-1} \times \exp[j(\pi/2)s_1^2]\mathscr{F}^*(s_1)\} - H_{\phi 2\,\text{image}} \tag{C-152}$$

$$E_{\rho\,\text{pseudo-surface}} = -E_{\rho 1\,\text{image}} - (\varepsilon'/2)Z_0 H_{\phi 1\,\text{image}} \times \{1 - j(\varepsilon'/2)\pi s_1[(\varepsilon'/2) + \cos\theta_1]^{-1} \times \exp[j(\pi/2)s_1^2]\mathscr{F}^*(s_1)\} - (E_{\rho 2\,\text{image}} + E_{\rho 3\,\text{image}}) \tag{C-153}$$

$$E_{z\,\text{pseudo-surface}} = -E_{z1\,\text{image}}\{1 + j(\varepsilon'/2)\pi s_1[(\varepsilon'/2) + \cos\theta_1]^{-1} \times \exp[j(\pi/2)s_1^2]\mathscr{F}^*(s_1)\} - (E_{z2\,\text{image}} + E_{z3\,\text{image}}) \tag{C-154}$$

where $H_{\phi 1\,\text{image}}$, $E_{\rho 1\,\text{image}}$, and $E_{z1\,\text{image}}$ are given by Eqs. (C-86)–(C-88) and $H_{\phi 2\,\text{image}}$, $E_{\rho 2\,\text{image}}$, $E_{\rho 3\,\text{image}}$, $E_{z2\,\text{image}}$, and $E_{z3\,\text{image}}$ are given by the unnumbered equations following Eq. (C-110).

Substituting Eqs. (C-152)–(C-154) into Eqs. (C-91)–(C-93),

$$H_{\phi\,\text{surface}} = -H_{\phi 1\,\text{image}}\{R_{\text{v}}(\theta_1) + j(\varepsilon'/2)\pi s_1[(\varepsilon'/2) + \cos\theta_1]^{-1} \times \exp[j(\pi/2)s_1^2]\mathscr{F}^*(s_1)\} - H_{\phi 2\,\text{image}}R_{\text{v}}(\theta_1) \tag{C-155}$$

$$E_{\rho\,\text{surface}} = -E_{\rho 1\,\text{image}}R_{\text{v}}(\theta_1) - (\varepsilon'/2)Z_0H_{\phi 1\,\text{image}} \times \{1 - j(\varepsilon'/2)\pi s_1[(\varepsilon'/2) + \cos\theta_1]^{-1}\exp[j(\pi/2)s_1^2]\mathscr{F}^*(s_1)\} - (E_{\rho 2\,\text{image}} + E_{\rho 3\,\text{image}})R_{\text{v}}(\theta_1) \tag{C-156}$$

$$E_{z\,\text{surface}} = -E_{z1}\,\text{image}\{R_{\text{v}}(\theta_1) + j(\varepsilon'/2)\pi s_1[(\varepsilon'/2) + \cos\theta_1]^{-1} \times \exp[j(\pi/2)s_1^2]\mathscr{F}^*(s_1)\} - (E_{z2\,\text{image}} + E_{z3\text{i}\,\text{mage}})R_{\text{v}}(\theta_1) \tag{C-157}$$

The parameter ε' in Eqs. (C-152)–(C-157) determines the functional form of the fields whereas the parameter s_1 (which is a function of ε') determines the argument of the functional form. The functional form is determined by satisfying a far-field constraint [see Eq. (C-137a and b)]. Just as the parameter ε was determined by expanding $\mathscr{F}^*(s_0)$ in an asymptotic series and then requiring that the surface-wave fields *vanish* in the far-field for the lowest-order term of the series, the same criterion holds for determining the parameter ε'. Substituting $\mathscr{F}^*(s_1) \approx (j\pi s_1)^{-1}\exp[-j(\pi/2)s_1^2]$ [analogous to Eq. (C-98)] into Eqs. (C-155)–(C-157) and requiring that the surface-wave fields vanish in the far-field for the lowest-order term,

$$H_{\phi 1\,\text{surface}} = -H_{\phi 1\,\text{image}}\{R_{\text{v}}(\theta_1) + (\varepsilon'/2)[(\varepsilon'/2) + \cos\theta_1]^{-1}\} = 0 \tag{C-158}$$

$$\begin{aligned} \text{E}_{\rho 1\,\text{surface}} &= -E_{\rho 1\,\text{image}}R_{\text{v}}(\theta_1) - (\varepsilon'/2)Z_0H_{\phi\,\text{image}}\{1 - [\varepsilon'/2][(\varepsilon'/2) + \cos\theta_1]^{-1}\} \\ &= -E_{\rho 1\,\text{image}}\{R_{\text{v}}(\theta_1) + (\varepsilon'/2)(\cos\theta_1)^{-1}\{1 - [\varepsilon'/2][(\varepsilon'/2) + \cos\theta_1]^{-1}\}\} \\ &= -E_{\rho 1\,\text{image}}\{R_{\text{v}}(\theta_1) + [\varepsilon'/2](\varepsilon'/2) + \cos\theta_1]^{-1}\} = 0 \end{aligned} \tag{C-159}$$

$$E_{z1\,\text{surface}} = -E_{z1\,\text{image}}\{R_{\text{v}}(\theta_1) + [\varepsilon'/2][(\varepsilon'/2) + \cos\theta_1]^{-1}\} = 0 \tag{C-160}$$

where, in the second line of Eq. (C-159), $H_{\phi\,\text{image}} = (Z_0\cos\theta_1)^{-1}E_{\rho\,\text{image}}$.

Since the image fields are nonzero, Eqs. (C-158)–(C-160) are satisfied if and only if

$$R_{\mathrm{v}}(\theta_1) + (\varepsilon'/2)[(\varepsilon'/2) + \cos\theta_1]^{-1} = 0 \tag{C-161}$$

Solving for ε' in Eq. (C-161),

$$\begin{aligned}\varepsilon' = \varepsilon'|_{\text{far-field constraint}} &= -2[R_{\mathrm{v}}(\theta_1)][1 + R_v(\theta_1)]^{-1}\cos\theta_1 \\ &= -\cos\theta_1 + n^{-1}[1 - n^{-2}\sin^2\theta_1]^{1/2}, \quad |n^2| \approx 1\end{aligned} \tag{C-162}$$

Substituting Eq. (C-162) into Eqs. (C-152)–(C-157),

$$\begin{aligned}H_{\phi\,\text{pseudo-surface}} = H_{\phi 1\,\text{image}}[R_{\mathrm{v}}(\theta_1)](j\pi s_1)\exp[j(\pi/2)s_1^2]\mathscr{F}^*(s_1) \\ - (H_{\phi 1\,\text{image}} + H_{\phi 2\,\text{image}}), \quad |n^2| \approx 1\end{aligned} \tag{C-163}$$

$$\begin{aligned}E_{\rho\,\text{pseudo-surface}} &= [R_{\mathrm{v}}(\theta_1)][1 + R_{\mathrm{v}}(\theta_1)]^{-1}\cos\theta_1 Z_0 H_{\phi 1\,\text{image}} \\ &\quad \times \{1 + [R_{\mathrm{v}}(\theta_1)](j\pi s_1)\exp[j(\pi/2)s_1^2]\mathscr{F}^*(s_1)\} \\ &\quad - (E_{\rho 1\,\text{image}} + E_{\rho 2\,\text{image}} + E_{\rho 3\,\text{image}}) \\ &= E_{\rho 1\,\text{image}}[R_{\mathrm{v}}(\theta_1)][1 + R_{\mathrm{v}}(\theta_1)]^{-1} \\ &\quad \{1 + [R_{\mathrm{v}}(\theta_1)](j\pi s_1)\exp[j(\pi/2)s_1^2]\mathscr{F}^*(s_1)\} \\ &\quad - (E_{\rho 1\,\text{image}} + E_{\rho 2\,\text{image}} + E_{\rho 3\,\text{image}}), \quad |n^2| \approx 1\end{aligned} \tag{C-164}$$

$$\begin{aligned}E_{z\,\text{pseudo-surface}} = E_{z1\,\text{image}}[R_{\mathrm{v}}(\theta_1)](j\pi s_1)\exp[j(\pi/2)s_1^2]\mathscr{F}^*(s_1) \\ - (E_{z1\,\text{image}} + E_{z2\,\text{image}} + E_{z3\,\text{image}}), \quad |n^2| \approx 1\end{aligned} \tag{C-165}$$

$$\begin{aligned}H_{\phi\,\text{surface}} = -H_{\phi 1\,\text{image}}[R_{\mathrm{v}}(\theta_1)]\{1 - (j\pi s_1)\exp[j(\pi/2)s_1^2]\mathscr{F}^*(s_1)\} \\ - H_{\phi 2\,\text{image}}R_{\mathrm{v}}(\theta_1), \quad |n^2| \approx 1\end{aligned} \tag{C-166}$$

$$\begin{aligned}E_{\rho\,\text{surface}} &= -E_{\rho 1\,\text{image}}[R_{\mathrm{v}}(\theta_1)]^2[1 + R_{\mathrm{v}}(\theta_1)]^{-1} \\ &\quad \times \{1 - (j\pi s_1)\exp[j(\pi/2)s_1^2]\mathscr{F}^*(s_1)\} \\ &\quad - (E_{\rho 2\,\text{image}} + E_{\rho 3\,\text{image}})R_{\mathrm{v}}(\theta_1), \quad |n^2| \approx 1\end{aligned} \tag{C-167}$$

$$E_{z\,\text{surface}} = -E_{z1\,\text{image}}[R_v(\theta_1)]\{1 - (j\pi s_1)\exp[j(\pi/2)s_1^2]\mathcal{F}^*(s_1)\} - (E_{z2\,\text{image}} + E_{z3\,\text{image}})R_v(\theta_1), \quad |n^2| \approx 1 \tag{C-168}$$

where s_1 is yet to be specified.

The value of $\varepsilon'|_{\text{far-field constraint}}$ given by Eq. (C-162) agrees with $\varepsilon' = \varepsilon' - (\gamma_0/k_0)$ given by Eq. (C-123) where ε and γ_0 are given by Eqs. (C-103) and (C-112), respectively. However, for $|n^2| \approx 1$, Eqs. (C-103) and (C-112) are restricted to angles $0 \leq \theta_1 \ll (1/3)$ rad [see Eq. (C-135a)]. For such small angles, $\varepsilon'|_{\text{far-field constraint}} \approx n^{-1} - 1 = \varepsilon'(0)$ where $\varepsilon'(0)$ is given by Eq. (C-127). The ratio $\varepsilon'|_{\text{far-field constraint}}/\varepsilon'(0)$ is given by

$$\varepsilon'|_{\text{far-field constraint}}/\varepsilon'(0) = \{-\cos\theta_1 + n^{-1}[1 - n^{-2}\sin^2\theta_1]^{1/2}\} \times (n^{-1} - 1)^{-1}, \quad \text{arbitrary } \theta_1, \quad |n^2| \approx 1 \tag{C-169a}$$

$$\varepsilon'|_{\text{far-field constraint}}/\varepsilon'(0) \approx 1; \quad 0 \leq \theta_1 \ll (1/3)\,\text{rad}, \; |n^2| \approx 1 \tag{C-169b}$$

$$\varepsilon'|_{\text{far-field constraint}}/\varepsilon'(0) \approx -[2/(n-1)]^{1/2}; \quad \theta_1 \approx \pi/2\,\text{rad}, \quad |n^2| \approx 1 \tag{C-169c}$$

Therefore, $\varepsilon'|_{\text{far-field constraint}} \approx \varepsilon'(0)$ only for small angles θ_1 measured from the normal to the air–earth interface. However, integrity of the stationary phase method requires that the argument s_1 in Eqs. (C-163)–(C-168) be a function of $\varepsilon' \approx \varepsilon'(0)$ at all angles θ_1 [see Eq. (C-137a and b)]. Substituting Eq. (C-127) into Eq. (C-142),

$$s_1 = (1/2)(n^{-1} - 1)(k_0 r_1/\pi)^{1/2}; \quad \varepsilon' \approx \varepsilon'(0), \quad |n^2| \approx 1 \tag{C-170}$$

Equations (C-163)–(C-168) together with Eq. (C-170) constitute the surface-wave field equations for the case $|n^2| \approx 1$.

A more precise value of s_1, applicable only for $0 \leq \theta_1 \ll (1/3)\,\text{rad}$, is obtained by substituting Eq. (C-162) into Eq. (C-142). Accordingly,

$$s_1 = [1 + R_v(\theta_1)]^{-1}(\cot\theta_1)(k_0 r_1/\pi)^{1/2} = s_0/2; \quad 0 \leq \theta_1 \ll (1/3)\,\text{rad}, \quad |n^2| \approx 1 \tag{C-171}$$

where s_0 is given by Eq. (C-104). For small angles θ_1, Eq. (C-171) reduces to Eq. (C-170). However, Eq. (C-171) cannot be considered to be more general than Eq. (C-170) because Eq. (C-170) is applicable at all angles whereas Eq. (C-171) is restricted to small angles. Numerical results obtained by substitution of Eq. (C-171) into Eq. (C-168) with $\theta_1 = \pi/2$ rad and $|n^2| = 1.05,\ 1.01$ gave poor

agreement with accurate results obtained by numerical integration of the Sommerfeld integral whereas substitution of Eq. (C-170) gave good agreement [140]. For $n = 1$, Eq. (C-170) reduces to $s_1 = 0$ for arbitrary θ_1 whereas Eq. (C-171) reduces to $s_1 = 0$ for $\theta_1 = \pi/2$ rad only.

Equations (C-163)–(C-171) are subject to three approximations:

1. A partially implemented modified variational method, realized in Eqs. (C-136), (C-137a and b);
2. Method of stationary phase, realized in Eqs. (C-143)–(C-145) that provides an asymptotic evaluation of the integrals analogous to the integrals of Eqs. (C-53) and (C-54); and
3. Neglect of the $(jk_0r_1)^{-2}$ and $(jk_0r_1)^{-3}$ higher-order terms in Eqs. (C-143)–(C-145), analogous to those terms neglected in Eq. (C-62c and d).

For $0 \leq \theta_1 \ll (1/3)\,\text{rad}$, $|n^2| \approx 1$, the parameters ε, λ, γ_0, γ_1, N_0, N, γ_0/N, and ε/N are given by the same expressions as for $|n^2| \gg 1$, namely, Eqs. (C-103) and (C-111)–(C-117), respectively. For $(\ll 1/3) \leq \theta_1 \leq (\pi/2)$ rad and $|n^2| \approx 1$, the parameters ε, λ, γ_0, γ_1, N_0, N, γ_0/N, and ε/N are undetermined.

Appendix D

Beam Pointing Errors Caused by a Nonhomogeneous Earth

Consider a plane wave that is incident from the true direction (θ, ϕ) at the kth element of a large array of m randomly distributed elements within a circular area of radius r_A. The elements are in proximity to nonhomogeneous earth whose nonhomogeneities are not necessarily randomly distributed over the circular area. A systematic distribution of nonhomogeneities causes beam pointing errors B_θ, B_ϕ that in turn cause a linear phase shift. The beam pointing errors reduce the tracking accuracy of the array. The linear phase shift causes a mean phase-squared error α_B^2 which should be subtracted from the array mean phase-squared error computed at the diffraction focus of the array. Expressions for the beam pointing errors B_θ, B_ϕ, and RMS phase error α_B are derived in this appendix.

The true phase advance $\delta_{\text{true},\,k}$, of the direct field at the kth element, relative to that of an element at the center of the array, is given by Ref. [189] as

$$\begin{aligned}\delta_{\text{true},k} &= (2\pi/\lambda_0)(x_k \sin\theta\cos\phi + y_k \sin\theta\sin\phi) \\ &= (2\pi/\lambda_0)(x_k u + y_k v)\end{aligned} \tag{D-1}$$

where

x_k, y_k = coordinates of the kth element along the x and y axes, respectively with the origin at the center of the array.

$u = \sin\theta\cos\phi$

$v = \sin\theta\sin\phi$

The measured phase delay δ_k at the kth element, in the presence of an indirect field reflected from the earth, is given by

$$\delta_k = \delta_{\text{true},\,k} + (\alpha_k - \bar{\alpha}) \tag{D-2}$$

where α_k, $\bar{\alpha}$ are given by Eqs. (13.2.9) and (13.2.10), respectively, of Sec. 13.2.2.

The estimates $\hat{u} = \sin\theta\cos\phi$, $\hat{v} = \sin\theta\sin\phi$ may be determined from the least squares algorithm given by

$$\text{minimize with respect to } \hat{u},\hat{v}: \sum_{k=1}^{m}[\delta_k - (2\pi/\lambda_0)(x_k\hat{u} + y_k\hat{v})]^2 \tag{D-3}$$

The minimization in Eq. (D-3) is executed by

$$\frac{\partial}{\partial\hat{u}}\sum_{k=1}^{m}[\delta_k - (2\pi/\lambda_0)(x_k\hat{u} + y_k\hat{v})]^2 = 0 \tag{D-4}$$

$$\frac{\partial}{\partial\hat{v}}\sum_{k=1}^{m}[\delta_k - (2\pi/\lambda_0)(x_k\hat{u} + y_k\hat{v})]^2 = 0 \tag{D-5}$$

Eqs. (D-4) and (D-5) reduce to

$$\sum_{k=1}^{m}[\delta_k x_k - (2\pi/\lambda_0)x_k^2\hat{u} - (2\pi/\lambda_0)x_k y_k\hat{v}] = 0 \tag{D-6}$$

$$\sum_{k=1}^{m}[\delta_k x_k - (2\pi/\lambda_0)x_k y_k\hat{u} - (2\pi/\lambda_0)y_k^2\hat{v}] = 0 \tag{D-7}$$

The projections x_k and y_k are uncorrelated (because the element locations are randomly distributed). Accordingly,

$$\sum_{k=1}^{m} x_k y_R \approx 0, \quad \text{elements randomly distributed} \tag{D-8}$$

Substituting Eq. (D-8) into Eqs. (D-6) and (D-7),

$$\begin{aligned}\hat{u} &= \frac{\lambda_0}{2\pi}\frac{\sum_{k=1}^{m} x_k\delta_k}{\sum_{k=1}^{m} x_k^2} = \frac{\lambda_0}{2\pi}\frac{\sum_{k=1}^{m} x_k[(2\pi/\lambda_0)x_k u + (\alpha_k - \bar{\alpha})]}{\sum_{k=1}^{m} x_k^2} \\ &= u + \frac{\lambda_0}{2\pi r_A}\frac{\sum_{k=1}^{m}(x_k/r_A)(\alpha_k - \bar{\alpha})}{\sum_{k=1}^{m}(x_k/r_A)^2}; \; x_k, y_k \text{ are uncorrelated}\end{aligned} \tag{D-9}$$

$$\hat{v} = \frac{\lambda_0}{2\pi}\frac{\sum_{k=1}^{m} y_k \delta_k}{\sum_{k=1}^{m} y_k^2} = \frac{\lambda_0}{2\pi}\frac{\sum_{k=1}^{m} y_k[(2\pi/\lambda_0)x_k v + (\alpha_k - \bar{\alpha})]}{\sum_{k=1}^{m} y_k^2}$$

$$= v + \frac{\lambda_0}{2\pi r_A}\frac{\sum_{k=1}^{m}(y_k/r_A)(\alpha_k - \bar{\alpha})}{\sum_{k=1}^{m}(y_k/r_A)^2}; \quad x_k, y_k \text{ are uncorrelated} \tag{D-10}$$

It should be noted that $\hat{u} = u$, $\hat{v} = v$ for the cases of homogeneous earth ($\alpha_k = \bar{\alpha}$) and nonhomogeneous earth with randomly-distributed elements and nonhomogeneities ($\sum x_k(\alpha_k - \bar{\alpha}) = \sum y_k(\alpha_k - \bar{\alpha}) = 0$). However, for nonhomogeneous earth with systematically-distributed elements or nonhomogeneities ($\sum x_k(\alpha_k - \bar{\alpha}) = \sum y_k(\alpha_k - \bar{\alpha}) \neq 0$), then $\hat{u} \neq u$, $\hat{v} \neq v$.

The RMS phase error α_B contributed by beam pointing errors is given by

$$\alpha_B = (1/m)\sum_{k=1}^{m}(2\pi r_A/\lambda_0)^2[(x_k/r_A)(\hat{u} - u) + (y_k/r_A)(\hat{v} - v)]^2 \tag{D-11}$$

where $\hat{u} = u$, $\hat{v} = v$ are given by Eqs. (D-9) and (D-10), respectively.

Since x_k and y_k have been assumed to be uncorrelated, Eq. (D-11) reduces to

$$\alpha_B = (2\pi r_A/\lambda_0)[(1/m)(\hat{u} - u)^2\sum_{k=1}^{m}(x_k/r_A)^2 + (1/m)(\hat{v} - v)^2\sum_{k=1}^{m}(y_k/r_A)^2]^{1/2}, \quad x_k, y_k \text{ are uncorrelated} \tag{D-12}$$

Substituting Eqs. (D-9) and (D-10) into Eq. (D-12),

$$\alpha_B = \left\{ \frac{(1/m)\left[\sum_{k=1}^{m}(x_k/r_A)(\alpha_k - \bar{\alpha})\right]^2}{\sum_{k=1}^{m}(x_k/r_A)^2} + \frac{(1/m)\left[\sum_{k=1}^{m}(y_k/r_A)(\alpha_k - \bar{\alpha})\right]^2}{\sum_{k=1}^{m}(x_k/r_A)^2} \right\}^{1/2}, \tag{D-13}$$

x_k, y_k are uncorrelated

The beam pointing errors B_θ, B_ϕ in the elevation and azimuthal directions, respectively, are defined as

$$B_\theta = \theta_{\text{apparent}} - \theta \tag{D-14}$$

$$B_\phi = \phi_{\text{apparent}} - \phi \tag{D-15}$$

where $(\theta_{\text{apparent}}, \phi_{\text{apparent}})$ is the apparent beam direction when the beam has a true direction (θ, ϕ). The beam pointing errors B_θ, B_ϕ are related to $\hat{u}$, $\hat{v}$ by

$$\begin{aligned}
\hat{u} = \widehat{\sin\theta\cos\phi} &= \overline{\sin(\theta_{\text{apparent}} - B_\theta)\cos(\phi_{\text{apparent}} - B_\phi)} \\
&= \text{estimate}[(\sin\theta_{\text{apparent}}\cos B_\theta - \sin B_\theta\cos\theta_{\text{apparent}}) \\
&\quad \times (\cos\phi + B_\phi\sin\phi + \sin\phi_{\text{apparent}}\sin B_\phi)] \\
&\approx (\sin\theta - B_\theta\cos\theta)(\cos\phi - B_\phi\sin\phi) \\
&\approx \sin\theta\cos\phi - B_\theta\cos\theta\cos\phi + B_\phi\sin\theta\sin\phi\,; \quad B_\theta \ll 1\ rad,\ B_\phi \ll 1\ rad
\end{aligned} \tag{D-16}$$

$$\begin{aligned}
\hat{v} = \widehat{\sin\theta\cos\phi} &= \overline{\sin(\theta_{\text{apparent}} - B_\theta)\sin(\phi_{\text{apparent}} - B_\phi)} \\
&= \text{estimate}[(\sin\theta_{\text{apparent}}\cos B_\theta - \sin B_\theta\cos\theta_{\text{apparent}}) \\
&\quad \times (\sin\phi_{\text{apparent}}\cos B_\phi - \cos\phi_{\text{apparent}}\sin B_\phi)] \\
&\approx (\sin\theta - B_\theta\cos\theta)(\sin\phi - B_\phi\cos\phi) \\
&\approx \sin\theta\sin\phi - B_\theta\cos\theta\cos\phi - B_\phi\sin\theta\cos\phi\,; \\
&\quad B_\phi \ll 1\,\text{rad},\ B_\phi \ll 1\,\text{rad}
\end{aligned} \tag{D-17}$$

Rearranging terms,

$$\hat{u} - u = -(\cos\theta\cos\phi)B_\theta + (\sin\theta\sin\phi)B_\phi \tag{D-18}$$

$$\hat{v} - v = -(\cos\theta\sin\phi)B_\theta + (\sin\theta\cos\phi)B_\phi \tag{D-19}$$

Denoting $\Delta = \begin{vmatrix} -\cos\theta\cos\phi & \sin\theta\sin\phi \\ -\cos\theta\sin\phi & -\sin\theta\cos\phi \end{vmatrix} = \cos\theta\sin\theta$

$$
\begin{aligned}
B_\theta &= \frac{1}{\Delta}\begin{vmatrix} \hat{u}-u & \sin\theta\sin\phi \\ \hat{v}-v & -\sin\theta\cos\phi \end{vmatrix} \\
&= (1/\Delta)[(\hat{u}-u)(-\sin\theta\cos\phi) - (\hat{v}-v)(\sin\theta\sin\phi)] \\
&= -(1/\cos\theta)[(\hat{u}-u)\cos\phi + (\hat{v}-v)\sin\phi],\ B_\theta \ll 1\,\text{rad}
\end{aligned}
\tag{D-20}
$$

$$
\begin{aligned}
B_\phi &= \frac{1}{\Delta}\begin{vmatrix} \cos\theta\ \cos\phi & \hat{u}-u \\ -\cos\theta\ \sin\phi & \hat{v}-v \end{vmatrix} \\
&= (1/\Delta)[(\hat{v}-v)(-\cos\theta\ \cos\phi) - (\hat{u}-u)(\cos\theta\ \sin\phi)] \\
&= -(1/\sin\theta)[(\hat{u}-u)\sin\phi + (\hat{v}-v)\cos\phi],\ \ B_\phi \ll 1\,\text{rad}
\end{aligned}
\tag{D-21}
$$

where $\hat{u}-u$, $\hat{v}-v$ are given by Eqs. (D-9) and (D-10), respectively.

References

CHAPTER 1

1. J Bardeen. The diffraction of a circularly symmetrical electromagnetic wave by a co-axial circular disc of infinite conductivity. Phys Rev 36:1482–1488, 1930.
2. JH Richmond. Monopole Antenna on Circular Disk. Technical Report 711639-1. Electro Science Laboratory, July 1979. See also IEEE Trans Antennas Propagation AP-32(12):1282-1287, 1984.
3. A Leitner, RD Spence. The oblate spheroidal wave functions. Franklin Inst J 249(4):299–321, 1950.
4. A Leitner. Effect of a Circular Groundplane on Antenna Radiation. Research Report No EM-19. Mathematics Research Group, New York University, April 1950.
5. A Leitner. Effect of a circular groundplane on antenna radiation. J Appl Phys 21:1001–1006, 1950.
6. CL Tang. On the Radiation Pattern of a Base-Driven Antenna over a Circular Conducting Screen. Technical Report No 301. Cruft Laboratory, Harvard University, May 1959.
7. JE Storer. The impedance of an antenna over a large circular screen. J Appl Phys 22(Aug):1058–1066, 1951. See also Techical Report No 119, Cruft Laboratory, Harvard University, Nov 1950.
8. JE Storer. The Radiation Pattern of an Antenna over a Circular Ground Screen. Technical Report No 126. Cruft Laboratory, Harvard University, June 1951.
9. KH Awadalla, TSM Maclean. Input impedance of a monopole antenna at the center of a finite groundplane. IEEE Trans Antennas Propagation AP-26(2):244–248, 1978.
10. KH Awadalla, TSM Maclean. Monopole antenna at the center of a circular groundplane: Input impedance and radiation pattern. IEEE Trans Antennas Propagation AP-27(2):151–153, 1979.

11. GA Thiele, TH Newhouse. A hybrid technique for combining moment methods with the geometrical theory of diffraction. IEEE Trans Antennas Propagation AP-23(1):62–69, 1975.

CHAPTER 2

12. RF Harrington. Time-Harmonic Electromagnetic Fields. New York: McGraw-Hill, 1961, pp 106–112. Please note that the signs of the radial field *E* on p 111 and the circumferential magnetic frill M on p 112 in 12 differ from those in Eqs. (2.4.9) and (2.4.8), respectively, because in 12 the voltage at the outer conductor is positive with respect to that at the inner conductor.
13. RWP King. The Theory of Linear Antennas. Cambridge, MA: Harvard University Press, 1956, p 87.
14. RS Elliot. Antenna Theory and Design. Englewood Cliffs, NJ: Prentice-Hall, 1981, pp 290–291.
15. CA Balanis. Antenna Theory: Analysis and Design. New York: Harper and Row, 1982, p 315.
16. CA Balanis. Antenna Theory: Analysis and Design. New York: Harper and Row, 1982, p 101, Eq. (4-2).

CHAPTER 3

17. L Brillouin. Origin of radiation resistance. Radioelectricite 3:147–152, 1922.
18. JA Stratton. Electromagnetic Theory. New York: McGraw-Hill, 1941, pp 454–457.
19. M Abramowitz, IA Stegun. Handbook of Mathematical Functions. New York: Dover Publications, 1972, pp 231, 244.
20. CA Balanis. Antenna Theory: Analysis and Design. New York: Harper and Row, 1982, p 292.
21. W Magnus, F Oberhettinger. Formulas and Theorems for the Functions of Mathematical Functions. New York: Chelsea Publishing, 1954, p 34.
22. IS Gradshteyn, IM Ryzhik. Tables of Integrals, Series and Products. New York: Academic Press, 1965.
23. JB Thomas. An Introduction of Statistical Communication Theory. New York: John Wiley and Sons, 1969, Appendix B: The Dirac Delta Function.
24. M Abramowitz, IA Stegun. Handbook of Mathematical Functions. New York: Dover Publications, 1972, p 763.
25. CA Balanis. Antenna Theory: Analysis and Design. New York: Harper and Row, 1982, pp 502–522, 529–531.
26. CA Balanis. Antenna Theory: Analysis and Design. New York: Harper and Row, 1982, pp 118–126, 133–135, 285–295.

CHAPTER 4

27. RS Elliot. Antenna Theory and Design. Englewood Cliffs, NJ: Prentice-Hall, 1981, p 29.

28. WJ Stutzman, GA Thiele. Antenna Theory and Design. New York: John Wiley and Sons, 1981, pp 489–495, 500–507.
29. W Magnus, F Oberhettinger. Formulas and Theorems for the Functions of Mathematical Functions. New York: Chelsea Publishing, 1954, pp 158–159.

CHAPTER 6

30. LJ Chu. Physical limitations of omni-directional antennas. J Appl Phys 19:1163–1175, 1948.
31. RF Harrington. Time-Harmonic Electromagnetic Fields. New York: McGraw-Hill, 1961, p 316, Chapter 6, problem 6–31.
32. RC Hansen. Fundamental limitations in antennas. Proc IEEE 69(2):170–182, 1981. Please note the error in Hansen's fifth equation. It should read

$$Q_n = (FF^*/2)(kr\,X_n' - X_n) = ((FF^*/2)(kr\,X_n)' - 2X_n)$$

where the prime indicates differentiation with respect to the variable *kr*.
33. JS McLean. A re-examination of the fundamental limits on the radiation Q of electrically small antennas. IEEE Trans Antennas Propagation 44(5):672–676, 1996.
34. G Ploussios. An electronically tuned HF/VHF helical antenna. Microwave J May:223–240, 1991.
35. G Ploussios, A Strugatsky. The ETH (electronically tuned helix) antenna. IEEE Communications Society, IEEE Military Communications Conference, Proceedings, November 5–8, 1995, pp 39.3-1–39.3-6.
36. RE Webster. A single-control tuning circuit for electrically small antennas. IRE Trans Antennas Propagation 3:12–15, 1955.
37. "Man-Made Noise" presented at the 14th Plenary Assembly of the International Radio Consultative Committee (French) (CCIR) Kyoto, Japan, 1978. Report 258-3. International Radio Consultative Committee, International Telecommunication Union, Geneva, 1980.
38. AD Spaulding, RT Disney. Man-made radio noise, Part 1: estimates for business, residential, and rural areas. Report 74-28. Office of Transportation, Department of Commerce, Boulder, CO, 1974.
39. HA Haus, et al. IRE standards on methods of measuring noise in linear two-ports. Proc Inst Radio Eng 48:61–68, 1960.
40. HA Haus, et al. Representation of noise in linear two-ports. Proc Inst Radio Eng 48:69–74, 1960.
41. AH Radjy, RC Hansen. S/N performance of aperiodic monopoles. IEEE Trans Antennas Propagation 27(2):259–261, 1979.
42. International Radio Consultative Committee (CCIR, in French). Operating noise threshold of a radio receiving system. Presented at the 11th Plenary Assembly, Oslo, Norway, 1966. Report 413. International Telecommunication Union, Geneva, Switzerland, 1967.
43. J Aitchison, J Brown. The Lognormal Distribution. Cambridge, England: Cambridge University Press, 1969, p 8.

44. PL Rice, AG Longley, KA Norton, AP Barsis. Transmission Loss Prediction for Tropospheric Communication Circuits. NBS Tech Note 101. Vols. I and II (revised), Jan 1967, NTIS, AD 687820 (Vol. I) and AD 687821 (Vol. II).
45. AG Longley, PL Rice. Prediction of Tropospheric Radio Transmission Loss over Irregular Terrain: A Computer Method—1968. ESSA Technical Report ERL-79-ITS 67. U.S. Department of Commerce, Boulder, CO, 1968, NTIS, AD 676874.
46. GA Hufford. The Longley–Rice Model—An Implementation, 1979 Programmer's and User's Guide. Boulder, Co: Inst. Telecommun. Sci., 1979.
47. GD Gierhart, ME Johnson. Computer Programs for Air/Ground Propagation and Interference Analysis, 0.1 to 20 GHz. ITS Technical Report FAA-RD-77-60. Sept 1973, NTIS, AD 770335.
48. GD Gierhart, ME Johnson. Applications Guide, Propagation and Interference Analysis Computer Programs (0.1 to 20 GHz). ITS Technical Report FAA-RD-77-60. Mar 1978, NTIS, AD A053242.
49. GD Gierhart, ME Johnson. Propagation Model (0.1 to 20 GHz) Extensions for 1977 Computer Programs. ITS Technical Report FAA-RD-77-129. May 1978, NTIS, AD A055605.
50. International Radio Consultative Committee (CCIR, in French). The Concept of Transmission Loss in Studies of Transmission Loss in Studies of Radio Systems, Recommendation 341. 14th Plenary Assy, Kyoto (1978). Vol. 1, Annex 1, Int Telecommun Union, Geneva, Switzerland, 1978, p 148.
51. GH Hagn. VHF radio system performance model for predicting communications operational ranges in irregular terrain. IEEE Trans Commun COM-28(9):1637–1644, 1980.
52. AG Longley. Radio propagation in urban areas. Conf Rec 28th IEEE Vehicular Technol Conf Denver, CO, Mar 22–24, 1978.
53. Y Okumura, E Ohmori, K Fukuda. Field strength and its variability in VHF and UHF land-mobile radio service. Rev Elec Commun Lab (Tokyo, Japan) 16:325–873, 1968.
54. K Bullington. Radio propagation fundamentals. Bell System Tech J 36:593–636, 1957.
55. JR Wait, RH Ott, T Telfer, eds. Workshop on Radio Systems in Forested and or Vegetated Environments. Technical Report ACC-ACO-1-74, Fort Huachuca, AZ: Advanced Concepts Office, U.S. Army Communications Command, 1974, AD 780712.
56. AH LaGrone. Propagation of VHF and UHF electromagnetic waves over a grove of trees in full leaf. IEEE Trans Antennas AP-25(6):866–869, 1977.
57. ML Meeks. Radar Propagation at Low Altitudes: A Review and Bibliography. Technical Report 580. MIT Lincoln Lab, July 1981, NTIS, AD A103773. Also available in book form (Dedham, MA: Artech House, 1982).
58. MI Miles, AP Barsis. Summary of 20–100 MHz Propagation Measurement Results over Irregular Terrain Using Low Antenna Heights. U.S. Department of Commerce, ESSA Technical Report. IER 10-ITSA 10, 1966.

59. AG Longley, RL Reasoner, VL Fuller. Measured and Predicted Long-Term Distributions of Tropospheric Transmission loss. OT Telecommun Res Eng Rep OT/TRER 16. Washington, DC: U.S. Government Printing Office, 1971.
60. MM Weiner, GA Robertshaw. Coherent Scatter of Microwaves from Moderately Rough Surfaces. Bedford, MA: The MITRE Corporation, 1981, ESD-TR-81-147, NTIS, AD A106133.
61. MM Weiner. A Comparison of the Longley–Rice Semi-Empirical Model with Theoretical Models for Coherent Scatter. Bedford, MA: The MITRE Corporation, 1982, ESD-TR-82-133, NTIS, AD A114644.
62. MM Weiner. Terrain and Sea Surface Truth: Profile Distributions. Bedford, MA: The MITRE Corporation, 1981, ESD-TR-81-387, NTIS, AD A110219.
63. GA Hufford, AG Longley, WA Kissick. A Guide to the Use of the ITS Irregular Terrain Model in the Area Prediction Mode. NTIA Report 82-100. Boulder, CO: U.S. Department of Commerce, 1982.
64. MM Weiner, E Jappe, NJ Johnson. Input Parameter Specification for the Longley–Rice and Johnson–Gierhart Tropospheric Radio Propagation Programs, 0.02–40 MHz. Bedford, MA: The MITRE Corporation, 1982, NTIS, AD-A122582.
65. GA Hufford. Modifications to the Use of the ITS Irregular Terrain Model in the Point-to-Point Mode. Boulder, CO: U.S. Department of Commerce, Jan 30, 1985, NTIA Memo.
66. MN Lustgarten, JA Madison. An empirical propagation model (EPM-73). IEEE Trans Electromagn Compat EMC-19(3):301–309, 1977.
67. M Weissberger, R Meidenbauer, H Riggens, S Marcus. Radio wave propagation: a handbook of practical techniques for computing basic transmission loss and field strength. Electromagn Compat Analysis Cen Rep ECAC-HDBK-82-049, Sept 1982, NTIS, AD A122090.
68. JP Murray. An Atlas of propagation curves for tactical electronic warfare planning in ground-to-ground scenarios. 30th Symposium Electromagnetic Wave Propagation Panel, Copenhagen, Denmark, May 24–28, 1982. In: HJ Albrecht, ed. Propagation Effects of ECM Resistant Systems in Communication and Navigation. AGARD Conf Proc No CP-331, Aug 1982, pp 16.1–16.14, NTIS, AD A123251.
69. ML Meeks. A propogation experiment combining reflection and diffraction. IEEE Trans Antennas Propagation AP-30:318–321, 1982.
70. ML Meeks. VHF propagation over hilly forested terrain. IEEE Trans Antennas Propagation AP-31:483–489, 1983.
71. ML Meeks. Radar Propagation at Low Altitudes. Dedham, MA: Artech House, 1982.
72. S Ayasli. SEKE: a computer model for low altitude radar propagation over irregular terrain. IEEE Trans Antennas Propagation AP-34(8):1013–1023, 1986.
73. Institute for Telecommunication Sciences. The IF-77 electromagnetic wave propagation model. NTIS, ADA-134504.
74. Institute for Telecommunication Sciences. Comparison of measured data with IF-77 propagation model predictions. NTIS, ADA-076508.
75. Institute for Telecommunication Sciences. An atlas of basic transmission loss of 0.125 to 15.5 GHz. NTIS, ADA-088153.

76. Institute for Telecommunication Sciences. Aerospace propagation prediction capabilities associated with the IF-77 Model. NTIS, ADA-063792.

CHAPTER 7

77. A Sommerfeld. Propagation of waves in wireless telegraphy. Ann Phys 28:665–736, 1909; 81:1135–1153, 1926.
78. A Sommerfeld. Wireless telegraphy. Die Differential und Integralgleichungen der Mechanik und Physik. Vol. 2. Braunschweig, Germany: F Vieweg, 1935, Chapter 23.
79. KA Norton. The propagation of radio waves over the surface of the earth and in the upper atmosphere. Proc IRE 24:1367–1387, 1936; 25(pt. II):1203–1236.
80. KA Norton. The calculations of ground-wave field intensity over a finitely conducting spherical earth. Proc IRE 29:623–639, 1941.
81. A Banos, Jr. Dipole Radiation in the Presence of a Conducting Half-Space. New York: Pergamon Press, 1966.
82. JR Wait, LL Campbell. The fields of an electric dipole in a semi-infinite conducting medium. J Geophys Res 58:21–28, 1953.
83. PM Hansen. The radiation efficiency of a dipole antenna located above an imperfectly conducting ground. IEEE Trans Antennas Propagation AP-20(6):766–770, 1972.
84. RWP King. New formulas for the electromagnetic field of a vertical electric dipole in a dielectric or conducting half-space near its horizontal interface. J Appl Phys 53:8476–8482, 1982; (erratum) 56:3366, 1984.
85. RWP King (with TT Wu). Electromagnetic field of a vertical dipole over an imperfectly conducting half-space. Radio Sci 25(2):149–160, 1990.
86. HG Booker, PC Clemmow. A relation between the Sommerfeld theory of radio propagation over a flat earth and the theory of diffraction of a straight edge. Proc IEE 97(pt. III):18–27, 1950.
87. PC Clemmow. The Plane Wave Spectrum Representation of Electromagnetic Fields. Oxford: Pergamon Press, 1966.
88. LM Brekhovskikh. Waves in Layered Media. 1st ed. New York: Academic Press, 1960, Chapter 4. Also available in a revised 2nd edition, 1980.
89. RP Rafuse, J Ruze. Low-angle radiation from vertically polarized antennas over radially heterogeneous flat ground. Radio Sci 10:1011–1018, 1975.
90. JR Wait, WA Pope. The characterization of a vertical antenna with a radial conductor ground system. Appl Sci Res, The Hague 4(Sec. B):177–195, 1954.
91. JR Wait, WJ Surtees. Impedance of a top-loaded antenna of arbitrary length over a circular ground screen. J Appl Phys 25:553–555, 1954.
92. JR Wait, LC Walters. Influence of a sector ground screen on the field of a vertical antenna. US National Bureau of Standards, Monograph 60, 1963, pp 1–11.
93. DA Hill, JR Wait. Calculated pattern of a vertical antenna with a finite radial-wire ground system. Radio Sci 8(1):81–86, 1973.
94. JR Wait. The theory of an antenna over an inhomogeneous ground plane. In: EC Jordan, ed. Electromagnetic Theory. Oxford: Pergamon Press, 1963, pp 1079–1097.

95. GD Monteath. Application of the Electromagnetic Reciprocity Principle. Oxford: Pergamon Press, 1973.
96. JR Wait, WA Pope. The characterization of a vertical antenna with a radial conductor ground system. Appl Sci Res, The Hague 4(Sec. B):177–195, 1954, [Eq. (7.62)].
97. JR Wait. Antenna performance influenced by the finite extent and conductivity of ground planes: a collection of reprints by JR Wait, et al. MITRE Report M90-79. Sept 1990, NTIS, AD-A232132/1/XAB.
98. JH Richmond. Monopole antenna on circular disk over flat earth. IEEE Trans Antennas Propagation AP-33(6):633–637, 1985.
99. GJ Burke, AG Poggio. Numerical electromagnetic code (NEC)—method of moments. Vol. 1: Theory and Code, Vol. 2: User's Guide. Report UCID-18834. Lawrence Livermore National Laboratory, 1981.
100. GJ Burke, EK Miller. Modeling antennas near to and penetrating a lossy interface. IEEE Trans Antennas Propagation AP-32:1040–1049, 1984.
101. GJ Burke. User's Guide Supplement for NEC-3 for Modeling Buried Wires. Report UCID-19918. Lawrence Livermore National Laboratory, 1983.
102. GJ Burke, EK Miller. Numerical modeling of monopoles on radial-wire ground screens. Proceedings of 1989 IEEE Antennas and Propagation Society Symposium, San Jose, CA, Vol. 1, 1989, pp 244–247.
103. MM Weiner, SP Cruze, CC Li, WJ Wilson. Monopole Elements on Circular Ground Planes. Norwood, MA: Artech House, 1987.

CHAPTER 8

104. ITU Recommendation P-527-3. Electrical Characteristics of the Surface of the Earth, P Series—Part 1, 1997, pp 140–142. International Telecommunication Union, Place des Nations—CH-1211, Geneva 20, Switzerland.
105. GH Hagn. HF ground and vegetation constants. Military Uses of High Frequency Spectrum. Burke, VA: Armed Forces Communications and Electronics Association (AFCEA) Professional Development Center Course, 1985.
106. GH Hagn. Ground constants at high frequencies (HF). Proceedings of Third Review of Progress in Applied Computational Electromagnetics, Monterey, CA, March 24–26, 1987.
107. S Ramo, JR Whinnery. Fields and Waves in Modern Radio. 2nd ed. New York: John Wiley & Sons, 1960, p 306.
108. J deBettencourt, D Davidson, JR Wait. IEEE guide for radio methods of measuring earth conductivity. IEEE Standard 356-1974. New York: Institute of Electrical and Electronics Engineers, 1974.
109. F Jay, ed. IEEE Standard Dictionary of Electrical and Electronic Terms. 4th ed. New York: Institute of Electrical and Electronic Engineers, 1988.

CHAPTER 9

110. JA Stratton. Electromagnetic Theory. New York: McGraw-Hill, 1941, p 494.

111. HR Reed, CM Russell. Ultra-High Frequency Propagation. Lexington, MA: Boston Technical Publishers, 1964, p 90.
112. RB Adler, LJ Chu, RM Fano. Electromagnetic Energy Transmission and Radiation. New York: John Wiley & Sons, pp 566–576.
113. P Beckmann, A Spizzochino. The Scattering of Electromagnetic Waves from Rough Surfaces. Oxford: Pergamon Press, 1963, pp 17–33.
114. RWP King. On the radiation efficiency and the electromagnetic field of a vertical electric dipole in the air above a dielectric or conducting half-space. Progress in Electromagnetic Research (PIER 4). New York: Elsevier, 1991, pp 1–42, Chapter 1.
115. GJ Burke. Private communication. Lawrence Livermore National Laboratory, June 19, 1990.
116. MM Weiner. Performance of ground-based high-frequency receiving arrays. Progress in Electromagnetic Research (PIER 8). Cambridge, MA: EMW Publishing, 1994, pp 109–159, Chapter 4.
117. JR Wait. Characteristics of antennas over lossy earth. In: RC Collin, FZ Zucker, eds. Antenna Theory, Part 2. New York: McGraw-Hill, 1969, pp 386–389, Chapter 23.
118. RWP King, SS Sandler. The electromagnetic field of a vertical electric dipole over the earth or sea. IEEE Trans Antennas Propagation AP-42(3):382–389, 1994.
119. JE Storer. The impedance of an antenna over a large circular screen. J Appl Phys 22(Aug):1063–1065, 1951, Sec. 5. See also Techical Report No 119, Cruft Laboratory, Harvard University, Nov 1950.
120. FB Hildebrand. Advanced Calculus for Engineers. New York: Prentice-Hall, 1949, p 8.
121. JD Jackson. Classical Electrodynamics. 2nd ed. New York: John Wiley & Sons, 1975, pp 316–317.
122. Reference Data for Radio Engineers. 6th ed. Indianapolis: Howard W Sams, 1983, Ch. 46, p. 37.
123. IV Lindell, E Alanen. Exact image theory for the sommerfeld half-space problem. IEEE Trans Antennas Propagation, Part I: Vertical Magnetic Dipole AP-32(2):126–133, 1984; Part II: Vertical Electric Dipole AP-32(8):841–847, 1984; Part III: General Formulation AP-32(10):1027–1032, 1984.
124. M Abramowitz, IA Stegun. Handbook of Mathematical Functions. New York: Dover Publications, 1972, p 300, items 7.3.1–7.3.2, 7.3.7.
125. JR Wait. Characteristics of antennas over lossy earth. In: RC Collin, FZ Zucker, eds. Antenna Theory. Part 2. New York: McGraw-Hill, 1969, p 391, eqs. (23.32) and (23.33). In [125], Sommerfeld's attenuation function is denoted by $F(p)$.
126. Reference Data for Radio Engineers. 6th ed. Indianapolis: Howard W Sams, 1983, Ch. 36, p 46.
127. GJ Burke. Private communication. LLNL, September 19, 2000.
128. TT Wu, RWP King. Radio Science. Vol. 17, No. 3, May–June 1982. Part I Lateral Waves: a New Formula (for $E_{1\rho}$) and Interference Patterns, pp 521–531; Part II Lateral Waves: New Formulas for $E_{1\phi}$ and E_{1z}, pp 532–538.
129. JR Wait. The ancient and modern history of EM ground-wave propagation. IEEE Antennas Propagation Mag 40(5):7–24, 1998.
130. A Fresnel. Mem Acad Sci 11:393, 1832.

131. H Hertz. Ann Physik 36:1, 1888.
132. MM Weiner. Total field of a vertically polarized Hertzian dipole above a half-space of either large or near-unity complex relative permittivity. IEEE Antennas and Propagation Magazine 2003 (submitted for publication).
133. V Houdzoumis. Scattering of electromagnetic missiles—Part I; Vertical electric dipole radiation over spherical earth—Part II. PhD dissertation, Harvard University, Cambridge, MA, 1994.
134. RW King, CW Harrison. Electromagnetic ground-wave field of vertical antennas for communication at 1 to 30 MHz. IEEE Trans Antennas Propagation AP-40(4):342–357, 1998.
135. KA Norton. The Polarization of Downcoming Ionospheric Radio Waves. Federal Communications Commission Rept 60047, declassified (National Bureau of Standards project sponsored by the National Defense Research Committee), Boulder, CO, 1942; Catalog, U.S. Department of Commerce, Information Resources Division, Library Branch MC5, 325 Broadway, Boulder, CO 80303.
136. KA Norton. Radio-wave propagation during world war II. Proc IRE 50(5):698–704, 1962, reference [40] and citation preceding references [31]–[40].
137. RJ King. Electromagnetic wave propagation over a constant impedance plane. Radio Sci 4(3):255–268, 1969.
138. RE Collin. Antennas and Radiowave Propagation. New York: McGraw-Hill, 1985, Sec. 6.5, Figure 6.35.
139. JR Wait. Electromagnetic Waves in Stratified Media. 1st ed. New York: Pergamon Press, 1996, second enlarged edition 1970; first edition reprinted by IEEE Press.
140. GJ Burke. Private communication. Lawrence Livermore National Laboratory, May–June, 2001.
141. M Abramowitz, IA Stegun. Handbook of Mathematical Functions. New York: Dover Publications, 1972, pp 231–244, compare Tables 7.7 and 7.9.
142. MM Weiner. Systems and Components for the Utilization of Electromagnetic Waves in Discrete, Phase-Ordered (Coherent) Media. U.S. Patent 3,765,773, Oct 16, 1973, Appendix A.

CHAPTER 10

143. JR Wait. Low angle radiation from HF antennas. Symposium on Antenna Technology and Applied Electromagnetics, Winnipeg, Canada, 15–17 August 1990.
144. JR Wait. Characteristics of antennas over lossy earth. In: RC Collin, FZ Zucker, eds. Antenna Theory. Part 2. New York: McGraw-Hill, 1969, pp 424–437, Chapter 23.
145. JR Wait. Electromagnetic Wave Theory. 3rd ed. Harper & Row/Wiley, 1992, Eq. (7.62).
146. MM Weiner, S Zamoscianyk, GJ Burke. Radiation efficiency and input impedance of monopole elements with radial-wire ground planes in proximity to earth. Electron Lett 28(16):1550–1551, 1992; "Comment" by JR Wait and "Reply" by MM Weiner, 3 December 1992, p 2329.

147. MM Weiner. Radiation efficiency and directivity of monopole elements with disc ground planes on flat earth. Electron Lett 28(25):2282–2283, 1992.
148. MM Weiner. Monopole element at the center of a circular ground plane whose radius is small or comparable to a wavelength. IEEE Trans Antennas Propagation AP-35(5):488–495, 1987.
149. JH Richmond. Far-Zone Field of Monopole Antenna on Circular Disk over Flat Earth. Report. MITRE Project 91260 HF Antenna Element Modeling, November 1990.
150. JR Carson. A generalization of the reciprocal theorem. Bell Systems Tech J 3(July):393–399, 1924.
151. JR Carson. Reciprocal theorems in radio communication. Proc IRE 17:952–956, 1929.
152. LL Tsai. Analysis and measurement of a dipole antenna mounted symmetrically on a conducting sphere or cylinder. PhD dissertation, Department of Electrical Engineering, Ohio State University, Columbus, Ohio, 1970.
153. LL Tsai. A numerical solution for the near and far fields of an annular ring of magnetic current. IEEE Trans Antennas Propagation AP-20(5):569–576, 1972.
154. GJ Burke. Private communication. Lawrence Livermore National Laboratory, April 1, 1992
155. RWP King. The Theory of Linear Antennas. Cambridge, MA: Harvard University Press, 1956, pp 158–159.
156. JH Richmond. Computer program WAIT–SURTEES. Report. MITRE Project 91260 HF Antenna Element Modeling, November 1990.

CHAPTER 11

157. GJ Burke. Modeling monopoles on radial-wire ground screens. Appl Comput Electromagn Newslett 1(1), 1986.
158. GJ Burke. User's Guide Supplement for NEC-GS. Report UCID-21301. Lawrence Livermore National Laboratory, 1988.
159. GJ Burke. Private communication. Lawrence Livermore National Laboratory, November 21, 1990.
160. A Ludwig. Wire grid modeling of surfaces. IEEE Trans Antennas Propagation AP-35(9):1045–1048, 1987.
161. RJ Paknys. The near field of a wire grid model. IEEE Trans Antennas Propagation AP-39:994–999, 1991.
162. EK Miller, AJ Poggio, GJ Burke, ES Selden. Analysis of wire antennas in the presence of a conducting half space: Part I. The vertical antenna in free space. Can J Phys 50:879–888, 1972.
163. EK Miller, AJ Poggio, GJ Burke, ES Selden. Analysis of wire antennas in the presence of a conducting half space: Part II. The horizontal antenna in free space. Can J Phys 50:2614–2627, 1972.
164. GJ Burke. User's Guide Supplement for NEC-3 for Modeling Buried Wires. Report UCID-19918. Lawrence Livermore National Laboratory, October 1983.

165. GJ Burke. A Model for Insulated Wires in the Method of Moments Code NEC. Report UCID-21301. Lawrence Livermore National Laboratory, 1988.
166. GJ Burke. Private communication. Lawrence Livermore National Laboratory, January 15, 1991.
167. GJ Burke. Numerical Electromagnetcs Code–NEC-4, Method of Moments, Part I: User's Manual, Part II: Program Description—Theory. Report UCRL-MA-109338. Lawrence Livermore National Laboratory, January 1992.
168. GJ Burke. Validation of NEC for Antennas Near Ground. Report UCRL-101190. Lawrence Livermore National Laboratory, 1989.
169. MM Weiner. Validation of the numerical electromagnetics code (NEC) for antenna wire elements in proximity to earth. Appl Comput Electromagn Soc J 8(2):44–71, 1993.
170. RL Lagace. Performance of the Monopole Antenna Element for the 96-Element Receiving Array of the High-Frequency High Resolution Experimental Site: Vol. 1 Theory and Results. Bedford, MA: The MITRE Corporation, 1991, NTIS AD-A259500, MTR-11291.
171. RL Lagace. Performance of the Monopole Antenna Element for the 96-Element Receiving Array of the High-Frequency High Resolution Experimental Site: Vol. 2 Appendices. Bedford, MA: The MITRE Corporation, 1991, NTIS AD-A259486, MTR-11291.
172. GH Hagn. Comparison of Full-Scale Measurements with Theory of a Monopole Element on a Radial-Wire Groundscreen in Imperfect Earth. 2nd Quarterly Review, Project 91260, High Frequency Antenna Element Modeling. Bedford, MA: The MITRE Corporation, 1990.
173. RH Stehle, GA DesBrisay, AL Whitson, GH Hagn. RELEDOP: a full-scale antenna pattern measurement system for high-powered HF transmitting antennas. IEEE Trans Broadcasting 34(2):210–220, 1988.
174. LO Harnish, M Lee, GH Hagn. Comparison of measured and NEC-calculated characteristics of a vertical monopole with buried radials. Conference Proceedings of 3rd Annual Review of Progress in Applied Computational Electromagnetics, Monterey, CA, March 24–26, 1987.

CHAPTER 12

175. GJ Burke. Private communication. Lawrence Livermore National Laboratory, December 9, 1992.
176. JR Wait. Effective impedance of a wire grid parallel to the earth's surface. IRE Trans Antennas Propagation AP-10(5):538–542, 1963.
177. LW Parker. Groundscreen Characterization. Report M91-82. The MITRE Corporation, 1991, NTIS, AD-A243164.
178. JR Wait. The impedance of a wire grid parallel to a dielectric interface. IRE Trans Microwave Theory Tech MTT-5:99–102, 1957
179. D Fan. A new approach to diffraction analysis of conductor grids. IEEE Trans Antennas Propagation AP-37(1):84–89, 1989.

180. GA Otteni. Plane wave reflection from a rectangular-mesh ground screen. IEEE Trans Antennas Propagation AP-21(6):843–851, 1973.
181. JK Skwirzynski, JC Thackray. Transmission of electromagnetic waves through wire gratings (theory). Marconi Rev 22:77–90, 1959.

CHAPTER 13

182. MM Weiner. Noise factor and antenna gains in the signal/noise equation for over-the-horizon radar. IEEE Trans Aerospace Electron Systems 27(6):886–890, 1991; "Addendum" Vol. 30, No. 2, April 1994, p 648.
183. MI Skolnik, ed. Radar Handbook. 2nd ed. New York: McGraw-Hill, 1990, pp 15.59, 24.3.
184. FE Nathanson. Radar Design Principles. New York: McGraw-Hill, 1969, p 522. Ref. [184] gives the reciprocal of f_{range} and f_{Doppler} in Eq. (13.1.10) because [184] defines loss factor as a gain instead of an attenuation.
185. DK Barton, HR Ward. Handbook of Radar Measurement. Englewood Cliffs, NJ: Prentice-Hall, 1969, p 348.
186. International Radio Consultative Committee (CCIR, in French). World distribution and characteristics of atmospheric radio noise. Report 322, 10th Plenary Assembly, Geneva (1963), Int Telecommunication Union, Geneva, Switzerland, 1964.
187. International Radio Consultative Committee (CCIR, in French). Characteristics and applications of atmospheric radio noise data. Report 322-2, 15th Plenary Assembly, Geneva (1982), Int Telecommunication Union, Geneva, Switzerland, 1983.
188. International Radio Consultative Committee (CCIR, in French). Recommendations and reports of the CCIR, Vol. 6, Man-Made Radio Noise. Report 258-4, 16th Plenary Assembly, Dubrovnik (1983), Int Telecommunication Union, Geneva, Switzerland, 1986.
189. RS Elliot. Antenna Theory and Design. Englewood Cliffs, NJ: Prentice-Hall, 1981, p 114.
190. M Born, E Wolf. Principles of Optics. 2nd ed. Oxford: Pergamon Press, 1964, pp 204–205, 460–462.
191. PJD Gething. Radio Direction Finding and the Resolution of Multi-Component Wave-Fields. London: Peter Peregrinus, 1978, Chapter 14.
192. WH Ahlbeck, WQ Crichlow, RT Disney, FF Fulton, Jr., CA Samson. Instruction Book for ARN-2 Radio Noise Recorder. Serial Nos. 1 to 10. Report 5545, National Bureau of Standards. U.S. Department of Commerce, 1985.